

Pertanika Journal of
**SCIENCE &
TECHNOLOGY**

JST

VOL. 29 (1) JAN. 2021



A scientific journal published by Universiti Putra Malaysia Press

Pertanika Journal of Science & Technology

About the Journal

Overview

Pertanika Journal of Science & Technology (PJST) is the official journal of Universiti Putra Malaysia published by UPM Press. It is an open-access online scientific journal which is free of charge. It publishes the scientific outputs. It neither accepts nor commissions third party content.

Recognized internationally as the leading peer-reviewed interdisciplinary journal devoted to the publication of original papers, it serves as a forum for practical approaches to improving quality in issues pertaining to science and engineering and its related fields.

PJST is a **quarterly** (January, April, July and October) periodical that considers for publication original articles as per its scope. The journal publishes in **English** and it is open to authors around the world regardless of the nationality.

The Journal is available world-wide.

Aims and scope

Pertanika Journal of Science and Technology aims to provide a forum for high quality research related to science and engineering research. Areas relevant to the scope of the journal include: bioinformatics, bioscience, biotechnology and bio-molecular sciences, chemistry, computer science, ecology, engineering, engineering design, environmental control and management, mathematics and statistics, medicine and health sciences, nanotechnology, physics, safety and emergency management, and related fields of study.

History

Pertanika was founded in 1978. A decision was made in 1992 to streamline *Pertanika* into three journals as *Pertanika Journal of Tropical Agricultural Science*, *Pertanika Journal of Science & Technology*, and *Pertanika Journal of Social Sciences & Humanities* to meet the need for specialised journals in areas of study aligned with the interdisciplinary strengths of the university.

After almost 28 years, as an interdisciplinary Journal of Science & Technology, the journal now focuses on research in science and engineering and its related fields.

Goal of *Pertanika*

Our goal is to bring the highest quality research to the widest possible audience.

Quality

We aim for excellence, sustained by a responsible and professional approach to journal publishing. Submissions are guaranteed to receive a decision within 14 weeks. The elapsed time from submission to publication for the articles averages 5-6 months.

Abstracting and indexing of *Pertanika*

The journal is indexed in SCOPUS (Elsevier), Clarivate-Emerging Sources Citation Index [ESCI (Web of Science)], BIOSIS, National Agricultural Science (NAL), Google Scholar, MyCite and ISC.

Future vision

We are continuously improving access to our journal archives, content, and research services. We have the drive to realise exciting new horizons that will benefit not only the academic community, but society itself.

Citing journal articles

The abbreviation for *Pertanika Journal of Science & Technology* is *Pertanika J. Sci. Technol.*

Publication policy

Pertanika policy prohibits an author from submitting the same manuscript for concurrent consideration by two or more publications. It prohibits as well publication of any manuscript that has already been published either in whole or substantial part elsewhere. It also does not permit publication of manuscript that has been published in full in Proceedings.

Code of Ethics

The *Pertanika* Journals and Universiti Putra Malaysia takes seriously the responsibility of all of its journal publications to reflect the highest in publication ethics. Thus all journals and journal editors are expected to abide by the Journal's codes of ethics. Refer to *Pertanika's Code of Ethics* for full details, or visit the Journal's web link at http://www.pertanika.upm.edu.my/code_of_ethics.php

International Standard Serial Number (ISSN)

An ISSN is an 8-digit code used to identify periodicals such as journals of all kinds and on all media—print and electronic. All *Pertanika* journals have ISSN as well as an e-ISSN.

Pertanika Journal of Science & Technology: ISSN 0128-7680 (*Print*); ISSN 2231-8526 (*Online*).

Lag time

A decision on acceptance or rejection of a manuscript is reached in 3 to 4 months (average 14 weeks). The elapsed time from submission to publication for the articles averages 5-6 months.

Authorship

Authors are not permitted to add or remove any names from the authorship provided at the time of initial submission without the consent of the Journal's Chief Executive Editor.

Manuscript preparation

Refer to *Pertanika's Instructions to Authors* at the back of this journal.

Editorial process

Authors are notified with an acknowledgement containing a *Manuscript ID* on receipt of a manuscript, and upon the editorial decision regarding publication.

Pertanika follows a **double-blind peer-review** process. Manuscripts deemed suitable for publication are usually sent to reviewers. Authors are encouraged to suggest names of at least three potential reviewers at the time of submission of their manuscript to *Pertanika*, but the editors will make the final choice. The editors are not, however, bound by these suggestions.

Notification of the editorial decision is usually provided within ten to fourteen weeks from the receipt of manuscript. Publication of solicited manuscripts is not guaranteed. In most cases, manuscripts are accepted conditionally, pending an author's revision of the material.

The Journal's peer-review

In the peer-review process, three referees independently evaluate the scientific quality of the submitted manuscripts.

Peer reviewers are experts chosen by journal editors to provide written assessment of the **strengths** and **weaknesses** of written research, with the aim of improving the reporting of research and identifying the most appropriate and highest quality material for the journal.

Operating and review process

What happens to a manuscript once it is submitted to *Pertanika*? Typically, there are seven steps to the editorial review process:

1. The Journal's Chief Executive Editor (CEE) and the Editorial Board Members (EBMs) examine the paper to determine whether it is appropriate for the journal and should be reviewed. If not appropriate, the manuscript is rejected outright and the author is informed.
2. The CEE sends the article-identifying information having been removed, to 2 or 3 reviewers who are specialists in the subject matter represented by the article. The CEE requests them to complete the review within 3 weeks.

Comments to authors are about the appropriateness and adequacy of the theoretical or conceptual framework, literature review, method, results and discussion, and conclusions. Reviewers often include suggestions for strengthening of the manuscript. Comments to the editor are in the nature of the significance of the work and its potential contribution to the research field.

3. The Editor-in-Chief (EiC) examines the review reports and decides whether to accept or reject the manuscript, invites the author(s) to revise and resubmit the manuscript, or seek additional review reports. Final acceptance or rejection rests with the CEE and EiC, who reserve the right to refuse any material for publication. In rare instances, the manuscript is accepted with almost no revision. Almost without exception, reviewers' comments (to the author) are forwarded to the author. If a revision is indicated, the editor provides guidelines to the authors for attending to the reviewers' suggestions and perhaps additional advice about revising the manuscript.
4. The authors decide whether and how to address the reviewers' comments and criticisms and the editor's concerns. The authors return a revised version of the paper to the CEE along with specific information describing how they have answered the concerns of the reviewers and the editor, usually in a tabular form. The author(s) may also submit a rebuttal if there is a need especially when the authors disagree with certain comments provided by reviewer(s).
5. The CEE sends the revised paper out for re-review. Typically, at least 1 of the original reviewers will be asked to examine the article.
6. When the reviewers have completed their work, the EiC examines their comments and decides whether the paper is ready to be published, needs another round of revisions, or should be rejected. If the decision is to accept, the CEE is notified.
7. The CEE reserves the final right to accept or reject any material for publication, if the processing of a particular manuscript is deemed not to be in compliance with the S.O.P. of *Pertanika*. An acceptance letter is sent to all authors.

The editorial office ensures that the manuscript adheres to the correct style (in-text citations, the reference list, and tables are typical areas of concern, clarity, and grammar). The authors are asked to respond to any minor queries by the editorial office. Following these corrections, page proofs are mailed to the corresponding authors for their final approval. At this point, **only essential changes are accepted**. Finally, the manuscript appears in the pages of the journal and is posted online.

Pertanika Journal of

**SCIENCE
& TECHNOLOGY**

Vol. 29 (1) Jan. 2021



A scientific journal published by Universiti Putra Malaysia Press



EDITOR-IN-CHIEF

Luqman Chuah Abdullah
Chemical Engineering

CHIEF EXECUTIVE EDITOR

Abu Bakar Salleh
Biotechnology and Biomolecular Science

UNIVERSITY PUBLICATIONS COMMITTEE

CHAIR

Zulkifli Idrus

EDITORIAL STAFF

Journal Officers:

Kanagamalar Silvarajoo, *ScholarOne*
Siti Zuhaila Abd Wahid, *ScholarOne*
Tee Syin-Ying, *ScholarOne*
Ummi Fairuz Hanapi, *ScholarOne*

Editorial Assistants:

Ku Ida Mastura Ku Baharom
Siti Juridah Mat Arip
Zulinaardawati Kamarudin

PRODUCTION STAFF

Pre-press Officers:

Nur Farrah Dila Ismail
Wong Lih Jiu

WEBMASTER

IT Officer:

Munir Hayat Md Bahrin

EDITORIAL OFFICE

JOURNAL DIVISION

Putra Science Park,
1st Floor, IDEA Tower II
UPM-MTDC Technology Centre
Universiti Putra Malaysia
43400 Serdang, Selangor, Malaysia

General Enquiry
Tel: +603 9769 1622 | 1616
E-mail:

executive_editor.pertanika@upm.edu.my
URL: www.journals-ijd.upm.edu.my

PUBLISHER

UPM PRESS

Universiti Putra Malaysia
43400 UPM, Serdang, Selangor, Malaysia.
Tel: +603 9769 8855 | 8854
Fax: +603 9679 6172
E-mail: penerbit@upm.edu.my
URL: <http://penerbit.upm.edu.my>



EDITORIAL BOARD 2020-2022

Abdul Latif Ahmad
Chemical Engineering
Universiti Sains Malaysia, Malaysia

Adem Kilicman
Mathematical Sciences
Universiti Putra Malaysia, Malaysia

Ahmad Zaharin Aris
Hydrochemistry, Environmental Chemistry, Environmental Forensics, Heavy Metals
Universiti Putra Malaysia, Malaysia

Azlina Harun@Kamaruddin
Enzyme Technology, Fermentation Technology
Universiti Sains Malaysia, Malaysia

Bassim H. Hameed
Chemical Engineering: Reaction Engineering, Environmental Catalysis & Adsorption
Qatar University, Qatar

Biswajeet Pradhan
Digital image processing, Geographical Information System (GIS), Remote Sensing
University of Technology Sydney, Australia

Daud Ahmad Israf Ali
Cell Biology, Biochemical, Pharmacology
Universiti Putra Malaysia, Malaysia

Hari M. Srivastava
Mathematics and Statistics
University of Victoria, Canada

Ho Yuh-Shan
Water research, Chemical Engineering and Environmental Studies
Asia University, Taiwan

Hsiu-Po Kuo
Chemical Engineering
National Taiwan University, Taiwan

Ivan D. Rukhlenko
Nonlinear Optics, Silicon Photonics, Plasmonics and Nanotechnology
The University of Sydney, Australia

Lee Keat Teong
Energy Environment, Reaction Engineering, Waste Utilization, Renewable Energy
Universiti Sains Malaysia, Malaysia

Mohamed Othman
Communication Technology and Network, Scientific Computing
Universiti Putra Malaysia, Malaysia

Mohammad Jawaid
Polymers and Plastics, Colloid and Surface Chemistry, Composite and Hybrid Materials, Chemical Engineering
Universiti Putra Malaysia, Malaysia

Mohd. Ali Hassan
Bioprocess Engineering, Environmental Biotechnology
Universiti Putra Malaysia, Malaysia

Mohd Sapuan Salit
Concurrent Engineering and Composite Materials
Universiti Putra Malaysia, Malaysia

Najafpour Darzi Ghasem
Bioprocess Technology, Chemical Engineering, Water and Wastewater Treatment Technology, Biochemical Engineering and Biotechnology, Bioethanol, Biofuel, Biohydrogen, Enzyme and Fermentation Technology
Babol Noshirvani University of Technology, Iran

Nor Azah Yusof
Biosensors, Material Sensor, Functional Material
Universiti Putra Malaysia, Malaysia

Norbahiah Misran
Communication Engineering
Universiti Kebangsaan Malaysia, Malaysia

Roslan Abd-Shukur
Physics & Materials Physics, Superconducting Materials
Universiti Kebangsaan Malaysia, Malaysia

Wing Keong Ng
Aquaculture, Aquatic Animal Nutrition, Aqua Feed Technology
Universiti Sains Malaysia, Malaysia

INTERNATIONAL ADVISORY BOARD 2018-2021

Adarsh Sandhu
Editorial Consultant for Nature Nanotechnology and Contributing Writer for Nature Photonics, Physics, Magneto-resistive Semiconducting Magnetic Field Sensors, Nano-BioMagnetism, Magnetic Particle Colloids, Point of Care Diagnostics, Medical Physics, Scanning Hall Probe Microscopy, Synthesis and Application of Graphene Electronics-Inspired Interdisciplinary
Research Institute (EIIRIS), Toyohashi University of Technology, Japan

Graham Megson
Computer Science
The University of Westminster, U.K

Kuan-Chong Ting
Agricultural and Biological Engineering
University of Illinois at UrbanaChampaign, USA

Malin Premaratne
Advanced Computing and Simulation
Monash University, Australia

Mohammed Ismail Elnaggar
Electrical Engineering
Ohio State University, USA

Peter J. Heggs
Chemical Engineering
University of Leeds, U.K

Ravi Prakash
Vice Chancellor, JUIT, Mechanical Engineering, Machine Design, Biomedical and Materials Science
Jaypee University of Information Technology, Indian

Said S.E.H. Elnashaie
Environmental and Sustainable Engineering
Penn. State University at Harrisburg, USA

Suhash Chandra Dutta Roy
Electrical Engineering
Indian Institute of Technology (IIT) Delhi, India

Vijay Arora
Quantum and Nano-Engineering Processes
Wilkes University, USA

Yi Li
Chemistry, Photochemical Studies, Organic Compounds, Chemical Engineering
Chinese Academy of Sciences, Beijing, China

ABSTRACTING AND INDEXING OF PERTANIKA JOURNALS

The journal is indexed in SCOPUS (Elsevier), Clarivate-Emerging Sources Citation Index (ESCI), BIOSIS, National Agricultural Science (NAL), Google Scholar, MyCite, ISC. In addition, Pertanika JSSH is recipient of "CREAM" Award conferred by Ministry of Higher Education (MoHE), Malaysia.



Pertanika Journal of Science & Technology
Vol. 29 (1) Jan. 2021

Contents

Foreword <i>Abu Bakar Salleh</i>	i
Engineering Sciences	
<i>Review Article</i>	
Former and Current Trend in Subsurface Irrigation Systems <i>Yasir Layth Alrubaye and Badronnisa Yusuf</i>	1
Forecasting Wind Speed in Peninsular Malaysia: An Application of ARIMA and ARIMA-GARCH Models <i>Nor Hafizah Hussin, Fadhilah Yusof, 'Aaishah Radziah Jamaludin and Siti Mariam Norrulashikin</i>	31
Harmonic Current Distortion Using the Linear Quadratic Regulator for a Grid-Connected Photovoltaic System <i>Oscar Andrew Zongo and Anant Oonsivilai</i>	59
Statistical Analysis of AC Dielectric Strength for Palm Oil under the Influence of Moisture <i>Muhammad Safwan Shukri, Norhafiz Azis, Jasronita Jasni, Robiah Yunus and Zaini Yaakub</i>	77
Performance Analysis of the Linear Launcher Motor via Modelling and Simulation for Light Electric Vehicles <i>Norramlee Mohamed Noor, Ishak Aris, Norhisam Mison, Suhaidi Shafie and Parvez Iqbal</i>	95
Implementation of Artificial Neural Network to Predict the Permeability and Solubility Models of Gypseous Soil <i>Imad Habeeb Obead, Hassan Ali Omran and Mohammed Yousif Fattah</i>	107
Public Tendering Practices, Issues and Directions - A Case of Pakistan Construction Sector <i>Ali Raza Khoso, Md Aminah Yusof, Muhammad Aslam Leghari, Fida Siddiqui and Samiullah Sohu</i>	123
Modeling of Inactivation of Biofilm Composing Bacteria with Low Intensity Electric Field: Prediction of Lowest Intensity and Mechanism <i>Mokhammad Tirono and Suhariningsih</i>	149

Bifurcation Analysis of an Exothermic Biocatalytic Reaction System <i>'Afifi Md Desa, Mohd Hafiz Mohd and Mohamad Hekarl Uzir</i>	165
Mathematical Sciences	
Predictive Performance of Logistic Regression for Imbalanced Data with Categorical Covariate <i>Hezlin Aryani Abd Rahman, Yap Bee Wah and Ong Seng Huat</i>	181
Elastic-Net Regression based on Empirical Mode Decomposition for Multivariate Predictors <i>Abdullah Suleiman Al-Jawarneh and Mohd. Tahir Ismail</i>	199
A New Parametric Function-Based Dynamic Lane Changing Trajectory Planning and Simulation Model <i>Md. Mijanoor Rahman, Mohd. Tahir Ismail, Norhashidah Awang and Majid Khan Majahar Ali</i>	217
Combined Impacts of Predation, Mutualism and Dispersal on the Dynamics of a Four-Species Ecological System <i>Murtala Bello Aliyu and Mohd Hafiz Mohd</i>	233
Revisited the Critical Load Assessment of Huang et al. on Willems Tested Beck Column <i>Peter Praveen Jakkana, Nageswara Rao Boggarapu, Mahaboob Bodanapu, Appa Rao Bhogapurapu Venkata, Narayana Cherukuri and Harnath Yeddala</i>	251
Modelling High Dimensional Paddy Production Data using Copulas <i>Nuranisyha Mohd Roslan, Wendy Ling Shinyie and Sim Siew Ling</i>	263
Logic Learning in Adaline Neural Network <i>Nadia Athirah Norani, Mohd Shareduwan Mohd Kasihmuddin, Mohd. Asyraf Mansor and Noor Saifurina Nana Khurizan</i>	285
Applied Sciences and Technologies	
Improvement of Bioethanol Production in Consolidated Bioprocessing (CBP) via Consortium of <i>Aspergillus niger</i> B2484 and <i>Trichoderma asperellum</i> B1581 <i>Mona Fatin Syazwane Mohamed Ghazali, Muskhazli Mustafa, Nur Ain Izzati Mohd Zainudin and Nor Azwady Abd Aziz</i>	301
Drying Characteristics of Jackfruit and Snake Fruit using Freeze Dryer <i>Joko Nugroho Wahyu Karyadi, Siti Rahma, Ronal Sitindaon, Dionisia Gusda Primadita Putri and Dwi Ayuni</i>	317

Shoreline Change and its Impact on Land use Pattern and Vice Versa-A Critical Analysis in and Around Digha Area between 2000 and 2018 using Geospatial Techniques <i>Anindita Nath, Bappaditya Koley, Subhajit Saraswati, Basudeb Bhatta and Bidhan Chandra Ray</i>	331
Surface Treatment of Cement based Composites: Nano Coating Technique <i>Isam Mohamad Ali, Tholfekar Habeeb Hussain and Ahmed Samir Naje</i>	349
Environmental Sciences	
Quantifying Suspended Sediment using Acoustic Doppler Current Profiler in Tidung Island Seawaters <i>Henry Munandar Manik and Randi Firdaus</i>	363
Carbon Footprint of Built Features and Planting Works during Construction, Maintenance and Renewal Stages at Urban Parks in Petaling Jaya, Selangor <i>Nurzuliza Jamirsah, Ismail Said, Badrulzaman Jaafar and Mohd Haniff Mohd Hassani</i>	387
Optimisation of Culture Conditions for PLA-food-packaging Degradation by <i>Bacillus</i> sp. SNRUSA4 <i>Suwapha Sawiphak and Aroon Wongjiratthiti</i>	407
Synthesis of Magnetic Activated Carbon Treated with Sodium Dodecyl Sulphate <i>Palsan Sannasi Abdullah, Huda Awang and Jayanthi Barasarathi</i>	427
Information, Computer & Communication Technologies	
<i>Review Article</i>	
Multilingual Sentiment Analysis: A Systematic Literature Review <i>Nur Atiqah Sia Abdullah and Nur Ida Aniza Rusli</i>	445
<i>Review Article</i>	
Internet of Things (IoT) Implementation in Learning Institutions: A Systematic Literature Review <i>Ruth Chweya and Othman Ibrahim</i>	471
LTE Network Analysis in Frequency Reuse Recycling Techniques <i>Muhammad Sabir Hussain, Nasri Suleiman and Nor Kamariah Noordin</i>	519
Algorithm for B-scan Image Reconstruction in Optical Coherence Tomography <i>Kranti Patili, Anurag Mahajan, Balamurugan Subramani, Arulmozhivarman Pachiyappan and Roshan Makkar</i>	533

Medical and Health Sciences

Molecular Markers and Phylogenetic Analysis of UPMT27, a Field Isolate of the Malaysian Fowl Adenovirus Associated with Inclusion Body Hepatitis 547
Salisu Ahmed, Abdul Razak Mariatulqabtiah, Mohd Hair Bejo, Abdul Rahman Omar, Aini Ideris and Nurulfiza Mat Isa

Optimisation and Evaluation of Antibacterial Topical Preparation from Malaysian Kelulut Honey using Guar Gum as Polymeric Agent 565
Mohd Amir Shahlan Mohd-Aspar, Raihana Zahirah Edros and Norul Amilin Hamzah

Identification and Antibiotic Resistance Profile of *Salmonella* spp. and *Citrobacter* spp. Isolated from Street-Vended Beverages 593
Siti Shahara Zulfakar, Noraziah Mohamad Zin, Siti Nur Shafika Mat Zalami and Nur Syakirah Mohd Nawawee

Short Communication

In Silico Designing of a Multi-Epitope Based Vaccine Candidate Against Human Adenovirus Type B3 Respiratory Infections by Utilising Various Immunoinformatics Approaches 607
Somnath Panda, Urmila Banik and Arun Kumar Adhikary

Earth Sciences

Comparison of Proximate Composition of Raw and Cooked Intramuscle Tissue of *Thunnus tonggol* from Terengganu, Malaysia 629
Norhazirah Abd Aziz, Ahmad Shamsudin Ahmad, Adiana Ghazali, Nurul Izzah Ahmad, Ahmad Ali and Meng-Chuan Ong

Distribution of Benthic Macroinvertebrates in Seafloor Northward of Pulau Indah, Klang 641
Mohd Sophian Mohd Kasihmuddin and Zaidi Che Cob

Flood-Modeling and Risk Map Simulation for Mae Suai Dam-Break, Northern Thailand 663
Anurak Busaman, Somporn Chuai-Aree, Salang Musikasuwana and Rhysa McNeil

Chemical Sciences

Differentiation Unclean and Cleaned Edible Bird's Nest using Multivariate Analysis of Amino Acid Composition Data 677
Nurul Alia Azmi, Ting Hun Lee, Chia Hau Lee, Norfadilah Hamdan and Kian Kai Cheng

Material Sciences

Effect of Sodium Hydroxide (NaOH) Treatment on Coconut Coir Fibre and its Effectiveness on Enhancing Sound Absorption Properties 693
Ida Norfaslia Nasidi, Lokman Hakim Ismail and Emedya Murniwaty Samsudin

Foreword

Welcome to the 1st 2021 issue of the Pertanika Journal of Science and Technology (PJST)!

PJST is an open-access journal for studies in Science and Technology published by Universiti Putra Malaysia Press. It is independently owned and managed by the university for the benefit of the world-wide science community.

This issue contains 37 articles; 3 review articles, 1 short communication and the rest are regular articles. The authors of these articles come from different countries namely Bangladesh, India, Indonesia, Iraq, Kenya, Malaysia, Nigeria, Pakistan and Thailand.

Articles submitted for this issue cover various scopes of Science and Technology including: applied sciences and technologies; chemical sciences; earth sciences; engineering sciences; environmental sciences; information, computer and communication technologies; material sciences; mathematical sciences; and medical and health sciences.

An article in this issue discussed the comparison between a proportional-integral controller, low pass filters, and the linear quadratic regulator in dealing with the task of eliminating harmonic currents in the grid-connected photovoltaic system. The DC/DC converter was controlled by perturb and observed technique with maximum power point tracking that concentrated on maximizing the available solar power and maintained an acceptable efficiency around the full load condition. The simulation results obtained had proven the robustness of the linear quadratic regulator over proportional-integral controller and low pass filters. The total harmonic distortion found in the grid current fell from 7.85% to 2.13% when the linear quadratic regulator was applied. Details of this study are available on page 59.

A regular article titled “Performance Analysis of the Linear Launcher Motor via Modelling and Simulation for Light Electric Vehicles” was presented by Norramlee Mohamed Noor and his colleagues. In this study, the analytical method to predict the linear launcher motor was described by using 2D-Jmag and MATLAB/Simulink. The performance of the linear launcher motor can generate axial force, speed, and displacement of with and without load. The authors stated that the maximum force without load was ~1.6kN and force with load was ~1.4kN at 100A. The detailed information of this study is available on page 95.

An investigation to determine a multi-epitope based vaccine candidate against Human Adenovirus Type B3 (HAdV-B3) respiratory infections by utilising various immunoinformatic approaches was conducted by Somnath Panda and co-researchers from AIMST University, Malaysia. Considering

the heterogeneity of HAdV-B3 and the complexity of generating conventional vaccines, an in-silico multi-epitope vaccine construct incorporating all epitopes of four major HAdV-B3 hexon variants was built. The constructed vaccine had 23 different epitopes which showed non-allergic but antigenic nature with 30hours of half-life in vitro and exhibited thermostable nature. The researchers believed that this construct would considerably reduce the time and expense of biological work needed for future vaccine development. Further details of the investigation can be found on page 607.

We anticipate that you will find the evidence presented in this issue to be intriguing, thought-provoking and useful in reaching new milestones in your own research. Please recommend the journal to your colleagues and students to make this endeavour meaningful.

All the papers published in this edition underwent Pertanika's stringent peer-review process involving a minimum of two reviewers comprising internal as well as external referees. This is to ensure that the quality of the papers justifies the high ranking of the journal, which is renowned as a heavily-cited journal not only by authors and researchers in Malaysia but by those in other countries around the world as well.

A special appreciation to all the Editorial Board Members of PJST (2018-2020) for serving the journal for the past two years in ensuring Pertanika plays a vital role in shaping the minds of researchers, enriching their lives, and encouraging them to continue their quest for new knowledge. Also, we welcome the new Editorial Board Members on board. We hope that their involvement and contributions towards Pertanika would not only improve its quality but also support the development efforts in making it an international journal of good standing.

PJST is currently accepting manuscripts for upcoming issues based on original qualitative or quantitative research that opens new areas of inquiry and investigation.

Chief Executive Editor

Dato' Dr. Abu Bakar Salleh

executive_editor.pertanika@upm.edu.my

Review Article

Former and Current Trend in Subsurface Irrigation Systems

Yasir Layth Alrubaye* and Badronnisa Yusuf

Department of Civil Engineering, Faculty of Engineering, Universiti Putra Malaysia, 43400 UPM, Serdang, Selangor, Malaysia

ABSTRACT

The main purpose of this review is to find the diversity in research studies of subsurface irrigation systems in the past two decades. Two periods of five years were selected to reflect the research studies at the beginning and the end of the comparing periods range. A statistical sorting was used to investigate the distribution of papers according to objectives, types of irrigation systems, research methods, and limitations of the studies. Results showed that the measurements and evaluations were the most presented objectives of the selected papers for both periods. Furthermore, almost 90 percent of the recent papers used multiple research methods, unlike the papers published in the former period which only 56 percent of them used multiple methods. Also, more than 90 percent of the recent papers used a single irrigation system. In conclusion, knowledge of subsurface irrigation systems had been

advanced in the former studies mostly by analyzing the measurements and evaluations of the traditional irrigation systems. Unlike the former period, the advancement in knowledge has been produced in the current period by introducing new subsurface irrigation systems and more concentration by the order of measurements, evaluation, and designing, respectively.

ARTICLE INFO

Article history:

Received: 01 June 2020

Accepted: 01 September 2020

Published: 22 January 2021

DOI: <https://doi.org/10.47836/pjst.29.1.01>

E-mail addresses:

gs55714@student.upm.edu.my (Yasir Layth Alrubaye)

nisa@upm.edu.my (Badronnisa Yusuf)

*Corresponding author

Keywords: Irrigation Systems, sub-Irrigation, subsurface irrigation, water movement in soil, wetting patterns

INTRODUCTION

Subsurface irrigation defined by Camp (1998) is the method of applying irrigation water directly into the root zone of the soil profile. In contrast with surface irrigation systems, subsurface irrigation systems highly reduce human contact with irrigation water which sometimes is not freshwater (Qiu et al., 2017). According to Massatbayev et al. (2016) the main components structured the properties of subsurface irrigation are emission products, construction methods, materials, and packing of the soil. Furthermore, the vital advantage of subsurface irrigation systems is reducing the losses such as evaporation and surface runoff comparing to the surface irrigation (Montazar et al., 2017). Over the past two decades, subsurface irrigation systems had widely developed. Researchers discussed various aspects of subsurface irrigation systems such as design, operation, evaluation, measuring the wetting fronts, or producing new irrigation products. Also, methods of research studies used to achieve these purposes has been changed.

Various methods have been used to review subsurface irrigation systems by researchers. In this aspect some review papers can be mentioned. Ayars et al. (1999) summarized 15 years of research studies in a subsurface drip irrigation system to identify limitations and future studies, where they addressed the impact of soil type on selecting irrigation interval needed to be further research. Bastiaanssen et al. (2007) used a technique of SWOT to analyze the flow of water in unsaturated soils and described the solutions methods for managing irrigation systems. They concluded that common sense was not enough for developing irrigation systems as it needed the optimal solutions as well. Furman (2008) reviewed the subsurface flow of irrigation systems using mathematical forms whereas they concluded that both accuracy and applicability were required for subsurface irrigation systems to measure the water distribution in the soil profile. Ayars et al. (2015) discussed the status of subsurface drip irrigation systems in California by reviewing the current research studies and the on-farm practices and they found that subsurface drip irrigation had many advantages and could be considered as an effective tool to increase water usage efficiency. Rudnick et al. (2019) reported the results and highlighted future research areas of limited irrigation strategies conducted by research studies in irrigation systems where they noted that the optimal practice of irrigation depended mainly upon irrigation system type, soil moisture content, market value, and initial cost.

Research studies of subsurface irrigation systems need successive contributions (Singh, 2014c) and periodic overview because of the continuous development. Recently, researchers developed various subsurface irrigation systems by introducing either a new component or new systems. Engineering applications in automated and mechanized irrigation systems are still under research and development (Hudzari et al., 2013). Besides, irrigation systems are modified to overcome the topographical obstacles (Razali et al., 2016). Furthermore, a comparison between outcome benefits of using different subsurface irrigation systems is

the main factor of continued and increased usability of these systems (Camp et al., 2000). Also, a substantial amount of irrigation water can be saved using innovation strategies compared to traditional irrigation systems (Azhar et al., 2014). Diversity in research studies is not only in irrigation systems but also in the objectives and methods of the research. Likewise, this diversity may change from each period to another because of the technological and knowledge development. Therefore, a comparison and general overview of former and current research studies is required to discover the diversity of research regions of subsurface irrigation systems.

The main purpose of this review is to preview the trend and diversity in research studies of subsurface irrigation systems by comparing the advancement in knowledge of subsurface irrigation systems in the past two decades. For instance, the trend represents the popularity of different topics in subsurface irrigation systems. Two periods of five years 1995-1999 and 2015-2019 were selected to reflect the research studies at the beginning and end of the comparison period. The former period indicates the later studies and the current period indicates the recent studies. Additionally, the objectives, methods, limitations, and the irrigation systems of the research studies in subsurface irrigation systems are analyzed.

MATERIALS AND METHODS

In this paper, a statistical sorting method was used to analyze and compare published research papers of subsurface irrigation systems. The general criteria used to select the papers and the description of the analysis method can be explained in detail in the following two sections.

General Criteria of Papers Selection

Two periods of time were selected of 20-years in range to represent the trend of research at each period. The first period was from 1995 to 1999 and the second period was from 2015 to 2019. A period of five-years had been used to represent the nature of the research published in the past and present as it was sufficient time to clarify the common research path. Moreover, to the absence of significant technological changes during the five-year period, which would not affect the nature of scientific research. The range of 20-years was used as a separation time range of the present period from the earliest past which was long enough to represent the differences because of the cognitive developments in the research trend.

Papers selected to be presented in this review were found using keywords which were directly related to the subject of the review. Since the subject of this review is the subsurface irrigation systems, keywords used to find the required papers were subsurface irrigation, wetting fronts, and irrigation systems. Furthermore, a research type of paper was selected to identify the required papers. These keywords had been searched in the Science Direct and Springer database.

Literature Classification Method

Research papers were classified by their objectives, methods of research, limitations, and the types of irrigation systems. This classification method presents the advancement in knowledge of the research studies by the categories of objectives and irrigation systems. Categories of methods and limitations represent the technological effectiveness of the research. These four categories give a good indication to compare the development of research trends in a 20-years range.

The first category is the research objectives which describe the distribution of selected papers according to their purpose which presents the general trend of knowledge. Four subcategories for classifying papers according to the objectives. The subcategories are design (DE), evaluation (EV), measurements (ME), and management (MA). These subcategories indicate the popularity of knowledge directions by presenting the distribution of research objectives per each period.

The second category is the research methods that present the common methods used by researchers to achieve their aims. This category indicates the technological development effectiveness specially to illustrate the differences between former and current research studies. Seven subcategories of research methods can be used to classify the research papers which are laboratory and on-field experiments (EX), numerical (NU), analytical (AN), optimization (OP), statistical (ST), economical (EC), and other (OT). Laboratory and on-field experiments usually adopt the case study or validate simulation models which is extremely helpful to understand what is the real behavior of the system in the real test (Fernández-Gálvez, et al., 2019). Simulation and optimization are commonly used in research methods for designing, managing, planning, and operating irrigation systems (Hantush & Marino, 1989; Huang & Loucks, 2000; Huang et al., 2012; Kite & Droogers, 2000; Loucks, et al. 1981; Mantoglou, 2003; Matanga & Mariño, 1979; Singh, 2013, 2014a, 2014b, 2014c; Tabari & Soltani, 2013). Also, mathematical and numerical approaches are widely used by researchers to represent specific purposes such as calculating the wetting fronts in soil profiles (Dawood & Hamad, 2016). Some researchers prefer to use more than one method for validating or comparing purposes therefore, research studies that used more than one method were classified and added into the existing methods. These subcategories of research methods can also indicate the reliability and the popularity of the adopted methods which can be interpreted from the rate of usage.

The third category is the research limitation. This category explains how technological development overcomes the difficulties faced the research. The research limitation reported in the literature is mainly on the dimensional presentation of the results and the soil types used in the research. The reason for using 2D or 3D representation is to show the ability of technological development in overcoming the research difficulties such as on-field measuring wetting fronts and simulation of water movement through time in the soil profile.

This category is usually considered as a challenge for researchers to overcome because the flow in the soil profile is unsaturated and needs visualization to be measured. Thus, presenting this category introduces the advancements in research methods and how it has impacted the quality and quantity of the result.

The fourth category is the type of irrigation system used in the research papers. Irrigation systems are developed through years of research projects. Therefore, it is important to sort the research papers according to the type of irrigation systems that indicate both the technological and knowledge developments. Irrigation systems which mentioned in this category are surface drip irrigation (SDI), subsurface drip irrigation (SSDI), subsurface membrane irrigation (SMI), subsurface irrigation pipe (SIP), optimized subsurface irrigation system (OPSIS), subsurface line source (SLS), surface irrigation (SI), irrigation basin (IB), micro-irrigation (MI), sprinkler irrigation systems (SIS) and baked clay pipes (BCP). Similarly, system products can be considered as a valuable addition to modify the typical system such as ceramic emitter (CE), suction emitter (SE), and rubber-based emitter (RB). Some research studies used more than one irrigation system for comparison purposes, so the classification considers all systems used per the research paper.

RESULTS AND DISCUSSION

In this paper, 81 papers had been statistically reviewed with 41 research papers classified into former (1995-1999) and 40 papers in the current (2015-2019) period. In the following subsections, summarized literature review of the both periods, results, and brief discussions are provided according to the classifications that have been explained earlier.

The literature review can be summarized in the two periods of five-years to show the sequence and type of resultant developments of each period. In the following paragraphs, the literature review is presented according to the sequence of the years which gives a good overview to compare between these two periods.

Review of Literature of 1995-1999

In 1995, most of the selected papers in subsurface irrigation systems were focused on management and measurements. For example, a research paper by Varshney (1995) discussed irrigation methods such as surface irrigation systems, sprinkler irrigation, drip irrigation, micro-sprinkler irrigation, and subsurface irrigation. He concluded that although subsurface irrigation could control the water content in the soil profile, it was still limited to be used just in arid areas because this method was uncommon for the farmers to be used in that time. Another paper conducted by Singh et al. (1995) presented the main idea of an automated irrigation schedule system that tested at the field to compare the results with a typical irrigation schedule. The system showed the ability to optimize irrigation water use.

In 1996, the majority of the research studies in subsurface irrigation systems were in measurements and evaluation. A study by Lacroix et al. (1996) introduced a measuring method to estimate the water balance which was verified by on-field experiments. They concluded that the method needed further calibration with field experiments to be more precise. Besides, Snyder et al. (1996) performed a survey of irrigation methods in California and compared them with previous surveys. The results showed that drip and sprinklers irrigation systems became popular more than before in contrast with the traditional methods.

In 1997, the objective presented in most of the selected papers was measurement techniques. For instance, a research paper by Esfandiari and Maheshwari (1997) developed an optimization method to estimate infiltration parameters of furrow irrigation method which gave a good accuracy by comparing with on-field results. Witelski (1997) analyzed the relation between wetting fronts with the boundary condition in soil profile using the perturbation method which indicated a high accuracy by comparing to solutions produced by numerical simulations.

In 1998, selected papers of subsurface irrigation were also focused on measurement. For example, Parlange et al. (1998) solved the nonlinear diffusion equation using an approximate analytical method for arbitrary boundary conditions which presented a well accurate performance. Also, Felsot et al. (1998) used on-field best management practices for reducing deep percolation of surface and subsurface drip irrigation. They concluded that it was difficult to measure the water distribution around the emitters.

In 1999, research studies of subsurface irrigation concentrated in measurement and design. For instance, a paper conducted by Meshkat et al. (1999) introduced a sand tube irrigation technique to reduce evaporation effectiveness on drip irrigation. Experiments and 3D simulations had been conducted in this study. The results showed that the technique could be used to reduce evaporation by more than 25 percent comparing to the typical surface drip irrigation. Furthermore, Barth (1999) developed a subsoil irrigation system that could be used to improve the performance of irrigation with minimum maintenance and a longer life span comparing to other irrigation systems.

The classification of research papers published in the former period is as presented in Table 1.

Table 1
Literatures classification of the former period (1995-1999)

Author (year)	Objectives	Methods	Limitations		Irrigation system
			Dimension	Soil type*	
Lacroix et al. (1996)	ME, MA	NU	OT	NM	MI, SI

Table 1 (Continued)

Author (year)	Objectives	Methods	Limitations		Irrigation system
			Dimension	Soil type*	
Varshney (1995)	MA	OT	OT	NM	SDI, SI, SIS, MI,
Singh et al. (1995)	MA, DE	OP, EX	OT	SC	SIS
Kandil et al. (1995)	MA	NU	OT	SC	SDI
Lockington and Parlange (1995)	ME	AN	1-D	NM	SI
Oad and Sampath (1995)	ME, EV, MA	EX, AN	OT	NM	SI
Ross et al. (1995)	ME, EV	AN, NU	2-D	S	NM
Scaloppi et al. (1995)	ME	NU, EX	OT	NM	SI
Snyder et al. (1996)	ME, EV	ST, OT	OT	NM	SI, MI, SDI, SSDI
Warrick and Shani (1996)	ME	EX, ST, AN	OT	SL	SSDI
Batchelor et al. (1996)	MA, EV	EX	OT	SCL	MI, SDI, BCP
Hansona et al. (1997)	ME, EV	EX, ST	OT	SL	SI, SDI, SSDI
Hilfer and Øren (1996)	ME	AN, EX	NM	S	NM
Izadi et al. (1996)	ME, EV	EX,	1-D, 2-D	SiL	SI
Kapoor (1996)	EV	AN	2-D, 3-D	S, L, C	NM
McClymont and Smith (1996)	EV, ME	OP, AN	OT	NM	SI
Panda et al. (1996)	MA	OP, AN	OT	SL, LS	SI
Rimmer et al. (1996)	EV, ME	EX	2-D	NM	NM
Ross et al. (1996)	ME,	NU, AN	1-D	S, C	NM
Shani et al. (1996)	EV, ME	EX, AN	OT	SL, SiL, CL	SSDI
Witelski (1997)	EV	AN, NU	OT	NM	NM
Willis et al. (1997)	ME	EX	OT	C	SI

Table 1 (Continued)

Author (year)	Objectives	Methods	Limitations		Irrigation system
			Dimension	Soil type*	
Esfandiari and Maheshwari (1997)	DE, EV, ME	EX, OP	OT	C	SI
Andreu et al. (1997)	ME, MA	EX	3-D	LS, SL	SDI
Amali et al. (1997)	ME, EV	EX, ST	OT	CL, SCL	SSDI, SI
Burt et al. (1997)	MA, EV, DE	OT	OT	NM	SI, SDI, SSDI, SIS, MI
Clemmens and Burt (1997)	EV, ME	ST	OT	NM	NM
Comparini and Mannucci (1997)	ME	AN	1-D	GPM	NM
Dale et al. (1997)	ME, DE	AN	1-D	GPM	NM
Furati (1997)	ME, EV	AN	1-D	GPM	NM
Kerkides et al. (1997)	EV, DE	AN,	1-D	GPM	SIS
Parseval et al. (1997)	ME	AN, EX	1-D	GPM	NM
Valiantzas (1997)	ME	NU, AN	OT	GPM	SI
Parlange et al. (1998)	ME	AN	1-D	GPM	SI
Felsot et al. (1998)	ME	EX	1-D	SL	SSDI
Ghanem and Dham (1998)	DE, EV	NU, ST	2-D	GPM	SI
Alazba (1999)	DE, ME	AN	OT	GPM	SI
Meshkat et al. (1999)	DE, ME	NU, EX	2-D	SiL, S	SDI
Barth (1999)	DE, MA	EX,	OT	NM	SLS
Connell (1999)	ME	AN, NU	1-D	S, L, C	NM
Coelho and Or (1999)	ME, EV	EX	2-D	SiL	SDI

*Symbols indicating the type of soil are: not mansion (NM), general pours media (GPM), sand (S), clay (C), silt (Si), loam (L), sandy clay (SC), sandy loam (SL), sandy clay loam (SCL), silty loam (SiL), loamy sand (LS), clay loam (CL), and sandy clay loam (SCL).

Review of Literature of 2015-2019

In 2015 and 2016, the selected research studies in subsurface irrigation systems focused mainly on the measurements. For example, Han et al. (2015) conducted on-field experiments and 2D simulation studies to measure the distribution of soil moisture content, which created by drip irrigation with mulch on the soil. Analysis of moisture content distribution that was created by 2D Hydrus showed a good agreement with the on-field experimental results. The 2D Hydrus model was found suitable to support the design and development process of a drip irrigation system in case of mulch on the soil surface. Another study conducted by Ali and Ghosh (2015) proposed a method for estimating the size-changing of wetting fronts in different soil types using numerical analysis and on-field verification where the results showed a high accuracy and could be applied into irrigation field to compute wetting fronts. Dawood and Hamad (2016) formed a set of equations by performing a set of numerical simulations using 2D Hydrus and on-field experiments to forecast the wetting fronts created by surface point source considering the variety of soil types which indicated highly accurate results.

In 2017, the selected papers in subsurface irrigation systems concentrated mainly on measurements, design, and evaluation. Honari et al. (2017) conducted a statistical approach to evaluate the ability of 3D Hydrus to simulate soil water content in field conditions which the results showed that the program could be used for simulating these kinds of cases. Also, Adams and Zeleke (2017) performed an on-field experimental study to illustrate the diurnal effects on irrigation efficiency and the study results pointed out that irrigation process for shallow root zone needed to be at the afternoon time to increase the irrigation efficiency.

In 2018, the majority of selected papers were also focused on measurements. As Al-Ghobari and Dewidar (2018) performed on-field experiments to test the strategy of deficit irrigation combined with surface and subsurface drip irrigation systems. The results of this study showed that combining deficit irrigation strategy with each of these irrigation systems could improve the irrigation productivity. Ren et al. (2018) derived a mathematical model for drip irrigation lateral and formulated an equation to represent the emitters discharge. They concluded that one of the main affected parameters on the hydraulic performance of laterals was the soil properties. Also, Fan et al. (2018b) simulated a vertical line source in HYDRUS to study the effect of influencing factors on the accumulating infiltration. The created empirical forms required further on field research studies to measure the wetting patterns and evaluate the created empirical models.

In 2019, the majority of papers of subsurface irrigation systems were concentrated in measurements. For example, an optimization study of designing subsurface irrigation systems conducted by Sakaguchi et al. (2019). They concluded that the recommended design parameters depended upon soil type, climate condition, irrigation intensity, and plant type. Another paper conducted by Cai et al. (2019a) was to test a ceramic patch in a subsurface irrigation line to control the saturated zone in soil profile created by the

pressure head applied on emitters. They found there was a relationship between pressure head, ceramic properties, and soil properties. Also, Lima et al. (2019) indicated that using a new irrigation product named permeable membrane could be used as a solution to increase water use efficiency and maximize the irrigation management. Furthermore, paper published by Elnesr and Alazba (2019) to simulate wetting fronts created by subsurface drip irrigation using 3D and 2D HYDRUS. They concluded that 2D simulation could be used confidently by simulators.

The classification of research papers published in the former period is as presented in Table 2.

Table 2
Literatures classification of the current period. (2015-2019)

Author (year)	Objectives	Methods	Limitations		Irrigation system
			Dimension	Soil type*	
Sakaguchi et al. (2019)	DE	NU, OP	2-D	NM	SIP
Al-Ghobari and Dewidar (2018)	ME, EV	EX, EC	OT	CS	SDI, SSDI
Saefuddin et al. (2019)	ME, EV, DE	NU, EX	3-D	Si, S	SSDI
Cai et al. (2019a)	ME, DE	AN, EX	OT	Si, L	SSDI, CE
Elnesr and Alazba (2019)	ME, EV	NU	2-D, 3-D	S, LS, SL, L, Si, SiL, SCL	SSDI
Gu et al. (2017)	DE, MA	NU, EX, OP, OT	OT	NM	SSDI
Lima et al. (2019)	ME, DE	EX	OT	NM	SMI
Feng et al. (2017)	ME	EX, ST	OT	CL, C	SIP
Ren et al. (2018)	ME, DE	AN, EX	OT	S, L, SL	SSDI
Ren et al. (2017)	ME, DE	AN	OT	NM	SSDI
Cai et al. (2017)	ME, DE	EX, NU, ST	OT	CL	CE
Liu et al. (2019)	ME, EV	EX, ST	OT	L	SSDI
Grecco et al. (2019)	ME, EV	NU, EX, ST	2-D	SL	SSDI
Jiang et al. (2019)	ME	NU, EX, ST	2-D, 3-D	S, Si, C	RB

Table 2 (Continued)

Author (year)	Objectives	Methods	Limitations		Irrigation system
			Dimension	Soil type*	
Cai et al. (2018)	ME, DE	NU, EX, ST	2-D	L	CE
Fan and Li (2018)	ME	EX, ST	OT	C, SiL, S	SSDI
Ghazouani et al. (2019)	ME, EV	EX, NU, ST	2-D	NM	SSDI
Cai et al. (2019b)	ME, EV	EX, NU, ST	2-D	CL, SL, S, LS, Si, SiL, SCL, CL, SiCL, SC, SiC, C	CE
Gunarathna et al. (2018)	ME, EV	EX, ST, OT	OT	NM	OPSIS
Gunarathna et al. (2017)	EV, DE	NU, ST, OP	OT	NM	OPSIS
Ding et al. (2019)	EV	EX, OT	OT	SL, S	SDI
Li et al. (2019)	ME, EV	EX, ST, OT	2-D	LSi, Si, LS, SL, S	SDI
Zhang et al. (2017)	ME, EV	EX, NU, ST	2-D	L, SiL, SL	SDI, SI
Castanedo et al. (2019)	EV	NU, ST	2-D	SL, SiL, CL	SI
Fan et al. (2018a)	ME	EX, NU, ST	2-D	S, SiL	CE
Fan et al. (2018b)	ME	NU, ST	2-D	CL, SiL, L, SL, S	SLS
Han et al. (2015)	ME, EV	EX, NU, ST	2-D	SiL	SSDI
Adams and Zeleke (2017)	ME	EX, ST	OT	SCL	SDI
Dawood and Hamad (2016)	ME	AN, EX, NU, ST	2-D	SiCL, S, LS, SL, SCL, L, SiL, Si, C, SC, SiCL, SiC, SSiL, CL	SDI

Table 2 (Continued)

Author (year)	Objectives	Methods	Limitations		Irrigation system
			Dimension	Soil type*	
Martínez de Azagra Paredes and Del Río San José (2019)	DE, ME	AN	2-D	GPM	SE
Khalil and Abid (2019)	ME	AN, EX, NU, ST	2-D	SL	SDI
Abid and Abid (2019)	ME	AN, NU, ST	2-D	LS, SL, L	SSDI
Ali and Ghosh (2015)	ME	AN, ST	OT	LS, L, CL, SC	IB
Hatiye et al. (2018)	ME	AN, NU, EX, ST	1-D	SL	SI
Honari et al. (2017)	EV	EX, NU, ST	3-D	L	SIP
Kacimov et al. (2018)	ME	AN, NU	2-D	L	SIP
Naghedifar et al. (2019)	ME	NU	2-D	C, L, S	SI
Reyes-Esteves and Slack (2019)	ME	EX, NU	2-D	CL, SCL	SIP
Soulis and Elmaloglou (2016)	MA	EX, NU, ST	2-D	LS, Si, SiL	SDI
Zheng et al. (2017)	MA, ME	EX, NU, ST	1-D	LS, S, LS, SiC, S	SI

*Symbols indicating the type of soil are: not mansion (NM), general pours media (GPM), sand (S), clay (C), silt (Si), loam (L), sandy clay (SC), sandy loam (SL), clay sand (CS), silty clay (SiC), loamy silt (LSi), silty loam (SiL), loamy sand (LS), clay loam (CL), sandy clay loam (SCL), silty clay loam (SiCL), sandy silty loam (SSiL), and sandy clay loam (SCL).

Research Objectives Category

The classification of research papers made based on their objectives was divided into main four subcategories. These subcategories were used to represent alternatives that had been adopted by researchers to express their research aim. For instance, the subcategory of measurement includes terms such as determine, predict, calculate, and relate. Subcategories management and evaluation used keywords such as schedule and examination, respectively. While the category of design covers terms like develop and introduce. These four

subcategories can be represented a general themes of research objectives. The distribution of research papers according to the objective's categories for former and current periods is as shown in Figure 1.

Figure 1 indicates the main directions of knowledge produced by research studies for former and current periods. All objectives mentioned in the papers accounted to be a part of the final percentage for each objective category. As shown in Table 1 and Table 2, some papers for both former and current periods were aimed for multiple objectives, as illustrated in Figure 2. For this reason, percentages cannot be integrated to obtain 100 percent in resultant.

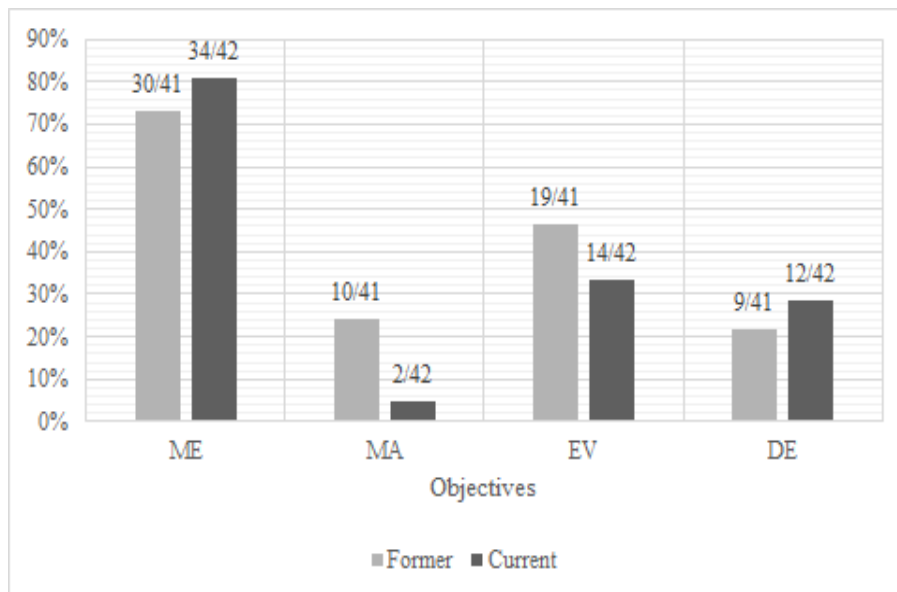


Figure 1. Research papers sorted according to the research objectives for former and current periods.

Papers published in the former period were distributed none uniformly throughout the four categories, which indicates that the general characterization of that period. More than 70 percent of the scientific research of the former period was interested in the measurement field. The evaluation field had gotten the second highest interests with 46 percent. Both categories of management and design had almost the same percentages of interests with 22 percent and 24 percent, respectively.

In the current period, the objectives of the research papers are also not uniformly distributed through the four categories but in a slightly different trend. Again, the measurement field had the highest percentage of 80 percent where it increased by almost

10 percent from the former period. Additionally, one-third of the research papers were concerned in the evaluation category which decreased more than 10 percent from the former period. The design category had been increased to 28 percent than in the former period, the most noticeable change was in the management category which highly decreased from 24 percent in the former period to 5 percent in the current period of the selected papers of subsurface irrigation systems.

As a result, the focusing of the papers in both periods were on measurements in the most of them and they had moderate concentration in evaluation and designing objectives.

Papers aimed for single or multiple objectives depending upon how these objectives are connected. Sometimes, the main objective needs for obtaining more data which produces another supportive goal. The use of single or multiple objectives has also been changed during the past 20 years as shown in Figure 2. Whereas, 60 percent of the papers were published in the past were aimed for multiple objectives. This percent had been reduced in recent research studies to be 48 percent. This difference may indicate that the researchers were focused more on the branches of the single objective research.

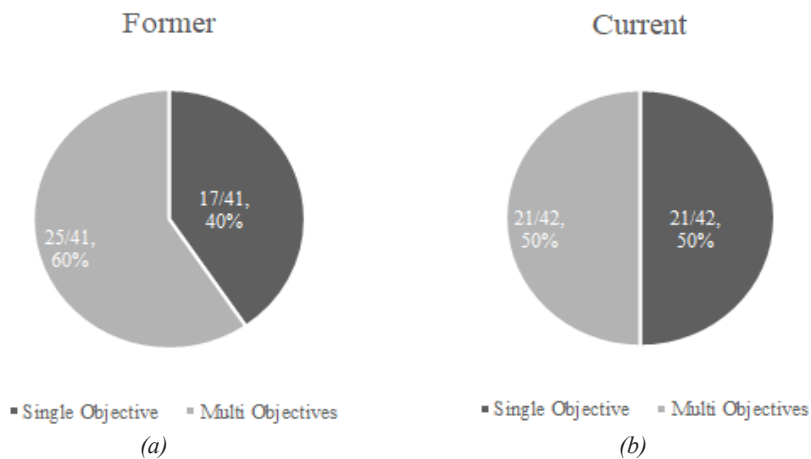


Figure 2. Percentage of research papers using single or multiple objectives in a) former and b) current periods.

Research Methods Category

Researchers used different methodologies available at their time to achieve the research objectives. In this subsection, a statistical overview of the methodologies of research papers is provided. The distribution of research papers according to research methods is presented in Figure 3. Since some papers used more than one method to achieve the research aim as presented in Figure 4, all methodologies used per paper had been accounted for. For this reason, percentages presented cannot be integrated into 100 percent.

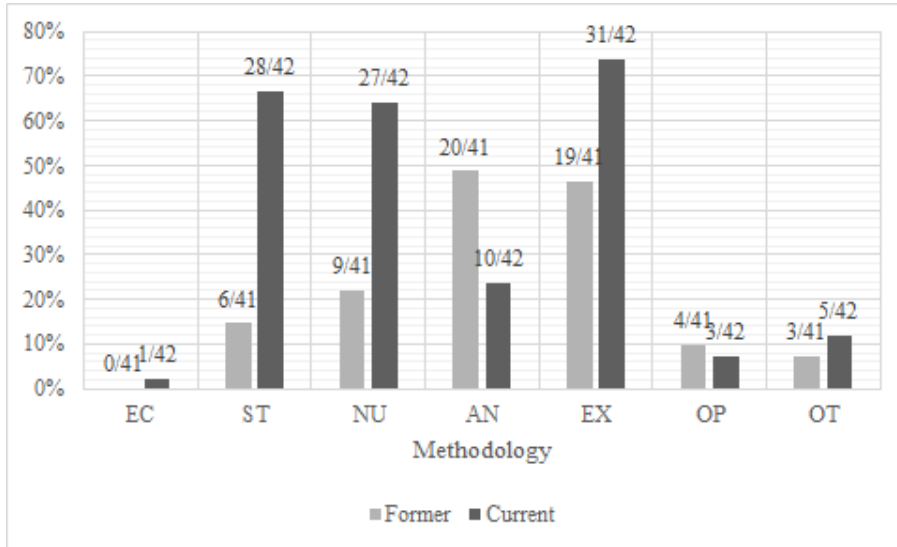


Figure 3. Research papers distributed according to research methods for former and current periods.

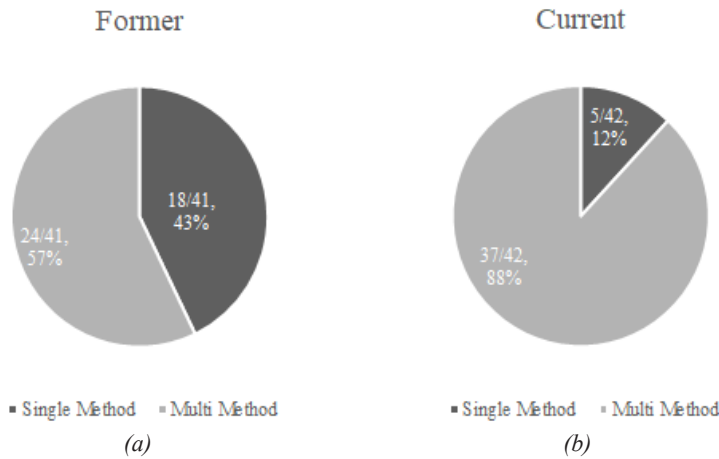


Figure 4. Percentage of research papers that used single or multiple methods for a) former and b) current periods.

The two foremost methods in the former period were experimental and analytical methods in which 46 and 49 percent of research adopted these methodologies, respectively. On the other hand, the economic study was not used by any research of the selected papers. Percentage of research papers reported statistical, numerical and optimization methods in subsurface irrigation systems are 15, 22, and 10 percent, respectively, of the total selected papers. Research studies used survey, explanations, or discussing the subsurface irrigation systems were summarized in other methods which are covered in 7 percent of the selected

papers. Two indications can be recognized from this distribution. The first indication is the analytical and experimental methods were popular in the former period which is a reason that may be due to the availability of these methods compared to the others. The second indication is the reliability of these methods that encourages the researchers to use them.

Research papers in the current period show a wide distribution of research methods. However, the experimental method was still preferred with an increase of usage by more than one-quarter to 73 percent. The analytical method decreased with the same ratio to 25 percent of the selected papers. In addition, both statistical and numerical methods increased used by 65 percent of the total research studies. On the other hand, optimization and economical methods adopted in 8 and 3 percent of the research, respectively. Other methods increased comparing to the former period to 10 percent of the current papers.

Technological development over the past 20 years has allowed researchers to use research methods such as numerical and statistical more than before. As these methods became available, more accurate, and easier to use, which made these methods more popular among researchers.

Figure 4 shows research papers that presented a single or multiple method to achieve the research aim. Single and multiple methods presented in 44 and 56 percent of the papers published in the former period respectively. That indicates a good availability of various types of methodologies in the former period. In the current period, researchers using more multiple methods in which the multiple methods were presented in 88 percent of the recently published papers. This change can be considered a huge step in scientific development which supported by technological developments. Using multiple methods gives a good chance for researchers to calibrate these methods to get more accurate results. According to Table 2, one of the notable things in the recent period is that the experimental, numerical, and statistical methods commonly used together, and this approach exists together in 29 percent of the recently published papers. This fact indicates the calibration development to create a larger tested area, accurate results, minimum cost of testing trials, and more models design.

Types of Irrigation Systems

In this subsection, irrigation systems used by researchers are sorted according to the subcategories as presented in Figure 5 is discussed. Although the main subject of this review is subsurface irrigation systems, some researchers use other irrigation systems to accomplish the research objectives, thus, irrigation systems that are not categorized under subsurface irrigation systems are also mentioned and accounted for in this statistical review. There are 15 categories of irrigation systems that have been accounted for that presented in the selected research papers for both former and current periods. Although, some research papers used more than one irrigation system, others did not mention the type of irrigation

system or discussed the supplying system as a general point or line source. Nevertheless, irrigation systems was not mentioned or the general sources of the selected papers were accounted for under the not mentioned category.

In the former period, typical types of irrigation systems such as surface and subsurface drip irrigation, baked clay pipes, surface irrigation, micro-irrigation, sprinklers irrigation were presented in 32, 17, 2, 46, 10 and 10 percent of the selected research papers, respectively. While another 29% did not mention any category. Although the main subject of this review is the subsurface irrigation systems, it is worth mentioning that the surface irrigation was the most researched topics in the former period. While the subsurface drip irrigation, baked clay pipes, and subsurface line system represented the subsurface irrigation system. In summary, it can be said that past researchers had concentrated more on the existing irrigation systems and less focused on using new irrigation methods.

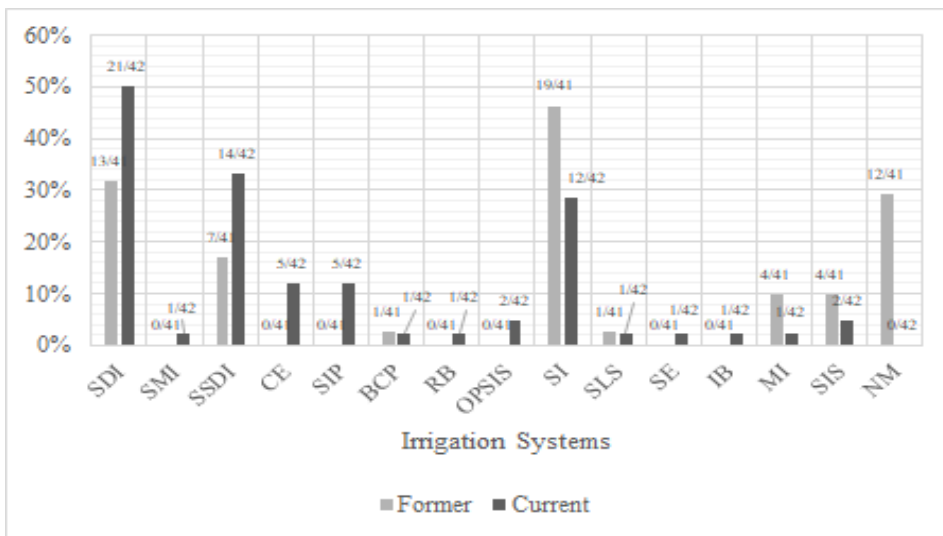


Figure 5. Research papers distributed according to irrigation systems used for former and current periods.

Recent papers present 14 types of irrigation systems which doubled the number of irrigation systems used by former papers. The current period witnessed a rise in developing new systems or new irrigation products. In addition, irrigation systems such as subsurface membrane irrigation, ceramic emitter, subsurface irrigation pipe, rubber-based emitter, optimized subsurface irrigation system, suction emitter, and irrigation basin are presented in 3, 13, 13, 3, 5, 3, and 3 percent of the current period respectively. Moreover, typical irrigation systems were presented differently in the papers of the current period in which surface drip irrigation system were presented in the half of the recent papers. Also, the

subsurface drip irrigation research increased more than 15 percent and presented in the one-third of the research papers. It is also observed that the research on surface irrigation systems reported in the papers of the current period decreased by 29 percent of the papers. All the selected research papers in the current period had mentioned the irrigation systems and none of them used the general point or line sources. Some research papers used more than one irrigation system for both former and current periods as can be shown in Figure 6.

Not only that more than half of the research papers in the former period used a single irrigation system but also 17 percent of them used multiple irrigation systems as shown in Figure 6. On the other hand, a high concentration of using a single irrigation system was presented in research papers in which 93 percent of the papers used a single irrigation system, and only 7 percent used multiple irrigation systems. These statistics results give a good sign to indicate the direction of knowledge advancement. The trend shows the subsurface irrigation systems have developed to a new efficient irrigation systems or irrigation products.

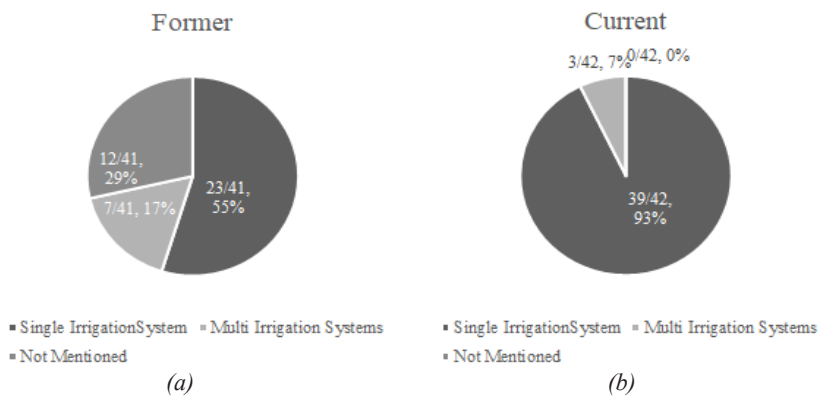


Figure 6. Percentage of research papers that used single or multiple irrigation systems for a) former and b) current periods.

Limitations

Two main limitations faced by researchers in the study of irrigation systems are discussed in this section. The first limitation is the soil type which represents one of the important components in the irrigation process. The second limitation is the dimension of the analysis.

Soil Type. Soil types had a lot of attention to the papers in both former and current periods to study subsurface irrigation systems. Research papers used different types of soils depending upon the availability and agricultural requirements. Figure 7 shows the distribution of research papers according to the soils type presented. However, some research papers used more than one type of soil, others used a general porous material as shown in Figure 8.

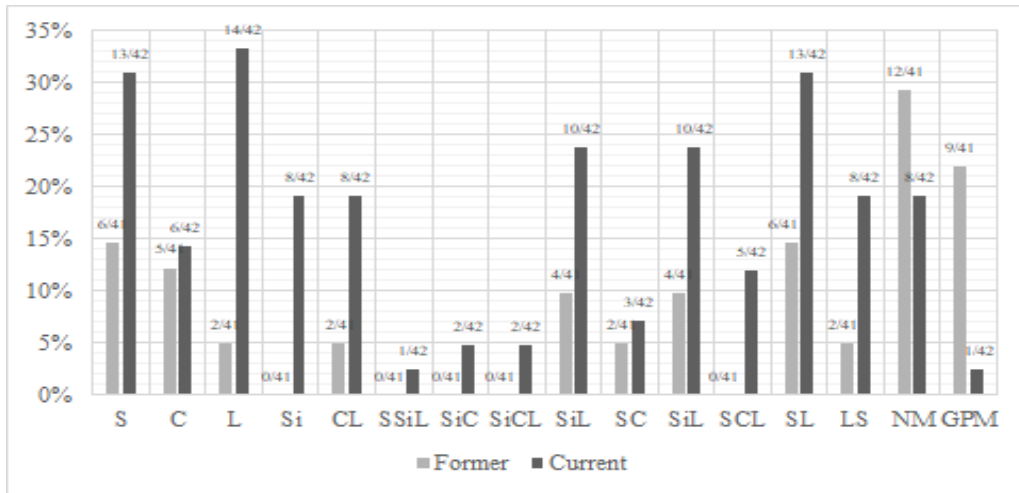


Figure 7. Research papers distributed according to soil type which used for former and current periods.

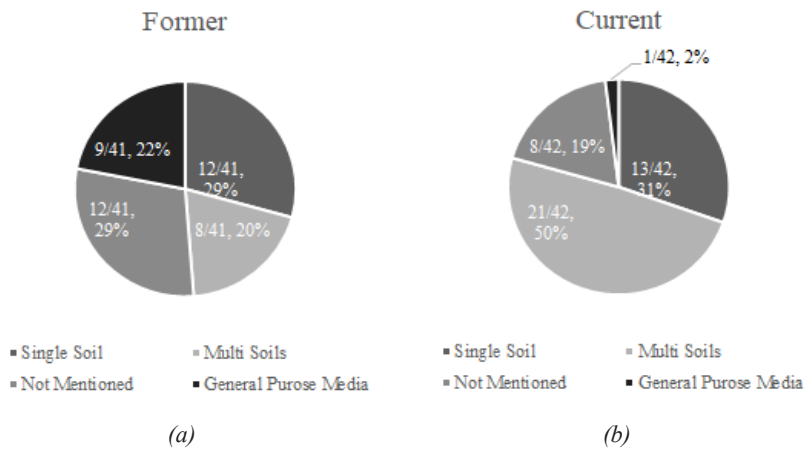


Figure 8. Percentage of research papers that used single or multiple soils for a) former and b) current periods.

A wide range of soil types had been used in research papers of both former and current periods which 16 types of soils accounted for in this statistical view. Even though 10 types of soil were presented in the papers of the former period, 15 soil types had been presented in the current period. Due to the technological developments which allowed the researchers in the recent period to present more soils than the past period.

According to the former period, items of “general porous media” and “not mentioned” were the highest two among the other items with 29 and 22 percent, respectively. Soil types such as sand, clay, silty loam, and sandy loam were presented in between 10-15 percent of the research papers. Other soil types such as loam, clay loam, sandy clay, and loamy sand were presented in 5 percent of the total selected papers.

According to the current period, soil types such as sand, loam, and loamy sand were the highest presented in the research papers which 33 percent of the papers used these types of soils. In addition, items of clay, silt, clay loam, sandy clay loam, and sandy loam existed between 5 and 20 percent of the selected papers. Other soil types such as sandy silt loam, silty clay, silty clay loam, and sandy clay were presented in less than 10 percent of the research papers.

Recent papers were presented soil types more than the former research papers which indicate the effectiveness of technological developments. For example, computer programming such as Hydrus was widely used by recent papers to simulate the subsurface flow for different soil types which allowed the researchers to create simulating models more easily than before.

As shown in Figure 8, papers used single soil type, multiple soil types, general porous media, or not mention the soil type for both published papers of former and current. Single and multiple soil types were mentioned by the former papers in 29 and 20 percent respectively. However, papers of the current period had mentioned single soil type in almost the same percentage of 31, the multiple soil types had widely increased, used by 50 percent of the recent papers. In addition, general porous media reduced from 29 percent of the former papers into 19 percent of the recent papers. Also, the item of “not mentioned” has been reduced by 20 percent over the 20 years. In conclusion, recent papers used the advantages of technological development to test more types of soil per research. Programming software is one of the important technological developments which allow researchers to simulate types of soils more than before.

Dimensions. Dimensions are another important limitation issue in scientific research. Studying subsurface flow is considered as a challenge because it cannot easily be visualized and difficult to be measured. This is the main reason for simplifying the flow in the soil profile by specifying dimensions. Figure 9 shows the distribution of former and current papers according to dimensions of the subsurface flow presented in these papers.

Four items presented in Figure 9 of one (1-D), two (2-D), three dimensions (3-D) and other limitations (OT). However, one dimension presented in 27 percent of the former papers, only 5 percent of the recent papers presented the one-dimension flow analysis. In contrast, two-dimensional analysis had been used in 17 percent of the former papers and it is highly increased to be more than 50 percent of the recent papers. Likewise, using three-dimensional analysis had been increased over the 20 years from 5 to 10 percent of the selected papers. High portion of the papers mentioned other types of limitation such as experimental period, specific treatment, shape and size of introduced products, hydraulic properties of the ceramic emitters or sometimes not mentioned the limitation.

Research papers of subsurface irrigation systems in the current period have the following advantages comparing to the former period. Firstly, they introduce new irrigation

components that will give the designers alternative options to provide users with an adequate subsurface irrigation system. Secondly, they are used more analysis methods per research which gives more reliability of the results than the former research studies. Thirdly, modern research papers have more focus on multiple objectives than the former papers. Fourthly, the latest papers tested much more soil types than the previous ones which improves the accuracy of measurements and prediction of subsurface flow.

On the other hand, recent research papers have disadvantages comparing to the previous papers. Firstly, in the most of papers in the current period used a single irrigation system per paper which reduced the chances of comparison with other irrigation systems. Secondly, the analytical method was less in use by the recent papers comparing to the latest papers which might reduce the opportunity of producing generalization forms. Thirdly, research in management and evaluation of the performance of subsurface irrigation systems had less focus on the current papers comparing to the former papers.

Technological development assists researchers in modifying the research methods to explore new research areas and investigate more materials with different methods. As a result, knowledge advancement is directly connected to technological development. Also, technological development increases the type of detail research but reduces the type of general research. Therefore, the trend of the subsurface irrigation systems in the current period is to measure the performance of novel irrigation systems components using experimental, numerical, and statistical analysis. On the other hand, the trend in subsurface irrigation systems for the former period is to measure and evaluate the performance of traditional irrigation systems using analytical and experimental methods.

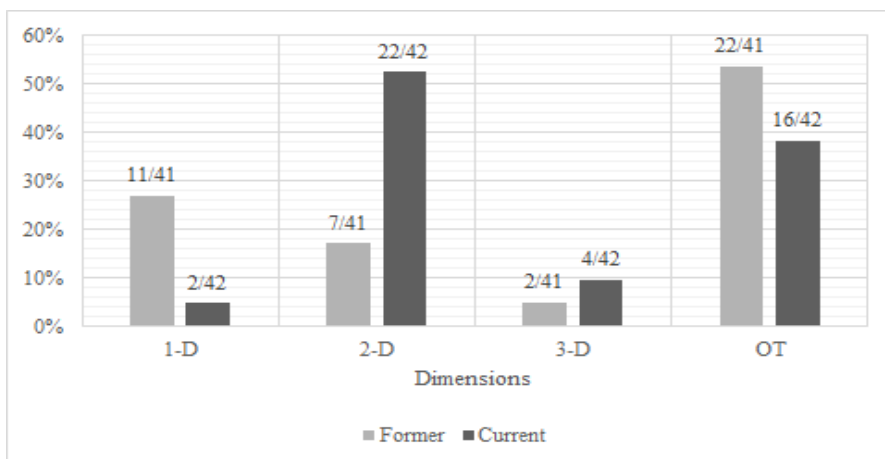


Figure 9. Research papers distributed according to dimensions which analyzed for former and current periods.

SUMMARY AND CONCLUSIONS

There are many differences between the papers of subsurface irrigation systems in former and current periods. In this review, the research papers had been classified by four categories to identify the trend of research topics and compare the differences in the advancement of knowledge resulted from the research studies and the effectiveness of the technological development on the research methodologies. Papers of former and current periods were classified by its objectives, method of study, irrigation systems, and research limitation.

In conclusion, papers of the both periods were focusing on measurements in the most of them and they have moderate concentration in evaluation and designing objectives. Multiple objective papers were presented in the former period more than the current period which gave more opportunity for using more research method and materials.

Even though, the selected papers were in the subject of subsurface irrigation systems, most of the papers in former period were presenting surface irrigation systems. In contrast with the recent papers which presented not only the higher in subsurface irrigation systems types but also lesser in using surface irrigation systems. Furthermore, more than 90 percent of the research papers in the current period used single irrigation system more than the past by almost 40 percent. The reason of this distribution is that the papers in the current period presented new irrigation systems such as subsurface membrane irrigation, ceramic emitter, subsurface irrigation pipe, rubber-based emitter, optimized subsurface irrigation system, and suction emitter.

Knowledge of subsurface irrigation systems had been advanced in the former studies mostly by analyzing the measurements and evaluations the traditional irrigation systems. On the other hand, knowledge had been advanced in the current period by introducing new subsurface irrigation systems and more concentration by the order of measurements, evaluation, and designing respectively.

In addition, almost 90 percent of the research papers in subsurface irrigation systems used multiple research methods higher than the past which presented 56 percent of the published papers. Experimental, numerical, and statistical methods were the major methods recently used by researchers. One of the noticeable changes was that the main research method widely used in the former period was the analytical method which was reduced by 25 percent of recent research studies.

The variation of soil types and dimensions of the analysis adopted in the research shows the effectiveness of the technological developments. Fifty percent of the recent research papers used multiple soil types more than the former research papers which presented in only 20 percent of the published papers. With respect to the dimensions of analysis adopted it has been observed that the one-dimensional analysis was commonly used in the former studies, but two-dimensional was the most used in the current period. These can

be considered as good indications of the effectiveness of the technological developments which advances some research methods to become easier to be used by the researchers.

ACKNOWLEDGEMENT

The authors are grateful to the reviewers for providing useful comments to improve the paper.

REFERENCES

- Abid, H. N., & Abid, M. B. (2019). Predicting wetting patterns in soil from a single subsurface drip irrigation system. *Journal of Engineering*, 25(9), 41-53.
- Adams, W. R., & Zeleke, K. T. (2017). Diurnal effects on the efficiency of drip irrigation. *Irrigation Science*, 35(2), 141-157. doi: 10.1007/s00271-016-0529-1
- Alazba, A. (1999). Dimensionless advance curves for infiltration families. *Agricultural Water Management*, 41(2), 115-131. Doi: [https://doi.org/10.1016/S0378-3774\(98\)00113-9](https://doi.org/10.1016/S0378-3774(98)00113-9)
- Al-Ghobari, H. M., & Dewidar, A. Z. (2018). Integrating deficit irrigation into surface and subsurface drip irrigation as a strategy to save water in arid regions. *Agricultural Water Management*, 209, 55-61. doi: <https://doi.org/10.1016/j.agwat.2018.07.010>
- Ali, S., & Ghosh, N. C. (2015). Methodology for the estimation of wetting front length and potential recharge under variable depth of ponding. *Journal of Irrigation and Drainage Engineering*, 142(1), 04015027. doi: [https://doi.org/10.1061/\(ASCE\)IR.1943-4774.0000921](https://doi.org/10.1061/(ASCE)IR.1943-4774.0000921)
- Amali, S., Rolston, D., Fulton, A., Hanson, B., Phene, C., & Oster, J. (1997). Soil water variability under subsurface drip and furrow irrigation. *Irrigation Science*, 17(4), 151-155. doi: <https://doi.org/10.1007/s002710050033>
- Andreu, L., Hopmans, J. W., & Schwankl, L. (1997). Spatial and temporal distribution of soil water balance for a drip-irrigated almond tree. *Agricultural Water Management*, 35(1-2), 123-146. doi: [https://doi.org/10.1016/S0378-3774\(97\)00018-8](https://doi.org/10.1016/S0378-3774(97)00018-8)
- Ayars, J., Fulton, A., & Taylor, B. (2015). Subsurface drip irrigation in California - Here to stay? *Agricultural Water Management*, 157, 39-47. doi: <https://doi.org/10.1016/j.agwat.2015.01.001>
- Ayars, J., Phene, C., Hutmacher, R., Davis, K., Schoneman, R., Vail, S., & Mead, R. (1999). Subsurface drip irrigation of row crops: a review of 15 years of research at the water management research laboratory. *Agricultural Water Management*, 42(1), 1-27. doi: [https://doi.org/10.1016/S0378-3774\(99\)00025-6](https://doi.org/10.1016/S0378-3774(99)00025-6)
- Azhar, M. A., Nashriyah, M., Hudzairi, M. H., Moneruzzaman, M. K., Amir, H., Rohaizad, M. M., & Ali, A. (2014). Effects of irrigation frequencies on aerial agro-morphological parameters of *Dioscorea hispida* dennst. (dioscoreaceae). *Journal of Applied Science research*, 8(9), 27-37.
- Barth, H. (1999). Sustainable and effective irrigation through a new subsoil irrigation system (SIS). *Agricultural Water Management*, 40(2-3), 283-290. doi: [https://doi.org/10.1016/S0378-3774\(99\)00003-7](https://doi.org/10.1016/S0378-3774(99)00003-7)

- Bastiaanssen, W. G., Allen, R. G., Droogers, P., D'Urso, G., & Steduto, P. (2007). Twenty-five years modeling irrigated and drained soils: State of the art. *Agricultural Water Management*, 92(3), 111-125. doi: <https://doi.org/10.1016/j.agwat.2007.05.013>
- Batchelor, C., Lovell, C., & Murata, M. (1996). Simple microirrigation techniques for improving irrigation efficiency on vegetable gardens. *Agricultural Water Management*, 32(1), 37-48. doi: [https://doi.org/10.1016/S0378-3774\(96\)01257-7](https://doi.org/10.1016/S0378-3774(96)01257-7)
- Burt, C. M., Clemmens, A. J., Strelkoff, T. S., Solomon, K. H., Bliesner, R. D., Hardy, L. A., ... & Eisenhauer, D. E. (1997). Irrigation performance measures: efficiency and uniformity. *Journal of Irrigation and Drainage Engineering*, 123(6), 423-442. doi: [https://doi.org/10.1061/\(ASCE\)0733-9437\(1999\)125:2\(97\)](https://doi.org/10.1061/(ASCE)0733-9437(1999)125:2(97))
- Cai, Y., Wu, P., Zhang, L., Zhu, D., Chen, J., Wu, S., & Zhao, X. (2017). Simulation of soil water movement under subsurface irrigation with porous ceramic emitter. *Agricultural Water Management*, 192, 244-256. doi: <https://doi.org/10.1016/j.agwat.2017.07.004>
- Cai, Y., Wu, P., Zhang, L., Zhu, D., Wu, S., Zhao, X., ... & Dong, Z. (2018). Prediction of flow characteristics and risk assessment of deep percolation by ceramic emitters in loam. *Journal of Hydrology*, 566, 901-909. doi: <https://doi.org/10.1016/j.jhydrol.2018.07.076>
- Cai, Y., Zhao, X., Wu, P., Zhang, L., Zhu, D., & Chen, J. (2019a). Effect of soil texture on water movement of porous ceramic emitters: A simulation study. *Water*, 11(1), 1-13. doi: <https://doi.org/10.3390/w11010022>
- Cai, Y., Zhao, X., Wu, P., Zhang, L., Zhu, D., Chen, J., & Lin, L. (2019b). Ceramic patch type subsurface drip irrigation line: Construction and hydraulic properties. *Biosystems Engineering*, 182, 29-37. doi: <https://doi.org/10.1016/j.biosystemseng.2019.03.005>
- Camp, C. (1998). Subsurface drip irrigation: A review. *Transactions of the ASAE*, 41(5), 1353-1367.
- Camp, C., Lamm, F., Evans, R., & Phene, C. (2000, November 14-16). Subsurface drip irrigation—Past, present and future. In *Proceedings of the 4th Decennial National Irrigation Symposium* (pp. 363-372). Phoenix, Arizona.
- Castanedo, V., Saucedo, H., & Fuentes, C. (2019). Modeling two-dimensional infiltration with constant and time-variable water depth. *Water*, 11(2), 1-16. doi: <https://doi.org/10.3390/w11020371>
- Clemmens, A. J., & Burt, C. M. (1997). Accuracy of irrigation efficiency estimates. *Journal of Irrigation and Drainage Engineering*, 123(6), 443-453. doi: [https://doi.org/10.1061/\(ASCE\)0733-9437\(1997\)123:6\(443\)](https://doi.org/10.1061/(ASCE)0733-9437(1997)123:6(443))
- Coelho, E. F., & Or, D. (1999). Root distribution and water uptake patterns of corn under surface and subsurface drip irrigation. *Plant and Soil*, 206(2), 123-136. doi: 10.1023/a:1004325219804
- Comparini, E., & Mannucci, P. (1997). Penetration of a wetting front in a porous medium interacting with the flow. *Nonlinear Differential Equations and Applications NoDEA*, 4(3), 425-438. doi: <https://doi.org/10.1007/s000300050023>
- Connell, L. D. (1999). A quasilinear based procedure for saturated/unsaturated water movement in soils. *Transport in Porous Media*, 36(1), 1-21. doi: 10.1023/a:1006504816562
- Dale, M., Ekrann, S., Mykkeltveit, J., & Virnovsky, G. (1997). Effective relative permeabilities and capillary pressure for one-dimensional heterogeneous media. *Transport in Porous Media*, 26(3), 229-260. doi: <https://doi.org/10.1023/A:1006536021302>

- Dawood, I. A., & Hamad, S. N. (2016). Movement of irrigation water in soil from a surface emitter. *Journal of Engineering*, 22(9), 103-114.
- Ding, Y., Gao, X., Qu, Z., Jia, Y., Hu, M., & Li, C. (2019). Effects of Biochar Application and Irrigation Methods on Soil Temperature in Farmland. *Water*, 11(3), 1-18. doi: <https://doi.org/10.3390/w11030499>
- Elnesr, M., & Alazba, A. (2019). Computational evaluations of HYDRUS simulations of drip irrigation in 2D and 3D domains (ii-subsurface emitters). *Computers and Electronics in Agriculture*, 163, 189-205. doi: <https://doi.org/10.1016/j.compag.2019.03.035>
- Esfandiari, M., & Maheshwari, B. (1997). Application of the optimization method for estimating infiltration characteristics in furrow irrigation and its comparison with other methods. *Agricultural Water Management*, 34(2), 169-185. doi: [https://doi.org/10.1016/S0378-3774\(97\)00007-3](https://doi.org/10.1016/S0378-3774(97)00007-3)
- Fan, W., & Li, G. (2018). Effect of soil properties on Hydraulic characteristics under subsurface drip irrigation. *IOP Conference Series: Earth and Environmental Science*, 121(5), 1-12. doi: <https://doi.org/10.1088/1755-1315/121/5/052042>
- Fan, Y. W., Huang, N., Zhang, J., & Zhao, T. (2018a). Simulation of soil wetting pattern of vertical moistube-irrigation. *Water*, 10(5), 1-19. doi: <https://doi.org/10.3390/w10050601>
- Fan, Y., Huang, N., Gong, J., Shao, X., Zhang, J., & Zhao, T. (2018b). A simplified infiltration model for predicting cumulative infiltration during vertical line source irrigation. *Water*, 10(1), 1-12. doi: <https://doi.org/10.3390/w10010089>
- Felsot, A., Cone, W., Yu, J., & Ruppert, J. (1998). Distribution of imidacloprid in soil following subsurface drip chemigation. *Bulletin of Environmental Contamination and Toxicology*, 60(3), 363-370.
- Feng, G., Zhang, Z., Wan, C., Lu, P., & Bakour, A. (2017). Effects of saline water irrigation on soil salinity and yield of summer maize (*Zea mays* L.) in subsurface drainage system. *Agricultural Water Management*, 193, 205-213. doi: <https://doi.org/10.1016/j.agwat.2017.07.026>
- Fernández-Gálvez, J., Pollacco, J., Lassabatere, L., Angulo-Jaramillo, R., & Carrick, S. (2019). A general beerkan estimation of soil transfer parameters method predicting hydraulic parameters of any unimodal water retention and hydraulic conductivity curves: Application to the kosugi soil hydraulic model without using particle size distribution data. *Advances in Water Resources*, 129, 118-130. doi: <https://doi.org/10.1016/j.advwatres.2019.05.005>
- Furati, K. M. (1997). Effects of relative permeability history dependence on two-phase flow in porous media. *Transport in Porous Media*, 28(2), 181-203. doi:10.1023/a:1006556018950
- Furman, A. (2008). Modeling coupled surface-subsurface flow processes: A review. *Vadose Zone Journal*, 7(2), 741-756. doi: <https://doi.org/10.2136/vzj2007.0065>
- Ghanem, R., & Dham, S. (1998). Stochastic finite element analysis for multiphase flow in heterogeneous porous media. *Transport in Porous Media*, 32(3), 239-262. doi:10.1023/a:1006514109327
- Ghazouani, H., Rallo, G., Mguidiche, A., Latrech, B., Douh, B., Boujelben, A., & Provenzano, G. (2019). Assessing Hydrus-2D model to investigate the effects of different on-farm irrigation strategies on potato crop under subsurface drip irrigation. *Water*, 11(3), 1-18. doi: <https://doi.org/10.3390/w11030540>

- Grecco, K. L., de Miranda, J. H., Silveira, L. K., & van Genuchten, M. T. (2019). HYDRUS-2D simulations of water and potassium movement in drip irrigated tropical soil container cultivated with sugarcane. *Agricultural Water Management*, 221, 334-347. doi: <https://doi.org/10.1016/j.agwat.2019.05.010>
- Gu, J., Yin, G., Huang, P., Guo, J., & Chen, L. (2017). An improved back propagation neural network prediction model for subsurface drip irrigation system. *Computers and Electrical Engineering*, 60, 58-65. doi: <https://doi.org/10.1016/j.compeleceng.2017.02.016>
- Gunarathna, M., Sakai, K., Nakandakari, T., Kazuro, M., Onodera, T., Kaneshiro, H., ... & Wakasugi, K. (2017). Optimized subsurface irrigation system (OPSIS): Beyond traditional subsurface irrigation. *Water*, 9(8), 1-11. doi: <https://doi.org/10.3390/w9080599>
- Gunarathna, M., Sakai, K., Nakandakari, T., Momii, K., Onodera, T., Kaneshiro, H., ... & Wakasugi, K. (2018). Optimized subsurface irrigation system: The future of sugarcane irrigation. *Water*, 10(3), 1-14. doi: <https://doi.org/10.3390/w10030314>
- Han, M., Zhao, C., Feng, G., Yan, Y., & Sheng, Y. (2015). Evaluating the effects of mulch and irrigation amount on soil water distribution and root zone water balance using HYDRUS-2D. *Water*, 7(6), 2622-2640. doi: <https://doi.org/10.3390/w7062622>
- Hansona, B., Schwankl, L., Schulbach, K., & Pettygrove, G. (1997). A comparison of furrow, surface drip, and subsurface drip irrigation on lettuce yield and applied water. *Agricultural Water Management*, 33(2-3), 139-157. doi: [https://doi.org/10.1016/S0378-3774\(96\)01289-9](https://doi.org/10.1016/S0378-3774(96)01289-9)
- Hantush, M. M., & Marino, M. A. (1989). Chance-constrained model for management of stream-aquifer system. *Journal of Water Resources Planning and Management*, 115(3), 259-277. doi: [https://doi.org/10.1061/\(ASCE\)0733-9496\(1989\)115:3\(259\)](https://doi.org/10.1061/(ASCE)0733-9496(1989)115:3(259))
- Hatiye, S. D., Hari Prasad, K., & Ojha, C. (2018). Deep percolation under irrigated water-intensive crops. *Journal of Irrigation and Drainage Engineering*, 144(8), 1-13. doi: [https://doi.org/10.1061/\(ASCE\)IR.1943-4774.0001326](https://doi.org/10.1061/(ASCE)IR.1943-4774.0001326)
- Hilfer, R., & Øren, P. (1996). Dimensional analysis of pore scale and field scale immiscible displacement. *Transport in Porous Media*, 22(1), 53-72. doi: <https://doi.org/10.1007/BF00974311>
- Honari, M., Ashrafzadeh, A., Khaledian, M., Vazifedoust, M., & Mailhol, J. (2017). Comparison of HYDRUS-3D soil moisture simulations of subsurface drip irrigation with experimental observations in the south of France. *Journal of Irrigation and Drainage Engineering*, 143(7), 1-7. doi: [https://doi.org/10.1061/\(ASCE\)IR.1943-4774.0001188](https://doi.org/10.1061/(ASCE)IR.1943-4774.0001188)
- Huang, G., & Loucks, D. P. (2000). An inexact two-stage stochastic programming model for water resources management under uncertainty. *Civil Engineering Systems*, 17(2), 95-118. doi: <https://doi.org/10.1080/02630250008970277>
- Huang, Y., Huang, G., Liu, D., Zhu, H., & Sun, W. (2012). Simulation-based inexact chance-constrained nonlinear programming for eutrophication management in the Xiangxi Bay of Three Gorges Reservoir. *Journal of Environmental Management*, 108, 54-65. doi: <https://doi.org/10.1016/j.jenvman.2012.04.037>
- Hudzari, R., Noorman, M., Asimi, M., Atar, M., & Nashriyah, M. (2013). Engineering technological in agriculture research and education. *Advanced Materials Research*, 705, 493-498. doi: <https://doi.org/10.4028/www.scientific.net/AMR.705.493>

- Izadi, B., King, B., Westermann, D., & McCann, I. (1996). Modeling transport of bromide in furrow-irrigated field. *Journal of Irrigation and Drainage Engineering*, 122(2), 90-96. doi: [https://doi.org/10.1061/\(ASCE\)0733-9437\(1996\)122:2\(90\)](https://doi.org/10.1061/(ASCE)0733-9437(1996)122:2(90))
- Jiang, X. J., Chen, C., Zhu, X., Zakari, S., Singh, A. K., Zhang, W., ... & Yu, S. (2019). Use of dye infiltration experiments and HYDRUS-3D to interpret preferential flow in soil in a rubber-based agroforestry systems in Xishuangbanna, China. *Catena*, 178, 120-131. doi: <https://doi.org/10.1016/j.catena.2019.03.015>
- Kacimov, A., Obnosov, Y. V., & Šimůnek, J. (2018). Steady flow from an array of subsurface emitters: Kornev's irrigation technology and Kidder's free boundary problems revisited. *Transport in Porous Media*, 121(3), 643-664. doi: <https://doi.org/10.1007/s11242-017-0978-x>
- Kandil, H., Skaggs, R., Dayem, S. A., & Aiad, Y. (1995). DRAINMOD-S: Water management model for irrigated arid lands, crop yield and applications. *Irrigation and Drainage Systems*, 9(3), 239-258. doi: <https://doi.org/10.1007/BF00880866>
- Kapoor, V. (1996). Criterion for instability of steady-state unsaturated flows. *Transport in Porous Media*, 25(3), 313-334. doi: <https://doi.org/10.1007/BF00140986>
- Kerkides, P., Poulouvassilis, A., Argyrokastritis, I., & Elmaloglou, S. (1997). Comparative evaluation of analytic solutions in predicting soil moisture profiles in vertical one-dimensional infiltration under ponded and constant flux boundary conditions. *Water Resources Management*, 11(5), 323-338. doi:10.1023/a:1007978714468
- Khalil, L. A., & Abid, M. B. (2019). Numerical simulation of unsaturated soil water from a trickle irrigation system for sandy loam soils. *Journal of Engineering*, 25(3), 38-52. doi: <https://doi.org/10.31026/j.eng.2019.03.04>
- Kite, G., & Droogers, P. (2000). Comparing evapotranspiration estimates from satellites, hydrological models and field data. *Journal of Hydrology*, 229(1-2), 3-18. doi: [https://doi.org/10.1016/S0022-1694\(99\)00195-X](https://doi.org/10.1016/S0022-1694(99)00195-X)
- Lacroix, M., Wang, H., & Blavoux, B. (1996). Water-table modelling to estimate irrigation losses: application to the Lower Durance, France. *Agricultural Water Management*, 30(3), 283-300. doi: [https://doi.org/10.1016/0378-3774\(95\)01227-3](https://doi.org/10.1016/0378-3774(95)01227-3)
- Li, P., Tan, H., Wang, J., Cao, X., & Yang, P. (2019). Evaluation of water uptake and root distribution of cherry trees under different irrigation methods. *Water*, 11(3), 1-18. doi: <https://doi.org/10.3390/w11030495>
- Lima, V., Keitel, C., Sutton, B., & Leslie, G. (2019). Improved water management using subsurface membrane irrigation during cultivation of *Phaseolus vulgaris*. *Agricultural Water Management*, 223, 1-11. doi: <https://doi.org/10.1016/j.agwat.2019.105730>
- Liu, Y., Zhou, Y., Wang, T., Pan, J., Zhou, B., Muhammad, T., ... & Li, Y. (2019). Micro-nano bubble water oxygation: Synergistically improving irrigation water use efficiency, crop yield and quality. *Journal of Cleaner Production*, 222, 835-843. doi: <https://doi.org/10.1016/j.jclepro.2019.02.208>
- Lockington, D., & Parlange, J. Y. (1995). Approximate formulae for the wetting front position and boundary water-content during horizontal infiltration. *Transport in Porous Media*, 18(2), 95-105. doi: <https://doi.org/10.1007/BF01064673>

- Loucks, D. P., Stedinger, J. R., & Haith, D. A. (1981). *Water resource systems planning and analysis*. Englewood Cliffs, New Jersey: Prentice-Hall.
- Mantoglou, A. (2003). Pumping management of coastal aquifers using analytical models of saltwater intrusion. *Water Resources Research*, 39(12), 1-12. doi: <https://doi.org/10.1029/2002WR001891>
- Martínez de Azagra Paredes, A., & Del Río San José, J. (2019). Pitcher Irrigation: Some Theoretical and Practical Aspects. *Irrigation and Drainage*, 68(3), 542-550. doi: <https://doi.org/10.1002/ird.2330>
- Massatbayev, K., Izbassov, N., Nurabaev, D., Musabekov, K., Shomantayev, A., & Massatbayev, M. (2016). Technology and regime of sugar beet drip irrigation with plastic mulching under the conditions of the jambyl region. *Irrigation and Drainage*, 65(5), 620-630. doi: <https://doi.org/10.1002/ird.2084>
- Matanga, G. B., & Mariño, M. A. (1979). Irrigation planning: 1. Cropping pattern. *Water Resources Research*, 15(3), 672-678. doi: <https://doi.org/10.1029/WR015i003p00672>
- McClymont, D., & Smith, R. (1996). Infiltration parameters from optimisation on furrow irrigation advance data. *Irrigation Science*, 17(1), 15-22.
- Meshkat, M., Warner, R. C., & Workman, S. R. (1999). Modeling of evaporation reduction in drip irrigation system. *Journal of Irrigation and Drainage Engineering*, 125(6), 315-323. doi: [https://doi.org/10.1061/\(ASCE\)0733-9437\(1999\)125:6\(315\)](https://doi.org/10.1061/(ASCE)0733-9437(1999)125:6(315))
- Montazar, A., Zaccaria, D., Bali, K., & Putnam, D. (2017). A model to assess the economic viability of alfalfa production under subsurface drip irrigation in California. *Irrigation and Drainage*, 66(1), 90-102. doi: <https://doi.org/10.1002/ird.2091>
- Naghedifar, S. M., Ziaei, A. N., Playán, E., Zapata, N., Ansari, H., & Hasheminia, S. M. (2019). A 2D curvilinear coupled surface–subsurface flow model for simulation of basin/border irrigation: theory, validation and application. *Irrigation Science*, 37(2), 151-168. doi: <https://doi.org/10.1007/s00271-018-0609-5>
- Oad, R., & Sampath, R. (1995). Performance measure for improving irrigation management. *Irrigation and Drainage Systems*, 9(4), 357-370.
- Panda, S., Khepar, S., & Kaushal, M. (1996). Interseasonal irrigation system planning for waterlogged sodic soils. *Journal of Irrigation and Drainage Engineering*, 122(3), 135-144. doi: [https://doi.org/10.1061/\(ASCE\)0733-9437\(1996\)122:3\(135\)](https://doi.org/10.1061/(ASCE)0733-9437(1996)122:3(135))
- Parlange, J. Y., Hogarth, W., Parlange, M., Haverkamp, R., Barry, D. A., Ross, P., & Steenhuis, T. (1998). Approximate analytical solution of the nonlinear diffusion equation for arbitrary boundary conditions. *Transport in Porous Media*, 30(1), 45-55. doi: <https://doi.org/10.1023/A:1006508721609>
- Parseval, Y. D., Pillai, K. M., & Advani, S. G. (1997). A simple model for the variation of permeability due to partial saturation in dual scale porous media. *Transport in Porous Media*, 27(3), 243-264. doi: [10.1023/a:1006544107324](https://doi.org/10.1023/a:1006544107324)
- Qiu, Z., Li, J., & Zhao, W. (2017). Effect of applying sewage effluent with subsurface drip irrigation on soil enzyme activities during the maize growing season. *Irrigation and Drainage*, 66(5), 723-737. doi: <https://doi.org/10.1002/ird.2124>

- Razali, M. H., Roslan, S., Halim, A. S. M. A., Shokeri, A. F. M., & Husin, N. A. (2016). Design and Development of Innovative Highland Water Filtration System. *World Journal of Engineering and Technology*, 4(3), 383-390. doi: 10.4236/wjet.2016.43037
- Ren, C., Zhao, Y., Dan, B., Wang, J., Gong, J., & He, G. (2018). Lateral hydraulic performance of subsurface drip irrigation based on spatial variability of soil: Experiment. *Agricultural Water Management*, 204, 118-125. doi: <https://doi.org/10.1016/j.agwat.2018.03.034>
- Ren, C., Zhao, Y., Wang, J., Bai, D., Zhao, X., & Tian, J. (2017). Lateral hydraulic performance of subsurface drip irrigation based on spatial variability of soil: Simulation. *Agricultural Water Management*, 193, 232-239. doi: <https://doi.org/10.1016/j.agwat.2017.08.014>
- Reyes-Esteves, R. G., & Slack, D. C. (2019). Modeling approaches for determining appropriate depth of subsurface drip irrigation tubing in alfalfa. *Journal of Irrigation and Drainage Engineering*, 145(10), 1-7. doi: [https://doi.org/10.1061/\(ASCE\)IR.1943-4774.0001409](https://doi.org/10.1061/(ASCE)IR.1943-4774.0001409)
- Rimmer, A., Parlange, J. Y., Steenhuis, T. S., Darnault, C., & Condit, W. (1996). Wetting and nonwetting fluid displacements in porous media. *Transport in Porous Media*, 25(2), 205-215. doi: <https://doi.org/10.1007/BF00135856>
- Ross, P., Haverkamp, R., & Parlange, J. Y. (1996). Calculating parameters for infiltration equations from soil hydraulic functions. *Transport in Porous Media*, 24(3), 315-339. doi: <https://doi.org/10.1007/BF00154096>
- Ross, P., Parlange, J. Y., & Haverkamp, R. (1995). Two-dimensional interaction of a wetting front with an impervious layer: Analytical and numerical solutions. *Transport in Porous Media*, 20(3), 251-263. doi: <https://doi.org/10.1007/BF01073175>
- Rudnick, D., Irmak, S., West, C., Chávez, J., Kisekka, I., Marek, T., ... & Djaman, K. (2019). Deficit irrigation management of maize in the High Plains Aquifer Region: A review. *JAWRA Journal of the American Water Resources Association*, 55(1), 38-55. doi: <https://doi.org/10.1111/1752-1688.12723>
- Saefuddin, R., Saito, H., & Šimůnek, J. (2019). Experimental and numerical evaluation of a ring-shaped emitter for subsurface irrigation. *Agricultural Water Management*, 211, 111-122. doi: <https://doi.org/10.1016/j.agwat.2018.09.039>
- Sakaguchi, A., Yanai, Y., & Sasaki, H. (2019). Subsurface irrigation system design for vegetable production using HYDRUS-2D. *Agricultural Water Management*, 219, 12-18. doi: <https://doi.org/10.1016/j.agwat.2019.04.003>
- Scaloppi, E. J., Merkle, G. P., & Willardson, L. S. (1995). Intake parameters from advance and wetting phases of surface irrigation. *Journal of Irrigation and Drainage Engineering*, 121(1), 57-70. doi: [https://doi.org/10.1061/\(ASCE\)0733-9437\(1995\)121:1\(57\)](https://doi.org/10.1061/(ASCE)0733-9437(1995)121:1(57))
- Shani, U., Xue, S., Gordin-Katz, R., & Warrick, A. (1996). Soil-limiting flow from subsurface emitters. I: Pressure measurements. *Journal of Irrigation and Drainage Engineering*, 122(5), 291-295. doi: [https://doi.org/10.1061/\(ASCE\)0733-9437\(1996\)122:5\(291\)](https://doi.org/10.1061/(ASCE)0733-9437(1996)122:5(291))
- Singh, A. (2013). Groundwater modelling for the assessment of water management alternatives. *Journal of Hydrology*, 481, 220-229. doi: <https://doi.org/10.1016/j.jhydrol.2012.12.042>

- Singh, A. (2014a). Irrigation planning and management through optimization modelling. *Water Resources Management*, 28(1), 1-14. doi: <https://doi.org/10.1007/s11269-013-0469-y>
- Singh, A. (2014b). Optimizing the use of land and water resources for maximizing farm income by mitigating the hydrological imbalances. *Journal of Hydrologic Engineering*, 19(7), 1447-1451. doi: [https://doi.org/10.1061/\(ASCE\)HE.1943-5584.0000924](https://doi.org/10.1061/(ASCE)HE.1943-5584.0000924)
- Singh, A. (2014c). Simulation–optimization modeling for conjunctive water use management. *Agricultural Water Management*, 141, 23-29. doi: <https://doi.org/10.1016/j.agwat.2014.04.003>
- Singh, B., Boivin, J., Kirkpatrick, G., & Hum, B. (1995). Automatic irrigation scheduling system (AISSUM): Principles and applications. *Journal of Irrigation and Drainage Engineering*, 121(1), 43-56. doi: [https://doi.org/10.1061/\(ASCE\)0733-9437\(1995\)121:1\(43\)](https://doi.org/10.1061/(ASCE)0733-9437(1995)121:1(43))
- Snyder, R., Plas, M., & Grieshop, J. (1996). Irrigation methods used in California: Grower survey. *Journal of Irrigation and Drainage Engineering*, 122(4), 259-262. doi: [https://doi.org/10.1061/\(ASCE\)0733-9437\(1996\)122:4\(259\)](https://doi.org/10.1061/(ASCE)0733-9437(1996)122:4(259))
- Soulis, K. X., & Elmaloglou, S. (2016). Optimum soil water content sensors placement in drip irrigation scheduling systems: Concept of time stable representative positions. *Journal of Irrigation and Drainage Engineering*, 142(11), 1-9. doi: [https://doi.org/10.1061/\(ASCE\)IR.1943-4774.0001093](https://doi.org/10.1061/(ASCE)IR.1943-4774.0001093)
- Tabari, M. M. R., & Soltani, J. (2013). Multi-objective optimal model for conjunctive use management using SGAs and NSGA-II models. *Water Resources Management*, 27(1), 37-53. doi: <https://doi.org/10.1007/s11269-012-0153-7>
- Valiantzas, J. D. (1997). Surface irrigation advance equation: Variation of subsurface shape factor. *Journal of Irrigation and Drainage Engineering*, 123(4), 300-306. doi: [10.1061/\(ASCE\)0733-9437\(1997\)123:4\(300\)](https://doi.org/10.1061/(ASCE)0733-9437(1997)123:4(300))
- Varshney, R. S. (1995). Modern methods of irrigation. *GeoJournal*, 35(1), 59-63.
- Warrick, A., & Shani, U. (1996). Soil-limiting flow from subsurface emitters. II: Effect on uniformity. *Journal of Irrigation and Drainage Engineering*, 122(5), 296-300. doi: [https://doi.org/10.1061/\(ASCE\)0733-9437\(1996\)122:5\(296\)](https://doi.org/10.1061/(ASCE)0733-9437(1996)122:5(296))
- Willis, T. M., Black, A. S., & Meyer, W. S. (1997). Estimates of deep percolation beneath cotton in the Macquarie Valley. *Irrigation Science*, 17(4), 141-150. doi: <https://doi.org/10.1007/s002710050032>
- Witelski, T. P. (1997). Perturbation analysis for wetting fronts in Richard's Equation. *Transport in Porous Media*, 27(2), 121-134. doi: <https://doi.org/10.1023/A:1006513009125>
- Zhang, H., Liu, H., Sun, C., Gao, Y., Gong, X., Sun, J., & Wang, W. (2017). Root development of transplanted cotton and simulation of soil water movement under different irrigation methods. *Water*, 9(7), 1-21. doi: <https://doi.org/10.3390/w9070503>
- Zheng, C., Lu, Y., Guo, X., Li, H., Sai, J., & Liu, X. (2017). Application of HYDRUS-1D model for research on irrigation infiltration characteristics in arid oasis of northwest China. *Environmental Earth Sciences*, 76(23), 785-795. doi: <https://doi.org/10.1007/s12665-017-7151-2>

Forecasting Wind Speed in Peninsular Malaysia: An Application of ARIMA and ARIMA-GARCH Models

Nor Hafizah Hussin^{1,2*}, Fadhilah Yusof², 'Aaishah Radziah Jamaludin² and Siti Mariam Norrulashikin²

¹Faculty of Electrical and Electronic Engineering Technology, Universiti Teknikal Malaysia Melaka, Hang Tuah Jaya, 76100, Durian Tunggal, Melaka, Malaysia

²Department of Mathematical Sciences, Faculty of Science, Universiti Teknologi Malaysia, 81300, Johor Bahru, Johor, Malaysia

ABSTRACT

In the global energy context, renewable energy sources such as wind is considered as a credible candidate for meeting new energy demands and partly substituting fossil fuels. Modelling and forecasting wind speed are noteworthy to predict the potential location for wind power generation. An accurate forecasting of wind speed will improve the value of renewable energy by enhancing the reliability of this natural resource. In this paper, the wind speed data from year 1990 to 2014 in 18 meteorological stations throughout Peninsular Malaysia were modelled using the Autoregressive Integrated Moving Average (ARIMA) to forecast future wind speed series. The Ljung-Box test was used to determine the presence of serial autocorrelation, while the Engle's Lagrange Multiplier (LM) test was used to investigate the presence of Autoregressive Conditional Heteroscedasticity (ARCH) effect in the residual of the ARIMA model.

In this study, three stations showed good fit using the ARIMA modelling since no serial correlation and ARCH effect were present in the residuals of the ARIMA model, while the ARIMA-GARCH had proven to precisely capture the nonlinear characteristic of the wind speed daily series for the remaining stations. The forecasting accuracy measure used was based on the value of root mean square error (RMSE) and mean absolute percentage error (MAPE). Both ARIMA and

ARTICLE INFO

Article history:

Received: 6 July 2020

Accepted: 5 November 2020

Published: 22 January 2021

DOI: <https://doi.org/10.47836/pjst.29.1.02>

E-mail addresses:

norhafizah.hussin@graduate.utm.my (Nor Hafizah Hussin)

fadhilahy@utm.my (Fadhilah Yusof)

['Aaishah Radziah Jamaludin](mailto:aishahjamaludin85@gmail.com)

sitimariam@utm.my (Siti Mariam Norrulashikin)

*Corresponding author

ARIMA-GARCH model proposed provided good forecast accuracy measure of wind speed series in Peninsular Malaysia. These results will help in providing a quantitative measure of wind energy available in the potential location for renewable energy conversion.

Keyword: Forecasting, modelling, renewable energy, time series method, wind speed

INTRODUCTION

In this rapid population growth, the energy demand has increased to support human consumption. The negative effect is energy usage has increased the demand on energy resulting in depletion of natural resources and will cause a harmful effect towards the environment (Ajayi et al., 2014). To overcome this issue, many developed countries are now focusing on conserving the non-renewable energy by switching to renewable energy sources like wind and solar. Wind power is one of the natural sources of renewable energy that is experiencing the fastest growth is the wind energy. Unlike solar energy, wind power can provide energy throughout day and night since it does not require any sunlight (Petinrin & Shaaban, 2015).

Many researchers have studied wind speed modelling and forecasting using various models which were developed in improving the wind speed forecasting accuracy (Chang et al., 2016; De Freitas et al., 2018; Norrulashikin et al., 2018; Sharma & Singh, 2018). According to Erdem et al. (2014), there are two main aspects to be considered in building a wind speed prediction model which is to predict the mean wind speed and the wind speed volatility. Commonly used models include autoregressive (AR) model, moving average (MA) model (Akcan, 2017), autoregressive moving average (ARMA) model (Lujano-Rojas et al., 2011), and autoregressive integrated moving average (ARIMA) model (Radziukynas & Klementavicius, 2014). These models assume that the occurrence of turbulence in the wind speed is constant or in other words, homoscedastic. However, wind speed series can exhibit the characteristics of nonlinear variance where it is often referred to as volatility and may vary over time. Therefore, the presence of nonlinear variance in a model needs to be investigated before any prediction is performed. If the error estimation for this variation of wind speed is underestimated, the prediction model might fail to provide accurate wind speed forecasting that will cause serious problems in the operation of wind turbine (Engle, 2001).

Hence, this study was conducted to propose a forecasting model using the ARIMA model. The proposed model with the presence of serial autocorrelation and effect of heteroscedasticity in the residual part of the series would be treated using the Generalized Autoregressive Conditional Heteroskedastic (GARCH) model. A related study by Masseran (2016) used an ARIMA-ARCH model to investigate the effect of mean and volatility of

the wind speed. Yan et al. (2016) suggested the ARIMA-GARCH model for forecasting a short-term wind speed series. The proposed model had successfully managed to capture the heteroscedasticity of wind speed series and gave a higher prediction accuracy compared to the ARIMA model. Based on Lojowska et al. (2010), the advantage of modelling using ARMA-GARCH model is that it has the capability to handle the dominant criteria of the data series, which is distribution, time dependence structure as well as periodicity. For the purpose of wind speed forecasting, Grigonytė & Butkevičiūtė (2016) used the ARIMA model to forecast a short-term wind speed in Latvia and the forecasting accuracy for the proposed model was based on root mean square error (RMSE) and mean absolute percentage error (MAPE) and mean absolute error (MAE) which allowed to establish an optimal model structure. While Sharma and Ghosh (2016) used MAPE in measuring the short-term wind speed forecasting in India and the finding suggested that ARIMA-GARCH model yielded smallest value of MAPE compared to other proposed models.

The aim of this study was to develop a time series model of daily wind speed series in Peninsular Malaysia. Box-Jenkins ARIMA model was used to model the series of each 18 stations and 15 stations were found to have a serial correlation and heteroscedastic effect in the residuals of the proposed model. Therefore, an ARIMA-GARCH model that is proven to help in capturing the serial autocorrelation and the heteroscedastic effects of a time series process was used. This hybrid model would help to overcome the linear limitation of ARIMA model for the purpose of obtaining a time series model that yielded higher accuracy of forecasting results.

MATERIALS AND METHODS

This research used a daily wind speed series collected from Malaysian Meteorological Department (MMD) which consisted of data from 1990 to 2014. Data of daily wind speed series from 18 meteorological stations throughout the Peninsular Malaysia were chosen for this study from different regions. The last 365 days of daily wind speed data for each station would be considered as the out-sample data which will be compared with the forecasted daily wind speed series based on the best fitted model. In this study, time series analysis was applied due to the ability to interpret the presence of internal structure that might occur to the data point taken over time. For instance, the condition of serial autocorrelation and heteroscedastic effects should be taken into account in the analysis.

Data Description

The daily wind speed data from 18 different locations in Peninsular Malaysia with a duration from 1/1/1990 to 31/12/2014 were used in this study. The location in Peninsular Malaysia were divided into 4 regions, namely: northern, east coast, central, and southern. The northern region consists of stations that are located in Perlis, Kedah, Pulau Pinang

and Perak, while the east coast region consists of stations that are located in the state of Kelantan, Terengganu, and Pahang. The central region consists of stations that are located in Selangor, Kuala Lumpur, and Putrajaya, and the southern region consists of stations that are located in Negeri Sembilan, Melaka, and Johor. The detailed information on the stations used in this study are given in Table 1 while Figure 1 shows the location of the stations on the map of Peninsular Malaysia.

Table 1

Coordinates for 18 stations used for wind speed data collection in Peninsular Malaysia

Location	Station	Latitude	Longitude
Chuping	NS1	6°28'47.0"N	100°15'36.1"E
Langkawi	NS2	6°20'13.0"N	99°43'35.4"E
Bayan Lepas	NS3	5°17'43.4"N	100°16'06.6"E
Butterworth	NS4	5°27'53.9"N	100°22'59.2"E
Lubok Merbau	NS5	4°47'42.9"N	100°53'46.6"E
Sitiawan	NS6	4°13'17.1"N	100°42'05.5"E
Kota Bharu	ES7	6°09'12.6"N	102°18'41.0"E
Kuala Terengganu	ES8	5°22'59.3"N	103°06'28.8"E
Cameron Highland	ES9	4°29'04.0"N	101°22'17.4"E
Kuantan	ES10	3°46'22.9"N	103°12'42.3"E
Subang	CS11	3°07'52.0"N	101°33'09.8"E
Petaling Jaya	CS12	3°06'26.0"N	101°38'52.9"E
Sepang	CS13	2°43'54.2"N	101°42'10.5"E
Melaka	SS14	2°15'17.2"N	102°14'36.0"E
Mersing	SS15	2°26'42.6"N	103°49'52.6"E
Batu Pahat	SS16	1°52'14.5"N	102°59'25.6"E
Kluang	SS17	2°01'41.6"N	103°19'14.0"E
Senai	SS18	1°38'20.3"N	103°39'57.0"E

ARIMA Model

In time series analysis, the Box-Jenkins method is the commonly used method to model a wind speed time series data. The first step is model identification which include measuring the stability of the mean and the stationarity of the time series. The transformation approach is needed if the data does not satisfy these conditions. This can be done by observing the time series and ACF plots of the collected wind speed data. A hypothesis testing using the

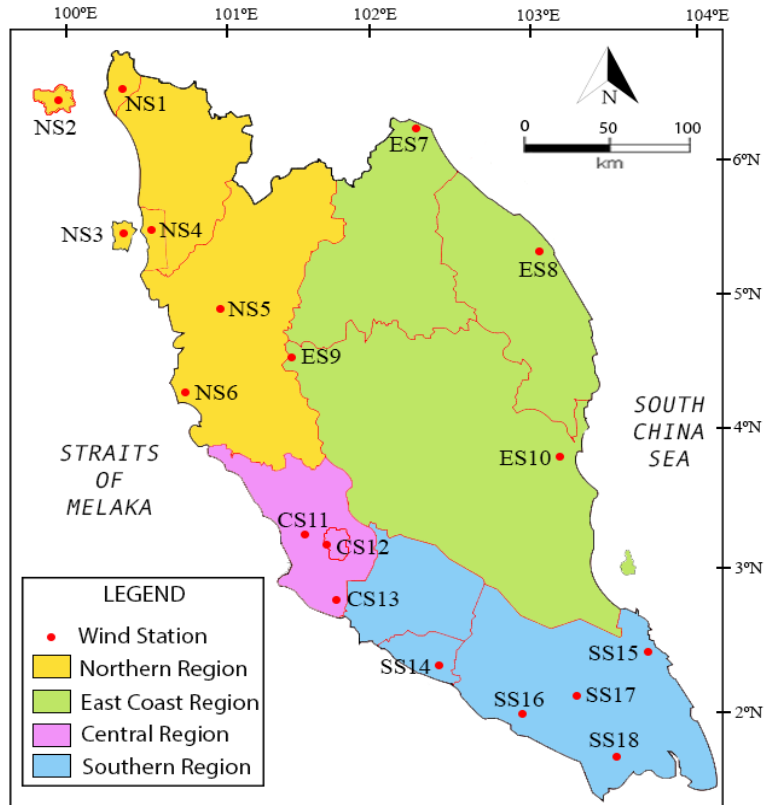


Figure 1. Location of wind stations in Peninsular Malaysia

Kwiatkowski–Phillips–Schmidt–Shin (KPSS) test can be used to determine the stationarity of the wind speed time series data, where the null hypothesis is the data series is stationary (Kwiatkowski et al., 1992). The formulation for the KPSS test is given by Equation 1:

$$y_t = \beta t + r_t + \varepsilon_t. \quad [1]$$

Note that $r_t = r_{(t-1)} + u_t$, where r_t represents a random walk while u_t are iid $(0, \sigma_u^2)$. For a p-value that is significantly low than 0.05, the null hypothesis will be rejected which indicates that the wind speed series is not stationary and requires a differencing approach. For the model selection, autocorrelation function (ACF) and partial autocorrelation function (PACF) plot provides the information on the potential models where it identifies the number of terms for autoregressive order p and moving average order q (Miswan et al., 2015).

The general form of autoregressive integrated moving average ARIMA (p, d, q) can be defined as Equation 2:

$$\varphi(B)(1 - B)^d y_t = \theta(B)\varepsilon_t \quad [2]$$

where y_t and ε_t are the observed values of wind speed series and the random error terms at time period t , respectively. $\varphi_1, \varphi_2, \varphi_3, \dots, \varphi_p$ are the autoregressive coefficients with order p . d is the order of differencing, and $\theta_1, \theta_2, \theta_3, \dots, \theta_q$ are the moving average coefficients with order q . B is the backward shift operator, while, $\varphi(B)$ and $\theta(B)$ are polynomials of order p and q respectively, and defined as follows (Wang et al., 2015):

$$\varphi(B) = 1 - \varphi_1 B - \varphi_2 B^2 - \dots - \varphi_p B^p$$

$$\theta(B) = 1 - \theta_1 B - \theta_2 B^2 - \dots - \theta_q B^q.$$

Serial Correlation

A statistical inference of time series analysis will be affected by the presence of serial correlation. A fitted model is appropriate or accurate if the residuals has the conditions of zero mean, homoscedastic, independent, and normally distributed (Jamaludin et al., 2016; Yürekli et al., 2005). One of the very useful diagnostic tools to measure the existence of a serial autocorrelation for residuals in the stationary ARIMA model is using the Ljung-Box (LB) test (Kim et al., 2004). The null hypothesis was set to the absence of serial autocorrelation in the residuals from the ARIMA model and was performed towards the residuals of a fitted ARIMA model instead of the original time series data. The decision making for the test is based on Equation 3:

$$Q = T(T + 2) \sum_{k=1}^L \frac{r_k^2}{(T-k)}; \quad [3]$$

where T is denoted as the length of the time series, k represents the number of parameters to be estimated in the model, r_k^2 denotes the sample autocorrelation at lag k , and L is the number of autocorrelation lag to be tested. The Q -statistics in Equation 3 approximately follows a chi-square distribution with L degree of freedom (Wang et al., 2015).

The Autoregressive Conditional Heteroscedasticity (ARCH) Effect

Besides checking for the presence of serial correlation, the test to check on the existence of heteroscedasticity in the residual of the model should also be performed. The result can

also be supported by performing ARCH Lagrange Multiplier (LM) test to determine the existence of heteroscedasticity in the residuals of the model.

Engle's Lagrange Multiplier Test for the ARCH Effect

Uncorrelated time series models might still have a serial dependence due to the dynamic conditional variance process. The existence of an ARCH effect in the ARIMA model occur if the model exhibits autoregressive conditional heteroscedasticity. If the ARCH effect is neglected, the consequences might result to large arbitrary loses in asymptotic efficiency which will lead to an extreme rejection of the standard test for the mean autocorrelation (Sjölander, 2011). To assess the significance of an ARCH effect, Engle (1982) proposed a methodology using Lagrange Multiplier (LM) test to assess the presence of ARCH effect based on the regression. The decision making of this test is based on Equation 4:

$$e_t^2 = \hat{a}_0 + \sum_{s=1}^q \hat{a}_s e_{t-s}^2 \quad [4]$$

where e_t is the residual series and a_s is the estimated coefficients of the fitted model. In this test, the null hypothesis is set to be that there is no existing ARCH component up to order q ; i.e. $a_s=0$ for all $s=1, 2, \dots, q$. The alternative hypothesis is there are presence of ARCH components in at least one of the estimated a_s coefficients (Yusof et al., 2013). The test statistics for this test is given by TR_2 . It follows a chi-square distribution with q degree of freedom, where R denotes the sample multiple correlation coefficient based on the computation from the regression in Equation 4, and T is the number of observations (Wang et al., 2005).

The GARCH Model

Generalized Autoregressive Conditional Heteroscedastic (GARCH) model was developed by Bollerslev (1986). It helps the ARIMA (p, d, q) model to capture the heteroscedastic effect in a time series process. In modelling a univariate time series, let $y_t = \mu_t + \varepsilon_t$ denote the mean equation with respect to time t , where the conditional mean of y_t is represented by μ_t , while ε_t is denoted as the shock at time t and the equation is $\varepsilon_t = v_t \sigma_t$ where it follows a distribution of $\varepsilon_t \sim \text{iid } N(0,1)$. Then, the conditional variance of y_t denoted by σ_t^2 , that follows a GARCH (p, q) model can be expressed in Equation 5:

$$\sigma_t^2 = \alpha_0 + \sum_{i=1}^p \alpha_i \varepsilon_{t-i}^2 + \sum_{i=1}^q \beta_i \sigma_{t-i}^2 \quad [5]$$

where the value of α_0 is always positive, while the sum of α_i and β_i is less than 1 up to order p and q . The coefficient of parameters that represent ARCH and GARCH are represented by α_i and β_i , respectively.

The ARIMA-GARCH Model

The ARIMA-GARCH model is known to have two procedures where the first part models the linear part of the wind speed series using ARIMA model, while the residual part consists of the nonlinear data (Yaziz et al., 2013). Then, using the GARCH model, the residuals that display only the nonlinear pattern will be modelled and the combination of the ARIMA model and GARCH error component will give a model that can capture the dynamics of the wind speed series which can be used to forecast wind series. The standard GARCH (1,1) model was used to capture the heteroscedastic effect of the time series process in this study.

Forecasting Accuracy Measures

The final part of this study was to forecast the wind speed data based on the best fitted proposed model as well as examine the adequacy and accuracy of the proposed model. The adequacy and accuracy checking involve the investigation of the error terms in the proposed model. This study would use RMSE and MAPE as forecasting accuracy measures which are given by Equation 6 and 7:

$$RMSE = \sqrt{\frac{1}{n} \sum_{j=1}^n (\hat{y}_j - y_j)^2} ; \tag{6}$$

$$MAPE = \frac{1}{n} \sum_{j=1}^n \frac{|\hat{y}_j - y_j|}{y_j} \times 100 ; \tag{7}$$

where the sample size is denoted by n , while \hat{y}_j is the predicted value based on proposed model at time j and y_j is the observed value at time j . According to a study by Moreno et al. (2013), the MAPE can be considered as one of the commonly used methods to measure forecasting accuracy since it has a feature that is reliable, easy to interpret, clarity of presentation, support of statistical evaluation, and it uses all the information related to the error (Moreno et al., 2013). The interpretation for the typical MAPE value which was explained by Lewis (1982) are presented in Table 2.

Table 2
Interpretation of typical MAPE values

MAPE	Interpretation	MAPE	Interpretation
< 10	Highly accurate forecasting	20 – 50	Reasonable forecasting
10 – 20	Good forecasting	> 50	Inaccurate forecasting

RESULTS AND DISCUSSION

Descriptive Statistics

Figure 2 illustrates the central tendency, the dispersion, and the skewness of the wind speed data. The outliers present in the boxplot for each station represent a high wind speed reading in a certain time and location. The presence of these extreme values in wind speed data is very pronounced in data processing. Based on Figure 2, the median of the data for all wind stations were in the range of 6 m/s to 9 m/s. The dispersion of the data that represented by the tail of the boxplot showed a wide dispersion which also indicates volatility. The boxplot also shows that all stations exhibited a positive skewness. It means that the wind speed series for all stations in Peninsular Malaysia were not normally distributed. Therefore, in order to capture the variability and volatility, the Box-Jenkins methodology was applied to model the wind speed data for all wind stations in Peninsular Malaysia.

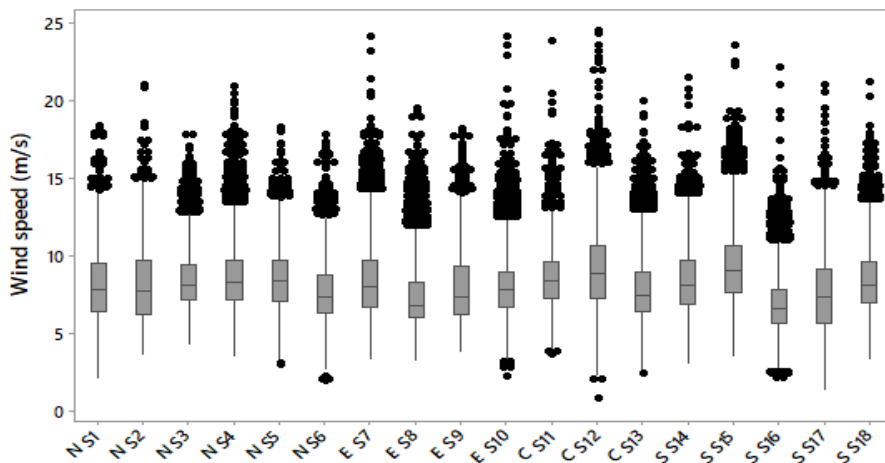


Figure 2. Boxplot of 18 wind stations in Peninsular Malaysia

ARIMA Model

The first step in building a time series model using the Box-Jenkins methodology is the model identification. This step is intended to determine whether the differencing is required in order to obtain a stationary time series. In practical sense, a stationary time series is known to vary around a constant mean level over time, with a constant variance. This can be determined by observing the time series plot and ACF plot of the wind speed data. It also can be done by performing the Kwiatkowski–Phillips–Schmidt–Shin (KPSS) test, where it tests the presence of a unit root in a time series data.

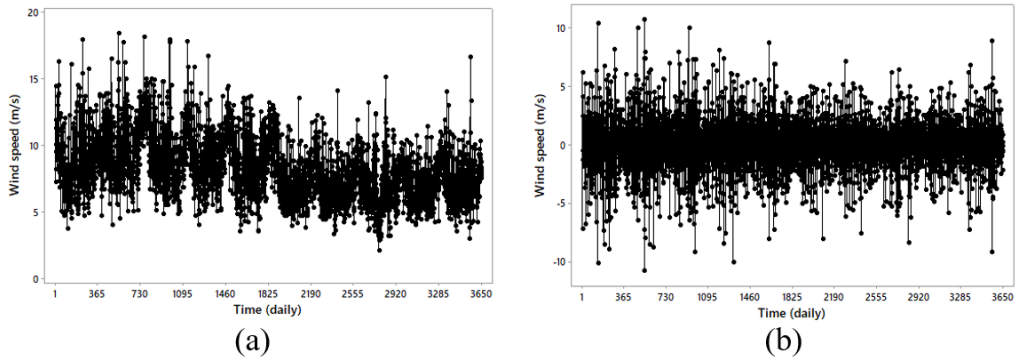


Figure 3. Time series plot of station NS1; (a) observation data and (b) after first difference.

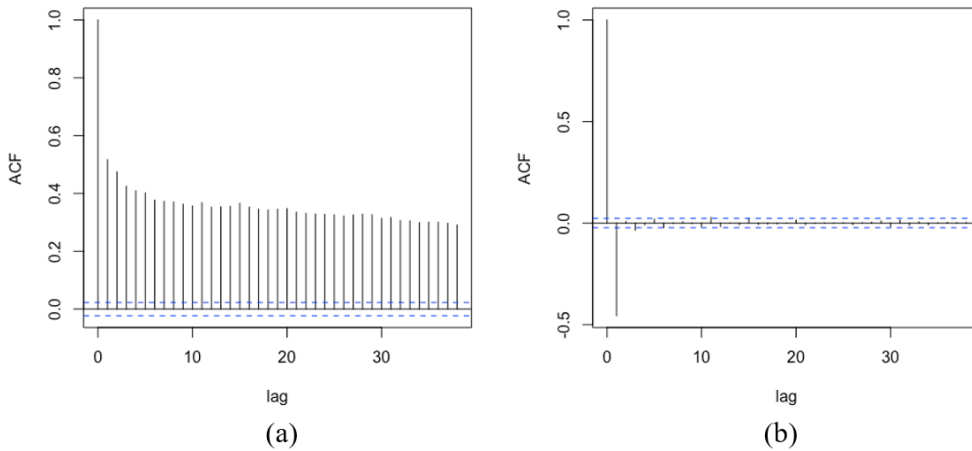


Figure 4. ACF plot for station NS1; (a) observation data and (b) after first difference.

The time series plot in Figure 3 (a) shows that the mean and variance of wind speed series in station NS1 change over time. This indicates that the time series was not stationary. The plot presented in Figure 4 (a) also proves that station NS1 was not stationary due to the slow decay displayed in the ACF plot. This suggest that the data must undergo differencing. A non-stationary time series can be transformed to stationary if the differences among pairs of observation at lags are calculated. After the first differencing approach was applied, Figure 3 (b) and Figure 4 (b) show that the wind speed data in station NS1 are stationary. To support the findings, the KPSS test was performed to determine the stationarity of the daily wind speed time series data, where the null hypothesis was the data series is stationary. For a p-value that was significantly lower than 0.05, the null hypothesis would be rejected which indicated that the wind speed series was not stationary and required a differencing

approach. The results of KPSS test for stationarity are presented in Table 3 where the findings concluded that five stations showed a stationary wind speed series, while 12 other stations satisfied this condition after first differencing ($d=1$).

Table 3

The KPSS test for stationarity of the daily wind speed series

Station	Observation Data			First Differencing		
	KPSS Level	p-value	Stationary	KPSS Level	p-value	Stationary
NS1	20.699	< 0.01	NO	0.0012	> 0.1	YES
NS2	0.0619	> 0.1	YES	-	-	-
NS3	0.0827	> 0.1	YES	-	-	-
NS4	3.8562	< 0.01	NO	0.0028	> 0.1	YES
NS5	3.1419	< 0.01	NO	0.0011	> 0.1	YES
NS6	20.181	< 0.01	NO	0.0015	> 0.1	YES
ES7	14.028	< 0.01	NO	0.0012	> 0.1	YES
ES8	24.312	< 0.01	NO	0.0010	> 0.1	YES
ES9	0.2554	> 0.1	YES	-	-	-
ES10	25.534	< 0.01	NO	0.0008	> 0.1	YES
CS11	0.0848	> 0.1	YES	-	-	-
CS12	2.000	< 0.01	NO	0.0015	> 0.1	YES
CS13	3.0304	< 0.01	NO	0.0013	> 0.1	YES
SS14	9.7655	< 0.01	NO	0.0009	> 0.1	YES
SS15	5.3813	< 0.01	NO	0.0011	> 0.1	YES
SS16	1.9574	< 0.01	NO	0.0026	> 0.1	YES
SS17	22.39	< 0.01	NO	0.0016	> 0.1	YES
SS18	0.2095	> 0.1	YES	-	-	-

After satisfying the stationarity condition, the next step in Box-Jenkins method is the parameter estimation. In this step, the orders of AR(p) and MA(q) for each station were identified using the PACF and ACF plots, respectively. Figure 5 illustrates the ACF plot and PACF plot of station NS1 after first differencing approach is done.

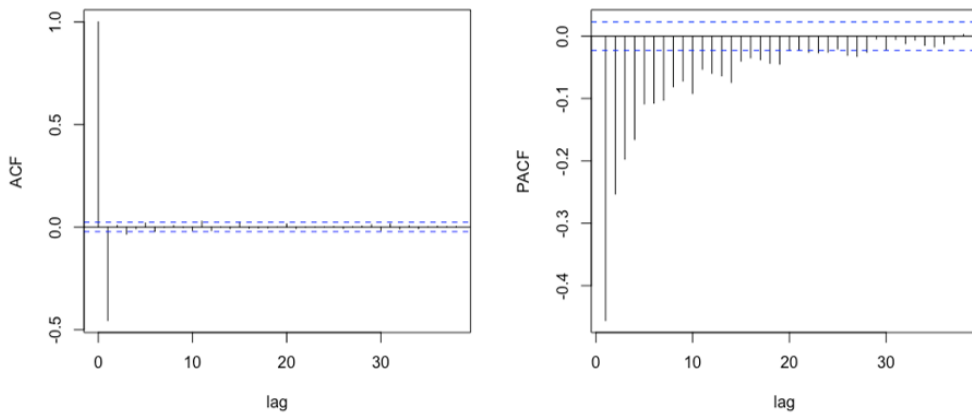


Figure 5. ACF and PACF plot for station NS1 after first difference

Few models were selected for ARIMA (p, d, q) based on these two plots, and the best model was selected based on the Akaike information criterion (AIC) values where the model with the lowest AIC value was selected as the best model for ARIMA model estimation. These steps were repeated on the remaining stations and the results of the best fitted ARIMA model for wind speed series for each station are shown in the Table 4.

Table 4

Model parameter estimates using the ARIMA (p, d, q) model for daily wind speed series

Location	Station	Model	Coefficient	Estimates	Standard Error
Chuping	NS1	ARIMA (2,1,1)	AR(1)	0.1858	0.0134
			AR(2)	0.1031	0.0132
			MA(1)	- 0.9329	0.0057
Langkawi	NS2	ARIMA (1,0,1)	AR(1)	0.5106	0.0628
			MA(1)	-0.2069	0.0709
Bayan Lepas	NS3	ARIMA (1,0,1)	AR(1)	0.8738	0.0892
			MA(1)	-0.8338	0.1008
Butterworth	NS4	ARIMA (1,1,2)	AR(1)	0.4906	0.0583
			MA(1)	-1.3395	0.0625
			MA(2)	0.3432	0.0621

Table 4 (Continued)

Location	Station	Model	Coefficient	Estimates	Standard Error
Lubok Merbau	NS5	ARIMA (1,1,2)	AR(1)	0.6452	0.0863
			MA(1)	-1.5047	0.0930
			MA(2)	0.5198	0.0883
Sitiawan	NS6	ARIMA (3,1,1)	AR(1)	0.0910	0.0127
			AR(2)	0.0246	0.0126
			AR(3)	-0.0184	0.0126
			MA(1)	-0.9557	0.0043
Kota Bharu	ES7	ARIMA (1,1,2)	AR(1)	0.5605	0.0322
			MA(1)	-1.3219	0.0367
			MA(2)	0.3249	0.0365
Kuala Terengganu	ES8	ARIMA (2,1,1)	AR(1)	0.2803	0.0125
			AR(2)	0.0915	0.0124
			MA(1)	-0.9849	0.0062
Cameron Highland	ES9	ARIMA (2,0,0)	AR(1)	0.4921	0.0261
			AR(2)	0.0305	0.0262
Kuantan	ES10	ARIMA (2,1,1)	AR(1)	0.0919	0.0118
			AR(2)	0.0675	0.0117
			MA(1)	-0.9770	0.0048
Subang	CS11	ARIMA (1,0,1)	AR(1)	0.9522	0.0291
			MA(1)	-0.9254	0.0355
Petaling Jaya	CS12	ARIMA (2,1,1)	AR(1)	0.0552	0.0155
			AR(2)	0.0343	0.0154
			MA(1)	-0.9513	0.0062
Sepang	CS13	ARIMA (1,1,1)	AR(1)	0.1224	0.0137
			MA(1)	-0.9888	0.0033
Melaka	SS14	ARIMA (1,1,2)	AR(1)	0.7459	0.0377
			MA(1)	-1.5496	0.0429
			MA(2)	0.5629	0.0401
Mersing	SS15	ARIMA (1,1,2)	AR(1)	0.6731	0.0362
			MA(1)	-1.4005	0.0408
			MA(2)	0.4196	0.0370

Table 4 (Continued)

Location	Station	Model	Coefficient	Estimates	Standard Error
Batu Pahat	SS16	ARIMA (1,1,2)	AR(1)	0.8653	0.0469
			MA(1)	-1.7653	0.0529
			MA(2)	0.7686	0.0517
Kluang	SS17	ARIMA (1,1,2)	AR(1)	0.7066	0.0524
			MA(1)	-1.5504	0.0580
			MA(2)	0.5648	0.0549
Senai	SS18	ARIMA (1,0,1)	AR(1)	0.9352	0.0214
			MA(1)	-0.8738	0.0301

After parameter estimation, the next step of the Box-Jenkins methodology is model diagnostic checking. In this step, the residual of a fitted ARIMA model was tested for the presence of serial autocorrelation and heteroscedasticity.

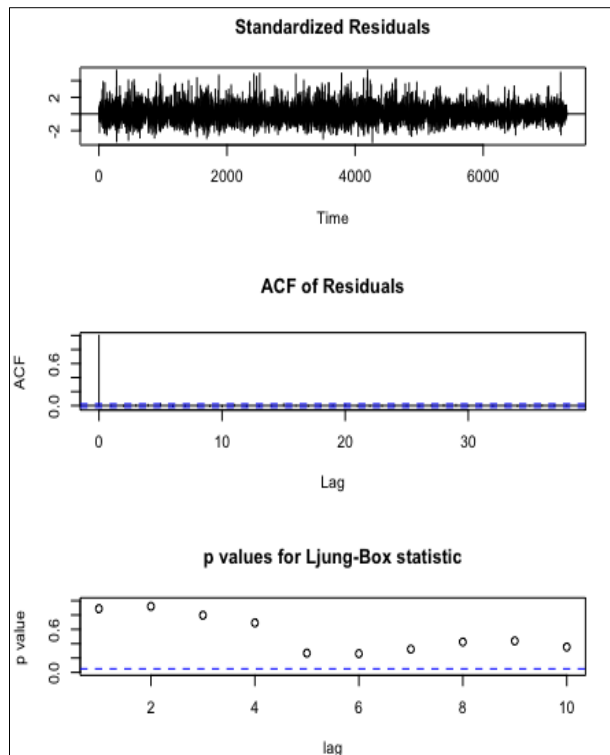


Figure 6. Diagnostic checking results for station NS1

Figure 6 shows the results of diagnostic checking using the Ljung-Box test for station NS1. The null hypothesis for the Ljung-Box test was set to be no serial autocorrelation in the residual of the fitted ARIMA (p, d, q) model. Based on the plot, the residuals of the wind speed series in station NS1 has a zero mean and constant variance. The ACF plot exhibits no correlation in the residuals of the series. The p-value for Ljung-Box test also confirmed that the residuals of the series were uncorrelated. This step was performed towards the remaining stations and the results are simplified in Table 5. The results of Ljung-Box test for the residuals in Table 5 are given into two parts; the figures represent the p-values for residuals up to lag 10 followed by the p-value for residuals up to lag 20. In addition, to prove that the square residuals are not a sequence of white noise, the Ljung-Box test was also performed on the squared residual of the wind speed series.

Table 5

The Ljung-Box test for the residuals and squared residuals of the fitted ARIMA (p, d, q) model of daily wind speed series

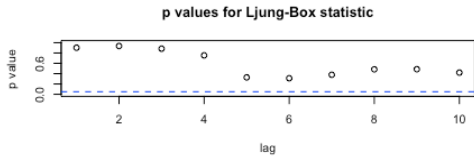
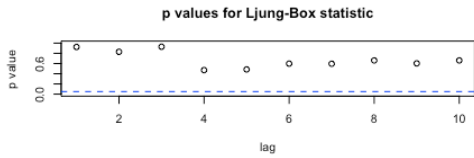
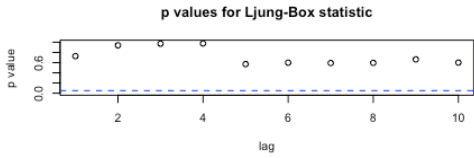
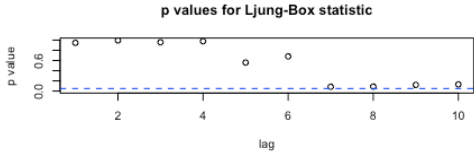
Station	ARIMA Model	p-value for Ljung-Box Statistics		
		Residuals	Squared Residuals	
NS1	ARIMA (2,1,1)		0.4028	2.2e-16
NS2	ARIMA (1,0,1)		0.0011	2.2e-16
NS3	ARIMA (1,0,1)		0.7637	0.00167
NS4	ARIMA (1,1,2)		0.2838	2.2e-16

Table 5 (Continued)

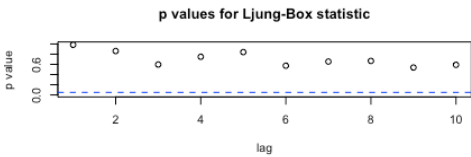
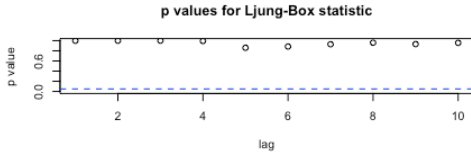
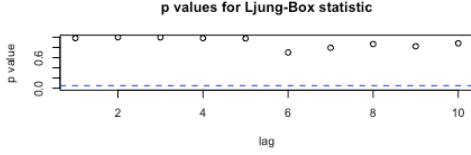
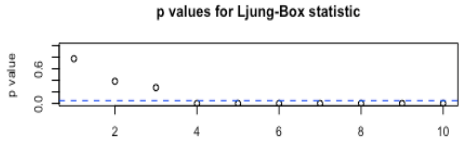
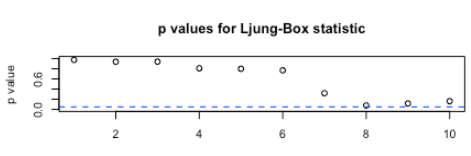
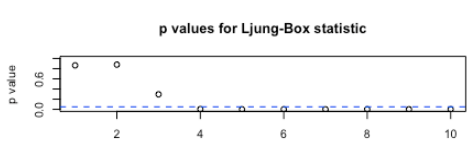
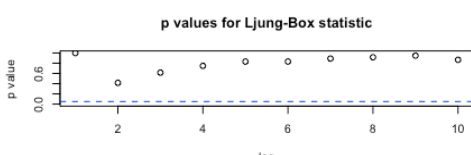
Station	ARIMA Model	p-value for Ljung-Box Statistics		
		Residuals	Squared Residuals	
NS5	ARIMA (1,1,2)		0.211	0.4394
NS6	ARIMA (3,1,1)		0.8291	2.2e-16
ES7	ARIMA (1,1,2)		0.4634	2.2e-16
ES8	ARIMA (2,1,1)		0.0037	2.2e-16
ES9	ARIMA (2,0,0)		0.0608	0.01968
ES10	ARIMA (2,1,1)		0.0048	2.2e-16
CS11	ARIMA (1,0,1)		0.7672	0.985

Table 5 (Continued)

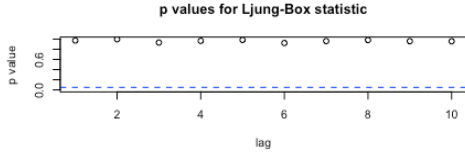
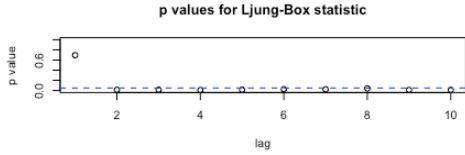
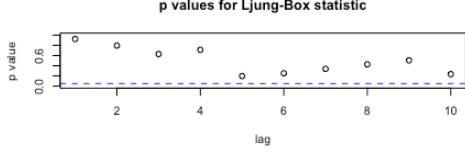
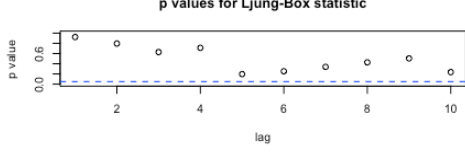
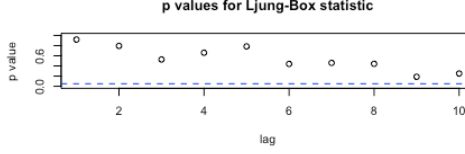
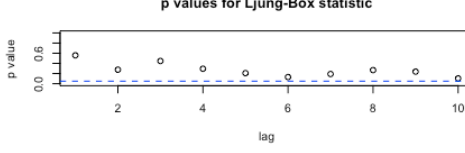
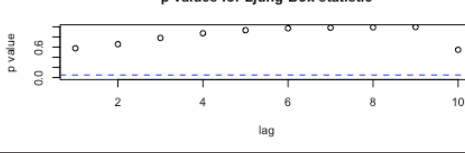
Station	ARIMA Model	p-value for Ljung-Box Statistics		
		Residuals	Squared Residuals	
CS12	ARIMA (2,1,1)		0.9718	0.00294
CS13	ARIMA (1,1,1)		0.0486	0.00587
SS14	ARIMA (1,1,2)		0.1366	1.098e-13
SS15	ARIMA (1,1,2)		0.1366	1.098e-13
SS16	ARIMA (1,1,2)		0.3976	2.2e-16
SS17	ARIMA (1,1,2)		0.1932	2.2e-16
SS18	ARIMA (1,0,1)		0.6180	0.157

Table 5 shows that the p-values of the Ljung-Box test for stations NS2, ES8, ES10, and CS13 show a clear evidence to reject the null hypothesis of no serial autocorrelation. It means that the wind speed daily series in these stations shows the presence of autocorrelation in the residual of the series. Other stations did not show the presence of serial autocorrelation in the residual of the daily wind speed series. On the other hand, the Ljung-Box test for the squared residuals with a p-value less than 0.05 indicates the presence of ARCH effect in the residuals of the series. Based on the results presented in Table 5, three stations were found to be not affected by ARCH effect, which was station NS5, CS11, and SS18. The remaining 15 stations showed that the residuals were a sequence of white noise which also indicated the presence of ARCH effect in the daily wind speed series. Therefore, to conclude on the presence of heteroscedasticity in the series, the LM test was applied towards the residuals of the fitted ARIMA models and the result are presented in Table 6. The null hypothesis for this test is there is no ARCH effect presence in the residual of the models. For a p-value that is lower than 0.05, the null hypothesis is rejected which indicates that the model residuals significantly exhibit an ARCH effect.

Table 6

The LM test for the residuals of the fitted ARIMA (p, d, q) model of daily wind speed series

Station	ARIMA Model	Residuals	Squared Residuals
		p-value	p-value
NS1	ARIMA (2,1,1)	2.2e-16	1.928e-05
NS2	ARIMA (1,0,1)	1.029e-08	0.9162
NS3	ARIMA (1,0,1)	0.0449	0.0471
NS4	ARIMA (1,1,2)	2.2e-16	0.0110
NS5	ARIMA (1,1,2)	0.4922	1
NS6	ARIMA (3,1,1)	2.2e-16	2.2e-16
ES7	ARIMA (1,1,2)	2.2e-16	0.9999
ES8	ARIMA (2,1,1)	2.2e-16	0.2241
ES9	ARIMA (2,0,0)	0.0414	0.9448
ES10	ARIMA (2,1,1)	2.2e-16	0.9847
CS11	ARIMA (1,0,1)	0.9865	1
CS12	ARIMA (2,1,1)	0.0056	0.9338
CS13	ARIMA (1,1,1)	0.0175	0.9995
SS14	ARIMA (1,1,2)	3.228e-06	0.5071
SS15	ARIMA (1,1,2)	2.997e-11	1
SS16	ARIMA (1,1,2)	2.834e-16	0.3848

Table 6 (Continued)

Station	ARIMA Model	Residuals	Squared Residuals
		p-value	p-value
SS17	ARIMA (1,1,2)	2.2e-16	0.0007
SS18	ARIMA (1,0,1)	0.1865	1

The results in Table 6 show that the 3 stations; NS5, CS11, and SS18 were not affected by the heteroscedasticity effect based on the p-values of the residuals of the LM test. This was also supported by the Ljung-Box test in Table 5 for squared residuals. Hence, it can be concluded that the proposed ARIMA model for these 3 stations are suitable for forecasting the daily wind speed series in the respective location. On the other hand, the remaining 15 stations verify that the ARCH effect was established in the wind speed daily series for these stations. Therefore, to cater the issue of the presence of serial autocorrelation and ARCH effect in the residual of fitted ARIMA (p, d, q) model, GARCH modelling is necessary to model the nonlinear part of the daily wind speed series.

ARIMA-GARCH Modelling

The ARIMA model explains the linear part of the data, while the nonlinear characteristics is explained using the GARCH model which is derived based on the residual series of an ARIMA model. In this study, the method used to model the variance behavior was using the standard GARCH (1,1) model.

Table 7

The result for the estimated ARIMA-GARCH model for wind speed data in Malaysia

Station	Model	Parameter Estimates				Ljung-Box Test	LM Test
		μ	ω	α	β	p-value	p-value
NS1	ARIMA (2,1,1) – GARCH (1,1)	0.0053	0.3363	0.0975	0.8176	0.0521	0.0131
NS2	ARIMA (1,0,1) – GARCH (1,1)	8.1178	1.0888	0.1384	0.6731	0.9053	0.9722

Table 7 (Continued)

Station	Model	Parameter Estimates				Ljung-Box Test	LM Test
		μ	ω	α	β	p-value	p-value
NS3	ARIMA (1,0,1) – GARCH (1,1)	8.4873	0.3458	0.0638	0.8489	0.9762	0.9510
NS4	ARIMA (1,1,2) – GARCH (1,1)	0.0003	0.0645	0.0258	0.9615	0.0000	0.1256
NS6	ARIMA (3,1,1) – GARCH (1,1)	0.0018	0.0936	0.0362	0.9376	0.2195	0.0812
ES7	ARIMA (1,1,2) – GARCH (1,1)	-0.0010	0.2578	0.1092	0.8551	0.0077	0.0902
ES8	ARIMA (2,1,1) – GARCH (1,1)	-0.0020	0.1026	0.1191	0.8763	0.0000	0.0007
ES9	ARIMA (2,0,0) – GARCH (1,1)	7.7551	1.7030	0.1552	0.4489	0.6530	0.3274
ES10	ARIMA (2,1,1) – GARCH (1,1)	0.0017	0.0707	0.0543	0.9390	0.7439	0.5164
CS12	ARIMA (2,1,1) – GARCH (1,1)	0.0005	1.6691	0.0647	0.6595	0.4033	0.4569
CS13	ARIMA (1,1,1) – GARCH (1,1)	0.0002	0.0795	0.0169	0.9655	0.6070	0.7862

Table 7 (Continued)

Station	Model	Parameter Estimates				Ljung-Box Test	LM Test
		μ	ω	α	β	p-value	p-value
SS14	ARIMA (1,1,2) – GARCH (1,1)	0.0004	0.0115	0.0124	0.9853	0.0119	0.3177
S S15	ARIMA (1,1,2) – GARCH (1,1)	-0.0011	1.5383	0.1468	0.6303	0.13388	0.22325
S S16	ARIMA (1,1,2) – GARCH (1,1)	0.0000	0.2179	0.0679	0.8831	0.7664	0.4526
S S17	A R I M A (1,1,2) – G A R C H (1,1)	0.0001	0.0103	0.0294	0.9691	0.14448	0.7983

Table 7 gives the result of the ARIMA-GARCH model. The mean behaviour of the daily wind speed series was modelled using ARIMA model, while the standard GARCH (1,1) model captured the conditional variance in the residuals of the series. In this case, the GARCH model was used to cater the existence of the ARCH effect in the residual of daily wind speed series. The diagnostic checking was conducted once again on the ARIMA-GARCH model. The Ljung-Box test was used to check the presence of serial autocorrelation in the standardized squared residuals from the GARCH model. Based on the p-values in Table 7, it can be concluded that the serial autocorrelation no longer existed in the model except for 4 stations which were NS4, ES7, ES8, and SS14. The test was performed on the residuals of the hybrid model using the LM test to investigate the existence of remaining ARCH effect in the residuals of the model. The results in Table 7 prove that there was still ARCH effect in stations NS1 and ES8. For the stations NS2, NS3, NS6, ES9, ES10, CS12, CS13, SS15, SS16, and SS17, there was enough evidence to conclude that the daily wind speed series were free from the conditional heteroscedasticity. This shows that the ARIMA-GARCH model has precisely captured the dynamics in the wind speed daily series. However, further investigation should be done to treat the presence of serial autocorrelation in time series data collected from the stations NS4, ES7, ES8, and SS14, and the presence of ARCH effect in time series data collected from the stations NS1 and

ES8 using other type of GARCH family models since it has proven to be very successful in describing the volatility dynamics in a short period of time (Jamaludin et al., 2016).

Forecasting Capabilities using ARIMA Model and ARIMA-GARCH Model

The performance of the proposed model was tested based on the capability of forecasting future daily wind speed series. The model was built using the in-sample data and then was projected for 365 days ahead. This forecasted series that is estimated based on the best fitted model was compared with the last 365 of out-sample data and the accuracy of the forecasting model was evaluated from the RMSE and MAPE values where the lowest value indicates a better performance. The results of RMSE and MAPE between the in-sample and out-sample data are given in Table 8. Forecasting interpretation based on Table 1 is also included in the Table 8.

Table 8
The result of forecast accuracy using RMSE and MAPE and forecasting interpretation

Station	Model	In-Sample		Out-Sample		Forecasting Interpretation
		RMSE	MAPE	RMSE	MAPE	
NS2	ARIMA (1,0,1) - GARCH (1,1)	2.4554	23.7161	2.3163	23.7408	Reasonable
NS3	ARIMA (1,0,1) - GARCH (1,1)	1.9921	16.907	2.1799	16.3708	Good
NS5	ARIMA (1,1,2)	1.4156	13.7443	1.4401	15.4814	Good
NS6	ARIMA (3,1,1) - GARCH (1,1)	1.4584	13.7489	1.3166	15.2564	Good
ES9	ARIMA (2,0,0) - GARCH (1,1)	2.1346	19.8658	2.3821	20.3147	Reasonable
ES10	ARIMA (2,1,1) - GARCH (1,1)	1.8198	14.9371	1.6481	14.0077	Good

Table 8 (Continued)

Station	Model	In-Sample		Out-Sample		Forecasting Interpretation
		RMSE	MAPE	RMSE	MAPE	
CS11	ARIMA (1,0,1)	2.1572	18.8206	1.7758	17.3518	Good
CS12	ARIMA (2,1,1) - GARCH (1,1)	1.9336	17.2430	1.8117	15.9246	Good
CS13	ARIMA (1,1,1) - GARCH (1,1)	1.5761	14.8005	1.8743	14.3288	Good
SS15	ARIMA (1,1,2) - GARCH (1,1)	1.9593	15.0709	1.7438	13.7584	Good
SS16	ARIMA (1,1,2) - GARCH (1,1)	1.5367	14.8042	1.3239	13.3581	Good
SS17	ARIMA (1,1,2) - GARCH (1,1)	1.6702	16.0472	1.2368	13.4531	Good
SS18	ARIMA (1,0,1)	2.0314	19.685	1.9686	17.7601	Good

Table 8 shows that the proposed model could forecast the daily wind speed series where the values of RMSE and MAPE of the out-sample data followed closely the in-sample data for ARIMA model and ARIMA-GARCH model. The values of MAPE for the proposed model shows that 11 out of 13 station (85%) gave good forecasts while the other 2 stations (15%) forecasted reasonably well as mentioned in Lewis (1982). Figure 7 shows the distribution of the best fitted model for 13 locations of wind stations in Peninsular Malaysia.

Table 9 shows that the ARIMA and ARIMA-GARCH model could modelled most of the stations in the northern, east coast, central and southern regions. There were 3 stations (16.68%) in the northern, central, and southern regions that could be modelled using ARIMA modelling. For ARIMA-GARCH modelling, 10 stations (55.56%) out of 18 were able to be modelled using the hybrid model. This shows that 13 stations (72.24%) out of 18 wind stations in Peninsular Malaysia were successfully modelled using a time

series modelling. These results have proven the ability of the proposed models for wind speed forecasting and may be used to predict the future pattern of daily wind speed series in Peninsular Malaysia. The results of wind speed prediction can be used to provide a quantitative measure of wind energy available in the potential location for renewable energy conversion (Barbosa de Alencar et al., 2017). Further studies are required for the remaining 5 stations (27.78%) that give a non-conclusive result due to failure in modelling the volatility of the daily wind speed using both ARIMA and ARIMA-GARCH.

To check the forecasting performance of ARIMA-GARCH modelling, the 3 stations that had an adequate model of ARIMA was tested once again using ARIMA-GARCH. The forecasting accuracy measure as mentioned in Lewis (1982) for the out-sample for each station are illustrated in Table 10.

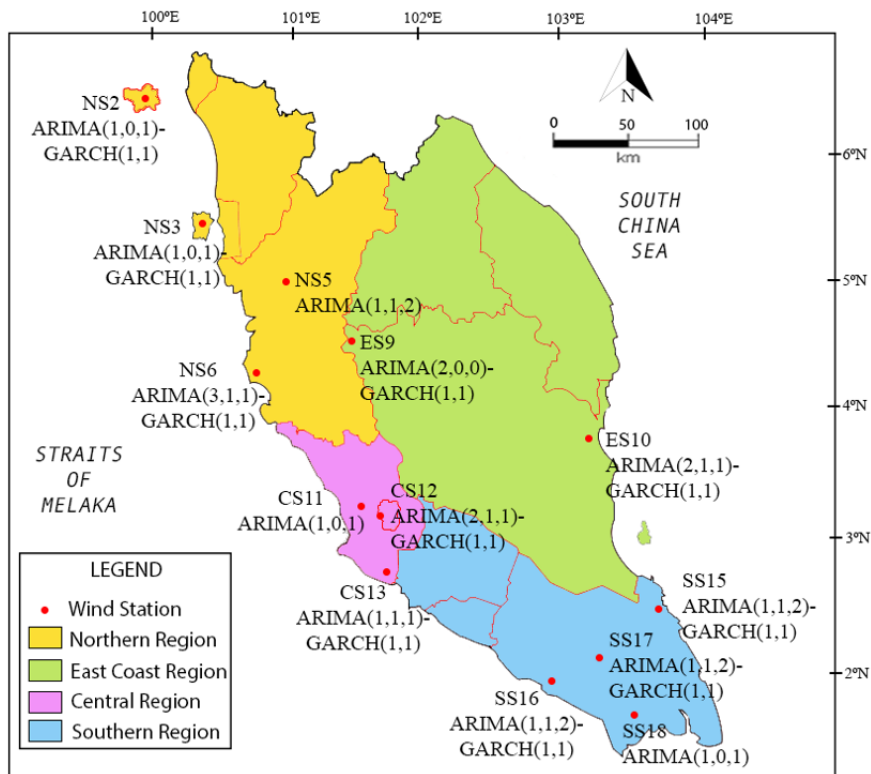


Figure 7. Results of ARIMA and ARIMA-GARCH models

Table 9

Percentage of proposed model based on region of wind stations

Region	Total Station	ARIMA		ARIMA-GARCH		Non- Conclusive	
		Station	Percent	Station	Percent	Station	Percent
North	6	1	5.56%	3	16.67%	2	11.11%
East Coast	4	0	0%	2	11.11%	2	11.11%
Central	3	1	5.56%	2	11.11%	0	0%
South	5	1	5.56%	3	16.67%	1	5.56%
Total	18	3	16.68%	10	55.56%	5	27.78%

Table 10

The result of forecasting performance of ARIMA-GARCH modelling

Location	Station	ARIMA		ARIMA-GARCH		Forecasting Interpretation
		RMSE	MAPE	RMSE	MAPE	
Lubok Merbau	NS5	1.4401	15.4814	1.4529	15.6325	Good
Subang	CS11	1.7758	17.3518	1.7697	16.6947	Good
Senai	SS18	1.9686	17.7601	2.0671	17.6552	Good

Based on these results, it shows that even though the ARIMA model has proven to be adequate in modelling these 3 stations, the ARIMA-GARCH modelling also gives a good forecasting accuracy based on the forecasting interpretation by Lewis (1982). These models can be used in forecasting the daily wind speed in the wind station with a good forecasting result.

CONCLUSION AND FUTURE WORK

This study led to the construction of a time series model of daily wind speed series of 18 meteorological stations in Peninsular Malaysia. The Box-Jenkins ARIMA modelling was

used to build a model of wind speed series for each station. In measuring the adequacy of the proposed ARIMA model, 3 stations: NS5, CS11, and SS18, were proven to be suitable for forecasting the wind speed series using the ARIMA model while the 15 other stations are affected by the presence of serial autocorrelation as well as ARCH effects. To overcome the issue, we used the ARIMA-GARCH model for 15 stations. The results show that 10 stations were successfully modelled using the ARIMA-GARCH model while 5 stations required other methods of modelling. Future work is needed to improve the limitation of the ARIMA-GARCH model for the remaining 5 stations. As for the 13 stations that had successfully been modelled using the time series, future work can be done by calculating the wind power density of each stations in Peninsular Malaysia in order to provide a quantitative measure of wind energy available in the potential location for renewable energy conversion.

ACKNOWLEDGEMENT

The authors would like to acknowledge Universiti Teknikal Malaysia Melaka, Universiti Teknologi Malaysia, and those who gave support in carrying out this research under the grant vote number Q.J130000.2654.17J30.

REFERENCES

- Ajayi, O. O., Ohijeagbon, O. D., Nwadialo, C. E., & Olasope, O. (2014). New model to estimate daily global solar radiation over Nigeria. *Sustainable Energy Technologies and Assessments*, 5, 28-36. doi: <https://doi.org/10.1016/j.seta.2013.11.001>
- Akcan, S. (2017). Wind speed forecasting using time series analysis methods. *Çukurova University Journal of the Faculty of Engineering and Architecture*, 32(2), 161-172.
- Barbosa de Alencar, D., de Mattos Affonso, C., Limão de Oliveira, R. C., Moya Rodriguez, J. L., Leite, J. C., & Reston Filho, J. C. (2017). *Different models for forecasting wind power generation: Case study. Energies*, 10(12), 1-27. doi: <https://doi.org/10.3390/en10121976>
- Bollerslev, T. (1986). Generalized autoregressive conditional heteroskedasticity. *Journal of Econometrics*, 31(3), 307-327.
- Chang, G. W., Lu, H. J., Hsu, L. Y., & Chen, Y. Y. (2016, July 17-21). A hybrid model for forecasting wind speed and wind power generation. In *2016 IEEE Power and Energy Society General Meeting (PESGM)* (pp. 1-5). Boston, MA, USA. doi: 10.1109/PESGM.2016.7742039
- De Freitas, N. C., Silva, M. P. D. S., & Sakamoto, M. S. (2018). Wind Speed Forecasting: A Review. *International Journal of Engineering Research and Application*, 8(1), 4-9. doi: 10.9790/9622-0801010409
- Engle, R. (2001). GARCH 101: The use of ARCH/GARCH models in applied econometrics. *Journal of Economic Perspectives*, 15(4), 157-168. doi: 10.1257/jep.15.4.157

- Engle, R. F. (1982). Autoregressive conditional heteroscedasticity with estimates of the variance of United Kingdom inflation. *Econometrica: Journal of the Econometric Society*, 50(4), 987-1007. doi: <https://doi.org/10.2307/1912773>
- Erdem, E., Shi, J., & She, Y. (2014). Comparison of Two ARMA-GARCH Approaches for Forecasting the Mean and Volatility of Wind Speed. In *International Congress on Energy Efficiency and Energy Related Materials (ENEFM2013)* (pp. 65-73). Cham, Switzerland: Springer. doi: https://doi.org/10.1007/978-3-319-05521-3_9
- Grigonytė, E., & Butkevičiūtė, E. (2016). Short-term wind speed forecasting using ARIMA model. *Energetika*, 62(1-2), 45-55. doi: <https://doi.org/10.6001/energetika.v62i1-2.3313>
- Jamaludin, A. R., Yusof, F., Kane, I. L., & Norrulasikin, S. M. (2016, June). A comparative study between conventional ARMA and Fourier ARMA in modeling and forecasting wind speed data. In *AIP Conference Proceedings* (Vol. 1750, No. 1, p. 060022). New York, USA: AIP Publishing LLC. doi: <https://doi.org/10.1063/1.4954627>
- Kim, E., Ha, J., Jeon, Y., & Lee, S. (2004). Ljung-Box test in unit root AR-ARCH model. *Communications for Statistical Applications and Methods*, 11(2), 323-327.
- Kwiatkowski, D., Phillips, P. C., Schmidt, P., & Shin, Y. (1992). Testing the null hypothesis of stationarity against the alternative of a unit root. *Journal of Econometrics*, 54(1-3), 159-178.
- Lewis, C. D. (1982). *Industrial and business forecasting methods: A practical guide to exponential smoothing and curve fitting*. Penang, Malaysia: Heinemann Publisher.
- Lojowska, A., Kurowicka, D., Papaefthymiou, G., & van der Sluis, L. (2010, June 14-17). Advantages of ARMA-GARCH wind speed time series modeling. In *2010 IEEE 11th International Conference on Probabilistic Methods Applied to Power Systems* (pp. 83-88). Singapore. doi: 10.1109/PMAPS.2010.5528979
- Lujano-Rojas, J. M., Bernal-Agustín, J. L., Dufo-López, R., & Domínguez-Navarro, J. A. (2011). Forecast of hourly average wind speed using ARMA model with discrete probability transformation. In M. Zhu (Ed.), *Electrical Engineering and Control* (pp. 1003-1010). Heidelberg, Germany: Springer. doi: https://doi.org/10.1007/978-3-642-21765-4_125
- Masseran, N. (2016). Modeling the fluctuations of wind speed data by considering their mean and volatility effects. *Renewable and Sustainable Energy Reviews*, 54, 777-784. doi: <https://doi.org/10.1016/j.rser.2015.10.071>
- Miswan, N. H., Said, R. M., Hussin, N. H., Hamzah, K., & Ahmad, E. Z. (2015). Comparative performance of ARIMA and DES models in forecasting electricity load demand in Malaysia. *International Journal of Electrical and Computer Sciences IJECS-IJENS*, 16(1), 6-9.
- Moreno, J. J. M., Pol, A. P., Abad, A. S., & Blasco, B. C. (2013). Using the R-MAPE index as a resistant measure of forecast accuracy. *Psicothema*, 25(4), 500-506.
- Norrulashikin, S. M., Yusof, F., & Kane, I. L. (2018). Meteorological multivariable approximation and prediction with classical VAR-DCC approach. *Sains Malaysiana*, 47(2), 409-417.
- Petinrin, J. O., & Shaaban, M. (2015). Renewable energy for continuous energy sustainability in Malaysia. *Renewable and Sustainable Energy Reviews*, 50, 967-981. doi: <https://doi.org/10.1016/j.rser.2015.04.146>

- Radziukynas, V., & Klementavicius, A. (2014, October 14). Short-term wind speed forecasting with ARIMA model. In *2014 55th International Scientific Conference on Power and Electrical Engineering of Riga Technical University (RTU CON)* (pp. 145-149). Riga, Latvia. doi: 10.1109/RTU CON.2014.6998223
- Sharma, R., & Singh, D. (2018). A review of wind power and wind speed forecasting. *Journal of Engineering Research and Application*, 8(7), 1-9. doi: 10.9790/9622-0807030109
- Sharma, S. K., & Ghosh, S. (2016). Short-term wind speed forecasting: Application of linear and non-linear time series models. *International Journal of Green Energy*, 13(14), 1490-1500. doi: <https://doi.org/10.1080/15435075.2016.1212200>
- Sjölander, P. (2011). A stationary unbiased finite sample ARCH-LM test procedure. *Applied Economics*, 43(8), 1019-1033. doi: <https://doi.org/10.1080/00036840802600046>
- Wang, J., Hu, J., Ma, K., & Zhang, Y. (2015). A self-adaptive hybrid approach for wind speed forecasting. *Renewable Energy*, 78, 374-385. doi: <https://doi.org/10.1016/j.renene.2014.12.074>
- Wang, W., Van Gelder, P. H. A. J. M., Vrijling, J. K., & Ma, J. (2005). Testing and modelling autoregressive conditional heteroskedasticity of streamflow processes. *Nonlinear Processes in Geophysics*, 12(1), 55-66.
- Yan, J., Guoqing, H., Xinyan, P., & Yongle, L. (2016). Method of short-term wind speed forecasting based on generalized autoregressive conditional heteroscedasticity model. *Journal of Southwest Jiaotong University*, 51(4), 663-669.
- Yaziz, S. R., Azizan, N. A., Zakaria, R., & Ahmad, M. H. (2013, December 1-6). The performance of hybrid ARIMA-GARCH modeling in forecasting gold price. In *20th International Congress on Modelling and Simulation* (pp. 1201-1207). Adelaide, Australia.
- Yürekli, K., Kurunç, A., & Öztürk, F. (2005). Testing the residuals of an ARIMA model on the Cekerek Stream Watershed in Turkey. *Turkish Journal of Engineering and Environmental Sciences*, 29(2), 61-74.
- Yusof, F., Kane, I. L., & Yusop, Z. (2013). Hybrid of ARIMA-GARCH modeling in rainfall time series. *Jurnal Teknologi*, 63(2), 27-34.

Harmonic Current Distortion Using the Linear Quadratic Regulator for a Grid-Connected Photovoltaic System

Oscar Andrew Zongo^{1*} and Anant Oonsivilai²

¹Walailak University International College, Walailak University, 222 Thaiburi, Tha sala, Nakhon Si Thammarat, Thailand

²School of Electrical Engineering, Suranaree University of Technology, 111 University Avenue, Muang, Nakhon Ratchasima, Thailand

ABSTRACT

This paper presents a comparison between a proportional-integral controller, low pass filters, and the linear quadratic regulator in dealing with the task of eliminating harmonic currents in the grid-connected photovoltaic system. A brief review of the existing methods applied to mitigate harmonic currents is presented. The Perturb & Observe technique was employed for maximum power point tracking. The PI control, low pass filters, and the linear quadratic regulator are discussed in detail in terms of their control strategies. The grid current was analyzed in the system with all three of the controllers applied to control the voltage source inverter of the solar photovoltaic system connected to the grid through an L filter and LCL filter and simulated in MATLAB/SIMULINK. The simulation

results obtained have proven the robustness of the linear quadratic regulator over other methods. The technique lowers the grid current total harmonic distortion from 7.85% to 2.13%.

ARTICLE INFO

Article history:

Received: 17 August 2020

Accepted: 13 October 2020

Published: 22 January 2021

DOI: <https://doi.org/10.47836/pjst.29.1.03>

E-mail addresses:

oscar.zongo1981@gmail.com (Oscar Andrew Zongo)

anant.oo141@gmail.com (Anant Oonsivilai)

*Corresponding author

Keywords: Harmonic current distortion, linear quadratic regulator, nonlinear load, photovoltaic system

INTRODUCTION

Solar photovoltaic (PV) systems convert solar radiation into electrical power (Arora & Arora, 2018). They can be used to supply power to customers as standalone units or connected to the grid. One of the sources of harmonic currents in a PV system is the presence of nonlinear loads (Khomsni et al., 2018). Harmonic currents affect the control of interfaced inverters. The interfaced inverters used in PV systems behave like current sources when they are connected to the main grid (Singh et al., 2018). The voltage source inverter (VSI) is responsible for controlling the power injected into the grid. Therefore, appropriate control strategies are needed for VSI to eliminate the effects of current harmonics which degrade the quality of the output power.

Azzam-Jai and Ouassaid (2018) had shown the effectiveness of active power filters (APF) in dealing with harmonic currents caused by nonlinear loads and power electronic converters. Although the hybrid compensation (HC) method using passive and active filters developed by Naderipoura et al. (2015) solved the power quality problems, it was expensive.

Mohamed et al. (2017) proposed various methods to compensate for current harmonics in the grid-connected PV systems by applying a three-phase voltage-fed shunt active power filter. The conventional p-q theory for the harmonic current distortion presented by Krama et al. (2016) is capable of reducing the total harmonic distortion (THD) of the source current from 23.15% to 3.03% and compensating for the reactive power of the system. Jannesar et al. (2018) proposed a control strategy based on the optimal passive harmonic filter (PHF) to deal with the problem of lower active power and higher voltage total harmonic distortion THDV which led to an increased percentage of harmonic current in the LV distribution system located in Yazd province, Iran. Kumar (2015) used an LCL third-order filter to reduce the THD in the load current to within 1.74% and that of voltage to 0.05%. Active power filters were employed to damp harmonic currents by Colque et al. (2018). Belaidi et al. (2016) used grid current drawn by the nonlinear load to calculate the compensator reference current applying the controller based on the p-q theory. The application of VSI as an active power filter for harmonic current distortion can be found in the work of Bag et al. (2016).

To overcome power quality problems in the distribution system caused by harmonic distortion, Peterson et al. (2017) applied the phasor aggregation technique in a high voltage network of 132 kV. Jain and Singh (2019) used a decoupled network of harmonics to filter out the harmonics from load current, thereby compensating for the reactive power consumed by nonlinear loads. An extended Kalman filter (EKF) state estimator was used to estimate the fundamental load currents in the control strategy developed by Srinivas et al. (2019). Chtouki et al. (2016) compared three passive filters L, LC, and LCL with an LCL filter with series and parallel resistors in the harmonic distortion of the system. A technique known as frequency-domain block least-mean square (FBLMS) was presented

by Kandpal et al. (2017). This method corrects the power factor, regulates the voltage, and drops the harmonic distortion of grid currents to below 5% when applied to the IEEE-519 standard system. A method based on an n-stage second-order generalized integrator phase-locked loop (SOGI-PL) was presented by Pereira et al. (2019). The technique was fast in the selection of the highest harmonic components. Additionally, in the study, copper and magnetic losses caused by the LCL filter were taken into account.

In this present study, a comparison is made of minimizing the effects of harmonic currents using a proportional-integral (PI) controller, low pass filter (LPF), and the linear quadratic regulator (LQR). The focus of this paper is the reduction of grid current THD.

The contribution of this research is the application of the LCL filter and the linear quadratic regulator in the minimization of THD and the control of VSI.

METHODOLOGY

In this work, PI control, LPF, and the LQR are discussed and used to design control schemes to control the grid current. The PV system used for testing, PI control, and LPF control schemes is shown in Figure 1 and includes the PV source, DC/DC boost converter, DC/AC converter, and *L* filter.

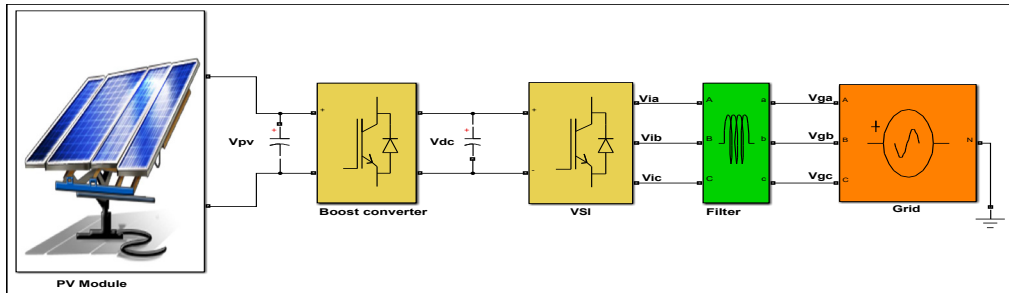


Figure 1. PV system is connected to the grid through VSI

PI Control Scheme

This control methodology is the conventional control strategy that has been used for decades to control several systems. The function of the PI controller (Upaphai et al., 2019) is to make the measured output track the reference input of the controlled system by minimizing the errors between them.

From Figure 1, the grid-side voltage Equation 1 can be written as Fekkak et al. (2018):

$$\begin{bmatrix} v_{ia} \\ v_{ib} \\ v_{ic} \end{bmatrix} = \begin{bmatrix} v_{ga} \\ v_{gb} \\ v_{gc} \end{bmatrix} - L \frac{d}{dt} \begin{bmatrix} i_{ga} \\ i_{gb} \\ i_{gc} \end{bmatrix} \tag{1}$$

Where v_{ia}, v_{ib}, v_{ic} are inverter voltages, v_{ga}, v_{gb}, v_{gc} are grid voltages, i_{ga}, i_{gb}, i_{gc} are grid currents, and L is the filter inductance. The dq transformation of Equations 2 and 3 is,

$$v_{id} = v_{gd} - L \frac{di_{gd}}{dt} + \omega_s L i_{gq} \tag{2}$$

$$v_{iq} = v_{gq} - L \frac{di_{gq}}{dt} + \omega_s L i_{gd} \tag{3}$$

Where:

v_{id} = direct axis inverter voltage.

v_{iq} = quadrature axis inverter voltage.

The abc reference voltages to control the VSI are calculated as shown in Figure 2 (Colque et al., 2018).

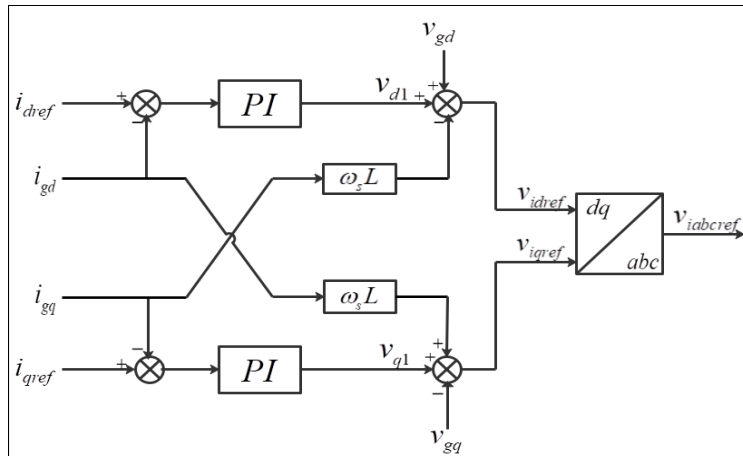


Figure 2. Cross-coupling control of current loops

In Figure 2, the output voltages of the PI-Controllers are (Equations 4 and 5):

$$v_{d1} = k_p \left(1 + \frac{k_i}{s} \right) (i_{dref} - i_d) \tag{4}$$

$$v_{q1} = k_p \left(1 + \frac{k_i}{s} \right) (i_{qref} - i_q) \tag{5}$$

Therefore, the dq components of the voltage references can be deduced as Equations 6 and 7:

$$v_{dref} = v_{dg} + v_{d1} - \omega_s L i_{iq} \tag{6}$$

LPF Control Scheme

In this control mechanism, two LPFs were used to filter the load currents separately and then the filtered currents were subtracted from the original components of the load currents to obtain the harmonic components as shown in Figure 4 (Colque et al., 2018).

Harmonic Current Extraction

The three-phase load currents (i_{la}, i_{lb}, i_{lc}) were converted into their dq components (i_{ld}, i_{lq}) and then the two LPFs were used to filter the currents separately. The filtered currents were subtracted from the original three-phase load currents to obtain the harmonic components as shown in Figure 4 (Colque et al., 2018).

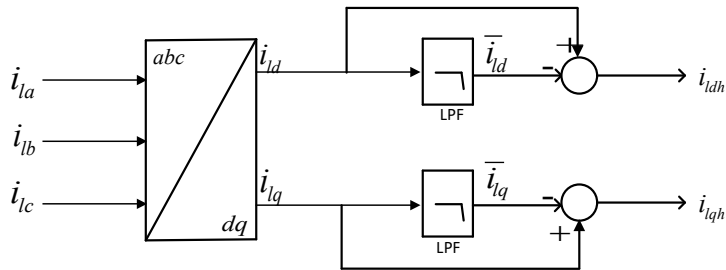


Figure 4. Extraction of harmonic currents

The outputs in Figure 4 are added to the reference currents in Equation 12 to obtain Equations 13 and 14,

$$i_{drefl} = i_{dref} + i_{ldh} \tag{13}$$

$$i_{qrefl} = i_{qref} + i_{lqh} \tag{14}$$

These become the new reference currents. The developed control strategy is shown in Figure 5.

LQR Control Scheme

The LCL filter added to the PV system is shown in Figure 6 (Pereira et al., 2019). The filter damps the harmonic currents caused by nonlinear loads and the electronic components in VSI. Proper modeling of the filter is crucial in the design of a suitable controller for the VSI so that it contributes to the mitigation of the THD in the system.

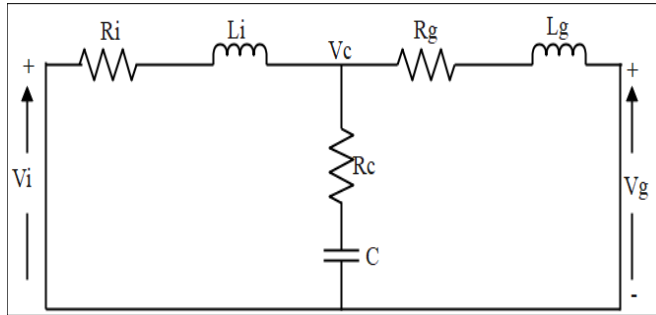


Figure 7. LCL filter equivalent circuit

The per-phase circuit dynamics of Figure 7 can be represented in the stationary reference frame by Equations 15-18

$$L_i \frac{di_i}{dt} = v_i - v_c - R_i i_i \tag{15}$$

$$L_g \frac{di_g}{dt} = v_c - v_g - R_g i_g \tag{16}$$

$$v_c = \frac{1}{C} \int i_c \cdot dt + i_c R_C \tag{17}$$

$$i_i = i_c + i_g \tag{18}$$

Taking the Laplace transform of Equations 15-18 results in Equation 19,

$$i_g(s) = \frac{sR_C C + 1}{a_0 s^3 + a_1 s^2 + a_2 s + a_3} v_i(s) - \frac{Cs^2 + CR_i s + 1}{a_0 s^3 + a_1 s^2 + a_2 s + a_3} v_g(s) \tag{19}$$

The LCL filter transfer function is then defined by Equation 20:

$$G(s) = \frac{i_g(s)}{v_i(s)} = \frac{sR_C C + 1}{a_0 s^3 + a_1 s^2 + a_2 s + a_3} \tag{20}$$

Where:

$$\begin{aligned} a_0 &= L_i L_g C \\ a_1 &= C(L_g(R_C + R_i) + L_i(R_C + R_g)) \\ a_2 &= L_g + L_i + C(R_C R_i + R_C R_g + R_i R_g) \\ a_3 &= R_i + R_g \end{aligned}$$

Where:

i_g = grid-side current,

The LQR can be represented by the block diagram shown in Figure 8. In this controller, r is the reference input, e is the state error, K is the controller gain vector, u is the plant input, P is the controlled plant, x is the state vector, and y is the measured output. In this study, the reference input is the reference grid current i_{gref} ; the state error e is the difference between the reference and the measured grid current i_g ; the controller K is the LQR; and the plant input u is the inverter voltag V_i .

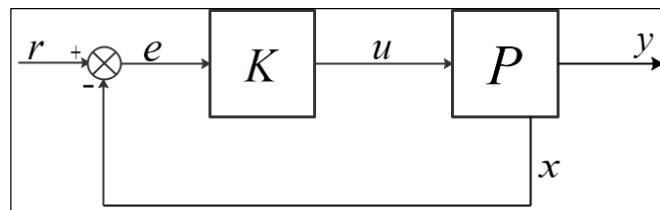


Figure 8. LQR control system

The problem is to find the vector $K(t)$ of the control law (Equation 21) (Xie et al., 2020, Arab et al., 2020 & Oonsivilai et al., 2019),

$$u(t) = -K(t)x(t) \tag{21}$$

that minimizes the value of a quadratic performance index J of the form (Equation 22),

$$J = \int_{t=0}^{t=f} (x'Qx + u'Ru)dt \tag{22}$$

The controller is obtained by solving the Algebraic Riccati Equation (ARE) (Equation 23),

$$\dot{p}(t) = -p(t)A - A'p(t) - Q + p(t)BR^{-1}B'p(t) \tag{23}$$

The closed-loop dynamics under state feedback law with $u(t) = -K(t)x(t)$ is given by Equation 24,

$$\dot{x}(t) = (A - BK)x = A_{CL}x \tag{24}$$

RESULTS, VERIFICATION, AND DISCUSSION

The simulation was performed in MATLAB/Simulink for a grid-connected PV system with the parameters shown in Table 1.

Table 1

Parameters of the PV system

Parameter	Value
The line to line voltage V_{L-L}	380 V
DC bus voltage V_{dc}	650 V
Grid frequency f	50 Hz
Inverter-side resistance R_i	0.5 Ω
Inverter-side inductance L_i	1.7 mH
Grid-side resistance R_g	0.5 Ω
Grid-side inductance L_g	0.1 mH
Filter capacitance R_C	5 μF
Capacitor resistance C	20 Ω

The LCL filter transfer function in Equation 20 was converted into state space. MATLAB function *lqr* was used to search for the controller K gains used to control the plant. The gains were $K = [41.4389 \quad 133.2036 \quad 255.0779]$.

The step response and linear analysis results of the system with and without LQR are shown in Figure 9 and Table 2 respectively. The step response shows that the system with LQR control is faster, settles to steady-state earlier, and permits lower steady-state error than when the system is without it. The results in Table 2 show that the system with LQR is four times faster than without it, and the difference in steady-state error with and without LQR is significantly big enough to prove the effectiveness of the proposed controller.

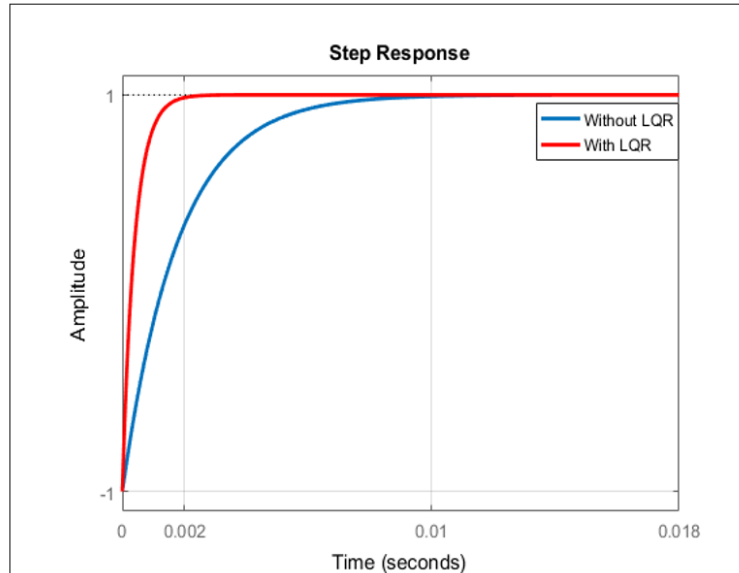


Figure 9. Step response of the system with and without LQR

Table 2

Linear analysis results

Performance	Without LQR	With LQR
Rise time	0.00395	0.000886
Settling time	0.00704	0.00159
Steady state error	1	0.212

RESULTS

The systems which are shown in Figure 3, Figure 5, and Figure 8 were run. The THD recorded with PI control was 7.85% in Figure 10. After the addition of the LPFs in the control strategy, the THD was reduced to 4.27% as shown in Figure 11. Optimal control based on LQR managed to decrease the THD to 2.13% (Figure 12). The results above were verified by the behavior of the grid current shown in Figures 13 to 15.

DISCUSSION

The results presented in Figures 10 to 15 show the robustness of the LQR control strategy compared to the other controllers. With the PI controller, the grid current has serious damaging oscillations.

The application of a filter has shown positive effects in previous studies (i.e., Mohamed et al., 2017; Belaidi et al., 2016; Ouchen et al., 2016) as it also did in this present research

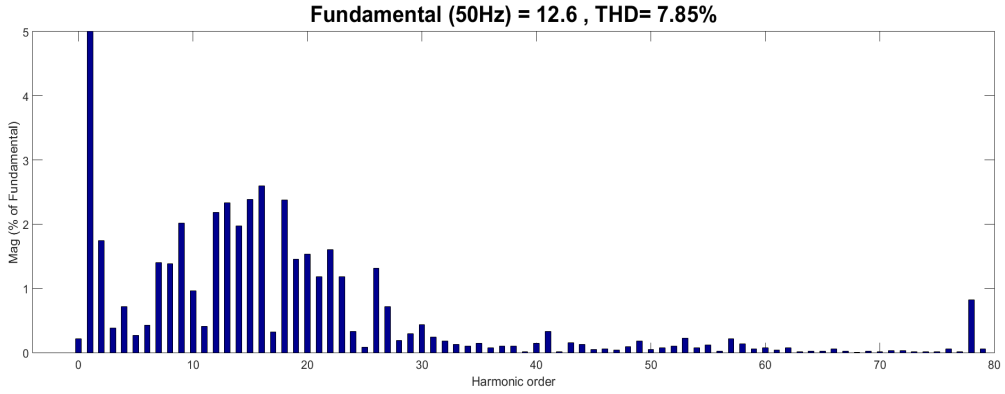


Figure 10. FFT analysis for THD of grid current with the PI control scheme

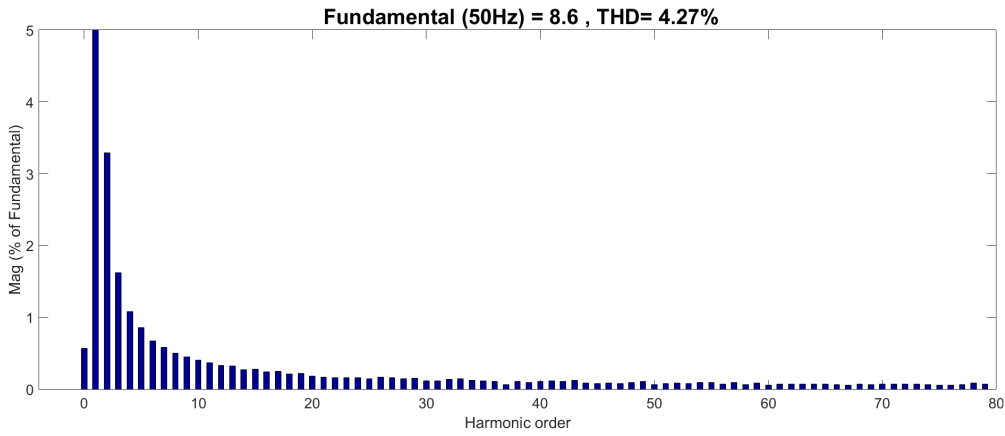


Figure 11. FFT analysis for THD of grid current with the LPF control scheme

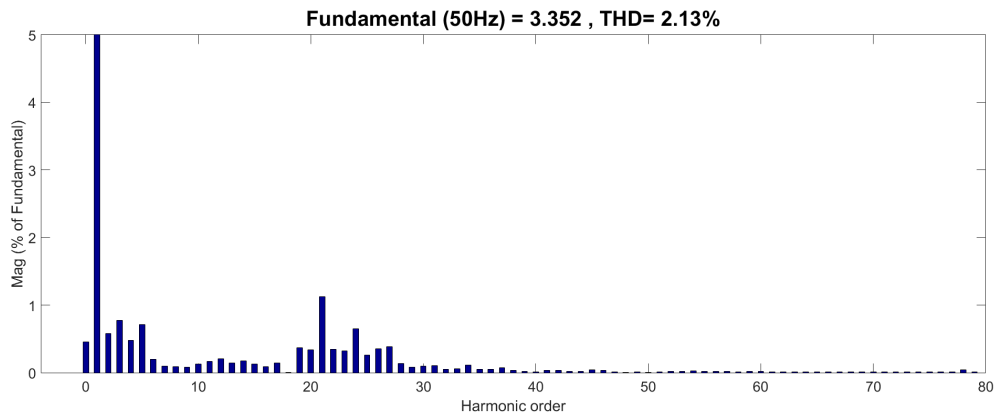


Figure 12. FFT analysis for THD of grid current with the LQR control scheme

Harmonic Current Distortion

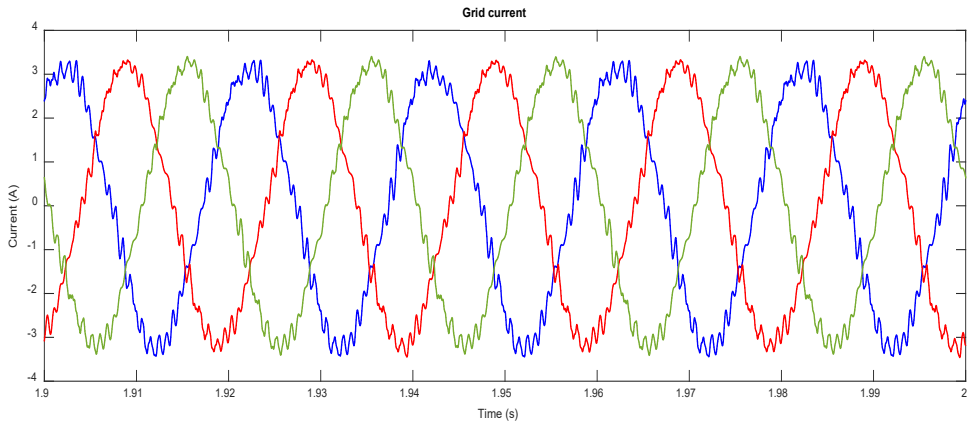


Figure 13. Highly-distorted grid current with a PI controller

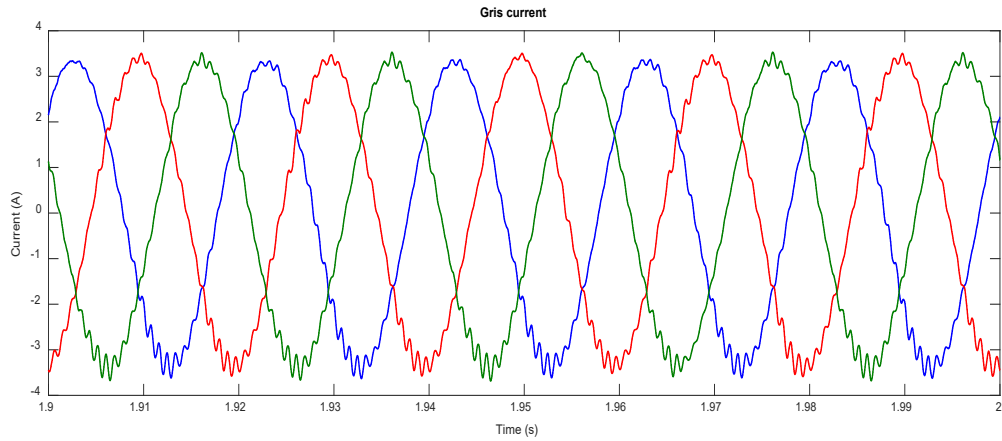


Figure 14. Grid current with the LPF control scheme

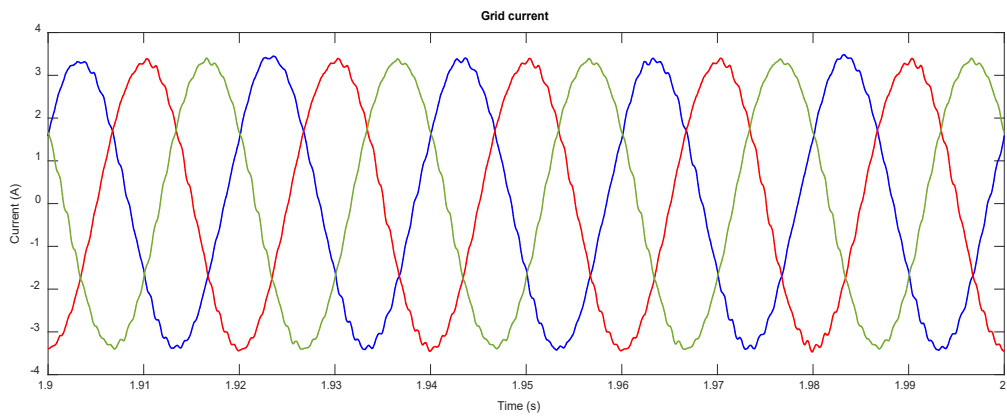


Figure 15. Grid current with the LQR control scheme

even though the control strategies are different. In this research, an LCL filter was used while in the studies of Mohamed et al. (2017), Belaidi et al. (2016) and Ouchen et al. (2016), shunt active power filters were applied. In all cases, THD was highly reduced and there was a significant improvement in the current after the application of the proposed controllers. When LPF and LCL filters were applied, there was a reduction in THD similar to the results obtained by Yousef et al. (2018), in which a shunt active power filter (APF) was applied to eliminate the harmonic currents caused by the nonlinear load. Additionally, there was a significant reduction in harmonic content in the grid current after the application of the LPF scheme (4.27%) and the LQR control (2.13%), meeting the 5% requirement as per the IEEE-519 standard. This experiment had applied LPF and LCL filters with LQR as in the previous study of Pereira et al. (2019), who also employed LCL filters for THD. In both studies, there have been significant distortion of the harmonic currents by the LCL filter. This study had applied L, LPF, and LCL filters in its control schemes, while the study of Chtouki et al. (2016) employed L, LC, and LCL for two comparative studies with and without passive damping. In both types of research, there have been optimum results in terms of harmonic reduction. The use of the L-C-L third-order filter reduced the THD to 1.74%, slightly lower than the results obtained in this work which managed to reduce THD to 2.13% by applying an LCL filter and LQR control for the VSI.

CONCLUSION

The paper has presented a control strategy for VSI that takes care of the presence of harmonics caused by nonlinear loads in the photovoltaic system integrated with the power system. In this paper, the DC/DC converter was controlled by P & O MPPT that concentrated on maximizing the available solar power and maintained an acceptable efficiency around the full load condition. The results obtained from tests with PI, LPF, and an LCL filter with LQR proved the robustness of the proposed controller. The LCL filter and the control scheme based on LQR assisted in removing harmonics from the grid current due to the non-linear load and the VSI. Through the simulation exercise, the total harmonic distortion found in the grid current fell from 7.85% to 2.13% when the optimal controller was applied.

ACKNOWLEDGMENTS

This work is sponsored by Walailak University International College, Walailak University, Nakhon si Thammarat, Thailand.

REFERENCES

- Arab, N., Vahedi, H., & Al-Haddad, K. (2020). LQR control of single-phase grid-tied PUC5 inverter with LCL filter. *IEEE Transactions on Industrial Electronics*, 67(1), 297-307. doi: 10.1109/TIE.2019.2897544
- Arora, R., & Arora, R. (2018). Experimental investigations and exergetic assessment of 1 kW solar PV plant. *Pertanika Journal of Science and Technology*, 26(4), 1881-1897.
- Azzam-Jai, A., & Ouassaid, M. (2018, November 21-23). A multifunctional PV-based shunt active power filter using neural network controller. In *Proceedings of International Symposium on Advanced Electrical and Communication Technologies (ISAECT)* (pp. 1-6). Rabat, Morocco. doi: 10.1109/ISAECT.2018.8618848
- Bag, A., Subudhi, B., & Ray, P. K. (2016, January 28-30). Grid integration of PV system with active power filtering. In *Proceedings of 2016 2nd International Conference on Control, Instrumentation, Energy & Communication (CIEC)* (pp. 372-376). Kolkata, India. doi: 10.1109/CIEC.2016.7513810
- Belaidi, R., Haddouche, A., Fathi, M., Larafi, M. M., & Kaci, G. M. (2016, November 14-17). Performance of grid-connected PV system based on SAPF for power quality improvement. In *Proceedings of 2016 International Renewable and Sustainable Energy Conference (IRSEC)* (pp. 542-545). Marrakech, Morocco. doi: 10.1109/IRSEC.2016.7984050
- Chtouki, I., Zazi, M., Feddi, M., & Rayyam, M. (2016, November 14-17). LCL filter with passive damping for PV system connected to the network. In *Proceedings of 2016 International Renewable and Sustainable Energy Conference (IRSEC)* (pp. 692-697). Marrakech, Morocco. doi: 10.1109/IRSEC.2016.7984020
- Colque, J. C., Ruppert, E., & Azcue, J. L. (2018, November 12-14). Performance analysis of a three-phase photovoltaic generation system with active filtering functions connected to the electrical grid. In *Proceedings of 13th IEEE International Conference on Industry Applications (INDUSCON)* (pp. 249-255). São Paulo, Brazil, Brazil. doi: 10.1109/INDUSCON.2018.8627249
- Darwish, A., Abdel-Khalik, A. S., Elserougi, A., Ahmed, S., & Massoud, A. (2013). Fault current contribution scenarios for grid-connected voltage source inverter-based distributed generation with an LCL filter. *Electric Power Systems Research*, 104(November 2013), 93-103. doi: <https://doi.org/10.1016/j.epsr.2013.06.020>
- Fekkak, B., Mena, M., & Boussahoua, B. (2018). Control of transformerless grid-connected PV system using average models of power electronics converters with MATLAB/Simulink. *Solar Energy*, 173(October 2018), 804-813. doi: <https://doi.org/10.1016/j.solener.2018.08.012>
- Geddada, N., Mishra, M. K., & Kumar, M. V. M. (2015). LCL filter with passive damping for DSTATCOM using PI and HC regulators in dq0 current controller for load compensation. *Sustainable Energy, Grids and Networks*, 2(June 2015), 1-14. doi: <https://doi.org/10.1016/j.segan.2015.02.001>
- Jain, V., & Singh, B. (2019). A multiple improved notch filter-based control for a single-stage PV system tied to a weak grid. *Proceedings of 2019 IEEE Transactions on Sustainable Energy*, 10(1), 238-247. doi: 10.1109/TSTE.2018.2831704
- Jannesar, M. R., Sedighi, A., Savaghebi, M., Moghaddam, A. A., & Guerrero, J. M. (2018, September 17-21). Optimal passive filter planning in distribution networks with nonlinear loads and photovoltaic systems. In *Proceedings of 20th European Conference on Power Electronics and Applications (EPE'18 ECCE Europe)* (pp. 1-9). Riga, Latvia.

- Kandpal, B., Tomar, K. P., Hussain, I., & Singh, B. (2017, October 26-28). Adaptive control of a grid-connected SPV system with DSTATCOM capabilities. In *Proceedings of 4th IEEE Uttar Pradesh Section International Conference on Electrical, Computer, and Electronics (UPCON)* (pp. 452 - 456). Mathura, India. doi: 10.1109/UPCON.2017.8251090
- Khomsi, C., Bouzid, M., Jelassi, K., & Champenois, G. (2018, March 20-22). Harmonic current compensation in a single-phase grid-connected photovoltaic system supplying nonlinear load. In *Proceedings of The 9th International Renewable Energy Congress (IREC)*. Hammamet, Tunisie. doi: 10.1109/IREC.2018.8362520
- Krama, A., Zellouma, L., & Rabhi, B. (2016, November 15-17). Improved control of shunt active power filter connected to a photovoltaic system using the technique of direct power control. In *Proceedings of 8th International Conference on Modelling, Identification, and Control (ICMIC)* (pp. 880-885). Algiers, Algeria. doi: 10.1109/ICMIC.2016.7804239
- Kumar, D. (2015, March 5-7). Modeling, simulation, and performance analysis of a grid-tied voltage source inverter based photovoltaic system underbalanced and non-linear load conditions. In *Proceedings of 2015 IEEE International Conference on Electrical, Computer, and Communication Technologies (ICECCT)* (pp. 1-5). Coimbatore, India. doi: 10.1109/ICECCT.2015.7225965
- Mohamed, J. M., Rasul, A., Khang, H. V., & Kolhe, M. (2017, August 11-14). Harmonic mitigation of a grid-connected photovoltaic system using shunt active filter. In *Proceedings of 20th International Conference on Electrical Machines and Systems (ICEMS)* (pp. 1-5). Sydney, NSW, Australia. doi: 10.1109/ICEMS.2017.8056401
- Naderipoura, A., Zinb, A. A. M., Habibuddin, M. H., Khokhar, S., & Kazemi, A. (2015, October 19-20). Improved control of shunt active power filter using harmony search algorithm. In *Proceedings of 2015 IEEE Conference on Energy Conversion (CENCON)* (pp. 90-95). Johor Bahru, Malaysia. doi: 10.1109/CENCON.2015.7409519
- Oonsivilai, A., Zongo, O. A., & Oonsivilai, R. (2019). Stability enhancement of doubly fed induction generator using a linear quadratic regulator. *GMSARN International Journal*, 13(4), 194-201.
- Ouchen, S., Abdeddaim, S., Betka, A., & Menadi, A. (2016). Experimental validation of sliding mode-predictive direct power control of a grid-connected photovoltaic system, feeding a nonlinear load. *Solar Energy*, 137(November 2016), 328-336. doi: <https://doi.org/10.1016/j.solener.2016.08.031>
- Pereira, H. A., da Mataa, G. L. E., Xavier, L. S., & Cupertino, A. F. (2019). Flexible harmonic current compensation strategy applied in single and three-phase photovoltaic inverters. *Electrical Power and Energy Systems*, 104(January 2019), 358-369. doi: <https://doi.org/10.1016/j.ijepes.2018.07.017>
- Peterson, B., Rens, J., Meyer, J., & Botha, G. (2017, September 20-22). Evaluation of harmonic distortion from multiple renewable sources at a distribution substation. In *Proceedings of 2017 IEEE International Workshop on Applied Measurements for Power Systems (AMPS)* (pp. 1-6). Liverpool, UK. doi: 10.1109/AMPS.2017.8078327
- Singh, A. K., Hussain, I., & Singh, B. (2018, January 31-February 2). An improved adaptive P&O technique for two-stage grid interfaced SPVECS. In *Proceedings of 2018 IEEE International Conference on Industrial Electronics for Sustainable Energy Systems (IESES)* (pp. 320-325). Hamilton, New Zealand. doi: 10.1109/IESES.2018.8349896

- Srinivas, V. L., Singh, B., & Mishra, S. (2019). Fault ride-through strategy for two-stage GPV system enabling load compensation capabilities using EKF algorithm. *Proceedings of 2019 IEEE Transactions on Industrial Electronics*, 66(11), 8913-8924. doi: 10.1109/TIE.2019.2899546
- Upaphai, W., Bunyawanichakul, P., & Janthong, M. (2019). Design of self-tuning fuzzy PID controllers for position tracking control of autonomous agricultural tractor. *Pertanika Journal of Science and Technology*, 27(1), 263-280.
- Xie, B., Mao, M., Zhou, L., Wan, Y., & Hao, G. (2020). Systematic design of linear quadratic regulator for digitally controlled grid-connected inverters. *IET Power Electron*, 13(3), 557-567.
- Yousef, M. Y., Ismail, M. M., & El-Masry, S. M. (2018, December 18-20). The effect of grid-connected photovoltaic location and penetration level on total harmonic distortion. In *Proceedings of Twentieth International Middle East Power Systems Conference (MEPCON)* (pp. 141-145). Cairo, Egypt. doi: 10.1109/MEPCON.2018.8635252



Statistical Analysis of AC Dielectric Strength for Palm Oil under the Influence of Moisture

Muhammad Safwan Shukri^{1,2*}, Norhafiz Azis^{1,2}, Jasronita Jasni¹, Robiah Yunus³ and Zaini Yaakub⁴

¹Advanced Lightning, Power and Energy Research Centre (ALPER), Faculty of Engineering, Universiti Putra Malaysia, 43400 UPM, Serdang, Selangor, Malaysia

²Institute of Advanced Technology (ITMA), Faculty of Engineering, Universiti Putra Malaysia, 43400 UPM, Serdang, Selangor, Malaysia

³Department of Chemical and Environmental Engineering, Faculty of Engineering, Universiti Putra Malaysia, 43400 UPM, Serdang, Selangor, Malaysia

⁴Hyrax Oil Sdn. Bhd., Lot 4937, Batu 51/2, Jalan Meru, Mukim Kapar, 41050 Klang, Selangor, Malaysia

ABSTRACT

This paper presents a statistical study on the AC Breakdown Voltage (BDV) of Refined, Bleached and Deodorized Palm Oil (RBDPO) olein under the influence of moisture. Different moisture contents of the RBDPO were prepared by drying the RBDPO in the oven at different time intervals. The AC BDV test of RBDPO was performed whereby the distance between 2 electrodes was set to 1 mm. The statistical analyses of AC BDV data for RBDPO were carried out based on normal, lognormal and Weibull distributions. It was shown that as the moisture content increased, the AC BDV of RBDPO decreased exponentially. Statistical analyses revealed that the AC BDV data with different moisture contents had platykurtic distributions. Moisture could influence the skewness of the distribution whereby the tail shifted from right to left as the content increased. At different moisture contents of RBDPO, most of the AC BDV data of RBDPO could be represented by Weibull distribution.

ARTICLE INFO

Article history:

Received: 28 September 2020

Accepted: 26 November 2020

Published: 22 January 2021

DOI: <https://doi.org/10.47836/pjst.29.1.04>

E-mail addresses:

safwannshukri@gmail.com (Muhammad Safwan Shukri)

norhafiz@upm.edu.my (Norhafiz Azis)

jas@upm.edu.my (Jasronita Jasni)

robiah@upm.edu.my (Robiah Yunus)

zaini@hyraxoil.com (Zaini Yaakub)

*Corresponding author

Keywords: AC breakdown voltage, moisture, palm oil, statistical distribution

INTRODUCTION

Among the main insulation materials in transformers is Mineral oil (MO). MO has an excellent electrical insulation and cooling properties, and it could act as an information carrier to determine the condition of transformers (Heathcore, 2007). It has been extensively used for decades due to its good performance to provide the necessary insulation to transformers (Martins, 2010; Oommen, 2002).

However, MO has several issues such as low fire/flash points and moisture tolerance (Tenbohlen & Koch, 2010). It has poor biodegradability, and it could cause contamination issues if serious spills occur in the soils and waterways (Mohamad et al., 2015). In addition, MO is a non-renewable source (Azis et al., 2014). Recently, the interests on environmental considerations in electrical industries are increasing which prompt for serious efforts to seek alternatives for MO.

Several types of Vegetable Oil (VO) have been identified as viable alternatives for MO whereby extensive laboratories experimental works and in-services testing have been carried out previously (Rafiq et al., 2015). Palm Oil (PO) is among the VOs that have been considered as alternative of MO for dielectric insulating liquid application (Mohamad et al., 2014). Different types of POs have been investigated where promising results have been obtained (Suwarno et al., 2003). Refined, Bleached and Deodorized Palm Oil (RBDPO) has been established as one of the promising POs which can be used as dielectric insulating fluid in transformers (Suleiman & Muhamad, 2011). RBDPO is environment friendly and it has high fire safety as compared to the MO (Aditama, 2005; Kiasatina et al., 2011). It is widely available in Malaysia and its characteristics such as biodegradability and non-toxicity are similar to other types of VO (Azis et al., 2014).

Previous studies have shown that the AC Breakdown Voltage (BDV)s of the MO and VO could be affected by the moisture (Takaaki et al., 2008). Previous study on MO showed that the AC BDV could decrease by 78% as the moisture increased from 12 ppm to 41 ppm (Suwarno & Prakoso, 2015). The study had shown that the AC BDV of MO maintained almost unchanged at low level as the relative water content increased higher than 50% (Suwarno & Prakoso, 2015). Wang & Wang (2008) had shown that the highest percentage of decrement for AC BDV for MO was 68% and a decrement trend was observed as the relative humidity increased from 3 % and 98%. Martin & Wang (2006) revealed that the AC BDV of MO decreased from 29 kV to 20 kV as the moisture increased from 5 ppm to 17 ppm.

On the other hand, it is shown that higher moisture content is required to cause significant reduction of AC BDV for VO as compared to MO. Martin & Wang (2006) showed that the AC BDV strength of natural ester decreased from 38 kV to 34 kV as the moisture increased from 31 ppm to 340 ppm. Other study showed that the AC BDV of natural ester decreased from 82 kV to 15.3 kV as the moisture increased from 128 ppm

to 776 ppm (Primo et al., 2019). A previous study on rapeseed oil also showed that the increment of moisture from 40 ppm to 3,000 ppm caused the reduction of AC BDV from 61 kV to 8 kV (Mehmood et al., 2018). Another study had shown that 100 ppm of moisture could cause 11%, 37% and 17% reductions of AC BDVs for red palm oil, RBDPO and Palm Fatty Acid Ester (PFAE) (Suleiman et al., 2014). Murad et al. (2013) showed that the introduction of 700 ppm moisture in RBDPO, carotino oil and PFAE could caused reduction 67%, 49% and 82% of AC BDV, respectively. At the moment, there is a limited study that has been performed to examine the overall pattern of AC BDV of RBDPO versus moisture. The knowledge could be useful especially on identifying the AC BDV saturation level for RBDPO as compared to other types of VO.

In this study, the influence of moisture on the AC BDV of RBDPO was investigated. RBDPOs with different moisture contents were prepared by controlling the drying times of RBDPO in the oven. All RBDPOs were measured for moisture contents and AC BDVs and the parametric statistical techniques were used to analyze the AC withstand voltages.

MATERIALS AND METHODS

Samples Preparation

A membrane filter with a pore size of 0.2 μm was used to filter the RBDPO. In total, 3 times of filtration process was carried out to ensure the number of particles in the sample could be reduced as low as possible (Wang & Wang, 2008). The first sample of RBDPO was defined as “as-received”. The RBDPO was dried in an air circulating oven at 85°C for 6, 12, 18, 24, 30, 36, 42 and 48 hours individually to obtain different moisture contents. The volume for each of the samples was set to 500ml. After the drying process, all samples were further rested at ambient temperatures for at least 6 hours before the moisture and AC breakdown measurements were carried out.

Moisture Measurement

The moisture in RBDPO was measured by a Metrohm 831 Karl Fischer (KF) Coulometer as per ASTM D6304-16e1 (2016). For each of the moisture measurements, 1 ml of RBDPO was extracted and injected into titration vessel that contain CombiCoulomat fritless Karl Fischer reagent as seen in Figure 1. In total, 2 measurements were taken, and the average value was used for the analysis.

AC BDV Measurement

AC BDV of RBDPO was performed by an automatic BAUR DPA 75C breakdown tester based on ASTM D1816-12 (2019). The test was conducted at ambient temperatures. The gap distance between 2 VDE electrodes with a diameter of 36 mm was set to 1 mm. In total, 400 ml of RBDPO was used for the AC BDV test and it was carefully poured into

the test cell in order to ensure there was no bubble formation as shown in Figure 2. The samples were rested for 15 minutes before the test was carried out. The test cell containing the RBDPO was placed in the test slot located within the BAUR DPA 75C breakdown tester. The voltage was automatically increased at 0.5 kV/s until the breakdown occurs between the 2 VDE electrodes and its corresponding breakdown voltage was recorded by the tester. Next, the RBDPO was automatically continuously stirred with a magnetic stirrer without any application of voltage for 5 minutes before the next breakdown test was carried out. The process was automatically repeated until 50 measurements were recorded for each of the samples.

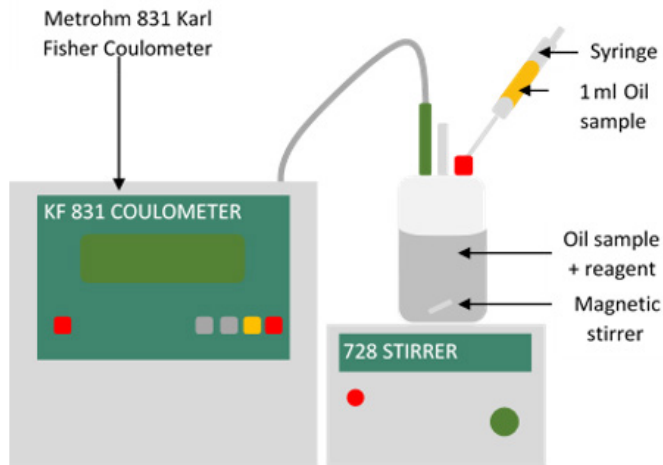


Figure 1. Moisture content test of the RBDPO

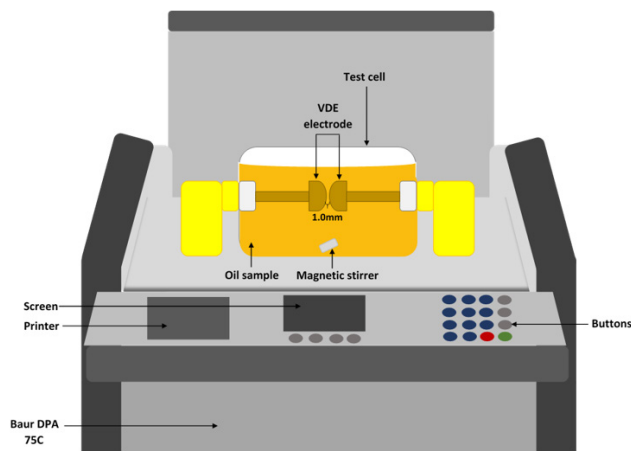


Figure 2. AC BDV test of the RBDPO

RESULTS AND DISCUSSION

Moisture Versus Drying Time

Moisture in RBDPO at different drying times can be seen in Figure 3a. It was observed that as the drying times increased, the moisture decreased exponentially. Apparent reduction of moisture up to 41% was found after 6 hours of drying. After 18 hours of drying, the reduction rate of moisture started to decrease. Between 18 hours and 48 hours of drying, the moisture decreased from 326 ppm to 199 ppm. The highest variation of the moisture content was observed for “as-received” samples as shown in Table 1. The variation decreased to a range between 1% and 3% with the increment of the drying time.

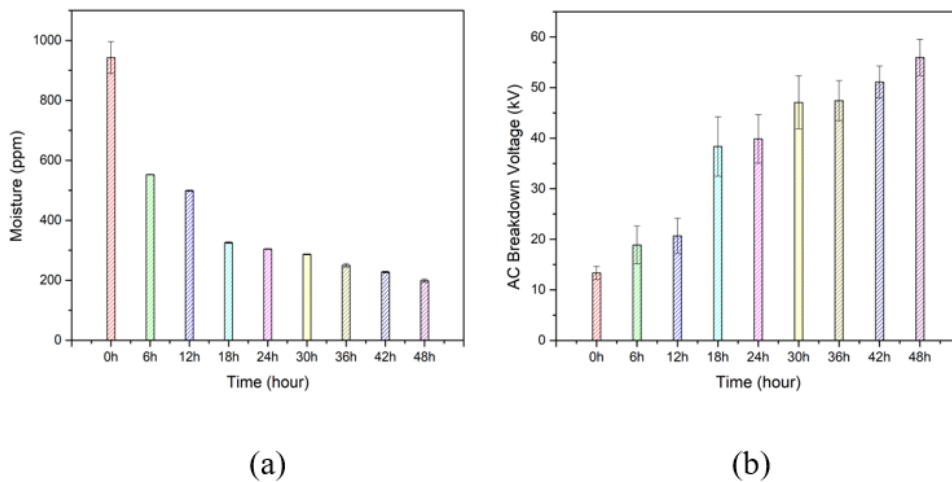


Figure 3. Relationship between (a) Moisture and drying time for RBDPO; (b) AC BDV and drying time for RBDPO

Table 1

Moisture content, standard deviation, and coefficient of variation according to drying time

Drying time (h)	Moisture content (ppm)	Standard deviation (ppm)	Coefficient of variation (%)
0	943	53.60	6
6	553	0.85	1
12	499	1.84	1
18	326	2.12	1
24	305	1.34	1
30	287	1.41	1
36	250	6.01	2
42	228	2.26	1
48	199	5.87	3

AC BDV Versus Drying Time

Linear increment of the AC BDV was found as the drying time increased as shown in Figure 3b. After 48 hours of drying, the AC BDV of RBDPO increases to 55.95 kV. The variation of AC BDVs is slightly different than moisture content as shown Table 2. The highest variation of AC BDV occurred after 6 hours of drying. After 42 hours of drying, the variation of AC BDV stabilized whereby it was maintained at 6%.

Table 2

Mean AC BDV, standard deviation, and coefficient of variation according to drying time

Drying time (h)	Mean AC BDV (kV)	Standard deviation (kV)	Coefficient of variation (%)
0	13.34	1.31	10
6	18.88	3.75	20
12	20.68	3.50	17
18	38.37	5.87	15
24	39.86	4.82	12
30	47.06	5.27	11
36	47.41	3.97	8
42	51.09	3.16	6
48	55.95	3.58	6

AC BDV Versus Moisture

It is apparent that the moisture has an apparent effect on the AC BDV of RBDPO as shown in Figure 4. The AC BDV of RBDPO decreased exponentially with the increment of the moisture. The highest percentage of AC BDV decrement could be up to 76% as the moisture increased from 199 ppm to 943 ppm.

The variation of AC BDV at different instance intervals and moisture contents can be seen in Figure 4. It was observed that the variation of AC BDV for RBDPO at moisture of 943 ppm was quite low as shown in Figure 5a. On the other hand, high variations of AC BDVs for RBDPO were observed at moisture of 326 ppm, 305 ppm and 287 ppm as shown in Figure 5d, e, and f. The variations of AC BDVs for RBDPO were observed to be quite moderate at moisture of 553 ppm, 499 ppm, 250 ppm, 228 ppm and 199 ppm as seen in Figure 5b, c, g, h, and i, respectively.

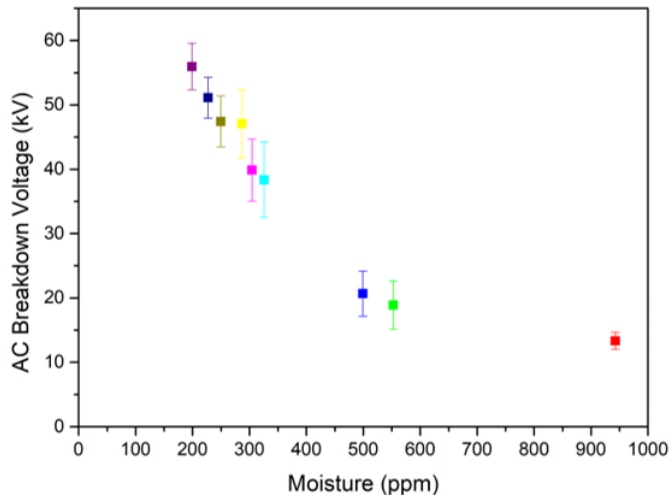


Figure 4. AC BDV versus moisture for RBDPO

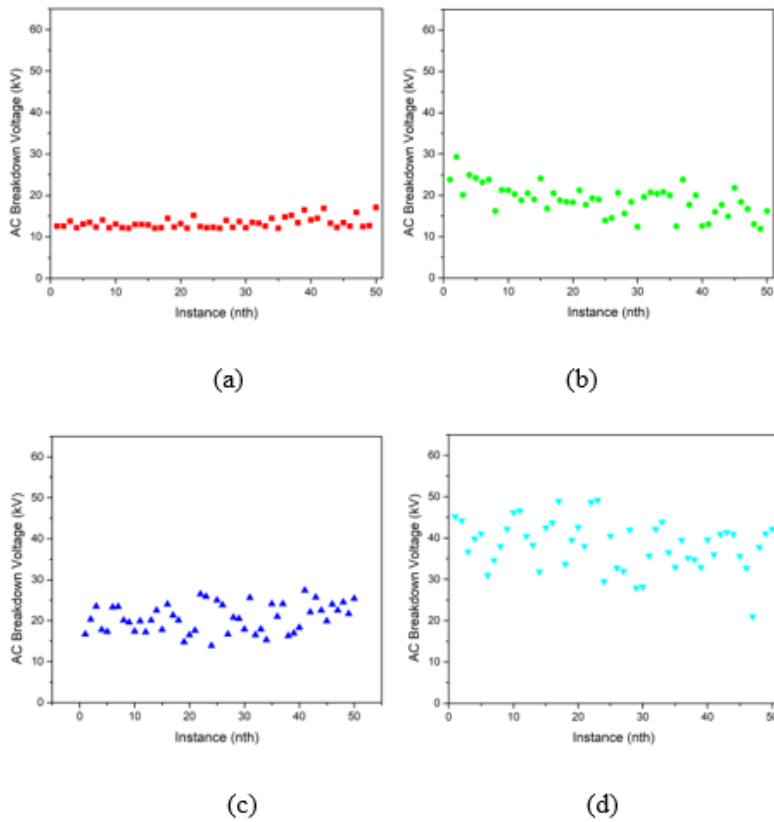
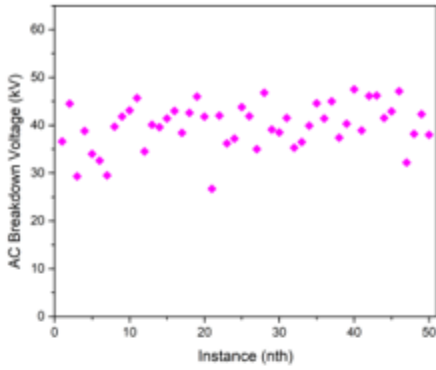
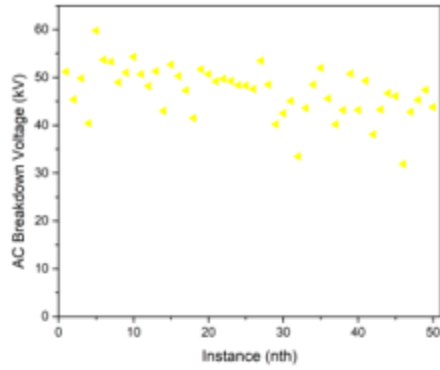


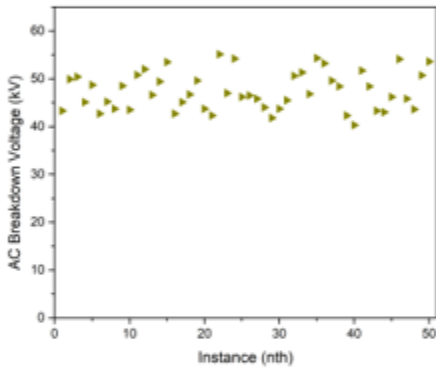
Figure 5. Distribution of AC BDV of RBDPO at moisture of (a) 943 ppm; (b) 533 ppm; (c) 499 ppm; (d) 326 ppm



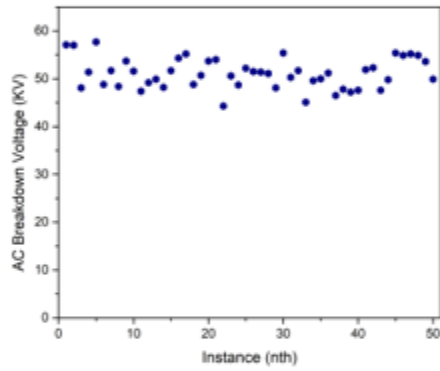
(e)



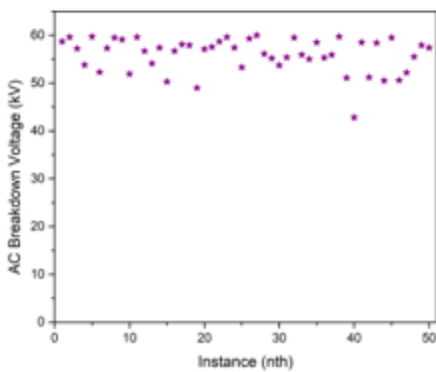
(f)



(g)



(h)



(i)

Figure 5. Distribution of AC BDV of RBDPO at moisture of (e) 305 ppm; (f) 287 ppm; (g) 250 ppm; (h) 228 ppm; (i) 199ppm

Statistical Analysis of AC BDV

Normal, lognormal and Weibull Cumulative Distribution Function (CDF) were the parametric techniques used to analyze the AC BDV data at different moisture contents. Equations 1 to 3 show the CDF models for normal, lognormal and Weibull distributions. For Equations 1 and 2, “ x ”, “ μ ” and “ σ ” represent of data, mean and standard deviation respectively. On the other hand, the “ x ”, “ α ” and “ β ” represents data, scale, and shape parameter for Equation 3.

$$F(x|\mu,\sigma) = \frac{1}{\sigma\sqrt{2\pi}} \int_{-\infty}^x e^{-\frac{(t-\mu)^2}{2\sigma^2}} dt \tag{1}$$

$$F(x|\mu,\sigma) = \left(\frac{1}{\sigma\sqrt{2\pi}}\right) \int_0^x \frac{1}{t} e^{-\frac{(\log t - \mu)^2}{2\sigma^2}} dt \tag{2}$$

$$F(x|\alpha,\beta) = \int_0^x b\alpha^{-b} t^{b-1} e^{-\left(\frac{t}{\alpha}\right)^b} dt \tag{3}$$

Normal distribution or also well known as Gaussian distribution assumes that the data lie symmetrically close the mean of the data obtained (Martin & Wang, 2008). Kurtosis can be used to analyzed the extreme or less extreme values around the distribution based on Equation 4 (Martin & Wang, 2008). The symmetrical of the data is determined by analyzing the skewness as seen in Equation 5 (Martin & Wang, 2008). For Equations 4 and 5, the “ n ”, “ x_i ” and “ \bar{X} ” represents of the sample size, individual value, and the mean of the sample, respectively.

$$g = \frac{n \sum_{i=1}^n (x_i - \bar{x})^4}{(\sum_{i=0}^n (x_i - \bar{x})^2)^2} \tag{4}$$

$$s = \frac{\sqrt{n} \sum_{i=0}^n (X_i - \bar{X})^3}{(\sum_{i=0}^n (X_i - \bar{X})^2)^{3/2}} \tag{5}$$

The skewness and kurtosis of the data for all samples can be seen in Table 3. Normally distributed data has the kurtosis of 3 and skewness of 0. If the kurtosis is less than 3, it means that the kurtosis is plytokurtic which indicates less extreme tail of the distribution. Kurtosis higher than 3 indicates leptokurtic distribution which mean extreme tail of the distribution. If the skewness is less than 0, the left tail of distribution is longer than right tail and vice versa if the value is higher than 0. Based on Table 3, it is apparent that the AC BDV data of RBDPO at different moisture contents had plytokurtic distribution whereby the tail was less extreme and concentrated mainly at the mean. Skewness analysis revealed that as the moisture decreased, the distribution tail shifted from right to left. Figure 6 shows the illustration of the AC BDV data distribution. It is shown the distribution of AC BDV data at moisture of 943 ppm has long right tail as shown in Figure 6a. The distributions of AC BDV data had no apparent extreme right or left tail as the moisture decreased from 553

ppm to 228 ppm as shown in Figure 6b, c, d, e, f, g, and h. As the moisture reached 199 ppm, the AC BDV data distribution started to exhibit long left tail as shown in Figure 6i.

Table 3

Kurtosis and skewness based on AC BDV data

Moisture content (ppm)	Mean AC BDV (kV)	Kurtosis for AC BDV data	Skewness for AC BDV data
943	13.34	1.31	1.36
553	18.88	0.11	0.11
499	20.68	-1.07	0.03
326	38.37	0.39	-0.44
305	39.86	0.24	-0.66
287	47.06	1.02	-0.61
250	47.41	-1.01	-0.30
228	51.09	-0.51	0.16
199	55.95	2.28	-1.34

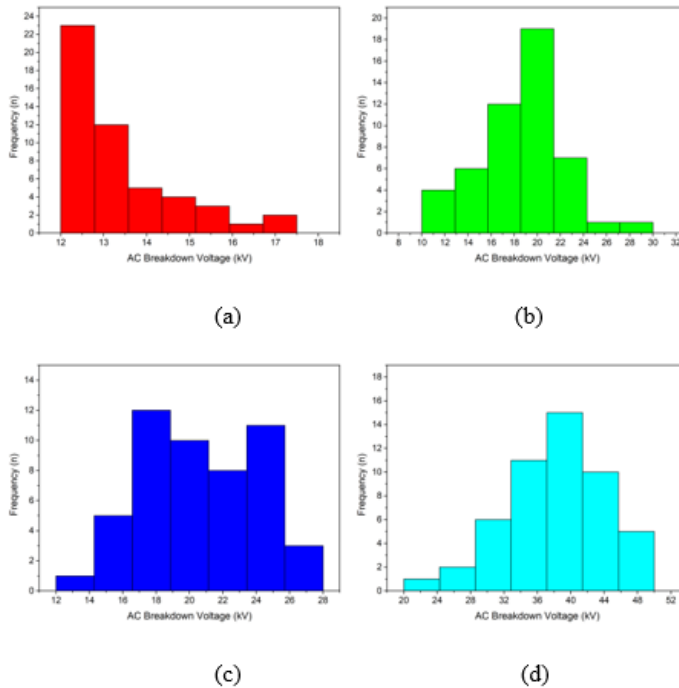
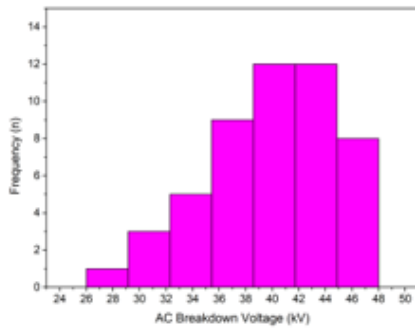
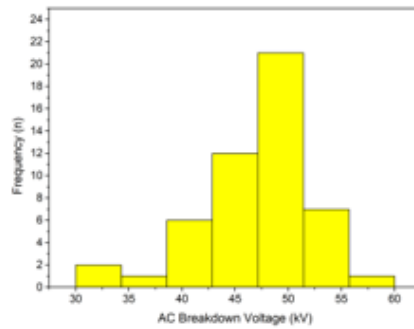


Figure 6. Histogram of frequency versus AC BDV of RBDPO at moisture of (a) 943 ppm; (b) 533 ppm; (c) 499 ppm; (d) 326 ppm

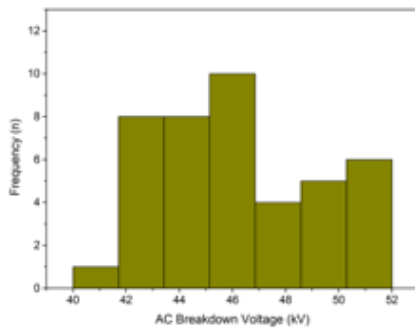
Statistical Analysis of AC Dielectric Strength for Palm Oil



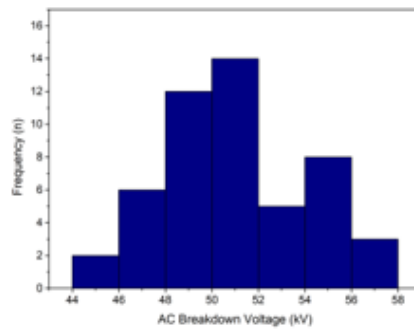
(e)



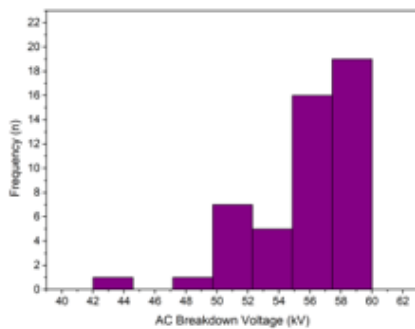
(f)



(g)



(h)



(i)

Figure 6. Histogram of frequency versus AC BDV of RBDPO at moisture of (e) 305 ppm; (f) 287 ppm; (g) 250 ppm; (h) 228 ppm; (i) 199ppm

The comparison among the fitted AC BDV data by normal, lognormal and Weibull distributions can be seen in Figures 7 to 9. Weibull distribution could represent most of the AC BDV data at moisture from 499 ppm to 199 ppm. The AC BDV data at moisture of 943 ppm and 553 ppm could not be represented by Weibull distribution whereby the data deviations occurred at lower probability. Normal and lognormal distributions could represent the AC BDV at moisture of 943 ppm, 553 ppm and 499 ppm quite well as compared to Weibull distribution. However, as the moisture decreased, apparent data deviations occurred at both lower and higher probabilities. Lognormal distribution performed better than normal distribution in term of representation the whole AC BDV data.

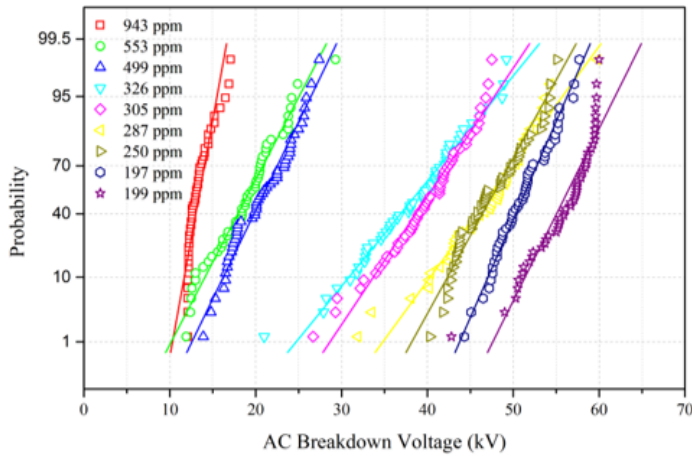


Figure 7. Normal probability plots of RBDPO

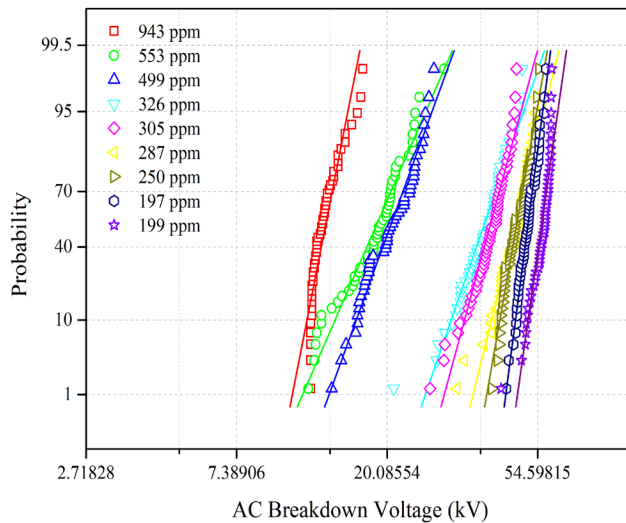


Figure 8. Lognormal probability plots of RBDPO

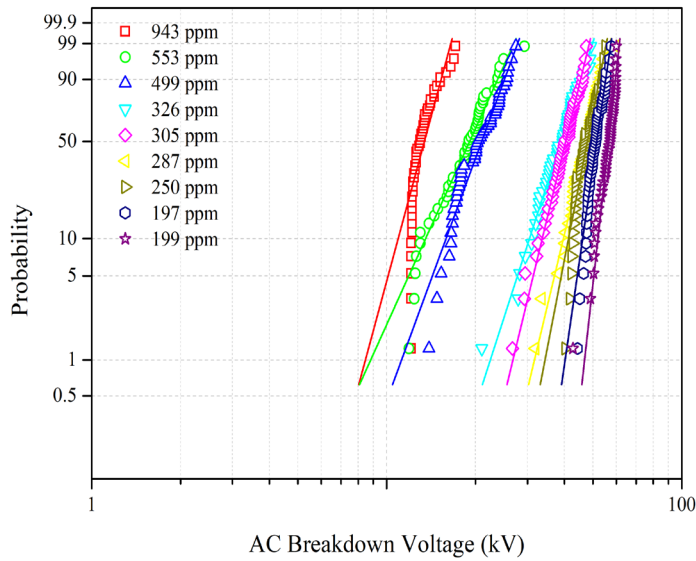


Figure 9. Weibull probability plots of RBDPO

The AC BDVs at 1%, 10%, 50% and 90% probabilities can be seen in Tables 4 to 7. It was found that the AC BDVs at 1%, 10% and 90% by lognormal distribution were slightly higher than other distributions. On the other hand, the AC BDV at 50% probability by Weibull distribution was slightly higher than other distributions. At 1%, 10% and 50% probabilities, the AC BDVs obtained by the Weibull distribution had the highest increments as moisture decreased from 943 ppm to 199 ppm with percentages of 453%, 375% and 321%. At 1% and 10% probabilities, the AC BDVs obtained by the normal distribution had the second highest of increment of 362% and followed by the lognormal distribution of 346% and 334%. At 50% probability, the AC BDV increment for lognormal distribution was slightly higher than normal distribution of 320%. At 90% probability, the AC BDV by lognormal distribution had the highest increment of 307%. The second highest of increment at 90% probability was normal distribution followed by Weibull distribution of 303% and 289% respectively.

Table 4
AC BDV at 1% probability according to parametric methods

Drying times (h)	Moisture content (ppm)	1% probability (kV)		
		Normal	Lognormal	Weibull
0	943	10.30	10.70	8.47
6	553	10.16	11.46	8.82

Table 4 (Continued)

Drying times (h)	Moisture content (ppm)	1% probability (kV)		
		Normal	Lognormal	Weibull
12	499	12.56	13.66	11.21
18	326	25.05	25.88	22.45
24	305	28.65	29.36	26.77
30	287	34.81	35.52	31.68
36	250	38.18	38.94	34.38
42	228	43.75	44.18	40.25
48	199	47.62	47.75	46.82

Table 5

AC BDV at 10% probabilities according to parametric methods

Drying times (h)	Moisture content (ppm)	10% probability (kV)		
		Normal	Lognormal	Weibull
0	943	11.67	11.79	10.93
6	553	14.07	14.21	13.53
12	499	16.21	16.35	15.87
18	326	31.18	30.72	30.46
24	305	33.69	33.56	33.65
30	287	40.31	40.18	39.71
36	250	42.32	42.47	41.31
42	228	47.05	47.12	46.13
48	199	51.36	51.22	51.97

Table 6

AC BDV at 50% probability according to parametric methods

Drying times (h)	Moisture content (ppm)	50% probability (kV)		
		Normal	Lognormal	Weibull
0	943	13.34	13.28	13.42
6	553	18.88	18.45	19.08
12	499	20.68	20.38	20.98
18	326	38.70	37.89	38.91

Table 6 (Continued)

Drying times (h)	Moisture content (ppm)	50% probability (kV)		
		Normal	Lognormal	Weibull
24	305	39.86	39.55	40.42
30	287	47.06	46.75	47.59
36	250	47.41	47.24	47.87
42	228	51.09	50.99	51.47
48	199	55.95	55.83	56.51

Table 7

AC BDV of 90% probability based on parametric method

Samples	Moisture content (ppm)	90% probability (kV)		
		Normal	Lognormal	Weibull
0	943	15.01	14.96	15.29
6	553	23.68	24.08	23.74
12	499	25.15	25.41	25.04
18	326	46.22	46.75	45.47
24	305	46.04	46.61	45.43
30	287	53.81	54.39	53.41
36	250	52.49	52.56	52.58
42	228	55.13	55.19	55.18
48	199	60.54	60.86	59.60

CONCLUSION

According to the current study, it is found that the drying process does help with the improvement of the AC BDV of RBDPO through reduction of moisture. The AC BDV of RBDPO decreases exponentially with the increment of the moisture. The AC BDV data of RBDPO has a platykurtic distribution whereby the distribution tail shift from right to left as the moisture increases. Weibull distribution can represent most of the AC BDV data of RBDPO at different moisture contents quite well as compared to the normal and lognormal distributions.

ACKNOWLEDGEMENTS

The authors would like to thank the Ministry of Higher Education for the funding provided for this study under the FRGS scheme FRGS/1/2019/TK07/UPM/02/3 (03-01-19-2071FR).

REFERENCES

- Aditama, S. (2005). Dielectric properties of palm oils as liquid insulating materials: Effects of fat content. In *Proceedings of 2005 International Symposium on Electrical Insulating Materials, 2005. (ISEIM 2005)* (Vol. 1, pp. 91-94). Tokyo, Japan: Yasuo Muraoka. doi: 10.1109/ISEIM.2005.193334
- ASTM D1816-12. (2019). *Standard test method for dielectric breakdown voltage of insulating liquids using VDE electrodes*. West Conshohocken, USA: ASTM International
- ASTM D6304-16e1. (2016). *Standard test method for determination of water in petroleum products, lubricating oils, and additives by Coulometric Karl Fischer Titration*. West Conshohocken, USA: ASTM International
- Azis, N., Jasni, J., Kadir, M. Z. A., & Mohtar, M. N. (2014). Suitability of palm based oil as dielectric insulating fluid in transformers. *Journal of Electrical Engineering and Technology*, 9(2), 662-669. doi: 10.5370/jeet.2014.9.2.662
- Heathcore, M. K. (2007). *The J and P transformer book*. Oxford, United Kingdom: Elsevier.
- Kiasatina, Kamarol, M., Zuhlilmey, M., & Arief, Y. A. (2011, June 21-22). Breakdown characteristics of RBDPO and soybean oil mixture for transformer application. In *Proceedings of the International Conference on Electrical, Control and Computer Engineering 2011 (InECCE)* (pp. 219-222). Pahang, Malaysia. doi: 10.1109/INECCE.2011.5953879
- Martin, D., & Wang, Z. D. (2006, October 15-18). A comparative study of the impact of moisture on the dielectric capability of esters for large power transformers. In *Proceedings of 2006 Annual Report Conference on Electrical Insulation and Dielectric Phenomena* (pp. 409 - 412). Kansas City, MO, USA. doi: 10.1109/CEIDP.2006.311956.
- Martin, D., & Wang, Z. D. (2008). Statistical analysis of the AC breakdown voltages of ester based transformer oils. *IEEE Transactions on Dielectrics and Electrical Insulation*, 15(4), 1044-1050. doi: 10.1109/TDEI.2008.4591226
- Martins, M. A. G. (2010). Vegetable oils, an alternative to mineral oil for power transformers-experimental study of paper aging in vegetable oil versus mineral oil. *IEEE Electrical Insulation Magazine*, 8(3), 7-13. doi: 10.1109/MEI.2010.5599974
- Mehmood, M. A., Li, J., Huan, Z., Wang, F., Li, X., Bhutta, M. S., & Li, X. (2018, September 10-13). Effects of suspended moisture particles on AC breakdown voltage and electric field distribution of vegetable insulation oil. In *Proceedings of 2018 IEEE International Conference on High Voltage Engineering and Application (ICHVE)* (pp. 1-4). Athens, Greece. doi: 10.1109/ICHVE.2018.8641957

- Mohamad, N. A., Azis, N., Jasni, J., Kadir, M. Z. A., Yunus, R., Ishak, M. T., & Yaakub, Z. (2015). A study on the dielectric properties of RBDPO olein under low temperature thermal ageing. *Applied Mechanics and Materials*, 793, 14-18. doi: 10.4028/www.scientific.net/AMM.793.14
- Mohamad, N. A., Azis, N., Jasni, J., Kadir, M. Z. A., Yunus, R., Ishak, M. T., & Yaakub, Z. (2014, December 1-3). A study on the dielectric properties of palm oil and coconut oil. In *Proceedings of the 2014 IEEE International Conference on Power and Energy (PECon)* (pp. 109-112). Kuching, Malaysia. doi: 10.1109/PECON.2014.7062423
- Murad, N. S., Muhamad, N. A., Suleiman A. A., & Jamail, N. A. M. (2013, October 20-23). A study on palm oil-based oil moisture absorption level and voltage breakdown. In *Proceedings of 2013 Annual Report Conference on Electrical Insulation and Dielectric Phenomena* (pp. 925-928). Shenzhen, China. doi: 10.1109/CEIDP.2013.6748188
- Oommen, T. V. (2002). Vegetable oils for liquid-filled transformers. *IEEE Electrical Insulation Magazine*, 18(1), 6-11. doi: 10.1109/57.981322
- Primo V. A., García, B., Pérez, D., & Burgos, J. C. (2019, June 23-27). Analysing the impact of moisture on the AC breakdown voltage on natural ester based nanodielectric fluids. In *Proceedings of 2019 IEEE 20th International Conference on Dielectric Liquids (ICDL)* (pp. 1-4). Roma, Italy. doi: 10.1109/ICDL.2019.8796675
- Rafiq, M., Lv, Y. Z., Zhou, Y., Ma, K. B., Wang, W., Li, C. R., & Wang, Q. (2015). Use of vegetable oils as transformer oils - A review. *Renewable and Sustainable Energy Reviews*, 52, 308-324. doi: <https://doi.org/10.1016/j.rser.2015.07.032>
- Suleiman, A. A., Muhamad, N. A., Bashir, N., Murad, N. S., Arief, Y. Z., & Phung, B. T. (2014). Effect of moisture on breakdown voltage and structure of palm based insulation oils. *IEEE Transactions on Dielectrics and Electrical Insulation*, 21(5), 2119-2126. doi: 10.1109/TDEI.2014.004431
- Suleiman, A., & Muhamad, N. A. (2011). A case for the establishment of Malaysian standard for biodegradable insulation oil in Malaysia transformers. *International Review on Modelling and Simulations*, 4(6), 2756-2763.
- Suwarno, S., & Prakoso, M. (2015). Effects of water content on dielectric properties of mineral transformer oil. *International Journal of Electrical and Computer Engineering*, 9(10), 1142-1146. doi: 10.5281/zenodo.1109353
- Suwarno, S., Sitinjak, F., Suhariadi, I., & Imsak, L. (2003, June 1-5). Study on the characteristics of palm oil and its derivatives as liquid insulating materials. In *Proceedings of the 7th International Conference on Properties and Applications of Dielectric Materials* (Vol. 2, pp. 495-498). Nagoya, Japan. doi: 10.1109/ICPADM.2003.1218461
- Takaaki, K., Hiroyuki, I., Yoshiyuki, H., Junichi, Y., Tomoyuki, H., Akina, Y., ... & Yasunori, H. (2008, June 30 - July 3). Analyses of electro-chemical characteristics of palm fatty acid esters as insulating oil. In *Proceedings of 2008 IEEE International Conference on Dielectric Liquids* (pp. 1-4). Futuroscope-Chasseneuil, France. doi: 10.1109/ICDL.2008.4622456

- Tenbohlen, S., & Koch, M. (2010). Aging performance and moisture solubility of vegetable oils for power transformers. *IEEE Transactions on Power Delivery*, 25(2), 825-830. doi: 10.1109/TPWRD.2009.2034747
- Wang, X., & Wang, Z. D. (2008, October 26-29). Particle effect on breakdown voltage of mineral and ester based transformer oils. In *Proceedings of 2008 Annual Report Conference on Electrical Insulation and Dielectric Phenomena* (pp. 598-602). Quebec, Canada. doi: 10.1109/CEIDP.2008.4772859

Performance Analysis of the Linear Launcher Motor via Modelling and Simulation for Light Electric Vehicles

Norramlee Mohamed Noor^{1,2*}, Ishak Aris^{1*}, Norhisam Misron¹, Suhaidi Shafie¹ and Parvez Iqbal³

¹Department of Electrical and Electronics, Faculty of Engineering, Universiti Putra Malaysia, 43400 Serdang, Selangor, Malaysia

²Electrical Electronic Automation Section, University Kuala Lumpur, Malaysian Spanish Institute, Kulim Hi-Tech Park, 09000 Kulim, Kedah, Malaysia

³International University of Business Agriculture and Technology – IUBAT, 4 Embankment Drive Road, Sector 10, Uttara Model Town, Dhaka 1230, Bangladesh

ABSTRACT

This research aimed to analyse the linear launcher motor (LM) for the light electric vehicle (EV) application that generated a linear movement. LM will replace the piston engine and eliminate the internal combustion engine (ICE) issues namely engine weight and friction at piston wall. The finite element magnetic softwares (FEMs) for a magnetic field was described in this study by predicting the magnetic flux relationship using a 2D J-Mag software. In addition the finite element (FE) analysis was used to simulate the linear launcher motor by using MATLAB/Simulink software. The results show that the linear launcher motor can generate the axial force, speed, and displacement of with and without load. The maximum force without load was ~1.6kN while force with load was ~1.4kN at 100A supplied. The comparison between the force without load and load force was different by 12.5%.

Keywords: Electric vehicle, finite element magnetic softwares, linear launcher motor

ARTICLE INFO

Article history:

Received: 28 November 2019

Accepted: 30 March 2020

Published: 22 January 2021

DOI: <https://doi.org/10.47836/pjst.29.1.05>

E-mail addresses:

norramlee@unikl.edu.my (Norramlee Mohamed Noor)

ishak_ar@upm.edu.my (Ishak Aris)

norhisam@upm.edu.my (Norhisam Misron)

suhaidi@upm.edu.my (Suhaidi Shafie)

akm.parvez.iqbal@gmail.com (Parvez Iqbal)

* Corresponding author

INTRODUCTION

The automobile industry in the coming years will face serious problems such as global warming and fossil fuel resources. This is because most vehicles on the road today use a large amount of internal combustion engine (ICE), which is the burning engine process that causes environmental pollution. According to a recent study, ICE by using

gasoline combustion is the most polluted air at about 28% (Andersson, 1991; Noor et al., 2019a). Compression piston rings and cylinder walls are represented by a significantly higher power loss in modern ICE that accounts for about 35% of the overall mechanical friction engine (Noor et al., 2019b; Bolander et al., 2005). To overcome these problems, various types of research and development for next-generation vehicles have been pursued from different angles (Chan, 1996).

This research aimed to provide the opportunity to develop the analytical study of a linear launcher motor (LM) for electric vehicle (EV) application, known as the linear electromagnetic motor (EMM). The finite element magnetic softwares (FEMs) for a magnetic field are described by predicting the magnetic flux relationship using 2D J-Mag software. In addition, the finite element (FE) analysis was used to simulate the linear launcher motor by using MATLAB/Simulink software. Finally, the results show that the linear launcher motor could generate axial force, speed, and displacement of with and without load.

LINEAR MOTIONS

The application of linear motion is currently more challenging than ever due to faster methods, more accurate positioning, longer life, less maintenance, less moving parts, and endless lists (Miler, 2006). There are various types of engines in the global market that have a different number of cylinders namely the inline engine, V engine, and flat-opposed engine. Every cylinder contains a piston that moves up and down inside the engine, where it is connected through an individual connecting rod to a universal crankshaft.

Concept of Linear Launcher Motor

The linear launcher motor is a conventional motor in which projectile moves in a linear direction rather than in the rotation (Bedajangam & Jadhav, 2013; Mclean, 1988; Say & Taylor, 1982; Matsch & Morgan, 1986; Sgobba, 2011). This kind of linear launcher may have a set of solenoids placed alongside the moving object. This linear launcher looks like a tubular launcher, which primarily consists of a simple row of coaxial coils. The linear launcher is divided into three categories including coil-gun, rail-gun, and induction launcher (Laithwaite, 1975; Gieras & Piech, 1999; Beaty & Kirtley, 1998).

Structure Linear Launcher Motor Model

The structure of linear LM is similar to a linear motor that is a solenoid actuator. A York and mover are the key components of this linear LM as shown in Figure 1. They are fabricated using materials such as mild steel AISI 1008 due to its good magnetic properties that contain 8-13% of carbon (Chemerys, 2001). The coil used is a copper wire material. Table 1 presents the parameter of the linear LM model.

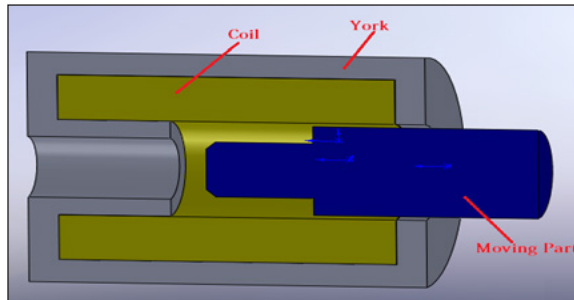


Figure 1. Structure of linear LM model

Table 1
The parameter of the linear LM model

Item	Parts	Unit (mm)
Coil	Diameter wire	4.1
	Height of coil	39.75
	Length of coil	224.5
Yoke	Back Yoke Inner	20
	Back Yoke length	265
Moving Part	Plunger diameter	80
	Plunger length	121.2
Parts		Materials
Coil wire		Copper
Yoke		Mild steel AISI 1008
Plunger		Mild steel AISI 1008

Method of the linear LM calculation

There are two types of calculations used to predict the linear LM, which are induction of coil and axial fields of finite coil.

Inductance of Coil

Figure 2 shows the air core coil and magnetic flux surrounding the conductor.

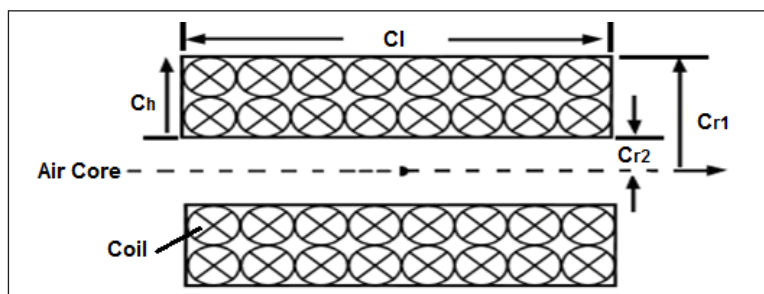


Figure 2. Cross-section of the multi-layer coil

The inductance of an air-core coil can be calculated using Equation 1, the Wheeler's formula (Johnson & Francis, 2007; Wheeler, 1982).

$$L = \frac{0.0315 (NCr)^2}{6Cr+9C_l+10C_h} \quad (1)$$

Where, L = inductance in μH ; N = Total number of turns; $Cr = (Cr_1 + Cr_2)$ = average radius in mm; C_l = Coil Length (along axis) in mm; $C_h = Cr_2 - Cr_1$ = Thickness of the winding is in mm.

Axial Fields of Finite Coil

Figure 3 shows the finite coil of the solenoid. The magnetic is measured according to x-plane.

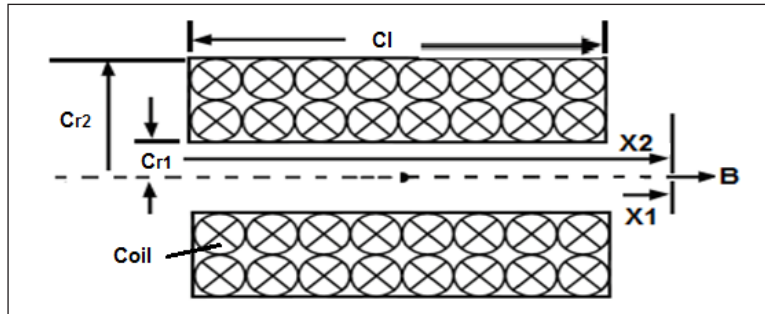


Figure 3: Solenoid in the cross-section view

The fields of a finite solenoid show that at each point, the axes are determined using Equation 2 (Engle et al., 2005; Wheeler, 1982).

$$B = \frac{\mu_0 I n}{2(Cr_2 - Cr_1)} \left[x_2 \ln \frac{\sqrt{Cr_2^2 + X_2^2 + Cr_2}}{\sqrt{Cr_1^2 + X_2^2 + Cr_1}} - x_1 \ln \frac{\sqrt{R_2^2 + X_1^2 + R_2}}{\sqrt{R_1^2 + X_1^2 + R_1}} \right] \quad (2)$$

Where, B = magnetic fields; μ_0 = Permeability constant; I = Current flow in the coil; n = number of turns; C_l = coil Length in mm; Cr_1 = Inside radius in mm, Cr_2 = Outside radius in mm, X_1 and X_2 = Distance in mm.

SIMULATIONS, RESULT AND DISCUSSION

Dynamic Simulation

The experiment aimed to revise the possible measures of the electromagnetic flux properties in the coil and to validate the simulation of the linear LM model. The coil was made using

copper wire (type 12 AWG) and the diameter of the coil was 4.1 mm with 400 turns. Figures 4, 5 and 6 display the view of the 2D-JMag model implemented in the FEMs program. Figure 4 shows the magnetic flux density is as shown in a contrasting colour and spectrum. The red colour of the magnetic flux density had the highest value that should be avoided followed by the blue region occurred in the air. Therefore, the overall magnetic flux density contour in this research was acceptable and below 2.0 Tesla when 150A current was applied.

Figure 5 is the flux line model that is implemented as a function of time for a better analysis of the simulation result. Figure 6 shows the mesh size on edge of mover at 1mm, for the coil at 6mm and for iron at 5mm.

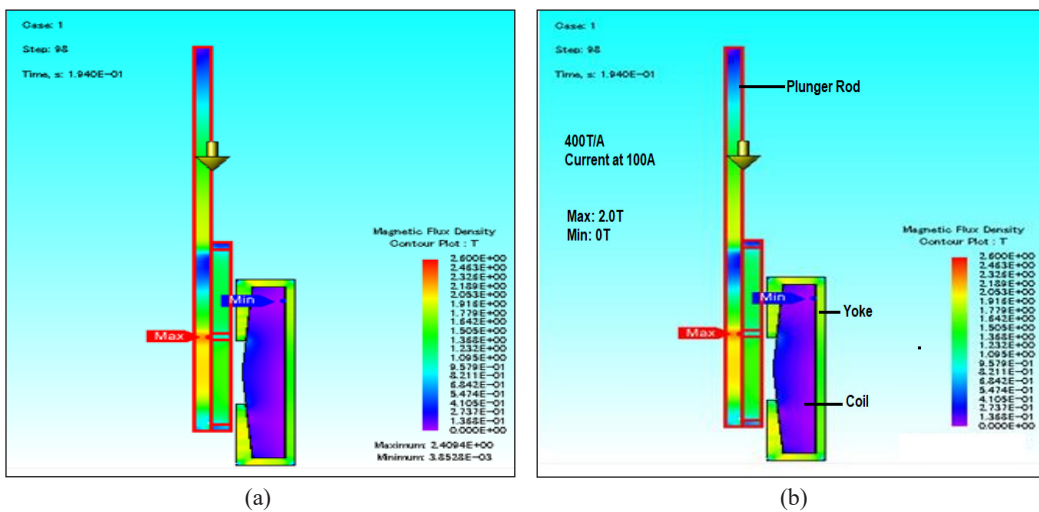


Figure 4. Magnetic flux density: (a) Before; and (b) After

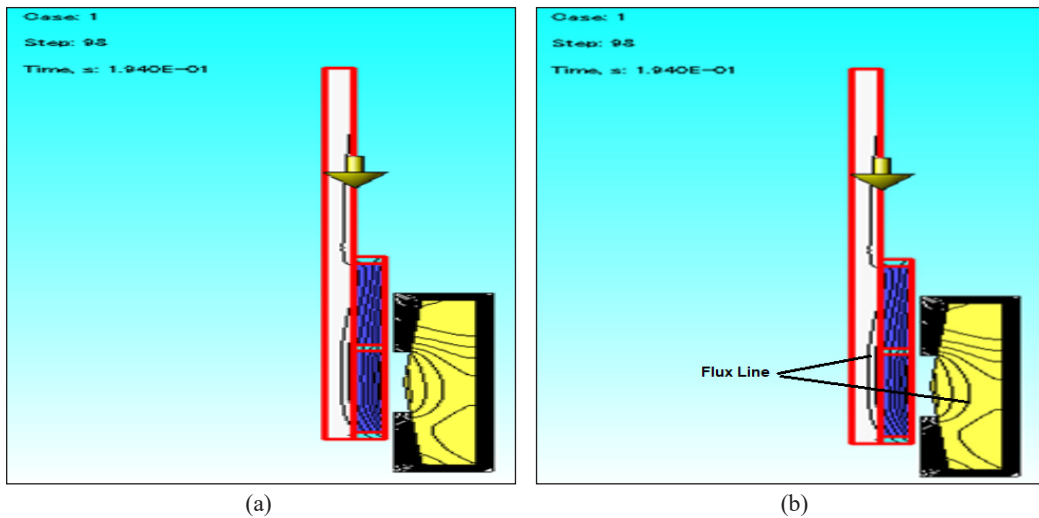


Figure 5. Flux Line: (a) Before; and (b) After

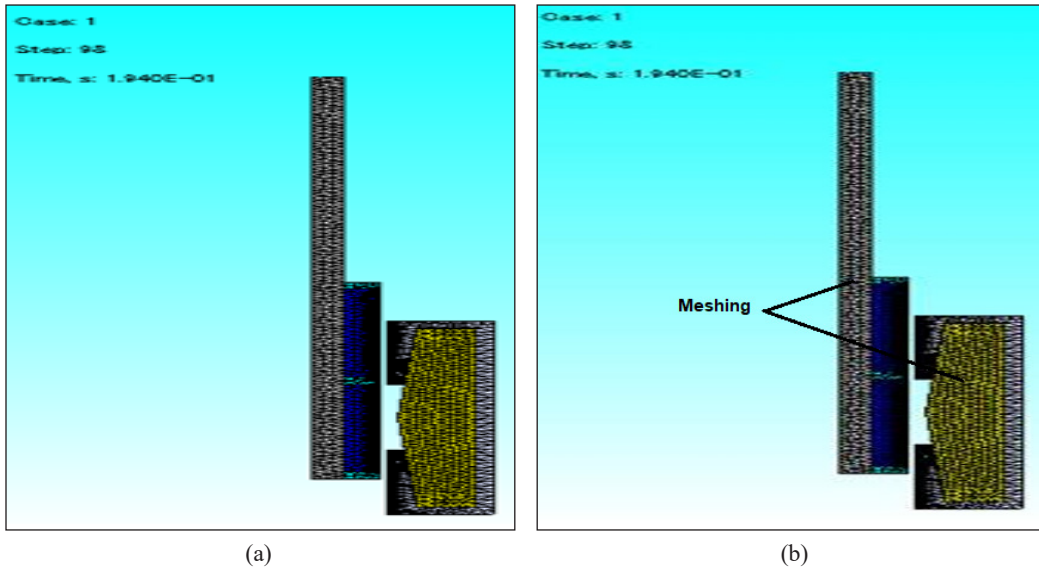


Figure 6. Meshing: (a) Before; and (b) After

Static Simulation

The combination of JMAG_RT file to MatLab/Simulink shown in Figure 7 was conducted for two situations; with load and without load. The simulation result of the linear LM model without load and with load in terms of force, speed, and displacement.

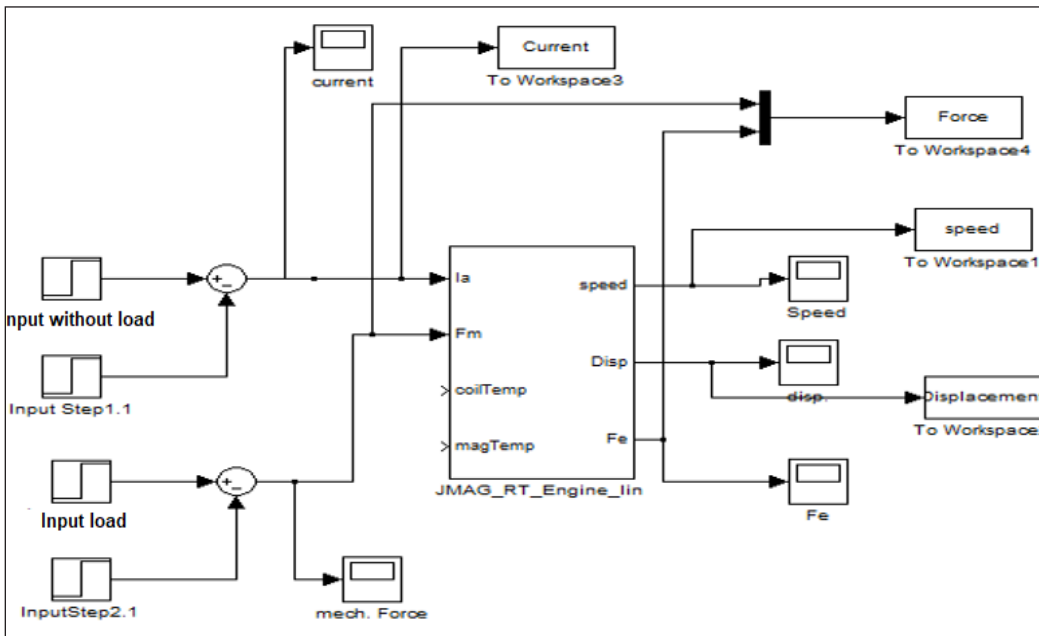


Figure 7. MATLAB/Simulink for linear LM model

Force

The graphs in Figures 8 and 9 show the relationship between force without load and load against time. Both graphs showed that the maximum force of linear LM without load was ~1.6kN while the force load was ~1.4kN at 100A supplied. Therefore, if the current is rising, the force is also increasing for both without load and load. The comparison between the force without load and load force is 12.5%.

Speed

The graphs in Figures 10 and 11 show the relationship between the speed of without load and load against time. Both graphs showed that the maximum speed of linear LM without load was ~6.1m/s while the speed load was ~2.5m/s at 100A supplied. Therefore, if the current is rising the speed is increasing for both without load and load. The comparison between the speed without load and load speed was ~59%.

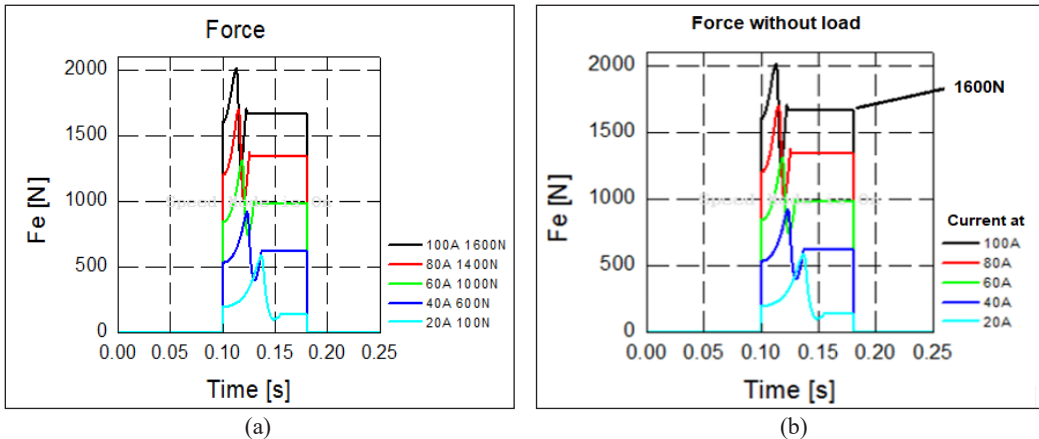


Figure 8. Force without load: (a) Before; and (b) After

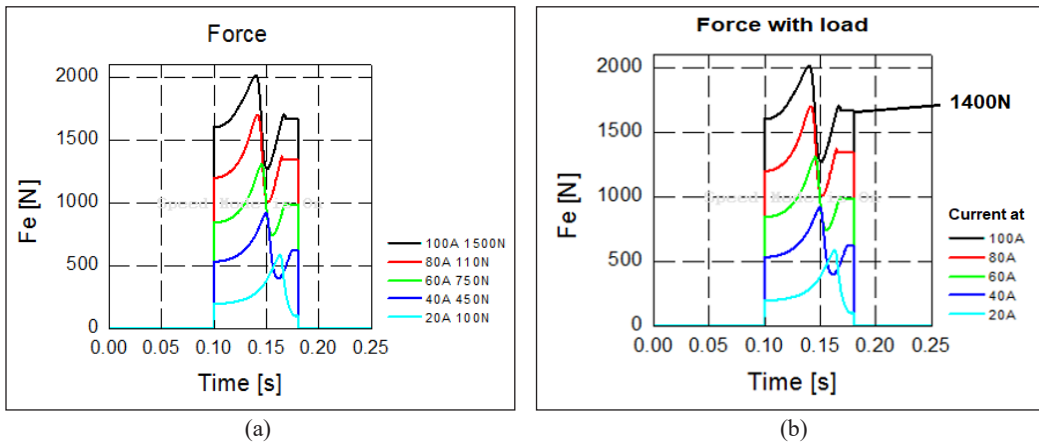


Figure 9. Force with load: (a) Before; and (b) After

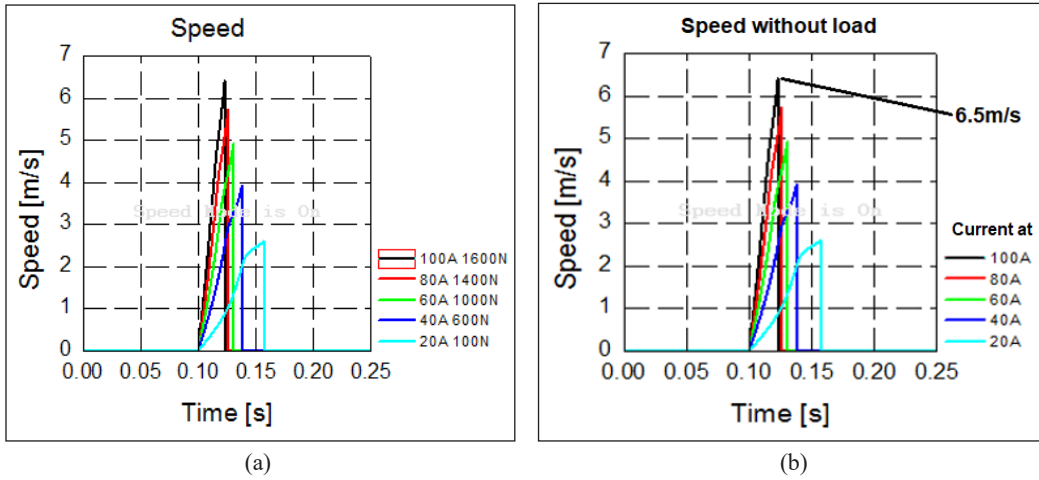


Figure 10. Speed without load: (a) Before; and (b) After

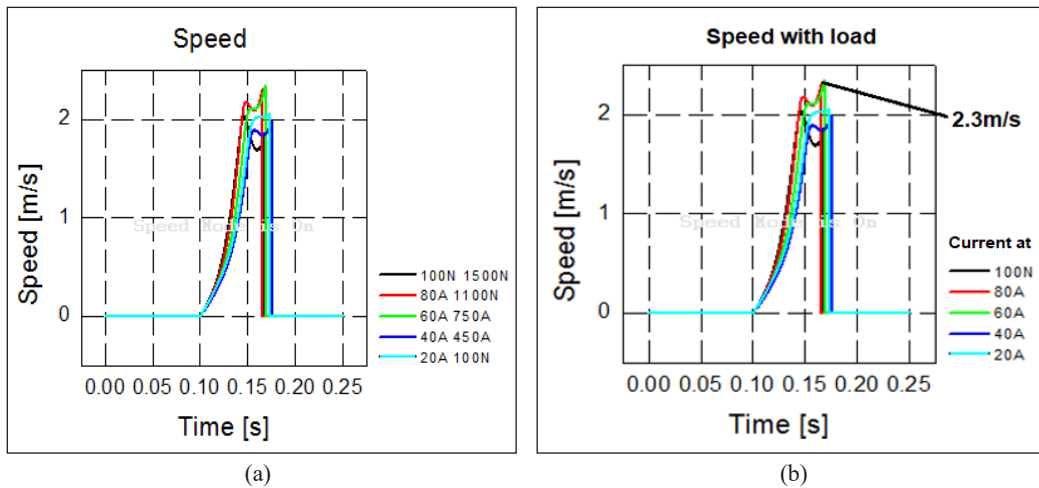


Figure 11. Speed with load: (a) Before; and (b) After

Displacement

The graphs in Figures 12 and 13 present the relationship between the plunger displacement of without load and load against time. Both graphs showed that maximum distance produced was 75mm at 100A supplied. If the current was increased, therefore the value of the plunger distance was constantly fixed at 75mm for both with and without load.

CONCLUSIONS

The design and simulation of linear launcher motor were discussed in this study. The analytical method to predict the linear launcher motor was presented by using 2D-Jmag and MATLAB/Simulink. The performance of the linear launcher motor can generate axial

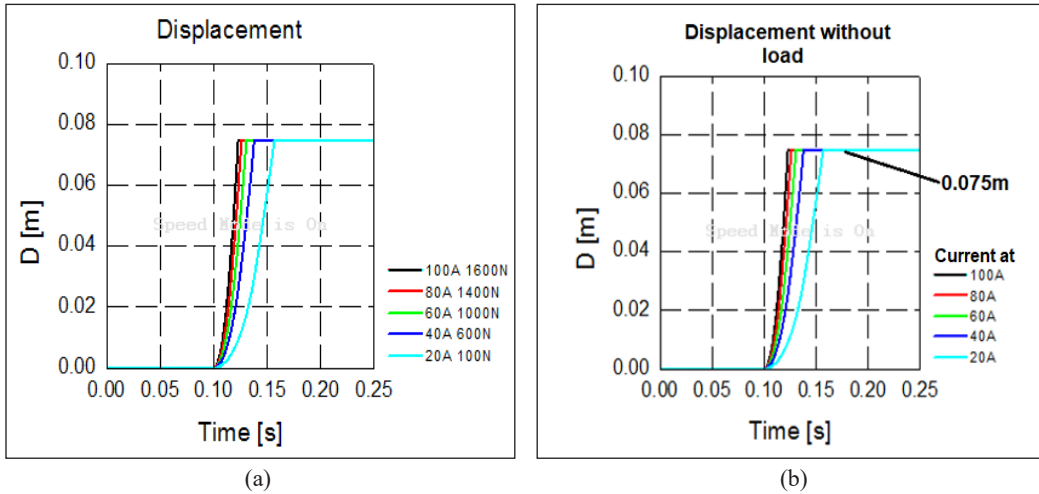


Figure 12. Displacement without load: (a) Before; and (b) After

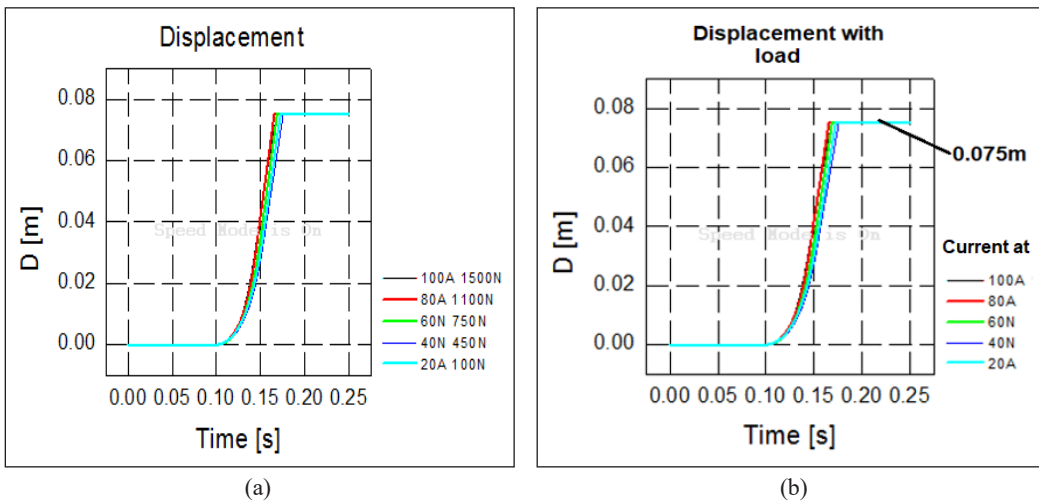


Figure 13. Displacement with load: (a) Before; and (b) After

force, speed, and displacement of with and without load such as the maximum force without load was $\sim 1.6\text{kN}$ and force with load was $\sim 1.4\text{kN}$ at 100A. Therefore, the comparison between the force without load and load force was 12.5%.

ACKNOWLEDGEMENT

The authors would like to thank Universiti Putra Malaysia (UPM) and UniKL MSI for providing financial support to carry out the research project. We would also like to express our gratitude to all my friends at UPM and UniKL MSI who have guided us during the research period

REFERENCES

- Andersson, B. S., (1991). Company perspectives in vehicle tribology-Volvo. *Tribology Series, Elsevier*, 18, 503-506. doi: [https://doi.org/10.1016/S0167-8922\(08\)70168-8](https://doi.org/10.1016/S0167-8922(08)70168-8)
- Beaty, H. W., & Kirtley, J. L. (1998). *Electric motor handbook*. New York, USA: McGraw-Hill Education.
- Bedajangam, S. K., & Jadhav, N. P. (2013). Friction losses between piston ring-liner assembly of internal combustion engine: A review. *International Journal of Scientific and Research Publications*, 3(6), 1-3.
- Bolander, N.W., Steenwyk, B. D., Sadeghi F., & Gerber, G. R., (2005). Lubrication regime transitions at the piston ring-cylinder linear interface. *Proceedings IMechE Part J: Engineering Tribology*, 219(1),19-31. doi: <https://doi.org/10.1243/135065005X9664>
- Chan, C. (1996, August 9). An overview of electric vehicle technology-challenges and opportunities. In *Proceedings of the 22nd International Conference on Industrial Electronics, Control, and Instrumentation* (pp. 1-6). Taipei, Taiwan. doi: 10.1109/IECON.1996.570892
- Chemerys, V. T. (2001). Review of the recent works of Ukrainian authors in the fields of electromagnetic acceleration and related topics. *IEEE Transactions on Magnetics*, 37(1), 16-24. doi: 10.1109/20.911782
- Engle, T. G., Nunnally, W. C., & Neri, J. M. (2005). Development of a medium-bore high-efficiency helical coil electromagnetic launcher. *IEEE Transactions on Magnetics*, 41(11), 4299-4303. doi: 10.1109/TMAG.2005.857900
- Gieras, J. F., & Piech, Z. J. (1999). *Linear synchronous motors: Transportation and automation systems*. Boca Raton, Florida: CRC Press.
- Johnson, A. J., & Francis, C. M. (2007). Elastic waves in electromagnetic launchers. *IEEE Transactions on Magnetic*, 43(1),141-144. doi: 10.1109/TMAG.2006.887443
- Laithwaite, E. R. (1975). Linear electric machines-A personal view. *Proceedings of the IEEE*, 63(2), 250-290. doi: 10.1109/PROC.1975.9734
- Matsch, L. W., & Morgan, J. D. (1986). *Electromagnetic and electromechanical machines*. New York, USA: Wiley.
- McLean, G. W. (1988). Review of recent progress in linear motors. *IEEE Proceedings B - Electric Power Applications*, 135(6), 380-416. doi: 10.1049/ip-b.1988.0042
- Miler, J. M. (2006). Hybrid electric vehicle propulsion system architectures of the e-CVT type. *IEEE Transactions on Power Electronics*, 21(3), 756-767. doi: 10.1109/TPEL.2006.872372
- Noor, N. M., Aris, I., Arof, S., Ismail, A. K., Shamsudin, K. A., & Misron, N. (2019a). Analytical study of a cylindrical linear electromagnetic pulsing motor for electric vehicles, progress in engineering technology. In M. H. A. Bakar, M. S. M. Sidik & A. Öchsner (Eds.), *Progress in Engineering Technology* (pp. 67-82). Cham, Switzerland: Springer. doi: https://doi.org/10.1007/978-3-030-28505-0_6
- Noor, N. M., Aris, I., Arof, S., Norhisam, M., & Iqbal, A. K. M. P. (2019b). Design and analytical study of tubular linear electromagnetic pulsing motor as an alternative for electric vehicle. In *Proceedings of the 3rd International Conference on Automotive Innovation Green Energy Vehicle* (Vol. 2059, No. 1, p. 020016). Maryland, USA: American Institute of Physics Inc. doi: <https://doi.org/10.1063/1.5085959>

- Say, M. G., & Taylor, E. O. (1982). *Direct current machines in introductory*. London, UK: Pitman.
- Sgobba, S. (2011). Physics and measurements of magnetic materials. In *Proceedings, 2009 CAS-CERN Accelerator School: Specialised course on Magnets* (pp. 39-63). Geneva, Switzerland: CERN.
- Wheeler, H. A. (1982). Inductance formulas for circular and square coils. *Proceedings of the IEEE*, 70(12), 1449-1450. doi: 10.1109/PROC.1982.12504



Implementation of Artificial Neural Network to Predict the Permeability and Solubility Models of Gypseous Soil

Imad Habeeb Obead¹, Hassan Ali Omran² and Mohammed Yousif Fattah^{2*}

¹Department of Civil Engineering, College of Engineering, University of Babylon, Hillah, Iraq

²Department of Civil Engineering, University of Technology, Baghdad, Iraq

ABSTRACT

The objective of the present study is to make a database that describes the leaching-permeability behavior of collapsible gypseous soil. The data will be implemented to develop ANN prediction models for predicting the saturated coefficient of permeability and percentage of solubility by weight. The complex soil behavior and tedious and time consume in soil testing have driven researchers to use Artificial Neural Network (ANN) as tool for prediction. The objectives of the study were to investigate leaching-permeability behavior of collapsible gypseous soils and to develop ANN models for estimating the saturated coefficient of permeability and solubility of the soils. The MATLAB R2015a software was used to predict the saturated coefficient of permeability and the solubility percentage by weight of gypseous soils. The dataset used in this work included (513) records of experimental measurements extracted from leaching-permeability tests conducted on gypseous soil samples taken from Baher Al-Najaf in Iraq. Four input variables were investigated to have the most important influence on the permeability and solubility percentage by weight. According to the achieved statistical analysis, the ANNs model have a

reliable capability to find out the predictions with a high-level of accuracy. The gypseous soils exhibited a high rate of dissolution of soluble minerals content, which caused increase in the coefficient of permeability as the soil samples reach the state of long-term full saturation.

Keywords: Artificial neural networks, electric conductivity, gypseous soil, leaching-permeability tests, MATLABR2015a, solubility of gypsum, total dissolved salts

ARTICLE INFO

Article history:

Received: 12 February 2020

Accepted: 23 July 2020

Published: 22 January 2021

DOI: <https://doi.org/10.47836/pjst.29.1.06>

E-mail addresses:

eng.imadh2005@yahoo.com (Imad Habeeb Obead)

hassan7745@gmail.com (Hassan Ali Omran)

myf_1968@yahoo.com (Mohammed Yousif Fattah)

* Corresponding author

INTRODUCTION

Collapsible soils or metastable soils are unsaturated soils that undergo a considerable volume change upon saturation with or without additional load. Generally, collapsible soils maintain an open “honey-combed” structure that can induce negative pore water pressure and cementing agents that result in considerable shear strength. As a result of wetting, effective stresses are reduced due to the dissipation of the negative pore water pressure.

The prevalent of Gypseous soils of higher gypsum content (more than 25%) for shallow depth less than 2 m according to Barazanji (1973) with particularly northwest and southwest parts of Iraq. Also, for lower content of gypsum in the central and southern parts of Iraq, it is the major problem. This was pointed out in the surrounding area of hydraulic structures in specific, and constructions in general. Numerous researchers investigated and discussed the many factors influencing the behavior of gypseous soils and their hydro-mechanical properties.

Ibrahim and Schanz (2017) examined the improvement of gypsiferous soil properties by using silicone oil to minimize the effects of moisture and gypsum loss. The work was conducted on artificial gypsiferous soil (30% Silber sand and 70% pure gypsum) treated with silicone oil in different percentages. Silicone oil was selected as an additive because of leakages of oil-related products from an oil refinery north of Iraq built on gypsiferous soil. Thus, this oil product provided a suitable analogue for oil that had infiltrated the foundation soil of the refinery buildings. The results showed that the silicone oil was a suitable material for modifying the basic properties of the gypsiferous soil, such as collapsibility and shear strength.

Fattah and Dawood (2020) tried to investigate the behavior of the gypseous soils and the effect of factors on the collapsibility characteristics such as initial conditions. Three types of gypseous soils had been experimented in this study, sandy gypseous soil from different parts of Iraq. Large-scale model with soil dimensions (700*700*600) mm was used to show the effect of water content-changes in different relations (collapse, stress and suction with time relations). The study showed that the collapse-potential, the soil-suction and the soil-strength were affected by the initial-conditions (water-content and dry unit weight). The collapse potential for all soil types increased when the water content increased due to a reduction in matric suction of the soil. The small value of the collapse that was obtained for all models was related to a number of factors such as dense condition, high compaction, capillary tension and cementing agent between soil particles. All these reasons make soil strong and more rigid to collapse.

The study carried out by Ashour et al. (2020) included large numbers of sandy and silty specimens of collapsible soils with different initial conditions to develop a correlation that evaluated the collapse potential C_p of the soil due to inundation. The presented model

reflected the significant influence of degree of saturation S_r on C_p of inundated soil which considerably decreased by the increase of S_r . The determined properties of inundated collapsed soil, such as void ratio and angle of friction were employed to construct the post-inundation stress-strain curve. Comparisons between predicted and measured stress-strain curves of inundated collapsible soils were presented for validation. A brief review of some of these ANNs related researches is presented in this paper.

Al-Janabi (2006) utilized multilayer perception training using the back propagation algorithm to build two ANN models, one for dissolved gypsum (DG) and the other for leaching strain (L.S). It was found that ANNs had the ability to predict the dissolved gypsum and leaching strain through process in gypseous soils with a good degree of accuracy.

Sinha and Wang (2008) presented artificial neural network models relating to permeability, maximum dry density and optimum moisture content as output variables with classification properties of the soils. Their study was based on the experimental results for samples of clayey soil. They introduced three ANNs models, one for each maximum dry density, optimum moisture content and coefficient of permeability. In addition to the combined ANNs model to estimate the above output variables together. The prediction models showed good accuracy.

Al-Ani et al. (2009) used artificial neural networks to relate the properties of gypseous soils and evaluated the values of compression of soils under different conditions of soaking and washing. ANNs were used for modeling the settlement ratio for wetting process, $(S/B)_w$, and the settlement ratio for soaking process, $(S/B)_s$ (where S is the settlement of footing of width B and w and s refer to washing and soaking, respectively). It was found that ANNs had the ability to predict the compression of gypseous soil due to soaking and washing process with high degree of accuracy. The results also showed that the initial gypsum content, stress level and time had smaller impact on the settlement ratio than other variables. It was concluded that the ANNs had the ability to predict the $(S/B)_w$ and $(S/B)_s$ of gypseous soil with high degree of accuracy. The equations obtained using ANNs for $(S/B)_w$ and $(S/B)_s$ showed excellent correlation with experimental results where the coefficients of correlation were (0.9541) and (0.991), respectively.

Tizpa et al. (2015) presented ANNs prediction models that correlated compaction parameters, permeability, and shear strength with the soil index characteristics that could be measured easily. They utilized the datasets of the geotechnical laboratory of the University of Bahia in Brazil. Their obtained results showed high accuracy for ANNs prediction models when compared with the experimental datasets.

The objectives of the study were to investigate leaching-permeability behavior of collapsible gypseous soils and to develop ANN models for estimating the saturated coefficient of permeability and solubility of the soils.

MATERIALS AND METHODS

Materials and Testing Procedures

The leaching-permeability experiments were carried out on disturbed mixed soil specimens taken from Baher Al-Najaf west of Iraq, the gypsum content ranged between 17% and 36%. Hydraulic experiments of leaching – permeability were conducted to investigate the saturated permeability and solubility of soil specimens. The soil samples were remolded to match the natural soil condition, i.e., the field density state. In this work, the soil specimens were leached in the constant head permeameter, initially carried out by permitting the soil specimen to saturate by maintaining the same water level in the inlet and outlet. Then, the water level in the inlet was raised and preserved at a constant level to output flow at a specific hydraulic gradient. A hydraulic gradient of 6.67, corresponding to a head of 1.0 m was considered to produce a significant fluctuation in groundwater elevation in the studied area. The testing procedures used by Ismael (1993) and Ismael and Mollah (1998) were modified to suit the present work conditions.

The testing procedures were conducted according to Ismael (1993) and Ismael and Mollah (1998). The samples were 70 mm in diameter and 150 mm in height, the main parts of the leaching device used comprised of constant head permeameter, water reservoir, and graduated cylinder to collect the leached water. The soil samples were poured inside the permeameter cylinder in layers with the vibration to reach the desired field density. Water from the reservoir was passed through the specimen at its bottom to drain at the top in order to simulate the soil saturation in the field due to rising of ground water table. Readings for total dissolved salts (TDS), temperature, pH, and electrical conductivity (EC) of the of leachate discharge that was accumulated in cylinder every one hour during the experiment period. The variations in the above parameters were recorded and used to evaluate the degree of salts dissolution of the soil samples. Leaching was assumed to have been terminated when the reading of these measuring units showed no further decrease. The experiments were conducted utilizing the setup shown in Figure 1.

The leaching period extended for seven days per each tested soil sample, the process in the laboratory was accomplished using ordinary drinking water.

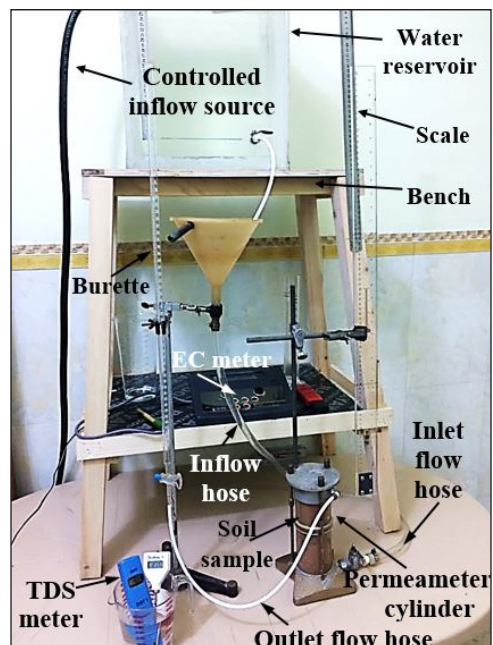


Figure 1. Experiment setup for permeability-leaching tests

Three devices were used to measure the dissolved materials, namely: the EC214 an electrical conductivity meter, and two portable devices which were the total dissolved-solids tester (TDS) and pH tester as shown in Figure 2. They were manufactured by Hanna Instruments Company, Romania.

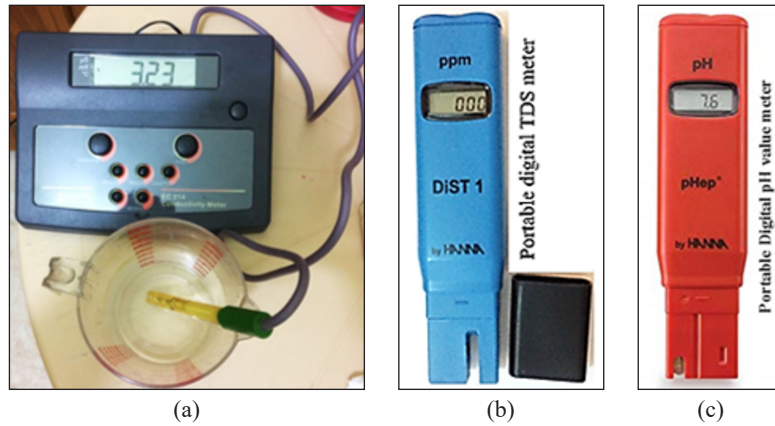


Figure 2. (a) EC; (b) TDS; and (c) pH value testers

Artificial Neural Network Technique

The artificial neural networks (ANNs) are preferably suitable for use in the field of water resources and geotechnical engineering since it can make use of heuristic knowledge or pattern matching method instead of resolving the mathematical equations. ANNs considered as computational tools that have the ability to learn with time and adjust the trend of varying of definite parameter in an explicit data (Al-Lamy, 2008). The ANNs structure and operation contain of a number of artificial neurons identified as "nodes" or "units" that is typically organized in layers namely; input layer, output layer and one or more hidden layers as shown in Figure 3.

According to Shahin et al., (2001) and Sinha and Wang (2008), the above architecture is termed multilayer perceptrons (MLPs) that consist of three layers ANNs, which is the furthestmost widely used in geotechnical engineering. In this study, the four input variables per each site involved to implement the ANNs model are; total dissolved salts (TDS) expressed in part per millions (ppm), electric conductivity (EC) in ms, time (t) in hrs, and temperature of leachate (T) in °C. Consequently, the input

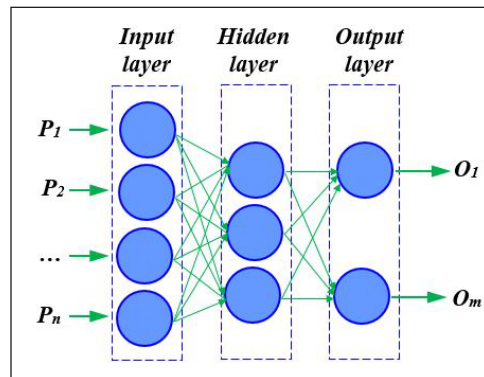


Figure 3. Structure and operation layout of the neural networks

layer contains four neurons. A typical neural network was established in this study in MATLABR2015a software in which, the saturated coefficient of permeability (K_{sat}), and the solubility of the gypsum (S) which were expressed as weight percentage and trained with the input variables. The leaching-permeability test results were analyzed together with the percentage of solubility of gypsum to be used as dataset as listed in Table 1 to develop the artificial neural network models.

Table 1
Descriptive statistics of gypseous soil parameters used in the permeability and solubility models

Site No.	Parameter Statistics	K_{sat} (cm/s.)	S% by wt.	TDS (ppm)	EC (ms)	T (°C)
#1	Max.	1.502×10^{-2}	24.421	1577.0	3.440	24.40
	Min.	2.148×10^{-3}	0.517	1261.0	2.450	22.30
	Mean	8.61×10^{-3}	14.973	1425.643	2.831	23.001
	Standard deviation	2.818×10^{-3}	5.955	65.057	0.20	0.464
#2	Max.	2.59×10^{-2}	8.754	1529.0	3.360	23.0
	Min.	2.01×10^{-3}	1.772	1419.0	2.90	21.500
	Mean	2.07×10^{-3}	7.008	1447.526	3.092	22.071
	Standard deviation	4.37×10^{-3}	1.287	23.061	0.124	0.374
#3	Max.	2.91×10^{-3}	7.280	1503.0	3.306	21.60
	Min.	2.10×10^{-3}	4.072	1461.0	2.94	20.41
	Mean	2.69×10^{-3}	6.546	1472.942	3.193	21.126
	Standard deviation	2.24×10^{-4}	0.784	9.294	0.081	0.346

RESULTS AND DISCUSSION

The results of physical and chemical properties of the natural soil samples are presented in Table 2.

During leaching, the leached soil sample is subjected to progressive dissolution of soluble salts within the soil matrix, the leaching effect becomes clearer in soils of high gypsum content. This is due to the fractional abstraction of soluble materials, and the inter-particle binding related to it. The losses in the original weight of the soil sample after starting of the leaching process can be idealized mathematically as Equation 1:

$$W_n = W_o - W_l \quad [1]$$

where, W_n = the new weight of soil sample after the leaching process at time step Δt , (N), W_o = the original weight of soil sample before the leaching process, (N) and W_l = the weight lost from soil sample after the period of Δt from starting of the leaching process, (N).

Table 2
Summary of physical properties and chemical tests for the natural soil samples (after Fattah et al., 2019)

Site No.	Field density ρ_d (gm/cm ³)	Natural moisture content (%)	Initial void ratio e_o	Gravel (> 4.75) (mm)	Sand (4.75-0.075) (mm)	Silt and Clay (<0.075) (mm)	D_{30} (mm)	Gypsum content γ (%)	Chloride, Cl- (%)	pH*	Classification USCS
1	1.417	1.25	0.79	20.50	78.90	0.58	1.80	40.11	0.117	8.0	SP, Poorly graded sand with gravel
2	1.507	1.13	0.63	4.35	88.20	7.45	0.43	20.42	0.107	8.22	SP- SM, Poorly graded clean sand with silt
3	1.404	0.83	0.78	12.45	84.60	2.95	2.60	28.98	0.097	8.15	SP, Poorly graded sand

* Averaged values for soil samples per each site

Based on the principle of conservation of mass and due to the dissolution of gypsum and other soluble salts in the soil matrix, the dissolved salts will be diffused in the solution (Equation 2).

$$W_l = \gamma Q \Delta t \quad [2]$$

where, γ = the unit weight of leachate in (F/L³),
 Q = the flow rate of water through soil sample in (L³/T), and
 Δt = time step in (T).

Simplifying Equation 2 yields Equation 3 and Equation 4:

$$W_l = \gamma \times K_{sat} \cdot i \cdot A \times \Delta t \quad [3]$$

where, K_{sat} = saturated coefficient of permeability for the soil in (L/T),
 i = the hydraulic gradient (dimensionless), and
 A = the cross sectional area of the soil sample in (L²).

$$W_\ell = (TDS_L - TDS_w) \times K_{sat} \cdot iA \times \Delta t \quad [4]$$

where, TDS_L = the total dissolved salts in the leachate in F/L³, and
 TDS_w = the total dissolved salts in the water in F/L³. The range for TDS_w considered in this work is 590 to 630 ppm for a range of temperatures (22 to 24.5°C).

Rearranging both sides of Equation 4 for the next time step, gives Equation 5:

$$W_{lt_{j+1}} = W_{lt_j} - K_{sat}.iA \times (TDS_L^{t_{j+1}} - TDS_w)(t_{j+1} - t_j) \quad [5]$$

where, W_{lt_j} = the weight of soil sample leachate from the previous time step.

Substitution Equation 4 in Equation 1, then the net weight of leachate soil at the end of leaching process can be expressed as Equation 6:

$$W_n = W_o - iA \times \sum_{j=0}^{j=n} (TDS_L^j - TDS_w)(t_{j+1} - t_j) \times K_{sat}. \quad [6]$$

The percentage of the soluble weight at any time of leaching period pointed out as solubility percentage (Equation 7):

$$\% S_{by\ wt.}^{t_{j+1}} = \frac{W_{\ell}^{t_{j+1}}}{W_o} \times 100 \quad [7]$$

where, $\% S_{by\ wt.}^{t_{j+1}}$ is the percentage of the soluble weight, and

t_{j+1} is the time step within leaching period at which removal weight is calculated.

It is noticed that Equation 5 may use an average value of K_{sat} that is obtained at the end of the leaching period. For more precise results, the value of K_{sat} could be measured and used at the end of each time step from the starting of the leaching process as adopted in Equation 6. Figure 4 presents the removal or soluble weight (averaged at one day intervals up to seven days testing period of leaching process) due to the dissolution of minerals

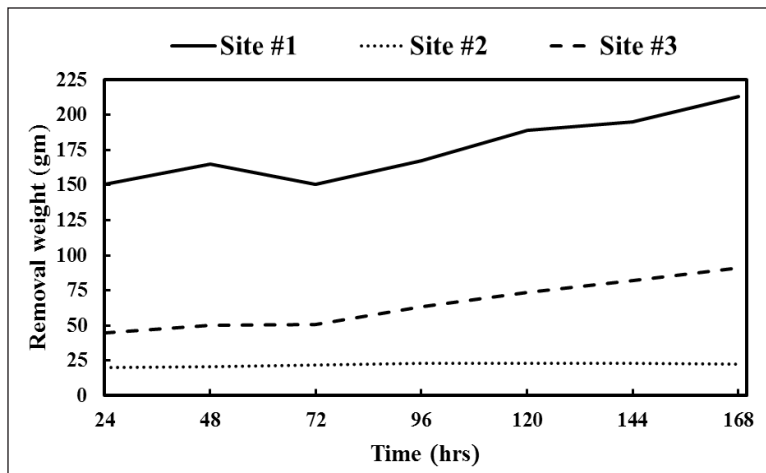


Figure 4. Removal weight for gypseous soil from different sites with leaching time

from leached soil sample versus time of leaching for the three sites. The original weights of soil samples before the leaching process per each site were 6.29 N, 6.69 N, and 6.24 N, respectively. Figure 4 shows the variation of removal weights from gypseous soil samples taken from different sites.

Results from Figure 4 show increasing the dissolution with time for soils at both sites #1 and #3 before roughly reaching a steady value. While for site #2, the dissolution was not increased significantly with time and the trend was maintained constant. The initial content of gypsum and the presence of perceptible content of chloride salts play a significant role as they change during the leaching process. In addition, the mutual interaction of soluble salts leads to a higher increase of the solubility rates that implies the expansion of voids and increasing the soil's permeability, while for field condition, the permeability probably

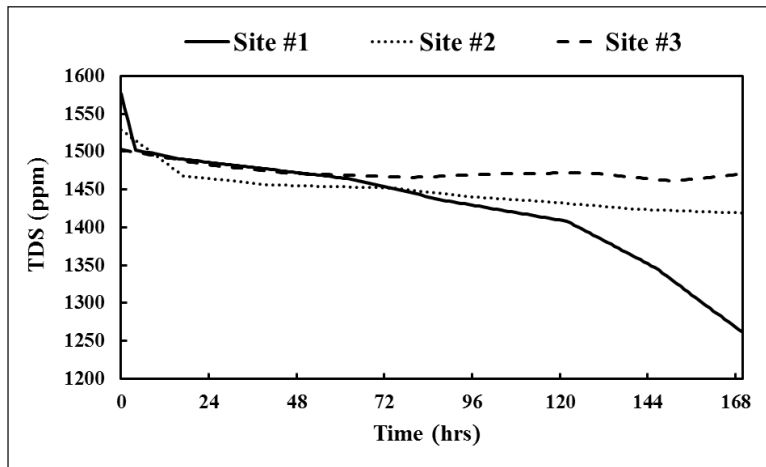


Figure 5. Variation of TDS of gypseous soils from different sites with leaching time

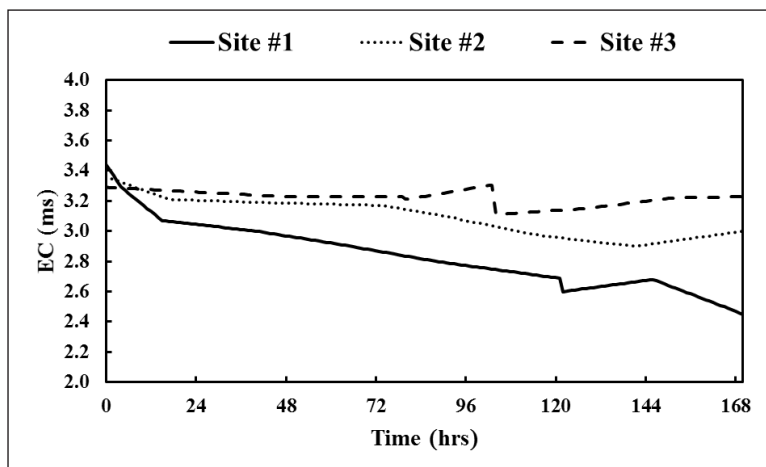


Figure 6. Variation of EC of gypseous soils from different sites versus leaching time

decreases as a consequence to the collapse of soil structure under the impact of applied loads (Fattah et al., 2019). Figure 5 to 8 show the variations of studied parameters [i.e., TDS in ppm, EC in ms, the percent the percent of solubility S% by weight, and saturated coefficient of permeability (K_{sat}) in cm/s.] with leaching time.

The TDS and EC versus time curves at different sites are shown in Figure 5 and 6, respectively. It is evident that TDS and EC measures decreased rapidly to around (20% and 29%) for site # 1 throughout the seven days of leaching process, whereas the measured TDS and EC values decreased slightly to about 7% and 11% for site #2 and the rates were about 2.2% and 1.9% for site #3. It is expected that the infiltrated water into the soil specimen for each site dissolved the concentrated soluble salts causing the release of ions and elements, which affected the electric conductivity of the leachate, but this did not reflect the similar declining trend for all sites. Eventually, the rapid trends of decrease were more widely clear for site #1 than those of the other sites as it is obvious from Figure 5 and 6, respectively. The initial gypsum content was lumped and compacted on grains of sand and gravel. Later, the leaching process caused structural weakness and loss of the bonds provided by gypsum. The voids were enlarged and occupied by the increased water as stated by Nashat (1990).

Figure 7 shows the variations of the coefficient of permeability under saturated condition versus leaching time. The initial value of steady-state coefficients of permeability was around a value of 1.5×10^{-3} cm/s per each site, the rates of increase in K_{sat} were 1.4%, 2.4% and 0.07% for these sites, respectively. The higher rate for site #2 was probably attributed to the progressive erosion of fines due to piping. In addition to the dissolution of salts contributed to a weight loss of this sample. Despite that the Site #2 samples had a rather lower gypsum content (Table 2).

Results in Figure 8 reveal the percentage of solubility for three different sites versus time. It is evident that the Site #1 sample yielded higher %S of 24.2% in comparison with 7.0% and 3.1% for Sites #2 and #3, respectively. Subsequently the soil samples taken from site #1, which had the higher content of soluble minerals as given in Table 2, then lost more gypsum/salt by weight. The pH measurements of the leachate from the soil samples taken from three sites investigated in this work were roughly constant as given in Table 2. These results are indicating the slight sensitivity of the pH values of the various contents of soluble salts. The pH measurements of the leachate from the soil samples taken from three sites investigated in this work were roughly constant as given in Table 2. These results indicate the slight sensitivity of the pH values for various contents of soluble salts.

As noticed from the forgoing results and discussion, in addition to results given in Table 3, the traditional nonlinear correlation equations for permeability and solubility per each site are proposed. The results showed that prediction model of the saturated coefficient of permeability did not provide strong relation. Hence, there is a difficulty to develop a general precise model for permeability and/or solubility via the traditional statistical techniques

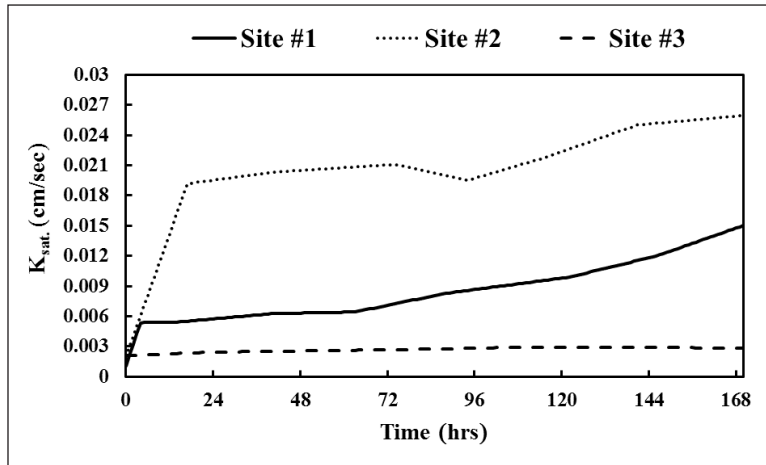


Figure 7. Variation of K_{sat} of gypseous soils from different sites with leaching time

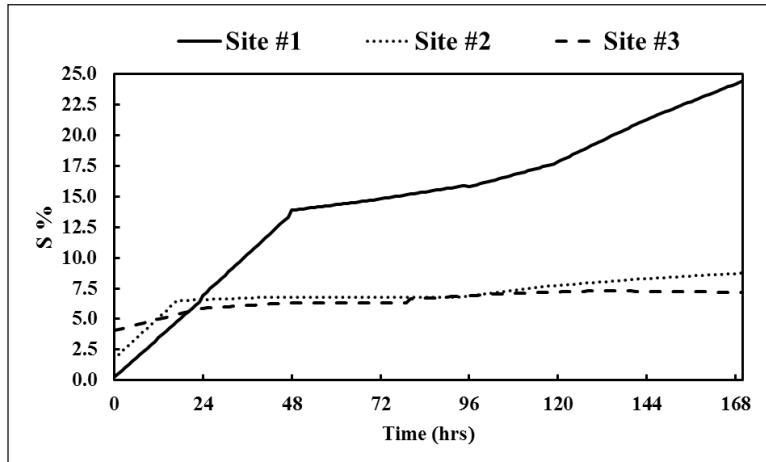


Figure 8. Variation of %S of gypseous soils from different sites with leaching time

in order to correlate overall affecting variables to include the studied sites although that the data include sufficient geotechnical and chemical properties in addition to the gypsum contents.

Comparisons between Figure 4 to 8 reveals that the decrease in TDS and EC with time was related to the increase of removal of soil weight, saturated permeability, and solubility percent.

Collapse may not induce the real problem of collapsible soil because full saturation of soil samples is not maintained. Fattah et al. (2017) concluded that the collapse potential resulted from complete wetting of soil layer might not be achieved in the field, due to the inability to reach full saturation state through a single step wetting. Therefore, the multi-step wetting procedure is more convenient due to the slowly rising of ground water by

Table 3
Traditional correlation models

Site No.	Dependent Variable	Correlation Model	Coefficient of Determination (R ²)
#1	$K_{sat.} (cm/s.)$	$K_{sat.} (TDS) = -4.0 \times 10^{-4}TDS + 0.0707$	0.9876
		$K_{sat.} (EC) = 0.0127EC^2 + 0.0861EC + 0.1501$	0.9418
	%S	$\%S (TDS) = -0.0004TDS^2 + 0.9501TDS - 587.98$	0.8986
		$\%S (EC) = -28.429EC + 95.334$	0.929
#2	$K_{sat.} (cm/s.)$	$K_{sat.} (TDS) = -1.0 \times 10^{-6}TDS^2 + 0.0026TDS - 1.7556$	0.9374
		$K_{sat.} (EC) = -0.1393EC^2 + 0.8334EC - 1.2226$	0.8074
	%S	$\%S (TDS) = -0.0545TDS + 85.835$	0.9524
		$\%S (EC) = -36.511EC^2 + 216.93EC - 314.12$	0.8719
#3	$K_{sat.} (cm/s.)$	$K_{sat.} (TDS) = 487.28e^{-0.008TDS}$	0.7721
		$K_{sat.} (EC) = -0.4831EC^2 + 3.1041EC - 4.9833$	0.9605
	%S	$\%S (TDS) = 1 \times 10^{09}e^{-0.013TDS}$	0.8171
		$\%S (EC) = 1438.1EC^3 - 13933EC^2 + 44975EC - 48364$	0.5277

capillary forces, especially in the low rainfall regions. So that, the results of leaching are more appropriate to present the problem of collapsible soil.

Estimation of the Separated ANN Models for $K_{sat.}$ and S% by Weight

Determination of the ANNs architecture is considered as a major and difficult objective in ANN’s model derivation (Shahin, 2003). Four variables were involved as input, the throughout dataset consisting of 513 samples which were divided into two subsets as training set and test set, thus randomly about 11% of the throughout data (56 inputs) were extracted as test set, the remaining 457 inputs or 89% of the over data were used as training set. The neural network properties used in this study were as follows. The training network type was a feed-forward back propagation technique. The multilayer perceptron network was adopted including three layers, four to ten neurons were experienced in order to reach to the best number of neurons in hidden layer per each model, the models consisted of eight neurons. The training function is “TRAINGDX” which updates weights and bias values by gradient descent rule to back- propagation errors through the network, the transfer (activation) function is ”LOGSIG” which calculates a layer’s output from its net input. A detailed demonstration of this function is available in the literature such as Shahin (2003). The performance of training was maintained by the mean squared error (MSE) criterion for an epochs number of 1000. The architecture of an ANN for estimating both $K_{sat.}$ and S% by weight is shown in Figure 9.

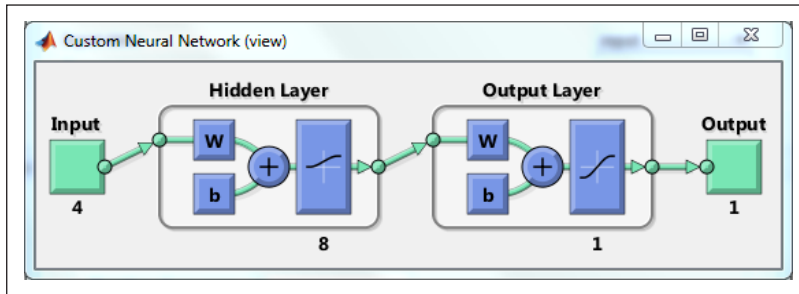


Figure 9. Architecture of ANN model predictions for K_{sat} and $S\%$ by weight

Statistical Evaluation of the ANN Models

In this study, some statistical approaches were used to evaluate the ANN models, these statistics are coefficient of correlation (R), root mean square error (RMSE), and coefficient of residual mass (RM).

The coefficient of correlation (R) can be calculated as Equation 8:

$$R = \frac{\sum_{i=1}^n (x_i - \bar{X})(y_i - \bar{Y})}{\sqrt{\sum_{i=1}^n (x_i - \bar{X})^2 \sum_{i=1}^n (y_i - \bar{Y})^2}} \quad [8]$$

where, x_i is the desired (measured) output, $x_i = x_1, x_2, \dots, x_n$, y_i is the model (predicted) output, $y_i = y_1, y_2, \dots, y_n$, \bar{X} and \bar{Y} are the mean measured and predicted output, respectively, and n is the number of data.

The root mean square error (RMSE) can be calculated as Equation 9:

$$RMSE = \sqrt{\frac{\sum_{i=1}^n (y_i - x_i)^2}{n}} \quad [9]$$

The coefficient of residual mass (RM) can be determined as Equation 10 (Tizpa et al., 2015):

$$RM = 1 - \frac{\sum_{i=1}^n y_i}{\sum_{i=1}^n x_i} \quad [10]$$

The coefficient of correlation is a measure that is used to determine the relative correlation and the goodness of fit between the predicted and measured data; while, the RMSE is the most popular measure of error and has the advantage that large error receives much greater attention than small errors (Al-Lamy, 2008). Tizpa et al. (2015) stated that the RMSE expressed the residual error variance; if the output fitted a dataset,

its value was minimum. When the value of RMSE is lower, the accuracy of the predicted model accordingly is higher, for the value RMSE is equal zero, a perfect fit is the case. The coefficient of residual mass, RM, is a different analysis of the measured and predicted outputs. The ideal value of RM is zero, whereas negative values indicate overestimation and vice versa. For evaluating the overall validity of ANN prediction models, assessments were performed by the ANN training regression plots as shown in Figure 10 that shows the comparing values for the coefficient of correlation between training and testing of the

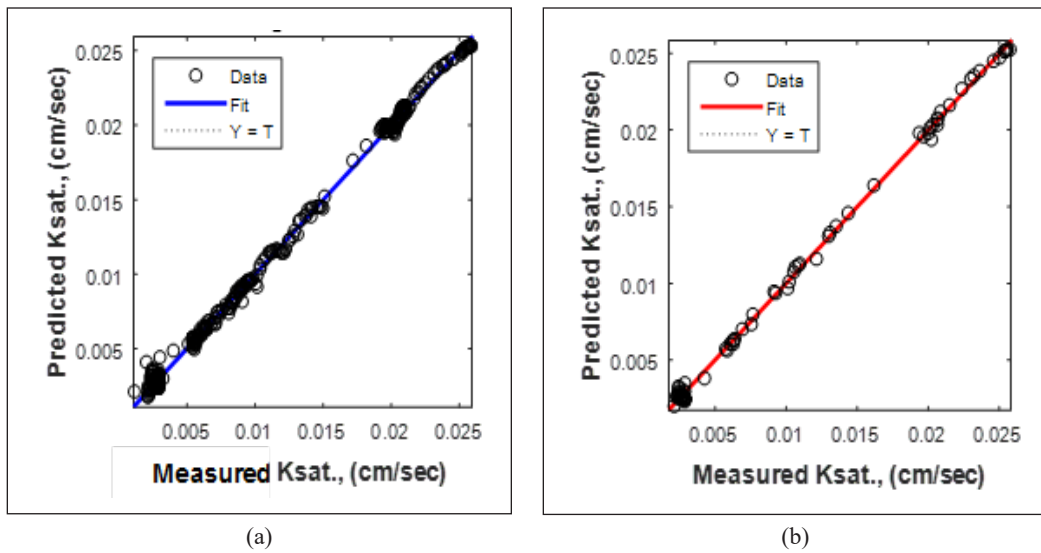


Figure 10. Neural network training regression of ANN model for the coefficient of permeability: (a) Training for $K_{sat.}$ model; and (b) Test of $K_{sat.}$ model

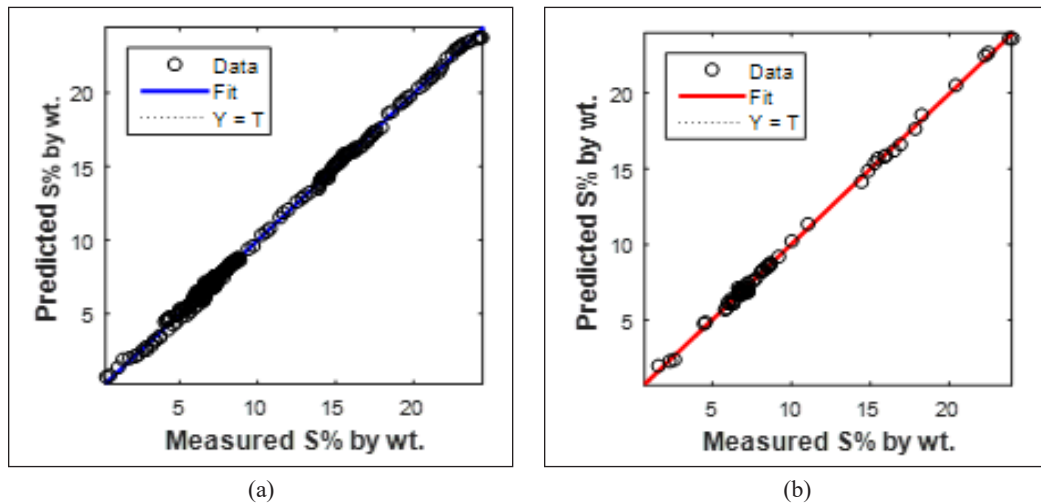


Figure 11. Neural network training regression of ANN model for the solubility percentage by weight: (a) Training for $K_{sat.}$ model; and (b) Test of $K_{sat.}$ model

Table 4
Models evaluation criterion

Model	Statistics	R%	RMSE	RM
	K_{sat} (cm/s.)	99.9912	3.41×10^{-04}	7.16×10^{-04}
	S% by weight	99.93	0.1957	1.52×10^{-04}

model. It is evident that acceptable correlation is obtained, and Figure 10 indicates a good correlation since R approaches to unity. Also, a perfect agreement was obtained between the measured and predicted values as indicated by the overall correlation coefficient.

Figure 11 shows the training regression plots for ANN model of the percent of solubility S% by weight. Results of Figure 11 reveal that as for K_{sat} model, a higher correlation is obtained between the training and testing of the S% model. As well as, a complete covenant between the measured and predicted values occurs as shown by the overall correlation coefficient.

Table 4 summarizes the statistical evaluation criterion for both ANN models. It can be noticed that acceptable values for the statistic parameters are obtained. It is concluded that strong correlations for prediction of both K_{sat} and S% could be obtained.

CONCLUSIONS

Based on the results of this study, the following conclusions may be drawn:

- The gypseous soils exhibited a high rate of dissolution of soluble minerals content, which caused increase in the coefficient of permeability as the soil samples reached the state of long-term full saturation.
- Artificial neural networks had the capabilities to predict the saturated coefficient of permeability (K_{sat}) and solubility percentage by weight (S) as a function to TDS, EC, T, and t of gypseous soil with higher accuracy according to the statistical parameters as the coefficient of correlation ranged between 99.99% and 99.93%.
- The leaching-permeability behavior of collapsible gypseous soils had been dealt with to develop ANN models for estimating the saturated coefficient of permeability and solubility of the soils. The datasets used in the model development had involved significantly the most influencing factors that might affect both the permeability of gypseous soils and solubility percentage which were TDS, EC, the temperature of leachate (T), and leaching time (t) of gypseous soil. These factors are usually faced in the practice of engineering.

ACKNOWLEDGEMENT

The authors would like to acknowledge the Civil Engineering Department of the University of Technology – Iraq for support and encouragement.

REFERENCES

- Al-Ani, M. M., Fattah, M. Y., & Al-Lamy, M. T. A. (2009). Artificial neural networks analysis of treatment process of gypseous soils. *Engineering and Technology Journal*, 27(9), 1811-1832.
- Al-Janabi, K. R. M. (2006). *Laboratory leaching modelling in gypseous soils using artificial neural network (ANN)* (PhD Thesis). University of Technology, Baghdad, Iraq.
- Al-Lamy, M. T. A. (2008). *The use of acrylate in grouting some Iraqi gypseous soils* (PhD Thesis). University of Technology, Baghdad, Iraq.
- Ashour, M., Abbas, A., Altahrany, A., & Alaaeldin, A., (2020). Modelling the behavior of inundated collapsible soils. *Engineering Reports*, 2(2), 1-14. doi: <https://doi.org/10.1002/eng2.12156>.
- Barzanji, A. (1973). *Gypsiferous soils in Iraq* (PhD thesis). University of Ghent, Belgium.
- Fattah, M. Y., & Dawood, B. A. (2020). Time-dependent collapse potential of unsaturated collapsible gypseous soils. *World Journal of Engineering*, 17(2), 283-294. doi: 10.1108/WJE-09-2019-0276.
- Fattah, M. Y., Hameedi, M. K., & Aswad, M. F. (2017). Determination of collapse potential of gypseous soil from field and laboratory tests. *Diyala Journal of Engineering Sciences*, 10(2), 75-85.
- Fattah, M. Y., Obead, I. H., & Omran, H. A. (2019). A study on leaching of collapsible gypseous soils. *International Journal of Geotechnical Engineering*, 2019, 1-11. doi: 10.1080/19386362.2019.1647664
- Ibrahim, A. N., & Schanz, T. (2017). Improvement of gypseous soil strength by silicone oil. *Soil Mechanics and Foundation Engineering*, 54(2), 117-121. doi: <https://doi.org/10.1007/s11204-017-9443-7>
- Ismael, N. F. (1993). Laboratory and field leaching tests on coastal salt-bearing soils. *Journal of Geotechnical Engineering*, 119(3), 53-470. doi: [https://doi.org/10.1061/\(ASCE\)0733-9410\(1993\)119:3\(453\)](https://doi.org/10.1061/(ASCE)0733-9410(1993)119:3(453))
- Ismael, N. F., & Mollah, M. A. (1998). Leaching effects on properties of cemented and sands in Kuwait. *Journal of Geotechnical and Geoenvironmental Engineering*, 124(10), 997-1004. doi: [https://doi.org/10.1061/\(ASCE\)1090-0241\(1998\)124:10\(997\)](https://doi.org/10.1061/(ASCE)1090-0241(1998)124:10(997))
- Nashat, I. H. (1990). *Engineering characteristics of some gypseous soils in Iraq* (PhD Thesis). University of Baghdad, Baghdad.
- Shahin, M. A. (2003). *Use of artificial neural networks for predicting settlement of shallow foundations on cohesionless soils* (PhD Thesis). University of Adelaide.
- Shahin, M. A., Jaska, M. B., & Maier, H. R. (2001). Artificial neural networks application in geotechnical engineering. *Australian Geomechanics*, 36(1), 49-62.
- Sinha, S. K., & Wang, M. C. (2008). Artificial neural network prediction models for soil compaction and permeability. *Geotechnical and Geological Engineering*, 26(1), 47-64. doi: <https://doi.org/10.1007/s10706-007-9146-3>
- Tizpa, P., Chenari, R. J., Fard, M. K., & Machado, S. L. (2015). ANN prediction of some geotechnical properties of soil from their index parameters. *Arabian Journal of Geosciences*, 8, 2911-2920. doi: <https://doi.org/10.1007/s12517-014-1304-3>

Public Tendering Practices, Issues and Directions - A Case of Pakistan Construction Sector

Ali Raza Khoso^{1*}, Md Aminah Yusof¹, Muhammad Aslam Leghari², Fida Siddiqui³ and Samiullah Sohu⁴

¹Department of Structure and Materials, School of Civil Engineering, Faculty of Engineering, Universiti Teknologi Malaysia, 81310 UTM, Johor Bahru, Malaysia

²National Engineering Services Pakistan (NESPAK), Hyderabad, 71500, Pakistan

³Department of Civil Engineering, Mehran University of Engineering & Technology Jamshoro, 76062, Pakistan

⁴Department of Civil Engineering, Quaid-e-Awam University of Engineering Science & Technology, Larkana Campus, 67480, Pakistan

ABSTRACT

Outdated tendering system is a significant obstacle in the momentum of public sector development in Pakistan. This study aims to examine various undiscovered part of public tendering through a detailed survey from key professionals, experts, and decision-makers of public projects. Furthermore, research covers the present status of public tendering in Pakistan and provides recommendations as per experts' opinion. This paper exhaustively highlights how the classical customs of the public tendering in Pakistan could track the old-fashioned sector to an upright path. Intensive interviews and questionnaire surveys were carried out throughout the country for data compilation. The one-way ANOVA test was performed to verify the perception of various participants and to reject the null hypothesis. The study revealed various interesting facts of present-day situations of public tendering. Various pitfalls in public tendering were underlined in the speculation of experts. The study concluded that public tendering in Pakistan is crowded with severe threats that may be alarming for the future of the industry. Un-discovering of alarming facts about public

tendering in Pakistan opens the directions for several researchers in terms of exploring project case studies further. The research is an eye-opener for policymakers, experts, decision-makers and governmental bodies to regulate the public tendering system accordingly.

Keywords: Contractor selection, current practices, Pakistan, public tendering, tendering issues

ARTICLE INFO

Article history:

Received: 22 July 2020

Accepted: 05 November 2020

Published: 22 January 2021

DOI: <https://doi.org/10.47836/pjst.29.1.07>

E-mail addresses:

raza.ali@graduate.utm.my (Ali Raza Khoso)

aminahyusof@utm.my (Md Aminah Yusof)

leghariaslam@gmail.com (Muhammad Aslam Leghari)

fida.siddiqui@faculty.muets.edu.pk (Fida Siddiqui)

sohoosamiullah@gmail.com (Samiullah Sohu)

* Corresponding author

INTRODUCTION

Public tendering principally integrates the fragmented supply of construction teams such as project managers, engineers, architects, contractors, suppliers and labourers. The public tendering encounters the challenges of right decision making which has predominant role in the construction project life cycle (Khoso & Yusof, 2020). A typical tendering process normally follows an extensive process, for executing infrastructures in public projects, by embroiling the right construction team at the right time at the right place. A public sector is predominantly considered a larger employer because it engages in mega projects in any country. Comparing to the private sector counterpart, the leading sector of construction projects is a public sector in any country and so in Pakistan. According to the annual report (2014-2015) of Pakistan Public Procurement Regulatory Authority (PPRA), a total of 31,844 public tenders were profitably allocated to various contractors, thus making this sector the largest in the country (PPRA, 2015).

The public sector in Pakistan must abide by the government's laws and legal boundaries. These official acts sometimes negatively affect the progress of the sector and driving the sector into more convoluted nexus owing to large legal formalities and strict procedures. Kog and Yaman (2016) compared the private and public sectors and stated that the private sectors were less concerned about legal procedures and were more flexible towards the tendering processes. However, the public sector projects are relatively more complicated, possessing high social involvement, extremely strict rules, and legal boundaries, and having diverse nature of work, and involving an inflexible tendering process. Further, they demonstrated that the private sector clients are reluctant and follow their own developed tendering process, whereas, in the public sector owing to public accountability, the project bid price is a key concern. This is also confirmed by Jobling and Smith (2018) who agreed that there were different mandates for public sector compared to the private one especially in developing countries.

Traditionally, most of the time in the public sector the project is awarded to the lowest bidder (Cheaitou et al., 2019; Lo & Yan, 2009). This lowest bid award scheme is a widespread practice in the competitive bidding system. Lo et al. (2007) believed that the competitive bidding system had been blamed for accepting abnormally low bids and also a prime cause of inferior quality in the projects. In contrast to the lowest bid award, the clients are more interested in exploring the best value for money along with the bid price. Ayoti (2012) stated that the tender which offered the best value for money would have to win the business in a public environment. This confrontation between the lowest price and the best value for money remained a debate for several years in the public construction history of many countries. Many researchers believe that the lowest bid award is one of the pillars of the best value for money strategy. On the contrary, several researchers agreed

that this system would not guarantee the maximum output and causes serious problems (Cheaitou et al., 2019; Horat et al., 2013; Wong et al., 2000) and further creates unhealthy competition in the market.

Besides the aforementioned issue of the lowest bid scheme in public sector, an additional major obstacle and dilemma in the process is the right and competent contractor selection. The importance of appropriate contractor selection in public tendering can never be ignored as the successful delivery of project depends on the contractors (Khosro & Yusof, 2020). Kog et al. (2014) believed that the choice of a capable contractor was one of the challenging decisions in the tendering process. Also, Jaskowski et al. (2009) stressed on precise assessment of the contractors through extensive evaluation. The precise decision entails that extensive qualification criteria must be designed for the selection. A research investigates that many issues in a project may have been due to the absence of suitable selection criteria consideration which allows selection of appropriate contractor (Elsayah, 2016). In public tendering apart from other goals, the client is expected to evaluate contractors based on several criteria other than bid price to ensure the capability of the contractors for the specific project and further to restrict the bidders at a later stage. But on account of several characteristics among contractors, the clients are tormented to select a contractor from a large pool of bidders (Liu et al., 2015). Therefore, an extensive evaluation of contractors in a public project leads to better decisions. Furthermore, in several cases, the correct information from contractor on quality criteria is not possible. Birjandi et al. (2019) pointed out that decision makers confront the issue of appropriate assessment owing to some vague criteria, and reliable information from contractors on criteria was problematic to collect. Wondimu et al. (2020) also confirmed that the contractor manipulated the information on certain criteria and presented the information according to their own advantages.

The issue of improper evaluation of contractors is prevailing globally. Traditionally, client sets excessive weight on price and lowers emphasis on soft parameters (Kadefors, 2005). This practice is more specific in public departments (Kumaraswamy & Anvuur, 2008) and the relation between the price and other criteria is not perfectly understood. Thus, many researchers believe that the tendering process is very intricate, for example; Ng and Skitmore (2001) exclaimed that the process was multifaceted because of high technical and financial evaluation. Similarly, Watt et al. (2010) claimed the process was full of risk and entailed higher uncertainty while also Bochenek (2014) also favored the same claim. Furthermore, Hochstetter et al. (2004) observed numerous issues in tendering process and noted that high-level requirements from bidders, intricate evaluation process, extremely short deadlines to bidders, and less expected completion time for project delivery were some loopholes in a tendering system inherently. Liu et al. (2015) investigated the

gaps in the tendering process and highlighted a number of problems as the root causes of tender complication. They included a very short deadline to deliver the project, distinct characteristics of bidders and diverse experience and knowledge of decision-makers in the tender evaluation.

Pertaining to the said problems, the tendering phase of the public projects is still encountering several serious issues and yet the right direction is still unclear especially in Pakistan where limited research is conducted to draw attention to this issue. This is consequently opening the gates for more research in this less discovered area. One such attempt is undertaken in this research in the form of unfolding serious reservations of professionals working in the public sector construction projects in Pakistan. The construction sector in Pakistan is advancing in optimistic directions but the industry unfortunately is not enjoying the expected positive outcome and reputation globally. Many researchers believed that shaky public tendering practices in Pakistan are key triggers of these issues. Farooqui et al. (2008) believed that in Pakistan public sector, the lowest bid award system was the most prevailing reason for poor performance in the country. Similarly, Khan and Khan (2015) asserted that the lowest bid award was a major reason for public sector downfall. Apart from the issue of the lowest bid, Maqsoom et al. (2014) stressed that poor public tendering policies were responsible for several mishaps in the public sector. Besides this, Azhar et al. (2008) mentioned that alongside other problems, the contract management and wrong bidding strategies in Pakistan are accountable for project issues. Looking at several shreds of evidence against the traditional public tendering practices, this study strives for the following research questions:

RQ1. What are the prevailing practices of public tendering in various organizations in Pakistan?

RQ2. What are the issues in public tendering traditional practices that impede the industry hike?

RQ3. How can the current loopholes in the traditional system be resolved?

This study aims to address the aforementioned research questions. This work is novel in many aspects as none of the past research has exhaustively addressed the issues of public tendering of Pakistan exhaustively until now. The studies of Farooqui et al. (2008) and Khan & Khan (2015) are only master pieces of the works in the literature where authors concentrated on the lowest bid flaws in the system. Moreover, none of the research until now has yet comprehensively discussed the issues of public tendering except the ones targeting this lowest bid award. This study is a step beyond highlighting the current practices, and the earlier issues in the existing system, and exhaustively discussed the possible recommendation from the viewpoint of experts.

METHODS

This research aims to investigate the current tendering practices and problems in Pakistan and their possible solutions. Inherent issues of public tendering were examined through a meticulous overview of literature around the globe. Facts of public tendering obtained through literature were discussed to justify the study for the Pakistan public sector. Not limited to this, the regularly published magazines, articles, and reports from various organizations in Pakistan were consistently reviewed. The explored organizations in Pakistan includes Pakistan Public Procurement Regulatory Authority (PPRA), Pakistan Bureau of Statistics (PBS), State Bank of Pakistan (SBP), and Pakistan Engineering Council (PEC). Furthermore, this study seeks to pursue exhaustive knowledge in the context of public tendering in Pakistan. In this connection, the expert surveys in the form of interviews were carried out with the key and top hierarchy experts in various public and private organizations in Pakistan. Such studies rely on shared perspectives from different groups of people such as clients, consultants and contractors as suggested by (Murtagh & Brooks, 2019). For this present research, an expert sampling technique of purposive sampling method was adopted. Fundamentally, this was a non-probabilistic sampling approach which is mutually based on the population characteristics and the study objectives. The high-profile decision makers and policy makers from client, consultants and contractors participated in present study. A special focus was kept on the experts in public organizations those having rich experience in public tendering.

To meet the intended research goals, issues of public tendering in Pakistan were presented in a pilot survey. The pilot survey was basically conducted to verify the viability of the study before the actual data collection process on a large sample size. Melody (2008) defined a pilot study as an informal way on a handful of participants to validate the studies. The shared groups of experts further pointed out the local prevailing problems of the industry apart from those mostly cited in the literature. An exhaustive survey instrument was designed in two different sections for the intention of achieving the significant outcomes of this research. The first section comprises the current practices and problems of Pakistan public tendering whereas, the later part is reserved for the possible opinion of experts on the current situation of public tendering in the form of possible solutions. The instrument was thus prepared and distributed to pertinent professionals working in public projects and especially with the experts those deal with the tendering matters. Collected responses were analyzed in SPSS and later kept under discussion with the experts. The differences of opinion of all respondents' group (i.e., client, consultants, and contractors) were investigated by computing a one-way ANOVA test. Henceforth a hypothesis is developed as follows.

H_1 : There is a substantial difference in the perception of each group on current practices, issues, and recommendations provided by experts on public tendering.

The research method flow is illustrated further in Figure 1 for further reference.

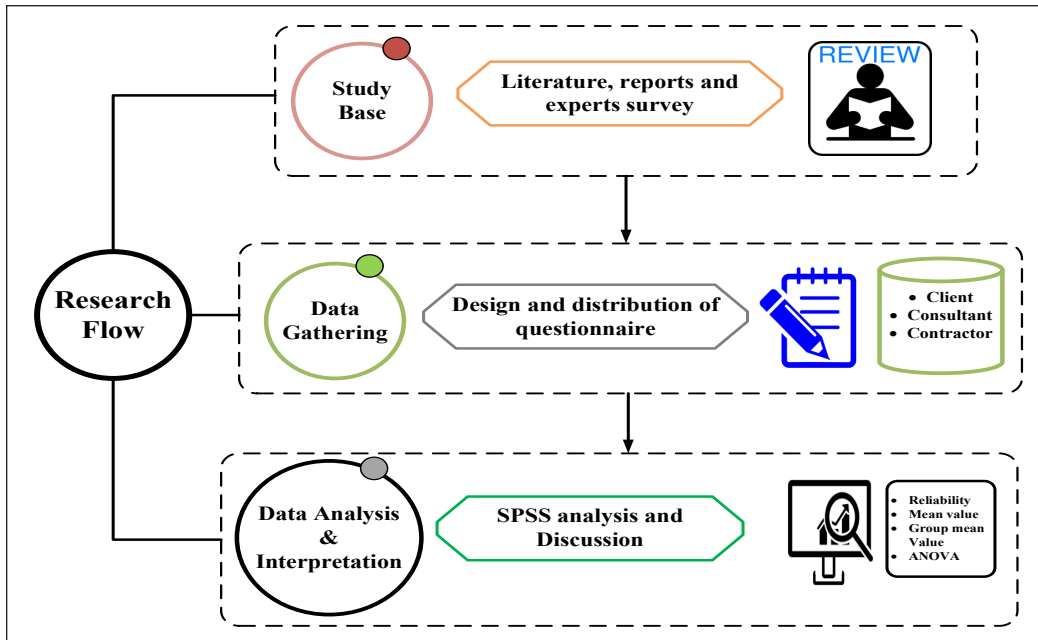


Figure 1. Research method flow diagram

Data Collection and Analysis Method

Data collection on a larger sample size begins after the successful completion of the pilot study. The data collection process involved various experienced participants from different groups i.e. client, consultants and contractors. Melody (2008) suggested that the opinion with the relevant participants based on their experience was sufficient for investigating the procedures and method. Before commencing with data collection, the targeted organizations are listed out from various public sector organizations in Pakistan. To ensure the participation of highly credible and pertinent respondents, vastly experienced professionals are approached in the data collection stage. The sample size was confirmed from the study of Morenikeji (2006). According to this study, below 30 respondents are deemed small size, while above 30 is viewed as a larger sample. However, to receive a high response from participant is also another problem. Wahlberg and Poom (2015) believed that all kinds of survey research where human participants were involved, the response rate of the questionnaire was relatively low, and researchers were often reliant on the respondents. Fortunately for this study, 109 responses were gathered from different provinces (states) and regions of the country. The demographic information of survey respondents is illustrated in Table 1.

Table 1 demonstrates that public sector clients are mostly targeted in the survey. Furthermore, the quality of respondents can be depicted from the high-level experience of respondents. According to the frequency analysis of respondents, over 50% of respondents

Table 1
Demographic information of survey respondents

Data types	No. of respondents					
	Public	Private	Semi-Public	NGO/INGO		
Ownerships of respondents	53	42	8	6		
Type of organization	Client	Consultant	Contractors			
	58	23	28			
Experience in Construction sector	1-5 yrs.	6-10 yrs.	11-15 yrs.	Above 15 yrs.		
	37	17	17	38		
Experience in public tendering	46	26	12	25		
Firm's Geographical Location	Sindh	Punjab	KPK	Baluchistan	Gilgit & AJK	
	70	7	5	18	3	
Position of respondents	Project Manager	Assistant/Executive Engineer	Chief Executive Officer	Procurement/Contract Engineer	Project Director	others
	8	47	15	13	5	21
Highest Educational Level	Diploma	Bachelor	Masters/M.Phil.			
	1	59	49			

have above ten years' experience in the construction. Furthermore, around 34% of respondents have similar experience in public tendering which is a reasonably significant number. The position of respondents further witnesses the quality of the data sample. As discussed earlier, top hierarchy personnel from the various organizations in Pakistan were pursued.

Survey responses were gathered on a five-point level of agreement and disagreement scale, where 1 represents strongly disagree and 5 represents strongly agree. An undecided option was also offered on the scale for those participants who have no information on particular question. SPSS (Statistical Packages for Social Sciences) was employed for the data analysis where reliability analysis, mean values and group mean values are supported to validate the responses. The mean value in the form of Average Index (AI) equal and greater than 3 was considered as benchmark and any value above 3 is recognized in the category of agree and strongly agree as per (Kim et al., 2018). Furthermore, the one-way ANOVA test was performed to cross-check the perception of client, consultant, and contractor on different issues and current situations of public tendering in the country. Therefore, the ANOVA test was presented to validate that there was no major difference in the opinion of all stakeholders on raised concerns. This test was verified at a 5% level of significance i.e. significant value of any case lesser than 5% (i.e., > 0.05) was considered a divergence in the opinion of stakeholders (Ng et al., 2009).

RESULTS AND DISCUSSION

Data Reliability

The reliability of data sample depends on the internal measures of reliability (Wang et al., 2019). To validate the quality of data, Cronbach's alpha test was carried out in SPSS. The Cronbach's alpha values lay between 0 to 1, where the value of 0.7 was considered the basis for the internal consistency, and 0.6 was also considered satisfactory (Phogat & Gupta, 2019). For this data sample, 0.783 value was found for the first section of questionnaire and 0.889 for the second part. Henceforth, the data sample was quite satisfactory for conducting a scientific research.

Analysis and Discussion on Current Practices of Public Tendering in Pakistan

In the first part of the study, multiple questions were raised in connection to current practices in various organizations of the public sector in Pakistan alongside with prevalent issues associated with current practices. A one-way ANOVA test was performed to examine the significant values of the responses. The results reveals that there was no significant difference in the majority of arguments except for two questions namely, "sometimes contractors provide wrong information on given criteria to client" and "public client accepts the abnormally low bid from contractors" with sig. values of 0.001 (<0.05) and 0.012 (<0.05) respectively. The one-way ANOVA test results confirmed that the null hypothesis (H_0) was rejected on the majority of arguments. However, a small difference in the opinion of participants' groups was observed in the said arguments. Owing to the opinion differences, a *post hoc* test was performed in SPSS using Tukey's test to detect which group had different opinions, among others.

Analysis of the post hoc test revealed that there was a disagreement of opinion between client and contractor on both said arguments. To explore this further, the group mean values of both cases from clients and contractors could be referred (Table 2). According to the obtained mean values, the client's group is more inclined toward the opinion that the contractor provides wrong information to them, but the contractor's group rejects the argument. However, the case is different in the second query as per the opinion of both participant groups. Therefore, no large difference in the opinion is observed for this case. Further discussion on the obtained results is discussed below.

A contractor is a key stakeholder in the construction industry and his/her role in the successful delivery of a project can never be ignored. Analysis of survey shows that the currently nature of construction projects is turning out to be complicated in Pakistan owing to several reasons such as market demands in the form of innovative designs, construction methods and modern skills. Such challenges are the impediment to a successful delivery of a project. Looking at these challenges, a client ought to focus on the selection of a

Table 2

Total mean value and group mean value results of current practices of public tendering in Pakistan

Questions/Arguments		N	Mean	Std. Deviation
The nature of construction projects in Pakistan is becoming more complicated.	Client	58	3.50	1.158
	Consultant	23	3.48	0.790
	Contractor	28	3.50	0.839
	Total	109	3.50	1.006
The contractors need to be more capable of meeting the demand for complicated projects.	Client	58	4.28	0.854
	Consultant	23	4.30	0.470
	Contractor	28	3.96	0.693
	Total	109	4.20	0.755
Public organizations are bound to follow strict legal process and formalities in tendering and procurement.	Client	58	4.45	0.680
	Consultant	23	4.30	0.876
	Contractor	28	4.18	0.772
	Total	109	4.35	0.750
Public organization follows PPRA rules/guidelines in tendering.	Client	58	4.43	0.920
	Consultant	23	4.48	0.593
	Contractor	28	4.18	0.905
	Total	109	4.38	0.858
Public organizations follow their own developed rules or process in tendering.	Client	58	2.97	1.401
	Consultant	23	2.83	0.984
	Contractor	28	2.61	1.066
	Total	109	2.84	1.241
Public organizations assess contractors based on the following evaluation criteria during the prequalification stage. a) Experience	Client	58	4.50	0.755
	Consultant	23	4.57	0.507
	Contractor	28	4.46	0.793
	Total	109	4.50	0.715
Public organizations assess contractors based on the following evaluation criteria during the prequalification stage. b) Financial Soundness	Client	58	4.45	0.776
	Consultant	23	4.52	0.511
	Contractor	28	4.57	0.504
	Total	109	4.50	0.661
Public organizations assess contractors based on the following evaluation criteria during the prequalification stage. c) Technical Personnel	Client	58	4.41	0.795
	Consultant	23	4.52	0.593
	Contractor	28	4.57	0.504
	Total	109	4.48	0.688
Public organizations assess contractors based on the following evaluation criteria during the prequalification stage. d) Equipment	Client	58	4.24	0.904
	Consultant	23	4.26	0.619
	Contractor	28	4.57	0.690
	Total	109	4.33	0.806
Public organizations assess contractors based on the following evaluation criteria during the prequalification stage. e) Management Capability	Client	58	4.00	0.991
	Consultant	23	4.30	0.765
	Contractor	28	4.25	0.844
	Total	109	4.13	0.914

Table 2 (continue)

Questions/Arguments		N	Mean	Std. Deviation
Public organizations assess contractors based on the following evaluation criteria during the prequalification stage. f) Quality	Client	58	4.03	1.008
	Consultant	23	4.35	0.573
	Contractor	28	4.04	1.036
	Total	109	4.10	0.942
Public organizations assess contractors based on the following evaluation criteria during the prequalification stage. g) Health & Safety	Client	58	3.57	1.110
	Consultant	23	3.96	0.638
	Contractor	28	3.61	0.994
	Total	109	3.66	1.002
Contractor's evaluation criteria in public organization are not sufficient.	Client	58	3.93	0.915
	Consultant	23	3.70	1.020
	Contractor	28	3.57	0.959
	Total	109	3.79	0.953
Clients evaluate contractors on certain criteria where right data/information from the contractor is not obtained.	Client	58	3.79	1.120
	Consultant	23	3.74	0.752
	Contractor	28	3.71	0.810
	Total	109	3.76	0.971
Sometimes contractors provide wrong information on given criteria to clients.	Client	58	4.19	0.888
	Consultant	23	3.96	0.475
	Contractor	28	3.50	0.793
	Total	109	3.96	0.838
All contractor passing the threshold marks are treated equally during the bid price stage in public tendering.	Client	58	3.83	1.157
	Consultant	23	3.83	0.937
	Contractor	28	3.89	0.497
	Total	109	3.84	0.973
Your organization select contractors; a) that offers least bid price but responsive	Client	58	4.16	1.225
	Consultant	23	4.39	0.722
	Contractor	28	4.46	0.922
	Total	109	4.28	1.064
b) without considering bid price only qualification criteria-based	Client	58	2.22	0.974
	Consultant	23	2.17	1.154
	Contractor	28	1.82	0.945
	Total	109	2.11	1.012
c) based on weightage of technical and price bid by considering multiple criteria selection	Client	58	3.38	1.240
	Consultant	23	3.83	0.834
	Contractor	28	3.82	0.819
	Total	109	3.59	1.082
Special consideration in assigning threshold (minimum passing marks) during the prequalification stage is not made in public tendering.	Client	58	3.17	1.286
	Consultant	23	3.17	0.887
	Contractor	28	3.46	0.881
	Total	109	3.25	1.115

Table 2 (continue)

Questions/Arguments		N	Mean	Std. Deviation
Public clients accept the abnormally low bid from contractors.	Client	58	3.09	1.315
	Consultant	23	3.70	0.765
	Contractor	28	3.75	0.752
	Total	109	3.39	1.130
Tender is always awarded to one who quotes lesser than ceiling price (estimation by client).	Client	58	3.38	1.309
	Consultant	23	3.61	0.988
	Contractor	28	3.89	0.737
	Total	109	3.56	1.134
Traditionally, the final contract award is made on the lowest cost basis.	Client	58	3.98	1.116
	Consultant	23	4.00	0.674
	Contractor	28	4.29	0.460
	Total	109	4.06	0.905
In your organization, contractors are rejected on the consent of high officials.	Client	58	2.74	1.117
	Consultant	23	2.78	1.166
	Contractor	28	3.25	1.041
	Total	109	2.88	1.120
Your organization follows a decision-making system for assessing the contractors.	Client	58	2.69	1.301
	Consultant	23	3.22	1.166
	Contractor	28	2.43	1.230
	Total	109	2.73	1.274

capable contractor in its team. The availability of capable contractors can be ensured when an exhaustive assessment from contractor is made possible during the public tendering process. Therefore, the extensive and exhaustive selection of a contractor is a key to a successful project outcome.

According to the survey results, the current tendering system in Pakistan for the contractor's assessment, evaluation, and final selection is ambiguous and inconsistent in many aspects. Clients in the construction sector of Pakistan throughout the country strictly follow PPRA 2004 rules. These regulations restrict the public clients in many situations such as in quotation of the bid price. Nevertheless, some limited organizations are developing the system with their own modification in PPRA 2004 regulations despite the strict requirements in the legislation. Discussing the facts with experts revealed loopholes in implementation of the governmental regulations. A similar claim was made by Ibrahim et al. (2017) that in the developing countries, public regulations were sometimes modified due to weakness in the system.

Further analysis on current evaluation criteria revealed that Experience, Financial Soundness, Technical Personnel, Equipment, Management Capability, Quality and Health & Safety criteria are considered currently in evaluating or pre-qualifying the contractors in

Pakistan. The survey also focused on associated issues with traditional quality criteria set by governmental bodies. Experts in Pakistan believe that these contractor selection criteria are outdated and furthermore not extensive enough to qualify a capable contractor especially in today's construction when the industry is changed at three sixty degrees. The matter is further worsened by the incorrect information provided by the contractor when asked for the available sources in the form of selection criteria. From the analysis of results, it is found that clients in the public sector in Pakistan are confronting the issue of receiving incorrect information from the contractors. This issue is prevailing because of inappropriate design of criteria by the client. In many cases, the right information from contractors on certain criteria is difficult to gather which creates problems in their true analyses.

While investigating the current selection mechanism in the country, the most adopted method is found as the least, and responsive price bid-based selection followed by weightage consideration of price and quality criteria. The survey further unwraps that the quality-based method is infrequent in public organizations. From the survey analysis, it is confirmed that in Pakistan, the least bid price mechanism is most common and many times abnormally bids are also considered for the award which is a great threat and further leads to project failure in many cases. Several reservations and differences of opinion were observed in the analysis. Despite the rules as per the PPRA 2004 which prohibits the acceptance of abnormal bid, it is still a common practice in the country which has adverse consequences. It is also evident from the results that the contract winner is always the one who quotes a bid lesser than estimation by the client. This method is followed by weightage consideration of price and quality where the weightages are measured based on a certain threshold values set by the client. Clients will normally set this number in the initial stage of preparation of tender documents. Some guidelines in Pakistan i.e. PEC suggests different values of these threshold marks for pre-qualifying the contractor such as 60 or 70 (out of 100). However, clients have further privilege to choose these marks reliant on the type of project within prescribed boundaries. The contractors attaining the threshold are qualified to bid for the project at the final stage. To unveil the current situation in Pakistan, a few questions were included in the questionnaire related to threshold marks. Results of the survey analysis found that in Pakistan, all the contractors attaining the threshold limit are considered equivalent and have equal opportunity to win the project. Even a contractor A with the highest marks for example, 95, is treated equally to a contractor B having marks, for example, 70. This basically reflects that qualification mark is irrelevant as long as they are passing threshold. Thus, there is no further importance of prequalification criteria and multi-characteristic qualities among the contractors. Henceforth, the process of public tendering in Pakistan is a discontinuous progression that partially recognizes the importance of quality criteria.

While investigating the availability of the decision-making system and their application in the public sector, a discouraging response in the form of unavailability of such a system

is obtained. Clients assign the responsibility of assessing the bids to a small group of experts who have the right to select or reject the competitors based on certain conditions. However, the entire judgement is based on a paperwork without any justified system or decision-making mechanism. Henceforth, there emerge chances of unjustified and unequal assessments on all cases as a result of human error. The aforementioned section unveils the current practices and relevant issues in public tendering in Pakistan which later help in developing the theoretical outcome from this research.

Analysis on Opinion of Construction Industry Experts on Current Tendering Issues in Pakistan

This section underlines the analysis and discussion part on the experts' opinion over the current practices in public tendering presently. Additionally, the section also covers various solutions for the prevailing issues in public sector in Pakistan. A significant number of questions and proposed solutions are enlisted in the 2nd part of the questionnaire. The gathered data was analyzed in SPSS using mean values, group mean values and standard deviation (Table 3).

A one-way ANOVA test was also performed to verify the significant values of each variable. The result presents that there was no significant difference in majority of interrogations, except the two namely; "contractor's assessment process could be improved if the benefits of prequalification (PQ) phase is provided in the final contract award" and "the human-based assessment system causing problem in contractor's selection process" with respective sig. value of 0.007 (<0.05) and 0.017 (<0.05). From the sig. values of the cases, the one-way ANOVA test confirmed that the null hypothesis (H₀) was rejected on the majority of suggestions. Due to the identified variations in opinion from different groups, a post hoc test was performed in SPSS. Analysis of post hoc test results uncovered that there was a significant difference in the opinion of consultants compared to other groups (i.e., client and contractor) on the first suggestion. Moreover, on the second query, the contractor's viewpoint was much different from the other two groups. The consultant was unwilling to accept suggestions in the first question. However, in the second question, the contractors' viewpoint was much different than the clients and consultants which clarified that contractors had more issues with the human-based assessment system of the public client. To explore further, the group mean values of both questions from clients and contractors were referred to. According to the group mean value, all groups of respondents agreed with both recommendations. The higher mean value (above 3) further indicated the validity of queries. The survey results on the opinion and recommendations of experts over the present condition in public sector in Pakistan is discussed below.

The survey result reveal that nowadays construction projects are of a complicated nature in Pakistan and the assessment of contractors is still based on earlier concepts. This further

Table 3
Total mean and group mean value analysis results of opinion of construction industry experts on current tendering issues in Pakistan

Suggestions	Type of respondents	N	Mean	Std. Deviation
The nature of construction projects nowadays requires extensive contractor's assessment in meeting project demands.	Client	58	4.28	0.523
	Consultant	23	4.17	0.834
	Contractor	28	3.93	0.858
	Total	109	4.17	0.701
The success of a project is greatly depending on the capability of a contractor.	Client	58	4.28	0.720
	Consultant	23	4.48	0.593
	Contractor	28	4.25	0.518
	Total	109	4.31	0.648
A contractor is more responsible for project success than other parties, for instance, client and consultant.	Client	58	3.93	1.090
	Consultant	23	3.96	0.976
	Contractor	28	4.39	0.832
	Total	109	4.06	1.017
Public projects fail because of selecting incapable contractors.	Client	58	4.09	0.978
	Consultant	23	3.96	1.065
	Contractor	28	4.32	0.819
	Total	109	4.12	0.960
Right contractor selection is still a problem in public projects.	Client	58	4.07	1.024
	Consultant	23	4.00	0.953
	Contractor	28	4.21	0.738
	Total	109	4.09	0.938
The ultimate solution to public projects lies in the proper selection of capable contractors.	Client	58	4.21	0.894
	Consultant	23	4.04	0.638
	Contractor	28	4.21	0.917
	Total	109	4.17	0.848
In comparison to the private sector, public organizations have more complicated tendering process owing to legal boundaries.	Client	58	4.00	1.170
	Consultant	23	4.00	0.674
	Contractor	28	4.04	1.071
	Total	109	4.01	1.050
The multi-characteristic requirement from contractors is making the tendering process more complicated.	Client	58	3.60	1.337
	Consultant	23	3.87	0.869
	Contractor	28	3.89	0.956
	Total	109	3.73	1.160
Flaws in evaluation process in public tendering are responsible for projects' failure in Pakistan.	Client	58	3.88	1.215
	Consultant	23	4.09	0.900
	Contractor	28	3.86	0.803
	Total	109	3.92	1.055
In your opinion which can be a reason for project failure in Pakistan in the context of public tendering? a) Lowest bid price selection	Client	58	4.36	0.873
	Consultant	22	4.36	0.790
	Contractor	28	4.29	1.013
	Total	108	4.34	0.888

Table 3 (continue)

Suggestions	Type of respondents	N	Mean	Std. Deviation
b) Insufficient contractor's technical evaluation	Client	58	4.26	0.890
	Consultant	23	4.17	0.491
	Contractor	28	4.29	0.763
	Total	109	4.25	0.784
c) Poor weightage consideration of technical and bid price criteria	Client	58	4.02	0.982
	Consultant	22	4.00	0.617
	Contractor	28	4.11	0.567
	Total	108	4.04	0.819
d) Improper decision support system for contractor's evaluation	Client	58	3.84	1.040
	Consultant	22	4.00	0.617
	Contractor	28	4.18	0.670
	Total	108	3.96	0.885
Several problems in the tendering phase are occurring in public projects because of ignoring standard procurement guidelines.	Client	58	3.84	0.933
	Consultant	23	3.96	0.638
	Contractor	28	4.14	0.448
	Total	109	3.94	0.780
Contractors are not properly evaluated because of insufficient quality criteria set by organizations.	Client	58	3.81	0.888
	Consultant	23	4.04	0.638
	Contractor	28	4.04	0.429
	Total	109	3.92	0.747
Clients are facing an issue of getting incorrect information on qualification criteria from contractors.	Client	58	3.95	0.981
	Consultant	23	3.91	0.793
	Contractor	28	3.61	0.786
	Total	109	3.85	0.901
Contractor's evaluation is becoming difficult due to the absence of proper screening at an early stage.	Client	58	4.00	1.009
	Consultant	23	4.04	0.767
	Contractor	28	4.04	0.881
	Total	109	4.02	0.923
The client must consider proper threshold marks (minimum passing marks) during prequalification.	Client	58	4.26	0.762
	Consultant	23	4.39	0.583
	Contractor	28	4.18	0.548
	Total	109	4.27	0.676
Capable contractors are not selected because of improper weightages are given to cost in comparison to other qualification criteria.	Client	58	3.97	1.092
	Consultant	23	4.22	0.736
	Contractor	28	4.32	0.548
	Total	109	4.11	0.916
A more capable contractor can be selected if technical parameters are given high importance/weightage.	Client	58	4.52	0.628
	Consultant	23	4.26	0.689
	Contractor	28	4.21	0.686
	Total	109	4.39	0.665

Table 3 (continue)

Suggestions	Type of respondents	N	Mean	Std. Deviation
The contractor assessment process can be improved if the benefits of prequalification or technical phase are given in the final contract award.	Client	58	4.45	0.776
	Consultant	23	3.87	0.869
	Contractor	28	4.43	0.573
	Total	109	4.32	0.780
The lowest bid award system in public project is responsible for several mishaps in any project.	Client	58	4.36	0.742
	Consultant	23	4.17	0.778
	Contractor	28	4.43	0.504
	Total	109	4.34	0.697
Other than price-based selection method must be developed in Pakistan.	Client	58	4.48	0.504
	Consultant	23	4.35	0.487
	Contractor	28	4.32	0.670
	Total	109	4.41	0.548
Contractors must be given flexibility in bid price quotation within the ceiling price limit.	Client	58	4.03	0.837
	Consultant	23	4.13	0.548
	Contractor	28	4.36	0.559
	Total	109	4.14	0.726
The client should accept any bid lies within the limit of ceiling price to make process more flexible.	Client	58	4.02	0.827
	Consultant	23	3.96	0.825
	Contractor	28	4.36	0.678
	Total	109	4.09	0.800
Public projects are suffering several problems because of poor mechanism of public tendering.	Client	58	3.90	1.003
	Consultant	23	3.96	0.878
	Contractor	28	4.14	0.591
	Total	109	3.97	0.887
Contractor selection issues are pertaining because of improper traditional contractor's assessment system.	Client	58	4.05	0.944
	Consultant	23	4.04	0.878
	Contractor	28	4.11	0.497
	Total	109	4.06	0.831
The human-based assessment system causing problems in contractors' selection process.	Client	58	3.60	0.972
	Consultant	23	3.83	1.154
	Contractor	28	4.25	0.752
	Total	109	3.82	0.992
Contractor's assessment system during the evaluation phase can help in smooth and justified assessments.	Client	58	4.14	0.712
	Consultant	23	3.96	0.562
	Contractor	28	4.21	0.418
	Total	109	4.12	0.620
The complexity of the tendering process can be minimized with the help of automated decision-making system.	Client	58	3.97	1.008
	Consultant	23	3.74	1.054
	Contractor	28	4.04	0.637
	Total	109	3.94	0.936

confirms that an extensive assessment of contractors is needed of the hour in construction sector in Pakistan. Further examination reveals that no doubt clients, consultants, and contractors are key personnel of a project, but the project accomplishment is more reliant upon the shoulders of a contractor in Pakistan. These results are in accordance with many past studies such as Alzahrani and Emsley (2013), and Lundberg and Bergman (2017), who believed that performance of project was highly dependent on the shoulders of contractors. In this continuation, furthermore, impressive results were found. According to the results, in Pakistan, mostly public projects fail because of selecting incapable contractors. Results confirm that the significance of selecting capable contractor for a public project is still not taken seriously. Apart from the capable contractor selection, owing to several governmental formalities as the funds belong to the public, public tendering is believed to be more complicated than its private counterpart projects bidding. Survey results found that the private sector is relatively more straightforward in process. The public tendering is bounded in more legal formalities and procedures. This is owing to a large number of formalities in public tendering; a higher number of requirements are asked from the contractors that are making the process obscure. Lundberg and Bergman (2017) also confirmed that public tendering complexity resulted in a lesser quality project compared to its private counterpart. The results also confirmed findings from the studies of Judit (2017) and Long et al. (2004). This leads to the suggestion that an easier and straightforward process with lesser formalities needs to be designed to get rid of various inherent issues of public tendering.

Several other problems tend to persist from the evaluation of contractors until its final award that is based on price. Referring to the survey results, the problematic evaluation process of contractors is to be blamed for project failures in the country. Several complications happened when wrong contractors entered the bidding and being awarded the project. Liu et al. (2015) assumed that a contractor whose capabilities did not match the project requirement creates problems of time, cost, and quality in project later on. Ultimately, the end goal of every client is to have a successful end to projects where a contractor plays a major role (Watt et al., 2010). Further reasons for project failure in the context of public tendering were reported as; “lowest bid price selection” which was discussed earlier. These results are consistent with the earlier findings of Cheaitou et al. (2019) and Zhang et al. (2015). Exploration of results further divulges that public clients are ignoring the standard procurement guidelines while designing, evaluating, and awarding the tenders. The survey found that the issue is most prevailing in the country, and experts believe this is one of the major causes of public tendering failure. Therefore, it is suggested that the lowest bid system is abolished. This can further be improved through extensive contractor’s evaluation before the bid stage. In this regard, an effective tool can be a standard procurement guideline. The second most critical reason of project failure was found as “insufficient contractor’s technical evaluation,” and the other similar causes

were stated as “poor weightage consideration of technical and bid price” and “improper decision support system for contractor’s evaluation.”

Proper evaluation of contractors is still a dominant issue in Pakistan as reported in the survey. Incapable contractors often became part of the competition owing to insufficient criteria set by the organizations. The study indicated that the existing evaluation criteria (Experience, Financial Soundness, Technical Personnel, Equipment, Management Capability, Quality and Health & Safety) received very high critics. Patil (2017) also, believed that proper screening in terms of evaluation criteria was necessary. Apart from the issues of insufficient criteria, designing and keeping the ambiguous criteria is another subject of matter where correct information from contractors is challenging to obtain is another subject of matter. Furthermore, results have proven that in the evaluation process, clients did not get accurate information from the contractors and this was due to improper designing of quality criteria. According to the survey results, due to the deficiency of proper screening, the contractor’s evaluation has become problematic. The experts believed that appropriate screening criteria in the preliminary phase can decrease more burdensome participation in the evaluation stage. Thus, this leads to the design of an extensive set of tougher criteria for initial scrutiny of contractors with higher weight on technical parameters over the cost. The results are in accordance with the assertion of Lundberg & Bergman (2017) who believed that quality parameters must be weighted more than cost considerations if the quality was ultimate expectations from the outcome.

As discussed above, the role of threshold marks is only limited to technical assessment phase (or prequalification stage) only. In this regard, many experts and professionals believed that proper calculation of threshold marks is not considered anywhere in public tendering practice. Henceforth, they believe that the proper understanding of such marks must be incorporated. The experts believe that the contractor’s assessment process can be improved further if the contractors are given the benefits of their higher marks in the final award of work. This suggests that certain percentages of technical phase process must be kept for the final award. This can offer the equal opportunity to a contractor for winning a project who will quote a right bid price over the least bid.

While addressing the issues to get rid of the lowest bid award system in Pakistan, the survey found interesting results. From the survey results, it was revealed that the lowest bid price selection is causing the problem in public projects and alternative to the price-based methods are grievously needed to be designed respectively. Zhang et al. (2015) also stressed that evaluation of bid was a significant concern in public tendering. This is also according to the study by Mamavi et al. (2017) which claims that apart from reality, several basic models of bid evaluation suggest that cost should not be the parameters for contractor selection. The problem of lowest bid selection can be resolved with an alternative suggestion. It is

suggested that contractors are offered flexibility while quoting their bid within the ceiling price limit. Clients are recommended to accept any bid from the contractors that is within the upper limit of ceiling price irrespective of the lowest value in the competition. This situation would not create any problem of over utilizing public funds and would further enhance the chances of fair competitions. The contractors will also be given their due right in the form of sufficient return on its investment. Therefore, the chances of providing bad quality outcome can also be minimized.

The long-lasting issues in public tendering in Pakistan are the results of certain traditional practices. Moreover, the human-based assessment system has created many flaws in the form of unjustified decisions and biases in the assessment process. Based on the survey, it was found that the tendering process in Pakistan is largely affected by traditional customs and human-based assessment. The absence of more objective evaluation led to unjustified decisions and biases in assessment processes. Thus, an assessment for the purpose of selecting contractors for public projects in Pakistan requires serious attention and more objective approach is needed. Nowadays, the world has entered the era of modernization, where the use of advanced tools and techniques is within reach for everyone. Unfortunately, the tendering department in many organizations in Pakistan are still in its old-fashioned way. This is especially so in the contractor's assessment system where a person or a team decides on the future of contractors with no or fewer means of alternative modern assessment methods or techniques, and with and with no guarantee of precision. The data analysis of respondents suggested that an automated decision support system can be a helpful tool in public organizations. Respondents agreed that such a system, if developed, could further simplify one of the difficult phases of public tendering i.e. justified assessment. Furthermore, they decided that many difficulties arising during the assessment process that is a hurdle in equal treatment of the contractors could be minimized with the system. With the aforementioned discussions on opinion on present practices and their solution in the form recommendations, a theoretical framework is developed to pave a road map for public tendering.

Public Tendering Theoretical Outcome for Pakistan Construction Projects

Referring to the research questions raised in the beginning, the exhaustive survey propagates in three different directions i.e. issues, practices, and recommendations in public tendering in Pakistan. In the first part i.e. current practices of public tendering in Pakistan, the issues and practices are investigated. The third direction of recommendations is computed from the second part of survey. Therefore, the results obtained from the analysis propagates in three different directions and helped in the development of theoretical framework. The novel research contribution is thus achieved in this research that can fill the wide gaps in current body of knowledge (Figure 2).

Figure 2 exemplifies that several ill practices in public projects in Pakistan are prevailing. These outdated customs of tendering process are a key hindrance in the development of the industry. The theoretical outcome interlinked each ill designed process to current issues facing the industry. Several inherent issues are emphasized that are the outcome of poor practices in Pakistan. Following up the issues, industry experts were called for their suggestions. Experts emphasized on various helpful recommendations those are mentioned under the analysis and discussion section. The recommendations are linked with each case of practices and issues and illustrated in Figure 2. The theoretical outcome of public tendering is a blueprint in construction sector. The recommendations drawn in the

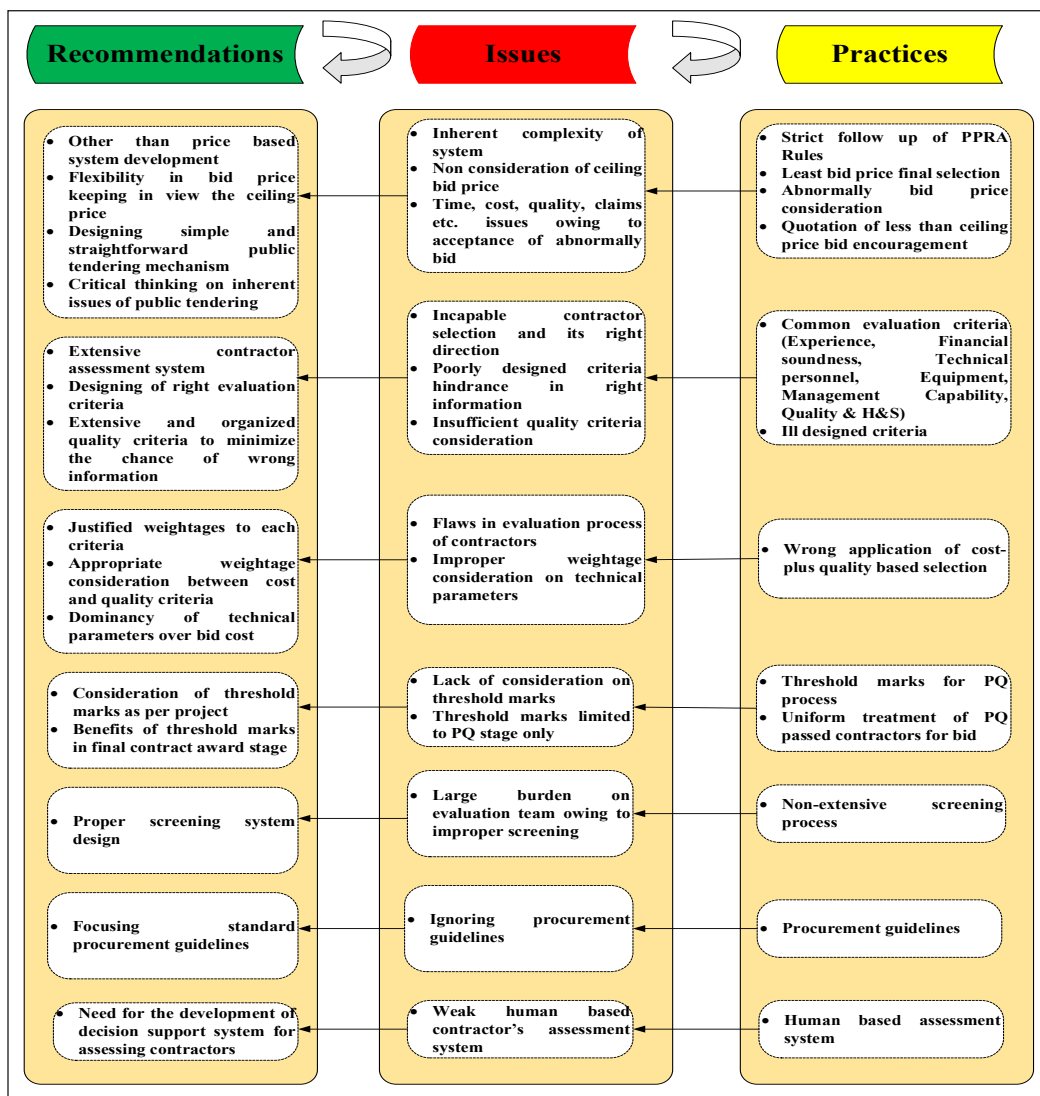


Figure 2. Public tendering theoretical outcome for Pakistan construction projects

end are fruitful in filling the wide gaps and pitfalls for public sector in Pakistan. Especially, a critical thought is required to overcome the issues of human assessment system that received a lot of critics. Construction sector in Pakistan is suggested to strictly follow the outcome for a better and prosperous construction sector.

CONCLUSION AND RECOMMENDATION

Public tendering in Pakistan is still at the embryonic stage. Exhaustive research was carried out to ascertain the current practices in public tendering and expert opinion on current issues of public tendering in Pakistan and various recommendations are put forward. A one-way ANOVA test clarified the divergence in the opinion of different stakeholders. Henceforth null hypothesis formulated in the beginning is rejected based on sig. values obtained in the one-way ANOVA test. The study results revealed several threatening results on a ground reality basis. The study concludes that in Pakistan, construction projects are turning into a modern phase and contractors are not capable enough to confront to meet the demands of new challenges. This has resulted in the failure of several projects in Pakistan. Further results revealed that a capable contractor selection is still an unresolved issue of public tendering. This is because the quality criteria on which contractors were assessed are not enough and not correctly designed. Also, a proper weightage on quality criteria and cost is not developed yet, leading to incapable contractor selection.

Furthermore, contractors passing the prequalification criteria are treated equally, which is not in favor of the system. Currently, clients are not interested in redesigning the threshold marks that would result in severe negative outcome soon. Several such reasons are responsible for complexity in public tendering comparing to the private sector. Many alarming results were obtained on bid price selection also. For instance, in Pakistan, the concept of accepting abnormal bid is prevailing and the clients offer the project to one who quotes the least bid price, dodging the clauses of PPRA. This system is believed to be a significant failure of public projects. The study concludes that competent contractor is vital in undertaking projects especially to cope with the advancement of technology and the complex nature of nowadays project. As such rigorous criteria must be included in the assessment stage to truly reflect the capacity and the capability of the contractor. In addition to this, decision making should be aided by automated decision making which will help to eliminate the biasness created in the human-judgement as per current practices in Pakistan. The study ends up with a theoretical outcome for public sector that is a novel contribution in the current knowledge. This study calls for exploring detailed project case studies to validate the findings further. Moreover, it recommends developing a decision support model for improving the current flaws in public tendering in Pakistan.

ACKNOWLEDGMENT

All praise to Almighty God, without His support, we would not be able to write a single sentence.

REFERENCES

- Alzahrani, J. I., & Emsley, M. W. (2013). The impact of contractors' attributes on construction project success: A post construction evaluation. *International Journal of Project Management*, 31(2), 313-322. doi: <https://doi.org/10.1016/j.ijproman.2012.06.006>
- Ayoti, B. (2012). *Factors influencing effectiveness in tendering process in public sector; The case of Nyeri County, Kenya* (Doctoral dissertation). University of Nairobi, Kenya.
- Azhar, N., Farooqui, R. U., & Ahmed, S. M. (2008, August 4-5). Cost overrun factors in construction industry of Pakistan. In *First International Conference on Construction in Developing Countries (ICCIDC-I), Advancing and Integrating Construction Education, Research & Practice* (pp. 499-508). Karachi, Pakistan.
- Birjandi, A. K., Akhyani, F., Sheikh, R., & Sana, S. S. (2019). Evaluation and selecting the contractor in bidding with incomplete information using MCGDM method. *Soft Computing*, 23(20), 10569-10585. doi: <https://doi.org/10.1007/s00500-019-04050-y>
- Bochenek, J. (2014). The contractor selection criteria in open and restricted procedures in public sector in selected EU countries. *Procedia Engineering*, 85, 69-74. doi: <https://doi.org/10.1016/j.proeng.2014.10.530>
- Cheaitou, A., Larbi, R., & Al-Housani, B. (2019). Decision making framework for tender evaluation and contractor selection in public organizations with risk considerations. *Socio-Economic Planning Sciences*, 68(January 2017), 1-12. doi: <https://doi.org/10.1016/j.seps.2018.02.007>
- Elsayah, O. S. (2016). *A framework for improvement of contractor selection procedures on major construction project in Libya*. Retrieved October 27, 2018, from <https://www.napier.ac.uk/~media/worktribe/output-453191/a-framework-for-improvement-of-contractor-selection.pdf>
- Farooqui, R. U., Saqib, M., Arif, F., & Lodi, S. H. (2008, August 4-5). An assesment of general trends adopted for bidding and procurement in the construction indystry of Pakistan. In *First International Conference on Construction In Developing Countries (ICCIDC-I) "Advancing and Integrating Construction Education, Research & Practice"* (pp. 153-160). Karachi, Pakistan.
- Hochstetter, J., Cachero, C., Cares, C., & Sepúlveda, S. (2004). *Call for tenders challenges in practice: A field study*. Retrieved January 27, 2019, from http://www.inf.puc-rio.br/~cibse/CIBSEpapers/artigos/artigos_CIBSE12/paper_60.pdf
- Horat, I. M., Camanho, A. S., & Lima, A. F. (2013). Design of performance assessment system for selection of contractors in construction industry E-marketplaces. *Journal of Construction Engineering and Management*, 139(8), 910-917. doi: [https://doi.org/10.1061/\(ASCE\)CO.1943-7862.0000691](https://doi.org/10.1061/(ASCE)CO.1943-7862.0000691)
- Ibrahim, M., Bawole, J. N., Obuobisa-Darko, T., Abubakar, A. B., & Kumasey, A. S. (2017). The legal regime and the compliance façade in public procurement in Ghana. *International Journal of Public Sector Management*, 30(4), 370-390. doi: <https://doi.org/10.1108/IJPSM-09-2016-0156>

- Jaskowski, P., Biruk, S., & Bucon, R. (2009). Assessing contractor selection criteria weights with fuzzy AHP method application in group decision environment. *Automation in Construction, 19*, 120-126. doi: <https://doi.org/10.1016/j.autcon.2009.12.014>
- Jobling, P. E., & Smith, N. J. (2018). Experience of the role of contracts in megaproject execution. *Proceedings of the Institution of Civil Engineers-Management, Procurement and Law, 171*(1), 18-24. doi: <https://doi.org/10.1680/jmapl.17.00006>
- Judit, S. (2017, November 8-10). Days of EU law. In *Proceedings of the International Scientific Conference* (pp. 76-85). Győr, Hungary.
- Kadefors, A. (2005). Fairness in interorganizational project relations: Norms and strategies. *Construction Management and Economics, 23*(8), 871-878. doi: <https://doi.org/10.1080/01446190500184238>
- Khan, T. H., & Khan, A. Q. (2015). Effects of lowest bidding bid awarding system in public sector construction projects in Pakistan. *Developing Country Studies, 5*(3), 132-147.
- Khoso, A. R., & Yusof, A. M. (2020). Extended review of contractor selection in construction projects. *Canadian Journal of Civil Engineering, 47*(7), 771-789. doi: <https://doi.org/10.1139/cjce-2019-0258>
- Kim, S. Y., Tuan, N. K., Lee, J. D., Pham, H., & Luu, V. T. (2018). Cost overrun factor analysis for hospital projects in Vietnam. *KSCE Journal of Civil Engineering, 22*(1), 1-11. doi: <https://doi.org/10.1007/s12205-017-0947-5>
- Kog, F., & Yaman, H. (2016). A multi-agent systems-based contractor pre-qualification model. *Engineering, Construction and Architectural Management, 23*(6), 709-726. doi: <https://doi.org/10.1108/ECAM-01-2016-0013>
- Kog, F., Yaman, H., & Kog, F., & Yaman, H. (2014). A meta classification and analysis of contractor selection and prequalification. *Procedia Engineering, 84*, 302-310. doi: <https://doi.org/10.1016/j.proeng.2014.10.555>
- Kumaraswamy, M. M., & Anvuur, A. M. (2008). Selecting sustainable teams for PPP projects. *Building and Environment, 43*, 999-1009. doi: <https://doi.org/10.1016/j.buildenv.2007.02.001>
- Liu, B., Huo, T., Meng, J., Gong, J., Shen, Q., & Sun, T. (2015). Identification of key contractor characteristic factors that affect project success under different project delivery systems. *Journal of Management in Engineering, 32*(1), 1-11. doi: [https://doi.org/10.1061/\(ASCE\)ME.1943-5479.0000388](https://doi.org/10.1061/(ASCE)ME.1943-5479.0000388)
- Long, N. D., Ogunlana, S., Quang, T., & Lam, K. C. (2004). Large construction projects in developing countries: A case study from Vietnam. *International Journal of Project Management, 22*(7), 553-561. doi: <https://doi.org/10.1016/j.ijproman.2004.03.004>
- Lo, W., Lin, C. L., & Yan, M. R. (2007). Contractor's opportunistic bidding behavior and equilibrium price level in the construction market. *Journal of Construction Engineering and Management, 133*(6), 409-416. doi: [https://doi.org/http://dx.doi.org/10.1061/\(ASCE\)07339364\(2007\)133:6\(409\)](https://doi.org/http://dx.doi.org/10.1061/(ASCE)07339364(2007)133:6(409))
- Lo, W., & Yan, M. R. (2009). Evaluating qualification-based selection system. *Journal of Construction Engineering and Management, 135*(6), 458-465. doi: [https://doi.org/https://doi.org/10.1061/\(ASCE\)CO.1943-7862.0000013](https://doi.org/https://doi.org/10.1061/(ASCE)CO.1943-7862.0000013)
- Lundberg, S., & Bergman, M. A. (2017). Tendering design when price and quality is uncertain. *International Journal of Public Sector Management, 30*(4), 310-327. doi: <https://doi.org/10.1108/IJPSM-04-2016-0063>

- Mamavi, O., Meier, O., & Zerbib, R. (2017). How do strategic networks influence awarding contract? Evidence from French public procurement. *International Journal of Public Sector Management*, 30(4), 357-369. doi: <https://doi.org/10.1108/IJPSM-05-2016-0091>
- Maqsoom, A., Charoenngam, C., Masood, R., & Awais, M. (2014). Foreign market entry considerations of emerging economy firms: An example of Pakistani contractors. *Procedia Engineering*, 77, 222-228. doi: <https://doi.org/10.1016/j.proeng.2014.07.020>
- Melody, A. H. (2008). Considerations in determining sample size for pilot studies. *Research in Nursing and Health*, 31(2), 180-191. doi: <https://doi.org/10.1002/nur.20247>
- Morenikeji, W. (2006). *Research and analytical methods for social scientist, planners and environmentalist* (1st Ed.). Jos, Nigeria: Jos University Press Ltd.
- Murtagh, S. R., & Brooks, T. (2019). Critical success factors for social value in construction procurement in Northern Ireland. *Proceedings of the Institution of Civil Engineers-Management, Procurement and Law*, 172(5), 183-196. doi: <https://doi.org/10.1680/jmapl.19.00005>
- Ng, S. T., & Skitmore, R. M. (2001). Contractor selection criteria: A cost-benefit analysis. *IEEE Transactions on Engineering Management*, 48(1), 96-106. doi: <https://doi.org/10.1109/17.913169>
- Ng, S. T., Tang, Z., & Palaneeswaran, E. (2009). Factors contributing to the success of equipment-intensive subcontractors in construction. *International Journal of Project Management*, 27(7), 736-744. doi: <https://doi.org/10.1016/j.ijproman.2008.09.006>
- Patil, K. (2017). Public procurement policy for small and medium enterprises in developing countries: Evidence from India. *International Journal of Public Sector Management*, 30(4), 391-410. doi: <https://doi.org/10.1108/IJPSM-10-2016-0160>
- Phogat, S., & Gupta, A. K. (2019). Evaluating the elements of just in time (JIT) for implementation in maintenance by exploratory and confirmatory factor analysis. *International Journal of Quality and Reliability Management*, 36(1), 7-24. doi: <https://doi.org/10.1108/IJQRM-12-2017-0279>
- PPRA. (2015). *Annual report 2014-15-public procurement regulatory authority*. Retrieved May 13, 2020, from <https://www.ppra.org.pk/areports.asp>
- Wahlberg, A. E., & Poom, L. (2015). An empirical test of nonresponse bias in internet surveys. *Basic and Applied Social Psychology*, 37(6), 336-347. doi: <https://doi.org/10.1080/01973533.2015.1111212>
- Wang, J., Yu, B., Tam, V. W. Y., Li, J., & Xu, X. (2019). Critical factors affecting willingness of design units towards construction waste minimization: An empirical study in Shenzhen, China. *Journal of Cleaner Production*, 221, 526-535. doi: <https://doi.org/10.1016/j.jclepro.2019.02.253>
- Watt, D. J., Kayis, B., & Willey, K. (2010). The relative importance of tender evaluation and contractor selection criteria. *International Journal of Project Management*, 28(1), 51-60. doi: <https://doi.org/10.1016/j.ijproman.2009.04.003>
- Wondimu, P. A., Klakegg, O. J., Lohne, J., & Lædre, O. (2020). Experiences with best-value procurement in Norway and the Netherlands. *Journal of Construction Engineering and Management*, 146(5), 1-13. doi: [https://doi.org/10.1061/\(ASCE\)CO.1943-7862.0001814](https://doi.org/10.1061/(ASCE)CO.1943-7862.0001814)

- Wong, C. H., Holt, G. D., & Cooper, P. A. (2000). Lowest price or value? Investigation of UK construction clients' tender selection process. *Construction Management and Economics*, 18(7), 767-774. doi: <https://doi.org/10.1080/014461900433050>
- Zhang, Y., Luo, H., & He, Y. (2015). A system for tender price evaluation of construction project based on big data. *Procedia Engineering*, 123, 606-614. doi: <https://doi.org/10.1016/j.proeng.2015.10.114>



Modeling of Inactivation of Biofilm Composing Bacteria with Low Intensity Electric Field: Prediction of Lowest Intensity and Mechanism

Mokhammad Tirono^{1*} and Suhariningsih²

¹Physics Department, Faculty of Science and Technology, Universitas Islam Negeri Maulana Malik Ibrahim Malang, Malang, East Java, Indonesia

²Physics Department, Faculty of Science and Technology, Airlangga University, Surabaya, East Java, Indonesia

ABSTRACT

Sterilization using high-intensity electric fields is detrimental to health if safety is inadequate, so it is necessary to study the possibility of sterilization using low-intensity electric fields. This study aims to determine the lowest electric field intensity and treatment time to deactivate the bacteria that make up the biofilms and explain the mechanism of inactivation. The study samples were biofilms from the bacteria *Pseudomonas aeruginosa* and *Staphylococcus epidermidis* grown on the catheter. The modeling formula was developed from the Pockels effect and the Weibull distribution with the treatment using a square pulse-shaped electric field with a pulse width of 50 μ s and an intensity of 2.0-4.0 kV/cm. The results showed that the threshold for irreversible electroporation of both samples occurred in the treatment using an electric field with an intensity of 3.5 kV/cm and 3.75 kV/cm, respectively, where the size and type of Gram of bacteria influenced. Moreover, the time of the treatment had an effect when irreversible electroporation occurred. However, when there was reversible electroporation, the effect of treatment time on the reduction in the number of bacteria was not significant. Also, changes in conductivity affected the reduction in the number of bacteria when reversible electroporation occurred.

Keywords: Bacteria, biofilms, electric field, electroporation, reduction

ARTICLE INFO

Article history:

Received: 17 August 2020

Accepted: 25 November 2020

Published: 22 January 2021

DOI: <https://doi.org/10.47836/pjst.29.1.08>

E-mail addresses:

tirono.uin.malang@gmail.com (Mokhammad Tirono)

suhariningsih.unair@gmail.com (Suhariningsih)

* Corresponding author

INTRODUCTION

Bacteria often form biofilms on the surfaces of medical devices such as venous catheters, breast implants, pacemakers, and others (Lazăr & Chifriuc, 2010). Unfortunately, materials used in these medical devices generally cannot withstand high temperature.

Moreover, biofilms have proven to be very resistant to several types of antibiotics and chemical disinfectants (Eriksson, 2011), making it difficult to inhibit their growth. Therefore, a right sterilization technique that can reduce the number of bacteria quickly but also does not cause heat to the materials of medical devices is highly needed, such as sterilization using high-intensity electric fields (Ramaswamy et al., 2019; Bonetta et al., 2014). In fact, the interaction between high-intensity electric fields with bacteria causes irreversible electroporation to the cell membrane (Miklavčič, 2017), which in turn induces bacterial death (Rosin & Kurrasch, 2018). However, exposure to these high-intensity electric fields can harm the organs of the human body or other living things around the exposure if the security is less than optimal. Negative effects that can occur are complaints on the face (Skulberg et al., 2001), decreased red blood cells (Di et al., 2018), reduction in sperm count and motility, damage to Deoxyribose Nucleic Acid (DNA), and oxidative stress (Aslankoc et al., 2018).

To reduce the negative impacts of sterilization on medical devices and human body, sterilization using low-intensity electric fields can be done, particularly for one that does not require short period of time in its treatment process. This, therefore, requires data on the lowest electric field intensity and treatment time for inactivating bacteria as well as data on a deactivation mechanism for their development. For the effectiveness of its implementation, it requires mathematical modeling that can predict the lowest electric field intensity and treatment time for the inactivation of the bacteria that make up the biofilms, and that can be used to explain the mechanism of deactivation.

Several studies have been conducted on mathematical modeling of the use of electric fields. Previously, a study was conducted on mathematical modeling of the use of electric fields to predict the growth of *Escherichia coli* bacteria in carrot juice (Singh et al., 2017). There has also been another modeling to predict the effect of the electric field on changes in spore morphology in *Bacillus atropheus* bacteria (Qiu et al., 2014), ion transport inside and outside the soft layer in Gram-positive bacteria (Moran et al., 2018), and changes in the bacterial pore radius (Mescia et al., 2019). Specifically, a model developed by Singh et al. (2017) still used a high electric field intensity at 9-21 kV/cm, while a model developed by Qiu et al. (2014), Moran et al. (2018), and Mescia et al. (2019) had not reported a reduction in the number of bacteria that occurred. Therefore, modeling to predict the lowest intensity in order to reduce the number of bacteria is highly needed.

In this study, a mathematical model developed from the Pockels effect and the Weibull distribution has been formulated. The present study aims at predicting the lowest electric field intensity and treatment time for inactivating bacteria and explaining the deactivation mechanism.

METHODS

Theory

This study used an electric field generated using parallel plates, so the field intensity between the plates is (Equation 1):

$$\mathbf{E} = \frac{\Delta V}{d} \quad [1]$$

where \mathbf{E} is the electric field between parallel plates, d is the distance between the plates, and ΔV is the potential difference between the plates. Bacterial cell membranes, especially those in the lipid bilayer, have anisotropic (Pogozheva et al., 2013; Huh et al., 2016) and electro-optical properties (Bunin et al., 2005), so when they interact with an external electric field, they experience a change in the refractive index (Eismann, 2012), which satisfies the Equation 2:

$$n(\mathbf{E}) = n - \frac{1}{2} r n^3 \mathbf{E} \quad [2]$$

where r is called the Pockel coefficient, n and $n(\mathbf{E})$ are the refractive index before and after being subjected to an electric field, respectively, and \mathbf{E} is the electric field.

Bacteria, especially lipid bilayers, are media that tend to be uniaxial (Galdiero et al., 2013), so when interacting with electric fields their refractive index is expressed as $n_x = n_y = n_o$ and $n_z = n_e$ (Eismann, 2012). If the electric field points to the z-axis, then $\mathbf{E}(x, y, z) = (0, 0, \mathbf{E})$. Therefore, the ellipsoid refractive index is expressed as Equation 3 and 4 (Eismann, 2012), i.e.:

$$n_o(\mathbf{E}) = n_o(0) - \frac{1}{2} n_o^3 r_{13} \mathbf{E} \quad [3]$$

$$n_e(\mathbf{E}) = n_e(0) - \frac{1}{2} n_e^3 r_{33} \mathbf{E} \quad [4]$$

For example, the electric field is changed by ΔE , so the extraordinary refractive index changes that occur is (Equation 5):

$$\Delta n_e = -\frac{1}{2} n_e^3 r_{33} \Delta E \quad [5]$$

where Δn_e is the change of the refractive index in z axis.

Diffusion of Water and Ions in the Cell Membrane

Exposure to the electric field in bacteria triggers changes in cell membrane permeability (Sweeney et al., 2018). Increased permeability causes changes in the diffusion of water and ions in the cell membrane (Kakorin & Neumann, 2002) expressed as Equation 6:

$$\Delta n_e = -\Delta f_W n_e + \Delta f_W n_a \quad [6]$$

The substitution of Equation 5 with 6 is done by changing the electric field from $E = 0$ to E , and then it is obtained as Equation 7:

$$\Delta f_W = \frac{1}{2} \frac{n_e^3 r}{n_e - n_a} E \quad [7]$$

where $\Delta f_W = f_W(E) - f_W(0)$ is the fraction of increasing volume of water and ion flow in the membrane, and n_a is the refractive index of water.

Cell Membrane Conductivity

Increased ion flow through the cell membrane will cause an increase in cell conductivity. The conductivity of the cell membrane is determined using the conductance of the permeable pore (m), assuming that the pore radius is R (Pavlin et al., 2005), so the conductivity of the cell membrane is obtained as Equation 8:

$$\sigma = m\pi R^2 \frac{\sigma_s}{d_m} = S_{por} \frac{\sigma_s}{d_m} \quad [8]$$

where σ_s is the conductivity of the pore, d_m is the thickness of the cell membrane, and S_{por} is the surface area of all conducting pores. Changes in the diffusion of water and ions that pass through the cell membrane change the conductivity of the pores in the cell membrane, which becomes Equation 9:

$$\sigma_s(E) = \sigma_s(0) + \Delta\sigma_s \quad [9]$$

where $\sigma_s(0)$ is the pore conductivity at condition $E = 0$, while $\sigma_s(E)$ is the pore conductivity at the electric field condition E . Thus, the conductivity of the cell membrane, when subjected to an electric field E , is (Equation 10)

$$\sigma(E) = \sigma \left(1 + \frac{1}{2} \frac{n_e^3 r}{n_e - n_a} m_{por} E \right) \quad [10]$$

where m_{por} is the number of pores in a bacterial cell. As a result of the increased conductivity of cell membranes, membrane damage occurs, which causes bacterial death (Pagán & Mackey, 2000).

The Reduction of the Number of Bacteria

The reduction in the number of bacteria in the logarithmic form is determined by modifying the Weibull distribution equation, thus obtaining the Equation 11 (Puértolas et al., 2009):

$$\log \frac{N(t)}{N_0} = - \left(\frac{W}{\delta} \right)^\rho \quad [11]$$

where the ρ value is the shape parameter. $N(t)$ is the number of bacteria that remain after exposure during t , N_0 is the number of bacteria before exposure, and W is the electrical energy used.

The amount of electrical energy W needed to deactivate bacteria (Monfort et al., 2012) is (Equation 12):

$$W = \sigma(E) E^2 t \quad [12]$$

The scale parameter (δ) is determined from a model based on the Gompertz function (Maria et al., 2011), which is expressed as Equation 13:

$$\delta = b e^{-e^{c(E-d)}} \quad [13]$$

where δ value represents the specific energy to do first inactivation, E is the electric field strength, b , c and d are the model parameters.

The reduction in the number of bacteria is determined by substituting Equation 10, 12, and 13 into Equation 11, to obtain Equation 14:

$$\log \frac{N(t)}{N_0} = \left(\frac{\sigma \left(1 + \frac{1}{2} \left(\frac{n_e^3 r}{n_e - n_a} \right) E m_{por} \right) E^2 t}{\delta} \right)^\rho \quad [14]$$

where ρ value accounts for upward concavity of a survival curve ($\rho < 1$), a linear survival curve ($\rho = 1$), and downward concavity ($\rho > 1$) (Puértolas et al., 2009). Equation 14 shows that the electric field intensity and treatment time affect the reduction in the number of bacteria.

Biofilm Growth

Study samples were *Pseudomonas aeruginosa* and *Staphylococcus epidermidis* bacteria grown on catheters. Pure isolates from the bacteria *Pseudomonas aeruginosa* and *Staphylococcus epidermidis* were each inserted into a tube containing 50 ml of sterile liquid Nutrient Broth (NB) and incubated in an incubator for 24 hours at a temperature of 37°C. A clean and sterile cut of the catheter was inserted into a tube that was covered with *Pseudomonas aeruginosa* and *Staphylococcus epidermidis* bacteria. The tube containing the bacteria was incubated again for 3 days at a temperature of 37°C and shaken at 100 rpm.

Treatment Process

The biofilm treatment was carried out using a pulsed electric field with an intensity of 2.0-4.0 kV/cm and a pulse width of 50 μ s for 5-25 minutes. Moreover, the space around the treatment area was sterilized, the ambient temperature was set to around 28°C, and the humidity was at around 70%. The treatment process for both control and treatment groups was repeated five times..

Bacterial Release from Biofilms

The taking of the catheter pieces that had been overgrown with biofilms was carried out using sterile tweezers, in both control and treatment groups, so as not to contaminate other bacteria. Before being treated and diluted, the sample was cleaned with purified water that had been sterilized to release planktonic cells. After being treated, the catheter piece was inserted into a test tube containing 10 ml of 0.9% NaCl, which was then added with 0.5-gram glass beads and vibrated using a vortex for 2 minutes to release the bacterial cells (Krysinski et al., 1992). After the bacteria were released, then 1.0 ml was taken to do the dilution.

Calculation of the Number of Colonies

Before doing the calculation, at first, a measure of the bacterial culture that had been released from the catheter was carried out. Dilution was done by taking 1.0 ml of bacterial culture and placing it in a bottle containing 9.0 ml of sterile distilled water, so the volume became 10 ml. The bacterial culture from the dilution was taken again as much as 1.0 ml and put into a bottle containing 9.0 ml sterile distilled water, so the volume was 10 ml. The dilution was repeated according to the calculation requirements. After the dilution process, a culture of 1.0 ml was taken and then sprinkled on a petri dish that had been given liquid plate count agar (PCA) media. Next, the Petri dishes that had been cultured were incubated in an incubator for 24 hours at 37°C. After the colony was formed, the colony count was calculated using a Colony Counter.

Variable Values in Modeling

The intensity of the electric field used to treat was 2.0 - 4.0 kV/cm, while the time of treatment was 5-25 minutes. The conductivity value (σ) of *Pseudomonas aeruginosa* bacterial cells was determined by referring to the conductivity of *Escherichia coli* (Gram-negative) bacteria, which was at a concentration of 1×10^9 - 4×10^9 cfu/ml; the conductivity was 2×10^{-6} - 1.4×10^{-5} mho/m. Meanwhile, the conductivity value (σ) of *Staphylococcus epidermidis* refers to the conductivity of *Bacillus subtilis* (Gram-positive), which was at a concentration of 1×10^8 - 8×10^8 cfu/ml; the conductivity was 0.5×10^{-5} - 5×10^{-5} mho/m (Fangxia et al., 2013). Pockels coefficient r of the cell membrane was 2.6 pm/V (Hajj et

al., 2009), lipid refractive index n_e was 1.384, water refractive index n_a was 1.342, and the number of pores was given the values as expressed by Martinac et al. (2008). Moreover, the ρ value was 0.75, while the δ value was obtained from Equation 13 by giving a d value depending on the shape and size of the bacteria and E was the electric field strength used for inactivation (Puértolas et al., 2009).

RESULTS

Electric Field Effect

Pseudomonas aeruginosa bacteria are Gram-negative, motile, and rod-shaped about 1-5 μm long and 0.5-1.0 μm wide (Diggle & Whiteley, 2020), while Gram-positive *Staphylococcus epidermidis* bacteria are cocci shaped and 0.5-1.5 μm in diameter. The reduction in the number of *Pseudomonas aeruginosa* bacteria in the log due to treatment with an electric field intensity of 2.0 - 4.0 kV/cm is shown in Figure 1, where the negative sign indicates a reduction. Figure 1 shows that the treatment using an electric field with an intensity of 2.0 - 3.25 kV/cm formed a line close to horizontal, which means that the reduction in the number of bacteria is relatively small, so it is not effective to be used in bacterial inactivation. Meanwhile, line deflection occurred on treatment with intensity from 3.5 kV/cm to 3.75 kV/cm, which means that the decrease in the number of bacteria increases or is at the threshold for irreversible electroporation. The line decreased when there was a treatment with an intensity of 4.0 kV/cm, so it is assumed that irreversible electroporation has occurred.

Figure 1 shows that the modeling result graph has the same pattern as the experimental result graph but has a R-squared of 0.923 for the 10-minute treatment time and 0.961 for the 25-minute treatment time. The modeling graph was obtained by entering the scale parameter values that changed along with changes in the electric field intensity as shown

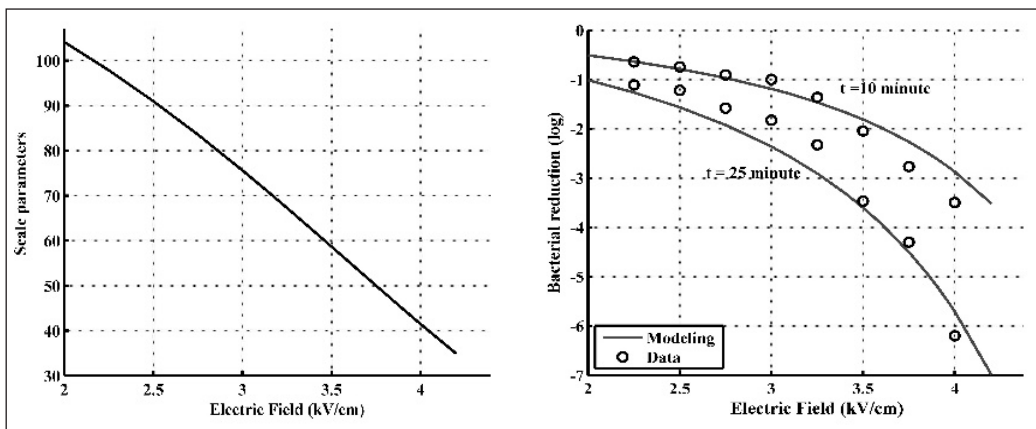


Figure 1. The reduction in the number of *Pseudomonas aeruginosa* bacteria after being treated with an electric field

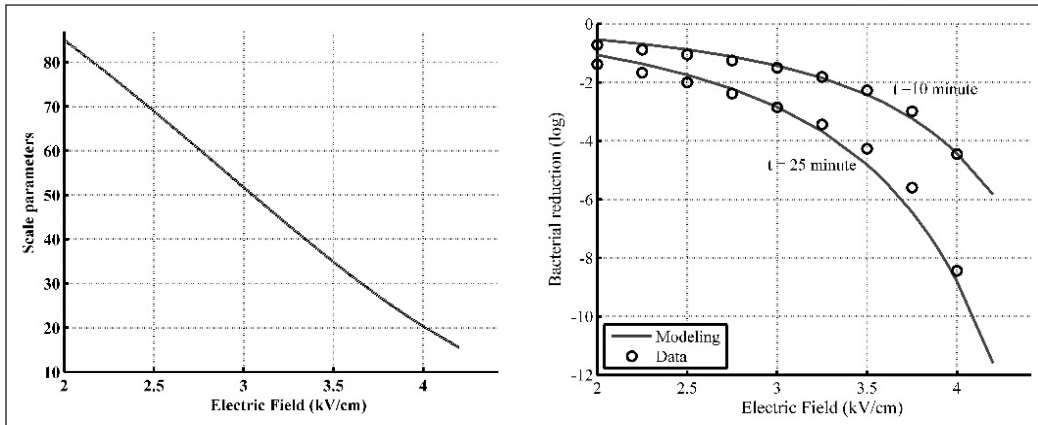


Figure 2. The reduction in the number of *Staphylococcus epidermidis* bacteria after being treated with an electric field

in Figure 1. Changes in scale parameters are identical to those reported by Puértolas et al. (2009), suggesting that the higher the intensity of electric field used, the lower the values of scale parameters. Scale parameters are considered as a measure of the resistance of bacteria to treatment using an electric field (Alvarez et al., 2003), which also depends on the temperature and PH of the medium (Huang et al., 2012). The constants b , c , and d from Equation 13, which were 150, 0.63 and 3.6, respectively, while the value of E changed according to changes in the intensity of the electric field used.

Staphylococcus epidermidis bacteria treated using an electric field with an intensity of 2.0 - 4.0 kV/cm experience a reduction in the number of bacteria, graphically the reduction is shown in Figure 2. The graph shows that biofilms treated using an electric field intensity of 2.0 - 3.25 kV/cm had a horizontal line because it was still below the irreversible electroporation threshold. The graph goes down when treated using an electric field with an intensity of 3.5 - 3.75 kV/cm, which means that the reduction in the number of bacteria increases because the bacterial cell membrane is at the threshold for irreversible electroporation. The reduction in the number of bacteria becomes large with a treatment using an electric field with an intensity of 4.0 kV/cm because the bacterial cell membrane had undergone irreversible electroporation.

Figure 2 shows a similar pattern with the graph of the modeling result and the experimental result, which means that a mathematical model can be used to predict the reduction in the number of bacteria on the biofilms from *Staphylococcus epidermidis*. The modeling result graph had a R-squared of 0.975 when given the 10-minute treatment and 0.980 when the treatment time was 25 minutes. The modeling graph was obtained by giving the scale parameter values as shown in Figure 2. The constants b , c , and d from Equation 13, which were 150, 0.63, and 2.9, respectively, while the E value changed according to changes in the intensity of the electric field used.

Treatment Time Effect

When the electric field used is different, the impact on bacteria is also different, which also impacts on the difference in the the reduction in the number of bacteria that occurs. Figure 3 is the effect of treatment time on reducing the number of *Pseudomonas aeruginosa* bacteria, and Figure 4 is the effect of treatment time on reducing the number of *Staphylococcus epidermidis* bacteria. The two graphs show that the treatment using an electric field with

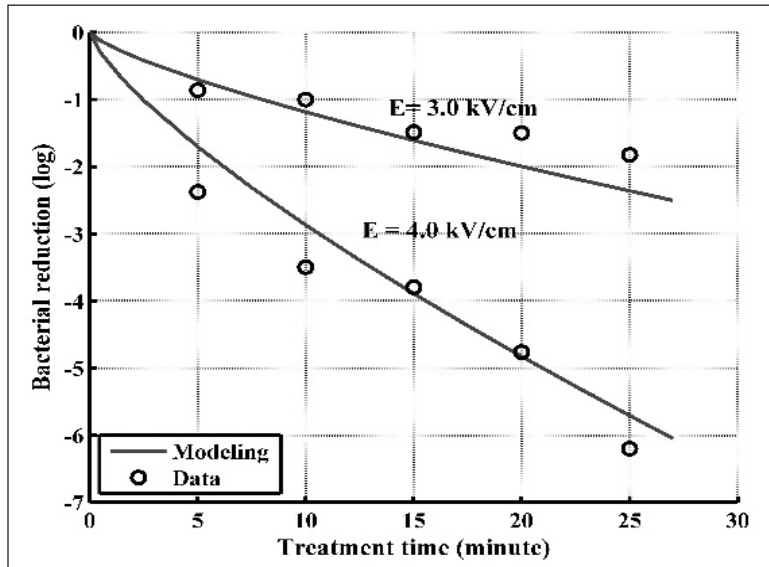


Figure 3. Reduction in the number of *Pseudomonas aeruginosa* due to changes in the treatment time

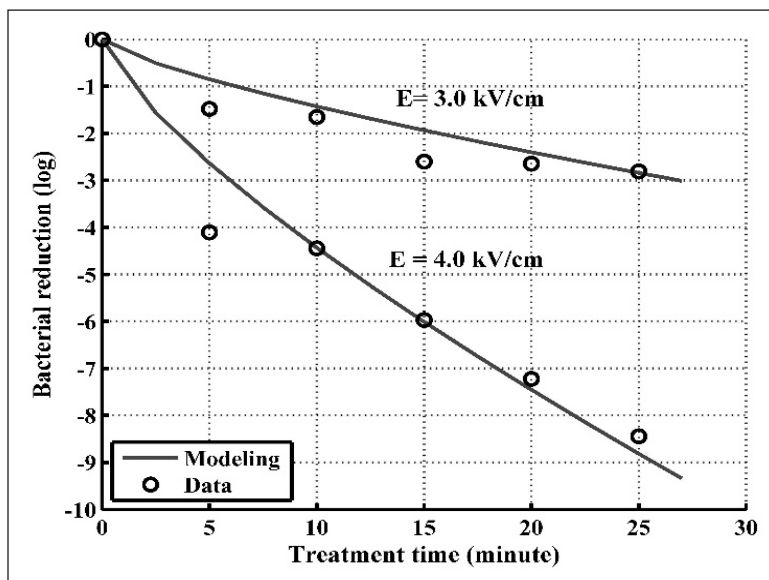


Figure 4. Reduction in the number of *Staphylococcus epidermidis* due to changes in the treatment time

an intensity of 3.0 kV/cm had a small effect on reducing the number of bacteria because it was still below the irreversible electroporation threshold. Meanwhile, the treatment using an electric field with an intensity of 4.0 kV/cm had a significant effect on reducing the number of bacteria because irreversible electroporation had occurred.

Figures 3 and 4 show the similarity of the pattern between the graph of the modeling result and the experimental result, which means that the mathematical model can be used to predict the decrease in the number of bacteria on biofilms from *Pseudomonas aeruginosa* and *Staphylococcus epidermidis* due to changes in treatment time. For *Pseudomonas aeruginosa*, the modeling R-squared were 0.991 and 0.999 for the electric field intensity of 3.0 kV/cm and 4.0 kV/cm, respectively, while for *Staphylococcus epidermidis* bacteria the modelling R-squared were 0.894 and 0.946 accordingly.

DISCUSSION

The outermost part of a bacterial cell is the plasma membrane, which is a barrier between the inside and outside of the cell, so it has a very important role (Silhavy et al., 2010). The cell membrane has a positive outer and inner negative charge, thus forming a potential difference between them (Gottenbos, 2001), which is called the transmembrane potential. In fact, the transmembrane potential becomes an obstacle for the circulation of substances from outside to inside or vice versa. However, in the cell membrane, there are ion channels that control the flow of solutes into the cells and organelles, playing an important role in maintaining homeostasis (Hohle et al., 2011). The interaction of the external electric field with the cell causes a shift in charge, especially the cell membrane, so the cell experiences electronic polarization. Electronic polarization itself causes a change in the refractive index of a cell, resulting in permeability changes. Due to the electrooptic nature of the cell membrane which tends to be anisotropic, the changes satisfy the Equation 3 and 4. Moreover, increased permeability, causing the flow of water and ions that pass through the cell membrane, also increases because the pore diameter enlarges (Kotnik et al., 2019), as formulated in Equation 7. Increased ion flow causes an increase in cell membrane conductivity (Pliquett et al., 2007), as in Equation 10. Furthermore, the part of the cell membrane with increased conductivity will cause damage (Silve et al., 2016), so the bacteria are inactive. Treatment using an electric field with an intensity of 2.0 - 3.25 kV/cm makes the conductivity of the cell membrane increases insignificantly, so the reduction in the number of bacteria is still low. In addition to the increase in conductivity, the interaction between the electric field and bacteria causes the transmembrane voltage to increase, where the increase satisfies the equation $\Delta\psi = 1.5 ER_a \cos\theta$ (Pavlin et al., 2005) where R_a is the cell radius and E is the electric field. When treated using an electric field with an intensity of 3.5 - 3.75 kV/cm, the channel porosity radius and transmembrane voltage are at the threshold of irreversible electroporation, so the reduction in the number of bacteria increases, and its visibility is

shown in Figures 5 and 6. Part A is the condition of the biofilms before being treated, while part B is the condition after being treated, so part A shows the adhering bacteria covered with carbohydrates, while part B has a few bacteria. Treating the bacteria using an electric field with an intensity of 4.0 kV/cm makes the conductivity of the cell membrane increase sharply, so the amount of reduction in bacteria is very large. Also, treated the bacteria using an electric field with an intensity of 4.0 kV/cm makes the conductivity of the cell membrane increase sharply, resulting in a potential breakdown in the cell membrane (Akinlaja & Sachs, 1998). Therefore, treatment using high-intensity electric fields requires a very short amount of time.

This modeling is effective for predicting the reduction in the number of bacteria due to treatment using low electric field intensity. The modeling error when compared with experimental data was at an average of 8.54% for *Pseudomonas aeruginosa* and 7.82% for *Staphylococcus epidermidis*. The error will increase when electric field intensities above 4.5 kV/cm is applied. The modeling conducted by Singh et al. (2017) has a lower error,

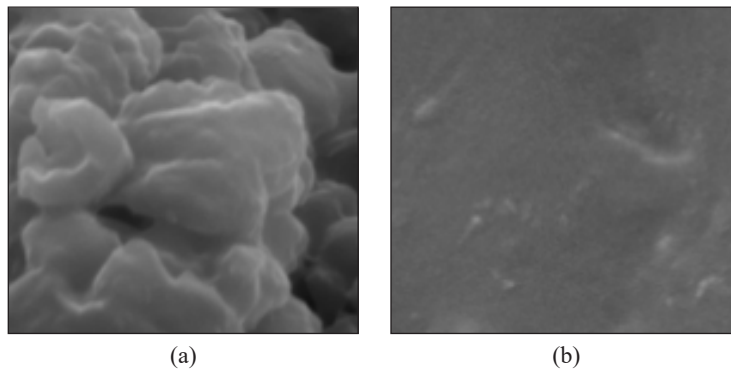


Figure 5. Biofilms from *Pseudomonas aeruginosa* bacteria: (a) before treatment; and (b) after treatment with an electric field intensity of 3.5 kV/cm for 25 minutes. Magnification of 10,000 x

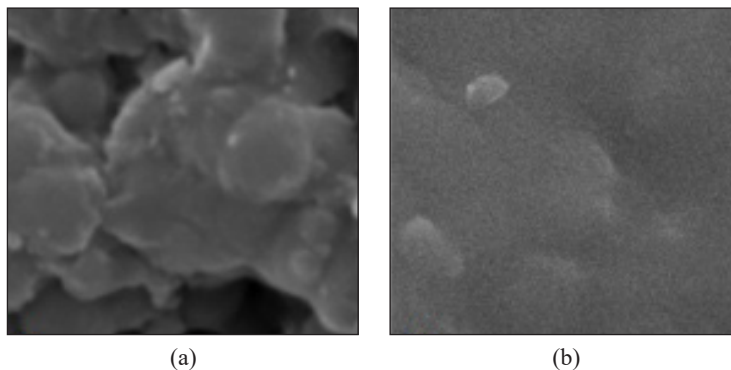


Figure 6. Biofilms from *Staphylococcus epidermidis* bacteria: (a) before treatment; and (b) after treatment with an electric field intensity of 3.5 kV/cm for 25 minutes. Magnification of 10,000 x

which is less than 5% with an electric field intensity of 9-21 kV/cm, but its application has not been reported at lower electric field intensities. Similar modeling was also carried out by Peleg (2017) by giving a treatment using an electric field of 8.0 - 20.0 kV/cm.

CONCLUSION

This study discusses the deactivation model of bacteria that have formed biofilms using the electrooptical principle combined with the Weibull distribution equation to predict a bacterial reduction. The model is used to predict the reduction in the number of bacteria due to treatment using an electric field at a low intensity. The study has found a threshold for irreversible electroporation on biofilms from *Pseudomonas aeruginosa* and *Staphylococcus epidermidis* bacteria at an electric field intensity of 3.5kV/cm and 3.75 kV/cm, respectively. In addition, the time of the treatment has an effect if the treatment uses an electric field with an intensity above the threshold, otherwise it does not affect. Also, the interaction of the electric field with bacteria causes electronic polarization, thereby lowering the refractive index and increasing the permeability of the cell membrane. The high permeability of the cell membrane causes the flow of water and ions through the cell membrane to increase, so the conductivity of the cell membrane increases. The high conductivity causes damage to the cell membrane, so the bacteria die.

ACKNOWLEDGMENT

This research was carried out on the financial assistance from the Directorate of Islamic Higher Education, Indonesian Ministry of Religious Affairs. Therefore, we thank the Minister of Religious Affairs along with his staff. We also thank the research and community service institution of State Islamic Universities of Maulana Malik Ibrahim Malang.

REFERENCES

- Akinlaja, J., & Sachs, F. (1998). The breakdown of cell membranes by electrical and mechanical stress. *Biophysical Journal*, 75(1), 247-254. doi: 10.1016/S0006-3495(98)77511-3
- Alvarez, I., Pagan, R., Condon, S., & Raso, J. (2003). The influence of process parameters for the inactivation of *Listeria monocytogenes* by pulsed electric fields. *International Journal of Food Microbiology*, 87(1-2), 87-95. doi: [https://doi.org/10.1016/S0168-1605\(03\)00056-4](https://doi.org/10.1016/S0168-1605(03)00056-4)
- Aslankoc, R., Gumral, N., Saygin, M., Senol, N., Asci, H., Cankara, F. N., & Comlekci, F. (2018). The impact of electric fields on testis physiopathology, sperm parameters and DNA integrity - The role of resveratrol. *Andrologia*, 50(4), 1-11. doi: 10.1111/and.12971
- Bonetta, S., Bonetta, S., Bellero, M., Pizzichemi, M., & Carraro, E. (2014). Inactivation of *Escherichia coli* and *Staphylococcus aureus* by pulsed electric fields increases with higher bacterial population and with agitation of liquid medium. *Journal of Food Protection*, 77(7), 1219-1223. doi: 10.4315/0362-028X.JFP-13-487

- Bunin, V. D., Ignatov, O. V., Guliy, O. I., Zaitseva, I. S., Neil, D. O., & Ivnikskii, D. (2005). The electrooptical parameters of suspensions of *Escherichia coli* XL-1 cells interacting with helper phage M13K07. *Microbiology*, 74(2), 164-168.
- Di, G., Gu, X., Lin, Q., Wu, S., & Kim, H. B. (2018). A comparative study on effects of static electric field and power frequency electric field on hematology in mice. *Ecotoxicology and Environmental Safety*, 166(September), 109-115. doi: 10.1016/j.ecoenv.2018.09.071
- Diggle, S. P., & Whiteley, M. (2020). Microbe profile: *Pseudomonas aeruginosa*: Opportunistic pathogen and lab rat. *Microbiology*, 166(1), 30-33. doi: 10.1099/mic.0.000860
- Eismann, M. T. (2012). Optical radiation and matter. In M. T. Eismann (Ed.), *Hyperspectral remote sensing* (pp. 37-82). Washington, USA: SPIE Press. doi: 10.1117/3.899758.ch2
- Eriksson, J. (2011). *Biofilm growth in strong electric fields* (Master Thesis). KTH Royal Institute of Technology, Sweden.
- Fangxia, S., Miaomiao, T., Hong, X., Zhencheng, X., & Maosheng, Y. (2013). Development of a novel conductance-based technology for. *Environmental Chemistry*, 58(4), 440-448. doi: 10.1007/s11434-012-5621-1
- Galdiero, S., Falanga, A., Cantisani, M., Vitiello, M., Morelli, G., & Galdiero, M. (2013). Peptide-lipid interactions: experiments and applications. *International Journal of Molecular Sciences*, 14(9), 18758-18789. doi: 10.3390/ijms140918758
- Gottenbos, B. (2001). Antimicrobial effects of positively charged surfaces on adhering Gram-positive and Gram-negative bacteria. *Journal of Antimicrobial Chemotherapy*, 48(1), 7-13. doi: 10.1093/jac/48.1.7
- Hajj, B., Pioufle, B. L., Osaki, T., & Suzuki, H. (2009). Electro-optical imaging microscopy of dye-doped artificial lipidic membranes. *Biophysical Journal*, 97(December), 2913-2921. doi: 10.1016/j.bpj.2009.08.055
- Hohle, T. H., Franck, W. L., Stacey, G., & O'Brian, M. R. (2011). Bacterial outer membrane channel for divalent metal ion acquisition. *Proceedings of the National Academy of Sciences of the United States of America*, 108(37), 15390-15395. doi: 10.1073/pnas.1110137108
- Huang, K., Tian, H., Gai, L., & Wang, J. (2012). A review of kinetic models for inactivating microorganisms and enzymes by pulsed electric field processing. *Journal of Food Engineering*, 111, 191-207. doi:10.1016/j.jfoodeng.2012.02.007
- Huh, K., Oh, D., Son, S. Y., Yoo, H. J., Song, B., Cho, D. I. D., ... & Kim, S. J. (2016). Laminar flow assisted anisotropic bacteria absorption for chemotaxis delivery of bacteria-attached microparticle. *Micro and Nano Systems Letters*, 4(1), 1-9. doi: 10.1186/s40486-016-0026-6
- Kakorin, S., & Neumann, E. (2002). Electrooptical relaxation spectrometry of membrane electroporation in lipid vesicles. *A: Physicochemical and Engineering Aspects*, 209(2-3), 147-165. doi: https://doi.org/10.1016/S0927-7757(02)00176-0
- Kotnik, T., Rems, L., Tarek, M., & Miklavčič, D. (2019). Membrane electroporation and electropermeabilization: Mechanisms and Models. *Annual Review of Biophysics*, 48(1), 63-91. doi: 10.1146/annurev-biophys-052118-115451

- Krysinski, E. P., Brown, L. J., & Marchisello, T. J. (1992). Effect of cleaners and sanitizers on *Listeria monocytogenes* attached to product contact surfaces. *Journal of Food Protection*, 55(4), 246-251. doi: <https://doi.org/10.4315/0362-028X-55.4.246>
- Lazăr, V., & Chifiriuc, M. C. (2010). Medical significance and new therapeutical strategies for biofilm associated infections. *Roumanian Archives of Microbiology and Immunology*, 69(3), 125-138
- Maria, M. G., Fatima, A. M., Teresa, R. S. B., & Cristina, L. M. S. (2011). On the use of the gompertz model to predict microbial thermal inactivation under isothermal and non-isothermal conditions. *Food Engineering Reviews*, 3, 17-25. doi: 10.1007/s12393-010-9032-2
- Martinac, B., Saimi, Y., & Kung, C. (2008). Ion channels in microbes. *Physiological Reviews*, 88(4), 1449-1490. doi: 10.1152/physrev.00005.2008.Ion
- Mescia, L., Chiapperino, M. A., Bia, P., Lamacchia, C. M., Gielis, J., & Caratelli, D. (2019, June 17-20). Multiphysics Modelling of Membrane Electroporation in Irregularly Shaped Cells. In *2019 Photonics & Electromagnetics Research Symposium-Spring (PIERS-Spring)* (pp. 2992-2998). Rome, Italy. doi: 10.1109/PIERS-Spring46901.2019.9017428
- Miklavčič, D. (2017). *Handbook of electroporation*. Cham, Switzerland: Springer International Publishing. doi: <https://doi.org/10.1007/978-3-319-32886-7>
- Monfort, S., Saldaña, G., Condón, S., Raso, J., & Álvarez, I. (2012). Inactivation of *Salmonella* spp. in liquid whole egg using pulsed electric fields, heat, and additives. *Food Microbiology*, 30(2), 393-399. doi: 10.1016/j.fm.2012.01.004
- Moran, J. L., Dingari, N. N., Garcia, P. A., & Buie, C. R. (2018). Numerical study of the effect of soft layer properties on bacterial electroporation. *Bioelectrochemistry*, 123, 261-272. doi: 10.1016/j.bioelechem.2017.09.004
- Pagán, R., & Mackey, B. (2000). Relationship between membrane damage and cell death in pressure-treated *Escherichia coli* cells: differences between exponential-and stationary-phase cells and variation among strains. *Applied and Environmental Microbiology*, 66(7), 2829-2834. doi: 10.1128/AEM.66.7.2829-2834.2000
- Pavlin, M., Rebers, M., Pucihar, G., Hart, F. X., & Magjarevic, R. (2005) Effect of cell electroporation on the conductivity of a cell suspension. *Biophysical Journal*, 88(June), 4378-4390. doi: 10.1529/biophysj.104.048975
- Peleg, M. (2017). Modeling microbial inactivation by pulsed electric field. In D. Miklavcic (Ed.), *Handbook of Electroporation* (pp.1269-1286). Cham, Swetzerland: Springer International Publishing. doi: 10.1007/978-3-319-32886-7_43
- Pliquett, U., Joshi, R. P., Sridhara, V., & Schoenbach, K. H. (2007). High electrical field effects on cell membranes. *Bioelectrochemistry*, 70(2), 275-282. doi: 10.1016/j.bioelechem.2006.10.004
- Pogozheva, I. D., Tristram-Nagle, S., Mosberg, H. I., & Lomize, A. L. (2013). Structural adaptations of proteins to different biological membranes. *Biochimica et Biophysica Acta (BBA)-Biomembranes*, 1828(11), 2592-2608. doi: 10.1016/j.bbamem.2013.06.023

- Puértolas, E., López, N., Condón, S., Raso, J., & Álvarez, I. (2009). Pulsed electric fields inactivation of wine spoilage yeast and bacteria. *International Journal of Food Microbiology*, 130(1), 49-55. doi: 10.1016/j.ijfoodmicro.2008.12.035
- Qiu, X., Lee, Y. T., & Yung, P. T. (2014, August 26-30). A bacterial spore model of pulsed electric fields on spore morphology change revealed by simulation and SEM. In *2014 36th Annual International Conference of the IEEE Engineering in Medicine and Biology Society* (pp. 6822-6825). Chicago, IL, USA. doi: 10.1109/EMBC.2014.6945195
- Ramaswamy, R., Ramachandran, R. P., & Gowrisree, V. (2019). High voltage pulsed electric field application using titanium electrodes for bacterial inactivation in unpurified water. *Japan Journal of Food Engineering*, 20(2), 63-70. doi: 10.11301/jsfe.19546
- Rosin, J. M., & Kurrasch, D. M. (2018). In utero electroporation induces cell death and alters embryonic microglia morphology and expression signatures in the developing hypothalamus. *Journal of Neuroinflammation*, 15(1), 1-15. doi: 10.1186/s12974-018-1213-6
- Silhavy, T. J., Kahne, D., & Walker, S. (2010). The bacterial cell envelope. In T. J. Silhavy, D. Kahne & S. Walker (Eds.), *Cold Spring Harbor perspectives in biology* (pp. 1-16). New York, USA: Cold Spring Harbor Laboratory Press. doi: 10.1101/cshperspect.a000414
- Silve, A., Leray, I., Poinard, C., & Mir, L. M. (2016). Impact of external medium conductivity on cell membrane electropermeabilization by microsecond and nanosecond electric pulses. *Scientific Reports*, 6, 1-15. doi: <https://doi.org/10.1038/srep19957>
- Singh, J., Singh, M., Singh, B., Nayak, M., & Ghanshyam, C. (2017). Comparative analyses of prediction models for inactivation of *Escherichia coli* in carrot juice by means of pulsed electric fields. *Journal of Food Science and Technology*, 54(6), 1538-1544. doi: 10.1007/s13197-017-2585-9.
- Skulberg, K. R., Skyberg, K., Eduard, W., Goffeng, L. O., Vistnes, A. I., Levy, F., & Kjuus, H. (2001). Effects of electric field reduction in visual display units on skin symptoms. *Scandinavian Journal of Work, Environment and Health*, 27(2), 140-145. doi: 10.5271/sjweh.601. doi: 10.5271/sjweh.601.
- Sweeney, D. C., Weaver, J. C., & Davalos, R. V. (2018). Characterization of cell membrane permeability *in vitro* part I : Transport behavior induced by single-pulse electric fields. *Technology in Cancer Research & Treatment*, 17, 1-15. doi: 10.1177/1533033818792491.



Bifurcation Analysis of an Exothermic Biocatalytic Reaction System

‘Afifi Md Desa^{1,2*}, Mohd Hafiz Mohd¹ and Mohamad Hekarl Uzir³

¹*School of Mathematical Sciences, Universiti Sains Malaysia, 11800 USM, Penang, Malaysia*

²*Institute of Engineering Mathematics, Universiti Malaysia Perlis, 02600 UniMAP, Arau, Perlis, Malaysia*

³*School of Chemical Engineering, Universiti Sains Malaysia, Engineering Campus, 14300 USM, Nibong Tebal, Pulau Pinang, Malaysia*

ABSTRACT

This paper focuses on the bifurcation analysis of an exothermic biocatalytic reaction system (EBRS). The objectives of the study were to provide a detailed dynamical systems analysis of an exothermic biocatalytic reaction and examine the long-term behaviours of the system using the techniques from phase portraits and bifurcation analysis. We investigated the combined influences of the proportional control constant and dilution rate on the dynamics of the model. Phase portraits relating to distinct outcomes of EBRS were computed to investigate the existence of different attractors in this system and its stability. Under a fixed dilution rate and different values of proportional control constant, there were four distinct outcomes in our model, which were stable steady states, bistability of two stable steady states, bistability between stable steady states and limit cycle and stable limit cycles. A bifurcation analysis (of codimensions one and two) was performed to examine how the overall dynamics change as chemically relevant parameters were varied. We observed that when the values of proportional control constant were high, the system would

achieve stable steady states regardless of how fast the dilution rate was. With lower magnitudes of proportional constant control, bistability occurred and the outcomes of this system depended on the initial conditions. Compared to higher dilution rates scenario, reactions that occurred at lower dilution rates provided higher reaction yields for this EBRS operation; it was also observed that both scenarios produced stable steady-state outcomes with different concentrations. In

ARTICLE INFO

Article history:

Received: 17 September 2020

Accepted: 30 October 2020

Published: 22 January 2021

DOI: <https://doi.org/10.47836/pjst.29.1.09>

E-mail addresses:

afifimddesa@gmail.com (*Afifi Md Desa)

mohdhafizmohd@usm.my (Mohd Hafiz Mohd)

chhekarl@usm.my (Mohamad Hekarl Uzir)

* Corresponding author

conclusion, the dynamical system analysis of the model improves our understanding of the EBRS under consideration and these insights may be beneficial for optimising operating conditions of this chemical system.

Keywords: Bifurcation, biocatalytic reaction, dynamical systems, nonlinear, phase-plane analysis

INTRODUCTION

An exothermic reaction occurs when the temperature of a system rises due to the evolution of heat (Petrucci et al., 2002). This is due to the reactant having more energy than the product, which causes the potential excess of energy to change into the kinetic energy of the product formed. During a chemical reaction, a catalyst is introduced to increase the speed of the reaction. A catalyst is an entity that accelerates a chemical reaction without being consumed (Guengerich, 2017). Often catalyst will lower the activation energy of a reaction, and this mechanism can increase the rate of the reaction. Normally, a catalyst does not react with reactants directly but if it does, in the case of enzymatic reaction systems, the intermediate complexes would either remain as bound complexes or they can reversibly dissociate and continue to catalyse the remaining substrate.

Most biocatalysts are protein known as enzymes. Enzymes are a type of biocatalysts and they can be obtained from living cells. Since the first biocatalyst was introduced nearly a century ago, different enzyme-based processes have been commercialised to manufacture several valuable products in many industries (Guan et al., 2011; Hu et al., 2010; Jestin & Kaminski, 2004; Sekhon et al., 2018; Uhr et al., 2014; Zhao et al., 2018). In contrast to a chemical catalyst, which produces side products, a biocatalyst usually produces a cleaner reaction. As the world is beginning to use green energy, biocatalytic processes will play an important role in the next generation of industrial revolutions for chemical production. The introduction of biocatalysts in chemical reactions can reduce several processing steps which will lead to higher efficiency and time (Tufvesson et al., 2010).

In a chemical reaction involving biocatalyst, the enzymes need to be blended with the reactant for a reaction to occur. Blending operations are frequently used in many industries to ensure that the final products meet customer requirements. A continuous stirred-tank reactor (CSTR) is shown in Figure 1. The CSTR are commonly used in industrial processing, primarily in homogeneous liquid-phase flow reactions where constant agitation is required. A CSTR is a continuous reactor that is equipped with

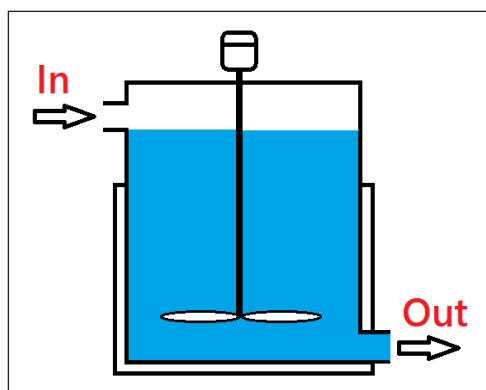


Figure 1. A diagram of a continuous stirred-tank reactor

an impeller or mixing device for efficient mixing. In a process involving a biocatalyst, a reactant enters the CSTR where the biocatalyst is prepared prior to the reaction and the product formed during the reaction flows through the outlet. There are a few factors influencing the reactor productivity such as substrate and enzyme concentration (Bommarius & Riebel, 2004), temperature (Devasena, 2010) and the dilution rate or time constant (De Gooijer et al., 1996). Increasing substrate and enzyme concentration will increase the enzyme reaction up to the limit of saturation. However, in practice it is very unlikely to increase to enzyme concentration due to certain constrain such as cost or excess of deactivated protein in the reactor where maximum limit of enzyme concentration is reached. Meanwhile, the effects of temperature on the reactor productivity depends on two factors which is the influence of temperature on the reaction rate and the thermal denaturation of enzyme at elevated temperature (Bommarius & Riebel, 2004). The vital aspect to achieve higher reactor productivity is to control temperature to the optimum temperature which was one of the focus of this study.

The most complete analysis of a CSTR behaviour was shown in the research by Aris and Amundson (1958a, 1958b). In their work, a simple CSTR model with associated control equipment was formulated to study the transient behaviour of a reaction. Even though many biocatalytic reactions are performed in CSTR, not many models and dynamical systems analyses of this reaction have been carried out in the literature. While there are several modelling studies on biocatalytic reactions, most of these studies focus on the other area than dynamical study including developing model and simulating transient behaviours of the systems (e.g. Petkevicius & Baronas, 2017), reactor selection for biocatalytic (e.g. Lindeque & Woodley, 2019), kinetic studies on immobilised enzymes (e.g. Mazzei et al., 2009) and industrial applications (e.g. Choi et al., 2015). One of the studies that explores the dynamics of biocatalytic reactions was conducted by Radzi and Uzir (2009), where they discussed the formulation of the model and the parameters that were involved. The dynamical analysis also covered the following three parameters: proportional control constant, dilution rate and enzyme concentration.

Inspired by the study of Radzi and Uzir (2009), we are interested to further explore the dynamical behaviours of exothermic biocatalytic reaction in CSTR by employing a similar model. One of the objectives of this study was to provide a detailed dynamical systems investigation of an exothermic biocatalytic reaction system (EBRS) using the techniques of phase portraits and bifurcation analysis. Furthermore, we would like to gain a better understanding of the influential roles of dilution rate and proportional control constant in determining the outcomes of this biocatalytic system. This study hopes to provide the researchers and engineers with a better understanding and control of the EBRS and to contribute to the existing body of knowledge in this area.

The article is organised as follows. The model of exothermic biocatalytic reaction is described under the Method section and then it is followed by the phase portrait analysis. We

illustrate the dynamical outcomes of the system at different values of proportional control constant, K_C . By using numerical continuation, we discuss some mathematical insight on the effect of proportional control constant and dilution rate on the dynamical outcomes of the system. Finally, we discuss the several CSTR operations implications of our results.

METHODS

In order to study the biocatalytic reaction, we would examine a dimensionless model of an exothermic biocatalytic reaction, in CSTR which was initially introduced by Radzi and Uzir (2009) (Equation 1).

$$\begin{aligned} \frac{dy}{d\tau} &= 1 - y - \frac{k_A y \alpha}{D} e^{\frac{\beta}{\theta}} \\ \frac{d\theta}{d\tau} &= \theta_0 - \theta + \frac{k_A y \alpha}{D} e^{\frac{\beta}{\theta}} - U(\theta - \theta_c) [1 + K_C(\theta - \theta_s)] \end{aligned} \quad [1]$$

In this model, the rate of change of substrate concentration is given by $\frac{dy}{d\tau}$ and the rate of change of the reactor temperature is given by $\frac{d\theta}{d\tau}$. The variable y is a dimensionless unit as it is the concentration of the outflow divided by the concentration of the inflow. If the value of y is close to one, it shows that the CSTR has a higher substrate concentration, and if the value is close to zero it shows that the CSTR has a lower substrate concentration. The term K_C is the proportional control constant on the cooling water flow rate. A high value of K_C means that the cooling water flow rate is set to a high value. Therefore, the higher cooling water flow rate will reduce the reactor temperature faster. The term D is the dilution rate, which is the rate that the existing medium in the reactor is replaced by a fresh medium. A high value of D means the rate of inflow and outflow from the CSTR is higher. The full interpretations of each variable and parameter values that used in this study were motivated by Radzi and Uzir (2009) and are shown in Table 1.

To achieve the objectives of the study, the first step was to determine the equilibria and their stability by using MAPLE® software. By using Pplane8, the solutions of the system were plotted for different set of parameters and the stability of the equilibria was also established. To gain better insight on the mechanisms that induced distinct solutions in this system for a different sets of parameters, we employed XPPAUT to conduct a codimension-one bifurcation analysis and this analysis tracks the stable and unstable equilibria together with their bifurcation points as parameters were varied. The bifurcation diagrams are important to understand the overall dynamics of this chemical system. Lastly, we also used MATCONT to plot a codimension-two bifurcation diagram to investigate the joint effects of K_C and D in determining the dynamics of the system.

Table 1
The variables and parameters of the model

Variable/ Parameter	Description	Value
y	Dimensionless substrate concentration	Variable
θ	Dimensionless reactor temperature on the stability of reaction	Variable
τ	Dimensionless time	Variable
k_A	Reaction velocity constant	e^{25}
α	Dimensionless total enzyme concentration	60
D	Dilution rate: the rate that the existing medium in the reactor is replaced by a fresh medium	$10 \leq D \leq 90$
	Dimensionless parameter for heat transfer	50
θ_0	Dimensionless initial reactor temperature on the stability of the reaction	1.75
θ_c	Dimensionless mean temperature of water in the cooling coil	1.75
θ_s	Desired steady-state temperature	2
U	Dimensionless analogue of U_oA , the overall heat transfer rate	1
K_C	Proportional control on the cooling water flow rate constant	$1 \leq K_C \leq 12$

RESULTS

In this section, we begin with the phase portrait analysis followed by the codimension-one and -two bifurcation analyses. The phase portrait analysis was performed using Pplane8 to visualise the equilibria of the system and identify the nature of stability of these solutions (i.e. whether they are stable or unstable). This could be performed for a given set of parameter values to reveal the dynamics of the system. With this analysis, we would be able to locate the nullclines, attractors, repellers and limit cycles for a given set of parameters as in Table 1 and this information should be in agreement with our theoretical analysis, e.g. local stability analysis.

To understand the changes in the dynamics of the system as chemically relevant parameters vary, we conducted a codimension-one bifurcation analysis of the system. This was performed using XPP software and Auto package. Two parameters, which are proportional control constant (K_C) and the dilution rate (D), had been chosen for this analysis as we would like to examine their combined influences on the dynamical behaviours of the system. The proportional control constant K_C , serves as a heat removal mechanism for the reaction. Since the biocatalytic reaction is an exothermic reaction, heat from the reaction will be released into the surroundings and this process will increase the temperature of the reactor. As the temperature increases, the enzyme activity will be affected because it needs to be operated at their optimal temperature (Devasena, 2010). By examining the influences of K_C on the dynamical behaviour of the system, we can control the temperature of the reactor to achieve the optimal operating conditions. On the other hand, the dilution rate, D is the rate at which the existing substrate in the reactor is replaced by a fresh substrate.

Since an enzyme is being used as a catalyst to speed up the reaction, the reaction will only occur when the substrate binds into the active sites of the enzymes. The duration that the substrate spends in the reactor can shape the efficiency of the reactor.

Bifurcation analysis will also identify the threshold values for D and K_C where the change in dynamics occur. We were also able to locate the tipping points where the distinct bifurcations emerged in the system. Further investigation was also carried out using a codimension-two bifurcation analysis to search for different stable regions of the model in a two-parameter space. For this analysis, we relied on MATCONT software to plot these stability regions and examine the interactions of different bifurcations in this CSTR system.

Phase Portrait Analysis

Since temperature is one of important factors that can influence enzyme activity, we will investigate the effects of changing temperature on the biocatalytic reaction system. This investigation corresponded to varying values of K_C to observe the dynamical outcomes of the system under a fixed dilution rate (e.g. $D = 50$). Our observations are as follows: (i) stable equilibrium; (ii) bistability of two stable steady states; (iii) bistability between the stable equilibrium and limit cycle; and (iv) stable limit cycles. These distinct dynamics are illustrated in Figure 1, which enable us to understand the long-term behaviours of the solution. It is also used to verify the dynamics in the codimension-one and two bifurcation diagrams which is described in a later section.

Figure 1a demonstrates the phase portrait when K_C is rather low (i.e., $K_C = 1$). The values of other parameters are listed in Table 1. Figure 1 shows the bistability of the system where there occurred two stable equilibria (E_1 and E_3) and an unstable saddle point E_2 . At E_2 , the stable manifold of the saddle-type solution (solid black curve) acted as a basin boundary and separated the basin of attractions for the two stable steady states, E_1 and E_3 . Depending on their initial conditions, the trajectories either converged to E_1 (lower substrate concentration) or E_3 (higher substrate concentration). For example, an initial condition below the stable manifold would converge to steady state E_3 . Otherwise, it would converge to a steady state E_1 .

At $K_C = 2$, the model exhibited another type of dynamical behaviour, which was the coexistence of a stable equilibrium with a stable limit cycle (Figure 2b). The previous stable equilibrium in E_1 (stable spiral) appeared to change a stability and consequently a stable limit cycle emerged with an increase in K_C ; any trajectories that started above the stable manifold of E_2 (solid black curve) would be attracted to this limit cycle. The occurrence of the limit cycle in this system indicates that an increase in heat removal would cause the stable equilibrium of E_1 (with high substrate concentration) to lose its stability and this also leads the appearance of a stable limit cycle.

Bifurcation Analysis of an Exothermic Biocatalytic Reaction System

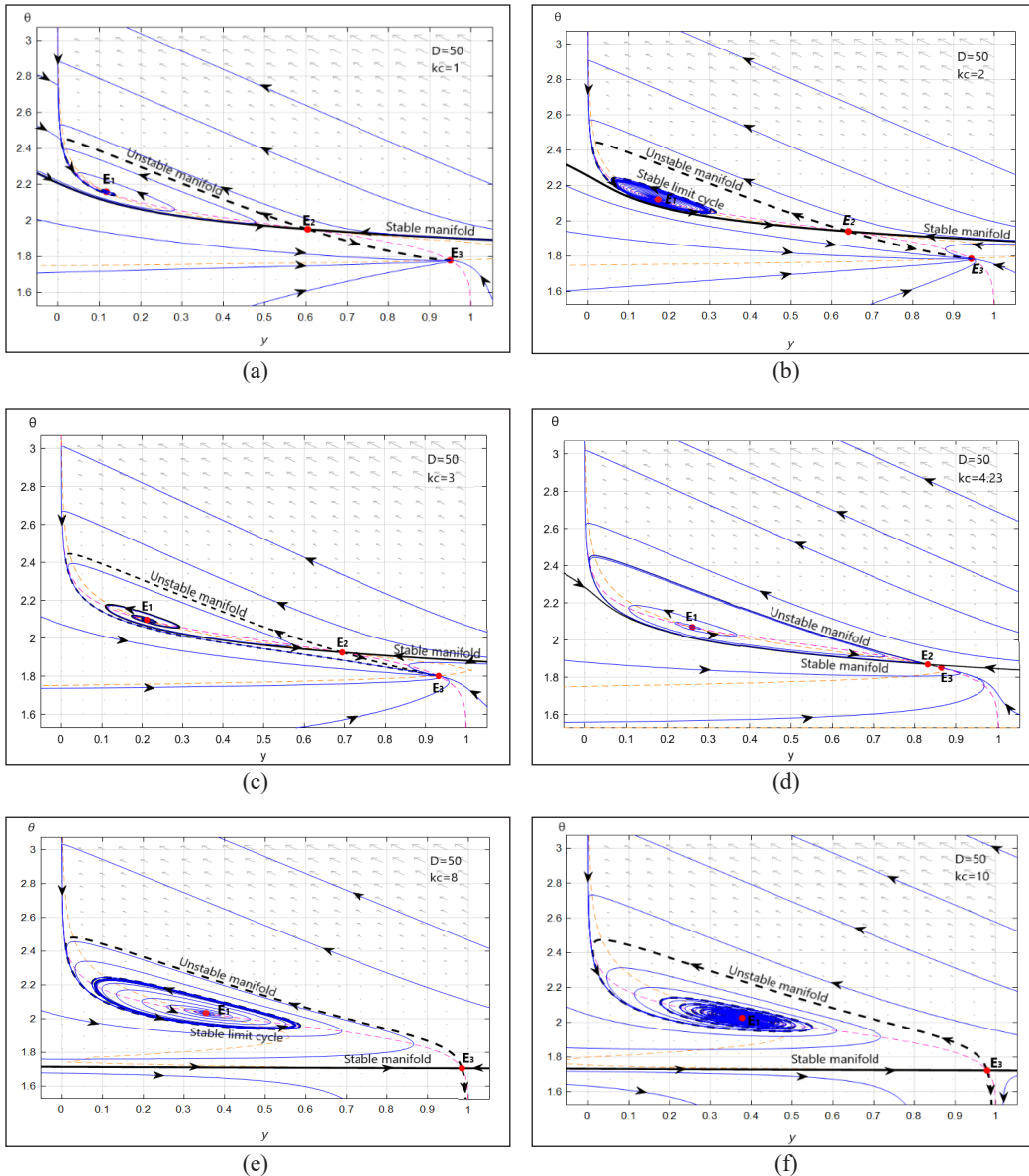


Figure 2. Phase portrait of the system at $D = 50$ and (a) $K_C = 1$, (b) $K_C = 2$, (c) $K_C = 3$, (d) $K_C = 4.5$, (e) $K_C = 8$ and (f) $K_C = 10$

At $K_C = 3$, the previous stable limit cycles could vanish and we observed the emergence of an unstable spiral at E_1 and hence due to this reason, the bistability phenomenon that we was previously also disappears. This situation results in the occurrence of single stable attractor E_3 (Figure 2c). In this case, all trajectories would converge to stable equilibrium E_3 .

There was another change in the dynamical behaviour of the model that we realised when the value of K_C increase e.g., $K_C = 4.23$ as in Figure 2d. The unstable spiral previously

at E_1 becoming stable limit cycle and hence the bistability phenomenon occurred where stable equilibrium at E_3 and stable limit cycle at E_1 coexisted. All trajectories above the stable manifold would be attracted to the limit cycle while trajectories below stable manifold would be attracted to stable equilibrium.

At higher values of K_C e.g., $K_C = 8$ (Figure 2e), we observed that the limit cycle decreased in size, which indicated that the amplitude of oscillation is getting smaller. Figure 3 shows the amplitude of oscillation in y when $K_C = 8$ had decreased compared to the amplitude at $K_C = 4.5$. This observation indicates that when K_C increases, this situation will reduce the amplitude of oscillatory solution and demonstrate that the conversion of reactant is more efficient. The biocatalytic reaction activity is increased due to the fact that more heat being released from the reactor. The reactor temperature becomes optimal for a biocatalytic process to occurs.

At higher values of K_C for instance, $K_C = 10$, the limit cycle disappeared, and the dynamics were replaced by a stable equilibrium (stable spiral) at E_1 is still a single attractor in the system, and for the system to reach this steady state the initial conditions must start above the stable manifold (Figure 2f). The system oscillated until it reached the steady state.

Codimension-One Bifurcation Analysis

To investigate the mechanism behind the emergence and disappearance of certain dynamic in this model, we employed codimension-one bifurcation analysis to track steady states of the model as parameter change. We were conducting the codimension-one bifurcation

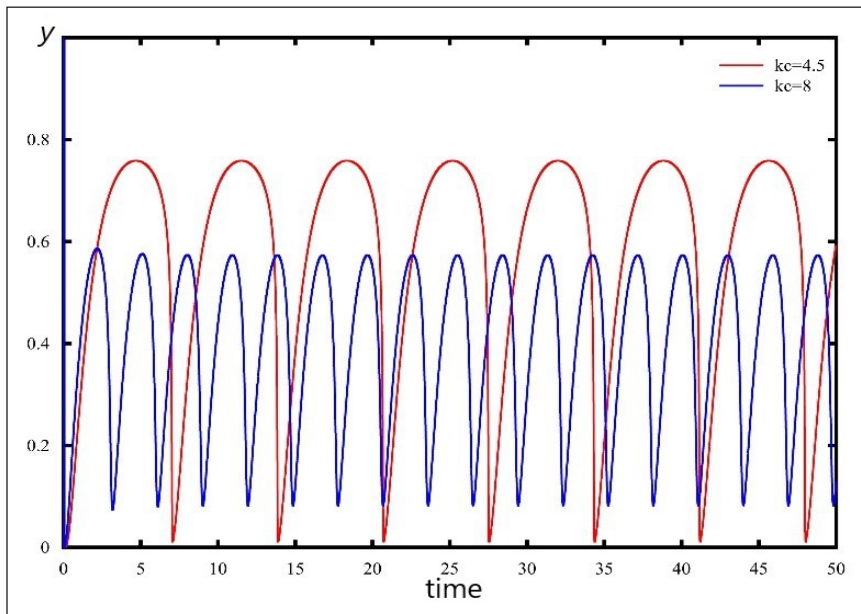


Figure 3. Time series plot at different values of K_C

analysis using two parameters which was the proportional control constant, K_C and the dilution rate, D .

Effects of Varying the Proportional Control Constant. In this section, we analyse the dynamical behaviour of the system as the parameter K_C changes. The term K_C refers to a heat removal control that regulates the cooling process of water in this system. An increase in the value of K_C cause a proportional increase in heat removal and hence lower the reactor temperature.

Figure 4 shows a bifurcation diagram at dilution rate $D = 50$ when K_C was varied from 0 to 12. Red (Black, respectively) curves corresponded to stable (unstable, respectively) steady states. The green curves demonstrated the occurrence of stable limit cycle in this EBRS model. There also occurred several threshold points i.e., H_1 , HB_1 , HB_2 , SN , and H_2 which corresponded to first Hopf bifurcation, first homoclinic bifurcation, second homoclinic bifurcation, saddle-node bifurcation and second Hopf bifurcation respectively as K_C increased to a higher value.

It was observed that at a very low K_C e.g., $K_C = 0$, the system had three steady state where the upper branch, E_3 and the lower branch E_1 , of steady states were stable. They were separated by an unstable steady state in the middle branch, E_2 . As K_C increased, there was a dynamical changes occurring on the lower branch of stable steady state E_1 at critical point H_1 ($K_C = 1.813$) corresponding to Hopf bifurcation. In this situation, the substrate

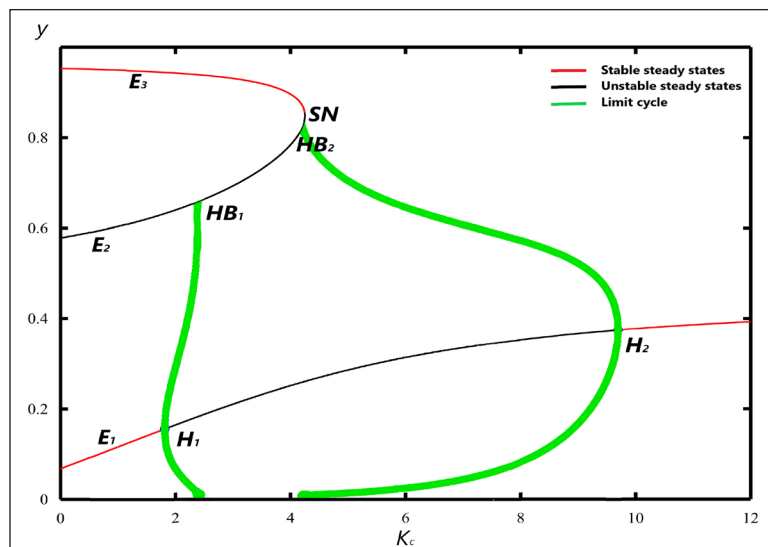


Figure 4. Bifurcation diagram for K_C at $D=50$. Red curves correspond to stable steady states. The black curves correspond to the unstable steady state. The green curves demonstrate the occurrence of stable limit cycle. E_1 is the lower branch of steady state, E_2 is the middle branch of steady state and E_3 is the upper branch of steady state. H_1 , HB_1 , HB_2 , SN , and H_2 correspond to first Hopf bifurcation, first homoclinic bifurcation, second homoclinic bifurcation, saddle-node bifurcation and second Hopf bifurcation respectively.

concentration started to oscillate between certain minimum and maximum values. This observation corresponded to creation of a stable limit cycle. There was also a change in dynamical behaviour as previous bistability between two stable steady state in the region $K_C < H_1$ was replaced by a bistability between stable steady states and stable limit cycle in the region $H_1 < K_C < HB_1$. As K_C increased, the amplitude of oscillations in the stable limit cycle were getting bigger in size and consequently collided with the unstable saddle point in the middle branch E_2 at critical point $HB(K_C = 2.396)$. This collision corresponded to a homoclinic bifurcation and resulting the disappearance of the previous stable limit cycle as K_C was increased. As K_C increased, there was another homoclinic bifurcation occurring at the critical point $HB(K_C = 4.203)$. There was a new dynamical behaviour observed in the region $HB_1 < K_C < HB_2$ as the previous bistability between stable limit cycle and stable steady state was replaced by single steady states. All trajectories would converge to a stable steady state in upper branch E_3 . As K_C increased pass the HB_2 , we observed another appearance of stable limit cycle. This limit cycle resulted from the second Hopf bifurcation occurring at critical point $H_2(K_C = 9.694)$ in the lower branch, E_1 . Meanwhile, in the upper branch E_3 there was another critical point at $SN(K_C = 4.251)$ corresponding to a saddle-node bifurcation. This saddle-node bifurcation resulted from the collision between stable steady state in upper branch, E_3 and unstable steady state in middle branch, E_2 . We also observed the dynamical behaviour changes in the region $HB_2 < K_C < SN$ as the bistability occurred between stable steady state and stable limit cycle. Another changes in dynamical behaviour was observed as the previous bistability was changed to single steady state in region $K_C > H_2$.

Effect of Varying the Dilution Rate. In this analysis, we investigated the influence of the dilution rate D on the outcomes of the system. Since the choice of the parameter K_C value was quite arbitrary, we set the outcome of the model for four distinct values of K_C so as to capture the overall dynamic of the model.

When the dilution rate, D increased, we observed the occurrence of different threshold values that would determine the dynamical behaviour of EBRS model. As we can see in Figure 5, there was a critical point occurring at $H(D = 40.59)$ which is corresponded to Hopf bifurcation. We observed as $D < H$, the system would be in stable steady state. On the other hand, as $D > H$, the stable steady state turned into unstable steady state, with corresponded to the creation of stable limit cycle. In this situation, the substrate concentration started to oscillate between certain minimum and maximum values. The stable limit cycle terminated at critical point $HB(D = 49.3)$ corresponding to homoclinic bifurcation. The homoclinic bifurcation occurred as a result from the collision of stable limit cycle with the saddle point. There was also another critical point occurring at $SN(D = 48.52)$ corresponding

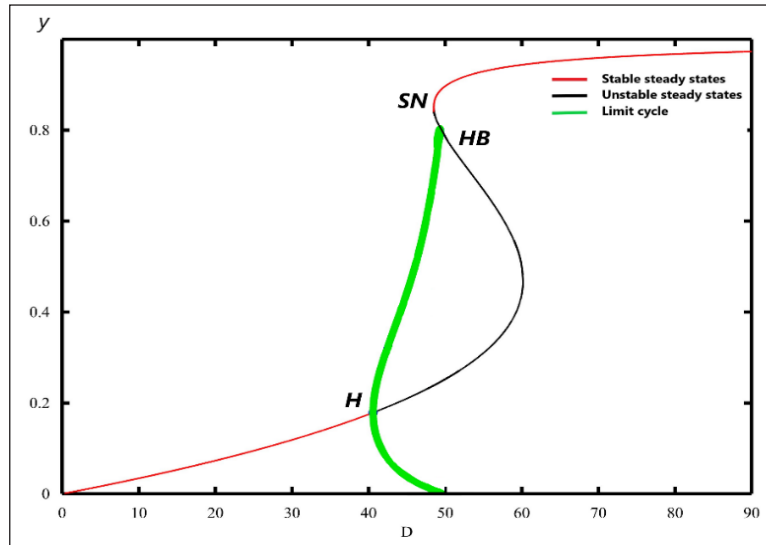


Figure 5. Bifurcation diagram for D at $K_C = 4$. Red curves correspond to stable steady states. The black curves correspond to the unstable steady state. The green curves demonstrate the occurrence of stable limit cycle. H , HB and SN correspond to Hopf bifurcation, homoclinic bifurcation, and saddle-node bifurcation respectively.

to the saddle node bifurcation as the stable steady state in the upper region collided with unstable steady state in the middle region. There existed a region of bistability between stable steady state and stable limit cycle in the region $SN < D < HB$.

Codimension-Two Bifurcation Analysis

Throughout this section, a codimension-two bifurcation analysis was conducted to continue the detected bifurcations through two parameter spaces and examined the boundary of the stable region. We would investigate the joint effects of proportional control constant, K_C and dilution rate, D on the dynamics of the system. To illustrate the effect of increasing the proportional control constant K_C on the dynamics of the system as dilution rate D varies, several bifurcation diagrams with different K_C values were plotted in Figure 6.

Figure 6a shows the bifurcation diagram with respect to parameter D and it was plotted at $K_C = 2$. There were three critical points observed in the bifurcation diagram corresponding to Hopf bifurcation, H at $D = 48.66$, homoclinic bifurcation, HB at $D = 51.61$ and saddle node bifurcation, SN at $D = 38.29$. There were two regions of bistability observed. The first bistability occurred in the region $SN < D < H$ between stable steady state in the higher concentration of y and the stable steady state in the lower concentration of y (red curve). Second bistability occurred in the region $H < D < HB$ between the stable steady state in the higher substrate concentration of y and the stable limit cycle emerging from the Hopf bifurcation in lower substrate concentration of y . Figure 6b shows the bifurcation diagram with respect to parameter D as we increased the value of $K_C = 5$. We observed a dynamical

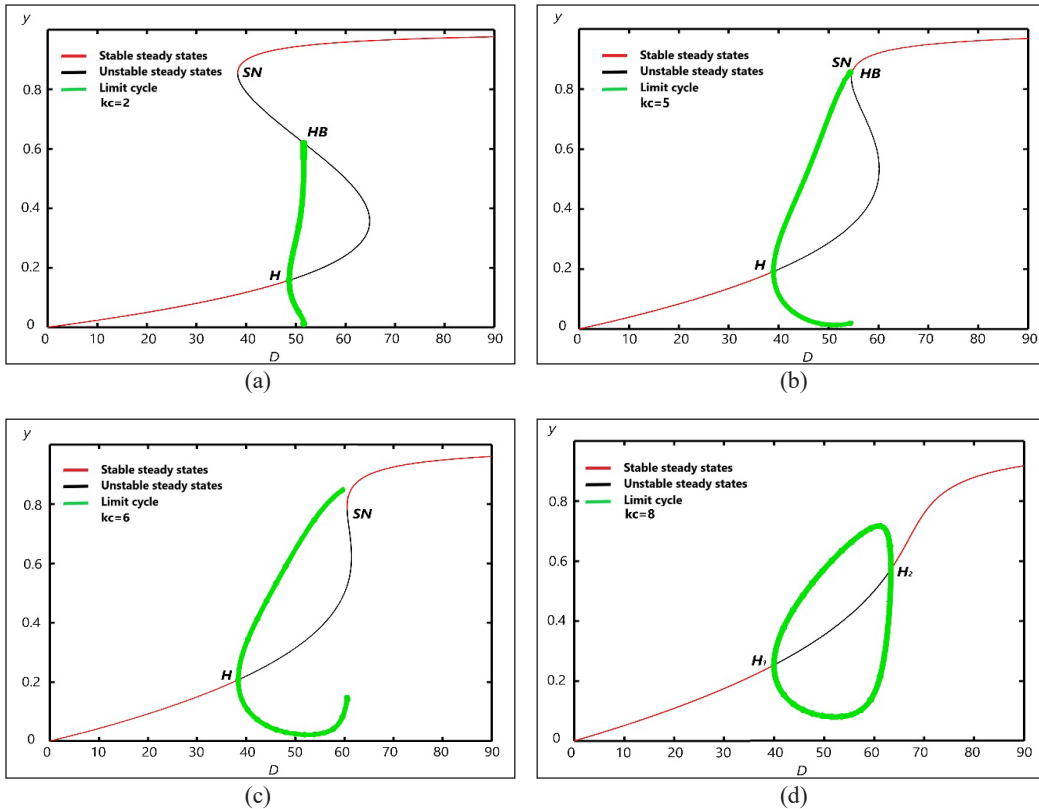


Figure 6. The effect of different K_C on the dynamics of the system as D increases. Red curves correspond to stable steady states. The black curves correspond to the unstable steady state. The green curves demonstrate the occurrence of stable limit cycle. H , H_1 , H_2 , HB , and SN correspond to Hopf bifurcation, first Hopf bifurcation, second Hopf bifurcation, homoclinic bifurcation, and saddle-node bifurcation respectively.

behaviour had changed compared to previous observation. There were three bifurcation observed in the bifurcation diagram corresponding to Hopf bifurcation, H occurring at $D = 38.99$, the homoclinic bifurcation, HB occurring at $D = 54.51$ and saddle node bifurcation, SN occurring at $D = 54.58$. We also observed the ‘S’ shape of the curve seemed to ‘unfold’ and this situation led to the previous bistability between two stable steady state in Figure 6a disappeared. Moreover, the bistability region between the stable steady state in the higher substrate concentration of y and the stable limit cycle emerged from the Hopf bifurcation in lower substrate concentration of y shrinking to a very small region in the region $HB < D < SN$. Figure 6c shows the bifurcation diagram with respect to parameter D as we increased the value of $K_C = 6$. We observed the disappearance of homoclinic bifurcation in the previous observation. Two bifurcations were observed in the bifurcation diagram corresponding to Hopf bifurcation, H at $D = 38.38$ and saddle node, SN bifurcation at $D = 60.55$. The ‘S’ shape of the curve became flatten with no more bistability phenomenon occurring in the system. Figure 6d shows the bifurcation diagram with respect to parameter D as we

increased the value of $K_C = 8$. Two Hopf bifurcation emerged from the system with the first Hopf bifurcation, H_1 occurring at $D = 39.98$ and second Hopf bifurcation, H_2 occurring at $D = 63.36$. This two Hopf bifurcation were connected by a stable limit cycle bifurcation from each critical point H_1 and H_2 . There was no bistability phenomenon occurring and the substrate concentration increased as the dilution rate increased.

There are three salient features we discovered from increasing the proportional control constant K_C on the dynamics of the system as dilution rate D varied. The first one was the disappearance of the bistability phenomenon; the bistability observed disappearing at higher K_C (Figure 6c to d). The second observation was the disappearance of the saddle node and homoclinic bifurcations; the ‘S’ shape of the equilibrium curve in lower K_C seemed to ‘unfold’ with increasing of K_C (Figure 6c). The third observation was the occurrence of two Hopf bifurcations. At high values of K_C , limit cycles which occurred was connected by two Hopf bifurcation points (Figure 6d). These three features are best described using a two-parameter bifurcation diagram.

Figure 7 shows a codimension-two bifurcation diagram as parameters D and K_C vary. The formation of Bogdanov–Takens point (BT) at $K_C = 6.25035$ and $D = 62.048275$ marked the meeting of the saddle node bifurcation and the Hopf bifurcations. The parameter space was divided into five regions by the Hopf, saddle node and homoclinic bifurcation curves. These regions (labelled I, II, III, IV and V) corresponded to distinct stable steady states of the system. Region I corresponded to the single stable steady state, region II corresponded

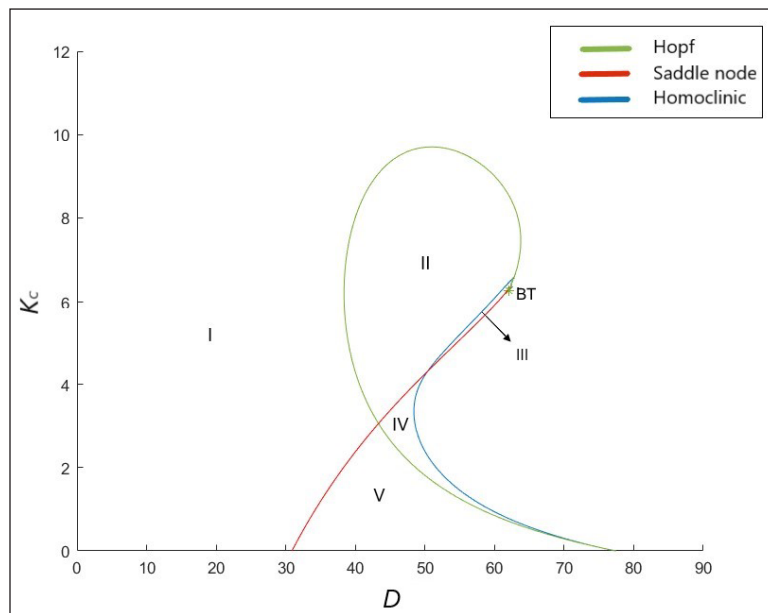


Figure 7. Codimension-two parameter bifurcation diagram. Green curve refers to Hopf bifurcation, red curve refers saddle node bifurcation and blue curve refers to homoclinic bifurcation. BT is the Bogdanov-Takens bifurcation point.

to the stable limit cycle, regions III and IV corresponded to the bistability between the steady states and limit cycle and region V corresponded to the bistability between two stable steady states.

DISCUSSION AND CONCLUSION

There is one limitation in our result. In order to analysis the stability of the solution in the EBRS model, it is very difficult to solve the model analytically since the model involves large set of parameters and highly nonlinear. We need to rely on the computer software such as MAPLE® and XPPAUT to compute the solutions of the model and determine their stability. Hence, all the results we present are computed numerically.

In a biocatalytic reaction, it is crucial to understand the dynamics of the reaction in CSTR by identifying the critical transitions between the possible dynamical regimes. Different parameters such as temperature and dilution rate are vital components in achieving high efficiency (productivity) of the reactor. Our results have shown that when the value K_C is high (e.g. $K_C > 10$) the system will achieve a stable steady state (Figure 7) regardless of how fast the dilution rate is. For higher values of K_C , more heat is removed from the system, lowering the reactor temperature level and providing optimal conditions for the biocatalytic reaction to operate. When the value of K_C is low (e.g., $K_C = 2$), minimal heat is removed from the system and the accumulated heat affects the biocatalytic reaction. At certain dilution rates D , the system exhibits different dynamics: (i) a stable steady state (e.g., $D = 20$), (ii) bistability between two stable steady states (e.g., $D = 40$) and (iii) bistability between the stable steady state and stable limit cycle (e.g., $D = 50$).

Controlling the dilution rate is also important in the CSTR operations. A reaction at higher and lower dilution rates provides better stability for the CSTR operations. For a higher dilution rate, the substrate concentration is high (Figure 6). This is due to the shorter duration that the substrate spends in the reactor. The enzymes are not fully utilised since the inflow and outflow of the reactant and product are at a higher rate. Lowering the dilution rate will result in a lower substrate concentration because the enzyme has more time to catalyse the reaction.

The finding of this study is also consistent with the result in Radzi and Uzir (2009). The dynamical behaviours are qualitatively the same. However, this study extends the previous knowledge in Radzi and Uzir (2009) by discovering the homoclinic bifurcation as a result of collision between stable limit cycle and saddle point in unstable steady state. Moreover, we have detected the region of bistability in which Radzi and Uzir (2009) missed. We also extending the bifurcation result into codimension-two bifurcations diagram and reveal more dynamical behaviours lies within the exothermic biocatalytic reaction model.

To conclude the discussion, the outcomes of the system depend on the joint influence of proportional control constant, K_C and the dilution rate, D . This study has provided a detailed analysis of the dynamical behaviours of an exothermic biocatalytic reaction as some chemically relevant parameters change. Using bifurcation analysis, the role of proportional control constant K_C and the dilution rate D in determining the outcomes of this chemical system is understood. For future research, other parameters could be taken into consideration such as enzyme concentration. Additionally, a specific inhibition model, such as competitive inhibition or uncompetitive inhibition, can be formulated and the results can be compared with this model.

ACKNOWLEDGEMENTS

Thanks to the School of Mathematical Sciences and the Universiti Sains Malaysia for the support. Mohd Hafiz Mohd is supported by Universiti Sains Malaysia (USM) Fundamental Research Grant Scheme (FRGS) No. 203/PMATHS/6711645.

REFERENCES

- Aris, R., & Amundson, N. R. (1958a). An analysis of chemical reactor stability and control—I: The possibility of local control, with perfect or imperfect control mechanisms. *Chemical Engineering Science*, 7(3), 121-131. doi: [https://doi.org/10.1016/0009-2509\(58\)80019-6](https://doi.org/10.1016/0009-2509(58)80019-6)
- Aris, R., & Amundson, N. R. (1958b). An analysis of chemical reactor stability and control—II: The evolution of proportional control. *Chemical Engineering Science*, 7(3), 132-147. doi: [https://doi.org/10.1016/0009-2509\(58\)80020-2](https://doi.org/10.1016/0009-2509(58)80020-2)
- Bommarius, A. S., & Riebel, B. R. (2004). *Biocatalysis, fundamentals and applications*. Weinheim, Germany: John Wiley & Sons.
- Choi, J. M., Han, S. S., & Kim, H. S. (2015). Industrial applications of enzyme biocatalysis: Current status and future aspects. *Biotechnology Advances*, 33(7), 1443-1454. doi: <https://doi.org/10.1016/j.biotechadv.2015.02.014>
- De Gooijer, C. D., Bakker, W. A. M., Beftink, H. H., & Tramper, J. (1996). Bioreactors in series: An overview of design procedures and practical applications. *Enzyme and Microbial Technology*, 18(3), 202-219. doi: [https://doi.org/10.1016/0141-0229\(95\)00090-9](https://doi.org/10.1016/0141-0229(95)00090-9)
- Devasena, T. (2010). *Enzymology*. New Delhi, India: Oxford University Press.
- Guan, D., Li, P., Zhang, Q., Zhang, W., Zhang, D., & Jiang, J. (2011). An ultra-sensitive monoclonal antibody-based competitive enzyme immunoassay for aflatoxin M1 in milk and infant milk products. *Food Chemistry*, 125(4), 1359-1364. doi: <https://doi.org/10.1016/j.foodchem.2010.10.006>
- Guengerich, F. P. (2017). Mechanisms of enzyme catalysis and inhibition. In D. L. Eaton (Ed.), *Comprehensive toxicology* (3rd Ed., Vol. 10-15). London, UK: Elsevier. doi: <https://doi.org/10.1016/B978-0-12-801238-3.10922-5>

- Hu, K., Huang, X., Jiang, Y., Fang, W., & Yang, X. (2010). Monoclonal antibody based enzyme-linked immunosorbent assay for the specific detection of ciprofloxacin and enrofloxacin residues in fishery products. *Aquaculture*, 310(1-2), 8-12. doi: <https://doi.org/10.1016/j.aquaculture.2010.08.008>
- Jestin, J. L., & Kaminski, P. A. (2004). Directed enzyme evolution and selections for catalysis based on product formation. *Journal of Biotechnology*, 113(1-3), 85-103. doi: <https://doi.org/10.1016/j.jbiotec.2004.03.032>
- Lindeque, R. M., & Woodley, J. M. (2019). Reactor selection for effective continuous biocatalytic production of pharmaceuticals. *Catalysts*, 9(3), 1-17. doi: <https://doi.org/10.3390/catal9030262>
- Mazzei, R., Giorno, L., Piacentini, E., Mazzuca, S., & Drioli, E. (2009). Kinetic study of a biocatalytic membrane reactor containing immobilized β -glucosidase for the hydrolysis of oleuropein. *Journal of Membrane Science*, 339(1-2), 215-223. doi: <https://doi.org/10.1016/j.memsci.2009.04.053>
- Petkevicius, L., & Baronas, R. (2017, October 8-12). Numerical simulation and analysis of enzyme-catalysed substrate conversion in a microbioreactor. In *SIMUL 2017: The Ninth International Conference on Advances in System Simulation* (pp. 1-6). Athens, Greece.
- Petrucci, R. H., Harwood, W. S., & Herring, F. G. (2002). *General chemistry: Principles and modern applications* (Vol. 1). Upper Saddle River, NJ: Prentice Hall.
- Radzi, M. R. M., & Uzir, M. H. (2009). Stability study of an exothermic biocatalytic reaction and its application in bioprocess systems. *Pertanika Journal of Science and Technology*, 17(1), 95-115.
- Sekhon, J. K., Rosentrater, K. A., Jung, S., & Wang, T. (2018). Effect of co-products of enzyme-assisted aqueous extraction of soybeans, enzymes, and surfactant on oil recovery from integrated corn-soy fermentation. *Industrial Crops and Products*, 121(December 2017), 441-451. doi: <https://doi.org/10.1016/j.indcrop.2018.05.033>
- Tufvesson, P., Fu, W., Jensen, J. S., & Woodley, J. M. (2010). Process considerations for the scale-up and implementation of biocatalysis. *Food and Bioprocess Processing*, 88(1), 3-11. doi: <https://doi.org/10.1016/j.fbp.2010.01.003>
- Uhr, L., Buchholz, T., Homann, T., Huschek, G., & Rawel, H. M. (2014). Targeted proteomics-based analysis of technical enzymes from fungal origin in baked products. *Journal of Cereal Science*, 60(2), 440-447. doi: <https://doi.org/10.1016/j.jcs.2014.04.007>
- Zhao, Y. M., Wang, L. H., Luo, S. F., Wang, Q. Q., Moaddel, R., Zhang, T. T., & Jiang, Z. J. (2018). Magnetic beads-based neuraminidase enzyme microreactor as a drug discovery tool for screening inhibitors from compound libraries and fishing ligands from natural products. *Journal of Chromatography A*, 1568, 123-130. doi: <https://doi.org/10.1016/j.chroma.2018.07.031>

Predictive Performance of Logistic Regression for Imbalanced Data with Categorical Covariate

Hezlin Aryani Abd Rahman^{1*}, Yap Bee Wah^{1,2} and Ong Seng Huat³

¹Centre of Statistical and Decision Science Studies, Faculty of Computer and Mathematical Sciences, Universiti Teknologi MARA, 40450 Shah Alam, Selangor, Malaysia

²Advanced Analytics Engineering Centre, Faculty of Computer and Mathematical Sciences, Universiti Teknologi MARA, 40450 Shah Alam, Selangor, Malaysia

³Department of Actuarial Science and Applied Statistics, UCSI University, 56000, Kuala Lumpur, Malaysia

ABSTRACT

Logistic regression is often used for the classification of a binary categorical dependent variable using various types of covariates (continuous or categorical). Imbalanced data will lead to biased parameter estimates and classification performance of the logistic regression model. Imbalanced data occurs when the number of cases in one category of the binary dependent variable is very much smaller than the other category. This simulation study investigates the effect of imbalanced data measured by imbalanced ratio on the parameter estimate of the binary logistic regression with a categorical covariate. Datasets were simulated with controlled different percentages of imbalance ratio (IR), from 1% to 50%, and for various sample sizes. The simulated datasets were then modeled using binary logistic regression. The bias in the estimates was measured using MSE (Mean Square Error). The simulation results provided evidence that the effect of imbalance ratio on the parameter estimate of the covariate decreased as sample size increased. The bias of the estimates depended on sample size whereby for sample size 100, 500, 1000 – 2000 and 2500 – 3500, the estimates were biased for IR below 30%, 10%, 5% and 2% respectively. Results also showed that parameter estimates were all biased at IR 1% for all sample size. An application using a real dataset supported the simulation results.

ARTICLE INFO

Article history:

Received: 13 February 2020

Accepted: 27 July 2020

Published: 22 January 2021

DOI: <https://doi.org/10.47836/pjst.29.1.10>

E-mail addresses:

hezlin@tmsk.uitm.edu.my (Hezlin Aryani Abd Rahman)

beewah@tmsk.uitm.edu.my (Yap Bee Wah)

ongsh@ucsiuniversity.edu.my (Ong Seng Huat)

* Corresponding author

Keywords: Categorical covariate, imbalanced data, logistic regression, parameter estimates, predictive analytics, simulation

INTRODUCTION

Imbalanced data are a condition where the dependent variable contains one class which has more observations than the other. Imbalanced data will have prominent effect on the classification performance of classifiers such as logistic regression, decision trees, support vector machine (SVM) and artificial neural network (ANN). Imbalanced data also affects the classification “power” of various classifiers. The effect of imbalanced data has been reported by researchers through the application of real data sets (Blagus & Lusa, 2010; Longadge et al., 2013; Ramyachitra & Manikandan, 2014).

Logistic regression (LR) is frequently used in predictive modeling as a benchmark model when other classifiers’ performances were evaluated. It is a conventional statistical model used widely in business, engineering, and social science research (Hamid, 2016 ; Hamid et al., 2018; Ahmad et al., 2011; Shariff et al., 2016; Yap et al., 2014), and medical and healthcare studies (Longadge et al., 2013; Mena & Gonzalez, 2006; Oztekin et al., 2009; Pourahmad et al., 2011; Rothstein, 2015; Roumani et al., 2013; Srinivasan & Arunasalam, 2013; Uyar et al., 2010). However, the presence of imbalanced data challenges LR’s ability to classify, whereby majority of classifiers normally focus in the prediction without consideration on the relative distribution between the classes (Dong et al., 2014). Normally, when imbalance data are present, classification results from standard classifiers are biased towards the majority class. As a result, if the event of interest is the minority class, the sensitivity of the classifier will be zero and the specificity will be 100%. The real dataset in reality often suffers from some imbalance problem (Goel et al., 2013) and the minority class is often misclassified (Chawla et al., 2004; He & Garcia, 2009; Weiss & Provost, 2003). Thus, whenever imbalance problem is found in healthcare and medical datasets, the credibility of the models generated by the classifiers are often misleading.

Imbalanced problem affects standard classifiers (Chawla, 2003; Cohen et al., 2006; Galar et al., 2011) and logistic regression based on application to real datasets studies (Blagus & Lusa, 2010; Burez & Van den Poel, 2009; Mena & Gonzalez, 2006; Van Hulse et al., 2007). In our previous study, we performed simulation to study the impact of imbalanced ratio (IR) on LR parameter (β) estimates and the odds ratio (e^β) of the LR model using a continuous covariate (Rahman & Yap, 2016). The results provided enough evidence to conclude that extreme imbalanced ratio (IR = 1%, 2%, 5%) and small sample size have more serious effect on parameter estimates of LR model. Imbalanced ratio is the ratio of the number of cases in minority class to the majority class. For example, if the response variable is the presence of cancer and has two categories Cancer or No Cancer the imbalanced ratio is n_1/n_0 , where n_1 is the number of patients diagnosed with cancer while n_0 is the number of patients who do not have cancer.

The effect of imbalanced data on the performance of the classifiers can be determined through simulation studies. In addition, the various types (categorical or continuous) of

variables in a set of data might show different effects. In this simulation study, we focus on the logistic regression model, a useful statistical model for classification problem and investigate the imbalanced effects on the parameter estimate of the model with a single categorical covariate.

The aim of this study was to determine the effects of different IR on the logistic regression parameter estimate via simulation and an application to real dataset. The results of this study will guide practitioners on the severity of bias in estimates as a result imbalanced data.

MATERIALS AND METHOD

Review on Methods

Machine learning techniques i.e. LR, DT, ANN and SVM, may have great classification performance if it involves a balanced data. However, these techniques performs poorly when imbalanced problem arises (Anand et al., 2010).

Most studies concluded that there was an effect of IR towards the performance of standard classifiers (Rahman et al., 2012; Chawla, 2003; Lemnaru et al., 2012; Mena & Gonzalez, 2006; Prati et al., 2014; Van Hulse et al., 2007; Yap et al., 2014). A study by Mena and Gonzalez (2006) introduced a 3-step algorithm using simple LR called REMED (Rule Extraction Medical Diagnosis) which enabled users to select attributes for the model and improved the accuracy of the model by adjusting the percentage of the partition. Although REMED's algorithm claimed to improve the prediction accuracy, it is limited to medical diagnostics. Lemnaru et al. (2012) reported that IR, size and complexity of the dataset affects the predictive performance of different classifiers [(k-nearest neighbor (KNN), C4.5, SVM, multi-layered perceptron (MLP), Naïve Bayes (NB), and Adaboost (AB)]. In their extensive study, the IR was categorized into three categories (balance, small, large), four categories of dataset size (very small, small, medium, and large) and four categories of complexity of the dataset (small, medium, large and very large). They concluded that the-performance of the classifiers was lower when the IR was high. Another extensive experiment performed by Van Hulse et al. (2007), using different sampling strategies (random oversampling (ROS), random undersampling (RUS), one-sided selection (OSS), cluster-based oversampling (CBOS), Wilson's editing (WE), SMOTE (SM), and borderline-SMOTE (BSM) on different classifiers (NB, DT C4.5, LR, random forest (RF), and SVM) on 35 real datasets with different ratio of imbalance (1.33% - 34.90%), concluded that sampling strategy improved the performance of the chosen classifiers. However, their study also concluded that there was no one universal sampling strategy that worked best for all classifiers. Chawla (2003) experimented on five real datasets using C4.5 as the classifier and reported that their synthetic sampling method, SMOTE, improved the performance of the classifier better than other sampling strategies. He also concluded that RUS was better

than ROS with replication. Prati et al. (2014) also experimented on 22 real datasets with different IR on different classifiers (C4.5, C4.5Rules, CN2 and RIPPER, Back-propagation Neural Network, NB and SVM) and by using different sampling strategies (ROS, SMOTE, borderline-SMOTE, AdaSyn, and MetaCost). They concluded that in terms of accuracy (AUC), the rule-based algorithm (C4.5Rule, RIPPER) was the most affected while Support Vector Machine (SVM) was least affected by imbalanced data. However, the authors also stated that severe imbalanced class distributions would have a strong influence on SVM and any classifier for that matter.

Thus, in a nutshell, we can conclude that the predictive performance of different standard classifiers compared by the mentioned studies arrived at different conclusions as to which classifier and sampling strategies performed better (Blagus & Lusa, 2010; Lemnar et al., 2012; Mena & Gonzalez, 2006; Prati et al., 2014; Sarmanova & Albayrak, 2013).

In classification and predictive analytics, LR is normally considered a very informative classifier as it provides important information about the effect of an independent variable (IV) on the dependent variable (DV) through the odds ratio (Hosmer & Lemeshow, 2004). However, the presence of imbalanced problem hinders the predictive “power” of LR (Wallace & Dahabreh, 2012). Blagus & Lusa (2010) performed a simulation study to evaluate the performance of six types of classifiers (ANN, Linear Discriminant Analysis (LDA), RF, SVM and penalized logistic regression (PLR)) on highly imbalanced data. However, their results showed that the PLR with ROS method, failed to remove the biasness towards the majority class.

A simulation study by Hamid et al. (2015) discovered that when sample size was large (at least 500) the parameter estimates accuracy for LR improved. In addition, the estimation of LR parameters is severely affected by types of covariates; either continuous, categorical, or count data. Simulation studies, usually, enables us to provide a more conclusive evidence on the effect of IR, as the simulated datasets were mold perfectly to cater specific problem types. In our previous study (Rahman & Yap, 2016), our results were consistent with the study by Hamid et al., 2015, which reported that the performance of LR is affected by sample size. However, Hamid et al. (2015) did not consider imbalanced data. Simulation studies are important to obtain empirical evidence on the impacts of IR on the estimate of logistic regression parameter, β -value and the odds ratio of the LR model.

Simulation Methods

This study considered a simple binary logistic regression (LR). In the LR model, two unknown parameters, β_0 and β_1 , are estimated using the maximum likelihood method. Assuming observations to be independent, the likelihood function is given by the following Equation 1 (Hosmer & Lemeshow, 2004):

$$L(\beta_0, \beta_1) = \prod_{i=1}^n \pi(x_i)^{y_i} [1 - \pi(x_i)]^{1-y_i} \quad (1)$$

To estimate β_0 and β_1 , the maximization of the likelihood function is required. Therefore, the maximization of the natural logarithm of the likelihood function is denoted by the following Equation 2:

$$\log[L(\beta_0, \beta_1)] = \sum_{i=1}^n \{y_i \log[\pi(x_i)] + (1 - y_i) \log[1 - \pi(x_i)]\} \quad (2)$$

By referring to the simple LR Equation 1, the Equation 2 can also be expressed as Equation 3 (Hosmer & Lemeshow, 2004):

$$\log[L(\beta_0, \beta_1)] = \sum_{i=1}^n y_i (\beta_0 + \beta_1 x_i) - \sum_{i=1}^n \log[1 + \exp(\beta_0 + \beta_1 x_i)] \quad (3)$$

By differentiating $\log[L(\beta_0, \beta_1)]$ with respect to β_0 and β_1 and setting the resulting Equation 4 to zero, we can obtain β that maximizes Equation 3.

$$\sum_{i=1}^n [y_i - \pi(x_i)] = 0 \quad \text{and} \quad \sum_{i=1}^n x_i [y_i - \pi(x_i)] = 0 \quad (4)$$

The maximum likelihood estimates of β_0 and β_1 , are denoted by $\hat{\beta}_0$ and $\hat{\beta}_1$ and is obtained using Newton-Raphson method. The probability that the event occurs, $\pi(x_i)$ for case i is then obtained as Equation 5:

$$\hat{\pi}(x_i) = \frac{e^{\hat{\beta}_0 + \hat{\beta}_1 x_i}}{1 + e^{\hat{\beta}_0 + \hat{\beta}_1 x_i}} \quad (5)$$

In addition, $\hat{\pi}(x_i)$ is also known as fitted or predicted value and the sum of $\hat{\pi}(x_i)$ is equal to the sum of the observed values as in Equation 6:

$$\sum_{i=1}^n y_i = \sum_{i=1}^n \hat{\pi}(x_i) \quad (6)$$

The final estimated simple logistic regression model is written as Equation 7:

$$\log \left[\frac{\hat{\pi}(x_i)}{1 - \hat{\pi}(x_i)} \right] = \hat{\beta}_0 + \hat{\beta}_1 x_i \quad (7)$$

We assessed the effect of various percentages of IR and sample size on estimation of the parameter coefficient, β for binary LR model with one categorical independent variable. The estimate, $\hat{\beta}_1$ were compared with the true β_1 value. The simulations were performed using R-Studio. The value of the regression coefficient (β_0) for the logistic model was set at 2.08 which gave a significant odds ratio (OR) of 8.004 for X ($OR = e^{2.08} = 8.004$). The R code developed for this simulation is available at <https://github.com/hezlin/simulationx1cat.git>. It is also provided in the Appendix.

Odds-ratio provide important information of the effect of the covariate on the event (dependent variable). Given a binary Y (1=Died, 0=Survived) and a categorical covariate X (Hypertension-HPT) with two categories (1=Yes and 0=No), an odds-ratio of 1 will indicate both patients with or without HPT has equal chance of $Y=1$ (Died). Meanwhile, an odds-ratio greater than 1 will indicate that patients with HPT are more likely to die, and if odds-ratio is less than 1, patients with no HPT are more likely to die.

Eight imbalance ratios were considered for this simulation study: 1%, 2%, 5%, 10%, 20%, 30%, 40%, and 50%. Imbalance ratio (IR) is the percentage of occurrence of minority class between the two predictor classes. For example, in this simulation, if we generated a dataset $N=100$, if the $IR = 1\%$ means that 1 out of 100 has $y=1$ and the rest 99 out of 100 has $y=0$. The IR 5% or less represents high IR in the response variable. However, due to the complexity of generating the simulated dataset, especially for fixing definite percentages of IR, the simulation model required β_0 values to be flexible for different IR ratio. Thus, the full LR model used for this study is denoted as Equation 8:

$$\log \left[\frac{\pi(x)}{1-\pi(x)} \right] = \beta_{0k} + 2.08x_{ik} \tag{8}$$

where β is determined by the IR and is not fixed at one value.

The data for the covariate (X) considered in this study were generated using a binomial distribution, $Bin(n = \text{sample size}, p=0.5)$. We considered sample size of 100, 500, 1000, 1500, 2000, 2500, 3000, 3500, 4000, 4500, and 5000. This simulation study involved 10,000 replications. The simulation algorithm is as follows:

Step 1: Generate random data for the categorical covariate X , for sample size, n and imbalance ratio, IR .

Step 2: Set β at 2.08 and obtain $f(x) = \beta_{0k} + 2.08x_{1k}$, where $k = 1, 2, \dots, 10,000$. β_{0k} is not fixed to create a fix percentage of imbalance accordingly, whereby the confidence interval of β_{0k} is set within the range of (-2, 10).

Step 3: Fit binary logistic regression to the generated data in Step 2.

Step 4: Obtain the parameter estimate, $\hat{\beta}$.

Step 5: Repeat Steps 1-4 for 10,000 replications.

Step 6: Calculate the MSE where
$$MSE = \frac{\sum_{i=1}^{10000} (\beta - \hat{\beta})^2}{10,000}$$

Repeat Steps 1 – 6 for different sample size and imbalanced ratio.

RESULTS AND DISCUSSION

Simulation Results

Table 1 presents the simulation results for the LR parameter estimates for various sample sizes and IR. (%). The effect of IR was reduced when sample size increased. The results showed that the estimates for β_0 and β_1 were very far from the true parameter values for smaller sample size ($n=100$) and for IR 1%, 2%, 5%, 10%, 20% and 30%. The bias in estimate was clearly seen for IR 20% or less for $n=500$. Meanwhile, for $n=1000$, the bias was seen for IR 10% or less. However, the effect of IR was less for sample size more than 3000 and above was only affected by IR of 1% and 2%. Table 2 summarizes the findings.

Figure 1 presents the effect of sample size and IR on the parameter estimate values. It clearly shows the parameter estimates was biased for IR 30% and below for $n=100$. The Figure 1 also shows that for all sample sizes, the estimate was close to the true parameter values at IR=30% and above. In Figure 2, we focused on high IR, 1% to 10% and omitting 20% to 50% so that visualization of the effect is clearer. The Figure 2 shows threshold of effect of IR decreases as sample size increases. For example, estimates are biased for $n=500$ for IR 5% and below, while for $n=1000$, estimates are biased at IR % and below. When estimates are biased the MSE will be larger. Figure 3 illustrates the effect of IR and sample size through the MSE and Figure 4 further emphasizes results in Figure 3 by focusing on the IR of 1% to 10%, by omitting the 20% to 50% ratios. In Figure 3, the effect of imbalance is less (lower MSE) at IR=30%, similar to the illustration in Figure 1. Further focusing on highly imbalanced ratios, Figure 4 illustrates that the MSE values are the largest for small sample sizes ($n=100$ and $n=500$).

Figures 5 and 6 illustrate the effects of imbalanced using a clustered boxplot. As shown in Figure 5, the effect of imbalanced data is obvious for sample size $n=500$ (IR=1% and 2%) and $n=1000$ (IR=1%). In Figure 6, we omit the imbalanced ratio 1% and 2%, and now there are no huge spikes in the boxplots. Figures 5 and 6 clearly showed the effect of IR for various sample sizes, whereby the patterns show that the effect of IR on the bias of parameter estimates depend on sample size. The estimates get closer to the true value when the sample size and IR increases. The dispersion (standard deviation) of $\hat{\beta}_1$ also improves as sample size and IR increases.

Table 1
Parameter estimates for categorical covariate ($\beta=2.08$) for model with different n and IR

Size	IR	$\hat{\beta}_1$	C.I (lower)	C.I (upper)	β_0	$\hat{\beta}_1$	Size	IR	C.I (lower)	C.I (upper)	β_0	$\hat{\beta}_1$	Size	IR	C.I (lower)	C.I (upper)	β_0	$\hat{\beta}_1$			
100	1	13.8056	13.5891	14.0222	-6.5778	-19.6347	2000	1	3.5815	3.4914	3.6717	-6.1199	-7.5977	4000	1	2.3202	2.2895	2.3508	-6.1038	-6.3349	
	2	14.1244	13.9647	14.2841	-5.6621	-17.6550		2	2.3260	2.2945	2.3574	-5.3962	-5.6309		2	2.1316	2.1241	2.1391	-5.3910	-5.4365	
	5	10.3026	10.1344	10.4707	-4.5099	-12.6521		5	2.1204	2.1140	2.1269	-4.4212	-4.4580		5	2.0982	2.0938	2.1026	-4.4184	-4.4357	
	10	6.0332	5.8896	6.1768	-3.6729	-7.5887		10	2.0970	2.0927	2.1013	-3.6369	-3.6524		10	2.0874	2.0844	2.0905	-3.6363	-3.6427	
	20	2.8190	2.7535	2.8845	-2.7598	-3.4784		20	2.0864	2.0835	2.0894	-2.7453	-2.7514		20	2.0850	2.0830	2.0871	-2.7445	-2.7494	
	30	2.2406	2.2164	2.2648	-2.1098	-2.2586		30	2.0836	2.0812	2.0860	-2.1130	-2.1151		30	2.0823	2.0806	2.0839	-2.1116	-2.1138	
	40	2.1501	2.1394	2.1607	-1.5605	-1.6111		40	2.0837	2.0816	2.0858	-1.5612	-1.5645		40	2.0810	2.0796	2.0825	-1.5623	-1.5631	
	50	2.1370	2.1275	2.1464	-1.0423	-1.0704		50	2.0822	2.0802	2.0842	-1.0402	-1.0411		50	2.0801	2.0787	2.0815	-1.0402	-1.0399	
	500	1	10.2400	10.0788	10.4011	-6.1980	-14.2681	2500	1	3.0220	2.9515	3.0924	-6.1132	-7.0367	4500	1	2.2362	2.2144	2.2579	-6.1051	-6.2509
	2	6.7500	6.6006	6.8993	-5.4361	-10.0587		2	2.1933	2.1766	2.2100	-5.3953	-5.4988		2	2.1231	2.1161	2.1301	-5.3879	-5.4281	
5	2.8327	2.7680	2.8975	-4.4340	-5.1721		5	2.1088	2.1029	2.1146	-4.4198	-4.4469		5	2.0964	2.0922	2.1006	-4.4192	-4.4340		
10	2.1722	2.1581	2.1863	-3.6419	-3.7273		10	2.0933	2.0895	2.0972	-3.6371	-3.6486		10	2.0878	2.0850	2.0906	-3.6362	-3.6431		
20	2.1168	2.1107	2.1229	-2.7487	-2.7787		20	2.0842	2.0816	2.0869	-2.7455	-2.7489		20	2.0824	2.0805	2.0843	-2.7454	-2.7474		
30	2.0902	2.0854	2.0950	-2.1131	-2.1219		30	2.0821	2.0800	2.0842	-2.1111	-2.1137		30	2.0825	2.0809	2.0841	-2.1112	-2.1139		
40	2.0912	2.0870	2.0954	-1.5615	-1.5692		40	2.0838	2.0819	2.0856	-1.5616	-1.5647		40	2.0812	2.0798	2.0826	-1.5619	-1.5630		
50	2.0928	2.0887	2.0968	-1.0390	-1.0458		50	2.0817	2.0799	2.0835	-1.0393	-1.0409		50	2.0804	2.0791	2.0817	-1.0400	-1.0405		
1000	1	6.4870	6.3443	6.6298	-6.1395	-10.5075	3000	1	2.6591	2.6051	2.7132	-6.1100	-6.6739	5000	1	2.2074	2.1893	2.2254	-6.1037	-6.2219	
	2	3.5189	3.4285	3.6094	-5.4078	-6.8257		2	2.1619	2.1493	2.1746	-5.3902	-5.4671		2	2.1176	2.1111	2.1242	-5.3905	-5.4227	
	5	2.1924	2.1767	2.2081	-4.4262	-4.5303		5	2.1020	2.0968	2.1072	-4.4196	-4.4398		5	2.0928	2.0888	2.0968	-4.4193	-4.4305	
	10	2.1163	2.1099	2.1227	-3.6365	-3.6712		10	2.0920	2.0885	2.0955	-3.6365	-3.6474		10	2.0874	2.0847	2.0901	-3.6372	-3.6429	
	20	2.0976	2.0933	2.1018	-2.7460	-2.7619		20	2.0867	2.0843	2.0891	-2.7457	-2.7511		20	2.0841	2.0823	2.0860	-2.7450	-2.7487	
	30	2.0883	2.0850	2.0917	-2.1118	-2.1192		30	2.0833	2.0814	2.0852	-2.1121	-2.1146		30	2.0825	2.0809	2.0841	-2.1112	-2.1139	
	40	2.0861	2.0832	2.0891	-1.5620	-1.5665		40	2.0814	2.0797	2.0831	-1.5626	-1.5634		40	2.0817	2.0803	2.0832	-2.1118	-2.1133	
	50	2.0844	2.0816	2.0872	-1.0401	-1.0418		50	2.0809	2.0793	2.0825	-1.0399	-1.0402		50	2.0804	2.0791	2.0817	-1.0400	-1.0402	
	1500	1	4.6278	4.5124	4.7431	-6.1250	-8.6452	3500	1	2.4233	2.3839	2.4628	-6.1072	-6.4387							
	2	2.5863	2.5351	2.6376	-5.3983	-5.8921		2	2.1460	2.1361	2.1559	-5.3877	-5.4511								
5	2.1322	2.1246	2.1322	-4.4223	-4.4704		5	2.1011	2.0963	2.1059	-4.4195	-4.4386									
10	2.1034	2.0984	2.1085	-3.6382	-3.6587		10	2.0913	2.0881	2.0946	-3.6369	-3.6466									
20	2.0894	2.0860	2.0929	-2.7467	-2.7541		20	2.0858	2.0835	2.0880	-2.7457	-2.7501									
30	2.0855	2.0827	2.0883	-2.1102	-2.1162		30	2.0817	2.0799	2.0834	-2.1118	-2.1134									
40	2.0835	2.0810	2.0859	-1.5618	-1.5649		40	2.0811	2.0796	2.0827	-1.5612	-1.5626									
50	2.0841	2.0818	2.0864	-1.0405	-1.0424		50	2.0808	2.0793	2.0823	-1.0400	-1.0404									

Table 2
 Summary of findings on the effect of IR and associated sample size

Sample Size	Estimates biased if IR is
100	30% and below
500	10% and below
1000 – 2000	5% and below
2500 – 3500	2% and below
4000 and above	1% and below

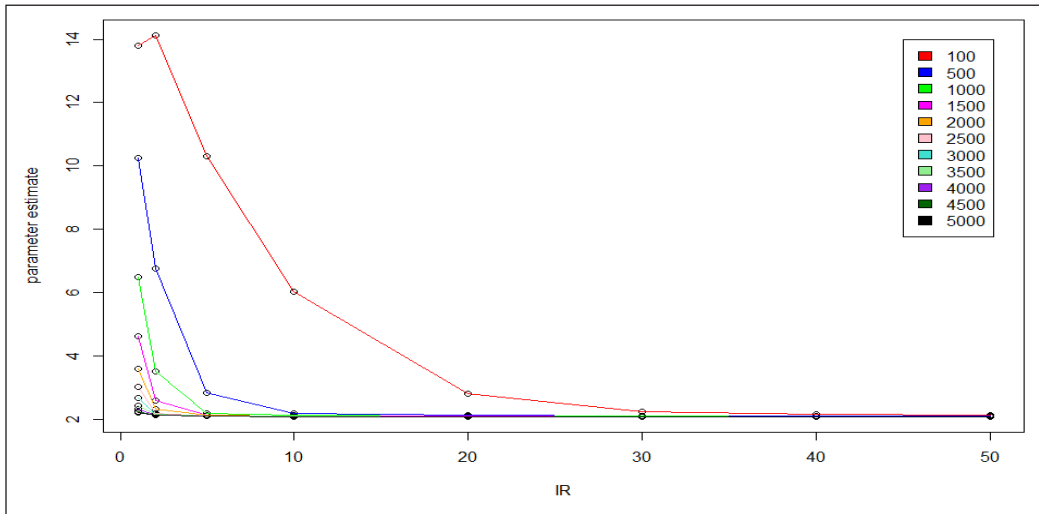


Figure 1. Categorical covariate’s parameter estimates, $\hat{\beta}_1$, for different sample size and imbalance ratio (Imbalance Ratio (IR): 1% to 50%).

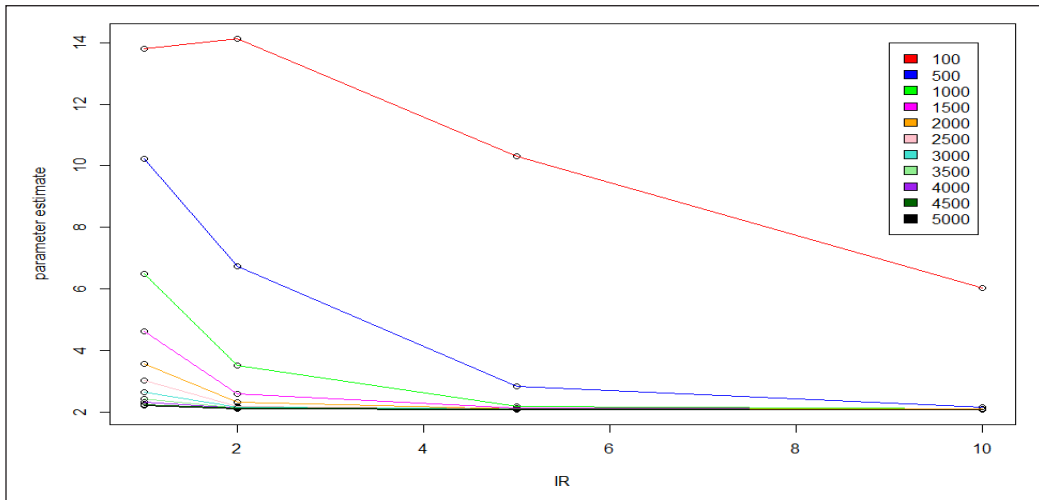


Figure 2. Categorical covariate’s parameter estimates, $\hat{\beta}_1$, for different sample size and highly imbalance ratio (IR : 1-10%).

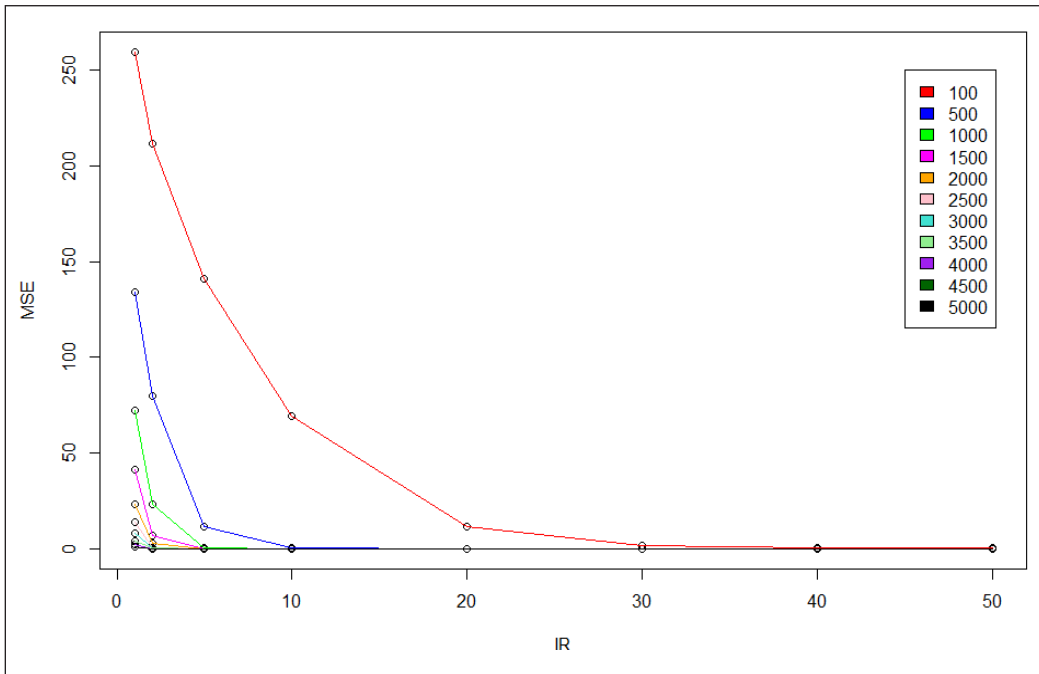


Figure 3. Mean square error (MSE) of categorical covariate's parameter estimates, $\hat{\beta}_1$, for different sample sizes and imbalance ratio

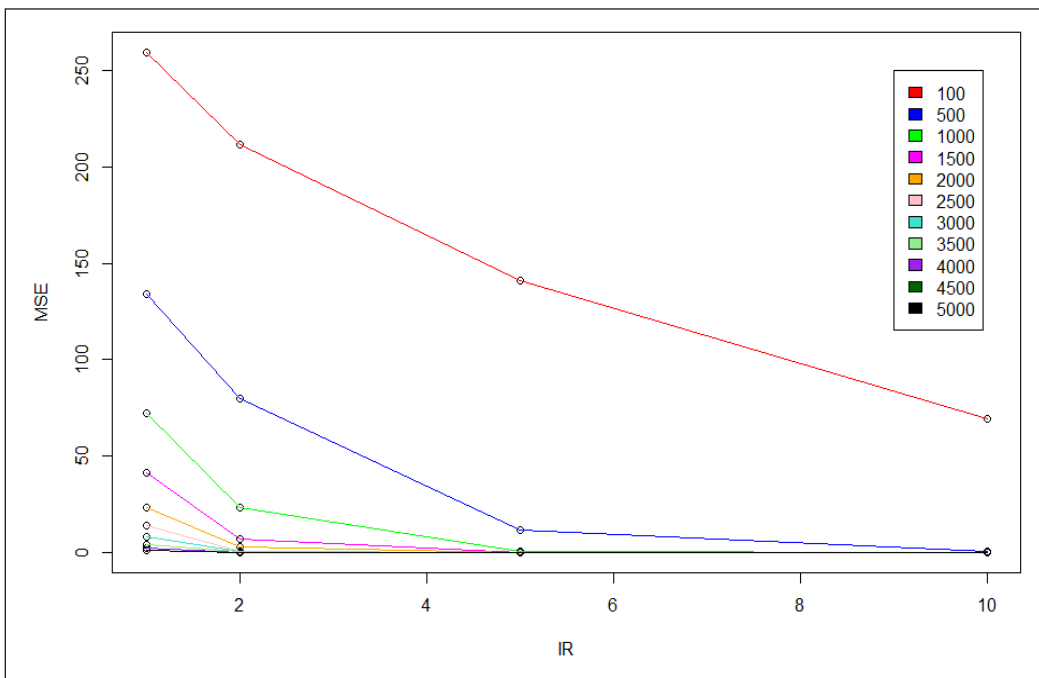


Figure 4. Mean square error (MSE) categorical covariate's parameter estimates, $\hat{\beta}_1$, for different sample size and highly imbalance ratio (IR : 1-10%).

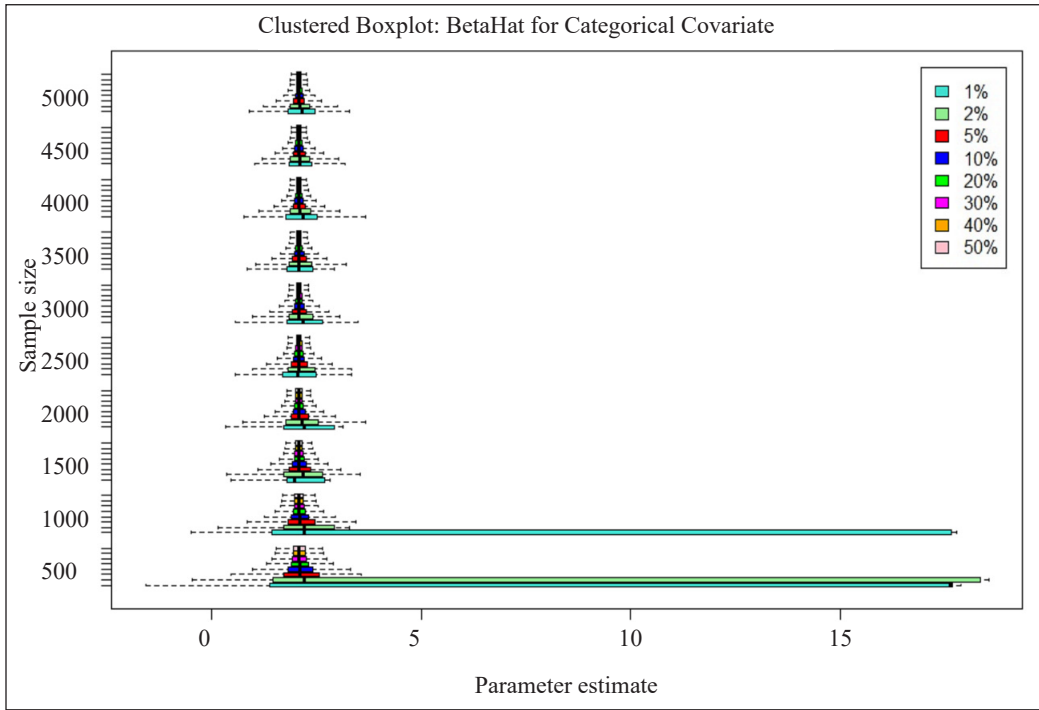


Figure 5. Clustered boxplots of $\hat{\beta}_1$ for a categorical covariate

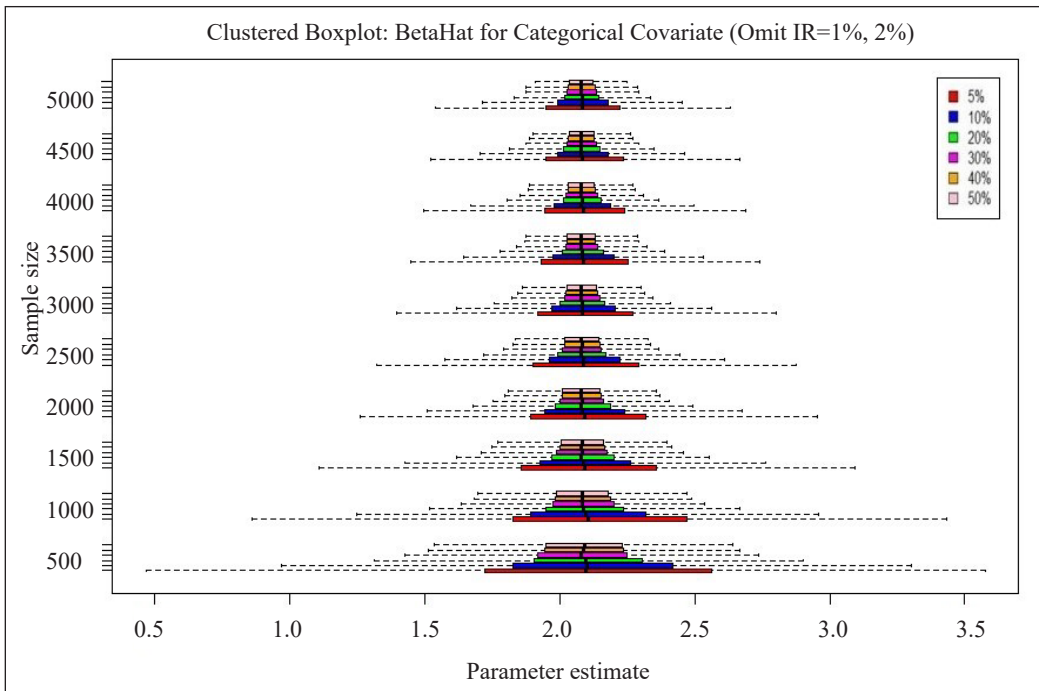


Figure 6. Clustered boxplots for $\hat{\beta}_1$ for a categorical covariate (omit IR=1%, 2%)

Hence, by referring to all the figures (Figures 1 to 6), it can be concluded that the effect of the imbalanced problem on the categorical covariate's parameter estimation was most severe for smaller sample sizes ($n \leq 500$) and for highly imbalanced ratios ($IR \leq 5\%$). The severity of the imbalanced problem was identified by the difference between the parameter estimated values and the fixed true beta value ($\beta_j=2.08$), as well as larger value of MSE. MSE is a good indicator of the bias in parameter estimates of the model. A larger MSE will indicate estimates are biased.

From this simulation results, the effect of IR for small sample size was very prominent with large MSE. Even for larger sample size ($n=1000$ and 1500), the effect of imbalance towards the parameter estimation was still apparent. For small sample size, $n=100$, only at $IR = 30\%$ onwards the value of the estimates became closer to the actual parameter value. Sample size $n=500$, the estimates improve at $IR = 10\%$ onwards. For other sample sizes $1000 \leq n \leq 2000$, $2500 \leq n \leq 3500$ and $n \geq 4000$, the parameter estimation improved at $IR = 5\%$, 2% and 1% onwards. The summary of these findings is shown in Table 2.

Application to Real Data Results

This section illustrates and application using a real medical dataset (Diabetes Messidor dataset) from the UCI repository which has 16 covariates and known as "The Diabetes Messidor" dataset (Antal & Hajdu, 2014), consists of 1151 observations. This dataset contains features extracted from the Messidor image set to predict whether an image contains signs of diabetic retinopathy or not (DR status). All features represent either a detected lesion, a descriptive feature of an anatomical part or an image-level descriptor. The two categorical covariates selected for this illustration are the *retinal abnormality* and *AMFM status*. We modeled the binary dependent variable, *DR status* (1=with DR (53%) and 0=without DR (47%)). We used retinal abnormality (1 = yes, 0 = no) and AMFM status (0 = AM, 1 = FM) as the independent variable in Model 1 and Model 2 respectively. Using stratified sampling on the original dataset, we obtained the IR percentage as shown in Table 3.

Results in Table 3 show that the estimate $\hat{\beta}_1$ in Model 1 was affected for IR 5% and below. The p-values for $\hat{\beta}_1$ increases (leading to independent variable becoming insignificant) as imbalance becomes more severe thus leading to misleading results. Results of Model 2 shows the effect of imbalance on odds-ratio. The odds-ratios were extremely large at IR 1% and 2%. This application to real dataset confirmed the results of the simulation study, which strengthened the conclusion that imbalanced problem will be misleading on the effect of the independent variable on the response variable.

Table 3
Effect of imbalanced with application to real dataset (Diabetes Messidor)

Independent Variable	Data/ IR	$\hat{\beta}_0$, [p-value] C.I (lower, upper)	$\hat{\beta}_1$, [p-value] C.I (lower, upper)	Odds-Ratio (OR) C.I (lower, upper)	
Retinal Abnormality (1 = yes, 0 = no)	Original (540:611)	0.6614, [0.002] (0.6613, 0.6614)	-0.5838, [0.010] (-0.5837, -0.5838)	0.5578 (0.5577, 0.5578)	
	40% (407:611)	0.9477, [0.000] (0.9414, 0.9539)	-0.5872, [0.026] (-0.5938, -0.5805)	0.5591 (0.5554, 0.5626)	
	30% (261:611)	1.4151, [0.000] (1.4033, 1.427)	-0.6110, [0.075] (-0.6236, -0.5983)	0.5537 (0.5470, 0.5604)	
	20% (152:611)	1.9717, [0.000] (1.9527, 1.9906)	-0.6262, [0.178] (-0.6462, -0.6062)	0.5609 (0.5506, 0.5712)	
	10% (68:611)	2.9467, [0.007] (2.8593, 3.0342)	-0.7962, [0.345] (-0.8846, -0.7078)	0.5700 (0.5528, 0.5871)	
	5% (35:611)	4.6431, [0.080] (4.3845, 4.9016)	-1.8264, [0.502] (-2.0863, -1.5664)	0.5920 (0.5680, 0.6159)	
	2% (13:611)	10.5126, [0.418] (10.0310, 10.9941)	-6.7028, [0.806] (-7.1881, -6.2176)	0.6347 (0.5902, 0.6792)	
	1% (7:611)	13.9315, [0.631] (13.4669, 14.3960)	-9.5009, [0.856] (-9.9711, -9.0306)	0.6799 (0.6137, 0.7461)	
	AMFM status (1 = FM, 0 = AM)	Original (540:611)	0.1837, [0.011] (0.1836, 0.1837)	-0.1785, [0.153] (-0.1784, -0.1785)	0.8364 (0.8364, 0.8365)
		40% (407:611)	0.4669, [0.000] (0.4657, 0.4680)	-0.1787, [0.219] (-0.1820, -0.1754)	0.8375 (0.8348, 0.8403)
30% (261:611)		0.9124, [0.000] (0.9104, 0.9143)	-0.1804, [0.307] (-0.1860, -0.1750)	0.8381 (0.8335, 0.8428)	
20% (152:611)		1.4515, [0.000] (1.4483, 1.4548)	-0.1721, [0.404] (-0.1811, -0.1630)	0.8510 (0.8432, 0.8587)	
10% (68:611)		2.2623, [0.000] (2.2570, 2.2677)	-0.1785, [0.451] (-0.1934, -0.1635)	0.8615 (0.8480, 0.8749)	
5% (35:611)		2.9268, [0.000] (2.9193, 2.9343)	-0.1601, [0.480] (-0.1816, -0.1387)	0.9061 (0.8850, 0.9272)	
2% (13:611)		3.9382, [0.000] (3.9240, 3.9525)	-0.0850, [0.500] (-0.1557, -0.0143)	79921.66 (-10534.34, 170377.67)	
1% (7:611)		4.5989, [2.0000e-03] (4.5452, 4.6526)	0.5738, [5.4100e-01] (0.3403, 0.8074)	1676700 (1185601, 2167798)	

CONCLUSIONS

Imbalanced data has effect on the parameter estimates and classification performance of binary logistic regression model with a categorical covariate. The optimal IR for different sample size for less biased estimates was determined via a simulation study. It was concluded that all samples are affected by imbalanced even for larger sample sizes. The effect of imbalanced data on parameter estimates reduces as sample size increases. The imbalanced ratio in the response variable will not only affect the parameter estimates,

but the p-value and odds- ratio for the covariate as well. Hence, imbalanced data can lead to inaccurate findings. There are approaches recommended for handling imbalanced problem such as resampling strategies (ROS (Random Oversampling), RUS, (Random Undersampling) and SMOTE (Synthetic Minority Oversampling Technique). Future simulation studies can investigate which sampling techniques can improve the parameter estimates and predictive performance of the binary logistic regression when data is highly imbalanced.

ACKNOWLEDGEMENT

Our gratitude goes to Universiti Teknologi MARA for the indirect contribution of this publication. We also thank Prof. Dr. Haibo He (Rhodes Island University), Prof. Dr. Ronaldo Prati (Universidade Federal do ABC), Dr. Pam Davey and Dr. Carolle Birrell (University of Wollongong) for sharing their knowledge and providing valuable comments for this study. Not to forget Dr. Hamzah Abdul Hamid (Univeristi Malaysia Perlis) for his indirect contribution to the simulation studies.

REFERENCES

- Ahmad, S., Midi, H., & Ramli, N. M. (2011). Diagnostics for residual outliers using deviance component in binary logistic regression. *World Applied Sciences Journal*, 14(8), 1125-1130.
- Anand, A., Pugalenth, G., Fogel, G. B., & Suganthan, P. N. (2010). An approach for classification of highly imbalanced data using weighting and undersampling. *Amino Acids*, 39(5), 1385-1391. doi: <https://doi.org/10.1007/s00726-010-0595-2>
- Antal, B., & Hajdu, A. (2014). An ensemble-based system for automatic screening of diabetic retinopathy. *Knowledge-Based Systems*, 60, 20-27. doi: <https://doi.org/10.1016/j.knosys.2013.12.023>
- Blagus, R., & Lusa, L. (2010). Class prediction for high-dimensional class-imbalanced data. *BMC Bioinformatics*, 11(1), 1-17. doi: <https://doi.org/10.1186/1471-2105-11-523>
- Burez, J., & Van den Poel, D. (2009). Handling class imbalance in customer churn prediction. *Expert Systems with Applications*, 36(3), 4626-4636. doi: <https://doi.org/10.1016/j.eswa.2008.05.027>
- Chawla, N. V. (2003, August 21). C4. 5 and imbalanced data sets: Investigating the effect of sampling method, probabilistic estimate, and decision tree structure. In *Proceedings of the International Conference on Machine Learning, Workshop Learning from Imbalanced Data Set II* (Vol. 3, p. 66). Washington, DC.
- Chawla, N. V., Japkowicz, N., & Kotcz, A. (2004). Editorial: Special issue on learning from imbalanced data sets. *ACM SIGKDD Explorations Newsletter*, 6(1), 1-6. doi: <https://doi.org/10.1145/1007730.1007733>
- Cohen, G., Hilario, M., Sax, H., Hugonnet, S., & Geissbuhler, A. (2006). Learning from imbalanced data in surveillance of nosocomial infection. *Artificial Intelligence in Medicine*, 37(1), 7-18. doi: <https://doi.org/10.1016/j.artmed.2005.03.002>

- Dong, Y., Guo, H., Zhi, W., & Fan, M. (2014, October 13-15). Class imbalance oriented logistic regression. In *2014 International Conference on Cyber-Enabled Distributed Computing and Knowledge Discovery* (pp. 187-192). Shanghai, China. doi: <https://doi.org/10.1109/CyberC.2014.42>
- Galar, M., Fernandez, A., Barrenechea, E., Bustince, H., & Herrera, F. (2011). A review on ensembles for the class imbalance problem: Bagging-, boosting-, and hybrid-based approaches. *IEEE Transactions on Systems, Man, and Cybernetics, Part C (Applications and Reviews)*, 42(4), 463-484. doi: 10.1109/TSMCC.2011.2161285
- Goel, G., Maguire, L., Li, Y., & McLoone, S. (2013). Evaluation of sampling methods for learning from imbalanced data. *Intelligent Computing Theories*, 7995, 392-401. doi: https://doi.org/10.1007/978-3-642-39479-9_47
- Hamid, H. A. (2016). Effects of different type of covariates and sample size on parameter estimation for multinomial logistic regression model. *Jurnal Teknologi*, 78(12-3), 155-161. doi: <https://doi.org/10.11113/jt.v78.10036>
- Hamid, H. A., Yap, B. W., Xie, X. J., & Rahman, H. A. A. (2015). Assessing the effects of different types of covariates for binary logistic regression. In *AIP Conference Proceedings 1643* (Vol. 425, pp. 425-430). New York, USA: American Institute of Physics. doi: <https://doi.org/10.1063/1.4907476>
- Hamid, H. A., Yap, B. W., Xie, X. J., & Ong, S. H. (2018). Investigating the power of goodness-of-fit tests for multinomial logistic regression. *Communications in Statistics: Simulation and Computation*, 47(4), 1039-1055. doi: <https://doi.org/10.1080/03610918.2017.1303727>
- He, H., & Garcia, E. E. A. (2009). Learning from imbalanced data. *IEEE Transactions on Knowledge and Data Engineering*, 21(9), 1263-1284. doi: <https://doi.org/10.1109/TKDE.2008.239>
- Hosmer, D. W., & Lemeshow, S. (2004). *Applied logistic regression, second edition*. New York, NY: John Wiley & Sons, Inc. doi: <https://doi.org/10.1002/0471722146>
- Lemnaru, C., Potolea, R., Lenmaru, C., & Potolea, R. (2012). Imbalanced classification problems: Systematic study, issues and best practices. *Enterprise Information Systems: Lecture Notes in Business Information Processing*, 102, 35-50. doi: <https://doi.org/10.1007/978-3-642-29958-2>
- Longadge, R., Dongre, S. S., & Malik, L. (2013). Class imbalance problem in data mining: Review. *International Journal of Computer Science and Network*, 2(1), 83-87. doi: <https://doi.org/10.1109/SIU.2013.6531574>
- Mena, L., & Gonzalez, J. A. (2006, May 11-13). Machine learning for imbalanced datasets: Application in medical diagnostic. In *Proceedings of the Nineteenth International Florida Artificial Intelligence Research Society Conference (FLAIRS 2006)* (pp. 574-579). Florida, USA.
- Oztekci, A., Delen, D., & Kong, Z. J. (2009). Predicting the graft survival for heart-lung transplantation patients: An integrated data mining methodology. *International Journal of Medical Informatics*, 78(12), e84-e96. doi: <https://doi.org/10.1016/j.ijmedinf.2009.04.007>
- Pourahmad, S., Ayatollahi, S. M. T., & Taheri, S. M. (2011). Fuzzy logistic regression: A new possibilistic model and its application in clinical vague status. *Iranian Journal of Fuzzy Systems*, 8(1), 1-17.

- Prati, R. C., Batista, G. E. A. P. A., & Silva, D. F. (2014). Class imbalance revisited: A new experimental setup to assess the performance of treatment methods. *Knowledge and Information Systems*, 45(1), 247-270. doi: <https://doi.org/10.1007/s10115-014-0794-3>
- Rahman, H. A. A., & Yap, B. W. (2016). Imbalance effects on classification using binary logistic regression. In *International Conference on Soft Computing in Data Science* (pp. 136-147). Singapore: Springer. doi: https://doi.org/https://doi.org/10.1007/978-981-10-2777-2_12
- Rahman, H. A. A., Yap, B. W., Khairudin, Z., & Abdullah, N. N. (2012, September 10-12). Comparison of predictive models to predict survival of cardiac surgery patients. In *2012 International Conference on Statistics in Science, Business and Engineering (ICSSBE)* (pp. 1-5). doi: <https://doi.org/10.1109/ICSSBE.2012.6396534>
- Ramyachitra, D., & Manikandan, P. (2014). Imbalanced dataset classification and solutions: A review. *International Journal of Computing and Business Research*, 5(4), 1-29.
- Rothstein, M. A. (2015). Ethical issues in big data health research: Currents in contemporary bioethics. *The Journal of Law, Medicine and Ethics*, 43(2), 425-429. doi: <https://doi.org/10.1111/jlme.12258>
- Roumani, Y. F., May, J. H., Strum, D. P., & Vargas, L. G. (2013). Classifying highly imbalanced ICU data. *Health Care Management Science*, 16(2), 119-128. doi: <https://doi.org/10.1007/s10729-012-9216-9>
- Sarmanova, A., & Albayrak, S. (2013, April 24-26). Alleviating class imbalance problem in data mining. In *2013 21st Signal Processing and Communications Applications Conference (SIU)* (pp. 1-4). Haspolat, Turkey. doi: 10.1109/SIU.2013.6531574
- Shariff, S. S. R., Rodzi, N. A. M., Rahman, K. A., Zahari, S. M., & Deni, S. M. (2016). Predicting the “graduate on time (GOT)” of PhD students using binary logistics regression model. In *AIP Conference Proceedings* (Vol. 1782, No. 1, p. 050015). New York, USA: AIP Publishing LLC. doi: <https://doi.org/10.1063/1.4966105>
- Srinivasan, U., & Arunasalam, B. (2013). Leveraging big data analytics to reduce healthcare costs. *IT Professional*, 15(6), 21-28. doi: <https://doi.org/10.1109/MITP.2013.55>
- Uyar, A., Bener, A., Ciracy, H. N., & Bahceci, M. (2010). Handling the imbalance problem of IVF implantation prediction. *IAENG International Journal of Computer Science*, 37(2), 164-170.
- Van Hulse, J., Khoshgoftaar, T. M., & Napolitano, A. (2007). Experimental perspectives on learning from imbalanced data. In *Proceedings of the 24th international conference on Machine learning* (pp. 935-942). New York, USA: Association for Computing Machinery. doi: <https://doi.org/10.1145/1273496.1273614>
- Wallace, B. C., & Dahabreh, I. J. (2012, December 10-13). Class probability estimates are unreliable for imbalanced data (and how to fix them). In *2012 IEEE 12th International Conference on Data Mining* (pp. 695-704). Brussels, Belgium. doi: 10.1109/ICDM.2012.115
- Weiss, G. M., & Provost, F. (2003). Learning when training data are costly: The effect of class distribution on tree induction. *Journal of Artificial Intelligence Research*, 19, 315-354. doi: <https://doi.org/10.1613/jair.1199>
- Yap, B. W., Rani, K. A., Rahman, H. A. A., Fong, S., Khairudin, Z., & Abdullah, N. N. (2014). An application of oversampling, undersampling, bagging and boosting in handling imbalanced datasets. In *Proceedings of the first international conference on advanced data and information engineering (DaEng-2013)* (pp. 13-22). Singapore: Springer. doi: <https://doi.org/10.1007/978-981-4585-18-7>

APPENDIX

```

#fitting the model
set.seed(54321)
ndata <- 100
nrep <- 10000 #set the number of replications
start <- -10 #set initial value of bnot
end <- 10 #set end value for bnot
n <- 1 #set initial value for the loop
perc <- 40 #set the percentage of imbalance

#replication setup
beta0Hat<-rep(NA,nrep)
beta1Hat<-rep(NA,nrep)
betanot<-rep(NA,nrep)
betaone <- 2.08

while(n<=nrep)
{
  #set bnot value
  for(i in seq(start,end,0.001))
  {
    x <- rbinom(ndata,1,1/2)
    rx <-chartr("\01", "AB", x)
    dummy(x)
    k <-dummy(x)
    linpred <- cbind(1,dummy(x)[,-1])%*% c(i,betaone) # (b)
    pi<-exp(linpred)/(1+exp(linpred))
    ru <- runif(ndata,0,1)
    u<-as.vector(ru)
    ry <- ifelse( (u<=pi),1,0)
    m_y <- (mean(ry)*100)
    if(m_y == perc && n <=nrep)
    {
      dt <-data.frame(x=rx, y=ry) #fit the logistic model
      #print(dt)
      betanot[n]<-i
      mod <- glm(y~x, family="binomial", data=dt)
      beta0Hat[n]<-mod$coef[1]
      beta1Hat[n]<-mod$coef[2]
      n <- n + 1
    }
  }
}

Round1<-round(c(beta0=mean(beta0Hat),beta1Hat=mean(beta1Hat)),3)
mean(beta1Hat)
ci.b1 <- CI(beta1Hat,ci=0.95)
MSEbeta1Hat <- round(sum((beta1Hat-2.08)^2/nrep),3)
meanb0 <- mean(betanot)
mean(beta0Hat)
ci.b0 <- CI(beta0Hat,ci=0.95)

```



Elastic-Net Regression based on Empirical Mode Decomposition for Multivariate Predictors

Abdullah Suleiman Al-Jawarneh* and Mohd. Tahir Ismail

School of Mathematical Sciences, Universiti Sains Malaysia, 11800 USM, Penang, Malaysia

ABSTRACT

The empirical mode decomposition (EMD) method is used to decompose the non-stationary and nonlinear signal into a finite set of orthogonal non-overlapping time scale components that include several intrinsic mode function components and one residual component. Elastic net (ELN) regression is a statistical penalized method used to address multicollinearity among predictor variables and identify the necessary variables that have the most effect on the response variable. This study proposed the use of the ELN method based on the EMD algorithm to identify the decomposition components of multivariate predictor variables with the most effect on the response variable under multicollinearity problems. The results of the numerical experiments and real data confirmed that the EMD-ELN method is highly capable of identifying the decomposition components with the presence or absence of multicollinearity among the components. The proposed method also achieved the best estimation and reached the optimal balance between the variance and bias. The EMD-ELN method also improved the accuracy of regression modeling compared with the traditional regression models.

Keywords: Elastic-net regression, empirical mode decomposition, LASSO, model selection, multicollinearity, ridge regression

ARTICLE INFO

Article history:

Received: 04 June 2020

Accepted: 11 September 2020

Published: 22 January 2021

DOI: <https://doi.org/10.47836/pjst.29.1.11>

E-mail addresses:

a_aljawarneh86@student.usm.my;

abdssj2004@yahoo.com (Abdullah Suleiman Al-Jawarneh)

m.tahir@usm.my (Mohd. Tahir Ismail)

* Corresponding author

INTRODUCTION

Regression analysis methods assume that the variables have stationary and linear properties and that the predictor variables are free from multicollinearity to achieve reliability and accuracy of results. Transformation (modification) methods can be used to convert the variables to become stationary and linearized; however, these

methods can lead to the loss of valuable information and features of the original dataset. Moreover, few statistical methods can handle variables selection when multicollinearity exists (Hamid et al., 2018; Hashibah & Mahat, 2013).

The empirical mode decomposition (EMD) method focuses on non-stationary and nonlinear variables and decomposes the variable into a set of decomposition components with different information (Huang, 2014). These components represent new predictor variables that can be used to study their effects on the response variable. Unlike traditional analysis methods, such as Fourier decomposition (Titchmarsh, 1948) and wavelet decomposition (Chui, 1995), the EMD method does not assume that the dataset is either stationary or linear.

Multicollinearity is one of the fundamental issues in variables selection. The presence of multicollinearity between predictor variables increases variance, highlights the wrong sign of coefficients, and misleads the selected model (Jadhav et al., 2014). To address this gap, Zou and Hastie (2005) proposed the technical penalized regularization method, which is a double shrinkage called elastic net regression (ELN). The ELN method is a combination of ridge regression (RR) (Hoerl & Kennard, 1970) and least absolute shrinkage and selection operator (LASSO) regression (Tibshirani, 1996). The ELN can achieve the best estimation of optimal balance between the variance and bias terms. It can also choose between predictors that exhibit a high correlation in the final model.

The EMD method and the penalized regularization regression method analysis have been used in several scientific fields to understand the significance of decomposition components on the response variable. Examples include the forward stepwise regression methods with EMD (Yang et al., 2011), the LASSO regression based on ensemble EMD (EEMD) (Shen & Lee, 2012), ridge regression with EEMD (Shen et al., 2012). LASSO regression based on EMD (Qin et al., 2016), LASSO regression, deep belief networks (DBN) with EEMD (Chu et al., 2018), kernel ridge regression and EMD (Naik et al., 2018), and LASSO regression based on noise-assisted multivariate EMD (NA-MEMD) (Masselot et al., 2018).

This article is an expansion of the study by Al-Jawarneh et al. (2020) that used the EMD-ELN method for univariate original predictor cases. Al-Jawarneh, et al. (2020) explored the relationship of the orthogonal decomposition components of the nonlinear and non-stationary original predictor with the response variable extracted through the EMD method. This article focused on the cases of the multivariate original predictors by applying the EMD method based on the ELN regression method. For the multivariate case, the effects of the decomposition components extracted through the EMD method of the nonlinear and non-stationary original multivariate predictor variables on the response variable are investigated. When multicollinearity among the decomposition components is determined, the proposed method removes the multicollinearity to arrive at a model free from multicollinearity, and to produce more accurate results

The rest of the paper is organized as follows. Section 2 describes the EMD algorithm, ELN regression, and EMD-ELN algorithm methods. Section 3 discusses and applies the method through numerical experiments using stock market data. Section 4 provides the conclusions of the study.

METHODS

This section describes the methods used in this study. The first method is the EMD algorithm method, which is employed to decompose the original signal (predictor variable) of the dataset. The second method is the regularization method by ELN regression. The proposed EMD-ELN algorithm is discussed in this section.

Empirical Mode Decomposition

Empirical mode decomposition (EMD) algorithm was presented by Huang et al. (1998). The EMD algorithm is a new technique analysis method that aims to decompose the non-stationary and nonlinear signal into a finite set of orthogonal decomposition components called intrinsic mode function (IMF) components. One component called the residual and represents the trend of the signal. The principle of the EMD algorithm is that it analyzes the original signal through an iterative process called the sifting process, which maintains the time domain of the signal (Huang, 2014). These decomposition components represent the temporal modes existing in the original signal, which have different physical significant meanings.

Each of the orthogonal decomposition components should satisfy the following IMF conditions: (1) Over the entire length of a signal, the number of local extrema (EX) (i.e. maximum and minimum) and the number of zero-crossing (Z) should be equal or differ at most by one ($|\#EX - \#Z| \leq 1$), where this condition indicates that each IMF has only one local extrema between two consecutive zero-crossing or vice versa. (2) At any point on a signal, the mean envelope (m) value between the upper (Ue) envelope defined by the local maximum and the lower (Le) envelope defined by the local minimum are zero ($m = \frac{Ue+Le}{2} = 0$), which explains that all IMF are stationary components (Huang, 2014).

The original signal $x(t)$ is the linear combination of the finite set of orthogonal IMF components and monotonic residual component through the EMD algorithm as indicated in the following Equation 1:

$$x(t) = \sum_{k=1}^K C_k(t) + r(t) \quad [1]$$

where symbol t represent the sample index (time domain) $\{C_k(t)\}$, $k = 1, 2, \dots, K$ denotes the finite set of IMF components, and $r(t)$ is the residual component.

The iterative process of the EMD algorithm to decompose $x(t)$ into orthogonal $C_k(t)$ and $r(t)$ components of a non-overlapping time scale are summarized in Algorithm 1 and Figure 1.

Algorithm 1: EMD algorithm

Input: $x(t)$

Output: $\{C_k(t)\}; k = 1, 2, \dots, K$ and $r(t)$ components

- (1) Initializations: $r_0(t) = x(t); j = 1$ and $k = 1$.
- (2) Identify all local maximum and a local minimum of $x(t)$.
- (3) Determine the upper $Ue_j(t)$ and lower $Le_j(t)$ envelopes through the cubic spline curve of the local maximum and minimum of the $x(t)$, respectively.
- (4) Compute the mean envelope: $m_j(t) = [Ue_j(t) + Le_j(t)]/2$.
- (5) Compute: $h_j(t) = x(t) - m_j(t)$.
- (6) Check that $h_j(t)$ satisfies the conditions of IMF.
 - Yes:** $h_j(t) = C_k(t)$, save output $C_k(t)$ and go to the next step (7).
 - No:** $j = j + 1$ and repeat steps (2)–(6).
- (7) Compute: $r_k(t) = r_{k-1}(t) - C_k(t)$.
- (8) Check that $r_k(t)$ satisfies the stoppage criterion.

$$SD_j = \sum_{t=0}^T (h_{j-1}(t) - h_j(t))^2 / h_{j-1}^2(t); 0.2 \leq SD_j \leq 0.3$$

Yes: Go to the next step (9).

No: $k = k + 1$ and repeat steps (2)–(8).

- (9) Save the output: $\sum_{k=1}^K C_k(t) + r_k(t)$.

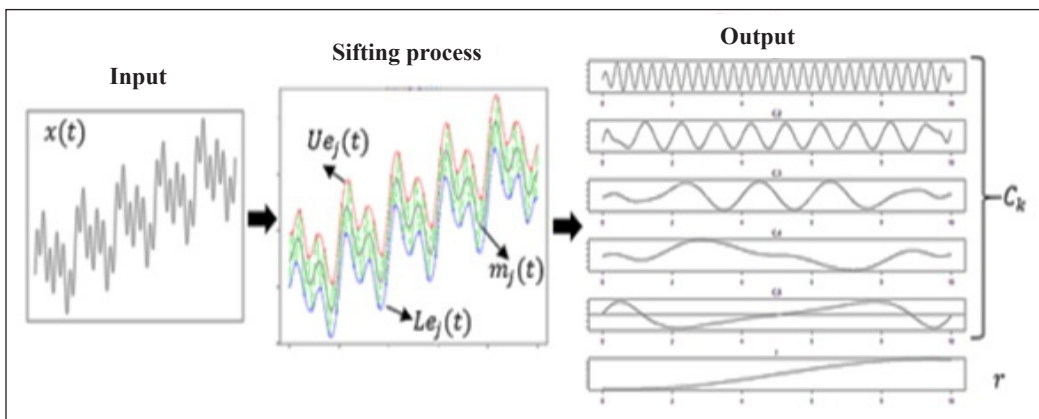


Figure 1. EMD algorithm process

Elastic Net Regression

Elastic net regression (ELN) was introduced by Zou and Hastie (2005). The ELN is a hybrid technology of the penalized least squares regression method that involves regularization and variables selection and was developed to improve and overcome the limitations of the LASSO regression in some situations (i.e., when the number of observations (n) is larger than the number of predictors (p) and the predictor variables have a multicollinearity problem) (Zou & Hastie, 2005).

Penalized regressions methods, such as the ELN method introduce little increase to the bias and contribute to the decrease in the variance by adding penalties to the estimation regression, which leads to the treatment of the multicollinearity and the enhancement of the accuracy of the selection compared to the other methods, such as the ordinary least square (OLS). The ELN is a combination of the two more commonly used penalized regression methods: (1) LASSO method, which uses the sum of the absolute values of the coefficient variables (l_1 -norm) with the tuning parameter and (2) the RR method, which uses the sum of the squared coefficient variables (l_2 -norm) with the tuning parameter (Javaid et al., 2020). The practical principles of the ELN method are similar to LASSO and involve the shrinkage of the coefficient regression toward zero or should be equal to zero for unnecessary predictors, leading to a reduction in the number of predictor variables (Al-Jawarneh et al., 2020). In a multicollinearity case, the ELN method can remove or select the predictor variables that exhibit high correlation in the final model, unlike the LASSO, which lacks the tools to deal with multicollinearity.

The model structure of the multiple linear regression with n observations and p predictors is derived as Equation 2:

$$y_i = \beta_0 + x_{i1}\beta_1 + x_{i2}\beta_2 + \dots + x_{ip}\beta_p + \varepsilon_i,$$

$$y = \sum_{j=0}^p x_j \beta_j + \varepsilon \quad [2]$$

where $i = 1, 2, \dots, n; j = 1, 2, \dots, p, \beta_0$ is the intercept, x_{ij} is the i -th observation of the j -th predictor variable x_j , and β_j is the unknown regression coefficient of the j -th predictor variable, which represents the average effect on y of per one unit change in the j -th predictor variable x_{ij} , while ε_i is the error term.

In the penalized regression methods, the predictors and response variables should be standardized to have zero mean and unit standard deviation (i.e. centered and normalized) before model fitting (Yan & Su, 2009; Zhou, 2013) as Equation 3:

$$\bar{y} = \frac{1}{n} \sum_{i=1}^n y_i, \bar{x}_j = \frac{1}{n} \sum_{i=1}^n x_{ij}, S_y = \sqrt{\sum_{i=1}^n (y_i - \bar{y})^2}, \text{ and } S_{x_j} = \sqrt{\sum_{i=1}^n (x_{ij} - \bar{x}_j)^2} \quad [3]$$

Then, the predictors and response variables are standardized as Equation 4:

$$y'_i = (y_i - \bar{y})/S_y, \text{ and } x'_{ij} = (x_{ij} - \bar{x}_j)/S_{x_j} \quad [4]$$

The classical OLS estimator is used to estimate the unknown regression coefficients by minimizing the residual sum of squares (*RSS*). The *RSS* is the sum of the squared differences between the actual value and the estimated value and is obtained as Equation 5:

$$RSS = \sum_{i=1}^n \left(y'_i - \beta_0 - \sum_{j=1}^p x'_{ij} \beta_j \right)^2 \quad [5]$$

Using Equation 5, the OLS regression for the *j*-th element $\hat{\beta}$ (i.e., $\beta_j: j = 0, 1, 2, \dots, p$) (Montgomery et al., 2012) is obtained as Equation 6:

$$\hat{\beta}^{OLS} = \underset{\beta}{\operatorname{argmin}} \sum_{i=1}^n \left(y'_i - \beta_0 - \sum_{j=1}^p x'_{ij} \beta_j \right)^2 \quad [6]$$

The ELN regression method is the penalized version of the OLS estimator and produces the coefficients regression $\hat{\beta}$ (Zou & Hastie, 2005) given by Equation 7:

$$\hat{\beta}^{ELN} = \underset{\beta}{\operatorname{argmin}} \sum_{i=1}^n \left(y'_i - \beta_0 - \sum_{j=1}^p x'_{ij} \beta_j \right)^2 + \lambda_1 \sum_{j=1}^p |\beta_j| + \lambda_2 \sum_{j=1}^p (\beta_j)^2 \quad [7]$$

where λ_1 and λ_2 are the tuning parameters ($\lambda_1, \lambda_2 > 0$), which are automatically selected by using cross-validation (CV). Another way is to denote $\lambda_1 = 2n\lambda\alpha$ and $\lambda_2 = n\lambda(1 - \alpha)$ (Haws et al., 2015), Equation 6 is equivalent to Equation 8:

$$\hat{\beta}^{ELN} = \underset{\beta}{\operatorname{argmin}} \frac{1}{2n} \sum_{i=1}^n \left(y'_i - \beta_0 - \sum_{j=1}^p x'_{ij} \beta_j \right)^2 + \lambda \left(\alpha \sum_{j=1}^p |\beta_j| + \frac{1 - \alpha}{2} \sum_{j=1}^p (\beta_j)^2 \right) \quad [8]$$

where α is a regularization parameter ($0 \leq \alpha \leq 1$) and λ is a tuning parameter ($\lambda \geq 0$). When $\lambda = 0$, the ELN estimation follows the OLS method in Equation 6 while the ELN estimation follows RR regression shown in Equation 9 when $\alpha = 0$, but when $\alpha = 1$ the

ELN estimation performed using the LASSO regression shown in Equation 10. Thus, the RR and LASSO regressions are cases from the ELN regression. Therefore, the ELN regression sets the appropriate value for α between zero and one.

$$\hat{\beta}^{RR} = \operatorname{argmin}_{\beta} \frac{1}{2n} \sum_{i=1}^n \left(y_i - \beta_0 - \sum_{j=1}^p x_{ij} \beta_j \right)^2 + \frac{\lambda}{2} \sum_{j=1}^p (\beta_j)^2 \quad [9]$$

$$\hat{\beta}^{LASSO} = \operatorname{argmin}_{\beta} \frac{1}{2n} \sum_{i=1}^n \left(y_i - \beta_0 - \sum_{j=1}^p x_{ij} \beta_j \right)^2 + \lambda \sum_{j=1}^p |\beta_j| \quad [10]$$

The coordinate descent method and soft-thresholding operator (Friedman et al., 2010) are used to solve Equation 8 with given values of λ and α . The coordinate descent method is used to optimize each predictor separately and solves exactly for one predictor x_{ij} while the rest of the predictors x_{if} except the j -th predictor are fixed in each coordinate descent step. Equation 7 can be rearranged to isolate β_j (Equation 11):

$$\hat{\beta}^{ELN} = \operatorname{argmin}_{\beta} \frac{1}{2n} \sum_{i=1}^n \left(y_i - \beta_0 - \sum_{f \neq j}^p x_{if} \beta_f - x_{ij} \beta_j \right)^2 + \lambda \alpha \sum_{j=1}^p |\beta_j| + \lambda \frac{1-\alpha}{2} \sum_{j=1}^p (\beta_j)^2 \quad [11]$$

where $y_i - \beta_0 - \sum_{f \neq j}^p x_{if} \beta_f$ is the partial residual \mathbf{r}_f that represents the differences between the actual and estimated values that does not involve x_{ij} . Let $X_j = \sum_{i=1}^n x_{ij} \beta_j$, then Equation 11 can be rearranged as Equation 12:

$$\hat{\beta}^{ELN} = \operatorname{argmin}_{\beta} \frac{1}{2n} (\mathbf{r}_f - X_j \beta_j)^2 + \lambda \alpha \sum_{j=1}^p |\beta_j| + \lambda \frac{1-\alpha}{2} \sum_{j=1}^p (\beta_j)^2 \quad [12]$$

Using the coordinate descent to compute Equation 12, the partial derivative for β_j is as Equation 13:

$$\frac{\partial \hat{\beta}^{ELN}}{\partial \beta_j} = \frac{1}{n} X_j^T (\mathbf{r}_f - X_j \beta_j) + \lambda \alpha \operatorname{sign}(\beta_j) + \lambda (1 - \alpha) \beta_j \quad [13]$$

Solving Equation 13 in terms of $\hat{\beta}_j$ yields the following Equation 14:

$$\hat{\beta}_j = S \left(\frac{1}{n} X_j^T \mathbf{r}_f, \lambda \alpha \right) / (1 + \lambda (1 - \alpha)) \quad [14]$$

where $\frac{1}{n} \mathbf{X}_j^T r_f$ is the simple OLS method to estimate the coefficient $\hat{\beta}_j$ and $S\left(\frac{1}{n} \mathbf{X}_j^T r_f, \lambda \alpha\right)$ is the soft-thresholding function with the value (Equation 15):

$$S\left(\frac{1}{n} \mathbf{X}_j^T r_f, \lambda \alpha\right) = \begin{cases} \frac{1}{n} \mathbf{X}_j^T r_f + \lambda \alpha & , \quad \frac{1}{n} \mathbf{X}_j^T r_f < -\lambda \alpha \\ 0 & , \quad \left| \frac{1}{n} \mathbf{X}_j^T r_f \right| \leq \lambda \alpha \\ \frac{1}{n} \mathbf{X}_j^T r_f - \lambda \alpha & , \quad \frac{1}{n} \mathbf{X}_j^T r_f > \lambda \alpha \end{cases} \quad [15]$$

The mean square error (*MSE*) is a measure of the average squared difference between the actual and estimated values as Equation 16:

$$MSE = \frac{1}{n} \sum_{i=1}^n \left(y_i - \sum_{j=1}^p x_{ij} \beta_j \right)^2 \quad [16]$$

The *MSE* is written as the sum of the variance and bias squared terms of the estimator $\hat{\beta}$ as Equation 17:

$$\begin{aligned} MSE(\hat{\beta}) &= E[\hat{\beta} - \beta] \\ &= E\left[(\hat{\beta} - E(\hat{\beta}))^2 \right] + [E(\hat{\beta}) - \beta]^2 \\ &= var(\hat{\beta}) + Bias^2(\hat{\beta}, \beta) \end{aligned} \quad [17]$$

where the bias and variance have a trade-off, and thus, the ELN regression aims to achieve the best estimator through an optimal balance between the variance and bias terms by increasing the bias value, leading to a decrease in the variance value to investigate the minimum *MSE*.

Proposed EMD-ELN Method

The proposed EMD-ELN method is intended to understand the significance of the decomposition components, $\{C_{jk}(t)\}; k = 1, 2, \dots, K$ and $r_j(t) j = 1, 2, \dots, p$, that have the most effect on response variable *y* in two case studies. In the first case, the components are free from multicollinearity while in the second case, high multicollinearity can be observed among the components. The EMD-ELN method is summarized in Algorithm 2 and Figure 2.

Algorithm 2: EMD-ELN algorithm**Input:** $x_j(t)$ and $y(t)$; $j = 1, 2, \dots, p$, and $y(t)$.**Output:** $\beta_{jk} \neq 0$; $j = 1, 2, \dots, p$ and $k = 1, 2, \dots, K, K + 1$.

- (1) Decompose
- $x_j(t)$
- via EMD separately.

$$x_j(t) = \sum_{k=1}^K C_{jk}(t) + r_j(t)$$

- (2) Use all
- $C_{jk}(t)$
- and
- $r_j(t)$
- components as new predictor variables to explain
- $y(t)$
- .

$$y(t) = \sum_{j=1}^p \left(\sum_{k=1}^K C_{jk}(t) \beta_{jk} + r_j(t) \beta_{jK+1} \right) + \varepsilon(t)$$

- (3) Check the multicollinearity by using the variance inflation factor (VIF) test,

$$VIF_{jk} = \frac{1}{1 - R_{jk}^2},$$

where R_{jk}^2 is the coefficient of determination.

- (4) Select the variables via the ELN:

$$\hat{\beta}^{ELN} = \operatorname{argmin}_{\beta} \frac{1}{2n} \sum_{i=1}^n \left(y(t) - \beta_0 - \sum_{j=1}^p \left(\sum_{k=1}^K C_{jk}(t) \beta_{jk} \right) - r_j(t) \beta_{jK+1} \right)^2 + \lambda P_{\alpha}(\beta);$$

$$P_{\alpha}(\beta) = \alpha \left(\sum_{j=1}^p \left(\sum_{k=1}^{K+1} |\beta_{jk}| \right) \right) + \frac{1 - \alpha}{2} \left(\sum_{j=1}^p \left(\sum_{k=1}^{K+1} (\beta_{jk})^2 \right) \right)$$

- (5) Build the final model by
- $\beta_{jk} \neq 0$
- .

APPLICATION

We explain the numerical experiments comprehensively using the sine waves function and the daily close stock market data to apply the EMD-ELN method and discuss the results.

Numerical Experiments

This study uses the sine function to demonstrate the use of the EMD-ELN method. The datasets are generated for the predictors and response signals with the length of a sample size $n = 250$ and time-domain between zero and seven ($0 \leq d \leq 7$) in the first experiment

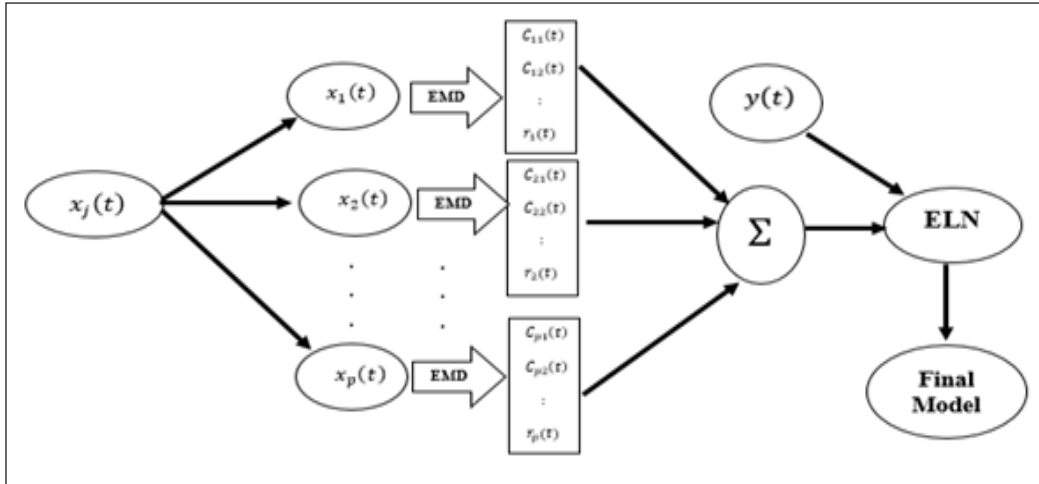


Figure 2. EMD-ELN modeling process

(Experiment 1) and $n = 450$ and $(0 \leq d \leq 9)$ second experiment (Experiment 2). The formulas of the function test in two experiments of the response and predictor variables are as follows.

Experiment 1:

$$x(d) = 0.5d + \sin(\pi d) + \sin(2\pi d) + \sin(6\pi d)$$

$$y(d) = \sin(2\pi d) + \sin(6\pi d) + \sin(8\pi d) + \sin(13\pi d)$$

Experiment 2:

$$x_1(d) = 0.8d + \sin(0.3\pi d) + \sin(2\pi d) + \sin(7\pi d) + \sin(9\pi d)$$

$$x_2(d) = 0.4d + \sin(0.2\pi d) + \sin(6\pi d) + \sin(7\pi d) + \sin(9\pi d)$$

$$x_3(d) = 0.6d + \sin(\pi d) + \sin(7\pi d) + \sin(9\pi d)$$

$$y(d) = 0.5d + \sin(\pi d) + \sin(2\pi d) + \sin(6\pi d)$$

RESULTS AND DISCUSSION

Table 1 presents the number of decomposition components extracted through the EMD algorithm and the multicollinearity test among the components in two experiments. In the first experiment, the original $x(t)$ had three IMFs and one residual component. The VIF test also showed that the components were free from multicollinearity where all values were less than 10. In the second experiment, the results of the EMD algorithm for the original multiple predictors $x_1(t)$, $x_2(t)$, and $x_3(t)$ were as follows: each one of the $x_1(t)$ and $x_2(t)$ has four IMFs and one residual component, while the $x_3(t)$ has five IMFs and one residual component. Based on the VIF test values for this experiment, several decomposition

components had values of more than 10, indicating that high multicollinearity existed among the decomposition components in the second experiment.

Table 2 illustrates the results of the comparison of the methods that depended on the values of lambda, which were selected by 10-fold CV. In the two experiments, the results showed that EMD-ELN had the smallest values of *RSS*. The penalty value increase appeared to cause a negligible increase in the bias, which contributed to the decrease in the variance of the two experiments. This result indicates that the optimal balance between variance and bias was achieved. For the variable selection in the first experiment, which was free from multicollinearity, the END-ELN method similar to END-LASSO method selected variables C_1 and C_2 and had the most effect on the response variable. In the second experiment, the EMD-ELN was the best method for selecting the decomposition components that exhibited a high correlation and included C_{12} , C_{14} , C_{21} , C_{32} , and C_{33} in the final model, whereas the EMD-LASSO selected C_{21} , C_{32} , and C_{33} . Hence, the EMD-LASSO failed to select any decomposition components from the predictor $x_1(t)$ because of multicollinearity, while the EMD-ELN selected, two components C_{12} and C_{14} , from the $x_1(t)$.

Table 1
Output of EMD and VIF tests

Experiment 1								
	$C_1(t)$	$C_2(t)$	$C_3(t)$	$r(t)$				
EMD								
VIF	1.00	1.01	1.00	1.01				
Experiment 2								
	$C_{11}(t)$	$C_{12}(t)$	$C_{13}(t)$	$C_{14}(t)$	$r_1(t)$	$C_{21}(t)$	$C_{22}(t)$	$C_{23}(t)$
EMD								
VIF	2414	25.27	6.71	1.36	325.54	3.59	1.34	7.54
	$C_{24}(t)$	$r_2(t)$	$C_{31}(t)$	$C_{32}(t)$	$C_{33}(t)$	$C_{34}(t)$	$C_{35}(t)$	$r_3(t)$
EMD								
VIF	42.33	7.61	2380	24.28	1.47	38.75	3.38	384.26

Table 2
Comparison of different methods for numerical experiments

Method	Parameter(s)	RSS	Bias ²	Var	Variable Selection
Experiment 1					
EMD-OLS	$\lambda = 0$	42.91298	5.89e-35	0.566789	All
EMD-RR	$\lambda = 0.05401, \alpha = 0$	42.43922	1.05e-36	0.512713	All
EMD-LASSO	$\lambda = 0.05405, \alpha = 1$	41.25816	2.59e-36	0.442239	C_1, C_2
EMD-ELN	$\lambda = 0.06434, \alpha = 0.84$	41.24562	4.81e-35	0.432979	C_1, C_2
Experiment 2					
EMD-OLS	$\lambda = 0$	124.2361	4.67 e-3	0.136539	All
EMD-RR	$\lambda = 0.083389, \alpha = 0$	118.4152	3.97 e-5	0.084286	All
EMD-LASSO	$\lambda = 0.039912, \alpha = 1$	115.2839	3.48 e-4	0.048209	C_{21}, C_{32}, C_{33}
EMD-ELN	$\lambda = 0.276647, \alpha = 0.12$	114.9694	8.83 e-4	0.033481	$C_{12}, C_{14}, C_{21}, C_{32}, C_{33}$

Figure 3 shows the graphs of the decomposition components selected using the EMD-ELN method and the response variable in the two experiments. In each graph, the solid black line represents the response variable and other lines are the selected components. The response variable in the first experiment was stationary while the second experiment had modifications (i.e. transformed to be stationary). We showed similarities and matching lines between the components selected and the response variables for the two experiments.

Table 3 illustrates that the results of the compared methods with noise structure errors $\varepsilon \sim iid N(0,1)$ added to the predictor variables in the first and second experiments with 2000 replications modeled. The value of the tuning parameter was chosen automatically using a 10-fold CV. The results show that EMD-ELN had the smallest error value in terms of RSS and achieved the optimal balance between variance and bias in two experiments.

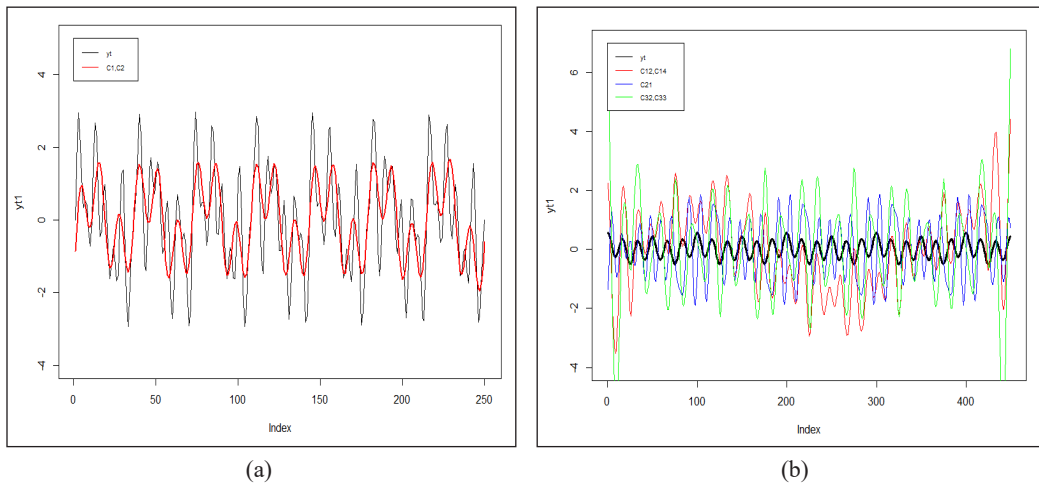


Figure 3. Variable selection and response variable: (a) experiment 1; and (b) experiment 2

Table 3
Comparison of different methods for simulation

Method	RSS	Bias ²	Var
Experiment 1			
EMD-OLS	52.03	4.99e-33	0.353
EMD-RR	51.77	9.06e-34	0.273
EMD-LASSO	51.51	8.36e-34	0.264
EMD-ELN	50.93	8.08e-34	0.263
Experiment 2			
EMD-OLS	131.22	0.010120	0.164156
EMD-RR	129.58	0.009838	0.060295
EMD-LASSO	128.40	0.009749	0.066662
EMD-ELN	126.71	0.009629	0.076161

Stock Market

In this study, the daily close stock market from March 26, 2010 to September 25, 2017 for three countries, namely, Japan (JAP), China (CH), and Singapore (SNG), were employed to evaluate the performance of the proposed EMD-ELN and traditional methods. All datasets were collected from the Yahoo finance database (<https://finance.yahoo.com/>). In this application, the response variable was the daily close stock market of SNG, while the predictor variables were the daily close stock markets of JAP and CH. Each dataset was divided into two parts: 70% for training (from March 26, 2010 until June 24, 2015) and the remaining 30% for testing.

Stock Market Results and Discussion

Figure 4 shows a graphical view of the original close daily stock market signals for CH, JAP, and SNG. Figure 4 shows that the signals did not show any constant value over time or straight lines, thereby indicating that the signals were non-stationary and nonlinear.

Figure 5 shows the plots of the decomposing components extracted by the EMD algorithm from the original predictor variables CH and JAP. The CH signal was decomposed into nine IMFs $\{C_{11}(t), C_{12}(t), C_{13}(t), C_{14}(t), C_{15}(t), C_{16}(t), C_{17}(t), C_{18}(t), C_{19}(t)\}$ and one residual $r_1(t)$ component, while the JAP signal was decomposed into seven IMFs $\{C_{21}(t), C_{22}(t), C_{23}(t), C_{24}(t), C_{25}(t), C_{26}(t), C_{27}(t)\}$ and one residual $r_2(t)$ component with different characteristics (i.e. frequency and wavelength).

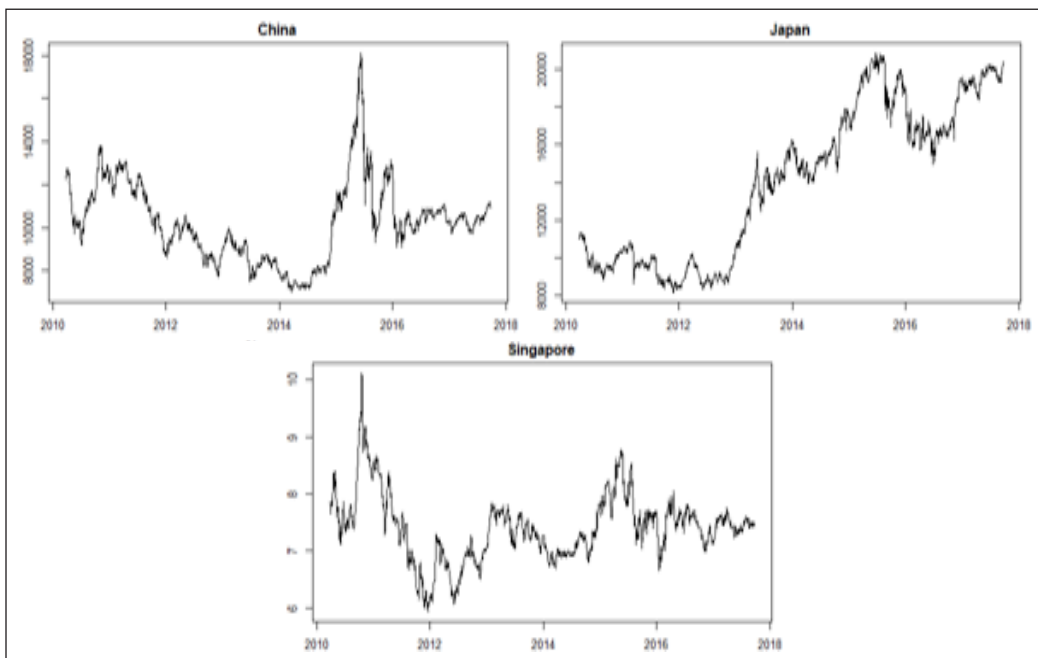


Figure 4. Plots of original signals

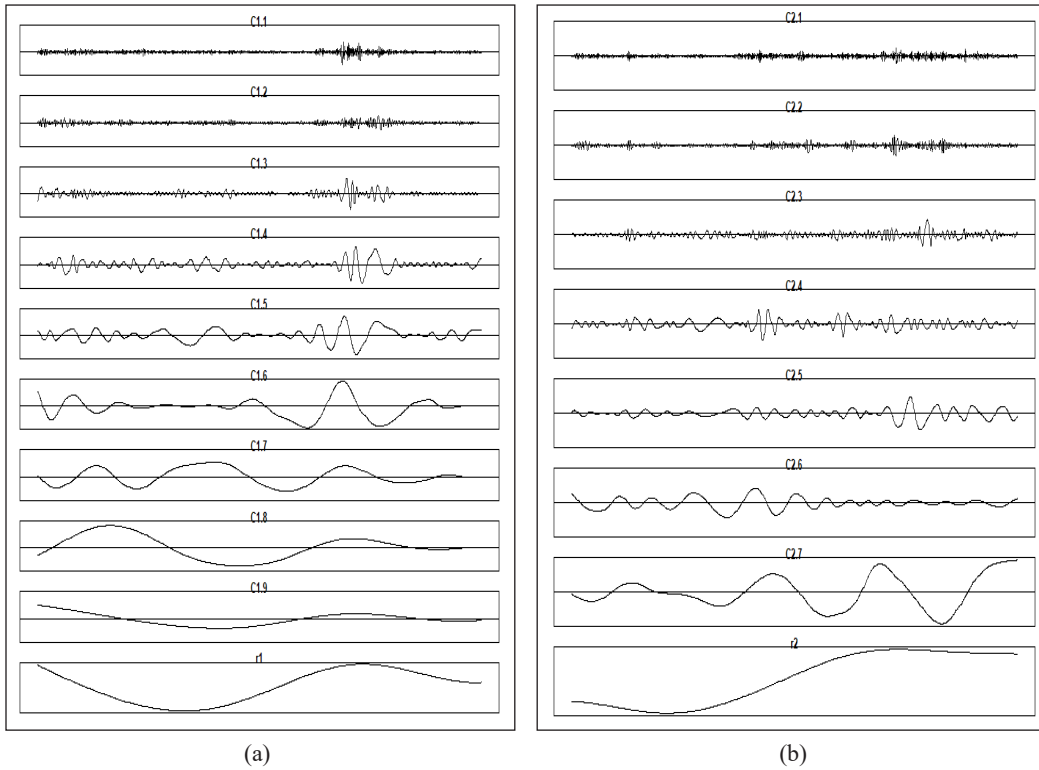


Figure 5. Decomposition of: (a) CH; and (b) JAP signals via EMD

Table 4 illustrates the values of the VIF test of multicollinearity among the decomposition components. The results of the VIF test shows that several decomposition components obtained values larger than 10 ($C_{19}(t)$, $r_1(t)$, and $r_2(t) > 10$), which indicates that high multicollinearity exists among the decomposition components.

Table 5 illustrates the results of the compared methods, which depend on the values of λ and were selected by 10-fold CV. The results show that the EMD-ELN outperformed its competitors. It had the smallest RSS ($RSS = 486.5276$ at that resulted in an optimal balance between variance and bias-square. For the variable selection, the EMD-ELN was the best method for selecting decomposition components that exhibit high multicollinearity. These chosen components included the eleven components in the

Table 4
VIF test

EMD	$C_{11}(t)$	$C_{12}(t)$	$C_{13}(t)$	$C_{14}(t)$	$C_{15}(t)$	$C_{16}(t)$	$C_{17}(t)$	$C_{18}(t)$	$C_{19}(t)$
VIF	1.04	1.02	1.05	1.23	1.12	1.52	1.52	4.19	172.0
EMD	$r_1(t)$	$C_{21}(t)$	$C_{22}(t)$	$C_{23}(t)$	$C_{24}(t)$	$C_{25}(t)$	$C_{26}(t)$	$C_{27}(t)$	$r_2(t)$
VIF	326.4	1.03	1.02	1.01	1.09	1.14	1.13	2.14	138.5

final model that had different signs on the response variable. The EMD-LASSO failed to select any decomposition components with high correlation, while the EMD-ELN could remove (like C_{19}) or chose the components that exhibited high correlation (like r_1 and r_2 components) in the final model.

Table 5
Comparison of different methods for stock market application

Method	Parameter(s)	RSS	Bias ²	Var	Variable Selection
EMD-OLS	$\lambda = 0$	759.3457	2.168e-29	0.5784	All
EMD-RR	$\lambda = 0.33320, \alpha = 0$	487.0063	2.005e-32	0.0424	All
EMD-LASSO	$\lambda = 0.04205, \alpha = 1$	489.6050	1.632e-34	0.0382	$\{C_{11}(t), C_{14}(t), C_{21}(t), C_{11}(t)\}$
EMD-ELN	$\lambda = 0.43233, \alpha = 0.02$	486.5276	5.545e-33	0.0320	$\{C_{11}(t), C_{12}(t), C_{24}(t), C_{18}(t), r_1(t), C_{21}(t), C_{22}(t), C_{23}(t), C_{26}(t), C_{27}(t), r_2(t)\}$

CONCLUSION

In this paper, we developed a hybrid EMD-ELN method using non-stationary and nonlinear predictor variables. The proposed method can be used to determine which of decomposition components through the EMD of the original non-stationary and nonlinear predictors have the most effect on the response variable.

The results of the numerical experiments and stock market applications prove that the EMD-ELN method is highly capable of identifying the decomposition components with the most effect on the response variable in the presence or absence of multicollinearity and building a model free from multicollinearity. The proposed EMD-ELN also achieves a balance between bias and variance.

ACKNOWLEDGEMENT

The authors thank the anonymous referees for their valuable recommendations that helped to improve the quality of the manuscript.

REFERENCE

- Al-Jawarneh, A. S., Ismail, M. T., Awajan, A. M., & Alsayed, A. R. (2020). Improving accuracy models using elastic net regression approach based on empirical mode decomposition. *Communications in Statistics-Simulation and Computation*, 2020, 1-20. doi: <https://doi.org/10.1080/03610918.2020.1728319>
- Chu, H., Wei, J., & Qiu, J. (2018). Monthly streamflow forecasting using EEMD-Lasso-DBN method based on multi-scale predictors selection. *Water*, 10(10), 1-15. doi: <https://doi.org/10.3390/w10101486>
- Chui, C. (1995). *Wavelet basics*. Boston, Massachusetts: Kulwer Academic Publishers.

- Friedman, J., Hastie, T., & Tibshirani, R. (2010). Regularization paths for generalized linear models via coordinate descent. *Journal of Statistical Software*, 33(1), 1-22.
- Hamid, H., Ngu, P., & Alipiah, F. (2018). New smoothed location models integrated with PCA and two types of MCA for handling large number of mixed continuous and binary variables. *Pertanika Journal of Science and Technology*, 26(1), 247-260.
- Hashibah, H., & Mahat, N. I. (2013). Using principal component analysis to extract mixed variables for smoothed location model. *Far East Journal of Mathematical Sciences*, 80(1), 33-54.
- Haws, D. C., Rish, I., Teysse, S., He, D., Lozano, A. C., Kambadur, P., ... & Parida, L. (2015). Variable-selection emerges on top in empirical comparison of whole-genome complex-trait prediction methods. *PLoS One*, 10(10), 1-22. doi: 10.1371/journal.pone.0138903
- Hoerl, A. E., & Kennard, R. W. (1970). Ridge regression: Biased estimation for nonorthogonal problems. *Technometrics*, 12(1), 55-67.
- Huang, N. E. (2014). Introduction to the Hilbert–Huang transform and its related mathematical problems. In *Hilbert–Huang transform and its applications* (pp. 1-26). Singapore: World Scientific. doi: https://doi.org/10.1142/9789814508247_0001
- Huang, N. E., Shen, Z., Long, S. R., Wu, M. C., Shih, H. H., Zheng, Q., ... & Liu, H. H. (1998). The empirical mode decomposition and the Hilbert spectrum for nonlinear and non-stationary time series analysis. *Proceedings of the Royal Society of London. Series A: Mathematical, Physical and Engineering Sciences*, 454(1971), 903-995. doi: <https://doi.org/10.1098/rspa.1998.0193>
- Jadhav, N. H., Kashid, D. N., & Kulkarni, S. R. (2014). Subset selection in multiple linear regression in the presence of outlier and multicollinearity. *Statistical Methodology*, 19, 44-59. doi: <https://doi.org/10.1016/j.stamet.2014.02.002>
- Javaid, A., Ismail, M., & Ali, M. K. M. (2020). Efficient model selection of collector efficiency in solar dryer using hybrid of LASSO and robust regression. *Pertanika Journal of Science and Technology*, 28(1), 193-210.
- Masselot, P., Chebana, F., Bélanger, D., St-Hilaire, A., Abdous, B., Gosselin, P., & Ouarda, T. B. (2018). EMD-regression for modelling multi-scale relationships, and application to weather-related cardiovascular mortality. *Science of The Total Environment*, 612, 1018-1029. doi: <https://doi.org/10.1016/j.scitotenv.2017.08.276>
- Montgomery, D. C., Peck, E. A., & Vining, G. G. (2012). *Introduction to linear regression analysis* (Vol. 821). Hoboken, New Jersey: John Wiley & Sons.
- Naik, J., Satapathy, P., & Dash, P. (2018). Short-term wind speed and wind power prediction using hybrid empirical mode decomposition and kernel ridge regression. *Applied Soft Computing*, 70(1), 1167-1188. doi: <https://doi.org/10.1016/j.asoc.2017.12.010>
- Qin, L., Ma, S., Lin, J. C., & Shia, B. C. (2016). Lasso regression based on empirical mode decomposition. *Communications in Statistics-Simulation and Computation*, 45(4), 1281-1294. doi: <https://doi.org/10.1080/03610918.2013.826361>

- Shen, Z., Feng, N., & Shen, Y. (2012). Ridge regression model-based ensemble empirical mode decomposition for ultrasound clutter rejection. *Advances in Adaptive Data Analysis*, 4(1-2), 1-7. doi: <https://doi.org/10.1142/S1793536912500136>
- Shen, Z., & Lee, C. H. (2012, March 25-30). A lasso based ensemble empirical mode decomposition approach to designing adaptive clutter suppression filters. In *2012 IEEE International Conference on Acoustics, Speech and Signal Processing (ICASSP)* (pp. 757-760). Kyoto, Japan.
- Tibshirani, R. (1996). Regression shrinkage and selection via the lasso. *Journal of the Royal Statistical Society: Series B (Methodological)*, 58(1), 267-288. doi: <https://doi.org/10.1111/j.2517-6161.1996.tb02080.x>
- Titchmarsh, E. C. (1948). *Introduction to the theory of fourier integrals* (Vol. 950). Oxford, UK: Clarendon Press.
- Yan, X., & Su, X. (2009). *Linear regression analysis: Theory and computing*. Singapore: World Scientific.
- Yang, A. C., Fuh, J. L., Huang, N. E., Shia, B. C., Peng, C. K., & Wang, S. J. (2011). Temporal associations between weather and headache: Analysis by empirical mode decomposition. *PloS One*, 6(1), 1-6. doi: <https://doi.org/10.1371/journal.pone.0014612>
- Zhou, D. X. (2013). On grouping effect of elastic net. *Statistics and Probability Letters*, 83(9), 2108-2112. doi: <https://doi.org/10.1016/j.spl.2013.05.014>
- Zou, H., & Hastie, T. (2005). Regularization and variable selection via the elastic net. *Journal of the Royal Statistical Society: Series B (Statistical Methodology)*, 67(2), 301-320. doi: <https://doi.org/10.1111/j.1467-9868.2005.00503.x>



A New Parametric Function-Based Dynamic Lane Changing Trajectory Planning and Simulation Model

Md. Mijanoor Rahman^{1,2}, Mohd. Tahir Ismail¹, Norhashidah Awang¹ and Majid Khan Majahar Ali^{1*}

¹School of Mathematical Sciences, Universiti Sains Malaysia, 11800 USM, Pulau Penang, Malaysia

²Department of Mathematics, Mawlana Bhashani Science and Technology University, Tangail-1902, Bangladesh

ABSTRACT

Lane-changing (LC) problem may cause serious accidents or create a painful traffic jam at multi-lane roads. Existing LC simulation model was created with some limitations (less fitted, without velocity and acceleration profiles, high curvature) by using well known trajectory curve such as Hyperbolic Tangent Curve (HTC), Sine-Based Curve (SC), Polynomial Curve (PC). In this study, a new parametric curve had been proposed by using curvilinear coordinate system and fitted against Next Generation Simulation (NGSIM) real dataset. Further, new profiles of velocity and acceleration were designed using the proposed LC trajectory curve. The curvature of proposed model was zero-based curvature both at LC starting and ending points. This proposed curvature was compared with two models such as HTC and SC. The average root-mean-square-error of proposed model decreased with 1.84% for left LC and 15.48% for right LC compared to HTC model and 1.74% for left LC and 15.60% for right LC compared to SC model. Similarly, the proposed model for velocity and acceleration profiles improved significantly from PC model. The proposed parametric curve solves the gap and collision points of LC vehicle with a front vehicle and rear vehicle at target lane and can be used in real LC path planning.

Keywords: Acceleration profiles, parametric curve, speed, trajectory planning

ARTICLE INFO

Article history:

Received: 20 June 2020

Accepted: 20 October 2020

Published: 22 January 2021

DOI: <https://doi.org/10.47836/pjst.29.1.12>

E-mail addresses:

mijanoor.math@student.usm.my (Md. Mijanoor Rahman)

m.tahir@usm.my (Mohd. Tahir Ismail)

shidah@usm.my (Norhashidah Awang)

majidkhanmajaharali@usm.my (Majid Khan Majahar Ali)

* Corresponding author

INTRODUCTION

Lane Changing Trajectory (LCT) planning is an important model for identifying and ensuring the safeness in any traffic systems where this model helps to predict the gap acceptance, and to plan LC dynamical

trajectory about the longitudinal and lateral movements (Yang et al., 2018). The trajectory planning has been developed from more than two decades. Few simulation models were developed for LCT system such as Quintic Bezier Curves (QBC), Spline-Based Curve (SBC), non-smooth Dijkstra algorithm and Multi Order Polynomial Curve (MOPC) for urban and freeway roads. Testing the simulation model by real trajectory data is required for this development, because the model based on simulation data poorly fits in the real traffic data (Zhou et al., 2017).

The QBC is used in LCT planning for shortest-distance and smoothness path, time-optimal and comfortable journey. Shen et al. (2017) addressed the trajectory planning based on the fifth order QBC for a comfortable journey. They implemented this curve with a few mini-mature vehicles in LC scenarios to test comfort measurement. However, their results were unrealistic as there was no error testing between the proposed path planning and real trajectory planning for longitudinal and lateral path positions. Meanwhile, González et al. (2016) and Kawabata et al. (2013) found that although QBC was very smooth, it was only applied on unicycle trajectory and agreed that high-degree QBC lost flexibility at the trajectory.

The parameters of MOPC are described by acceleration, speed and position constraints. Sometimes, inexperienced driving causes uncomfortable journey at the time of LC. Wang and Zheng (2013) provided a simulation model for LCT planning using MOPC without testing the with real vehicle trajectory. A few researches only assumed that the acceleration and velocity at the starting and ending points were zeros to generate the PC-based lateral trajectory model (Resende & Nashashibi, 2010; Wang & Zheng, 2013; You et al., 2015; Ntousakis et al., 2016; Chebly et al., 2017).

Heil et al. (2016) developed the PC-based LCT planning and found the computational cost by using maximum acceleration and overshooting behaviour. Connors and Elkaim (2007) had successfully overcome collision points during LC. They used the trajectory planning based on SBC to overcome any obstacle point. SBC is very important for smoothness at the corner between two straight lines with limitation that the continuous velocity was not possible at this corner point (Sanchez-Reyes & Chacón, 2018). Therefore, the most of LCT model developed using the MOPC model, but most of the research still only assumed its velocity and acceleration profiles at the starting and ending points were zeros, in which these assumptions were unrealistic. Wang et al. (2018) explored another lateral trajectory path based on SC and a longitudinal trajectory line. Their trajectory model still assumed zeros for lateral velocity and acceleration.

Zhou et al. (2017), modified a reference angle-based trajectory planning model using HTC. The curvature and fitted values were compared with PC and SBC, in which modified HTC performed better than other two models. They suggested that the reference angle could only be determined by vehicle traveling data recorders. So, data extracted from still

video camera cannot be employed in reference angle adopted trajectory model whereas this type of data is very popular (Wan et al. 2020). Yang et al. (2018) modified the MPOC model in order to determine LCT curve and found that the starting and ending points were non-zeros as assumed previously by other researchers. However, they assumed the vehicle at ending point was parallel to the target lane. If a vehicle is parallel to the target lane, then the lateral velocity should be zero as non-lateral movements. Therefore, that assumption is also unrealistic.

Katrakazas et al., (2015) discovered that there were two important types of findings for LCT problems

1. The best geometric trajectory was necessary for LC vehicle. It indicates that the curvature at every point on the curve was to be as small as possible, besides the curvatures at starting and ending points were nearly zero for comfortable journey.
2. The realistic vehicle dynamical system was very important for path planning. The vehicle LC time versus position, vehicle LC time versus velocity and vehicle LC time versus acceleration should be validated by real trajectory.

In this study, a new parametric trajectory curve, velocity and acceleration profiles were proposed by using curvilinear motion planning. The proposed trajectory curve was fitted with NGSIM data. Further, the curvature of the trajectory curve was calculated and compared with HTC and SC models. Furthermore, the velocity and acceleration profiles were compared with PC model.

METHODS

The Curvilinear Motion Planning (Rectangular Coordinates)

Let X, Y be the coordinate frame where the horizontal direction is represented by the x -axis and the vertical direction is represented by the y -axis. The rectangular coordinate system represents the vehicle's longitudinal and lateral positions, respectively, $X(t)$ and $Y(t)$. So, the position of the vehicle, at any given time t , is $P(t) = [X(t), Y(t)]$, where is the position of the cartesian system and t is the time during LC.

Trajectory Curve

The parametric function for LCT planning is identified due to the nature of the function, which is continuous, low curvature; and because they ensure easy computation and time-saving trajectories. The parameters of this functions represent the positioned coordinates of the LCT with respect to time. But for the aggressive driver, parameters' values must be changed quickly to reach the target point. Further, we propose a lateral velocity and acceleration profiles for vehicle motion. Equation 1 and 2 represent for longitudinal movement and lateral movement respectively to identify velocity and acceleration:

Longitudinal position (Y. Y. Wang, Pan, Liu & Feng, 2018),

$$X(t) = u_0 t + L_0, \text{ for } T_{origin} \leq t \leq T_{target} \quad (1)$$

Lateral position of proposed curve,

$$Y(t) = \frac{L_{YD}}{2} (\tanh t_1 - t) + L_{YID}, \text{ for } T_{origin} \leq t \leq T_{target} \quad (2)$$

where, u_0 is initial velocity, L_0 is initial longitudinal position during LC, T_{origin} and T_{target} are starting time and ending time of LC respectively. In Equation 2, the parameter L_{YD} represents to the total lateral displacement during LC wherein it is positive for Left LC (LLC) and negative for Right LC (RLC). The range of total lateral displacement, L_{YD} is [2.8,4] for LLC and [-4,-2.8] for RLC scenarios. L_{YID} is ordinate of middle position of LC starting and ending points and t_1 is the such time that vehicle arrives at middle position of starting and ending positions. Where, σ is a weighted parameter represents to be estimated. Figure 1 depicts the parameters movement on RLC and LLC scenario using Equations 1 and 2. These parametric functions are fitted the LLC and RLC in order to find LCT in lane width, middle position of LC starting and ending points are initially used, when a driver needs to change the lane. Figures 2 and 3 are time versus RLC and LLC positions respectively using Equation 2 where the vehicle lateral position is decreasing for RLC, and increasing for LLC.

Velocity Profile

The longitudinal and the lateral positions are represented by Equation 1 and 2 with respect to time respectively. The lateral displacement per unit time was found by taking the derivative with respect to time, then the lateral velocity of the vehicle comes out. Similarly, longitudinal velocity was calculated by differentiation with respect to time.

The vehicle velocity vector is parallel to the tangent line on the position vector of the parametric path, where the lateral velocity is zero and the longitudinal velocity is linear motion before LC. When LC starts, the value of lateral velocity increases, but the longitudinal speed remains in the previous speed. However, for the motion control and path planning of the vehicle, this velocity profile is suitable to overcome the smoothness and curvature limitation.

If a LC starts from zero second and finishes at eighth second, then time interval is [0,8] seconds, but some aggressive vehicles are very fast, and their LC time interval is [0,6] seconds (Zhou et al., 2017). The LC processing starts from time, $t = 0$, and the velocity function is increasing until vehicles arrive at the middle position of two lanes. After that, velocity decreases for merging with the target lane. Since, the lateral velocity is not very

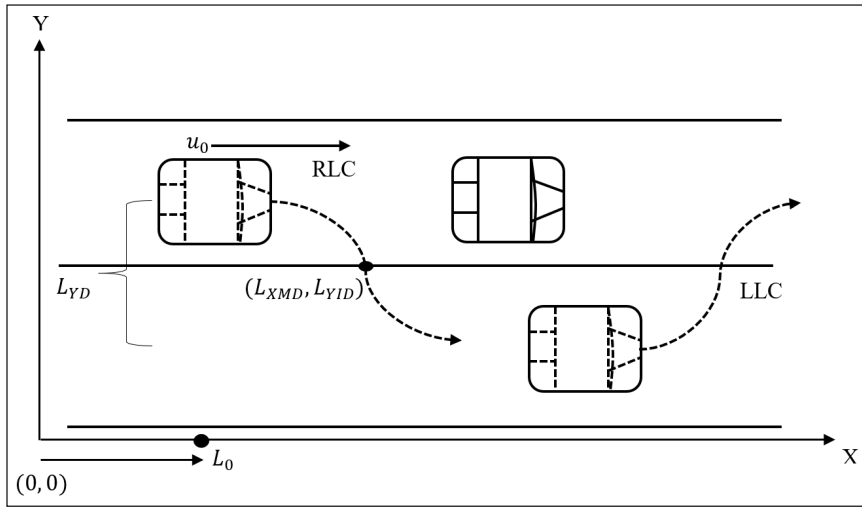


Figure 1. RLC and LLC traffic scenarios

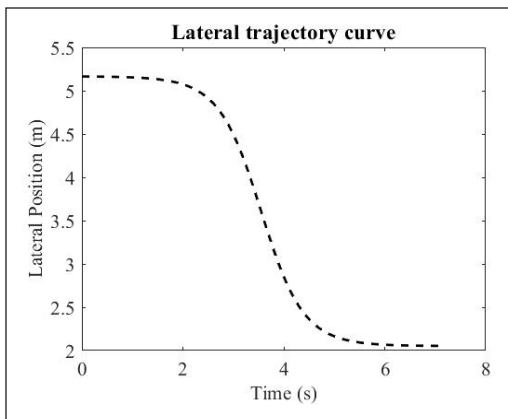


Figure 2. Parametric RLC path planning for lateral position

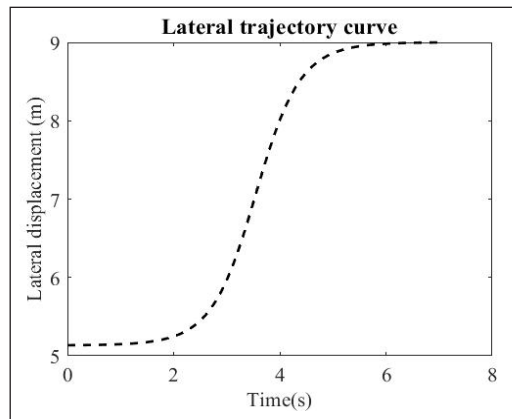


Figure 3. Parametric LLC path planning for lateral position

fast, the total LC velocity mostly depends on the longitudinal velocity for arriving at target lane in time. The longitudinal and lateral velocities shown in Equation 3 and 4 respectively where the Equation 1 and 2 are differentiated with respect to t .

Longitudinal velocity,

$$v_X(t) = u_0, \text{ for } T_{origin} \leq t \leq T_{target} \quad (3)$$

Lateral velocity,

$$v_Y(t) = -\sigma \frac{L_{YD}}{2} \operatorname{sech}^2 \sigma (t_1 - t) \text{ for } T_{origin} \leq t \leq T_{target} \quad (4)$$

Figure 4 represents the longitudinal and lateral velocities by using Equations 3 and 4 where longitudinal velocity is parallel to the horizontal line, and lateral velocity is a smooth curve during LC.

Acceleration Profile

A comfortable journey should adopt low lateral acceleration according to Katrakazas et al. (2015) work. Since, this study uses the smooth lateral velocity and constant longitudinal velocity based on Equation 3 and 4, respectively. The longitudinal and lateral accelerations presented in Equations 5 and 6 respectively by using the differentiation of Equations 3 and 4 during LC.

Longitudinal acceleration,

$$a_x(t) = 0 \text{ for } T_{origin} \leq t \leq T_{target} \tag{5}$$

Lateral acceleration,

$$a_y(t) = \sigma^2 L_{YD} \text{sech}^2 \sigma(t_1 - t) \tanh \sigma(t_1 - t) \text{ for } T_{origin} \leq t \leq T_{target} \tag{6}$$

Figure 5 represents the longitudinal and lateral acceleration where longitudinal acceleration is zero according to Equation 5, and lateral acceleration is a smooth curve using Equation 6.

DATA PROCESSING

Dong et al. (2017) had estimated the starting and ending points of LC with less standard deviation and limited mean error from US 101, NGSIM dataset. This data set included the longitudinal and lateral position of LC vehicle with other surrounding vehicles, such as a

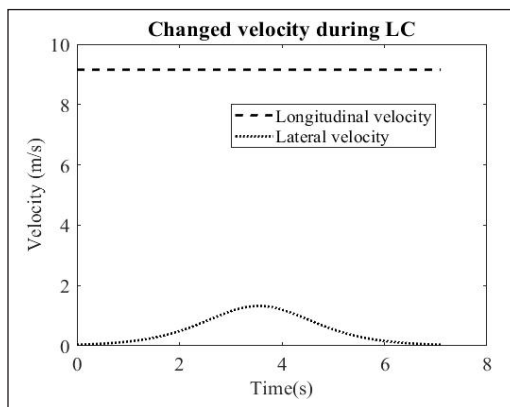


Figure 4. Longitudinal and lateral velocities of the parametric curve LC times

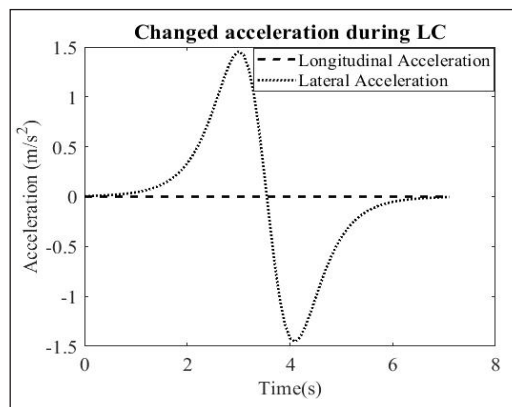


Figure 5. Longitudinal and lateral accelerations of parametric curve during LC

front vehicle, lag vehicle on the current lane and front vehicle, rear vehicle on the target lane. This dataset included groups of LC vehicle with surrounding. Every group had five vehicles, such as a front vehicle, lag vehicle on the current lane and front vehicle, rear vehicle on the target lane. The study used 200 LC vehicles to fit the proposed LCT model during LC.

Every vehicle in a group had 20 s longitudinal and lateral velocity and longitudinal and lateral acceleration profiles time series microscopic data where the data resolution was 0.1 second (Li et al., 2016). This dataset also included the LC starting and ending position of LC vehicle, and the movement position of other surrounding vehicles. The LC duration depended on the starting and ending points of the trajectory data. Before starting point, the longitudinal and lateral positions were before LC data, and after the ending point, the positioning data were after LC data. During LC, for getting the average longitudinal velocity and lateral velocity of every vehicle, the total longitudinal and lateral displacement was divided by the total time. Similarly, longitudinal acceleration and lateral acceleration were found from longitudinal velocity and lateral velocity respectively.

RESULTS AND DISCUSSION

As mentioned previously, one of the limitations of reference angle, the value only can be collected from vehicle traveling data recorders, but not from still video camera as in NGSIM. So, Zhou et al. (2017) adopted parameters (average velocity, longitudinal distance and reference angle) were modified using coordinate geometrical system, as shown in Appendix A. In addition, another SC model is proposed by Wang et al. (2018) also shown in Appendix B. Both of HTC and SC were used to compare the efficiency of the proposed parametric curve.

Equations 1 and 2 present a longitudinal and lateral positions of the LC. By using parameters' values- L_{YD} and L_{YID} , t_1 , u_0 and L_0 , the proposed curve was fitted to 200 LC vehicles' trajectories. The only parameter's value, σ was tested by using initial value 0 to 1 because it was a weighted parameter. So, this study found the more fitted value of σ is 0.56. In addition, the fitted curves and real trajectory curves were compared.

Curvature Estimation

Equation 7 (Léger, 1999) was applied for determining the curvature value of proposed parametric curve, and compared to HTC and SC curves.

$$\text{Curvature, } k = \frac{y''}{(1 + y'^2)^{3/2}} \quad (7)$$

where, y' and y'' are first and second differentiations respectively of lateral displacement, y' with respect to longitudinal displacement, x by using Equations 1 and 2. The maximum

values of the curvature were not more than 0.006 for LLC and 0.009 for RLC shown in Figure 6 and Figure 7. These curvature values were nearly zeros at the starting and ending points of the curve. Therefore, the proposed curve provided the comfortable journey according to the small curvatures at the starting and ending points during LC as a challenge of Ktrakazas et al. (2015) study.

The curvature of the proposed curve is shown in Figures 6 and Figure 7 by using Equation 7, and these curvatures are lower than the HTC and SC proposed curvatures. However, by using the LCT in the parametric curve, the driver not only determines the vehicle path, but also follows the longitudinal and lateral velocity and acceleration profiles with respect to their desired dynamics and gaps at the target lane. Many other information can also be collected by using the prediction curve besides the proposed model can generate different trajectories which follow the aggressive and non-aggressive drivers by changing the values of the initial parameters of the prediction curve.

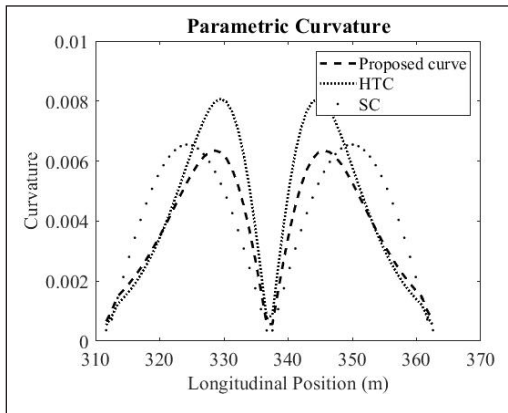


Figure 6. The curvature for LLC

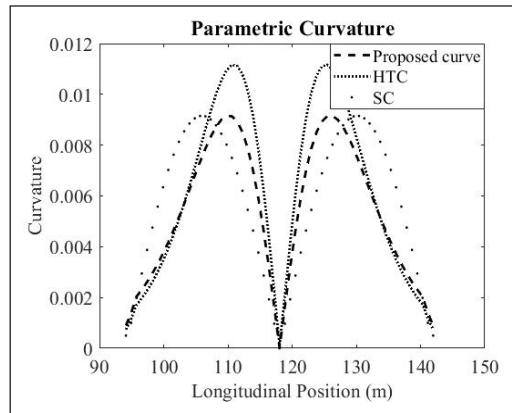


Figure 7. The curvature for RLC

Trajectory Curve Validation

For validation test, the total of 200 LC real trajectory data (100 LLC and 100 RLC data) were randomly taken from 200 groups of vehicles LC scenarios for NGSIM data. The parameters' values of prediction trajectory curve were used to adjust with the real trajectory vehicle position. Table 1 shows that the average Root Mean Square Error (RMSE) values where the intervals of total lateral distance of RLC and LLC were [3.3, 4.4] meters and [2.7, 5.4] meters respectively. The middle longitudinal point and the middle lateral point were situated in the middle coordinate of the trajectory curve. The middle coordinate changed for every trajectory curve, because the LC position of every trajectory was different. But the ranges of total longitudinal LC distance were [25, 85] meters for RLC and [30, 93] meters for LLC real data. The total LC time depended on aggressive driving or regular driving. Here, the ranges of total LC time are [5.5, 8.9] seconds for RLC and [4.8, 8.8]

seconds for LLC appeared in the dataset. These dynamical parameters of the curve were collected from real dataset to fit this curve with real trajectory planning.

The total 100 LLC and 100 RLC vehicles data were tested by using proposed trajectory model, HTC model and SC model. The HTC and SC models used the Equation 8 and 9 respectively where Equation 8 was adopted in Appendix A, and Equation 9 was adopted in Appendix B. The average RMSE values of used models are presented in Table 1 for comparison of the proposed model. The average RMSE of proposed parametric curve for LLC and RLC were 0.2795 and 0.2179 respectively, where proposed model improved 1.84% from HTC, and 1.74% from SC for LLC, and 15.48% from HTC, and 15.60% from SC.

Figure 8 shows the lateral displacements of RLC vehicles along our proposed curve, HTC, SC and real trajectories of NGSIM data sets. The real trajectory of a vehicle (randomly selected from 100 groups of vehicles) for RLC are represented. Figure 9 shows the longitudinal movements according to Equation 1 and the same vehicle longitudinal movements. This study used the Wang et al. (2018) proposed longitudinal movements line due to use the determination of the curvature, velocity and acceleration. Figure 8 clearly shows that the lateral displacements of parametric curve are similar to that of the real trajectory curve, and better than the HTC and SC due to movement of the proposed curve and real trajectory.

Table 1
The parametric curve fitting RMSE value using 200 vehicles data

	Proposed (LLC)	HTC (LLC)	SC (LLC)	Proposed (RLC)	HTC (RLC)	SC (RLC)
Average RMSE (m)	0.2795	0.2848	0.2845	0.1719	0.2033	0.2036
Improved proposed model		From 1.84%	From 1.74%		From 15.48%	From 15.60%

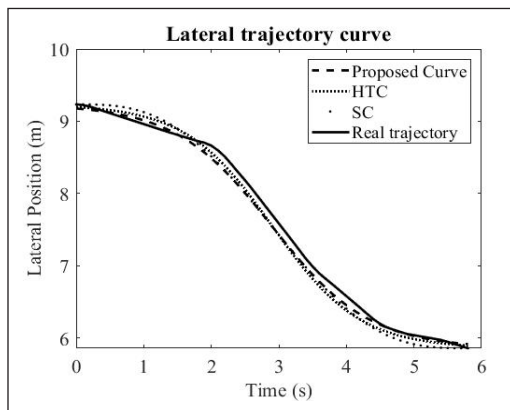


Figure 8. Lateral movement of RLC

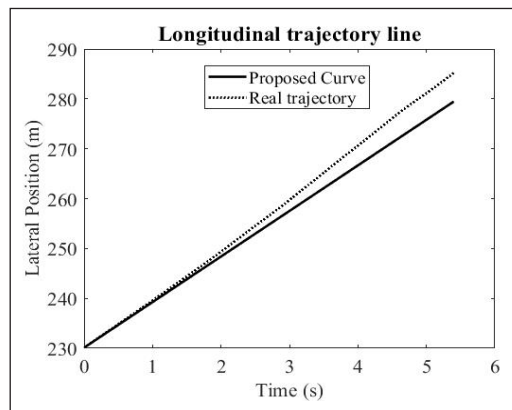


Figure 9. Longitudinal movement of RLC

Similarly, Figure 10 represents the lateral displacements of our proposed curve, HTC, SC and real trajectory of a vehicle (randomly selected from 100 groups of vehicles) for LLC. Figure 11 shows the Wang et al. (2018) proposed longitudinal movements and real vehicle longitudinal movements. Figure 10 also clearly shows that the lateral displacements of parametric curve are similar to that of the real trajectory curve, and better than the HTC and SC due to similar reason as mentioned above for Figure 8. This research does not consider any modification model for longitudinal movements.

Velocity and Acceleration Profiles Validation

Recently, Ali et al. (2019), Gu et al. (2019), and Li et al. (2016) applied the data smoothing process for using NGSIM data on other traffic researches. The velocity and acceleration data cannot be applied directly in any model because they have many noises. In addition, these two trajectories were derived from positional information (Thiemann et al., 2008). In this reason, the above-mentioned studies employed the data smoothing technique. Therefore, for validation testing of velocity and acceleration profiles, this study applied the spline-based interpolation by using MATLAB Curve Fitting Package. This similar procedure was applied for trajectory model testing by Wang et al. (2018).

The Equation 4 represents the simulated lateral velocity, and real lateral movements generated the real lateral velocity wherein every LC vehicle has velocity and acceleration trajectories. To test the validation, this study compared the simulated and real lateral velocities and accelerations by using RMSE value. The validation tests considered 100 LLC vehicles and 100 RLC vehicles. These trajectories were formed in a same time frame. Therefore, every LC vehicle adopted the RMSE value whereas Table 2 shows the average RMSE values in which proposed velocity and acceleration models were better than PC-based velocity and acceleration models.

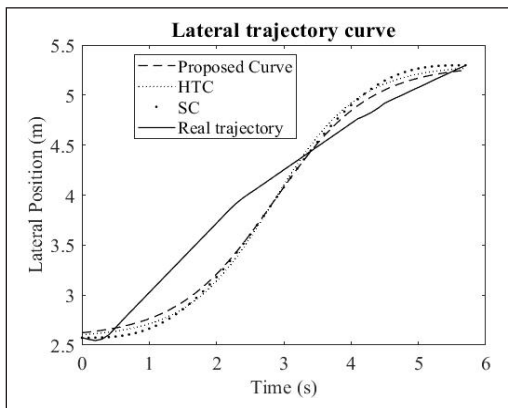


Figure 10. Lateral movement of LLC

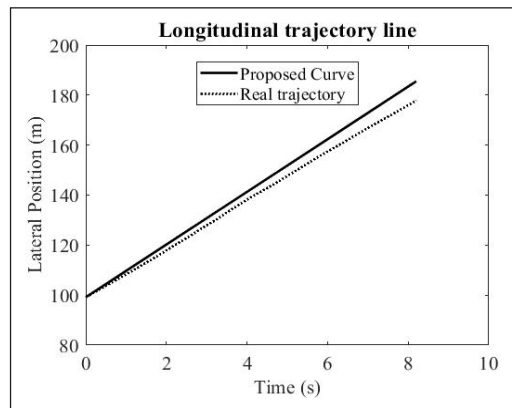


Figure 11. Longitudinal movement of LLC

The test results for our proposed model revealed that respectively, the average RMSE of velocity and acceleration were 0.218 and 0.314 for LLC, and 0.148 and 0.238 for RLC. Respectively, the average RMSE for PC model of velocity and acceleration were 0.236 and 0.362 for LLC, and 0.188 and 0.302 for RLC. Therefore, the proposed model improved from PC model 7.75% (velocity profile) and 13.28% (acceleration profile) for LLC, and 21.43% (velocity profile) and 21.13% (acceleration profile) for RLC.

Table 2
Comparative validation test results for velocity and acceleration profiles

Model	RMSE(LLC) 100 vehicles		RMSE (RLC) 100 vehicles	
	Velocity	Acceleration	Velocity	Acceleration
Proposed	0.218	0.314	0.148	0.238
PC	0.236	0.362	0.188	0.302
Improved proposed model (%)	7.75%	13.28%	21.43%	21.13%

The second challenge of Katrakazas et al. (2015) adopted in introduction of this study was to test the validation against real data set. Table 2 shows the validation test results using real data and comparisons with PC-based velocity and acceleration models. This section also shows the graphical comparison among real data, proposed simulation model, and PC model for velocity and acceleration profiles. Therefore, Figure 12 (LLC) and Figure 13 (RLC) show the velocity profiles of proposed lateral movements using Equations 4, 11 (Appendix C) and real vehicle data.

Our proposed velocity was smoothly increasing before the middle of the lane and smoothly decreasing after the middle of the lane as shown in Figure 12 (LLC) and Figure 13 (RLC). The dashed line represents proposed model velocity, dotted line represents PC model velocity while solid line represents real velocity (Figures 12 and 13). So, the proposed velocity profile fits more than PC model with real data. In addition, the longitudinal velocity is almost constant velocity because of linear movements, a similar result showed by Chebly et al. (2017). Figures 12 and 13 show that the velocities at starting and ending points were not always zeros for real vehicle, whereas PC model considered zeros at these points. This similar statement was proven by Yang et al. (2018).

Further, Figure 14 (LLC) and Figure 15 (RLC), show the lateral accelerations of proposed lateral movements of Equations 6, 12 (Appendix C) and real vehicle. Although, the longitudinal acceleration of prediction movements was zero shown in Equation 5 due to the constant longitudinal velocity as like Chebly et al. (2017). So, the acceleration of simulated vehicle depended on only lateral acceleration where the lateral acceleration of our proposed model was smooth and flexible. The accelerations at starting and ending points were non-zeros, although PC model considered zeros at these points shown in Figures 14 and 15. Therefore, the proposed model of velocity and acceleration profiles referred better than PC model as fitted with real trajectory.

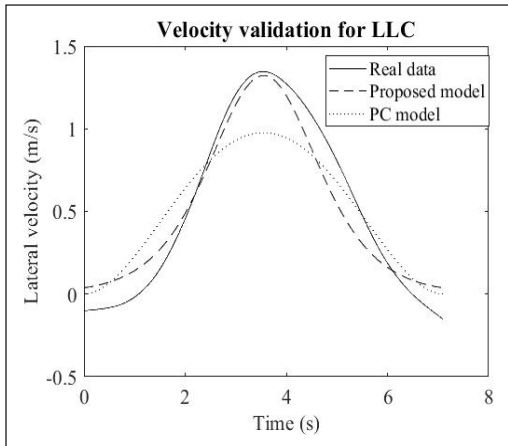


Figure 12 Velocity profiles

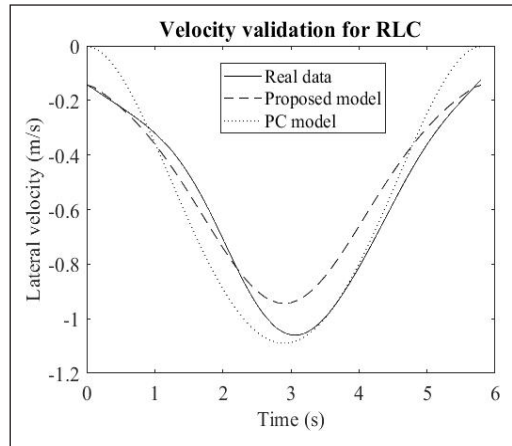


Figure 13 Velocity profiles

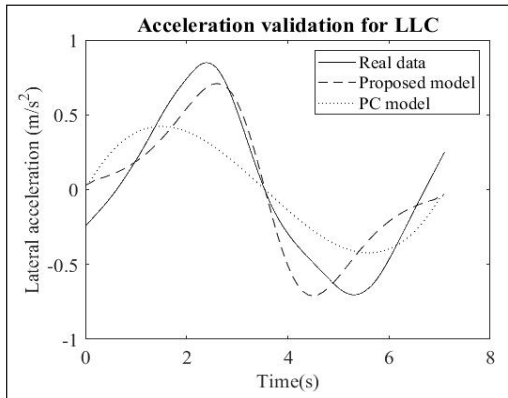


Figure 14. Acceleration profiles

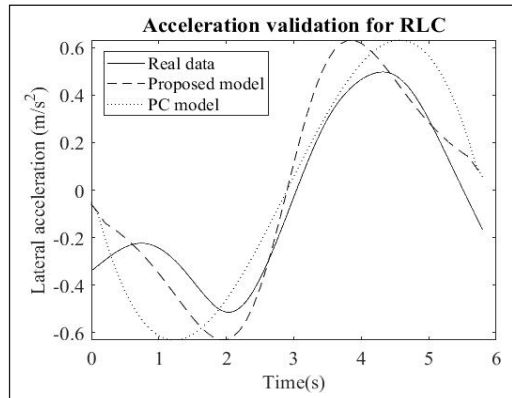


Figure 15. Acceleration profiles

CONCLUSION

The dynamical systems such as position movement, lateral velocity, lateral acceleration and curvature can be simplified by adopting the LCT planning model. Katrakazas et al. (2015) explored the challenges such as more fitted geometric curve, the continuous and zero-based curvatures at the initial position and ending position, and more realistic velocity and acceleration profiles. The curvatures of the proposed curve for LLC and RLC are lower than the HTC and SC curvatures. In addition, the curvature at LC starting and ending positions are very small and near zeros. Although, some previous LCT models were developed and tested by simulated vehicles, but our model is tested with 200 real vehicles, and shown the significant improvement. The validation test results show that the average RMSE of proposed trajectory model decreases with 1.84% for LLC and 15.48% for RLC compared to HTC model and 1.74% for LLC and 15.60% for RLC compared to SC model. Furthermore, the proposed model improved from PC model 7.75% (velocity

profile) and 13.28% (acceleration profile) for LLC, and 21.43% (velocity profile) and 21.13% (acceleration profile) for RLC. Therefore, the proposed model adopted longitudinal and lateral position trajectory and velocity and acceleration profiles overcome challenges of Katrakazas et al. (2015) work. The lateral trajectory model includes a weighted parameter as aggressive driving behavior tested manually in some fixed values. Therefore, future research should purpose findings optimum parameters by using more real trajectory data.

ACKNOWLEDGEMENT

All the authors acknowledge Universiti Science Malaysia (School of Mathematical Sciences) and Mawlana Bhashani Science and Technology University for funding this research.

REFERENCES

- Ali, Y., Zheng, Z., Haque, M., & Wang, M. (2019). A game theory-based approach for modelling mandatory lane- changing behaviour in a connected environment. *Transportation Research Part C, 106*(February), 220-242. doi: <https://doi.org/10.1016/j.trc.2019.07.011>
- Chebly, A., Talj, R., & Charara, A. (2017, October 16-19). Maneuver planning for autonomous vehicles , with clothoid tentacles for local trajectory planning. In *20th IEEE International Conference on Intelligent Trans- Portation (ITSC 2017)* (pp. 1-6). Yokohama, Japan. doi: 10.1109/ITSC.2017.8317856
- Connors, J., & Elkaim, G. (2007, April 22-25). Analysis of a spline based, obstacle avoiding path planning algorithm. In *IEEE Vehicular Technology Conference* (pp. 2565-2569). Dublin, Ireland. doi: <https://doi.org/10.1109/VETECS.2007.528>
- Dong, C., Zhang, Y., & Dolan, J. M. (2017, September 24-28). Lane-change social behavior generator for autonomous driving car by non-parametric regression in reproducing kernel hilbert space. In *IEEE International Conference on Intelligent Robots and Systems, 2017-Septe* (pp. 4489-4494). Vancouver, BC, Canada. doi: <https://doi.org/10.1109/IROS.2017.8206316>
- González, D., Pérez, J., Milanés, V., & Nashashibi, F. (2016). A review of motion planning techniques for automated vehicles. *IEEE Transactions on Intelligent Transportation Systems, 17*(4), 1135-1145. doi: <https://doi.org/10.1109/TITS.2015.2498841>
- Gu, X., Yu, J., Han, Y., Han, M., & Wei, L. (2019, July 12-14). Vehicle lane change decision model based on random forest. In *2019 IEEE International Conference on Power, Intelligent Computing and Systems, ICPICS 2019* (pp. 115-120). Shenyang, China. doi: <https://doi.org/10.1109/ICPICS47731.2019.8942520>
- Heil, T., Lange, A., & Cramer, S. (2016, November 1-4). Adaptive and efficient lane change path planning for automated vehicles. In *2016 IEEE 19th International Conference on Intelligent Transportation Systems (ITSC)* (pp. 479-484). Rio de Janeiro, Brazil. doi: <https://doi.org/10.1109/ITSC.2016.7795598>
- Katrakazas, C., Quddus, M., Chen, W. H., & Deka, L. (2015). Real-time motion planning methods for autonomous on-road driving: State-of-the-art and future research directions. *Transportation Research Part C: Emerging Technologies, 60*, 416-442. doi: <https://doi.org/10.1016/j.trc.2015.09.011>

- Kawabata, K., Ma, L., Xue, J., & Zheng, N. (2013, July 9-12). A path generation method for automated vehicles based on Bezier curve. In *2013 IEEE/ASME International Conference on Advanced Intelligent Mechatronics: Mechatronics for Human Wellbeing, AIM 2013* (pp. 991-996). Wollongong, NSW, Australia. doi: <https://doi.org/10.1109/AIM.2013.6584223>
- Léger, J. C. (1999). Menger curvature and rectifiability. *Annals of Mathematics*, *149*(3), 831-869. doi: <https://doi.org/10.2307/121074>
- Li, L., Chen, X. M., & Zhang, L. (2016). A global optimization algorithm for trajectory data based car-following model calibration. *Transportation Research Part C: Emerging Technologies*, *68*, 311-332. doi: <https://doi.org/10.1016/j.trc.2016.04.011>
- Ntousakis, I. A., Nikolos, I. K., & Papageorgiou, M. (2016). Optimal vehicle trajectory planning in the context of cooperative merging on highways. *Transportation Research Part C*, *71*, 464-488. doi: <https://doi.org/10.1016/j.trc.2016.08.007>
- Resende, P., & Nashashibi, F. (2010, September 19-22). Real-time dynamic trajectory planning for highly automated driving in highways. In *IEEE Conference on Intelligent Transportation Systems, Proceedings, ITSC* (pp. 653-658). Funchal, Portugal. doi: <https://doi.org/10.1109/ITSC.2010.5625194>
- Sanchez-Reyes, J., & Chacón, J. M. (2018). Representation of polynomial nonparametric B e transition curves. *Journal of Surveying Engineering*, *144*(2), 1-8. doi: [https://doi.org/10.1061/\(ASCE\)SU.1943-5428.0000251](https://doi.org/10.1061/(ASCE)SU.1943-5428.0000251)
- Shen, P., Zhang, X., & Fang, Y. (2017). Essential properties of numerical integration for time-optimal path-constrained trajectory planning. *IEEE Robotics and Automation Letters*, *2*(2), 888-895. doi: <https://doi.org/10.1109/LRA.2017.2655580>
- Thiemann, C., Treiber, M., & Kesting, A. (2008). Estimating acceleration and lane-changing dynamics from next generation simulation trajectory data. *Transportation Research Record*, *2088*(1), 90-101. <https://doi.org/10.3141/2088-10>
- Wan, Q., Peng, G., Li, Z., Hiroshi, F., & Inomata, T. (2020). Spatiotemporal trajectory characteristic analysis for traffic state transition prediction near expressway merge bottleneck. *Transportation Research Part C*, *117*, 1-24. doi: <https://doi.org/10.1016/j.trc.2020.102682>
- Wang, C., & Zheng, C. Q. (2013). Lane change trajectory planning and simulation for intelligent vehicle. In Y. Huang, T. Bao & H. Wang (Eds.), *Advanced materials research* (Vol. 671-674, pp. 2843-2846). New York, USA: Trans Tech Publications Ltd. doi: <https://doi.org/10.4028/www.scientific.net/AMR.671-674.2843>
- Wang, Y. Y., Pan, D., Liu, Z., & Feng, R. (2018). *Study on lane change trajectory planning considering of driver characteristics* (No. 2018-01-1627). SAE Technical Papers. doi: <https://doi.org/10.4271/2018-01-1627>
- Yang, D., Zheng, S., Wen, C., Jin, P. J., & Ran, B. (2018). A dynamic lane-changing trajectory planning model for automated vehicles. *Transportation Research Part C: Emerging Technologies*, *95*(June), 228-247. doi: <https://doi.org/10.1016/j.trc.2018.06.007>
- You, F., Zhang, R., Lie, G., Wang, H., Wen, H., & Xu, J. (2015). Expert systems with applications trajectory planning and tracking control for autonomous lane change maneuver based on the cooperative vehicle infrastructure system. *Expert Systems With Applications*, *42*(14), 5932-5946. doi: <https://doi.org/10.1016/j.eswa.2015.03.022>

Zhou, B., Wang, Y., Yu, G., & Wu, X. (2017). A lane-change trajectory model from drivers' vision view. *Transportation Research Part C: Emerging Technologies*, 85(October), 609-627. doi: <https://doi.org/10.1016/j.trc.2017.10.013>

APPENDIX

Hyperbolic Tangent curve-based path planning approach:

The HTC model was proposed by Zhou et al. (2017) converted in Equation 8 using mathematical transformation. The lateral movements of vehicle represented by $Y_z(t)$ with respect to time t .

$$Y_z(t) = \frac{S_f}{z} \left(\tanh \left(\frac{\sigma}{l_d / v_d} \left(\frac{l_d}{2v_d} - t \right) \right) \right) + T_f \quad (8)$$

where, S_f is a scale factor, σ is driver aggressiveness, l_d is total longitudinal distance, V_d average velocity and T_f is a translation factor during LC action, where parameters are generated from dynamical trajectories except σ . This research tested four values (3, 4.3, 4.5, 7) of σ according to Zhou et al. (2017) suggestion. The optimized parameter value is 4.5.

Sine curve-based path planning approach:

Wang et al. (2018) proposed Equation 9 of lateral movements $Y_w(t)$, where t is time.

$$Y_w(t) = T_1 \frac{t}{t_1} - \frac{T_1}{2\pi} \sin \left(2\pi \frac{t}{t_1} \right) + T_f \quad (9)$$

where, T_1 is total lateral displacement, t_1 is total LC time and T_f is a translation factor, where all parameters are produced from dynamical trajectories.

Polynomial curve-based path planning approach:

Chebly et al. (2017) proposed Equation 10 of lateral movements $Y_p(t)$, where t is time.

$$Y_p(t) = 10T_1 \frac{t^3}{t_1^3} - 15T_1 \frac{t^4}{t_1^4} + 6T_1 \frac{t^5}{t_1^5} + T_f \quad (10)$$

where, T_1 is total lateral displacement, t_1 is total LC time and T_f is a translation factor, where all parameters are created from dynamical trajectories.

The lateral velocity profile is derived from Equation 10 shown in Equation 11:

$$V_p(t) = 30T_1 \frac{t^2}{t_1^3} - 60T_1 \frac{t^3}{t_1^4} + 30T_1 \frac{t^4}{t_1^5} \quad (11)$$

The lateral acceleration profile is shown in Equation 12: (Chebly et al., 2017)

$$A_p(t) = 60T_1 \frac{t}{t_1^3} - 180T_1 \frac{t^2}{t_1^4} + 150T_1 \frac{t^3}{t_1^5} \quad (12)$$

Combined Impacts of Predation, Mutualism and Dispersal on the Dynamics of a Four-Species Ecological System

Murtala Bello Aliyu^{1,2*} and Mohd Hafiz Mohd^{1,3}

¹*School of Mathematical Sciences, Universiti Sains Malaysia, 11800 USM, Penang, Malaysia*

²*Department of Mathematics, Nigerian Defence Academy, Afaka, PMB 2019, Kaduna, Nigeria*

³*School of Mathematical Sciences, Faculty of Science and Technology, Universiti Kebangsaan Malaysia, 43600 UKM, Bangi, Selangor, Malaysia*

ABSTRACT

Multi-species and ecosystem models have provided ecologist with an excellent opportunity to study the effects of multiple biotic interactions in an ecological system. Predation and mutualism are among the most prevalent biotic interactions in the multi-species system. Several ecological studies exist, but they are based on one-or two-species interactions, and in real life, multiple interactions are natural characteristics of a multi-species community. Here, we use a system of partial differential equations to study the combined effects of predation, mutualism and dispersal on the multi-species coexistence and community stability in the ecological system. Our results show that predation provided a defensive mechanism against the negative consequences of the multiple species interactions by reducing the net effect of competition. Predation is critical in the stability and coexistence of the multi-species community. The combined effects of predation and dispersal enhance the multiple species coexistence and persistence. Dispersal exerts a positive effect on the system by supporting multiple species coexistence and stability of community structures. Dispersal process also

reduces the adverse effects associated with multiple species interactions. Additionally, mutualism induces oscillatory behaviour on the system through Hopf bifurcation. The roles of mutualism also support multiple species coexistence mechanisms (for some threshold values) by increasing the stable coexistence and the stable limit cycle regions. We discover that the stability and coexistence mechanisms are controlled by the transcritical and Hopf bifurcation that

ARTICLE INFO

Article history:

Received: 21 June 2020

Accepted: 18 September 2020

Published: 22 January 2021

DOI: <https://doi.org/10.47836/pjst.29.1.13>

E-mail addresses:

murtalabelloaliyu@gmail.com (Murtala Bello Aliyu)

mohdhafizmohd@usm.my (Mohd Hafiz Mohd)

* Corresponding author

occurs in this system. Most importantly, our results show the important influences of predation, mutualism and dispersal in the stability and coexistence of the multi-species communities.

Keywords: Dispersal, Hopf bifurcation, limit cycle, multi-species, stability, transcritical bifurcation

INTRODUCTION

The population dynamics of multi-species systems are substantially driven by interspecific interactions (Gause & Witt, 1935; Ojonubah & Mohd, 2020). There has been renewed interest in the role of predation in conservation (Soulé & Terborgh, 1999; Sala, 2006; Schmitz, 2006; Johnson et al., 2007). Several work on empirical and theoretical studies have addressed the effects of predation on the dynamics of the multi-species communities (Rosenzweig & MacArthur, 1963; Chesson, 2000). For instance, Hixon & Menge (1991) showed in their study that predation strength (i.e., rate at which the predator feeds on the prey) had a direct effect on the diversity of prey species. Predation in the multi-species community has been shown to preserve species coexistence when its effects are more prevalent than competitive interactions; on the other hand, predation can also lead to species exclusion (Chesson & Kuang, 2008).

Recently, some researchers have shed some light on the dynamics of mutualistic interactions; (i.e., symbiotic interaction between two-species where each benefits from the other) (Bronstein, 2001a; Holland et al., 2002; Bever, 2003; Bruno et al., 2003). These studies of mutualism were carried out in one-or two-species system. In real life, multiple species interact in different ways. Some other studies on mutualism arrived at two generalisations (Holland et al., 2002); (i) the stability of the multi-species systems depends on how the positive feedback from mutualism is balanced with the negative feedback (Chesson, 2000; Bever, 2003); (ii) mutualism has direct cost and benefits that are dependent on density of populations (Addicott, 1979; Morales, 2000; Bronstein, 2001b). In reality, the maintenance of the ecosystem, ecological structure and biodiversity are well-known benefits that can be gained from mutualism (Aslan et al., 2013). Predation and mutualism are among important biotic interactions that occur in nature. The dynamics of these interactions are intertwined, and this has hampered the understanding of their combined effects in isolation (Fontaine et al., 2011; Georgelin & Loeuille, 2014). Moreover, information on the combined effects of predation, mutualism and dispersal on multi-species coexistence and community stability are poorly understood, and thus warrant further studies.

Predation and mutualism have a stabilising impact on the negative feedback when species population density is abundant (Holland et al., 2002; Schmitt & Holbrook, 2003; Holland & DeAngelis, 2010; Holland et al., 2013). An essential ecological question is what effects dispersal has on the interplay between predation and mutualism in a four-species ecological system. To address this problem, we used a system of partial differential

equations (PDE) to gain insight on the combined effects of predation, mutualism, and dispersal in the ecological systems. In general, dispersal plays a vital role in conservation biology and spatial ecology (Hanski, 1998; Kindlmann & Burel, 2008; Kool et al., 2012). Dispersal facilitates the mobility of species to new environments (Bonte et al., 2003). Low dispersal strength has a synchronisation effect (i.e., variation in an ecological context and population dynamics) on large amplitude population cycles across space (Bjørnstad, 2000; Vasseur & Fox, 2009; Vogwill et al., 2009). The chances for dispersal-induced stability is low when the population cycle goes through spatial synchrony (i.e., the abundance of different geographical populations) (Yaari et al., 2012; Lampert & Hastings, 2016). Several studies have demonstrated how antagonistic interactions facilitate dispersal (Mondor et al., 2004; Green, 2009; Poethke et al., 2010; Chaianunporn & Hovestadt, 2015; Amarasekare, 2015). A well-known effect of antagonistic interaction is strong population cycles which consequencely lead to changes in species fitness (Green, 2009; Chaianunporn & Hovestadt, 2012).

Some studies also report that dispersal lessens the variability in species population and extinction (Briggs & Hoopes, 2004; Vogwill et al., 2009; Abbott, 2011). Nevertheless, there are conflicting evidence on how dispersal affects the multi-species communities. Varying abundances in species population in various geographical areas are one of the benefits derives from dispersal among local populations (Kendall et al., 2000; Abbott, 2011). It has also been demonstrated that the effect of dispersal on the multi-species community could either be no effects, stabilising, or destabilising (Dey & Joshi, 2006; Steiner et al., 2013). A more recent study shows that dispersal could have both stabilising and destabilising effect on a multi-species ecological system (Mohd et al., 2018). Given all these different perspectives on predation, mutualism, and dispersal, it becomes crucial to investigate the combined effects of predation, mutualism and dispersal on the species coexistence and community stability in these multi-species systems. In general, the joint effects of predation, mutualism and dispersal on the multi-species communities are still unclear and need to be further explored.

To cover this knowledge gap, we extended the four-species interactions model (Mitani & Mougi, 2017) to investigate the effects of predation, mutualism, and dispersal. We numerically showed the impact of predation, mutualism and dispersal on the multiple species coexistence dynamics. Furthermore, we discussed the implications of our results from the perspectives of multiple species coexistence and community stability.

MATERIAL AND METHODS

Model Description

We proposed a system of PDE for the densities $X(x, t)$, $W(x, t)$, $Y(x, t)$ and $Z(x, t)$ in one-dimension $0 \leq x \leq 1$ (Equation 1) (Mitani & Mougi, 2017; Mohd et al., 2017):

$$\begin{aligned}
\frac{\partial X}{\partial t} &= X(r_k - X - \beta W - \alpha Y + \frac{uZ}{h_z + Z}) + D_1 \frac{\partial^2 X}{\partial x^2} \\
\frac{\partial W}{\partial t} &= W(r_w - W - \alpha X) + D_2 \frac{\partial^2 W}{\partial x^2} \\
\frac{\partial Y}{\partial t} &= Y(gaX - d) + D_3 \frac{\partial^2 Y}{\partial x^2} \\
\frac{\partial Z}{\partial t} &= Z(r_z - Z + \frac{vX}{h_x + X}) + D_4 \frac{\partial^2 Z}{\partial x^2}
\end{aligned} \tag{1}$$

where X , W , Y , Z represent the population densities of resource, competitor, exploiter, and mutualist species, respectively. The parameter r_k is the rate at which the resource species grows; r_w is the rate at which the competitor species grows; r_z is the rate at which the mutualist species grows; α and β represent the strength of competition (i.e., resource and competitor species, respectively); a represents capture rate (i.e., the rate at which the exploiter species capture the prey). The term g represents the conversion efficiency; d represents exploiter species death; u and v represent the benefits from the mutualistic interactions (i.e., mutualistic strength of the resource and mutualist species, respectively); h_x and h_z represent the half-saturation constant of resource and mutualist species, respectively (i.e., density at which half the average intake of prey is achieved, irrespective of the prey population available). It is assumed that the self-regulation mechanism of mutualist species (net effect of a mutualist on the other mutualist species) is unity for theoretical simplicity. Equation 1 is a spatial extension of the multiple interactions type model (Mitani & Mougi, 2017). The system of ordinary differential equations (ODE) becomes systems of PDE with the addition of the diffusion term. The term D_i ($i = 1, 2, 3, 4$) represents the dispersal strength along spatial domain (x). We assumed equal dispersal strength for all the interacting species ($D_1 = D_2 = D_3 = D_4 = 0.005$). Also, we applied zero-flux boundary conditions for each of the interacting species (Equation 2) (i.e., no movement is allowed across the boundaries):

$$\begin{aligned}
D_1 \frac{\partial X(0,t)}{\partial x} &= D_1 \frac{\partial X(1,t)}{\partial x} \\
D_2 \frac{\partial W(0,t)}{\partial x} &= D_2 \frac{\partial W(1,t)}{\partial x} \\
D_3 \frac{\partial Y(0,t)}{\partial x} &= D_3 \frac{\partial Y(1,t)}{\partial x}
\end{aligned} \tag{2}$$

$$D_4 \frac{\partial Z(0, t)}{\partial x} = D_4 \frac{\partial Z(1, t)}{\partial x}$$

To solve Equation 1 with the boundary conditions as in Equations 2, we used the method of line. This numerical approach was implemented in XPPAUT, which provides a good platform for solving PDE systems in one spatial variable x . The spatial domain was divided into meshes of $M + 1$ equivalent points of $x_i = ih$ for $i = 0, 1, \dots, M$ ($0 \leq x \leq 1$). The central difference approximation was then employed to replace the spatial derivative in Equation 1. In this numerical method, the zero-flux boundary conditions were encoded into the scheme using finite difference approximation. The resulting transformation resulted in a $4(N+1)$ ODE scheme, one for each species at spatial location x_i . The regular ODE solver, *cvode*, was used for solving the resulting ODE system for $t = 1000$ (i.e., until steady state). The size of the mesh used in the numerical simulation was $h = 0.09$. We had also used AUTO to continue the steady state, in which case we tracked the stable, unstable and bifurcation points that arose as the parameters changed in this ecological system. It was also verified that the numerical results were insensitive to changes in grid spacing (i.e., by increasing and decreasing the number of finite difference points).

RESULT

Effects of Predation on the Dynamics of ODE and PDE Models

Here, we discuss the vital features of the system (1) in the absence of dispersal ($D=0$). The dynamical behaviour of the ODE model (in the absence of dispersal) is represented

Table 1
Symbols, their definitions and the parameter values used for the numerical simulations

Symbol	Definition	Parameter value
r_k	The intrinsic growth rate of resource species	1
r_w	The intrinsic growth rate of competitor species	1
r_z	The intrinsic growth rate of the mutualist species	1
u	Maximum benefit of the mutualistic interaction	3
v	Maximum benefit of the mutualistic interaction	2
a	Capture rate	1.8
g	Conversion efficiency of the exploiter species	0.25
d	Death rate of the exploiter	0.05
h_x	Half saturation constant of the hyperbolic functional response	1
h_z	Half saturation constant of the hyperbolic functional response	1
β	Competitive strength of the competitor species	0.7
a	Competitive strength of the resource species	0.2
D	Dispersal strength	0.005

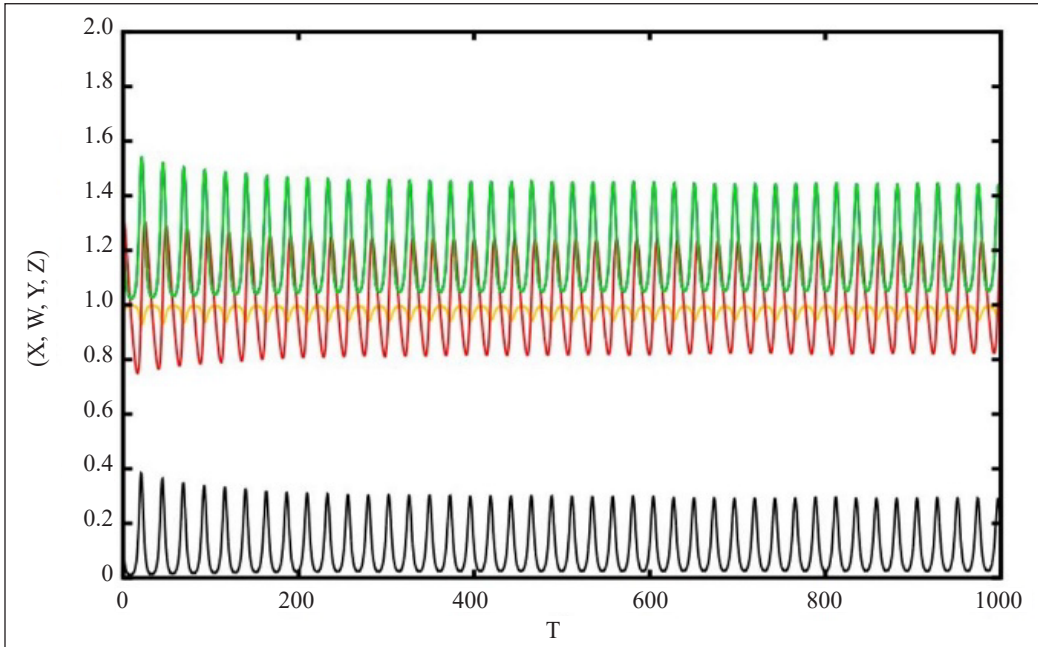


Figure 1. The time series of Equation 1 with $D=0$. Initial species density $X(0) = 0.9$, $W(0) = 0.3$, $Y(0) = 0.2$, $Z(0) = 0.8$. X (black), W (yellow), Y (red) and Z (green). The diagram was plotted using XPPAUT and the parameter values as in Table 1.

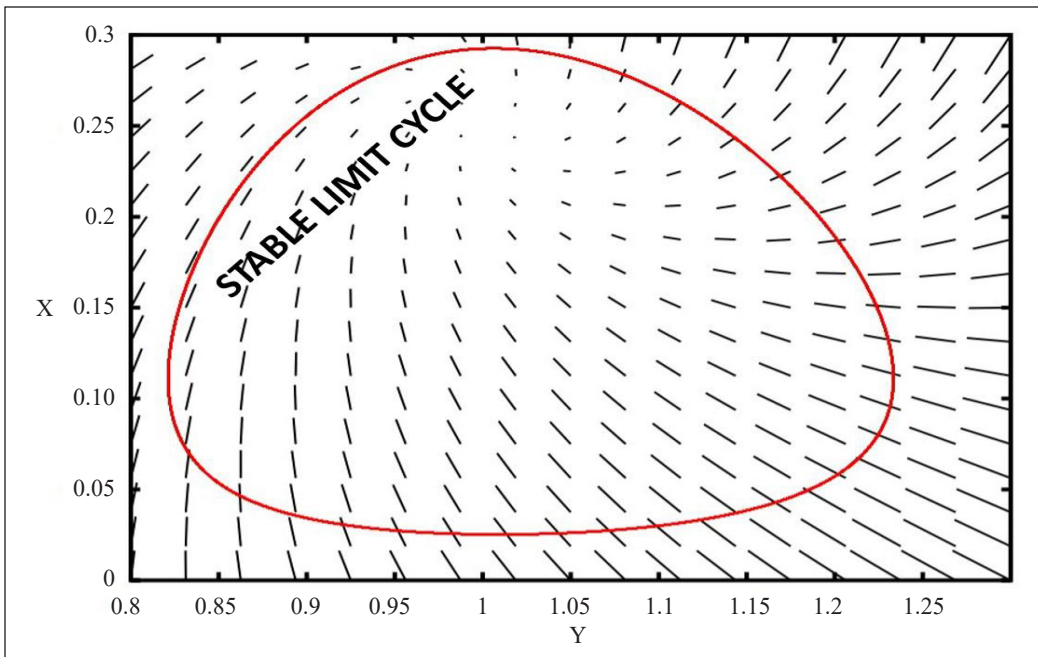


Figure 2. Stable limit cycle of Equation 1 with $D=0$. Initial species density $X(0) = 0.9$, $W(0) = 0.3$, $Y(0) = 0.2$, $Z(0) = 0.8$. X (black), W (yellow), Y (red) and Z (green). The diagram was plotted using XPPAUT and the parameter values in Table 1.

in Figures 1 and 2 using the parameter values as in Table 1. Figure 1 shows the oscillatory dynamics in this ecological system, which are crucial properties of multi-species interactions. This oscillatory behaviour arises due to the salient interplay of different biotic factors, i.e., resource-competitor-exploiter-mutualist interactions. Subsequently, all the steady state is unstable, and this leads to the emergence of a stable limit cycle (Figure 2) in which case the species population densities oscillate between some maximum and minimum densities.

Since we aimed to explore how predation and mutualism shape species coexistence and community stability, we carried out one-parameter bifurcation analysis using a and u (i.e., the strength of predation and mutualistic strength, respectively). For instance, Figure 3 illustrates the species population densities in the absence of dispersal as a varies. There occurred a threshold point ($a=1.437$) in this co-dimension one bifurcation (Figure 3) conforming to Hopf bifurcation (i.e., HB). This Hopf bifurcation gave births to the oscillatory behaviour in the ecological Equation 1. Thus, the strength of predation directly affects the coexistence of multiple species and the stability of community structures in this multiple interaction type system. As an example, when $a < HB$, a four-species steady-state emerged and when $a > HB$, stable limit cycle occurred. The transition from a four-species steady-state to a stable limit cycle occurred at the Hopf bifurcation point. Further, since the first Lyapunov coefficient was negative, this implies that the Hopf bifurcation is supercritical, and the limit cycle is of stable type (Figure 3).

The inclusion of dispersal qualitatively changes the dynamics of this multiple interactions type system. There occurred a critical value ($a=0.4759$) corresponding to a transcritical bifurcation (i.e., BP) as the parameter a changed in the system (Figure 4). At

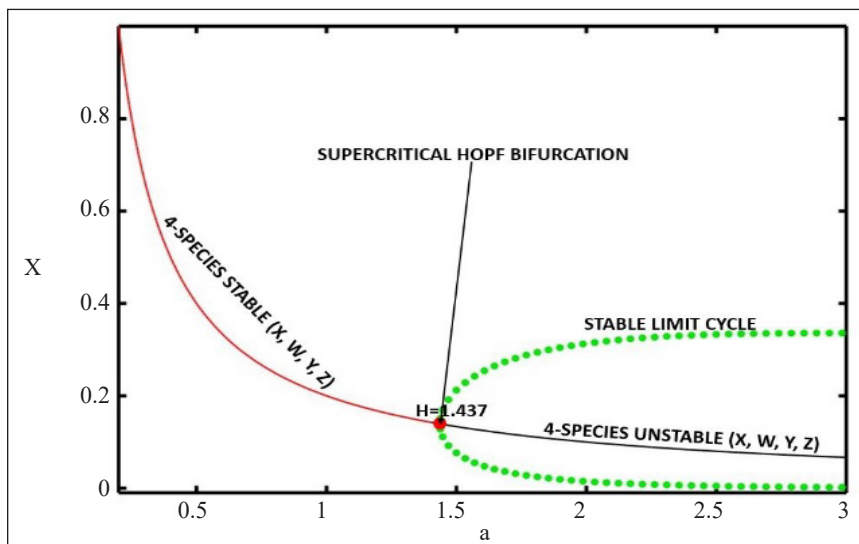


Figure 3. Bifurcation diagram showing the stability behaviour of the system as we vary a . $D = 0$. The diagram was plotted using XPPAUT package and the parameter values in Table 1.

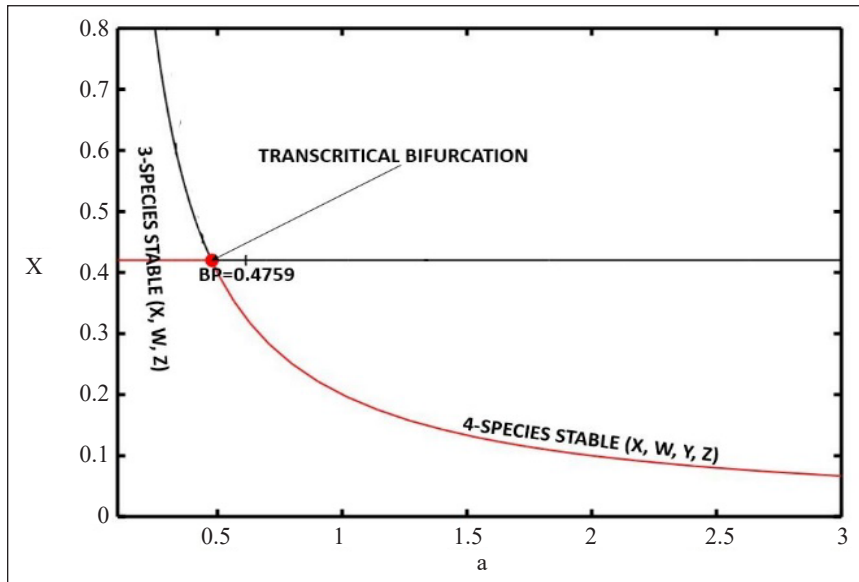


Figure 4. Bifurcation diagram showing the stability behaviour of the system as we vary a . $D = 0.005$. The diagram was plotted using XPPAUT package and the parameter values in Table 1.

this transcritical bifurcation point, we observed the exchange of stability between steady-states (i.e., from three-species steady-state to four-species steady-state). The emergence of transcritical bifurcation affected species coexistence and community stability mechanisms of this ecological system. We discovered three-species steady-state (i.e., when $a < BP$) and four-species steady-state (i.e., when $a > BP$) as a changed in the presence of dispersal (Figure 4). We also observed that weak predation strength interacted with dispersal affecting species persistence (i.e., a species goes extinct) in this multiple interactions type system. However, for the broader region of a ($a > BP$), the species persistence was maintained as four-species steady-state occurred. Most importantly, this observation suggested that intense predation in the presence of dispersal supported multi-species coexistence in this ecological system. By comparing Figures 3 and 4, we observed an apparent qualitative change in the dynamics of the multiple interactions type system. Oscillatory behaviour dominated the dynamics of the ecological system without dispersal (Figure 3) and multi-species coexistence steady state dominated in the presence of dispersal (Figure 4). This result illustrates that dispersal promotes coexistence of multiple species through the occurrence of stable steady-states and also limit cycles.

Effects of Mutualism on the Dynamics of ODE and PDE Models

We first studied the effects of mutualism in the ODE system. Figure 5 shows the dynamics of the ecological system in the absence of dispersal as u changes. There emerged a critical bifurcation point as the parameter u (i.e., at $u=2.741$) varied, and this point corresponded to

supercritical Hopf bifurcation (i.e., HB). The supercritical Hopf bifurcation affects species coexistence and community stability in this multiple interaction type model. For example, there occurred a four-species steady-state when $u < HB$, and stable limit cycles when $u > HB$. The first Lyapunov coefficient at the Hopf bifurcation point was negative; thus, this confirms that the Hopf bifurcation is supercritical and the limit cycle that emerges is stable.

In the presence of dispersal, the PDE model exhibited qualitatively similar dynamics compared to no dispersal case (Figure 6). There existed a bifurcation point that corresponded to a supercritical Hopf bifurcation (i.e., at $u=2.865$). The Hopf bifurcation affected multi-species composition (i.e., presence-absence of species) as u changed. The first Lyapunov coefficient was negative, and this indicates that the limit cycle is stable. These species compositions include: (i) a four-species steady-state (i.e., $u < HB$); (ii) stable limit cycles (i.e., $u > HB$). We further compared the result in Figures 5 and 6. We discovered a qualitative similar effect of dispersal which determined coexistence dynamics of this ecological system. The inclusion of dispersal shifted the threshold of mutualistic interaction strength to higher values (i.e., from $u=2.741$ to $u=2.865$), thus multi-species coexistence outcomes could be observed for more values of u . Overall, in the presence of dispersal, mutualism enhances species coexistence and community stability, compared to no-dispersal case.

We investigated the joint effects of predation and mutualism on the species coexistence and community stability by conducting a co-dimension two bifurcation analysis, as shown in Figures 7 and 8. Figure 7 depicts the effects of varying a and u in the absence of dispersal (i.e., $D=0$ in the Equation 1). We observed species compositions as follows: (i)

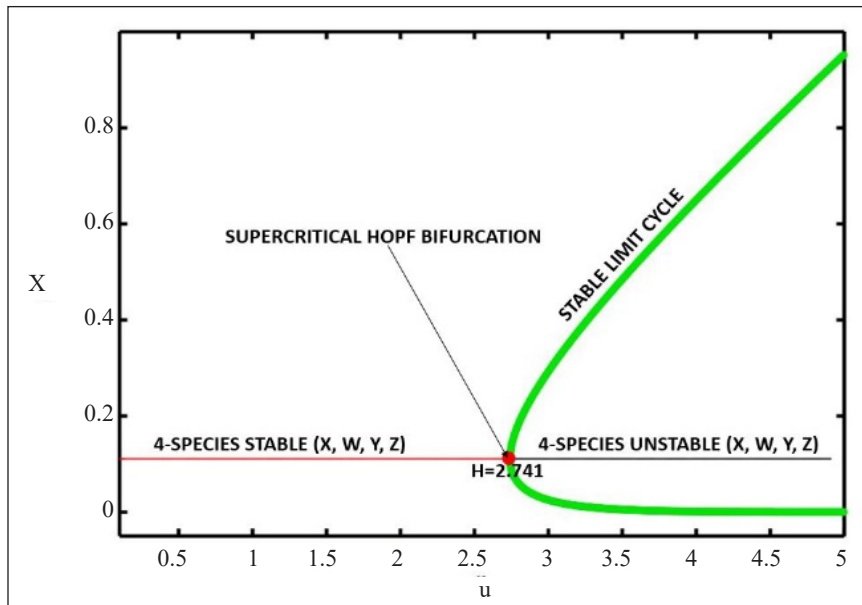


Figure 5. Bifurcation diagram showing the stability behaviour of the system as we vary u . $D = 0$. The diagram was plotted using XPPAUT package and the parameter values in Table 1.

four-species stable coexistence region (ii) stable limit cycles (four-species unstable) region. In the presence of dispersal (Figure 8), we had three-species stable coexistence region, four-species stable coexistence region and stable limit cycle region. Most importantly, by comparing Figures 7 and 8, we discovered that predation, mutualism, and dispersal mediate more species coexistence outcomes compared to no-dispersal case.

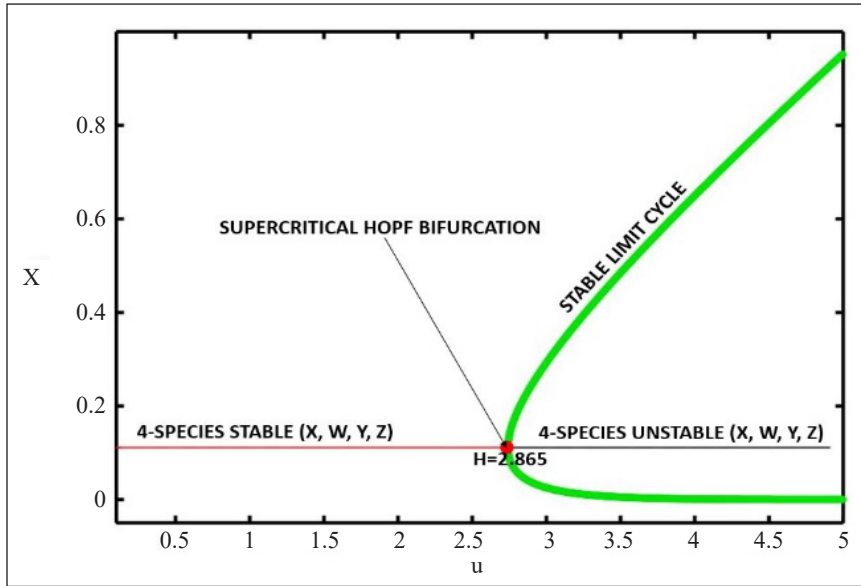


Figure 6. Bifurcation diagram showing the stability behaviour of the system as we vary u . $D = 0.005$. The diagram was plotted using XPPAUT package and the parameter values in Table 1.

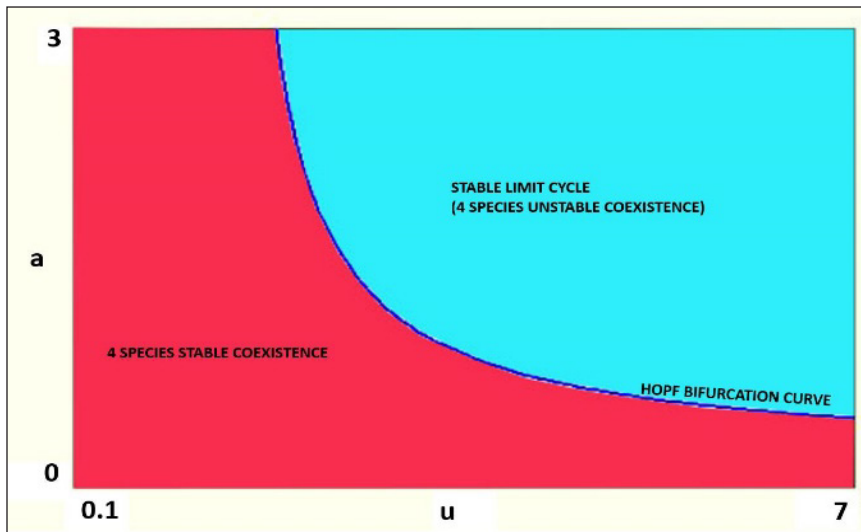


Figure 7. Bifurcation diagram showing the different coexistence dynamics in the system with no-dispersal ($D=0$) as a and u are varied. $D = 0$. The diagram was plotted using XPPAUT package and the parameter values as in Table 1.

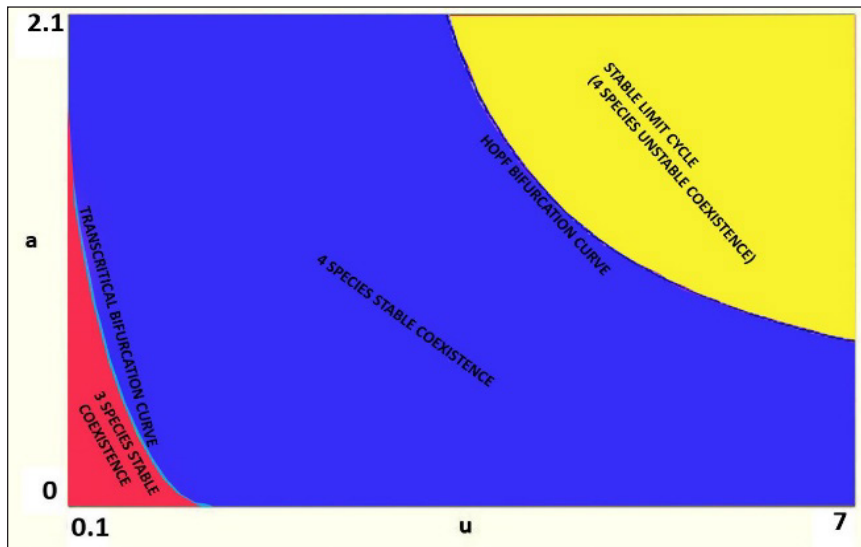


Figure 8. Bifurcation diagram showing the different coexistence dynamics in the PDE system (1) with $D=0.005$ as a and u were varied. The diagram was plotted using XPPAUT package and the parameter values as in Table 1.

DISCUSSION AND CONCLUSION

Our numerical simulation results show that the effects of predation, mutualism, and dispersal in the presence of other biotic interactions can affect the community stability and stable coexistence of species in this ecological system. Predation supports the community stability of multiple species in the systems (Caro & Stoner, 2003). A significant ecological benefit of predation is that it promotes the spatial and structural diversity of species in the ecosystem (Carter et al., 2015; Swanson et al., 2016). Fundamentally, our results show that weak predation strength in a multiple interactions type system affects species diversity negatively in the presence of dispersal. Specifically, weak predation endangers the exploiter species in these multiple species model. Although moderate and intense predation strength supports the stable coexistence and stability of multiple species in this ecological system, there are some conflicting reports on the effects of predation from experimental studies (Cheng et al., 2018; Quinn et al., 2016). We observed that there was a gradual reduction in the equilibrium population densities of the interacting species as the predation strength continued to increase in the absence of dispersal. However, predation can provide a buffer against extinction in the presence of dispersal, even when the interactions are intense. In general, our results show that predation coupled with dispersal in the multiple interactions type model are crucial for species coexistence and persistence.

Mutualism has dual effects on the stability and stable coexistence of the multiple species community. Our results show that for some threshold values of u , multiple species stability and persistence can be preserved. For other values of mutualistic strength, the system exhibits oscillatory behaviour. These dual effects of mutualism shown in our results have

been reported in several studies (Kooi et al., 2004; Valdovinos et al., 2016; Valdovinos et al., 2018; Addicott, 1998; Herrera, 1998; Parker, 1999). Overall, our results provide insights into the significance of mutualism in the understanding of the natural world. We caution that there is a high probability of extinction of species in the occurrence of stable limit cycles as population density continues to fluctuate between some maximum to minimum densities which are close to zero (Mohd, 2019). In contrast to our finding, earlier studies carried out by Rosenzweig (1971) and Wright (1989) reported that mutualism had no impacts on the diversity of species in an ecological system. From the conservation viewpoint, mutualism supports multiple species coexistence for some critical values in this ecological system. This finding is in agreement with the reports that mutualism supports species richness (Pascual-García & Bastolla, 2017; Chomicki et al., 2019; Bascompte, 2019; Martignoni et al., In Press).

The results in this work also show that dispersal has a qualitative effect on these multiple interactions type model. Dispersal increases the initial amplitude of oscillation in the ecological system. This result is in contrast with the report of (Laan & Fox, 2019) which observed that dispersal had no effect on the amplitude of oscillation in a multiple interactions type system. The positive effects of dispersal on these multiple interactions type system support the persistence and coexistence mechanisms of species (Kot et al., 1996; Kerr et al., 2002; Mohd et al., 2018). An exciting consequence of dispersal is that it increases the extent of geographical areas for interacting species, and this supports the notion of biodiversity of species (Godsoe et al., 2015; Dytham, 2009). The occurrence of oscillatory behaviour in this system suggests that there are other mechanisms outside the paradox of enrichment that drive population cycle (Rozhnova et al., 2013; Barraquand et al., 2017).

The bifurcation results in this work have demonstrated the role of bifurcation analysis in understanding the coexistence and stability behaviour of a multi-species community. Specifically, our bifurcation result shows the dynamics that occur in this ecological system and the threshold values at which they occur. Furthermore, the bifurcation results illustrate the presence of transcritical and Hopf bifurcation as we vary a and u , respectively. The transcritical bifurcation affects the extinction and survival of the exploiter species from the system as a result of stability change, and the Hopf bifurcation causes a transition from a stable steady-state to limit cycles with increasing amplitude over time. These two dynamics have shed some light on the possible outcomes of multiple interactions type system. In particular, our results show that predation, mutualism and dispersal are essential forces that determine the stability and coexistence of multiple species.

In conclusion, the numerical simulations result in this study shows the influential roles of predation, mutualism and dispersal in the maintenance of the multi-species ecological systems. The results in this work will serve as valuable reference material for species conservationists and managers in maintaining the biodiversity of species.

ACKNOWLEDGEMENT

This research is supported by the Universiti Sains Malaysia (USM) Fundamental Research Grant Scheme (FRGS) No. 203/PMATHS/6711645.

REFERENCES

- Abbott, K. C. (2011). A dispersal-induced paradox: Synchrony and stability in stochastic metapopulations. *Ecology Letters*, 14(11), 1158-1169. doi: 10.1111/j.1461-0248.2011.01670.x.
- Addicott, J. F. (1979). A multispecies aphid-ant association: Density dependence and species-specific effects. *Canadian Journal of Zoology*, 57(3), 558-569. doi: 10.1139/z79-066.
- Addicott, J. F. (1998). Regulation of mutualism between yuccas and yucca moths: Population level processes. *Oikos*, 81(1), 119-129. doi: 10.2307/3546474.
- Amarasekare, P. (2015). Evolution of dispersal in a multi-trophic community context. *Oikos*, 125(4), 514-525. doi: 10.1111/oik.02258.
- Aslan, C. E., Zavaleta, E. S., Tershy, B., & Croll, D. (2013). Mutualism disruption threatens global plant biodiversity: A systematic review. *PLoS ONE*, 8(6), 1-11. doi: 10.1371/journal.pone.0066993.
- Barraquand, F., Louca, S., Abbott, K. C., Cobbold, C. A., Cordoleani, F., DeAngelis, D. L., ... & Murray, D. L. (2017). Moving forward in circles: Challenges and opportunities in modelling population cycles. *Ecology Letters*, 20(8), 1074-1092. doi: 10.1111/ele.12789.
- Bascompte, J. (2019). Mutualism and biodiversity. *Current Biology*, 29(11), R467-R470. doi: 10.1016/j.cub.2019.03.062.
- Bever, J. D. (2003). Soil community feedback and the coexistence of competitors: Conceptual frameworks and empirical tests. *New Phytologist*, 157(3), 465-473. doi: 10.1046/j.1469-8137.2003.00714.x.
- Bjørnstad, O. N. (2000). Cycles and synchrony: Two historical "experiments" and one experience. *Journal of Animal Ecology*, 69(5), 869-873. doi: 10.1046/j.1365-2656.2000.00444.x.
- Bonte, D., Vandenbroecke, N., Lens, L., & Maelfait, J. P. (2003). Low propensity for aerial dispersal in specialist spiders from fragmented landscapes. *Proceedings of the Royal Society of London. Series B: Biological Sciences*, 270(1524), 1601-1607. doi: doi.org/10.1098/rspb.2003.2432.
- Briggs, C. J., & Hoopes, M. F. (2004). Stabilizing effects in spatial parasitoid-host and predator-prey models: A review. *Theoretical Population Biology*, 65(3), 299-315. doi: 10.1016/j.tpb.2003.11.001.
- Bronstein, J. L. (2001a). The exploitation of mutualisms. *Ecology Letters*, 4(3), 277-287. doi: 10.1046/j.1461-0248.2001.00218.x.
- Bronstein, J. L. (2001b). The costs of mutualism. *American Zoologist*, 41(4), 825-839. doi: 10.1093/icb/41.4.825.
- Bruno, J. F., Stachowicz, J. J., & Bertness, M. D. (2003). Inclusion of facilitation into ecological theory. *Trends in Ecology and Evolution*, 18(3), 119-125. doi: 10.1016/s0169-5347(02)00045-9.
- Caro, T., & Stoner, C. (2003). The potential for interspecific competition among African carnivores. *Biological Conservation*, 110(1), 67-75. doi: 10.1016/s0006-3207(02)00177-5.

- Carter, N., Jasny, M., Gurung, B., & Liu, J. (2015). Impacts of people and tigers on leopard spatiotemporal activity patterns in a global biodiversity hotspot. *Global Ecology and Conservation*, 3, 149-162. doi: 10.1016/j.gecco.2014.11.013.
- Chaianunporn, T., & Hovestadt, T. (2012). Evolution of dispersal in metacommunities of interacting species. *Journal of Evolutionary Biology*, 25(12), 2511-2525. doi: 10.1111/j.1420-9101.2012.02620.x.
- Chaianunporn, T., & Hovestadt, T. (2015). Evolutionary responses to climate change in parasitic systems. *Global Change Biology*, 21(8), 2905-2916. doi: 10.1111/gcb.12944.
- Cheng, B. S., Ruiz, G. M., Altieri, A. H., & Torchin, M. E. (2018). The biogeography of invasion in tropical and temperate seagrass beds: Testing interactive effects of predation and propagule pressure. *Diversity and Distributions*, 25(2), 285-297. doi: 10.1111/ddi.12850.
- Chesson, P. (2000). Mechanisms of maintenance of species diversity. *Annual Review of Ecology and Systematics*, 31(1), 343-366. doi: 10.1146/annurev.ecolsys.31.1.343.
- Chesson, P., & Kuang, J. J. (2008). The interaction between predation and competition. *Nature*, 456(7219), 235-238. doi: 10.1038/nature07248.
- Chomicki, G., Weber, M., Antonelli, A., Bascompte, J., & Kiers, E. T. (2019). The impact of mutualisms on species richness. *Trends in Ecology and Evolution*, 34(8), 698-711. doi: doi.org/10.1016/j.tree.2019.03.003.
- Dey, S., & Joshi, A. (2006). Stability via asynchrony in drosophila metapopulations with low migration rates. *Science*, 312(5772), 434-436. doi: 10.1126/science.1125317.
- Dytham, C. (2009). Evolved dispersal strategies at range margins. *Proceedings of the Royal Society B: Biological Sciences*, 276(1661), 1407-1413. doi: 10.1098/rspb.2008.1535.
- Fontaine, C., Guimarães Jr, P. R., Kéfi, S., Loeuille, N., Memmott, J., van Der Putten, W. H., ... & Thébaud, E. (2011). The ecological and evolutionary implications of merging different types of networks. *Ecology Letters*, 14(11), 1170-1181. doi: 10.1111/j.1461-0248.2011.01688.x.
- Gause, G. F., & Witt, A. A. (1935). Behavior of mixed populations and the problem of natural selection. *The American Naturalist*, 69(725), 596-609. doi: 10.1086/280628.
- Georgelin, E., & Loeuille, N. (2014). Dynamics of coupled mutualistic and antagonistic interactions, and their implications for ecosystem management. *Journal of Theoretical Biology*, 346, 67-74. doi: 10.1016/j.jtbi.2013.12.012.
- Godsoe, W., Murray, R., & Plank, M. J. (2015). Information on biotic interactions improves transferability of distribution models. *The American Naturalist*, 185(2), 281-290. doi: 10.1086/679440.
- Green, D. M. (2009). Coevolution of dispersal in a parasitoid-host system. *Population Ecology*, 51(2), 253-260. doi: 10.1007/s10144-008-0131-3.
- Hanski, I. (1998). Metapopulation dynamics. *Nature*, 396(6706), 41-49. doi: 10.1038/23876.
- Herrera, C. M. (1998). Long-term dynamics of Mediterranean Frugivorous birds and fleshy fruits: A 12-year study. *Ecological Monographs*, 68(4), 511-538. doi: 10.1890/0012-9615(1998)068[0511:ltomf]2.0.c.
- Hixon, M. A., & Menge, B. A. (1991). Species diversity: Prey refuges modify the interactive effects of predation and competition. *Theoretical Population Biology*, 39(2), 178-200. doi: 10.1016/0040-5809(91)90035-e.

- Holland, J. N., & DeAngelis, D. L. (2010). A consumer–resource approach to the density-dependent population dynamics of mutualism. *Ecology*, *91*(5), 1286-1295. doi: 10.1890/09-1163.1.
- Holland, J. N., DeAngelis, D. L., & Bronstein, J. L. (2002). Population dynamics and mutualism: Functional responses of benefits and costs. *The American Naturalist*, *159*(3), 231-244. doi: 10.1086/338510.
- Holland, J. N., Wang, Y., Sun, S., & DeAngelis, D. L. (2013). Consumer–resource dynamics of indirect interactions in a mutualism–parasitism food web module. *Theoretical Ecology*, *6*(4), 475-493. doi: 10.1007/s12080-013-0181-9.
- Johnson, C. N., Isaac, J. L., & Fisher, D. O. (2007). Rarity of a top predator triggers continent-wide collapse of mammal prey: Dingoes and marsupials in Australia. *Proceedings of the Royal Society B: Biological Sciences*, *274*(1608), 341-346. doi: 10.1098/rspb.2006.3711.
- Kendall, B. E., Bjørnstad, O. N., Bascompte, J., Keitt, T. H., & Fagan, W. F. (2000). Dispersal, environmental correlation, and spatial synchrony in population dynamics. *The American Naturalist*, *155*(5), 628-636. doi: 10.1086/303350.
- Kerr, B., Riley, M. A., Feldman, M. W., & Bohannan, B. J. M. (2002). Local dispersal promotes biodiversity in a real-life game of rock–paper–scissors. *Nature*, *418*(6894), 171-174. doi: 10.1038/nature00823.
- Kindlmann, P., & Burel, F. (2008). Connectivity measures: A review. *Landscape Ecology*, *23*(8), 879-890. doi: 10.1007/s10980-008-9245-4.
- Kooi, B. W., Kuijper, L. D. J., & Kooijman, S. A. L. M. (2004). Consequences of symbiosis for food web dynamics. *Journal of Mathematical Biology*, *49*(3), 227-271. doi: 10.1007/s00285-003-0256-0.
- Kool, J. T., Moilanen, A., & Treml, E. A. (2012). Population connectivity: Recent advances and new perspectives. *Landscape Ecology*, *28*(2), 165-185. doi: 10.1007/s10980-012-9819-z.
- Kot, M., Lewis, M. A., & van den Driessche, P. (1996). Dispersal data and the spread of invading organisms. *Ecology*, *77*(7), 2027-2042. doi: 10.2307/2265698.
- Laan, E., & Fox, J. W. (2019). An experimental test of the effects of dispersal and the paradox of enrichment on metapopulation persistence. *Oikos*, *129*(1), 49-58 doi: 10.1111/oik.06552.
- Lampert, A., & Hastings, A. (2016). Stability and distribution of predator-prey systems: Local and regional mechanisms and patterns. *Ecology Letters*, *19*(3), 279-288. doi: 10.1111/ele.12565.
- Martignoni, M. M., Hart, M. M., Tyson, R. C., & Garnier, J. (In Press). Diversity within mutualist guilds promotes coexistence and reduces the risk of invasion from an alien mutualist. *Proceedings of the Royal Society B: Biological Sciences*. doi: 10.1098/rspb.2019.2312.
- Mitani, N., & Mougi, A. (2017). Population cycles emerging through multiple interaction types. *Royal Society Open Science*, *4*(9), 1-7. doi: 10.1098/rsos.170536.
- Mohd, M. H. (2019). Diversity in interaction strength promotes rich dynamical behaviours in a three-species ecological system. *Applied Mathematics and Computation*, *353*, 243-253. doi: 10.1016/j.amc.2019.02.007.
- Mohd, M. H., Murray, R., Plank, M. J., & Godsoe, W. (2017). Effects of biotic interactions and dispersal on the presence-absence of multiple species. *Chaos, Solitons and Fractals*, *99*, 185-194. doi: 10.1016/j.chaos.2017.04.012.

- Mohd, M. H., Murray, R., Plank, M. J., & Godsoe, W. (2018). Effects of different dispersal patterns on the presence-absence of multiple species. *Communications in Nonlinear Science and Numerical Simulation*, *56*, 115-130. doi: 10.1016/j.cnsns.2017.07.029.
- Mondor, E. B., Rosenheim, J. A., & Addicott, J. F. (2004). Predator-induced transgenerational phenotypic plasticity in the cotton aphid. *Oecologia*, *142*(1), 104-108. doi: 10.1007/s00442-004-1710-4.
- Morales, M. A. (2000). Mechanisms and density dependence of benefit in an ant–membracid mutualism. *Ecology*, *81*(2), 482-489. doi: 10.1890/0012-9658(2000)081[0482:MADDOB]2.0.CO;2.
- Ojonubah, J. O., & Mohd, M. H. (2020). Impacts of asymmetric biotic interactions and environmental factors on the presence-absence of multispecies. *Pertanika Journal of Science and Technology*, *28*(1), 245-261.
- Parker, M. A. (1999). Mutualism in metapopulations of legumes and rhizobia. *The American Naturalist*, *153*(S5), S48-S60. doi: 10.1086/303211.
- Pascual-García, A., & Bastolla, U. (2017). Mutualism supports biodiversity when the direct competition is weak. *Nature Communications*, *8*(1), 1-13. doi: 10.1038/ncomms14326
- Poethke, H. J., Weisser, W. W., & Hovestadt, T. (2010). Predator-induced dispersal and the evolution of conditional dispersal in correlated environments. *The American Naturalist*, *175*(5), 577-586. doi: 10.1086/651595.
- Quinn, T. P., Cunningham, C. J., & Wirsing, A. J. (2016). Diverse foraging opportunities drive the functional response of local and landscape-scale bear predation on Pacific salmon. *Oecologia*, *183*(2), 415-429. doi: 10.1007/s00442-016-3782-3.
- Rosenzweig, M. L. (1971). Paradox of enrichment: Destabilization of exploitation ecosystems in ecological time. *Science*, *171*(3969), 385-387. doi: 10.1126/science.171.3969.385.
- Rosenzweig, M. L., & MacArthur, R. H. (1963). Graphical representation and stability conditions of predator-prey interactions. *The American Naturalist*, *97*(895), 209-223. doi: 10.1086/282272.
- Rozhnova, G., Metcalf, C. J. E., & Grenfell, B. T. (2013). Characterizing the dynamics of rubella relative to measles: The role of stochasticity. *Journal of The Royal Society Interface*, *10*(88), 20130643-20130643. doi: 10.1098/rsif.2013.0643.
- Sala, E. (2006). Top predators provide insurance against climate change. *Trends in Ecology and Evolution*, *21*(9), 479-480. doi: 10.1016/j.tree.2006.07.006.
- Schmitt, R. J., & Holbrook, S. J. (2003). Mutualism can mediate competition and promote coexistence. *Ecology Letters*, *6*(10), 898-902. doi: 10.1046/j.1461-0248.2003.00514.x.
- Schmitz, O. J. (2006). Predators have large effects on ecosystem properties by changing plant diversity, not plant biomass. *Ecology*, *87*(6), 1432-1437. doi: 10.1890/0012-9658(2006)87[1432:phleoe]2.0.co;2.
- Soulé, M. E., & Terborgh, J. (1999). Conserving nature at regional and continental scales-a scientific program for North America. *BioScience*, *49*(10), 809-817. doi: 10.2307/1313572.
- Steiner, C. F., Stockwell, R. D., Kalaimani, V., & Aqel, Z. (2013). Population synchrony and stability in environmentally forced metacommunities. *Oikos*, *122*(8), 1195-1206. doi: 10.1111/j.1600-0706.2012.20936.x.

- Swanson, A., Arnold, T., Kosmala, M., Forester, J., & Packer, C. (2016). In the absence of a “landscape of fear”: How lions, hyenas, and cheetahs coexist. *Ecology and Evolution*, *6*(23), 8534-8545. doi: 10.1002/ece3.2569.
- Valdovinos, F. S., Berlow, E. L., Moisset de Espanés, P., Ramos-Jiliberto, R., Vázquez, D. P., & Martínez, N. D. (2018). Species traits and network structure predict the success and impacts of pollinator invasions. *Nature Communications*, *9*(1), 1-8. doi: 10.1038/s41467-018-04593-y.
- Valdovinos, F. S., Brosi, B. J., Briggs, H. M., Moisset de Espanés, P., Ramos-Jiliberto, R., & Martínez, N. D. (2016). Niche partitioning due to adaptive foraging reverses effects of nestedness and connectance on pollination network stability. *Ecology Letters*, *19*(10), 1277-1286. doi: 10.1111/ele.12664.
- Vasseur, D. A., & Fox, J. W. (2009). Phase-locking and environmental fluctuations generate synchrony in a predator–prey community. *Nature*, *460*(7258), 1007-1010. doi: 10.1038/nature08208.
- Vogwill, T., Fenton, A., & Brockhurst, M. A. (2009). Dispersal and natural enemies interact to drive spatial synchrony and decrease stability in patchy populations. *Ecology Letters*, *12*(11), 1194-1200. doi: 10.1111/j.1461-0248.2009.01374.x.
- Wright, D. H. (1989). A simple, stable model of mutualism incorporating handling time. *The American Naturalist*, *134*(4), 664-667. doi: 10.1086/285003.
- Yaari, G., Ben-Zion, Y., Shnerb, N. M., & Vasseur, D. A. (2012). Consistent scaling of persistence time in metapopulations. *Ecology*, *93*(5), 1214-1227. doi: 10.1890/11-1077.1.s.



Revisited the Critical Load Assessment of Huang et al. on Willems Tested Beck Column

Peter Praveen Jakkana^{1*}, Nageswara Rao Boggarapu², Mahaboob Bodanapu¹, Appa Rao Bhogapurapu Venkata¹, Narayana Cherukuri³ and Harnath Yeddala⁴

¹Department of Mathematics, Koneru Lakshmaiah Education Foundation, Vaddeswaram, Guntur, 22502, India

²Department of Mechanical Engineering, Koneru Lakshmaiah Education Foundation, Vaddeswaram, Guntur, 522502, India

³Department of Mathematics, Sri Harsha Institute of P.G Studies, Nellore, Andhra Pradesh, 524137, India

⁴Department of Mathematics, Audhisankara College of Engineering, Gudur, Andhra Pradesh 524101, India

ABSTRACT

Dynamic stability of elastic structures is a fascinating topic. Many researchers have examined the problem theoretically considering a cantilever column under a tip-concentrated tangential load, the so-called Beck column. Experimental verification is demanded since the critical load of Beck column is found to be approximately eight times to that of the classical Euler column. Different types of testing procedures are being adopted to create the follower force. Among them, notable Willems experimentation provides the critical load close to that of Beck column. Investigations made by other researchers indicate the controversy associated with modeling and testing of Willems on Beck column. Such an intriguing problem of structures loaded by non-conservative forces is revisited here through a simple mathematical formulation. This paper confirms the adequacy of Willems approach on Beck column and the wrong critical load assessment of others. It indicates the possibility on the practical realization of follower forces

Keywords: Beck column, coalescence frequency parameter, critical load parameter, dynamic stability, frequency parameter, tip-angle, tip-concentrated tangential load

ARTICLE INFO

Article history:

Received: 20 July 2020

Accepted: 28 September 2020

Published: 22 January 2021

DOI: <https://doi.org/10.47836/pjst.29.1.14>

E-mail addresses:

jprraveen17@kluniversity.in (Peter Praveen Jakkana)

bnrao52@rediffmail.com (Nageswara Rao Boggarapu)

mahaboob@kluniversity.in (Mahaboob Bodanapu)

bvardr2010@kluniversity.in (Appa Rao Bhogapurapu Venkata)

nareva.nlr@gmail.com (Narayana Cherukuri)

yeddala@gmail.com (Harnath Yeddala)

* Corresponding author

INTRODUCTION

Space launch vehicles subjected to aerodynamic (drag) forces acting at the top and along the axis of the vehicle are modeled as columns under compressive

loads. To assess their structural integrity, overall stability analysis will be performed for the flight conditions. After Beck in 1952, the problem of a cantilever column subjected to a follower load at its free-end has been solved adopting different techniques (Anderson & Thomsen, 2002; Langthjem & Sugiyama, 2000a; Langthjem & Sugiyama, 2000b; Rao & Rao, 1989a; Rao & Rao, 1989b; Rao & Rao, 1990; Rao & Rao, 1991; Madhusudan et al., 2003; Zahharov et al., 2004; Kwasniewski, 2010; Mutyalarao et al., 2012). Timoshenko and Gere (2012) had emphasized experimental verification on the critical load of Beck column. Sugiyama et al. (2000), Sugiyama (2002), and Sugiyama et al. (2019) had mounted a solid rocket motor at a free-end of the cantilever column for generating a tip-concentrated sub-tangential follower force and conducted experiments. They had demonstrated the stabilization of the system due to rocket thrust. However, their test results were found to be well below the critical load estimates (Mutyalarao et al., 2017). Tomski and Uzny (2013) had considered a slender system under a conservative load (in which the direction of force was towards the positive pole) and a non-conservative load (generating the Beck's load through a reaction engine), whose investigations were well documented in (Tomski et al., 1998; Tomski et al., 2007; Tomski & Szmidia, 2004; Tomski & Uzny, 2008; Tomski & Uzny, 2010; Tomski & Uzny, 2011). Willems (1966) had adopted a simple procedure to perform experiments. Though the critical load of Willems configuration was close to that of Beck's column, Huang et al. (1967) had presented theoretical analyses of Willems column and Beck column creating difference only in the fourth boundary condition. They recommended that Willems test results were not representing the Beck column. Augusti et al. (1967) had made discussion on the Willems experimental investigations. In his author's closure (Augusti et al., 1967), Willems accepted the difference in the treatment of Beck's problem and his experimentation. He claimed that his experimentation fulfilled the boundary conditions of the Beck's problem. Huang et al. (1967) had created a fourth boundary condition for the Willems column, which provided the same load versus frequency curve for the first mode of the Beck column, whereas for the second mode, the curve cut the load axis instead of coalescing with the first mode curve. Coincidentally, the second mode curve cut the load axis matched with the Willems test results. It should be noted that the fixed point of the column axis at a distance δ from the free end should be same only at the coalescence point, whereas it changed with the load parameter and the frequency parameter. Huang et al. (1967) had considered same δ value in the Willems column for the first and second modes. Due to this reason, the load versus frequency curve matched well with the first mode of the Beck column and differed drastically with the second mode. However, Huang et al. (1967) analysis results with fictitious fourth boundary condition for Willems column created great confusion for many researchers including Willems.

Elishakoff (2005a, 2005b) had stated that Willems experiment was "deposed". The load by the follower force directed towards the pole is not representing the Beck's force (Tomski et al., 1998; Tomski & Uzny, 2008). Motivated by the work of the Willems (1966)

and Huang et al. (1967), a simple mathematical formulation is presented here to resolve the controversy associated with the approach of Willems on applying tangential load to cantilever column at free end.

MATHEMATICAL FORMULATION

Figure 1 shows the deformation of a cantilever column subjected to a tip-concentrated follower load (P) having tip-angle $\phi(0)$. 's' is the length of the deflection curve from the tip. $\phi(s)$ is the angle between the tangent to the deformed column and its vertical axis.

From the moment-curvature ($M - \rho^{-1}$) relationship, Mutyalarao et al. (2017) have presented a system of nonlinear differential equations for large deflections of a cantilever column. They are briefly presented below as Equation 1, 2 and 3 for clarity.

$$\frac{M}{EI} = \frac{1}{\rho} = \frac{d\phi}{ds} \tag{1}$$

Here,

$$M = M_p + M_A + M_T \tag{2}$$

The bending moment produced by the tangential load (M_p), and by the action of inertia forces (M_A, M_T) are as in Equation 3, 4 and 5

$$M_p = -P \cos \phi(0) \times (Y_a - Y) + P \sin \phi(0) \times (X_a - X) \tag{3}$$

$$M_A = \int_0^s m \ddot{u} \{Y(s,t) - Y(\zeta,t)\} d\zeta = -\Omega^2 \int_0^s m \{Y(s,t) - Y(\zeta,t)\} d\zeta \tag{4}$$

$$M_T = \int_0^s m \ddot{v} \{X(s,t) - X(\zeta,t)\} d\zeta = -\Omega^2 \int_0^s m v \{X(s,t) - X(\zeta,t)\} d\zeta \tag{5}$$

E is the Young's modulus of the column material. I is the moment of inertia. L is the column length. m is the mass per unit length of the column. $(u, v) = (X - L + s, Y)$, are the column deflections. (X, Y) are the deformed column coordinates. Harmonic motion assumed for the deflections (u, v) in Equation 4 and 5, which obey Equation 6 and 7

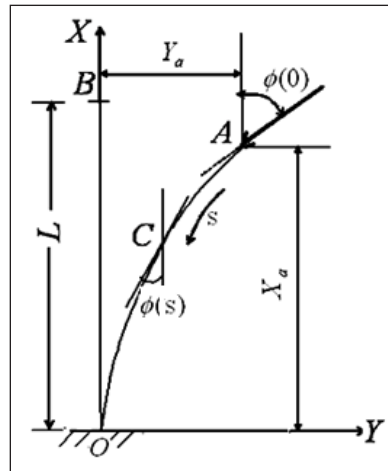


Figure 1. Deformation of a cantilever column subjected to a concentrated Follower load at its free-end (Mutyalarao et al., 2012; Mutyalarao et al., 2017)

$$\ddot{u} + \Omega^2 u = 0 \quad [6]$$

$$\ddot{v} + \Omega^2 v = 0 \quad [7]$$

Ω is the circular frequency and over dots denotes differentiation with respect to time, t . The deformed column coordinates can be obtained from

$$(X, Y) = \int_s^L (\cos \phi, \sin \phi) ds \Rightarrow (x, y) = \left(\frac{X}{L}, \frac{Y}{L} \right) = \int_\eta^1 (\cos \phi, \sin \phi) d\eta \quad [8]$$

Here, $\eta = \frac{s}{L}$. At $s = 0$, Equation 8 gives the column tip-coordinates (X_a, Y_a) .

Equation 1 and 8 are differentiated with respect to s . Defining; $H = \int_0^\eta (1 - \xi - x) d\xi$; $V = \int_0^\mu y d\xi$; load parameter, $\lambda = \frac{PL^2}{EI}$; frequency parameter, $\omega = \Omega L^2 \sqrt{\frac{m}{EI}}$, the governing equations are written in non-dimensional form as Equation 9, 10, 11, 12 and 13 (Mutyalarao et al., 2012; Mutyalarao et al., 2017)

$$\phi'' + \lambda \sin(\phi - \phi(0)) + \omega^2 (H \sin \phi + V \cos \phi) = 0 \quad [9]$$

$$H' - (1 - \eta - x) = 0 \quad [10]$$

$$V' - y = 0 \quad [11]$$

$$x' + \cos \phi = 0 \quad [12]$$

$$y' + \sin \phi = 0 \quad [13]$$

The boundary conditions for Equation 9 - 13 are as in Equation 14 and 15

$$\phi = \phi(0), \phi' = H = V = 0 \text{ at } \eta = 0 \quad [14]$$

$$\phi = x = y = 0 \quad \eta = 1 \quad [15]$$

Primes denote differentiation with respect to η . Following Willems (1966), the tangent at the free end of the deformed column in Figure 1 makes the angle $\phi(0)$, which can be related to Equation 16

$$\tan \phi(0) = \frac{Y_a}{X_a - (L - \delta)} \quad [16]$$

Here δ is the distance from the tip of the un-deformed column to the point where the tangent line at the free end of the deformed column intersects the column axis. In case of small deflections (i.e., $\phi \rightarrow 0$), $\cos \phi \approx 1$ and $\sin \phi \approx \phi$. Equation 8 gives $X(s) = L - s \Rightarrow X_a = L$ and Equation 16 becomes Equation 17

$$\phi(0) = \frac{Y_a}{\delta} \Rightarrow \delta = \frac{Y_a}{\phi(0)} \Rightarrow \frac{\delta}{L} = \frac{Y_a}{L\phi(0)} = \frac{y_a}{\phi(0)} \quad [17]$$

Defining $\tilde{y} = \frac{y}{\phi(0)}$, the nonlinear differential Equation 9 - 15 for small deflections are in the form of Equation 18

$$\tilde{y}^{iv} + \lambda \tilde{y}'' - \omega^2 \tilde{y} = 0 \quad [18]$$

The boundary conditions for Equation 18 arrived are as in Equation 19 and 20

$$\tilde{y}' = -1, \tilde{y}'' = \tilde{y}''' = 0 \text{ at } \eta = 0 \quad [19]$$

$$\tilde{y} = \tilde{y}' = 0 \text{ at } \eta = 1 \quad [20]$$

The general solution of the Equation 18 is Equation 21

$$\tilde{y}(\eta) = A \cosh(\lambda_1 \eta) + B \sinh(\lambda_1 \eta) + C \cos(\lambda_2 \eta) + D \sin(\lambda_2 \eta) \quad [21]$$

Here (Equation 22 and 23),

$$\lambda_1 = \sqrt{-0.5\lambda + \sqrt{\omega^2 + 0.25\lambda^2}} \quad [22]$$

$$\lambda_2 = \sqrt{0.5\lambda + \sqrt{\omega^2 + 0.25\lambda^2}} \quad [23]$$

From Equation 19 and 21, one obtains Equation 24, 25 and 26

$$\lambda_1 B + \lambda_2 D = -1 \quad [24]$$

$$\lambda_1^2 A - \lambda_2^2 C = 0 \Rightarrow C = \lambda_1^2 \lambda_2^{-2} A \quad [25]$$

$$\lambda_1^3 B - \lambda_2^3 D = 0 \Rightarrow D = \lambda_1^3 \lambda_2^{-3} B \quad [26]$$

Using Equation 20, 21, 25 and 26 one obtains Equation 27 and 28

$$(\sinh \lambda_1 - \lambda_1 \lambda_2^{-1} \sin \lambda_2)A + (\cosh \lambda_1 + \lambda_1^2 \lambda_2^{-2} \cos \lambda_2)B = 0 \quad [27]$$

$$(\cosh \lambda_1 + \lambda_1^2 \lambda_2^{-2} \cos \lambda_2)A + (\sinh \lambda_1 + \lambda_1^3 \lambda_2^{-3} \sin \lambda_2)B = 0 \quad [28]$$

From Equation 27 and 28, the transcendental equation relating λ and ω is in the form $(\sinh \lambda_1 - \lambda_1 \lambda_2^{-1} \sin \lambda_2)(\sinh \lambda_1 + \lambda_1^3 \lambda_2^{-3} \sin \lambda_2) - (\cosh \lambda_1 + \lambda_1^2 \lambda_2^{-2} \cos \lambda_2)^2 = 0$, which can be further simplified to Equation 29

$$\lambda^2 + 2\omega^2(1 + \cosh \lambda_1 \cos \lambda_2) + \lambda\omega \sinh \lambda_1 \sin \lambda_2 = 0 \quad [29]$$

Equation 29 is solved for ω by specifying λ using the Mathematica®.

Using Equation 24 - 28, one can find the arbitrary constants A, B, C and D in Equation 21. From Equation 17, one can find Equation 30

$$\frac{\delta}{L} = \frac{y_a}{\phi(0)} = \frac{y(0)}{\phi(0)} = \tilde{y}(0) = A + C = A(1 + \lambda_1^2 \lambda_2^{-2}) = \frac{\lambda_2^3 \sinh \lambda_1 + \lambda_1^3 \sin \lambda_2}{\omega(\lambda_2^2 \cosh \lambda_1 + \lambda_1^2 \cos \lambda_2)} \quad [30]$$

Following Mutyalarao et al. (2017), stability of the column is assessed from λ versus ω eigencurve. Critical load parameter (λ_c) is a minimum value where the eigencurve cuts the λ -axis. The dynamic stability load is the minimum load where two branches of eigencurve coalesce. A simple procedure is presented below for generating the eigencurves from the first two frequency parameters (ω_1 and ω_2) specifying the load parameter (λ). Setting $\lambda = 0$ in Equation 29, ω_1 and ω_2 are found for the unloaded column. The eigencurves are generated considering the first two frequencies by specifying the values of λ varying from 0 in steps of 1. When λ value is reached to 21, Mathematica® provides bifurcated frequency values. Each time, the step size is reduced to half for obtaining the frequency values prior to the bifurcation load parameter. At $\lambda_c = 20.0509$, the two positive frequency values are tending to the coalescing frequency parameter (ω_c) value of 11.011. Variation of λ with ω is shown in Figure 2. Figure 3 shows variation of δ/L with λ . It should be noted that the results are presented in non-dimensional form for the non-dimensional load parameter (λ) and frequency parameters (ω_1 and ω_2) useful for any specified column dimensions and material.

For the specific λ , Figure 2 gives the first two frequency parameters (ω_1, ω_2). Hence Figure 3 shows two δ/L values for each value of λ . At the coalescence frequency ω_c these two values of δ/L are identical. It is noted from Figure 3 that δ/L should be 0.42312. λ versus ω curve shown in Figure 2 closely matches to that of Huang et al. (1967) for the Beck column. For the specific λ , the frequencies (ω_1 and ω_2) and δ/L are obtained from

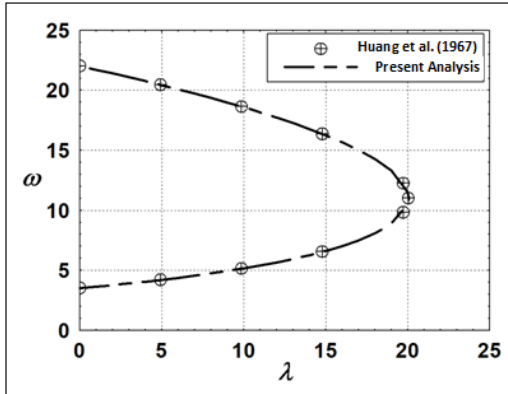


Figure 2. Variation of λ with ω

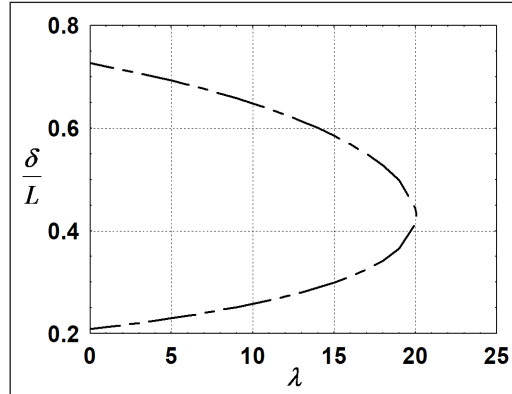


Figure 3. Variation of δ/L with λ

Equation 29 and 30. Table 1 gives the comparison of present analysis results with those of Willems (1966).

Values of δ for the specific λ and ω_1 in Table 1 are reasonably in good agreement with those of Willems (1966). However, the transcendental Equation 29 for the specific λ , gives slightly different ω_1 and ω_2 . This is the reason why δ values of Willems (1966) in Table 1 slightly differ from the present analysis results. Figure 4 and 5 show the first and second mode shapes generated from Equation 21 for the unloaded column ($\lambda = 0$) and for the specific λ and the corresponding ω_1 and ω_2 . Figure 4 and 5 clearly indicate different mode shapes due to different frequencies (ω_1 and ω_2 for the same load parameter (λ)). In case of critical load parameter (λ_c), these two frequencies (ω_1 and ω_2) tend to ω_c . Hence, the first and second mode shapes in Figure 6 are identical, which result the same δ/L .

Willems (1966) had used only the boundary conditions of the Beck column to arrive δ for the applied the load (P). A slight impact was given to the column and observed vibrations of a stable character (when P is less than the critical load) and damped out. Vibrations caused excessive amplitudes resulting in failure at the critical load. For the

Table 1
Comparison of frequencies (ω_1 and ω_2) and δ for the specified λ

$\frac{\lambda}{\pi^2}$	First Mode				Second Mode		
	λ	ω_1	δ/L		λ	ω_2	δ/L
			Present Analysis	Willems (1966)			
0	0	3.5160	0.7265	0.727	0	22.0344	0.2092
0.5	4.9348	4.2071	0.6931	0.750	4.9348	20.4578	0.2296
1.0	9.8696	5.1461	0.6496	0.676	9.8696	18.6395	0.2570
1.5	14.8044	6.5545	0.5884	0.585	14.8044	16.3664	0.2977
2.0	19.7392	9.8282	0.4665	0.464	19.7392	12.2545	0.3936
2.0315	20.0509	11.01	0.4252	-----	20.0509	11.01	0.4252

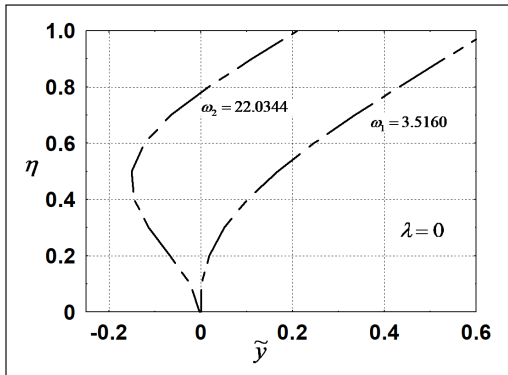


Figure 4. Mode shapes for the unloaded cantilever column

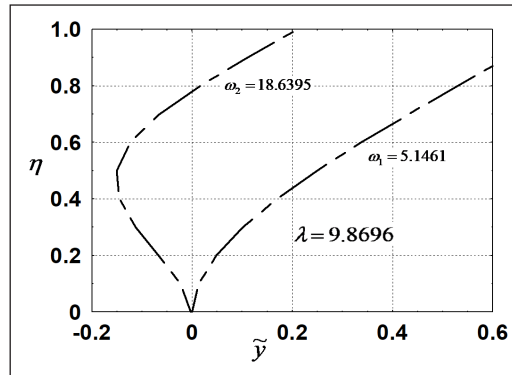


Figure 5. Mode shapes for the loaded cantilever column

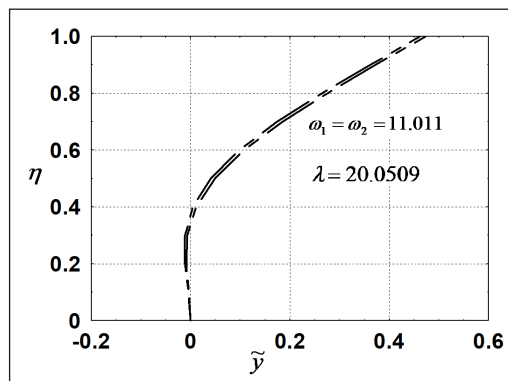


Figure 6. Mode shapes for the critically loaded cantilever column

steel column of size $304.8 \times 7.62 \times 2.54$ mm, the critical load parameter reported by Willems (1966) was 18.61, whereas the present analysis was 20.05. The discrepancy in the results might be due to inaccurate calculations of δ by Willems (1966), mass and stiffness of the column. However, Willems (1966) experimental results are within 7% of the analysis results. It should be noted from Willems (1966) that Willems had concentrated on the critical load alone. The fast camera might had been used to capture the individual displacement stages of column during flutter phenomena. The eigencurve of the first frequency obtained by Willems (1966) and that of the Beck column were same. The upper curve of δ in Figure 3 corresponds to λ and ω_1 , whereas the lower curve of δ corresponds to λ and ω_2 . For the case of λ_c and ω_c , δ value is $0.423L$. By imposing correctly, the passage through this fixed point yield λ_c .

The curvilinear coordinate system simplifies the complexity of the mathematical formulation for large deflections. The above small deflection analysis results are obtained by specifying the tip-angle $\phi(0)$ as 0.01° and solving Equation 9 - 15. Being a non-linear

nature of the problem, it has to be solved numerically. As in Mutyalarao et al. (2013), the post-critical load parameter (λ_c), coalesce frequency parameter ω_c , and the tip- coordinates of the Beck column as in Equation 31:

$$(x_a, y_a) = \left(\frac{X_a}{L}, \frac{Y_a}{L} \right) \tag{31}$$

for different values of the tip-angle $\phi(0)$ are evaluated numerically by solving the nonlinear differential Equation 9 - 15 using the fourth-order Runge-Kutta integration scheme. The boundary value problem is converted to an initial value problem adopting shooting method. For large deflection analysis, Equation 16 can be written as Equation 32

$$\tan \phi(0) = y_a \left\{ x_a - 1 + \frac{\delta}{L} \right\}^{-1} \tag{32}$$

which implies as in Equation 33

$$\frac{\delta}{L} = \frac{y_a}{\tan \phi(0)} - x_a + 1 \tag{33}$$

Using Equation 33, δ is computed and values are presented in Table 2. It is noted that δ increases marginally with increasing the tip-angle $\phi(0)$. From the above observations, one can conclude that Willems has considered in his experimentation only the Beck column.

Table 2
Post-critical load parameter (λ_c) for the specific tip-angle, $\phi(0)$

$\phi(0)$ (degree)	λ_c	ω_c	x_a	y_a	δ / L Eq. (33)
10	20.1888	11.0294	0.9944	0.0747	0.4292
20	20.1623	11.0634	0.9776	0.1484	0.4301
30	21.3529	11.1211	0.9499	0.2201	0.4313
40	22.4690	11.2269	0.9117	0.2887	0.4323
50	24.0584	11.3828	0.8636	0.3534	0.4329
60	26.2815	11.6238	0.8062	0.4128	0.4321

CONCLUSION

Dynamic stability of elastic structures is a fascinating topic, which is being examined theoretically by many researchers considering a cantilever column under a tip-concentrated tangential load. The load versus frequency curve is essential for assessing the dynamic stability of such columns. Timoshenko and Gere (2012) had emphasized experimental validation since the critical load was found to be approximately eight times to that of the

classical Euler column. Different types of testing procedures are followed to create the follower force. Among them, notable Willems (1966) experimentation provided the critical load close to that of Beck column. But, Huang et al. (1967) had specified wrong input in the analysis and drawn wrong conclusions on Willems experimentation, which had created great confusion for many researchers including Willems in 1966 (Augusti et al., 1967).

This paper resolves the controversy associated with the Willems experiments on the stability of Beck column through a simple mathematical modeling. It should be noted that Willems (1966) had aimed only on the critical load of the column and demonstrated its value close to that of the Beck column. Use of the fast camera in Willems experimentation might have captured the individual displacement stages of column during flutter phenomena. Large deflection analysis results indicate marginal increase in δ with increasing the tip-angle $\phi(0)$. Equation 16 can be used to obtain the position of the point of intersection corresponding to the critical load for small as well as large deflections of the cantilever column subjected to a tip-concentrated follower load.

The controversial articles of Koiter (1996) and Sugiyama et al. (1998) on unrealistic and realistic follower forces remains a matter of debate (Mascolo, 2019). The problem in such cases is in the practical realization of follower forces (Bolotin, 1963; Elishakoff, 2005b). Mullagulov (1994) had successfully created follower forces and performed tests. Approaches of Willems (1966) and Mullagulov (1994) confirmed the demands of Koiter (1996) on experimental validation of Beck column for the practical realization of follower forces.

ACKNOWLEDGEMENT

The authors are grateful to the reviewers for their constructive criticism to improve the clarity of presenting the work in the paper and the journal for encouragement.

REFERENCES

- Anderson, S. B., & Thomsen, J. J. (2002). Post-critical behavior of Beck's column with a tip mass. *International Journal of Nonlinear Mechanics*, 37(1), 135-151. doi: [https://doi.org/10.1016/S0020-7462\(00\)00102-5](https://doi.org/10.1016/S0020-7462(00)00102-5)
- Augusti, G., Roorda, J., Herrmann, G., & Levinson, M. (1967). Discussion: Experimental verification of the dynamic stability of a tangentially cantilever column. *Transactions of ASME Journal of Applied Mechanics*, 34(2), 523-524. doi: <https://doi.org/10.1115/1.3607729>
- Bolotin, V. V. (1963). *Non-conservative problems of the theory of elastic stability*. New York, NY: Macmillan.
- Elishakoff, I. (2005a). Essay on the contributors to the elastic stability theory. *Meccanica*, 40(1), 75-110. doi: <https://doi.org/10.1007/s11012-004-2199-y>
- Elishakoff, I. (2005b). Controversy associated with the so-called 'Follower Forces': Critical overview. *Applied Mechanics Reviews*, 58(2), 117-142. doi: <https://doi.org/10.1115/1.1849170>

- Huang, N. C., Nachabar, W., & Nemat-Nasser, S. (1967). On Willems' experimental verification of the critical load in Beck's problem. *Transactions of ASME Journal of Applied Mechanics*, 34(1), 243-245. doi: <https://doi.org/10.1115/1.3607646>
- Koiter, W. T. (1996). Unrealistic follower forces. *Journal of Sound and Vibration*, 194(4), 636-638. doi: <https://doi.org/10.1006/jsvi.1996.0383>
- Kwasniewski, L. (2010). Numerical verification of post-critical Beck's column behavior. *International Journal of Nonlinear Mechanics*, 45(3), 242-255. doi: <https://doi.org/10.1016/j.ijnonlinmec.2009.11.007>
- Langthjem, M. A., & Sugiyama, Y. (2000a). Optimum design of cantilevered columns under the combined action of conservative and non-conservative loads, Part-I: The undamped case. *Computers and Structures*, 74(4), 385-398. doi: [https://doi.org/10.1016/S0045-7949\(99\)00050-4](https://doi.org/10.1016/S0045-7949(99)00050-4)
- Langthjem, M. A., & Sugiyama, Y. (2000b). Dynamic stability of columns subjected to follower loads: A survey. *Journal of Sound and Vibration*, 238(5), 809-851. doi: <https://doi.org/10.1006/jsvi.2000.3137>
- Mascolo, I. (2019). Recent developments in the dynamic stability of elastic structures. *Frontiers in Applied Mathematics and Statistics*, 5, 1-16. doi: 10.3389/fams.2019.00051.
- Madhusudan, B. P., Rajeev, V. R., & Rao, B. N. (2003). Post-buckling of cantilever columns having variable cross-section under a combined load. *International Journal of Non-Linear Mechanics*, 38(10), 1513-1522. doi: [https://doi.org/10.1016/S0020-7462\(02\)00086-0](https://doi.org/10.1016/S0020-7462(02)00086-0)
- Mutyalarao, M., Bharathi, D., & Rao, B. N. (2012). Dynamic stability of cantilever columns under a tip-concentrated sub tangential follower force. *Mathematics and Mechanics of Solids*, 18(5), 449-463. doi: <https://doi.org/10.1177/1081286512442436>
- Mutyalarao, M., Bharathi, D., Narayana, K. L., & Rao, B. N. (2017). How valid are Sugiyama's experiments on follower forces? *International Journal of Non-linear Mechanics*, 93, 122-125. doi: <https://doi.org/10.1016/j.ijnonlinmec.2014.12.007>
- Mullagulov, M. K. (1994). Experimental-theoretical study of the stability of rods, compressed by follower forces. *Strength of Materials*, 26(6), 441-446. doi: <https://doi.org/10.1007/BF02209415>
- Rao, B. N., & Rao, G. V. (1989a). Post-critical behaviour of a uniform cantilever column under a tip concentrated follower force. *Journal of Sound and Vibration*, 132(2), 350-352.
- Rao, B. N., & Rao, G. V. (1989b). Some studies on buckling and post-buckling of cantilever columns subjected to conservative or non-conservative loads. *The Journal of the Aeronautical Society of India*, 41(2), 165-182.
- Rao, B. N., & Rao, G. V. (1990). Stability of tapered cantilever columns subjected to a tip concentrated sub tangential follower force. *Forschung Im Ingenieurwesen*, 56(3), 93-96.
- Rao, B. N., & Rao, G. V. (1991). Post-critical behaviour of a tapered cantilever column subjected to a tip-concentrated follower force. *Journal of Applied Mathematics and Mechanics*, 71(11), 471-473. doi: <https://doi.org/10.1002/zamm.19910711116>
- Sugiyama, Y., Langthjem, M. A., & Ryu, B. J. (1998). Realistic follower forces. *Journal of Sound and Vibration*, 225(4), 779-782.

- Sugiyama, Y., Katayama, K., & Kiriyama, K. (2000). Experimental verification of dynamic stability of vertical cantilever columns subjected to a sub-tangential force. *Journal of Sound and Vibration*, 236(2), 193-207. doi: <https://doi.org/10.1006/jsvi.1999.2969>
- Sugiyama, Y. (2002). Experimental approach to non-conservative stability problems. In A. P. Seyranian & I. Elishakoff (Eds.), *Modern problems of structural Stability* (pp. 341-394). Vienna, Austria: Springer. doi: 10.1007/978-3-7091-2560-1
- Sugiyama, Y., Langthjem, M. A., & Katayama, K. (2019). *Dynamic stability of columns under non-conservative forces: Theory and experiments*. Cham, Switzerland: Springer International Publishing. doi: 10.1007/978-3-030-00572-6
- Timoshenko, S. P., & Gere, J. M. (2012). *Theory of elastic stability*. New Delhi, India: Tata Mc Graw-Hill Education Private Limited.
- Tomski, L., Przybylski, J., Golebiowska-Rozanow, M., & Szmidla, J. (1998). Vibration and stability of a cantilever column subject to a follower force passing through a fixed point. *Journal of Sound and Vibration*, 214(1), 67-81. doi: <https://doi.org/10.1006/jsvi.1998.1528>
- Tomski, L., & Szmidla, J. (2004). Theoretical and experimental investigations of the natural vibrations of the divergence and divergence pseudoflutter type systems. In *PAMM: Proceedings in Applied Mathematics and Mechanics* (Vol. 4, No. 1, pp. 418-419). Berlin, Germany: WILEY-VCH Verlag.
- Tomski, L., Szmidla, J., & Uzny, S. (2007). The local and global instability and vibration of systems subjected to non-conservative loading. *Thin-Walled Structures*, 45(10-11), 945-949. doi: <https://doi.org/10.1016/j.tws.2007.08.019>
- Tomski, L., & Uzny, S. (2008). Free vibrations and the stability of a geometrically non-linear column loaded by a follower force directed towards the positive pole. *International Journal of Solids and Structures*, 45(1), 87-112. doi: <https://doi.org/10.1016/j.ijsolstr.2007.07.011>
- Tomski, L., & Uzny, S. (2010). Chosen slender systems in aspect of possibility of specific load realization. *Vibrations in Physical Systems*, 24, 429-434.
- Tomski, L., & Uzny, S. (2011). The regions of flutter and divergence instability of a column subjected to Beck's generalized load, taking into account the torsional flexibility of the loaded end of the column. *Mechanics Research Communications*, 38(2), 95-100. doi: <https://doi.org/10.1016/j.mechrescom.2011.01.013>
- Tomski, L., & Uzny, S. (2013). Free vibrations and stability of a new slender system subjected to a conservative or nonconservative load. *Journal of Engineering Mechanics*, 139(8), 1133-1148. doi: [https://doi.org/10.1061/\(ASCE\)EM.1943-7889.0000463](https://doi.org/10.1061/(ASCE)EM.1943-7889.0000463)
- Willems, N. (1966). Experimental verification of the dynamic stability of a tangentially loaded cantilever column. *Transactions of ASME Journal of Applied Mechanics*, 33(2), 460-461. doi: <https://doi.org/10.1115/1.3625073>
- Zakharov, Y. V., Okhotkin, K. G., & Skorobogatov, A. D. (2004). Bending of bars under a follower load. *Journal of Applied Mechanics and Technical Physics*, 45(5), 756-763. doi: <https://doi.org/10.1023/B:JAMT.0000037975.91152.01>

Modelling High Dimensional Paddy Production Data using Copulas

Nuranisyha Mohd Roslan¹, Wendy Ling Shinyie^{1*} and Sim Siew Ling²

¹*Department of Mathematics, Faculty of Science, Universiti Putra Malaysia, 43400 UPM, Serdang, Selangor, Malaysia*

²*School of Business and Management, University College of Technology Sarawak, Jalan Universiti, 96000 Sibu Sarawak, Malaysia*

ABSTRACT

As the climate change is likely to be adversely affecting the yield of paddy production, thence it has brought a limelight of the probable challenges on human particularly regional food security issues. This paper aims to fit multivariate time series of paddy production variables using copula functions and predicts the next year event based on the data of five countries in southeast Asia. In particular, the most appropriate marginal distribution for each univariate time series was first identified using maximum likelihood parameter estimation method. Next, we performed multivariate copula fitting using two types of copula families, namely, elliptical copula family and Archimedean copula family. Elliptical copula family studied are normal and t copula, while Archimedean copula family considered are Joe, Clayton and Gumbel copulas. The performance of marginal distribution and copula fitting was examined using Akaike information criterion (AIC) values. Finally, we used the best fitted copula

model to forecast the succeeding event. In order to assess the performance of copula function, we computed the forecast means and estimation errors of copula function with a generalized autoregressive conditional heteroskedasticity model as reference group. Based on the smallest AIC, the majority of the data favoured the Gumbel copula, which belongs to Archimedean copula family as well as extreme value copula family. Likewise, applying the historical data to forecast the future trends may assist

ARTICLE INFO

Article history:

Received: 28 September 2020

Accepted: 17 November 2020

Published: 22 January 2021

DOI: DOI: <https://doi.org/10.47836/pjst.29.1.15>

E-mail addresses:

aliakisyah9731@gmail.com (Nuranisyha Mohd Roslan)

sy_ling@upm.edu.my (Wendy Ling Shinyie)

simsiewling@ucts.edu.my (Sim Siew Ling)

* Corresponding author

all relevant stakeholders, for instance government, NGO agencies, and professional practitioners in making informed decisions without compromising the environmental as well as economical sustainability in the region.

Keywords: Archimedean copula family, dependence structure, elliptical copula family, paddy production

INTRODUCTION

Paddy is an essential crop and a staple food for more than half of the universal population. Particularly nearly 90% of the world's paddy production likewise consumption takes place in Asia (Bandumula, 2017). Abreast of the heedfulness about global climate change whereby scrutinising the Intergovernmental Panel on Climate Change (IPCC) most recently released report has articulated that the agricultural products' yields are highly correlated with atmospheric indicators, wherein the extreme whether such as droughts and flooding would eventuate grievous repercussion on the livelihood of small scale farmers particularly in Southeast Asia region (IPCC, 2019). An accelerating temperature due to the shifting of climate pattern could resultant in the decline of crop yields which may eventually shed the limelight on the shortage of global food supply. Subsequently, it may trigger food security issue wherein on the grounds of the estimated world population which is envisioned to be 9.7 billion in the next three decades despite the projection indicating a stagnant growth ever since 1950 (United Nations, 2019).

The variability of climatic factors such as total rainfall and maximum temperature has direct impacts on paddy productivity, as the extreme weather such as flood and drought can retard normal growth and grain yield (Nyang'au et al., 2014). For instance, El Nino affects the components of grain production ranging from cropping area (area planted) as well as cropping intensity (volume of production per year) in Southern Asian regions. Furthermore, the importance of soil fertility on paddy production has been well validated in previous literature whereby the farming practices in maintaining adequate input such as fertilizer is important to ensure good quality of crop (Putri et al., 2019).

In ASEAN countries, there is approximately 46.171 million (M) ha of paddy planted area in 2019 (ASEAN Food Security Information System, 2019). The largest area is found in Indonesia (10.290 M ha), followed by Thailand (11.356 M ha), Vietnam (7.478 M ha), Myanmar (7.228 M ha) and Malaysia (0.700 M ha). In general, the cultivation of paddy in Southeast Asian consists of three main systems which are (i) upland or so called as aerobic rice that is planted in dry fields; (ii) lowland rice which farmed in irrigated field for the most part of the crop growing period; and (iii) floating rice that is grown in water depths between 0.5-4.5 m (Muhammad, & Abdullah, 2013). Although approximately 55 percent of the paddy production in Southeast Asia is cultivated using floating rice system, yet the rest (i.e. upland and lowland) is highly dependent on the timely and consistent rainfall particularly during the reproductive growth stage (USDA, 2015). In term of the fertilizer

usage, Vietnam recorded the highest increment in fertilizer consumption (15.1%), followed by Myanmar (12.2%), Thailand (6.2%), Indonesia (4.6%), and Malaysia (3.7%) in the interval period of 1990-1999 (Mutert & Fairhurst, 2002).

Agriculture is a crucial economic sector that contributed approximately \$3 trillion real global gross domestic production (GDP) in 2017 (Food and Agriculture Organisation, 2019). However, Hsiang et al. (2017) had revealed the simulation findings about the likelihood of global GDP to shrink in between one to three percent every year if the global warming issue persisted beyond the 21st century. A recent publication of OECD divulges that the trading volume amongst ASEAN countries merely comprises 2% of their regional yielding despite the fact that greater extent of integration between the territorial rice market can improve the malnourishment plight by 1% and even up to 6% when there are constraints in production factors (OECD, 2018).

While contemplating the level of production of paddy in 2018, the top four ranking ASEAN countries comprise Indonesia (83,037,000 tons), Vietnam (44,046,250 tons), Thailand (32,190,090 tons), and Myanmar (25,418,140 tons) while Malaysia is merely producing 2,718,990 tons (Moore, 2020). Though an observation of a declining trend apropos the consumption of table rice in some countries such as Japan and South Korea due to the diversification of choice for caloric diets, yet such incident does not betide in Malaysia wherein rice ingestion has reached triple times or more in comparison with other sources of carbohydrate such as wheat over the past four decades (OECD, 2020; Khazanah Research Institute, 2019). Thenceforth, this study has included Malaysia as one of study countries on the ground that the adverse weather condition has further reduced the paddy production along with the restricted paddy harvested area due peninsular geographical landscape. However, based on past research, the paddy harvested area had declined by 2.7% on year over year (y-o-y) in 2019 as compared to year 2018. This has made Malaysia a net importer of rice in spite of improving in paddy yield ensuing of enhancement of seed variability (ASEAN Food Security Information System, 2019).

The extraction statistics from the similar report in year 2019 manifesting that even with an upsurge of paddy planted area in countries such as Indonesia (y-o-y increment of 6.90%) and Vietnam (y-o-y increment of 0.93%), after all the paddy yield has not improved accordingly i.e. Indonesia (y-o-y declined by 1.36%) and Vietnam (y-o-y fallen by 0.17%). Nearly 80% of destructed paddy planted plots in ASEAN have been affected by adverse climate conditions, for an illustration purpose, a shrinkage of harvested area (y-o-y decreased by 0.86%) has slumped Thailand's paddy production by 2.33%, wherewith approximately 187,118 hectares and 364,773 hectares of paddy area have been damaged by flood and drought respectively (ASEAN Food Security Information System, 2019). Almost all of the paddy cultivation grown in irrigated and rainfed lowland, the aquatic environment has been further impelled the importance of having proper nutrient management as inefficient utilisation of fertilizer may constraint the grain yield (Singh & Singh, 2017).

This study intends to furnish the policy maker with intuitiveness about how the variability of condition such as rice area, fertilizer usage, total annual average rainfall and highest average temperature could affect the paddy production in the key rice producing ASEAN nations expressly Indonesia, Vietnam, Thailand, Myanmar and Malaysia with the interval between 1961 and 2014. Likewise, applying the historical data to forecast the future trends may assist all relevant stakeholders, for instance government, NGO agencies, and professional practitioners in making informed decisions without compromising the environmental as well as economical sustainability in the region. On the whole, the database is retrieved from well-organised, international repositories namely World Bank climate data portal and *ricepedia*.

The objective of this study is to compare and determine the best copula for modelling the paddy production variables, which are paddy production ('000 ton), planted area ('000 hectare), fertilizer used ('000 ton), total annual average rainfall (mm) and maximum average temperature (°C). This analysis was employed for five countries in South East Asia, i.e. Malaysia, Thailand, Indonesia, Vietnam and Myanmar. In particular, ten univariate distributions were fitted to each variable and the distribution with minimal Akaike information criterion (AIC) value would be selected for copula modelling. Two copulas from elliptical copula family and three copulas from Archimedean copula family were selected for statistical modelling of five variables. The copula which give consistent results, namely, the copula that provide smallest AIC values for all five countries, will be proposed as guidelines for practitioners in the paddy industry. Paddy planting has been the main economic activity of the rural community in ASEAN countries, hence the dependence modelling findings in this study aim to provide an efficient tool in order to increase the production and income generation for farmers and also to provide sufficient grains for the nations.

MATERIALS AND METHODS

Study Area and Data

This research focused on five variables, which were, paddy production, planted area, fertilizer usage, total annual average rainfall and maximum average temperature collected from Malaysia, Thailand, Indonesia, Vietnam, and Myanmar. The data variables used in this study were from year 1961 to 2013, which were collected from *ricepedia* and World Bank climate data portal. In this study, our main interest was paddy production. The other four variables were the factors that might affect the production. Paddy planted area is positively related with the production. Water and nutrients are important to improve aerobic conditions and support the yields. Although the optimum weather for paddy cultivation is in tropical countries, which is between 25-35°C, higher temperature will reduce the weight and quality of paddy produced. Hence, we would like to use copula functions to analyse the effects of these variables on paddy production.

Marginal Distributions

Copula is a multivariate probability distribution function for two or more variables, and their marginal probability distribution are uniformly distributed on the interval $[0,1]$. Most researchers have opted probability distribution functions as the marginal distributions, rather than using empirical distribution function. The plausible elucidation is the restrictions that may encountered when using empirical distributions i.e. they are relatively inefficient as they require actual values of probability to describe the full distribution and they are incapable to estimate the distribution of higher amplitudes in the long term (Sørensen, 2011). The main advantage of copula is that the marginal distribution can come from different distribution families and there is no need to assume a specific distribution to model the data. Therefore, for this research, we examined the most suitable probability distribution function for each variable using continuous probability distributions. Since there was no single suitable probability distribution for all countries and variables, we would examine the performance of fitting for ten probability distributions, namely, exponential, gamma, Weibull, Pareto, Gumbel, Laplace, normal, inverse Gaussian, log normal and logistic distributions. The marginal parameters would be estimated using maximum likelihood method. The Akaike information criterion (AIC) values would be identified and compared to select the most suitable univariate distribution for each variable. A smaller value of AIC indicates a better fit.

Copula Theory

Copulas are models for the dependence between two or more random variables when their joint distribution function is not explicitly known. The fundamental theorem of copulas states that, with F be a d -dimensional cumulative distribution function with marginal distributions $F_i, i = 1, \dots, d$. This exists a unique decomposition $F(x_1, \dots, x_d) = C(F_1(x_1), \dots, F_d(x_d))$ and the copula

$$C(u_1, \dots, u_d) = P(U_1 \leq u_1, \dots, U_d \leq u_d), \quad U_i \equiv F_i(X_i)$$

on $[0,1]^d$ which comprises the information on the underlying dependence structure.

Types of Copulas Used

In this study, we would focus on two families of parametric copulas, which are:

Elliptical Copula Family. Normal and t -distribution are the two most commonly used univariate distributions whereby through the incorporation of Sklar's theorem, the bivariate and multivariate elliptical copula family had been constructed (Fouque & Zhou, 2008; Luo & Shevchenko, 2012). Elliptical copula family has been substantially employed by keeping

the identical elliptical copula function and varying the marginal distributions (Okhrin et al., 2017). The main advantage of elliptical copula family is that different levels of correlation between the marginals can be specified, however, elliptical copula family does not have closed form expressions and are restricted to have radial symmetry.

(a) Normal copula

The normal copula with correlation matrix Σ is defined as

$$C(u_1, \dots, u_d) = \Phi_{\Sigma}(\Phi^{-1}(u_1), \dots, \Phi^{-1}(u_d))$$

With Φ is denoted as the cumulative distribution function of the standard normal variable and Φ^{-1} signifies as its inverse.

(b) *t* copula

According to Okhrin et al. (2017), the *t* copula with correlation matrix Σ is defined as

$$C(u_1, \dots, u_d) = \int_0^1 \Phi_{\Sigma}(z_1(u_1, s), \dots, z_d(u_d, s)) ds$$

where Φ as the cumulative distribution function of the standard normal variable and $z_i(u_i, s) = t_{v_i}^{-1}(u_i)/G_{v_i}^{-1}(s)$, with t_v^{-1} denotes the inverse for cumulative distribution function of a Student's *t* variable with degree of freedom *v* and G_v^{-1} denote the inverse for cumulative distribution function of $\sqrt{v/\chi_v^2}$.

Archimedean Copula Family. Archimedean copula family is one of the most popular copula family that has been extensively employed. This is mainly because most of the copulas in Archimedean copula family admit an explicit formula, while the elliptical copula family does not comply. Archimedean copula family has been studied in numerous research fields, for example, rainfall frequency analysis (Zhang & Singh, 2007; Zhang & Singh, 2012), intensity-duration-frequency relationship (Ariff et al., 2012), modelling wind speed dependence (Xie et al., 2012), modelling option pricing (Cherubini & Luciano, 2002) and probabilistic estimates of heat stress for rice (Zhang et al., 2018).

(a) Joe copula

According to Joe (1997) (Equation 1),

$$C(u_1, \dots, u_d) = 1 - \left(\sum_{i=1}^d (1 - u_i)^\theta - \prod_{i=1}^d (1 - u_i)^\theta \right)^{1/\theta} \quad (1)$$

for $\theta \geq 1$.

(b) Clayton copula

Clayton (1978), Cook and Johnson (1981) and Oakes (1982) had defined the copula as in Equation 2

$$C(u_1, \dots, u_d) = \left(\sum_{i=1}^d u_i^{-\theta} - d + 1 \right)^{-1/\theta} \quad (2)$$

for $\theta > 0$. Independence will lead $\theta \rightarrow 0$. A complete dependence corresponds to $\theta \rightarrow \infty$.

(c) Gumbel copula

Gumbel (1960) had derived the Gumbel copula as in Equation (3)

$$(u_1, \dots, u_d) = \exp \left(- \left(\sum_{i=1}^d (-\log u_i)^\theta \right)^{\frac{1}{\theta}} \right) \quad (3)$$

for $\theta \geq 1$, $\theta = 1$ if the structure is independent. Besides that, Gumbel copula is the only copula that was grouped as an Archimedean copula family as well as an extreme value copula family.

Estimating Copula Parameter

The parameter for the five selected copulas will be estimated using maximum likelihood estimator (Equation 4). Given a sample $u_i, i \in \{1, \dots, d\}$,

$$\hat{\theta} = \underset{\theta \in \Theta}{\operatorname{argsup}} \sum_{i=1}^d \log c(u_i) \quad (4)$$

where $c(u_i)$ is the density function of C .

By using the derived likelihood value, we will compare the performance of copulas using Akaike Information Criterion (AIC) values. The best fit copula would be the copula with minimal AIC value.

Prediction Method using Best Fit Copula

The identification of best fit copula is useful for researchers and practitioners to predict the next year event as well as extreme quantiles. For each country, the d -dimensional time series for n years is denoted as (x_1, \dots, x_d) and the marginal distribution of x_i is F_i .

The following prediction algorithm was proposed by Simard and Remillard (2015) to forecast the x_{n+1} :

1. Let $u = (u_1, \dots, u_d)$ be the copula data of d -dimensional for the best fit copula. Then the Rosenblatt's transformation of u , will be denoted as $y = (y_1, \dots, y_d)$. As mentioned in Schepsmeier (2015), $y_1 := u_1, y_2 := C(u_2|u_1), \dots, y_d := C(u_d|u_1, \dots, u_{d-1})$.
2. Simulate k realizations for conditional copula, which is $C_{u_n|u_{n-1}}(y)$. Set the simulation result as $U^{(j)}, j \in \{1, \dots, k\}$.
3. Set $x_{n+1}^{(j)} = F^{-1}(U^{(j)})$ and determine the predicted value using $\hat{x}_{n+1} = \frac{1}{k} \sum_{j=1}^k x_{n+1}^{(j)}$. Hence, we will use $\hat{x}_{i,n+1}$ as the predictor for $x_{i,n+1}$.
4. Determine the mean and standard error of the prediction value.

RESULTS AND DISCUSSIONS

Exploratory Data Analysis

The annual time series for five countries in southeast Asia, namely Malaysia, Thailand, Indonesia, Vietnam and Myanmar, were used in this study. Five adopted variables were paddy production, planted area, fertilizer used, total annual average rainfall and maximum average temperature. The summary statistics for the five countries are shown in Table 1. Among the five countries, Malaysia has the smallest paddy planted area as well least outputs of paddy production, while Indonesia ranks the highest for both aforementioned indicators. For the climatological variables, Thailand has the lowest total annual rainfall and the highest maximum temperature. By observing the maximum paddy production of Thailand (in year 2012) and Indonesia (in year 2013), we found that although the difference for paddy planted area was only 1880 ('000 hectare), the paddy production harvested in Indonesia was almost twice that of Thailand. This might be due to the variation in climatology factors (amount of annual rainfall difference is almost twice) or other unperceived factors.

Figures 1 to 5 present the plot of five variables studied for Malaysia, Thailand, Indonesia, Vietnam, and Myanmar. These plots can be used to provide preliminary insights about the trend and relationship of the variables. In general, a clear linear pattern is visible in paddy production, planted area and fertilizer usage variable. For total annual rainfall and maximum temperature, only slight linear pattern can be observed. Multivariate Mann-Kendall trend test were performed to analyse data collected over time for consistently increasing or decreasing trends. All five countries are having small p-value which are approximately zero. This indicates that the multivariate data are all having monotonic trends which also means that the data are showing a trend, that can be either positive, negative or non-null.

Figures 6 to 10 provide the boxplot for each country. We can observe the shape of distribution for each time series and have an initial understanding of the data. For paddy production variable, Malaysia and Indonesia are showing left-skewed distribution, while the rest are right-skewed. For paddy planted area, only Malaysia and Thailand are showing negative skewness. Based on the fertilizer usage data, only Indonesia's data is left-skewed,

Table 1
 Summary statistics of variables used for five countries

Country	Variables used	Min.	Q1	Median	Mean	Q3	Max
Malaysia	Paddy Production	1089	1696	1995	1913	2141	2604
	Planted Area	516.5	659	676.2	669.6	693.4	766.2
	Fertilizer Usage	93.71	228.5	723.7	825	1270	2241
	Annual Rainfall	2498	2830	3008	3036	3250	3733
	Maximum Temperature	25.36	25.76	26.13	26.11	26.42	27.32
Thailand	Paddy Production	10150	13920	19550	20720	25840	38000
	Planted Area	6120	7743	9147	8971	9913	11960
	Fertilizer Usage	1.72	12.16	35.13	59.41	108.1	167.7
	Annual Rainfall	1268	1472	1565	1564	1651	1974
	Maximum Temperature	27.84	28.55	29.09	29.1	29.63	30.49
Indonesia	Paddy Production	11600	22340	40080	38280	51100	71280
	Planted Area	6731	8369	9988	10030	11570	13840
	Fertilizer Usage	5.25	27.17	105.5	93.57	142.7	205.4
	Annual Rainfall	2163	2647	2934	2861	3073	3581
	Maximum Temperature	25.83	26.23	26.46	26.45	26.65	27.44
Vietnam	Paddy Production	8366	10600	16000	21000	32110	44040
	Planted Area	4497	5030	5718	6116	7329	7903
	Fertilizer Usage	8.29	45.93	94.08	153.6	292.3	403.9
	Annual Rainfall	1525	1638	1834	1825	1978	2146
	Maximum Temperature	26.79	27.17	27.41	27.43	27.7	28.17
Myanmar	Paddy Production	6636	8602	14150	15990	21320	32680
	Planted Area	4254	4672	4884	5519	6302	8078
	Fertilizer Usage	0.61	4.71	8.95	9.743	15.82	20.76
	Annual Rainfall	1527	1868	1988	1992	2100	2483
	Maximum Temperature	24.88	25.43	25.77	25.87	26.24	27.24

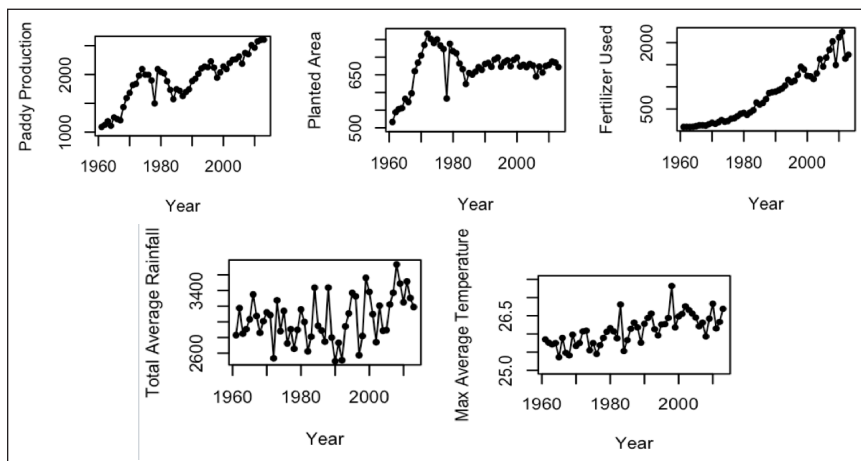


Figure 1. Scatterplots of five variables used for Malaysia

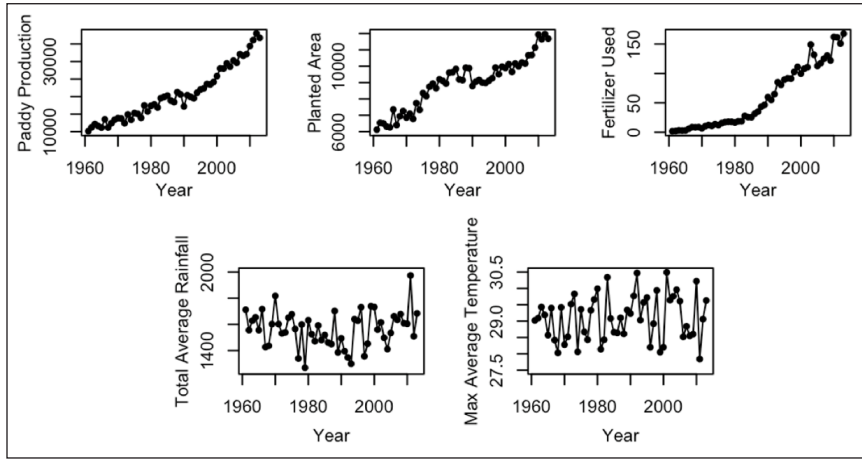


Figure 2. Scatterplots of five variables used for Thailand

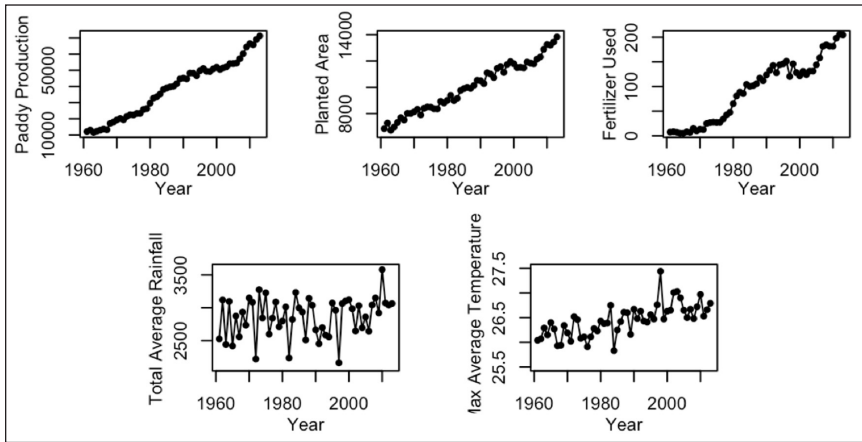


Figure 3. Scatterplots of five variables used for Indonesia

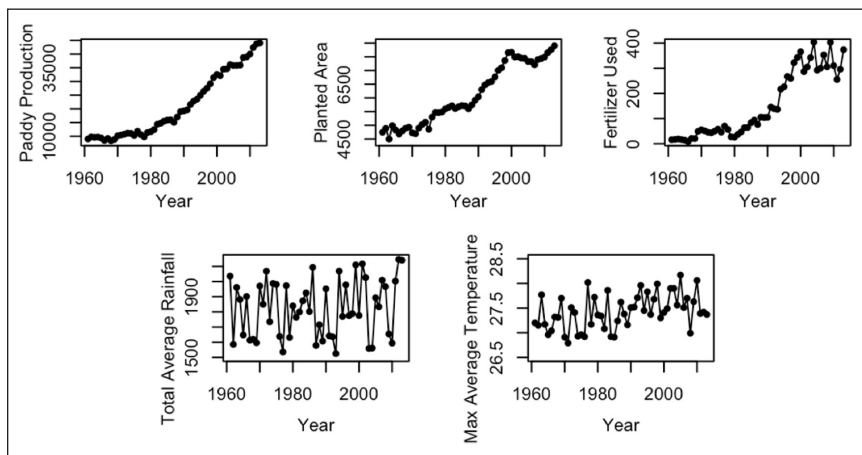


Figure 4. Scatterplots of five variables used for Vietnam

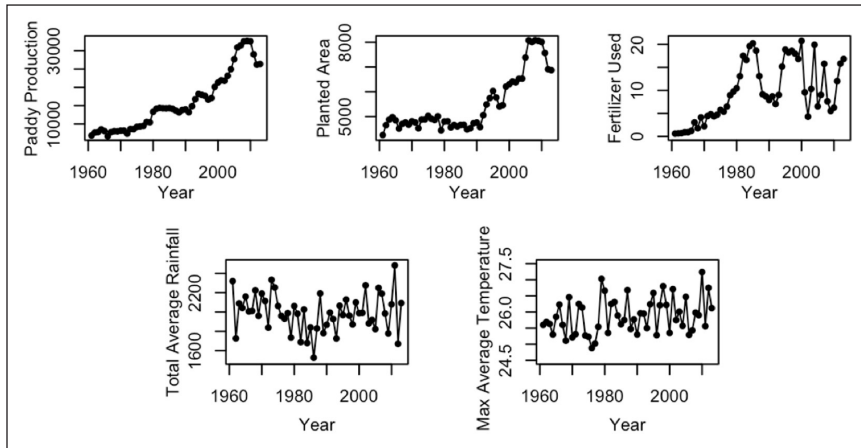


Figure 5. Scatterplots of five variables used for Myanmar

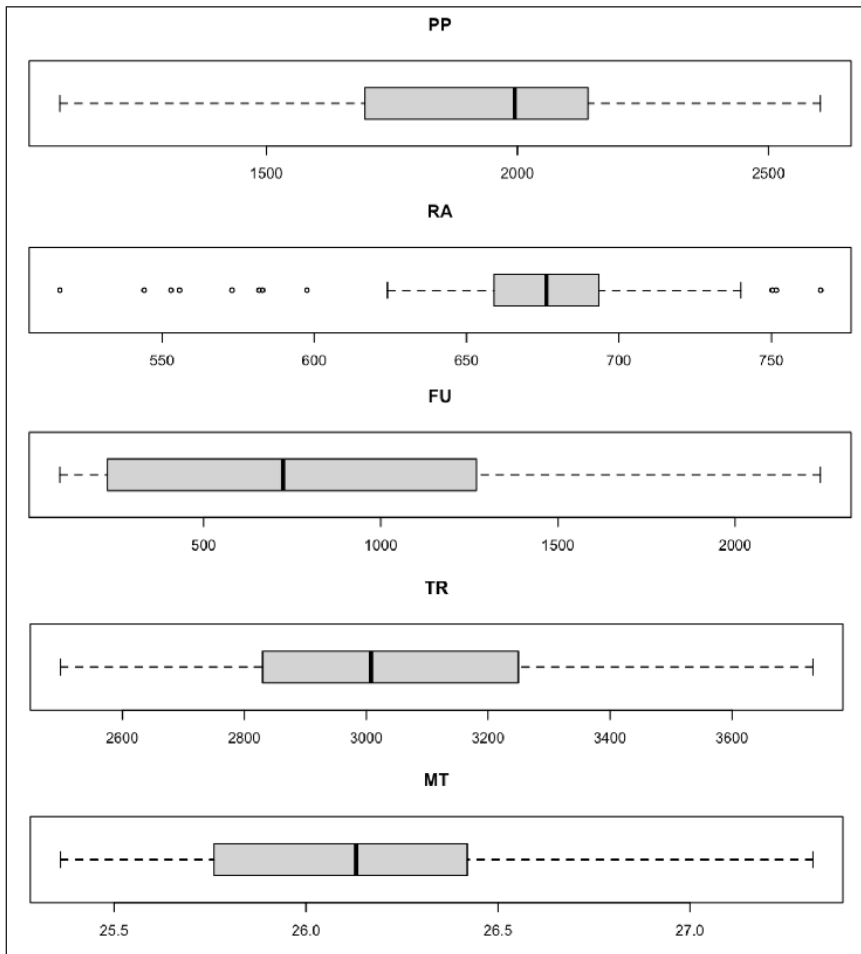


Figure 6. Boxplot of variables used for Malaysia

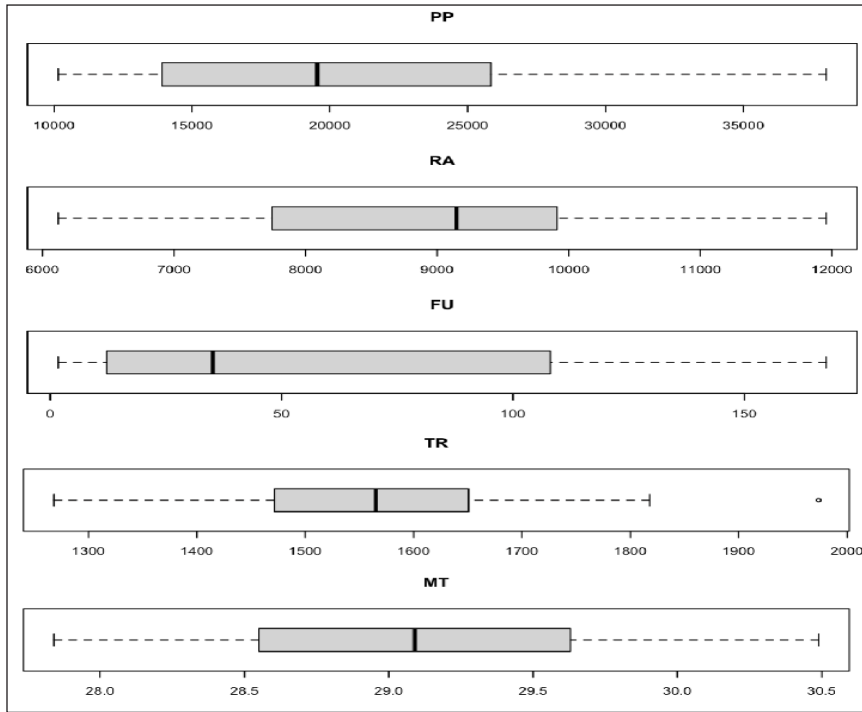


Figure 7. Boxplot of variables used for Thailand

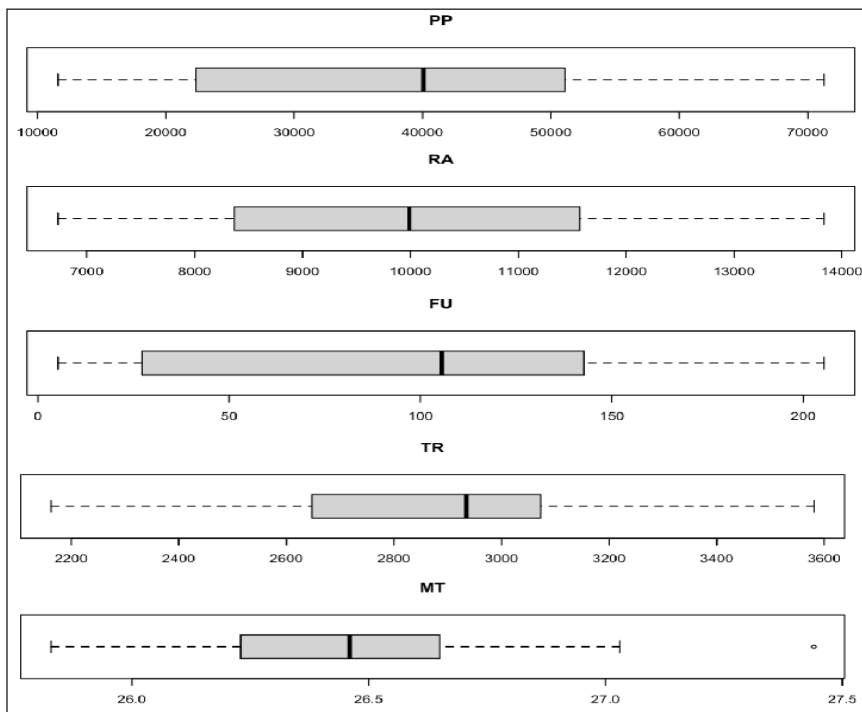


Figure 8. Boxplot of variables used for Indonesia

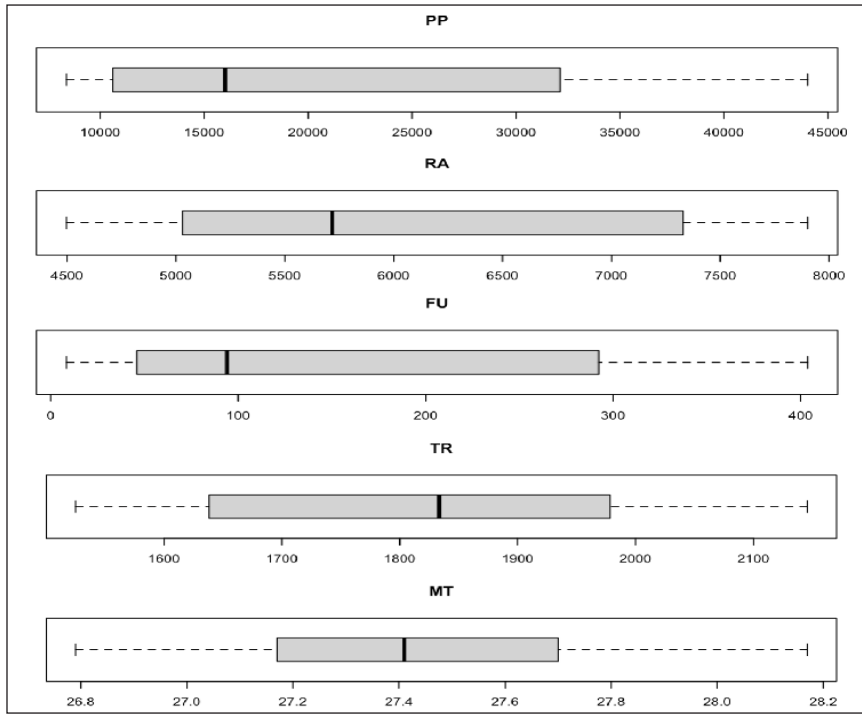


Figure 9. Boxplot of variables used for Vietnam

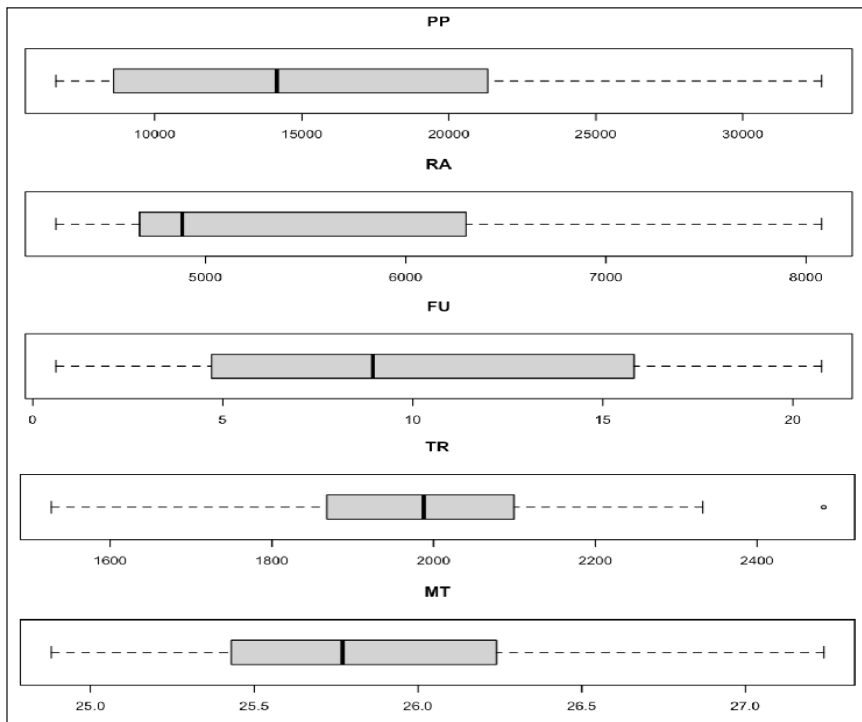


Figure 10. Boxplot of variables used for Myanmar

the other four countries are right-skewed. The average of total annual rainfall time series in Malaysia and Myanmar are having positive skewness behaviour, while Thailand, Indonesia and Vietnam have longer tail at the left. For the fifth adopted variable, which is maximum average temperature, only Malaysia and Indonesia are indicating negative skewness.

After understanding the data variables, we proceeded with determining best fit marginal distribution for each variables. Variables used were paddy production (PP), paddy planted area (RA), fertilizer used (FU), total annual rainfall (TR) and maximum temperature (MT). The distributions tested were exponential, gamma, Weibull, Pareto, Gumbel, Laplace, normal, inverse Gaussian, log normal and logistic. Table 2 provides the best fit distributions and their respective parameter estimates. Rate parameter shown is also the inverse of scale parameter, it is one of the parameters for exponential and gamma distributions. Generally,

Table 2
Parameter estimates of best fit distributions for each univariate time series

		Parameters				
	Best fit distribution	Location	Scale	Shape	Rate	
Malaysia	PP	Weibull		2069.768	5.752	
	RA	Laplace	676.2	36.33		
	FU	Weibull		886.54	1.26	
	TR	Inverse Gaussian	3036		0.0003049	
	MT	Inverse Gaussian	26.11		0.0009491	
Thailand	PP	Inverse Gaussian	20722		0.00000654	
	RA	Weibull		9613.993	6.672	
	FU	Exponential			0.01683	
	TR	Gamma			133.08559	0.08511
	MT	Inverse Gaussian	29.1		0.0001882	
Indonesia	PP	Weibull		43290.981	2.416	
	RA	Gamma			26.927714	0.002684
	FU	Weibull		99.922	1.269	
	TR	Weibull		2989.7	11.21	
	MT	Normal	26.4466	0.3179		
Vietnam	PP	Inverse Gaussian	20997		0.0000163	
	RA	Inverse Gaussian	6116		0.0000053	
	FU	Exponential			0.006509	
	TR	Gamma			96.59	0.05292
	MT	Inverse Gaussian	27.43		0.0005807	
Myanmar	PP	Inverse Gaussian	15993		0.0000159	
	RA	Pareto		4253.7	4.148	
	FU	Weibull		10.701	1.475	
	TR	Normal	1991.7	191.4		
	MT	Gumbel	25.611	0.4616		

Weibull and inverse Gaussian were most suitable distribution for the variables studied. These two distributions have similar shape as both are positively skewed and having long tail. Besides, the gamma distribution which is a family of right-skewed probability distributions is the third most suitable distribution. This indicates that most of the data studied in this research are skewed to the right and exhibiting heavy tail.

Table 3 provides the further details of model fitting. The models listed in second column are used to represent the different variables used for model fitting. Variables studied for their respective models are as listed below:

- Model 1 : Paddy production and planted area
- Model 2 : Paddy production and fertilizer usage
- Model 3 : Paddy production and total annual rainfall
- Model 4 : Paddy production and maximum temperature
- Model 5 : Paddy production, planted area and fertilizer usage
- Model 6 : Paddy production, planted area and total annual rainfall
- Model 7 : Paddy production, planted area and maximum temperature
- Model 8 : Paddy production, fertilizer usage and total annual rainfall
- Model 9 : Paddy production, fertilizer usage and maximum temperature
- Model 10 : Paddy production, total annual rainfall and maximum temperature
- Model 11 : Paddy production, planted area, fertilizer usage and total annual rainfall
- Model 12 : Paddy production, planted area, fertilizer usage and maximum temperature
- Model 13 : Paddy production, planted area, total annual rainfall and maximum temperature
- Model 14 : Paddy production, fertilizer usage, total annual rainfall and maximum temperature
- Model 15 : Paddy production, planted area, fertilizer usage, total annual rainfall and maximum temperature

The purpose of studying different combinations are to measure the relationship for these variables and to compare the performance of different variables combination for three types of model fitting approaches. Multiple correlation (Corr) for the models are shown in third column which signifying as model 3 and 4 whereby these models with only paddy production and climatological variables have low correlation. However, when we included more variables, the correlation magnitude had increased and became strongly correlated. In addition, model 15 exhibited the highest correlation values for all five countries although for clarity only the nearest thousandth are shown (as presented in bold font in Table 3).

Apart from modelling using high dimensional copulas, we have included the AIC values for multiple regression model (MRM) and multivariate normal distribution (MVN). Multiple regression model is the simplest method to distinguish relationship between multiple independent variables and one dependent variable. From the results shown in

Table 3
Results for all methods

		AIC							
	Model	Corr	MRM	MVN	Normal	t	Joe	Clayton	Gumbel
Malaysia	1	0.647	761.88	-15.81	-19.20	-17.19	2.00	-41.14	-6.11
	2	0.800	736.46	8.97	-60.39	-58.28	-51.78	-48.23	-58.47
	3	0.298	785.67	-32.16	-3.51	-1.33	-7.67	7.55	-5.64
	4	0.569	769.82	-9.90	-18.61	-16.62	-7.21	-18.09	-13.87
	5	0.952	667.60	33.96	-99.63	-94.43	-103.22	-101.86	-110.12
	6	0.716	754.42	-29.24	-24.82	-17.87	-48.50	-48.38	-37.34
	7	0.788	741.27	-6.16	-38.60	-32.18	-68.38	-70.24	-57.07
	8	0.801	738.32	-7.13	-62.47	-55.78	-60.73	-61.28	-63.90
	9	0.802	738.02	33.44	-92.75	-86.73	-84.10	-87.03	-92.47
	10	0.645	764.12	-23.43	-23.44	-16.60	-21.48	-24.51	-23.06
	11	0.952	669.38	21.00	-103.53	-92.57	-107.63	-107.40	-113.80
	12	0.952	669.59	59.05	-130.51	-118.74	-133.54	-134.12	-142.12
	13	0.847	727.73	-14.34	-48.29	-34.37	-74.40	-76.55	-53.71
	14	0.802	740.01	22.96	-99.68	-86.60	-94.05	-96.43	-100.26
	15	0.952	671.37	51.15	-138.74	-118.54	-138.66	-141.01	-147.78
Thailand	1	0.929	997.41	95.28	-131.77	-129.65	-87.93	-131.53	-112.39
	2	0.955	973.36	79.88	-128.83	-126.62	-101.77	-105.38	-120.35
	3	0.192	1100.60	-37.89	1.04	3.08	-0.03	2.94	0.47
	4	0.123	1101.80	-43.60	0.85	2.86	1.01	1.47	0.90
	5	0.982	928.62	205.93	-264.23	-257.47	-233.96	-235.21	-261.60
	6	0.940	990.48	80.68	-130.31	-123.71	-130.95	-132.41	-138.05
	7	0.929	999.41	72.96	-129.24	-123.00	-128.15	-128.98	-135.44
	8	0.956	974.58	65.10	-131.17	-124.45	-104.40	-107.38	-124.28
	9	0.955	975.31	56.74	-126.02	-119.31	-102.66	-103.91	-119.02
	10	0.270	1100.59	-58.09	-1.79	4.67	-7.29	-6.68	-5.42
	11	0.985	921.64	198.96	-269.56	-256.38	-234.77	-237.66	-267.01
	12	0.982	930.24	183.62	-259.70	-246.61	-230.32	-231.97	-257.45
	13	0.941	991.50	62.58	-132.21	-120.01	-137.57	-137.79	-143.86
	14	0.956	976.57	44.90	-132.37	-119.29	-114.98	-117.81	-133.20
	15	0.985	923.50	181.72	-270.70	-249.42	-244.04	-248.81	-275.33
Indonesia	1	0.992	970.25	172.35	-214.97	-212.72	-204.44	-73.69	-221.12
	2	0.987	998.13	124.24	-160.81	-158.43	-125.14	-122.94	-148.88
	3	0.065	1190.50	-39.54	-0.99	1.03	0.36	0.31	-0.14
	4	0.127	1189.86	5.39	-31.45	-29.39	-15.72	-27.36	-24.31
	5	0.997	917.49	349.71	-392.55	-384.97	-345.17	-344.85	-386.04
	6	0.993	962.88	165.14	-222.04	-215.12	-211.12	-211.20	-229.30
	7	0.992	972.15	201.58	-244.92	-238.88	-233.44	-233.55	-252.92
	8	0.987	997.96	110.09	-162.79	-155.64	-126.44	-125.50	-151.67
	9	0.987	997.20	154.01	-190.54	-183.18	-149.87	-153.81	-178.42
	10	0.719	1154.19	-7.55	-31.57	-25.28	-23.61	-26.90	-29.46

Table 3 (continue)

		AIC							
	Model	Corr	MRM	MVN	Normal	t	Joe	Clayton	Gumbel
	11	0.997	915.19	343.20	-397.69	-383.79	-351.97	-352.03	-392.22
	12	0.997	919.21	379.73	-420.53	-410.27	-368.02	-370.89	-413.83
	13	0.993	964.71	197.81	-252.06	-240.20	-238.62	-240.94	-261.05
	14	0.988	996.00	143.23	-192.02	-178.88	-149.84	-154.50	-181.70
	15	0.997	917.19	376.37	-425.77	-408.19	-374.16	-378.19	-420.09
Vietnam	1	0.964	1007.36	89.40	-42.63	-79.83	-106.82	-7.41	-97.85
	2	0.951	1022.93	79.61	-40.07	-79.97	-101.16	-5.90	-94.68
	3	0.212	1145.00	-41.28	0.03	3.17	-2.12	1.25	-1.05
	4	0.408	1137.81	-26.18	-3.87	-1.34	-5.23	1.47	-5.89
	5	0.970	999.75	214.66	-162.97	-195.56	-229.15	-231.66	-232.91
	6	0.965	1007.37	62.60	-40.60	-72.30	-107.46	-106.80	-97.14
	7	0.965	1008.17	80.97	-51.83	-84.11	-110.82	-112.82	-105.12
	8	0.953	1023.36	53.25	-38.07	-72.70	-101.28	-101.00	-93.73
	9	0.951	1024.93	69.54	-47.86	-82.03	-104.26	-106.83	-99.80
	10	0.524	1132.46	-45.72	-8.72	-0.64	-7.68	-10.38	-14.83
	11	0.971	999.64	188.75	-159.13	-184.15	-230.50	-231.79	-231.96
	12	0.971	1000.54	206.24	-170.18	-195.73	-231.15	-235.00	-238.17
	13	0.965	1009.01	61.85	-55.63	-85.28	-120.44	-120.83	-113.94
	14	0.953	1025.13	51.51	-51.95	-82.00	-109.69	-111.47	-107.45
	15	0.971	1001.28	188.25	-172.29	-193.06	-238.76	-241.00	-244.99
Myanmar	1	0.946	987.50	36.35	-31.69	-38.20	-86.55	-1.83	-65.60
	2	0.422	1096.38	-17.90	-24.01	-21.88	-4.50	-33.25	-14.55
	3	0.009	1106.75	-33.49	1.77	2.94	2.00	1.55	1.91
	4	0.250	1103.33	-39.95	-2.37	-0.26	-1.02	-2.39	-2.01
	5	0.973	953.38	55.95	-54.23	-63.54	-118.84	-120.36	-92.26
	6	0.958	976.68	33.09	-27.93	-35.18	-88.14	-88.63	-64.51
	7	0.952	983.43	22.01	-33.25	-34.92	-89.26	-90.47	-67.78
	8	0.448	1096.90	-23.46	-27.03	-22.20	-34.06	-36.19	-31.31
	9	0.450	1096.75	-35.54	-24.93	-18.17	-32.39	-34.12	-29.03
	10	0.265	1104.89	-45.75	-3.40	2.83	-0.83	-1.91	-2.13
	11	0.976	949.92	54.34	-55.26	-60.74	-122.46	-124.29	-94.38
	12	0.975	951.45	41.64	-54.22	-55.97	-119.55	-122.45	-92.50
	13	0.960	976.31	22.28	-32.29	-30.64	-86.49	-87.98	-65.89
	14	0.491	1096.15	-35.71	-30.20	-18.40	-34.18	-36.51	-33.49
	15	0.977	949.84	-42.36	-57.57	-53.09	-126.48	-127.63	-96.52

Table 3, multiple regression method is the least fitted model. As for multivariate normal distribution, it is an approach to generalize univariate normal distribution to higher dimensions and is derived from the multivariate central limit theorem. Since the sample sizes of variables used are sufficiently large, the central limit theorem assumption is fulfilled. Based upon the AIC values shown, we can conclude that the multivariate normal

distribution fits the data relatively better than multiple regression model. Most of the AIC values are negative, this indicates that there is less information loss as compared to MRM.

Subsequently, we discuss the performance of the copulas fitted to different combination of variables. Generally, for all five countries, model 15 performed the best as the AIC values produced were generally lower than other models (as shown as bold font in Table 3). Apart from that, we also found that the Gumbel copula performed best for Malaysia, Thailand and Vietnam. Since Gumbel copula typically signifies as an extreme value copula, we can further presume that the variables for Malaysia, Thailand and Vietnam exhibit a heavy tail behaviour. But for Myanmar, both Clayton and Joe copulas for model 15 were performing identically well, with Clayton copula having a relatively lower AIC value. Besides that, the best fit copula for Indonesia was the normal copula, with AIC value equal to -425.77. Therefore, the best fit marginal distributions and copula for each countries would be utilised for further prediction.

Finally, we predicted the next year event using best fit marginal distributions for each variables and best fit copula function for the countries. For each country, one thousand simulations were performed and the average together with estimation error of the predictions were computed. In order to identify the performance of prediction results, we also forecasted the next year event using univariate generalized autoregressive conditional heteroskedasticity (GARCH) time series model. The GARCH model is selected as the reference group for prediction using copula modelling as it is a most common forecasting method for time series and GARCH model is known as an effective model that aims to minimize errors in forecasting. For this study, the number of autocorrelation term used for the GARCH model was 1 (also known as AR(1)), and GARCH(1,1) was used to model the variance term. This AR(1)-GARCH(1,1) model was selected as it is one of the most prevalent GARCH model and the error approximation is relatively smaller as compared to other models that examined using our existing data.

Table 4 shows the mean and standard error of predicted values for copula and GARCH model. Based on the values of standard error, copula model behaved reasonably well compared to GARCH model since fifteen out of the total of twenty-five predictions of copula showed lower figure. Other than that, the predicted means are provided in the same table for comparative purpose. It can be seen that copula model produces higher mean than the GARCH model in nineteen predictions.

The result of prediction has indicated that the forecasting method based on copula models are also capable in detecting autocorrelation and volatility of multivariate time series. The findings in this research can be useful for practitioners and other related stakeholders in monitoring the variables that will affect paddy production and to predict the future trend.

Table 4
Mean and standard error for predicted values

	Variables	Copula		GARCH	
		Mean	SE	Mean	SE
Malaysia	PP	2610.1	58.4	2626.3	80.3
	RA	719.4	20.0	671.0	13.1
	FU	1859.6	362.5	1732.8	395.1
	TR	3414.9	180.3	3078.2	305.3
	MT	27.94	0.57	26.49	0.38
Thailand	PP	31267.0	3312.0	31498.6	3665.8
	RA	10967.0	522.5	11660.9	442.6
	FU	133.5	20.2	125.0	54.8
	TR	1716.4	65.1	1571.2	146.5
	MT	30.77	0.85	29.07	0.74
Indonesia	PP	59006.0	7345.9	58789.3	7243.0
	RA	12601.8	1668.9	12351.3	809.6
	FU	191.9	25.6	162.7	31.6
	TR	3186.6	148.5	2831.6	298.0
	MT	26.72	0.221	26.65	0.26
Vietnam	PP	35584.8	3651.0	37520.7	3892.9
	RA	7444.8	334.4	7504.9	185.4
	FU	385.3	109.1	374.8	81.5
	TR	2066.4	55.9	1812.7	202.6
	MT	27.76	0.17	27.42	0.34
Myanmar	PP	26936.2	4417.2	27330.1	4277.2
	RA	6997.2	267.5	6874.2	272.4
	FU	19.2	3.205	17.1	2.4
	TR	2221.8	100.5	1979.1	199.1
	MT	26.38	0.36	25.88	0.56

CONCLUSION

Rice is important for human consumption as well as for economic growth particularly for countries that produce rice in tropical region. Therefore, the objective of this study was to identify the best fit model and perform prediction using the model. We had compared the high dimensional copulas with multiple regression model and multivariate normal distribution by using several variables which were paddy production, paddy planted area, fertilizer usage, total annual rainfall and maximum temperature for five countries in southeast Asia. The five countries were Malaysia, Thailand, Indonesia, Vietnam, and Myanmar located in the tropical region in southeast Asia. Prior to multivariate analysis,

we had to determine the best fit univariate marginal distributions for all variables using maximum likelihood estimation method. The results indicate that Weibull and inverse Gaussian probability distributions fitted well to most of the variables.

Based on the results of model fitting, copulas produced the lowest AIC values while multivariate normal distribution produced a moderate AIC and multiple regression model has the highest AIC. For Malaysia, Thailand and Vietnam, Gumbel copula is the most suitable copula for the model that consists of all five variables. On the contrary, although the model contains of all five variables performs best for Myanmar and Indonesia too, the best fit copula for Myanmar is Clayton copula whilst for Indonesia is normal copula. In general, we can conclude that copulas are able to reduce the information loss in model fitting. Besides that, planted area, fertilizer usage, rainfall and temperature do play an important role in paddy production.

The forecasted values of the following year event were computed based on best fit marginal distribution and copula functions. In order to compare the effectiveness of copula, we have also computed the mean and standard error of forecasted values using AR(1)-GARCH(1,1) model. GARCH model is treated as reference group due to its ability to minimize errors in forecasting and to enhance the accuracy of further predictions. Based on the results, we found that the performance of the prediction is relatively similar with GARCH model. Hence, this proves that the effectiveness of multivariate copula model is comparable to univariate GARCH model.

ACKNOWLEDGEMENT

We acknowledge the financial support of Universiti Putra Malaysia (UPM-GP-IPM-9587800).

REFERENCES

- Ariff, N. M., Jemain, A. A., Ibrahim, K., & Zin, W. Z. W. (2012). IDF relationships using bivariate copula for storm events in peninsular Malaysia. *Journal of Hydrology*, 470, 158-171. doi: <https://doi.org/10.1016/j.jhydrol.2012.08.045>
- ASEAN Food Security Information System. (2019). *ASEAN Agricultural Commodity Outlook, No. 22, June 2019*. Retrieved July 11, 2020, from <http://www.apfisis.org/uploads/normal/ACO%20Report%2022/ACO%20Report22.pdf>
- Bandumula, N. (2017). Rice production in Asia: Key to global food security. In *Proceedings of the Natural Academy of Sciences, India, Section B: Biological Sciences*, 88(4), 1323-1328. doi: <https://doi.org/10.1007/s40011-017-0867-7>
- Cherubini, U., & Luciano, E. (2002). Bivariate option pricing with copulas. *Applied Mathematical Finance*, 9(2), 69-86.

- Clayton, D. G. (1978). A model for association in bivariate life tables and its application in epidemiological studies of familial tendency in chronic disease incidence. *Biometrika*, 65(1), 141-151. doi: <https://doi.org/10.1093/biomet/65.1.141>
- Cook, R. D., & Johnson, M. E. (1981). A family of distributions for modeling nonelliptically symmetric multivariate data. *Journal of the Royal Statistical Society: Series B*, 4(2)3, 210-218. doi: <https://doi.org/10.1111/j.2517-6161.1981.tb01173.x>
- Food and Agriculture Organization of the United Nations. (2019). *Macroeconomic statistics: Global trends in GDP, agriculture value added, and food-processing value added (1970-2017)*. Retrieved June 28, 2020, from <http://www.fao.org/economic/ess/ess-economic/gdpagriculture/en/>
- Fouque, J. P., & Zhou, X. (2008). Perturbed gaussian copula. In J. P. Fouque, T. B. Fomby & K. Solna (Eds.), *Econometrics and risk management* (pp. 103-121). Bingley, England: Emerald Group Publishing Limited. doi: [https://doi.org/10.1016/S0731-9053\(08\)22005-0](https://doi.org/10.1016/S0731-9053(08)22005-0)
- Gumbel, E. J. (1960). Bivariate exponential distributions. *Journal of the American Statistical Association*, 55(292), 698-707.
- Hsiang, S., Kopp, R., Jina, A., Rising, J., Delgado, M., Mohan, S., ... & Oppenheimer, M. (2017). Estimating economic damage from climate change in the United States. *Science*, 356(6345), 1362-1369. doi: 10.1126/science.aal4369
- IPCC. (2019). Summary for policymakers. In *Global Warming of 1.5°C. An IPCC Special Report on the impacts of global warming of 1.5°C above pre-industrial levels and related global greenhouse gas emission pathways, in the context of strengthening the global response to the threat of climate change, sustainable development, and efforts to eradicate poverty*. Intergovernmental Panel on Climate Change (IPCC), Geneva, Switzerland. Retrieved June 28, 2020, from https://www.ipcc.ch/site/assets/uploads/sites/2/2019/06/SR15_Full_Report_High_Res.pdf
- Joe, H. (1997). *Multivariate models and dependence concepts*. London, UK: Chapman and Hall.
- Khazanah Research Institute. (2019). *The status of the paddy and rice industry in Malaysia*. Retrieved July 11, 2020, from http://www.krinstitute.org/assets/contentMS/img/template/editor/20190409_RiceReport_Full%20Report_Final.pdf
- Luo, X., & Shevchenko, P. V. (2012). Bayesian model choice of grouped t-copula. *Methodology and Computing in Applied Probability*, 14(4), 1097-1119. doi: <https://doi.org/10.1007/s11009-011-9220-4>
- Muhammad, M., & Abdullah, M. H. H. (2013). Modelling and forecasting on paddy production in Kelantan under the implementation of system of rice intensification (SRI). *Academic Journal of Agricultural Research*, 1(7), 106-113. doi: <http://dx.doi.org/10.15413/ajar.2013.0112>
- Moore, M. (2020). *Rice paddy production in the Asia Pacific region in 2018, by country*. Retrieved July 11, 2020, from <https://www.statista.com/statistics/681740/asia-pacific-rice-paddy-production-by-country/#statisticContainer>
- Mutert, E., & Fairhurst, T. H. (2002). Developments in rice production in Southeast Asia. *Better Crops International*, 15(Suppl), 12-17.

- Nyang'au, W., Mati, B., Kalamwa, K., Wanjogu, R., & Kiplagat, L. (2014). Estimating rice yield under changing weather conditions in Kenya using CERES rice model. *International Journal of Agronomy*, 2014, 1-12. doi: <https://doi.org/10.1155/2014/849496>
- Oakes, D. (1982). A model for association in bivariate survival data. *Journal of the Royal Statistical Society: Series B*, 44(3), 414-422. doi: <https://doi.org/10.1111/j.2517-6161.1982.tb01222.x>
- OECD. (2018). *Joint working party on agriculture and trade. ASEAN rice market integration: Findings from a feasible study*. Organisation for Economic Co-operation and Development. Retrieved July 11, 2020, from [http://www.oecd.org/officialdocuments/publicdisplaydocumentpdf/?cote=TAD/TC/CA/WP\(2018\)7/FINAL&docLanguage=En](http://www.oecd.org/officialdocuments/publicdisplaydocumentpdf/?cote=TAD/TC/CA/WP(2018)7/FINAL&docLanguage=En)
- OECD. (2020). *OECD-FAO agricultural outlook 2019 – 2028: OECD-FAO agricultural outlook 1990-2028, by country*. Retrieved July 7, 2020, from <https://stats.oecd.org/>
- Okhrin, O., Ristig, A., & Xu, X. F. (2017). Copulae in high dimensions: An introduction. In W. Härdle, C. H. Chen & L. Overbeck (Eds.), *Applied quantitative finance, statistics and computing*. Heidelberg, Germany: Springer. doi: https://doi.org/10.1007/978-3-662-54486-0_13
- Putri, R. E., Yahya, A., Adam, N. M., & Aziz, S. A. (2019). Rice yield prediction model with respect to crop healthiness and soil fertility. *Food Research*, 3(2), 174-180. doi: [http://doi.org/10.26656/fr.2017.3\(2\).117](http://doi.org/10.26656/fr.2017.3(2).117)
- Simard, C., & Rémillard, B. (2015). Forecasting time series with multivariate copulas. *Dependence Modeling*, 3, 59-82.
- Singh, B., & Singh, V. K. (2017). Fertilizer management in rice. In B. Chauhan, K. Jabran & G. Mahajan (Eds.), *Rice production worldwide* (pp. 217-253). Cham, Switzerland: Springer. doi: https://doi.org/10.1007/978-3-319-47516-5_10
- Sørensen, M. (2011). Estimating functions for diffusion-type processes. In M. Kessler, A. Lindner & M. Sørensen (Eds.), *Statistical methods for stochastic differential equations*. London, UK: Chapman & Hall.
- United Nations. (2019). *World Population Prospects 2019: Highlights*. Department of Economic and Social Affairs, Population Division. Retrieved June 28, 2020, from https://population.un.org/wpp/Publications/Files/WPP2019_Highlights.pdf
- USDA. (2015). *Southeast Asia: 2015/16 rice production outlook at record levels*. Commodity Intelligence Report. United State Department of Agriculture.
- Xie, K., Li, Y., & Li, W. (2012). Modelling wind speed dependence in system reliability assessment using copulas. *IET Renewable Power Generation*, 6(6), 392-399.
- Zhang, L., & Singh, V. P. (2007). Bivariate rainfall frequency distributions using Archimedean copulas. *Journal of Hydrology*, 332, 93-109. doi: <https://doi.org/10.1016/j.jhydrol.2006.06.033>
- Zhang, L., & Singh, V. P. (2012). Bivariate rainfall and runoff analysis using entropy and copula theories. *Entropy*, 14, 1784-1812. doi: <https://doi.org/10.3390/e14091784>
- Zhang, L., Yang, B., Guo, A., Huang, D., & Huo, Z. (2018). Multivariate probabilistic estimates of heat stress for rice across China. *Stochastic Environmental Research and Risk Assessment*, 32, 3137-3150. doi: <https://doi.org/10.1007/s00477-018-1572-7>

Logic Learning in Adaline Neural Network

Nadia Athirah Norani¹, Mohd Shareduwan Mohd Kasihmuddin^{2*}, Mohd. Asyraf Mansor³ and Noor Saifurina Nana Khurizan⁴

^{1,2,4}*School of Mathematical Sciences, Universiti Sains Malaysia, 11800, Penang, Malaysia*

³*School of Distance Education, Universiti Sains Malaysia, 11800, Penang, Malaysia*

ABSTRACT

In this paper, Adaline Neural Network (ADNN) has been explored to simulate the actual signal processing between input and output. One of the drawback of the conventional ADNN is the use of the non-systematic rule that defines the learning of the network. This research incorporates logic programming that consists of various prominent logical representation. These logical rules will be a symbolic rule that defines the learning mechanism of ADNN. All the mentioned logical rule are tested with different learning rate that leads to minimization of the Mean Square Error (MSE). This paper uncovered the best logical rule that could be governed in ADNN with the lowest MSE value. The thorough comparison of the performance of the ADNN was discussed based on the performance MSE. The outcome obtained from this paper will be beneficial in various field of knowledge that requires immense data processing effort such as in engineering, healthcare, marketing, and business.

Keywords: Adaline neural network, logic programming, logical rule

ARTICLE INFO

Article history:

Received: 4 August 2020

Accepted: 28 September 2020

Published: 22 January 2021

DOI: <https://doi.org/10.47836/pjst.29.1.16>

E-mail addresses:

nadiaathirahnorani@gmail.com (Nadia Athirah Norani)

shareduwan@usm.my (Mohd Shareduwan Mohd Kasihmuddin)

asyrafman@usm.my (Mohd. Asyraf Mansor)

saifurina@usm.my (Noor Saifurina Nana Khurizan)

*Corresponding author

INTRODUCTION

Artificial Neural Network (ANN) was inspired by the biological neuron model. ANN consists of interconnected neurons with distinctive input and output layer. Despite the various development of the ANN in many field of studies, ANN experience lack of representation during learning and retrieval phase. One of the unique direction in the work of ANN is the

use of the optimal learning system via symbolic rule. Initially, Abdullah (1992) proposed logic programming in special case of ANN called Hopfield Neural Network (HNN). The proposed network introduced an innovative connection weight by comparing cost function and energy function. This pursuit was continued by Sathasivam (2010) where this work capitalized special case of logic called Horn Satisfiability. Since then, several propositional logical rules were proposed in ANN such as 2 Satisfiability (Kasihmuddin et al., 2017), 3 Satisfiability (Mansor et al., 2017) and Random 2 Satisfiability (Sathasivam et al. 2020a). The proposed methods played an important role in the emergent of several related applications such as Very Large Scale Integration (Sathasivam et al., 2020b), Bezier reconstruction (Kasihmuddin et al., 2016), logic mining (Kho et al., 2020) and many more. In another development, Alzaemi et al. (2020) proposed 2 Satisfiability logical rule in Radial Basis Function Neural Network (RBFNN) by utilizing the value of the parameters in the hidden layers. The comparative study between HNN and RBFNN has been reported in (Mansor et al. 2020). All the mentioned logical rule utilizes only the Satisfiable logic except in the work of Kasihmuddin et al. (2018) that proposed non-Satisfiable logic. As far as the logical rule is concern, the proposed ANN only implemented limited type of propositional logical rule. This is due to the redundant nature of the logic that prevent the previous studies to produce optimal synaptic weight that corresponds to the goal of the logic.

Popularized by Widrow and Hoff (1960), Adaline Neural Network (ADNN) is designed to cater a simple data processing unit that serves as an intermediate layer between pre-processing input and input (Sharma et al., 2019). ADNN is a single layer network with multiple nodes where each node receives multiple inputs and produces one output. ADNN is a self-adaptive algorithm that can automatically modify the current structure in order to optimize performance based on previous input (Widrow & Hoff, 1960). This network adapts to the input data, learn from the data, and produce the final output based on the minimized synaptic weight. This network is based on the Delta rule that utilizes least mean squares learning error to minimize the error during the training phase (Widrow & Lehr, 1990). Due to the simplicity of the ADNN, this network endured rapid development in term of architecture and data processing. Pajares and Jesús (2001) proposed ADNN in optimizing the stereovision matching problem. The proposed ADNN managed to increase a good decision by learning the optimal weight design when considering relative importance of the attribute. In another development, Negarestani et al. (2003) proposed ADNN to estimate the environmental parameters of the radon concentration in the soil. The proposed ADNN has a good agreement with the similar established work. Recently, Sujith and Padma (2020) utilized ADNN to estimate the harmonics for Pulse Width Modulation. The proposed ADNN optimized the crucial parameter of the system such as load voltage, current and reactive power. In some areas, ADNN became a useful method in adaptive signal processing due to the simplicity of the modelling method (Widrow &

Stearns, 1985; Wang et al., 2000; Kavak et al., 2005). Unfortunately, the above studies only utilize ADNN as a tool rather than self-adaptive ANN by using pre-defined symbolic rule. In this case, very limited effort to establish another variant of logical rule embodied into ADNN. In this paper, we implemented logical programming in ADNN by embedding several established logical rule. Hence, this combination provides a good understanding of the ADNN governed by logical structure.

The remaining part of this paper is as follows. In section 1, we explore the logical representation that consists of newly proposed logical rule. The proposed logical rule consists of both redundant and non-redundant variables. In section 2, the general structure of ADNN is explained in detail. Next, the implementation of various logical rule in ADNN is demonstrated. Finally, the performance of different logical rule in ADNN is discussed thoroughly and we conclude the paper with some remarks and future work.

MATERIALS AND METHOD

Logical Representation

Logic programming transformed the knowledge representation into mathematical derivation. Logic programming is declarative because this representation requires the user to state the desired task while putting minimal emphasis on the underlying process (Somogyi et al., 1996). In another perspective, logic programming represent fact both explicitly and implicitly depending on the nature of the desired problem. According to Kowalski (1978), logic programming is expressed symbolically according the following Equation 1:

$$\textit{Algorithm} = \textit{Logic} + \textit{Control}. \quad [1]$$

In Equation 1, logic signifies the issue of “what” and control explains the “how” which can be determined using the method defined by the user. In this case, optimal logic programming has to be able to clearly define the end goal that corresponds to the logical statement and control the system accordingly (Hamadneh, 2013). In practice, logical representation can “communicate” with the user by assigning the logical state for each variable in the logic. Hence, listing all the possible logical instance optimize the “control” part by identifying the logical inconsistencies that deviates from the goal.

In this paper, we only consider propositional logical rule where the output consists of only bipolar (1 or -1). In this case, the output reads 1 (True) or -1 (False). The goal of each logic formulation is to produce only 1 (True) statement. One of the most prominent representations of Propositional logic is in Boolean algebra form. Boolean algebra is a logical algebra in which symbols are used to describe the complexity of the logical representation (Riche, 2011). This representation consists of individual unit called variable and connectives (Table 1). Similar to the output of the logical rule, variable is a symbolic

unit that can be defined as 1 (True) and -1 (False). The relationship of the variable is define by connectives manipulate the behaviour of the problem that leads to the final output (goal).

Table 1
List of logic programming connections

Connective	Representation
T	True
\wedge	False
\wedge	Conjunction
\vee	Disjunction
\neg	Negation
\leftarrow	Implication

To further illustrate the connection in Table 1, we first describe two logical variables A and B that serve as input and P as an output P where $B \in \{-1, 1\}$, $B \in \{-1, 1\}$ and $P \in \{-1, 1\}$. The variants of the logical rule that relates A and B can be shown in Table 2. Note that, different logical formulations require different logical states which lead to $P = 1$.

Table 2
List of logical variants

Logical Statement	Conventional Formulation	Propositional Formulation
A AND B	$P = A \cdot B$	$P = (A \wedge B)$
A OR B	$P = A + B$	$P = (A \vee B)$
NOT A	$P = \overline{A}$	$P = \overline{A}$
A NAND B	$P = \overline{A \cdot B}$	$P = \neg(A \wedge B)$
A NOR B	$P = \overline{A + B}$	$P = \neg(A \vee B)$
A EX-OR B	$P = A \oplus B$	$P = (A \wedge \neg B) \vee (\neg A \wedge B)$
A EX-NOR B	$P = \overline{A \oplus B}$	$P = (A \wedge B) \vee \neg(A \wedge B)$

Since each variable in P is binary in nature, the logical structure can be implemented in ANN. In this paper, we will utilize logical structure in Table 2 as a learning rule that governs the ADNN model.

Adaline Neural Network (ADNN)

ADNN consists of single interconnected layer neurons with n inputs and one output. The determination of the output is based on the linear combinations of the inputs (Jannati et al., 2016). The main feature of ADNN is the ability to be self-adapting algorithm usually used for the weights training.

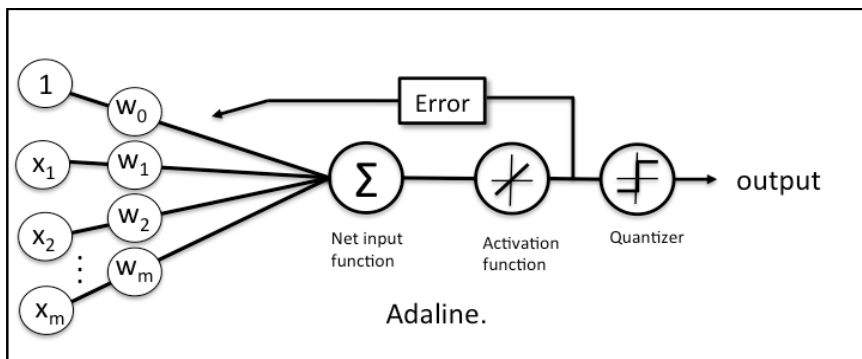


Figure 1. Symbolic illustration of Adaline Neural Network (Raschka, 2015)

Figure 1 shows an ADNN with multiple nodes where each node receives multiple inputs and generate one output, $y(k)$. Note that, k is the sampling time index ($k = 0, 1, \dots$). The updating rule of the output is based on the following Equation 2:

$$y(k) = b + \sum_{i=0}^r w_i x(k-i), \quad i = 0, 1, 2, \dots, r, \quad [2]$$

where b, w_i, r are denoted as bias, weight and the order of adaptive linear combiner respectively. In ADNN, the activation function must be non-linear (such as sigmoid activation function) to ensure nonlinearity of the output. Sigmoid activation will give smooth gradient and help to adapt with variety of data (Sharma, 2017). The output classification of $y(k)$ is based on the following Equation 3:

$$y(k) = \begin{cases} 1 & , y(k) \geq 0 \\ -1 & , y(k) < 0 \end{cases} \quad [3]$$

Optimal value of w_i is crucial to ensure the input will always approach the optimal $y(k)$. The training pattern will undergo pre-defined number of iteration until the optimal value of were obtained. In this case, the weight updating is carried out by applying Delta rule.

Delta rule use in ADNN will evaluate the difference between $d(k)$ with the target output $d(k)$, in order to adjust the weight and threshold of the neuron. The error $e(k)$ is given by Equation 4:

$$e(k) = d(k) - y(k). \quad [4]$$

The value of $e(k)$ is vital for the change of weight and bias (Equation 5):

$$\begin{aligned} w_{i+1} &= w_i + \alpha e(k) x(k-i) \\ b_{i+1} &= b_i + \alpha e(k), \end{aligned} \quad [5]$$

where, w_{i+1} and b_{i+1} are the new value of weights and bias respectively. α is the learning rate that accelerate the searching of optimal value for w_{i+1} and b_{i+1} where $\alpha \in (0, 1)$. $x(k-i)$ is set of activation input at time k . The proposed ADNN is structurally different than traditional Hebb Rule since the value of weights is adjusted as the training progress. In general, ADNN is based upon an idea that decrement in the value of $e(k)$ will reinforce the input-output connection. By reducing the value of $e(k)$, the back-spreading from one layer to the other layer can be reduced dramatically. Algorithm 1 shows the step based training algorithm for ADNN.

Algorithm 1: Adaline Neural Network

- Step 1:** Initialize weights w_i with small random value that is not equal to zero (Sivanandam & Deepa, 2006). Assign learning rate α .
- Step 2:** Set activation of input $x(k-i) = s(k-i)$, for $i = 1$ to r from Equation (3).
- Step 3:** With every bipolar training pair conduct Step 4-6.
- Step 4:** Measure the net input to output unit from Equation (2).
- Step 5:** Update bias and weights, $i = 1$ to r from Equation (5).
- Step 6:** Calculate the error from Equation (4).
- Step 7:** Test for stopping condition. Depending the stopping conditions, the number of iterations and epochs take place.

Logic Programming in ADNN

Logic programming can play a part as a representational knowledge that can be “learned” by ADNN. Apparent knowledge should be held as well as recuperated on the off chance that essential. The most thought here is to break the situation into smaller parts and after that hunt for logical rules which can demonstrate with a computer. This neuron model is oversimplified, and it has substantial computing potential and bipolar in nature. Based on Table 2, this could conduct the basic logic operations NOT, OR, and AND, with suitable chosen weights and thresholds. Every multivariable combinational function could be done using either the NOT and OR, or on the other hand the NOT and AND logical rules.

Coherent run this logical rule is one of the perfect ways to clarify the black box model of neural network. Neural network is a black box throughout the way that while it would approximate any function, studying the structure will not provide any insight into the nature of the function being approximated. The poor design practices which unintentionally result in logically redundant and may cause an unnecessary increase in network complexity.

The list of logical rules through Table 2 are used to develop logic programming in ADNN. These logical rules utilized as bipolar inputs and bipolar targets. The conventional ADNN utilizes bipolar $\{1, -1\}$ neuron representation that corresponds to $\{TRUE, FALSE\}$. Figure 2 shows the training process of logical rules can be implemented in ADNN. ADNN is capable of performing only a small subset of function known as linearly separable (Widrow & Lehr, 1990).

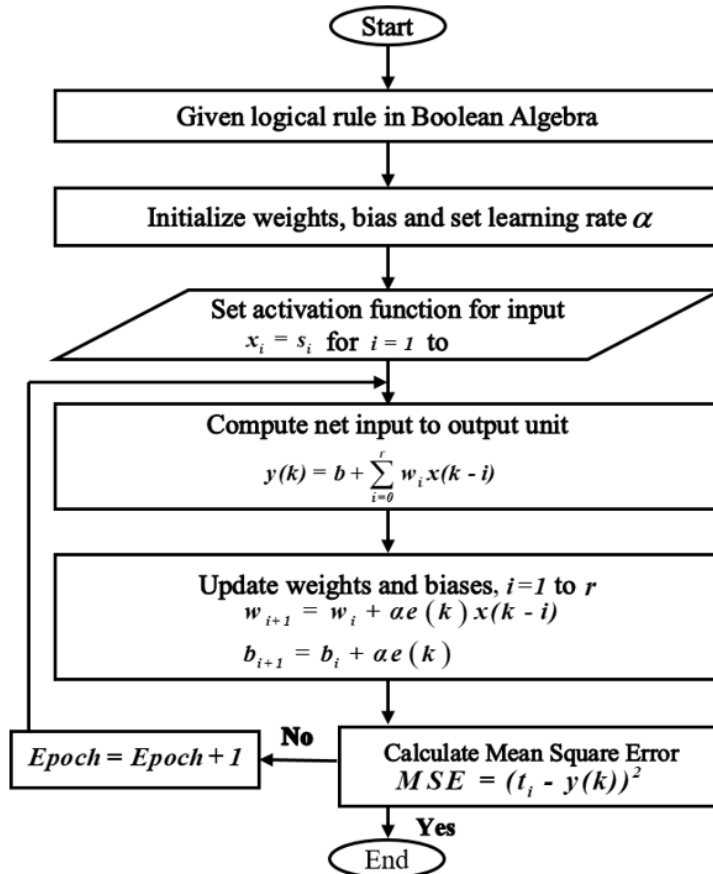


Figure 2. Flowchart of logic programming in Adaline Neural Network

With two inputs, ADNN can realize possible bipolar logical rules. Combination of elements and network of components can be utilized to perform functions which are not linearly separable.

Figure 3 demonstrates the distinctive situation that can be considered when logical rule in ADNN configuring the learning rate. However, learning rate will have an impact on how successfully ADNN will converge to arrive at the finest possible accuracy. The determination value of learning rate in the training process has a significant impact on the learning process. The learning rate decides how quickly ADNN is adjusted to the logical rule. ADNN was trained with diverse optimizer which is logical rule. For each optimizer it was trained with distinctive learning rate between $0 \leq \alpha \leq 1$ at logarithmic intervals. ADNN is trained until it achieves minimum mean square error. According to Smith (2017), we can approximate the optimal learning rate by increasing exponentially the learning rate at each iteration. In this case, the initial learning rate must be low in order to cater the increment of the α .

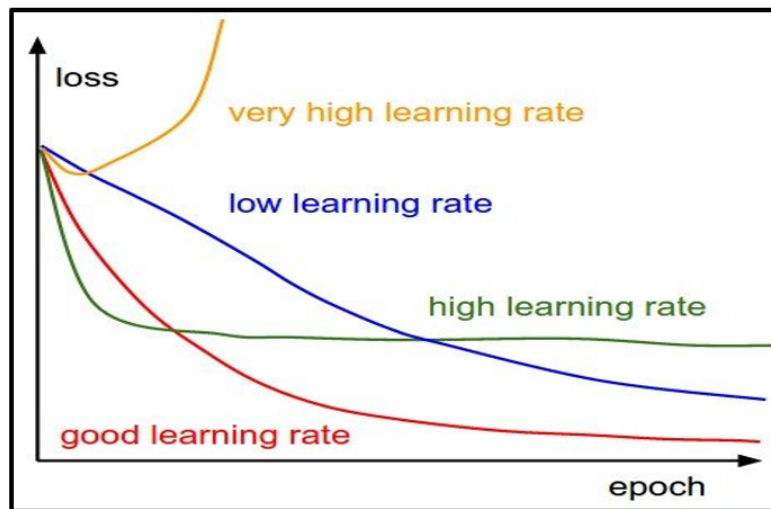


Figure 3. Symbolic illustration effect of different learning rate (Zulkiffi, 2018)

IMPLEMENTATION

Performance Evaluation

In this section, ADNN is evaluated based on mean square error. During the simulation, the value of learning rate would be introduced during the learning phase of the logical rule in ADNN. The proposed ADNN is compared with logical rule and learning rate.

Mean Square Error (MSE)

Mean square error (MSE) was used as a standard metric to evaluate the correlation between the target value and the net input to the output (Chen et al., 2010). This is supposed to minimize average of the squared difference between the estimated value and the target value. Least mean square error (LMS) algorithm proposed by Widrow and Hoff in 1959, is an adaptive algorithm. The LMS algorithm is relatively straightforward and LMS also an example of supervised training. The supervised training that uses MSE cost function may use formal statistical methods to determine the confidence of a trained model. The value can be used to calculate the confident interval of the output of the network (Equation 6).

$$\{p_1, t_1\}, \{p_2, t_2\}, \dots, \{p_q, t_q\}. \quad [6]$$

Here, $p_i = y(k)$ is an input to the network and t_i is the corresponding target output. The error is calculated as the difference between the target output and network output (Equation 7).

$$MSE = (t_i - y(k))^2. \quad [7]$$

The LMS algorithm will adjust the weights and bias of the ADNN to minimize the mean square error which is the difference between the target output t , and the net input y_{in} . The mean square error performance index for ADNN is quadratic. The performance index will either have a global minimum, a weak minimum or no minimum depending on characteristic of the input vector (Asha & Anuja, 2010).

Experimental Setup

This research based on simulated data set, where the initial neuron state was generated randomly. Based on Table 2, the variant of the logical rule would have applied in ADNN with several conditions that would take place where the learning process may run 50 epochs and 4 number of iteration. As stated in Table 3, a small random value of initial weights and bias was chosen because this may impact the error factor (Sivanandam & Deepa, 2006). There was no optimal number of iteration. In order to avoid overfitting, need to iterate until the error does not significantly decrease. The learning rate is hyperparameter may control how much the model can react to the evaluated error each time the weight is updated. The output from logical rules in ADNN would be compared with the target output until the weight change came to a small value.

RESULT AND DISCUSSION

Efficiency can be demonstrated by examining the value of MSE produced by ADNN with different logical rule. In term of stability, learning rate can be a metric to examine the stability of the proposed logical rule. Figures 4-8 reveal the MSE result for logical rule in ADNN with different value of learning rate respectively. The MSE was minimized

Table 3

Table of parameters for logical rules in ADNN

Parameter	Value
Initial Weight (w_i)	0.1
Bias (b)	0.1
Stopping Criteria	1. Number of iteration = 4 2. Number of Epoch ≤ 50
Learning Rate	$0.01 \leq \alpha \leq 0.4$
Number of Layer	Single Layer
Neuro State	$S_i = \{-1, 1\}$

based on the number of registered epochs. In order to make a fair comparison among all logical rule, the simulations are carried out until 50 epochs. As shown in Figure 4, logical rule in ADNN such as OR, AND, NAND, and NOR take fewer number of epoch during the learning phase to minimized the error. Conventional ADNN that employed a higher number of epochs during the learning phase might come to a point where the network became over-adapted to training data and losses performance in terms of generalization such as in Figure 6-8. Based on the value of MSE, the solution in NAND-Function in ADNN revealed the lowest error compared to the other logical rule. Based on Figure 5, the value of learning rate $\alpha = 0.01$ is lower compared to Figure 4 value of learning rate $\alpha = 0.1$. The value of learning rate will determine how quickly or slowly ADNN can learn from the problem. EXOR-Function and EXNOR-Function in Figure 5 showed the lowest learning rate but the training process took significantly longer to train and the error was not well minimized. Very small learning rate will not only be time consuming but will increase the probability for the ADNN to stuck in local minima MSE value (Goodfellow et al., 2016). Nevertheless, another four logical rules in ADNN revealed that the network took a shorter time to train and the error was optimally minimized. The result demonstrates that the training algorithm is precisely designed to find an approximate solution to minimize errors although there is no guarantee that the proposed ADNN will always arrive to the optimal solution. Hence according to the experimental value, we obtained $\alpha = 0.1$ as an optimal learning rate.

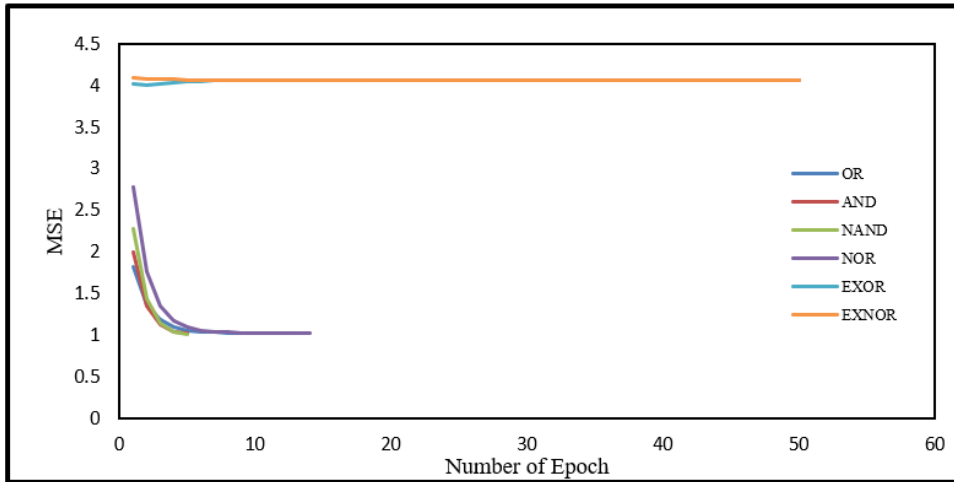


Figure 4. MSE for OR, AND, NAND, NOR, EXOR and EXNOR Function in ADNN with $\alpha = 0.1$

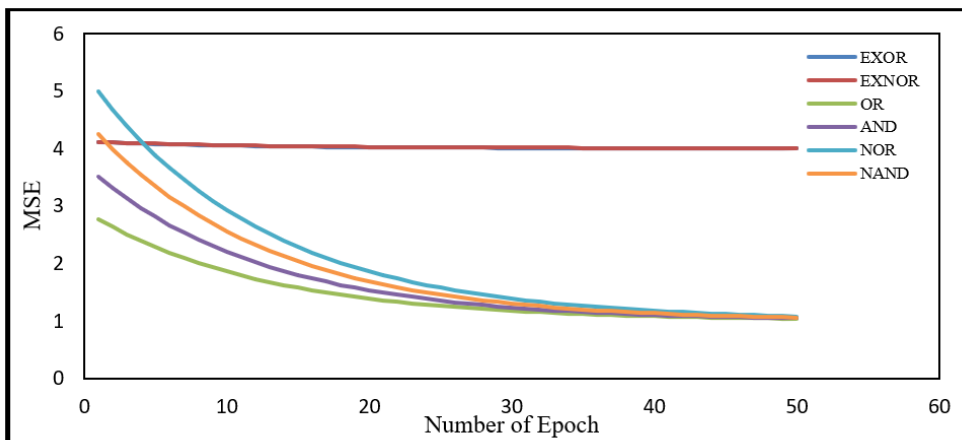


Figure 5. MSE for OR, AND, NAND, NOR, EXOR and EXNOR Function in ADNN with $\alpha = 0.01$

According to Figures 4-8, the lowest MSE value that governs the ADNN is NAND function. In the case of $P = 1$, NAND function works effectively in producing the final neuron state $P = 1$. In this case, ADNN produces the least MSE value in order to achieve the optimal weight for the output neurons. This is considered as an interesting result because this is the first logical that utilized redundant variable and being implemented in ANN. This is a major breakthrough over the result obtained by Kasihmuddin et al. (2017) that considered the redundant logical with $P = 1$ as an outcome. As of simple propositional logical rule

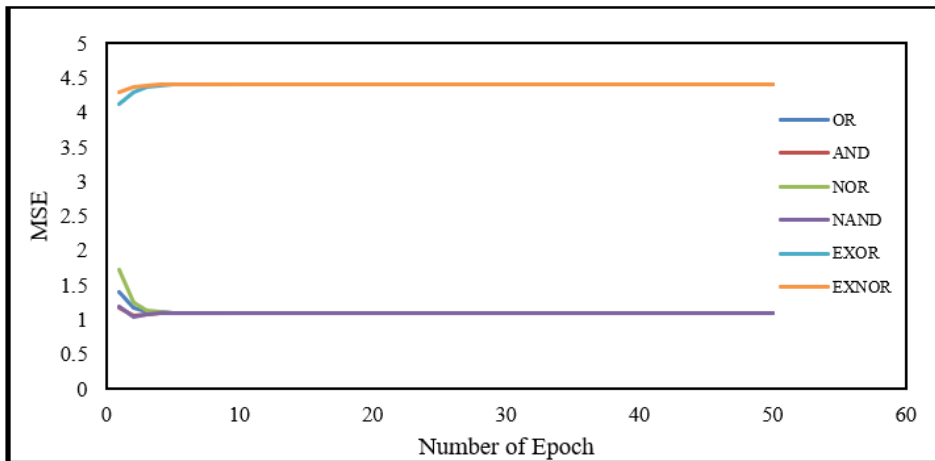


Figure 6. MSE for OR, AND, NAND, NOR, EXOR and EXNOR Function in ADNN with $\alpha = 0.2$

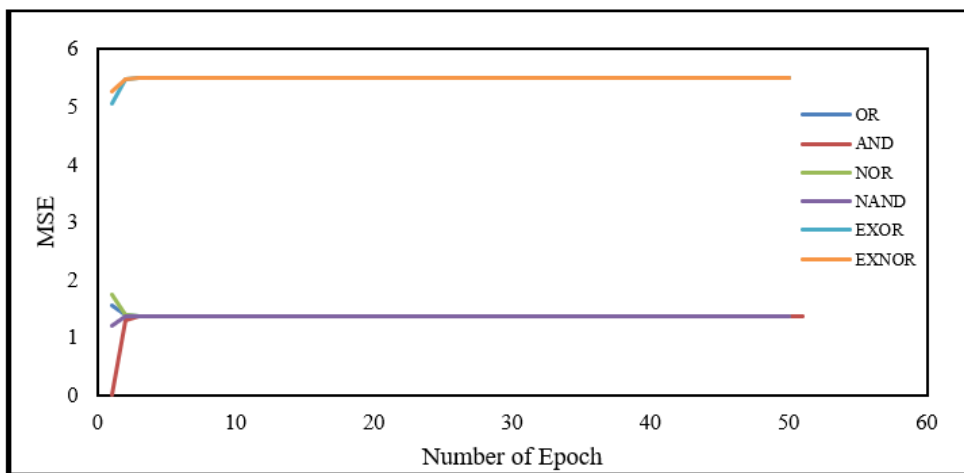


Figure 7. MSE for OR, AND, NAND, NOR, EXOR and EXNOR Function in ADNN with $\alpha = 0.3$

such as OR and AND had converge effectively and has a good agreement with the work of Mansor et al. (2020) that used similar logical rule. The proposed ADNN with NAND logical rule is shown to be more effective than the work of Alzaeemi et al. (2020) because ADNN incorporated with logical rule does not requires any complex hidden layer and specialized parameters where Alzaeemi et al. (2020) presented 2SAT logic programming in Radial Basis Function Neural Network. The proposed ADNN also does not require any rigid cost function that leads to $P = 1$ and computational clause checking. Hence,

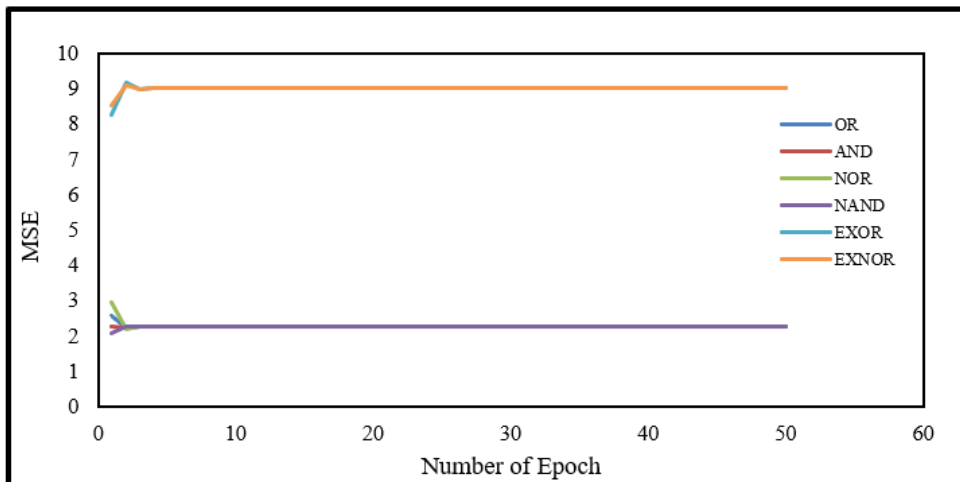


Figure 8. MSE for OR, AND, NAND, NOR, EXOR and EXNOR Function in ADNN with $\alpha = 0.4$

parameter tuning is required to reduce the error accumulation for other logical rule such as EXOR and EXNOR. ADNN is tends to converge to suboptimal weight when dealing with EXOR and EXNOR due to the structure of the clause involved. Although the value of error is high, the final output of the neuron is consistently $P = 1$. In practice, the training of EXOR and EXNOR can be further optimized by implementing accelerating algorithm such as Metaheuristics Algorithm. The limitation of logic programming in ADNN are the logical rule and the learning rate depending on the complexity of the learning process.

CONCLUSION

The primary aim for logic programming in ANN is to create flexible ANN that can govern both non-redundant and redundant logical rule. In this paper, the implementation of various logical rule in ADNN is proposed. The result obtained demonstrates the effectiveness of ADNN in governing redundant logical rule. This study has successfully uncovered the best logical rule that can be governed in ADNN with the lowest MSE value. In this case, NAND has been observed to has the lowest MSE value which leads to $P = 1$ with regards to other redundant logic. Hence, this profound logical rule is only a tip of the iceberg in creating ANN that is governed by logical rule. For future work, ADNN can utilize the non-differentiable signum function for non-linearity feature or Madaline network. In this network, multiple unit of ADNN in parallel will be utilized to process the training data. Despite the success by the proposed paradigms, robust and continuous efforts are needed especially on the complexity and application of these paradigms to obtain more feasible solutions.

ACKNOWLEDGEMENT

This research was funded by Fundamental Research Grant Scheme (FRGS), Ministry of Education Malaysia, grant number 203/PJJAUH/6711751 and Universiti Sains Malaysia.

REFERENCES

- Abdullah, W. A. T. W. (1992). Logic programming on a neural network. *International Journal of Intelligent Systems*, 7(6), 513-519. doi: <https://doi.org/10.1002/int.4550070604>
- Alzaeemi, S., Mansor, M. A., Kasihmuddin, M. S. M., Sathasivam, S., & Mamat, M. (2020). Radial basis function neural network for 2 satisfiability programming. *Indonesian Journal of Electrical Engineering and Computer Science*, 18(1), 459-469. doi: 10.11591/ijeecs.v18.i1.pp459-469
- Asha, P., & Anuja, J. (2010). *Benchmarking the competency mapping process with special reference to manufacturing industry*. Retrieved November 25, 2019, from <https://www.asmedu.org/incon/INCON6HRRP.pdf>
- Chen, B., Zhu, Y., & Hu, J. (2010). Mean-square convergence analysis of ADALINE training with minimum error entropy criterion. *IEEE Transactions on Neural Networks*, 21(7), 1168-1179. doi: 10.1109/TNN.2010.2050212
- Goodfellow, I., Bengio, Y., & Courville, A. (2016). *Deep learning*. Cambridge, USA: MIT press. doi: <https://doi.org/10.4258/hir.2016.22.4.351>
- Hamadneh, N. (2013). *Logic programming in radial basis function neural networks* (PhD thesis). Universiti Sains Malaysia, Malaysia.
- Jannati, M., Hosseinian, S. H., Vahidi, B., & Li, G. J. (2016). ADALINE (Adaptive Linear Neuron)-based coordinated control for wind power fluctuations smoothing with reduced BESS (battery energy storage system) capacity. *Energy*, 101, 1-8. doi: <https://doi.org/10.1016/j.energy.2016.01.100>
- Kasihmuddin, M. S. M., Mansor, M. A., & Sathasivam, S. (2016). Bezier curves satisfiability model in enhanced Hopfield network. *International Journal of Intelligent Systems and Applications*, 8(12), 9-17. doi: 10.5815/ijisa.2016.12.02
- Kasihmuddin, M. S. M., Mansor, M. A., & Sathasivam, S. (2017a). Hybrid genetic algorithm in the Hopfield network for logic satisfiability problem. *Pertanika Journal of Science and Technology*, 25(1), 139-152.
- Kasihmuddin, M. S. M., Mansor, M. A., & Sathasivam, S. (2018). Discrete Hopfield neural network in restricted maximum k-satisfiability logic programming. *Sains Malaysiana*, 47(6), 1327-1335. doi: <http://dx.doi.org/10.17576/jism-2018-4706-30>
- Kavak, A., Yigit, H., & Ertunc, H. M. (2005). Using ADALINE neural network for performance improvement of smart antennas in TDD wireless communications. *IEEE Transactions on Neural Networks*, 16(6), 1616-1625. doi: 10.1109/TNN.2005.857947
- Kho, L. C., Kasihmuddin, M. S. M., Mansor, M., & Sathasivam, S. (2020). Logic mining in league of legends. *Pertanika Journal of Science and Technology*, 28(1), 211-225.

- Kowalski, R. (1978). Logic for data description. In *Logic and data bases* (pp. 77-103). Boston, MA: Springer. doi: https://doi.org/10.1007/978-1-4684-3384-5_4
- Mansor, M. A., Jamaludin, S. Z. M., Kasihmuddin, M. S. M., Alzaeemi, S. A., Basir, M. F. M., & Sathasivam, S. (2020). Systematic boolean satisfiability programming in radial basis function neural network. *Processes*, 8(2), 1-16. doi: <https://doi.org/10.3390/pr8020214>
- Mansor, M. A., Kasihmuddin, M. S. M., & Sathasivam, S. (2017). Artificial immune system paradigm in the Hopfield network for 3-satisfiability problem. *Pertanika Journal of Science and Technology*, 25(4), 1173-1188.
- Negarestani, A., Setayeshi, S., Ghannadi-Maragheh, M., & Akashe, B. (2003). Estimation of the radon concentration in soil related to the environmental parameters by a modified Adaline neural network. *Applied Radiation and Isotopes*, 58(2), 269-273. doi: [https://doi.org/10.1016/S0969-8043\(02\)00304-4](https://doi.org/10.1016/S0969-8043(02)00304-4)
- Pajares, G., & Jesús, M. (2001). Local stereovision matching through the ADALINE neural network. *Pattern Recognition Letters*, 22(14), 1457-1473. doi: [https://doi.org/10.1016/S0167-8655\(01\)00097-6](https://doi.org/10.1016/S0167-8655(01)00097-6)
- Raschka, S. (2015). *Adaptive linear neuron*. Retrieved July 13, 2019, from https://rasbt.github.io/mlxtend/user_guide/classifier/Adaline/
- Riche, J. (2011). Logic in Whitehead's universal algebra. *Logique and Analyse*, 214(6), 135-159.
- Sathasivam, S. (2010). Upgrading logic programming in Hopfield network. *Sains Malaysiana*, 39(1), 115-118.
- Sathasivam, S., Mamat, M., Mansor, M., & Kasihmuddin, M. S. M. (2020b). Hybrid discrete Hopfield neural network based modified clonal selection algorithm for VLSI circuit verification. *Pertanika Journal of Science and Technology*, 28(1), 227-243.
- Sathasivam, S., Mansor, M. A., Kasihmuddin, M. S. M., & Abubakar, H. (2020a). Election algorithm for random k satisfiability in the Hopfield neural network. *Processes*, 8(5), 1-19. doi: <https://doi.org/10.3390/pr8050568>
- Sharma, P., Raghuvanshi, A., & Pachori, R. (2019). *Artificial intelligence and soft computing: Soft computing techniques: Artificial intelligence, neural networks, fuzzy logic and genetic algorithm*. Chhattisgarh, India: Educreation Publishing.
- Sharma, S. (2017). *Activation functions in neural networks*. Retrieved September 8, 2020, from <https://towardsdatascience.com/activation-functions-neural-networks-1cbd9f8d91d6>
- Sivanandam, S. N., & Deepa, S. N. (2006). *Introduction to neural networks using Matlab 6.0*. New Delhi, India: Tata McGraw-Hill Education.
- Smith, L. N. (2017, March 24-31). Cyclical learning rates for training neural networks. In *2017 IEEE Winter Conference on Applications of Computer Vision (WACV)* (pp. 464-472). Santa Rosa, CA, USA. doi: 10.1109/WACV.2017.58
- Somogyi, Z., Henderson, F., & Conway, T. (1996). The execution algorithm of mercury, an efficient purely declarative logic programming language. *The Journal of Logic Programming*, 29(1), 17-64. doi: [https://doi.org/10.1016/S0743-1066\(96\)00068-4](https://doi.org/10.1016/S0743-1066(96)00068-4)

- Sujith, M., & Padma, S. (2020). Optimization of harmonics with active power filter based on ADALINE neural network. *Microprocessors and Microsystems*, 73(2020), 1-17. doi: <https://doi.org/10.1016/j.micpro.2019.102976>
- Wang, Z. Q., Manry, M. T., & Schiano, L. (2000). LMS learning algorithms: Misconceptions and new results on convergence. *IEEE Transactions on Neural Network*, 11(1), 47-56. doi: 10.1109/72.822509
- Widrow, B., & Hoff, M. E. (1960). *Adaptive switching circuits*. Stanford, California: Stanford University CA Stanford Electronics Labs.
- Widrow, B., & Hoff, M. E. (1959). Adaptive sampled-data systems - A statistical theory of adaptation. *I.R.E. Wescon Convention Record*, 4, 96-104.
- Widrow, B., & Lehr, M. A. (1990). 30 years of adaptive neural networks: Perceptron, madaline, and backpropagation. *Proceedings of the IEEE*, 78(9), 1415-1442. doi: 10.1109/5.58323
- Widrow, B., & Stearns, S. D. (1985). *Adaptive signal processing*. Englewood Cliffs, N.J: Prentice-Hall.
- Zulkifli, H. (2018). *Understanding learning rates and how it improves performance in deep learning*. Retrieved July 16, 2019, from <https://towardsdatascience.com/understanding-learning-rates-and-howit-improves-performance-in-deep-learning-d0d4059c1c10>.

Improvement of Bioethanol Production in Consolidated Bioprocessing (CBP) via Consortium of *Aspergillus niger* B2484 and *Trichoderma asperellum* B1581

Mona Fatin Syazwanee Mohamed Ghazali, Muskhazli Mustafa*, Nur Ain Izzati Mohd Zainudin and Nor Azwady Abd Aziz

Department of Biology, Faculty of Science, Universiti Putra Malaysia, 43400 UPM, Serdang, Selangor, Malaysia

ABSTRACT

Consolidated bioprocessing (CBP) in bioethanol production involves the combination of four essential biological procedures in a single bioreactor, using a mixture of organisms with favourable cellulolytic ability without the addition of exogenous enzymes. However, the main disadvantage of this process is the complexity to optimise all factors considering both enzymes and microbial activity at the same time. Hence, this study aimed to optimise suitable culture conditions for both organisms to work efficiently. Six single factors that are considered crucial for bioethanol production were tested in one-factor-at-a-time (OFAT) analysis and analysed using Response Surface Methodology (RSM) software for *Aspergillus niger* B2484 and *Trichoderma asperellum* B1581 strains. The formulation of a new consortia setting was developed based on the average of two settings generated from RSM testing several combinations of consortia concentrations (5:1, 2:4, 3:3, 4:2, and

1:5). The combination of 5:1 *Aspergillus niger* B2484 and *Trichoderma asperellum* B1581 produced the most ethanol with 1.03 g/L, more than *A. niger* B2484, alone with 0.34 g/L of ethanol, indicating the potential of the combination of *A. niger* B2484 and *T. asperellum* B1581 co-culture for bioethanol production in CBP.

ARTICLE INFO

Article history:

Received: 9 September 2020

Accepted: 30 November 2020

Published: 22 January 2021

DOI: <https://doi.org/10.47836/pjst.29.1.17>

E-mail addresses:

mfsyazwanee_ghazali@yahoo.com (Mona Fatin Syazwanee

Mohamed Ghazali)

muskhazli@upm.edu.my (Muskhazli Mustafa)

ainizzati@upm.edu.my (Nur Ain Izzati Mohd Zainudin)

azwady@upm.edu.my (Nor Azwady Abd Aziz)

*Corresponding author

Keywords: Bioethanol, consolidated bioprocessing, consortium; one-factor-at-a-time analysis, response surface methodology

INTRODUCTION

Bioethanol, commonly known as ethyl alcohol (C_2H_5OH), is generated from the fermentation of fermentable sugars, such as glucose and sucrose, from plant sources using microorganisms (Chin & H'ng, 2013). The production of bioethanol represents as an alternative source of energy which also helps to minimise greenhouse gases effects (Artifon et al., 2018). The first-generation bioethanol production was based on food crops but due to competition between the food supply and bioethanol development, there was a sudden increase in food prices (Naik et al., 2010). This led to the development of second-generation bioethanol production using non-food based and readily available resources, such as lignocellulosic materials (Singh & Trivedi, 2013). These materials primarily originate from biomass sources, such as wheat straw, corn stover, and paddy straw, which comprise two structural polysaccharides, namely cellulose and xylan, that can be transformed into simple sugars (Park et al., 2010). Biodegradation of cellulose into glucose has become more popular as it offers low investment costs and is a non-polluting bioprocess (Liu et al., 2011).

Consolidated bioprocessing (CBP) in bioethanol production involves the combination of four biological procedures, secretion of cellulolytic enzymes, degradation of polysaccharides present in biomass, and the fermentation of hexose (C6) and pentose sugars (C5), in a single bioreactor (Kaneko et al., 2012). The challenge in the development of CBP is to identify an appropriate microorganism, which has all crucial properties for the utilisation of lignocellulosic materials, such as cellulolytic enzymes for degradation and capacity to ferment all mono-saccharides available, to produce ethanol via fermentation (Huang et al., 2014; Suhag & Singh, 2014).

Due to unavailability of a single strain to produce all essential enzymes for efficient lignocellulose degradation, a recent study focussed on the development of fungal consortia with benefits of evading feedback regulations and metabolite suppression (Wongwilaiwalin et al., 2010; Cui et al., 2015). The 'on-site' production of cellulolytic enzyme results from the co-cultivation of fungi in a single system (Ray & Behera, 2017), which can be achieved by co-cultivation of compatible fungal strains in a single bioreactor, cultivation of genetically modified strain with some good cellulolytic genes, or cultivation of several monocultures by blending enzymes (Kolasa et al., 2014). In comparison to single cultures, co-cultivation cultures of fungi may result in better utilisation of substrate, enhanced adaptability to changing conditions, improved resistance to contamination by undesirable microbes and most importantly, increased production yield (Tesfaw & Assefa, 2014). Before fungi application as consortia, a compatibility test is mandatory to avoid further complication during CBP. According to Syazwanee et al. (2019) there was mutual interaction between *Aspergillus niger* B2484 and *Trichoderma asperellum* B1581, indicating that these species can mutually live together in the same medium or environment without suppressing each

other's growth. However, the major obstacle in using microbial consortia for CBP is the difficulty in controlling both single microbes and the whole system simultaneously (Shong et al., 2012). The initiation of a stable co-culture system involves a complex process, in which all culture conditions, such as the pH of the medium, temperature of saccharification, the concentration of the substrates and enzyme, substrates size, carbon sources and pressure must be adjusted to be optimal for each strain (Cheng & Zhu, 2013; Shah et al., 2016). Hence, determination of the appropriate and stable conditions for fungi consortium to produce the maximal amount of bioethanol is required. This study aimed to develop a fungi consortium of *A. niger* B2484 and *T. asperellum* B1581 to produce bioethanol.

MATERIALS AND METHODS

Fungi Stock Culture

Aspergillus niger B2484 and *Trichoderma asperellum* B1581 were obtained from the Mycology Laboratory, Faculty of Science, Universiti Putra Malaysia. All strains were grown on Potato Dextrose Agar (PDA) at $28^{\circ}\text{C} \pm 2^{\circ}\text{C}$ for 7 days.

Preparation of Culture

The culture was prepared using 1% (w/v) paddy straw with size 5 mm and pretreated with 2% (w/v) NaOH (Syazwanee et al., 2018). The compositions of paddy straw after pretreatment were; 72.47% cellulose, 19.42% hemicellulose, 1.02% lignin and 5.44% ash content. The paddy straw was mixed in 25 mL of 10% (v/v) basal medium ($(\text{NH}_4)_2\text{SO}_4$ 1.4 g/L; KH_2PO_4 2.0 g/L; CaCl_2 0.3 g/L; $\text{MgSO}_4 \cdot 7\text{H}_2\text{O}$ 0.3 g/L; CoCl_2 2.0 g/L) with 1 mL of trace elements ($\text{MnSO}_4 \cdot \text{H}_2\text{O}$ 1.56 g/L; $\text{FeSO}_4 \cdot 7\text{H}_2\text{O}$ 5.0 g/L; $\text{ZnSO}_4 \cdot 7\text{H}_2\text{O}$ 1.4 g/L) and sterilised at $121 \pm 0.5^{\circ}\text{C}$ for 15 min (Ja'afaru, 2013). The culture medium was inoculated with fungal spore suspensions of *T. asperellum* B1581 and *A. niger* B2484 once it had cooled. In order to ensure the growth of both fungi were constant throughout the entire experiment, the concentrations of the spore suspensions were calculated using haemocytometer and the concentrations were adjusted to 1×10^6 spore/mL (Mauch et al., 1988).

One-factor-at-a-time (OFAT) Analysis

The culture conditions were based on a preliminary study and are as follows: 150 rpm, $30^{\circ}\text{C} \pm 0.5^{\circ}\text{C}$ for saccharification and fermentation processes, 3 days of saccharification and 3 days of fermentation. Six parameters, duration of saccharification, saccharification temperature ($^{\circ}\text{C}$), duration of fermentation, fermentation temperature ($^{\circ}\text{C}$), media level (% v/v), and substrate level (% w/v), were tested using a Megazyme® Ethanol Assay Kit (Table 1). In this study, both saccharification and fermentation process were carried out in

Infors HT- Multitron incubator shaker; the only difference during fermentation process was the samples were allowed to rest at controlled temperature without any agitation occurs. This approach was performed sequentially to identify the level of the factors influencing the yield (Shaw et al., 2002). The data obtained from OFAT was analysed using mean \pm standard deviation at the 95% confidence limit ($p < 0.05$).

Table 1

The pre-determine ranges for each of the parameters in one-factor-at-a-time (OFAT)

Parameters tested	Control setting	Ranges
Temperature of fermentation	$30 \pm 0.5^{\circ}\text{C}$	$25^{\circ}\text{C} - 45 \pm 0.5^{\circ}\text{C}$
Days of saccharification	3 days	1 day – 5 days
Days of fermentation	3 days	1 day – 5 days
Substrate level	1%	1% - 7%
Media level	10%	10% - 90%
Temperature of saccharification	$30 \pm 0.5^{\circ}\text{C}$	$25^{\circ}\text{C} - 45 \pm 0.5^{\circ}\text{C}$

Response Surface Methodology (RSM)

The optimisation of RSM was performed using a Central Composite Design (CCD) via Design-Expert software Version 6.0.8 (Stat-Ease Inc., Minneapolis, MN, USA) with the full expression of the quadratic model. For each response, optimum points were predicted based on the variable input, followed by the second-order polynomial in the quadratic model. The amount of ethanol was quantified for each set-up and was subjected to analysis of variance (ANOVA) to determine the optimum set-up for bioethanol production.

Consortium Development

The compatibility of *A. niger* B2484 and *T. asperellum* B1581 was tested before the development of fungal consortia. The consortia of *A. niger* B2484 and *T. asperellum* B1581 was designed based on 6% v/v (10^6 spores/mL) in the combination of 1:5, 2:4, 3:3, 4:2 and 5:1. The amount of ethanol produced was quantified by the Megazyme® ethanol assay kit according to the manufacturer's instructions at 340 nm.

RESULTS AND DISCUSSION

Determination of Parameters via OFAT Analysis

The optimisation of all parameters is essential to ensure the maximum production of bioethanol. The classical method of optimisation involves varying one-factor-at-a time

(OFAT) while keeping the others constant (Czitrom, 1999). In the OFAT analysis, the parameter range was tested from large scale and narrowed down to a smaller scale, which was later used in the RSM software. The analysis also allows fast identification of the influence of the factors involved and the experimental results can be easily understood (Pambi & Musonge, 2016). One of the main disadvantages in the SSF process and CBP is the identification of the optimal temperature required for the saccharification and fermentation stages (Hasunuma & Kondo, 2012). Hence, the first parameter tested was the fermentation temperature. All samples were incubated at different temperatures from 25°C to 45 ± 0.5°C, with the most ethanol produced by both *A. niger* B2484 (0.04 ± 0.01 g/L) and *T. asperellum* B1581 (0.06 ± 0.02 g/L) at 30°C (Figure 1a), thus, narrowing the range of fermentation temperature for RSM to 27–32°C ± 0.5°C. The fermentation process in this study was carried out by filamentous fungi under aerobic condition. As this process is an exergonic, controlling the fermentation temperature with proper handling has become a compulsory (Cutzu & Bardi, 2017). According to Satyakala et al. (2017) maximum growth for *A. niger* and *Trichoderma harzianum* are recorded at 30°C and it is significantly highest over all other temperature tested between 20°C to 35°C. The unsuitable temperature for the microbial growth causes an inhibitory effect on the production of bioethanol (Selim et al., 2018). The increment of temperature improves the rate of biological reactions up to a certain temperature but further increment in temperature may cause in lesser product formation (Kanagasabai et al., 2019). The duration of saccharification was manipulated from 1 day to 5 days using the optimal fermentation temperature, with *A. niger* B2484 producing 0.04 ± 0.01 g/L ethanol after 3 days, while *T. asperellum* B1581 produced most ethanol (0.05 ± 0.01 g/L) after 2 days of saccharification (Figure 1b). Regarding the amount of ethanol produced, *T. asperellum* B1581 produced more ethanol than *A. niger* B2484, which is in line with Jena and Satpathy (2017) who showed that *Trichoderma* strains produced more ethanol from the fermentation of cellulose into ethanol than *Aspergillus*.

The duration of fermentation was shorter than saccharification, especially for *A. niger* B2484, with most ethanol produced after 1 day of fermentation (0.03 ± 0.00 g/L), decreasing thereafter (Figure 1c), whereas *T. asperellum* B1581 produced most ethanol after 2 days of fermentation (0.03 ± 0.00 g/L), with no ethanol detected from day 3 onwards. The fermentation time influences fungal growth, hence, a shorter fermentation time will cause inefficient fermentation due to insufficient fungal growth, while a longer period of fermentation results has toxic effects on growth due to the high concentration of ethanol in the fermented broth (Azhar et al., 2017). Even though the OFAT analysis was performed sequentially, it fails to consider the interactions between variables (Kanmani et al., 2013), explaining why the amount of ethanol produced suddenly drops. Therefore, to explore the relationships between several explanatory operating variables, RSM has been extensively used to optimise parameters for the production of ethanol from different substrates (Dasgupta et al., 2013).

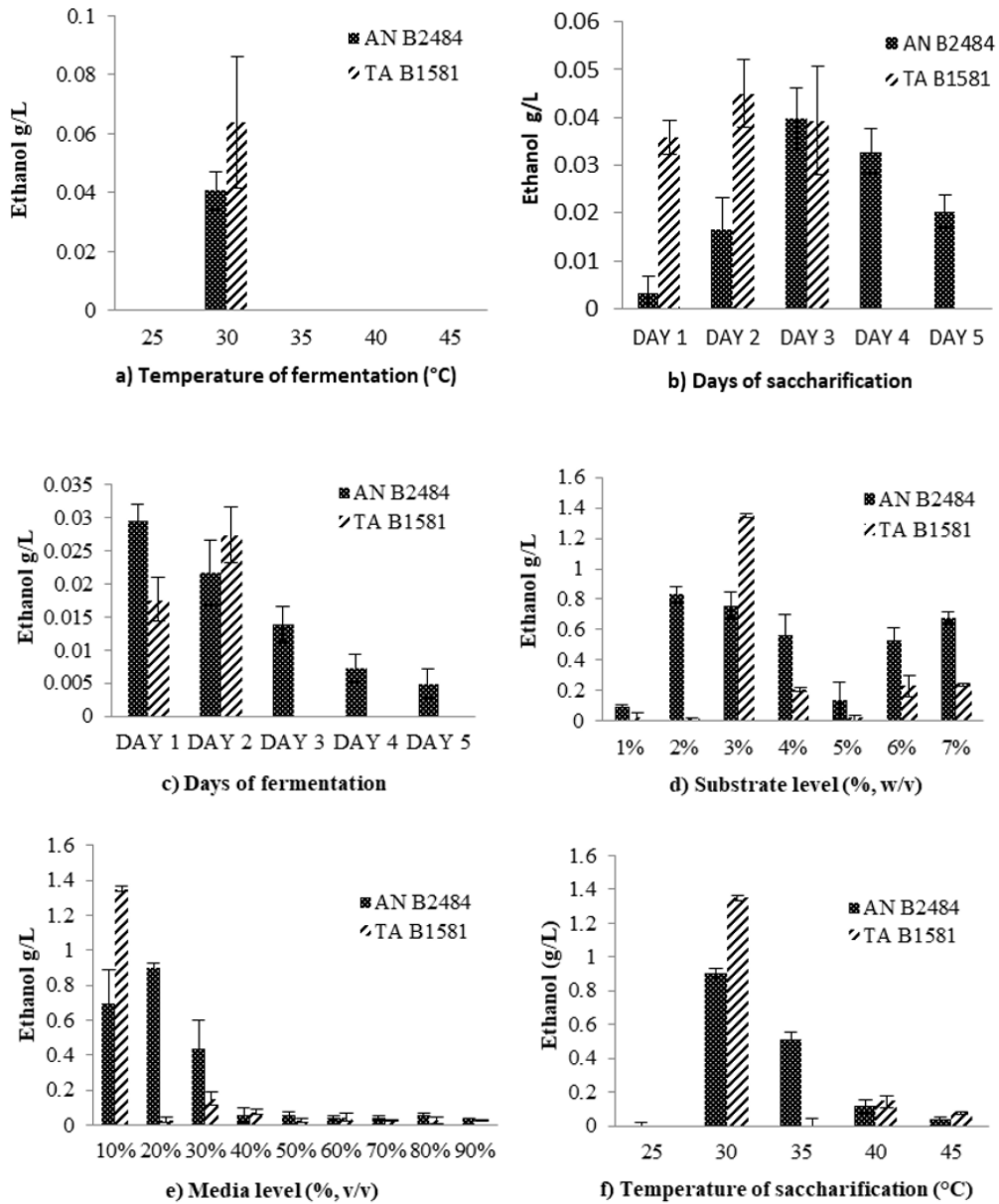


Figure 1. Optimization of all significant parameters using OFAT analysis, which were carried out in sequential pattern from parameter (a) to parameter (f) for both *A. niger* B2484 and *T. asperellum* B1581

The substrate was paddy straw pretreated with 2% NaOH and the range was set below 10% (w/v). In this study, *A. niger* B2484 produced 0.83 ± 0.05 g/L ethanol using 2% substrate loading and *T. asperellum* B1581 produced 1.35 ± 0.02 g/L ethanol using 3%

substrate loading mixed 10% (v/v) basal media (Figure 1d). Next, the media level (% v/v), also referred to as the amount of basal media, was manipulated from 10% to 90% (v/v), with the amount of ethanol produced by *A. niger* B2484 increasing from 0.83 ± 0.05 g/L to 0.90 ± 0.03 g/L using 20% (v/v) media (Figure 1e). However, there was no improvement in the volume of ethanol produced by *T. asperellum* B1581. The optimal temperature in normal CBP for saccharification was 50°C, 30°C for fermentation, thus, a compromise was required to achieve both processes (Mutreja et al., 2011). In this study, the last parameter tested was the saccharification temperature, which ranged from 25°C to $45 \pm 0.5^\circ\text{C}$, showing that the optimal temperature for saccharification for *A. niger* B2484 and *T. asperellum* B1581 was $30 \pm 0.5^\circ\text{C}$ (Figure 1f). This analysis suggested a compromised optimal temperature for both the saccharification and fermentation process of $30 \pm 0.5^\circ\text{C}$ in CBP. However, the OFAT approach proved to be time consuming and unreliable, leading to inaccurate optimal conditions without considering the interactions between factors (Wahid & Nazir, 2013). Such complications can be reduced by varying several variables at the same time, by designing experiments using statistical methods such as RSM (Bhaumik et al., 2013; Biswas et al., 2017). Despite the drawbacks, the OFAT analysis played an important role in determining the selection range for RSM evaluation for bioethanol production.

Response Surface Methodology (RSM)

The OFAT analysis results were used to optimise bioethanol production using *A. niger* B2484 and *T. asperellum* B1581 by RSM. To measure how adequate the suggested model suits the experimental data, the parameters such as R^2 , p-value, standard deviation and adequate precision are used to describe the quadratic model. The p-value (the values of “Prob > F”) is the probability of a given statistical model, whether it is similar to or larger than the actual experimental results when the null hypothesis is true. If the p-value is small, the probability of the null hypothesis is small, hence, a smaller p-value corresponds to more significant results (Liu et al., 2018). In this study, the p-value for both organisms (*A. niger* B2484 and *T. asperellum* B1581) was <0.0001 , indicating significant bioethanol production. For *A. niger* B2484, the quadratic regression model yielded a determination coefficient (R^2) of 0.60, with the fit explaining 60% of the total variation in the data, while the R^2 value for *T. asperellum* B1581 was 0.79, explaining 79% of the results (Table 2). A value of R^2 which is close to 1 indicates an almost flawless relationship with all data points falls perfectly on the regression line, while a value of R^2 close to 0 indicates that the mean is corresponding to the model fitted (Saunders et al., 2012). Nevertheless, a high coefficient of determination is not a definite guarantee in indicating a ‘goodness of fit’ and similarly there is also no guarantee that a small R^2 value specifies a weak relationship as the statistic is mostly influenced by variation in the independent variable (Hamilton, 2015). In this study, despite having a low R^2 value, the independent variables were significant

and important relationship between variables can be clearly seen in the Equations 1 (Y_1) and 2 (Y_2).

Table 2

The summary of quadratic model statistics of *A. niger* B2482 and *T. asperellum* B1581

Source	Std.dev	Mean	R ²	Adjusted R ²	Predicted R ²	Adequate Precision
1. AN B2484	0.19	0.22	0.60	0.42	-0.01	8.23
2. TA B1581	0.19	0.26	0.79	0.69	0.39	11.82

1. *Aspergillus niger* B2484

2. *Trichoderma asperellum* B1581

The signal to noise ratio was evaluated by adequacy precision, which involved the predicted value at the design points and the average prediction error (Behera et al., 2018). In the present study, the adequacy precision ratio for *A. niger* B2484 was 8.23, 11.82 for *T. asperellum* B1581, which was desirable as the required ratio should be greater than 4. Hence, the developed model can be used to guide the design space.

To simultaneously optimise the responses, the RSM uses a set of mathematical and statistical procedures to explain a polynomial equation that relates to the experimental data (Bezerra et al., 2008; Akintunde et al., 2015). Y_1 and Y_2 represent the ethanol production by *A. niger* B2484 and *T. asperellum* B1581 respectively in the CBP process. The symbols A, B, C, D, E, F represent coded variables used in CCD: (A) duration of saccharification, (B) saccharification temperature, (C) duration of fermentation, (D) fermentation temperature, (E) media level and lastly, (F) substrate level.

$$Y_1 = + 0.58 + 0.11A + 0.02B + 0.02C + 0.03D + 0.02E + 0.03F - 0.07A^2 - 0.07B^2 - 0.06C^2 - 0.05D^2 - 0.07E^2 - 0.06F^2 - 0.01AB + 0.02AC + 9.25E-003AD + 7.25E-003AE + 0.01AF - 5.50E-003BC + 0.01BD - 4.97E-003BE - 0.02BF + 0.02CD - 0.01CE + 0.02CF + 8.75E-004DE + 9.41E-003DF - 7.03E-003EF$$

[1]

$$Y_2 = + 0.93 + 0.11A + 0.02B + 0.02C + 0.02 D - 0.03E + 0.05F - 0.12A^2 - 0.14B^2 - 0.13C^2 - 0.08D^2 - 0.13E^2 - 0.12F^2 + 0.01AB + 0.01AC + 0.04AD - 0.03AE + 0.04AF - 2.70E-003BC - 0.03BD - 6.72E-004BE - 0.02BF + 2.52E-003CD - 5.45E-003CE + 0.03CF - 0.01DE + 9.55E-003DF - 0.037EF$$

[2]

The positive and negative signs in Equations 1 and 2 represent synergy and antagonistic effects among the variables. Hence, the model terms showing a positive synergistic effect in ethanol production by *A. niger* B2484 (Y_1 or Equation 1) were A, B, C, D, E, F, AC, AD, AE, AF, BD, CD, CF, DE, DF, with the interaction between A, B, C, D, F, AB, AC, AD, AF, CD, CF, DF showing positive synergy in ethanol production by *T. asperellum* B1581, with the other terms showing antagonistic effects (Y_2 or Equation 2).

The standard deviation for both models was 0.19, indicating that the predicted and actual values were close. To test the adequacy of the model developed, the numerical optimisation of ethanol production by *A. niger* B2484 and *T. asperellum* B1581 were tested, in which the model predictions were compared with the actual outcome for validation purposes (Table 3). To check the optimal points predicted by the software, a series of five replicate experiments were performed and the outcome analysed using a one-sample t-test (Safa et al., 2017). The values of the predicted amount of ethanol showed no significant difference to the actual amount of ethanol produced, confirming that the experimental values were in agreement with the predicted values, thus the model was validated.

Table 3

The optimization settings recommended by RSM for A. niger B2484 and T. asperellum B1581 along with formulation of new consortia setting based from the average settings

	RSM Settings						Outcome	
	Saccharification		Fermentation		Basal Media		Ethanol (g/L)	
No.	Hour (h)	Temp (°C)	Hour (h)	Temp (°C)	Media (%v/v)	Subs. (%w/v)	Predicted	Actual
1.	66.75	29.76	32.3	30.18	14.74	2.59	0.61 ± 0.11	0.63 ± 0.19
2.	67.72	29.58	32.9	29.79	12.42	2.84	0.96 ± 0.14	0.94 ± 0.27
Avg	67.24	29.67	32.6	29.99	13.58	2.72		

1. *Aspergillus niger* B2484

2. *Trichoderma asperellum* B1581

The new RSM setting for both strains suggests the same saccharification and fermentation temperature, $30^{\circ}\text{C} \pm 0.5$ with an average total time of 99.84 h or approximately 4 days. The optimum level of media (% v/v) used for *A. niger* B2484 and *T. asperellum* B1581 were 14.74% and 12.42% respectively. Theoretically, the usage of high substrate concentration should achieve a great ethanol yield during fermentation but the concentrated

substrate creates an inhibitory effect to the fermentation process owing to the osmotic stress (Hamouda et al., 2015). With optimum amount of substrate level used, 2.59% managed to produce approximately 0.63 g/L ethanol using *A. niger* B2484 in CBP. As for *T. asperellum* B1581, 0.94 g/L ethanol was produced using 2.84% substrate. In this study, the optimized RSM set-up helped to provide better result with good reproducibility and reliable estimation as it evaluated the effects and learn the interactions between all the important parameters involved for an efficient bioethanol production using paddy straw.

Formation of the Fungal Consortium

Generally, different strains of fungi have different optimal growth conditions, so the most appropriate optimal conditions for both strains to mutually co-exist for bioethanol production must be determined (Table 3). The combination of different species influences the productivity of biomass degradation through species interactions, such as mutual intermingling, inhibition and mutual intermingling with inhibition (Correa et al., 2018). The compatibility of the fungi from different genera, *Trichoderma* and *Aspergillus* have been studied, indicating that both species show mutual intermingling interactions and can co-exist in the same environment for the production of ethanol (Syazwanee et al., 2019). This led to the development of a consortium of 6% v/v (10^6 spores/mL) *A. niger* B2484 and *T. asperellum* B1581 in the ratio of 1:5, 2:4, 3:3, 4:2 and 5:1 (Table 4).

Table 4

The amount of ethanol produced from different consortium composition between A. niger B2484 and T. asperellum B1581

Species	Consortium ratio (10^6 spore/mL)	Species	Ethanol (g/L) \pm S.D
<i>A. niger</i> B2484	1:5	<i>T. asperellum</i> B1581	0.93 \pm 0.16 ^a
<i>A. niger</i> B2484	2:4	<i>T. asperellum</i> B1581	0.17 \pm 0.04 ^{bc}
<i>A. niger</i> B2484	3:3	<i>T. asperellum</i> B1581	0.04 \pm 0.02 ^c
<i>A. niger</i> B2484	4:2	<i>T. asperellum</i> B1581	0.16 \pm 0.03 ^{bc}
<i>A. niger</i> B2484	5:1	<i>T. asperellum</i> B1581	1.03 \pm 0.10^a

Values are means of three replicates with \pm SD.

Conventionally, ethanol is manufactured from processing starch, followed by fermentation of glucose using *Saccharomyces cerevisiae*, but this particular yeast failed to fully utilise the main C5 sugar (xylose) of the hydrolysate produced from agricultural waste hydrolysis (Sarkar et al., 2012; Ire et al., 2016). In comparison with pure cultures, co-cultivation systems could widen up the substrate utilisation scales (Jiang et al., 2019). Based on the advantages of these two fungi, their combination performs better in reducing sugar (Kartini & Dhokhikah, 2018). Indeed, the co-cultivation of fungi has been suggested to be more efficient for CBP compared to mono-cultivation (Grewal et al., 2020). However, fine-tuning and balancing the inoculation ratio significantly affects overall production and can be very challenging (Jawed et al., 2019). Hence, several combination ratios of *A. niger* B2484 and *T. asperellum* B1581 were tested, demonstrating that the combination of *A. niger* B2484 and *T. asperellum* B1581 in the ratio 5:1 produced the most ethanol, 1.03 g/L, compared to the single culture of *A. niger* B2484, 0.63 g/L. These results indicate that CBP for bioethanol production from cellulosic material can be accomplished by the combination of *A. niger* B2484 and *T. asperellum* B1581 in the ratio 5:1 without using microbes with gene recombinant (Horisawa et al., 2019). The enhancement of the ethanol titre occurred only within a proper range and appropriate proportion (Du et al., 2015). Under these circumstances, the beneficial effects of microbial consortium could become limited due to environmental stress factors and competition for the same resources (Bradáčová et al., 2019). In a microbial consortium, interactions such as mutualism and competition between two different species in the same ecological environment will affect the metabolism and influence the production of the target product in the fermentation process (Jiang et al., 2017).

Instead of using gas chromatography (GC) analysis, the overall process of ethanol quantification was done using Megazyme® Ethanol Assay Kit as the process was more cost efficient and time saving considering the large number of samples that needed to be quantified. The Single Lab Validation from Ivory et al. (2020) demonstrates that the Ethanol Assay Kit is suitable and relevant for the quantification of ethanol in low alcohol samples, fruit juices as well as fermented drinks with quick, easy and robust method. Hence, suggesting the fitness of this kit for the measurement of ethanol in this study.

CONCLUSION

The assessment of consolidated process for ethanol production using fungal consortium between *A. niger* B2484 and *T. asperellum* B1581 has been carried out using newly formulated setting derived from an average of initial settings suggested by RSM for both strains. Out of five possible combination ratios, the 5:1 combination of *A. niger* B2484 and *T. asperellum* B1581 produced the most ethanol, 1.03 g/L; verifying the potential of *A. niger* B2484 and *T. asperellum* B1581 as co-culture for bioethanol production in CBP.

ACKNOWLEDGEMENT

The authors would like to acknowledge Universiti Putra Malaysia for financial support through Grant No. GP-IPS/2016/9485600 and all staff of the Plant Systematic and Microbe Laboratory, Biology Department, Universiti Putra Malaysia for their efforts.

REFERENCES

- Akintunde, A. M., Ajala, S. O., & Betiku, E. (2015). Optimization of *Bauhinia monandra* seed oil extraction via artificial neural network and response surface methodology: A potential biofuel candidate. *Industrial Crops and Products*, 67, 387-394. doi: <https://doi.org/10.1016/j.indcrop.2015.01.056>
- Artifon, W., Bonatto, C., Bordin, E. R., Bazoti, S. F., Dervanoski, A., Alves, S. L., & Treichel, H. (2018). Bioethanol production from hydrolyzed lignocellulosic after detoxification via adsorption with activated carbon and dried air stripping. *Frontiers in Bioengineering and Biotechnology*, 6, 1-6. doi: <https://doi.org/10.3389/fbioe.2018.00107>
- Azhar, S. H. M., Abdulla, R., Jambo, S. A., Marbawi, H., Gansau, J. A., Faik, A. A. M., & Rodrigues, K. F. (2017). Yeasts in sustainable bioethanol production: A review. *Biochemistry and Biophysics Reports*, 10, 52-61. doi: <https://doi.org/10.1016/j.bbrep.2017.03.003>
- Behera, S. K., Meena, H., Chakraborty, S., & Meikap, B. C. (2018). Application of response surface methodology (RSM) for optimization of leaching parameters for ash reduction from low-grade coal. *International Journal of Mining Science and Technology*, 28(4), 621-629. doi: <https://doi.org/10.1016/j.ijmst.2018.04.014>
- Bezerra, M. A., Santelli, R. E., Oliveira, E. P., Villar, L. S., & Escaleira, L. A. (2008). Response surface methodology (RSM) as a tool for optimization in analytical chemistry. *Talanta*, 76(5), 965-977. doi: <https://doi.org/10.1016/j.talanta.2008.05.019>
- Bhaumik, R., Mondal, N. K., Chatteraj, S., & Datta, J. K. (2013). Application of response surface methodology for optimization of fluoride removal mechanism by newly developed biomaterial. *American Journal of Analytical Chemistry*, 4(8), 404-419. doi: 10.4236/ajac.2013.48051
- Biswas, G., Kumari, M., Adhikari, K., & Dutta, S. (2017). Application of response surface methodology for optimization of biosorption of fluoride from groundwater using *Shorea robusta* flower petal. *Applied Water Science*, 7, 4673-4690. doi: <https://doi.org/10.1007/s13201-017-0630-5>
- Bradáčová, K., Florea, A. S., Bar-Tal, A., Minz, D., Yermiyahu, U., Shawahna, R., ... & Pošta, G. (2019). Microbial consortia versus single-strain inoculants: An advantage in PGPM-assisted tomato production? *Agronomy*, 9(2), 1-23. doi: <https://doi.org/10.3390/agronomy9020105>
- Cheng, J. R., & Zhu, M. J. (2013). A novel co-culture strategy for lignocellulosic bioenergy production: A systematic review. *International Journal of Modern Biology and Medicine*, 1(3), 166-193.
- Chin, K. L., & H'ng, P. S. (2013). A real story of bioethanol from biomass: Malaysia perspective. In M. D. Matovic (Ed.), *Biomass now: Sustainable growth and use* (pp. 329-346). Rijeka, Croatia: InTech Open Access Publisher. doi: <http://dx.doi.org/10.5772/51198>

- Correa, S. J., Jaramillo, A. C., Merino, R. A., & Hormaza, A. (2018). Evaluation of individual fungal species and their co-culture for degrading a binary mixture of dyes under solid-state fermentation. *Biotechnology, Agronomy and Society and Environment*, 22(4), 242-251. doi: 10.25518/1780-4507.16675
- Cui, Y., Dong, X., Tong, J., & Liu, S. (2015). Degradation of lignocellulosic components in un-pretreated vinegar residue using an artificially constructed fungal consortium. *BioResources*, 10(2), 3434-3450.
- Cutzu, R., & Bardi, L. (2017). Production of bioethanol from agricultural wastes using residual thermal energy of a cogeneration plant in the distillation phase. *Fermentation*, 3(2), 1-8. doi: <https://doi.org/10.3390/fermentation3020024>
- Czitrom, V. (1999). One-factor-at-a-time versus designed experiments. *American Statistician*, 53(2), 126-131.
- Dasgupta, D., Suman, S. K., Pandey, D., Ghosh, D., Khan, R., Agrawal, D., ... & Adhikari, D. K. (2013). Design and optimization of ethanol production from bagasse pith hydrolysate by a thermotolerant yeast *Kluyveromyces* sp. IPE453 using response surface methodology. *SpringerPlus*, 2, 1-10. doi: <https://doi.org/10.1186/2193-1801-2-159>
- Du, R., Yan, J., Li, S., Zhang, L., Zhang, S., Li, J., ... & Qi, P. (2015). Cellulosic ethanol production by natural bacterial consortia is enhanced by *Pseudoxanthomonas taiwanensis*. *Biotechnology for Biofuels*, 8, 1-10. doi: <https://doi.org/10.1186/s13068-014-0186-7>
- Grewal, J., Tiwari, R., & Khare, S. K. (2020). Secretome analysis and bioprospecting of lignocellulolytic fungal consortium for valorization of waste cottonseed cake by hydrolase production and simultaneous gossypol degradation. *Waste and Biomass Valorization*, 11, 2533-2548. doi: <https://doi.org/10.1007/s12649-019-00620-1>
- Hamilton, D. F. (2015). Interpreting regression models in clinical outcome studies. *Bone and Joint Research*, 4(9), 152-153. doi: <https://doi.org/10.1302/2046-3758.49.2000571>
- Hamouda, H. I., Nassar, H. N., Madian, H. R., Abu-Amr, S. S., & El-Gendy, N. S. (2015). Response surface optimization of bioethanol production from sugarcane molasses by *Pichia veronae* strain hsc-22. *Biotechnology Research International*, 2015, 1-10. doi: <https://doi.org/10.1155/2015/905792>
- Hasunuma, T., & Kondo, A. (2012). Development of yeast cell factories for consolidated bioprocessing of lignocellulose to bioethanol through cell surface engineering. *Biotechnology Advances*, 30(6), 1207-1218. doi: <https://doi.org/10.1016/j.biotechadv.2011.10.011>
- Horisawa, S., Inoue, A., & Yamanaka, Y. (2019). Direct ethanol production from lignocellulosic materials by mixed culture of wood rot fungi *Schizophyllum commune*, *Bjerkandera adusta* and *Fomitopsis palustris*. *Fermentation*, 5(1), 1-8. doi: <https://doi.org/10.3390/fermentation5010021>
- Huang, J., Chen, D., Wei, Y., Wang, Q., Li, Z., Chen, Y., & Huang, R. (2014). Direct ethanol production from lignocellulosic sugars and sugarcane bagasse by a recombinant *Trichoderma reesei* strain HJ48. *The Scientific World Journal*, 2014, 1-9. doi: <https://doi.org/10.1155/2014/798683>
- Ire, F. S., Ezebuiro, V., & Ogugbue, C. J. (2016). Production of bioethanol by bacterial co-culture from agro-waste-impacted soil through simultaneous saccharification and co-fermentation of steam-exploded bagasse. *Bioresources and Bioprocessing*, 3, 1-12. doi: <https://doi.org/10.1186/s40643-016-0104-x>

- Ivory, R., Delaney, E., Mangan, D., & McCleary, B. V. (2020). Determination of ethanol concentration in kombucha beverages: Single-laboratory validation of an enzymatic method, first action method 2019.08. *Journal of AOAC International*, *qsaa122*, 1-25. doi: doi.org/10.1093/jaoacint/qsaa122 doi: https://doi.org/10.1093/jaoacint/qsaa122
- Ja'afaru, M. I. (2013). Screening of fungi isolated from environmental samples for xylanase and cellulase production. *International Scholarly Research Notices*, *2013*, 1-7.
- Jawed, K., Yazdani, S. S., & Koffas, M. A. G. (2019). Advances in the development and application of microbial consortia for metabolic engineering. *Metabolic Engineering Communications*, *9*, 1-10. doi: https://doi.org/10.1016/j.mec.2019.e00095
- Jena, N., & Satpathy, S. (2017). Production of ethanol by *Trichoderma* spp. in solidstate fermentation of sugarcane molasses. *International Journal of Engineering Mathematics*, *6*(6), 281-288.
- Jiang, L. L., Zhou, J. J., Quan, C. S., & Xiu, Z. L. (2017). Advances in industrial microbiome based on microbial consortium for biorefinery. *Bioresources and Bioprocessing*, *4*(1), 1-10. doi: https://doi.org/10.1186/s40643-017-0141-0
- Jiang, Y., Wu, R., Zhou, J., He, A., Xu, J., Xin, F., ... & Dong, W. (2019). Recent advances of biofuels and biochemicals production from sustainable resources using co-cultivation systems. *Biotechnology for Biofuels*, *12*, 1-12. doi: https://doi.org/10.1186/s13068-019-1495-7
- Kanagasabai, M., Maruthai, K., & Thangavelu, V. (2019). Simultaneous saccharification and fermentation and factors influencing ethanol production in SSF process. In Y. Yun (Ed.), *Alcohol fuels - Current technologies and future prospect* (pp. 1-15). London, UK: InTech Open Access Publisher. doi: 10.5772/intechopen.86480
- Kaneko, S., Mizuno, R., Maehara, T., & Ichinose, H. (2012). Consolidated bioprocessing ethanol production by using a mushroom. In M. A. P. Lima (Ed.), *Bioethanol* (pp. 191-208). Rijeka, Croatia: InTech Open Access Publisher.
- Kanmani, P., Karthik, S., Aravind, J., & Kumaresan, K. (2013). The use of response surface methodology as a statistical tool for media optimization in lipase production from the dairy effluent isolate *Fusarium solani*. *International Scholarly Research Notices*, *2013*, 1-8. doi: https://doi.org/10.5402/2013/528708
- Kartini, A. M., & Dhokhikah, Y. (2018). Bioethanol production from sugarcane molasses with simultaneous saccharification and fermentation (SSF) method using *Saccaromyces cerevisiae*-*Pichia stipites* consortium. *IOP Conference Series: Earth and Environmental Science*, *207*(1), 1-9.
- Kolasa, M., Ahring, B. K., Lübeck, P. S., & Lübeck, M. (2014). Co-cultivation of *Trichoderma reesei* RutC30 with three black *Aspergillus* strains facilitates efficient hydrolysis of pretreated wheat straw and shows promises for on-site enzyme production. *Bioresource Technology*, *169*, 143-148. doi: https://doi.org/10.1016/j.biortech.2014.06.082
- Liu, D., Zhang, R., Yang, X., Wu, H., Xu, D., Tang, Z., & Shen, Q. (2011). Thermostable cellulase production of *Aspergillus fumigatus* Z5 under solid-state fermentation and its application in degradation of agricultural wastes. *International Biodeterioration and Biodegradation*, *65*(5), 717-725. doi: https://doi.org/10.1016/j.ibiod.2011.04.005

- Liu, J., Wang, J., Leung, C., & Gao, F. (2018). A multi-parameter optimization model for the evaluation of shale gas recovery enhancement. *Energies*, *11*(3), 1-29. doi: <https://doi.org/10.3390/en11030654>
- Mauch, F., Mauch-Mani, B., & Boller, T. (1988). Antifungal hydrolases in pea tissue and inhibition of fungal growth by combinations of chitinase and β -1,3-glucanase. *Plant Physiology*, *88*, 936-942. doi: <https://doi.org/10.1104/pp.88.3.936>
- Mutreja, R., Das, D., Goyal, D., & Goyal, A. (2011). Bioconversion of agricultural waste to ethanol by SSF using recombinant cellulase from *Clostridium thermocellum*. *Enzyme Research*, *2011*, 1-6.
- Naik, S. N., Goud, V. V., Rout, P. K., & Dalai, A. K. (2010). Production of first and second generation biofuels: A comprehensive review. *Renewable and Sustainable Energy Reviews*, *14*(2), 578-597. doi: <https://doi.org/10.1016/j.rser.2009.10.003>
- Pambi, R. L. L., & Musonge, P. (2016). Application of response surface methodology (RSM) in the treatment of final effluent from the sugar industry using Chitosan. In C. A. Brebbia (Ed.), *WIT Transactions on Ecology and the Environment* (Vol. 209 pp. 209-219). Southampton, UK: WIT Press.
- Park, J. Y., Shiroma, R., Al-Haq, M. I., Zhang, Y., Ike, M., Arai-Sanoh, Y., ... & Tokuyasu, K. (2010). A novel lime pretreatment for subsequent bioethanol production from rice straw - Calcium capturing by carbonation (CaCCO) process. *Bioresource Technology*, *101*(17), 6805-6811. doi: <https://doi.org/10.1016/j.biortech.2010.03.098>
- Ray, R. C., & Behera, S. S. (2017). Solid state fermentation for production of microbial cellulases. In G. Brahmachari, A. L. Demain & J. L. Adrio (Eds.), *Biotechnology of microbial enzymes: Production, biocatalysis, and industrial applications* (pp. 43-79). Amsterdam, Netherland: Academic Press. doi: <https://doi.org/10.1016/B978-0-12-803725-6.00003-0>
- Safa, Z. J., Aminzadeh, S., Zamani, M., & Motallebi, M. (2017). Significant increase in cyanide degradation by *Bacillus* sp. M01 PTCC 1908 with response surface methodology optimization. *AMB Express*, *7*, 1-9. doi: <https://doi.org/10.1186/s13568-017-0502-2>
- Sarkar, N., Ghosh, S. K., Bannerjee, S., & Aikat, K. (2012). Bioethanol production from agricultural wastes: An overview. *Renewable Energy*, *37*(1), 19-27. doi: <https://doi.org/10.1016/j.renene.2011.06.045>
- Satyakala, K., Alladi, A., & Thakur, K. D. (2017). Effect of physiological parameters on growth of *Aspergillus niger* and *Trichoderma harzianum*. *Indian Journal of Pure and Applied Biosciences*, *5*(4), 1808-1812.
- Saunders, L. J., Russell, R. A., & Crabb, D. P. (2012). The coefficient of determination: What determines a useful R² statistic? *Investigative Ophthalmology and Visual Science*, *53*, 6830-6832. doi: <https://doi.org/10.1167/iovs.12-10598>
- Selim, K. A., El-Ghwas, D. E., Easa, S. M., & Hassan, M. I. A. (2018). Bioethanol a microbial biofuel metabolite: New insights of yeasts metabolic engineering. *Fermentation*, *4*(1), 1-27. doi: <https://doi.org/10.3390/fermentation4010016>
- Shah, S. R., Ishmael, U. C., Palliah, J. V., Asras, M. F. F., & Ahmad, S. S. N. W. (2016). Optimization of the enzymatic saccharification process of empty fruit bunch pretreated with laccase enzyme. *Bioresources*, *11*(2), 5138-5154.

- Shaw, R., Festing, M. F. W., Peers, I., & Furlong, L. (2002). Use of factorial designs to optimize animal experiments and reduce animal use. *ILAR Journal*, 43(4), 223-232. doi: <https://doi.org/10.1093/ilar.43.4.223>
- Shong, J., Diaz, M. R. J., & Collins, C. H. (2012). Towards synthetic microbial consortia for bioprocessing. *Current Opinion in Biotechnology*, 23(5), 798-802. doi: <https://doi.org/10.1016/j.copbio.2012.02.001>
- Singh, D. P., & Trivedi, R. K. (2013). Acid and alkaline pretreatment of lignocellulosic biomass to produce ethanol as biofuel. *International Journal of ChemTech Research*, 5(2), 727-734.
- Suhag, M., & Singh, J. (2014). Recent Advances in fermentation of lignocellulosic biomass hydrolysate to ethanol. *Journal of Advances in Science and Technology*, 7(13), 1-8.
- Syazwane, M. M. F., Izzati, M. N. A., Azwady, A. N., & Muskhazli, M. (2019). Screening of lignocellulolytic fungi for hydrolyzation of lignocellulosic materials in paddy straw for bioethanol production. *Malaysian Journal of Microbiology*, 15(4), 379-386. doi: <http://dx.doi.org/10.21161/mjm.180250>
- Syazwane, M. M. F., Shaziera, A. N., Izzati, M. N. A., Azwady, A. N., & Muskhazli, M. (2018). Improvement of delignification, desilication and cellulosic content availability in paddy straw via physico-chemical pretreatments. *Annual Research and Review in Biology*, 26(6), 1-11. doi: <https://doi.org/10.9734/ARRB/2018/40947>
- Tesfaw, A., & Assefa, F. (2014). Co-culture: A great promising method in single cell protein production. *Biotechnology and Molecular Biology Reviews*, 9(2), 12-20. doi: <https://doi.org/10.5897/BMBR2014.0223>
- Wahid, Z., & Nadir, N. (2013). Improvement of one factor at a time through design of experiments. *World Applied Sciences Journal*, 21, 56-61. doi: 10.5829/idosi.wasj.2013.21.mae.99919
- Wongwilaiwalin, S., Rattanachomsri, U., Laathanachareon, T., Eurwilaichitr, L., Igarashi, Y., & Champreda, V. (2010). Analysis of a thermophilic lignocellulose degrading microbial consortium and multi-species lignocellulolytic enzyme system. *Enzyme and Microbial Technology*, 47(6), 283-290. doi: <https://doi.org/10.1016/j.enzmictec.2010.07.013>

Drying Characteristics of Jackfruit and Snake Fruit using Freeze Dryer

Joko Nugroho Wahyu Karyadi*, Siti Rahma, Ronal Sitindaon, Dionisia Gusda Primadita Putri and Dwi Ayuni

Departement of Agricultural and Biosystems Engineering, Faculty of Agriculture Technology, Universitas Gadjah Mada, Jl. Flora No. 1 Bulaksumur, Yogyakarta 55281, Indonesia

ABSTRACT

Jackfruit (*Artocarpus heterophyllus* Lam.) and snake fruit [*Salacca zalacca* (Gaert.) Voss] are tropical fruits that are rich in vitamins and minerals. Due to their specific aroma and unique taste, jackfruit and snake fruit have great potential to be processed into dried fruits and healthy snacks. In this work, jackfruit and snake fruit were freeze-dried using a self-designed laboratory-scale freeze dryer. The freeze dryer was constructed with a stainless-steel plate (3 mm thickness). The drying rates were determined with three different heating temperatures: 50, 60, and 70°C. This study also investigated the effect of the freeze-drying process on the characteristics of dried fruit such as moisture content, texture, color, ascorbic acid content, and morphological of dried samples. Results showed that the heating temperatures were revealed to affect characteristics such as drying rate, final moisture content, texture, and ascorbic acid content. Increased drying rate and decreased drying time were observed with an increase in the dryer temperature. The sample resulted from 70°C of heating temperature exhibited the optimum results in terms of hardness and ascorbic content preservation. The first-order kinetic model was the best fit for the prediction of drying kinetics of all materials.

Keywords: Drying rate, freeze drying, jackfruit, physical and chemical characteristics, snake fruit

ARTICLE INFO

Article history:

Received: 29 April 2020

Accepted: 07 October 2020

Published: 22 January 2021

DOI: <https://doi.org/10.47836/pjst.29.1.18>

E-mail addresses:

jknugroho@ugm.ac.id (Joko Nugroho Wahyu Karyadi)

sitirahmalabente@gmail.com (Siti Rahma)

ronalsitindaon@gmail.com (Ronal Sitindaon)

dionisiagusdaa@gmail.com (Dionisia Gusda Primadita Putri)

dwi.ayuni@mail.ugm.ac.id (Dwi Ayuni)

* Corresponding author

INTRODUCTION

Jackfruit (*Artocarpus heterophyllus* Lam.) and snake fruit (*Salacca zalacca*) may not yet be considered as well-known tropical fruits globally, but they are widely cultivated in Asia, including Indonesia (Palupi et al., 2019; Zumaidar & Miftahuddin, 2018).

Jackfruit and snake fruit were proven to be a great source of nutrition for human health (Ranasinghe et al., 2019; Suica-Bunghez et al., 2016). Regardless of all benefits offered, tropical fruits such as jackfruit and snake fruit are known as highly perishable and susceptible to deterioration due to its high respiration rate and water activity (Fundo et al., 2015). Extreme conditions such as high pressure and temperature can also affect the quality, like the changes in fruit firmness, color, and other physical quality traits (Liu et al., 2019). Especially for jackfruit, around 60% portion of this fruit is inedible (Rana et al., 2018), so it is less profitable to sell whole fruit to the export market. Therefore, the marketing and transportation of these fruits remain a big challenge. They need to be processed to be able to have a long shelf life as well as easy to handle.

A fruit processing that can be done is drying (Fernandes et al., 2011; Soebiantoro et al., 2018). Among all drying methods, freeze-drying seems to be the superior method to remove the water as well as retain the nutrients and physicochemical characteristics of fruits (Kang et al., 2014; Turkiewicz et al., 2019). Freeze-drying is a process in which the moisture content inside the fruit is crystallized at a low temperature and subsequently sublimated from the solid-state directly into the vapor phase (Cieurzyńska & Lenart, 2011). In general, The temperature and drying time can improve the reaction rates and affect the water activity of the product. Because of the water evaporation process, ascorbic acid content can be increased. The good quality of ascorbic acid can be retained by the freeze-drying process (Prabhakar & Mallika, 2014).

Several studies have focused on the evaluation of the freeze-drying process to the widely known tropical fruits such as soursop (Ceballos et al., 2012) and mango (Rahman et al., 2015). However, there are still very few studies focused on the freeze-drying of jackfruit and snake fruit. The processing of jackfruit and snake fruit using a freeze-drying method can open up opportunities for these fruits to be produced into healthy snacks that are easy to handle and transported to the export market. Therefore, this study was aimed to evaluate the performance of mini freeze-dryer for jackfruit and snake fruit. The effect of the heating temperatures on the characteristics of the freeze-dried fruits like moisture content, colour, texture, and ascorbic acid contents was also investigated.

MATERIALS AND METHODS

Materials

Ripen jackfruit and snake fruit (cultivar name: Salak Pondoh) were purchased from a local market of Sleman Regency, Yogyakarta, Indonesia. One distributor was picked to maintain the same variety and quality of fruits used. Ripen jackfruit was shown by its bright yellow colour of the flesh and its distinctive aroma. Selected jackfruit had an average weight of 10 – 15 kg. Meanwhile, ripen snake fruit had a yellowish-brown skin colour, with an average weight of 60 – 80 g. Fruits were processed on the same day they were bought,

to avoid any undesired changes in fruit quality. The average total soluble solid (TSS) of fresh jackfruit and snake fruit ranged from 18 to 30 and 16 to 19°Brix, respectively. The approximate moisture content of fresh jackfruit and snake fruit were 77.38 ± 4.97 % wb and 81.61 ± 1.01 % wb, respectively. All the fruits were washed and peeled. Fruits were cut into uniform shapes of 2×5 cm² with an average thickness of 5 mm, then put on a tray to be dried using freeze-drying.

Experimental Freeze Dryer

Figure 1 shows the laboratory freeze-drying system used in this work. The freeze dryer had $0.7 \times 0.5 \times 1$ m³ of the total dimension as well as 0.4 m diameter x 0.6 m length of the drying chamber. There were three main systems in the freeze dryer, namely: the vacuum chamber system, the cooling system, and the heating system. The vacuum chambers, doors, and steam traps were made using stainless steel with 3 mm thickness. The vacuum pump used in this study was a two-stage vacuum pump with 1 HP (horsepower) power (VALUE VE2100N, Zhejiang, China). The cooling system was constructed using ¼ HP compressor refrigerant compressor (Fuji - Kobe SR91, Fuji Electric, Tokyo, Japan), to cool the vacuum chambers and water traps. Whereas the heating system used four rectangular heater mats (40×20 cm²) with the power of 2000 watt for each, arranged in series to 500 watts. The heater mats were installed above and below the material rack.

Experiments were performed with a total pressure of 75.5 cmHg vacuum, as well as the freezing time and the total drying time of 6 hours and 36 hours, respectively. The freeze-drying process was run with the heating temperature set for 50, 60, and 70°C. The heating

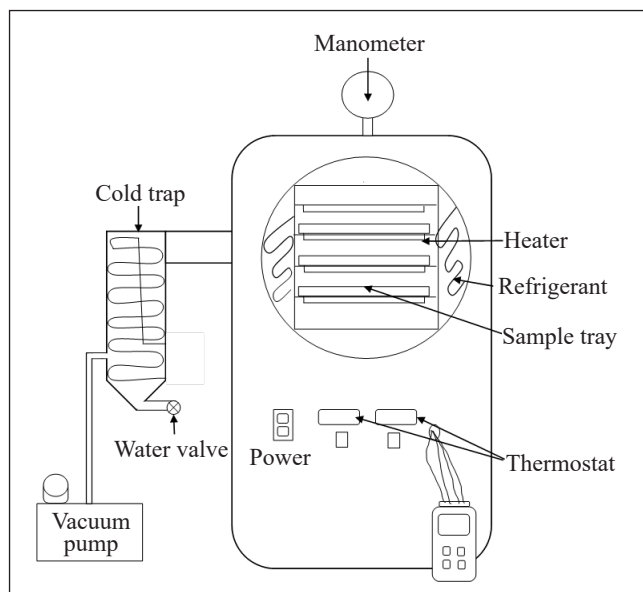


Figure 1. Laboratory freeze-drying system

temperature was set to improve the secondary drying, therefore the evaporation process of bound water can be done as quickly as possible. Based on the results of the preliminary test, the use of heating temperatures above 70°C caused non-enzymatic browning, while temperatures below 50°C were time-consuming and were not optimal to dry samples.

A pressure gauge (Wiebrock EN 837-1, Wiebrock, Herford, Nort Rhine-Westphalia) and thermometer (Lutron TM-946, Lutron Electronic Enterprise Co., LTD, Taipei, Taiwan, with the standard error of 2.2 °C) were used to measure and monitor the pressure and the temperatures during the drying, respectively. The products obtained from the freeze-drying process were weighed, and their physical properties were determined. The freeze-dried fruits were stored in an aluminum bag until they were used for the next analyses.

Moisture Content

The moisture content of the samples was measured using the methods explained by Park (2008), based on the Official Methods of Analysis of AOAC International with slight modification. The initial samples were weighed for 2 g and were dried in an oven (Memmert UM-400, Memmert GmbH + Co.KG, Schwabach, Germany) at 105°C for 24 hours to get a bone dry sample. The weight reduction from the initial to the bone dry was considered as the water amount contained in the sample. The calculation to determine the moisture content was presented by Equation 1.

$$M = \frac{W_0 - W_1}{W_1} \quad [1]$$

where M was the moisture content (g/g dry solid), W_0 was the initial mass sample at the pre-determined time during drying (g), and W_1 was a dry matter of sample after 24 hours oven drying (g).

To collect the drying kinetic data, the moisture ratio of the samples measured for 12, 18, 24, and finally 36 hours of drying. Since the equilibrium moisture content M_e was very low and imperceptible, the moisture ratio MR was simplified (Liu et al., 2016), as presented by Equation 2.

$$MR = \frac{M - M_e}{M_0 - M_e} \approx \frac{M}{M_0} \quad [2]$$

where M and M_0 were the moisture content at pre-determined time and the initial moisture content, respectively (g / g dry solid).

The moisture ratio during drying was then described by a first-order kinetic model. The first-order model is the most common and well-understood model used for exponential modelling in engineering investigations (Singh et al., 2018). The model was presented by Equation 3 (Orikasa et al., 2018).

$$MR = e^{-kt} \quad [3]$$

where MR was the moisture ratio (-), k was the drying rate constant (h^{-1}) and t was drying time (h).

The drying constant, k , was estimated by fitting the obtained moisture content data to Equation 3 using the least-squares method. To evaluate the goodness of fit, the determination coefficient (R^2) was calculated using Equation 4 (Saberian et al., 2014).

$$R^2 = 1 - \frac{\sum_{i=1}^N (MR_{pre,i} - MR_{exp,i})^2}{\sum_{i=1}^N (MR_{pre} - MR_{exp,i})^2} \quad [4]$$

where N was the number of observations, m was the number of constants, $MR_{pre,i}$ and $MR_{exp,i}$ were the i -th predicted and experimental moisture ratio, respectively.

Shrinkage

Shrinkage (%) was calculated using the formula presented by Equation 5

$$Shrinkage = \frac{(D_0 - D_1)}{D_0} \times 100\% \quad [5]$$

where D_0 was dimension (length, width, or thickness) before drying, and D_1 was dimension after drying.

Color Analysis

The color analysis was performed using Color Meter (Color Meter TES-135A, TES Electrical Electronic Corp., Taipei, Taiwan). The lightness (L^*), redness/greenness (a^*), and yellowness/blueness (b^*) were evaluated. These parameters were used to calculate the color changes (ΔE) (Ceballos et al., 2012), which was presented by Equation 6.

$$\Delta E = \sqrt{(L^* - L_0)^2 + (a^* - a_0)^2 + (b^* - b_0)^2} \quad [6]$$

where L_0 , a_0 , and b_0 were the lightness, redness/greenness, and yellowness/blueness of the fresh sample, respectively.

Texture Analysis

Texture analysis was carried out by measuring the deformation force with a Texture Analyser (Brookfield CT3 Texture Analyser, Middleboro, MA, USA), using a cylindrical probe TA39 (diameter = 2 mm). Freeze-dried fruit was placed on the texture analyser

plate and compressed at a rate of 1 mm/s until 20 mm penetration was achieved using one compression cycle. The force (N) required to deform the sample was defined as hardness.

Ascorbic Acid Content

The ascorbic acid content was determined using a 2.6D method from AOAC (Nielsen, 2017). Especially for freeze-dried samples, 200 – 300 g samples were crushed using a Waring blender to get slurry. About 10 g of the slurry was dissolved in 100 ml of distilled water. After that, the dilution was put into a centrifuge to separate the filtrate. 100 ml filtrate of fresh and freeze-dried samples were homogenized with 100 ml of HPO₃-HOAc and then filtered through filter paper. About 10 ml of filtrate was titrated with 2,6-dichloroindophenol (DCPIP) indicator. The ascorbic acid contents measured were presented in mg/100 g in dry matter (DM) of the samples.

Scanning Electron Microscopy (SEM)

The magnified image of the cross-sectional morphology of freeze-dried fruits was observed using Scanning electron microscopy (SEM; JSM 6510LA JEOL Ltd., Tokyo, Japan). The sample was coated with Platinum/Palladium metal using an Auto Fine Coater before placed over the SEM sample holder using double-sided tape.

Statistical Analysis

Statistical analysis was performed using IBM SPSS Statistics 23 software (SPSS Inc., Chicago, IL). The characteristics of freeze-dried fruits were introduced to variance analysis (ANOVA) with a 95 % significance level. When the conditions were achieved, the Duncan test was used to test the homogeneity of variances among samples.

RESULTS AND DISCUSSION

Drying Temperature and Pressure

Figure 2 shows the temperature and pressure during the freeze-drying process. In general, it can be seen from all graphs that for all heating temperatures, the product temperature reached -5°C during the freezing stage. The freezing rates should be kept low to allow simultaneous dehydration and inhibit the increase of vapor flux during the next stage (Marques & Freire, 2005). According to Shukla (2011), during the primary stage of drying, the increased temperature warms the sample, yet the low pressure below 0.06 atm (71.44 cmHg vacuum) prevents the liquid forming. As a consequence, the ice crystal became vapor, and the sublimation started to occur. Several other studies used even lower pressure and temperature during their freeze-drying process. Valentina et al. (2016) freeze-dried several types of food with the pressure and freezing temperature were set at 60 millitorrs (75.94

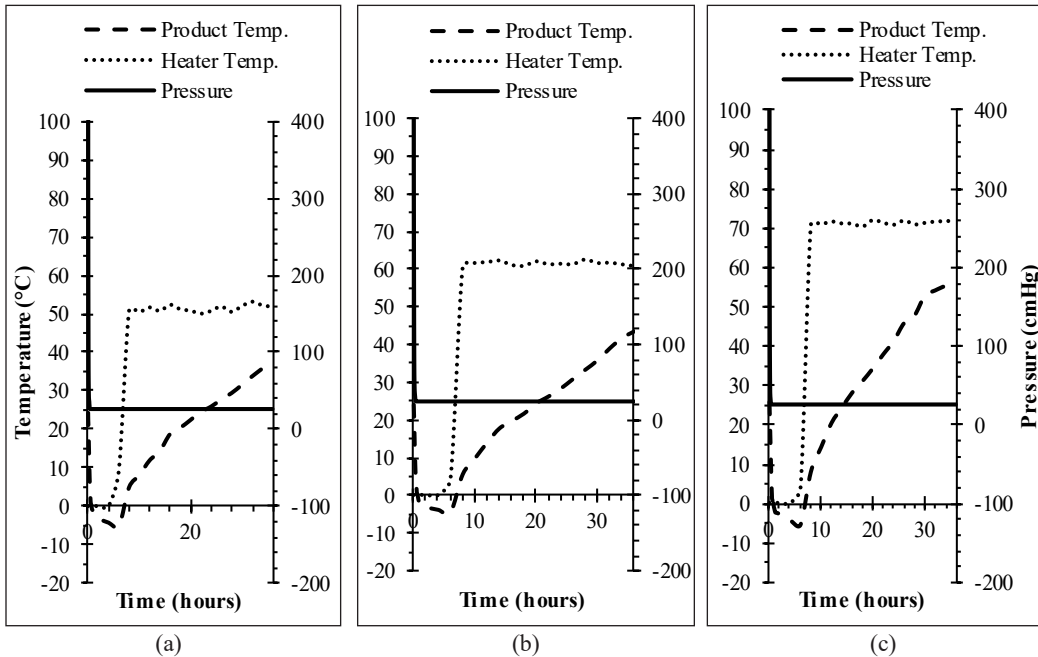


Figure 2. Temperature and pressure during freeze drying of jackfruit for different heating temperatures setting of (a) 50, (b) 60, and (c) 70°C

cm Hg vacuum) and -40°C , respectively. According to Figure 2, during the second stage of drying, the final product temperatures were varied, depending on the heating temperature applied. The product temperature after the drying process ranged from 35 – 55°C. This result was similar to the study of tropical fruits freeze-drying done by Marques et al. (2006) which reached the product final temperature of 38°C.

Moisture Content

The moisture content ratio of the jackfruit of 0.1 was fitted to the first-order kinetic model (Equation 3), shown in Figure 3, to evaluate the drying process in this study. The calculated results (shown by the solid lines) seem to agree with the measured results ($R^2 = 0.99$), indicating the suitability of the model to explain the degradation of moisture ratio during freeze-drying. From the graph, it can be seen that the drying rate decreased linearly after the first few hours of drying. The drying rate constants calculated for temperatures of 50, 60, and 70°C were 0.1296, 0.1623, and 0.1957 %/h, respectively. The results show that different increasing heating temperatures increased the drying rate of jackfruit in the first falling rate period. These results confirm that higher drying temperature would produce greater heat transfer, therefore induced moisture evaporation (Sanwiriya & Suleiman, 2019).

The final moisture content of dried jackfruit by the heating temperature of 70°C was 4.29 % db. This result was similar to that obtained by Yi et al. (2016), who applied the

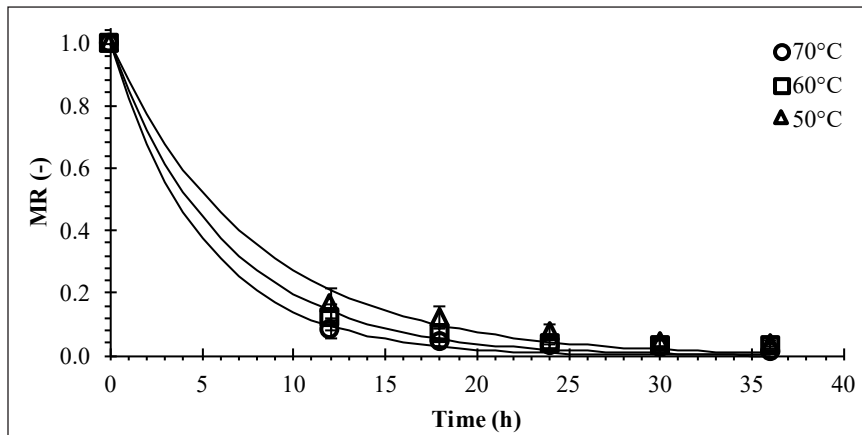


Figure 3. Plot of Moisture Ratio (MR) at three different heating temperatures for freeze-drying process of jackfruit

freeze-drying to dry jackfruit, with the pressure of 0.1 kPa (75.93 cmHg vacuum) and the secondary drying temperature of 25°C, and got the final moisture content of 4.9 % db. Meanwhile, the final moisture contents of dried jackfruit by the heating temperature of 50 and 60°C were 14.04 and 11.33 % db, respectively. Meanwhile, the final moisture content of dried snake fruit was 10.52, 4.59, and 2.18 % db for the heating temperature of 50, 60, and 70°C, respectively.

The higher the heating temperature, the lower the final moisture contents obtained for each fruit sample ($p < 0.05$). Lower moisture content may provide to the crispness of freeze-dried chips. The moisture content should be lowered to below 4% to have a good shelf life and quality. Moreover, the conventional freeze-drying permits reduction of moisture to less than 2% (Prabhakar & Mallika, 2014). Therefore, from the results obtained, 70°C was chosen as the best temperature applied to get the optimum final moisture content.

Characteristics of Freeze-dried Jackfruit and Snake Fruit

Table 1 shows the characteristics of freeze-dried jackfruit and snake fruit. Ratti (2001) who reviewed the comparison of hot air and freeze-drying of high-value foods, stated that shrinkage during freeze-drying was ranged from 5 to 15%, while during air-drying shrinkage was around 80%. However, from this study, the shrinkages obtained during freeze-drying were quite excessive (20 – 40%), with the effect of heating temperature not giving any tendency of significant difference to the results ($p > 0.05$). The shrinkage could be happen due to the short freezing time in the process, which was 6 hours. One study reported that a longer freezing time could decrease drying shrinkage (Cieurzyńska & Lenart, 2011).

Table 1
Characteristics of freeze-dried fruits

Heating Temperature (°C)	Final moisture content (% db)	Shrinkage (%)		Hardness (N)	Color Parameter		Ascorbic Acid (mg / 100 g DM)			
		Length	Width		Thickness	L*		ΔE		
Jackfruit										
50	12.30 ± 0.10 ^c	19.71 ± 4.20 ^a	19.41 ± 1.80 ^a	40.00 ± 0.00 ^b	1.99 ± 0.62 ^a	70.75 ± 2.62 ^b	14.19 ± 2.75 ^a	178.37 ± 8.50 ^a		
60	10.16 ± 0.19 ^b	19.46 ± 6.30 ^a	21.49 ± 0.70 ^a	31.75 ± 2.75 ^a	17.14 ± 9.62 ^b	74.49 ± 1.97 ^b	12.98 ± 2.96 ^a	263.56 ± 9.79 ^c		
70	4.11 ± 0.07 ^a	20.44 ± 7.25 ^a	24.69 ± 5.66 ^a	36.05 ± 2.58 ^{ab}	43.38 ± 15.15 ^c	73.14 ± 0.76 ^b	12.47 ± 5.07 ^a	272.44 ± 8.80 ^c		
Fresh sample								57.24 ± 1.80 ^a	226.62 ± 2.85 ^b	
Snake fruit								82.50 ± 0.39 ^b	8.08 ± 5.23 ^a	174.59 ± 7.61 ^a
50	10.52 ± 1.01 ^c	20.43 ± 0.74 ^a	18.46 ± 3.71 ^a	29.13 ± 0.49 ^b	2.79 ± 0.92 ^a	83.54 ± 0.36 ^b	3.71 ± 0.94 ^a	227.54 ± 17.48 ^b		
60	4.59 ± 0.14 ^b	24.77 ± 2.69 ^{ab}	36.56 ± 7.46 ^b	22.83 ± 1.88 ^a	16.57 ± 2.93 ^b	83.25 ± 0.70 ^b	3.79 ± 0.37 ^a	223.05 ± 7.06 ^b		
70	2.18 ± 0.28 ^a	29.02 ± 3.20 ^b	29.08 ± 3.60 ^b	40.66 ± 1.95 ^c	54.03 ± 13.98 ^c	74.02 ± 1.42 ^a		445.97 ± 4.70 ^c		
Fresh sample								74.02 ± 1.42 ^a		445.97 ± 4.70 ^c

Mean values ± standard deviation (n = 3)

Different superscripts per parameter indicate significant differences (p < 0.05) for each fruit sample.

According to Table 1, the higher temperature would result in a more rigid texture, marked by the higher hardness results ($p < 0.05$). The lower final moisture obtained at low temperature could reduce the glass transition point, leading to a stronger matrix of the fruits (Mounir et al., 2012). The hardness results of the 70°C heating temperature for snake fruit and jackfruit were 54.03 ± 13.98 and 43.38 ± 15.15 N, respectively. The results obtained were higher than those done by previous studies of jackfruit freeze-drying (Yi et al., 2016).

Both snake fruit and jackfruit showed a significant increase of L^* value, showed rising brightness after drying ($p < 0.05$). These results confirmed one of the merits of freeze-drying to preserve the color of products. Similar results were also obtained by previous studies done for soursop (Ceballos et al., 2012), apple, banana, potato, and carrot (Krokida et al., 2001). There was no difference in ΔE data among different heat temperatures ($p > 0.05$).

For the analysis of ascorbic acid content, the freeze-dried fruits from 50°C of heating temperature were significantly lower in ascorbic acid content than other variations ($p < 0.05$). Besides oxygen and temperature, moisture content also affects the degradation of ascorbic acid. Final moisture content that was still high in products would generate high water activity, leading to a decrease of ascorbic acid content (Lee & Kader, 2000). A previous study had proven that freeze-drying was more effective in preserving ascorbic content in products since its degradation was approximately 40% lower than that in air drying (Orak et al., 2012).

Scanning Electron Microscopy

Good appearance, adequate rehydration, and crisp texture are the characteristic of freeze-drying products. Figure 4 shows the cross-sectional of SEM micrographs of the freeze-dried fruits operated at 100× magnification. Figure 4a, c, and e correspond to the heating temperatures of 50, 60, and 70°C for jackfruit, respectively. Figure 4b, d, and f correspond to the heating temperatures of 50, 60, and 70°C for snake fruit, respectively.

In general, there was a qualitative difference in pore size among different heat temperatures. Commonly in freeze-drying, the material is in the glassy state, and the ice sublimation creates pores (Ismail et al., 2016; Rahman, 2001). Therefore, the final product of freeze-drying is very porous (as can be seen in 70°C). On the other hand, the SEM results for the temperature of 50 and 60°C seemed dense and withered. The minimum appearances of the pores suggest the products still in the rubbery state, which confirms the low hardness results discussed above. High porosity helps to maintain the structure without the deformations, allowing a fast rehydration process due to that water easily reoccupies the empty spaces (Pieniazek & Messina, 2017).

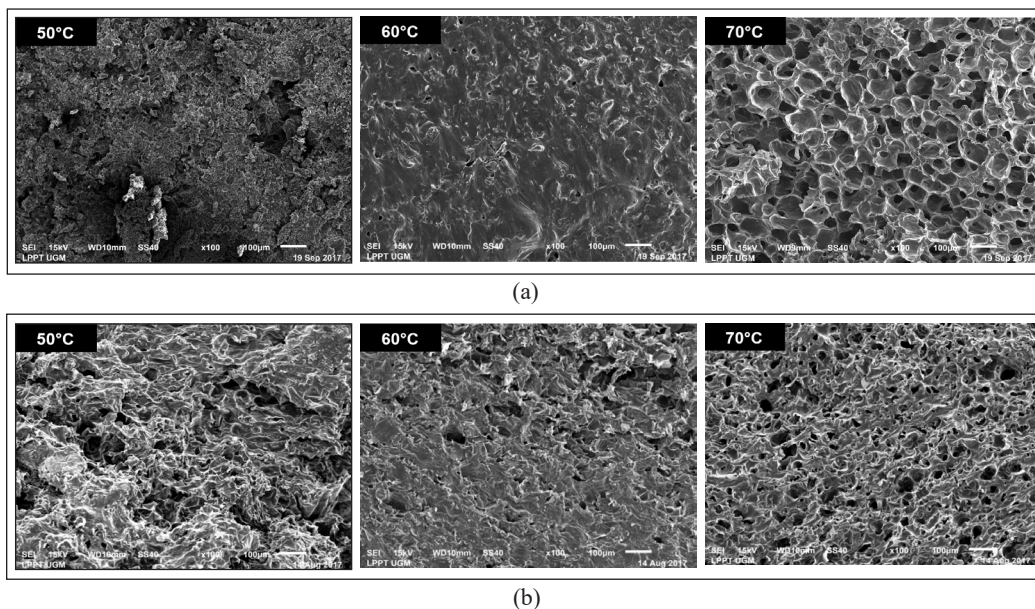


Figure 4. 100× SEM micrographs of freeze-dried fruits for (a) jackfruit and (b) snake fruit

CONCLUSIONS

This study investigated the effect of temperature on the characteristic changes for snake fruit and jackfruit during freeze-drying. A mathematical model based on first-order kinetic function was developed to simulate the moisture ratio of fruits undergoing freeze-drying. The simulation results showed that first-order kinetic could predict freeze-drying kinetics of jackfruit with adequate accuracy. The highest drying rate was reported from the heating temperature of 70°C, which was 0.1957 %/h. The lowest moisture content of freeze-dried jackfruit and snake fruit were 4.11 ± 0.07 and 2.18 ± 0.28 %, respectively. From the experiment carried out, it can be adequately stated that freeze-drying may be a suitable method for processing jackfruits and snake fruit, based on its ability to retain the color, aroma, and nutritional value after the drying.

ACKNOWLEDGEMENT

We thank Prof. Bambang Purwantana for his supervision during the design and construction of freeze-dryer. This research was funded by the Ministry of Research and Technology of Indonesia, through a program named “Excellent Researches of the University” in 2017 to 2019.

REFERENCES

- Ceballos, A., Giraldo, G. I., & Orrego, C. E. (2012). Effect of freezing rate on quality parameters of freeze dried soursop fruit pulp. *Journal of Food Engineering*, *111*, 360-365. doi: <https://doi.org/10.1016/j.jfoodeng.2012.02.010>
- Ciurzyńska, A., & Lenart, A. (2011). Freeze-drying application in food processing and biotechnology - A review. *Polish Journal of Food and Nutrition Sciences*, *61*(3), 165-171. doi: <https://doi.org/10.2478/v10222-011-0017-5>
- Fernandes, F. A. N., Rodrigues, S., Law, C. L., & Mujumdar, A. S. (2011). Drying of exotic tropical fruits: A comprehensive review. *Food and Bioprocess Technology*, *4*(2), 163-185. doi: <https://doi.org/10.1007/s11947-010-0323-7>
- Fundo, J. F., Amaro, A. L., Madureira, A. R., Carvalho, A., Feio, G., Silva, C. L. M., & Quintas, M. A. C. (2015). Fresh-cut melon quality during storage: An NMR study of water transverse relaxation time. *Journal of Food Engineering*, *167*, 71-76. doi: <https://doi.org/10.1016/j.jfoodeng.2015.03.028>
- Ismail, M. H., Law, C. L., & Hii, C. L. (2016). Transparency phenomena of flat-rice noodles (kuew teow) at drying at soaking variation. *International Food Research Journal*, *23*(December), S195-S202.
- Kang, O. L., Yong, P. F., Ma'aruf, A. G., Osman, H., & Nazaruddin, R. (2014). Physicochemical and antioxidant studies on oven-dried, freeze-dried and spray-dried agaro-oligosaccharide powders. *International Food Research Journal*, *21*(6), 2363-2367.
- Krokida, M. K., Maroulis, Z. B., & Saravacos, G. D. (2001). The effect of the method of drying on the colour of dehydrated products. *International Journal of Food Science and Technology*, *36*(1), 53-59. doi: <https://doi.org/10.1046/j.1365-2621.2001.00426.x>
- Lee, S. K., & Kader, A. A. (2000). Preharvest and postharvest factors influencing vitamin C content of horticultural crops. *Postharvest Biology and Technology*, *20*(3), 207-220. doi: [https://doi.org/10.1016/S0925-5214\(00\)00133-2](https://doi.org/10.1016/S0925-5214(00)00133-2)
- Liu, B., Wang, K., Shu, X., Liang, J., Fan, X., & Sun, L. (2019). Changes in fruit firmness, quality traits and cell wall constituents of two highbush blueberries (*Vaccinium corymbosum* L.) during postharvest cold storage. *Scientia Horticulturae*, *246*, 557-562. doi: <https://doi.org/10.1016/j.scienta.2018.11.042>
- Liu, Y. H., Li, X. F., Zhu, W. X., Luo, L., Duan, X., & Yin, Y. (2016). Drying characteristics, kinetics model and effective moisture diffusivity of vacuum far-infrared dried Rehmanniae. *International Journal of Agricultural and Biological Engineering*, *9*(5), 208-217. doi: <https://doi.org/10.3965/j.ijabe.20160905.2082>
- Marques, L. G., & Freire, J. T. (2005). Analysis of freeze-drying of tropical fruits. *Drying Technology*, *23*, 2169-2184. doi: <https://doi.org/10.1080/07373930500212438>
- Marques, L. G., Silveira, A. M., & Freire, J. T. (2006). Freeze-drying characteristics of tropical fruits. *Drying Technology*, *24*(4), 457-463. doi: <https://doi.org/10.1080/07373930600611919>
- Mounir, S., Allaf, T., Mujumdar, A. S., & Allaf, K. (2012). Swell drying: Coupling instant controlled pressure drop DIC to standard convection drying processes to intensify transfer phenomena and improve quality - An overview. *Drying Technology*, *30*, 1508-1531. doi: <https://doi.org/10.1080/07373937.2012.693145>

- Nielsen, S. S. (2017). Vitamin C determination by indophenol method. In *Food Analysis Laboratory Manual* (pp. 143-146). Cham, Switzerland: Springer International Publishing. doi: <https://doi.org/10.1007/978-3-319-44127-6>
- Orak, H. H., Aktas, T., Yagar, H., Isbilir, S. S., Ekinci, N., & Sahin, F. H. (2012). Effects of hot air and freeze drying methods on antioxidant activity, colour and some nutritional characteristics of strawberry tree (*Arbutus unedo* L) fruit. *Food Science and Technology International*, 18(4), 391-402. doi: <https://doi.org/10.1177/1082013211428213>
- Orikasa, T., Ono, N., Watanabe, T., Ando, Y., Shiina, T., & Koide, S. (2018). Impact of blanching pretreatment on the drying rate and energy consumption during far-infrared drying of paprika (*Capsicum annum* L.). *Food Quality and Safety*, 2(2), 97-103. doi: <https://doi.org/10.1093/fqsafe/fy006>
- Palupi, D., Rahayu, S. S. B., & Daryono, B. S. (2019). Genetic diversity in jackfruit (*Artocarpus Heterophyllus* Lam.) based on molecular characters in Indonesia. *Sabrao Journal of Breeding and Genetics*, 51(1), 57-67.
- Park, Y. (2008). Moisture and water activity. In L. M. L. Nollet & F. Toldrá (Eds.), *Handbook of processed meats and poultry analysis* (pp. 35-67). London, UK: CRC Press. doi: <https://doi.org/10.1201/9781420045338.ch3>
- Pieniazek, F., & Messina, V. (2017). Texture and color analysis of freeze-dried potato (cv. Spunta) using instrumental and image analysis techniques. *International Journal of Food Properties*, 20(6), 1422-1431. doi: <https://doi.org/10.1080/10942912.2016.1211143>
- Prabhakar, K., & Mallika, E. N. (2014). Dried foods. In C. A. Batt & M. L. Tortorello (Eds.), *Encyclopedia of food microbiology: Second edition* (Vol. 1, pp. 574-576). San Diego, USA: Academic Press. doi: <https://doi.org/10.1016/B978-0-12-384730-0.00085-9>
- Rahman, M. M., Das, R., Hoque, M. M., & Zzaman, W. (2015). Effect of freeze drying on antioxidant activity and phenolic contents of mango (*Mangifera indica*). *International Food Research Journal*, 22(2), 613-617.
- Rahman, M. S. (2001). Toward prediction of porosity in foods during drying: A brief review. *Drying Technology*, 19(1), 1-13. doi: <https://doi.org/10.1081/DRT-100001349>
- Rana, S. S., Pradhan, R. C., & Mishra, S. (2018). Optimization of chemical treatment on fresh cut tender jackfruit slices for prevention of browning by using response surface methodology. *International Food Research Journal*, 25(1), 196-203.
- Ranasinghe, R. A. S. N., Maduwanthi, S. D. T., & Marapana, R. A. U. J. (2019). Nutritional and health benefits of jackfruit (*Artocarpus heterophyllus* Lam.): A review. *International Journal of Food Science*, 2019, 1-12. doi: <https://doi.org/10.1155/2019/4327183>
- Ratti, C. (2001). Hot air and freeze-drying of high-value foods: A review. *Journal of Food Engineering*, 49, 311-319. doi: [https://doi.org/10.1016/S0260-8774\(00\)00228-4](https://doi.org/10.1016/S0260-8774(00)00228-4)
- Saberian, H., Amooi, M., & Hamidi-Esfahani, Z. (2014). Modeling of vacuum drying of loquat fruit. *Nutrition and Food Science*, 44(1), 24-31. doi: <https://doi.org/10.1108/NFS-08-2012-0087>
- Sanwiriya, P., & Suleiman, N. (2019). The effects of drying method and temperature on the nutritional quality of watermelon rinds. *International Food Research Journal*, 26(3), 953-958.

- Shukla, S. (2011). Freeze drying process: A review. *International Journal of Pharmaceutical Sciences and Research*, 2(12), 3061-3068.
- Singh, A. P., Siddiqui, J., & Diosady, L. L. (2018). Characterizing the pH-dependent release kinetics of food-grade spray drying encapsulated iron microcapsules for food fortification. *Food and Bioprocess Technology*, 11(2), 435-446. doi: <https://doi.org/10.1007/s11947-017-2022-0>
- Soebiantoro, F. A., Tarigan, E., Hwa, L., Halim, V. P., & Sapei, L. (2018). Drying characteristics of *Curcuma longa* using solar dryer. *Pertanika Journal of Science and Technology*, 26(3), 1265-1274.
- Suica-Bunghez, I. R., Teodorescu, S., Dulama, I. D., Voinea, O. C., Imionescu, S., & Ion, R. M. (2016). Antioxidant activity and phytochemical compounds of snake fruit (*Salacca Zalacca*). *IOP Conference Series: Materials Science and Engineering*, 133(1), 1-18. doi: <https://doi.org/10.1088/1757-899X/133/1/012051>
- Turkiewicz, I. P., Wojdyło, A., Lech, K., Tkacz, K., & Nowicka, P. (2019). Influence of different drying methods on the quality of Japanese quince fruit. *LWT - Food Science and Technology*, 114, 1-8. doi: <https://doi.org/10.1016/j.lwt.2019.108416>
- Valentina, V., Pratiwi, R. A., Hsiao, P. Y., Tseng, H. T., Hsieh, J. F., & Chen, C. C. (2016). Sensorial characterization of foods before and after freeze-drying. *Austin Food Sciences*, 1(6), 1-5.
- Yi, J., Wang, P., Bi, J., Liu, X., Wu, X., & Zhong, Y. (2016). Developing novel combination drying method for jackfruit bulb chips: Instant controlled pressure drop (DIC)-assisted freeze drying. *Food and Bioprocess Technology*, 9(3), 452-462. doi: <https://doi.org/10.1007/s11947-015-1643-4>
- Zumaidar, & Miftahuddin. (2018). Species distribution of genus *Salacca*. *Journal of Physics: Conference Series*, 1116(2018), 1-8. doi: <https://doi.org/10.1088/1742-6596/1116/5/052083>

Shoreline Change and its Impact on Land use Pattern and Vice Versa – A Critical Analysis in and Around Digha Area between 2000 and 2018 using Geospatial Techniques

Anindita Nath^{1*}, Bappaditya Koley², Subhajit Saraswati¹, Basudeb Bhatta³ and Bidhan Chandra Ray⁴

¹Departments of Construction Engineering, Jadavpur University, Kolkata, West Bengal, 700106 India

²School of Oceanographic Studies, Jadavpur University, Kolkata, West Bengal, 700032 India

³Computer Aided Design Centre, Jadavpur University, Kolkata, West Bengal, 700032 India

⁴Department of Chemistry, Jadavpur University, Kolkata, West Bengal, 700032 India

ABSTRACT

The shoreline is a very unpredictable, uncertain, and forever changing landscape for any coastal process. Due to erosional and accretional activities, the shoreline has continuously fluctuated with the continual process of waves and tides. Shore boundaries are determined by the shoreline at its furthest towards the sea (low tide) and extreme towards land (high tide). The present research aimed to identify the temporal alterations of shoreline and changes in land-cover between the areas of Rasulpur to Subarnarekha estuary, east coast of India with 70.04 km length of shoreline. An area amounting to 143sq.km had been selected for showing the land-cover changing and this area had witnessed the rapid growth of population and increasing industrial activities causing an unsurpassable impact on the environment. The present study used three multi dated imageries for land use/ land cover (LULC) map and seven multi-resolution satellite images were applied to estimate the long-term shoreline change rate by dividing the coastal area into three “littoral zones”

(LZ). The Digital shoreline analysis system (DSAS) was applied to identify the shoreline change rate of the year 2000 to 2018. Several statistical methods, linear regression rate (LRR), net shoreline movement (NSM), End Point Rate (EPR) were used to find out the erosion and accretion rate. The result showed that maximum erosion had been found in LZ III, rate of -2.22 m/year. Maximum accretion had been identified in

ARTICLE INFO

Article history:

Received: 07 July 2020

Accepted: 28 September 2020

Published: 22 January 2021

DOI: <https://doi.org/10.47836/pjst.29.1.19>

E-mail addresses:

aninditan286@gmail.com (Anindita Nath)

bappadiyakoley2012@gmail.com (Bappaditya Koley)

subhajitsaraswati@gmail.com (Subhajit Saraswati)

basubhatta@gmail.com (Basudeb Bhatta)

drbidhanray@gmail.com (Bidhan Chandra Ray)

* Corresponding author

LZ I, at the rate of 35.5 m/year. The LULC showed that maximum vegetation area had been decreased in the year of 2010 (14.21sq.km) but 38.96sq.km vegetation area had increased in 2018. The prominent increase had been identified in built up and shallow water. Built up had been expanded from 25.59sq.km (2000) to 41.26sq.km (2018). Shallow water was increased from 5.53sq.km (2000) to 18.90sq.km (2018). Sand and soil showed a decreasing pattern from 2000 – 2018. The outcome acquired from the present study will play a significant role to estimate the shoreline migration rate and will be helpful for sustainable land use management. The shoreline change rate will be also useful for coastal planners to adopt mitigation measures.

Keywords: Digital shoreline analysis system, end point rate, land use/land cover, littoral zone, linear regression rate, net shoreline movement

INTRODUCTION

Shoreline is relatively narrow strip of land adjacent to water bodies like sea or lake. Components of shoreline is controlled by the wave dynamics and sediment characteristics, slope, climate, vegetation, tide fluctuation and overall a littoral behavior. Equilibrium shoreline changes its configuration over a time period due to changing behavior of the agent (Pandian et al., 2004). Removal of sediment by erosional process is more vulnerable than accretion and widening of shoreline. Analysis of shoreline change leads to understanding coastal processes operating in a particular area in terms of frequency and magnitude. Anthropogenic factors also influence coastal morphology. Every coastal zone has its specific natural properties like, coastal slope, bathymetry and water density. Shoreline changes are the effects of some coastal processes like, breaking zone, breaker types of wave, breaking energy and so on. The surf zone where wave losses its energy and breaks are called the breaking wave zone. Braking type means the level of unstable movement within the wave (Koloa & Samanta, 2013).

Coastal zones require a huge amount of spatial research to assess and predict the geomorphic changes (Murali & Kumar, 2015). The land use/land cover (LULC) of an area that is a combined output of physical and manmade variable and processes. The present study fulfill the two main objectives, (i) to observe the shoreline changes and calculate the shoreline change rate along the area of Rasulpur river estuary to Subarnarekha river estuary in eastern coast of India, (ii) to identify and quantify the land-cover classes for the bench mark years 2000, 2010 and 2018 by using different GIS tools. The present study area has been subjected to many geo-environmental factors like beach sand loss, lack of sediment transport, shoreline retreat or transgression (erosion), destruction of mangroves, rapid growth of urbanization near shore areas, decreasing soil area and increase of water level which is become significant cause of concern. Identification and estimation of shoreline shifting is an important phenomenon for coastal management and coastal environment

monitoring (Van & Bihn, 2008). The output of the present study is the shoreline change and LULC maps that can be useful for coastal authority for coastal zone management plan for the study area.

Various studies can be found in the existing literature for the study of shoreline change and land use/land cover change using geospatial analysis. Present work is based on the scientific approach and methodology of several research details given in Table 1.

Table 1
Scientific approach and methodology of several research details

Scientific approach and methodology	Research
Geospatial analysis of shoreline and LULC changes through remote sensing and GIS techniques.	Samanta & Paul, 2016
Shoreline identification using satellite images	Garcia-Rubio et al., 2009
Study of the land use and land cover changes and CRZ in the coastal area of Ganjam district, Odisha.	Guru et al., 2014
Assessment of shoreline changes along Nagapattinam coast using geospatial techniques.	Mageswaran et al., 2015
Sea level rise and shoreline changes: a geo-informatics appraisal of Chandipur coast, Orissa.	Mukhopadhyay et al., 2011
Long and short-term shoreline changes along mangalore coast, India.	Kumar & Jayappa, 2009
Analysis of land use /land cover using remote sensing techniques –A case study of Karur district, Tamil Nadu, India.	Balachandar et al., 2011
Automatic shoreline detection and future prediction: a case study on Puri Coast, Bay of Bengal, India.	Mukhopadhyay et al., 2012
Coastline change detection using remote sensing.	Alesheikh et al., 2007

STUDY AREA

The length of 70.04 km shoreline in east coast of India, area between Rasulpur to Subarnarekha estuary part of West Bengal and Orissa respectively was selected for the present study (Figure 1). East coast of India along with Bay of Bengal is more inundation prone and various shocked related to ocean than west coast of India (Chatterjee, 1995). The study area is located between latitudes of 21°34'25" N to 21°47'16" N and longitudes 87°22'36" E to 87°52'55" E. Elevation of is less than 3 m in average above sea level (Umitsu & Sen, 1987; Goodbred & Kuehl, 2000; Khan & Islam, 2008). Beach sand in the study area has been observed as similar to Subarnarekha sand which is mainly quartz and yellowish in color tone. The general conception is contracted that the beach sand has been supplied from Subarnarekha River not from Ganga (River Research Institute, 2009). The entire coastal zone is predominated by south west monsoon with subtropical humid climate and three several climate pattern identified these are (i) per-monsoon (March – June), (ii) monsoon (June – October) and (iii) retreat monsoon (November – February) (Dey et al., 2005). Five important estuary areas have been observed in the study zone.

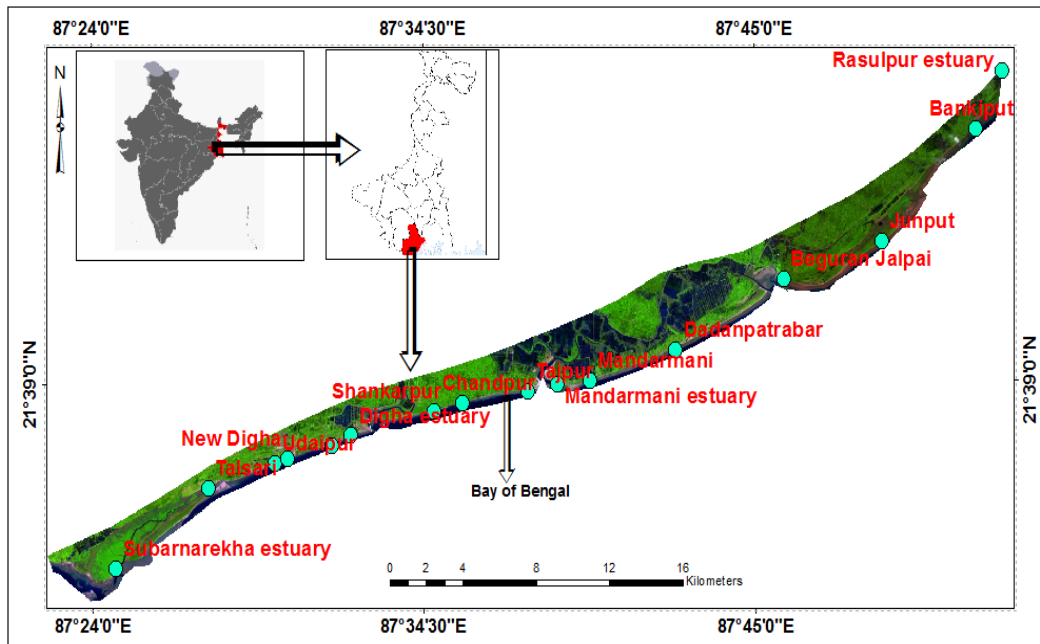


Figure 1. Geographical setting of study area

These are: Subarnarekha estuary (Subarnarekha River), Digha estuary (Digha canal and Champa River), Mandarmani estuary (Balisai canal and Sapua canal), BeguranJalpai (Pichabani canal and Contai canal) and Rasulpur estuary (Rasulpur River). The study area has witnessed rapid growth of urbanization due to development of tourism industry and various commercial activities are found in hinterland of the study area.

METHODS

Various methods of shoreline identification and shoreline retreat measures are available in the existing literature (Jana et al., 2013; Kuleli, 2009; Nguyen et al., 2010; Mujabar & Chandrasekar, 2011; Selvan et al., 2014). The shoreline change detection is primarily based on the actual positioning of tidal datum that is mainly termed as mean high water (MHW) on a map (Everts et al., 1983). In this study, various remote sensing, and GIS methods (explained later) were applied to determine the shoreline position; land use/land cover changes. Different statistical analyses were also performed for estimating the shoreline retreatment rate. The following subsections explain different modules of methodology.

Data Analysis

The study was carried out using three multi-temporal and multi resolution images of Landsat ETM⁺ (Enhanced thematic Mapper) with a spatial resolution of 30m for bands 1 to 7 and band 8 for 15m and Landsat 8 (Operational Land Imager / OLI) and thermal

infrared sensor (TIR) with a spatial resolution of 30m for band 1 to 7 and 9, 15m for band 8, band 10 and 11 are thermal bands with a spatial resolution of 100m. In Landsat 8, band 1 is useful for coastal studies.

Available data over the selected period (2000 – 2018) had differences in their resolutions. Since the images were visually interpreted for mapping purpose, these differences of resolution did influence the accuracy to obtaining the real information about land cover features. Satellite image of 2000 is low resolution image with some atmospheric errors which create some problem in identifying the LULC features. The effect of low resolution has been observed especially in built up area of 2000 image. Landsat data are very much reliable in coastal studies and being used for decades (Munday & Alfodi, 1979; Chand & Acharya, 2010). Use of satellite images also proved its reliability in identifying the shoreline position and coastal changes (Boak & Turner, 2005). The selected satellite images, for the years 2000, 2006, 2007, 2009, 2010, 2015 and 2018 were downloaded from USGS Global visualization viewer (<https://glovis.usgs.gov>).

Identification and Estimation of Shoreline Change

The shoreline was identified by interpreting the differences in shades of tone between the land and ocean. Brightness, contrast adjustment and histogram stretch techniques were applied on the satellite images for better visual identification. The pixels which represent the shoreline were converted into a polyline vector format in ArcGIS environment. In image of 2000, some errors were observed related to atmospheric disturbances which generate some problem in extracting shoreline; and therefore, correction method was applied for this particular image. The least brightness value in every band was detected and this value was deducted from all pixel values (DN values) in the corresponding band that comport to atmospherically rectified image (Chavez, 1988; Trinh et al., 2020; Emran et al., 2016).

Prerequisite for change detection analysis are precise geometric correction (Saha et al., 2005). All of the satellite images were rectified geometrically in GIS application. Geometrically corrected images were projected by Universal Transverse Mercator (UTM) projection (WGS 84, Zone: 45N) based on nearest-neighbor interpolation technique. Then, standard false color composites (infrared color composites) were created for the satellite images.

To estimate the shoreline shifting rate, the Digital Shoreline Analysis System (DSAS) was most useful system available at USGS earth explorer website that performed with Arc GIS software in collaboration where shoreline change rate had been calculated following the “linear regression” (LR) method (Maiti & Bhattacharya, 2009). The vector layers (.shp) of shoreline for the years 2000 – 2018 were used in DSAS to estimate the rate of shoreline shifting. Transect information were required to estimating the change rate of shoreline and 2682 transects (in the form of shape file) were placed at 50 m interval along

the shoreline. The DSAS tool was used to estimate the NSM (Net shoreline movement), EPR (End point rate) and LRR (Linear Regression Rate). The distance between youngest and oldest shorelines was demarcating the estimation of NSM. The LRR was demarcated by compatible least squares regression line to all the relative shoreline points of various years for a single transect. The EPR was estimated from the horizontal change rate of shorelines. The EPR was calculated by dividing the distance of horizontal shoreline change rate by the NSM (Thieler et al., 2009). The negative (-) values indicate the retreat of shoreline and positive (+) values indicate the advance of shoreline or sea ward movement of shoreline. The total area (Subarnarekha estuary to Rasulpur river estuary) was divided into 3 littoral zones (LZ) for prominent identification of erosion and accretion pattern. The littoral zone is very close area to shoreline. This zone is influenced by the process of transportation and sedimentation. The total area was divided into different littoral segment based on important estuaries in the study area that were the main source of sediment supply over the area. First zone was selected Subarnarekha estuary to Digha estuary area (length of 23.04 km) and 932 transects were drawn in this LZ I. Second zone was chosen from Digha estuary to BeguranJalpai (length of 31.15 km) and 1051 number of transect were drawn to calculate the Shoreline change rate. Final zone was BeguranJalpai to Rasulpur river estuary area (length of 16.23km) with 699 number of transects. Three littoral zones were calculated by statistical method and finally a zonation map was prepared with five different zones according to LRR values and classes were defined based on their values in three littoral zones. Two specific classes were obtained: low erosion zone (range -100 to 0) and low accretion (range varies from 0 to 100). The entire study area has been observed by these two classes. The study shows the changes between 2000 – 2018 time periods (18 years) in a long-term method. The analysis was performed based on LRR and EPR method to showing the variation of shoreline change rate. LRR method was more compatible to showing the long-term changes than EPR method because in EPR method could not access more than two shorelines so when additional shorelines were assigned to calculate the change rate extra (more than two) shorelines were neglected. Due to this reason rate of shoreline migration might be overlooked. In case of LRR method, all shoreline data (more than two) were computed in regardless and the accurate rate of shoreline shifting was obtained using acceptable statistical techniques (Dolan et al., 2007). The present study had been applied both methods (EPR and LRR) to calculate the shoreline change rate and variation in both methods.

To justify the location of shoreline a validation method was applied for 2000, 2006, 2007, 2009, 2010, 2015 and 2018 shoreline. These three shorelines were converted into Google earth (.kml) version; and then by the using of Google earth historical imagery system these three shorelines were validated.

Study of Land Use/ Land Cover

Satellite images and field data were used to classify land cover features (Pal et al., 2012). The image classification resulted in the classified land-cover maps for the years 2000, 2010 and 2018. Image classification was performed in Arc GIS software for following land-cover classes: vegetation, soil, shallow water, sand and built-up. To preparing the LULC map approximate 143sq.km area was chosen. The total area was divided into three littoral zones (LZ) for each year. The LULC classification was performed for these three zones of each year to make a comparative study between 2000 – 2018 time periods. The maximum likelihood classification algorithm was used to create this land use/ land cover map. Maximum likelihood classification is a process where known classes are distributed as the maximum for a certain statistic (Scott & Symons, 1971; Mukhopadhyay et al. 2013; Mukhopadhyay et al. 2018). The training samples or signatures were collected from the images by means of visual image interpretation with appropriate ground truthing. From the LULC data, some statistical techniques were adopted to find out the drastic changes between 2000 – 2018 timwere. No classified map has been considered as accurate without performing the accuracy assessment (Bradley, 2009). To assess any classified image, confusion matrix is the most suitable method (Story & Congalton, 1986; Biging et al., 1998; Oumer, 2009; Zhang et al., 2000; Mujabar & Chandrasekar, 2013). Based on this method, similar and dissimilar pixels are assembled to compare the ground truth pixel along the location in classified map. Ground truth data are represented through column and classified pixel data are represented by row (SCGE, 2011). The matrix was performed by calculating user's accuracy, producer's accuracy and overall accuracy measures based on the commission and omission error (Coppin & Bauer, 1996; Boschetti et al., 2004; Carlotto, 2009). Finally, the accuracy assessment was performed to determinethe overall accuracy and Kappa co-efficient accuracy (Rossiter, 2014). The result of accuracy assessment is given in Table 2.

Overall accuracy as in Equation 1:

$$\frac{\sum_{a=1}^U C_a}{Q} * 100\% \quad (1)$$

Where, Q and U is the number of total pixel and classes, respectively. The acceptable overall accuracy has been considered 85% (Congalton & Green, 1999; Lu & Weng, 2007; Li & Zhou, 2009).

Kappa confusion matrix is demarcated as in Equation 2:

$$K = \frac{\sum_{a=1}^U \frac{C_a}{Q} \sum_{a=1}^U \frac{C_a C_a}{Q^2}}{1 - \sum_{a=1}^U \frac{C_a \cdot C_a}{Q^2}} \quad (2)$$

Where, C_a =Row sum

Table 2
Showing the accuracy assessment by Kappa Co-efficient

LULC feature name	Producer's accuracy			User's accuracy		
	2000	2010	2018	2000	2010	2018
Built up	100%	100%	71.43%	37.5%	90%	71.43%
Vegetation	100%	90%	100%	87.50%	100%	100%
Soil	66.66%	100%	71.43%	100%	85.71%	100%
Sand	77.77%	90%	100%	100%	100%	90%
Shallow water	100%	100%	100%	100%	100%	89%
	Overall accuracy			85%	95%	90%
	Kappa co-efficient			81.25%	93.67%	87.43%

RESULT AND DISCUSSION

Shoreline Change Analysis

The shoreline change or shoreline recession had been estimated for the area under Subarnarekha to Rasulpur river estuary area using Digital Shoreline Analysis System (DSAS) tool in Arc GIS 10.3 software. In the study area, shoreline length of 70.04 km observed both erosion and accretion (Figure 2, 3, 4). The shorelines of different years were drawn in ArcGIS. From the DSAS analysis, EPR and LRR for every transect length over the shoreline is shown in Figure 5, 6 and 7. From the DSAS transect analysis it was observed that in the LZ I (Figure 2) maximum area was under low erosion to low accretion regime. But near Subarnarekha estuary a prominent accretion zone was found but at the same area also experiences the erosional tendency (Figure 2). The average positive LRR value was found as 35.5 m/year near Subarnarekha estuary and average negative changes of LRR value was -1.5 m/year was observed in the extent part of Subarnarekha estuary to before Talsari area and near Old Digha, New Digha and Digha estuary area which is under low accretion zone. A tetrapod groin was constructed near Digha estuary area for the purpose of sedimentation which protects the beach area from coastal erosion in the year of 2007 by fishery Dept, Govt. of West Bengal (Figure 8). While in the LZ II (Figure 3) it was noticed that maximum area was dominated by low accretional formation and some area near Tajpur and Mandarmani estuary was under low erosional regime. The erosion rate was varying between -0.64 to -1.85 m/year and positive changes rate was 10.15 m/year in LRR value. In the LZ III reflects that the area had experienced low erosional pattern (Figure 4). Junput area was under accretion regime with average 32.33 m/year LRR value whereas Rasulpur river estuary was under low erosional regime with -2.22 m/year LRR value. Bankiput area was under accretion zone but some part of Bankiput shoreline remarked as domination of erosion with rate of -3.23 m/year. Figures 5, 6 and 7 explain the prominence of LRR method to estimating the long-term shoreline migration compare to EPR method in LZ I, II and III. In LRR statistics every change magnitude had been computed which was absence in EPR method and accurate change rate was obtained by LRR method. In case of LZ

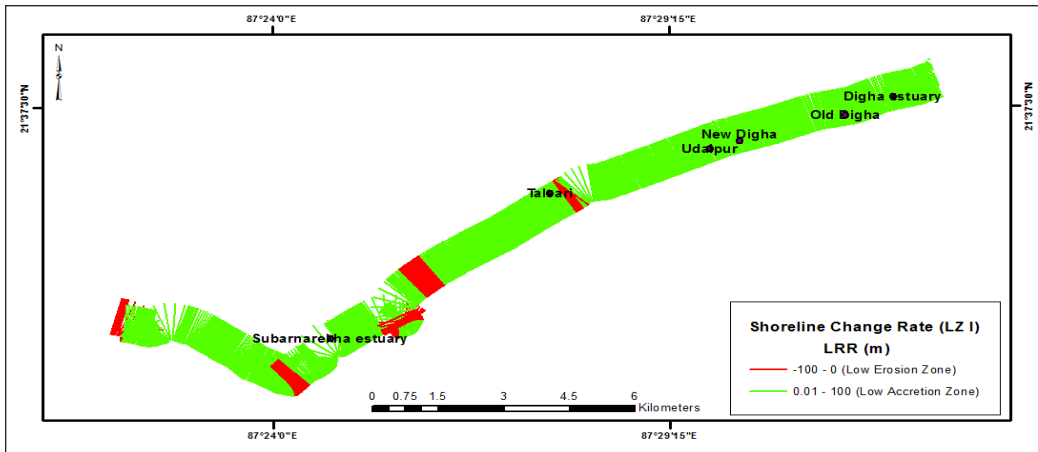


Figure 2. Shoreline change dynamics of LZ 1 (2000-2018)

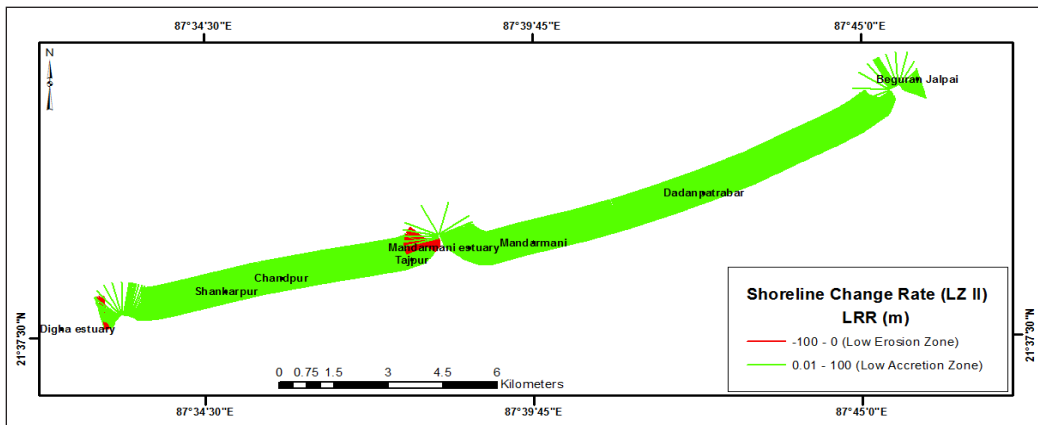


Figure 3. Shoreline change dynamics of LZ 2 (2000-2018)

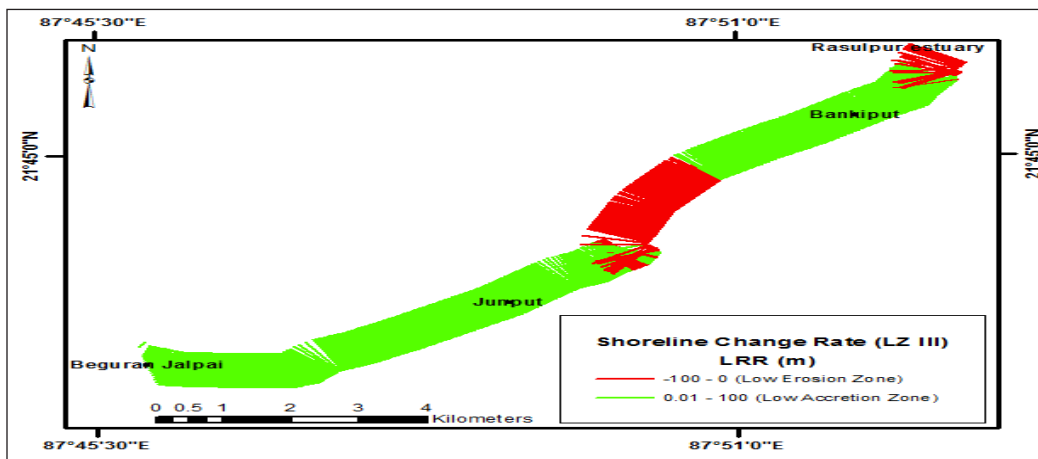


Figure 4. Shoreline change dynamics of LZ 3 (2000-2018)

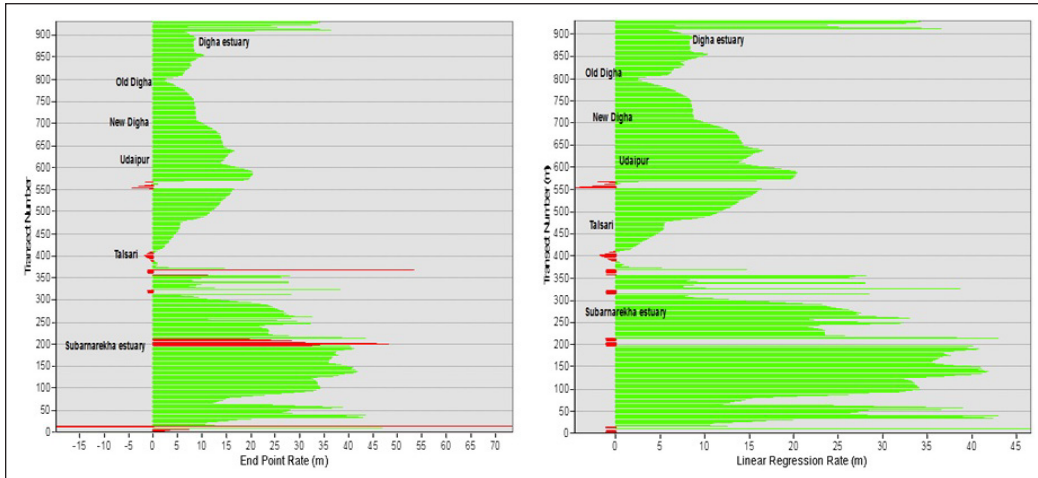


Figure 5. Graphical representation of shoreline changes in LZ I by EPR & LRR (2000 - 18)

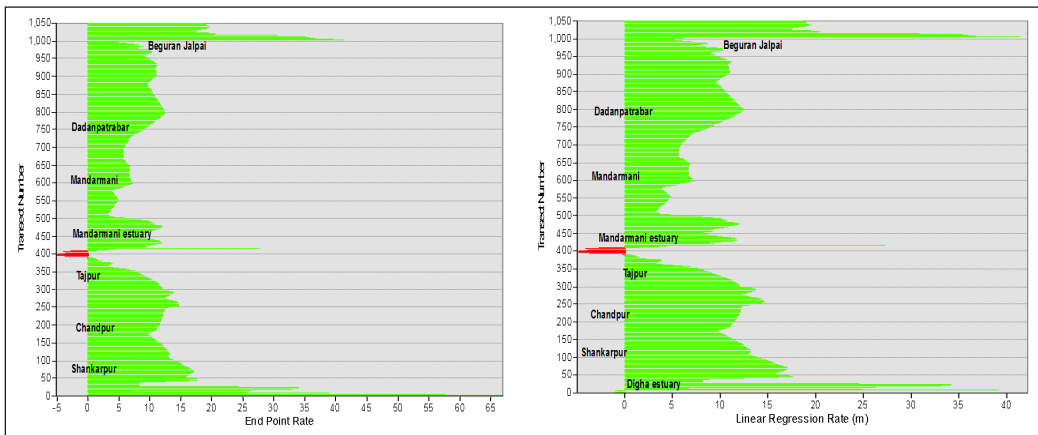


Figure 6. Graphical representation of shoreline changes in LZ II by EPR & LRR (2000 - 18)

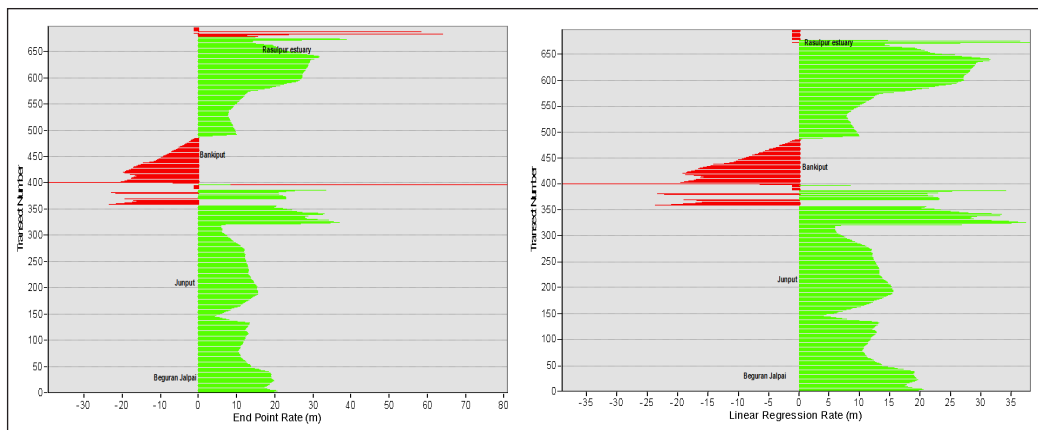


Figure 7. Graphical representation of shoreline changes in LZ III by EPR & LRR (2000-18)



Figure 8. Google earth image of Digha estuary and tetrapod groin

III, the LRR graph showed the prominent erosion in Bankiput and Rasulpur estuary with signified value but in EPR method the values were distracted from erosion to accretion zone due to its adaptation problem in multiple shoreline data. LZ I also experienced the same in Subarnarekha estuary area (Figure 5). Due to this problem, to estimate the long-term shoreline change rate LRR was the most compatible method.

Spatial Changes in Land Use/ Land Cover Mapping

The land use/land cover classification was done for an area of approximate 143sq.km. From this LULC map it was observed that drastic changes occurred from 2000 to 2018 (Figures 9, 10, 11). To identify the prominent change, total area was divided into three littoral zones (LZ) as stated earlier. LZ I (Figure 9) of 2000, 2010, 2018 LULC maps showed that the maximum soil area could be found in the year 2000 but it was reduced rapidly from 2010 to 2018. This zone also showed that how built-up area was enhanced within the time span 2000 to 2018. However, the growth of vegetation was observed after 2010 and it was increased in 2018. It happened because plantation initiative was adopted to protect the shoreline from coastal erosion by West Bengal Govt. after 2010. In the year 2000, shallow water was observed in few areas but from 2010 the increasing trend of water level was found prominently. In LZ II (Figure 10) it was observed that built-up area was low in 2010 but in 2018 LULC map built-up increased again. In this zone, soil area was low in 2000 and 2018, but in the year 2010 maximum soil area was found. Shallow water area was increased from 2010. Maximum sand area was observed in the year 2000. Vegetation was increased after 2010. Most of the built-up area found in Mandarmani to Dadanpatrabar region. The LZ III (Figure 11) was most accreted area where high vegetation cover was found in 2000 and 2018 but in 2010 vegetation cover was reduced. Sand area of higher coverage was observed clearly in 2000 but from 2010 it was decreased. Built-up area was found mostly in 2010 and 2018. This zone clearly showed that water level was high in 2010 and 2018 map. Maximum soil area was found in 2010.

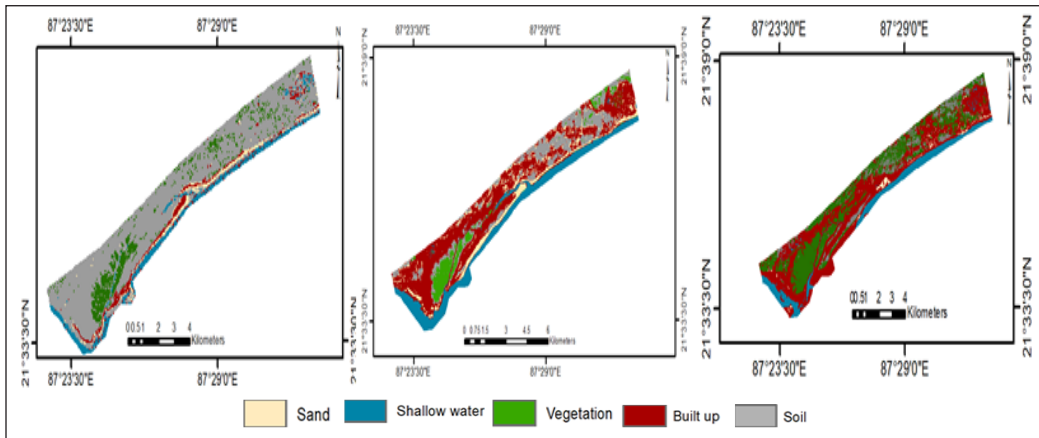


Figure 9. LULC map of LZ I in 2000, 2010, 2018

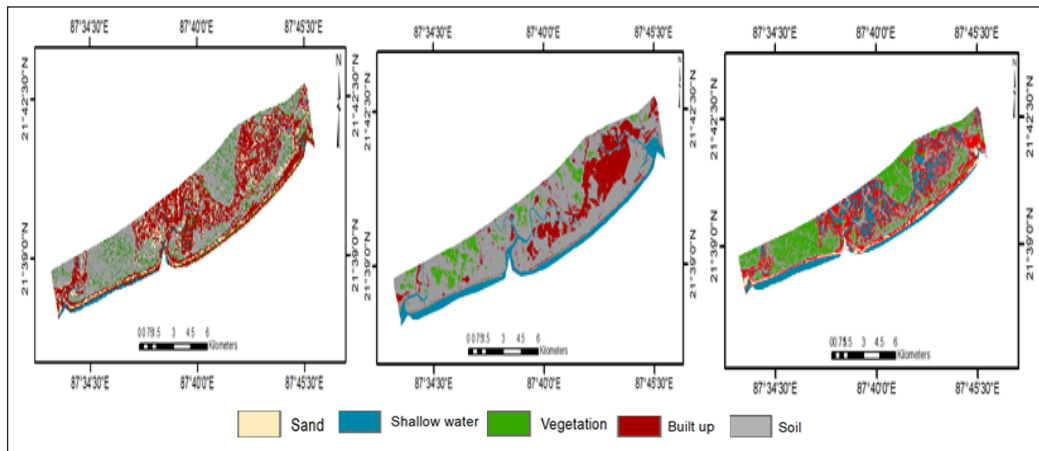


Figure 10. LULC map of LZ II in 2000, 2010, 2018

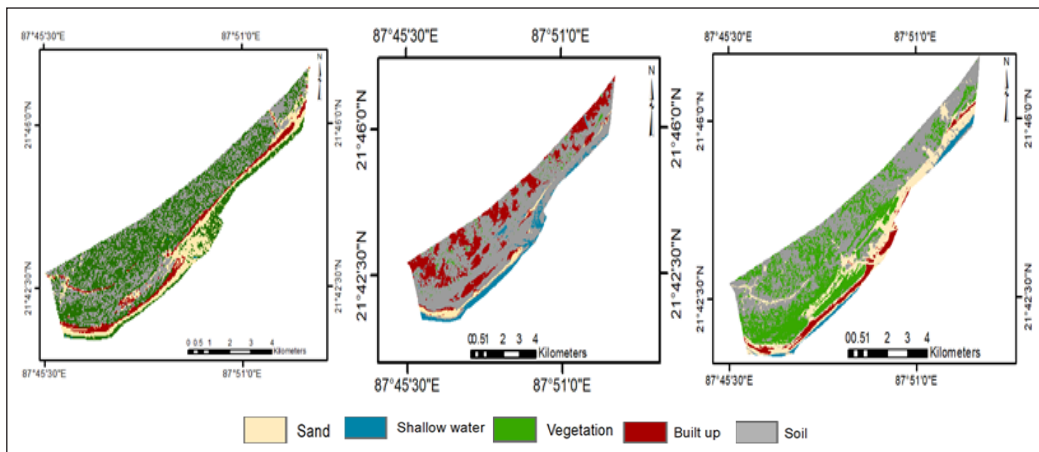


Figure 11. LULC map of LZ III in 2000, 2010, 2018

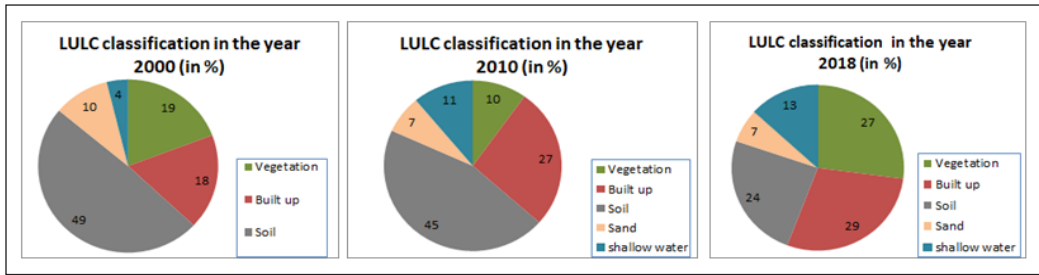


Figure 12. LULC area in percentage (2000 – 2018)

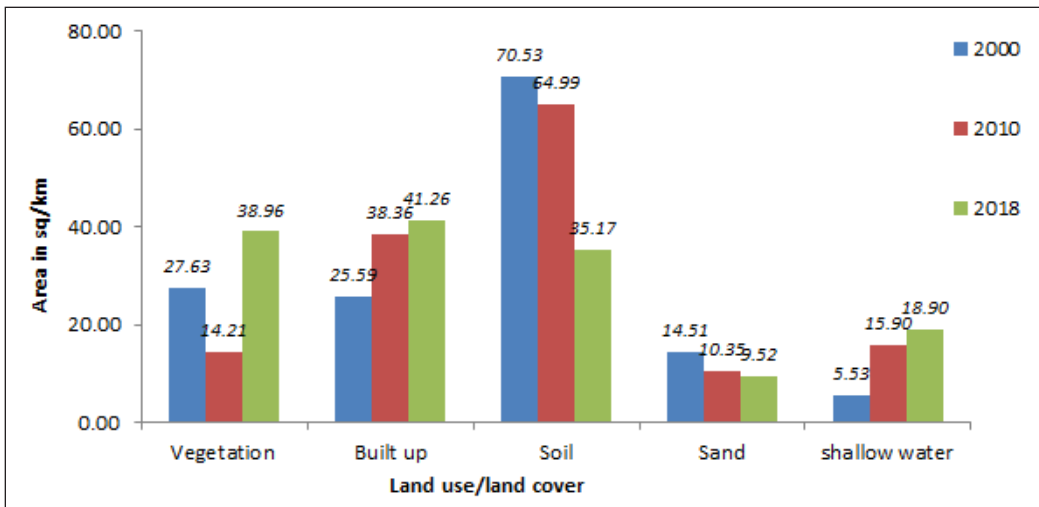


Figure 13. LULC area in sq.km (2000 – 2018)

Figure 12 shows the total changes in percentage. Figure 12 explains the drastic changes that occurred between 2000 – 2018 time span. The built-up area increased in 2000 – 2018 from 18% to 29% where shallow water level also increased in these 18 years from 4% to 13%. But soil area was reduced from 49% in 2000 to 45% in 2010 and 24% in 2018. Sand area was observed 10% in 2000 but decreased 7% in 2018. Vegetation was 19% in 2000 but it decreased to 10% in 2010. Sand area increased again in 2018 to 27%.

Figure 13 shows the LULC area in sq.km from 2000 – 2018 in approx. 143sq.km. This distribution shows that vegetation area was increased from 27.63sq.km to 38.96sq.km. Built-up area was enhanced from 25.69sq.km to 41.26sq.km. Maximum drastic changes were observed in soil area that was decreased rapidly from 70.59sq.km to 35.17sq.km in 18 years. Shallow water was also increased from 5.5sq.km to 18.90sq.km during the same time span.

From the accuracy assessment, it has been observed that maximum producer’s accuracy was obtained in built up, vegetation and shallow water, whereas the maximum user’s accuracy was obtained in class of soil, sand, and shallow water area (2000, 2010, 2018).

The overall accuracy of 85% and Kappa co-efficient 81.25% has been obtained from the assessment. The built-up area showed the lowest user's accuracy in 2000 map (37.5%) due to the low resolution of the image. In the classified map of 2010, the highest producer's accuracy was found in built up, soil and shallow water area and accurate user's accuracy was reflects in vegetation, sand and shallow water area with 95% overall accuracy and 93.67% Kappa co-efficient. The classified image of 2018 remarked the highest producer's accuracy in vegetation, sand and shallow water area and highest user's accuracy reached in vegetation and soil area where the overall accuracy was 90% and Kappa co-efficient accuracy was 87.43% (Table 2).

CONCLUSION

The use of remote sensing data to find out the erosion – accretion patterns and LULC changes has been presented in this work. The research presented multi-temporal LULC status of the study area with coverage of 143sq.km and it also presented shoreline shifting analysis for a length of 70.04 km. Over the last 18 years the entire area has been facing shoreline advance and retreat related problems, resulting in destructions to the environmental situation of the coastal area. The entire area under observation had been broadly divided into three “littoral zones” (LZ I to LZ III). The LZ I zone shows an average negative LRR value of -0.45 m/year and positive change rate value of 15.5 m/year. The LZ I also showed erosion of -1 m/year LRR and 10.15 m/year positive LRR change values. The LZ III was under accretion and erosional situation. The erosion change rate was found an average of -2.22 m/year and accretion change rate was 32 m/year LRR value. The LULC analysis showed that maximum built-up areas were concentrated in LZ 1 and built-up areashave been enhanced after the year 2000. Subarnarekha estuary to Digha estuary area observed immense pressure of urbanization from 2010. From these three LZ maps it could be observed prominently that shallow water was increased from 2010 to 2018. Finally, the present work shows the shoreline changes and prepares LULC maps that will play a very significant role for decision makers to identify and protect the susceptible zones and invent better mitigation methods for associated coastal problems.

ACKNOWLEDGEMENT

I would like to express my special thanks to Irrigation & Waterways Department and River Research Institute, West Bengal, India for their cooperation in date collection and field survey. I am thankful to Mr. Amiya Bera, Deputy Director (Structure), Irrigation & Waterways Department, West Bengal, Kolkata and Dr. Bibhas Chandra Barman, Deputy Director, River Research Institute, Mohanpur, Nadia, West Bengal, India for their heartfelt contribution. I also thankful to Mr. Bimal Adak, field investigator at Digha, (RRI) West Bengal, India for his support during field visit.

REFERENCES

- Alesheikh, A. A., Ghorbanali, A., & Nouri, N. (2007). Coastline change detection using remote sensing. *International Journal of Environmental Science and Technology*, 4(1), 61-66. doi: <https://doi.org/10.1007/BF03325962>
- Balachandar, D., Rutharvel M. K., Muruganandam, R., Sumathi, M., Sundararaj, P., & Kumaraswamy, K. (2011). Analysis of land use/ land covers using remote sensing techniques-A case study of Karur district, Tamil Nadu, India. *International Journal of Current Research*, 3(12), 226-229.
- Biging, G. S., Colby, D. R., & Congalton, R. G. (1998). Sampling systems for change detection accuracy assessment, remote sensing change detection. In R. S. Lunetta & C. D. Elvidge (Eds.), *Environmental monitoring methods and applications* (pp. 281-308). Michigan, USA: Ann Arbor Press.
- Boak, E., & Turner, I. (2005). Shoreline definition and detection: A review. *Journal of Coastal Research*, 21(4), 688-703. doi: <https://doi.org/10.2112/03-0071.1>
- Boschetti, L., Flasse, S. P., & Brivio, P. A. (2004). Analysis of the conflict between omission and commission in low spatial resolution dichotomic thematic products: The pareto boundary. *Remote Sensing of Environment*, 91(3-4), 280-292. doi: <https://doi.org/10.1016/j.rse.2004.02.015>
- Bradley, B. A. (2009). Accuracy assessments of mixed land cover using a GIS-designed sampling scheme. *International Journal of Remote Sensing*, 30(13), 3515-3529. doi: <https://doi.org/10.1080/01431160802562263>
- Carlotto, M. J. (2009). Effect of errors in ground truth on classification accuracy. *International Journal of Remote Sensing*, 30(18), 4831-4849. doi: <https://doi.org/10.1080/01431160802672864>
- Chand, P., & Acharya, P. (2010). Shoreline change and sea level rise along coast of Bhitarkanika wildlife sanctuary, Orissa: An analytical approach of remote sensing and statistical techniques. *International Journal of Geomatics and Geosciences*, 1(3), 436-455.
- Chatterjee, R. K. (1995). A comparative study between East and West Indian Coast: A geographical account. *Geographical Review of India*, 12(1), 23-25.
- Chavez, J. R. (1988). An improved dark-object subtraction technique for atmospheric scattering correction of multispectral data. *Remote Sensing of Environment*, 24(3), 459-479. doi: [https://doi.org/10.1016/0034-4257\(88\)90019-3](https://doi.org/10.1016/0034-4257(88)90019-3)
- Congalton, R. G., & Green, K. (1999). *Assessing the accuracy of remotely sensed data: Principles and practices*. Boca Raton, Florida: CRC Press, Taylor & Francis Group.
- Coppin, P. R., & Bauer, M. E. (1996). Digital change detection in forest ecosystems with remote sensing imagery. *Remote Sensing Reviews*, 13(3-4), 207-234. doi: <https://doi.org/10.1080/02757259609532305>
- Dey, S., Ghosh, P., & Nayak, A. (2005). The influences of natural environment upon the evolution of sand dunes in tropical environments along Medinipore coastal area, India. *Indonesian Journal of Geography*, 37(1), 51-68.
- Dolan, R., Fenster, M. S., & Holme, S. J. (1991). Temporal analysis of shoreline recession and accretion. *Journal of Coastal Research*, 7(3), 723-744.

- Emran, A., Rob, M. A., Kabir, M. H., & Islam, M. N. (2016). Modeling spatio-temporal shoreline and areal dynamics of coastal island using geospatial technique. *Modeling Earth Systems and Environment*, 2(4), 1-11. doi: 10.1007/s40808-015-0060-z.
- Everts, C. H., Battley Jr, J. P., & Gibson, P. N. (1983). *Shoreline movements. Report 1. Cape Henry, Virginia, to Cape Hatteras, North Carolina, 1849-1980* (No. CERC-83-1-1). Technical Report. Coastal Engineering Research Center Vicksburg MS.
- Garcia-Rubio, G., Huntley, D., Kingston, K., & Esteves, L. S. (2009). Shoreline identification using satellite images. *Coastal Dynamics*, 2009, 1-10. doi: 10.1142/9789814282475_0117
- Goodbred Jr, S. L., & Kuehl, S. A. (2000). The significance of large sediment supply, active tectonism, and eustasy on margin sequence development: Late quaternary stratigraphy and evolution of the Ganges–Brahmaputra delta. *Sedimentary Geology*, 133(3-4), 227-248. doi: [https://doi.org/10.1016/S0037-0738\(00\)00041-5](https://doi.org/10.1016/S0037-0738(00)00041-5)
- Guru, B., Neha, M., & Anubhooti, Y. (2014, December 9-12). Study the land use and land cover changes and CRZ in the coastal area of Ganjam District, Odisha. In *International Society of Photogrammetry and Remote Sensing (ISPRS), Mid-Term Symposium of the Technical Commission VIII* (pp. 1-5). Hyderabad, India.
- Jana, A., Biswas, A., & Maiti, S. (2013). Shoreline changes in response to sea level rise along Digha Coast, Eastern India: An analytical approach of remote sensing, GIS and statistical techniques. *Journal of Coastal Conservation*, 18(3), 145-155. doi: <https://doi.org/10.1007/s11852-013-0297-5>
- Khan, S. R., & Islam, B. (2008). Holocene stratigraphy of the lower Ganges-Brahmaputra river delta in Bangladesh. *Frontiers of Earth Science in China*, 2(4), 393-399. doi: <https://doi.org/10.1007/s11707-008-0051-8>
- Koloa, C., & Samanta, S. (2013). Development impact assessment along Merkhram River through remote sensing and GIS technology. *International Journal Asian Academy Research Association*, 5(1), 26-41.
- Kuleli, T. (2009). Quantitative analysis of shoreline changes at the Mediterranean Coast in Turkey. *Remote Sensing of Environment*, 167(1-4), 387-397. doi: <https://doi.org/10.1007/s10661-009-1057-8>
- Kumar, A., & Jayappa, K. S. (2009). Long and short-term shoreline changes along Mangalore Coast, India. *International Journal Environmental Research*, 3(2), 177-188.
- Li, B., & Zhou, Q. (2009). Accuracy assessment on multi-temporal land-cover change detection using a trajectory error matrix. *International Journal of Remote Sensing*, 30(5), 1283-1296. doi: <https://doi.org/10.1080/01431160802474022>
- Lu, D., & Weng, Q. (2007). A survey of image classification methods and techniques for improving classification performance. *International Journal of Remote Sensing*, 28(5), 823-870. doi: <https://doi.org/10.1080/01431160600746456>
- Mageswaran, T., Mohan, V. R., Selvan, S. C., Arumugam, T., Usha, T., & Kankara, R. S. (2015). Assessment of shoreline changes along Nagapattinam coast using geospatial techniques. *International Journal of Geomatics and Geosciences*, 5(4), 555-563.

- Maiti, S., & Bhattacharya, A. K. (2009). Shoreline change analysis and its application to prediction: A remote sensing and statistics based approach. *Marine Geology*, 257(1-4), 11-23. doi: <https://doi.org/10.1016/j.margeo.2008.10.006>
- Mujabar, P. S., & Chandrasekar, N. (2011). Coastal erosion hazard and vulnerability assessment for southern coastal Tamil Nadu of India by using remote sensing and GIS. *Natural Hazards*, 69(3), 1295-1314. doi: <https://doi.org/10.1007/s11069-011-9962-x>
- Mujabar, P. S., & Chandrasekar, N. (2013). Shoreline change analysis along the coast between Kanyakumari and Tuticorin of India using remote sensing and GIS. *Arabian Journal of Geosciences*, 6(3), 647-664. doi: <https://doi.org/10.1007/s12517-011-0394-4>
- Mukhopadhyay, A., Hornby, D. D., Hutton, C. W., Lázár, A. N., Johnson, F. A., & Ghosh, T. (2018). Land cover and land use analysis in coastal Bangladesh. In *Ecosystem Services for Well-Being in Deltas* (pp. 367-381). Cham, Switzerland: Palgrave Macmillan.
- Mukhopadhyay, A., Mukherjee, S., Garg, R. D., & Ghosh, T. (2013). Spatio-temporal analysis of land use - land cover changes in Delhi using remote sensing and GIS techniques. *International Journal of Geomatics and Geosciences*, 4(1), 212-223.
- Mukhopadhyay, A., Mukherjee, S., Hazra, S., & Mitra, D. (2011). Sea level rise and shoreline changes: A geo-informatics appraisal of Chandipur coast, Orissa. *International Journal of Geology, Earth and Environmental Sciences*, 1(1), 9-17.
- Mukhopadhyay, A., Mukherjee, S., Mukherjee, S., Gosh, S., Hazra, S., & Mitra, D. (2012). Automatic shoreline detection and future prediction: A case study on Puri Coast, Bay of Bengal, India. *European Journal of Remote Sensing*, 45(1), 201-213. doi: <https://doi.org/10.5721/EuJRS20124519>
- Munday, J. C., & Alfoldi, T. T. (1979). LANDSAT test of diffuse reflectance models for aquatic suspended solids measurement. *Remote Sensing Environment*, 8(2), 169-183. doi: [https://doi.org/10.1016/0034-4257\(79\)90015-4](https://doi.org/10.1016/0034-4257(79)90015-4)
- Murali, R. M., & Kumar, P. D. (2015). Implications of sea level rise scenarios on land use/land cover classes of the coastal zones of Cochin, India. *Journal of Environmental Management*, 148, 124-133. doi: <https://doi.org/10.1016/j.jenvman.2014.06.010>
- Nguyen, H. H., Pullar, D., Duke, N., McAlpine, C., Nguyen, H. T., & Johansen, K. (2010, November 1-5). Historic shoreline changes: An indicator of coastal vulnerability for human landuse and development in Kien Giang, Vietnam. In *31st Asian Conference on Remote Sensing* (pp. 1835-1843). Hanoi, Vietnam.
- Oumer, H. A. (2009). *Land use and land cover change, drivers and its impact: A comparative study from Kuhar Michael and LencheDima of Blue Nile and Awash Basins of Ethiopia* (Unpublished thesis). Cornell University, NY, USA.
- Pal, B., Samanta, S., & Pal, D. K. (2012). Morphometric and hydrological analysis and mapping for Watut watershed using Remote Sensing and GIS techniques. *International Journal of Advances in Engineering and Technology*, 2(1), 357-368.
- Pandian, P. K., Ramesh, S., Murthy, M. V. R., Ramachandran, S., & Thayumanavan, S. (2004). Shoreline changes and near shore processes along Ennore coast, east coast of South India. *Journal of Coastal Research*, 20(203), 828-845. doi: [https://doi.org/10.2112/1551-5036\(2004\)20\[828:SCANSP\]2.0.CO;2](https://doi.org/10.2112/1551-5036(2004)20[828:SCANSP]2.0.CO;2)

- River Research Institute. (2009). *Report on the beach profile survey at Digha form West Bengal-Orissa Border to Mandermoni*. Report [Hard Copy].
- Rossiter, D. G. (2014). *Statistical methods for accuracy assessment of classified thematic maps*. Technical Note. International Institute for Geo-information Science and Earth Observation (ITC).
- Saha, A. K., Arora, M. K., Csaplovics, N. E., & Gupta, R. P. (2005). Land covers classification using IRS LISS III Image and DEM in a Rugged Terrain: A case study in Himalayas. *Geocarto International*, 20(2), 33-40. doi: <https://doi.org/10.1080/10106040508542343>
- Samanta, S., & Paul, S. (2016). Geospatial analysis of shoreline and land use/land covers changes through remote sensing and GIS techniques. *Modeling Earth Systems and Environment*, 2(3), 1-8. doi: <https://doi.org/10.1007/s40808-016-0180-0>
- SCGE. (2011). *Supervised/unsupervised land use land cover classification using ERDAS imagine*. Summer course computational geocology. Retrieved May 30, 2015, from <http://horizon.science.uva>
- Scott, A. J., & Symons, M. J. (1971). Clustering methods based on likelihood ratio criteria. *Biometrics*, 27(2), 387-397.
- Selvan, S. C., Kankara, R. S., & Rajan, B. (2014). Assessment of shoreline changes along Karnataka coast, India using GIS and Remote sensing techniques. *Indian Journal of Marine Sciences*, 43(7), 1286-1291
- Story, M., & Congalton, R. (1986). Accuracy assessment: A user's perspective. *Photogrammetric Engineering and Remote Sensing*, 52(3), 397-399.
- Thieler, E. R., Himmelstoss, E. A., Zichichi, J. L., & Ayhan, E. (2009). *Digital shoreline analysis system (DSAS) version 4.3. An Arc GIS extension for calculating shoreline change: U.S. Geological Survey Open-File Report 2008-1278*. Retrieved November 5, 2018, from <http://pubs.usgs.gov/of/2008/1278>.
- Trinh, L. H., Le, T. G., Kieu, V. H., Tran, T. M. L., & Nguyen, T. T. N. (2020). Application of remote sensing technique for shoreline change detection in Ninh Binh and Nam Dinh provinces (Vietnam) during the period 1988 to 2018 based on water indices. *Russian Journal of Earth Sciences*, 20(2), 1-36. doi: 10.2205/2020ES000686.
- Umitsu, M., & Sen, B. (1987). Late quaternary sedimentary environment and landform evolution in the Bengal low land. *Geographical Review of Japan, Series B.*, 60(2), 164-178. doi: <https://doi.org/10.4157/grj1984b.60.164>
- Van, T. T., & Binh, T. T. (2008, December 4-6). Shoreline change detection to serve sustainable management of coastal zone in Cu Long Estuary. In *Proceedings of the International Symposium on Geoinformatics for Spatial Infrastructure Development in Earth and Allied Sciences* (pp. 1-6). Hanoi, Vietnam.
- Zhang, S., Zhang, S., & Zhang, J. (2000). A study on wetland classification model of remote sensing in the Sangjiang plain. *Chinese Geographical Science*, 10(1), 68-73. doi: <https://doi.org/10.1007/s11769-000-0038-1>

Surface Treatment of Cement based Composites: Nano Coating Technique

Isam Mohamad Ali¹, Tholfekar Habeeb Hussain² and Ahmed Samir Naje^{2*}

¹Karbala Technical Institute, Al-Furat Al-Awsat Technical University, 56001 Karbala, Iraq

²College of Water Resources Engineering, Al-Qasim Green University, Babylon, Iraq

ABSTRACT

Geometry, size, and shape of the surface pores, as well as, capillarity, and exposure environment are directly influence strength and durability of cementitious composites. The current research aimed to improve the resistance to abrasion and decrease the surface porosity of cement-based composites by nano surface coating technique. All samples were coated with a mixture of methanol alcohol, ordinary Portland cement and nano powder of (TiO₂, MgO, ZnO and ZrO₂) separately in percentages of (1, 1.5, and 2 %) by weight of cement. The hardness, abrasion, water absorption, density, porosity, and microstructural analysis: Scanning Electron Microscopy and X-Ray Diffraction (SEM & XRD) were studied for all coated and control specimens. Results showed an improvement in mechanical properties for all coated specimens as compared to control. The highest Vickers micro hardness value had reached 29%, while the largest value of abrasion resistance had increased by 39% for coated samples with 2% ZrO₂. Also, the results showed a reduction in the porosity and water absorption of all coated samples, having highest scores obtained from the coated samples with 2% MgO. While the total water absorption rate decreased by 45% and the density had increased by 1% and the porosity had decreased by 46%. Additionally, the results of microstructural tests revealed pattern and images for each of SEM and XRD. Also,

results indicated that the nano coating leads to significant consumption of Portlandite (CH) associated with production of a stable structure of CSH and reduction of voids, and this is evident from the enhancement in the physical properties.

ARTICLE INFO

Article history:

Received: 19 September 2020

Accepted: 25 September 2020

Published: 22 January 2021

DOI: <https://doi.org/10.47836/pjst.29.1.20>

E-mail addresses:

ali_isam@ymail.com (Isam Mohamad Ali)

ahmednamesamir@gmail.com (Tholfekar Habeeb Hussain)

ahmednamesamir@yahoo.com (Ahmed Samir Naje)

* Corresponding author

Keywords: Abrasion resistance, cement composites, hardness, microstructure, nano coating, porosity

INTRODUCTION

Harmful agents present in the medium that concrete is subjected to, were the main reasons for degradation and low service life of concrete. Sulfates, carbon dioxide and chlorides from industrial and marine environments penetrate into pores and react chemically, causing expansive reactions and corrosion of steel bars (Quraishi et al., 2017). However, the porosity of the cement- based composites is influenced by many factors that may be due to its raw materials, the production procedure, and water / cement ratio, type of curing, compaction, and degree of hydration (de la Cruz Barroso et al., 2015). According to what was mentioned by Mehta and Monteiro (2006), “the empty pores present in the concrete could be classified according to their size to: gel pores: of 1 to 5 μm diameter; capillary pores: of 5 to 30 μm diameter; small air bubbles; of 30 μm to 1 mm diameter; and large air bubbles: of greater than or equal to 1 mm diameter”. The absorption rate investigated on concrete is governed by the capillary pressure of its pores, which is determined by the diameter, shape and connection of the pores present in the surface (Pellegrini-Cervantes et al., 2013). In the case of ion penetration, the capillary absorption of concrete is a very fast process, being considered a hundred times faster than its permeability (Aperador et al., 2016). The dispersion method impact for CaCO_3 nanoparticles on hydration rate, setting, and compressive strength of concrete. Nanoparticles can be used to increase the mechanical features of cement composites (Camilletti et al., 2013). Another study was made to assess the capability of concrete containing nano TiO_2 to degrade organic molecules. The extent of nano TiO_2 in the concrete mixes was 3, 6, 9, 12, and 15% by cement weight. The resulting concrete samples were subjected to sunlight for 24, 48, 72, and 96 hrs. The nano TiO_2 extinguish the organic molecules, by reducing the surface permeability and, as a result, resists certain kinds of air pollution (Elia et al., 2018). The compositions of nano coatings are nano powders dissolved in a fluid to reach an excessive surface area to volume ratio (Birgisson et al., 2012). Due to nanoparticles coatings, corrosion resistance, antivirus features are improved due to enhanced properties of hardness, adhesion, and wear (Mendes et al., 2015). In India, this coating technique was extensively utilized in the strengthening of New Delhi wealth Games building (Glenn, 2013). Thus, the use of organic coatings on concrete is the most common withstand method of concrete and reinforcements versus weathering and corrosion (Vera et al., 2013). Further, the inclusion of nano SiO_2 as thin film on aggregate surfaces enhances the efficiency of concrete. Mortar formed accompanying to nano SiO_2 of 0.32 by wt. % of cement, as a coating on aggregate surfaces exhibited an average 35% enhancement in compressive, flexural, and tensile strengths with a decline in chloride permeability (Zhuang & Chen, 2020). The previous and most nanotechnology researchers’ studies were focused on characterizing of concrete when nano particles were added in the concrete during mixing to increase strength (Ltifi et al., 2011; Zhang et al., 2019a; Zhang et al., 2019b; Rezania et al., 2019; Ali et al., 2020). Meanwhile, it is the

surface pores, which control the rate of entry and movement of detrimental agents that can alter concrete properties and causing a deterioration of its microstructure. Thus, the surface porosity of cement-based composites is vital in the durability of concrete, which is the main characteristic that determines the life for which they were designed. Further, the reason behind using nanomaterials was to enhance mortar performance is that the properties of the particles at the nanoscale are extremely better than the conventional particle size for the same chemical component. This means that novel building materials with superior properties could be produced by using nanoparticles.

The objectives of this research were to study the impact of nano coating on the performance of cement-based composite and to improve the resistance to the chemical as well as biological agent ingress using different types and doses of nanoparticles as coating layer and as a protective shield.

MATERIALS AND METHOD

Materials Characteristics

The raw materials used were type I cement, micro silica, fine aggregate, water, and super plasticizer. Ordinary Portland cement, conforming to I.Q.S 5/1984, was used to produce the specimens. Micro silica was used as pozzolanic admixture associated with 124% pozzolanic strength activity index. Results revealed that micro silica used in this study conformed to the requirements of ASTM C-1240-05 standard. A high range water reducer superplasticizer (Sika ViscoCrete 5930) with a density of 1.095 g/cm³ was used to increase dispersing of mixes, which had been classified as type G according to ASTM C494-14. The sand conforming to the Iraqi Specification No.45/1984 zone 2, was of 4.75 mm maximum size. The nano powders in addition to methanol alcohol used in this study were provided by Nanoshel Company (USA), and Table 1 presents their properties according to manufacturing origin.

Experimental Analysis

In this study, cement based composite boards with a density of 2200 kg/m³ were made and tested for 28 days following the ASTM C1185-12. In light of past research, the experimental factors were: three different percentages of nanoparticles (1, 1.5, and 2 %) by cement weight, and nano particle type (TiO₂, MgO, ZnO and ZrO₂). All the cement mixes used in this investigation had a constant water-to-cement ratio of 35%, superplasticizer-to-cement ratio of 1%, the replacement of microsilica by cement weight of 10%, and a cement-to-sand ratio of 1:2.75. All samples with dimension (305*152*12 mm), were preserved in the molds covered with wet burlap secured with a plastic sheet for one day to prevent moisture loss. After 28 days of moist curing, coating suspensions were prepared following

the procedure described by Ibrahim (2016). Using airbrush spray gun technique at 10 bar compressed air at laboratory temperature, sprayed distance 25 cm, feeding rate 300 ml/min and primary heating of the specimens to 100 °C before coating for 30 minutes to improve the bond between the coating layer and the substrate surface. After that, density, water absorption and porosity were determined in accordance to ASTM C642-06 using the water displacement method.

Table 1
The properties of used materials according to Nanoshel Company (USA)

Properties	Titanium dioxide nano powder	Zirconium oxide nano powder	Zinc oxide nano powder	Magnesium oxide nano powder	Methanol Alcohol
Chemical composition	TiO ₂	ZrO ₂	ZnO	MgO	CH ₃ OH
Purity (%)	99.9	99.9	99.9	99.9	99.8
particle size (nm)	50	50	50	50	/
Specific surface area (m ² /gm)	35	45	65	40	/
Color	White	White	White	White	colorless
Phase	Rutile	Tetragonal	Hexagonal	Cubic	liquid
Density (g/cm ³)	4.3	5.9	5.6	3.6	0.79

The abrasion test machine consists of rotating disc made of tool steel carried out by four parameters (load, time, sliding speed, and sliding distance). Applied load was 5 N, applied time was 1 min, and the constant sliding speed was 1000 rpm with constant sliding distance of 5 cm following ASTM C779-03. Vickers micro hardness tester was used to measure the hardness at indentation load of 0.1N for 15 second. Four values for the hardness were taken on each specimen surface and the average diagonal dimensions of this indent were measured to find the Vickers hardness according to ASTM E 384-99. In addition, the microstructural properties were investigated in terms of X-ray diffraction (XRD), and scanning electron microscope (SEM), for all coated and control specimens.

RESULTS AND DISCUSSION

Effect of Nano Coating on Vickers Hardness

The trends observed during the testing were similar to those seen by other researchers using the same nano particles. The increase observed was almost linear in nature for TiO₂, ZnO and ZrO₂ and nonlinear for MgO nano particles. Figure 1 demonstrates the correlation between Vickers hardness and nano particle type for both coated and control specimens. Higher hardness for coated cement composite specimens were directly related to their higher dosage in the coating film. When comparing between nano particles types, ZrO₂ specimens yielded 29 % higher hardness with the higher dosage in the coating film, despite

of convergence of results. Whilst ZnO specimens yielded only 13 % higher hardness as compared to control specimens. Zirconium oxide nano powder yielded the highest values of hardness due to both the accelerated pozzolanic activity between nano oxides and calcium hydroxide from cement hydration, which led to harder products and to the filling effect by the very tiny particles, thus reducing the number and size of surface pores. This trend is similar to that found by Ibrahim (2016).

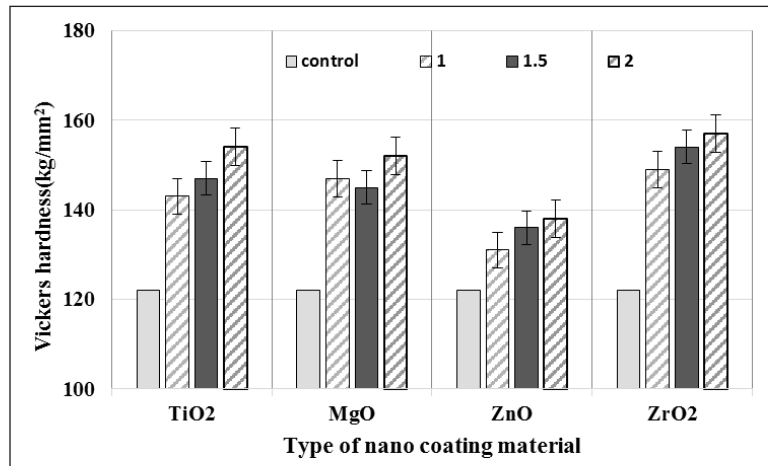


Figure 1. Effect of nanoparticles on the Vickers micro hardness for all cement specimens

Effect of Nano Coating on Abrasion

The word abrasion mainly points to dry wearing action, like in case of wear on pavements and concrete floors by vehicles. There is an essential inverse correlation between porosity and strength of all solid materials. Figure 2 shows histogram of the abrasion test results for all specimens after 28 days of curing. From Figure 2, it can be seen that the abrasion rate reached to the half of control specimen and often quarter that after coating by 2% ZrO₂, as compared with that of the control. It is also obvious that higher doses of 2% for all types were very beneficial to long term abrasion rate and, the lowered 1 % dose might be more desirable than high rate for economy consideration, hence decreasing the abrasion rate of the final composite. This could be due to the filling effect by the very tiny particles which reduced the volume and number of surface pores resulting in solidification of specimen surface. Moreover, as compared to control, an increase in the nano particles concentration in the coating film from (1 to 2%) decreased the abrasion rate by (21-28%), (14-26%), (9-23%) and (28-39%) for TiO₂, MgO, ZnO and ZrO₂, respectively. It was also noticed 1% ZnO showed the lower decrease in the abrasion of 39 g/min *10⁻⁸, while 1% ZrO₂ nano particles showed the higher decrease of 26 g/min *10⁻⁸. This trend is comparable to that found by Othman et al., (2016).

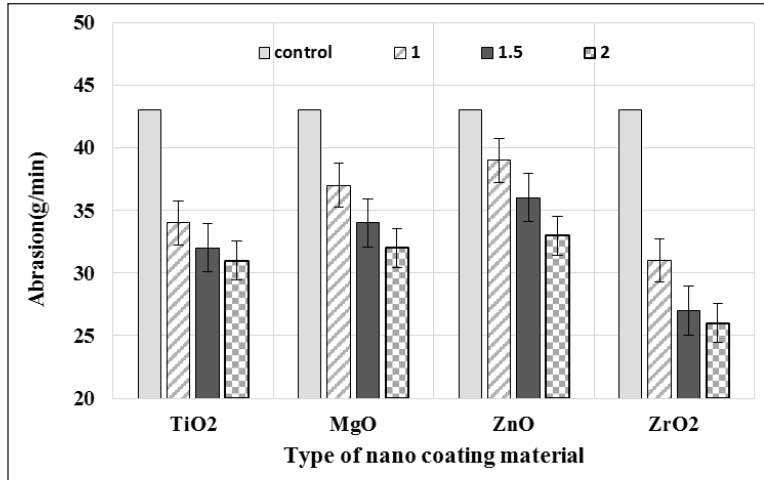


Figure 2. Effect of nanoparticles on the abrasion rate for all cement specimens

Effect of Nano Coating on Density

Figure 3 shows the average densities of all specimens after 28 days of curing. As discussed above, all of the mechanical properties calculated improved as the nano content increased in the coating film. The density for each nano particle type varied differently depending on the percentage of their mass addition in the coating film and to the density of each type. According to Figure 3, all coated specimens were heavier than the control, especially for 2% zirconium oxide nano particles which had the highest density of 2.262 g/cm³. This could be attributed to the high density of (ZrO₂) compared to other types. Else ways, 2% (MgO) showed the lower improvement in density in comparison to control due to the low density of nano MgO particles. However, all the nano coated films showed pozzolanic reactivity between nano oxides and calcium hydroxide from cement hydration leading to

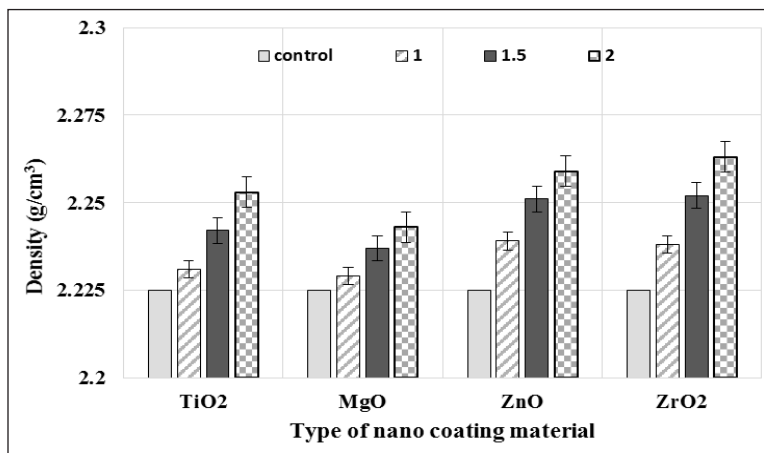


Figure 3. Effect of nanoparticles on the density for all cement specimens

further hydration products that altered the final density. Hence, increasing the nano particle dosage in the coating film (1 to 1.5 to 2 %) increased the density of specimen 0.3, 0.8 & 1.3 % for TiO₂; 0.2, 0.5 & 0.8 % for MgO; 0.6, 1.2 & 1.5 % for ZnO; 0.6, 1.2 & 1.7 % for ZrO₂. These results are in line with the values obtained by Khitab and Arshad (2014).

Effect of Nano Coating on Porosity

From Figure 4, it is observed that all coated specimens would show lower porosity especially MgO at 2% by weight of cement. A stronger adhesion between the coating film and the substrate surface besides the low density of nano MgO particles was assumed to be responsible for this. At higher doses, there would be a chemical interaction between the coating film and the specimen surface that filled the empty pores on the surface and beyond. However, the ability of mineral nano oxides to react at normal temperatures with CH (present in the hydrated Portland cement) and to form additional calcium silicate hydrate were responsible for the decrement in porosity of the final composite. As shown in Figure 4, all coated specimens had porosities in the range of 8-45 %, which was smaller than that of control without coating film. It was interesting to find that there existed a reverse linear relationship between the nano particle dosage in the coating film and the void ratio. The lowest porosity was achieved in 2% MgO (1.92%), and the highest was gained for ZrO₂ (3.26%) at 1% dose of addition.

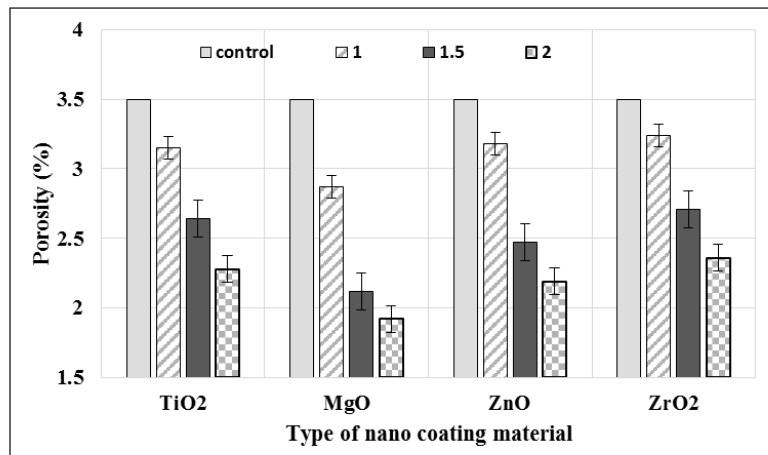


Figure 4. Effect of nanoparticles on the porosity for all cement specimens

Effect of Nano Coating on Water Absorption

Figure 5 represents the water absorption of all cement coated and the control specimens after 28 days of curing. It is obvious that the water absorption for all coated specimens was lower than the control, particularly for nano MgO coating of 2% has the lowest water absorption (45%) as compared to control. This could be attributed to the low density of nano

MgO particles leading to higher volume fraction in the coating film which decreased the surface porosity of specimens. Meanwhile, the lowest water absorption for 2% TiO₂, ZnO and ZrO₂ were 34, 37 and 31% respectively. Test results indicated that the water absorption of all specimens decreased continuously with increasing the nano particles dosage in the coating film. This could be due to the filling effect by the very tiny particles which reduced the volume and number of surface pores. Nevertheless, additional hydration products were gained during the pozzolanic activity between nano oxides and calcium hydroxide from cement hydration as indicated in SEM and XRD images.

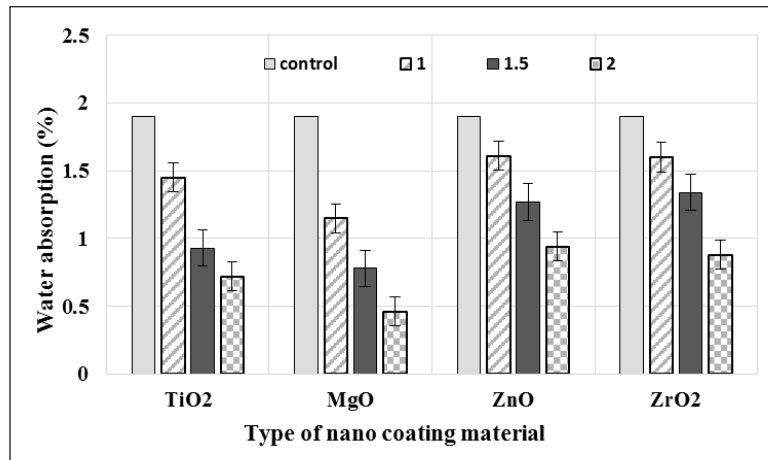


Figure 5. Effect of nanoparticles on the water absorption for all cement specimens

XRD Patterns

After 28 days of curing, XRD analyses were conducted to investigate the activity of incorporating nanoparticles for control and coated cement composite specimens. According to “Joint Committee on Powder Diffraction Standards (JCPDS)”, the components shown in the Figure 1 to 6 were: Portlandite: Ca(OH)₂, hexagonal crystallized, Tobermorite: Ca₅Si₆(O, OH, F)₁₈.5H₂O, orthorhombic crystallized, Ettringite: Ca₆A₁₂(SO₄)₃(OH)₁₂. 26H₂O, hexagonal crystallized, CSH: CaO.SiO₂.H₂O, poor crystallized, CS: CaSiO₃, monoclinic crystallized, Zirconium Oxide: ZrO₂, tetragonal crystallized, Titanium Dioxide: TiO₂, rutile, Magnesium Oxide: MgO, cubic crystallized, and Zinc Oxide: ZnO, hexagonal crystallized. The results of the X-ray diffraction spectra presented in Figure 6 to 10 include data from representative mixtures from the testing matrix control and coated with four types of nano powders. According to Figure 6, major peak humps of Ca(OH)₂ was observed in the diffraction pattern 2θ values of 21.5°, 29.5° and 37° for control mixes. Meanwhile, a minor peak of (CSH, CS and ettringite) were noticed in the diffraction pattern between 2θ values of 22°, 25° and 52°. It is also evident from XRD patterns in Figures 7 to 10 that the CH intensity decreased with the ZrO₂, TiO₂, MgO, and ZnO coated nanoparticles.

However, the results are agreeable with those of obtained by Ahmed et al. (2017). It is therefore concluded from Figure 7 to 10 that the nanoparticles chemically reacted with CH produced during the hydration of cement. The pozzolanic reactivity of nanoparticles can significantly improve the microstructure, so enhancing the mechanical performance of the cement composites (Othman et al., 2016).

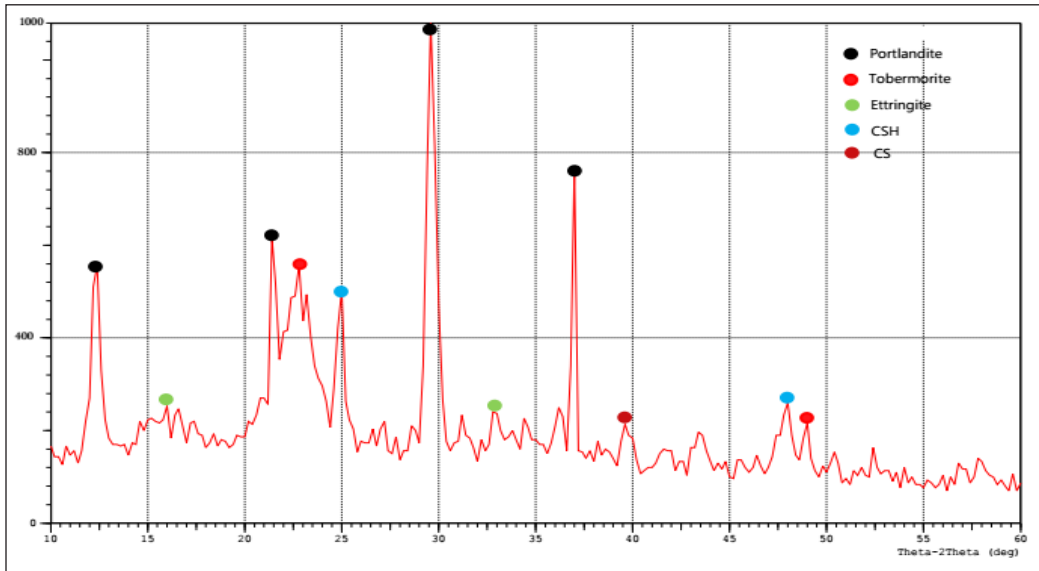


Figure 6. The XRD patterns for the control cement specimen

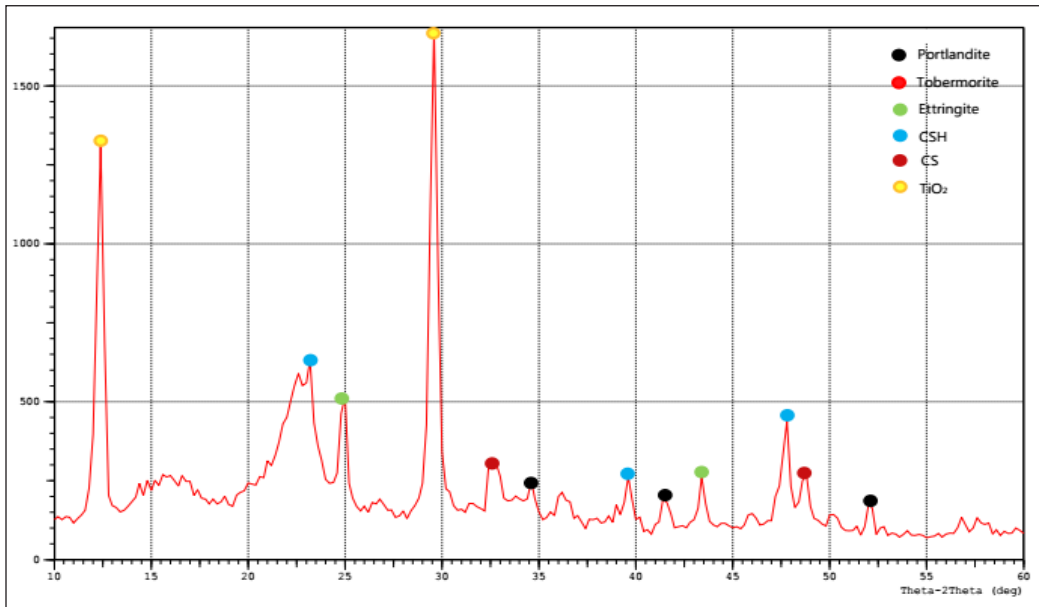


Figure 7. The XRD patterns for the cement coated specimen with 2% TiO₂ nanoparticles

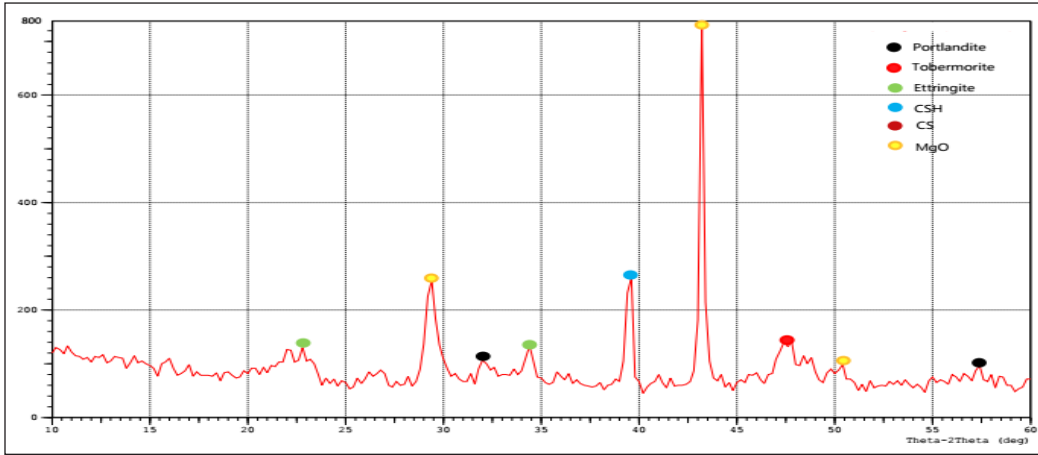


Figure 8. The XRD patterns for the cement coated specimen with 2% MgO nanoparticles

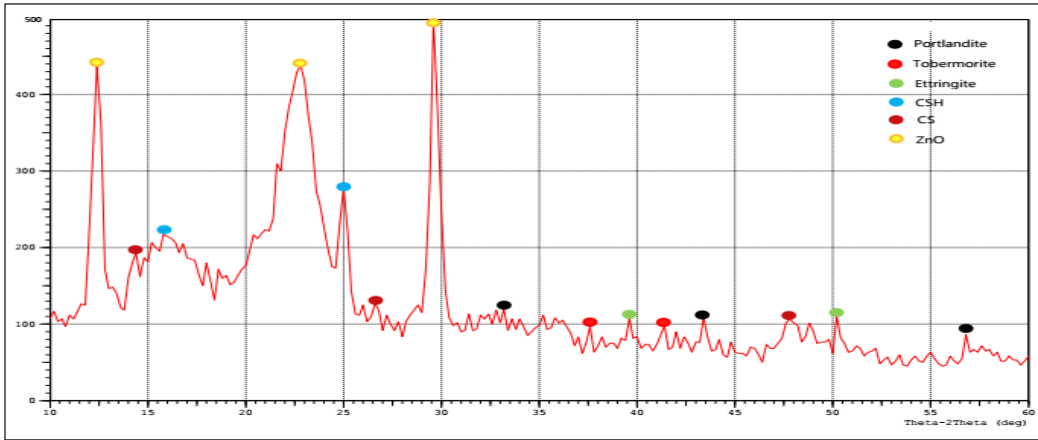


Figure 9. The XRD patterns for the cement coated specimen with 2% ZnO nanoparticles

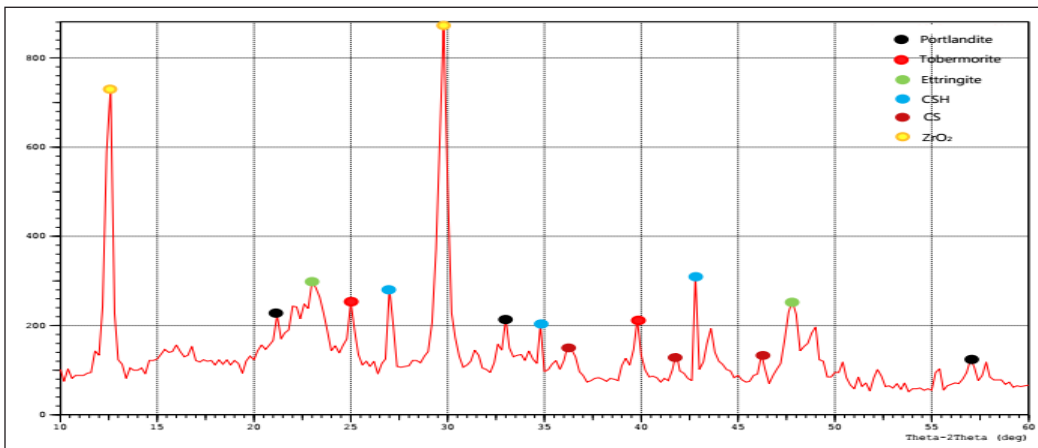


Figure 10. The XRD patterns for the cement coated specimen with 2% ZrO₂ nanoparticles

SEM Analysis

SEM analysis of the cementitious composites offered a good qualitative view of the mineralogy that lies inside the composite structure. Figure 11 views the SEM micrographs of control and coated with four types of nano powders fractured surface after 28 days of moist curing. Four representative images for each specimen were obtained and only one SEM micrograph was chosen from them. The existence of CH crystals connected to the CSH gel (arrow 1/a) indicates that the microstructure was weak and also explains the reduction of mechanical properties for the control mix. Whereas it seems clear that the surface pores were partially filled with 2% TiO₂ nano particles and/or additional hydration products from the pozzolanic activity (arrow 2/b). Also, it is obvious that after 2% MgO nano coating, there was a good adhesion force between CSH and CS, so no cracks appeared within ITZ (arrows 3/c). However, the cross section of 2% ZnO used here, was composed of large crystals of CH, so the fracture crack at failure initiated rapidly within ITZ so reducing the final composite strength (arrows 4/d). This is an indication of low pozzolanic activity for Zinc oxide nano powder. This is the opposite of what happened to the composite after ZrO₂ nano coating (arrows 5/e). The surface black holes were completely filled with extra CSH from the pozzolanic activity and there was no indication for CH crystals in

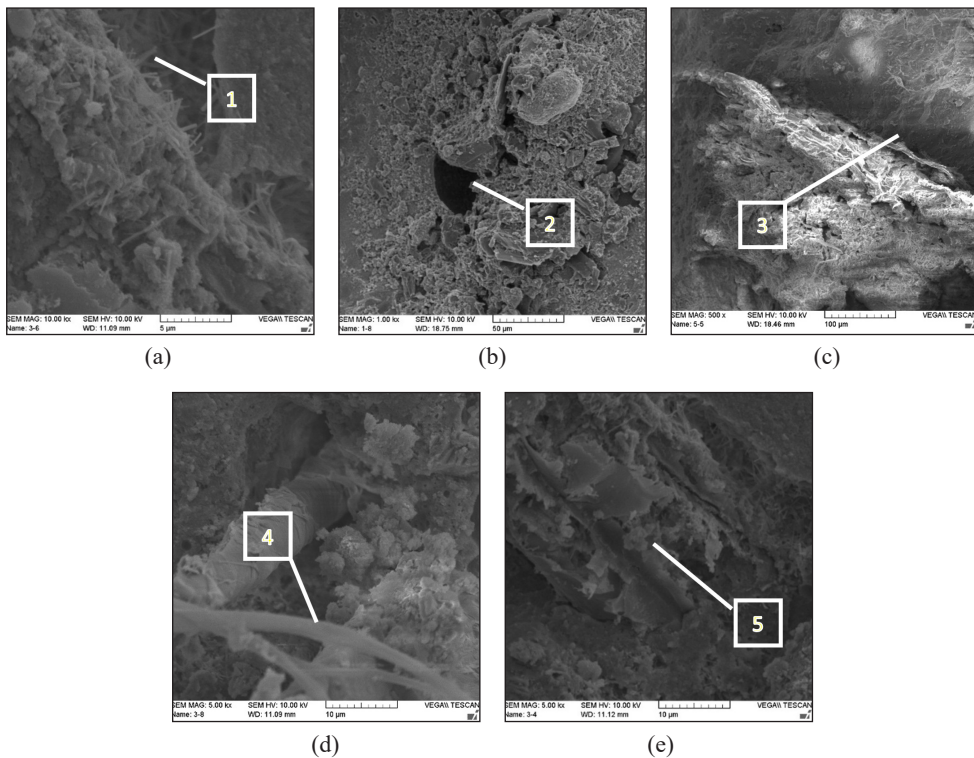


Figure 11. SEM images of fractured surface at 28-day for specimens: (a) control; (b) coated with 2% TiO₂; (c) coated with 2% MgO; (d) coated with 2% ZnO and (e) coated with 2% ZrO₂

the morphology. Therefore, the coated cement matrix is denser than control mix that can enhance the interfacial transition zone, and certainly promote the strength and density of the end composite. The results are in accordance with prior work done by Du et al. (2019).

CONCLUSION

Based on the analysis of data compiled throughout this study, these conclusions are summarized as follows:

1. Higher hardness was observed for coated specimens that directly related to their higher dosage in the coating film. 2% ZrO₂ yielded 29 % the superior hardness whilst, ZnO specimens yielded only 13 % higher hardness as compared to control.
2. The abrasion rate reduced after coating by nano particles, as compared to control. Higher doses of 2% for all types were very beneficial to long term abrasion rate, thereby decreasing the abrasion rate of the final composite.
3. All coated specimens were heavier than the control, especially for 2% ZrO₂ nano particles which had the highest density of 2.262 g/cm³.
4. All coated specimens showed lower porosity, especially MgO at 2% by weight of cement due to both the accelerated pozzolanic activity between nano oxides and calcium hydroxide and to the filling effect by the very tiny particles leading to the reduction in the number and size of pores.
5. 2% MgO coating had the highest water absorption (45%) as compared to control. Meanwhile, the water absorption for 2% TiO₂, ZnO and ZrO₂ were 34, 37 and 31% respectively.
6. It was evident from XRD patterns that the CH intensity decreased with the coated ZrO₂, TiO₂, MgO, and ZnO nanoparticles.
7. The surface black holes were completely filled with nano particles and/or extra CSH from the pozzolanic activity and there was no indication for CH crystals in the morphology except for ZnO.
8. ZrO₂ was the best nano material that improve the performance of cement-based composites. For economic consideration, 1.5 % was the preferable dose that maximize the performance of cement-based composites. Over this dose (2%) a low improvement was noticed.

ACKNOWLEDGEMENT

The authors thank the Kerbala Technical Institute, Al-Furat Al-Awsat Technical University for helping in the preliminary examination of raw materials.

REFERENCES

- Ahmed, H. E. D., Sabrah, B. A. E. G., Mohamed, S. A. E. A., & Mostafa, N. M. (2017). Chemical and engineering properties of blended cement containing micro-and nano-silica. *American Journal of Chemical Engineering*, 5(5), 111-121. doi: 10.11648/j.ajche.20170505.13
- Ali, I. M., Nasr, M. S., & Naje, A. S. (2020). Enhancement of cured cement using environmental waste: particleboards incorporating nano slag. *Open Engineering*, 10(1), 273-281. doi: <https://doi.org/10.1515/eng-2020-0031>
- Aperador, W., Delgado, A., & Bautista-uiz, J. (2016). Effect of durability and chloride ion permeability in ternary cementitious concrete with additions of fly ash and blast furnace slag. *International Journal of Electrochemical Science*, 11, 2297-2305.
- Birgisson, B., Mukhopadhyay, A. K., Geary, G., Khan, M., & Sobolev, K. (2012). *Nanotechnology in concrete materials: A synopsis*. Washington, USA: Transportation Research Board. doi: 10.17226/22672
- Camiletti, J., Soliman, A. M., & Nehdi, M. L. (2013). Effect of nano-calcium carbonate on early-age properties of ultra-high-performance concrete. *Magazine of Concrete Research*, 65(5), 297-307. doi: <https://doi.org/10.1680/mac.12.00015>
- de la Cruz Barroso, J. C., del Campo, J. M., & Aranguren, D. C. (2015). Comparative study on porosity and permeability of conventional concrete and concrete with variable proportions of natural zeolite additions. *Revista de la Construcción*, 14(3), 72-78.
- Du, S., Wu, J., AlShareedah, O., & Shi, X. (2019). Nanotechnology in cement-based materials: A review of durability, modeling, and advanced characterization. *Nanomaterials*, 9(9), 1-29. doi: <https://doi.org/10.3390/nano9091213>
- Elia, H. N., Ghosh, A., Akhnoukh, A. K., & Nima, Z. A. (2018). Using nano- and micro-titanium dioxide (TiO₂) in concrete to reduce air pollution. *Journal of Nano Medicine and Nanotechnology*, 9(3), 1-5. doi: 10.4172/2157-7439.1000505
- Glenn, J. (2013). *Nanotechnology in concrete: Critical review and statistical analysis* (MSc Thesis). Florida Atlantic University, Boca Raton, Florida.
- Ibrahim, S. I. (2016). *Studying the effect of nano additives materials in cement coating for building applications* (PhD Thesis). University of Technology, Baghdad, Iraq.
- Khitab, A., & Arshad, M.T. (2014). Nano construction materials: Review. *Reviews on Advanced Materials Science*, 38(2), 181-189.
- Ltifi, M., Guefrech A., Mounanga P., & Khelidj A. (2011). Experimental study of the effect of addition of nano-silica on the behavior of cement mortars. *Procedia Engineering*, 10, 900-905. doi: <https://doi.org/10.1016/j.proeng.2011.04.148>
- Mehta, P. K., & Monteiro, P. J. (2006). *Concrete microstructure, properties, and materials* (3rd Ed.). New York, USA: McGraw-Hill.
- Mendes, T. M., Hotza, D., & Repette, W. L. (2015). Nanoparticles in cement based materials: A review. *Revision Advance Materials Science*, 40(1), 89-96.

- Othman, F. M., Hameed, A. A., & Ibrahim, S. I. (2016). Studying the effect of nano additives and coating on some properties of cement mortar mixes. *Engineering and Technology Journal*, 34(3 Part (A) Engineering), 553-566.
- Pellegrini-Cervantes, M. J., Almeraya-Calderon, F., Borunda-Terrazas, A., Bautista-Margulis, R. G., Chacón-Nava, J. G., Fajardo-San-Miguel, G., ... & Martinez-Villafañe, A. (2013). Corrosion resistance, porosity and strength of blended portland cement mortar containing rice husk ash and nano-SiO₂. *International Journal of Electrochemical Science*, 8(1), 10697-10710.
- Quraishi, M. A., Nayak, D. K., Kumar, R., & Kumar, V. (2017). Corrosion of reinforced steel in concrete and its control: An overview. *Journal of Steel Structures and Construction*, 3(1), 1-6.
- Rezania M., Panahandeh M., Razavi S. M. J., & Berto F. (2019). Experimental study of the simultaneous effect of nano-silica and nano-carbon black on permeability and mechanical properties of the concrete. *Theoretical and Applied Fracture Mechanics*, 104, 1-10. doi: <https://doi.org/10.1016/j.tafmec.2019.102391>
- Vera, R., Apablaza, J., Carvajal, A. M., & Vera, E. (2013). Effect of surface coatings in the corrosion of reinforced concrete in acid environments. *International Journal of Electrochemical Science*, 8, 11832-11846.
- Zhang, A., Ge Y., Yang, W. C., Cai, X. P., & Du, Y. B. (2019a). Comparative study on the effects of nano-SiO₂, nano-Fe₂O₃ and nano-NiO on hydration and microscopic properties of white cement. *Construction and Building Materials*, 228, 1-11. doi: <https://doi.org/10.1016/j.conbuildmat.2019.116767>
- Zhang, S., Qiao, W. G., Chen, P. C., & Xi, K. (2019b). Rheological and mechanical properties of microfine-cement-based grouts mixed with microfine fly ash, colloidal nanosilica and superplasticizer. *Construction and Building Materials*, 212, 10-18. doi: <https://doi.org/10.1016/j.conbuildmat.2019.03.314>
- Zhuang, C., & Chen, Y. (2020). The effect of nano-SiO₂ on concrete properties: A review. *Nanotechnology Review*, 8, 562-572. doi: <https://doi.org/10.1515/ntrev-2019-0050>

Quantifying Suspended Sediment using Acoustic Doppler Current Profiler in Tidung Island Seawaters

Henry Munandar Manik^{1*} and Randi Firdaus²

¹*Division of Ocean Acoustics and Instrumentation, Department of Marine Science and Technology, Faculty of Fisheries and Marine Sciences, Bogor Agricultural University (IPB University), Kampus IPB Dramaga, Bogor 16680 Indonesia*

²*Marine Technology Study Program, IPB University Graduate School, Kampus IPB Dramaga Bogor Indonesia, and Meteorological, Climatological, and Geophysical Agency, Indonesia*

ABSTRACT

Tidung Island, located near Jakarta Bay, is a tourism and conservation area. It is necessary to keep these seawaters unpolluted. To calculate the level of pollution, it is necessary to know the sediment concentration. Quantifying concentration suspended sediment is important for knowledge of sediment transport. Researchers usually use water sample analysis and optical method for quantifying suspended sediment in seawater. Less accuracies of these methods are due to under sample of seawater and the existence of biological fouling. One promising method to measure concentration of suspended sediment is using Acoustic Doppler Current Profiler (ADCP). ADCP is usually used by oceanographer and hydrographer to measure ocean current. In this research, ADCP with 300 kHz operating frequency was used effectively to measure suspended sediment concentration (SSC) and ocean current simultaneously. The echo intensity received from suspended sediment was computed using sonar equations to quantify SSC. The empirical equation between echo intensity and SSC was found. The SSC value obtained by ADCP was also compared with *in situ* measurement. The result showed that

quantified SSC value obtained by ADCP was nearly equal with SSC obtained from *in situ* measurement with coefficient correlation of 0.98. The high concentration ranged from 55 mg/L to 80 mg/L at the surface layer to a depth 12 m, moderate concentration ranged from 45 mg/L to 55 mg/L at a depth 12 m to 40 m, and low concentration less than 45 mg/L at a depth greater than 40 m. The distribution of SSC

ARTICLE INFO

Article history:

Received: 24 May 2020

Accepted: 05 October 2020

Published: 22 January 2021

DOI: <https://doi.org/10.47836/pjst.29.1.21>

E-mail addresses:

henrymanik@apps.ipb.ac.id (Henry Munandar Manik)

randi_firdaus@apps.ipb.ac.id (Randi Firdaus)

* Corresponding author

was correlated with ocean current condition. In small currents, suspended solids will settle faster so that the concentration in the water column will decrease. Conversely, if the velocity is high, suspended solids will continue to float carried by the current in the water column so that the concentration is high.

Keywords: Acoustic Doppler Current Profiler, suspended sediment concentration, Tidung Island

INTRODUCTION

Improvement of sediment transport monitoring is a crucial for coastal management. Knowledge of sediment concentration provides a better understanding of marine environment. Degradation of marine fisheries resources can damage coastal ecosystems such as fish, coral reefs, and another marine biota. Therefore, the study to quantify sediment concentration is vital to detecting and monitoring sediment in the ocean. The decrease of photosynthesis is caused by the high concentration of suspended sediment.

Suspended sediment is one of marine pollution indicator that is very important in the aquatic environment. In coral reef ecosystems in coastal areas, the life of underwater biota is strongly influenced by the concentration of suspended sediments. But until now, the measurement of suspended sediment concentrations is still constrained by conventional methods, which cannot be measured continuously. The Acoustic Doppler Current Profiler (ADCP) device, which was originally designed to measure the profile of ocean current speed and direction, can be used to measure suspended sediment concentrations simultaneously by converting echo intensity from sediment using Sonar equation.

Determination of suspended sediment concentrations is of fundamental importance in studying sediment transport (American Public Health Association, 2012). Measurement of suspended sediment concentration can be conducted in two ways, namely by gravimetry and acoustic methods. The conventional method using the gravimetric method in the laboratory has several disadvantages, namely requiring many water samples at each point and depth of the observation station, therefore it is not possible to gather time series data. Other reason is this method takes time to conduct and thus needs more budget (Medwin & Clay, 1997; Ainsle & McColm, 1998; Deines, 1999; Downing, 1996; Poerbandono & Mayerle, 2004; Ghaffari et al., 2011; Poerbandono & Suprijo, 2013). Therefore, ADCP instruments are used as an alternative since it can produce continuous suspended sediment concentration, (SSC) data with a long-time scale and broad distribution (Manik et al., 2020).

State of the Art

The current study demonstrates the application of sonar equation to quantify echo intensity of ADCP instrument and measure the suspended sediment concentration in Tidung Island seawaters, Indonesia. ADCP is usually to measure ocean current, however in this research

measurement of suspended sediment concentration and ocean current was simultaneously conducted.

The hydroacoustic technology utilizes sound waves for various purposes of underwater detection. The ADCP device is able to detect and quantify underwater objects accurately by emitting sound to the target then the target reflects back sound waves until they are received by acoustic devices (Holdaway et al., 1999; Gartner & Cheng, 2001; Gruber et al., 2016). Through acoustic signals obtained, the determination of spatial and temporal suspended sediment concentrations can be better obtained when compared to conventional methods.

This research is significant to monitor the condition of marine waters in the ecosystem of Jakarta Bay from the threat of suspended sediment pollution. The objective was to quantify real time and accurate of the acoustic intensity obtained from ADCP instrument to be used in determining the suspended sediments concentration (SSC).

METHODS

The procedure for collecting field data included data collection using ADCP and water sampling. Data processing carried out the conversion of data in the form of echo intensity from ADCP to the concentration of suspended sediments. In laboratory measurements, gravimetric analysis was compared to acoustic method for suspended sediment concentrations measurements. The value of suspended sediment concentration obtained from the results of analysis in the laboratory was in absolute value, so the level of confidence was very high.

Figure 1 shows data acquisition using one ADCP moves with downward-looking sound waves. Data acquisition was done with two lines that represent the characteristics of the waters of Tidung Island. Determination of the data collection transect line is based on the location in the field, namely the water near the port and in a location far from the port.

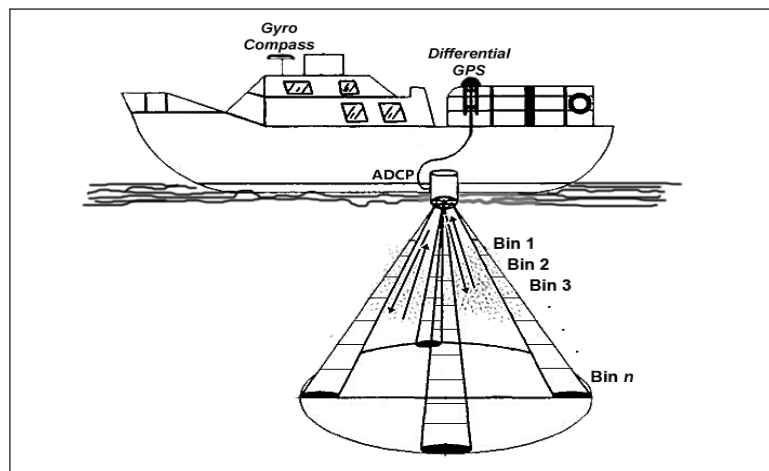


Figure 1. The method of data acquisition using the ADCP in a downward-looking method

Water sampling was carried out during the high tide and low tide period with the aim of comparing the measurement results from the ADCP.

The ADCP instrument was installed at 0.65 meters below the sea surface, the maximum depth of detection was 50 meters, and the thickness of the bin and hose data was 1 meter and 1 second. ADCP are designed for motion is relatively slow and unaffected by ocean waves. A flux-gate compass and inclinometers can measure pitch, roll, and heading effectively.

Echo intensity was derived from ADCP calibrated with the laboratory measurement and analyzed using a linear regression. The results of the analysis produce slope and intercept values could be used in the process of converting echo intensity (EI) values to SSC using Valeport Datalog X2 software to produce spreadsheets, then plotted in MATLAB.

In this research we also used a sensor to measure turbidity value of seawater and correlated it with SSC value.

Sonar Equation for ADCP

ADCP instrument transmits the acoustic signal into water column and hits the underwater object such as suspended sediment (Simmonds & MacLennan, 2005). The acoustic signal from suspended sediment was backscattered to the ADCP transducer. The value of acoustic backscatter was processed to quantify suspended sediment using Sonar Equation. The foundational sonar equation between *SSC* and the relative backscatter (*RB*) can be expressed as in decibel (dB) (Equation 1) (Gartner, 2004):

$$SSC = 10^{(A + B \cdot RB)} \text{ or } 10 \log (SSC) = A + B \cdot (RB) \quad (1)$$

where *A* and *B* are empirical parameters derived from known *SSC* and *RB* data pairs.

The relative backscatter is the measured acoustic backscatter corrected for transmission losses in units of dB. Acoustic waves in the water will experience sound propagation in the form of geometric attenuation and shrinkage due to the presence of suspended sediments in the water column.

Relating *RB* and *SSC* can be expressed as Equation 2:

$$RB = RL + 2 TL \quad (2)$$

where *RL* is the reverberation level and *2.TL* is the two way transmission loss. The *RL* is given as Equation 3:

$$RL = SL - 2 TL + TS \quad (3)$$

where SL is source level and TS is target strength of suspended sediment. Here TS depends on acoustic frequency, particle size and shape, and rigidity. ADCP instrument measures the RL using Equation 4:

$$RL = K_c (EI - E_r) \quad (4)$$

where K_c is the received signal strength indicator scale factor, EI is the echo strength (counts), E_r is the reference level for echo intensity (counts). K_c can be estimated using Equation 5:

$$K_c = \frac{127.3}{T + 273} \quad (5)$$

where T is the real time temperature of the amplification circuits in °C. Measuring Transmission Loss (TL) depends on spherical spreading of the beam and absorption of sound, and is given by Equation 6:

$$TL = 10 \Psi \log(R) + \alpha R \quad (6)$$

where Ψ is a near field correction factor, R is the slant range from transducer head to measured bin (m), α is absorption coefficient of sea water and attenuation from suspended sediment. (Francois & Garrison, 1982a; Francois & Garrison, 1982b; Sassi et al., 2012). The correction factor for near field spreading loss is (Equation 7):

$$\psi = \frac{1 + 1.35 Z + (2.5 Z)^{3.2}}{[1.35 Z + (2.5 Z)^{3.2}]} \quad (7)$$

where $Z = R / R_{critical}$ and $R_{critical} = \pi a^2 / \lambda$, a is the radius of transducer (cm) and λ is acoustic wavelength. Sound absorption in sea water is calculated by Equation 8:

$$\alpha_w = 8.687 \frac{3.38 \cdot 10^{-6} \cdot f^2}{f_r} \quad (8)$$

where f is operating frequency (Hz) of ADCP and f_r , the relaxation frequency (Hz) depends on sea water temperature (T) as in Equation 9:

$$f_r = 21,9 \times 10^{(6 - \frac{1520}{273+T})} \quad (9)$$

The attenuation due to absorption of sediment (α_s) is calculated in this research by Equation 10:

$$\alpha_s = -\frac{1}{2} \frac{d}{dr} (W) \quad (10)$$

where W is water corrected backscatter.

Final equation of SSC is expressed by Equation 11:

$$SSC = 10^A + B (K_c(EI - E_r) + 2(10 \log(R) + \alpha R)) \quad (11)$$

where echo intensity (EI), slant range (R) and reference level (E_r) can be measured with ADCP, while K_c and α are estimated.

The data used are scattered backwater water intensity data from four beams of ADCP type RDI Workhouse 307.2 kHz on lines 1 and 2 on the waters around Tidung Island showed in Figure 2. Line 1 is in the north of Tidung Island while line 2 is in the South of Tidung Island.

For gravimetric method, one liter of seawater was sampled and analyzed in the laboratory. A 500 ml of sub water sample was used and then processed with vacuum-filtered with a 1.5 μm particle retention. The filters were dried for 24 hours at 100 °C, reweighed to measure *in situ* concentration of suspended sediment.

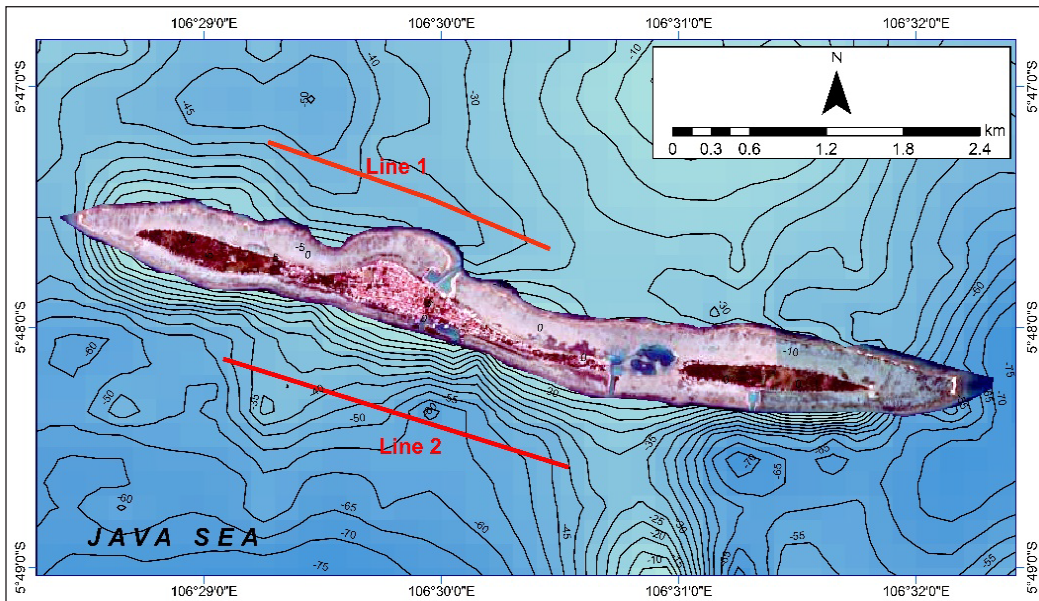


Figure 2. Analyzed track location (— Lines 1 and 2 are for collecting ADCP data). Sea water depth ranged from 5 to 60 m

RESULTS AND DISCUSSIONS

Figures 3 and 4 show the linear relationship between the scattering value of each beam with other beams. Figures 3 and 4 illustrate the echo intensity detection in Count unit resulted

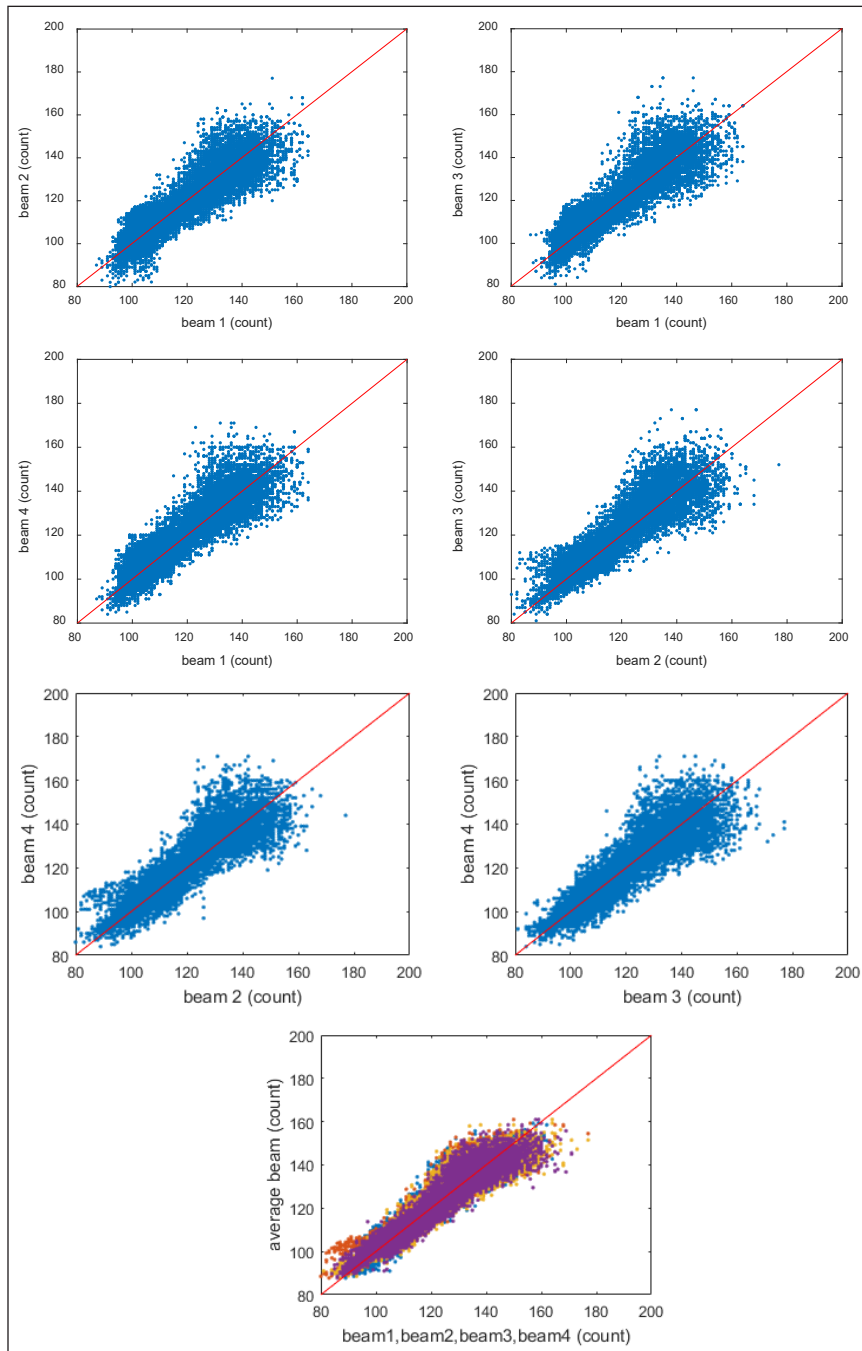


Figure 3. Comparison of backscatter values in line 1

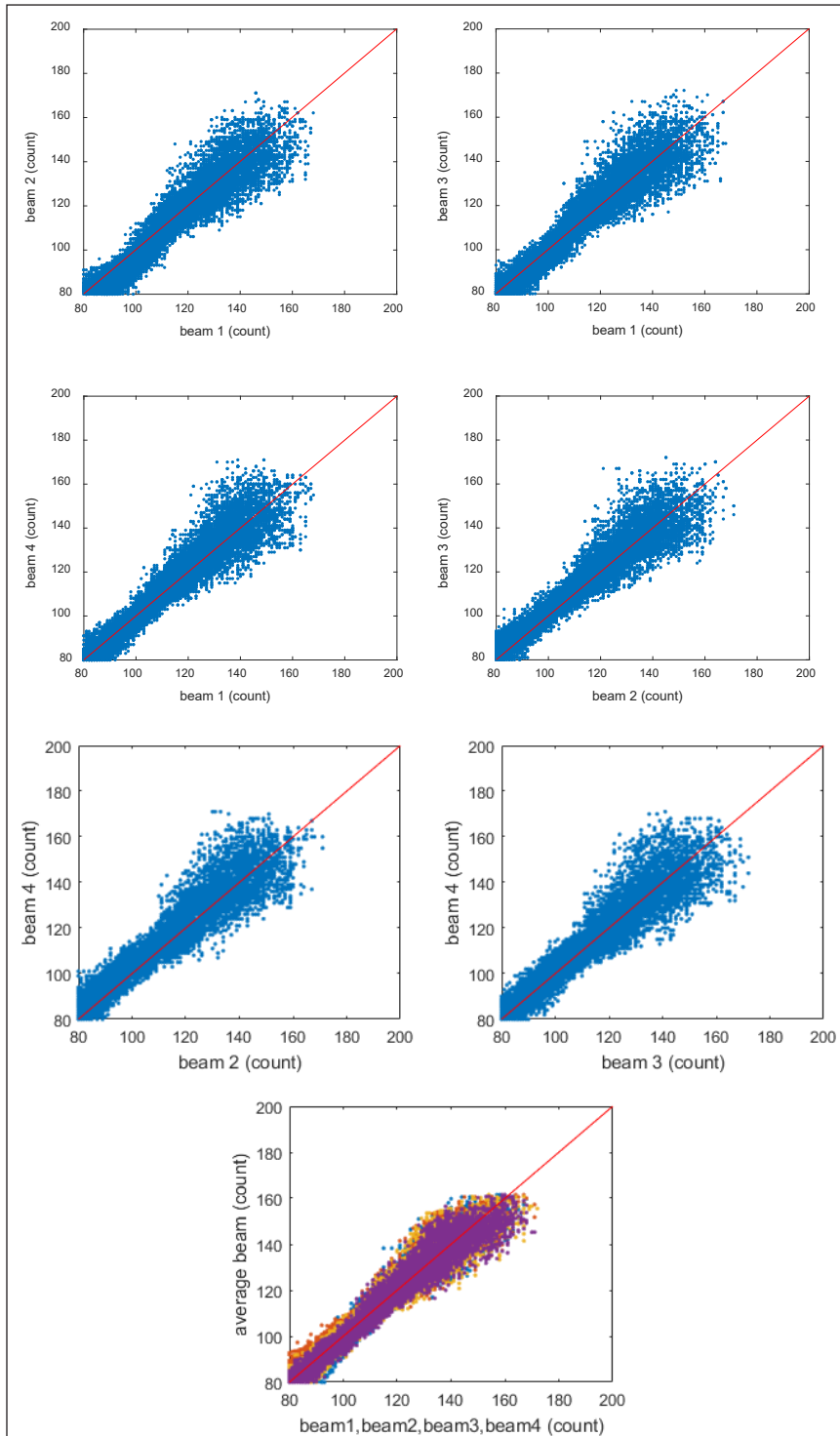


Figure 4. Comparison of backscatter values between beams in line 2

from the four beams of ADCP and comparison this echo for each beam from the ADCP transducer. Finally, the average signal of each beam was combined to further process of echo intensity to measure suspended sediment concentration.

The screening of data was performed on ADCP data recorded in each beam. A beam to beam comparison of the echo intensity value was conducted for all four ADCP beams. Figures 3 and 4 show the scatterplot of echo intensity (blue dot colour) for each beam and for combined ADCP beam (red dot colour). Echo intensity data were recorded in beam coordinated and the data quality were retained for ensemble of each beam. The applications of the comparison ADCP beams is to provide careful application of the instrument calibration and particular attention to the measurement of echo intensity of the beam-by-beam.

Figure 5 shows the curve of echo intensity against suspended sediment calibration obtained from ADCP with a high correlation coefficient (r) of 0.96 in Equation 12. Figure 6 shows the SSC estimated by ADCP compare to direct measurement of SSC using gravimetric analysis with $r = 0.98$ in Equation 13. Figure 7 shows the high relationship between turbidity (NTU) and SSC (mg/L) with $r = 0.91$ in Equation 14:

$$10 \log_{10} (SSC) = 0.2843 EI \text{ (dB)} - 46.66 \quad (12)$$

$$SSC_{est} = 10^{1.0607 RB - 2.32} \quad (13)$$

$$SSC = 1.8395 \text{ Turbidity}^{0.901} \quad (14)$$

The results of the conversion of counts into relative backscatter (relative dB) in line 1 are presented in Figures 8 and 9. Conversions were carried out by a scale factor of 0.43

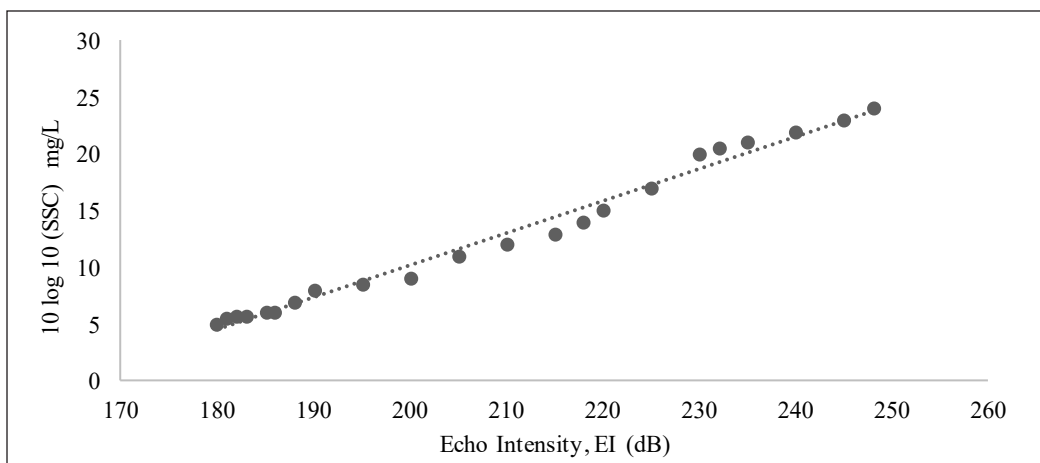


Figure 5. Echo intensity against direct sample of suspended sediment concentration (SSC)

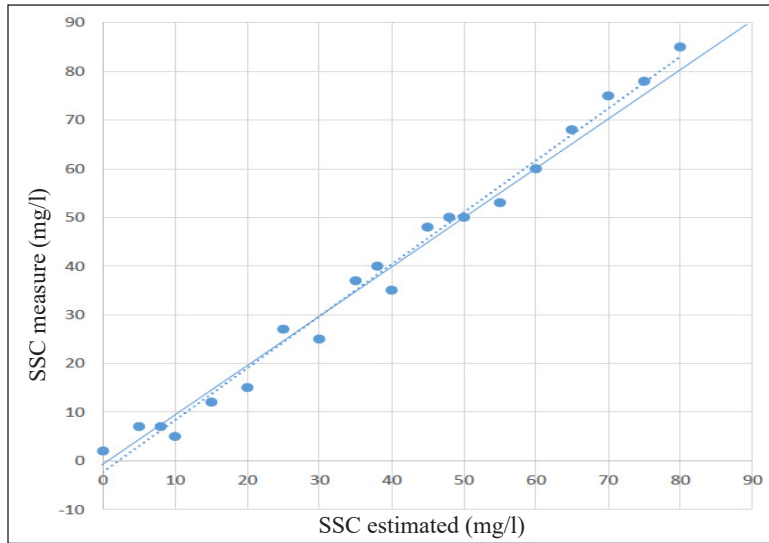


Figure 6. Validation of the estimated SSC using ADCP and measured SSC using gravimetric analysis

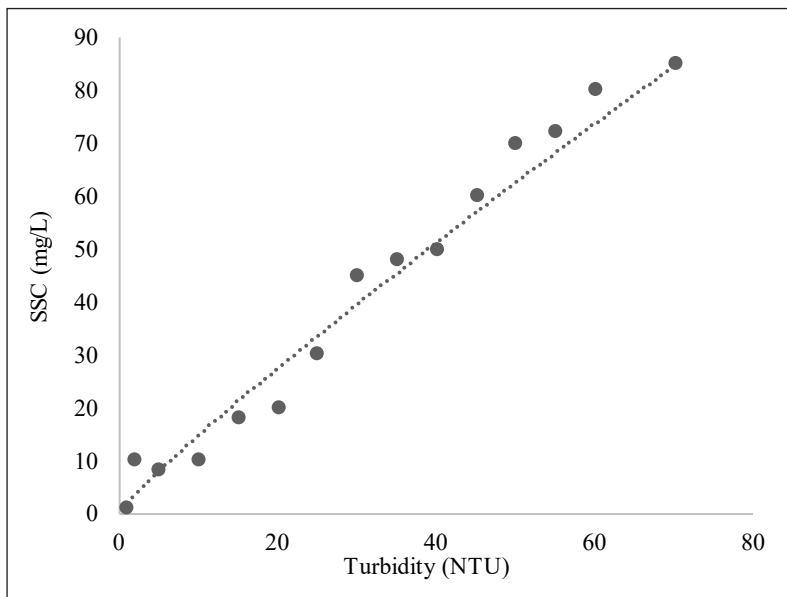
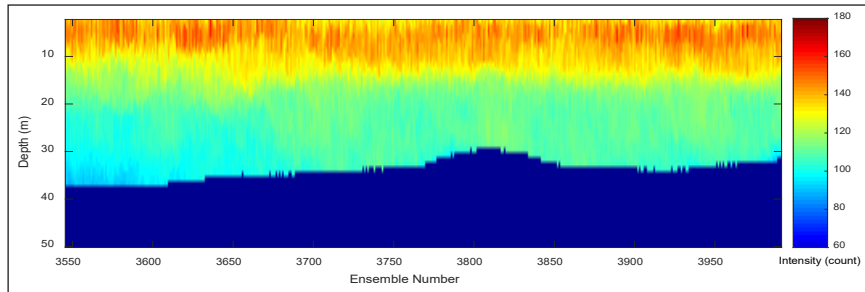


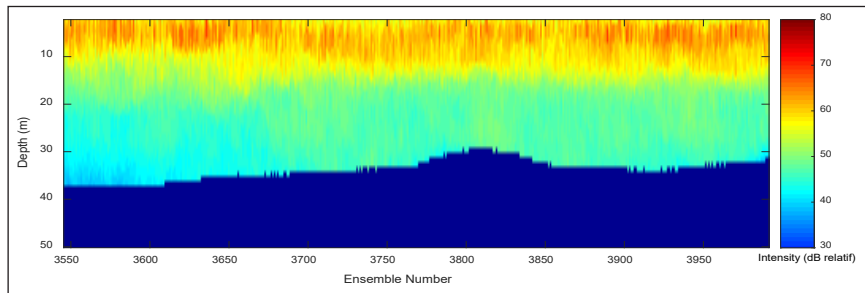
Figure 7. Suspended sediment calibration for a turbidity probe

for every 1 count. The intensity value (in count) ranged from 80 to 180 in line 1 where the high value was at the surface while the low value was near the bottom of the water. The intensity value in line 2 ranged from 60 in deep waters to 180 counts on the surface. Overall, the backscatter pattern in lines 1 and 2 had similarities, in the surface layer to a depth of 10 m was the layer with the highest intensity and the intensity decreased with increasing depth.

Suspended Sediment using Acoustic Doppler Current Profiler

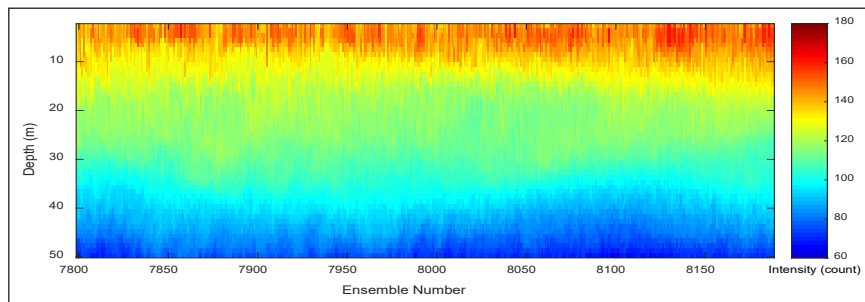


(a)

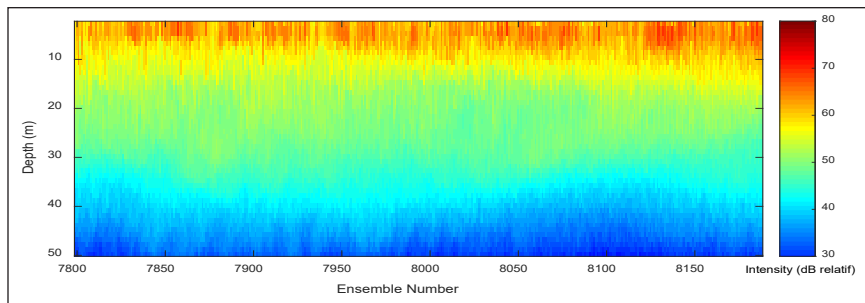


(b)

Figure 8. Example of the results of conversion of backscatter values in units of count (a) to relative dB units (b) using a scale factor of 0.43 in line 1



(a)



(b)

Figure 9. Example of the results of the conversion of backscatter values in units of count (a) into relative dB units (b) using a scale factor of 0.43 in line 2

The vertical profile of SSC in lines 1 and 2 of Tidung Island waters was obtained after the backscatter value (relative dB) (Figures 8 and 9) was changed to SSC (mg / L) concentration using Equation 10. The SSC concentration for each beam and the average on line 2 are presented in Figure 10 for line 1 and Figure 11 for line 2.

High SSC (> 55 mg / L) were in the surface layer to a depth of 12 m. At a depth of 15 m to the bottom of the water the SSC ranged from 40 mg / L to 50 mg / L. The area to the west (left) had a lower concentration than the east at the same depth.

In contrast to line 1, SSC on line 2 showed a variation between high, moderate, and low SSC. This is because the depth of the water on line 2 was quite deep (more than 50 m, but because the detection distance was only set to a maximum at a depth of 50 m, so that the bottom of the water was not detected). High concentrations (55 mg / L to 80 mg /

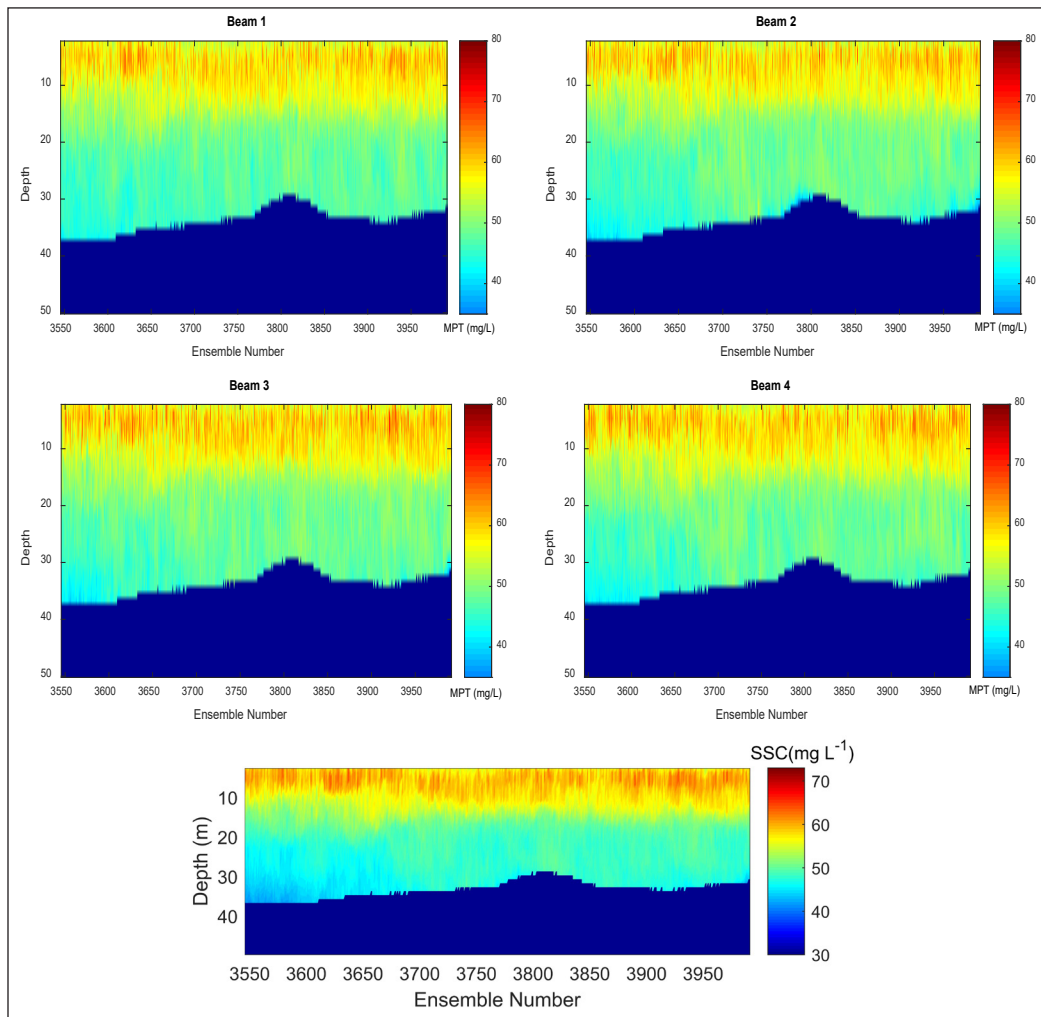


Figure 10. Distribution of SSC (mg / L) on each beam and the average in line 1.

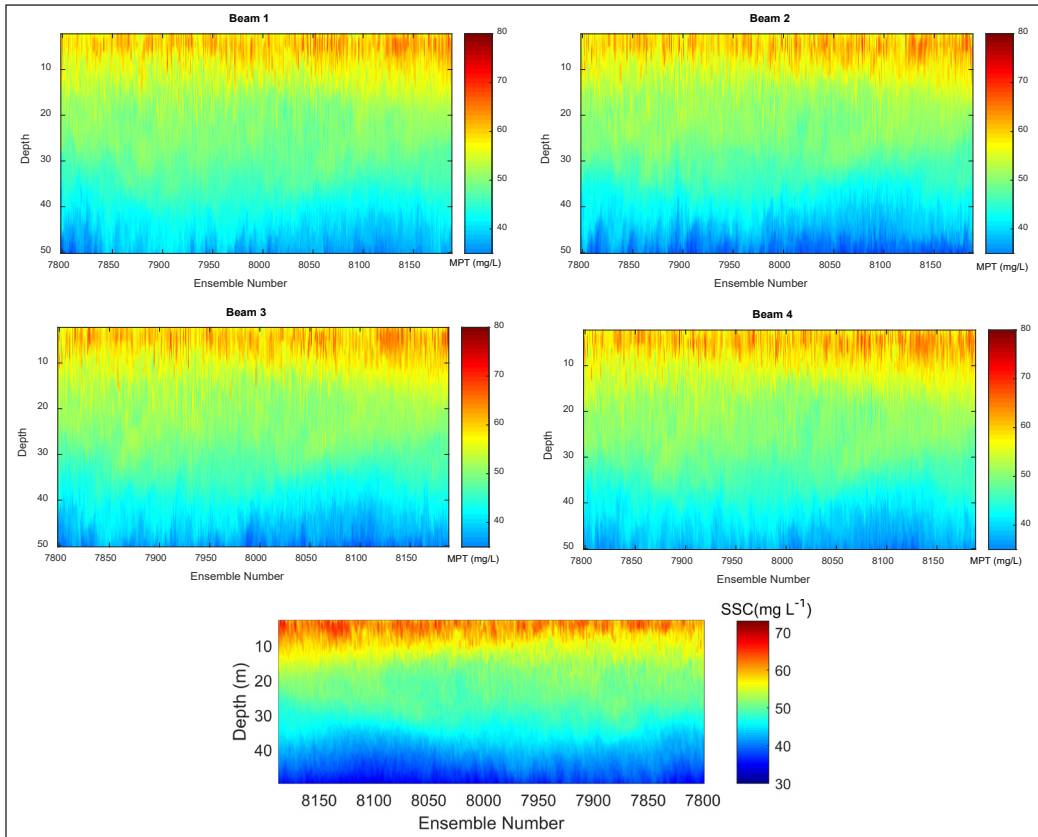


Figure 11. Distribution of SSC (mg / L) on each beam and the average in line 2

L) were found in the surface layer to a depth of 12 m, while moderate concentrations (55 mg / L to 45 mg / L) were at a depth of 12 m to a depth of 32 m, then low concentrations (<45 mg / L) at depths greater than 40 m. Near the sea bottom, the SSC had a wave-like contour. On the surface, the SSC in the western part was higher than the eastern part, contrasting with the SSC near the sea bottom where high concentrations were in the east. This indicates that there are different factors that affect the concentration of SSC on the surface and in deeper waters. The existence of suspended sediment in the surface bottom is coarse sediment. This is supported by the result of previous research (Li et al., 2005).

In general, the concentration of SSC on lines 1 and 2 had the same pattern where high concentrations were on the surface. This result is contrary to the results of the previous study in the Lembeh Strait which showed high concentration was located near the bottom of the water (Dwinovantyo et al., 2017). This is probably due to differences in oceanographic conditions in both waters. In addition, the concentration of SSC on line 2 (south of Tidung Island) was higher than that of line 1 (north of Tidung Island). This could be seen from the SSC of the surface layer to a depth of 10 m. This is probably because in the southern

part there is more have an anthropogenic activity because there are main ports and the construction of physical buildings. In addition, the southern part is also closer to Jakarta Bay which has a higher turbidity.

From this result, we had succeeded in converting echo intensity to suspended sediment concentration and validated its results with *in situ* measurement by using gravimetric method and turbidity sensor. By using Rayleigh scattering theory (Thorne et al., 1991), we estimated the particle size of detected suspended sediment was less than 1600 μm .

Relationship between SSC and Ocean Current

Extracting ADCP data resulted in the component of water current velocity and direction. The component data of the current velocity in the direction of x (u) and the velocity component in the direction y (v) are further processed to obtain the magnitude and direction of the current. The current magnitude is calculated by Equation 15 (Urick, 1996):

$$V = \sqrt{u^2 + v^2} \quad (15)$$

while the direction of the north direction as 0° is calculated through Equation 16:

$$Direction (^\circ) = 270^\circ - a \tan^2 (v, u) \quad (16)$$

where:

$$atan2 (v, u) = \begin{cases} \arctan \left(\frac{v}{u} \right) & \text{if } u > 0; \\ \arctan \left(\frac{v}{u} \right) + \pi & \text{if } u < 0 \text{ and } v \geq 0; \\ \arctan \left(\frac{v}{u} \right) - \pi & \text{if } u < 0 \text{ and } v < 0; \\ + \frac{\pi}{2} & \text{if } u = 0 \text{ and } v > 0; \\ - \frac{\pi}{2} & \text{if } u = 0 \text{ and } v < 0; \\ \text{undefined} & \text{if } u = 0 \text{ and } v = 0 \end{cases}$$

with π stand for 180° .

Because the current velocity and the concentration of suspended solids vary with depth, a correlation is performed for the average current data and suspended solids concentration (SSC) for all pinged data depths. The current relationship with SSC is expressed by Pearson linear correlation formulated as Equation 17:

$$r = \frac{\sum_{i=1}^n (X_i - \bar{X})(Y_i - \bar{Y})}{\{\sum_{i=1}^n (X_i - \bar{X})^2 \sum_{i=1}^n (Y_i - \bar{Y})^2\}} \quad (17)$$

where $\bar{X} = \sum_{i=1}^n \frac{X_i}{n}$ and $\bar{Y} = \sum_{i=1}^n \frac{Y_i}{n}$; n is the amount of data per depth, X is the current speed while Y is the SSC value.

A strong relationship if the value of r approaches 1 or -1, with a negative sign (-) stating the relationship between X and Y is the opposite. Correlations were also made for each individual ping on both lines.

Vertical distribution of suspended solids (SSC), velocity and direction of flow were shown in Figure 12. The current velocity on line 1 ranged between 0 and 0.9 m / s, but the dominant speed was 0.2 to 0.4 m / s (blue to light blue). Figure 12 also shows the current velocity variation as well as SSC variation. High speed on the surface to a depth

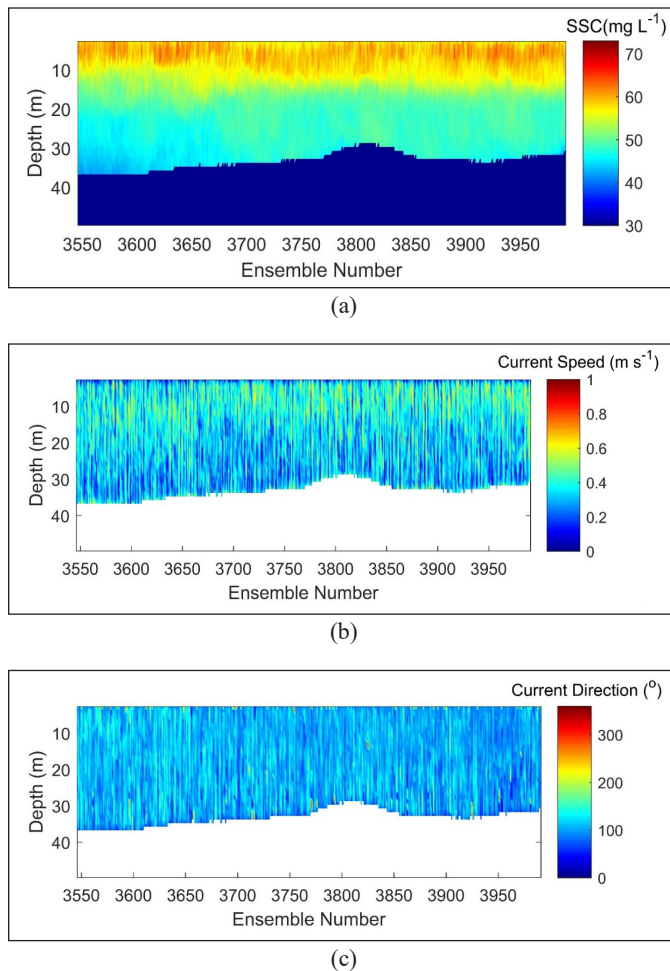


Figure 12. (a) Distribution of SSC; (b) current velocity; and (c) current direction on line 1

of 10 m while low speeds were near the bottom of the water. This is because one of the driving factors was the wind so that near the surface the influence of the wind in moving sea water was very large. The direction of the flow tended to be uniform on line 1 which was towards the east. This indicates that the current driving factor on the surface to the bottom is the same. These results are in good agreement with previous research (Gartner, 2004; Park & Lee, 2016).

The value of SSC in the eastern region had a higher value than the western region at the same depth. This is most likely caused by currents. The current direction was dominant to the east (Figure 13). This caused suspended solids to be carried eastward.

The value of current velocity on line 2 (which is in the south) was far greater than that of line 1 (which was in the north). This can be seen from the red color (the value of the high current velocity, > 0.6 m / s) on Figure 13 on line 2 which dominates more. On line 2 there was also a stratification of the current velocity. The highest ocean current velocity

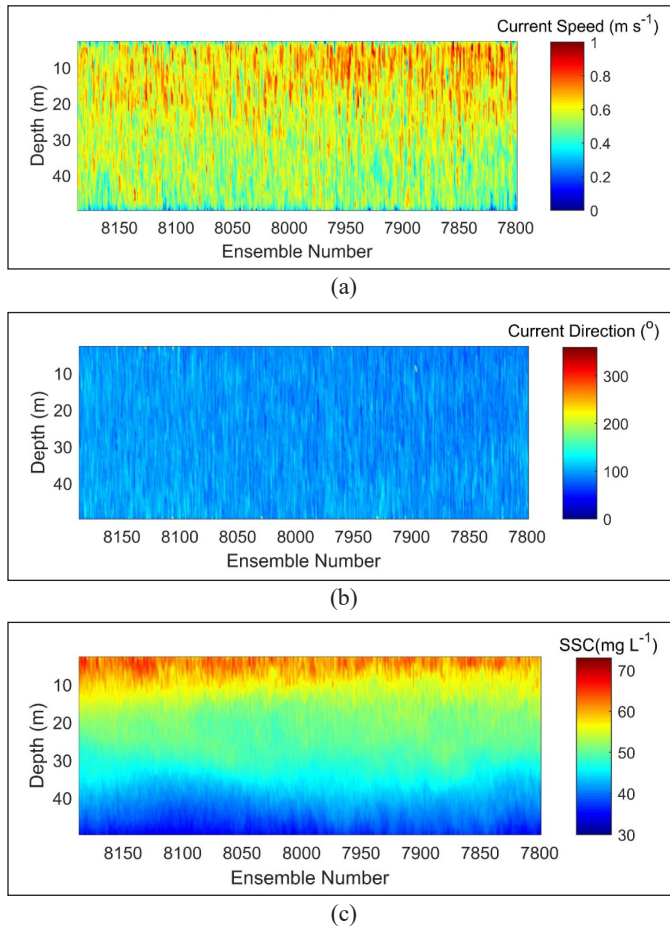


Figure 13. (a) Flow velocity distribution; (b) current direction; and (c) suspended sediment concentration

Suspended Sediment using Acoustic Doppler Current Profiler

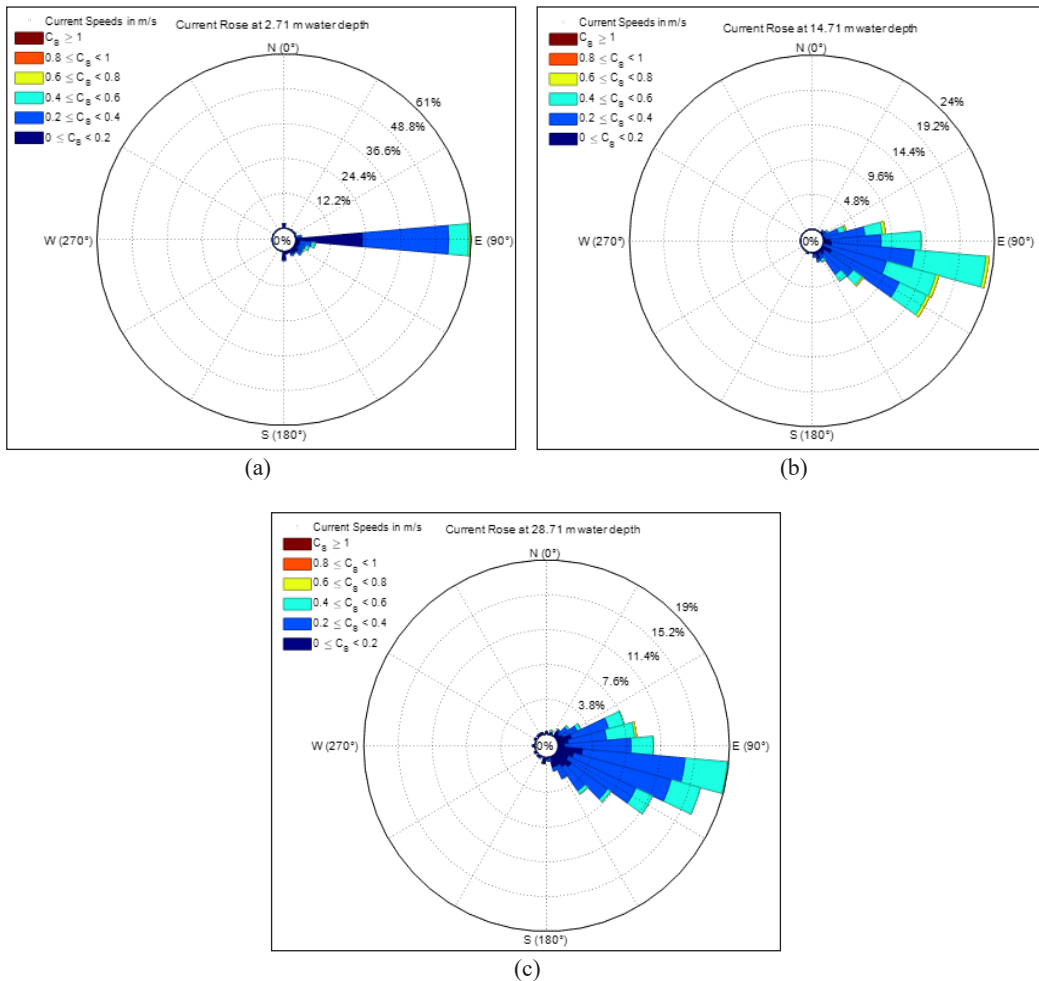


Figure 14. Current roses at: (a) 2.71 m; (b) 14.71 m; and (c) 28.71 m on line 1

value was at a depth of 10 m, the deeper, the lower the current speed. The direction of the dominant current on line 2 was also almost the same as line 1 which was eastward.

To see more clearly how the velocity and direction of the distribution were made current rose for both trajectories in three layers of depth were 2.71 m depth, 14.71 m and 28.71 m each of which represented the surface conditions, the middle layer and the deeper layers (Figures 14 and 15).

At a depth of 2.71 m, the dominant current direction went east with a speed of less than 0.6 m / s (Figure 14). The dominant speed at this depth was 0.2 to 0.4 m / s, while the frequency of speeds of 0.4 to 0.6 m / s was very small. At a depth of 14.71 m, the current speed was higher than at a depth of 2.71 m, where the speed of 0.4 to 0.6 m / s was high, even at this depth there was a current speed of 0.6 to 0.8 m / s. The direction of flow at a depth of 14.71 m was more varied with the direction from east to southeast. At a depth

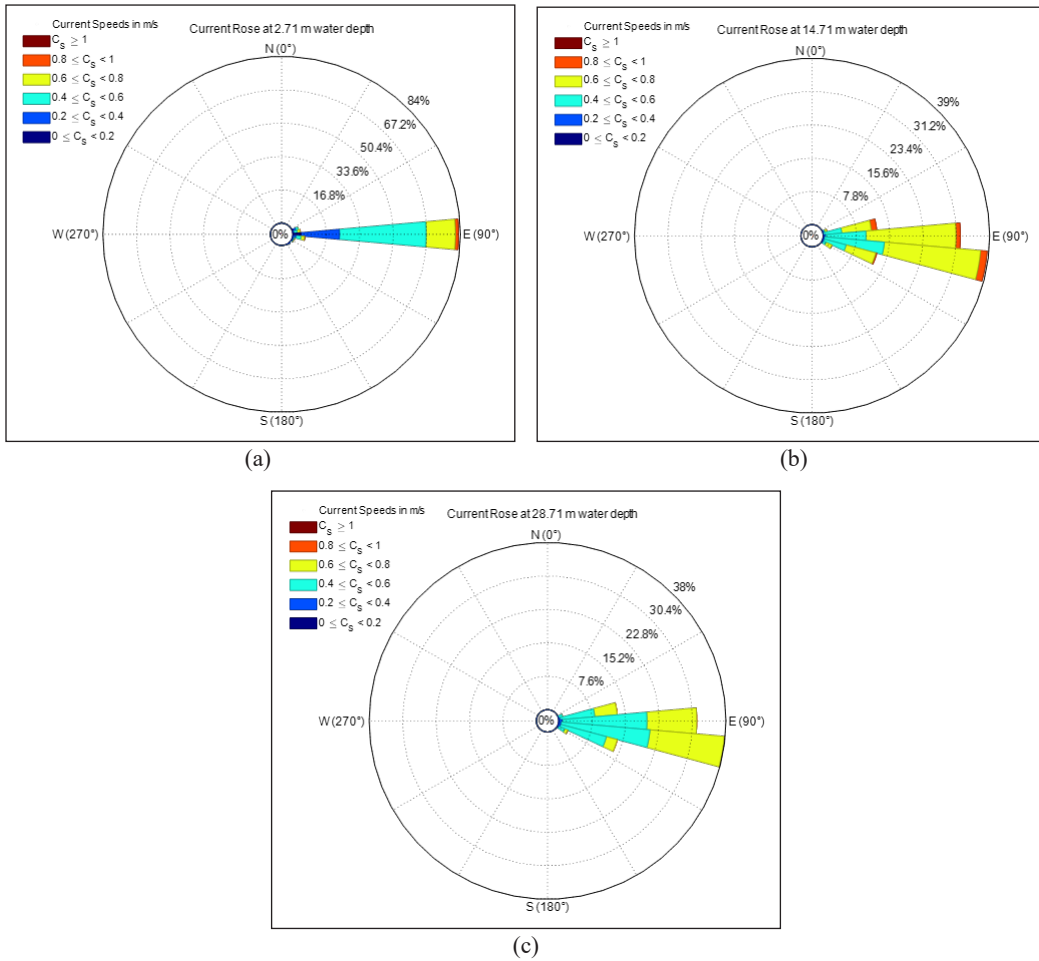
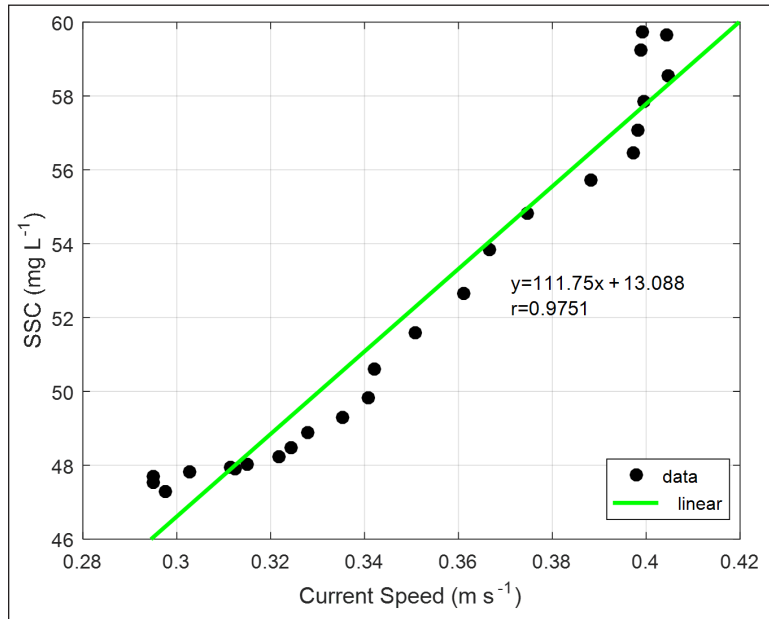


Figure 15. Current roses at: (a) 2.71 m; (b) 14.71 m; and (c) 28.71 m on line 2

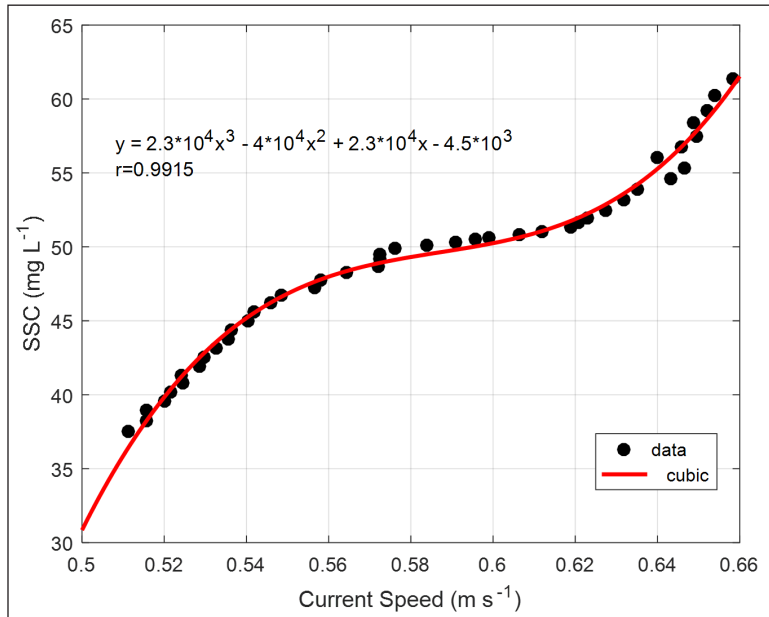
of 28.71 m, the current direction was almost the same as the depth of 14.71 m, but the speed was lower, and was dominated at speeds of 0.4 to 0.6 m / s. This pattern is due to the surface and near the bottom, the current will have a friction which will inhibit the flow of current. The SSC distribution was influenced by tidal current and this research was in good agreement with other researchers (Li et al., 2015).

The ocean current pattern on line 2 was similar to line 1, which was a low current velocity at a depth of 2.71 m and a maximum at a depth of 14.71 m. The current velocity on line 2 was higher for each layer compared to line 1. While the direction of the current was almost the same between line 16 and trajectory which was east to southeast (Figure 15).

The relationship between ocean current and SSC values is shown in Figure 16. This relationship is expressed by Pearson's correlation coefficient. Correlation was performed on the average data of current velocity and SSC.



(a)



(b)

Figure 16. Relationship between current velocity with the concentration of suspended solids on: (a) line 1; and (b) line 2

The average current velocity of each depth with the SSC value of each depth on lines 1 and 2 had a very high linear correlation of 0.97 for lines 1 (Figure 16a) and 0.99 for line 2 (Figure 16b). Based on Figure 16, the SSC value was high in a fast ocean current. This is related to the settling velocity of suspended particles which is influenced by the velocity of the fluid and the grain size of the particles. In small currents, suspended solids will settle faster so that the concentration in the water column will decrease. Conversely, if the velocity is high, suspended solids will continue to float carried by the current in the water column so that the concentration is high. This is confirmed from the vertical SSC profile and current. The effect of onshore SSC increased on the tidal pumping of sediment. This is also found by previous researchers (Wall et al., 2006; Yu et al., 2012). The highest SSC value on both lines was at a depth of 5 to 15 m, corresponding to the maximum current velocity value at that depth. In addition, the higher SSC value on the line 2 compared to the line 1 also confirms that it corresponds to the higher current velocity on line 2 higher than the line 2. This indicates that there is a difference in the transport mechanism or the size of the dissolved particles between the two lines. This research result is in agreement to previous research (Chen et al., 2006; Jiang et al., 2007; Moore et al., 2012; Rai & Kumar, 2015). They stated that ocean hydrodynamics and biological processes affected the distribution of suspended sediment. Sediment transport in coastal water is important because of the impact it has on water quality, turbidity, marine habitats (Tessier et al., 2008; Thorne et al., 2014). In the next research we suggest to measure the attenuation of suspended sediment for computing sonar equation to gain the SSC. We had effectively used a new technology using ADCP because it is recognized as having the capability of measuring suspended sediment with high spatial-temporal resolution and ocean current simultaneously.

CONCLUSION

Acoustic Doppler Current Profiler (ADCP) had been used to quantify the concentration of suspended sediments. The estimated SSC from the acoustic technique showed a high correlation coefficient of 0.98 with *in situ* measurement using gravimetric method. In general, the distribution of SSC for line 1 and line 2 for all ADCP beams had the same pattern where high SSC occurred at the sea surface.

ADCP measurements reliably assess SSC from the water column until the seabed. Sonar equation theory confirms the empirical calibration. By using Rayleigh scattering theory for 300 kHz frequency, the particle size of suspended sediment of less than 1600 μm was predicted.

The ocean hydrodynamic condition such as ocean current is the key factor responsible for SSC distribution in the study area.

ACKNOWLEDGMENT

The authors are grateful to Ministry of Education and Culture of Indonesia for providing research funding through Fundamental Research Scheme. The authors also thank the anonymous reviewers for their comments and suggestion to this manuscript.

REFERENCES

- Ainslie, M. A., & McColm, J. G. (1998). A simplified formula for viscous and chemical absorption in sea water. *The Journal of the Acoustical Society of America*, 103(3), 1671-1672. doi: <https://doi.org/10.1121/1.421258>
- American Public Health Association. (2012). *Standard methods for the examination of water and wastewater* (22nd Ed.). Washington, USA: APHA.
- Chen, S. L., Zhang, G. A., Yang, S. L., & Shi, J. Z. (2006). Temporal variations of fine suspended sediment concentration in the Changjiang River estuary and adjacent coastal waters, China. *Journal of Hydrology*, 331(1-2), 137-145. doi: <https://doi.org/10.1016/j.jhydrol.2006.05.013>
- Deines, K. L. (1999, March 13). Backscatter estimation using broadband acoustic Doppler current profilers. In *Proceedings of the IEEE Sixth Working Conference on Current Measurement* (pp. 249-253). San Diego, CA, USA. doi: 10.1109/CCM.1999.755249
- Downing, J. P. (1996, February 12-13). Suspended sediment and turbidity measurements in streams: What they do and do not mean. In *Automatic Water Quality Monitoring Workshop* (Vol. 12, p. 13). Richmond, Canada.
- Dwinovantyo, A., Manik, H. M., Prartono, T., & Ilahude, D. (2017). Estimation of suspended sediment concentration from Acoustic Doppler Current Profiler (ADCP) instrument: A case study of Lembeh Strait, North Sulawesi. In *IOP Conference Series: Earth and Environmental Science* (Vol. 54, No. 1, p. 012082). Bristol, UK: IOP Publishing. doi:10.1099/1755-1315/54/1/012082.
- Francois, R. E., & Garrison, G. R. (1982a). Sound absorption based on ocean measurements: Part I: Pure water and magnesium sulfate contributions. *The Journal of the Acoustical Society of America*, 72(3), 896-907. doi: <https://doi.org/10.1121/1.388170>
- Francois, R. E., & Garrison, G. R. (1982b). Sound absorption based on ocean measurements. Part II: Boric acid contribution and equation for total absorption. *The Journal of the Acoustical Society of America*, 72(6), 1879-1890. doi: <https://doi.org/10.1121/1.388673>
- Gartner, J. W., & Cheng, R. T. (2001, March 25-29). The promises and pitfalls of estimating total suspended solids based on backscatter intensity from acoustic Doppler current profilers. In *Proceedings of the Seventh Federal Interagency Sedimentation Conference* (Vol. 25, pp. 119-126). Reno, Nevada.
- Gartner, J. W. (2004). Estimating suspended solids concentrations from backscatter intensity measured by acoustic Doppler current profiler in San Francisco Bay, California. *Marine Geology*, 211(3-4), 169-187. doi: <https://doi.org/10.1016/j.margeo.2004.07.001>
- Ghaffari, P., Azizpour, J., Noranian, M., Chegini, V., Tavakoli, V., & Shah-Hosseini, M. (2011). Estimating suspended sediment concentrations using a broadband ADCP in Mahshahr tidal channel. *Ocean Science Discussions*, 8(4), 1601-1630. doi: <https://doi.org/10.5194/osd-8-1601-2011>

- Gruber, P., Felix, D., Storti, G., Lattuada, M., Fleckenstein, P., & Deschwenden, F. (2016). Acoustic measuring techniques for suspended sediment. In *IOP Conference Series: Earth and Environmental Science* (Vol. 49, No. 12, p. 1-11). Bristol, UK: IOP Publishing. doi: <https://doi.org/10.1088/1755-1315/49/12/122003>
- Holdaway, G. P., Thorne, P. D., Flatt, D., Jones, S. E., & Prandle, D. (1999). Comparison between ADCP and transmissometer measurements of suspended sediment concentration. *Continental Shelf Research*, 19(3), 421-441. doi: [https://doi.org/10.1016/S0278-4343\(98\)00097-1](https://doi.org/10.1016/S0278-4343(98)00097-1)
- Li, J., Li, J., Xu, J., Qiao, L., Dong, P., Ding, D., ... & Sun, P. (2015). Seasonal suspended particles distribution patterns in Western South Yellow Sea based on Acoustic Doppler Current Profiler observation. *Journal of Ocean University of China*, 14, 385-398. doi: <https://doi.org/10.1007/s11802-015-2762-2>
- Jiang, S., Dickey, T. D., Steinberg, D. K., & Madin, L. P. (2007). Temporal variability of zooplankton biomass from ADCP backscatter time series data at the Bermuda Testbed Mooring site. *Deep Sea Research Part I: Oceanographic Research Papers*, 54(4), 608-636. doi: <https://doi.org/10.1016/j.dsr.2006.12.011>
- Li, G. X., Yang, Z. G., & Liu, Y. (2005). *The research of the origin of the sea bottom sedimentary environment in China seas*. Beijing, China: The Science Publishing Company.
- Manik, H. M., Gultom, D. A., Firdaus, & Elson, L. (2020). Evaluation of ADCP backscatter computation for quantifying suspended sediment concentration. *IOP Conference Series: Earth and Environmental Science*, 429, 1-7.
- Medwin, H., & Clay, C. S. (1997). *Fundamentals of acoustical oceanography*. Massachusetts, USA: Academic press.
- Moore, S. A., Le Coz, J., Hurther, D., & Paquier, A. (2012). On the application of horizontal ADCPs to suspended sediment transport surveys in rivers. *Continental Shelf Research*, 46, 50-63. doi: <https://doi.org/10.1016/j.csr.2011.10.013>
- Park, H. B., & Lee, G. H. (2016). Evaluation of ADCP backscatter inversion to suspended sediment concentration in estuarine environments. *Ocean Science Journal*, 51(1), 109-125. doi: <https://doi.org/10.1007/s12601-016-0010-3>
- Poerbandono, R., & Mayerle, R. (2004, October 3-7). Assesment of approaches for converting acoustic echo intensity into suspended sediment concentration. In *Proceedings 3rd FIG Regional Conference* (pp. 1-13). Jakarta, Indonesia.
- Poerbandono, R., & Suprijo, T. (2013). Modification of attenuation rate in range normalization of echo levels for obtaining frequency-dependent intensity data from 0.6 MHz and 1.0 MHz devices. *Journal of Engineering and Technological Sciences*, 45(2), 140-152. doi: <http://dx.doi.org/10.5614%2Fj.eng.technol.sci.2013.45.2.3>
- Rai, A. K., & Kumar, A. (2015). Continuous measurement of suspended sediment concentration: Technological advancement and future outlook. *Measurement*, 76, 209-227. doi: <https://doi.org/10.1016/j.measurement.2015.08.013>
- Sassi, M. G., Hoitink, A. J. F., & Vermeulen, B. (2012). Impact of sound attenuation by suspended sediment on ADCP backscatter calibrations. *Water Resources Research*, 48(9), 1-14. doi: <https://doi.org/10.1029/2012WR012008>

- Simmonds, J., & MacLennan, D. N. (2005). *Fisheries acoustic: Theory and practice* (2nd Ed.). Oxford, UK: Blackwell Science.
- Tessier, C., Le Hir, P., Lurton, X., & Castaing, P. (2008). Estimation of suspended sediment concentration from backscatter intensity of Acoustic Doppler Current Profiler. *Comptes Rendus Geoscience*, 340(1), 57-67.
- Thorne, P. D., MacDonald, I. T., & Vincent, C. E. (2014). Modelling acoustic scattering by suspended flocculating sediments. *Continental Shelf Research*, 88, 81-91. doi: <https://doi.org/10.1016/j.csr.2014.07.003>
- Thorne, P. D., Vincent, C. E., Hardcastle, P. J., Rehman, S., & Pearson, N. (1991). Measuring suspended sediment concentrations using acoustic backscatter devices. *Marine Geology*, 98(1), 7-16. doi: [https://doi.org/10.1016/0025-3227\(91\)90031-X](https://doi.org/10.1016/0025-3227(91)90031-X)
- Urick, R. J. (1996). *Principles of underwater sound* (3rd Ed.). California, USA: Peninsula Publishing.
- Wall, G. R., Nystrom, E. A., & Litten, S. (2006). *Use of an ADCP to compute suspended-sediment discharge in the tidal Hudson River, New York*. Scientific Investigations Report 2006-5055. New York Water Science Center. doi: <https://doi.org/10.3133/sir20065055>
- Yu, Q., Wang, Y. P., Flemming, B., & Gao, S. (2012). Tide-induced suspended sediment transport: Depth-averaged concentrations and horizontal residual fluxes. *Continental Shelf Research*, 34, 53-63. doi: <https://doi.org/10.1016/j.csr.2011.11.015>



Carbon Footprint of Built Features and Planting Works during Construction, Maintenance and Renewal Stages at Urban Parks in Petaling Jaya, Selangor

Nurzuliza Jamirsah^{1*}, Ismail Said¹, Badruzaman Jaafar² and Mohd Haniff Mohd Hassani³

¹Department of Landscape Architecture, Faculty of Built Environment and Surveying, Universiti Teknologi Malaysia, 81310 UTM, Johor, Malaysia

²Department of Landscape, Majlis Bandaraya Petaling Jaya, 46675 Petaling Jaya, Selangor, Malaysia

³Department of Landscape, Khoo Soon Lee Realty Sdn Bhd, 41000 Klang, Selangor, Malaysia

ABSTRACT

Carbon emissions in Malaysia are escalating due to rapid urbanisation wherein their sources are claimed to be generated by the construction industry, including urban park development. Upon completion of the urban park project, the vegetation will supposedly function immediately as a carbon sequester. However, the processes of building, maintaining, and renewing built features and plantings can emit additional carbon dioxide (CO₂) than the storage. Rigorous CO₂ release across the maintenance and renewal stages may be contributed by park management activities, such as planting grooming, built feature rectification, and park maintenance works. This study investigated carbon footprint derived from built features and planting works during the construction, maintenance, and renewal stages of park management. Taman Bandaran Kelana Jaya and Taman Aman Petaling

Jaya were chosen as the study sites as they were located at urban areas. Continued use of the parks resulted in a swift deterioration of its facilities, whereby this scenario would ensure recurrent maintenance and renewal works were conducted for them. As-built drawings were utilised to identify the lists of inventories and work breakdown structure for every built feature and planting work to approximate the indirect CO₂ emissions, which was aided by EToolLCD software. This study revealed that the amount of CO₂

ARTICLE INFO

Article history:

Received: 24 July 2020

Accepted: 07 October 2020

Published: 22 January 2021

DOI: <https://doi.org/10.47836/pjst.29.1.22>

E-mail addresses:

nurzulizajamirsah@gmail.com (Nurzuliza Jamirsah)

ismailbinsaid@gmail.com (Ismail Said)

badruzaman@mbpj.gov.my (Badruzaman Jaafar)

mohdhaniff8731@gmail.com (Mohd Haniff Mohd Hassani)

* Corresponding author

sequestered by the manicured vegetation was only 28.7% out of the total CO₂ emission produced since its construction stage. Hence, urban parks can be perceived as a carbon source instead of a carbon sink medium.

Keywords: Carbon footprint, CO₂ emission, CO₂ sequestration, Project management life cycle, Urban parks

INTRODUCTION

The abundance of undesirable greenhouse gaseous remnants such as carbon dioxide (CO₂) is harmful to the climate. Malaysia's construction industry contributes 6% of CO₂ to the atmosphere owing to its rapid development of construction activities (Begum, 2017). Meanwhile, urban parks are known for their purpose as a carbon sinker, whereby the provision of urban parks and greenery is perceived as the mitigating solution towards reducing the atmospheric carbon content. Prior studies (Almeida et al., 2018; Braun & Bremer, 2019; Chen, 2015; Haq, 2011; Sun & Chen, 2017) have found that urban parks alleviate CO₂ emission within an urban setting, whereas their management procedures indirectly contribute to an additional release of atmospheric CO₂. Furthermore, other studies including Connor et al. (2011), Feltynowski et al. (2017), Pocock (2009), and Strohbach et al. (2012), have discovered that they are the source of CO₂ emission in urban areas, which originates from park management activities. Such activities include pruning, trimming, grass mowing, rubbish clearance, hardscape repairs, planting replacement, planting additions, planting treatment, soil treatment, watering, pest and disease control, weed control, and more.

Accordingly, the life cycle of urban park management consists of at least six stages, namely designing, construction, operation, maintenance, demolition, and renewal. These life cycle stages are allegedly contributing CO₂ content to the atmosphere. According to Hisham et al. (2018), a notable amount of CO₂ emissions is produced during the construction stage compared to the maintenance and operation stages. In particular, a significant one-off amount of CO₂ emitted is caused by the heavy use of machinery, transportation of materials, and labour. The stages, as mentioned earlier, often involve the use of machinery, especially during the early stage of project construction, and are associated with CO₂ emission due to fuel consumption. Moreover, the types of materials used as landscape element construction can further influence the carbon footprint of the projects. Besides, the function of urban parks as a CO₂ sink medium becomes null due to the CO₂ emitted by their maintenance activities. Figure 1 shows the conceptual framework of this study, where the studied boundary is limited to the construction, maintenance, and renewal stages (Figure 1). Meanwhile, the stages of design, operation, and demolition are dismissed due to inconsistent data records and documentation. It is hypothesised that the management of urban parks is attributable to the significant CO₂ liberation. Therefore, this study examines how much CO₂ is produced from urban park management by dissecting its life cycle stages into a detailed work breakdown structure.

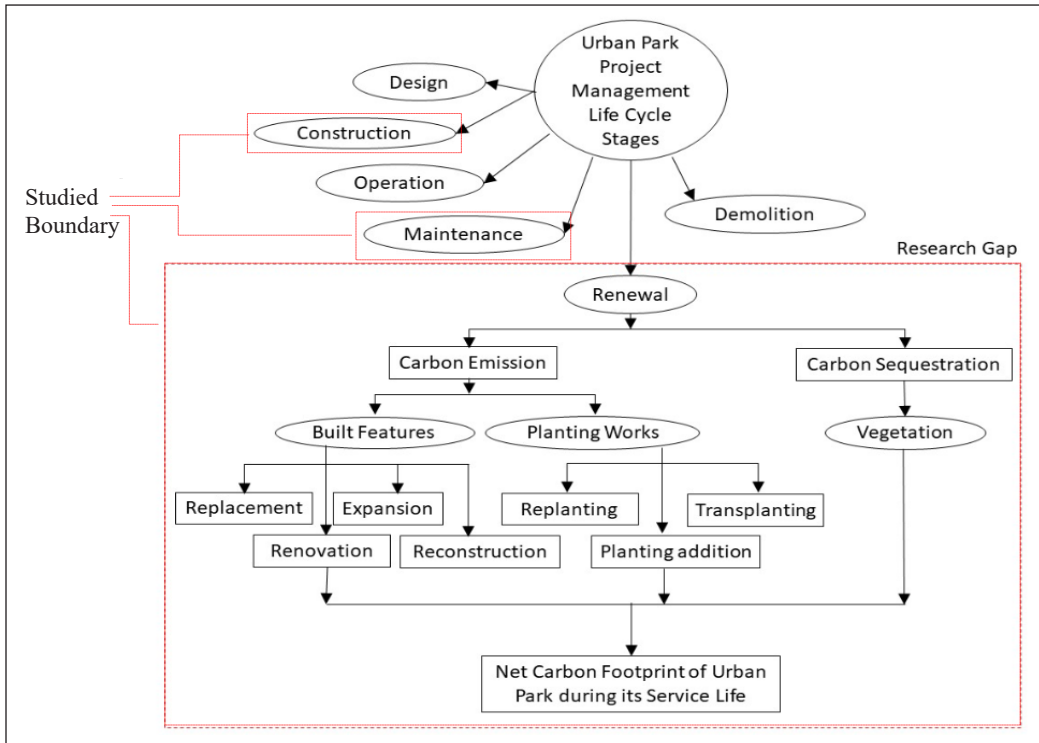


Figure 1. Urban park management carbon footprint conceptual framework

MATERIAL AND METHODS

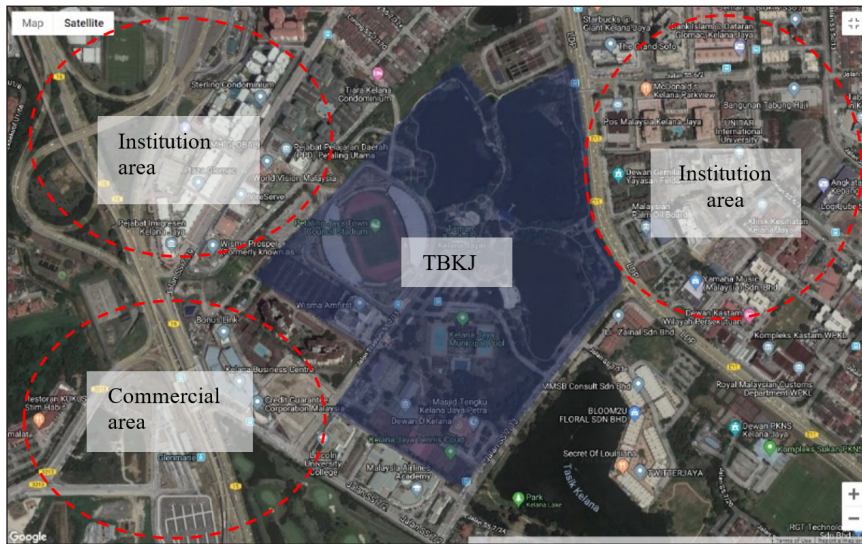
Taman Bandaran Kelana Jaya (TBKJ) and Taman Aman Petaling Jaya (TAPJ) are located in the urban part of Selangor district and thus chosen as the study sites. Table 1 shows the sizes of the parks, which are 361,169 m² and 80,339 m², respectively. Both parks possess similar built features and planting composition ranging between 10.4% to 13.5% (built features) and 86.5% to 89.5% (plantings). Figure 2 shows that these parks are located adjacent to residential, institutional, and commercial areas, thereby indicating that they are utilised frequently as an open green space for urban dwellers. The study sites are chosen according to the following factors; a) urban parks are for public usage; b) as-built drawing availability; c) unmanned aerial vehicle (UAV) drone flight use is permitted.

Table 1
Urban parks background

Park Name	Taman Bandaran Kelana Jaya	Taman Aman Petaling Jaya
Park Size, m ²	361,169	80,339
Park Age, year	24 years old (1995-2019)	18 years old (2001-2019)
Hardscape Composition	10.4%	13.5%
Softscape Composition	89.6%	86.5%

As-built Drawings of Urban Parks

Document retrieval of the old as-built drawings, construction drawings, and maintenance records was laborious. A representative of Petaling Jaya City Council (PJCC) acknowledged that they kept insufficient drawing documentation and records of preceding maintenance activities of the aged parks under their supervision. However, the parks being studied possessed sufficient as-built drawings to recognize the built features and planting inventories.



(a)



(b)

Figure 2. Site context of: (a) TBKJ; and (b) TAPJ

Work Breakdown Structure and Park Management Life Cycle

Every urban park is composed of built features and planting components. By referring to the as-built drawings, Table 2 shows the component inventory during the construction stage, which is fragmented to small-scale components, otherwise known as the work breakdown structure (WBS). The WBS was employed to predict the CO₂ content released by each urban park. Based on the construction CO₂ emission, this study predicted the CO₂ emissions for the maintenance and renewal stages accordingly. The renewal stage can be divided into two categories, namely built feature renewals and planting renewals.

Table 2

Work breakdown structure for several built features during construction stage of the studied urban parks

Built Features	Work Breakdown Structure	Work Packages (eToolLCD)	
Toilet	Site preparation	Small scale excavation	
	Foundation	Formwork (Foundations)	
	Services		Plumbing-100mm Insulated Pipework (22mm dia)
			Multi-Res Bedroom LED Lighting
	Floor	Concrete Floor, 125mm slab. 40MPa. 4% reo by volume	
	Column	Concrete column structural, 30Mpa 3% reo by volume	
	Wall		Concrete Walls (450mm, 40MPa, 25% BFS, 2% reo by volume)
			Partition wall hard resin
	Roof	Roof - TimberTruss/ClayTile/25°Pitch	
	Door	Internal Door - HollowCoreTimber/WoodenJam/painted (m2)	
Finishes		External Finish - Paint(SuperStructure)	
		Internal Finish - Paint (standard)	
Concrete Seating	Foundation	Crushed Rock infill & compaction	
	Floor	Concrete Floor, 100mm slab. 25MPa. 3.8% reo by volume	
	Wall	Assembly only pour concrete	
	Finishes	External Wall Finish - 10mm Render (clay)	
Shelter (Gazebo)	Site preparation	Small scale excavation	
	Foundation	Formwork (Foundations)	
	Floor	Concrete Floor, 125mm slab. 40MPa. 4% reo by volume	
	Column	Concrete column structural, 30Mpa 3% reo by volume	
	Roof	Roof - TimberTruss/ClayTile/25°Pitch	
	Finishes	External Finish - Paint (SuperStructure)	
Bridge	Site preparation	Small scale excavation	
	Foundation	Formwork (Foundations)	
	Floor	Bridge Deck Precast concrete	
	Handrail	Steel handrail 50mm diam	
	Finishes	Floor Finish - Coloured Epoxy Concrete Floor Coating	
Playground floor	Site preparation	Small scale excavation	
	Foundation	Formwork (Foundations)	

Table 2 (continue)

Built Features	Work Breakdown Structure	Work Packages (eToolLCD)
Playground floor	Floor	Concrete Floor - 100mm slab on ground/30MPa/1% reo by volume/no fd
	Finishes	Landscaping - Rubber Play Ground Surface
Parcourse floor	Site preparation	Small scale excavation
	Foundation	Formwork (Foundations)
	Floor	Concrete Floor - 100mm slab on ground/30MPa/1% reo by volume/no fd
	Finishes	Landscaping - Rubber Play Ground Surface
Plaza	Site preparation	Small scale excavation
	Foundation	Formwork (Foundations)
	Floor	Concrete Floor - 100mm slab on ground/30MPa/1% reo by volume/no fd
	Finishes	Floor Finish - Coloured Epoxy Concrete Floor Coating
Walkway	Site preparation	Small scale excavation
	Foundation	Formwork (Foundations)
	Floor	Concrete Floor - 100mm slab on ground/30MPa/1% reo by volume/no fd
	Finishes	Floor Finish - Coloured Epoxy Concrete Floor Coating
Lake	Site preparation	Bulk earthworks - cut (used on site)
Parking area	Site preparation	Large Scale Excavation Sand infill
	Floor	Paving/Road - Asphalt 80mm on 300mm aggregate base
Pole Lighting	Foundation	Crushed Rock infill & compaction
	Lighting	Lighting, 70W pedestrian area lighting on 4m pole, installed

* Work packages were derived from eToolLCD Software at www.etoollcd.com

Table 3 shows built feature renewal, which consists of four sub-stages, specifically replacement, renovation, expansion, and reconstruction. Meanwhile, Table 4 shows that the planting renewal category consists of three sub-stages, which are replanting, planting additions, and transplanting. Altogether, these seven renewal sub-stages were ranked based on the intensity of work: the amount of work performed by a team of workers divided by unit time (Kabanov, 2018).

A set of definition is justified to avoid an inconsistent understanding of the park management terminologies, construction, maintenance, and renewal. Firstly, construction in project management describes the act of erecting a large structure after which its completion is called a project. Examples of construction works include foundation excavation, flooring, column erection, beam fastening, roof works, and finishes. Regardless, the construction CO₂ emission is typically a one-off value and occurs once only throughout the entire urban park life cycle.

Table 3
Work breakdown structure for a shelter from the construction, maintenance and renewal stages

Example of Built Feature	Construction WBS	Maintenance WBS	Renewal WBS			
			Replacement WBS	Renovation WBS	Expansion WBS	Reconstruction WBS
Shelter	Site preparation					Demolition
	Foundation			Demolition	Foundation	Site preparation
	Floor	Finishes	Removal			Foundation
	Column			Roof		Floor
	Roof					Column
	Finishes			Roof	Finishes	Roof
					Finishes	Finishes

Table 4
Work breakdown structure for trees from the planting installation, planting maintenance and renewal stages

Example of Planting Work	Planting Installation WBS	Planting Maintenance WBS	Renewal WBS		
			Replanting WBS	Planting addition WBS	Transplanting WBS
Tree	Site preparation	Pruning/ Fertilizer/ Pest control	Site preparation	Site preparation	Site preparation
	Planting		Planting	Planting	Planting

Next, maintenance entails the preservation of a project or the facilities in the project to its original state post-completion to avoid decomposition. Examples of maintenance works are repainting jobs on built structures, park up-keeping, debris clearance, tree pruning, fertilising, and irrigation. It usually occurs monthly for plantings and yearly for built features.

Finally, renewal is defined as the act to renew a design when it fails to meet the expectation of the users. Examples of renewal works are revamping the existing built structures, park size extension, replanting perished or frail plantings, transplanting, and replanting softscapes according to the upgraded urban park design. This study found that renewal consisted of seven significant sub-stages, namely replacement, replanting, expansion, planting addition, renovation, reconstruction, and transplanting.

Moreover, replacement refers to solely replacing any damaged and defected items, such as timber material, door, roof, playmat, and more. Meanwhile, replanting can be described as solely replanting dead trees by using the number of dead trees (1.4% mortality rate) out of total tree numbers of the park. Next, renovation refers to only renovating any decayed or damaged structures once every five years. This ‘5-year’ period is acknowledged by the experts who had experienced in handling park management (PJCC and KSL

representatives). Expansion is defined by expanding the park with the assumption of urban park components numbers added were based on the park halved amount of total previous constructed item. Planting addition refers to the number of trees added halved the total numbers of trees previously planted. Reconstruction refers to the items reconstructed in the park to equal the amount of previously constructed items in total. At a minimum of every ten years, the urban park designs are usually revamped to achieve a fresher environment. Based on Google Earth satellite images of the studied parks, changes of park morphology had been detected by comparing satellite images from parks completion year until the year 2019. Thus far, several renewal works have been done. Next, transplanting refers to the works of moving healthy or heritage trees within or outside of the urban park. The number of transplanted trees can be calculated using 1.4% of the tree mortality numbers to be replanted on the park.

Following this, patterns of CO₂ liberation during the construction stage emerged, and the WBS pattern was extrapolated during the maintenance and renewal stages for predicting the CO₂ emission in the context of other urban parks with similar microclimate, built features, plant species, and management life cycles.

Built Features Inventory

The built feature is any built form or structure in an urban park categorised as free-standing elements, horizontal and vertical surfaces (Hisham et al., 2018; Connor et al., 2011). CO₂ release estimation of these built features for TBKJ and TAPJ was done using EToolLCD Software, an online paid software that aids in calculating the WBS for construction items, including foundation, column, wall, roof, and finishes (Eslamirad & Mahdavejad, 2018; De Wolf et al., 2017). The floor areas in square metre (m²) of each built feature were gathered from the as-built drawings. Height, length and width dimensions were collected using an unmanned aerial vehicle (UAV) drone flights over the parks using the decided transect paths (Figure 3a and 3b). The output of the UAV flights is orthophotos. This method is termed as Structure from Motion (SfM), where a series of two dimensional (2D) orthophotos is utilised to reconstruct the three dimensional (3D) model of a built object. The 3D models of the urban parks generated by MeshLab Software were used to measure the verifiable height, length and width in metre (m). The model is reliable as it is an accurate representation of the Earth's surface. These new techniques are practical for data collection at places that are difficult to reach, such as lush vegetation in urban parks (Shashi & Jain, 2007). A DJI Phantom 4 Pro drone was used to capture low-altitude photographs, and GPS devices were used to survey the reference points (Ground Control Points) (Figure 3c). These data were processed in an SfM workflow to create elevation point cloud to derive orthophotos and canopy height models (CHM). Thus, UAV flights data collection is reliable coequal with LiDAR but at an inexpensive cost (Ngadiman et al., 2018).

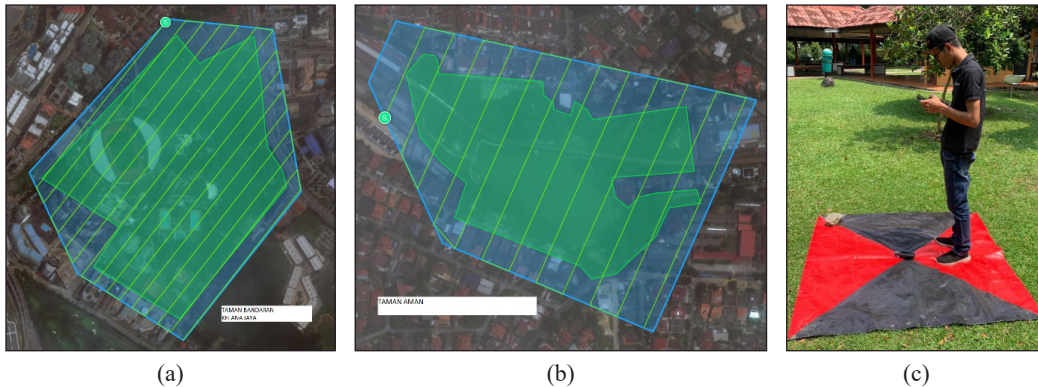


Figure 3. (a) TBKJ UAV drone transect path; (b) TAPJ UAV drone transect path; and (c) Ground Control Point coordinate tagging

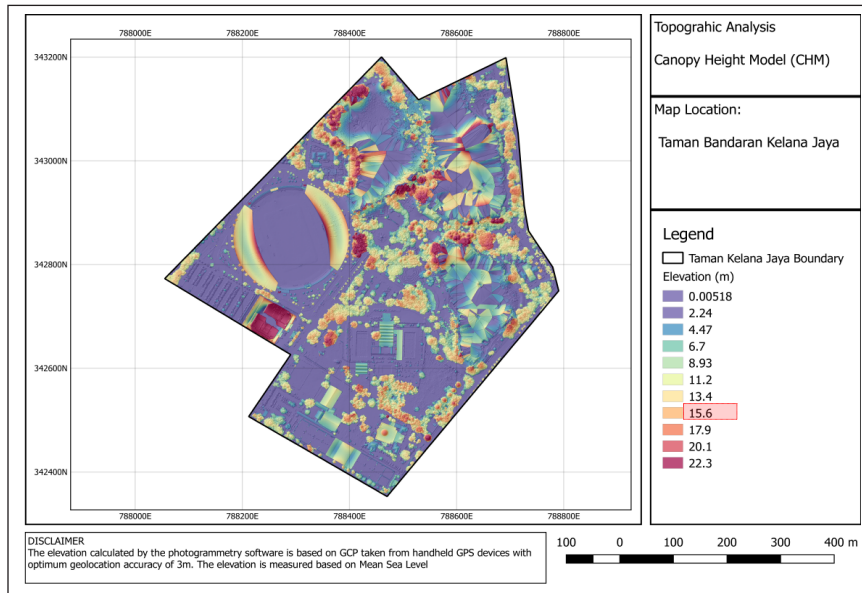
Planting Inventory

Planting is any vegetation prescribed during the design stage of an urban park, such as trees, ornamental flowers, edible plants, shrubs, groundcovers and turfs (Hisham et al., 2018). The tree numbers and species were accumulated from the as-built drawings. Tree heights and diameter at breast heights (DBH) were collected from the UAV flights and on-site measurements, respectively. The output of UAV flights was a Canopy Height Model (CHM) in which the average tree heights could be identified (Figure 4a and 4b). These urban parks have been in existence for 24 years (TBKJ) and 18 years (TAPJ) each, thereby both having matured vegetation with an average overall height of 15.6 m (Figure 4a) and 17.8 m (Figure 4b), respectively. Planting types observed were trees and turfs exclusively due to shrubs being frequently altered at the parks, and the records for any altered species and numbers altered were unavailable. Plantings CO₂ emission were calculated from the commencement of planting activities on-site until the growing process such as pruning, fertilising and weeding presently.

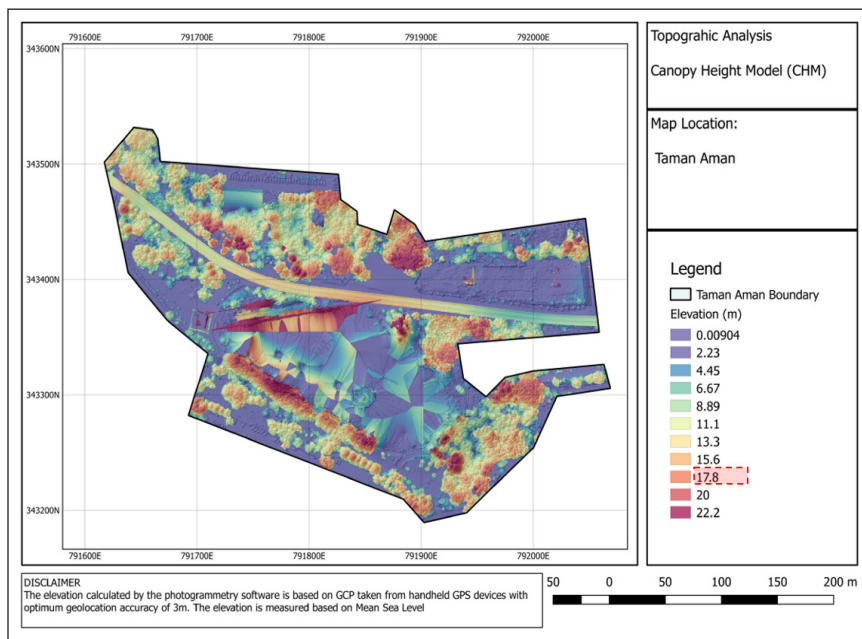
Trees were categorised into three; small (< 9m), medium (≤ 9 to 21m \geq) and large (> 21m) (Arbor Day Foundation, 2020). CO₂ sequestrations were calculated based on the DBH, height, numbers and years of the trees planted on the urban parks 1348 trees at TBKJ and 551 trees at TAPJ. Table 5 shows the formulae to estimate CO₂ sequestration by trees and turfs developed by Othman and Kasim (2016). Tree mortality rates depend on the year and type of microclimate where the vegetation is planted. In a tropical climate such as Malaysia, the value is low in the case of temperatures between 26.0 and 29.5 °C. This study adopted 1.40% tree mortality rate at a tropical climate out of total tree numbers at each urban park, which was as suggested by previous studies (Aleixo et al., 2019; Arellano et al., 2019; King et al., 2006).

Turf is commonly found in large areas of natural and agricultural lands. Due to urbanisation, such green spaces have been replaced with golf courses, public parks, private

lawns, and sports fields (Alig et al., 2004). Five urban parks were observed between the year 2018-2019, and only two parks were presented in this paper. Based on the observation conducted onto these parks, turf height must be kept at an optimum level of approximately 2.5 cm to 4.0 cm represented as κ in figure 6a (Marcum, 2010).



(a)



(b)

Figure 4. (a) CHM of TBKJ; and (b) CHM of TAPJ

Figure 5a shows the turf specimen height was measured as 4.95 cm. After two to three weeks, the turf reached approximately 7.5 cm to 12.0 cm tall represented as 3κ shown in Figure 6b. Turf exceeding 12.0 cm were cut and unfavourable due to pest infestation. At the optimum height, they can germinate seeds and retain moisture longer within the topsoil. At the same time, excessively short turf leads to inefficient photosynthesis, stressed root system, and is vulnerable for pathogen infestation. Thus, mowing was carried out every three weeks onto the turf at these parks.

Figure 5b shows the length of the grass cut was 1/3 of total grass height which was 4.03 cm. This cut height is equivalent to the κ grass height of 2.5cm to 4.0 cm delivered from nursery and previously planted on site (Figure 6a). The carbon emissions from mowing were estimated based on the number of cumulative annual mowing events (Braun & Bremer, 2019). This study applied 17 times of mowing events minimum required annually. Hence,

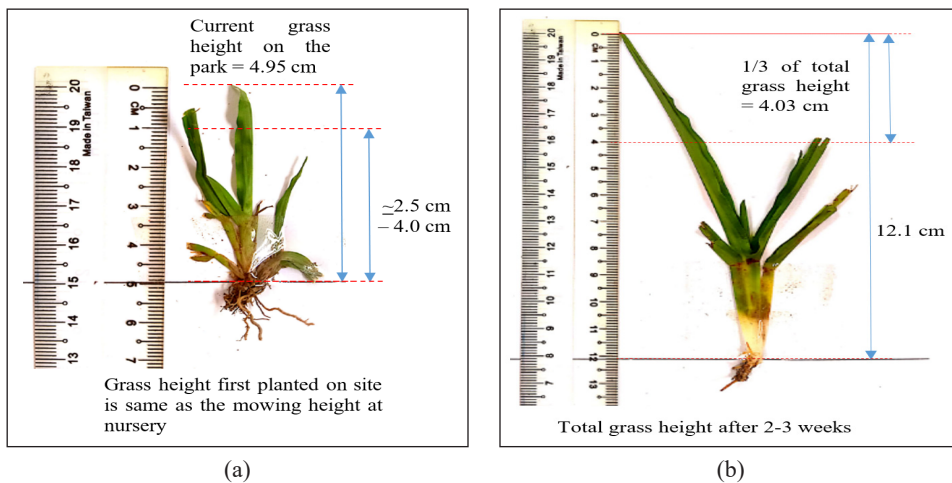


Figure 5. (a) Turf specimen of the park post mowing = 4.95cm; and (b) length of grass blade clipped at 1/3 of total turf height represent the turf height first planted on site

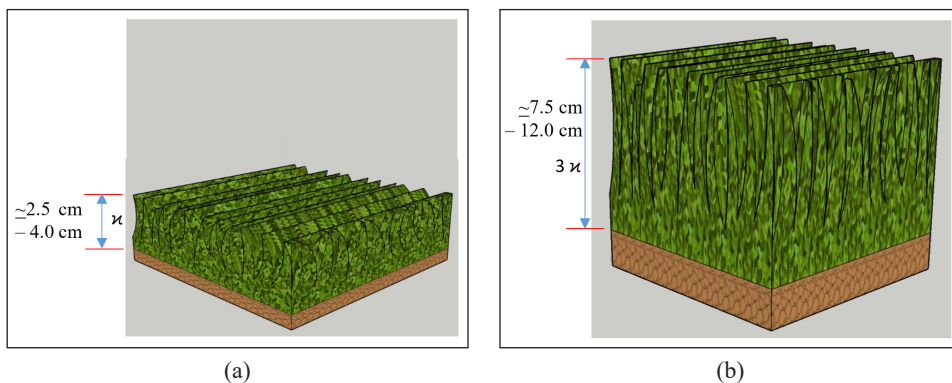


Figure 6. a) κ is turf mowing height at 2.5 cm to 4.0 cm (Marcum, 2010); and b) 3κ is turf height after 2 to 3 weeks at 7.5 cm to 12.0 cm

Table 5
CO₂ sequestration formula for trees and turf

CO ₂ Sequestration Rate formula for Trees	CO ₂ Sequestration Rate formula for Turf
Total Green Weight, TGW (D=<11 in), W=0.25D ² H (1.2)	Total Dry Weight, TDW = 0.56 x area in m ²
Total Green Weight, TGW (D=>11 in), W=0.15D ² H (1.2)	Total Carbon Weight, TCW = TDW x 0.427
Total Dry Weight, TDW = TGW x 0.725,	Total CO ₂ Weight, TCO ₂ W = TCW x 3.6663
Total Carbon Weight, TCW = TDW x 0.5	Exp 1 - TCO ₂ W to date =
Total CO ₂ Weight, TCO ₂ W = TCW x 3.6663	TCO ₂ W x 17 x park age x ***0.44 grass mortality rate
TCO ₂ W to date = TCO ₂ W x **1.4% x Tree nos	

* adaptation of Othman and Kasim (2016) trees and turf sequestration

** tree mortality rate adopted from Aleixo et al. (2019)

*** grass mortality rate adopted from Lauenroth and Adler (2008)

this study adopted the formula for turf CO₂ sequestration developed by Othman and Kasim (2016) with further multiplication of 17 times mowing events, park age and 0.44% grass mortality rate as expression 1 shown in Table 5.

RESULTS AND DISCUSSION

Built Features Inventory

According to Petaling Jaya City Council and KSL representatives, an urban park may have undergone replacement, replanting, renovation, expansion, planting addition, reconstruction, and transplanting at least once throughout its service life span. Carbon emission for TBKJ (24 years) and TAPJ (18 years) were estimated as 95,325,744 kgCO₂eq and 29,152,303 kgCO₂eq respectively.

CO₂ emission for the construction stage is estimated as a one-off emission. Maintenance stage emission was calculated from the park cleaning, and make-good works multiplied with park age. Built feature renewal emission consisted of four substages, namely replacement, renovation, expansion and reconstruction. The CO₂ emission of replacement works was considering the repairing work such as scrapping damaged playground mat and change it to a similar mat. The emission for renovation works, including changing the existing built feature to a different shape, material and finishes. The emission for expansion works, including the enlargement of park surface areas and addition of built features quantity. The emission of reconstruction works is focusing on revamping the whole park design with a refreshed design suitable for current urban users. This study assumed that the reconstructed design followed the previous design, material, finishes and quantities.

The built features produced a total of 38,850,190 kgCO₂eq (Table 6) and 8,330,614 kgCO₂eq (Table 7) of CO₂ emissions during the construction stage of the urban parks. The highest CO₂ emission identified was produced by site preparation including earthworks

Table 6
Built feature inventories and CO₂ emission estimation for TBKJ during construction, maintenance and renewal stages

Built Feature	Carbon Emissions for Built Feature at TBKJ					
	Construction Stage	Maintenance Stage (24 years)	Renewal Stage			
			Replacement Stage	Renovation Stage	Expansion Stage	Reconstruction Stage
Site Preparation/ Overall works	32,279,571	39,591	15,430	21,216	383,251	32,500,099
Toilet	32,195	908	1,939	13,889	16,396	32,657
Concrete seating	6,572	1,325	19	-	3,339	6,572
Planter box	6,324	1,111	-	-	3,162	6,325
Concrete structure	115,696	8,456	50,154	57,076	35,014	115,695
Shelter	24,671	809	10,149	10,958	11,693	23,604
Pergola	24,745	1,578	12,157	20,144	12,375	24,750
Bridge	6,938	381	282	-	3,406	6,938
Playground / Play court	222,529	187,920	20,782	189,081	110,864	222,889
Parcourse	11,620	10,281	1,083	10,302	5,846	11,620
Plaza	270,456	58,915	-	-	131,714	270,456
Walkway	447,855	124,450	256,521	-	221,398	447,855
Parking area	1,619,422	-	-	-	809,711	1,619,422
Lighting	2,594,673	-	2,591,113	-	1,295,696	2,591,113
Man-Made Lake	1,186,923	-	-	-	593,461	1,186,923
Total	38,850,190	435,724	2,964,691	322,667	3,660,343	39,070,477
Overall Built Feature	38,850,190	10,457,376	2,964,691	322,667	3,660,343	39,070,477
Carbon Emission, kgCO ₂ eq			95,325,744			

* CO₂ emission estimations were done using eToolLCD Software at www.etoollcd.com

excavation and movements, drainage ditching system and electrical cabling placement, with 32,279,571 kgCO₂eq and 7,180,299 kgCO₂eq, respectively. This emission is due to the high number of heavy machinery involved in the works. This was followed by lighting (TBKJ) and man-man lake (TAPJ) at 2,594,673 kgCO₂eq and 280,792 kgCO₂eq, respectively. Lighting CO₂ emission was the highest value due to 400 pedestrian lighting fixtures allocated at the TBKJ. Their energy usage during the operation phase assumed that the 70W/bulb was running for 12 hours (7 pm till 7 am) daily. Similarly, the man-made lake produced the highest CO₂ emission at TAPJ due to heavy machinery used during the

Table 7
Built feature inventories and CO₂ emission estimation for TAPJ during construction, maintenance and renewal stages

Built Feature	Carbon Emissions for Built Feature at TAPJ					
	Construction Stage	Maintenance Stage (18 years)	Renewal Stage			
			Replacement Stage	Renovation Stage	Expansion Stage	Reconstruction Stage
Site Preparation/ Overall works	7,180,299	11,489	8,850	4,768	85,639	7,254,583
Toilet	8,761	446	1,603	4,441	5,289	8,763
Concrete seating	3,130	114	19	-	1,539	3,130
Shelter	19,262	707	8,529	9,236	9,589	16,315
Bridge	16,726	3,137	11,819	-	27,027	16,727
Playground / Play court	183,693	153,584	16,979	154,533	90,611	182,153
Parcourse	102,504	92,754	9,688	92,759	52,450	102,503
Plaza	58,613	12,555	-	-	28,544	58,613
Walkway	256,086	67,667	142,246	-	120,406	243,532
Parking area	110,217	-	-	-	55,108	110,218
Lighting	110,531	-	110,452	-	55,344	110,530
Man-Made Lake	280,792	-	-	-	5,159,262	280,792
Total	8,330,614	342,453	310,185	265,736	5,690,809	8,390,805
Overall Built Feature Carbon Emission, kgCO ₂ eq	8,330,614	6,164,154	310,185	265,736	5,690,809	8,390,805
			29,152,303			

* CO₂ emission estimations were done using eToolLCD Software at www.etoollcd.com

construction stage. The machinery involved were the Front-End Loader (25 tonnes) (i.e. for lake excavation and backfilling), Loader (i.e. for loading bulk earthworks into the truck), and Dump Truck (i.e. for moving bulk earthworks to other sites within the construction site).

Planting Inventory

CO₂ emission for planting installation stage is also a one-time emission. Emission during the planting maintenance stage was estimated from the tree pruning, fertilizing and plant matter clearance and multiplied with park age. Planting renewal emission consisted of three substages, namely replanting, planting addition, and transplanting. The CO₂ emission of replanting works derived from the substituting sick or dead trees with similar species. The

emission for planting addition works, including adding more quantities of trees of similar or different species. The emissions were derived from transplanting works, including the transplanting existing trees at renovated, expanded or reconstructed areas to other location within the urban park.

A total of 1348 trees (TBKJ) and 551 trees (TAPJ) were found along the study transects. A sum of 9,397,508 kgCO₂eq (Table 8) and 1,868,777 kgCO₂eq (Table 9) of CO₂ emissions of planting works was produced during the construction, maintenance and renewal stages of the TBKJ and TAPJ, respectively. Planting work CO₂ estimation was dependent on the tree numbers and turf surface areas. Project supervisors of Petaling Jaya City Council suggested that the related works to planting a tree involved planting pit preparation, tree

Table 8
Planting inventories and CO₂ emission estimation for TBKJ during construction, maintenance and renewal stages

Planting Work	Carbon Emission for Planting Works at TBKJ				
	Planting Installation Stage	Planting Maintenance Stage (24 years)	Renewal Stage		
			Replanting Stage	Planting addition Stage	Transplanting Stage
Overall works	24,631	39,591	2,058	12,316	2,058
Tree	629,893	39,591	63,083	314,947	63,083
Turf	159,349	256,127	-	79,674	-
Total	813,873	335,309	65,141	406,937	65,141
Overall Planting Work Carbon Emission, kgCO ₂ eq	813,873	8,047,416	65,141	406,937	65,141
			9,397,508		

* CO₂ emission estimations were done using eToolLCD Software at www.etoollcd.com

Table 9
Planting inventories and CO₂ emission estimation for TAPJ during construction, maintenance and renewal stages

Planting Work	Carbon Emission for Planting Works at TAPJ				
	Planting Installation Stage	Planting Maintenance Stage (18 years)	Renewal Stage		
			Replanting Stage	Planting addition Stage	Transplanting Stage
Overall works	7,148	11,489	848	3,574	845
Tree	257,471	11,489	25,701	128,970	25,701
Turf	33,021	53,076	-	16,511	-
Total	297,640	76,055	26,548	149,054	26,545
Overall Planting Work Carbon Emission, kgCO ₂ eq	297,640	1,368,990	26,548	149,054	26,545
			1,868,777		

* CO₂ emission estimations were done using eToolLCD Software at www.etoollcd.com

lifting, topsoil backfilling, staking erection, mulching and watering. These works required labour as site supervisor and operating the small electrical equipment. Such works indirectly caused CO₂ liberation. Similarly, turf installation CO₂ emissions were acquired from site supervision during soil compacting, turf laying on-site, and watering.

The total CO₂ sequestration produced at TBKJ and TAPJ were 41,371,400 kgCO₂eq and 9,992,415 kgCO₂eq, respectively (Table 10). According to the maturity of vegetation, TAPJ had more matured vegetation despite its 18 years of park age compared to TBKJ (i.e. 24 years). Even though TBKJ was 24 years in age, the DBH and tree height were less matured compared to TAPJ.

Subsequent years of urban park completion require the parks to go through a series of maintenance and renewal stages throughout their management life cycle. These management activities are to ensure the parks are relevant to be used by visitors. Meanwhile, accumulated CO₂ emissions throughout the service life of an urban park commencing from construction, maintenance and renewal stages are justified in Table 11. The urban park itself is a carbon sink; conversely, the urban park management procedures implemented served as the carbon source.

The findings suggested that the net carbon footprint of the urban parks during the construction, maintenance, and renewal stages over 24 years (TBKJ) and 18 years (TAPJ) was not compensated for the CO₂ sequestration by its vegetation. TBKJ (146,094,652

Table 10
Planting inventory and CO₂ sequestration estimation for TBKJ and TAPJ according to age of the parks

Planting Inventory	Taman Bandaran Kelana Jaya (TBKJ)		Taman Aman Petaling Jaya (TAPJ)	
	Allometric Equation			
	Numbers, Nos	CO ₂ Sequestration Estimation, kgCO ₂ eq	Numbers, Nos	CO ₂ Sequestration Estimation, kgCO ₂ eq
Trees	1,348	3,272,628	551	4,121,649
U.P Age = 24 y and 18 y (1.40% tree mortality rate)	1,330	3,226,811	544	4,063,946
	Floor area, m ²	Carbon Sequestration Estimation, kgCO ₂ eq	Floor area, m ²	Carbon Sequestration Estimation, kgCO ₂ eq
Turf / year	242,368	212,481	50,225	44,032
24 y and 18 y (0.44% grass mortality rate)		38,144,589		5,928,469
Total Softscape CO ₂ Sequestration, kgCO ₂ eq		41,371,400		9,992,415

* CO₂ sequestration estimations were calculated using adaptation allometric equation developed by Othman and Kasim, (2016).

kgCO₂eq) reported a higher CO₂ emission by 90.7% than TAPJ (14,864,511 kgCO₂eq) due to its regular renewal compared to TAPJ (Table 12). TBKJ is a prominent spot for outdoor recreation among urban residents as the park offers a variety of park facilities. Whereby heavy usage of its facilities contributes to frequent wearing down of the built features and facilities, subsequently causing maintenance and repairing activities to be conducted. Damaged facilities trigger intense renewal works, which indicate that more CO₂ emission is generated indirectly and derived from material transportation, machinery, and labour. Plantings such as trees, shrubs, and turfs are manicured regularly to ensure visitors' safety and avoiding pest inhabitation within the urban parks. Besides, user visitation frequency contributes to waste accumulation as well, hence requiring maintenance works to meet the cleanliness standard accepted by the users. Although TBKJ was six years older than TAPJ, its vegetation dissipated CO₂ further due to the maintenance cycle as frequent as once every three weeks. Table 12 shows the amount of CO₂ sequestered by the established vegetation, which was stochastically below 28.7% out of the total of CO₂ emission produced since its previous construction stage. This study presented facts contrary to the general opinion of landscape architects and researchers who claimed urban parks to be a carbon sink medium.

The amount of carbon footprint per square metre of the urban parks is approximately 404.5 kgCO₂eq/m² for TBKJ and 185.0 kgCO₂eq/m² for TAPJ. Therefore, the amount

Table 11
Total urban park carbon emission of TBKJ and TAPJ to date

CO ₂ Emission for every Park Management Phase	Taman Bandaran Kelana Jaya (TBKJ), kgCO ₂ eq	Taman Aman Petaling Jaya (TAPJ), kgCO ₂ eq
Construction Phase	39,664,063	8,628,254
Maintenance Phase	18,504,792	1,368,990
Renewal Phase	46,554,397	14,859,682
Total Urban Park CO ₂ Emission to Date, kgCO ₂ eq	104,723,252	24,856,926

Table 12
Net urban park carbon footprint of TBKJ and TAPJ up to date

Urban Park Carbon Footprint	Taman Bandaran Kelana Jaya (TBKJ), kgCO ₂ eq	Percentage, %	Taman Aman Petaling Jaya (TAPJ), kgCO ₂ eq	Percentage, %
Total Urban Park CO ₂ Emission	104,723,252	71.7%	24,856,926	71.3%
Total Urban Park CO ₂ Sequestration	41,371,400	28.3%	9,992,415	28.7%
Net Carbon Footprint up to Date, kgCO ₂ eq	146,094,652		14,864,511	

* Net Carbon footprint = Total Urban Park CO₂ Emission – Total Urban Park CO₂ Sequestration

of tree emission was consistent as 467.3 kgCO₂eq/m² because of the works involved were similar such as tree pit preparation, machinery for tree lifting, and labour top-soil backfilling. In contrast, the amount of turf emission was consistent as 0.78 kgCO₂eq/m² due to works involved in handling turf, namely labour for turf laying, top-soil backfilling and compacting, and watering.

The amount of tree sequestration was irregular at 2427 kgCO₂eq/tree (TBKJ), and 7480 kgCO₂eq/tree (TAPJ) due to the different soil type, mostly since TBKJ was previously an ex-mining site, thus causing the vegetation's slow growth to be influenced by the nutrient-deficient soil. In contrast, TAPJ vegetation consisted of species such as *Syzygium grande* (0.65gcm⁻³), *Lagerstroemia speciose* (0.83gcm⁻³), and *Ficus roxburghii* (0.52gcm⁻³), which was fast-growing, suitable to local climate, and had a higher wood density. TBKJ consisted of species such as *Albizia saman* (0.46gcm⁻³), *Cocos nucifera* (0.58gcm⁻³), and *Acacia auriculiformis* (0.75gcm⁻³), which had a lower wood density. Besides, TAPJ locales were at the valleys where water collection occurred, whereby the high level of moisture in its soil supported rigorous tree growth. TBKJ had low sequestration rates as the park had a higher mortality rate caused by a natural disaster such as strong winds and floods. These events were depriving trees by damaging tree branches and water ponding at root areas.

CONCLUSION

This study concluded that urban park management procedures contributed to the release of CO₂ emission by 71.3% - 71.7% derived from the construction, maintenance, and renewal stages. Carbon storage by urban vegetation was only 28.3% - 28.7% for as long as 18 to 24 years of age parks. The studied urban parks serve as the carbon source instead of a carbon sink medium in the context of the urban location. This study discovered that built features and planting works of an urban park emitted additional carbon content than that being absorbed. The aggravated stage of carbon emitted can be mitigated by reducing the maintenance and renewal frequencies conducted in an urban park.

This study suggests several ways to reduce the carbon footprint of urban parks. First, retrofitting the existing light bulb to a more energy-efficient bulb and reduce its operating hours. Second, reducing earthwork excavation to alter landforms, instead of blend and adapt the proposed design with the existing site. It is encouraging to use eco-friendly or recyclable materials for constructing the built feature so that it can reduce resource wastage. Finally, reducing planting maintenance frequencies by focusing on the areas where people used the most. The CO₂ emission allowance was based on the amount of vegetation able to sequester yearly. It is advisable to identify the amount of CO₂ sequestration by greenery at the parks and use the sequestration value as carbon emission allowance to conduct management activities.

ACKNOWLEDGEMENT

The authors would like to acknowledge Majlis Bandaraya Petaling Jaya and Khoo Soon Lee Realty Sdn Bhd for support and data supplication of the studied urban parks.

REFERENCES

- Aleixo, I., Norris, D., Hemerik, L., Barbosa, A., Prata, E., Costa, F., & Poorter, L. (2019). Amazonian rainforest tree mortality driven by climate and functional traits. *Nature Climate Change*, 9(5), 384-388. doi: <https://doi.org/10.1038/s41558-019-0458-0>
- Alig, R. J., Kline, J. D., & Lichtenstein, M. (2004). Urbanization on the US landscape: looking ahead in the 21st century. *Landscape and Urban Planning*, 69(2-3), 219-234. doi: <https://doi.org/10.1016/j.landurbplan.2003.07.004>
- Almeida, C. M. V. B., Mariano, M. V, Agostinho, F., Liu, G. Y., & Giannetti, B. F. (2018). Exploring the potential of urban park size for the provision of ecosystem services to urban centres : A case study in São Paulo, Brazil. *Building and Environment*, 144(August), 450-458. doi: <https://doi.org/10.1016/j.buildenv.2018.08.036>
- Arbor Day Foundation. (2020). *The basic spacing guide from various distances and various tree heights*. Retrieved March 3, 2020, from <https://www.arborday.org/trees/rightTreeAndPlace/size.cfm>
- Arellano, G., Medina, N. G., Tan, S., Mohamad, M., & Davies, S. J. (2019). Crown damage and the mortality of tropical trees. *New Phytologist*, 221(1), 169-179. doi: <https://doi.org/10.1111/nph.15381>
- Begum, R. A. (2017). *Tackling climate change and Malaysia's emission reduction target*. Retrieved March 3, 2020, from <http://magazine.scientificmalaysian.com/issue-13-2017/tackling-climate-change-malaysias-emission-reduction-target/>
- Braun, R. C., & Bremer, D. J. (2019). Carbon sequestration in Zoysiagrass Turf under different irrigation and fertilization management regimes. *Agrosystems, Geosciences and Environment*, 2(1), 1-8. doi: <https://doi.org/10.2134/age2018.12.0060>
- Chen, W. Y. (2015). The role of urban green infrastructure in offsetting carbon emissions in 35 major Chinese cities: A nationwide estimate. *Cities*, 44, 112-120. doi: <https://doi.org/10.1016/j.cities.2015.01.005>
- Connor, K. O., Pocock, C., Barthelmeh, M., & Davis, S. (2011). *Carbon and environmental profiling of hard landscape materials* (Research Report). Lincoln University, New Zealand: Centre for Land Environment & People.
- De Wolf, C., Pomponi, F., & Moncaster, A. (2017). Measuring embodied carbon dioxide equivalent of buildings: A review and critique of current industry practice. *Energy and Buildings*, 140, 68-80. doi: <https://doi.org/10.1016/j.enbuild.2017.01.075>
- Eslamirad, N., & Mahdavejad, M. (2018, September 26-28). External shadings effect on operating energy based on lcea, case study: A residential building in Tehran. In *2018 Building Performance Analysis Conference and SimBuild* (pp. 494-501). Chicago, Illinois.

- Feltynowski, M., Kronenberg, J., Bergier, T., Kabisch, N., Łaskiewicz, E., & Strohbach, M. (2017). Challenges of urban green space management in the face of using inadequate data. *Urban Forestry and Urban Greening*, 31, 56-66. doi: <https://doi.org/10.1016/j.ufug.2017.12.003>
- Haq, S. M. A. (2011). Urban green spaces and an integrative approach to sustainable environment. *Journal of Environmental Protection*, 02(05), 601-608. doi: 10.4236/jep.2011.25069
- Hisham, F. D. B., Shahidan, M. F., & Ja'afar, M. F. Z. (2018). Stages and elements affecting development of low carbon parks in Malaysia: An expert review. *Alam Cipta*, 11(1), 2-8.
- Kabanov, V. (2018). Measurement of the intensity of construction and installation works taking into account the level of organizational and technological reliability. In *MATEC Web of Conferences* (Vol. 193, pp. 1-8). Les Ulis, France: EDP Sciences. doi: <https://doi.org/10.1051/mateconf/201819305056>
- King, D. A., Davies, S. J., & Noor, N. S. M. (2006). Growth and mortality are related to adult tree size in a Malaysian mixed dipterocarp forest. *Forest Ecology and Management*, 223(1-3), 152-158. doi: <https://doi.org/10.1016/j.foreco.2005.10.066>
- Lauenroth, W. K., & Adler, P. B. (2008). Demography of perennial grassland plants: Survival, life expectancy and life span. *Journal of Ecology*, 96(5), 1023-1032. doi: <https://doi.org/10.1111/j.1365-2745.2008.01415.x>
- Marcum, K. (2010). *Tropical turfgrass mowing*. Retrieved March 3, 2020, from <https://www.nparks.gov.sg/-/media/cuge/pdf/rtn-03-2010---tropical-turfgrass-mowing.pdf?la=en&hash=F99D23289A512EFFAFB61CBC69DA6C67091249C9>
- Ngadiman, N., Kaamin, M., Sahat, S., & Mokhtar, M. (2018). Production of orthophoto map using UAV photogrammetry: A case study in UTHM Pagoh campus. In *AIP Conference Proceedings 2016* (Vol. 020112, pp. 1-6). Melville, USA: AIP Publishing LLC. doi: <https://doi.org/10.1063/1.5055514>
- Othman, R., & Kasim, S. Z. A. (2016). Assessment of plant materials carbon sequestration rate for horizontal and vertical landscape design. *International Journal of Environmental Science and Development*, 7(6), 410-414. doi: 10.7763/IJESD.2016.V7.810
- Pocock, C. (2009). The carbon landscape: Managing the carbon impact in landscape design. *Pocock Design Environment*. Retrieved March 3, 2020, from <http://www.carbonlandscape.com/the-carbon-landscape-2007.html>
- Shashi, M., & Jain, K. (2007). Use of photogrammetry in 3D modeling and visualization of buildings. *Journal of Engineering and Applied Sciences*, 2(2), 37-40.
- Strohbach, M. W., Arnold, E., & Haase, D. (2012). The carbon footprint of urban green space-A life cycle approach. *Landscape and Urban Planning*, 104(2), 220-229. doi: <https://doi.org/10.1016/j.landurbplan.2011.10.013>
- Sun, R., & Chen, L. (2017). Effects of green space dynamics on urban heat islands: Mitigation and diversification. *Ecosystem Services*, 23(December 2016), 38-46. doi: <https://doi.org/10.1016/j.ecoser.2016.11.011>

Optimisation of Culture Conditions for PLA-food-packaging Degradation by *Bacillus* sp. SNRUSA4

Suwapha Sawiphak* and Aroon Wongjirathiti

Program of Biology, Faculty of Science and Technology, Sakon Nakhon Rajabhat University, Sakon Nakhon, 47000, Thailand

ABSTRACT

Polylactic acid (PLA) is increasingly used in food-packaging production. The screening of PLA-food-packaging-degrading bacteria and optimisation of culture conditions for the PLA-food-packaging degradation by PLA-food-packaging-degrading bacteria were investigated for bioplastic waste management purposes. Only bacterial strain SNRUSA4 exhibited an increase in optical density (OD) in Basal Medium (BM) supplemented with 1.0 g/L of PLA-food-packaging as sole carbon source after 4 weeks of incubation. A weight loss of 7.3% and the rough and porous surface of PLA-food-packaging indicated that SNRUSA4 was a PLA-food-packaging-degrading bacterium. SNRUSA4 was able to degrade pure PLA which was confirmed from the clear zone formation around its colony on emulsified pure PLA agar plate. The 16S rRNA gene sequence of SNRUSA4 showed the similarity with thirteen *Bacillus* species. Hence, the strain SNRUSA4 was assigned as *Bacillus* sp. SNRUSA4. Response surface methodology with Box-Behnken Design was used to optimise the culture conditions including yeast extract concentration, initial pH value, temperature and agitation speed for growth and PLA-food-packaging degradation of *Bacillus* sp.

SNRUSA4. The optimal conditions of *Bacillus* sp. SNRUSA4 was discovered in BM at initial pH value 7.02 with yeast extract concentration of 2.56% and agitated at 205.28 rpm at 31.68°C. Under optimal conditions, the OD of *Bacillus* sp. SNRUSA4 was up to 1.955, and the different OD between before and after optimisation was up to 1.752. Furthermore, the PLA-food-packaging weight loss also increased from 7.30% to 87.10% indicating that the

ARTICLE INFO

Article history:

Received: 11 September 2020

Accepted: 07 December 2020

Published: 22 January 2021

DOI: <https://doi.org/10.47836/pjst.29.1.23>

E-mail addresses:

ssuvapa@hotmail.com (Suwapha Sawiphak)

mic_610@hotmail.com (Aroon Wongjirathiti)

* Corresponding author

PLA-food-packaging degradation under optimal conditions was higher than the unoptimised conditions. Therefore, *Bacillus* sp. SNRUSA4 is an efficient strain for degradation of PLA and PLA-food-packaging.

Keywords: *Bacillus* sp. SNRUSA4, biodegradation, Box-Behnken design, response surface methodology

INTRODUCTION

Plastics made from petroleum such as polyamides (nylon), polyethylene, polystyrene, and poly(vinyl chloride). are non-degradable materials which lead to the accumulation of plastic wastes in environment. Polylactic acid (PLA) is considered as an alternative plastic to reduce the environmental problem. Lactic acid (monomer of PLA) was produced through the fermentation of renewable resources and biodegradable materials (Tawakkal, et al., 2014; Muller et al., 2017). PLA is a nontoxic compound and is accepted as generally recognized as safe by FDA (Food and Drug Administration) (Tawakkal et al., 2014). PLA-food-packaging is widely used in drinking cups (Farah et al., 2016) and various food grade containers (Zhong et al., 2020). The production of PLA had increased from 140,000 tonnes per annum in 2011 to 800,000 tonnes per annum in 2020 (Mirabal et al, 2013). The PLA-food-packaging degradation depends on the environmental conditions. The degradation of PLA in natural condition (soil and sludge) spends more than 90 days (Boonmee et al., 2016). The usage rate of PLA-food-packaging is greater than the PLA degradation rate, potentially causing additional environmental problems in the future.

The PLA degradation occurs by cleavage of ester bonds between two lactic acid molecules. Hydrolytic (Elsawy et al., 2017), photolytic (Janorkar et al., 2007) and microbial degradation (Apinya et al., 2015; Liang et al., 2016; Lipsa et al., 2016; Bubpachat et al., 2018) are three recognised mechanisms of PLA degradation. Microbial degradation is one of the interesting topics of PLA degradation research, as the complete degradability of PLA does not cause any pollution to the environment (Qi et al., 2017). Karamanlioglu et al. (2014) demonstrated that PLA-food-packaging did not degrade in sterile soil and suggested that microorganisms as biocatalyst could help to degrade PLA-food-packaging. Microbial degradation of PLA-food-packaging by the two fungi, *Aspergillus ustus* and *Penicillium verrucosum* was first found by Szumigaj et al. (2008). *Streptomyces* sp. K KU215 is the first actinomycete strain for PLA-food-packaging degradation (Yottakot & Leelavatcharamas, 2019). There have been no reports on PLA-food-packaging degradation by unicellular bacteria. Thus, isolation and screening of microorganisms capable of degrading PLA-food-packaging is an interesting research.

The utilisation of Response Surface Methodology (RSM) based on Box-Behnken Design (BBD) for the optimisation of culture conditions is the currently accepted method (Khatoon & Rai, 2020). This statistical technique can provide the information of interaction between parameters (Qi et al., 2015). Moreover, the degradation of PLA and PLA-food-

packaging has been significantly increased through the use of RSM with BBD (Chaisu et al., 2012; Yottakot & Leelavatcharamas, 2019).

Therefore, the aim of this research was to screen, identify and optimise culture conditions of PLA-food-packaging-degrading bacteria. RSM with BBD was used to determine the optimal culture conditions (concentration of yeast extract (*YE*), initial pH value (pH_{mi}), temperature (*T*) and agitation speed (*AS*)) of *Bacillus* sp. SNRUSA4 growth for PLA-packaging degradation.

MATERIALS AND METHODS

Screening of PLA-food Packaging-Degrading Bacteria

PLA-food-packaging was purchased from Dairy Home Co., Ltd, Thailand. PLA-food-packaging was cut into samples of size 1 cm x 1 cm, then PLA-food-packaging coupons was washed with 70% (v/v) ethanol and allowed to air-dry until completely dry. The samples were collected from soils and composts to isolate the PLA-packaging-degrading bacteria. These samples were kept at 4°C until required.

The sterile Basal Medium (BM) (pH 7.0) was prepared by adding 4 g of $(\text{NH}_4)_2\text{SO}_4$, 2 g of K_2HPO_4 , 2 g of KH_2PO_4 and 0.5 g of $\text{MgSO}_4 \cdot 7\text{H}_2\text{O}$ to 1 L of distilled water, and then autoclaved at 121°C for 15 minutes. The sterile BM was added 1 g of PLA-food-packaging coupons as sole carbon source.

In order to isolate PLA-food packaging degrading bacteria, 10 g of the samples was inoculated into 250 mL Erlenmeyer flask with 100 mL of sterilised BM containing 1 g of PLA-food-packaging coupons. The inoculated flask was incubated at 37°C and 180 rpm in an incubator shaker for 7 days. After incubation, 10 mL of the culture was inoculated into sterilised BM containing 1 g of PLA-food-packaging coupon as sole carbon source. This experiment was performed five times with the same method. Then, each of the PLA-food-packaging coupons was transferred onto BM agar plates. The plates were incubated at 37°C for 7 days (Yottakot & Leelavatcharamas, 2019). The colonies around PLA-food-packaging coupons were purified by streak plate technique on Nutrient Agar (NA) plate. The purified isolates were stored on NA slant at 4°C and in 30% glycerol at -10°C.

PLA-food packaging-degrading bacteria was screened by analysing the growth in the sterile BM containing 1 g of PLA-food-packaging coupons as sole carbon source using the optical density (OD) at wavelength 600 nm (Lee et al., 2013). The cell suspension of selected stains was transferred to Nutrient Broth (NB) medium and shaken at 180 rpm at 37°C for 24 hours, and then centrifuged for 10 min at 5,635 x g. The precipitated cells were washed twice with 0.85% (w/v) NaCl. The cell density was adjusted to $\text{OD}_{600} = 1.0$ with 0.85% (w/v) NaCl. The optical density was measured by spectrophotometer. Cell suspension (10 mL) of each isolate was inoculated into 100 mL of the sterile BM containing 1 g of PLA-food-packaging coupons as sole carbon source, and then incubated at 37°C and 180

rpm in an incubator shaker. The cell density was measured every week for 4 weeks. The sterilised BM, BM containing 1 g of PLA-food packaging coupons and BM with the cell were used as controls. The experiment was done in triplicate.

SNRUSA4, PLA-food-packaging-degrading bacterial strain was screened because of the increasing OD. The ability of SNRUSA4 to degrade PLA-food-packaging coupons was measured after 4 weeks of incubation by analysing weight loss and surface changes of the individual samples in the sterilised BM containing 1 g of PLA-food-packaging coupons as sole carbon source. The original PLA-food-packaging coupons and PLA-food-packaging coupons in BM without inoculation of SNRUSA4 after 4 weeks of incubation were used as controls.

Degradation of PLA-food-packaging coupons was assessed by measuring weight loss. The PLA-food-packaging coupons was washed with distilled water, and dried until constant weight in an electronic desiccator. The weight loss percentage of PLA-food-packaging coupons was calculated according to Equation 1 (Vey et al., 2007).

$$\% \text{ Weight loss} = \frac{m_{ini} - m_{dry}}{m_{ini}} \times 100\% \quad [1]$$

where m_{ini} is the initial weight of original PLA-food-packaging coupon; m_{dry} is the dry weight of PLA-food-packaging coupon after degrading.

The change in surface morphology of the PLA-food-packaging coupon was checked after 4 weeks of incubation by Scanning Electron Microscope (SEM) (SEC, model SNE-4500M). The PLA-food-packaging coupons were coated with gold before SEM examination.

The pure PLA degradability of PLA-food-packaging-degrading bacterial strain SNRUSA4 was confirmed by the clear zone around bacterial strain SNRUSA4 colony on emulsified PLA agar plate after 2 weeks of incubation at 37°C. PLA pellet (2003D grade, melting temperature 210°C, average molecular weight 200,000 g/mol) was obtained from NatureWorks LLC (U.S.A.). Emulsified PLA agar was prepared as follows by the method of Yottakot & Leelavatcharamas (2019).

Identification of Selected Strain

The PLA-food-packaging-degrading bacterial isolate SNRUSA4 was identified on the basis of 16S rRNA gene sequence analysis. DNA of SNRUSA4 was extracted using DNA mini kit (Geneaid Biotech Ltd., Taiwan). The 16S rRNA gene was amplified from the genomic DNA by PCR using the two primers, 20F and 1500R (Brosius et al., 1981). PCR was performed using a Taq polymerase (Cinnagen, Iran). The PCR program using following cycling step, initial denaturation at 96°C for 3 min, and then 25 cycles with denaturation at 94°C for 1 min, 50°C for 1 min, 72°C for 2 min. A final extension was performed at 72°C for 3 min.

The PCR product was purified through 1.0 % agarose gel using the GenepHlow™ Gel/PCR Kit (Geneaid). DNA sequencing of the purified PCR products was carried out on an ABI Prism® 3730XL DNA Sequence (Applied Biosystems, Foster City, California, USA). The sequences were aligned using program CLUSTAL X (version 1.8) (Thompson, 1997) in BioEdit program (Hall, 1999). Phylogenetic trees were reconstructed by the neighbor-joining method (Saitou & Nei, 1987) and maximum-likelihood (Felsenstein, 1985) tree-making algorithms by using the MEGA version 6.0 (Tamura et al., 2013).

Optimisation of *Bacillus* sp. SNRUSA4 Growth Conditions for PLA-food-packaging Degradation using Statistical Design

The optimisation of *Bacillus* sp. SNRUSA4 growth conditions for enhancement of degradation of PLA-food-packaging was investigated. RSM based on BBD was used to design and optimise the culture condition of *Bacillus* sp. SNRUSA4 by Design-Expert® Software Version 10 (Trial Version). *YE* concentration, pH_{ini} , T and AS were optimised in this research. The suitable ranges of each factor for RSM were selected based on the preliminary single factor experiments. The ranges of four independent variables including *YE* concentration (0.2-3.0 %), pH_{ini} (4.0-10.0), T (27-47°C) and AS (150-250 rpm) are shown in Table 1. The OD of *Bacillus* sp. SNRUSA4 was examined after 2 days of incubation.

Table 1
Coded and levels of factors in BBD

Independent variables	Code	Levels		
		-1	0	1
<i>YE</i> concentration (%)	X_1	0.2	1.6	3.0
pH_{ini}	X_2	4.0	7.0	10.0
T (C)	X_3	27	37	47
AS (rpm)	X_4	150	200	250

The results of optimisation were confirmed by OD after 2 days of cultivation and degradation of PLA-food-packaging after 4 weeks of cultivation under the optimal conditions based on the results of RSM.

RESULTS AND DISCUSSION

Screening of PLA-food-packaging-degrading Bacteria

Only one bacterial strain, SNRUSA4 revealed increasing OD at 0.203 in BM with PLA-food-packaging as sole carbon source after 4 weeks of cultivation (Figure 1). In contrast, the OD of all controls (the sterile BM, the sterile BM containing 1 g of PLA-food-packaging coupons and the sterile BM with SNRUSA4) did not increase after 4 weeks of cultivation (Figure 1). SNRUSA4 could grow in the BM medium with PLA-food-packaging coupons

which indicated that it was able to degrade the PLA-food-packaging material as a carbon source. The increase of cell density in BM medium supplemented with a bioplastic as a carbon source could indicate the capability of microbe to degrade bioplastic (Jeon & Kim, 2013; Lee et al., 2013; Yottakot & Leelavatcharamas, 2019).

The bacterial strain SNRUSA4 was isolated from compost. This result is also consistent with the study of Kim & Park (2010) and Jeon & Kim (2013). Kim & Park (2010) could isolate PLA-degrading bacteria, *Bordetella petrii* PLA-3 from compost. Jeon & Kim (2013) found *Stenotrophomonas maltophilia* LB 2-3 from compost which could degrade PLA. Therefore, compost is a suitable bacterial source sample to isolate and screening the PLA-degrading bacteria.

The PLA-food-packaging coupons had a weight loss of $7.30 \pm 0.11\%$ after degradation by SNRUSA4 for 4 weeks. The weight loss of PLA-food-packaging coupons did not decrease in the absence of bacterial cells. The weight loss can be applied to measure degradation of the plastics (Muhonja et al., 2018). Although, the SNRUSA4 strain can degrade the PLA-food-packaging coupon, the PLA-food-packaging degradation of this strain seems to be very low. The increasing nutrients such as YE and gelatin in BM medium can lead to an increase in PLA degradability of microorganism (Jarerat & Tokiwa, 2003; Jarerat et al., 2003; Konkit et al., 2012; Zhou et al., 2017; Bubpachet et al., 2018; Yottakot & Leelavatcharamas, 2019; Decorosi et al., 2019). Thus, the optimisation of culture conditions is essential for the degradation of PLA-food-packaging.

The scanning electron micrographs of the PLA-food-packaging coupons before and after 4 weeks of degradation are shown in Figure 2. There was no significant difference between the surface of PLA-food-packaging coupons before degradation (Figure 2a) and

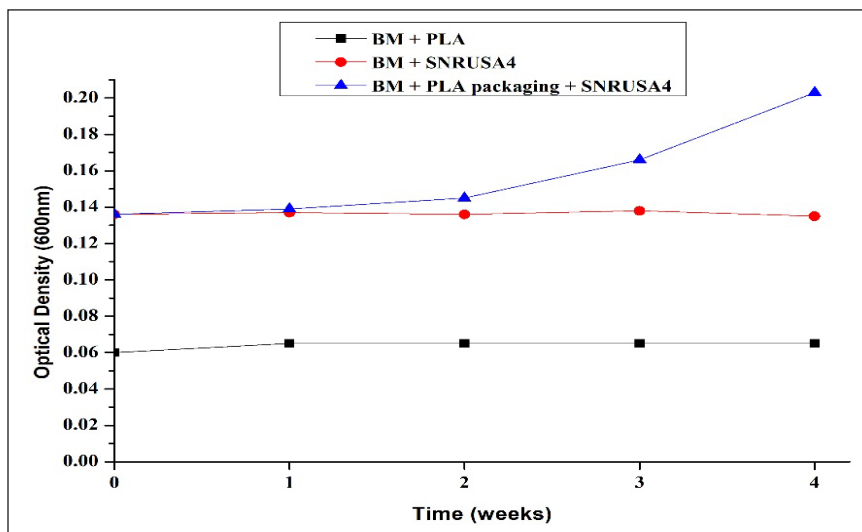


Figure 1. The increase in cell density of strain SNRUSA4 after incubated in the sterile BM medium containing PLA-food-packaging for 4 weeks

the surface of PLA-food-packaging coupons after degradation in BM medium without inoculation of SNRUSA4 (Figure 2b). Figure 2c showed the roughness and porosity on the surface of the PLA-food-packaging coupons after degradation in BM medium with inoculation of SNRUSA4. This finding is similar to the result of Kim et al. (2017) evaluating the morphological changes in the surface of PLA film after the degradation by using SEM.

The standard clear zone method was commonly used to analyse the PLA degradation by microorganism (Liang et al., 2016; Bubpachat et al., 2018; Butbunchu & Pathom-Aree, 2019). The clear zone formation around the colony was formed by microbe able to degrade suspended PLA in emulsified PLA agar medium. This method is therefore applicable for the confirmation of PLA degradation by PLA-food-packaging-degrading bacterial strain SNRUSA4. SNRUSA4 could degrade PLA in emulsified PLA agar plate due to the clear zone formation around the colony within 2 weeks of incubation at 37°C (Figure 3). The microorganisms can produce enzymes to degrade the biopolymers (Penkhrue et al., 2015;

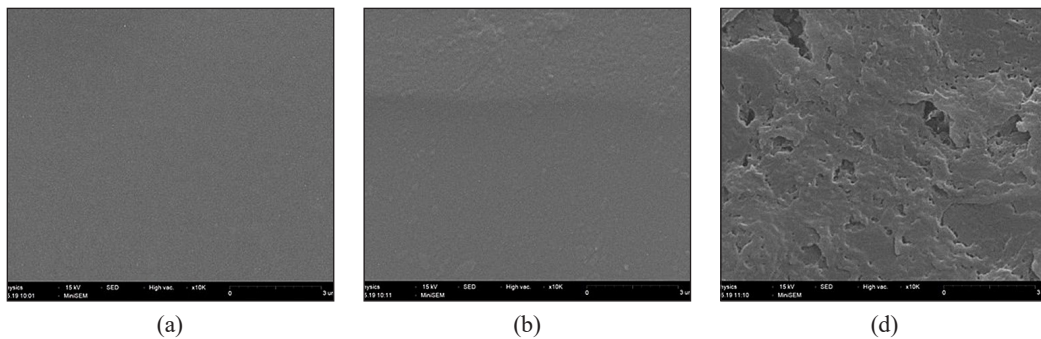


Figure 2. SEM micrographs of the surface of PLA-food-packaging coupons: (a) the surface before degradation; (b) the surface after incubation in BM medium without the strain; and (c) after the SNRUSA4 strain degradation

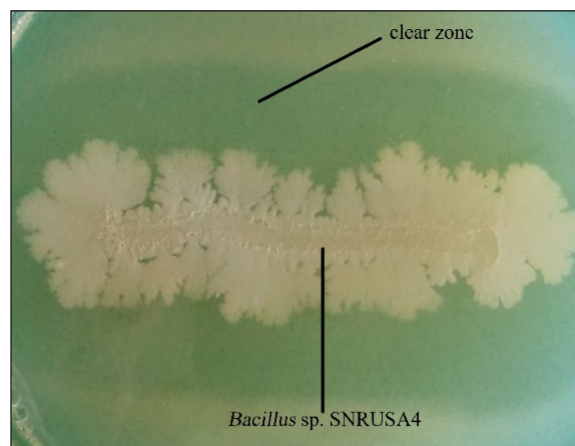


Figure 3. Clear zone formation by *Bacillus* sp. SNRUSA4 on emulsified PLA agar after 2 weeks of incubation at 37°C

Phukon et al., 2012). The formation of clear zone around SNRUSA4 colonies indicates that SNRUSA4 can use PLA as sole carbon source for growth.

Identification of SNRUSA4 Strain

The 16S rDNA sequence of the SNRUSA4 strain is related to more than 99% with the genus *Bacillus*. This isolate is named as *Bacillus* sp. SNRUSA4 (Figure 4). The 16S rDNA sequence of *Bacillus* sp. SNRUSA4 showed similarity with *Bacillus methylotrophicus* KACC 13105 (99.93%), *Bacillus siamensis* KCTC 13613 (99.85%), *Bacillus amyloliquefaciens* subsp. *plantarum* FZB42 (99.78%), *Bacillus subtilis* subsp. *subtilis* NCIB 3610 (99.70%), *Bacillus amyloliquefaciens* subsp. *amyloliquefaciens* DSM 7 (99.63%), *Bacillus subtilis* subsp. *inaquosorum* KCTC 13429 (99.63%), *Bacillus tequilensis* KCTC 13622 (99.63%), *Bacillus vallismortis* DV1-F-3 (99.55%), *Bacillus atrophaeus* JCM 9070 (99.48%), *Bacillus subtilis* subsp. *spizizenii* NRRL B-23049 (99.48%), *Brevibacterium halotolerans* DSM 8802 (99.48%), *Bacillus mojavensis* RO-H-1 (99.41%) and *Bacillus vanillea* XY18 (99.40%). The 16S rDNA sequence of *Bacillus* sp. SNRUSA4 was submitted in the GenBank database

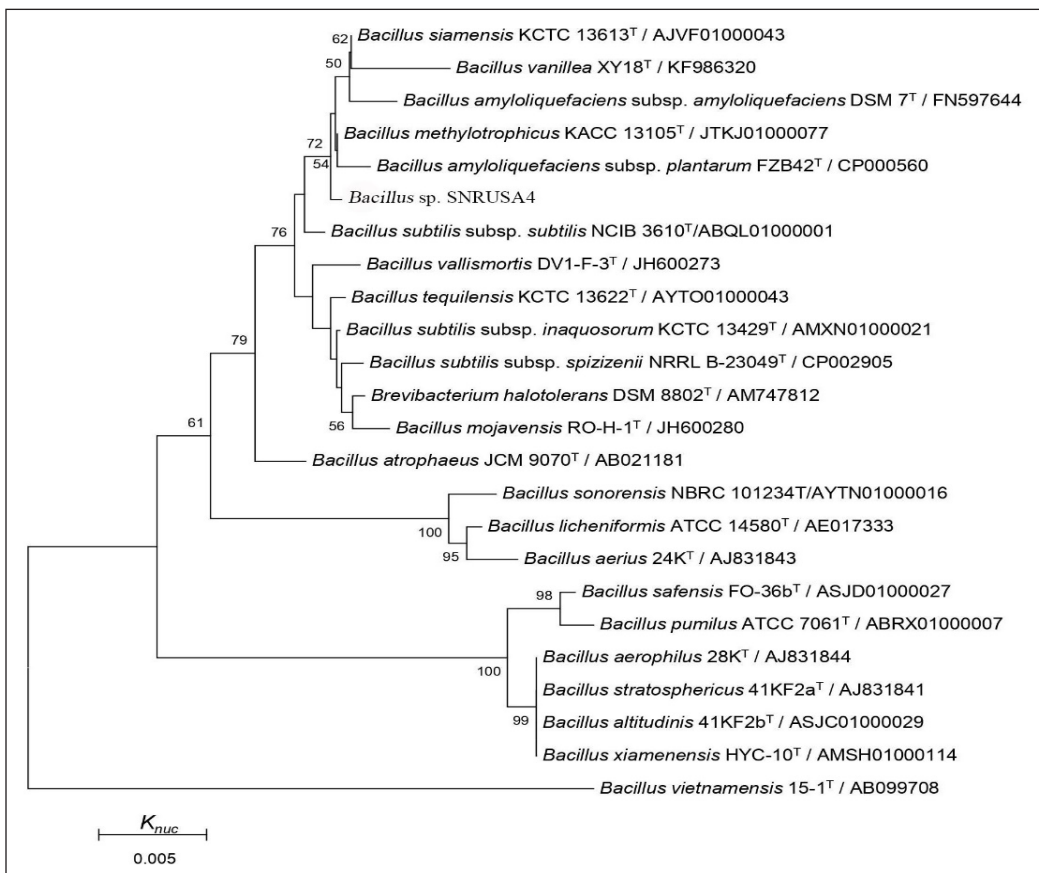


Figure 4. Phylogenetic tree of strain SNRUSA4 and related species of the genus *Bacillus*

system with the accession number MT913031. All of thirteen *Bacillus* species have not been reported yet to being able to degrade PLA. Therefore, *Bacillus* sp. SNRUSA4 is a novel species for PLA and PLA-food-packaging degradation.

Optimization of Growth Conditions by *Bacillus* sp. SNRUSA4

The four factors including YE concentration (%) (X_1), pH_{ini} (X_2), T ($^{\circ}C$) (X_3) and AS (rpm) (X_4) were optimised by RSM using BBD. Twenty-eight experiments with three levels of each factor and its responses are shown in Table 2.

Table 2

Experimental conditions of Box Behnken design for Bacillus sp. SNRUSA4 growth

Run No.	YE concentration (%)	pH_{ini}	T ($^{\circ}C$)	AS (rpm)	Optical Density (600nm)	
					Experiment	Predicted
1	3.0	7	37	250	1.912	1.687
2	0.2	4	37	200	0.007	-0.247
3	1.6	10	27	200	0.034	0.125
4	1.6	10	37	150	0.079	0.073
5	1.6	7	37	200	1.849	1.787
6	3.0	7	37	150	1.666	1.501
7	0.2	7	47	200	0.711	1.029
8	1.6	7	47	150	0.740	0.888
9	1.6	4	47	200	0.009	-0.268
10	1.6	7	27	150	1.545	1.503
11	0.3	10	37	200	0.029	0.242
12	0.2	7	37	250	1.250	1.228
13	1.6	10	47	200	0.011	-0.255
14	1.6	4	37	250	0.009	0.241
15	1.6	7	47	250	1.324	1.325
16	0.2	10	37	200	0.003	-0.232
17	1.6	7	27	250	1.638	1.449
18	3.0	4	37	200	0.014	0.208
19	1.6	7	37	200	1.743	1.787
20	3.0	7	27	200	1.953	1.863
21	0.2	7	27	200	0.621	0.772
22	1.6	4	27	200	0.010	0.900
23	0.2	7	37	150	0.991	1.030
24	1.6	7	37	200	1.819	1.787
25	3.0	7	47	200	0.794	0.868
26	1.6	10	37	250	0.051	0.253
27	1.6	7	37	200	1.738	1.787
28	1.6	4	37	150	0.014	0.037

The results of the experimentation obtained from BBD were fitted to a second order polynomial model to explain the dependence of *Bacillus* sp. SNRUSA4 growth on the four factors. The response surface regression model is shown as Equation 2:

$$\begin{aligned}
 Y = & - 13.47006 + (1.47093X_1) + (2.35354X_2) + (0.23731X_3) + \\
 & (0.014561X_4) + (0.00113095X_1X_2) - (0.022357X_1X_3) - (0.0000464286X_1X_4) - \\
 & (0.000183333X_2X_3) - (0.0000383333X_2X_4) + (0.0002455X_3X_4) - (0.14887X_1^2) \\
 & - (0.16692X_2^2) - (0.00361917X_3^2) - (0.00005.34667X_4^2) \quad [2]
 \end{aligned}$$

where Y is the predicted OD, and X_1 , X_2 , X_3 and X_4 are the independent variables of YE concentration, pH_{ini} , T and AS , respectively.

The significance and adequacy of the quadratic response surface model was tested by analysis of variance (ANOVA). The results of the second order response surface model fitting in the form of ANOVA are given in Table 3. Even though, the lack of fit was significant (0.0120), the response surface regression model was highly significant with P-value <0.0001 and F-value = 19.33. In addition, the coefficient of determination R^2 (0.9542) and the adjusted coefficient of determination R^2 (0.9048) were also found acceptable (> 0.90) (Chen et al., 2009), which indicated the suitability of the response surface regression model for accurate prediction and analysis of *Bacillus* sp. SNRUSA4 growth.

The linear effect of YE concentration and T showed significant impact on OD of *Bacillus* sp. SNRUSA4 with P-value of 0.0052 and 0.0194, respectively. The quadratic effect of YE concentration (p-value = 0.0106), pH_{ini} (p-value <0.0001) and T (p-value = 0.0027) presented great influence on the cell density, indicating that the effect of various factors on OD of *Bacillus* sp. SNRUSA4 was not a simple linear relationship but a significant surface relationship (Yun et al., 2018). There is an interaction between YE concentration and T because the interaction effect between two factors was significant.

RSM was used to predict the optimal culture conditions of *Bacillus* sp. SNRUSA4. The three-dimensional (3D) response surface plots were generated from regression equation by considering two test variables at one time, while the other two variables were maintained at their middle level. The relationship between the variables and response was visualised through 3D response surface or contour plot to analyse the effects of each factors on the growth of *Bacillus* sp. SNRUSA4. The optimal level of each factor for maximal response, the impact of independent factors and the impact of interaction effect of each factor were determined with the aid of 3D response surface plots. The 3D response surface plots and contour plots are demonstrated in Figure 5(A-F). The shape of 3D response surface plots was convex, which indicated that the well-defined optimal variables were found.

Table 3
 Analysis of variance (ANOVA) for BBD results used for optimizing growth by *Bacillus* sp. SNRUSA4

Source	SS	df	MS	F-value	P-value
Model	15.56	14	1.11	19.33	<0.0001
YE concentration	0.65	1	0.65	11.27	0.0052
pH_{ini}	0.001728	1	0.001728	0.030	0.8650
T	0.41	1	0.41	1.91	0.0194
AS	0.11	1	0.11	0.280	0.1899
YE concentration * pH_{ini}	0.00009025	1	0.00009025	0.00157	0.9690
YE concentration * T	0.39	1	0.39	6.82	0.0216
YE concentration * AS	0.00004225	1	0.00004225	0.0007348	0.9788
pH_{ini} * T	0.000121	1	0.000121	0.002105	0.9641
pH_{ini} * AS	0.0001323	1	0.0001323	0.0023	0.9625
T * AS	0.060	1	0.060	1.05	0.3246
YE concentration * YE concentration	0.51	1	0.51	8.89	0.0106
pH_{ini} * pH_{ini}	13.54	1	13.54	235.52	<0.0001
T * T	0.79	1	0.79	13.67	0.0027
AS * AS	0.11	1	0.11	1.86	0.1953
Lack of Fit	0.74	10	0.074	24.06	0.0120
Pure Error	0.009205	3	0.003068		
Cor Total	16.30	27			

$R^2 = 0.9542$
 Adjusted $R^2 = 0.9048$
 Predicted $R^2 = 0.7382$

YE is one of the important factors for the optimisation of the growth conditions. It is a complex organic nitrogen source not only contain nitrogen but also certain vitamin B, sulphur, and trace nutrients, and widely used as an ingredient in the media for microorganism cultivation (Kalil et al., 2008). As shown in Figure 5(A), (B) and (C), when we increased the concentration of YE up to 2.56%, a maximal growth of *Bacillus* sp. SNRUSA4 was observed. The results of this study indicate that YE is a necessary factor for *Bacillus* growth and are similar to other *Bacillus* spp. such as *Bacillus licheniformis* (Hassaan et al., 2014), *Bacillus subtilis* SF4-3 (Tian et al., 2016), *Bacillus* sp. (Biniarz et al., 2018) and *Bacillus aryabhatai* KIIT BE-1 (Ojha et al., 2020).

The pH_{ini} of culture medium plays significant role in bacterial growth. It was clear from Fig. 5(B), (D) and (E) that the medium with pH 7.02 was found to be the best pH_{ini} providing the highest *Bacillus* sp. SNRUSA4 growth. The optimal pH of most *Bacillus* was discovered at neutral pH such as *Bacillus megaterium* (Mohanrasu et al., 2020), *Bacillus cereus* sp. BNPI-92 (Mohammed et al., 2019) and *Bacillus subtilis* (Kim et al., 2020).

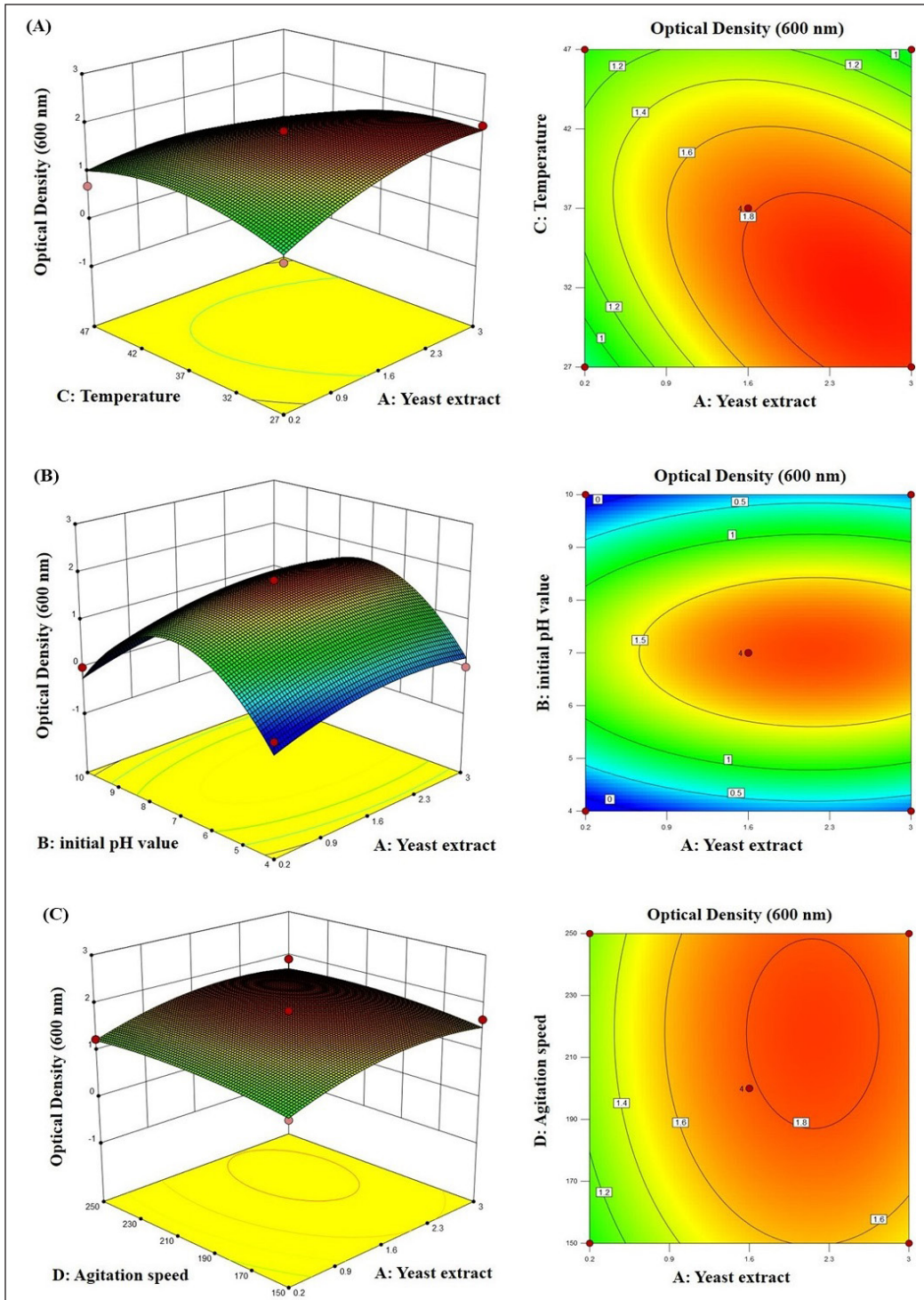


Figure 5. The 3D plots and contour plots showing the effect of (A) YE concentration and T , (B) YE concentration and pH_{ini} , and (C) YE concentration and AS

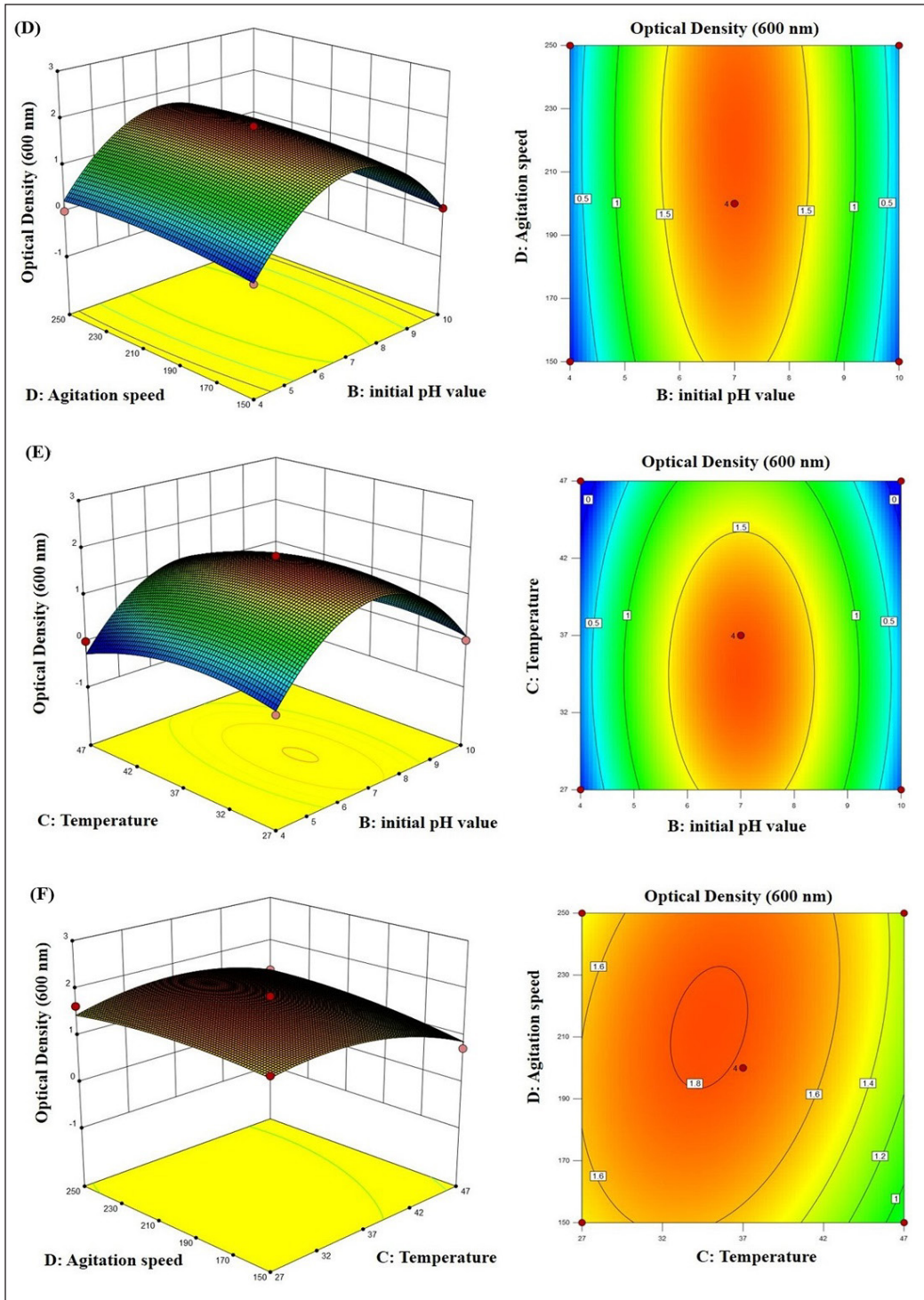


Figure 5. (continue) The 3D plots and contour plots showing the effect of (D) pH_{ini} and AS, (E) pH_{ini} and T , (F) T and AS.

T is an important environmental variable in microbial culture influencing enzyme activity, metabolite production and microbial growth (Logan & Vos, 2015). The optimal T of *Bacillus* sp. SNRUSA4 from the response surface analysis was 31.68°C [Figures 5(A), (E) and (F)]. *Bacillus* spp. are mesophilic bacteria that grow best at optimal T range of 30-37°C. (Khatoun & Rai, 2020; Naskar et al., 2020; Kim et al., 2020).

The AS directly affects the oxygen transfer rate (OTR), a parameter that plays an important role in metabolism of aerobic *Bacillus* spp. (Bratcher, 2018). The AS of 205.28 rpm was optimal AS for *Bacillus* sp. SNRUSA4 cultivation [Figure 5(C), (D) and (F)]. This result conforms with a previous report by Unrean et al. (2012) who found that the highest cell density of *Bacillus subtilis* K-C3 was achieved at AS of 200 rpm.

In conclusion, the predicted optimal conditions of YE concentration, pH_{ini} , T and AS from the response surface curves and contour plots were 2.56%, 7.02, 31.68°C and 205.28 rpm, respectively. At these conditions, predicted OD of *Bacillus* sp. SNRUSA4 was 1.921 (Table 4).

Table 4
The optimal values of test factors, and predicted maximum optical density

Variables	Value
YE concentration (%)	2.56
pH_{ini}	7.02
T (°C)	31.68
AS (rpm)	205.28
predicted maximum optical density	1.921

The verification experiment was carried out under the optimal conditions based on the results of RSM for the model validation. The OD after 2 days of cultivation and PLA-food-packaging degradation after 4 weeks of cultivation were investigated to confirm the accurate optimisation results. The predicted OD (1.921) was close to the OD of *Bacillus* sp. SNRUSA4 at optimal conditions (1.955). The result of this experiment proved that the model is reasonable. Moreover, regarding the PLA-food-packaging degradation, the weight loss of PLA-food-packaging under the optimal conditions by *Bacillus* sp. SNRUSA4 had greatly increased, up to 87.10±0.16%.

CONCLUSION

Bacillus sp. SNRUSA4 was discovered in this study as a novel PLA-food-packaging-degrading bacteria that could degrade both PLA and PLA-food-packaging. The optimal conditions from RSM based on BBD were YE concentration of 2.56%, pH 7.02, incubation T of 31.68°C and AS of 205.28 rpm. Under these conditions, the OD was found at 1.955, which was 1.752 more than that before optimisation (0.203). Furthermore, the degradation

of PLA-food-packaging under optimal conditions was also higher than before optimisation due to the increasing weight loss of PLA-food-packaging. The degradation of PLA-food-packaging under optimal conditions was almost twelve times greater than before the optimisation. Based on the current study, *Bacillus* sp. SNRUSA4 is a promising strain for the degradation of PLA-food-packaging. The degradation of PLA-food-packaging by *Bacillus* sp. SNRUSA4 in its natural state should be further studied.

ACKNOWLEDGEMENTS

This research was supported by the instrument used for study from Sakon Nakhon Rajabhat University, Thailand.

REFERENCES

- Apinya, T., Sombatsompop, N., & Prapagdee, B. (2015). Selection of a *Pseudonocardia* sp. RM423 that accelerates the biodegradation of poly (lactic) acid in submerged cultures and in soil microcosms. *International Biodeterioration and Biodegradation*, *99*, 23-30. doi: 10.1016/j.ibiod.2015.01.001
- Biniarz, P., Coutte, F., Gancel, F., & Łukaszewicz, M. (2018). High-throughput optimization of medium components and culture conditions for the efficient production of a lipopeptide pseudofactin by *Pseudomonas fluorescens* BD5. *Microbial Cell Factories*, *17*(1), 1-18. doi: 10.1186/s12934-018-0968-x
- Boonmee, C., Kositanont, C., & Leejarkpai, T. (2016). Degradation of poly (lactic acid) under simulated landfill conditions. *Environment and Natural Resources Journal*, *14*(2), 1-9. doi: 10.14456/ennrj.2016.8
- Bratcher, D. F. (2018). *Bacillus* species (Anthrax). In S. S. Long, C. G. Prober & M. Fischer (Eds.), *Principles and Practice of Pediatric Infectious Diseases* (pp. 770-773). Philadelphia, PA: Elsevier. doi: 10.1016/b978-0-323-40181-4.00129-8
- Brosius, J., Dull, T. J., Sleeter, D. D., & Noller, H. F. (1981). Gene organization and primary structure of a ribosomal RNA operon from *Escherichia coli*. *Journal of Molecular Biology*, *148*(2), 107-127. doi: [https://doi.org/10.1016/0022-2836\(81\)90508-8](https://doi.org/10.1016/0022-2836(81)90508-8)
- Bubpachat, T., Sombatsompop, N., & Prapagdee, B. (2018). Isolation and role of polylactic acid-degrading bacteria on degrading enzymes productions and PLA biodegradability at mesophilic conditions. *Polymer Degradation and Stability*, *152*, 75-85. doi: 10.1016/j.poly.mdegradstab.2018.03.023
- Butbunchu, N., & Pathom-Aree, W. (2019). Actinobacteria as promising candidate for polylactic acid type bioplastic degradation. *Frontiers in Microbiology*, *10*, 1-10. doi: 10.3389/fmicb.2019.02834
- Chaisu, K., Charles, A. L., Guu, Y. K., & Chiu, C. H. (2012). Optimization of polylactic acid (PLA) plastic degradation by *Aneurinibacillus migulanus* using response surface methodology. In *International Conference on Biological and Life Sciences* (pp. 22-27). Singapore: International Association of Computer Science and Information Technology (IACSIT) Press.
- Chen, X. C., Bai, J. X., Cao, J. M., Li, Z. J., Xiong, J., Zhang, L., ... & Ying, H. J. (2009). Medium optimization for the production of cyclic adenosine 3', 5'-monophosphate by *Microbacterium* sp. no. 205 using

- response surface methodology. *Bioresource Technology*, *100*(2), 919-924. doi: <https://doi.org/10.1016/j.biortech.2008.07.062>
- Decorosi, F., Exana, M. L., Pini, F., Adessi, A., Messini, A., Luciana Giovannetti, L., & Viti, C. (2019). The degradative capabilities of new *Amycolatopsis* isolates on polylactic acid. *Microorganisms*, *7*(590), 1-18. doi: [10.3390/microorganisms7120590](https://doi.org/10.3390/microorganisms7120590)
- Elsawy, M. A., Kim, K., Park, J., & Deep, A. (2017). Hydrolytic degradation of polylactic acid (PLA) and its composites. *Renewable and Sustainable Energy Reviews*, *79*, 1346-1352. doi: <https://doi.org/10.1016/j.rser.2017.05.143>
- Farah, S., Anderson, D. G., & Langer, R. (2016). Physical and mechanical properties of PLA, and their functions in widespread applications - A comprehensive review. *Advanced Drug Delivery Reviews*, *107*, 367-392. doi: [10.1016/j.addr.2016.06.012](https://doi.org/10.1016/j.addr.2016.06.012)
- Felsenstein, J. (1985). Confidence limits on phylogenies: An approach using the bootstrap. *Evolution*, *39*, 783-791. doi: [10.1111/j.1558-5646.1985.tb00420.x](https://doi.org/10.1111/j.1558-5646.1985.tb00420.x)
- Hall, T. A. (1999). BioEdit: A user-friendly biological sequence alignment editor and analysis program for Windows 95/98/NT. *Nucleic Acids Symposium Series*, *41*, 95-98.
- Hassaan, M. S., Soltan, M. A., & Ghonemy, M. M. R. (2014). Effect of synbiotics between *Bacillus licheniformis* and yeast extract on growth, hematological and biochemical indices of the Nile tilapia (*Oreochromis niloticus*). *The Egyptian Journal of Aquatic Research*, *40*(2), 199-208. doi: [10.1016/j.ejar.2014.04.001](https://doi.org/10.1016/j.ejar.2014.04.001)
- Janorkar, A. V., Metters, A. T., & Hirt, D. E. (2007). Degradation of poly(L-lactide) films under ultraviolet-induced photografting and sterilization conditions. *Journal of Applied Polymer Science*, *106*(2), 1042-1047. doi: <https://doi.org/10.1002/app.24692>
- Jarerat, A., & Tokiwa, Y. (2003). Poly (L-lactide) degradation by *Saccharothrix waywayandensis*. *Biotechnology Letters*, *25*(5), 401-404. doi: [10.1023/a:1022450431193](https://doi.org/10.1023/a:1022450431193)
- Jarerat, A., Tokiwa, Y., & Tanaka, H. (2003). Poly (L-lactide) degradation by *Kibdelosporangium aridum*. *Biotechnology Letters*, *25*(23), 2035-2038. doi: [10.1023/b:bile.00000004398.38799.29](https://doi.org/10.1023/b:bile.00000004398.38799.29)
- Jeon, J. H., & Kim, N. M. (2013). Biodegradation of poly(L-lactide) (PLA) exposed to UV irradiation by a mesophilic bacterium. *International Biodeterioration and Biodegradation*, *85*, 289-293. doi: [10.1016/j.jibiod.2013.08.013](https://doi.org/10.1016/j.jibiod.2013.08.013)
- Kalil, M. S., Alshiyab, H. S., & Yusoff, W. M. W. (2008). Effect of nitrogen source and carbon to nitrogen ratio on hydrogen production using *C. acetobutylicum*. *American Journal of Biochemistry and Biotechnology*, *4*(4), 393-401. doi: [10.3844/ajbbbsp.2008.393.401](https://doi.org/10.3844/ajbbbsp.2008.393.401)
- Karamanlioglu, M., Houlden, A., & Robson, G. D. (2014). Isolation and characterisation of fungal communities associated with degradation and growth on the surface of poly(lactic) acid (PLA) in soil and compost. *International Biodeterioration and Biodegradation*, *95*, 301-310. doi: [10.1016/j.jibiod.2014.09.006](https://doi.org/10.1016/j.jibiod.2014.09.006)
- Khatoon, H., & Rai, J. P. N. (2020). Optimization studies on biodegradation of atrazine by *Bacillusadius* ABP6 strain using response surface methodology. *Biotechnology Reports*, *26*, 1-10. doi: [10.1016/j.btre.2020.e00459](https://doi.org/10.1016/j.btre.2020.e00459)

- Kim, M. N., & Park, S. T. (2010). Degradation of poly (L-lactide) by a mesophilic bacterium. *Journal of Applied Polymer Science*, 117, 67-74. doi: 10.1002/app.31950
- Kim, M. Y., Kim, C., Moon, J., Heo, J., Jung, S. P., & Kim, J. R. (2017). Polymer film-based screening and isolation of polylactic Acid (PLA)- degrading microorganisms. *Journal of Microbiology and Biotechnology*, 27(2), 342-349. doi: [https://doi.org/ 10.4014/jmb.1610.10.015](https://doi.org/10.4014/jmb.1610.10.015)
- Kim, O. Y., Mahboob, S., Viayaraghavan, P., Biji, D., Ghanim, A. A. K., Misned, A. F., ... & Kim, H. J. (2020). Growth promoting activity of *Penaeus indicus* by secondary metabolite producing probiotic bacterium *Bacillus subtilis* isolated from the fish gut. *Journal of King Saud University-Science*, 32(2), 1641-1646. doi: 10.1016/j.jksus.2019.12.023
- Konkit, M., Jarerat, A., Khanongnuch, C., Lumyong, S., & Pathom-aree, W. (2012). Poly(lactide) degradation by *Pseudonocardia alni* AS4.1531(T). *Chiang Mai Journal of Science*, 39(1), 128-132.
- Lee, J. S., Park, H. E., Han, H. Y., Kim, O. Y., & Park, W. S. (2013). Isolation of a marine bacterium capable of biodegrading poly (butylene succinate). *Journal of Fisheries and Aquatic Sciences*, 16(1), 41-44. doi: 10.5657/FAS.2013.0041
- Liang, T. W., Jen, S. N., Nguyen, A. D., & Wang, S. L. (2016). Application of chitinous materials in production and purification of a poly (L-lactic acid) depolymerase from *Pseudomonas tamsuii* TKU015. *Polymers*, 8(98), 1-11. doi: 10.3390/polym8030098
- Lipsa, R., Tudorachi, N., Darie-Nita, R. N., Oprică, L., Vasile, C., & Chiriac, A. (2016). Biodegradation of poly (lactic acid) and some of its based systems with *Trichoderma viride*. *International Journal of Biological Macromolecules*, 88, 515-526. doi: 10.1016/j.ijbiomac.2016.04.017
- Logan, N. A., & Vos, P. D. (2015). *Bacillus*. In W. B. Whitman (Ed.), *Bergey's manual of systematics of archaea and bacteria* (pp. 1-163). Hoboken, NJ: John Wiley & Sons, Inc. doi: 10.1002/9781118960608.gbm.00530
- Mirabal, A. S., Scholz, L., & Carus, M. (2013). *Bio-based polymers in the world capacities, production and applications: Status quo and trends towards 2020*. Retrieved August 19, 2020, from http://bio-based.eu/market_study/media/files/13-06_21MSBiopolymersExcerpt.pdf
- Mohammed, S., Behera, H. T., Dekebo, A., & Ray, L. (2019). Optimization of the culture conditions for production of polyhydroxyalkanoate and its characterization from a new *Bacillus cereus* sp. BNPI-92 strain, isolated from plastic waste dumping yard. *International Journal of Biological Macromolecules*, 156, 1064-1080. doi: 10.1016/j.ijbiomac.2019.11.138
- Mohanrasu, K., Rao, R. G. R., Dinesh, G. H., Zhang, K., Prakash, G. S., Song, D. P., ... & Arun, A. (2020). Optimization of media components and culture conditions for polyhydroxyalkanoates production by *Bacillus megaterium*. *Fuel*, 271, 1-9. doi: 10.1016/j.fuel.2020.117522
- Muhonja, C. N., Makonde, H., Magoma, G., & Imbuga, M. (2018). Biodegradability of polyethylene by bacteria and fungi from Dandora dumpsite Nairobi-Kenya. *PLoS One*, 13(7), 1-17. doi: 10.1371/journal.pone.0198446
- Muller, J., González-Martínez, C., & Chiralt, A. (2017). Combination of poly (lactic) acid and starch for biodegradable food packaging. *Materials*, 10(952), 1-22. doi: 10.3390/ma10080952

- Naskar, A., Majumder, R., & Goswami, M. (2020). Bioaccumulation of Ni(II) on growing cells of *Bacillus* sp. response surface modeling and mechanistic insight. *Environmental Technology and Innovation*, 20, 1-39. doi: 10.1016/j.eti.2020.101057
- Ojha, S. K., Singh, P. K., Mishra, S., Pattnaik, R., Dixit, S., & Verma, S. K. (2020). Response surface methodology based optimization and scale-up production of amylase from a novel bacterial strain, *Bacillus aryabhatai* KIIT BE-1. *Biotechnology Reports*, 27, 1-9. doi: 10.1016/j.btre.2020.e00506
- Penkhrue, W., Khanongnuch, C., Masaki, K., Pathom-aree, W., Punyodom, W., & Lumyong, S. (2015). Isolation and screening of biopolymer-degrading microorganisms from northern Thailand. *World Journal of Microbiology and Biotechnology*, 3, 1431-1442. doi: 10.1007/s11274-015-1895-1
- Phukon, P., Saikia, J. P., & Konwar, B. K. (2012). Bio-plastic (P-3HB-co-3HV) from *Bacillus circulans* (MTCC 8167) and its biodegradation. *Colloids and Surfaces B: Biointerfaces*, 92, 30-34. doi: 10.1016/j.colsurfb.2011.11.011
- Qi, F. F., Huang, M. H., Zheng, Y., & Xu, Q. (2015). Optimization of an A2/O process for tetracycline removal via response surface methodology coupled with a Box–Behnken design. *Journal of Environmental Science and Health*, 50(7), 735-743. doi: 10.1080/10934529.2015.1011981
- Qi, X., Ren, Y., & Wang, X. (2017). New advances in the biodegradation of poly (lactic) acid. *International Biodeterioration and Biodegradation*, 117, 215-223. doi: 10.1016/j.ibiod.2017.01.010
- Saitou, N., & Nei, M. (1987). The neighbor-joining method: A new method for reconstructing phylogenetic trees. *Molecular Biology and Evolution*, 4, 406-425. doi: 10.1093/oxfordjournals.molbev.a040454
- Szumigaj, J., Zakowska, Z., Klimek, L., Rosicka-Kaczmarek, J., & Bartkowiak, A. (2008). Assessment of polylactide foil degradation as a result of filamentous fungi activity. *The Polish Journal of Environmental Studies*, 17(3), 335-341.
- Tamura, K., Stecher, G., Peterson, D., Filipinski, A., & Kumar, S. (2013). MEGA6: Molecular evolutionary genetics analysis version 6.0. *Molecular Biology and Evolution*, 30(12), 2725-2729. doi: 10.1093/molbev/mst197
- Tawakkal, I. S. M. A., Cran, M. J., Miltz, J., & Bigger, S. W. (2014). A Review of poly (lactic acid)-based materials for antimicrobial packaging. *Journal of Food Science*, 79(8), 1477-1490. doi: 10.1111/1750-3841.12534
- Thompson, J. (1997). The clustal_x windows interface: Flexible strategies for multiple sequence alignment aided by quality analysis tools. *Nucleic Acids Research*, 25(24), 4876-4882. doi: 10.1093/nar/25.24.4876
- Tian, Y., Fan, Y., Liu, J., Zhao, X., & Chen, W. (2016). Effect of nitrogen, carbon sources and agitation speed on acetoin production of *Bacillus subtilis* SF4-3. *Electronic Journal of Biotechnology*, 19, 41-49. doi: 10.1016/j.ejbt.2015.11.005
- Unrean, P., Nguyen, N. H. A., Visessanguan, W., & Kitsubun, P. (2012). Improvement of nattokinase production by *Bacillus subtilis* using an optimal feed strategy in fed-batch fermentation. *KKU Research Journal*, 17(5), 769-777.
- Vey, E., Miller, A. F., Claybourn, M., & Saiani, A. (2007). *In vitro* degradation of poly (lactic-co2-glycolic) acid random copolymers. *Macromolecular Symposia*, 251(1), 81-87. doi: 10.1002/masy.20075 0511

- Yottakot, S., & Leelavatcharamas, V. (2019). Isolation and optimisation of polylactic acid (PLA)-packaging degrading actinomycete for PLA-packaging degradation. *Pertanika Journal of Tropical Agricultural Science*, 42(3), 1111-1130.
- Yun, T. Y., Feng, R. J., Zhou, D. B., Pan, Y. Y., Chen, Y. F., Wang, F., ... & Xie, J. H. (2018). Optimization of fermentation conditions through response surface methodology for enhanced antibacterial metabolite production by *Streptomyces* sp. 1-14 from cassava rhizosphere. *PloS One*, 13(11), 1-21. doi: <https://doi.org/10.1371/journal.pone.0206497>
- Zhong, Y., Godwin, P., Jin, Y., & Xiao, H. (2020). Biodegradable polymers and green-based antimicrobial packaging materials: A mini-review. *Advanced Industrial and Engineering Polymer Research*, 3, 27-35. doi: 10.1016/j.aiepr.2019.11.002
- Zhou, Y., Sun, Y. B., He, H. W., Feng, J. T., Zhang, X., & Han, L. R. (2017). Optimization of medium compositions to improve a novel glycoprotein production by *Streptomyces kanasensis* ZX01. *AMB Express*, 7(1), 1-9. doi: 10.1186/s13568-016-0316-7



Synthesis of Magnetic Activated Carbon Treated with Sodium Dodecyl Sulphate

Palsan Sannasi Abdullah*, Huda Awang and Jayanthi Barasarathi

Faculty of Agro Based Industry, Universiti Malaysia Kelantan Jeli Campus, 17600 Jeli, Kelantan, Malaysia

ABSTRACT

Magnetic activated carbon (MAC) is found to be effective for the adsorption of methylene blue due to its physico-chemical properties such as strong adsorption of magnetization. The use of activated carbon (AC) for methylene blue adsorption was ineffective compared to MAC. MAC was prepared by incorporating different types of iron powder and chemicals [sodium dodecyl sulphate (SDS), citric acid (CA), dimethicone (D350), and epichlorohydrin (C_3H_5ClO)] to strengthen the magnetism and stabilize the MAC. The methylene blue test and iodine test were tested on different samples. Characterization test on physical and chemical properties was carried out using Scanning Electron Microscopy (SEM) and X-ray diffraction (XRD). The yield of MAC was higher because of the addition of magnetic particles. The incorporation of magnetic particles had been proven by the SEM and XRD analysis that showed the presence of iron compound. The performance study of the adsorbent sample showed that MAC_A3II presented better qualities with highest removal percentage (98.81 % of removal) in methylene blue adsorption and low magnetic contact time that showed strong magnetism. MAC_A3II was prepared by incorporating iron powder and treated by using sodium dodecyl sulphate (SDS). Among all the adsorbent sample, MAC_B2III performed the weakest quality because the dye removal percentage was low, and the preparation process was complicated compared with others.

Keywords: Iron powder, magnetic activated carbon, methylene blue adsorption, sodium dodecyl sulphate

ARTICLE INFO

Article history:

Received: 27 September 2020

Accepted: 25 November 2020

Published: 22 January 2021

DOI: <https://doi.org/10.47836/pjst.29.1.24>

E-mail addresses:

palsan.abdullah@umk.edu.my (Palsan Sannasi Abdullah)

hudaawang@gmail.com (Huda Awang)

jayne_barath@yahoo.com (Jayanthi Barasarathi)

* Corresponding author

INTRODUCTION

Batik is a traditional fabric craft with hand-painted and richly colored patterns. The batik industry is one of economic driven industries in east coast states of Malaysia- Kelantan and Terengganu (Jamaludin, 2020). Many

batik entrepreneurs built their manufacturing units along the adjoining riverside for disposal of wastewater such as dyes, grease, wax, and heavy metals (Ramakreshnan et al., 2020). Methylene blue (MB) is commonly used dye in batik industry. The presence of dye in rivers not only deteriorates aesthetic value of water but also compromises human health (Ewadh, 2020). Thus, a proper treatment for effluents rich in color and organic pollutants is required prior to discharging into the environment (Ramakreshnan et al., 2020). One of the methods applied to treat the wastewater is Advanced Oxidation Processes (AOP). In this method, the spent bleaching earth impregnated with Tungsten trioxide went through sonocatalytic to form hydroxyl radicals. The hydroxyl radicals therefore destruct pollution compounds. Although the percentage of pollutant degradation is 99.12% the process is expensive for a small cottage batik manufacture (Hindryawati et al., 2020). Therefore, adsorption is an effective method to treat wastewater. Many industries used commercial AC to treat effluents from factories, the drawbacks of AC are high cost and disposal problem (Vyavahare et al., 2019). Thus, current research found the potential of agricultural waste to produce activated carbon. By this way, it is not only cost effective but also environment- friendly (Shokry et al., 2020). Furthermore, production on magnetic activated carbon (MAC) from agricultural waste represents novel adsorbent for water purification. Activated carbon is a high-content carbon enriched with minerals adsorbent. By this way, it is not only cost effective but also environment- friendly (Shokry et al., 2020) Activated carbon can be produced through the pyrolysis of biomass in the absence of oxygen at $\leq 500^{\circ}\text{C}$ or carbonization process and it is a carbon rich residue. Activation step of activated carbon involved oxidizing gases such as steam, air, and carbon dioxide (Ooi et al., 2013). It has porous properties which can increase the removal of contaminants from aqueous solution. It also has large specific surface area and strong redox reactivity (Yao et al., 2015). Therefore, unique properties of activated carbon are widely used as a filter to improve the quality of water and wastewater whereby it increases efficiency of water treatment and reduces the spread of contamination from hazardous chemicals. Accordingly, MAC is proposed to improve effectiveness of separation process which aided by external magnetic field (Shokry et al., 2020). The key obstacle of impregnation process is magnetic particles does not fully impregnate with the AC. In order to encounter the problem, a surfactant is applied due to change the surface properties of adsorbent. The hydrophobic and hydrophilic characteristics of the surfactant enable improve adsorption capacity by affecting solubility of the organic pollutant. Thus, organic pollutants such as dye is suggested to test the performance of impregnation process with surfactant treatment (Li et al., 2019). An alternative method to produce magnetic activated carbon derived from coconut shell with sodium dodecyl sulfate treatment is proposed in this study. Besides, the methylene blue will be used as pollutant to test the adsorbent. The challenge of this study is to show that MAC is a competitive adsorbent by comparing with commercial AC. Hence, the objective of this study was to synthesis magnetic activated carbon treated with SDS and to test the performance of the novel adsorbent.

MATERIALS AND METHOD

Chemical and Reagents

The chemical and reagent used in the research were hydrochloric acid, HCl (37%), ammonium hydroxide, NH₄OH (28%), 2 M hydrochloric acid, HCl (2 M), ammonium hydroxide, NH₄OH (0.7 M), iodine solution (0.1 N), sodium thiosulphate solution, Na₂S₂O₃ (0.05 N), starch solution, sodium carbonate, Na₂CO₃, potassium iodide (KI), and distilled water. The magnetization of AC was carried out using iron powder (IFP) and labelled as Group A; Group B was γ -Fe₂O₃ (I30B), the gamma phase of ferrous oxide; Group C was α -Fe₂O₃ (I30) the alpha phase of ferrous oxide; Group D was ferrous chloride, FeCl₂ impregnated with ferric chloride, FeCl₃ and Group E was ferrous sulphate, FeSO₄ impregnate with Ferric Chloride, FeCl₃. In addition, sodium dodecyl sulphate (SDS), citric acid (CA), dimethicone 350 (D350) and epichlorohydrin, (C₃H₅ClO) used to strengthen the impregnation between magnetic particles and AC.

Synthesis of Activated Carbon

Raw coconut shell sample was collected from coconut milk manufacturer company, which is located at Tanah Merah district, Kelantan state. The raw coconut shell was carbonized by using modified drum method. Carbonization is a conversion of organic matters like biomass into carbon through destructive distillation. The activated carbon was produced through modified pyrolysis technique using an empty 55-gallon steel oil drum. The coconut shell was placed into the oil drum and lit from the bottom. Once the materials inside the drum were fully ignited and the water in the carbon source had evaporated, the drum was sealed to initiate the anoxic combustion process. The process would take about two to three hours for the material to be fully carbonized. Once the charcoal was completed, it was sorted by visual inspection to find material that had been thoroughly carbonized. Shells that retained a natural brown colour and that were difficult to break by hand were excluded. Any material that had not been completely carbonized was saved for the following batch. The drum method produced approximately 5 kg of carbon material. There is no fixed temperature in this process but can range from 400 to 500°C (Cobb et al., 2012). The schematic diagram on the preparation of activated carbon using carbonization drum method is illustrated in Figure 1. The carbonized coconut shells were grounded into the desired form and further subjected to activation with 1N concentration of potassium hydroxide (KOH) at a ratio of 1:3, with slow agitation at 75 rpm for 1 hour. To prepare 1N KOH, 56.11 g of KOH was dissolved in 300 mL water and then transferred to a 1 L measuring flask quantitatively and dilute until it reaches 1 liter (Cobb et al., 2012). The mixture was left to mature for about 5 to 6 hour and followed by filtration, later, rinsed with double distilled water (ddH₂O). The AC was dried in oven at temperature of 90 -100°C. The dried AC was placed in a muffle furnace (Carbolite ELF 11/6B) and heated to 800-900°C (10°C/min), and kept for 15-30

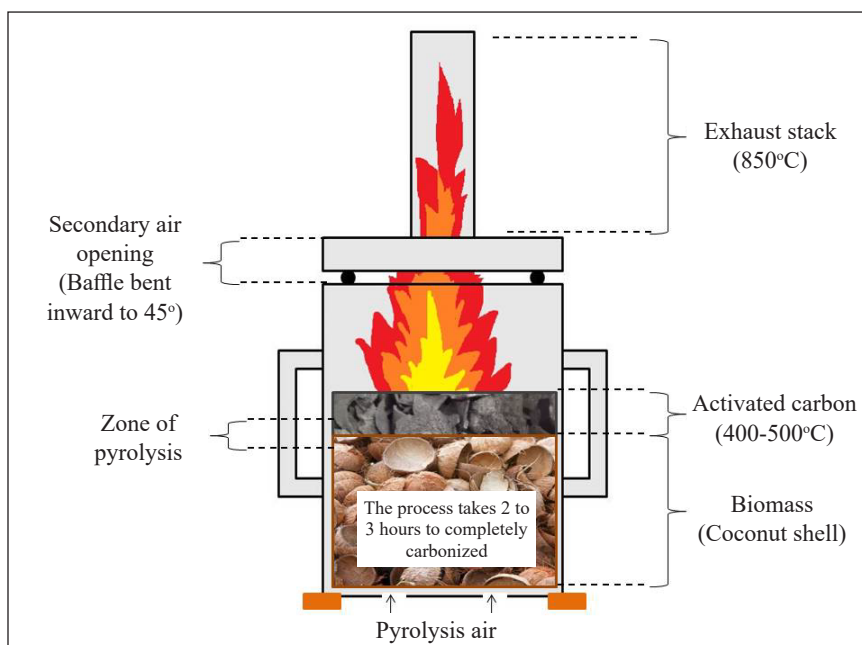


Figure 1. Schematic diagram on the synthesis of activated carbon from coconut shell via carbonization method

min (Lee et al., 2018). The cooled down sample was washed, neutralized with 5% HCl, dried and stored for further modification.

Preparation Method for Magnetization of Coconut Shell Activated Carbon

Table 1 displays the different combination of the final product by using different magnetic particles impregnated with different chemical and different sonicated treatment. The AC used was in mesh size of less than $45\mu\text{m}$. At first, 2.95 g of iron powder or iron (III) oxide powder, Fe_2O_3 (IFP, I30B, and I30) was dissolved in 45 mL of distilled water and placed in the orbital shaker for the agitation of 250 rpm for 30 min. For MAC, the experiment was continued with the addition of 6 mL of ammonium hydroxide solution, NH_4OH (28%) and agitated for 1 hour. Next, 1.5 g of AC was added and continued the agitation for 5 min. Then, the preparation was continued with addition of 0.6 ml of different chemical (control, Dimetricone 350, Sodium Dodecyl Sulphate, and Citric Acid) respectively as enhancer of magnetization and continue agitated for another 1 hour. All of the samples were continued with 3 different sonication for 1 hour which is non-sonicated, ultrasonic bath and sonicated respectively. Lastly, the final product, MAC was washed and collected using neodymium magnet. The MAC was dried at 50°C in the oven to obtain the dry MAC powder. Group C (I30) contained the lowest magnetism among all the group which the magnetic particles used was the alpha phase of ferric oxide, $\alpha\text{-Fe}_2\text{O}_3$ which was the lowest magnetism among

all magnetic particles. D350 was the worst chemical used to treat the sample which wasted lots of carbon sample during the washing process.

Table 1
Sample with different treatment combination using method 1

		Non-sonicated (I)	Ultrasonic bath (II)	Sonicated (III)
IFP (A)	Control (1)	MAC_A1I	MAC_A1II	MAC_A1III
	D350 (2)	MAC_A2I	MAC_A2II	MAC_A2III
	SDS (3)	MAC_A3I	MAC_A3II	MAC_A3III
	CA (4)	MAC_A4I	MAC_A4II	MAC_A4III
I30B (B)	Control (1)	MAC_B1I	MAC_B1II	MAC_B1III
	D350 (2)	MAC_B2I	MAC_B2II	MAC_B2III
	SDS (3)	MAC_B3I	MAC_B3II	MAC_B3III
	CA (4)	MAC_B4I	MAC_B4II	MAC_B4III
I30 (C)	Control (1)	MAC_C1I	MAC_C1II	MAC_C1III
	D350 (2)	MAC_C2I	MAC_C2II	MAC_C2III
	SDS (3)	MAC_C3I	MAC_C3II	MAC_C3III
	CA (4)	MAC_C4I	MAC_C4II	MAC_C4III

Notes: A = IFP (Iron Powder); B = I30B (γ -Fe₂O₃); C = I30 (α -Fe₂O₃); 1 = Control; 2 = D350; 3 = SDS; 4 = CA; I = Non-sonicated; II = Ultrasonic bath; III = Sonicated

Preparation Method for Magnetization of Coconut Shell Activated Carbon using Method 2

For the impregnation magnetization 1.95 g of FeCl₃ was mixed with 0.7 g of FeCl₂ (D) and then dissolved in 45 mL of distilled water and placed in the orbital shaker for the agitation at 250 rpm for 30 min (Table 2). The sample was further added with 6 mL of ammonium hydroxide solution, NH₄OH (28%) and continued agitation for another 1 hour. Then, 1.5 g of AC was added into the solution and the agitation continued for another 5 mins. The prepared solution was added with different chemical (control, SDS, and CA) and continued the agitation for another 1 hour. The sample were treated using three different method for 1 hour which was non-sonicated, ultrasonic bath and sonicated respectively. Lastly, the

Table 2
Sample with different treatment combination using method 2

		Non-sonicated (I)	Ultrasonic bath (II)
FeCl ₃ + FeCl ₃ (D)	Control (1)	MAC_D1I	MAC_D1II
	SDS (3)	MAC_D3I	MAC_D3II
	CA (4)	MAC_D4I	MAC_D4II
FeCl ₃ + FeSO ₄ (E)	Control (1)	MAC_E1I	MAC_E1II
	SDS (3)	MAC_E3I	MAC_E3II
	CA (4)	MAC_E4I	MAC_E4II

Notes: D = FeCl₂; E = FeSO₄; 1 = Control; 3 = SDS; 4 = CA; I = Non-sonicated; II = Ultrasonic bath

final product, was washed and collected using neodymium magnet. The treated MAC was dried at 50 °C in the oven to obtain the dry MAC powder. The magnetization method was repeated $\text{FeCl}_3 + \text{FeSO}_4$ (E) by replacing the preparation formula (i) with formula (ii) (1.95 g of FeCl_3 impregnated with 1.0 g of FeSO_4).

Process Performance

Yield (%). The total yield of MAC (%) estimated by using the following Equation 1,

$$\text{Total Yield of MAC (\%)} = \frac{\text{weight of MAC}_{XX} \text{ produced}}{\text{weight of activated carbon sample}} \times 100\% \quad (1)$$

Methylene Blue Test. Methylene blue test was carried out using method described by Jadhav and Mohanraj (2016). Methylene blue solution was prepared by diluting the stock solution with 1000 ppm to 2 ppm. A fixed parameter was measured in this adsorption experiment where the time taken of the MAC to decolorize the methylene blue (contact time) and the time taken of the sample fully attached to the magnet (magnetic contact time) were recorded. At first, 0.15 g of each sample were weighed and poured into 25 mL of methylene blue solution. The time taken to decolorize the methylene blue and the time of the sample fully attached to the magnet were recorded. The methylene blue test was conducted in triplicates under identical condition and average value was calculated. Next, the filtrate was analyzed using UV visible spectrophotometer (Thermo Scientific Genesys 20) at 668 nm (Islam et al., 2017). This was to further prove the effectiveness of the MAC in adsorption of methylene blue solution. The absorbance value was recorded in triplicate and the average value were also recorded. The percentage of dye removal by using different sample was calculated using mathematical Equation 2.

$$\text{Percentage of dye removal (\%)} = \frac{(B - S)}{S} \times 100 \quad (2)$$

Where B (mg/ L) and S (mg/ L) are MB concentration at initial and after added MAC. The steps were repeated by using different concentration of methylene blue dye which was 5 ppm and 10 ppm.

Iodine Test. Iodine number was used to determine the adsorption of iodine on the activated carbon (Mianowski et al., 2007). The main principle was to determine the residual iodine concentration by titration with sodium thiosulfate standard solution after the quantitative sample and iodine standard solution were fully shaken under specific conditions to determine the iodine adsorption amount. Iodine adsorption value can be used as a qualitative indicator of microporous structure of activated carbon (Yang et al., 2020).

Preparation of Iodine Solution (0.1 N). For the preparation of iodine solution (0.1 N), 12.7 g of iodine pearls and 19.1 g of potassium iodide (KI) were weighed. Next, around 2-5 mL of distilled water was added slowly and stirred using magnetic stirrer. Distilled water was added until 50 mL to completely dissolve the iodine pearl. The solution was allowed to stir for a minimum of 4 hours to make sure that all the crystals were completely dissolved. The solution was quantitatively transferred to a 1 L volumetric flask (ASTMD4607_14, 2014). The iodine solution 0.1 N must be stored in amber bottle due to its sensitivity to light.

Preparation of Sodium Thiosulphate, $\text{Na}_2\text{S}_2\text{O}_3$ (0.05 N). Around 12.4 g of sodium thiosulphate, $\text{Na}_2\text{S}_2\text{O}_3$ (0.05N) was dissolved in approximately 100 mL of freshly boiled distilled water and 0.1 g of sodium bicarbonate, NaHCO_3 was added to decrease the bacterial decomposition of the thiosulphate solution. The mixture was transferred quantitatively to a 1 L volumetric flask and diluted to the mark (ASTMD460714, 2014).

Preparation of Starch Solution. To prepare a starch solution, 1.0 ± 0.5 g of starch was mixed with 5 to 10 mL of cold water to make a paste. Additional of 25 ± 5 mL of water was added while stirring to the starch paste. The mixture was poured into a 1 L boiling water and boiled for 4 to 5 min (ASTMD460714, 2014).

Iodine Number. Iodine number was determined on iodine solution as blank, 45 μm of AC, 63 μm of AC, CMAC, the best and worst condition of sample, MAC_XX. The test divided into two parts as part a and b. Part b was a blank reading. At first, 10 mL of iodine solution (0.1 N) was measured and poured into conical flask. The solution was titrated with sodium thiosulphate solution, (0.05 N) until the solution turn to pale yellow. Then, 2 drops of starch solution were added, and the solution turned blue. The solution was continued with titration of sodium thiosulphate until the solution turned colorless. The burette reading corresponds to blank reading (b). For part a, around 0.2 g of sample (AC, MAC, MAC_XX) was weighed and dissolved in 40 mL of iodine solution 0.1N. The solution was shaken for 50 min at 200 rpm in the orbital shaker and filtered. Then, 10 mL of filtrate was measured and poured into another conical flask. The filtrate was titrated with sodium thiosulphate solution until the solution turns pale yellow. Next, 2 drops of starch solution were added into the solution until the solution turns blue. The solution was continued with the titration of sodium thiosulphate until the solution turned colorless. The burette readings were correspond to (a). The iodine value was calculated by using Equations 3 to 5 as stated below.

$$\text{Iodine value} = c \times \text{Conversion factor; mg/g} \quad (3)$$

Conversion factor =

$$\frac{\text{molecular weight of iodine} \times \text{normality of iodine} \times 40}{\text{weight of activated carbon}} \times \text{blank reading}$$

$$= \frac{127 \times 0.1 \text{ N} \times 40}{0.2 \text{ g}} \times b \quad (4)$$

$$c = b - a \quad (5)$$

Characterization of magnetic activated carbon

Scanning Electron Microscopy (SEM) Analysis. SEM was used to analyze the pore structure of AC and MAC sample that produced. The magnification used were 1000×. The sample was placed on the SEM holder and moulded into the mounting holed in a JEOL JSM-IT100 scanning electron microscope. The focus knob was adjusted and the selected image captured.

X-ray Diffraction (XRD). X-ray diffraction is method a that uses X-ray to characterize the crystalline properties of carbon material. The sample was packed into the sample holder and analyzed by using Bruker D2 Phaser. The sample was scanned from 20.0°C to 90.0°C at the scan speed of 2° min⁻¹. The XRD diffractogram patterns was obtained from the system.

RESULTS AND DISCUSSION

Weight and Yield of Magnetic Activated Carbon

Table 3 shows the weight and the total yield of the MAC. Magnetic activated carbon was produced by using different type of iron powder (A, B, C, D, and E), different chemical to treat MAC (1, 2, 3, and 4) and also different type of sonication (I, II, and III). The production yield was considered as an important parameter in the feasibility study under specified condition. The magnetism of these MAC sample was tested using neodymium magnet (NdFeB). The results showed that the magnetism of group C was the lowest. The results clearly showed that the MAC yield of all samples was more than 100 %. This is because the addition of different type of iron powder into different samples. The highest MAC yield, 417.33% was achieved by MAC_A4II (True yield: 140.67%). The lowest MAC yield among all sample was from MAC_E3II that recorded 86% (True yield: 28.99%). This happened because of the washing and cleaning process that washed away most of the AC. Besides, this could also be due to the failure of impregnation process to impregnate the FeSO₄ powder and the AC.

Table 3
 Weight and percentage of MAC yield (%)

No	Sample	Weight (g)	Total Yield of MAC (%)	True Yield (%)
1	MAC_A1I	3.29	219.33	73.93
2	MAC_A1II	4.74	316.00	106.52
3	MAC_A2I	3.34	222.67	75.06
4	MAC_A2II	3.85	256.67	86.52
5	MAC_A2III	3.28	218.67	73.71
6	MAC_A3I	4.80	320.00	107.87
7	MAC_A3II	4.94	329.33	111.01
8	MAC_A3III	4.66	310.67	104.72
9	MAC_A4I	4.61	307.33	103.60
10	MAC_A4II	6.26	417.33	140.67
11	MAC_A4III	4.16	277.33	93.48
1	MAC_B1I	4.14	276.00	93.03
2	MAC_B1II	4.31	287.33	96.85
3	MAC_B2I	3.71	247.33	83.37
4	MAC_B2II	3.53	235.33	79.33
5	MAC_B2III	3.82	254.67	85.84
6	MAC_B3I	3.50	233.33	78.65
7	MAC_B3II	3.61	240.67	81.12
8	MAC_B3III	3.93	262.00	88.31
9	MAC_B4I	3.12	208.00	70.11
10	MAC_B4II	4.71	314.00	105.84
11	MAC_B4III	3.61	240.67	81.12
12	MAC_C1I	4.08	272.00	91.69
13	MAC_C1II	4.17	278.00	93.71
14	MAC_C2I	3.87	258.00	86.97
15	MAC_C2II	4.21	280.67	94.61
16	MAC_C2III	4.32	288.00	97.08
17	MAC_C3I	4.36	290.67	97.98
18	MAC_C3II	4.23	282.00	95.06
19	MAC_C3III	4.11	274.00	92.36
20	MAC_C4I	4.09	272.67	91.91
21	MAC_C4II	4.21	280.67	94.61
22	MAC_C4III	4.71	314.00	105.84
23	MAC_D1I	2.55	170.00	57.30
24	MAC_D1II	2.17	144.67	48.76
25	MAC_D3I	2.16	144.00	48.54
26	MAC_D3II	2.60	173.33	58.43
27	MAC_D4I	2.13	142.00	47.87
28	MAC_D4II	2.15	143.33	48.31
29	MAC_E1I	2.08	138.67	46.74
30	MAC_E1II	2.03	135.33	45.62
31	MAC_E3I	2.07	138.00	46.52
32	MAC_E3II	1.29	86.00	28.99
33	MAC_E4I	2.12	141.33	47.64
34	MAC_E4II	2.38	158.67	53.48

Notes: A = IFP (Iron Powder); B = I30B (γ - Fe_2O_3); C = α - Fe_2O_3 ; D = FeCl_2 ; E = FeSO_4 ; 1 = Control; 2 = D350; 3 = SDS; 4 = CA; I = Non-sonicated; II = Ultrasonic bath; III = Sonicated.

Methylene Blue Test

The behavior of methylene blue and iodine test were closely related to surface area and pores volume of the carbon sample. The parameter used in methylene blue test were the time taken by MAC to decolorize methylene blue solution (contact time) and the time taken by MAC fully attached to magnet (magnetic contact time). For methylene blue test, the selected MAC samples were from group A, B, D and E. Group C was not selected because group C did not contain any magnetism which was considered as lowest quality if compared with others. Table 4 shows the contact time and the magnetic contact time between the MAC sample and 2 ppm methylene blue. Additionally, the absorbance value had been recorded that measured at 668 nm by using UV-VIS. Besides, the test had been done triplicates and the average result was calculated. The results showed the contact time, magnetic contact time of the MAC form by using the iron powder (IFP) and treated with different chemical (control, D350, SDS and citric acid) and sonicated way (non-sonicated, ultrasonic bath and sonicated). The sample that achieved the shortest contact time was MAC_A3I which recorded 5.38 s and on the other hand the longest contact time recorded was by MAC_A2III which was 156.73 s. This explained that MAC_A3I applied shorter time to decolorize the methylene blue whereas MAC_A2III applied the longest time. For the magnetic contact time, the shortest time, 17.43 s recorded by MAC_A2III and the longest time, 40.87 s recorded by MAC_A2I. The result clarifies that some MAC have good methylene blue adsorption but weak magnetism. The magnetism of the MAC sample was affected by different types of iron powder used and the treated chemical.

Group B was the MAC prepared by using gamma phase of ferric oxide, $\gamma\text{-Fe}_2\text{O}_3$ (I30B) and treated by different chemical (control, D350, SDS and citric acid) and sonicated way (non-sonicated, ultrasonic bath and sonicated). Based on Table 4, MAC_B3I had recorded the shortest contact time which was 3.90 s whereas on the other hand MAC_B2I had recorded the longest contact time, 50.54 s. Furthermore, for the longest and shortest magnetic contact time, MAC_B2III and MAC_B1I recorded were 6.283 s and 71.87 s respectively.

The MAC from group D was carried out by coporate ferrous chloride (FeCl_2) with ferric chloride (FeCl_3). For group D, MAC_D3I and MAC_D1I had recorded the shortest and longest contact time when dissolved in methylene blue solution. Moreover, for the magnetic contact time, MAC_D3I displayed the best magnetism and conversely MAC_D1I displayed the worst magnetism among category D. The time recorded were 28.64 s and 35.91 s respectively. MAC_E which the group E was MAC that were manufactured by mixing the ferric chloride (FeCl_2) with ferrous sulphate (FeSO_4). Lastly for treatment Group E, the results showed that MAC_E3I and MAC_E4II had presented the shortest and longest contact time when they dissolved in methylene blue solution. The time recorded were 3.73 s and 4.54 respectively which also explained that MAC_E3I was more effective

Table 4
Methylene blue (2 ppm) test using different treatments

No	Sample	Contact Time (s)	Magnetic Contact Time (s)	Absorbance Value (at wavelength of 668 nm)	Percentage of dye removal (%)
1	MAC_A1I	6.857	38.537	0.064±0.004	81.009
2	MAC_A1II	10.713	30.743	0.060±0.006	82.196
3	MAC_A2I	15.717	40.870	0.010±0	97.033
4	MAC_A2II	32.283	31.380	0.102±0.002	69.733
5	MAC_A2III	156.733	17.430	0.194±0.0005	42.433
6	MAC_A3I	5.357	35.140	0.013± 0.0011	96.142
7	MAC_A3II	7.427	33.420	0.004± 0.0005	98.81
8	MAC_A3III	10.437	30.310	0.003± 0.0005	99.110
9	MAC_A4I	21.107	19.790	0.009± 0.0005	97.329
10	MAC_A4II	11.883	35.110	0.015± 0.001	95.549
11	MAC_A4III	19.643	19.530	0.011± 0.001	96.736
1	MAC_B1I	5.533	71.867	0.017±0.0005	94.955
2	MAC_B1II	4.620	55.490	0.014±0.0005	95.846
3	MAC_B2I	50.540	10.723	0.080±0.0005	76.261
4	MAC_B2II	37.327	13.197	0.036±0	89.318
5	MAC_B2III	44.497	6.283	0.118±0.0015	64.985
6	MAC_B3I	3.903	54.997	0.005±0.001	98.516
7	MAC_B3II	4.040	53.527	0.009±0.0005	97.329
8	MAC_B3III	3.953	45.783	0.003±0.0005	98.110
9	MAC_B4I	5.737	49.437	0.030±0	91.098
10	MAC_B4II	3.953	42.993	0.019±0.0005	94.362
11	MAC_B4III	5.870	50.910	0.007±0	97.923
1	MAC_D1I	4.727	30.070	0.049±0.0005	85.460
2	MAC_D1II	3.917	35.910	0.082±0.001	75.668
3	MAC_D3I	3.600	28.640	0.067±0	80.119
4	MAC_D3II	4.423	34.120	0.098±0.0005	70.920
5	MAC_D4I	3.803	35.270	0.055±0.0005	83.680
6	MAC_D4II	4.183	34.510	0.059±0.0005	82.493
1	MAC_E1I	4.000	48.640	0.089±0.0017	73.591
2	MAC_E1II	4.533	46.680	0.074±0.001	78.042
3	MAC_E3I	3.733	47.450	0.060±0.0005	82.196
4	MAC_E3II	4.343	41.170	0.085±0.0005	74.777
5	MAC_E4I	4.183	54.290	0.103±0.00153	69.436
6	MAC_E4II	4.540	52.220	0.055±0.0005	83.680

Where n=3 for triplicate test of methylene blue test. Notes: A = IFP (Iron Powder); B = I30B (γ -Fe₂O₃); D = FeCl₂; E = FeSO₄; 1 = Control; 2 = D350; 3 = SDS; 4 = CA; I = Non-sonicated; II = Ultrasonic bath; III = Sonicated

if compared with MAC_E4II. Additionally, MAC_E3II and MAC_E4I had recorded 41.17 s and 54.29 s as the shortest and longest magnetic contact time. Table 5 showed the contact and magnetic contact time of the CMAC and AC. The result showed that the CMAC recorded the contact time of the sample in methylene blue solution as 4.13 s and 50.81 s as the magnetic contact time. On the other hand, due to AC not containing magnetism, the AC only recorded 9.58 s for the contact time of sample in methylene blue solution.

Table 5
Methylene blue (2 ppm) test

No	Sample	Contact Time (s)	Magnetic Contact Time (s)	Absorbance Value (668 nm)	
		Average	Average	Average	Percentage of dye removal (%)
1	CMAC	4.127	50.810	0.098	70.920
2	AC	9.580	-	0.244	27.596

Iodine Test

Iodine test for selected MAC sample were calculated by using Equation 3 to 5. The iodine number of the selected sample is shown in Table 6. The sample was selected based on the highest and the lowest of the percentage of dye removal from methylene blue test.

Table 6
Iodine number for selected MAC sample

No	Sample	Iodine Value (mg/g)
1	45 μ m AC	925.840
2	63 μ m AC	874.948
3	CMAC	657.301
4	MAC_A2III	821.627
5	MAC_A3II	652.606
6	MAC_B2III	368.710
7	MAC_B3I	275.069
8	MAC_D1I	719.862
9	MAC_D3II	737.419
10	MAC_E4I	795.945
11	MAC_E4II	782.240

Notes: A = IFP (Iron Powder); B = I30B (γ -Fe₂O₃); D = FeCl₂; E = FeSO₄; 1 = Control; 2 = D350; 3 = SDS; I = Non-sonicated; II = Ultrasonic bath; III = Sonicated

Iodine test was used to determine the surface area of the MAC and AC. Additionally, iodine test also act as a measure of micropore content of AC by observing the iodine adsorption from the solution. As shown in Tables 3 and 4, there are comparison between

AC and MAC. At first, the comparison between 45 μm AC and 63 μm AC was made. The result clearly showed that the iodine number of 45 μm AC was higher than 63 μm AC. 45 μm AC recorded 925.84 mg/g whereas 63 μm AC recorded 874.95 mg/g of iodine number. The higher iodine number indicates a higher degree of activation (Machrouhi et al., 2019). Besides, higher iodine number indicates that the 45 μm AC contain a larger porosity and higher number of porosity (Arslanoglu, 2019). The result showed that 45 μm AC had higher quality compared to 63 μm AC. The iodine test for MAC was also calculated for comparison. For group A, MAC_A3II recorded a lower iodine adsorption number, 652.606 mg/g which indicated it was better compared to MAC_A2III that recorded higher iodine adsorption number, 821.63 mg/g (Figure 2). Next, for the comparison of other group B, D and E, the more qualified MAC are MAC_B3I, MAC_D1I and MAC_E4II. The iodine adsorption number recorded are 275.07 mg/g, 719.86 mg/g and 782.24 mg/g respectively. MAC_B3I recorded the lowest iodine adsorption number which indicated that the surface of MAC_B3I are mostly covered by iron ion (Deng et al., 2010). The iodine adsorption number of MAC are much lower compared to AC because of the surface of MAC were mostly covered by iron ion depending on the type of magnetic agent used. Besides, this further explained that MAC_A3II having a lower iodine adsorption number had a smaller number of micropores and the surface of carbon were mostly covered by iron ion.

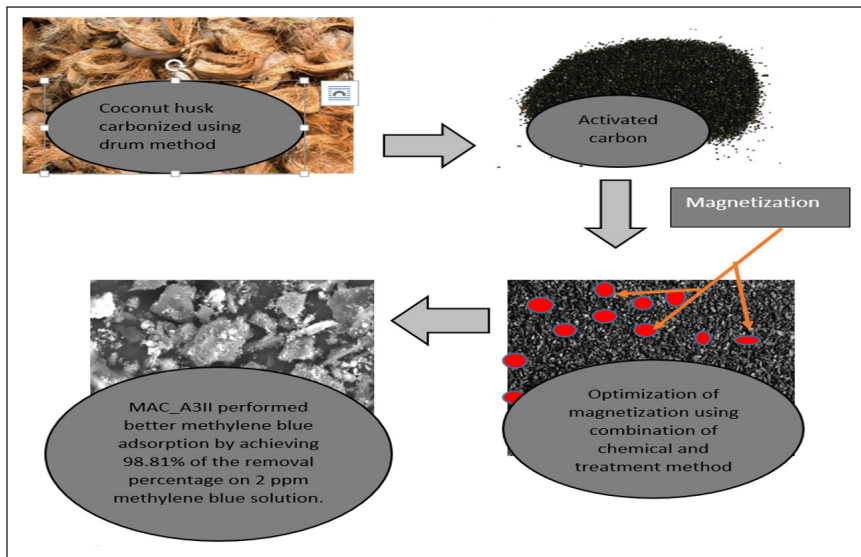


Figure 2. Process flow on the synthesis of magnetic activated carbon treated with sodium dodecyl sulphate

Characterization of Magnetic Activated Carbon

Scanning Electron microscope. Scanning electron microscopy analysis is an analytical technique to study the physical properties of the carbon. This analysis was mainly to illustrate the pore structure or the morphology of the carbon sample. Figure 3 depicts the

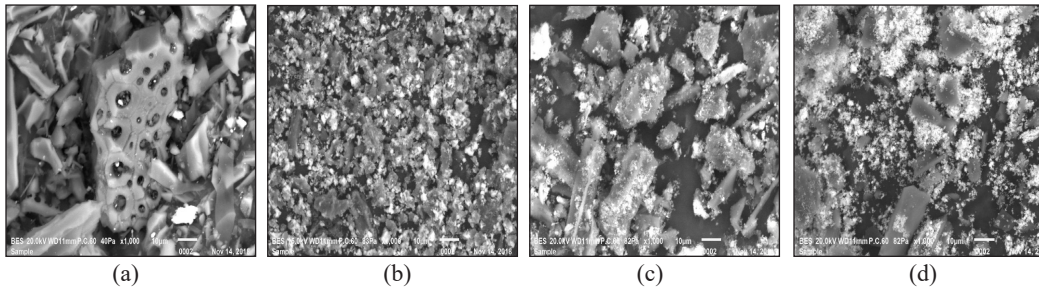


Figure 3. Micrograph of carbon material at magnification of 1000×: (a) AC; (b) CMAC; (c)MAC_A3II; and (d) MAC_B2III

micrograph and image of the chosen sample under the magnification of 1000x. The sample were chosen based on the best condition on iodine test and methylene blue test and samples chosen were the AC, CMAC, MAC_A3II and MAC_B2III. Figure 3 shows the micrograph related to AC. As seen on the micrograph, there were abundant pores developed on the AC (1000x). The pores were randomly scattered on the surface of the activated carbon with various size, diameter, and width of external pores. Besides, there was also some white particles spotted on the surface of the carbon. This might be due to the impurities that was not washed completely during the washing process (Anyika, et al., 2017). The micrograph of the AC showed many micropores and mesopores compared to other samples. This was certainly proof with the iodine number that are higher if compared to other samples. The micrographs of CMAC, MAC_A3II and MAC_B2III are depicted in Figure 3 b, c, and d, respectively. The micrograph of all MAC sample does not show obvious pores if compared to activated carbon. This is because the iron powder used have blocked the pores of the MAC (Suresh et al., 2017). Furthermore, the carbon surface of CMAC showed a homogeneous surface whereas micrograph of MAC_A3II and MAC_B2III showed that the particle size was not homogeneous.

The micrograph of MAC_A3II displayed bigger and uneven size of particle compared to CMAC. In addition, MAC_A3II also showed some needle like structure which represented the presence of ferrous oxide. Moreover, MAC_B2III contained less greyish layer compared to the others. The greyish layer might represent some of the chemical that added to strengthen the magnetism of the MAC. Next, there were some white spots scattered around the surface of each magnetized sample. The white spot was believed to act as the silica particles and MAC_B2III contained more white spots because of the addition of D350 chemical that were contained in silica particles (Wang, et al., 2017).

X-Ray Diffraction (XRD). X-ray diffraction is the analytical technique that mainly identify the crystalline phase of the sample tested. The selected samples were analyzed by using X-ray diffraction analysis as shown on Figure 4. Diffractogram of AC showed some intense

Synthesis of MAC Treated With SDS

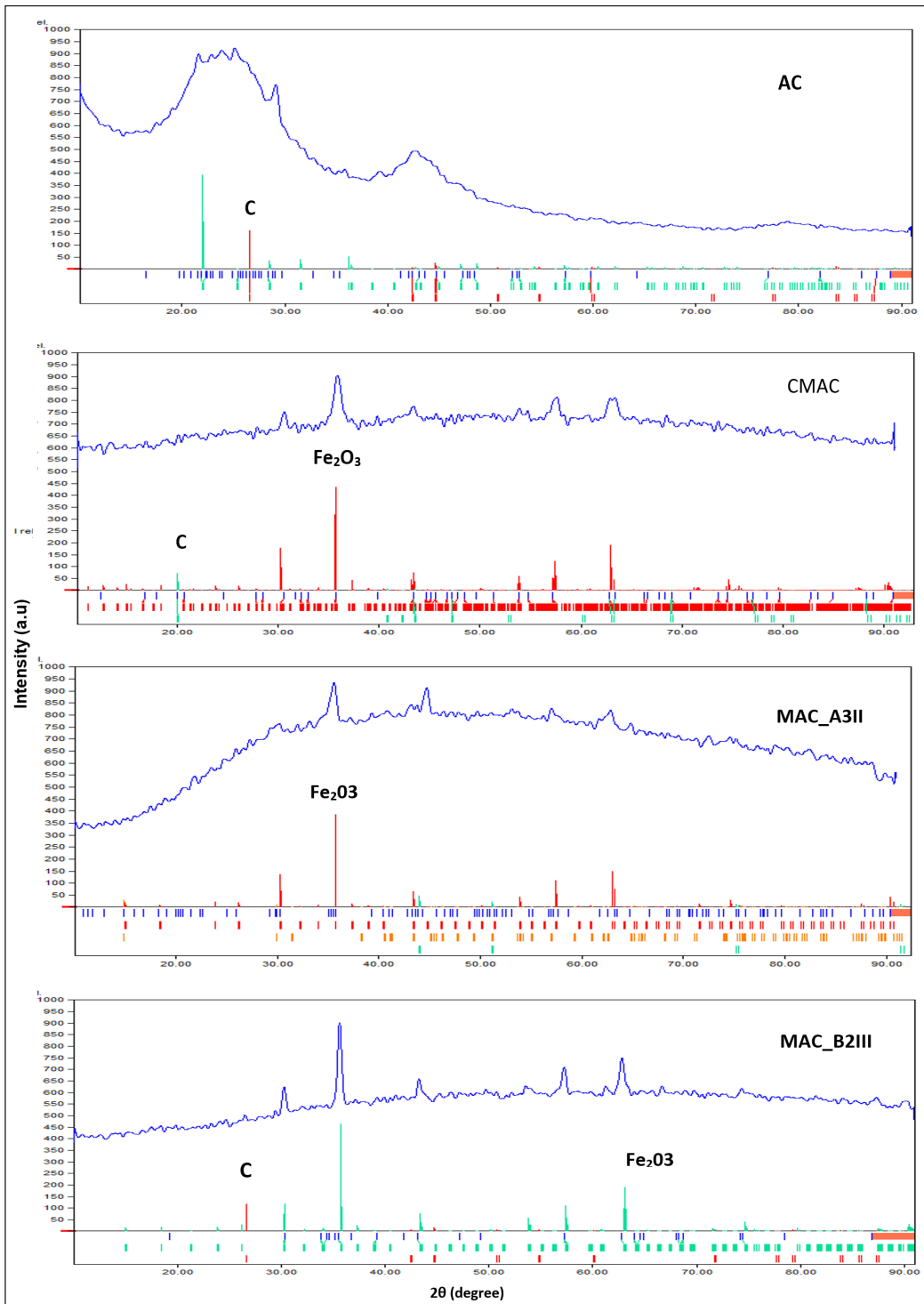


Figure 4. XRD diffractogram of AC, CMAC, MAC_A3II and MAC_B2III
 (Note: A = IFP (iron powder); B = I30B (γ -Fe₂O₃); 2 = D350; 3 = SDS; II = ultrasonic bath; III = Sonicate)

peaks which assigned to the presence of carbon at 2θ 26.54°, 42.42°, 59.74°, and 87.55° at intensity of 596.95, 483.38, 181.95 and 181.85, respectively. Diffractogram of AC shows that AC contained 47.8% of graphite compound. Diffractogram of CMAC had shown the main composition was iron oxide at 90.3%. The most important structure in MAC was the iron compound that leads to the magnetism of the AC. The diffractogram had shown a few peaks which matched to ferric oxide at 2θ 30.54°, 35.71° and 62.80° at the intensity of 418.86, 1000.00, and 456.86, respectively. The presence of iron oxides indicates that the CMAC contains magnetism. Furthermore, diffractogram of MAC_A3II displayed the many peaks that related to ferrous oxide. There were some intense peaks that matched to ferric oxide at 2θ 30.26° and 35.68° at the intensity of 394.73 and 853.49, respectively. Diffractogram of MAC_B2III shows some peaks at 2θ 35.55° and 63.96° that matched to maghemite and carbon whereas 2θ 26.54° that matched to carbon.

CONCLUSION

This study revealed that MAC_A3II had presented a better characteristic compared with other adsorbent samples, CMAC and the AC. MAC_A3II produced by impregnated the iron powder with SDS as the treated chemical and sonicated by using ultrasonic bath. Moreover, MAC_A3II performed better methylene blue adsorption by achieving 98.81% of the removal percentage on 2 ppm methylene blue solution. The iodine test of MAC_A3II, 626.61 mg/g was lower than the AC which was 925.84 mg/g. This showed that AC were highly porous and had larger surface area. On the other hand, MAC_A3II had lower iodine number because the iron had blocked the surface of the carbon. The SEM analysis clearly showed that AC contained many micropores and mesopores if compared with MAC. Besides, for SEM analysis of MAC, the micropores and mesopores were very hard to identified as the pores were blocked by the iron or silicone atom. From the analysis it can be concluded that MAC_A3II presented better qualities and characteristics on the methylene blue adsorption and magnetism if compared to AC and CMAC. MAC_A3II prepared by using the iron powder and treated by adding SDS, was proven as the best qualities of MAC. The presence of iron oxide had been verified by using XRD analysis.

ACKNOWLEDGEMENT

The authors acknowledge the support from Universiti Malaysia Kelantan (R/SGJP/A07.00/01397A/005/2018/00570).

REFERENCES

- Anyika, C., Asri, N. A. M., Majid, Z. A., Yahya, A., & Jaafar, J. (2017). Synthesis and characterization of magnetic activated carbon developed from palm kernel shells. *Nanotechnology for Environmental Engineering*, 2(1), 1-16. doi: <https://doi.org/10.1007/s41204-017-0027-6>

- Arslanoglu, H. (2019). Direct and facile synthesis of highly porous low cost carbon from potassium-rich wine stone and their application for high-performance removal. *Journal of Hazardous Materials*, 374, 238-247. doi: <https://doi.org/10.1016/j.jhazmat.2019.04.042>
- ASTM D4607-14. (2014). *Standard test method for determination of iodine number of activated carbon*. West Conshohocken, USA: ASTM International.
- Cobb, A., Warms, M., Maurer, E. P., & Chiesa, S. (2012). Low-tech coconut shell activated charcoal production. *International Journal for Service Learning in Engineering*, 7(1), 93-104.
- Deng, H., Li, G., Yang, H., Tang, J., & Tang, J. (2010). Preparation of activated carbons from cotton stalk by microwave assisted KOH and K₂CO₃ activation. *Chemical Engineering Journal*, 163(3), 373-381. doi: <https://doi.org/10.1016/j.cej.2010.08.019>
- Ewadh, H. M. (2020). Removal of methylene blue by coontail (*Ceratophyllum demersum*) using phytoremediation concept. *Plant Archives*, 20(1), 2677-2681.
- Hindryawati, N., Dirgarini, J. N. S. R. R., Panggabean, A. S., & Wilsoma. (2020). Ultrasound assisted the degradation of methylene blue using WO₃- deoiled spent bleaching earth as a catalyst. *IOP Conference Series: Earth and Environmental Science*, 854(1), 1-8.
- Islam, M. A., Ahmed, M. J., Khanday, W. A., Asif, M., & Hameed, B. H. (2017). Mesoporous activated coconut shell-derived hydrochar prepared via hydrothermal carbonization-NaOH activation for methylene blue adsorption. *Journal of Environmental Management*, 203, 237-244. doi: <https://doi.org/10.1016/j.jenvman.2017.07.029>
- Jadhav, A., & Mohanraj, G. (2016). Synthesis of activated carbon from *Cocos nucifera* leaves agrowaste by chemical activation method. *Chemistry and Chemical Technology*, 10(2), 201-208.
- Jamaludin, M. Z. (2020). Study on removal of pollutant from batik wastewater using coal bottomash (CBA). *IOP Conference Series: Earth and Environmental Science*, 476(1), 1-6.
- Lee, C. L., H'ng, P. S., Paridah, M. T., Chin, K. L., Rashid, U., Maminski, M., & Khoo, P. S. (2018). Production of bioadsorbent from phosphoric acid pretreated palm kernel shell and coconut shell by two-stage continuous physical activation via N₂ and air. *Royal Society Open Science*, 5(12), 1-19. doi: <https://doi.org/10.1098/rsos.180775>
- Li, C., Gao, Y., Li, A., Zhang, L., Ji, G., Zhu, K., & Wang, X. (2019). Synergistic effects of anionic surfactants on adsorption of norfloxacin by magnetic biochar derived from furfural residue. *Environmental Pollution*, 254, 1-8. doi: <https://doi.org/10.1016/j.envpol.2019.113005>
- Machrouhi, A., Alilou, H., Farnane, M., El Hamidi, S., Sadiq, M., Abdennouri, M., ... & Barka, N. (2019). Statistical optimization of activated carbon from *Thapsia transtagana* stems and dyes removal efficiency using central composite design. *Journal of Science: Advanced Materials and Devices*, 4(4), 544-553. doi: <https://doi.org/10.1016/j.jsamd.2019.09.002>
- Mianowski, A., Owczarek, M., & Marecka, A. (2007). Surface area of activated carbon determined by the iodine adsorption number. *Energy Sources part A*, 29(9), 839-850. doi: <https://doi.org/10.1080/00908310500430901>

- Ooi, C. H., Lee, T., Pung, S. Y., & Yeoh, F. Y. (2015) Activated carbon fiber derived from single step carbonization-activation process. *ASEAN Engineering Journal*, 4(1), 40-50. doi: <https://doi.org/10.11113/aej.v4.15426>
- Ramakreshnan, L., Rajandra, A., Aghamohammadi, N., Fong, C. S., & Nalatambi, S. (2020). A preliminary insight into the environmental awareness of community in the vicinity of batik manufacturing units in Kelantan, Malaysia. *GeoJournal*, 85, 1745-1753. doi: <https://doi.org/10.1007/s10708-019-10046-w>
- Shokry, H., Elkady, M., & Salama, E. (2020). Eco-friendly magnetic activated carbon nano-hybrid for facile oil spills separation. *Scientific Reports*, 10(1),1-17. doi: <https://doi.org/10.1038/s41598-020-67231-y>
- Suresh K. P., Prot, T., Korving, L., Keesman, K. J., Dugulan, I., van Loosdrecht, M. C. M., & Witkamp, G. J. (2017). Effect of pore size distribution on iron oxide coated granular activated carbons for phosphate adsorption - Importance of mesopores. *Chemical Engineering Journal*, 326, 231-239. doi: <https://doi.org/10.1016/j.cej.2017.05.147>
- Vyavahare, G., Jadhav, P., Jadhav, J., Patil, R., Aware, C., Patil, D., ... & Gurav, R. (2019). Strategies for crystal violet dye sorption on biochar derived from mango leaves and evaluation of residual dye toxicity. *Journal of Cleaner Production*, 207, 296-305. doi: <https://doi.org/10.1016/j.jclepro.2018.09.193>
- Wang, Z., Rorvik, S., Ratvik, A. P., & Grande, T. (2017). Formation of carbon build-up on the flue wall of anode baking furnace. In A. P. Ratvik (Ed.), *Light Metals 2017* (pp. 1265-1274). Cham, Switzerland: Springer. doi: https://doi.org/10.1007/978-3-319-51541-0_151
- Yang, Z., Ning, H. L., Jia, H., Li, Y., Meng, Z., & Chen, Z. (2020) Preparation of porous composite materials with semi-coke based activated carbon doped with graphene oxide. *IOP Conference Series: Material Science Engineering*, 729(1), 1-5.
- Yao, Y., Gao, B., Wu, F., Zhang, C., & Yang, L. (2015). Engineered biochar from biofuel residue: Characterization and its silver removal potential. *ACS Applied Material International*, 7(19), 10634-10640. doi: <https://doi.org/10.1021/acsami.5b03131>

Review Article

Multilingual Sentiment Analysis: A Systematic Literature Review

Nur Atiqah Sia Abdullah^{1*} and Nur Ida Aniza Rusli²

¹Faculty of Computer and Mathematical Sciences, Universiti Teknologi MARA,
40450 Shah Alam, Selangor, Malaysia

²Faculty of Computer and Mathematical Sciences, Universiti Teknologi MARA, Kampus Kuala Pilah,
Pekan Parit Tinggi, 72000 Kuala Pilah, Negeri Sembilan, Malaysia

ABSTRACT

With the explosive growth of social media, the online community can freely express their opinions without disclosing their identities. People with hidden agendas can easily post fake opinions to discredit target products, services, politicians, or organizations. With these big data, monitoring opinions and distilling their sentiments remain a formidable task because of the proliferation of diverse sites with a large volume of opinions that are portrayed in multilingual. Therefore, this paper aims to provide a systematic literature review on multilingual sentiment analysis, which summarises the common languages supported in multilingual sentiment analysis, pre-processing techniques, existing sentiment analysis approaches, and evaluation models that have been used for multilingual sentiment analysis. By following the systematic literature review, the findings revealed, most of the models supported two languages, and English is seen as the most used language in sentiment analysis

studies. None of the reviewed literature has catered the combination of languages for English, Chinese, Malay, and Hindi language on multilingual sentiment analysis. The common pre-processing techniques for the multilingual domain are tokenization, normalization, capitalization, N-gram, and machine translation. Meanwhile, the sentiment analysis classification techniques for multilingual sentiment are hybrid sentiment analysis, which includes localized

ARTICLE INFO

Article history:

Received: 08 September 2020

Accepted: 07 December 2020

Published: 22 January 2021

DOI: <https://doi.org/10.47836/pjst.29.1.25>

E-mail addresses:

atiqah684@uitm.edu.my (Nur Atiqah Sia Abdullah)

idaaniza@uitm.edu.my (Nur Ida Aniza Rusli)

* Corresponding author

language analysis, unsupervised topic clustering, and then followed by multilingual sentiment analysis. In terms of evaluation, most of the studies used precision, recall, and accuracy as the benchmark for the results.

Keywords: Machine learning, machine translation, multilingual sentiment analysis, opinion mining, pre-processing, sentiment analysis

INTRODUCTION

There is a well-known English saying “*The pen is mightier than the sword*” written by a novelist Edward Bulwer-Lytton in 1839 (as in Sykes et al., 2018), that emphasizes how the freedom of speech (including written and oral communications) has generally been a powerful tool than a weapon due to its capability to influence, persuade and control the society or situation (Mäntylä et al., 2018; Jing & Murugesan, 2018). The freedom of speech has opened opportunities for people to publicly voice out their feelings and opinions through various communication mediums without restrictions, which sometimes cause more damage and violated the right of free expressions.

Sentiment analysis is a method or process of detecting and extracting a given subject such as opinion and attitudes from written and spoken language. In general, sentiment analysis is about the ability to determine the sentiment of a topic and classify the overall polarity of the topic sentence in positive, negative, or neutral (Kang & Park, 2014). Sentiment analysis has been a popular research area over the past decade. It is gaining even more importance over time due to the emerging use of the internet and social media such as social networking sites; Twitter, forums, and blogs. Capturing public opinions about political issues, social events, products preferences, or services that they have used are valuable for understanding the concerns and to influence the decision-making process.

However, this sentiment analysis is facing an issue where the written opinions are often mixed with several languages which leads to the difficulties in fully capturing the text messages and consequently making the polarity of the text becomes harder to classify (Dashtipour et al., 2016; Devika et al., 2016). Hence, multilingual sentiment analysis is proposed to enhance the sentiment classification of texts in multiple languages. Recently, there has been considerable interest in multilingual sentiment analysis. Numerous methods and automatic tools have been developed to extract relevant information from various sources.

The purpose of this paper is to review different combination of strategies to develop a multilingual sentiment analysis that includes preprocessing techniques, sentiment analysis methods, and evaluation model that have been applied in the existing proposed models.

This paper is organized as follows. Section 2 briefly explains the concept of sentiment analysis. Section 3 presents the systematic literature review methods and processes. Section 4 and Section 5 present the results and discussions. Finally, Section 6 concludes the paper.

SENTIMENT ANALYSIS

The following sections describe the concept of sentiment analysis including pre-processing, sentiment analysis classification techniques, and evaluation models for multilingual sentiment analysis.

Pre-processing

Texts, especially in blogs, Twitter, and online chats are known to comprise various spelling errors, slang words, and multilingual words. Thus, pre-processing is important to remove irrelevant part of the texts, and to transform into a readable format to extract the sentiment. Some of pre-processing techniques in sentiment analysis are listed as follows (Dashtipour et al., 2016; Devika et al., 2016; Yadav & Elchuri, 2013).

Tokenization. A process of splitting text into words, phrases or other important parts called tokens. Tokens are separated by whitespace, punctuation marks, and line breaks; and characters such as punctuation marks are usually removed during the tokenization process. Tokenization is considered relatively easy compared to other preprocessing techniques.

Stopword Removal. A process of discarding words that do not have significant meaning such as 'a', 'of', and 'is'.

Stemming. A process of identifying the root of a specific word. For example, stemming puts variation of words such as 'greatly', 'greatest', and 'greater' to the root word 'great'.

N-gram Generation. A set of co-occurring words or letters taken from a body of text. The n-gram usually consists of bigram (n=2), for example, "honesty is", "is the", "the best", or "best policy" and trigram (n=3) like "honesty is the", "is the best" or "the best policy".

Lemmatization. A process of converting words to its initial form. Unlike stemming, lemmatization considers the context of the texts and translates the word into its relevant structure. For example, lemmatization would map the word 'caring' to the form of the word 'care', whereas stemming would transform the word 'caring' to 'car'.

POS (Part-of-speech) Tagging. A process of tagging a word in a text with its part of speech such as noun, verb, adverb, pronoun, preposition, and conjunction.

Noise Removal. A process of excluding noise such as HTML tags, keywords, scripts, or advertisements.

Normalization. A process of cleaning text and removing insignificant data such as word redundancy, spelling error, symbols, or tags.

Word Embedding/Text Vectors. A process to capture the similarities of words. In other words, it represents words in a coordinate system where related words, based on a corpus of relationships, are placed closer together. Word2Vec is the most common model for word embedding process.

Capitalization. A process of converting all letters to lowercase. Capitalization preprocessing technique is important to be employed especially for Twitter since Twitter users commonly use uppercase to express their emotions in texts.

Negation. A process of reversing the text polarity. A negation word can influence the structure of the whole sentence. When negation words such as ‘no’, ‘not’, and ‘never’ appear in a text, it is important to identify the scope of negation, as the presence of negations sometimes does not indicate the negative polarity.

Machine Translation. Several studies that adopt machine translation (to translate texts usually to English language) as a step to process texts and documents. Google Translate, Bing Translator, and Babylon translator are the most common machine translation tools used in sentiment analysis.

Sentiment Analysis Classification Techniques

Generally, the research on sentiment analysis is categorized into three approaches: machine learning, lexical based, and hybrid methods (Rajput & Solanki, 2016; Thakkar & Patel, 2015; Bahrainian & Dengel, 2013).

Machine Learning (ML). A method to teach a machine to learn and process data more efficiently. In this method, algorithms are used to train the computer to identify complex patterns, usually in big data and provide a decision based on the input given. These algorithms generally can be divided into two groups: supervised and unsupervised learning. Supervised learning is a type of system where data scientist or supervisor guides the algorithms to produce the aimed output. On the other hand, unsupervised learning can learn and recognize the pattern without human guidance. Support Vector Machine (SVM), Naive Bayesian (NB), Artificial Neural Network (ANN), and k-means algorithm are the common techniques used in ML (Sabbeh, 2018; Michie et al., 1994).

Lexicon Approach. A method that utilizes a predefined set of patterns, which is also known as sentiment dictionary or lexicon. Each data entry will be associated with sentiment orientation. For example, the word “great” is classified as positive sentiment word, and the word “bad” is classified as negative sentiment word. The sentiment classification for lexicon approach can be implemented either using dictionary-based or corpus-based approach. In dictionary-based approach, a dictionary which contains synonyms and antonyms of words are referred towards the opinion words from the texts. The dictionaries such as WordNet, SentiWordNet, SenticNet are usually used to classify the sentiment polarity of the words. Meanwhile, for corpus-based approach, the method works by relying on syntactic rules in large corpora. It provides a list of opinion words with relatively high precision of specific context (Hamouda & Rohaim, 2011; Esuli & Sebastiani, 2006).

Hybrid Method. The method combines the concept of machine learning and lexicon-based approach. The process generally started by analysing texts using lexicon-based approach. The produced results are then inserted into the machine learning as training data (Ardabili et al., 2019; Tsai & Wang, 2009).

Evaluation Methods

Evaluation methods are part of sentiment analysis proposals. There are many different evaluation models used for evaluating multilingual sentiment analysis. The most common evaluation models are as follows (Sokolova et al., 2006; Padmaja & Fatima, 2013):

Accuracy. Predictions of how often classifier makes correction prediction. It measures the ratio of correct predictions over the total number of instances evaluated.

$$Accuracy = \frac{Correct\ Prediction}{Total\ Number\ of\ Instance}$$

Precision. Calculates the exactness of a classifier the consistency of the results when the measurements are repeated. It measures the positive patterns that are correctly predicted from the total predicted patterns in a positive class.

$$Precision = \frac{True\ Positives}{True\ Positives + False\ Positives}$$

Recall. Computes the number of positive class predictions made out of all positive examples in the dataset. It measures the fraction of positive patterns that are correctly classified.

$$Recall = \frac{True\ Positives}{True\ Positives + False\ Negatives}$$

F-measure/ F1-score. Provides a single metric that balances both of precision and recall in one number. It measures the mean value between recall and precision value.

$$F1 = 2 * \frac{Precision * Recall}{Precision + Recall}$$

SYSTEMATIC LITERATURE REVIEW

Appropriate guidelines have been followed to conduct this systematic literature review, particularly the guidelines for SLRs in Software Engineering by Kitchenham and Charters (2007). The systematic literature review includes the research questions, data sources and search strategy, study selection, inclusion/exclusion criteria, and quality assessment as shown in Figure 1.

Research Questions

The research question addressed by this study is “What is the best sentiment analysis approach for multilingual sentiment analysis specific to English, Malay and Chinese?”

- What are the existing multilingual languages involved in sentiment analysis?
- Which pre-processing techniques are suitable to extract multilingual sentiment analysis?

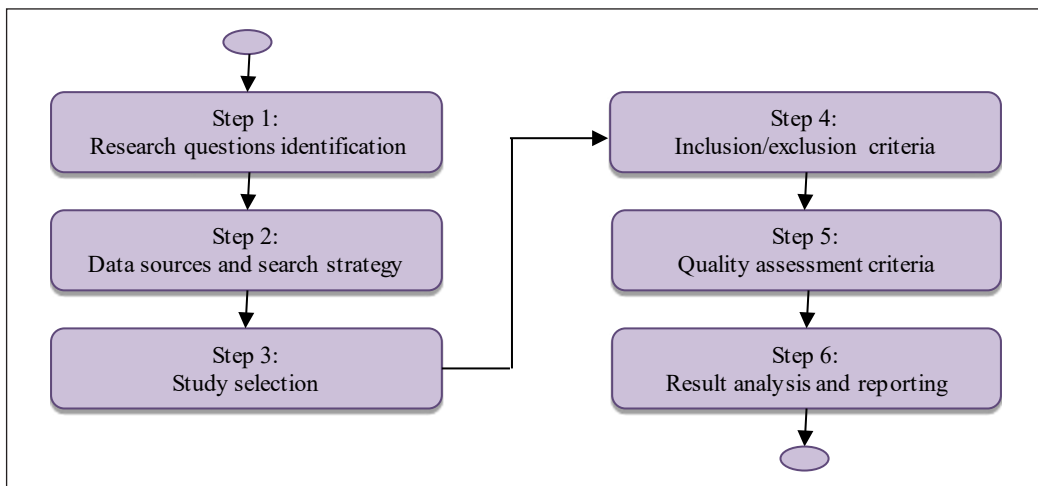


Figure 1. A systematic literature review flow for multilingual sentiment analysis

- What sentiment analysis classification methods are available for multilingual domain?
- How to evaluate the sentiment analysis classification methods in multilingual sentiment analysis?

Data Sources and Search Strategy

The planning stage also involved enumerating data sources which we searched for studies or previous works and used to define the query strings that would be executed on those sources. The following digital libraries were selected to carry out the search process of this review:

- IEEEXplore: <http://ieeexplore.ieee.org/>
- Science Direct: <http://www.sciencedirect.com/>.
- SpringerLink: <http://www.springerlink.com/>.
- ACM Digital Library: <http://portal.acm.org/>.
- Google Scholar: <http://scholar.google.com/>

We formulated the search terms using Population, Intervention, Contrast, and Outcome (Kitchenham & Charters, 2007). The following general search string was eventually used: “multilingual sentiment analysis” and (“pre-processing” or “lexicon-based” or “machine learning”). Table 1 shows that our initial searches elicited 336 articles.

Table 1
Search results

Digital Libraries	Search Results
IEEE Explore	64
Science Direct	57
Springer Link	66
ACM Digital Library	18
Google Scholar	131
Total	336

Study Selection

We obtained 336 articles in the first search process. Since many articles did not provide sufficient information to answer the research questions, we performed another filtration steps as follows:

- Step 1: remove the duplicated articles obtained by authors and/or different libraries.
- Step 2: apply inclusion and exclusion criteria to the candidate papers to avoid any irrelevant articles.
- Step 3: apply the quality assessment rules to include the qualified articles that give the best answers to the research questions.

Inclusion/Exclusion Criteria

After removing the duplicated articles, we obtained 248 articles. Next, we adopted the following inclusion/exclusion criteria. We went through the abstract and body of each paper to ensure their relevance according to these criteria. Defining inclusion and exclusion criteria helped to clarify the boundaries of the study.

The inclusion criteria:

- Primary studies published in journals, conferences, or workshop proceedings in the form of experiments, surveys, case studies, reports, and observation papers using multilingual sentiment analysis.
- Primary studies within the period from 2010 to 2019.

The exclusion criteria:

- Non-English publications
- Publications that did not include multilingual sentiment
- Informal studies (unknown conferences or journals)
- Articles that were irrelevant to the research questions

Quality Assessment

Once we had selected several works based on inclusion and exclusion criteria (51 articles), we assessed the quality of the research they presented. Six Quality Assessment (QA) questions (Indajat et al., 2016; Maita et al., 2015) had been defined to assess the quality of the research of each proposal and to provide a quantitative comparison between them. The scoring procedure used was Yes (Y) = 1, Partly (P) = 0.5 or No (N) = 0. The quality assessment questions defined in this systematic literature review, are as shown in Table 2.

Table 3 presents the results of the quality assessment score of each article. Each study could obtain a score ranging from zero to six points. Any study that awarded with a quality score three and lower was eliminated from the review. From the results, four articles were excluded since they did not satisfy the assessment criteria. There are 45 articles with grade four and higher that were considered as the resources for this review. The selected articles are listed in Table 4.

RESULTS

What are the Existing Multilingual Languages that involved in Sentiment Analysis?

A summary of results for research question RQ1 is presented in Tables 5 and 6. The results in Table 5 shows 31% (n=14) of selected studies used two languages in their proposed model, 27% (n=12) used three languages, 18% (n=8) used four languages, 13% (n=6) used five languages, 7% (n=3) used seven languages, and only 4% (n=2) used eight languages in their proposed method.

Table 2
Quality assessment checklist

Item	Assessment Criteria	Score	Description
QA1	Is there a clear statement in research aims?	0	No, aims are not described
		0.5	Partially, aims are described but unclearly
		1	Yes, aims are well described and clear
QA2	Does the pre-processing/feature used in the study is clearly described?	0	No, the pre-processing/feature are not described
		0.5	Partially, the pre-processing/feature are described but unclearly
		1	Yes, the pre-processing/feature are well described and clear
QA3	Does the study present a detailed description of the approach (classifier/techniques)?	0	No, details are missing
		0.5	Partially, if you want to use the approach, you need to read the references
		1	Yes, the approach can be used with presented details
QA4	Does the study present a detailed evaluation of the approach?	0	No, evaluation is missing
		0.5	Partially, evaluation process is described but unclearly
		1	Yes, the evaluation process is well described and clear
QA5	Is there a comparison with other approach?	0	No, comparison with other approach is missing
		0.5	Partially, comparison is described but unclearly
		1	Yes, the comparison with other approach is well described and clear
QA6	Is there a clear statement of the findings?	0	No, findings are not described
		0.5	Partially, findings are described but unclearly
		1	Yes, aims are well described and clear

Table 3
Quality assessment score

No	Author(s)	QA1	QA2	QA3	QA4	QA5	QA6	Total Score
1	Pessutto et al., 2018	1	0.5	1	1	1	1	5.5
2	Pustulka-Hunt et al., 2018	1	1	1	1	1	1	6
3	Vilares et al., 2018	1	0	1	1	0	1	4
4	Wehrmann et al., 2018	1	1	1	1	1	1	6
5	Vīksna and Jēkabsons, 2018	1	0	0	0	0	1	2
6	Bhargava and Sharma, 2017	1	1	1	1	0	1	6
7	Becker et al., 2017a	1	1	1	1	1	1	6
8	Lo et al., 2017b	1	1	1	1	0	1	5
9	Tellez et al., 2017	1	1	1	1	1	1	6
10	Vilares et al., 2017	1	1	1	1	0	1	5
11	Lo et al., 2017a	1	0	0	0	0	1	2
12	Becker et al. 2017b	1	1	1	1	1	1	6
13	Karima and Smaili, 2016	1	1	1	1	0	1	5
14	Lu and Mori, 2017	1	1	1	1	1	1	6
15	Kaity and Balakrishnan, 2017	1	0	1	0	0	0	2
16	Patel et al., 2017	1	1	1	1	1	1	6
17	Rosenthal et al., 2017	1	0	1	1	0	1	4

Table 3 (continue)

No	Author(s)	QA1	QA2	QA3	QA4	QA5	QA6	Total Score
18	Al-Shabi et al., 2017	1	0.5	1	1	1	1	5.5
19	Kaur et al., 2017	1	1	1	0	0	0	3
20	Deriu et al., 2017	1	1	1	1	1	1	6
21	Lo et al., 2016	1	1	1	1	1	1	6
22	Saravia et al., 2016	1	1	1	1	1	1	6
23	Araujo et al., 2016	1	0	1	1	1	1	5
24	Zhou et al., 2016	1	1	1	1	0	1	5
25	Pappas et al., 2016	1	0.5	1	1	0	1	4.5
26	Argueta et al., 2016	1	1	1	1	1	1	6
27	Shalunts and Backfried, 2016	1	0	1	0	1	1	4
28	Dadoun and Olsson, 2016	1	0.5	1	1	0	1	4.5
29	Balahur and Perea-Ortega, 2015	1	1	1	1	1	1	6
30	Nowson et al., 2015	1	1	1	1	0	1	5
31	Vilares et al., 2015	1	1	1	1	0	1	5
32	Shalunts and Backfried, 2015	1	1	1	1	1	1	6
33	Lin et al., 2014b	1	1	1	1	1	1	6
34	Balahur and Turchi, 2014	1	1	1	1	1	1	6
35	Cruz et al., 2014	1	1	1	1	1	1	6
36	Balahur et al., 2014	1	0.5	1	1	0	1	4.5
37	Abdel-Hady et al., 2014	1	0.5	1	1	0	1	4.5
38	Lin et al., 2014a	1	1	1	1	1	1	6
39	Erdmann et al., 2014	1	0.5	1	1	0	1	4.5
40	Volkova et al., 2013	1	0	1	1	0	1	4
41	Balahur and Turchi, 2013	1	1	1	1	0	1	5
42	Saad et al., 2013	1	1	1	1	1	1	6
43	Demirtas and Pechenizkiy, 2013	1	1	1	1	1	1	6
44	Balahur and Turchi, 2012a	1	1	1	1	1	1	6
45	Balahur and Turchi, 2012b	1	1	1	1	1	1	6
46	Tromp and Pechenizkiy, 2011	1	1	1	1	0	1	5
47	Cui et al., 2011	1	1	1	1	1	1	6
48	Gînscă et al., 2011	1	1	1	1	0	1	5
49	Steinberger et al., 2011	1	0	1	1	0	1	4

Table 4

List of selected articles

Study ID	Author (s)	Digital Library	Year
S1	Pessutto et al.	IEEE	2018
S2	Pustulka-Hunt et al.	IEEE	2018
S3	Vilares et al.	IEEE	2018
S4	Wehrmann et al.	Google Scholar	2018
S5	Bhargava, and Sharma	IEEE	2017
S6	Becker et al.	Science Direct	2017a
S7	Lo et al.	Science Direct	2017b
S8	Tellez et al.	Science Direct	2017
S9	Vilares et al.	Science Direct	2017

Table 4 (continue)

Study ID	Author (s)	Digital Library	Year
S1	Pessutto et al.	IEEE	2018
S2	Pustulka-Hunt et al.	IEEE	2018
S3	Vilares et al.	IEEE	2018
S4	Wehrmann et al.	Google Scholar	2018
S5	Bhargava, and Sharma	IEEE	2017
S6	Becker et al.	Science Direct	2017a
S7	Lo et al.	Science Direct	2017b
S8	Tellez et al.	Science Direct	2017
S9	Vilares et al.	Science Direct	2017
S10	Becker et al.	Google Scholar	2017b
S11	Karima and Smaili	Google Scholar	2016
S12	Lu and Mori	Google Scholar	2017
S13	Patel et al.	Google Scholar	2017
S14	Rosenthal et al.	Google Scholar	2017
S15	Al-Shabi et al.	Google Scholar	2017
S16	Deriu et al.	ACM	2017
S17	Lo et al.	Science Direct	2016
S18	Saravia et al.	Springer Link	2016
S19	Araujo et al.	ACM	2016
S20	Zhou et al.	ACM	2016
S21	Pappas et al.	ACM	2016
S22	Argueta et al.	Google Scholar	2016
S23	Shalunts and Backfried	Google Scholar	2016
S24	Dadoun and Olsson	Google Scholar	2016
S25	Balahur and Perea-Ortega	Science Direct	2015
S26	Nowson et al.	Google Scholar	2015
S27	Vilares et al.	Google Scholar	2015
S28	Shalunts and Backfried	Springer Link	2015
S29	Lin et al.	IEEE	2014b
S30	Balahur and Turchi	Science Direct	2014
S31	Cruz et al.	Science Direct	2014
S32	Balahur et al.	Google Scholar	2014
S33	Abdel-Hady et al.	Google Scholar	2014
S34	Lin et al.	ACM	2014a
S35	Erdmann et al.	Springer Link	2014
S36	Volkova et al.	Google Scholar	2013
S37	Balahur and Turchi	Google Scholar	2013
S38	Saad et al.	Google Scholar	2013
S39	Demirtas and Pechenizkiy	ACM	2013
S40	Balahur and Turchi	ACM	2012a
S41	Balahur and Turchi	Google Scholar	2012b
S42	Tromp and Pechenizkiy	IEEE	2011
S43	Cui et al.	Springer Link	2011
S44	Gînscă et al.	ACM	2011
S45	Steinberger et al.	Google Scholar	2011

Table 5
Number of languages supported in sentiment analysis

Number of Language	Study ID	Total	%
2 languages	S6, S7, S9, S11, S13, S14, S15, S24, S25, S27, S35, S38, S39, S42	14	31%
3 languages	S2, S12, S17, S18, S22, S28, S29, S30, S33, S36, S40, S44	12	27%
4 languages	S4, S5, S10, S16, S23, S26, S41, S43	8	18%
5 languages	S1, S3, S20, S31, S32, S37	6	13%
6 languages	-	0	0
7 languages	S19, S34, S45	3	7%
8 languages	S8, S21	2	4%

The detail languages supported in the selected studies are shown in Table 6. From the results, we can conclude that 91% (n=41) applied a combination of English with other languages, 13% (n=6) applied a combination of English, Chinese and other languages, and only one article (S17) that included English, Chinese and Malay on multilingual sentiment analysis. Meanwhile, two studies (S3 and S13) were using the combination of English, Hindi, and other languages.

Thus, from the literature review, we found out that none of the studies had catered the combination of languages for English, Chinese, Malay, and Hindi language on multilingual sentiment analysis. This is an important finding because based on the social environment in Malaysia, major races use languages like English, Malay, and Chinese language. Hindi language is not used in Malaysia. Most of the Indians in Malaysia use Tamil language. However, there seems to be a lag in Tamil language use among the younger generation. The younger generation tends to converse in Malay and English more than Tamil (Paramasivam & Farashaiyan, 2016).

Table 6
Languages used in the selected articles

Study ID	Target Languages
S1	English, Spanish, Dutch, Russian, and Turkish
S2	English, German, and French
S3	Spanish, Italian, Portuguese, Chinese, and Hindi
S4	English, Spanish, German, and Portuguese
S5	English, Spanish, German, and French
S6	English and Portuguese
S7	English and Chinese (dialect)
S8	English, Spanish, German, Italian, Portuguese, Russian, Arabic, and Swedish
S9	English and Spanish
S10	English, Spanish, German, and Portuguese
S11	English and Arabic
S12	English, Chinese, and Japanese

Table 6 (continue)

Study ID	Target Languages
S13	English and Hindi
S14	English and Arabic
S15	English and Arabic
S16	English, German, French, and Italian
S17	English, Chinese (dialect), and Malay
S18	English, Spanish, and French
S19	Spanish, German, French, Italian, Portuguese, Dutch, and Turkish
S20	English, Spanish, German, Portuguese, and Dutch
S21	English, Spanish, German, French, Italian, Chinese, Russian, and Turkish
S22	English, Spanish, and French
S23	English, Spanish, German, and Russian
S24	English and Swedish
S25	English and Spanish
S26	English, Spanish, Italian, and Dutch
S27	English and Spanish
S28	English, German, and Russian
S29	English, German, and French
S30	Spanish, German, and French
S31	English, Spanish, Catalan, Basque, and Galician
S32	English, Spanish, German, French, and Italian
S33	English, Spanish, and Portuguese
S34	English, Spanish, German, French, Italian, Chinese, and Dutch
S35	English and Japanese
S36	English, Spanish, and Russian
S37	English, Spanish, German, French, and Italian
S38	English and Arabic
S39	English and Turkish
S40	Spanish, German, and French
S41	English, Spanish, German, and French
S42	English and Dutch
S43	English, Spanish, German, and Portuguese
S44	English and Romanian
S45	English, Spanish, German, French, Italian, Czech, and Hungarian

Which Pre-processing Techniques are Suitable to Extract Multilingual Sentiment Analysis?

A quantitative summary of the results for research questions RQ2 is shown in Table 7. The results presented in Table 7 reveal that machine translation (49%) and tokenization (42%) were the most common preprocessing techniques in multilingual sentiment analysis;

Table 7
Pre-processing technique in sentiment analysis

Processing	Study ID	Total	%
Tokenization	S1, S2, S4, S6, S12, S15, S16, S17, S18, S20, S22, S24, S25, S26, S32, S34, S37, S43, S44	19	42%
Stop word removal	S5, S7, S8, S11, S15, S29, S31, S43	8	18%
Stemming	S5, S8, S11, S15, S28	5	11%
N-gram	S2, S9, S12, S13, S15, S26, S27, S30, S32, S33, S38, S39, S40, S41, S44	15	33%
Lemmatization	S9, S11, S20, S26, S27, S31, S44	7	16%
POS tagging	S5, S9, S11, S20, S26, S27, S42, S43	8	18%
Noise removal	S7, S35	2	4%
Normalization	S12, S17, S18, S22, S25, S26, S32, S37, S43, S44	10	22%
Word Embedding / Text Vectors	S1, S4, S5, S10, S12, S16, S21, S30	8	18%
Capitalization	S1, S2, S12, S16, S17, S25, S28, S37, S44	9	20%
Negation	S8, S28	2	4%
Machine translation	S3, S13, S15, S19, S20, S21, S23, S24, S25, S26, S30, S32, S33, S34, S35, S36, S37, S39, S40, S41, S43, S45	22	49%

this was followed by n-gram (33%), normalization (22%) and capitalization (20%). Next, POS tagging (18%), word embedding/text vectors (18%), lemmatization (16%), stemming (11%), noise removal (4%), and negation (4%).

Table 8 shows several pre-processing techniques used for English, Chinese, Malay, and Hindi language. Among the articles that had focused on English language, tokenization was the most pre-processing technique used for English language (n=19), followed by machine translation (n=18), n-gram (n=13), normalization (n=10) and capitalization (n=9). Meanwhile, in Chinese language, tokenization (n=3), machine translation (n=3), word embedding/text vector (n=2), normalization (n=2) and capitalization (n=2) were the most preprocessing techniques used in the proposals. S17, the only proposal that focused primarily on the Malay language, had adopted tokenization, normalization, and capitalization in their proposed model. Lastly, S13 used n-gram and machine translation to process Hindi text.

Based on Table 8, the pre-processing techniques, which are commonly used for multilingual sentiment analysis, include tokenization, normalization, and capitalization. These three pre-processing techniques are used to extract the sentiment in the multilingual languages like English, Chinese and Malay. However, for the combination of languages that include English, Chinese and Hindi, the suitable pre-processing techniques are N-gram and machine translation.

Table 8
Number of preprocessing techniques used for English, Chinese, Malay and Hindi language

Pre-processing	English	Chinese	Malay	Hindi
Tokenization	S1, S2, S4, S6, S12, S15, S16, S17, S18, S20, S22, S24, S25, S26, S32, S34, S37, S43, S44 Total: 19	S12, S17, S34 3	S17 1	- 0
Stopword removal	S5, S7, S8, S11, S15, S29, S31, S43 Total: 8	S7 1	- 0	- 0
Stemming	S5, S8, S11, S15, S28 Total: 5	- 0	- 0	- 0
N-gram	S2, S9, S12, S13, S15, S26, S27, S32, S33, S38, S39, S41, S44 Total: 13	S12 1	0 -	S13 1
Lemmatization	S9, S11, S20, S26, S27, S31, S44 Total: 7	- 0	- 0	- 0
POS tagging	S5, S9, S11, S20, S26, S27, S42, S43 Total: 8	- 0	- 0	- 0
Noise removal	S7, S35 Total: 2	S7 1	- 0	- 0
Normalization	S12, S17, S18, S22, S25, S26, S32, S37, S43, S44 Total: 10	S12, S17 2	S17 1	- 0
Word embedding/ text vector	S1, S4, S5, S10, S12, S16, S21 Total: 7	S12, S21 2	- 0	- 0
Capitalization	S1, S2, S12, S16, S17, S25, S28, S37, S44 Total: 9	S12, S17 2	S17 1	- 0
Negation	S8, S28 Total: 2	- 0	- 0	- 0
Machine translation	S13, S15, S20, S21, S23, S24, S25, S26, S32, S33, S34, S35, S36, S37, S39, S41, S43, S45 Total: 18	S3, S21, S34 3	- 0	S13 1

What Sentiment Analysis Classification Methods are Available for Multilingual Domain?

Table 9 shows a quantitative summary of the results for research questions RQ3. From the results in Table 9, machine learning (51%, n=23) was the most common sentiment analysis technique for multi-language; followed by lexicon (38%, n=17) and hybrid technique (11%, n=5).

From the results in Table 10, we can conclude that machine learning was the leading sentiment analysis technique for English language (n=21), followed by lexicon (n=16) and hybrid technique (n=4). Meanwhile, machine learning, lexicon-based, and hybrid method were equally adopted by two articles as the sentiment analysis method for the Chinese

Table 9
Methods for multilingual sentiment analysis

Sentiment Analysis	Study ID	Total	%
Machine learning	S1, S2, S4, S6, S7, S8, S9, S10, S12, S13, S15, S18, S25, S26, S27, S29, S30, S32, S37, S39, S40, S41, S44	23	51%
Lexicon	S3, S11, S14, S16, S20, S21, S22, S23, S28, S31, S33, S35, S36, S38, S42, S43, S45	17	38%
Hybrid	S5, S17, S24, S19, S34	5	11%

Table 10
Summary of sentiment analysis methods for English, Chinese, Malay and Hindi language

Language	Sentiment Analysis	StudyID	Total
English	Machine Learning	S1, S2, S4, S6, S7, S8, S9, S10, S12, S13, S15, S18, S25, S26, S27, S29, S32, S37, S39, S41, S44	21
	Lexicon	S11, S14, S16, S20, S21, S22, S23, S28, S31, S33, S35, S36, S38, S42, S43, S45,	16
	Hybrid	S5, S17, S24, S34	4
Chinese	Machine learning	S7, S12	2
	Lexicon	S3, S21	2
	Hybrid	S17, S34	2
Malay	Machine Learning	-	0
	Lexicon	-	0
	Hybrid	S17	1
Hindi	Machine Learning	S13	1
	Lexicon	S3	1
	Hybrid	-	0

language. For Malay language, S17 had used the hybrid technique in the proposed model, while the Hindi language had adopted machine learning and lexicon-based approach.

Based on Table 10, the sentiment analysis classification technique for multilingual sentiment that involves English, Chinese, and Malay is hybrid sentiment analysis. The hybrid sentiment analysis processes include the localized language analysis, unsupervised topic clustering, and followed by the multilingual sentiment analysis. Meanwhile, for the combination of languages that includes English, Chinese and Hindi, the classification techniques can be either machine learning or lexicon-based techniques.

How to Evaluate the Sentiment Analysis Methods in Multilingual Sentiment Analysis?

A quantitative summary of the results for research questions RQ4 is presented in Table 11. The results described that accuracy (36%, n=16) was the most common evaluation model for multilingual sentiment analysis, followed by precision (22%, n=10). In contrast, recall

Table 11
Evaluation model for multilingual sentiment analysis

Evaluation Criteria	Study ID	Total	%
Precision	S2, S5, S7, S17, S18, S33, S35, S36, S44, S45	10	22%
Recall	S2, S5, S7, S14, S17, S32, S33, S36, S45	9	20%
F measure/ F1 score	S6, S10, S16, S32, S33, S36, S43	7	16%
Accuracy	S2, S4, S10, S12, S13, S14, S18, S22, S27, S29, S31, S34, S37, S38, S39, S43	16	36%

Table 12
Evaluation model for English, Chinese, Malay, Hindi and Arabic language

Language	Evaluation Model	Study ID	Total
English	Precision	S2, S5, S7, S17, S18, S33, S35, S36, S44, S45	10
	Recall	S2, S5, S7, S14, S17, S32, S33, S36, S45	9
	F measure/ F1 score	S6, S10, S16, S32, S33, S36, S43	7
	Accuracy	S2, S4, S10, S12, S13, S14, S18, S22, S27, S29, S31, S34, S37, S38, S39, S43	16
Chinese	Precision	S7, S17	2
	Recall	S7, S17	2
	F measure/ F1 score	-	0
	Accuracy	S12, S34	2
Malay	Precision	S17	2
	Recall	S17	2
	F measure/ F1 score	-	0
	Accuracy	-	0
Hindi	Precision	-	0
	Recall	-	0
	F measure/ F1 score	-	0
	Accuracy	S13	1

(20%, n=9) and F-measure (16%, n=7) were found to have the lowest number of articles used for the evaluation process.

Table 12 illustrates the evaluation model used for English, Chinese, Malay, and Hindi language. According to the results, we can summarize that accuracy is the most common evaluation model for English language (n=16). Instead, for Chinese language, precision and recall are employed to evaluate S7 and S17. Malay language in S17 had also used precision and recall model, while S13 had used accuracy model for the Hindi language.

Based on Table 12, to evaluate the sentiment analysis methods for multilingual sentiment in English, Chinese, and Malay, the evaluation models include precision and recall. For English, Chinese, and Hindi, the evaluation model is more on the accuracy.

From the literature, there is an issue in terms of the evaluation model selected for the analysis process. There is no specific approach to evaluate sentiment analysis specifically for multilingual. It means the evaluation model is selected without academic justification and the evaluation criteria are solely decided by the researcher (Alsaeedi, 2009). Although these evaluation models are broadly applied in practices, it is important to find a set of generic evaluation criteria in which they are capable to accommodate various languages without producing biases towards given datasets.

DISCUSSION

The growth of the internet and social media has given users to share their thoughts and opinions on all kinds of topic in different languages. Sentiment analysis in only one language could increase the risks of missing important information if the texts are written using a combination of other languages. Furthermore, most research on sentiment analysis focuses on text written in English, and there is a significant lack regarding the information sources for other languages. Consequently, most of the resources, such as sentiment lexicons and corpora, have been developed for the English language. An effective sentiment analysis approach should be able to handle a variety of languages so that it could easily detect the content or specific word in different languages and improves the overall classification of sentiment in the data.

While increasing effort has been made in creating resources for other formal languages, there are not many resources available when it comes to languages that are not commonly used in informal communication. It is well-known that different languages have their unique way of expression; for example, in S17, Singaporeans generally speak and write in English with some Chinese dialects and Malay language; which are certainly mixed with informal languages. Thus, it is important to note that, future research should not only cater to formal multilingual texts, but it should be possible to process texts in informal representation too.

Preprocessing method plays an important role to extract the relevant content and eliminate unnecessary words. From the analysis, machine translation is the most common preprocessing technique in multilingual sentiment analysis, followed by tokenization. The performance of machine translation systems such as Google Translate and Bing Translator has proven effective to provide accurate translation for most spoken languages. Machine translation, however, occasionally faced problems where it does not fully translate the texts, which can bring the risk of missing relevant content in texts (Balahur & Turchi, 2012a; Al-Kabi et al., 2013). Whereas tokenization is generally considered as an easy preprocessing technique compared to other techniques, however, it is important to note that tokenization process can be hard to implement to the text that does not have any whitespace or other characters. Some of the languages are classified as space-delimited; by means, the words are separated from each other's blank space, while languages such as Chinese, Japanese

and Thai are referred as unsegmented word, where the languages do not have particular boundaries (Wang et al., 2017). Tokenization of unsegmented language can be difficult and would require additional technique or procedure. For example, instead of tokenized words using Chinese characters, S7 and S17 adapt the romanization of Chinese words to execute the tokenization process. Hence, researchers need to identify properly which preprocessing technique is suitable to process their target languages.

In terms of sentiment analysis technique, machine learning approaches for multi-language have been extensively studied due to their capability to adopt a variety of preprocessing techniques and features. Machine learning techniques like Naïve Bayes (NB), Support vector machine (SVM) and K-nearest neighbor (KNN) have been proven achieved great success in sentiment analysis. Among 23 literatures, S6, S13, S15, S29, S39 and S44 have adopted NB classifier in the proposal. The advantage of the Naïve Bayes classifier is that it requires a small amount of training data to estimate the parameters necessary for classification. However, empirical finding (Alsaleem, 2011; Hadi et al., 2010) indicated that SVM approaches are performed better compared to NB approach for multilingual sentiment analysis. Support vector machines (SVMs) are one of the classification methods that are well-known to be more accurate; thus, studies such as S6, S8, S12, S13, S15, S25, S30, S32, S37, S39, S40, and S41 have used SVM method in their proposal. Meanwhile, S13, S15, and S29 adopted KNN in their proposal. This method was said to be effective and easy to be implemented for multiple languages (Baro et al., 2019).

Choosing the right evaluation models is particularly important since the selection of the techniques can produce a potential positive or negative bias towards measuring the sentiment analysis characteristics. The analysis shows that accuracy is the most common method to measure the performance of sentiment analysis proposals due to its simplicity and straightforward process in generating the results. However, it should be noted that using accuracy model alone could be insufficient to ensure the results can be used solely as the indicator since it only yields a single number without describing the types of errors occur during the evaluation process. In addition, accuracy is highly affected by the imbalance number of instances in different classes (Dinsoreanu & Bacu, 2014; Al-Azani & El-Alfy, 2017). Thus, a combination of other evaluation models such as accuracy and precision, or accuracy and f-measure could draw the right conclusions on the performance of sentiment analysis models.

CONCLUSION

This paper has presented a systematic literature review of articles from 2010 to 2019, covering the aspects of common languages supported in multilingual sentiment analysis, pre-processing techniques, sentiment analysis approaches, and evaluation model that have been used to multilingual sentiment analysis. We have identified 45 primary studies that

are related to the four research questions (RQs) in this review. A vast majority (31%) of the 45 articles include two languages multilingual sentiment analysis, and most of the studies (91%) introduced a combination of English with other languages (RQ1). The most preferred preprocessing technique for answering RQ2 is machine translation (49%), followed by tokenization (42%). Overall, 51% of articles used machine learning as the method in multilingual sentiment analysis (RQ3), and finally, it is found that most of articles (36%) are likely to use accuracy to evaluate their proposed method (RQ4).

ACKNOWLEDGEMENTS

The authors would like to thank Ministry of Higher Education (MOHE) Malaysia for sponsoring this paper under the grant of FRGS/1/2018/ICT04/UITM/02/9. A special appreciation for Faculty of Computer and Mathematical Sciences, Universiti Teknologi MARA for supporting the publication of this paper.

REFERENCES

- Abdel-Hady, M., Mansour, R., & Ashour, A. (2014, August 24). Cross-lingual twitter polarity detection via projection across word-aligned corpora. In *Proceedings of WISDOM* (pp. 1-12). New York, USA.
- Al-Azani, S., & El-Alfy, E. S. M. (2017). Using word embedding and ensemble learning for highly imbalanced data sentiment analysis in short arabic text. *Procedia Computer Science*, 109, 359-366.
- Al-Kabi, M. N., Hailat, T. M., Al-Shawakfa, E. M., & Alsmadi, I. M. (2013). Evaluating English to Arabic machine translation using BLEU. *International Journal of Advanced Computer Science and Applications (IJACSA)*, 4(1), 66-73.
- Alsaeedi, A. (2019). EFTSA: Evaluation framework for Twitter sentiment analysis. *Journal of Software*, 14(1), 24-35. doi: 10.17706/jsw.14.1.24-35
- Alsalem, S. (2011). Automated Arabic text categorization using SVM and NB. *International Arab Journal of e-Technology*, 2(2), 124-128.
- Al-Shabi, A., Adel, A., Omar, N., & Al-Moslimi, T. (2017). Cross-lingual sentiment classification from English to Arabic using machine translation. *International Journal of Advanced Computer Science and Applications*, 8(12), 434-440. doi: 10.14569/IJACSA.2017.081257
- Araujo, M., Reis, J., Pereira, A., & Benevenuto, F. (2016). An evaluation of machine translation for multilingual sentence-level sentiment analysis. In *Proceedings of the 31st Annual ACM Symposium on Applied Computing* (pp. 1140-1145). New York, USA: ACM. doi: <https://doi.org/10.1145/2851613.2851817>
- Ardabili, S., Mosavi, A., & Várkonyi-Kóczy, A. R. (2019). Advances in machine learning modeling reviewing hybrid and ensemble methods. In *International Conference on Global Research and Education* (pp. 215-227). Cham, Switzerland: Springer. doi: https://doi.org/10.1007/978-3-030-36841-8_21
- Argueta, C., Calderon, F. H., & Chen, Y. S. (2016). Multilingual emotion classifier using unsupervised pattern extraction from microblog data. *Intelligent Data Analysis*, 20(6), 1477-1502. doi: 10.3233/IDA-140267

- Bahrainian, S. A., & Dengel, A. (2013, December 3-5). Sentiment analysis and summarization of twitter data. In *2013 IEEE 16th International Conference on Computational Science and Engineering* (pp. 227-234). Sydney, Australia. doi: 10.1109/CSE.2013.44
- Balahur, A., & Perea-Ortega, J. M. (2015). Sentiment analysis system adaptation for multilingual processing: The case of tweets. *Information Processing and Management*, *51*(4), 547-556. doi: <https://doi.org/10.1016/j.ipm.2014.10.004>
- Balahur, A., & Turchi, M. (2012a, September 28). Comparative experiments for multilingual sentiment analysis using machine translation. In *Proceedings of the 1st International Workshop in Sentiment Discovery from Affective Data* (pp. 75-86). Bristol, UK.
- Balahur, A., & Turchi, M. (2012b, July 12). Multilingual sentiment analysis using machine translation? In *Proceedings of the 3rd workshop in Computational Approaches to Subjectivity and Sentiment Analysis* (pp. 52-60). Jeju, Republic of Korea.
- Balahur, A., & Turchi, M. (2013, September 7-13). Improving sentiment analysis in twitter using multilingual machine translated data. In *Proceedings of the International Conference Recent Advances in Natural Language Processing 2013* (pp. 49-55). Hissar, Bulgaria.
- Balahur, A., & Turchi, M. (2014). Comparative experiments using supervised learning and machine translation for multilingual sentiment analysis. *Computer Speech and Language*, *28*(1), 56-75. doi: <https://doi.org/10.1016/j.csl.2013.03.004>
- Balahur, A., Turchi, M., Steinberger, R., Ortega, J. M. P., Jacquet, G., Küçük, D., & El Ghali, A. (2014). Resource creation and evaluation for multilingual sentiment analysis in social media texts. In *Proceedings of the Ninth International Conference on Language Resources and Evaluation 2014* (pp. 4265-4269). Reykjavik, Iceland: European Language Resources Association.
- Baro, R. A., Pagudpud, M. V., Padirayon, L. M., & Dilan, R. E. (2019, February). Classification of project management tool reviews using machine learning-based sentiment analysis. In *IOP Conference Series: Materials Science and Engineering* (Vol. 482, No. 1, p. 012041). Bristol, UK: IOP Publishing. doi: <https://doi.org/10.1088/1757-899X/482/1/012041>
- Becker, K., Moreira, V. P., & dos Santos, A. G. (2017a). Multilingual emotion classification using supervised learning: Comparative experiments. *Information Processing and Management*, *53*(3), 684-704. doi: <https://doi.org/10.1016/j.ipm.2016.12.008>
- Becker, W., Wehrmann, J., Cagnini, H. E., & Barros, R. C. (2017b). An efficient deep neural architecture for multilingual sentiment analysis in twitter. In *Proceedings of the Thirtieth International Flairs Conference* (pp. 246-251). Palo Alto, California: AAAI Press.
- Bhargava, R., & Sharma, Y. (2017, January 12-13). MSATS: Multilingual sentiment analysis via text summarization. In *Proceedings of 7th International Conference on Cloud Computing, Data Science and Engineering-Confluence 2017* (pp. 71-76). Noida, India. doi: 10.1109/CONFLUENCE.2017.7943126
- Cruz, F. L., Troyano, J. A., Pontes, B., & Ortega, F. J. (2014). Building layered, multilingual sentiment lexicons at synset and lemma levels. *Expert Systems with Applications*, *41*(13), 5984-5994. doi: <https://doi.org/10.1016/j.eswa.2014.04.005>

- Cui, A., Zhang, M., Liu, Y., & Ma, S. (2011). Emotion tokens: Bridging the gap among multilingual twitter sentiment analysis. In *Asia information retrieval symposium* (pp. 238-249). Heidelberg, Germany: Springer. doi: https://doi.org/10.1007/978-3-642-25631-8_22
- Dadoun, M., & Olsson, D. (2016). *Sentiment classification techniques applied to swedish tweets investigating the effects of translation on sentiments from Swedish into English* (Degree Project). KTH Royal Institute of Technology, Stockholm, Sweden.
- Dashtipour, K., Poria, S., Hussain, A., Cambria, E., Hawalah, A. Y., Gelbukh, A., & Zhou, Q. (2016). Multilingual sentiment analysis: State of the art and independent comparison of techniques. *Cognitive computation*, 8(4), 757-771. doi: <https://doi.org/10.1007/s12559-016-9415-7>
- Demirtas, E., & Pechenizkiy, M. (2013). Cross-lingual polarity detection with machine translation. In *Proceedings of the Second International Workshop on Issues of Sentiment Discovery and Opinion Mining* (pp. 9-17). Chicago, USA: ACM. doi: <https://doi.org/10.1145/2502069.2502078>
- Deriu, J., Lucchi, A., De Luca, V., Severyn, A., Müller, S., Cieliebak, M., ... & Jaggi, M. (2017). Leveraging large amounts of weakly supervised data for multi-language sentiment classification. In *Proceedings of the 26th International Conference on World Wide Web* (pp. 1045-1052). Geneva, Switzerland: International World Wide Web Conferences Steering Committee. doi: <https://doi.org/10.1145/3038912.3052611>
- Devika, M. D., Sunitha, C., & Ganesh, A. (2016). Sentiment analysis: A comparative study on different approaches. *Procedia Computer Science*, 87, 44-49. doi: <https://doi.org/10.1016/j.procs.2016.05.124>
- Dinsoreanu, M., & Bacu, A. (2014, October 21-24). Unsupervised twitter sentiment classification. In *Proceedings of the International Conference on Knowledge Management and Information Sharing 2014* (pp. 220-227). Rome, Italy. doi: 10.5220/0005079002200227
- Erdmann, M., Ikeda, K., Ishizaki, H., Hattori, G., & Takishima, Y. (2014). Feature based sentiment analysis of tweets in multiple languages. In *International Conference on Web Information Systems Engineering* (pp. 109-124). Cham, Switzerland: Springer. doi: https://doi.org/10.1007/978-3-319-11746-1_8
- Esuli, A., & Sebastiani, F. (2006). Sentiwordnet: A publicly available lexical resource for opinion mining. *Proceedings of Language Resources and Evaluation (LREC 2006)*, 6, 417-422.
- Gînscă, A. L., Boroş, E., Iftene, A., TrandabĂţ, D., Toader, M., Corîci, M., & Cristea, D. (2011, June 24). Sentimatrix: Multilingual sentiment analysis service. In *Proceedings of the 2nd workshop on computational approaches to subjectivity and sentiment analysis* (pp. 189-195). Portland, Oregon, USA.
- Hadi, W. E. M., Salam, M. A., & Al-Widian, J. A. (2010). Performance of NB and SVM classifiers in Islamic Arabic data. In *Proceedings of the 1st International Conference on Intelligent Semantic Web-Services and Applications* (pp. 1-6). New York, USA: ACM. doi: <https://doi.org/10.1145/1874590.1874604>
- Hamouda, A., & Rohaim, M. (2011). Reviews classification using sentiwordnet lexicon. *The Online Journal on Computer Science and Information Technology (OJCSIT)*, 2(1), 120-123.
- Injadat, M., Salo, F., & Nassif, A. B. (2016). Data mining techniques in social media: A survey. *Neurocomputing*, 214, 654-670. doi: <https://doi.org/10.1016/j.neucom.2016.06.045>
- Jing, T. W., & Murugesan, R. K. (2018). A theoretical framework to build trust and prevent fake news in social media using blockchain. In *International Conference of Reliable Information and Communication*

- Technology* (pp. 955-962). Cham, Switzerland: Springer. doi: https://doi.org/10.1007/978-3-319-99007-1_88
- Kaity, M., & Balakrishnan, V. (2017, July 18). A multi-layered framework for building multilingual sentiment lexicons. In *Proceedings of the Postgraduate Research Excellence Symposium 2017* (pp. 29-34). Kuala Lumpur, Malaysia.
- Kang, D., & Park, Y. (2014). Based measurement of customer satisfaction in mobile service: Sentiment analysis and VIKOR approach. *Expert Systems with Applications*, *41*(4), 1041-1050. doi: <https://doi.org/10.1016/j.eswa.2013.07.101>
- Karima, A., & Smaili, K. (2016, September 29 - October 1). Measuring the comparability of multilingual corpora extracted from Twitter and others. In *Proceedings of the Tenth International Conference on Natural Language Processing (HrTAL2016)*. Dubrovnik, Croatia.
- Kaur, H., Mangat, V., & Krail, N. (2017). Dictionary based sentiment analysis of hinglish text. *International Journal of Advanced Research in Computer Science*, *8*(5), 816-822. doi: 10.26483/ijarcs.v8i5.3438
- Kitchenham, B., & Charters, S. (2007). *Guidelines for performing systematic literature reviews in software engineering* (EBSE Technical Report). Keele University, UK.
- Lin, Z., Jin, X., Xu, X., Wang, W., Cheng, X., & Wang, Y. (2014a). A cross-lingual joint aspect/sentiment model for sentiment analysis. In *Proceedings of the 23rd ACM international conference on conference on information and knowledge management* (pp. 1089-1098). New York, USA: ACM. doi: <https://doi.org/10.1145/2661829.2662019>
- Lin, Z., Jin, X., Xu, X., Wang, Y., Tan, S., & Cheng, X. (2014b, August 11-14). Make it possible: Multilingual sentiment analysis without much prior knowledge. In *Proceedings of the 2014 IEEE/WIC/ACM International Joint Conferences on Web Intelligence (WI) and Intelligent Agent Technologies (IAT)-Volume 02* (pp. 79-86). Warsaw, Poland. doi: 10.1109/WI-IAT.2014.83
- Lo, S. L., Cambria, E., Chiong, R., & Cornforth, D. (2016). A multilingual semi-supervised approach in deriving Singlish sentic patterns for polarity detection. *Knowledge-Based Systems*, *105*, 236-247. doi: <https://doi.org/10.1016/j.knosys.2016.04.024>
- Lo, S. L., Cambria, E., Chiong, R., & Cornforth, D. (2017a). Multilingual sentiment analysis: From formal to informal and scarce resource languages. *Artificial Intelligence Review*, *48*(4), 499-527. doi: <https://doi.org/10.1007/s10462-016-9508-4>
- Lo, S. L., Chiong, R., & Cornforth, D. (2017b). An unsupervised multilingual approach for online social media topic identification. *Expert Systems with Applications*, *81*, 282-298. doi: <https://doi.org/10.1016/j.eswa.2017.03.029>
- Lu, Y., & Mori, T. (2017). Deep learning paradigm with transformed monolingual word embeddings for multilingual sentiment analysis. *Computing Research Repository*, *2017*, 1-10.
- Maita, A. R. C., Martins, L. C., Lopez Paz, C. R., Peres, S. M., & Fantinato, M. (2015). Process mining through artificial neural networks and support vector machines: A systematic literature review. *Business Process Management Journal*, *21*(6), 1391-1415. doi: <https://doi.org/10.1108/BPMJ-02-2015-0017>

- Mäntylä, M. V., Graziotin, D., & Kuuttila, M. (2018). The evolution of sentiment analysis - A review of research topics, venues, and top cited papers. *Computer Science Review*, 27, 16-32. doi: <https://doi.org/10.1016/j.cosrev.2017.10.002>
- Michie, D., Spiegelhalter, D. J., & Taylor, C. C. (1994). Machine learning. *Neural and Statistical Classification*, 13(1994), 1-298.
- Nowson, S., Perez, J., Brun, C., Mirkin, S., & Roux, C. (2015, September 8-11). XRCE personal language analytics engine for multilingual author profiling. In *Proceedings of the Working Notes of CLEF 2015 - Conference and Labs of the Evaluation Forum* (pp. 1412-1424). Toulouse, France.
- Padmaja, S., & Fatima, S. S. (2013). Opinion mining and sentiment analysis-an assessment of peoples' belief: A survey. *International Journal of Ad hoc, Sensor & Ubiquitous Computing*, 4(1), 21-33. doi: 10.5121/ijasuc.2013.4102
- Pappas, N., Redi, M., Topkara, M., Jou, B., Liu, H., Chen, T., & Chang, S. F. (2016). Multilingual visual sentiment concept matching. In *Proceedings of the 2016 ACM on International Conference on Multimedia Retrieval* (pp. 151-158). New York, USA: ACM. doi: <https://doi.org/10.1145/2911996.2912016>
- Paramasivam, M., & Farashaiyan, A. (2016). Language change and maintenance of Tamil language in the multilingual context of Malaysia. *International Journal of Humanities and Social Science Invention*, 5(12), 55-60.
- Patel, S., Nolan, B., Hofmann, M., Owende, P., & Patel, K. (2017). Sentiment analysis: Comparative analysis of multilingual sentiment and opinion classification techniques. *World Academy of Science, Engineering and Technology, International Journal of Computer, Electrical, Automation, Control and Information Engineering*, 11(6), 565-571.
- Pessutto, L. R. C., Vargas, D. S., & Moreira, V. P. (2018, December 3-6). Clustering multilingual aspect phrases for sentiment analysis. In *2018 IEEE/WIC/ACM International Conference on Web Intelligence (WI)* (pp. 182-189). Santiago, Chile. doi: 10.1109/WI.2018.00-91
- Pustulka-Hunt, E., Hanne, T., Blumer, E., & Frieder, M. (2018, August 27-29). Multilingual sentiment analysis for a swiss gig. In *2018 6th International Symposium on Computational and Business Intelligence (ISCBI)* (pp. 94-98). Basel, Switzerland. doi: 10.1109/ISCBI.2018.00028
- Rajput, R., & Solanki, A. K. (2016). Review of sentimental analysis methods using lexicon-based approach. *International Journal of Computer Science and Mobile Computing*, 5(2), 159-166.
- Rosenthal, S., Farra, N., & Nakov, P. (2017). SemEval-2017 task 4: Sentiment analysis in Twitter. In *Proceedings of the 11th International Workshop on Semantic Evaluation (SemEval-2017)* (pp. 502-518). Vancouver, Canada: Association for Computational Linguistics. doi: 10.18653/v1/S17-2088
- Saad, M. K., Langlois, D., & Smali, K. (2013). Comparing multilingual comparable articles based on opinions. In *Proceedings of the Sixth Workshop on Building and Using Comparable Corpora* (pp. 105-111). Sofia, Bulgaria: Association of Computational Linguistics.
- Sabbeh, S. F. (2018). Machine-learning techniques for customer retention: A comparative study. *International Journal of Advanced Computer Science and Applications*, 9(2), 273-281.

- Saravia, E., Argueta, C., & Chen, Y. S. (2016). Unsupervised graph-based pattern extraction for multilingual emotion classification. *Social Network Analysis and Mining*, 6(1), 1-21. doi: <https://doi.org/10.1007/s13278-016-0403-4>
- Shalunts, G., & Backfried, G. (2015). SentiSAIL: Sentiment analysis in English, German, and Russian. In *International Workshop on Machine Learning and Data Mining in Pattern Recognition* (pp. 87-97). Cham, Switzerland: Springer. doi: https://doi.org/10.1007/978-3-319-21024-7_6
- Shalunts, G., & Backfried, G. (2016, October 9-13). Multilingual sentiment analysis on data of the Refugee crisis in Europe. In *Proceedings of the Fifth International Conference on Data Analytics 2016* (pp. 45-50). Venice, Italy.
- Sokolova, M., Japkowicz, N., & Szapkowicz, S. (2006). Beyond accuracy, F-score and ROC: A family of discriminant measures for performance evaluation. In *Australasian Joint Conference on Artificial Intelligence* (pp. 1015-1021). Heidelberg, Germany: Springer. doi: https://doi.org/10.1007/11941439_114
- Steinberger, J., Lenkova, P., Kabadjov, M., Steinberger, R., & Van der Goot, E. (2011, September 12-14). Multilingual entity-centered sentiment analysis evaluated by parallel corpora. In *Proceedings of the International Conference Recent Advances in Natural Language Processing 2011* (pp. 770-775). Hissar, Bulgaria.
- Sykes, L. M., Evans, W. G., Buchanan, G., Warren, N., & Fernandes, N. (2018). To pen or to probe. Prescribing versus treating, how to decide. *South African Dental Journal*, 73(1), 53-55.
- Tellez, E. S., Miranda-Jiménez, S., Graff, M., Moctezuma, D., Suárez, R. R., & Siordia, O. S. (2017). A simple approach to multilingual polarity classification in Twitter. *Pattern Recognition Letters*, 94, 68-74. doi: <https://doi.org/10.1016/j.patrec.2017.05.024>
- Thakkar, H., & Patel, D. (2015). Approaches for sentiment analysis on twitter: A state-of-art study. *Computing Research Repository*, 2015, 1-8.
- Tromp, E., & Pechenizkiy, M. (2011, December 11). Senticorr: Multilingual sentiment analysis of personal correspondence. In *2011 IEEE 11th International Conference on Data Mining Workshops* (pp. 1247-1250). Vancouver, Canada. doi: 10.1109/ICDMW.2011.152
- Tsai, C. F., & Wang, S. P. (2009, March 18-20). Stock price forecasting by hybrid machine learning techniques. In *Proceedings of The International Multiconference of Engineers and Computer Scientists* (Vol. 1, No. 755, pp. 60-66). Hong Kong, China.
- Vīksna, R., & Jēkabsons, G. (2018). Sentiment analysis in Latvian and Russian: A survey. *Applied Computer Systems*, 23(1), 45-51. doi: <https://doi.org/10.2478/acss-2018-0006>
- Vilares, D., Alonso, M. A., & Gómez-Rodríguez, C. (2015, September 17). Sentiment analysis on monolingual, multilingual and code-switching twitter corpora. In *Proceedings of the 6th Workshop on Computational Approaches to Subjectivity, Sentiment and Social Media Analysis* (pp. 2-8). Lisboa, Portugal.
- Vilares, D., Alonso, M. A., & Gómez-Rodríguez, C. (2017). Supervised sentiment analysis in multilingual environments. *Information Processing and Management*, 53(3), 595-607. doi: <https://doi.org/10.1016/j.ipm.2017.01.004>

- Vilares, D., Peng, H., Satapathy, R., & Cambria, E. (2018, November 18-21). BabelSenticNet: A commonsense reasoning framework for multilingual sentiment analysis. In *2018 IEEE Symposium Series on Computational Intelligence (SSCI)* (pp. 1292-1298). Bangalore, India. doi: 10.1109/SSCI.2018.8628718
- Volkova, S., Wilson, T., & Yarowsky, D. (2013, October 18-21). Exploring demographic language variations to improve multilingual sentiment analysis in social media. In *Proceedings of the 2013 Conference on Empirical Methods in Natural Language Processing* (pp. 1815-1827). Washington, USA.
- Wang, X., Li, J., Yang, X., Wang, Y., & Sang, Y. (2017, October 21-23). Chinese text sentiment analysis using bilinear character-word convolutional neural networks. In *Proceedings of International Conference on Computer Science and Application Engineering (CSAE 2017)* (pp. 36-43). Shanghai, China. doi: 10.12783/dtcse/csae2017/17466
- Wehrmann, J., Becker, W. E., & Barros, R. C. (2018). A multi-task neural network for multilingual sentiment classification and language detection on Twitter. In *Proceedings of the 33rd Annual ACM Symposium on Applied Computing* (pp. 1805-1812). New York, USA: ACM. doi: <https://doi.org/10.1145/3167132.3167325>
- Yadav, V., & Elchuri, H. (2013, June 14-15). Serendio: Simple and practical lexicon-based approach to sentiment analysis. In *Second Joint Conference on Lexical and Computational Semantics (*SEM), Volume 2: Proceedings of the Seventh International Workshop on Semantic Evaluation (SemEval 2013)* (pp. 543-548). Atlanta, Georgia.
- Zhou, Y., Demidova, E., & Cristea, A. I. (2016, April). Who likes me more?: Analysing entity-centric language-specific bias in multilingual Wikipedia. In *Proceedings of the 31st Annual ACM Symposium on Applied Computing* (pp. 750-757). New York, USA: ACM. doi: <https://doi.org/10.1145/2851613.2851858>

Review Article

Internet of Things (IoT) Implementation in Learning Institutions: A Systematic Literature Review

Ruth Chweya^{1,2*} and Othman Ibrahim¹

¹*Department of Information Systems, School of Computing, Universiti Teknologi Malaysia, 81310 UTM Skudai, Johor, Malaysia*

²*Department of Computing, School of Information Science and Technology, Kisii University, 40200, Kisii, Kenya*

ABSTRACT

Internet of Things (IoT) is a computing concept facilitating the management of collaborative activities from one central area. Millennial learners, growth in enrolment numbers in universities, and the need for equity and quality learning necessitate the use of IoT technologies in education. The focus of this paper is to examine IoT implementations in learning institutes, their application areas, the themes presented, the models and methodologies used, and the benefits. This study concentrated on publications from 2008 to 2017. The outcomes revealed that the utilization of IoT for tracking and tracing a learner's attendance had been one of the application areas of IoT in education. This study further categorized the papers and presents novel research opportunities based on concentrated themes and areas that had not been fully exhausted. Most research studies employed qualitative methods, with a few utilizing a quantitative approach with surveys. Research themes exhibited a shortcoming in other important themes, such as the models and methodologies used for implementing IoT. Finally, the results of this study agree that IoT

implementation could help solve some issues in learning institutions like equity and quality learning. The results from this research also provide a base for future research works on the successful implementation of IoT in learning institutions.

ARTICLE INFO

Article history:

Received: 5 August 2020

Accepted: 5 November 2020

Published: 22 January 2021

DOI: <https://doi.org/10.47836/pjst.29.1.26>

E-mail addresses:

ruthchweya@gmail.com (Ruth Chweya)

othmanibrahim@utm.my (Othman Ibrahim)

*Corresponding author

Keywords: Adoption, information technology, intention, IoT, learning institutions

INTRODUCTION

Integrating information and communication technologies in education has altered the learning environment (Albion et al., 2015), resulting in several changes and various improvements (Uzelac et al., 2015). The advancement of new technologies is as a result of the Industrial Revolution (IR) 4.0 (Hussin, 2018). The expansion is guided by the advent of artificial intelligence, the internet of things, and robotics, among others. The aim is to align people and technologies for any upcoming possibilities.

Internet of Things (IoT) utilization has taken root in several aspects of life including smart homes, factories, cities and learning surroundings (Chin & Callaghan, 2013; Marquez et al., 2016; Uskov et al., 2016). More citations are in Appendix A. IoT projects have been embarked upon to expand technologies like social networking and email, among others (Want et al., 2015). This has been made possible by enabling IoT in objects to disseminate information (French & Shim, 2016). As users' needs grow, innovative applications are being presented to track, control and automate peoples' activities everywhere (Asghari et al., 2019). For learners and instructors, the aim is to provide personalized services in pedagogy to create an intelligent environment (Bagheri & Movahed, 2016; Bandara & Ioras, 2016; Kamar et al., 2016).

IoT utilizes numerous subcomponents from different gadgets to attain the intelligent surrounding (Uzelac et al., 2015). It also employs diversified gadgets to provide consistent data dissemination (Kamar et al., 2016). Being an internetwork, IoT is significant technologically, physically, and largely in the socioeconomic surroundings (Krotov, 2017). Furthermore, the outfitting of a Wi-Fi facility, connected lecture halls, telecasting conference amenities, online repository, and several improved applications are for educating better learners (ur Rahman et al., 2016).

In the current world, the educational climate revolution has led to an introduction of various modern kinds of learning and innovations (Bandara & Ioras, 2016). This has inspired the learning institutions to establish methods that can support learners and their growth using the current instruction techniques (Njeru et al., 2017). With the implementation of IoT in various environments, the main focus is to reshape every organization's operations, its objectives and policies (Onyalo et al., 2015). IoT aims to use heterogeneous networks to permit millions of people, places and things to participate (Hsu & Lin, 2018). In learning, the main objective is permitting physical space interactivity, to allow transmission of information or to enable learning (Veeramanickam & Mohanapriya, 2017). Hence, IoT needs to provide learner support in areas of personalized learning, interactivity, mobility, and also accessibility (Bagheri & Movahed, 2016; Farhan et al., 2017; Moreira et al., 2018). It can also lower the education costs and provision for quality education resources as compared to the existing channels (Bagheri & Movahed, 2016; Roy et al., 2016).

The most significant trial in education is the implementation of open, cheaper and quality guided global training environments (Jeffords et al., 2014). This comes amidst several hindrances in education that, if eliminated, would provision for access and immensely reduce the education costs (Aldowah et al., 2017). Hence, for the survival of institutions in the present era, there is a need for significant tools to impart better pedagogical actions to technology-savvy learners (Baker et al., 2016).

The key concentration areas of IoT applications have been smart cities, smart living, smart homes, smart health, smart security, and other approaches. For instance, the use of IoT in Smart homes (Stojkoska & Trivodaliev, 2017), IoT applications in Agriculture (Gómez-Chabla et al., 2019) for a clear perspective on IoT innovations, IoT in agro-industrial and environmental fields (Talavera et al., 2017) showing IoT utilization (monitoring, control, prediction, and logistics), IoT applications in healthcare (Ahmadi et al., 2019) showing various directions of IoT architecture in healthcare, IoT utilization in food safety (Bouzembrak et al., 2019), IoT for smart cities (Mijac et al., 2017) which reveals the infancy of IoT, and finally, IoT and supply chain management (Ben-Daya et al., 2019), which indicate gaps in frameworks and models in the supply chain. Apart from the mentioned, IoT has been speculated to enhance learning beyond the classroom area (Aldowah et al., 2017; Roy et al., 2016).

Nowadays, learners need to access education in a cheaper way while they are away from their study environments. Using gadgets that can allow anywhere and anytime access for learners can somehow overcome the aforementioned difficulties. IoT technologies, by supporting the learning process, can lower the cost for institutions (Bagheri & Movahed, 2016), ease resource sharing and also expand the quality of teaching (Farhan et al., 2017).

Looking at this area, there are several papers that have evaluated aspects of IoT in education, the significance and benefits, and correlated technologies. To the best of the researcher's knowledge as per this study, there is a lack of reviews addressing models and methodologies for implementing IoT in education. Hence, this paper presents a complete review of IoT models and theories in the context of learning from 2008 to 2017. In execution of the objective of this research, three research inquiries are presented below:

- i. What are the predominant investigations on IoT, and the research concepts already described?
- ii. What are the dominant models and theories employed in the study?
- iii. What key constraints and omissions are found in IoT investigation?

For this exploration, the review is organized as follows: Section 2 studies the method employed for review including the protocol used, and the inclusion and exclusion criteria. Section 3 illustrates the data synthesis and extraction, and highlights publication sources.

Additionally, the distribution of articles as per publication year is presented. Section 4 demonstrates the results, including the benefits and methodologies. Lastly, section 5 discusses the conclusion.

RELATED STUDIES

This subsection cross-examines similar reviews in IoT implementation in learning environments. The objective is also to bring out the importance of IoT in learning environments. Additionally, it purposes to show the extent of IoT implementation in the learning context.

An exploration was conducted on IoT in education by Ramlowat and Pattanayak (2019). It examined benefits of IoT and its implementation in different areas of education, for instance distance studies, medical studies, computer science studies, among others. The paper also discussed the application areas of IoT apart from education. Another study was undertaken to review IoT smart campuses and their implementation (Zhamanov et al., 2017). The study brought out the significance of IoT in flipped classes and gave a comparison of it with the traditional methods. A different research looked at IoT and Big Data (Kusuma & Viswanath, 2018). The researcher examined the significance of IoT and Big Data in eLearning environments, and various eLearning procedures. A review on IoT in education was done by (Kassab et al., 2020), concentrating on benefits and challenges of incorporating IoT in educational areas and the curriculum. It also highlighted the challenges hindering deployment of IoT, which were security, human issues, and scalability.

Incorporating IoT in learning environments is a promising solution to overcome difficulties linked with high enrolment numbers and attaining equity. Accordingly, designing a university campus with the incorporation of technology boosts the learner experience (Aldowah et al., 2017). For instance, IoT has been utilized as a base for lifelong learning with Radio Frequency Identification (RFID) and Near Field Communication (NFC) (Gómez et al., 2013) and also through learning analytics (Cheng & Liao, 2012). IoT has also been employed for underprivileged students in rural areas with sensors and wireless connections (Pruet et al., 2015). The outcome was an improved learner experience.

IoT has been incorporated in teaching and learning through pervasive technology (Chin & Callaghan, 2013). This contributed to an enhancement in the governing of campuses, while providing an effective delivery system for learning materials. IoT has been employed to enhance learning through data mining for efficient and effective online teaching and learning (Njeru et al., 2017). IoT has been applied to educational business models (Bagheri & Movahed, 2016), leading to minimizing the cost of firms, lowering time wastage, and bringing comfort to learners and educators. It eliminates the need for dedicated security

personnel by utilizing sensors and mobile gadgets. Finally, IoT has also been employed in vocational and university education due to its many benefits (Kortuem et al., 2013).

Hence, regarding the previous studies, this research explores uncovered areas through a comprehensive review. For instance, from the reviews undertaken, models and methodologies for adoption are minimally explored. Besides, implementations of IoT in learning have been maximally utilized.

REVIEW METHOD

Systematic literature inquiry is a methodical thorough analysis (Brereton et al., 2007). It is not about the aggregation of every available affirmation on a research inquiry. However, it aims to aid the creation of evidence-based suggestions for professionals. Research conducted by Kitchenham (2004) brought out the below mentioned points for performing similar evaluations:

- To give a summary of the already available evidence about technology. For instance, summarize pragmatic indicators of the advantages, inclusive of shortcomings of some definite procedure.
- To bring out any omissions in the latest explorations and to give suggestions for any supplemental investigations.
- For the provision of background to correctly place emerging research activities.

Conducting systematic literature reviews entails several discrete activities undertaken in three phases: planning, conducting the review, and reporting the review (Brereton et al., 2007). Furthermore, the steps mentioned are broken down into specific processes. They include: one, affirming the research inquiry; two, establishing a review protocol; three, validating the review protocol; four, identifying the appropriate research; five, determining paramount studies; six, evaluating the quality of the investigation; seven, extraction of required data; and eight, synthesizing the data.

Review Protocol

A review protocol outlines how a specific systematic review will take place to minimize researcher biases. It encompasses the rationale for the survey, investigation inquiries to be reported by the reviewer, the procedure to search the primary studies, procedures including the criteria for the study selection, quality assessments checklists for individual studies assessment, data extraction, and extracted data synthesis (Kitchenham, 2004). Figure 1 shows the selection process utilized in this research.

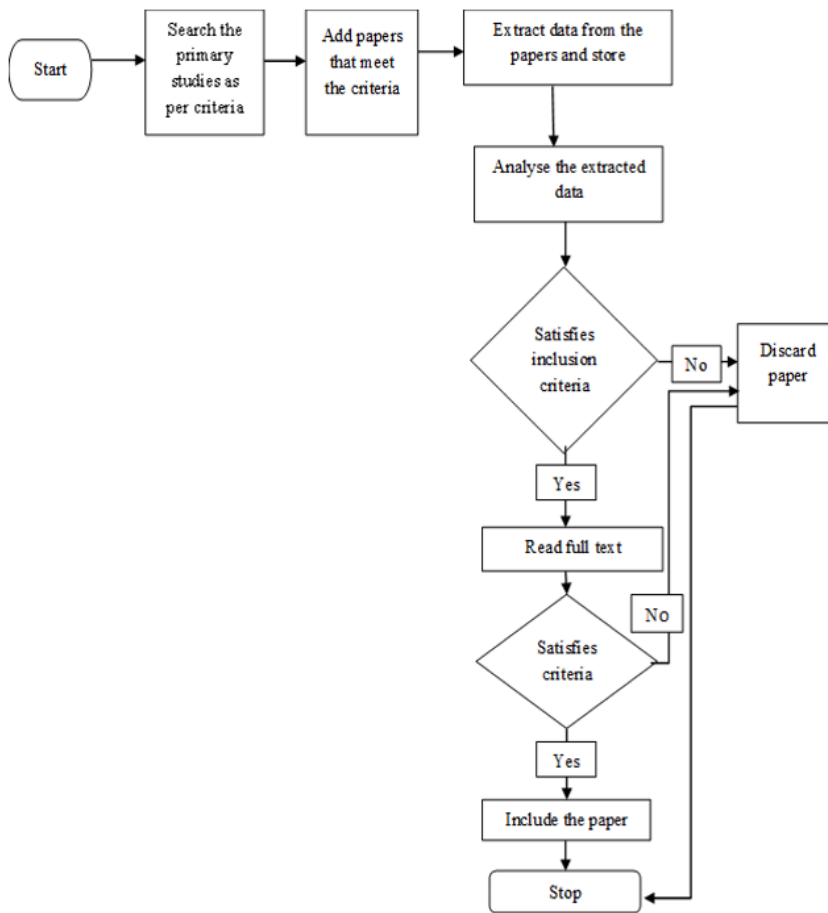


Figure 1. Paper selection process

Inclusion and Exclusion Criteria

This section ensures that the applicable analyses are utilized in the review procedure. To cover most of the relevant studies, papers were searched by querying different digital libraries. The purpose of this study is to understand the status of IoT in learning institutions. The procedure details examining published articles with future directions on the trends in this research area. Full papers written in English, published from 2008 to 2017 from peer-scrutinized reports, journals, book chapters, conference proceedings, and symposia reports were well-reviewed. The aim was to disqualify insignificant papers. A total of 200 journals were searched. A sum of 148 research papers was selected from the journals, conference proceedings, white papers, and articles. Table 1 recaps the basis.

Table 1

Inclusion and exclusion measure

Inclusion measure	Exclusion measure
Published from 2008 to 2017	External to IS research field
Papers that can be accessed full text	Papers with no access to the full text
Written in English	Not in English
Directly or indirectly answers the research question	Lacks the relationship to the defined research inquiries of the study
Papers with no direct term IoT but should address smart learning, smart education, IoT technologies used and focus on ubiquitous computing	Papers representing at least one key concepts (IoT, IoT adoption, IoT in learning, smart learning, smart education, IoT technologies among others) but not considering the term adoption
Papers proposing a model, a method, or methodology for adopting IoT and proposing practice mechanism	Papers with at least one of the concepts (method, model, methodology) but not considering learning domain
Published in the selected database	Publications that lacked a link to the inclusion criteria

Search Strategy

An orderly search starts with deducing keywords and search terms built from the study scope, literature, and discussions by the review team (Tranfield et al., 2003). The relevant strings for the search are then decided upon. The search strategy is thereafter relayed exhaustively to allow for future replication of the exploration. The examination procedure consists of manual and automatic stages. The automatic stages recognized studies related to IoT. In this study, the review was done from Scopus, Science direct, Taylor & Francis Online, Springer, and Web of Science journals like Computer Communications journal, International Journal of Development Research, Ad Hoc Networks and Wireless personal communications, Future generation computer systems, IEEE transactions on Industrial Informatics journal and others. Moreover, studies from conferences were also included (for instance ACM International Conference on Advances in Social Networks, enabling technologies: infrastructure for collaborative enterprises, Annual computer software and Applications conference, Applied System Innovation (ICASI)) for the study. Besides these, unpublished studies, conference proceedings, industry trials and even the internet material were considered. However, the key output of the research was a whole list of articles and papers where the review was grounded. Hence, the manual search process detailed the specific conference proceedings and journal papers from the year 2008.

Chosen journals encompassed either literature surveys or empirical research experiments. They also needed prior utilization as sources for other similar studies linked to information systems. Every journal or conference proceeding underwent review. Studies with a concentration on different literature surveys were recognized to be possibly applicable. All the papers were searched by applying the inclusion and exclusion criteria. The study was performed based on the following keywords: “IoT”, “Internet of Things”, “smart learning”, “WSNs”, “RFIDs”, “smart education” and “Internet of Things adoption” in the electronic journal databases.

Study Selection Process

At this stage, the choice of the suitable material for this literature review was done, as shown in Figure 2. The main search was performed via the search stream. It yielded 148 research papers using an automatic search method. Then, based on the inclusion and exclusion measure from the abstract and the close section of every paper, 64 papers were disqualified. A further manual scan was done, eliminating 18 more papers outside the specified criteria. Following this, a full scan was performed for the rest of the studies founded on the exclusion criteria. Manual steps were utilized to check any missing reports. Finally, a total of 49 papers were selected as the primary data. Thereafter, the classification by year and type of publication (journal article, conference proceedings) was done.

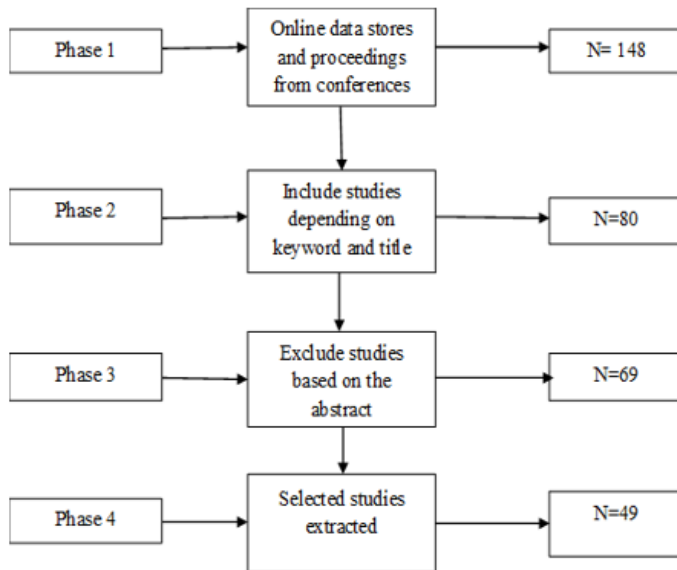


Figure 2. Study selection procedure

Quality Assessment

The quality assessment procedure outlines how to attain minimal biases with maximum internal and external validation (Brereton et al., 2007). This section aims to check the universal quality of the identified research articles. The full quality measure is in Appendix C. The four criteria about this study are:

QA1: Whether the topic in this article is related to IoT

QA2: If the research methodology is well outlined in this article

QA3: Whether enough illustration is provisioned for the setting where the study took place

QA4: If there is comprehensible information about the research intents

Each paper was assessed and later allocated a score of either high, medium, or low-quality level. A mark of 2 was allocated to the articles that attained the measure. A mark of 1 was given to those that partially satisfied the criteria while a mark of 0 was allocated to those that did not satisfy the criteria. High-quality papers scored a value of at least 5 and above, a score of 4 was given to a medium rated paper, and low to those whose score was below 4. As a result, 14 papers that did not meet the full criteria were removed from the list. Overall, the study chose 49 papers. From Figure 3, it can be seen that a good number of papers (62%) got a high score following these criteria, with 30% getting a medium score and 8% getting a low score.

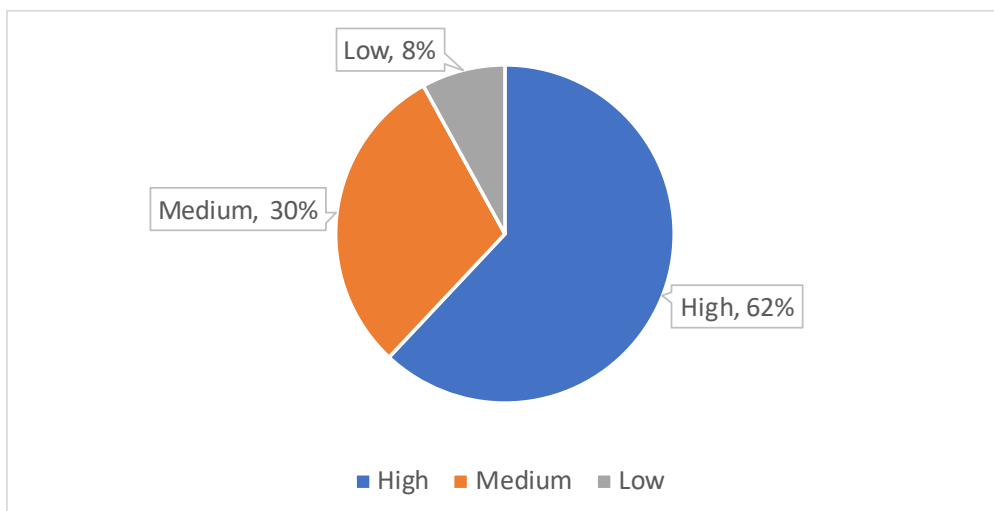


Figure 3. How studies are distributed

DATA EXTRACTION AND SYNTHESIS

To minimize errors and biases, data extraction forms are used in systematic reviews (Tranfield et al., 2003). They specify the general information, study aspects with other definite details, and emerging themes together with details of synthesis. Research synthesis entails making a summary, integrating, and accruing the outcomes of various studies on a concern. Here the main objective was getting a data extraction form to accurately record information from preliminary studies. The required details were extricated via endnote and Microsoft Excel spreadsheets. The extracted details are as shown in Table 2.

Table 2

Extraction of data from main studies

Extracted data	Detail
Article ID	Unique paper recognition
Writer and publishing Date	Author names and the publication year (2008-2017)
Article title	Paper name during a search
Article Subject	Objectives a paper address
Theory/Framework	Adopted theory/framework
Data gathering technique	Like a survey, experiment, observation, among others.
Data analysis process	A qualitative, quantitative, or mixed method
Group Origin	A description like benefits, adoption, strategies, among others Journal, book chapter, conference proceedings, among others

Publication Source Overview

Overall, 49 papers were chosen for the study (Appendix B), which included 45 articles from journal studies and 4 from conference studies. The earliest report was produced in 2010. Figure 4 shows the chosen articles from 2008 to 2017 by category type.

Temporal Outlook of the Publication

As per Figure 4, the extracted items concentrated on internet, things, IoT, learning, management, computing, education, technology, innovation adoption and learning, among others. Figure 5 shows how the articles were distributed. This study found little research on IoT adoption, more specifically centred on education from 2008 to 2010, with more

Citation Count

Table 3 shows that some of the chosen studies exhibited an elevated impact and some, a low impact. The statistics were obtained from Google Scholar and they show rough evidence on the paper citations. Likewise, there are not many studies that have been done on IoT in learning institutions before 2017. There are low rates in terms of adoption for learning institutions. About 12 studies have a citation count of more than 100, with the rest falling below 100. As low as 10 articles were cited as low as 10 times. One study lacked a citation. Conversely, as per this study, most of the papers have been published from 2015 and it is expected of them to have low citation count.

Table 3
Citation count

STUDY_ID	Study Title	Citations
I2	The Internet of Things: A survey	9826
I14	IoT: A perception, structural facets, and future requirements	57962
I23	The Internet of things vision: Key features, applications, and open issues	2362
I36	An authentication model for Internet of things clouds	1739
I41	Context aware computing for the Internet of Things: A survey	1731
I17	IoT: utilization, investments, and issues for enterprises	590
I10	A recap of IoT for individuals having impairment	380
I7	A vision of IoT: Applications, challenges, and opportunities with China perspective	304
I33	Enabling the internet of things	297
I46	Upcoming Internet of Things: open pitfalls and trials	138
I45	A blended view on the elements affecting consumer acceptance of IoT technology	121
I15	Educating the Internet-of-Things generation	111
I19	Developing a theoretical framework of strategic decision, to support ability and details dissemination under Internet of Things	96
I42	Why are not organizations adopting virtual worlds	92
I37	IoT grounded Smart environments: state of the Art, Taxonomy, and open investigations problems	85

Table 3 (Continued)

STUDY_ID	Study Title	Citations
I13	Interaction structure grounded on IoT as a pillar for Education	75
I43	A socio-technical structure for IoT blueprint: An individual engrossed blueprint for IoT	75
I12	An evaluation on Internet-of-Things	74
I35	A research structure for smart education	71
I38	Opportunistic IoT: Exploring the social side of IoT	55
I48	A study of the institutional forces influencing the adoption intention of RFID by suppliers	54
I6	Evolution is not enough: Revolutionizing current learning environments to smart learning environments	40
I49	Aspects of RFID adoption level with identified value	38
I27	IoT: being prepared for what is coming	38
I8	Smarter Universities: A vision for the fast-changing digital era	37
I25	A strategical process using IoT Smart data pricing models	36
I29	Conceptualizing and measuring quality of experience of the internet of things: Exploring how quality is perceived by users	33
I32	The growth of next generation bar code-RFID embrace	32
I40	Building trust in the Human-Internet of Things relationship	26
I44	IoT Business models	26
I24	Adoption of Internet of Things in India: a test of competing models using SEM	25
I16	The Internet of Things plus current business opportunities	25
I34	An integrated framework for RFID adoption and diffusion	22
I3	The result of IoT on Educational Business design	22
I11	IoT based student's interaction framework employing attention scoring assessment in e-learning	16
I30	Understanding the Internet of Things ecosystem: multi-level analysis of users, society, and ecology	14
I21	Establishing a unified model for RFID expansion	13

Table 3 (Continued)

STUDY_ID	Study Title	Citations
I18	Details about learning IoT: Research direction and upcoming trends from social science viewpoint	13
I1	IoTFLiP: IoT-based flipped learning platform for medical education	8
I26	Disrupting objects: a design to enable acquisition of IoT-based innovations by the urban poor	5
I28	The upcoming Technological and Theoretical models in Education: linking Cloud Computing (CC), Connectivism plus IoT	5
I22	The Application of WSNs and wearable technologies for education	2
I4	Benefits of “IoT” on E-learning in the Smart Cities	2
I20	Internet-of-Things-based Learning Framework to enable STEM Undergraduate Education	2
I39	Remote laboratory: using Internet of Things	2
I9	Investigating the Educational capability of IoT in Seamless instruction.	1
I31	The Internet of Things as an accelerator of progressing broadband networks in Thailand	1
I5	Democratizing AmI and the IoT: The Power and Influence of Social Innovation and Participative and Humanistic Design	0

Methodologies of Research

Figure 6 exhibits all the study methodologies employed in the initial exploration. It shows that most of the studies found in literature employed the qualitative methodology. Few studies employed the quantitative method. Besides, those that employed quantitative methodology utilized the survey method. Appendix D also gives the full details of the methodologies and methods.

OUTCOMES

R-Q1: What are the predominant investigations on IoT, and are the research concepts already described?

As from literature, there are three main categories of IoT: monitoring and control, big data and business analytics, and information sharing and collaboration (Lee & Lee, 2015). The detailed analysis of the selected studies was based on their similarities. This

is in terms of factors that influence IoT adoption or its related technologies in learning institutions. As per the evaluated publications and for feedback to the research inquiries, the investigation brings out five main categories of articles related to the subject of study, as shown in Figure 7.

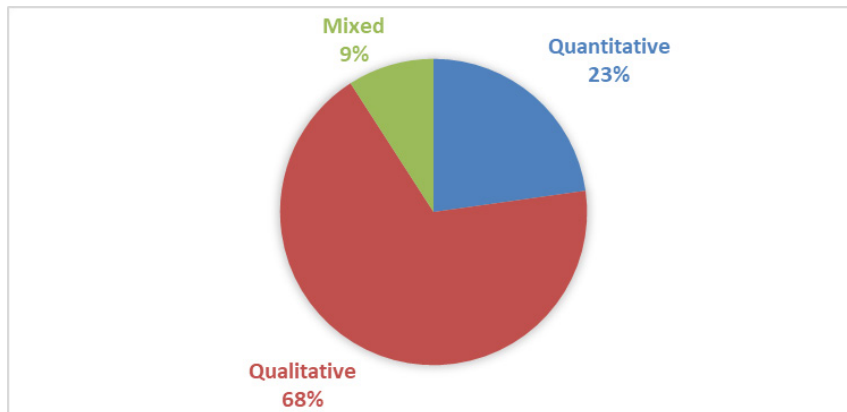


Figure 6. Research methodologies distribution chart

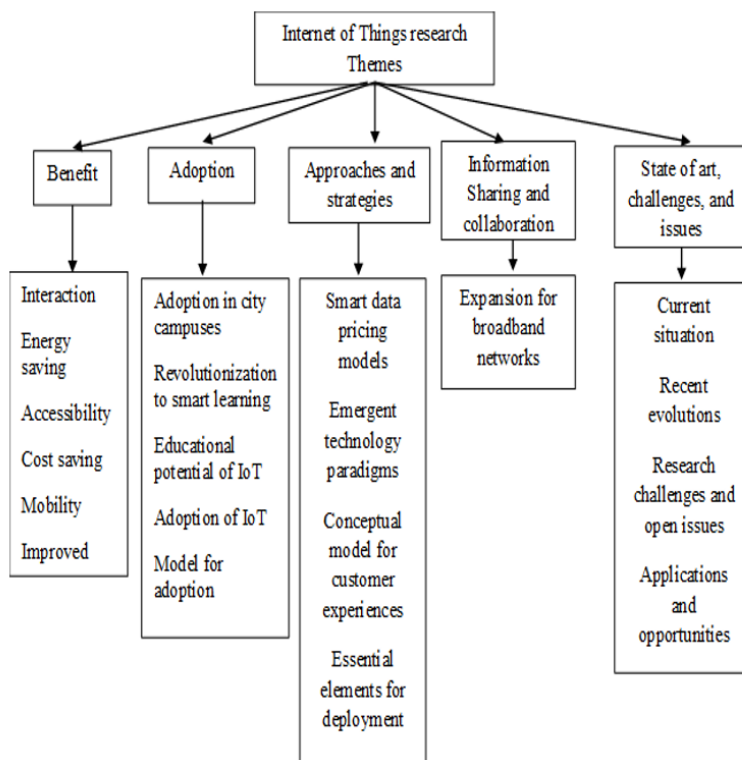


Figure 7. Themes for research and topics mentioned

Information Sharing and Collaboration

Most of the research conducted on IoT which was identified in this study detailed out a few things: the positive elements of utilizing IoT in limited resources environments, advantages of IoT in learning, the technical issues of IoT, tracking students' attendance using RFID technology, comparing outcomes of IoT learning platforms with traditional learning methods, use of IoT to stimulate learners' motivation, IoT as a subject of study in higher learning, and the important role of a teacher in using these applications. IoT brings in greater accessibility because of the high internet speed and lower gadget costs (Saritaş, 2015). This means better learning resources and immersive learning experiences with greater interaction. Accordingly then, IoT has a chance of lowering the education costs and expanding education material past the study rooms (Roy et al., 2016). It can facilitate quality educational resources at a fraction of the price of the prevailing mechanisms. Furthermore, IoT can be used to accelerate the expansion of broadband networks to reach out to many learners (Sudtasan & Mitomo, 2017).

Adoption

At the onset, we include studies with details on the adoption and inclusion of IoT in learning. Selected studies discuss elements that may impact the utilization of IoT. Few studies in this research have examined the adoption of IoT through models and frameworks, while highlighting important factors for successful implementation (Barreto et al., 2015; Kalashnikov et al., 2017; Li et al., 2012). However, research by Moreira et al. (2018) suggests that successful acceptance and introduction of IoT in learning institutions depends on the perception and inclination of educators, politicians, and society.

Benefits

Few studies have shown how to achieve benefits from IoT. Hence, IoT has attracted many in recent years, changing the landscape of disseminating information in the virtual world, interchanging details, convenience, and practicality (Ali et al., 2017). In global higher education, IoT is explicitly linked to the betterment of economic development, new research, and innovation (Bandara & Ioras, 2016). For example, IoT provides ways in which new opportunities can be utilized to merge various smart devices for learning (Niyato et al., 2016). The outcome is an advanced computing environment. Following this, system efficiency, safety, and security, upgraded trading opportunities and an income stream will be achieved. For instance, a study was done on developing a design to incorporate IoT-linked revolutions by the suburban poor (Roy et al., 2016). The result showed that IoT could improve the quality of education. This is through the acquisition of enhanced educational resources and the provision and availability of massively online open courses. Chen et al., (2014) in contrast looked at the benefits of IoT in terms of opportunities available for IoT.

Accordingly, IoT is believed to offer communication through existing technologies and new communication modes. The incorporation of IoT with the virtual and physical world will help realize utilization of various concepts and technical components.

Approaches and Strategies

Studies under this area outlined techniques and procedures used by IoT. They indicated the necessity to understand the users' connection between the social and technical perspectives for sustainability (Shin & Park, 2017; Shin, 2014). However, there is a need to address social innovation roles and the human approach participation (Bibri, 2015). Another research suggested the stimulation of people's thinking, creativity, and much of entrepreneurship.

State of art, Challenges, and Issues

Studies in this section bring out the modern state of IoT and any problems that need attention. For instance, universities confront challenges from the traditional learning systems (Coccoli et al., 2014). The outcome has resulted in recent evolutions in technology and networking, dramatically changing the way of life and knowledge accession. Hence, IoT can boost the role of technology as an innovation promoter in different markets of utilization (Miorandi et al., 2012). The IoT scenario and its facilitating technologies are also studied (Farooq et al., 2015). The human-centric perspective of IoT is also explained (Guo et al., 2012). Additionally, there are details on how data mining can be utilized with computational intelligence for future IoT applications (Tsai et al., 2014).

In summary, of the 148 articles on IoT revealed, only 49 that focused on the study area were retained. The 49 retained papers investigated IoT adoption and use in learning. However, most concentrated on the organizational level of adoption, and few on individual perception and preparedness. From the advantage category, most of the studies focussed on the benefit of IoT, issues, challenges, and future directions. Few studies focussed on the use of IoT to measure performance, track or monitor attendance and capture data.

R-Q2: What are the dominant models and theories employed in the study?

Most of the theories and models employed were grounded on the organizational level. However, some articles utilized individual-level theories. Many theories were related to technology adoption, entailing the incorporation of more than one single theory (Hameed et al., 2012). However, in this study, few researchers had utilized theories and theoretical models to expound on the adoption of IoT. A few theories that were employed included the Theory of Planned Behavior (TPB), Diffusion of Innovation (DOI), Technology Readiness Index (TRI), and Technology, Organization and Environment (TOE).

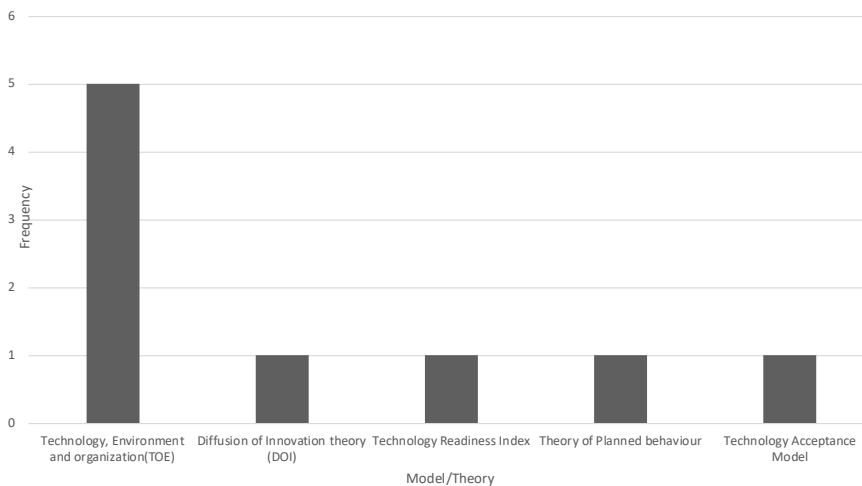


Figure 8. Theoretical frameworks and models used in selected studies

From Figure 8, TOE was found to be the most widely used theory in institutions planning, to adopt and use IoT. TOE by Tornatzky and Fleischer (1990) was developed to evaluate and analyse the present organization's conditions concerning the adoption and implementation of innovations. For instance, Aboelmaged (2014) mentioned that the TOE framework was strong theoretically and empirically, and hence helpful in the study of readiness, adoption, and implementation of various applications. The next theory is the DOI theory by Rogers (2003), that describes the willingness or non-willingness to adopt a new technology. Rogers (2003) argued that faster innovations to adopt were those that offered more relative advantage, compatibility, simplicity, trialability and observability. DOI tries to predict an innovation's adoption behaviour according to the personal characteristics related to the innovation (Samiee & Rezaei-Moghaddam, 2017).

TRI describes people's tendency to accept and use new technologies to achieve goals in home life and work (Parasuraman & Colby, 2015). The model assesses an individual's willingness to grab and utilize innovations at his quarters and duty (Parasuraman, 2000). Studies have applied TRI in assessing important factors for the successful implementation of technologies. For instance, Al-Shareem et al., (2015) emphasized on external reasons influencing preparedness to adopt public and private partnerships, Lin and Hsieh (2007) emphasized the role of technology readiness in self-service technology acceptance, and Thakur and Srivastava (2014) emphasized on readiness to adopt through TRI. TPB developed by Ajzen (1991) has been used to predict human behaviour in different fields. It hypothesizes that a person's conduct is as a result of three elements; a person's mentality toward behaviour, subjective standards, and perceived behavioural control (Cheon et al., 2012). TPB can be used to study wide areas of acceptance of technology (Oye et al., 2014).

The significant expectation of TPB is to catch those motivational variables and intentions, to speculate an individual effort (Ho et al., 2017).

R-Q3: What key constraints and omissions are found in the IoT investigation?

This study examined a sum of 148 papers to gather more knowledge and insight on IoT adoption in learning. However, it can be seen that the higher learning institutions have not fully utilized the technology. Only 49 papers were deemed relevant for this study. Therefore, there is a need for a better understanding of the technology to prepare organizations for its adoption. Possibly, the quantitative design approach would provide more insight into this analysis area.

Despite several articles on the adoption of IoT, recent academic literature on IoT adoption for learning institutions has shown a gap in models for readiness to adopt and use IoT. Researchers (Bourrie et al., 2015) argued that organizational readiness was reflected in the beliefs, attitudes, and intentions of members of an organization. Hence, much effort and detail are required to improve the impression and arrangements in institutions (Moreira et al., 2018). Sabi et al. (2016) also ascertained that consideration of the existing social and cultural conditions needed evaluation to avoid failure in the technology adoption process. Additionally, some studies pointed out the need to address privacy and security difficulties (Atzori et al., 2010; Bagheri & Movahed, 2016; Bibri, 2015). Very little research concentrated on the significance of user behaviour in IoT implementation; while other studies focused on the benefits, general discussion on IoT (including challenges, factors, technologies, and future directions), adoption and actual usage by organizations, and significance of the technology.

DISCUSSION AND CONCLUSION

This study has evaluated the implementation of IoT in learning. The study has examined the low usage of IoT in learning, and how only a few models have been used for adopting IoT. For greater insights, the few models and methodologies that have been used were brought out. It also exhibits the gaps in the literature to highlight the potential of IoT in helping tackle learning-related challenges. Amidst several benefits of IoT, innovations that handle learning and pedagogical issues are not fully in place. As highlighted in the introduction, IoT has numerous benefits for the educational environments to enable the tracking of learner activities. Hence, IoT can allow learning institutions to quickly address learner challenges through the study activities. Finally, this study shows the benefits and issues of utilizing IoT in learning.

The SLR method identified 49 primary studies published between 2008 and 2017. In addition, this study was to determine the utilization of IoT in other areas in learning with the themes and benefits. From the study, there has been noted a tremendous rise in the

number of papers in this field because of the significance of this subject in learning. It was noted that most studies were linked to monitoring learning activities. The rise in student population and need for quality learning requires the transition from traditional learning to personalized study. The level of device connectivity furnished by IoT necessitates an enriched learning process for students around the globe (Mrabet & Moussa, 2017). Besides, IoT technologies extend learning by generating sources of data for gathering and inspecting learners' studies individually (French & Shim, 2016). This is one way to transform the traditional pedagogy to the current learning methods through IoT. Another application of IoT is outdoor learning through RFID (Tan et al., 2007). Educators can design varying educational applications in areas with low capacity to relay information. The outcome is enhanced student creativity and improved skills from new knowledge.

Achieving quality learning in the face of continuous expansion is critical. As the learner's requirements have been altered with the evolvement of new technologies, using the best tools for strong pedagogy to the technology savvy population is important. Moreover, having the best decisions to improve the success of learners and institutions is also crucial. Hence, the need to utilize IoT, as per this study can help get valuable insights. There is a need for more research in learning environments.

From the review, the universal quality of the identified research articles yielded that 62% of the papers had a high score, 30% had a medium score, and 8% had a low score. Furthermore, most studies did not use any method, while majority (68%) used the qualitative technique. According to this study, very few authors used the quantitative method (23%), hence this is something that needs further exploration. This study may have failed to examine every existing literature item. Nevertheless, the aim is to furnish information on this growing technology to both, stakeholders, and practitioners. Based on this study's categorization of literature, it can be seen that using IoT for tracking and tracing objects and people has been the norm. Hence, the benefits and improvements resulting from IoT have still not been fully utilized in learning.

Concerning the predominant models and methodologies, this study found few utilizations. Since IoT can improve the society, making learners more linked while having independent control is key in the future eLearning vision. IoT can provision for improved infrastructure robustness, scalability, continuous communication and can save on learner costs. Furthermore, using IoT will create learner flexibility, expand learning materials, upgrade teaching and learning, and bring agility. It is crucial that stakeholders consider this evolving technology and actively deploy it in learning environments. With the continuous enrolment of learners in educational institutions, a major issue is extending learning services to a wider location. Implementing IoT has significant benefits that make it preferable for expanding teaching and learning. Therefore, selecting a good model and methodology for implementing IoT is crucial. Major issues like security and privacy need to be handled,

as they inhibit the spread of IoT. This study did research comprehensively on IoT for learning institutions through more than 120 authors and various studies. However, it was not possible to capture every research.

There are gaps identified concerning IoT in learning from this review, which are further elaborated on as follows:

- There is a miss on the models that provide direction on IoT adoption in education with defined guidelines. The aim is to help learning institutions in deploying IoT. IoT will impact planning, quality learning and decision making, among other issues.
- There are many barriers to implementing IoT in learning from the people and organizational context. There is a need to clearly understand the peoples' perspective and their preparedness. Research by Moreira et al. (2018) suggests the need for preparedness from stakeholders and educators. There are not many studies addressing the issue of preparedness among other challenges.

Overall, after all the analysis was done, the study concludes that the use of IoT can be of great benefit if more research is undertaken. The findings from this review will assist university policy makers to make better decisions regarding implementation and deployment of IoT. IoT is among the technologies that can play an important role in enhancing quality learning, increasing knowledge acquisition, and lowering study costs. IoT is expected to improve learning, enhance quality education, and save on costs while overcoming learning inequities. More study can be done on the technologies used in various IoT implementations in learning, with a comparison on which one suits best. This study acts as a basis for researchers in getting more research ideas on IoT in learning.

ACKNOWLEDGEMENT

Our appreciation goes to everyone who provided guidance and support to this study.

REFERENCES

- Aboelmaged, M. G. (2014). Predicting e-readiness at firm-level: An analysis of technological, organizational and environmental (TOE) effects on e-maintenance readiness in manufacturing firms. *International Journal of Information Management*, 34(5), 639-651. doi: <https://doi.org/10.1016/j.ijinfomgt.2014.05.002>
- Adhiarna, N., Hwang, Y. M., Park, M. J., & Rho, J. J. (2013). An integrated framework for RFID adoption and diffusion with a stage-scale-scope cubicle model: A case of Indonesia. *International Journal of Information Management*, 33(2), 378-389. doi: <https://doi.org/10.1016/j.ijinfomgt.2012.10.001>
- Ahmadi, H., Arji, G., Shahmoradi, L., Safdari, R., Nilashi, M., & Alizadeh, M. (2019). The application of internet of things in healthcare: A systematic literature review and classification. *Universal Access in the Information Society*, 18, 837-869. doi: <https://doi.org/10.1007/s10209-018-0618-4>

- Ahmed, E., Yaqoob, I., Gani, A., Imran, M., & Guizani, M. (2016). Internet-of-things-based smart environments: state of the art, taxonomy, and open research challenges. *IEEE Wireless Communications*, 23(5), 10-16. doi: 10.1109/MWC.2016.7721736
- Albion, P. R., Tondeur, J., Forkosh-Baruch, A., & Peeraer, J. (2015). Teachers' professional development for ICT integration: Towards a reciprocal relationship between research and practice. *Education and Information Technologies*, 20(4), 655-673. doi:10.1007/s10639-015-9401-9
- Ajzen, I. (1991). The theory of planned behavior. *Organizational Behavior and Human Decision Processes*, 50(2), 179-211.
- Aldowah, H., Rehman, S. U., Ghazal, S., & Umar, I. N. (2017). Internet of things in higher education: A study on future learning. *Journal of Physics: Conference Series*, 892, 1-11. doi :10.1088/1742-6596/892/1/012017
- Ali, M., Bilal, H. S. M., Razzaq, M. A., Khan, J., Lee, S., Idris, M., ... & Kang, B. H. (2017). IoTFLiP: IoT-based flipped learning platform for medical education. *Digital Communications and Networks*, 3(3), 188-194. doi: <https://doi.org/10.1016/j.dcan.2017.03.002>
- Al-Shareem, K. M., Yusof, N. A., & Kamal, E. M. (2015). External factors influencing the readiness for implementing public-private partnerships among public and private organizations in Yemen. *Journal of Science & Technology Policy Management*, 6(1), 56-75. doi: <https://doi.org/10.1108/JSTPM-07-2014-0030>
- Asghari, P., Rahmani, A. M., & Javadi, H. H. S. (2019). Internet of Things applications: A systematic review. *Computer Networks*, 148, 241-261. doi: <https://doi.org/10.1016/j.comnet.2018.12.008>
- Atabekov, A., He, J., & Bobbie, P. O. (2016, June). Internet of things-based framework to facilitate indoor localization education. In *2016 IEEE 40th Annual Computer Software and Applications Conference (COMPSAC)* (Vol. 2, pp. 269-274). Atlanta, GA, USA. doi: 10.1109/COMPSAC.2016.143
- Atzori, L., Iera, A., & Morabito, G. (2010). The Internet of Things: A survey. *Computer Networks*, 54(15), 2787-2805. doi: <https://doi.org/10.1016/j.comnet.2010.05.010>
- Bagheri, M., & Movahed, S. H. (2016, November 28-December 1). The effect of the Internet of Things (IoT) on education business model. In *2016 12th International Conference on Signal-Image Technology & Internet-Based Systems (SITIS)* (pp. 435-441). Naples, Italy. doi: 10.1109/SITIS.2016.74
- Baker, C., Nafukho, F. M., McCaleb, K., Becker, M., & Johnson, M. (2016). The tangible and intangible benefits of offering massive open online courses: Faculty perspectives. *Internet Learning*, 4(2), 52-68.
- Bandara, I., & Ioras, F. (2016, March 7-9). The evolving challenges of internet of everything: Enhancing student performance and employability in higher education. In *INTED2016 10th annual International Technology, Education and Development* (pp. 652-658). Valencia, Spain.
- Barreto, L., Celesti, A., Villari, M., Fazio, M., & Puliafito, A. (2015, August 25-28). An authentication model for IoT clouds. In *2015 IEEE/ACM International Conference on Advances in Social Networks Analysis and Mining (ASONAM)* (pp. 1032-1035). Paris, France. doi: 10.1145/2808797.2809361
- Bayani, M., Leiton, K., & Loaiza, M. (2017). Internet of things (IoT) advantages on e-learning in the smart cities. *International Journal of Development Research*, 7(12), 17747-17753.

- Ben-Daya, M., Hassini, E., & Bahroun, Z. (2019). Internet of Things and supply chain management: A literature review. *International Journal of Production Research*, 57(15-16), 4719-4742. doi: <https://doi.org/10.1080/00207543.2017.1402140>
- Bibri, S. E. (2015). Democratizing AmI and the IoT: The power and influence of social innovation and participative and humanistic design. In *The Shaping of Ambient Intelligence and the Internet of Things* (pp. 239-301). Paris, France: Atlantis Press. doi: https://doi.org/10.2991/978-94-6239-142-0_8
- Bourrie, D. M., Sankar, C. S., & Jones-Farmer, L. A. (2015). Conceptualizing interactions between innovation characteristics and organizational members' readiness to adopt educational innovations. *International Journal of Engineering Education*, 31(4), 967-985.
- Bouzemrak, Y., Klüche, M., Gavai, A., & Marvin, H. J. (2019). Internet of Things in food safety: Literature review and a bibliometric analysis. *Trends in Food Science and Technology*, 94, 54-64. doi: <https://doi.org/10.1016/j.tifs.2019.11.002>
- Brereton, P., Kitchenham, B. A., Budgen, D., Turner, M., & Khalil, M. (2007). Lessons from applying the systematic literature review process within the software engineering domain. *Journal of Systems and Software*, 80(4), 571-583. doi: <https://doi.org/10.1016/j.jss.2006.07.009>
- Chen, S., Xu, H., Liu, D., Hu, B., & Wang, H. (2014). A vision of IoT: Applications, challenges, and opportunities with china perspective. *IEEE Internet of Things Journal*, 1(4), 349-359. doi: 10.1109/JIOT.2014.2337336
- Cheng, H. C., & Liao, W. W. (2012, February 19-22). Establishing an lifelong learning environment using IOT and learning analytics. In *2012 14th International Conference on Advanced Communication Technology (ICACT)* (pp. 1178-1183). PyeongChang, South Korea
- Chen, N. S., Cheng, I. L., & Chew, S. W. (2016). Evolution is not enough: Revolutionizing current learning environments to smart learning environments. *International Journal of Artificial Intelligence in Education*, 26(2), 561-581.
- Cheon, J., Lee, S., Crooks, S. M., & Song, J. (2012). An investigation of mobile learning readiness in higher education based on the theory of planned behavior. *Computers and Education*, 59(3), 1054-1064. doi: <https://doi.org/10.1016/j.compedu.2012.04.015>
- Chin, J., & Callaghan, V. (2013, July 16-17). Educational living labs: a novel internet-of-things based approach to teaching and research. In *2013 9th International Conference on Intelligent Environments* (pp. 92-99). Athens, Greece. doi: 10.1109/IE.2013.48
- Coccoli, M., Guercio, A., Maresca, P., & Stanganelli, L. (2014). Smarter universities: A vision for the fast changing digital era. *Journal of Visual Languages and Computing*, 25(6), 1003-1011. doi: <https://doi.org/10.1016/j.jvlc.2014.09.007>
- Demirer, V., Aydın, B., & Çelik, Ş. B. (2017). Exploring the Educational Potential of Internet of Things (IoT) in Seamless Learning. In *The Internet of Things: Breakthroughs in Research and Practice* (pp. 1-15). Hershey, USA: IGI Global. doi: 10.4018/978-1-5225-1832-7.ch001
- Dijkman, R. M., Sprenkels, B., Peeters, T., & Janssen, A. (2015). Business models for the Internet of Things. *International Journal of Information Management*, 35(6), 672-678. doi: <https://doi.org/10.1016/j.ijinfomgt.2015.07.008>

- Domingo, M. C. (2012). An overview of the Internet of Things for people with disabilities. *Journal of Network and Computer Applications*, 35(2), 584-596. doi: <https://doi.org/10.1016/j.jnca.2011.10.015>
- Farhan, M., Jabbar, S., Aslam, M., Khalid, S., Hammoudeh, M., Khan, M., & Han, K. (2017). IoT-based students interaction framework using attention-scoring assessment in eLearning. *Future Generation Computer Systems*, 79, 909-919. doi: <https://doi.org/10.1016/j.future.2017.09.037>
- Farooq, M., Waseem, M., Mazhar, S., Khairi, A., & Kamal, T. (2015). A review on internet of things (IoT). *International Journal of Computer Applications*, 113(1), 1-7.
- French, A. M., & Shim, J. P. (2016). The digital revolution: Internet of Things, 5G, and beyond. *Communications of the Association for Information Systems*, 38(1), 840-850.
- Gao, L., & Bai, X. (2014). A unified perspective on the factors influencing consumer acceptance of internet of things technology. *Asia Pacific Journal of Marketing and Logistics*, 26(2), 211-231. doi: <https://doi.org/10.1108/APJML-06-2013-0061>
- Gómez-Chabla, R., Real-Avilés, K., Morán, C., Grijalva, P., & Recalde, T. (2019). IoT applications in agriculture: A systematic literature review. In *2nd International Conference on ICTs in Agronomy and Environment* (pp. 68-76). Cham, Switzerland: Springer. doi: https://doi.org/10.1007/978-3-030-10728-4_8
- Gómez, J., Huete, J. F., Hoyos, O., Perez, L., & Grigori, D. (2013). Interaction system based on Internet of Things as support for education. *Procedia Computer Science*, 21, 132-139. doi: <https://doi.org/10.1016/j.procs.2013.09.019>
- Gonzalez, G. R., Organero, M. M., & Kloos, C. D. (2008, July). Early infrastructure of an internet of things in spaces for learning. In *2008 Eighth IEEE International Conference on Advanced Learning Technologies* (pp. 381-383). Cantabria, Spain. doi: 10.1109/ICALT.2008.210
- Gubbi, J., Buyya, R., Marusic, S., & Palaniswami, M. (2013). Internet of Things (IoT): A vision, architectural elements, and future directions. *Future Generation Computer Systems*, 29(7), 1645-1660. doi: <https://doi.org/10.1016/j.future.2013.01.010>
- Guo, B., Yu, Z., Zhou, X., & Zhang, D. (2012, May 23-25). Opportunistic IoT: Exploring the social side of the internet of things. In *Proceedings of the 2012 IEEE 16th International Conference on Computer Supported Cooperative Work in Design (CSCWD)* (pp. 925-929). Wuhan, China. doi: 10.1109/CSCWD.2012.6221932
- Hameed, M. A., Counsell, S., & Swift, S. (2012). A conceptual model for the process of IT innovation adoption in organizations. *Journal of Engineering and Technology Management*, 29(3), 358-390. doi: <https://doi.org/10.1016/j.jengtecman.2012.03.007>
- He, J. S., Ji, S., & Bobbie, P. O. (2017). Internet of things (iot)-based learning framework to facilitate stem undergraduate education. In *Proceedings of the SouthEast Conference* (pp. 88-94). New York, USA: Association for Computing Machinery.
- Ho, S. M., Ocasio-Velázquez, M., & Booth, C. (2017). Trust or consequences? Causal effects of perceived risk and subjective norms on cloud technology adoption. *Computers and Security*, 70, 581-595. doi: <https://doi.org/10.1016/j.cose.2017.08.004>
- Hossain, M. A. (2014). Development of an integrated model for RFID extension. *Business Process Management Journal*, 20(5), 752-772. doi: <https://doi.org/10.1108/BPMJ-04-2013-0055>

- Hossain, M. A., & Quaddus, M. (2015). Radio frequency identification (RFID) adoption: A cross-sectional comparison of voluntary and mandatory contexts. *Information Systems Frontiers*, 17(5), 1057-1076. doi: <https://doi.org/10.1007/s10796-013-9482-1>
- Hsu, C. L., & Lin, J. C. C. (2018). Exploring factors affecting the adoption of Internet of Things services. *Journal of Computer Information Systems*, 58(1), 49-57. doi: <https://doi.org/10.1080/08874417.2016.1186524>
- Hussin, A. A. (2018). Education 4.0 made simple: Ideas for teaching. *International Journal of Education and Literacy Studies*, 6(3), 92-98. doi: <http://dx.doi.org/10.7575/aiac.ijels.v.6n.3p.92>
- Iyawa, G. E., Herselman, M., & Botha, A. (2017). The application of wireless sensor networks and wearable technologies for educational purposes: A scoping review. In *Proceedings of the Second International Conference on Advanced Wireless Information, Data, and Communication Technologies* (pp. 1-5). New York, USA: Association for Computing Machinery.
- Jeffords, J., Kane, P., Moghaddam, Y., Rucinski, A., & Temesgen, Z. (2014, December 3-6). Exponentially disruptive innovation driven by service science and the Internet of Things as a Grand Challenge enabler in Education. In *2014 International Conference on Interactive Collaborative Learning (ICL)* (pp. 1021-1025). Dubai, United Arab Emirates. doi: 10.1109/ICL.2014.7017922
- Kalashnikov, A., Zhang, H., Jennings, J., & Abramriuk, M. M. (2017, May 17-19). Remote laboratory: Using Internet-of-Things (IoT) for E-learning. In *Comparison of the responsiveness of ultrasonic oscillating temperature sensors (UOTSes) and conventional sensors to temperature inflection points* (pp. 43-46). Sumy, Ukraine.
- Kamar, I., Chatterjee, P., & Hamie, A. (2016). Internet of Things in learning systems-A perspective of platforms. *International Journal of Advanced Research in Computer Science*, 7(2), 52-56.
- Kassab, M., DeFranco, J., & Laplante, P. (2020). A systematic literature review on Internet of things in education: Benefits and challenges. *Journal of Computer Assisted Learning*, 36(2), 115-127. doi: <https://doi.org/10.1111/jcal.12383>
- Kitchenham, B. (2004). Procedures for performing systematic reviews. *Keele, UK, Keele University*, 33(2004), 1-26.
- Kortuem, G., Bandara, A. K., Smith, N., Richards, M., & Petre, M. (2013). Educating the Internet-of-Things generation. *Computer*, 46(2), 53-61. doi: 10.1109/MC.2012.390
- Kounelis, I., Baldini, G., Neisse, R., Steri, G., Tallacchini, M., & Pereira, A. G. (2014). Building trust in the human? internet of things relationship. *IEEE Technology and Society Magazine*, 33(4), 73-80. doi: 10.1109/MTS.2014.2364020
- Krotov, V. (2017). The Internet of Things and new business opportunities. *Business Horizons*, 60(6), 831-841. doi: <https://doi.org/10.1016/j.bushor.2017.07.009>
- Kusuma, S., & Viswanath, D. K. (2018). IOT and big data analytics in E-learning: A technological perspective and review. *International Journal of Engineering and Technology*, 7, 164-167.
- Lee, I., & Lee, K. (2015). The Internet of Things (IoT): Applications, investments, and challenges for enterprises. *Business Horizons*, 58(4), 431-440. doi: <https://doi.org/10.1016/j.bushor.2015.03.008>

- Lee, S. E., Choi, M., & Kim, S. (2017). How and what to study about IoT: Research trends and future directions from the perspective of social science. *Telecommunications Policy*, 41(10), 1056-1067. doi: <https://doi.org/10.1016/j.telpol.2017.09.007>
- Li, Y., Hou, M., Liu, H., & Liu, Y. (2012). Towards a theoretical framework of strategic decision, supporting capability and information sharing under the context of Internet of Things. *Information Technology and Management*, 13(4), 205-216. doi: <https://doi.org/10.1007/s10799-012-0121-1>
- Lin, J. S. C., & Hsieh, P. L. (2007). The influence of technology readiness on satisfaction and behavioral intentions toward self-service technologies. *Computers in Human Behavior*, 23(3), 1597-1615. doi: <https://doi.org/10.1016/j.chb.2005.07.006>
- Marquez, J., Villanueva, J., Solarte, Z., & Garcia, A. (2016). IoT in education: Integration of objects with virtual academic communities. In *New Advances in Information Systems and Technologies* (pp. 201-212). Cham, Switzerland: Springer. doi: https://doi.org/10.1007/978-3-319-31232-3_19
- Mijac, M., Androcec, D., & Picek, R. (2017). Smart city services driven by IoT: A systematic review. *Journal of Economic and Social Development*, 4(2), 40-50.
- Miorandi, D., Sicari, S., De Pellegrini, F., & Chlamtac, I. (2012). Internet of things: Vision, applications and research challenges. *Ad Hoc Networks*, 10(7), 1497-1516. doi: <https://doi.org/10.1016/j.adhoc.2012.02.016>
- Mital, M., Chang, V., Choudhary, P., Papa, A., & Pani, A. K. (2018). Adoption of Internet of Things in India: A test of competing models using a structured equation modeling approach. *Technological Forecasting and Social Change*, 136, 339-346. doi: <https://doi.org/10.1016/j.techfore.2017.03.001>
- Moreira, F. T., Magalhaes, A., Ramos, F., & Vairinhos, M. (2018). The power of the internet of things in education: an overview of current status and potential. In *Conference on Smart Learning Ecosystems and Regional Development* (pp. 51-63). Cham, Switzerland: Springer. doi: https://doi.org/10.1007/978-3-319-61322-2_6
- Mrabet, H. E., & Moussa, A. A. (2017). Smart classroom environment via IoT in basic and secondary education. *Transactions on Machine Learning and Artificial Intelligence*, 5(4), 274-279. doi: <https://doi.org/10.14738/tmlai.54.3191>
- Niyato, D., Hoang, D. T., Luong, N. C., Wang, P., Kim, D. I., & Han, Z. (2016). Smart data pricing models for the Internet of Things: A bundling strategy approach. *IEEE Network*, 30(2), 18-25. doi: 10.1109/MNET.2016.7437020
- Njeru, A. M., Omar, M. S., Yi, S., Paracha, S., & Wannous, M. (2017, May 13-17). Using iot technology to improve online education through data mining. In *2017 International Conference on Applied System Innovation (ICASI)* (pp. 515-518). Sapporo, Japan. doi: 10.1109/ICASI.2017.7988469
- Onyalo, N., Kandie, H., & Njuki, J. (2015). The Internet of Things, progress report for africa: A survey. *International Journal of Computer Science and Software Engineering*, 4(9), 230-237.
- Oye, N. D., Iahad, N. A., & Rahim, N. A. (2014). The history of UTAUT model and its impact on ICT acceptance and usage by academicians. *Education and Information Technologies*, 19(1), 251-270. doi: 10.1007/s10639-012-9189-9

- Parasuraman, A. (2000). Technology readiness index (TRI) a multiple-item scale to measure readiness to embrace new technologies. *Journal of Service Research*, 2(4), 307-320. doi: <https://doi.org/10.1177/109467050024001>
- Parasuraman, A., & Colby, C. L. (2015). An updated and streamlined technology readiness index: TRI 2.0. *Journal of Service Research*, 18(1), 59-74. doi: <https://doi.org/10.1177/1094670514539730>
- Patil, K. (2016, December 19-21). Retail adoption of Internet of Things: Applying TAM model. In *2016 International Conference on Computing, Analytics and Security Trends (CAST)* (pp. 404-409). Pune, India. doi: 10.1109/CAST.2016.7915003
- Perera, C., Zaslavsky, A., Christen, P., & Georgakopoulos, D. (2014). Context aware computing for the internet of things: A survey. *IEEE communications surveys & tutorials*, 16(1), 414-454. doi: 10.1109/SURV.2013.042313.00197
- Pruet, P., Ang, C. S., Farzin, D., & Chaiwut, N. (2015, June 24-27). Exploring the Internet of “Educational Things”(IoET) in rural underprivileged areas. In *2015 12th International Conference on Electrical Engineering/Electronics, Computer, Telecommunications and Information Technology (ECTI-CON)* (pp. 1-5). Hua Hin, Thailand. doi: 10.1109/ECTICon.2015.7207125
- Ramlowat, D. D., & Pattanayak, B. K. (2019). Exploring the internet of things (IoT) in education: A review. In *Information systems design and intelligent applications* (pp. 245-255). Singapore: Springer. doi: https://doi.org/10.1007/978-981-13-3338-5_23
- Reyes, P. M., Li, S., & Visich, J. K. (2016). Determinants of RFID adoption stage and perceived benefits. *European Journal of Operational Research*, 254(3), 801-812. doi: <https://doi.org/10.1016/j.ejor.2016.03.051>
- Roy, A., Zalzal, A. M. S., & Kumar, A. (2016). Disruption of things: A model to facilitate adoption of IoT-based innovations by the urban poor. *Procedia Engineering*, 159, 199-209. doi: <https://doi.org/10.1016/j.proeng.2016.08.159>
- Rogers, E. M. (2003). *Diffusion of innovations* (5th Ed.). Tampa, Florida: Free Press.
- Sabi, H. M., Uzoka, F. M. E., Langmia, K., & Njeh, F. N. (2016). Conceptualizing a model for adoption of cloud computing in education. *International Journal of Information Management*, 36(2), 183-191. doi: <https://doi.org/10.1016/j.ijinfomgt.2015.11.010>
- Samiee, S., & Rezaei-Moghaddam, K. (2017). The proposed alternative model to predict adoption of innovations: The case of no-till technology in Iran. *Journal of the Saudi Society of Agricultural Sciences*, 16(3), 270-279. doi: <https://doi.org/10.1016/j.jssas.2015.09.002>
- Sarıtaş, M. T. (2015). The emergent technological and theoretical paradigms in education: The interrelations of cloud computing (CC), connectivism and Internet of Things (IoT). *Acta Polytechnica Hungarica*, 12(6), 161-179. doi: 10.12700/aph.12.6.2015.6.10
- Saarikko, T., Westergren, U. H., & Blomquist, T. (2017). The Internet of Things: Are you ready for what's coming? *Business Horizons*, 60(5), 667-676. doi: <https://doi.org/10.1016/j.bushor.2017.05.010>

- Shin, D. (2014). A socio-technical framework for Internet-of-Things design: A human-centered design for the Internet of Things. *Telematics and Informatics*, 31(4), 519-531. doi: <https://doi.org/10.1016/j.tele.2014.02.003>
- Shin, D. H. (2017). Conceptualizing and measuring quality of experience of the internet of things: Exploring how quality is perceived by users. *Information & Management*, 54(8), 998-1011. doi: <https://doi.org/10.1016/j.im.2017.02.006>
- Shin, D. H., & Park, Y. J. (2017). Understanding the Internet of Things ecosystem: Multi-level analysis of users, society, and ecology. *Digital Policy, Regulation and Governance*, 19(1), 77-100. doi: <https://doi.org/10.1108/DPRG-07-2016-0035>
- Stojkoska, B. L. R., & Trivodaliev, K. V. (2017). A review of Internet of Things for smart home: Challenges and solutions. *Journal of Cleaner Production*, 140, 1454-1464. doi: <https://doi.org/10.1016/j.jclepro.2016.10.006>
- Sudtasan, T., & Mitomo, H. (2017). The Internet of Things as an accelerator of advancement of broadband networks: A case of Thailand. *Telecommunications Policy*, 42(4), 293-303. doi: <https://doi.org/10.1016/j.telpol.2017.08.008>
- Talavera, J. M., Tobón, L. E., Gómez, J. A., Culman, M. A., Aranda, J. M., Parra, D. T., ... & Garreta, L. E. (2017). Review of IoT applications in agro-industrial and environmental fields. *Computers and Electronics in Agriculture*, 142, 283-297. doi: <https://doi.org/10.1016/j.compag.2017.09.015>
- Tan, T. H., Liu, T. Y., & Chang, C. C. (2007). Development and evaluation of an RFID-based ubiquitous learning environment for outdoor learning. *Interactive Learning Environments*, 15(3), 253-269. doi: <https://doi.org/10.1080/10494820701281431>
- Thakur, R., & Srivastava, M. (2014). Adoption readiness, personal innovativeness, perceived risk and usage intention across customer groups for mobile payment services in India. *Internet Research*, 24(3), 369-392. doi: <https://doi.org/10.1108/IntR-12-2012-0244>
- Thiesse, F., Staake, T., Schmitt, P., & Fleisch, E. (2011). The rise of the “next-generation bar code”: an international RFID adoption study. *Supply Chain Management: An International Journal*, 16(5), 328-345. doi: <https://doi.org/10.1108/13598541111155848>
- Tornatzky, L., & Fleischer, M. (1990). *The process of technology innovation*. Lexington, MA: Lexington Books.
- Tranfield, D., Denyer, D., & Smart, P. (2003). Towards a methodology for developing evidence-informed management knowledge by means of systematic review. *British Journal of Management*, 14(3), 207-222. doi: <https://doi.org/10.1111/1467-8551.00375>
- Tsai, C. W., Lai, C. F., & Vasilakos, A. V. (2014). Future Internet of Things: Open issues and challenges. *Wireless Networks*, 20(8), 2201-2217. doi: 10.1007/s11276-014-0731-0
- Tsai, M. C., Lai, K. H., & Hsu, W. C. (2013). A study of the institutional forces influencing the adoption intention of RFID by suppliers. *Information & Management*, 50(1), 59-65. doi: <https://doi.org/10.1016/j.im.2012.05.006>
- ur Rahman, M., Deep, V., & Rahman, S. (2016, January 14-15). ICT and internet of things for creating smart learning environment for students at education institutes in India. In *2016 6th International Conference-*

- Cloud System and Big Data Engineering (Confluence)* (pp. 701-704). Noida, India. doi: 10.1109/CONFLUENCE.2016.7508209
- Uskov, V., Pandey, A., Bakken, J. P., & Margapuri, V. S. (2016, April 10-13). Smart engineering education: The ontology of Internet-of-Things applications. In *2016 IEEE Global Engineering Education Conference (EDUCON)* (pp. 476-481). Abu Dhabi, United Arab Emirates. doi: 10.1109/EDUCON.2016.7474596
- Uzelac, A., Gligoric, N., & Krco, S. (2015). A comprehensive study of parameters in physical environment that impact students' focus during lecture using Internet of Things. *Computers in Human Behavior*, *53*, 427-434. doi: <https://doi.org/10.1016/j.chb.2015.07.023>
- Veeramanickam, M., & Mohanapriya, M. (2017). Iot enabled futuristic smart campus with effective e-learning: i-campus. *GSTF Journal of Engineering Technology (JET)*, *3*(4), 8-87. doi: 10.5176/2251-3701_3.4.164
- Want, R., Schilit, B. N., & Jenson, S. (2015). Enabling the internet of things. *Computer*, *48*(1), 28-35. doi: 10.1109/MC.2015.12
- Whitmore, A., Agarwal, A., & Xu, L. D. (2015). The Internet of Things—A survey of topics and trends. *Information Systems Frontiers*, *17*(2), 261-274. doi: <https://doi.org/10.1007/s10796-014-9489-2>
- Xu, L. D., He, W., & Li, S. (2014). Internet of things in industries: A survey. *IEEE Transactions on Industrial Informatics*, *10*(4), 2233-2243. doi: 10.1109/TII.2014.2300753
- Yoon, T. E., & George, J. F. (2013). Why aren't organizations adopting virtual worlds? *Computers in Human Behavior*, *29*(3), 772-790. doi: <https://doi.org/10.1016/j.chb.2012.12.003>
- Zhamanov, A., Sakhiyeva, Z., Suliyev, R., & Kaldykulova, Z. (2017, November 28-29). IoT smart campus review and implementation of IoT applications into education process of university. In *2017 13th International Conference on Electronics, Computer and Computation (ICECCO)* (pp. 1-4). Abuja, Nigeria. doi: 10.1109/ICECCO.2017.8333334
- Zhu, Z. T., Yu, M. H., & Riezebos, P. (2016). A research framework of smart education. *Smart Learning Environments*, *3*(1), 1-17. doi: <https://doi.org/10.1186/s40561-016-0026-2>

Appendix A

Defining Internet of Things

Concept	Definition	Author
Internet of Things	The interconnectedness of numerous gadgets that have possibility of report, screen, or give other esteem or administrations that are of incentive to end clients	Atabekov et al. (2016)
Internet of Things	formation of inventive alternatives for learning and this is conceivable because of the expansion of concepts from ubiquitous computing and technologies as mobile, Radio Frequency Identification amidst the rest	Gonzalez et al. (2008)
Internet of Things	IoT involves interaction with heterogeneous devices along with seamless sharing of data with a specific end goal to give personalized services to the learners and instructors	Kamar et al. (2016)
Internet of Things	a dynamic worldwide system foundation that has the capability of self-conFigureuration based on standards and interoperable protocols where there is identification of physical and virtual things, physical attributes and virtual personalities to use intelligent interfaces by being coherently being part of the data network	Xu et al. (2014); Uzelac et al. (2015); Moreira et al. (2018)
Internet of Things	the enabling of internet presence for any person, place, or thing on the planet	Want et al. (2015)
Internet of Things	It comprises various gadgets part of the technological, physical, and broad socioeconomic environments. The physical surrounding has human and nonhuman objects connected by ubiquitous wireless network. They empower programmed correspondence and association among the items and the physical condition, and the mechanical condition contained equipment, programming, organizing advances, information, incorporated stages, and specialized benchmarks empower collaborations in the physical condition.	Krotov (2017)

Appendix B

Primary study references

Study ID	References
I1	Ali, M., Bilal, H. S. M., Razzaq, M. A., Khan, J., Lee, S., Idris, M., . . . Kang, B. H. (2017). IoTFLiP: IoT-based flipped learning platform for medical education. <i>Digital Communications and Networks</i> , 3(3), 188-194.
I2	Atzori, L., Iera, A., & Morabito, G. (2010). The Internet of Things: A survey. <i>Computer Networks</i> , 54(15), 2787-2805.
I3	Bagheri, M., & Movahed, S. H. (2016). The Effect of the Internet of Things (IoT) on Education Business Model. In <i>2016 12th International Conference on Signal-Image Technology & Internet-Based Systems (SITIS)</i> (pp. 435-441). IEEE.
I4	Bayani, M., Leiton, K., & Loaiza, M. (2017). Internet of Things (IoT) Advantages on E-learning in the Smart Cities. <i>International Journal of Development Research</i> , 7(12), 17747-17753.
I5	Bibri, S. E. (2015). Democratizing Aml and the IoT: The Power and Influence of Social Innovation and Participative and Humanistic Design <i>The Shaping of Ambient Intelligence and the Internet of Things</i> (pp. 239-301): Springer.
I6	Chen, N.-S., Cheng, I.-L., & Chew, S. W. (2016). Evolution is not enough: Revolutionizing current learning environments to smart learning environments. <i>International Journal of Artificial Intelligence in Education</i> , 26(2), 561-581.
I7	Chen, S., Xu, H., Liu, D., Hu, B., & Wang, H. (2014). A vision of IoT: Applications, challenges, and opportunities with china perspective. <i>IEEE Internet of Things Journal</i> , 1(4), 349-359.
I8	Coccoli, M., Guercio, A., Maresca, P., & Stanganelli, L. (2014). Smarter universities: A vision for the fast changing digital era. <i>Journal of Visual Languages & Computing</i> , 25(6), 1003-1011.
I9	Demirer, V., Aydın, B., & Çelik, Ş. B. (2017). Exploring the Educational Potential of Internet of Things (IoT) in Seamless Learning. <i>The Internet of Things: Breakthroughs in Research and Practice: Breakthroughs in Research and Practice</i> , 1.
I10	Domingo, M. C. (2012). An overview of the Internet of Things for people with disabilities. <i>Journal of Network and Computer Applications</i> , 35(2), 584-596.
I11	Farhan, M., Jabbar, S., Aslam, M., Khalid, S., Hammoudeh, M., Khan, M., & Han, K. (2017). IoT-based students interaction framework using attention-scoring assessment in eLearning. <i>Future Generation Computer Systems</i> , 79, 909-919.
I12	Farooq, M., Waseem, M., Mazhar, S., Khairi, A., & Kamal, T. (2015). A review on internet of things (IoT). <i>International Journal of Computer Applications</i> , 113(1).
I13	Gómez, J., Huete, J. F., Hoyos, O., Perez, L., & Grigori, D. (2013). Interaction System based on Internet of Things as Support for Education. <i>Procedia Computer Science</i> , 21, 132-139.
I14	Gubbi, J., Buyya, R., Marusic, S., & Palaniswami, M. (2013). Internet of Things (IoT): A vision, architectural elements, and future directions. <i>Future Generation Computer Systems</i> , 29(7), 1645-1660.
I15	Kortuem, G., Bandara, A. K., Smith, N., Richards, M., & Petre, M. (2013). Educating the Internet-of-Things generation. <i>Computer</i> , 46(2), 53-61.
I16	Krotov, V. (2017). The Internet of Things and new business opportunities. <i>Business Horizons</i> , 60(6), 831-841.
I17	Lee, I., & Lee, K. (2015). The Internet of Things (IoT): Applications, investments, and challenges for enterprises. <i>Business Horizons</i> , 58(4), 431-440.

Appendix B (Continued)

Study ID

References

- I18 Lee, S.-E., Choi, M., & Kim, S. (2017). How and what to study about IoT: Research trends and future directions from the perspective of social science. *Telecommunications Policy*, 41(10), 1056-1067.
- I19 Li, Y., Hou, M., Liu, H., & Liu, Y. (2012). Towards a theoretical framework of strategic decision, supporting capability and information sharing under the context of Internet of Things. *Information Technology and Management*, 13(4), 205-216
- I20 He, J. S., Ji, S., & Bobbie, P. O. (2017). Internet of Things (IoT)-based Learning Framework to Facilitate STEM Undergraduate Education. In *Proceedings of the SouthEast Conference* (pp. 88-94).
- I21 Hossain, M. A. (2014). Development of an integrated model for RFID extension. *Business Process Management Journal*, 20(5), 752-772.
- I22 Iyawa, G. E., Herselman, M., & Botha, A. (2017). The Application of Wireless Sensor Networks and Wearable Technologies for Educational Purposes: A Scoping Review. In *Proceedings of Second International Conference on Advanced Wireless Information, Data, and Communication Technologies (AWICT'17)*. ACM, Paris, France. doi:10.1145/1234567890
- I23 Miorandi, D., Sicari, S., De Pellegrini, F., & Chlamtac, I. (2012). Internet of things: Vision, applications and research challenges. *Ad hoc networks*, 10(7), 1497-1516.
- I24 Mital, M., Chang, V., Choudhary, P., Papa, A., & Pani, A. K. (2017). Adoption of Internet of Things in India: A test of competing models using a structured equation modeling approach. *Technological Forecasting and Social Change*. 136, 339-346.
- I25 Niyato, D., Hoang, D. T., Luong, N. C., Wang, P., Kim, D. I., & Han, Z. (2016). Smart data pricing models for the Internet of Things: A bundling strategy approach. *IEEE Network*, 30(2), 18-25.
- I26 Roy, A., Zalzal, A. M. S., & Kumar, A. (2016). Disruption of Things: A Model to Facilitate Adoption of IoT-based Innovations by the Urban Poor. *Procedia Engineering*, 159(Supplement C), 199-209.
- I27 Saarikko, T., Westergren, U. H., & Blomquist, T. (2017). The Internet of Things: Are you ready for what's coming? *Business Horizons*, 60(5), 667-676.
- I28 Sarıtaş, M. T. (2015). The Emergent Technological and Theoretical Paradigms in Education: The Interrelations of Cloud Computing (CC), Connectivism and Internet of Things (IoT). *Acta Polytechnica Hungarica*, 12(6), 161-179.
- I29 Shin, D.-H. (2017). Conceptualizing and measuring quality of experience of the internet of things: Exploring how quality is perceived by users. *Information & Management*, 54(8), 998-1011.
- I30 Shin, D.-H., & Jin Park, Y. (2017). Understanding the Internet of Things ecosystem: multi-level analysis of users, society, and ecology. *Digital Policy, Regulation and Governance*, 19(1), 77-100.
- I31 Sudtasan, T., & Mitomo, H. (2017). The Internet of Things as an accelerator of advancement of broadband networks: A case of Thailand. *Telecommunications Policy*, 42(4), 293-303.
- I32 Thiesse, F., Staake, T., Schmitt, P., & Fleisch, E. (2011). The rise of the "next-generation bar code": an international RFID adoption study. *Supply Chain Management: An International Journal*, 16(5), 328-345.
- I33 Want, R., Schilit, B. N., & Jenson, S. (2015). Enabling the internet of things. *Computer*, 48(1), 28-35.
- I34 Adhiarna, N., Hwang, Y. M., Park, M. J., & Rho, J. J. (2013). An integrated framework for RFID adoption and diffusion with a stage-scale-scope cubicle model: A case of Indonesia. *International Journal of Information Management*, 33(2), 378-389.
- I35 Zhu, Z.-T., Yu, M.-H., & Riezebos, P. (2016). A research framework of smart education. *Smart Learning Environments*, 3(1), 4.

Appendix B (Continued)

Study ID

References

- I36 Barreto, L., Celesti, A., Villari, M., Fazio, M., & Puliafito, A. (2015, 25-28 Aug. 2015). *An authentication model for IoT clouds*. Paper presented at the 2015 IEEE/ACM International Conference on Advances in Social Networks Analysis and Mining (ASONAM).
- I37 Ahmed, E., Yaqoob, I., Gani, A., Imran, M., & Guizani, M. (2016). Internet-of-things-based smart environments: state of the art, taxonomy, and open research challenges. *IEEE Wireless Communications*, 23(5), 10-16.
- I38 Guo, B., Yu, Z., Zhou, X., & Zhang, D. (2012, May). Opportunistic IoT: Exploring the social side of the internet of things. In *Proceedings of the 2012 IEEE 16th International Conference on Computer Supported Cooperative Work in Design (CSCWD)* (pp. 925-929). IEEE.
- I39 Kalashnikov, A., Zhang, H., Jennings, J., & Abramriuk, M. M. (2017). Remote laboratory: using Internet-of-Things (IoT) for E-learning. In: Comparison of the responsiveness of ultrasonic oscillating temperature sensors (UOTs) and conventional sensors to temperature inflection points, *Springer*, 43-46.
- I40 Kounelis, I., Baldini, G., Neisse, R., Steri, G., Tallacchini, M., & Pereira, A. G. (2014). Building trust in the human? internet of things relationship. *IEEE Technology and Society Magazine*, 33(4), 73-80.
- I41 Perera, C., Zaslavsky, A., Christen, P., & Georgakopoulos, D. (2013). Context aware computing for the internet of things: A survey. *IEEE communications surveys & tutorials*, 16(1), 414-454.
- I42 Yoon, T. E., & George, J. F. (2013). Why aren't organizations adopting virtual worlds? *Computers in Human Behavior*, 29(3), 772-790.
- I43 Shin, D. (2014). A socio-technical framework for Internet-of-Things design: A human-centered design for the Internet of Things. *Telematics and informatics*, 31(4), 519-531.
- I44 Dijkman, R. M., Sprenkels, B., Peeters, T., & Janssen, A. (2015). Business models for the Internet of Things. *International Journal of Information Management*, 35(6), 672-678.
- I45 Gao, L., & Bai, X. (2014). A unified perspective on the factors influencing consumer acceptance of internet of things technology. *Asia Pacific Journal of Marketing and Logistics*, 26(2), 211-231.
- I46 Tsai, C. W., Lai, C. F., & Vasilakos, A. V. (2014). Future Internet of Things: open issues and challenges. *Wireless Networks*, 20(8), 2201-2217. doi:10.1007/s11276-014-0731-0
- I47 Patil, K. (2016, December). Retail adoption of Internet of Things: Applying TAM model. In *2016 International Conference on Computing, Analytics and Security Trends (CAST)* (pp. 404-409). IEEE.
- I48 Tsai, M.-C., Lai, K.-H., & Hsu, W.-C. (2013). A study of the institutional forces influencing the adoption intention of RFID by suppliers. *Information & Management*, 50(1), 59-65.
- I49 Reyes, P. M., Li, S., & Visich, J. K. (2016). Determinants of RFID adoption stage and perceived benefits. *European Journal of Operational Research*, 254(3), 801-812.

Appendix C

Quality evaluation measure

QAF: "QUALITY ASSESSMENT FACTORS"					
S/ID	Q-A1	Q-A2	Q-A3	Q-A4	SCORE
I1	2	2	2	2	8
I2	2	0	0	2	4
I3	2	1	0	2	5
I4	2	0	2	1	5
I5	2	0	1	2	5
I6	2	0	0	2	4
I7	2	0	2	2	6
I8	2	0	2	1	5
I9	2	0	1	2	5
I10	2	0	1	2	5
I11	2	1	1	1	5
I12	1	1	1	1	4
I13	2	2	2	2	8
I14	2	0	2	1	5
I15	2	0	2	1	5
I16	2	0	1	1	4
I17	2	0	1	1	5
I19	2	0	2	2	6
I20	2	0	2	1	5
I21	2	2	1	1	6
I22	2	0	2	1	5
I23	1	1	1	1	4
I24	2	2	2	2	8
I25	2	1	2	2	7
I26	2	2	1	1	6
I27	2	0	1	1	4
I28	2	0	1	1	4
I29	2	2	2	2	8
I30	2	2	1	2	7
I32	2	2	2	2	8
I33	2	0	1	1	4

Appendix C (Continued)

QAF: "QUALITY ASSESSMENT FACTORS"					
S/ID	Q-A1	Q-A2	Q-A3	Q-A4	SCORE
I34	2	1	1	1	5
I35	2	0	1	1	4
I36	2	0	0	2	4
I37	2	1	0	1	4
I38	2	0	0	1	3
I39	2	1	0	1	4
I40	2	0	1	1	4
I41	2	0	1	1	4
I42	1	2	1	1	5
I43	2	2	1	1	6
I44	2	2	1	1	6
I45	1	2	1	1	5
I46	2	0	0	2	4
I47	2	2	1	2	7
I48	2	2	1	2	7
I49	2	2	2	2	8

Appendix D

Distribution of research methodologies

Distribution of research methodologies						
ID	Instigator(s)	Article Name	Intent	Theory/ Framework	Method	Details collection process
1	Dijkman et al. (2015)	Business models for internet of things	Presenting a framework for developing business models for IoT application	none	mixed	Interviews and Surveys

Appendix D (Continued)

Distribution of research methodologies						
ID	Instigator(s)	Article Name	Intent	Theory/ Framework	Method	Details collection process
2	Farhan et al. (2017)	IoT based student's interaction framework using attention scoring assessment in e-learning	To develop IoT-based interaction framework and analysis of the student experience of electronic learning (eLearning).	none	quantitative	experiment
3	Ali et al. (2017)	IoTFLiP: IoT-based flipped learning platform for medical education	Developing of an IoT flipped learning for improved learning	none	qualitative	none
4	Coccoli et al. (2014)	Smarter Insitutions: A vision for the quick digital era	Analyze the current situation of education in universities, with particular reference to the European scenario. Specifically, we observe that recent evolutions, such as pervasive networking and other enabling technologies, have been dramatically changing human life, knowledge acquisition, and the way works are performed, and people learn	none	qualitative	none

Appendix D (Continued)

Distribution of research methodologies						
ID	Instigator(s)	Article Name	Intent	Theory/ Framework	Method	Details collection process
5	Thiesse et al. (2011)	The rise of next generation bar code-RFID adoption	To find the causals of adopting RFID within initial standards adopters	TOE	quantitative	survey
6	Adhiarna et al. (2013)	An integrated framework for RFID adoption and diffusion	The main concern in this study is stages of adoption which covers tree phases in respect of the maturity of the RFID project and the sophisticated business applications and RFID technology	TOE	qualitative	none
7	Iyawa et al. (2017)	Utilizing WSNz and wearable technologies for education	To perform a scoping evaluation on utilizing WSNs and wearable innovations for instruction	none	qualitative	none
8	Reyes et al. (2016)	Determinants of RFID adoption stage and perceived benefits	This study identifies the determinants of radio frequency identification (RFID) adoption stage and explores the perceived benefits from RFID adoption	TOE	quantitative	survey

Appendix D (Continued)

Distribution of research methodologies						
ID	Instigator(s)	Article Name	Intent	Theory/ Framework	Method	Details collection process
9	Hossain and Quaddus (2015)	Development of an integrated model for RFID extension	To develop an integrated model that explains the adoption, continuance, and extension of a technological innovation – taking radio frequency identification (RFID) as the case.	TOE	quantitative	survey
10	Yoon and George (2013)	Why arent organizations adopting virtual worlds	To comprehend reasons for slowness in firm incorporation of virtual worlds than required, through empirical determination of elements significant for organizational need to incorporate virtual worlds	TOE	quantitative	survey
11	Gómez et al. (2013)	Interaction System Based on Internet of Things as Support for Education	The education field, where Internet of Things can be used to create more significant learning spaces.	none	qualitative	none
12	Gao and Bai (2014)	A unified perspective on the factors influencing consumer acceptance of internet of things technology	To develop and test an integrative model of factors determining consumers' acceptance of IoT technology.	TAM	quantitative	survey

Appendix D (Continued)

Distribution of research methodologies						
ID	Instigator(s)	Article Name	Intent	Theory/ Framework	Method	Details collection process
13	He et al. (2017)	Instruction founded on Internet of Things (IoT) Framework to ease STEM Undergraduate instruction	Implementation of an IoT-based learning model that enables STEM undergraduate instruction	none	qualitative	none
14	Mital et al. (2018)	Adoption of Internet of Things in India: a test of competing models using SEM	To satisfy a clear gap in the main field of research by proposing a Structured Equation Model (SEM) approach to test three competing models in the context of Internet of Things in India.	SEM	quantitative	survey
15	Roy et al. (2016)	Disruption of things: a model to facilitate adoption of IoT-based innovations by the urban poor	This study examines the adoption of the Internet of Things (IoT) based innovations by urban poor communities.	none	quantitative	survey
16	Shin and Park (2017)	Understanding the Internet of Things ecosystem: multi-level analysis of users, society, and ecology	To conduct socio-technical analysis of the rapidly evolving Internet of Things (IoT) ecosystem and industry, including such factors as market growth and user experiences, policy, and the impact of IoT on various areas.	none	Mixed	interview and survey

Appendix D (Continued)

Distribution of research methodologies						
ID	Instigator(s)	Article Name	Intent	Theory/ Framework	Method	Details collection process
17	Zhu et al. (2016)	A research framework for smart education	The definition of smart education and presents a conceptual framework.	none	qualitative	none
18	Tsai et al. (2014)	Future Internet of Things: open issues and challenges	An overview of IoT and FIoT, followed by discussions on how to apply data mining and computational intelligence to FIoT.	none	qualitative	none
19	Sudtasan and Mitomo (2017)	The Internet of Things as an accelerator of advancement of broadband networks: A case of Thailand	Illustrates effect of consumer decisions influenced by Internet of Things applications	none	qualitative	none
20	Shin (2014)	A socio-technical framework for Internet of Things design centered on humans	How Internet of Things will evolve and stabilize in a smart environment, relation linking social and technical elements of Internet of Things and challenges in design, deploying, and sustaining diverse components of IoT	none	Mixed methods	Interviews and Surveys

Appendix D (Continued)

Distribution of research methodologies						
ID	Instigator(s)	Article Name	Intent	Theory/ Framework	Method	Details collection process
21	Barreto et al. (2015)	An authentication model for Internet of things clouds	Present an architectural model and several use cases that allow different types of users to access IoT devices	none	qualitative	none
22	Perera et al. (2014)	Context aware computing for the Internet of Things	Context awareness from an IoT perspective.	none	qualitative	none
23	Kounelis et al. (2014)	Human-IoT relationship	Agency as a driver in building trusted human Internet of Things	none	qualitative	none
24	Kalashnikov et al. (2017)	Remote laboratory: via Internet of Things	Remote laboratory project for video streaming	none	qualitative	none
25	Guo et al. (2012)	Opportunistic IoT: Exploring the social side of	To present the IoT from the human-centric perspective	none	qualitative	none
26	Gubbi et al. (2013)	Internet of Things: A vision, architectural components, and future guidelines	A cloud centric vision for worldwide implementation of IoT	none	qualitative	none

Appendix D (Continued)

Distribution of research methodologies						
ID	Instigator(s)	Article Name	Intent	Theory/ Framework	Method	Details collection process
27	Farooq et al. (2015)	A review on Internet of things	A detailed examination of the IoT notion with its enabling innovations and the sensor networks	none	qualitative	none
28	Chen et al. (2014)	IoT perception in China: Applications, challenges, and opportunities	The status of IoT development in China, plus standards, R&D plans, applications, and standardization	none	qualitative	none
29	Miorandi et al. (2012)	The Internet of things vision: Key elements, uses, and open issues	Research challenges and open issues to be faced for the IoT realization in the real world	none	qualitative	none
30	Ahmed et al. (2016)	Internet-of-Things-Based Smart environments: state of the Art, Taxonomy, and open research challenges	Status on evaluation efforts to permit IoT based smart environments	none	qualitative	none
31	Bagheri and Movahed (2016)	The effect of the Internet of Things (IoT) on Educational Business model	To investigate and analyze change of IoT platform regarding education business model	none	qualitative	literature

Appendix D (Continued)

Distribution of research methodologies						
ID	Instigator(s)	Article Name	Intent	Theory/ Framework	Method	Details collection process
32	Atzori et al. (2010)	The Internet of Things: A survey	Allow the reader to understanding what has been done and what remains to be addressed, as well as which are the enabling factors of this evolutionary process and what are its weaknesses and risk factors.	none	qualitative	none
33	Bayani et al. (2017)	Internet of Things (IoT) Advantages on E-learning in the Smart Cities	The need of adopting IoT technologies in smart city campuses, analyzing the predictable advantages of the e-learning.	none	qualitative	none
34	Bibri (2015)	Democratizing AmI and the IoT: The power and Influence of Social Innovation and Participative and Humanistic Design	To explore the power and seminal role of social innovation and participative and humanistic design—as one holistic approach—in sustaining the success of AmI and the IoT technologies, and to identify and address the great challenges involved in the process of embracing this approach	none	qualitative	none
35	Chen et al. (2016)	Evolution is not enough: Revolutionizing present instruction environments to smart learning area	Challenges with a view towards revolutionizing current learning environments to smart learning environments and provides new suggestions for technological solutions	none	qualitative	none

Appendix D (Continued)

Distribution of research methodologies						
ID	Instigator(s)	Article Name	Intent	Theory/ Framework	Method	Details collection process
36	Demirer et al. (2017)	Exploring the Educational Potential of Internet of Things (IoT) in Seamless Learning.	Introduction of IoT technology pus its potentiality in seamless instruction.	none	qualitative	none
37	Domingo (2012)	An overview of the Internet of Things for people with disabilities	Overview of the Internet of Things for people with disabilities is provided	none	qualitative	none
38	Kortuem et al. (2013)	Educating the Internet-of-Things generation	To place the IoT at the core of the first-year computing curriculum and to prime students from the beginning to meet the coming changes in society and technology	none	qualitative	none
39	Krotov (2017)	The Internet of Things and upcoming business opportunities	To stimulate thinking, creativity, and entrepreneurship in relation to the IoT	none	qualitative	none
40	Lee and Lee (2015)	IoT Applications, investments, and challenges for enterprises	Essential IoT technologies for the deployment of IoT-based products and services and IoT categories for enterprise applications	none	qualitative	none

Appendix D (Continued)

Distribution of research methodologies						
ID	Instigator(s)	Article Name	Intent	Theory/ Framework	Method	Details collection process
41	Lee et al. (2017)	How and what to study about IoT: Research trends and future directions from the perspective of social science	Examines the status of scholarly discourse on IoT.	none	qualitative	none
42	Li et al. (2012)	Towards a theoretical framework of strategic decision, supporting capability and information sharing under the context of Internet of Things	That groups IoT into perspective of managers' strategic need and industrial driving force, and suggest that market-based exploratory necessities impact companies incorporating get-ahead strategy, and market-based exploitative possibilities are significant for organizations incorporating catch-up strategy in market	none	qualitative	none
43	Niyato et al. (2016)	Smart data pricing models for the Internet of Things: A bundling strategy approach	Suggest an improved pricing structure for IoT service providers to choose the sensory details initial cost and IoT service subscription price given to sensor owners and service individuals, separately	none	qualitative	none
44	Saariko et al. (2017)	The Internet of Things: Are you prepared for what is coming?	Reviewing the complexity of IoT, the issues in linked environments, plus the rising necessity to create links for innovative outcomes	none	qualitative	none

Appendix D (Continued)

Distribution of research methodologies						
ID	Instigator(s)	Article Name	Intent	Theory/ Framework	Method	Details collection process
45	Sarıtaş (2015)	The Emergent Technological and Theoretical Paradigms in Education: The Interrelations of Cloud Computing (CC), Connectivism and IoT	Background and fundamentals about emerging technology paradigms – Cloud Computing (CC) and Internet of Things (IoT), and an emerging learning theory – Connectivism.	none	qualitative	none
46	Shin (2017)	Conceptualizing and measuring quality of experience of the internet of things: Exploring how quality is perceived by users	Relationship between consumer experiences, the quality perception of IoT, and develops a conceptual model for QoE in personal informatics	TRA and TPB	Mixed method	Focus groups, brainstorming
47	Sudtasan and Mitomo (2017)	The Internet of Things as an accelerator of advancement of broadband networks: A case of Thailand	Show influence of consumer decisions on choices of advanced Internet access by the emergence of IoT applications	Bivariate probit model	quantitative	Survey
48	Want et al. (2015)	Enabling the internet of things	Benefits of IoT, future directions and challenges	none	qualitative	none
49	Tsai et al. (2013)	Examining institutional pressure for incorporating RFID by suppliers	How different institutional forces experienced by retailer's suppliers were related to their relational investment on inter-organizational information sharing	DOI	quantitative	survey

Appendix E

Additional article (Book Chapter)

ID	References	Name	Aspiration
81	Bibri (2015)	The Shaping of Ambient Intelligence and the Internet of Things	The book explains how Ambient Intelligence (AMI) and IoT utilizations of scientific discovery merge with various implementations in the spheres of the European society. It positions AmI and the IoT developments and innovations as modernist science-based innovation enterprises in a volatile and tense relationship.



LTE Network Analysis in Frequency Reuse Recycling Techniques

Muhammad Sabir Hussain*, Nasri Suleiman and Nor Kamariah Noordin

Department of Electrical and Electronics Engineering, Faculty of Engineering, University Putra Malaysia, 43400 UPM, Serdang, Selangor, Malaysia

ABSTRACT

In recent years, several researchers have embraced fractional frequency (FF) reuse as a strategy for resolving the inter-cell and co-channel interferences of adjacent cells (ICI, CCI) as the number of wireless networks grows. This technique is focused on the cell division of two parts, the inner and the outer, which enables multiple frequency bands to be assigned. The frequency advantages can be completely used in each inner zone, since there is no inter-cell disturbance for consumers in inner regions. According to this effective usage of the frequency spectrum available, FF will reduce the interruption of the channel and improve device efficiency. This manuscript presents a comprehensive study of different mechanisms to select the optimal FF scheme based on the user throughput. The analysis was conducted in order to obtain the optimal internal and external range for the cells as well as the optimal frequency distribution between the areas of the FR, Fractional Frequency Reuse 1 (FFR1) and Fractional Frequency Reuse 2 (FFR2) and evaluating their outputs and their number of users. In detail the overall consumer efficiency through the configured frequency distribution is analyzed. The FFR is a resource allocation technique that can effectively mitigate inter-cell interference (ICI) in LTE based HetNets and it is a promising solution. The proposal also employs high number sectors in a cell, low interference and good frequency reuse. The processes are tested by way of multiple modeling simulations.

Keywords: FFR, inner region, LTE network, maximum throughput, optimal radius, outer region

ARTICLE INFO

Article history:

Received: 23 June 2020

Accepted: 25 November 2020

Published: 22 January 2021

DOI: <https://doi.org/10.47836/pjst.29.1.27>

E-mail addresses:

engineersabir1@yahoo.com (Muhammad Sabir Hussain)

nasri_sulaiman@upm.edu.my (Nasri Suleiman)

nknordin@upm.edu.my (Nor Kamariah Noordin)

* Corresponding author

INTRODUCTION

The 3rd Generation Long Term Innovation Collaboration Project (3GPP-LTE) is the 4th Generation (4 G), a wireless network built to serve compact, powerful and high-performances end-users, providing a large

capacity, improved connectivity efficiency. In December 2007 3GPP published their first LTE research work in “release 7,” which now has a major topic (Hashima et al., 2014; Simonsson, 2007). LTE Multi-Access Orthogonal Frequency Division (OFDMA) technology for downlinks has attracted significant attention from researchers in recent years in achieving a high rate of data transfer in wireless and mobile communications. OFDMA provides a higher spectrum output in order to satisfy the growing demands of smartphone users because of its versatile frequency assignment (Zhang et al., 2020). In LTE, each OFDMA traffic channel is solely allocated to one individual, which provides the end-user frequency with a high degree of reliability and flexibility (Zhao et al., 2012). The device efficiency is significantly degraded by the Inter-cell Interference (ICI) dependent on a multi cell LTE OFDMA-related network because of the same frequency reuse and interference by the co-channel (CCI) when more than one radio transmitters use the same frequency (Chung et al., 2014; Elayoubi et al., 2008; Hindia et al., 2014; Mannweiler et al., 2020; Wang et al., 2014).

In order to address both ICI and CCI, FFR has become an area of intensive study by several OFDMA-based researchers (Bilios et al., 2013; Mao et al., 2008; Nuaymi, 2007). In order to minimize the CCI and ICI, FFR main target is to divide cells volume into inner and outer regions (Chang et al., 2009; Cong et al., 2020; Group, 2004; Saleh, 2020). FFR is a mixture of different types of frequency reuse scheme such as traditional frequency reuse (FR) factor and FFR3. One of the main objectives of LTE is to use the whole of the system’s bandwidth to achieve high spectral efficiency (Group, 2004; Mao et al., 2008). This method is known as traditional FR where all available bandwidth is fully assigned in each cell. In FFR3, on the other hand, the available bandwidth is divided into 3 equal sub-bands and each of these sub-bands will be allocated in a manner to the cells in a cluster so that no adjacent cells will have the same sub-bands. In addition, traditional FR can be used by the mobile stations (MSs) which are located around the base stations (BSs) or in particular in the cell inner region and FFR3 is allocated to the cell edge users, which will decrease the interference, but data rate also will be decreased due to the fact that the full frequency band is not used by this method (Ali & Leung, 2009; Chang et al., 2009; Kim et al., 2014; Soultan et al., 2020; Stiakogiannakis & Kaklamani, 2010). OFDMA allows the dynamic allocation of subcarriers (called OFDMA traffic channel) to different users at different time instances. For example, it utilizes 15 KHz subcarriers in LTE, which can be grouped into Resource Blocks (RBs) with each having 12 subcarriers (Kim et al., 2010; Lei et al., 2007; Sheu et al., 2015; Taranetz et al., 2011; Wang, 2013). To implement these for FFR scheme, one of the ways to allocate these RBs is to allocate them in a sector (Guo & Suárez, 2020; Hambebo et al., 2014). The main goal of this paper is to investigate the characteristics of three existing methods of FR, FFR1 and FFR2 to evaluate an interference management in LTE networks. The studied mechanism calculates the optimal FFR scheme based on user throughput. It then successively checks the inner cell radius and the inner

cell frequency and calculates the Signal to Interference Plus Noise Ratio (SINR), capacity and throughput. These values are then used in order to calculate the cell mean throughput. Finally, the mechanism selects the optimal center to cell radius ratio and optimal number of users in order to propose the best FFR scheme that maximizes the cell mean throughput (Rumney, 2013). The rest of the paper is organized as follows: Section 2 describes the related work to our study. Section 3 refers to our studied system model, Section 4 introduces the simulation, and Section 5 presents the simulation results and discussion.

RELATED WORK

The research on FFR focuses on the implementation of reuse of frequencies, which is the sub band divisioning for the BS area. OFDMA infrastructure has been used by several wireless network protocols, like GPP and 3GPP2. In recent study, the key topic of discussion is network efficiency, performance, rate, scope, and frequency distribution. Hindia et al. (2014) selected the frequency reuse pattern from four varying degrees of partitioning criteria (e.g. FRF1 and FRF3) to improve the performance of mobile and base station. FFR impact was presented in the cellular area division into inner and outer regions was suggested to avoid conflict in Bilioss et al. (2013) as an effect of FFR. The authors proposed partial frequency allocation for the cell edge region and full frequency spectrum for the cell inner region. The users are modulated more tightly than BSs, because different modulation instructions are taken into consideration according to the distance of the consumer from BSs and also the state of the signal, which indicates that the frequency reuse is higher. In most research, static or semi-static synchronization systems are introduced in BSs with little cellular performance benefit and needing advance frequency preparation. The system's efficiency is significantly diminished to increase the cell-end performance (Mao et al., 2008; Nuaymi, 2007). In contrast, prior frequency planning is not required in dynamic coordination technique. FFR was proposed in order to keep the stability between cell-edge throughput and overall network throughput (Chang et al., 2009; Group, 2004). In these works the authors partitioned cells into inner and edge zones which associated the low and high Frequency Reuse Factors In order to reduce interference, the total available frequency bandwidth was divided into two sub-bands such as center band and edge band where frequency bands are fully to Bfr and partly to Bpr allocated respectively. Ali and Leung (2009) implemented the super-group and the hierarchical organization of a standard community, which were divided in cells and sectors to ensure a greater device efficiency. The FFR efficiency improvement was analyzed by Stiakogiannakis and Kaklamani (2010) in three forms of zone distributions, such as SINR-based, distance-based and load-balance-based techniques. The combination of the load balancing with the SINR and the correct distribution of resources gives the machine a decent bit rate. Business technology had been suggested by Kim et al. (2014) for the frequency reuse component. This method is used in WiMAX to boost the 802.16j relay device that transmits the signals to the BS portfolio.

Based on the simulation test, this scheme improved the spectrum utilization and network output. Macro-femto networks with the idea of FFR, there is a novel hierarchical resource distribution method suggested by Lei et al. (2007). The three considerations in this scheme to minimize the CCI in macro and femtocells are size, time and place. To this end the method suggested a hybrid two-part grouping of macro cells and the deployment of femto BSs in each section of macro cells conducted in accordance with the objective of growing the average cell efficiency. Improved FFR technique (E-FFR) was introduced in WiMAX by Kim et al. (2010) for reducing ICI. The variety of users and frequency are viewed as strategies to boost device efficiency for mobile and fixed users. Such strategies improve the signal from the consumer against undesired noise. Downlink (DL) and Uplink (UL) frames were divided into WiMAX frames, and each frame was further divided into zones to quantify unused space to allow appropriate modulation and coding in order to improve device efficiency. However, overhead will occur at BS without continuous consumer input as the channel parameters alter over time. A new multiple access (B-OFDMA) biorthogonal frequency division system with the broad low-complexity Fourier transform fraction (FrFT) was proposed by Wang (2013). The variation of time and frequency is set at each BS in this scheme with multi-angle reuse (MADR). The program will efficiently reduce ICI and increase the efficiency of the device. A FFR optimization method based on capacity density was suggested by Tarantetz et al. (2011). In this work, the frequency sub-band with highest achievable capacity density was assigned to a given user. The authors then formulated the FFR optimization problem mathematical expressions. Here, the per-user capacity was mainly investigated from per-area capacity. The maximum average capacity density was aimed with the condition of least required cell-edge throughput c5% and minimizing the c95% peak user throughput loss.

METHOD AND SYSTEM MODEL

In this section, SINR and capacity of user x on subcarrier n are calculated based on theoretical approach in order to define the throughput. The N adjacent cells are considered as overall network where a number of users look forward to share a collection of subcarriers in each cell. In this case a distinction of a user which can be found in the inner or outer zone of the cell. In an OFDMA based network, we assume the user as x in a base station s on subcarrier c , the related SNIR can be calculated using Equation 1 (Chung et al., 2014; Hindia et al. 2014; Wang et al. 2014):

$$SINR_{x,n} = \frac{L_{s,x} \cdot P_{s,c} \cdot G_{s,x,c}}{\sigma_c^2 + \sum_{j=1}^k L_{j,x} \cdot P_{j,c} \cdot G_{j,x,c}} \quad [1]$$

where the path loss associated with channel between user x and base station s is defined as to $L_{s,x}$, the transmit power of the base station as $P_{s,c}$, exponentially distributed channel fast

fading power as $G_{s,x,c}$, the noise power of the additive White Gaussian Noise (AWGN) channel is defined as σ^2 . The sets of all interfering base stations are defined as symbol k and j . More precisely, k is the number of co-channel cell and j is the cell index. We consider the transmit power on subcarrier is equal as $P_{s,c} = P$ for all BSs. The coefficient $G_{s,x,c}$ is equal to 1 of its mean value.

The interference presents in the inner and the outer regions of the disjoint set of download links. A specific frequency band is assigned on transmission, which is a common band in every inner region, thus it brings interference in those regions. Moreover, it is required to distinguish two different types of BSs. The first type of consists of all interfering BSs, which transmits to the users of the cell-inner region on the same sub-band as user x and the second type consists of all interfering BSs transmits to the users of the cell-edge users on the same sub-band as user x . Now, in order to calculate the throughput, we first define the capacity of the user. The capacity of user x on subcarrier c is given by the following Equation 2 (Bilios et al., 2013):

$$E_{x,c} = \Delta f \cdot \log_2(1 + SINR_{x,c}) \quad [2]$$

Where, Δf denotes as the available bandwidth for each subcarrier. Here, the subcarrier is divided among the number of users to be shared. Finally, the throughput of the user x is expressed specifically in terms of $SINR$ and $E_{x,c}$ as in Equation 3

$$T_x = \sum_n \beta_{x,n} \cdot E_{x,n} \quad [3]$$

Where $\beta_{x,c}$ refers to the subcarrier assigned to user x . When, $\beta_{x,c}=1$, the subcarrier c is allocated to user x . Otherwise, $\beta_{x,c}=0$.

SIMULATION ENVIROMENT

The applications are tested and evaluated using the Matlab program. As detailed in Table 1, the simulation area consists of 7 cells network and the users randomly distributed in the cells and system bandwidth is 10 MHZ.

Figure 1 is the graphical representation of the network area for FFR1 scheme where it is being applied to investigate the optimum center ratio and the optimum number of users per cell. As we can observe from the Figure 1 how the users are distributed throughout the inner and outer cells where we assume the area of X-axis from -4000 m to 3000 m and Y-axis from -3000 m to 4000 m. The inner and outer cell have specific sub-band which is represented by band color. The different colors in Figure 1 correspond to bandwidth of the different cells. FFR1 is a heavy frequency and low frequency reuse hybrid. Strong frequency

reuse splits the bandwidth into different subbands(color) depending on the reuse factor selected such that the neighboring cells will communicate on different subbands(color). The entire bandwidth of FFR1 is split into internal and external subbands. The central area is allocated to local users residing outside BS on the basis of path failure with a decreased power that relates to the FRF1 of one that is fully utilized by all eNBs. The fraction of the outer bandwidth area is distributed for more than one frequency reuse factor. Both BSs are required to share the entire bandwidth of the soft frequency. However, the eNBs are restricted to a certain capacity constraint for increasing subcontractor transmission. In fact, the number of cell users is assigned arbitrarily.

Figure 2 is the demonstration of the total FFR2 network region to analyze the optimal center ratio and the optimal consumer number per node. The distribution of users in the internal and external cells of the cluster in the form of sub-bands (color) is shown in Figure

Table 1
Simulations inputs

Parameters	Settings
Cell Radius	750m
Bandwidth	10MHz
Number of Cell	7
Number of Subcarriers	50
Bearer Types	From QCI 1- QCI 15
eNodeB Height	50 m
UE Height	1m
eNodeB Tx power in cell Center	40 dBm
eNodeB Tx power in cell edge	46 dBm
Path loss	Cost 231 Hata Model (dB)
Power Noise Density	-174 dBm/Hz

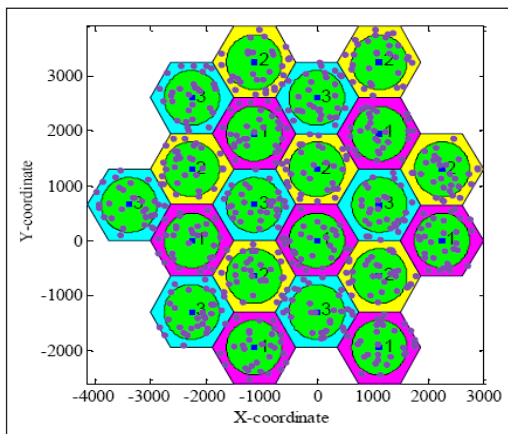


Figure 1. Network area of FFR1

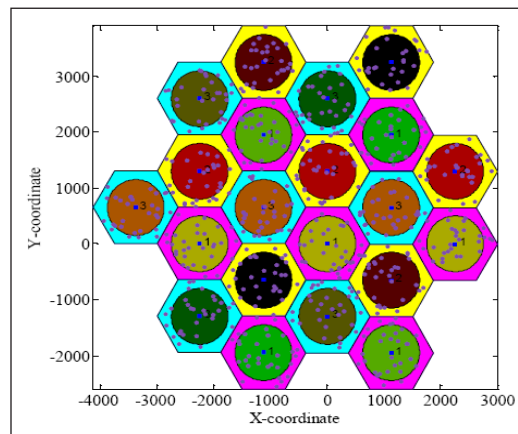


Figure 2. Network area of FFR2

2. The X-axis field from -4000 meters to 3000 meters and the Y-axis from -3000 meters to 4000 meters as for FFR1 are expected to be comparable. The frequency reuse component is greater than one for the proportion of the main and main regions of bandwidth. Except for inner and outer parts, the frequency bands vary.

RESULTS AND DISCUSSION

Figure 3 and Table 2 represent the average cell throughput according to the center radius to cell radius ratio with different number of users for FFR1. We can observe from the Figure 3 that the throughput is almost linearly increasing until cell radius ratio 0.5 for all groups of users except group of 10 users. However, the slope of the line graph varies based on the number of users. The average throughput of a group of 10, 20, 30, 40, 50, 60, 70, and 80

Table 2
The maximum throughput (Mbps) for the various cell center ratio and users for FFR1

Radius \ User	0.3	0.4	0.5	0.6	0.7	0.8	0.9
10	13	12.8	12.5	12	11.6	10.8	10.5
20	16	17.5	20.3	22	22.5	21.5	21
30	19	22	26	29.8	32.5	31.5	27.5
40	21	25.5	31.5	36.5	39	34	27.5
50	23	29.8	36	42	41.5	35	27.5
60	26	33	41.5	45	41.5	36.5	27.5
70	28	37.5	46	45.5	41.5	36.6	27.5
80	31	41	48	46	41.5	37	27.5

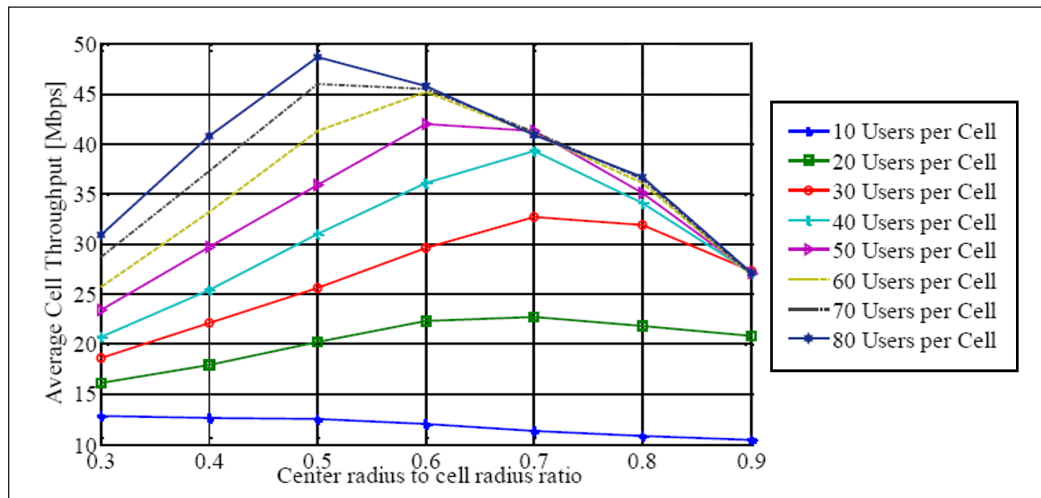


Figure 3. The average cell throughput according to the variation of cell radius to cell center ration with various user group for FFR1.

users are 12.5, 20.5, 26, 31.5, 36, 41.5, 46, 48 Mbps, respectively when the center to cell radius ratio (C_{rr}) is 0.5. Remarkably, the average throughput is highest for group of 80 and 70 users when the C_{rr} is 0.5 and the breakdown points for group of 60 and 50 users are at C_{rr} 0.6 and 40, 30, 20 users are at 0.7. After those points the throughput linearly decreases with the increase of the cell radius ratio. From the above scenario, this can be concluded that the highest average throughput observed when the C_{rr} is 50% for the group of 80 users.

The average cell throughput according to the number of users per cell with the various cell center radius ratio is being observed in Figure 4 more intuitively. The throughput linearly increases for the 30%, 40%, 50% and 60% of center radius ratio, respectively with the increase number of users. However, the throughput becomes saturated for the C_{rr} 70%, 80% and 90% after the certain number of users. The throughput is seen highest when the number of users are as higher as 80 at the C_{rr} 50%.

The average performance in Figure 5 and Table 3 is seen in terms of the number of FFR2 users with the center radius ratio. The linear rise in performance for the 80, 70, 60, 50 and 40 users until the specified center-ratio is shown in this chart. On the other side, the averages are almost the same for the community of 30 and 40 users, while the performance for the category of 10 users is often smaller. Like FFR1, a limit of 60 Mbps for the 80 users at C_{rr} 0.6 is available. Figures 3 and 5 demonstrate that the average FF2 efficiency is higher than FFR2 and the ideal cell center radius is 60%.

Figure 6 shows the representation of the average user output by the cell-to-center ratio. For the group of ten to twenty users, for all variations of center radius the variation of the throughput values are almost the same. With the center radius ratio from 30% to 70%, the output increases linearly with various slopes where 80% and 90% of the output for a given

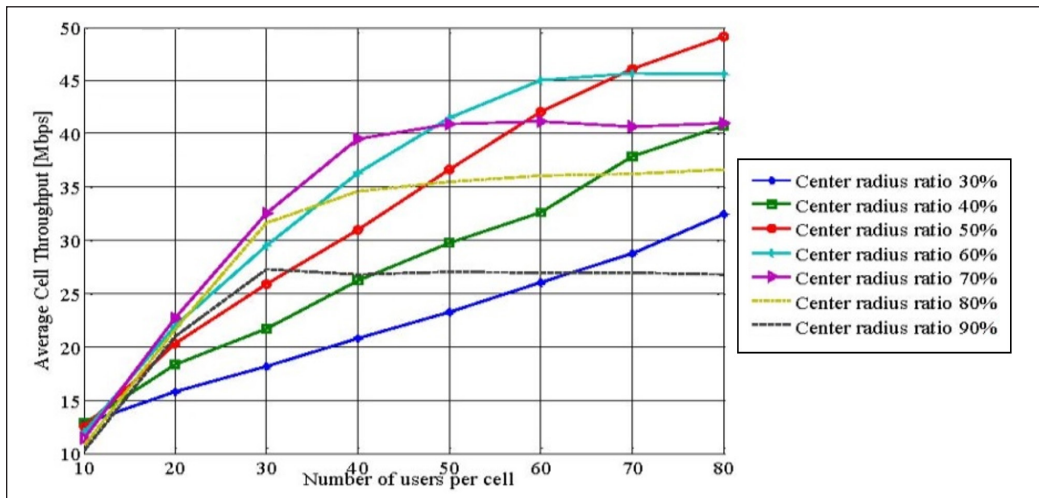


Figure 4. The average cell throughput at cell radius 750m according to the number of users per cell to center radius ratio

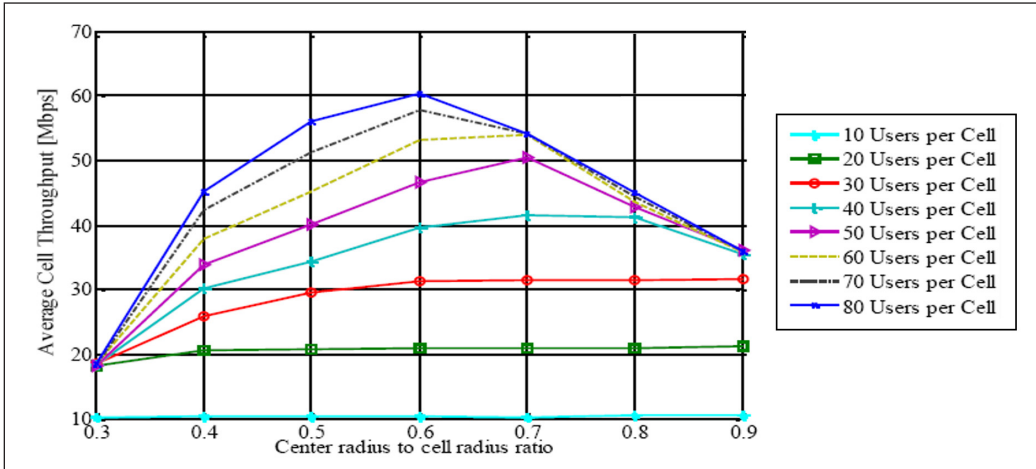


Figure 5. Average cell throughput at cell radius 750m according to the variation of cell radius to cell center ration with users for FFR2.

Table 3
The maximum throughput (Mbps) for the various cell center ratio (C_n) and users for FFR2

Radius \ User	0.3	0.4	0.5	0.6	0.7	0.8	0.9
10	10	10.1	10.1	10.1	10.1	111	11
20	19	20.5	20.5	20.5	20.5	20.5	21
30	19	25	29	31.5	31.6	31.8	32
40	19	30	34	40	42	41.6	36
50	19	34	40	46.5	50	43	36.5
60	19	38	45	54	54.5	43.2	36.5
70	19	42	52	57.6	54.5	43.4	36.5
80	19	45	56	60	54.5	44	36.5

number of users is saturated. Figure 6 also shows that the 0.6 center ratio is the highest throughput for a group of 80 users.

Figure 7 indicates that, for the initial distribution, the community of 80 cell users has been done. In the three systems up to 20 consumers, the performance is greater for the conventional FR system. The lowest performance for users is roughly 23 Mbps, irrespective of where they are in the FR unit, for 20 to 80 users. In comparison, the FFR1, with a linearly improvement in efficiency to 30 users, performs more than the FR, which stays practically the same for 30 to 80 users.

FFR2, on the other side, users from 10 to 40 linearly get the improved throughput values and it may go up to 36 Mbps for users 40 and is almost constant for about 40 and 80 users regardless of where they are placed. In addition, the above remarks are clearly illustrated in Figure 7, in the fractional frequency reuse 2 (FFR2) schemes due to the equal

distribution of resource blocks to the inner and outer cell regions that show the highest throughput. This mechanism ensures that applications from 40 applications and above have equal maximum performance values regardless of where they are. To make a description, Figure 7 indicates a clear distinction in cell mean throughput of all three forms of frequency reuse schemes, including conventional frequency reuse, FFR1 and FFR2. A significant observation is made here on the three distinct cell average scenarios. In terms of average throughput, in comparison with the two other frequencies reuse schemes, the FFR2 regime results in higher levels. The graph reveals that standard FR has a maximum speed of 23.80

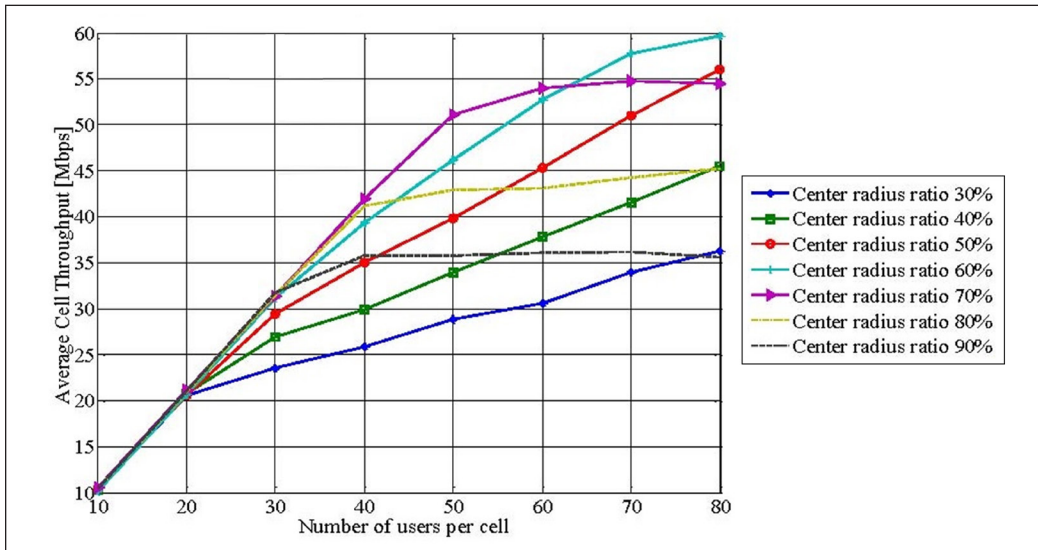


Figure 6. The average cell throughput at radius 750m according to the number of users per cell to center radius ratio for FFR2

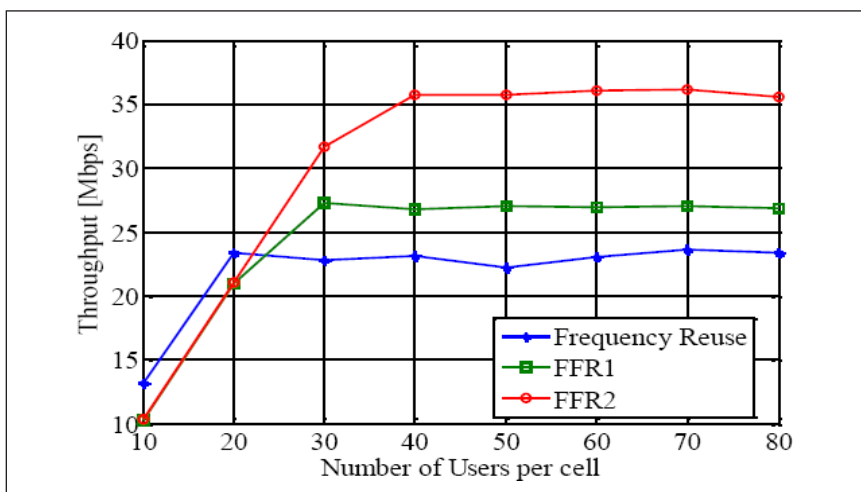


Figure 7. Comparison of FR, FFR1 and FFR2 scheme

Table 4

The summary of maximum throughput (Mbps) for users and center to cell radius ratio (C_{rr}) for both FFR1 and FFR2

Users	FFR1	FFR2
80	48 Mbps at C_{rr} 0.5	60 Mbps at C_{rr} 0.6
70	45 Mbps at C_{rr} 0.5	57.6 Mbps at C_{rr} 0.6
60	44 Mbps at C_{rr} 0.6	54.5 Mbps at C_{rr} 0.7
50	42 Mbps at C_{rr} 0.6	50 Mbps at C_{rr} 0.7
40	38 Mbps at C_{rr} 0.7	42 Mbps at C_{rr} 0.7
30	30 Mbps at C_{rr} 0.7	32 Mbps at C_{rr} 0.8
20	20 Mbps at C_{rr} 0.7	21 Mbps at C_{rr} 0.9
10	13 Mbps at C_{rr} 0.3	11 bps at C_{rr} 0.9

Mbps and FFR1 crosses 27.50 Mbps. FR reaches a cumulative flow value of 36.10 Mbps, on the other side. Table 4 summarizes the FFR1 and FFR2 potential performance along with a number of users and the cell radius node.

CONCLUSION

In this paper, the overall comparative evaluation on traditional Frequency Reuse (FR), FFR1 and FFR2 are presented. The general approach to avoid interference problem, the investigated mechanisms calculate the per-user SINR, capacity and throughput. It is found that the group of 80 users achieves the highest maximum throughput 48 Mbps and 60 Mbps for FFR1 and FFR2 at the cell radius ratio 0.5 and 0.6, respectively. However, at center to cell radius ratio 0.5, the maximum throughput is 55 Mbps for the same user group. Therefore, it can be concluded that among the schemes, FFR2 provides the best throughput at 0.6 cell radius ratio for 80 users, which are considered as the optimal center to cell radius ratio and users, respectively.

ACKNOWLEDGEMENT

The authors would like to thank the Universiti Putra Malaysia special grant.

REFERENCES

- Ali, S. H., & Leung, V. C. (2009). Dynamic frequency allocation in fractional frequency reused OFDMA networks. *IEEE Transactions on Wireless Communications*, 8(8), 4286-4295. doi: 10.1109/TWC.2009.081146
- Bilios, D., Bouras, C., Kokkinos, V., Papazois, A., & Tseliou, G. (2013). Selecting the optimal fractional frequency reuse scheme in long term evolution networks. *Wireless Personal Communications*, 71(4), 2693-2712. doi: <https://doi.org/10.1007/s11277-012-0965-z>

- Chang, R. Y., Tao, Z., Zhang, J., & Kuo, C. C. (2009, June 14-18). A graph approach to dynamic fractional frequency reuse (FFR) in multi-cell OFDMA networks. In *2009 IEEE International Conference on Communications* (pp. 1-6). Dresden, Germany. doi: 10.1109/ICC.2009.5198612
- Chung, S., Jang, S., & Joe, I. (2014). Selective clustering scheme based on user equipment path and frequency reuse scheme for coordinated multi-point joint processing. *IET Communications*, 8(17), 2961-2970. doi: 10.1049/iet-com.2013.1186
- Cong, L. S., Tuan, N. Q., & Sandrasegaran, K. (2020). A general model of fractional frequency reuse: Modelling and performance analysis. *VNU Journal of Science: Computer Science and Communication Engineering*, 36(1), 38-45. doi: <https://doi.org/10.25073/2588-1086/vnucsce.221>
- Elayoubi, S. E., Haddada, O. B., & Fourestie, B. (2008). Performance evaluation of frequency planning schemes in OFDMA-based networks. *IEEE Transactions on Wireless Communications*, 7(5), 1623-1633. doi: 10.1109/TWC.2008.060458.
- Group, I. W. (2004). *IEEE standard for local and metropolitan area networks-part 16: Air interface for fixed broad-band wireless access systems*. New Jersey, USA: Institute of Electrical and Electronics Engineers. doi: 10.1109/IEEESTD.2004.226664
- Guo, T., & Suárez, A. (2020). *Fine-grained frequency reuse in centralized small cell networks*. New Jersey, USA: IEEE Transactions on Mobile Computing. doi: 10.1109/TMC.2020.2981032
- Hambebo, B. M., Carvalho, M. M., & Ham, F. M. (2014, April 7-9). Performance evaluation of static frequency reuse techniques for OFDMA cellular networks. In *Proceedings of the 11th IEEE International Conference on Networking, Sensing and Control* (pp. 355-360). Miami, FL, USA. doi: 10.1109/ICNSC.2014.6819652
- Hashima, S., Muta, O., Alghonimey, M., Shalaby, H., Frkawa, H., Elnoubi, S., & Mahmoud, I. (2014, April 26-28). Area spectral efficiency performance comparison of downlink fractional frequency reuse schemes for MIMO heterogeneous networks. In *2014 International Conference on Information Science, Electronics and Electrical Engineering* (Vol. 2, pp. 1005-1010). Sapporo, Japan. doi: 10.1109/InfoSEEE.2014.6947820
- Hindia, M. N., Reza, A. W., & Noordin, K. A. (2014). Investigation of a New Handover Approach in LTE and WIMAX. *The Scientific World Journal*, 2014, 1-11. doi: <https://doi.org/10.1155/2014/246206>
- Kim, D. C., Kwon, Y. H., Kwak, J. S., Moon, S. H., & Han, S. H. (2014). *U.S. Patent No. 8,660,050*. Washington, DC: U.S. Patent and Trademark Office.
- Kim, Y. S., Choi, S. H., Jang, K. H., & Hwang, H. S. (2010). *U.S. Patent No. 7,821,976*. Washington, DC: U.S. Patent and Trademark Office.
- Lei, H., Zhang, L., Zhang, X., & Yang, D. (2007, September 3-7). A novel multi-cell OFDMA system structure using fractional frequency reuse. In *2007 IEEE 18th International Symposium on Personal, Indoor and Mobile Radio Communications* (pp. 1-5). Athens, Greece. doi: 10.1109/PIMRC.2007.4394228
- Mannweiler, C., Sartori, C., Wegmann, B., Flinck, H., Maeder, A., Goerge, J., & Winkelmann, R. (2020). Evolution of Mobile Communication Networks. In S. Mwanje & C. Mannweiler (Eds.), *Towards Cognitive Autonomous Networks: Network Management Automation for 5G and Beyond* (pp. 29-92). Croydon, UK: John Wiley & Sons Ltd. doi: <https://doi.org/10.1002/9781119586449.ch2>

- Mao, X., Maaref, A., & Teo, K. H. (2008, November 30 - December 4). Adaptive soft frequency reuse for inter-cell interference coordination in SC-FDMA based 3GPP LTE uplinks. In *IEEE GLOBECOM 2008-2008 IEEE Global Telecommunications Conference* (pp. 1-6). New Orleans, LO, USA. doi: 10.1109/GLOCOM.2008.ECP.916
- Nuaymi, L. (2007). *WiMAX: technology for broadband wireless access*. Chippenham, UK: John Wiley & Sons.
- Rumney, M. (2013). *LTE and the evolution to 4G wireless: Design and measurement challenges*. Singapore: John Wiley & Sons.
- Saleh, A. M. M. (2020). *Performance analysis of fractional frequency reuse schemes in downlink multi-relay multi-cell OFDMA and NOMA cellular networks* (PhD Thesis). University of Calgary, Canada.
- Sheu, T. L., Lin, B. J., & Chou, Z. T. (2015). Analytical models for call blocking and dropping in sectorized cellular networks with fractional frequency reuse. *Wireless Communications and Mobile Computing*, 15(17), 2125-2140.
- Simonsson, A. (2007, April 22-25). Frequency reuse and intercell interference co-ordination in E-UTRA. In *2007 IEEE 65th Vehicular Technology Conference-VTC2007-Spring* (pp. 3091-3095). Dublin, Ireland. doi: 10.1109/VETECS.2007.633
- Soultan, E. M., Nafea, H. B., & Zaki, F. W. (2020). Interference Management for Different 5G Cellular Network Constructions. *Wireless personal communications*, 115(3) 1-20. doi: <https://doi.org/10.1007/s11277-020-07805-1>
- Stiakogiannakis, I. N., & Kaklamani, D. I. (2010, September 26-30). Fractional frequency reuse techniques for multi-cellular WiMAX networks. In *21st Annual IEEE International Symposium on Personal, Indoor and Mobile Radio Communications* (pp. 2432-2437). Istanbul, Turkey. doi: 10.1109/PIMRC.2010.5671728
- Taranetz, M., Ikuno, J. C., & Rupp, M. (2011, November 6-9). Capacity density optimization by fractional frequency partitioning. In *2011 Conference Record of the Forty Fifth Asilomar Conference on Signals, Systems and Computers (ASILOMAR)*. Pacific Grove, CA.
- Wang, H. (2013). Biorthogonal frequency division multiple access cellular system with angle division reuse scheme. *Wireless Personal Communications*, 70(4), 1553-1573. doi: <https://doi.org/10.1007/s11277-012-0765-5>
- Wang, K., Li, H., Ma, J., Liu, P., & Pan, H. (2014). Two-level scheme to maximise the number of guaranteed users in downlink femtocell networks. *IET Communications*, 8(16), 2917-2924. doi: 10.1049/iet-com.2013.0944
- Zhang, H., Sun, Y., Lou, H. L., & Chu, L. (2017). *U.S. Patent No. 9,717,086*. Washington, DC: U.S. Patent and Trademark Office.
- Zhao, Y., Fang, X., Huang, R., & Fang, Y. (2012). Joint interference coordination and load balancing for OFDMA multihop cellular networks. *IEEE Transactions on Mobile Computing*, 13(1), 89-101. doi: 10.1109/TMC.2012.224



Algorithm for B-scan Image Reconstruction in Optical Coherence Tomography

Kranti Patil¹, Anurag Mahajan^{1*}, Balamurugan Subramani², Arulmozhivarman Pachiyappan³ and Roshan Makkar⁴

¹Department of Electronics and Telecommunication, Symbiosis Institute of Technology, Symbiosis International (Deemed University), (SIU) Lavale, Pune, (Maharashtra), India

²Department of Instrumentation, School of Electrical Engineering, VIT, Vellore, Tamil Nadu, India

³School of Electrical Engineering, VIT, Vellore, Tamil Nadu, India

⁴Department of Photonics, Society of Applied Microwave Electronics Engineering and Research (SAMEER) Mumbai, Maharashtra, India

ABSTRACT

Optical coherence tomography (OCT) is an evolving medical imaging technology that offers in vivo cross-sectional, sub-surface images in real-time. OCT has become popular in the medical as well as non-medical fields. The technique extensively uses for food industry, dentistry, dermatology, and ophthalmology. The technique is non-invasive and works on the Michelson interferometry principle, i.e., dependent on back reflections of the signal and its interference. The objective is to develop an algorithm for signal processing to construct an OCT image and then to enhance the quality of the image using image processing techniques like filtering. The image construction was primarily based on the Fourier transform (FT) of the dataset obtained by data acquisition. This FT could

be performed rapidly with the extensively used algorithm of fast Fourier transform (FFT). The depth-wise information could be extracted from each A-scan, i.e., axial scan and also the B-scan was obtained from the A-scan to see the structure of sample. The maximum penetration depth achieved with proposed system was 2.82mm for 1024 data points. First and second layer of leaf were getting at thickness of 1mm and 1.6mm, respectively. A-scans for Human fingertip gave its first, second and third layer was at a

ARTICLE INFO

Article history:

Received: 09 October 2020

Accepted: 16 November 2020

Published: 22 January 2021

DOI: <https://doi.org/10.47836/pjst.29.1.28>

E-mail addresses:

krantipatil1111@gmail.com (Kranti Patil)

anurag.mahajan@sitpune.edu.in (Anurag Mahajan)

sbalamurugan@vit.ac.in (Balamurugan Subramani)

arulmozhivarman@vit.ac.in (Arulmozhivarman Pachiyappan)

roshan@sameer.gov.in (Roshan Makkar)

* Corresponding author

thickness of 0.75mm, 0.9mm and 1.6mm, respectively. A-scans for foam sheet gave its first, second and third layer was at a thickness of 0.6mm, 0.75mm, and 0.85mm, respectively.

Keywords: A-scan, b-scan, depth profile, filtering, image processing, optical coherence tomography (OCT), signal processing

INTRODUCTION

With The rapid expansion in the field of medical imaging technologies, a huge amount of biomedical image data can be collected by several biomedical techniques like X-ray, Magnetic Resonance Imaging (MRI), 3D ultrasound, and Optical Coherence Tomography (OCT) (Lee et al., 2019; Drexler & Fujimoto, 2008). Three-dimensional medical modalities can examine numerous features of biological features, such as blood flow, structural information of organs, and molecular content, which gives a crisp of the scanned object (Zhang et al., 2018). The OCT system is also used to analyze the final B-scan image and get to a medical conclusion. The main analysis is on the retinal layers (Schönfeldt-Lecuona et al., 2020, Chua et al., 2020) and neural layer (Liu et al., 2020) to get the structural information.

The principle used for OCT system is Michelson Interferometry (Panta et al., 2019). A light source of low coherence is used in Michelson Interferometer, as displayed in Figure 1. As shown in Figure 1, the source of light beam having broadband spectrum is divided in two portions i.e., sample and reference arm by the beam splitter (Tomlins & Wang, 2005). Sample and reference arm reflect the signal which forms the pattern of interference and this pattern is detected by the spectrometer in which photocurrent of the pattern is measured by using the line scanning camera (Lee et al., 2020).

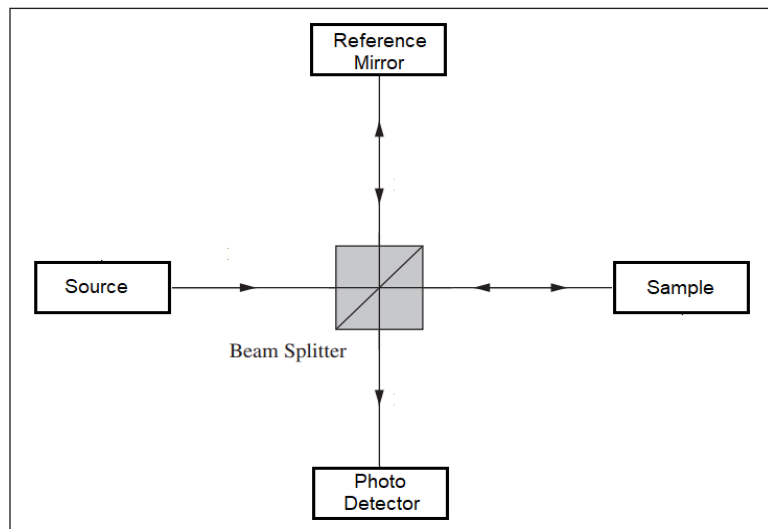


Figure 1. Principle of Michelson interferometer

The light falls on line scanning camera where the photocurrent of light is detected with the array of pixels to give the intensity corresponding to each wavelength in the bandwidth. This data is then taken for the signal processing for the image formation (Tang et al., 2018). Figure 1 describes the working principle of Michelson Interferometer, where half-silvered beam splitter is used (Kim et al., 2018; Lee et al., 2011).

Bhatia et al. (2016) described the core of the OCT systems and implemented the spectral-domain OCT(SD-OCT). The detected signal from the OCT gives three terms of getting in the data, which were constant term, autocorrelation and cross-correlation (Bhatia et al., 2016). The different applications of OCT in clinical and non-clinical fields are discovered. The spectrometer gives information about one-dimensional data by taking the interference signal as an input (Fujimoto & Swanson, 2016; Patil et al., 2020). The system uses the signal processing algorithm, which has the blocks of background removal, resampling, FFT and DC removal (Choudhari et al., 2017). The system uses the wavelength of 840nm with 40nm bandwidth and getting the depth profile which gives imaging depth of 0.5mm. Zhang et al. (2018) implemented the swept-source OCT (SS-OCT) for imaging the choriocapillaris and associated flow voids. The system works on the wavelength of 1060nm and bandwidth of 100nm. The final images of choriocapillaris give information regarding the diseases and the response of the body to therapies. Petrov et al. (2016) applied the short time Fourier transforms in the signal processing, using the window and this window slid along the time series. This algorithm takes more time to execute as it is having more point FFT, also we see the maximum penetration depth is not much and if we want to image the tissue to certain depth we need more penetration depth (Petrov et al., 2016).

From the literature survey, we have found that the imaging depth in the existing systems is typically in the range of 1-2 mm, hence there is a scope of improvement in the imaging depth. Therefore, in this paper, we proposed the system which worked on the wavelength of 840nm and bandwidth of 64nm and developed the algorithm to increase the maximum penetration depth. Also, in OCT, the speckle noise gets added to the final B-scan images. This noise is reduced by applying some image processing techniques so as to improve the quality of the image for the better interpretation.

MATERIALS AND METHODS

Signal Processing in OCT

The data acquisition process was executed by implementing Spectral-domain OCT (SD-OCT). In order to obtain the final OCT images the fundamental blocks were used as shown in Figure 2.

In every system some background noise gets added in the system due to reflections of room light and electronic devices (Rawat & Gaikwad, 2014). This background noise is an important factor in image formation as it disturbs the image, hence it needs to be removed.

The output of the Michelson interference is nothing but the interference pattern in the form of fringes. The interference pattern has the optical light; this optical intensity is measured by the spectrometer (Lee et al., 2011). As for image formation FFT is taken and for which the data must be evenly sampled in wavenumber space, for this resampling and interpolation blocks are followed. The image objects frequently used in OCT comprise of dispersive media, where the speed for optical frequencies are not the same as for different mediums speed is different. The individual reflections from the sample, and those reflections from specific scatters not likely to form the point images, rather they blurred by dispersion. Due to mismatch between the sample and reference arm of the interferometer the non-linear phase, which is dependent on frequency is introduced and by cancelling this phase, the dispersion can be compensated.

The phase correction is can be calculated as in Equation 1 (Ali & parlapalli, 2010)

$$\varphi(\omega) = -[(b * n^2) + (c * n^3)] \tag{1}$$

Where b and c are linear constants; n is a vector of linear elements from -1 to 1.

This phase which is equal and opposite to the physical wavelength-dependent path length shift is multiplied to each element of the spectrum in order to compensate the dispersion (Marks et al., 2002). The FFT is taken in the last to get the depth resolved profile (McKeown, 2010).

Formation of B-scan Image

The mechanism involves scanning the sample along the optical axis. One dimensional scanning is performed in the Z-direction, and it is known as the axial scanning or A-scan. One dimensional scanning can only give information about the single point of the sample. The two-dimensional scanning can be obtained by combining the multiple axial scans. The

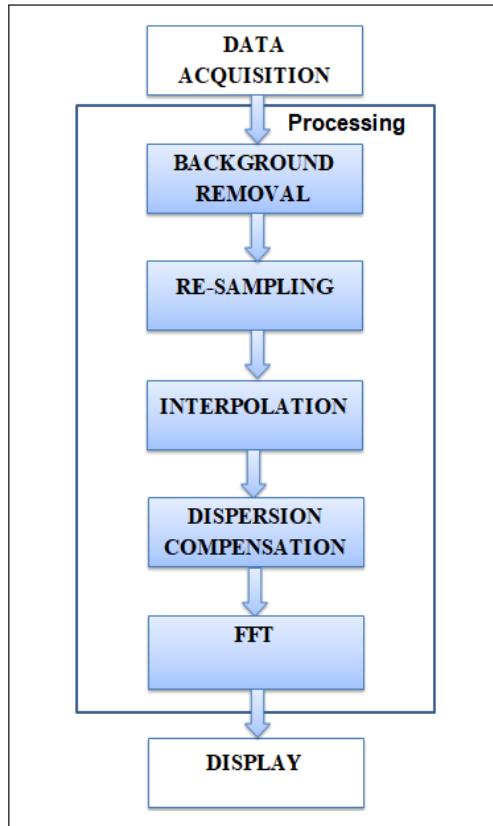


Figure 2. Signal processing algorithm

two-dimensional scan is also known as B-scan. A scan includes point scanning, whereas B scanning involves scanning the entire surface. The flowchart for getting B-scan is as shown in Figure 3. It follows the flow from acquisition of the data from the experimental setup of the OCT. The single point data is taken to signal processing algorithm to form a depth profile of that particular point. As the data can be processed and 512 axial scans are formed. Now for the formations of the B-scan image all these 512 A-scans are stacked sequentially to get the final OCT image

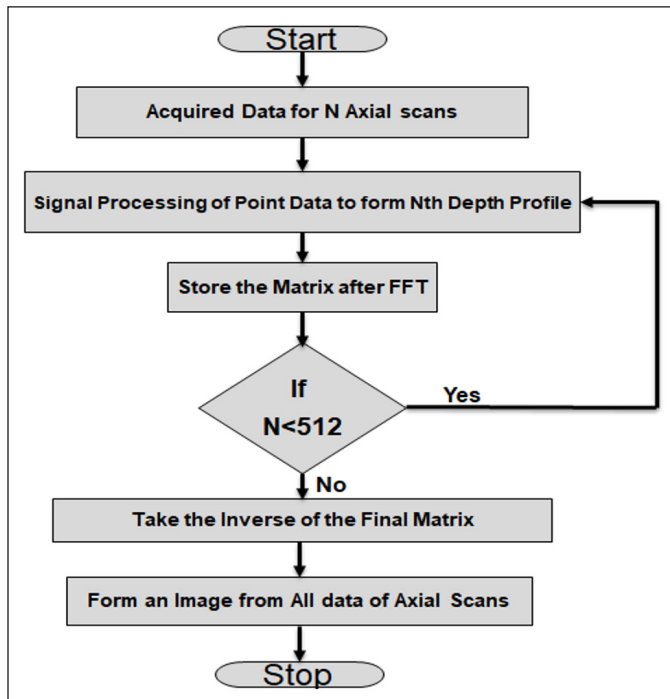


Figure 3. Flow chart for B-scan formation

Image Processing in OCT

Low-coherence interferometry is used in the OCT imaging, which introduces some speckle noise in the images, and this speckle-noise is the granular noise, seen as black and white spots on the images (Frosz et al., 2001). This speckle noise is a ubiquitous artifact that limits the interpretation as it profoundly affects the quality, contrast of the image and makes the difficulties in analyzing the exceptional features and structures. The back reflections of the incident light generates a signal which carries speckle, while due to scattering of photons in forwarding and backward direction generates the signal-degrading speckle (Petrov et al., 2016). The speckle is visible as grainy structures which blurs the details of the structural image (Murakami & Ogawa, 2018). As this speckle-noise needs to be removed but removing speckle noise removes some useful information also hence the special care should be taken.

Therefore, it is crucial to take out the speckle noise with care and for better interpretation, image enhancement and filtering techniques are used. Here the median filtering gives the best results from other filtering techniques.

Median Filtering

The median filter is an order statistics filter. This filtering technique is used to eliminate the noise by preserving the sharp edges in the images. This technique comes under non-linear filtering techniques. The impulse noise is also eliminated by the average filtering, in which centre pixel is replaced with average of neighbouring pixels, but in this filtering technique, the fine details of the image are not preserved and hence the loss of information occurs. While in the case of median filtering, the centre pixel is replaced by the median of the neighbouring pixel. Median filters are one-dimensional as well as two-dimensional. The results of two-dimensional median filters are better than that of one-dimensional median filter. The results are shown in the results section.

RESULTS AND DISCUSSION

We had acquired the data from the SD-OCT system setup for three different samples of a leaf, human fingertip, and foam sheet. The dataset was in terms of the intensities and the respective wavelengths. The data set was then applied to the several steps of signal processing algorithm like background subtraction, resampling interpolation, dispersion compensation and FFT. The Signal Processing Algorithm gives the Depth profile of the sample, i.e., Axial scan (A-scan). This A-scan was obtained after processing algorithm on the dataset. The dataset in our case was 512×1024 , i.e., a total of 512 A-scans each having 1024 pixels. The depth profiles for samples like a leaf, human fingertip and foam sheet are given in the following part.

Each A-scan gives the layer-wise depth information about the thickness. The proposed system provides maximum penetration depth at 2.82mm for each sample only differing in the position of the peaks which is shown in Figures 4, 5 and 6. As each sample had 512 A-scan in our case and four of them are shown for each sample. The first A-scan from Figure 4 gave information that the first and second layer were getting at thickness of 1mm and 1.6mm, respectively. Likewise, the depth information could be extracted from every A-scan.

A-scans for Human fingertip is shown in Figure 5. The information taken out from the first A-scan is the first, second and third layer is getting at a thickness of 0.75mm, 0.9mm and 1.6mm, respectively.

Another sample was the foam sheet. Foam sheet having multiple layers can be seen by the A-scans shown in Figure 6. Also, for foam sheet, the layers are different at each point. The layers are coming at 0.6mm, 0.75mm and 0.85mm thickness.

Algorithm for B-scan Image Reconstruction in OCT

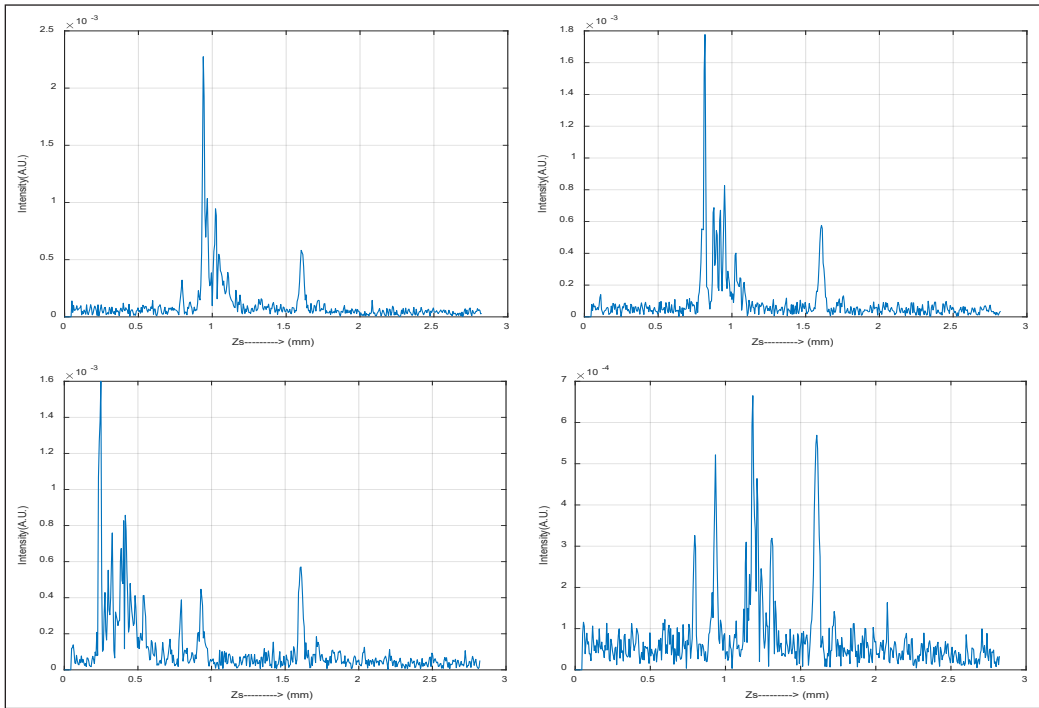


Figure 4. A-scans of leaf

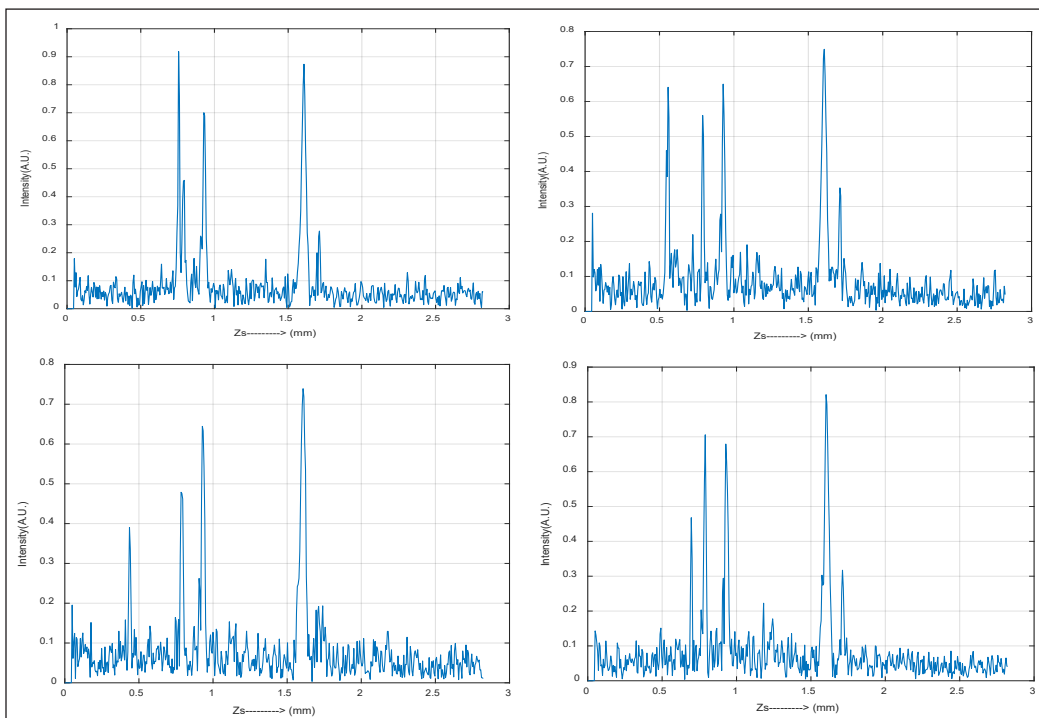


Figure 5. A-scans of human fingertip

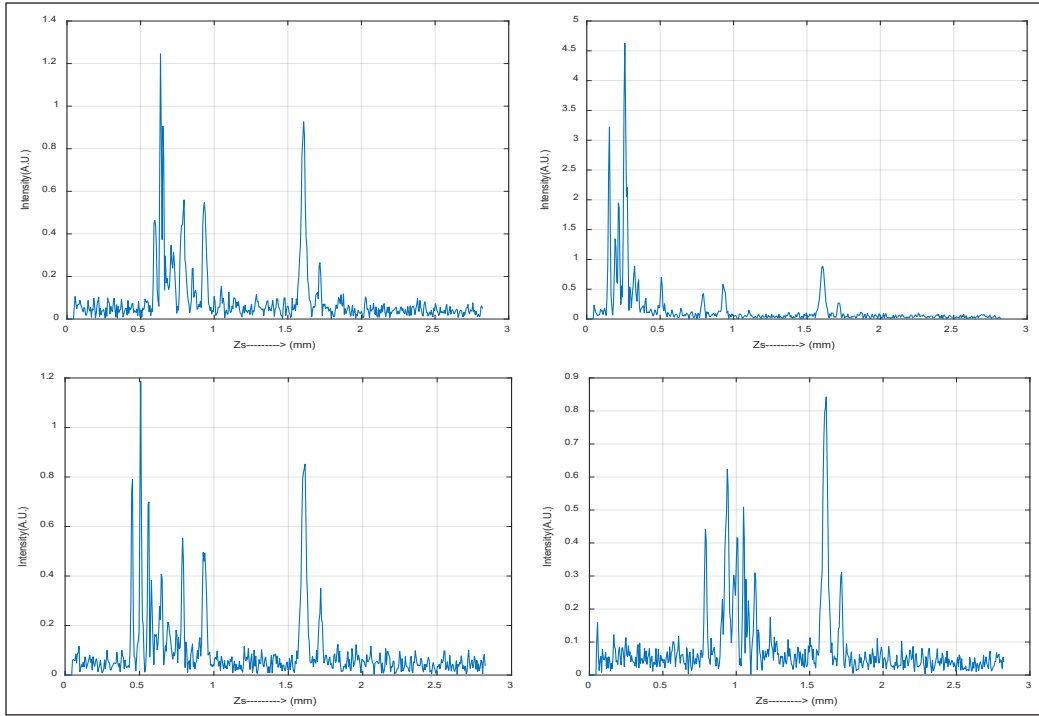


Figure 6. A-scans of foam sheet

Table 1
Comparison with existing systems

Year	Maximum Depth	Number of pixels per A-scan
Bhatia et al., 2016	0.5 mm	128
Lee et al., 2019	2.6 mm	1024
Zhang et al., 2018	3 mm	2048
Patil et al., 2020	2.75mm	1024
Proposed	2.82mm	1024

From Table 1, it is clear that the proposed system gave the maximum penetration depth as compared to the existing system for the same number of data points. As for imaging the tissues or some sample, the maximum penetration depth should be as high as possible with the minimum number of pixels, as with pixel numbers, the complexity increases. Now to form the B-scan image we had arranged all these 512 depth profiles, i.e., A-scans in a sequential manner followed by Figure 3 and the B-scan images as shown in Figure 7.

This 2-dimensional, i.e., B-scan image gives the structural information about the sample. The above B-scan is of a leaf, and the deep middle part indicates the axis of the leaf. Likewise, more information can be extracted after the feature extraction technique. In similar ways, B-scan for human fingertip, foam sheet and stack tape were obtained and

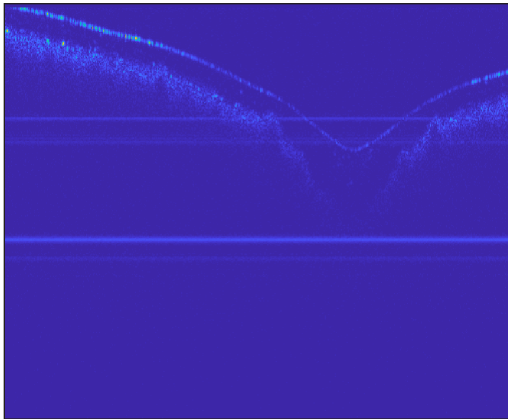


Figure 7. B-scan of leaf (512×512)

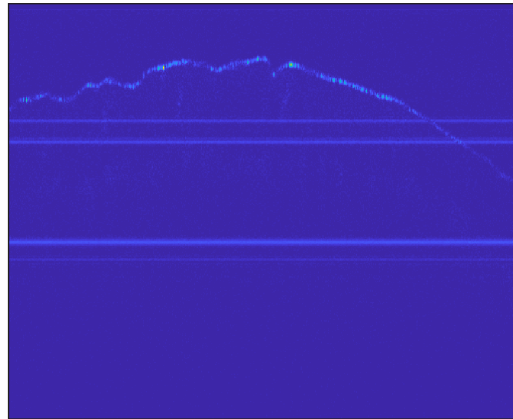


Figure 8. B-scan image of human fingertip (512×512)

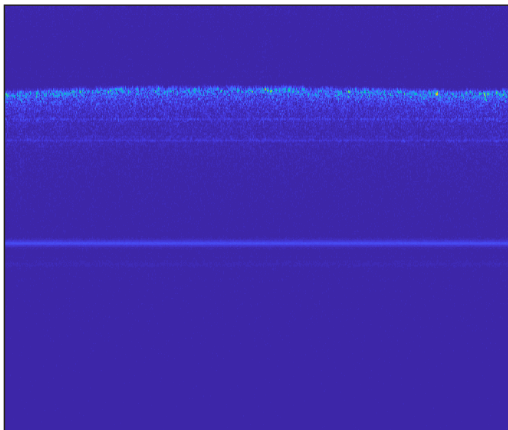


Figure 9. B-Scan of foam sheet (512×512)

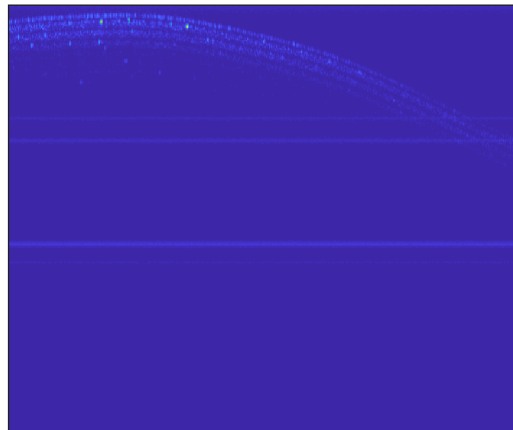


Figure 10. B-Scan of stack of tape (512×512)

shown in Figures 8, 9 and 10, respectively. Also, in every B-scan there are some horizontal lines, these horizontal lines are due to the system and those can be ignored.

The above B-scan in Figure 8 is of the human fingertip and having the pixel size 512×512. The image shows the skin layers of the fingertip. The above B-scan is of the foam sheet, and it has multiple layers at each point. B-scan image of the stack tape is shown in Figure 10.

These B-scan images can be enhanced by using some image processing technique like filtering. The impact of different filters on the B-scan image is studied by applying different filtering techniques on the sample image. The image quality is improved more with two-dimensional median filtering amongst the other techniques like average and 1-D filtering. The speckle noise is reduced to some amount after using the filtering technique. The results after filtering are shown in Figures 11 to 14.

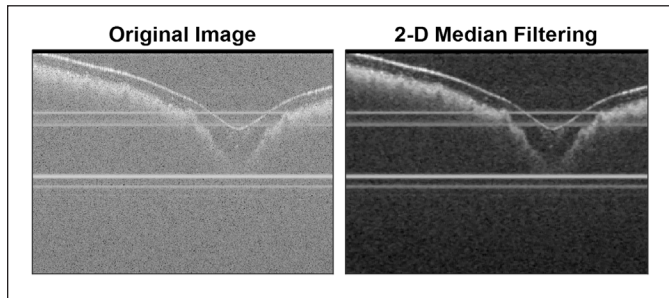


Figure 11. Filtering result for leaf (512x512)

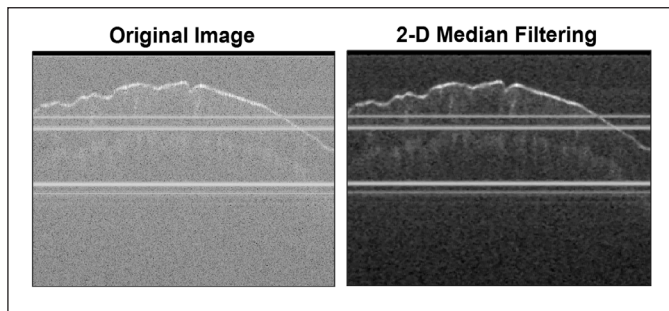


Figure 12. Filtering result for human fingertip (512x512)

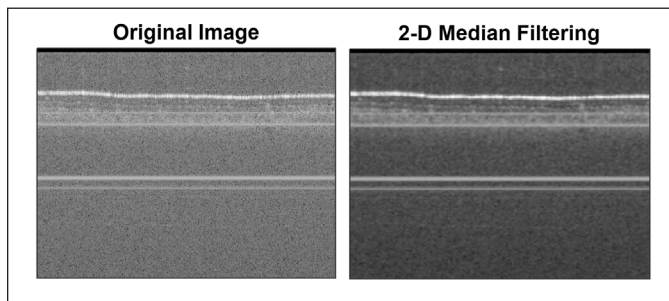


Figure 13. Filtering result for foam sheet (512x512)

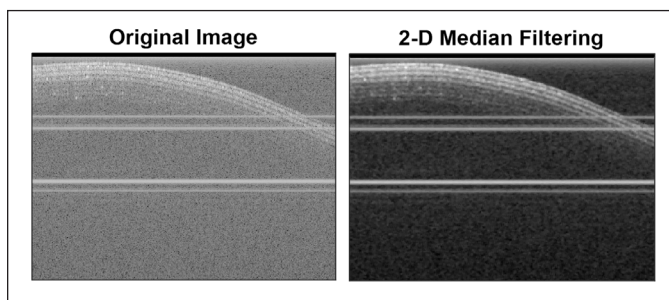


Figure 14. Filtering result for stack of tape (512x512)

The median filtering is applied in two ways, i.e., 1-dimensional and 2-dimensional. The results are better with 2-dimensional median filtering as the method gives the best quality images amongst other filtering technique.

CONCLUSIONS AND FUTURE SCOPE

The dataset is obtained by SD-OCT system setup for three different samples like human fingertip, leaf, and foam sheet. The signal processing algorithm is executed on the MATLAB to get the depth profile at each point. Thus, for every sample, 512 axial scans are collected, and each of A-scan is consisted of 1024 pixels, by combining these entire axial scans, B-scan image is formed. The maximum penetration depth calculated from the axial scan is 2.82mm for 1024 data points. The image processing technique of filtering applied on the sample image to see the impact of different filters on the B-scan image. The image quality is improved more with two-dimensional median filtering amongst all other techniques.

In future work, the detailed structural information can be obtained by feature extraction techniques and by applying some artificial intelligence (Kapoor et al., 2019) and machine learning algorithm, the automated analysis can be obtained.

ACKNOWLEDGEMENT

Mr. Kranti Patil is thankful to Director-General for the opportunity to work on the live project, Photonics Division, SAMEER, IIT Bombay for providing the necessary equipment required to carry out this work. Authors would like to thank Department of Science and Technology (DST) for funding support for the project sanction number IDP/MED/53/2016 under Biomedical Device and Technology (BDTD).

REFERENCES

- Ali, M., & Parlapalli, R. (2010). *Signal processing overview of optical coherence tomography systems for medical imaging* (SPRABB9–June). Texas Instruments. Retrieved October 09, 2020, from https://www.researchgate.net/publication/268356516_Signal_Processing_Overview_of_Optical_Coherence_Tomography_Systems_for_Medical_Imaging/link/54eb3d620cf25ba91c8652df/download
- Bhatia, P., Choudhari, S., Rodrigues, A., Patil, M., & Makkar, R. (2016, March 23-25). High resolution imaging system using spectral domain Optical Coherence Tomography using NIR source. In *2016 International Conference on Wireless Communications, Signal Processing and Networking (WiSPNET)* (pp. 2212-2216). Chennai, India. doi: 10.1109/WiSPNET.2016.7566535
- Choudhari, S., Patil, M., & Makkar, R. (2017). Modelling for spectral domain optical coherence tomography (SD-OCT) system. In I. Bhattacharya, S. Chakrabarti, H. Reehal & V. Lakshminarayanan (Eds.), *Advances in Optical Science and Engineering* (pp. 591-597). Singapore: Springer. doi: https://doi.org/10.1007/978-981-10-3908-9_74

- Chua, J., Sim, R., Tan, B., Wong, D., Yao, X., Liu, X., ... & Schmetterer, L. (2020). Optical coherence tomography angiography in diabetes and diabetic retinopathy. *Journal of Clinical Medicine*, 9(6), 1-28. doi: <https://doi.org/10.3390/jcm9061723>
- Drexler, W., & Fujimoto, J. G. (2008). *OCT Technology and Applications. Biomedical Engineering*. Heidelberg, Germany: Springer. doi: 10.1007/978-3-540-77550-8
- Frosz, M. H., Juhl, M., & Lang, M. H. (2001). *Optical coherence tomography: System design and noise analysis*. Roskilde, Denmark: Risø National Laboratory.
- Fujimoto, J., & Swanson, E. (2016). The development, commercialization, and impact of optical coherence tomography. *Investigative Ophthalmology and Visual Science*, 57(9), OCT1-OCT13. doi: <https://doi.org/10.1167/iovs.16-19963>
- Kapoor, R., Whigham, B. T., & Al-Aswad, L. A. (2019). Artificial intelligence and optical coherence tomography imaging. *The Asia-Pacific Journal of Ophthalmology*, 8(2), 187-194. doi: 10.22608/APO.201904
- Kim, S., Crose, M., Eldridge, W. J., Cox, B., Brown, W. J., & Wax, A. (2018). Design and implementation of a low-cost, portable OCT system. *Biomedical Optics Express*, 9(3), 1232-1243. doi: <https://doi.org/10.1364/BOE.9.001232>
- Lee, S. S., Song, W., & Choi, E. S. (2020). Spectral domain optical coherence tomography imaging performance improvement based on field curvature aberration-corrected spectrometer. *Applied Sciences*, 10(10), 1-15. doi: <https://doi.org/10.3390/app10103657>
- Lee, S. W., Song, H. W., Kim, B. K., Jung, M. Y., Kim, S. H., Cho, J. D., & Kim, C. S. (2011). Fourier domain optical coherence tomography for retinal imaging with 800-nm swept source: Real-time resampling in k-domain. *Journal of the Optical Society of Korea*, 15(3), 293-299.
- Lee, W. D., Devarajan, K., Chua, J., Schmetterer, L., Mehta, J. S., & Ang, M. (2019). Optical coherence tomography angiography for the anterior segment. *Eye and Vision*, 6(1), 1-9. doi: <https://doi.org/10.1186/s40662-019-0129-2>
- Liu, J., Zhu, J., Zhu, L., Yang, Q., Fan, F., & Zhang, F. (2020). Quantitative assessment of optical coherence tomography angiography algorithms for neuroimaging. *Journal of Biophotonics*, 13(9), 1-9. doi: <https://doi.org/10.1002/jbio.202000181>
- Marks, D. L., Oldenburg, A., Reynolds, J. J., & Boppart, S. A. (2002, July 7-10). Digital dispersion compensation in optical coherence tomography. In *Proceedings IEEE International Symposium on Biomedical Imaging* (pp. 621-624). Washington, DC, USA. doi: 10.1109/ISBI.2002.1029334
- McKeown, M. (2010). *FFT Implementation on the TMS320VC5505, TMS320C5505, and TMS320C5515 DSPs (SPRABB6B)*. Application report, Texas instruments. Retrieved October 9, 2020, from https://www.ti.com/lit/an/sprabb6b/sprabb6b.pdf?ts=1606467818116&ref_url=https%253A%252F%252Fwww.google.com%252F
- Murakami, T., & Ogawa, K. (2018, March 9-10). Speckle noise reduction of optical coherence tomography images with a wavelet transform. In *2018 IEEE 14th International Colloquium on Signal Processing & Its Applications (CSPA)* (pp. 31-34). Batu Feringghi, Malaysia. doi: 10.1109/CSPA.2018.8368680

- Panta, P., Lu, C. W., Kumar, P., Ho, T. S., Huang, S. L., Kumar, P., ... & John, R. (2019). Optical coherence tomography: Emerging *in vivo* optical biopsy technique for oral cancers. In P. Panta (ed.), *Oral Cancer Detection* (pp. 217-237). Cham, Switzerland: Springer. doi: https://doi.org/10.1007/978-3-319-61255-3_11
- Patil, K., Mahajan, A., Balamurugan, S., Arulmozhivarman, P., & Makkar, R. (2020, July 28-30). Development of signal processing algorithm for optical coherence tomography. In *2020 International Conference on Communication and Signal Processing (ICCCSP)* (pp. 1283-1287). Chennai, India. doi: 10.1109/ICCCSP48568.2020.9182121
- Petrov, D. A., Abdulkareem, S. N., Ghaleb, K. E., & Proskurin, S. G. (2016). An improved algorithm of structural image reconstruction with rapid scanning optical delay line for optical coherence tomography. *Journal of Biomedical Photonics and Engineering*, 2(2), 1-6.
- Rawat, C. S., & Gaikwad, V. S. (2014, July 10-11). Signal analysis and image simulation for optical coherence tomography (OCT) systems. In *2014 International Conference on Control, Instrumentation, Communication and Computational Technologies (ICCICCT)* (pp. 626-631). Kanyakumari, India. doi: 10.1109/ICCICCT.2014.6993037
- Schönfeldt-Lecuona, C., Kregel, T., Schmidt, A., Kassubek, J., Dreyhaupt, J., Freudenmann, R. W., ... & Pinkhardt, E. H. (2020). Retinal single-layer analysis with optical coherence tomography (OCT) in schizophrenia spectrum disorder. *Schizophrenia Research*, 219, 5-12. doi: <https://doi.org/10.1016/j.schres.2019.03.022>
- Tang, S. N., Hsiang, C. Y., & Huang, S. J. (2018, June 25-29). Hardware/software codesign for portable optical coherence tomography (OCT) applications. In *2018 Joint 7th International Conference on Informatics, Electronics & Vision (ICIEV) and 2018 2nd International Conference on Imaging, Vision & Pattern Recognition (icIVPR)* (pp. 24-28). Kitakyushu, Japan. doi: 10.1109/ICIEV.2018.8641052
- Tomlins, P. H., & Wang, R. K. (2005). Theory, developments and applications of optical coherence tomography. *Journal of Physics D: Applied Physics*, 38(15), 2519-2535. doi: <https://doi.org/10.1088/0022-3727/38/15/002>
- Zhang, Q., Zheng, F., Motulsky, E. H., Gregori, G., Chu, Z., Chen, C. L., & Wang, R. K. (2018). A novel strategy for quantifying choriocapillaris flow voids using swept-source OCT angiography. *Investigative Ophthalmology & Visual Science*, 59(1), 203-211. doi: <https://doi.org/10.1167/iovs.17-22953>



Molecular Markers and Phylogenetic Analysis of UPMT27, a Field Isolate of the Malaysian Fowl Adenovirus Associated with Inclusion Body Hepatitis

Salisu Ahmed^{1,4}, Abdul Razak Mariatulqabtiah^{1,3}, Mohd Hair Bejo^{2,3},
Abdul Rahman Omar^{2,3}, Aini Ideris^{2,3} and Nurulfiza Mat Isa^{1,3*}

¹Faculty of Biotechnology and Biomolecular Sciences, Universiti Putra Malaysia, 43400 UPM, Serdang, Selangor, Malaysia

²Faculty of Veterinary Medicine, Universiti Putra Malaysia, 43400 UPM, Serdang, Selangor, Malaysia

³Institute of Bioscience, Universiti Putra Malaysia, 43400 UPM, Serdang, Selangor, Malaysia

⁴Department of Science Laboratory Technology, Jigawa State Polytechnic, 7040 Dutse, Jigawa state, Nigeria

ABSTRACT

Inclusion body hepatitis (IBH) is considered one of the re-emerging diseases of avian virus that causes economic damage worldwide. IBH is caused by different serotypes of fowl adenovirus (FAdV), and most of the FAdV cases in Malaysia are related to the serotype 8b. The objective of this study was to determine the molecular markers of UPMT27 Malaysian FAdV isolate and to identify the evolutionary relationship through the phylogenetic approach. Propagation of the isolate was made in embryonated chicken eggs and chicken embryo liver (CEL cells) before it was subjected to viral DNA extraction. Both the fiber and hexon genes of the isolate were amplified and sequenced. The sequences were aligned

with the published FAdV sequences. The results showed 100% identity between UPMT27 and the previous Malaysian isolates. A phylogenetic study showed that UPMT27 was closely related to the previous Malaysian isolates. Interestingly, the substitution of the amino acids was consistent between the Malaysia isolates of both fiber protein at positions 72 (Serine-serine), 101 (Alanine-alanine), 125 (Glycine-glycine), and hexon protein 85 (Serine-serine) 160 (Glutamate-glutamate) and 205 (Alanine-alanine) respectively. It

ARTICLE INFO

Article history:

Received: 20 April 2020

Accepted: 11 November 2020

Published: 22 January 2021

DOI: <https://doi.org/10.47836/pjst.29.1.29>

E-mail addresses:

Sahmed@jippoly.edu.ng (Salisu Ahmed)

mariatulqabtiah@upm.edu.my (Abdul Razak Mariatulqabtiah)

mdhair@upm.edu.my (Mohd Hair Bejo)

aro@upm.edu.my (Abdul Rahman Omar)

aiini@upm.edu.my (Aini Ideris)

nurulfiza@upm.edu.my (Nurulfiza Mat Isa)

* Corresponding author

appeared that the amino acid variations were the indicators for genetic diversity. Thus, these findings provide information on the evolutionary relationship between FAdV subtypes for IBH prevention.

Keywords: Amino acids, fiber, fowl adenovirus, hexon, inclusion body hepatitis, PCR, phylogenetic analysis

INTRODUCTION

The global spread of fowl adenovirus (FAdV) cases is related to the varieties of the virus infection. These disease outbreaks cause significant economic lost in the poultry trade (Li et al., 2017). Commercial farm birds especially broilers are susceptible to FAdV infection. FAdV is characterized by a wide range of virulence (Mcferan & Smyth, 2000). FAdV has been classified as a member of genus of aviadenovirus and divided into 5 molecular subgroups (designated as FAdV -A to E). The virus is categorized into twelve serotypes (Serotype 1 {CELO}, 2, 3, 4, 5, 6, 7, 8a, 8b, 9 and 11) based on their restriction enzyme digest patterns, phylogenetic relationships, pathogenicities, neutralizations, molecular organizations, and recombinant potentials

The pathogenicity of the virus is associated with a wide range of avian diseases. Serotype 1 is associated with gizzard erosion and ulceration (GUE) (Niu et al., 2016), while serotype- 4 is the pre-dominant causative agent of hydropericardium syndrome (HHS) (Zhang et al., 2018). In addition, serotypes 2, 3, 8a, 8b, 9 and 11 are the etiological agents of inclusion body hepatitis (IBH) (Gupta et al., 2018).

Serotype 8b is a causative agent of most cases of inclusion body hepatitis (IBH) in all Asian countries and in South America, Australia, North America, Canada, and South Africa (Morshed et al., 2017).

In Malaysia, cases of IBH among commercial chickens is rising exponentially and a vaccine against IBH is not yet available to prevent the outbreaks (Juliana et al., 2014). Primary cells derived (chicken embryo liver cells) from 13-14 days SPF chicken embryonated eggs are frequently used for virus propagation and attenuation (Mansoor et al., 2011). IBH cases in Malaysia, were first isolated in 2005 from commercial broilers chickens with high mortality and poor broiler performance due to serotype 8b and caused significant impact to the poultry industry (Norfitriah et al., 2018). Since then, the outbreaks have also been reported in several states of Malaysia involving major poultry producing areas (Norina et al., 2016).

Previous studies revealed that the fiber and hexon proteins were the major structural proteins of fowl adenovirus, in which the serotype, group and subgroup-specific antigenic determinants were located as demonstrated in the virus virion surface (James & Edward, 2011). Subsequently, the major antigenic determinant was located on the fiber and hexon genes, the virus encoded those proteins during viral replication, which penetrated into the

nucleus of host cells (Wang & Zhao, 2019). Nevertheless, there is a scanty of information on the roles of these proteins. It has been speculated that the fiber protein may play a vital role for virus attachment and internalization of the virus into the host cell (Wang & Zhao, 2019).

Among the three major structural proteins, hexon comprises the largest portion of the virus protein and is divided into two major parts namely conserved and variable loops. Conserved regions are further divided into two fragments namely P1 and P2 located in the internal capsid side and play a major role in structural stability of hexon protein. The external capsid side of hexon forms three intertwined loops known as L1, L2 and L4 that are not conserved and exposing different surfaces between serotypes to form type-specific epitopes. Research indicates, that the L1 loop was found to be longest and complex in mastadenovirus while L3 loop buried internally and more conserved to stabilize the interface between P1 and P2 conserved regions. The antigenic specificity region or epitope is situated in the hypervariable region in loop 1 and loop 2 of the hexon. It is the predominant target for the induction of serotype specific neutralizing antibodies. Previous study indicates that the hexon gene is associated with the FAdV pathogenicity that plays a major role in virus neutralization antibody (Rux & Burnett, 2003). It has been reported that amino acid substitution in the variable region of L1 of a cell culture-based adapted FAdV strain resulted in complete attenuation (Majdi & Hair-Bejo, 2015).

The fiber protein is one of the major surface-exposed capsid structure of adenovirus, which is responsible for virus antigenicity and harbour type-specific epitopes. It is characterized by the formation of projection and bound noncovalently to the penton base involved in virus entry into the host cell and implicated in the variation of virulence of FAdVs. The fiber protein is divided into 3 domains which involve tail, shaft, and head or knob comprising some specific features (Grgić et al., 2013).

The fiber protein, specifically the head or the knob region is characterized as a receptor-binding domain and the fiber molecule is a critical factor associated with the infection properties of AdV, such as alterations in tissue tropism and virulence. In addition, it had been established that an amino acid substitution in the fiber protein of a FAdV serotype could cause a difference in pathogenicity (Pallister et al., 1996). The shaft domain is located between the tail and head of the fiber protein. The unique special, feature in the shaft domain of human adenovirus is the detection of 22 pseudo-repeats of 15 amino acid residues, most with a Proline (P) or Glycine (G) in a common position and with common substituting of hydrophobic and hydrophilic amino acids (aa) and play an important role in the b-strand formation. The shaft region constitutes the largest portion of the fiber protein its specific role toward virulence was not established but, the presence of corresponding amino acid motif "VYPF" at position (55-56 amino acid), involved in the penton base interaction (Grgić et al., 2014).

The penton protein enhances interactions with cellular components and the virus-neutralizing antibody (Wang & Zhao, 2019).

Therefore, the objectives of this study were to identify amino acid variations between the UPMT27 isolate and other previous isolates and to establish its evolutionary relationships with other FAdV isolates worldwide.

MATERIALS AND METHODS

Viral Strain

FAdV UPMT27 was isolated from the liver of a 27-day old broiler chicken in Tawau, Sabah, Malaysia in 2017 outbreak with 2% mortality. The infected broiler chicken exhibited classical IBH clinical signs such as severe depression, ruffled feathers, and crouching positions. On necropsy, the affected chickens had pale, swollen, friable, hemorrhagic livers with focal to extensive necrosis, gizzard erosions and basophilic intranuclear inclusion bodies in hepatocytes (Popowich et al., 2018).

Preparation of Chicken Embryo Liver Cells (CELS)

Primary chicken embryo liver (CEL) cells were derived from 13-15 days old SPF eggs based on Soumyalekshmi *et al.* (2014) with slight modifications. The livers of SPF embryonated chicken eggs were aseptically removed and washed twice with x1 ml of PBS, pH 7.4. The liver tissues were gently minced and transferred into a sterile beaker, 0.25% trypsin-EDTA solution was added, and the mixture shaken for 20 minutes. The trypsinised livers cells were gently decanted and sterile gauze tied to a beaker was used to filter the liver cells. Growth medium DMEM (High glucose, L-glutamine; sodium pyruvate, Biosera) supplemented with 10% foetal bovine serum (FBS; Hyclone) and 1x antibiotics penicillin streptomycin solution was added to the filtrate at the rate of 10 ml / 100ml to stop the activity of trypsin. Subsequently the cells were centrifuged at 350g for 5 minutes at 4°C. The supernatant was decanted, and growth medium was added to the cell pellet. The cell concentrations were adjusted to 5.0x10⁶ cell/ml of the medium and 5 ml of the cell suspension were seeded in 25cm² tissue culture flasks until a 70% monolayer was formed. Tissue culture flasks containing complete monolayers were infected with 0.1 ml FAdV (UPMT27), maintained at 37°C in a 5% CO₂ incubator and observed for cytopathic effect (CPE) daily. After CPEs was established, the flasks were freeze- thawed 3 times and the cells were transferred into 50 ml centrifuge tubes and centrifuge at 350 xg for 5 min and the supernatants were gently harvested by pipette and stored at -20°C until use.

Extraction of Virus Genomic DNA

The FAdV genomic DNA extraction was carried out using (Analytikjena innu PREP viral, Germany). DNA extraction was performed in a fresh 2.0 µl tube. A mixture containing

200 µl of CBV/ carrier mix, 200 µl of viral supernatant and 20 µl of the proteinase K were vigorously mixed and incubated at 70°C (water bath) for 10 minutes. After the incubation, 400 µl of the Binding solution (SBS) were added to the lysate cells and vortexed. The mixture was applied to the spin filter and centrifuged at 10, 000g for 5 minutes. The filtrate was discarded, and the spin filter was placed in a new 2.0 ml receiver tube. Then 650 µl washing solution (LS) was added to the spin column and centrifuged at 10, 000g for 5 minutes. The steps were repeated once and the spin filter was placed in a new 2.0 ml receiver tube and centrifuged at 10, 000g for 5 minutes. The receiver tube was also discarded to remove all traces of ethanol. The spin filter was placed into a new 1.5 ml elution tube. Then, 60 µl of preheated nuclease free water were added into the column and it was incubated at room temperature for 2 minutes and subsequently centrifuged at 8, 000 xg for 1 minute. The concentration of the genomic DNA was quantified by spectrophotometry (Beckman, USA).

DNA Amplifications of Fiber and Hexon Genes

The DNA amplifications of the fiber and hexon gene for the detection of FAdV were performed using MyTaqTMMix (Bioline, UK) based on the recommended protocol. Primers were designed based on FAdV accession numbers KT862811 retrieved from the GenBank (Marek et al., 2016) for the hexon and the fiber genes, respectively. HexonF/HexonR (HexonF: 5'-ATG GCC GCG TTT ACA CC-3' and HexonR: 5'-TTA CAC AGC GTT ACC GG -3') and FiberF/FiberR (FiberF: 5'-ATG GCG ACC TCG ACT CC-3' and FiberR: 5'-TTA AGG AGC GTT GGC GG-3') were used to amplify the complete hexon gene and the partial fiber gene.

PCR amplification was performed on a PCR thermocycler (C1000 TouchTM Thermal Cycler (BIO-RAD, USA). The PCR mixture of 50 µl containing 2 µl (10 pmol) of both forward and reverse primers, 25 µl MyTaqTMMix, 1 µl/ng DNA template and 22 µl nuclease-free water was subjected to the following thermal condition protocol: 95°C for 1min, followed by 30 cycles of 95°C for 15s, 51°C-60°C (Gradient) for 15s, and 72°C for 1 min, followed by a final elongation step of 1min at 72°C. Agarose gel electrophoresis (1% (w/v) agarose gel) was used to examine the PCR products of the isolate under study together with the positives controls isolates for hexon gene (KY305955) and fiber gene (KY305945) at 125 V for 40 min (iNtRON). The gel was then visualized under Gel doc (transillumination UV BIO- RAD). PCR products of the expected lengths, of fiber (882 bp) and hexon (2900 bp) were purified using a kit (Analytikjena innu PREP viral, Germany).

The PCR product of the positive samples was then subjected to the purification process. A mixture of 50 µl of PCR product and 500 µl of binding buffer were mixed in a reaction tube and vortexed. The mixture was transferred into a spin filter and centrifuged at 11, 000 xg for 3 minutes and flow-through was discarded. The spin filter was placed into a new elution tube, 50 µl of the RNase- free water were added directly onto the spin filter and

incubated for 1 minute at room temperature. After the 1 minute incubation, the mixture was centrifuged at 11, 000 xg for 1 minute. The purified PCR products were then sent for nucleotide sequencing using hexon and fiber primers (HexonF/HexonR) (FiberF/FiberR) respectively

Nucleotide, Amino Acid Sequencing and Phylogenetic Analysis

The nucleotide sequence results were assembled and examined using BioEdit (USA ver.6.0; Therapeutics, Ibis).

The nucleotide sequence determined were 882 bp-long, corresponds to 294 amino acid sequence covering the shaft region of the fiber gene. But only 558 bp –long of the fiber gene were used for further nucleotide sequence analysis which correspond to position 30644 to 31232 in the fiber gene of the reference strain KT862811 (Marek et al., 2016) encompassing the shaft region of the fiber gene. Meanwhile, the nucleotide sequence used for hexon analysis were 2900 bp-long corresponds to 996 amino acid sequence covering the Loop 1 of the gene. But only 556 bp long of the hexon were used for further analysis which correspond to position 26377 to 26933 in the hexon gene of the reference strain KT862811 (Marek et al., 2016) encompassing the Loop 1 region of the hexon gene. UPMT27 isolates was aligned with the 28 and 27 published sequences for fiber and hexon respectively to identify the nucleotides homology among the FAdV strains. The fiber and the hexon gene sequences were successively submitted to the NCBI database GenBank and were given the following accession numbers for fiber (MT233531) and hexon (MT233532).

A total of 28 and 27 complete FAdV fiber gene (Table 1) and hexon gene (Table 2) sequences were aligned with the reference sequences retrieved from Genbank were used for the construction of the phylogenetic tree. All sequences were aligned by CLUSTAL W'. Distance-based neighbor joining phylogenetic trees were constructed using the Tamura–Nei model available in the program MEGA 6.0 with 1,000 bootstrap replicates used to evaluate them (Niu *et al.*, 2016).

Nucleotide sequences of fiber and hexon genes generated from the UPMT27 and published FAdV isolates were translated into amino acids residues and analyse the similarity and variation of amino acid substitution between the isolate under study (UPMT27) and the published FAdV isolate.

RESULTS

DNA fragments of the expected lengths of the fiber gene 882 bp (Figure 1) and hexon genes 2900 bp (Figure 2) were observed in the agarose gel. Nucleotide sequence analysis revealed that the isolate of this study had high nucleotide identity [E value = 0, 99% identity] with the Malaysian isolates for fiber (KU517714, KY305954, KY305955 and KY305950) and hexon genes (KU517714, KY305954, KY305955, and KY305950) (Juliana et al., 2014; Norfitriah, 2018)

Table 1

Fowl adenovirus fiber gene sequences retrieved from NCBI for phylogenetic analysis

S/N	Strain	Accession Number	Group*	Reference
1	Strain 8b 764	KT862811	E	Marek et al., 2016
2	UPMT27*	MT233531	E	This study
3	UPM04217	KU517714	E	Juliana et al., 2014
4	UPM1137E15	KY305953	E	Norfitriah, 2018
5	UPM1137E10	KY305955	E	Norfitriah, 2018
6	UPM1137E5	KY305954	E	Norfitriah, 2018
7	UPM1137CEL35	KY305956	E	Norfitriah, 2018
8	UPM1137CEL25	KY305950	E	Norfitriah, 2018
9	UPM1137CEL10	KY305957	E	Norfitriah, 2018
10	QD2016	MF577036	E	Unpublished
11	Strain HG	GU734104	E	Grgić et al., 2011
12	SD1356	MG712775	E	Unpublished
13	Vac-2005	KT037704	E	Unpublished
14	VIC-2/430-06	KT037705	E	Unpublished
15	NSW-5/100931	KT037708	E	Unpublished
16	NZ-1/101151-1	KT037709	E	Unpublished
17	ON NP2	KP231537	D	Slaine et al., 2016
18	HBQ12	KM096545	D	Zhao et al., 2015
19	MX95-S11	KU746335	D	Unpublished
20	CH/HNJZ/2015	KU558760	C	Unpublished
21	AG234	MK572850	C	Unpublished
22	HLJFA15	KU991797	C	Unpublished
23	Strain-340	HE608155	B	Marek et al., 2012
24	40440-M/2015	MG953201	B	Unpublished
25	Isolate-340	FR872928	B	Marek et al., 2012
26	Strain-340	KC493646	B	Marek et al., 2013
27	Strain A-OTE	FN557183	A	Marek et al., 2010
28	CELO	U46933	A	Chiocca et al., 1996

Note. **UPMT27** * Indicate the isolate use in this present study

Group*= FAdV grouping (A-E)

Table 2

Fowl adenovirus hexon gene sequences retrieved from NCBI for phylogenetic analysis

S/N	Strain	Accession Number	Group*	Reference
1	Strain 8b 764	KT862811	E	Marek et al., 2016
2	UPM T27	MT233532	E	This study
3	UPM04217	KU517714	E	Juliana et al., 2014
4	UPM1137E10	KY911366	E	Norfitriah, 2018
5	UPM1137E15	KY911367	E	Norfitriah, 2018

Table 2 (continue)

S/N	Strain	Accession Number	Group*	Reference
6	UPM1137CEL15	KY305953.1	E	Norfitriah, 2018
7	UPM1137CEL 10	KY305944.1	E	Norfitriah, 2018
8	Strain HG	GU734104	E	Grgić et al., 2011
9	SD16-116	KY426984	E	Niu et al., 2016
10	SD1356	MG712775	E	Huang et al., 2019
11	ID-HCL-038	MG765468	E	Unpublished
12	USP-BR-420	KY229168	E	Unpublished
13	Strain-764	AF508958	D	Meulemans et al., 2004
14	SD15-24	KY426992	D	Unpublished
15	ON NP2	KP231537	D	Slaine et al., 2016
16	JL/1407	KY012057	D	Unpublished
17	ZZ-Isolate	MN337322	C	Unpublished
18	HN/151025	KU245540	C	Unpublished
19	SDSX1	KY636400	C	Unpublished
20	SD1601/FAV4	MH006602	C	Unpublished
21	AG234	MK572850	C	Unpublished
22	CH/GDYF/201706	MK387062	C	Unpublished
23	CH/HNJZ/2015	KU558760	C	Unpublished
24	CELO-CORR	MK572875	A	Schachner et al., 2019
25	CELO	U46933A	A	Chiocca et al., 1996
26	Strain-340	KC493646B	B	Marek et al., 2016
27	LYG	MK757473	B	Unpublished

Note. **UPMT27** * Indicate the isolate use in this present study
Group*= FAdV grouping (A-E)

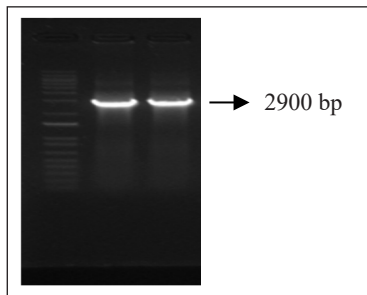


Figure 1. Amplification of hexon gene (2900 bp) using primer pair HexonF/HexonR of UPM T27 fowl adenovirus and reference isolates. M: DNA Ruler 1 kb⁺; Lane 1: Positive control [KY305955] (Norfitriah et al., 2018) and Lane 2: UPM T27.

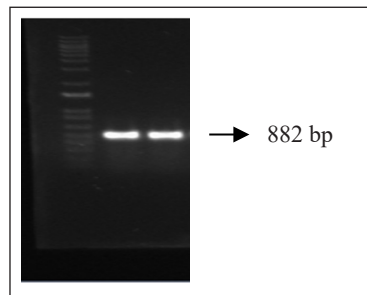


Figure 2. Amplification of fiber gene (882 bp) using primer pair FiberF/FiberR of UPM T27 fowl adenovirus and reference isolates. M: DNA Ruler 1 kb⁺; Lane 1: Positive control (KY305945) (Norfitriah et al., 2018) and Lane 2: UPMT27.

Phylogenetic analyses based on the nucleotide sequences of the fiber and hexon genes revealed that UPMT27 was closely related to the Malaysian isolates (Juliana et al., 2014; Norfitriah, 2018) for fiber gene (Figure 3) and hexon gene (Figure 4) and shared common ancestors with FAdV serotypes 8b under group E

The multiple sequence alignment in the fiber gene shows that UPMT27 and Malaysian isolates (KU517714, KY305954, KY305955 and KY305950) (Juliana et al., 2014; Norfitriah, 2018) exhibit identical patterns of amino acid substitution at positions 72

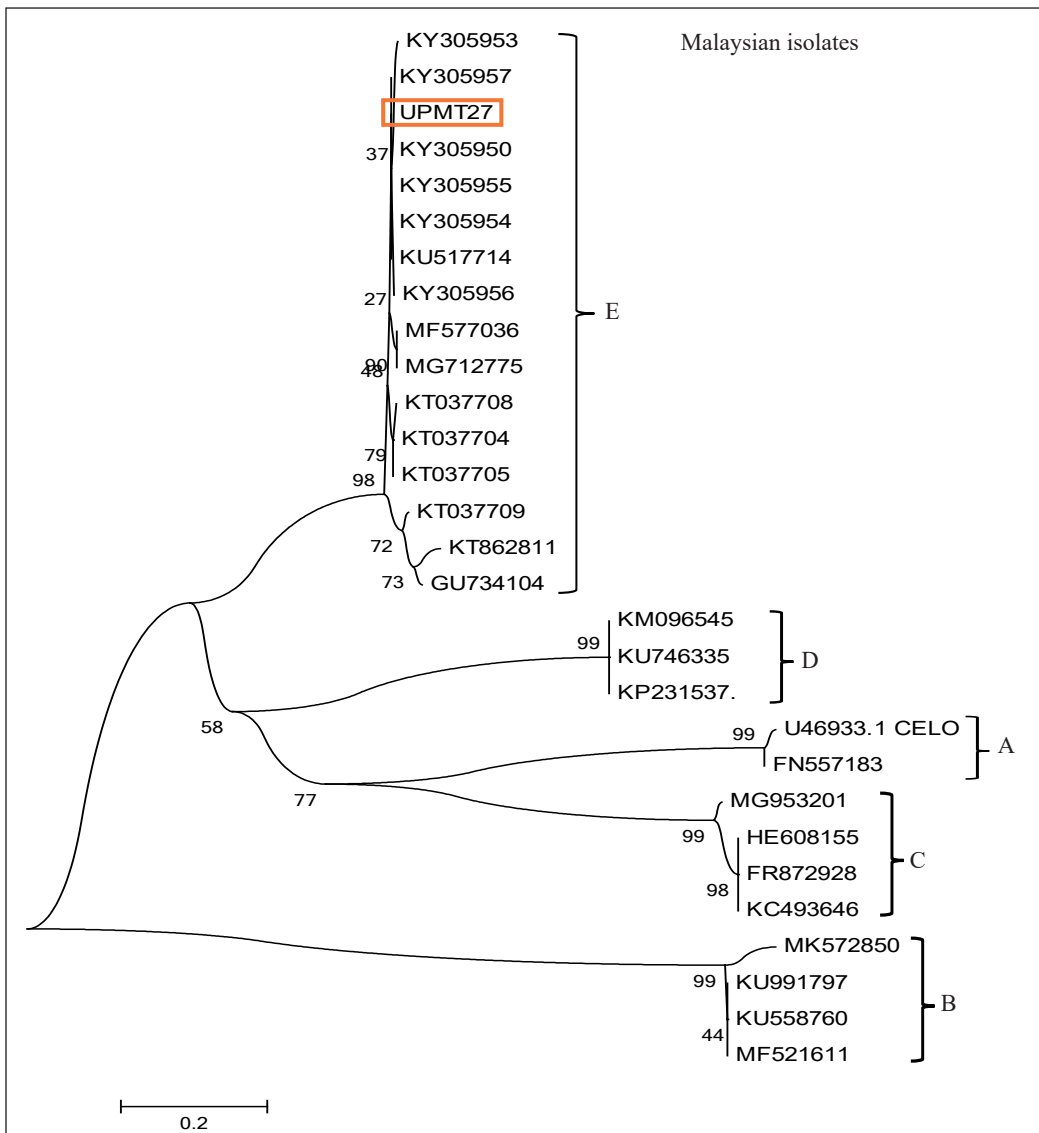


Figure 3. Sequence identity and phylogenetic analysis of partial fiber gene based on the 558 nucleotide bases in shaft region with 28 references isolates are labeled. At major nodes are indicated bootstrap values. UPMT27 is in red box

(Serine –serine), 101 (Alanine -alanine), 125 (Glycine-glycine) respectively (Table 3). The result shows consistent amino acid substitution between UPMT27 and reference isolate KT862811 (Marek et al., 2016).

However, multiple sequence alignment of amino acids of the hexon gene shows that UPMT27 and Malaysian isolates (KU517714, KY305954, KY305955, and KY305950) (Juliana et al., 2014; Norfitriah, 2018) exhibit similar pattern of amino acid substitution

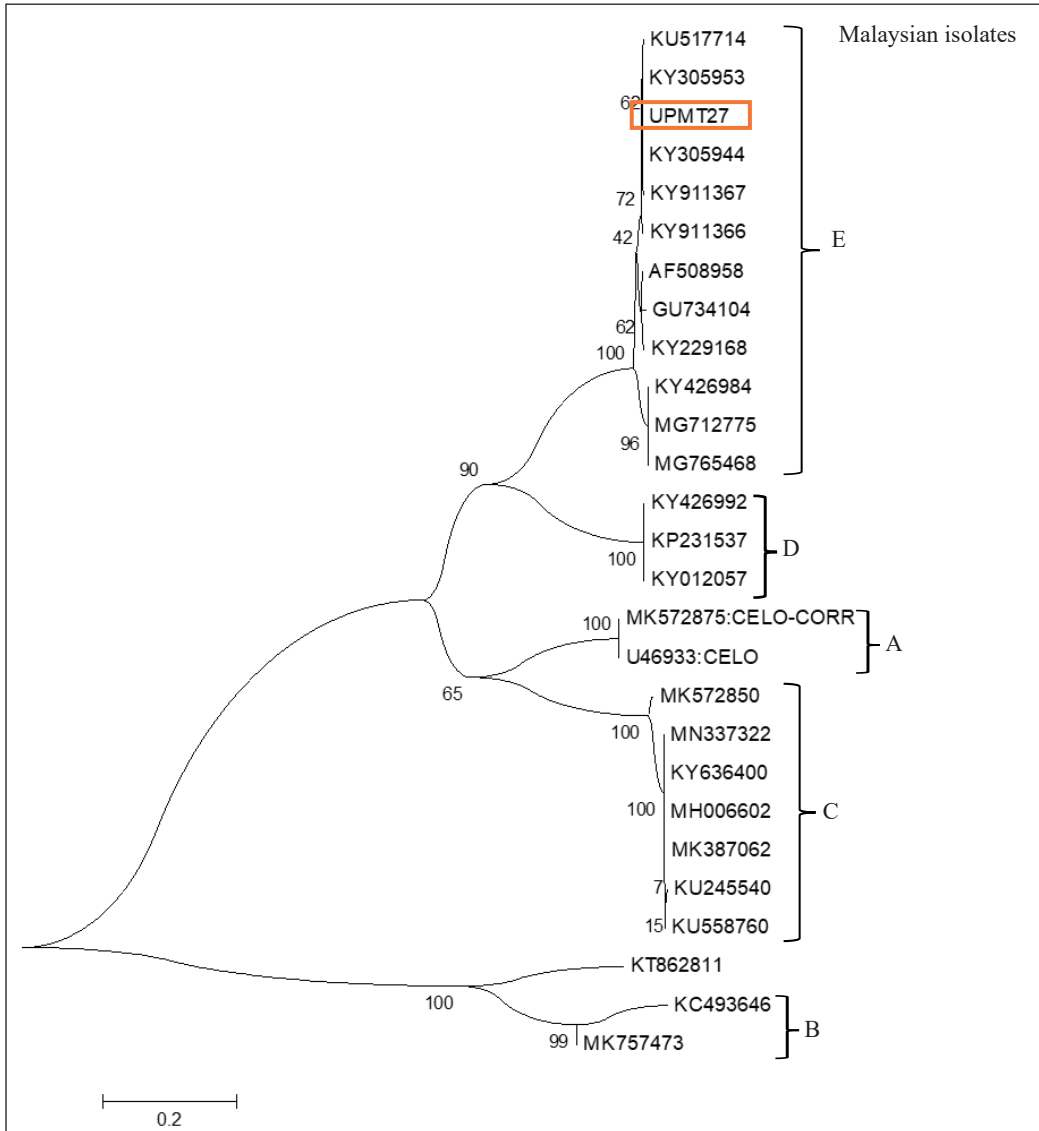


Figure 4. Sequence identity and phylogenetic analysis of partial hexon gene based on the 556 nucleotide bases in Loop 1 region with 27 reference isolates are labeled. At major nodes are indicated bootstrap values. UPMT27 is labeled in red box

(Table 4) at positions 79 (Alanine-alanine), 85 (Serine-serine) 160 (Glutamate- glutamate), 205 (Alanine-alanine) respectively. The result further revealed that there is variation in amino acid substitution between UPMT27 isolate and group B isolates [KC 493646; MK757473] (Marek et al., 2016) at positions 79 (Alanine-valine), 85 (Serine- alanine)

Table 3

Molecular marker substitutions in the fiber protein of UPMT27 and reference FAdV strains retrieved from the NCBI GenBank

S/N	Accession Number	Group*	Serotypes	Amino acid (aa) substitution and position			Reference
				72	101	125	
1	KT862811	E	Strain 8b	S	A	G	Marek et al., 2016
2	MT233531	E	Strain 8b	S	A	G	This study
3	KU517714	E	Strain 8b	S	A	G	Juliana et al., 2014
4	KY305953	E	Strain 8b	S	A	G	Norfitriah, 2018
5	KY305955	E	Strain 8b	S	A	G	Norfitriah, 2018
6	KY305954	E	Strain 8b	S	A	G	Norfitriah, 2018
7	KY305956	E	Strain 8b	S	A	G	Norfitriah, 2018
8	KY305950	E	Strain 8b	S	A	G	Norfitriah, 2018
9	KY305957	E	Strain 8b	S	A	G	Norfitriah, 2018
10	MF577036	E	Strain 8b	S	A	V	Unpublished
11	GU734104	E	Strain 8b	S	A	G	Grgić et al., 2011
12	MG712775	E	Strain 8b	S	A	V	Unpublished
13	KT037704	E	Strain 8b	S	A	G	Unpublished
14	KT037705	E	Strain 8b	S	A	G	Unpublished
15	KT037708	E	Strain 8b	S	A	G	Unpublished
16	KT037709	E	Strain 8b	S	A	G	Unpublished
17	KP231537	D	*	A	G	D	Slaine et al., 2016
18	KM096545	D	*	A	G	D	Zhao et al., 2015
19	KU746335	D	*	A	G	D	Unpublished
20	KU558760	C	Strain 4	G	D	G	Unpublished
21	MK572850	C	Strain 4	S	D	G	Unpublished
22	KU991797	C	Strain 4	S	D	G	Unpublished
23	HE608155	B	Strain 5	T	G	G	Marek et al., 2012
24	MG953201	B	Strain 5	T	G	G	Unpublished
25	FR872928	B	Strain 5	T	G	P	Marek et al., 2012
26	KC493646	B	Strain 5	T	G	P	Marek et al., 2013
27	FN557183	A	Strain 1	R	K	S	Marek et al., 2010
28	U46933	A	Strain 1	R	K	S	Chiocca et al., 1996

Note. **UPMT27** * Indicates the isolate used in this present study

Group*= FAdV grouping (A-E)

*= Non-classified strain

160 (Glutamate- leucine), 205 (Alanine-arginine) respectively as shown in Table 4. Subsequently, prominent amino acid changes were also observed in other FAdV groups (C, D and E) (Table 4).

Table 4

Molecular marker substitutions in the hexon protein of UPMT27 and reference FAdV strains retrieved from the NCBI GenBank

S/N	Accession Number	Group*	Serotypes	Amino acid (aa) substitution and position			Reference
				85	160	205	
1	KT862811	E	Strain 8b	A	L	V	Marek et al.,2016
2	MT233532	E	Strain 8b	S	E	A	This study
3	KU517714	E	Strain 8b	S	E	A	Juliana et al., 2014
4	KY911366	E	Strain 8b	S	E	A	Norfitriah, 2018
5	KY911367	E	Strain 8b	S	E	A	Norfitriah, 2018
6	KY305953	E	Strain 8b	S	E	A	Norfitriah, 2018
7	KY305944	E	Strain	S	E	A	Norfitriah, 2018
8	GU734104	E	Strain 8b	S	E	A	Grgić et al., 2011
9	KY426984	E	Strain 8b	S	E	A	Niu et al., 2016
10	MG712775	E	Strain 8b	S	E	A	Unpublished
11	MG765468	E	Strain 8b	S	E	A	Unpublished
12	KY229168	E	Strain 8b	S	E	A	Unpublished
13	AF508958	D	Strain -9	S	E	A	Meulemans et al., 2004
14	KY426992	D	*	V	K	A	Unpublished
15	KP231537	D	*	V	K	A	Slaine et al., 2016
16	KY012057	D	*	V	K	A	Unpublished
17	MN337322	C	Strain 4	V	Q	A	Unpublished
18	KU245540	C	Strain 4	V	Q	E	Unpublished
19	KY636400	C	Strain 4	V	Q	A	Unpublished
20	MH006602	C	Strain 4	V	Q	A	Unpublished
21	MK572850	C	Strain 4	V	R	A	Unpublished
22	MK387062	C	Strain 4	V	Q	A	Unpublished
23	KU558760	C	Strain 4	V	Q	A	Unpublished
24	MK572875	A	*	V	Q	A	Schachner et al., 2019
25	U46933	A	Strain 1	V	Q	A	Chiocca et al., 1996
26	KC493646	B	Strain 5	A	L	R	Marek et al., 2016
27	MK757473	B	Strain 5	A	L	A	Unpublished

Note. UPMT27 * Indicate the isolate use in this present study

Group*= FAdV grouping (A-E)

*= Non-classified strain

DISCUSSION

On a global scale, an incessant outbreak of FAdV has been reported, predominantly within the last 15 years (Schachner et al., 2019). To date, at least one, but more often a combination of more than one FAdV associated condition has been reported from every continent. The first cases of FAdV in Asian continent was reported by Hair-bejo, 2005 from the outbreak in commercial farm in Perak, Malaysia in 2004 and serotype 8b of group E is the predominant etiological agent of IBH which is an economically important disease for the poultry industry (Majdi & Hair-Bejo, 2015).

The PCR result showed that DNA fragments of the expected lengths of the fiber (882 bp) and hexon genes (2900 bp) were successfully amplified (Figure 1 & 2). This indicated the presence of the virus in the CELs. Also confirmed that CELs derived from embryonated eggs was a sensitive medium for the isolation and propagation of FAVs.

The phylogenetic analysis of the 588 nt bases of the fiber gene showed that UPMT27 was closely related to Malaysian isolates (KU517714, KY305954, KY305955, and KY305950) (Juliana et al., 2014; Norfitriah, 2018) (Figure 3). Similarly, high nucleotide identity was also observed (E value = 0, 99% identity) (Norfitriah, 2018). These results showed that UPMT27 shared common ancestors with FAdV serotypes 8b under group E which were the predominant serotypes of FAdV causing IBH in Asian continent

The multiple sequence alignment of the fiber and hexon sequences had categorized the FAdV references sequences into 5 diverse divisions. From the phylogenetic tree it has been observed that FAdV strain 7, 8a, and 8b are classified from the same ancestor under group E.

This topology agreed with the latest ICTV classification of FAdV with 5 independent clusters designated as Subgroup A-E.

Correspondingly, the phylogenetic analysis of the 556 nt bases of the hexon gene indicated that UPMT27 was clustered phylogenetically with the Malaysian isolates KU517714, KY305954, KY305955, and KY305950) (Juliana et al., 2014; Norfitriah, 2018). Nucleotide identity was also consistent with the Malaysian isolates (KU517714, KY305954, KY305955, and KY305950) (Juliana et al., 2014; Norfitriah, 2018) (E value = 0, 99% identity). It also shared common ancestors with FAdV serotypes 8b under group E which were the major serotypes of FAdV causing IBH in Asian continent.

Amino acids changes in the fiber and the hexon genes due to viral adaptation in the primary cell line played vital roles in virus attenuation (Shah et al., 2017). We postulated that amino acids changes might be considered as virus makers for pathogenicity. This agreed with the work reported by Zhang et al. (2018) which showed that amino acid differences in the fiber gene knob domain as well as in the hexon gene L1 loop domain were implicated in the differences in tissue tropism and virulence for human and canine adenoviruses.

The nucleotide sequencing results demonstrated that the UPMT27 isolate was genetically related to Malaysian isolates in both fiber and hexon genes. Multiple sequence

alignment results showed that there was no amino acid difference in the fiber gene between UPMT27 and Malaysian isolates exhibit similar amino acid substitution at positions 72 (Serine –serine), 101 (Alanine -alanine) and 125 (Glycine-glycine) respectively (Table 3). Hence, the amino acids similarities in the fiber gene between UPMT27 and the Malaysian isolates indicated that the result was consistent with the phylogenetic results, which showed that the isolate under study was genetically related to the Malaysian isolates and could also be categorized under serotype 8b and group E, the causative agent of inclusion body hepatitis outbreaks in Malaysia.

The amino acid changes were observed between UPMT27 and isolates in group C at different position (Table 3). Hence, these patterns of amino acid changes indicated the genetic variations that existed amongst FAdV isolates and this could be simply suggested as a determinant for pathogenicities differences among FAdV isolates. This result agreed with a previous work done by Ojkic and Nagy (2000) who reported that amino acid changes in the fiber protein alone in FAdV isolates within the same serotype might caused differences in their pathogenicities.

Based on the hexon gene, the results showed similarity between UPMT27 and the Malaysian isolates (Table 4). The consistency of similar amino acid substitution indicated that UPMT27 was genetically related to the Malaysian isolates. In addition, it was observed that there was a difference in amino acid substitution between UPMT27 and KC493646 and MK757473 at position 79 (Alanine-valine), 85 (Serine- alanine) 160 (Glutamate-leucine) and 205 (Alanine-arginine) respectively. This finding was expected as KC493646 and MK757473 are classified under serotype B. Nevertheless, the ability to make this distinction that they are not from the same serotype and group is important because not all 12 FAdV serotypes are pathogenic.

CONCLUSION

This study showed that UPMT27 is closely related to the other Malaysian isolates categorized under subtype 8b of group E which is the predominant subtype in Malaysia, causing inclusion body hepatitis outbreaks. In addition, amino acids changes indicated that the isolate under study was evolutionary related with the Malaysian isolates. That emerged as poultry threats in 2005. Our data suggest that molecular and phylogenetic studies based on the fiber and hexon genes may play important roles in characterizing FAdV isolates and identification of virulence markers.

ACKNOWLEDGEMENTS

This work was funded by the Higher Institute Centre of Excellent (HICoE) grant (6369101) from the Higher Education Ministry of the Malaysian Government. Also, the authors would like to thank the Laboratory of Vaccine and Immunotherapeutics, IBS, Universiti

Putra Malaysia for allowing us to conduct all the experiments there. The authors would also like to show appreciation to Professor Dr. Soon Guan Tan, formerly Associate Editor of Elsevier Editorial System, Gene, for proofreading the manuscript

REFERENCE

- Chiocca, S., Kurzbauer, R., Schaffner, G., Baker, A., Mautner, V., & Cotten, M. (1996). The complete DNA sequence and genomic organization of the avian adenovirus CELO. *Journal of Virology*, *70*(5), 2939-2949.
- Grgić, H., Yang, D. H., & Nagy, É. (2011). Pathogenicity and complete genome sequence of a fowl adenovirus serotype 8 isolate. *Virus Research*, *156*(1-2), 91-97. doi: <https://doi.org/10.1016/j.virusres.2011.01.002>
- Grgić, H., Poljak, Z., Sharif, S., & Nagy, É. (2013). Pathogenicity and cytokine gene expression pattern of a serotype 4 fowl adenovirus isolate. *PloS One*, *8*(10), 1-10. doi: <https://doi.org/10.1371/journal.pone.0077601>
- Grgić, H., Krell, P. J., & Nagy, É. (2014). Comparison of fiber gene sequences of inclusion body hepatitis (IBH) and non-IBH strains of serotype 8 and 11 fowl adenoviruses. *Virus Genes*, *48*(1), 74-80.
- Gupta, A., Popowich, S., Ojkic, D., Kurukulasuriya, S., Chow-Lockerbie, B., Gunawardana, T., ... & Tikoo, S. K. (2018). Inactivated and live bivalent fowl adenovirus (FAdV8b+ FAdV11) breeder vaccines provide broad-spectrum protection in chicks against inclusion body hepatitis (IBH). *Vaccine*, *36*(5), 744-750. doi: <https://doi.org/10.1016/j.vaccine.2017.12.047>
- Hair-Bejo, M. (2005). Inclusion body hepatitis in a flock of commercial broiler chickens. *Journal of Veterinary Malaysia*, *17*(1), 23-26.
- Huang, Q., Ma, X., Huang, X., Huang, Y., Yang, S., Zhang, L., ... & Xu, C. (2019). Pathogenicity and complete genome sequence of a fowl adenovirus serotype 8b isolate from China. *Poultry Science*, *98*(2), 573-580. doi: <https://doi.org/10.3382/ps/pey425>
- James, N. M., & Edward, J. D. (2011). *Fenner's veterinary virology* (4th Edition). San Diego, USA: Academic Press.
- Juliana, M. A., Nurulfiza, M. I., Hair-Bejo, M., Omar, A. R., & Aini, I. (2014). Molecular characterization of fowl adenoviruses isolated from inclusion body hepatitis outbreaks in commercial broiler chickens in Malaysia. *Pertanika Journal of Tropical Agriculture Science*, *37*(4), 483-497.
- Li, P. H., Zheng, P. P., Zhang, T. F., Wen, G. Y., Shao, H. B., & Luo, Q. P. (2017). Fowl adenovirus serotype 4: Epidemiology, pathogenesis, diagnostic detection, and vaccine strategies. *Poultry Science*, *96*(8), 2630-2640. doi: <https://doi.org/10.3382/ps/pex087>
- Mansoor, M. K., Hussain, I., Arshad, M., & Muhammad, G. (2011). Preparation and evaluation of chicken embryo-adapted fowl adenovirus serotype 4 vaccine in broiler chickens. *Tropical Animal Health and Production*, *43*(2), 331-338. doi: <https://doi.org/10.1007/s11250-010-9694-z>
- Majdi, A., & Hair-Bejo, M. (2015, February 23-27). Pathogenicity of Malaysian fowl adenovirus isolates in specific pathogen free chickens. In *10th Proceedings of the Seminar of Veterinary Sciences* (pp. 15-20). Faculty of Veterinary Medicine, Universiti Putra Malaysia, Malaysia.

- Marek, A., Kaján, G. L., Kosiol, C., Benkő, M., Schachner, A., & Hess, M. (2016). Genetic diversity of species Fowl aviadenovirus D and Fowl aviadenovirus E. *Journal of General Virology*, 97(9), 2323-2332. doi: <https://doi.org/10.1099/jgv.0.000519>
- Marek, A., Kosiol, C., Harrach, B., Kajan, G. L., Schlotterer, C., & Hess, M. (2013). The first whole genome sequence of a fowl adenovirus B strain enables interspecies comparisons within the genus aviadenovirus. *Journal Veterinary Microbiology*, 166(1-2), 250-256. doi: <https://doi.org/10.1016/j.vetmic.2013.05.017>
- Marek, A., Schulz, E., Hess, C., & Hess, M. (2010). Comparison of the fibers of fowl adenovirus A serotype 1 isolates from chickens with gizzard erosions in Europe and a pathogenic reference strains. *Journal of Veterinary Diagnostics*, 22(6), 937-941. doi: <https://doi.org/10.1177/104063871002200613>
- Marek, A., Nolte, V., Schachner, A., Berger, E., Schlötterer, C., & Hess, M. (2012). Two fiber genes of nearly equal lengths are a common and distinctive feature of Fowl adenovirus C members. *Veterinary Microbiology*, 156(3-4), 411-417. doi: <https://doi.org/10.1016/j.vetmic.2011.11.003>
- McFerran, J. B., & Smyth, J. A. (2000). Avian adenoviruses. *Revue Scientifique Et Technique (International Office of Epizootics)*, 19(2), 589-601.
- Meulemans, G., Couvreur, B., Decaesstecker, M., Boschmans, M., & van den Berg, T. P. (2004). Phylogenetic analysis of fowl adenoviruses. *Journal of Avian Pathology*, 33(2), 164-170. doi: <https://doi.org/10.1080/03079450310001652086>
- Morshed, R., Hosseini, H., Langeroude, A. G., Fard, M. H. B., & Charkhkar, S. (2017). Fowl adenoviruses D and E cause inclusion body hepatitis outbreaks in broilers and broilers breeder pullet flocks. *Avian Disease*, 61(2), 205-210. doi: <https://doi.org/10.1637/11551-120516-Reg.1>
- Niu, Y. J., Sun, W., Zhang, G. H., Qu, Y. J., Wang, P. F., Sun, H. L., & Liu, S. D. (2016). Hydropericardium syndrome outbreak caused by fowl adenovirus serotype 4 in China. *Journal of General Virology*, 97, 2684-2690. doi: <https://doi.org/10.1099/jgv.0.000567>
- Norfitriah, M. S. (2018). *Development of live attenuated Fowl adenovirus isolate of Malaysia for future production of vaccine* (PhD Thesis). Universiti Putra Malaysia, Malaysia.
- Norfitriah, M. S., Hair-Bejo, M., Omar, A. R., Aini, I., & Nurulfiza, M. I. (2018). Molecular detection and pathogenicity of fowl adenovirus isolated from disease outbreak in commercial layer farm. *International Journal of Agriculture Sciences and Veterinary Medicine*, 6(1), 73-84.
- Norina, L., Norsharina, A., Nurnadiah, A., Redzuan, I., Ardy, A., & Nor-Ismaliza, I. (2016). Avian adenovirus isolated from broiler affected with Inclusion body hepatitis. *Malaysian Journal of Veterinary Research*, 7(2), 121-126.
- Ojkic, D., & Nagy, É. (2000). The complete nucleotide sequence of fowl adenovirus type 8. *Journal of General Virology*, 81(7), 1833-1837. doi: <https://doi.org/10.1099/0022-1317-81-7-1833>
- Pallister, J., Wright, P. J., & Sheppard, M. (1996). A single gene encoding the fiber is responsible for variations in virulence in the fowl adenoviruses. *Journal of Virology*, 70(8), 5115-5122.
- Popowich, S., Gupta, A., Chow-lockerbie, B., Ayalew, L., Ambrose, N., Ojkic, D., ... & Suresh, K. (2018). Broad spectrum protection of broiler chickens against inclusion body hepatitis by immunizing their broiler

- breeder parents with a bivalent live fowl adenovirus vaccine. *Research in Veterinary Science*, *118*, 262-269. doi: <https://doi.org/10.1016/j.rvsc.2018.03.003>
- Rux, J. J., & Burnett, R. M. (2003). Structural and phylogenetic analysis of adenovirus hexons by use of high-resolution X-ray crystallographic, molecular modeling, and sequence based methods. *Journal of Virology*, *77*, 9553-9566. doi: [10.1128/JVI.77.17.9553-9566.2003](https://doi.org/10.1128/JVI.77.17.9553-9566.2003)
- Schachner, A., Gonzalez, G., Endler, L., Ito, K., & Hess, M. (2019). Fowl Adenovirus (FAdV) Recombination with Intertypic Crossovers in Genomes of FAdV-D and FAdV-E, Displaying Hybrid Serological Phenotypes. *Viruses*, *11*(12), 1-24. doi: <https://doi.org/10.3390/v11121094>
- Shah, M. S., Ashraf, A., Khan, M. I., Rahman, M., Habib, M., Chughtai, M. I., & Qureshi, J. A. (2017). Fowl adenovirus: history, emergence, biology and development of a vaccine against hydropericardium syndrome. *Archives of Virology*, *162*(7), 1833-1843. doi: <https://doi.org/10.1007/s00705-017-3313-5>
- Slaine, P. D., Ackford, J. G., Kropinski, A. M., Kozak, R. A., Krell, P. J., & Nagy, E. (2016). Molecular characterization of pathogenic and non-pathogenic fowl aviadenovirus serotype 11 isolates. *Journal of Microbiology*, *62*(12), 993-1002. doi: <https://doi.org/10.1139/cjm-2016-0297>
- Soumyalekshmi, S., Ajith, M. K., & Chandraprakash, M. (2014). Isolation of fowl adenovirus in chicken embryo liver cell culture and its detection by hexon gene based PCR. *Journal of Science Research and Technology*, *2*(3), 33-36.
- Wang, Z., & Zhao, J. (2019). Pathogenesis of Hypervirulent Fowl Adenovirus Serotype 4: The Contributions of Viral and Host Factors. *Viruses*, *11*(8), 1-10. doi: <https://doi.org/10.3390/v11080741>
- Zhang, Y., Liu, R., Tian, K., Wang, Z., Yang, X., Gao, D., ... & Zhao, J. (2018). Fiber2 and hexon genes are closely associated with the virulence of the emerging and highly pathogenic fowl adenovirus 4. *Emerging Microbes and Infections*, *7*(1), 1-10. doi: <https://doi.org/10.1038/s41426-018-0203-1>
- Zhao, J., Zhong, Q. I., Zhao, Y., Hu, Y. X., & Zhang, G. Z. (2015). Pathogenicity and complete genome characterization of fowl adenoviruses isolated from chickens associated with inclusion body hepatitis and hydropericardium syndrome in China. *PloS One*, *10*(7), 1-14. doi: <https://doi.org/10.1371/journal.pone.0133073>



Optimisation and Evaluation of Antibacterial Topical Preparation from Malaysian Kelulut Honey using Guar Gum as Polymeric Agent

Mohd Amir Shahlan Mohd-Aspar¹, Raihana Zahirah Edros^{1*} and Norul Amilin Hamzah²

¹Faculty of Chemical and Process Engineering Technology, Universiti Malaysia Pahang, Lebuhraya Tun Razak, 26300 Kuantan, Pahang, Malaysia

²The Pathology and Laboratory Medicine Department, International Islamic University Malaysia (IIUM) Medical Centre, 25200 Kuantan, Pahang, Malaysia

ABSTRACT

The study aims to formulate and optimise topical antibacterial preparation using Malaysian *kelulut* honey as the active ingredient and guar gum as the polymeric agent. Response surface methodology (RSM) was used to optimise the preparation. The acidity, honey concentration, and guar gum concentration were the independent variables. Meanwhile, the zone of inhibitions on *Staphylococcus aureus* ATCC6538 and *Escherichia coli* ATCC8739 were the response variables. The optimal preparation was evaluated on its physicochemical properties, viscosity, antibacterial efficacy, and stability. The antibacterial efficacy of the optimal preparation was compared to the commercial antibacterial gel (MediHoney™, Comvita). The optimal preparation was formulated at pH 3.5, honey concentration of 90% (w/v), and guar gum concentration of 1.5% (w/v). The inhibition zones measured on *S. aureus* ATCC6538 was 16.2 mm and *E. coli* ATCC8739 was 15.8 mm, respectively. The optimal preparation showed good physicochemical properties and effective antibacterial properties. However, the viscosity of the preparation was reduced by more than 50% during the six months of the stability study. Guar gum is a potential polymeric agent in preparing

kelulut as topical preparation with effective antibacterial properties. Consideration of additional stabilising or preservative agent is recommended to overcome the reduction of viscosity over time.

Keywords: Antibacterial properties, guar gum, Malaysian *kelulut*, topical preparation

ARTICLE INFO

Article history:

Received: 20 July 2020

Accepted: 07 December 2020

Published: 22 January 2021

DOI: <https://doi.org/10.47836/pjst.29.1.30>

E-mail addresses:

amirshahlan@ump.edu.my (Mohd Amir Shahlan Mohd-Aspar)

rzahirah@ump.edu.my (Raihana Zahirah Edros)

amilin@iium.edu.my (Norul Amilin Hamzah)

* Corresponding author

INTRODUCTION

Honey has been successfully applied as a topical preparation in the treatment of wound infection. Other than antibacterial properties, other additional characteristics of honey such as non-irritant, non-toxic, self-sterile, nutritive, and easy application (Boukraâ, 2014; Ismail, 2016) enhance its potential of being effectively utilised as a topical agent. Among various types of honey, manuka is most commonly used as an agent to prevent bacterial infection. Manuka, with its Unique Manuka Factor (UMF) of 10+ and above, is documented as the medical-grade honey used in clinical application as an antibacterial agent (Tan et al., 2009). In Malaysia, several types of honey are actively harvested, including tualang, kelulut, and acacia. These types of honey were studied and found to possess potent antibacterial properties, including bacteriostatic and bactericidal effects (Jalil et al., 2017; Tuksitha et al., 2018; Yaacob et al., 2018). Interestingly, kelulut was revealed to have higher antibacterial properties comparable to manuka honey for preventing the growth of common pathogenic bacterial species, such as *Pseudomonas aeruginosa* (Mohd-Aspar & Edros, 2019). Although described to possess potent antibacterial properties, the report of kelulut honey utilisation as an agent to prevent bacterial infection is lacking.

Honey harvested from the tropical rainforest in Malaysia contained high moisture content (exceeding 20%), causing it to be less viscous, diluted, and unsuitable to be directly applied without improving its rheological properties. The honey could not remain on the site of action for as long as necessary and maintain a concentration within an effective range to promote bacteriostatic and bactericidal effects (El-Kased et al., 2017; Zhu et al., 2019). In this study, the rheological properties of Malaysian honey have been improved for the topical application using natural polymeric agents, i.e., guar gum.

The objective of this study was to evaluate the potential development of a topical preparation from Malaysian kelulut honey with the employment of guar gum as the polymeric agent. To maximise the effect on the prevention of bacterial growth, the preparation was optimised by considering the most effective pH, honey concentration, and polymeric agent concentration used. The optimisation was performed through response surface methodology (RSM). The optimal preparation was evaluated on its physicochemical properties, antibacterial efficacy, and stability to confirm its quality. As for antibacterial efficacy, the commercially available antibacterial gel (MediHoney™) was used as a basis for comparison.

MATERIALS AND METHODS

Honey Samples

Kelulut honey sample was obtained from a local apiarist and aseptically stored in sterile bottles. The honey was harvested in March 2016 from the farm located at Guar Batu Hitam, Kodiang, Kedah, Malaysia. Information on the collected honey was recorded in

the Certificate of Analysis (CoA) obtained during the purchase of the honey, accredited by the authorised institution, the Malaysian Agriculture Research and Development Institute (MARDI). An additional assay using the RapidRaw™ method developed by the Malaysia Genome Institute (MGI) to confirm the purity of the honey sample was included. The honey was stored in sterile glass bottles for experimental work and kept away from direct sunlight at room temperature in a dark plastic container.

Materials and Reagents

The guar gum was purchased from Sigma, USA. Sodium benzoate and triethanolamine (TEA) were purchased from Bendosen, Malaysia.

Bacteria

The study had employed 8 standard strains and 14 clinically isolated strains of common wound-infecting bacteria. The eight standard bacterial strains obtained from the American Type Culture Collection (ATCC, USA) were kindly supplied by the Department of Pathology and Laboratory Medicine, International Islamic University Malaysia Medical Centre (IIUMMC) and Central Laboratory, Universiti Malaysia Pahang (UMP). The strains included three Gram-positive bacteria, i.e., *Staphylococcus aureus* ATCC 6538, *Streptococcus pyogenes* ATCC 19615, and *Enterococcus faecalis* ATCC 29212, and five Gram-negative bacteria, i.e., *Escherichia coli* ATCC 8739, *Pseudomonas aeruginosa* ATCC 9027, *Salmonella typhimurium* ATCC 14028, *Proteus mirabilis* ATCC 12453, and *Klebsiella pneumoniae* ATCC BAA 1144. The 14 clinically isolated bacteria were primarily obtained from the Department of Pathology and Laboratory Medicine, International Islamic University Malaysia Medical Centre (IIUMMC). These included five Gram-positive bacteria, i.e., *S. aureus*, *Staphylococcus hominis*, *Staphylococcus haemolyticus*, *S. pyogenes*, and *Streptococcus agalactiae* and another nine Gram-negative bacteria, i.e., *E. coli*, *P. aeruginosa*, *Salmonella sp.*, *P. mirabilis*, *Proteus vulgaris*, *K. pneumoniae*, *Acinetobacter baumannii*, *Enterococcus cloacae*, and *Enterococcus aerogenes*. The bacteria were re-cultured in nutrient or soy agar and incubated at 37°C for 24 h, known as primary culture.

The working bacterial culture was prepared by inoculating a loop of primary culture into sterile screw-capped test tubes containing 10 mL of broth and incubated in a shaking incubator for 24 h at 37°C and rotational speed of 150 rpm. The prepared working bacteria cultures were adjusted to 0.5 McFarland standard, equivalent to 1.5×10^8 CFU/mL. They were prepared based on optical density by diluting the working bacteria into the fresh sterile broth and adjusted to be in the absorbance range of 0.08 to 0.13 (Franklin et al., 2012). The absorbance of the prepared cultures was measured using Ultraviolet-Visible Spectrophotometer UV-1800 (Shimadzu, Japan) at the reference wavelength of 600 nm.

Preparation of the Antibacterial Topical Preparation

The preparation of kelulut honey was performed by dissolving the desired amount of guar gum in sterile deionised water with continuous stirring for 1 h until the polymer was completely soaked in water. This step was followed by the addition of 0.02% (w/v) sodium benzoate (Bendosen, Malaysia) as a preservative in the preparation. The desired amount of honey was added to the mixture with continuous stirring for another 30 min until the honey was dissolved. The final volume of each preparation was set to 100 mL by adding sterile deionised water. The preparation was kept in a sterile, wide-mouth glass container covered with a lid and stored at 28°C for 24 h for complete swelling.

Optimisation of the Preparation

The preparation was set at its optimum antibacterial properties through the RSM. The experimental domain is defined as the antibacterial properties of the preparation. The three independent variables are acidity, honey concentrations (% w/v), and guar gum concentrations (% w/v), designated as X_1 , X_2 , and X_3 , respectively. The inhibition zone (mm) on *S. aureus* ATCC 6538 and *E. coli* ATCC 8739 were collected as the response variables designated as Y_1 and Y_2 , respectively. *S. aureus* and *E. coli* were selected because these species were commonly isolated from infected wounds and had various mechanisms of resistance towards antibacterial agents (Brudzynski & Sjaarda, 2014; Peacock & Paterson, 2015).

In each of the independent variables X_1 , X_2 , and X_3 , the optimum parameters were determined within the range set during the optimisation work. The details of the values set during the optimisation process are tabulated in Table 1. The low and high levels were set between pH of 3.5 and 6.5 for acidity (X_1), 50% and 90% (w/v) for honey concentration (X_2), and 1.0% and 2.0% (w/v) for the guar gum concentration (X_3), respectively. The axial points were obtained based on the range defined for low and high levels which used to obtain an efficient estimation of the quadratic model (Morshedi & Akbarian, 2014; Wang et al., 2011).

Table 1
Actual values of the independent variables for the optimisation process

Factor	Low-level axial point	Low-level factorial	Centre point	High-level factorial	High-level axial point
X_1 : pH	2.48	3.50	5.00	6.50	7.52
X_2 : Honey concentration (% w/v)	36.36	50.00	75.00	90.00	103.64
X_3 : Guar gum concentration (% w/v)	0.66	1.00	1.50	2.00	2.34

In this study, the RSM based on central composite design (CCD) was used to optimise the antibacterial properties of the preparation. According to the CCD, the total number of experimental combinations is based on Equation 1 below (Anitha & Pandey, 2016; Shekar et al., 2014):

$$2^k + 2k + n_0 \quad [1]$$

Where k is the number of independent variables and n_0 is the number of repetitions of the experiments at the central points. In this study, three independent variables were involved ($k = 3$) with five replicates at the centre points ($n_0 = 5$), leading to a total of nineteen runs. The details of the 19 experimental runs are tabulated in Table 2.

The Design of Experts Software (DOE version, 7.1.3, STAT-EASE Inc., Minneapolis, USA) was used for Analysis of Variance (ANOVA), regression, and graphical analyses of the data obtained. The regression model, three-dimensional response graph, and desirability function to get the optimum combinations of independent variables were plotted using the same software. In ANOVA, the analysis included overall model significance, correlation coefficient (R), and determination coefficient (R^2) that measure the goodness of fit of the regression model.

Table 2
Experimental design of the central composite design

Run	Factor		
	X_1 : pH	X_2 : Honey concentration (% w/v)	X_3 : Guar gum concentration (% w/v)
1	3.50	50.00	1.00
2	6.50	50.00	1.00
3	3.50	90.00	1.00
4	6.50	90.00	1.00
5	3.50	50.00	2.00
6	6.50	50.00	2.00
7	3.50	90.00	2.00
8	6.50	90.00	2.00
9	2.48	70.00	1.50
10	7.52	70.00	1.50
11	5.00	36.36	1.50
12	5.00	103.64	1.50
13	5.00	70.00	0.66
14	5.00	70.00	2.34
15	5.00	70.00	1.50
16	5.00	70.00	1.50
17	5.00	70.00	1.50
18	5.00	70.00	1.50
19	5.00	70.00	1.50

Measurement of Inhibition Zone

This assay was used during the optimisation process and after optimisation of the preparation process. In this assay, soy agar was used to grow *E. faecalis* and *S. pyogenes*, while nutrient agar was used to grow the remaining bacteria, i.e., *S. aureus*, *E. coli*, *P. aeruginosa*, *S. typhimurium*, *P. mirabilis*, and *K. pneumonia*. The nutrient and soy agar were prepared by dissolving 23 g and 40 g of agar powder to 1 L of distilled water and later autoclaved at the pressure of 100 kPa and temperature of 121°C for 20 min. The agars were allowed to cool down slightly and was poured into 90 mm × 15 mm (Brandon™, Malaysia) Petri dishes.

The working bacterial culture, which was adjusted to 0.5 McFarland bacteria concentration, was prepared. A volume of 100 µL of the adjusted 0.5 McFarland culture was spread onto the agar using the pour plate technique. Upon inoculation, 6 mm diameter wells were cut on the agar surface. The plate was divided into four quadrants, and a single well was created in each quadrant to contain 80 µL of the preparation. The plates were incubated at 37°C for 24 h. The inhibition zones diameters were measured in millimetres (mm), based on the diameter of the circles formed around the tested well areas in which the bacterial colonies did not grow. This diameter is inclusive of the 6 mm well diameter that was used to occupy the tested preparation. Each test was carried out in triplicate, and the average values were calculated.

Based on the inhibition zones measured, the sensitivity of bacteria towards the preparation was categorised as not sensitive, sensitive, very sensitive, and extremely sensitive, as previously described (Moussa et al., 2012). The not sensitive category was denoted by the diameter of inhibition zone of lower than 8 mm, sensitive for the diameter between 8 to 14 mm, very sensitive for the diameter between 15 to 19 mm, and extremely sensitive for the diameter of 20 mm and above.

Evaluation of the Optimal Preparation

The optimal preparation resulting from the optimisation process was evaluated in terms of physicochemical properties, antibacterial efficacy, and stability. This is essential to decide on adequate and reliable preparation.

Physicochemical Properties

The physicochemical properties of the optimal preparation were evaluated in terms of physical appearance, colour, homogeneity, grittiness, lump formation, viscosity, and pH. The viscosity was measured using Viscometer VL210001 (Fungilab, Spain), spindle number R5, at 100 rotations per min. Meanwhile, the pH was measured using the pH meter SevenCompact™ (Mettler Toledo, USA).

Centrifugation Test

The centrifugation test was performed using a refrigerated centrifuge 5810R (Eppendorf, Germany), as previously described by Dantas et al. (2016). It was performed by adding 10 g of the preparation in a tapered test tube and was subjected to a cycle of 151g for 30 min at 25°C.

Antibacterial Efficacy

The antibacterial efficacy of the optimal preparation was evaluated for its inhibition effect and bactericidal effect. For both evaluations, the experiments were performed on 22 bacterial species, including 8 standard strains and 14 clinical strains, as previously listed.

Measurement of Inhibition Zone. Prior to investigating the potency to inhibit bacterial growth, a study was conducted to measure the inhibition zone of bacterial strains when exposed to the preparation. This was performed qualitatively using the agar well diffusion assay, as previously described, to gain an understanding of the sensitivity of bacteria towards the preparation (Moussa et al., 2012; Sherlock et al., 2010). The diameters of the inhibition zone were measured in mm, including the diameter of the well created. Each test was carried out in triplicate, and the average values were calculated. The commercially available topical preparation formulated using manuka honey (MediHoney™) was used as the basis of comparison.

Bactericidal Effect. The bactericidal effect of the optimal preparation was determined using a tube dilution method, which was adapted from a previous antibacterial study (Shagana & Geetha, 2017). An equal volume of 0.5 mL of the preparation was mixed with 0.5 mL of freshly prepared broth in a screw cap tube (Jain et al., 2016; Shagana & Geetha, 2017). Then, a loopful of the test organism adjusted to 0.5 McFarland was transferred into the tube (Dewanjee et al., 2008). A tube containing 1 mL of broth and seeded with the test organism was used as a control. The prepared tubes were then incubated in the incubator shaker at 37°C and a rotational speed of 150 rpm for 24 h. After overnight incubation, a loopful suspension was suspended and inoculated onto freshly prepared Trypticase Soy Agar (TSA) using the streak plate method. Then, the plate was incubated for another 24 h in 37°C before being observed for bacterial growth. A plate with no visible bacterial growth (indicated by the formation of the bacterial colony) was considered to possess a bactericidal effect. In contrast, the plate with visible bacterial colony formation was considered to have no bactericidal effect.

Stability Study

Evaluation of the stability of the optimal preparation was adapted from previous studies (Chen et al., 2016; Dantas et al., 2016; Majumdar et al., 2018) with slight modification. The preparation was kept in glass containers and stored for long-term and accelerated conditions, i.e., at $25^{\circ}\text{C} \pm 2/60\% \pm 5$ relative humidity (RH) and $40^{\circ}\text{C} \pm 2/75\% \pm 5$ RH, respectively, for 6 months and evaluated at 0, 1, 2, 3, and 6 months. The storage conditions were set according to the International Council of Harmonisation of Technical Requirement for Pharmaceuticals for Human Use (ICH) guideline (World Health Organisation, 2018). The evaluations were observed based on the colour, pH, homogeneity, viscosity, and antibacterial efficacy, which were conducted similar to the procedures described in the previous sections. In the measurement of the inhibition zone and bactericidal effect, three Gram-positive strains, i.e., *S. aureus* ATCC 6538, *E. faecalis* ATCC, and *S. pyogenes*; and three Gram-negative strains, i.e., *E. coli* ATCC 8739, *K. pneumonia*, and *E. aerogenes* were considered.

RESULTS AND DISCUSSION

Optimisation of the Antibacterial Topical Preparation

A total of 19 runs were generated from RSM with different combination levels of pH, the concentration of honey, and the concentration of guar gum. The observed responses from each run are tabulated in Table 3.

Based on the findings, the inhibition zones measured ranged from 7.8 ± 0.00 mm to 14.6 ± 0.58 mm on *S. aureus* and 8.0 ± 0.58 mm to 14.5 ± 0.50 mm on *E. coli*. The largest zones of inhibition of 14.6 ± 0.58 mm and 14.5 ± 0.50 mm were measured on *S. aureus* and *E. coli*, respectively, in run number 9. In contrast, the smallest zones of inhibition of 7.8 ± 0.29 mm and 8.0 ± 0.58 mm were measured on *S. aureus* and *E. coli*, respectively, in run number 4.

The relationship between independent and response variables was determined through the application of multiple regression analysis on the experimental data to generate a second-order polynomial model. The generated models were described as Equation 2 and Equation 3 representing the analysis of data for *S. aureus* and *E. coli*, respectively.

$$Y_1 = 9.13 - 2.09X_1 + 0.51X_2 + 0.12X_3 - 0.11X_1X_2 + 0.34X_1X_3 + 0.31X_2X_3 + 0.76X_1^2 + 0.14X_2^2 + 0.07X_3^2 \quad [2]$$

$$Y_2 = 8.97 - 1.98X_1 + 0.48X_2 - 0.023X_3 - 0.57X_1X_2 + 0.25X_1X_3 + 0.20X_2X_3 + 0.96X_1^2 + 0.17X_2^2 + 0.15X_3^2 \quad [3]$$

The effect of pH (X_1) is more prominent in both equations compared to the concentration of honey (X_2) and guar gum concentration (X_3). This is due to the coefficient of X_1 with the value of 2.09, which is 4-fold and 17-fold higher than the coefficient of X_2 and X_3 , with values of 0.51 and 0.12 for Equation 2. This also applies to Equation 3 with a value of 1.98 for X_1 , which is 4-fold and 86-fold higher compared to X_2 and X_3 , with values of 0.48 and 0.023, respectively.

The significant impact of each term in the second-order polynomial equation was evaluated through ANOVA, and the results are tabulated in Table 4. The degree of significance for every term in the equation, including linear (X_1 , X_2 , X_3), quadratic (X_1^2 , X_2^2 , X_3^2), and combination (X_1X_2 , X_1X_3 and X_2X_3) were analysed at 95% confident interval (P -value < 0.05) (Ammer et al., 2016; Madiha et al., 2017).

Among the linear terms, the effects of pH (X_1) and honey concentration (X_2) on the inhibition zones were highly significant, as shown by their respective P -values, with P_{X_1} < 0.0001 and P_{X_2} = 0.0051 for *S. aureus*, and P_{X_1} < 0.0001 and P_{X_2} = 0.0067 for *E. coli*. In contrast, guar gum concentration (X_3) had an insignificant effect on the inhibition zones

Table 3
Responses for the experimental runs

Run	Factor			Response of inhibition zone (mm)	
	X_1	X_2	X_3	<i>S. aureus</i> (Y_1)	<i>E. coli</i> (Y_2)
1	3.50	50.00	1.00	12.7 ±0.58	12.3 ±1.04
2	6.50	50.00	1.00	7.8 ±0.29	8.5 ±0.58
3	3.50	90.00	1.00	12.8 ±0.76	13.7 ±0.00
4	6.50	90.00	1.00	7.8 ±0.29	8.0 ±0.58
5	3.50	50.00	2.00	11.0 ±0.50	10.7 ±0.58
6	6.50	50.00	2.00	7.8 ±0.00	8.3 ±0.58
7	3.50	90.00	2.00	12.7 ±0.58	13.3 ±0.29
8	6.50	90.00	2.00	8.7 ±0.58	8.2 ±0.29
9	2.48	70.00	1.50	14.6 ±0.58	14.5 ±0.50
10	7.52	70.00	1.50	7.8 ±0.00	8.5 ±0.58
11	5.00	36.36	1.50	8.2 ±0.76	8.3 ±0.29
12	5.00	103.64	1.50	10.7 ±0.58	10.2 ±0.58
13	5.00	70.00	0.66	8.5 ±0.58	8.7 ±0.58
14	5.00	70.00	2.34	10.0 ±0.00	9.7 ±0.50
15	5.00	70.00	1.50	8.7 ±0.58	8.5 ±0.58
16	5.00	70.00	1.50	9.7 ±0.58	9.0 ±0.00
17	5.00	70.00	1.50	9.3 ±0.58	9.3 ±0.58
18	5.00	70.00	1.50	9.0 ±0.00	8.8 ±1.04
19	5.00	70.00	1.50	9.0 ±1.00	9.3 ±0.58

The symbol ± represents the standard deviation, which was calculated between three biological replicates. Student's t-test shows significant differences for the data collected (P -value < 0.05)

Table 4
 Analysis of variance (ANOVA) of the quadratic model

Factors	Inhibition zone on <i>S. aureus</i>		Inhibition zone on <i>E. coli</i>	
	P-value	Model term	P-value	Model term
X_1	<0.0001	Significant	<0.0001	Significant
X_2	0.0051	Significant	0.0067	Significant
X_3	0.4100	Not Significant	0.8696	Not Significant
X_1X_2	0.5468	Not Significant	0.0110	Not Significant
X_1X_3	0.0931	Not Significant	0.1989	Not Significant
X_2X_3	0.1160	Not Significant	0.2961	Not Significant
X_1^2	0.0004	Significant	<0.0001	Significant
X_2^2	0.3332	Not Significant	0.2598	Not Significant
X_3^2	0.6233	Not Significant	0.3105	Not Significant
Model	<0.0001	Significant	<0.0001	Significant
Lack of fit	0.2028	Not significant	0.1413	Not significant

Significant at 5% level (P -value < 0.05)

for both *S. aureus* and *E. coli*, with $P_{X_3} = 0.4100$ and $P_{X_3} = 0.8696$, respectively. As for quadratic terms, only X_1^2 was significant for both *S. aureus* and *E. coli*, with $P_{X_1^2} = 0.0004$ for *S. aureus* and $P_{X_1^2} < 0.0001$ for *E. coli*. Meanwhile, X_2^2 and X_3^2 were insignificant with $P_{X_2^2} = 0.3332$ and $P_{X_3^2} = 0.6233$ for *S. aureus*, and $P_{X_2^2} = 0.2598$ and $P_{X_3^2} = 0.3105$ for *E. coli*. Meanwhile, none of the combination terms had a significant effect on the inhibition zones. The results suggest that pH and honey concentrations have a significant relationship with the inhibition zones, as a small variation in the values considerably altered the inhibition zone for both *S. aureus* and *E. coli*. The results are in agreement with previous studies in which pH and honey concentration influenced antibacterial properties of honey (Johnston et al., 2018; Kateel et al., 2018).

According to Table 4, results of the ANOVA demonstrated that the model was highly significant, with P -value < 0.0001 for both *S. aureus* and *E. coli*, indicating that the polynomial models, as expressed by Equation 2 and Equation 3, provide a reliable description of the responses. In addition, the ANOVA also showed a statistically insignificant lack of fit with P -value = 0.2028 and 0.1413 for *S. aureus* and *E. coli*, respectively, indicating an adequate prediction of responses by the model (Wang et al., 2011).

The coefficients of determination $R^2 = 0.9691$ and 0.9689, as described in Table 5, imply that the zone of inhibition is attributed to the given independent variables. The R^2 values indicate that 97% of the total variation is explained by the model, and the remaining 3% of unexplained conditions is contributed by unknown factors. The adjusted determination coefficients (adjusted $R^2 = 0.9697$ and 0.9689) are also high, indicating good accuracy and ability of the polynomial model to predict the response trend. It can be concluded that the second-order polynomial models are adequate to describe the inhibition

Table 5
Coefficient of correlation (R) and coefficient of determination (R^2) of the quadratic model

	Inhibition zone on <i>S. aureus</i>	Inhibition zone on <i>E. coli</i>
R^2	0.9691	0.9689
Adjusted R^2	0.9383	0.9379

zone with the response to pH, honey concentration, and guar gum concentration as the independent variables.

Response Surface Analysis

The interaction between independent variables; X_1X_2 , X_1X_3 , and X_2X_3 , as indicated in Equation 2 and Equation 3, can be visualised using 3D response surface and 2D contour plots, as shown in Figure 1 for *S. aureus* ATCC 6538 and Figure 2 for *E. coli* ATCC 8739. These plots are important to illustrate the effects of independent variables and their interactions on the response variables.

Figure 1 (a) and Figure 2 (a) show the 3D plots and their corresponding contour plots, showing the effect of pH (X_1) and honey concentration (X_2) on the inhibition zones of *S. aureus* and *E. coli*, while the concentration of guar gum (X_3) was fixed at its middle level, which was 1.5% (w/v). At pH between 3.5 and 6.5, the concentration of honey was directly proportional to the inhibition zone for both *S. aureus* and *E. coli* regardless of the pH level. In contrast, the pH was inversely proportional to the inhibition zone at any concentration of honey between 50% and 90% (w/v). The analysis of Figure 1 (a) and Figure 2 (a) showed that the optimal pH was at the lowest pH, i.e., at 3.5 and the honey concentration was at 90% (w/v) due to the largest inhibition zone estimated at these conditions. The finding is congruent with a study that reported the effectiveness of acidity in preventing bacterial growth (El-Kased et al., 2017). The reason for larger inhibition zones at strong acidic pH compared to neutral pH could be due to the unbecoming bacterial growth condition, which required pH between 6.6 to 7.0 (Jones et al., 2015). Furthermore, the antimicrobial properties of compounds such as flavonoids and phenolic acids available in kelulut honey were reported to increase at lower pH (Sanchez-Maldonado et al., 2011). As for the concentration of honey, the increased diameter of the inhibition zone with an increased concentration of honey can be explained by the increase in antibacterial compounds, such as phenolic acids and flavonoids, which increased as the concentration of honey increased (Bakar et al., 2017; Tuksitha et al., 2018). In addition, the degree of sugar content naturally present in kelulut honey will also lead to a potential increase in osmotic pressure to inhibit the growth of bacteria (Dluya, 2016). These findings are similar to the previous study that found a higher inhibition zone in response to increments of honey concentration used in honey-based preparations (El-Kased et al., 2017).

Figure 1 (b) and Figure 2 (b) depict the 3D plots and their corresponding contour plots showing the effects of pH (X_1) and guar gum concentration (X_3) on inhibition zones of *S. aureus* and *E. coli*, while the honey concentration was fixed at its middle level, i.e., at 70% (w/v). There was a lack of interaction between pH and guar gum concentration on the zones of inhibition. As the preparations were formulated with guar gum concentration between 1.0% and 2.0% (w/v), the zones of inhibition remained unchanged for both *S. aureus* and *E. coli*, regardless of the variation in pH level. Similarly, as the pH was increased from 3.5 to 6.5, the inhibition was decreased without being affected by guar

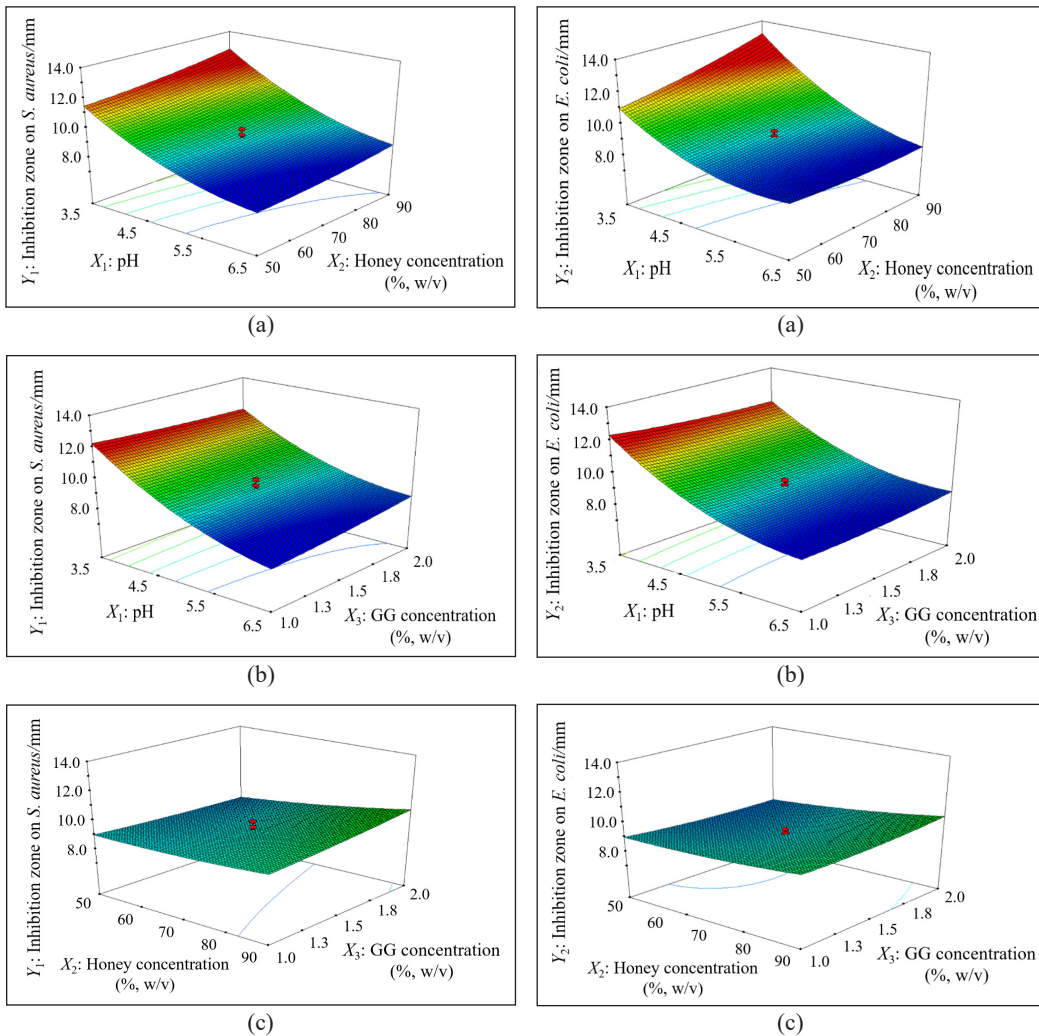


Figure 1. Response surface plot showing the effect of pH (X_1), honey concentration (X_2), and guar gum concentration (X_3) on inhibition zones against *S. aureus* ATCC 6538 (Y_1). (a) X_1X_2 , (b) X_1X_3 , and (c) X_2X_3

Figure 2. Response surface plot showing the effect of pH (X_1), honey concentration (X_2), and guar gum concentration (X_3) on inhibition zones against *E. coli* ATCC 8739 (Y_2). (a) X_1X_2 , (b) X_1X_3 , and (c) X_2X_3

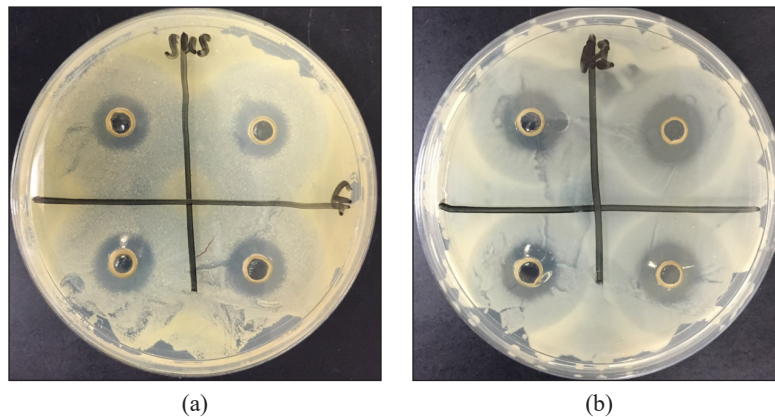


Figure 3. Formation of inhibition zone on: (a) *S. aureus* ATCC 6538; and (b) *E. coli* ATCC 8739 (right) in response to optimal preparation prepared using guar gum as polymeric agent

gum concentration. This indicates that the pH and guar gum concentration did not show any interaction affecting the zone of inhibition. The analysis of Figure 1 (b) and Figure 2 (b) revealed that there was no optimal concentration of guar gum in the inhibition zones of *S. aureus* and *E. coli*. The insignificant effect could be due to the use of a narrow range of guar gum concentration between 1% and 2%. Although the range has been reported to significantly affect the rheological properties of the preparation (Mulye et al., 2014), it does not significantly affect the zone of inhibition.

Figure 1 (c) and Figure 2 (c) present 3D plots and their corresponding contour plots showing the effect of honey concentration (X_2) and guar gum concentration (X_3) on the inhibition zones of *S. aureus* and *E. coli*, while the pH was fixed at its middle level, i.e., 5.0. Based on the results obtained, honey concentration is directly proportional to the inhibition zones of both *S. aureus* and *E. coli* regardless on the variation of guar gum concentrations between 1.0% and 2.0% (w/v). As for the guar gum concentration, the inhibition zones were consistent at any tested concentrations between 1.0% and 2.0% (w/v) regardless of the concentration of honey used. Thus, it can be concluded that there is a lack of interaction between the concentration of honey and guar gum in response to the inhibition zone.

According to the analysis, the inhibition zones of 12.7 mm for *S. aureus* and 13.1 mm for *E. coli* were predicted for the optimal preparation with pH of 3.5, the honey concentration of 90% (w/v), and guar gum concentration of 1.5% (w/v). The experiments were performed to verify the results, and the observed responses are tabulated in Table 6. Based on the conducted experiment, the inhibition zones obtained are 12.5 mm for *S. aureus* and 13.5 mm for *E. coli*, respectively (Figure 3). The results were congruent to the model's prediction, with the percentage of difference of 1.6% for *S. aureus* and 3.1% for *E. coli*, respectively. The findings confirmed the reliability of the models developed to predict the responses with less than 10% variation (Madiha et al., 2017; Shahzad et al., 2012).

Table 6
Summary of the predicted and observed responses for the optimal preparation

Factor	Optimal value			
pH	3.5			
Honey concentration (% w/v)	90			
Guar gum concentration (% w/v)	1.5			
Response	Predicted	Observed	Residual	Prediction error (%)
Inhibition zone on <i>S. aureus</i> (mm)	12.7	12.5	±0.2	1.6
Inhibition zone on <i>E. coli</i> (mm)	13.1	13.5	±0.4	3.1

Evaluations of the Optimal Preparation

The physicochemical properties of the optimal preparations were evaluated in terms of physical appearance, homogeneity, colour, grittiness, lump formation, pH, viscosity, and centrifugation test. The results are tabulated in Table 7.

Table 7
Physicochemical properties of the optimal preparation

Formulation	Guar gum
Physical appearance	Opaque
Homogeneity	Homogeneous
Colour	Dark brown
Grittiness	No
Lump formation	No
pH	3.53 ± 0.70
Viscosity at 100rpm (cps)	2470 ± 120.1
Centrifugation Test	No phase separation observed

The symbol \pm represents the standard deviation which was calculated between three biological replicates.

The preparation resulted in opaque, homogeneous, and dark brown colour, as shown in Figure 4. No grittiness and formation of the lump were observed in the preparation. The pH of the preparation was recorded at 3.53 ± 0.70 . The pH recorded can be considered suitable for topical preparation, as the pH ranging between 2.8 and 7.4 was acceptable for therapeutic effect with non-irritant effect on human skin (Dantas et al., 2016; Panther & Jacob, 2015).

The viscosity of the preparation was measured at 2470 ± 120.1 cps. The viscosity was within the range that was sufficient for good spreadability and clarity. The viscosity appropriate for topical preparation was recorded between 512 and 15000 cps (Chen et al., 2016; Pande et al., 2014; Singh et al., 2013).



Figure 4. Physical appearance of the optimal preparations prepared using guar gum



(a)



(b)

Figure 5. Appearance of the preparations: (a) before; and (b) after centrifugation test

The centrifugation test was also conducted to evaluate the gravitational effect on the preparation. This is essential to analyse the adequate quality and stability of the preparation (Dimeski et al., 2011; Iradhati & Jufri, 2017). Based on the results obtained, no noticeable instability was observed on the optimal preparation upon spinning at 151g for 30 min at 25°C. The preparation remained intact without phase separation, indicating adequate and stable formulation (Figure 5).

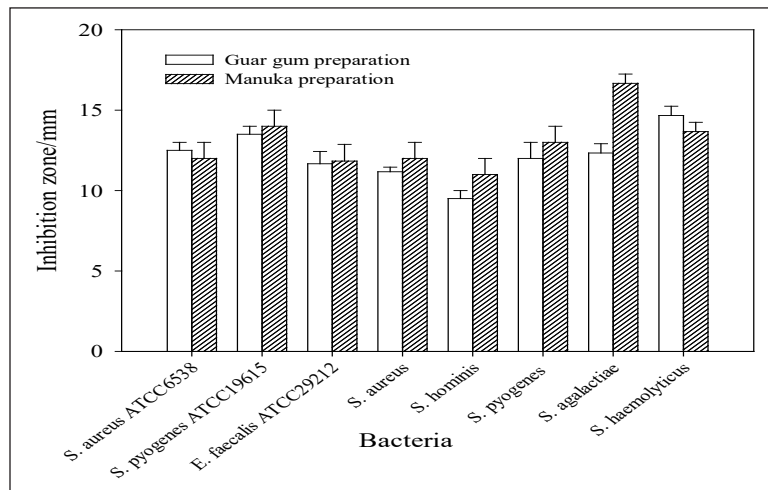
Antibacterial Efficacy

The antibacterial efficacy of the optimal preparation was evaluated through the measurement of the inhibition zone and formation of a bacterial colony to indicate the presence of bacteriostatic and bactericidal of the preparation.

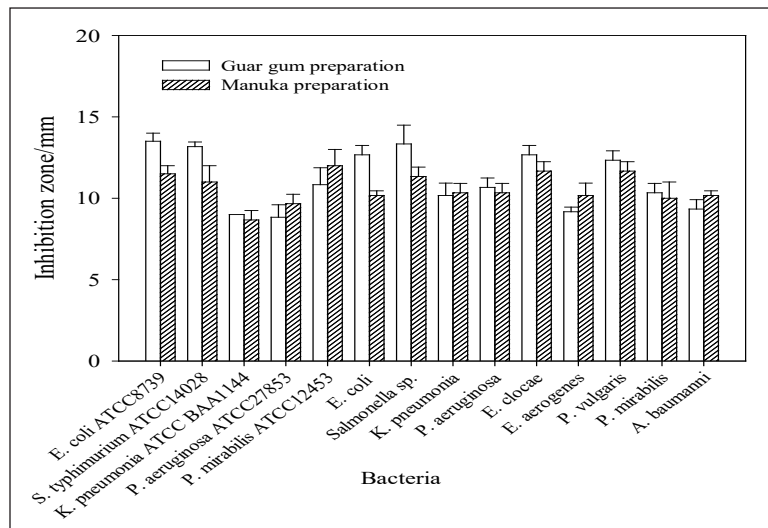
Measurement of Inhibition Zone. The results for the inhibition zone measurements are shown in Figure 6 (a) for Gram-positive, and Figure 6 (b) for Gram-negative bacteria. The range of inhibition zone measured for the optimal preparation was between 8.8 ± 0.76 mm and 14.7 ± 0.58 mm, indicating that the bacteria reacted as sensitive towards the preparation. The lowest inhibition zone was measured on *P. aeruginosa* ATCC 27853, while the largest inhibition zone was measured on *S. haemolyticus*.

In the commercially available preparation using manuka, the inhibition zone was measured in the range between 8.7 ± 0.58 mm and 16.7 ± 0.58 mm, with the smallest inhibition zone measured on *K. pneumonia*, while the largest on *S. agalactiae*, respectively. Based on the range of inhibition zones measured, the tested bacteria reacted between sensitive to very sensitive towards the manuka preparation.

In comparison with the guar gum preparation, none of the inhibition zones measured was larger than the manuka preparation for Gram-positive bacteria. Whereas for Gram-negative bacteria, out of 14 species, the preparation using guar gum showed the inhibition zone of 9.0 ± 0.00 mm and 12.7 ± 0.58 mm on *K. pneumonia* ATCC BAA 1144 and *E. cloacae*, which were 1.03 and 1.09-fold larger compared to manuka, with the inhibition zones of 8.7 ± 0.58 mm and 11.7 ± 0.58 mm, respectively. The remaining 12 species of Gram-negative bacteria were inhibited with larger inhibition zones by manuka preparation.



(a)



(b)

Figure 6. The inhibition zone measured by the preparations tested against the standard laboratory and clinical isolated bacteria of: (a) Gram-positive; and (b) Gram-negative. Error bars symbolise the errors calculated from three biological replicates. One sample t-test represent significant differences between the mean of the sampled population and the hypothesised population mean (P -value < 0.05)

Bactericidal Effect. An attempt was made to investigate the ability of the preparation to kill bacteria through the formation of a bacterial colony. The results are tabulated in Table 8 for Gram-positive, and Table 9 for Gram-negative, respectively.

In the 22 tested bacteria, no formation of the bacterial colony was observed on the surface of agar for guar gum preparation after 24 h of incubation, indicating the presence of bactericidal effect (Dewanjee et al., 2008; Shagana & Geetha, 2017). Figure 7 and Figure 8 show the absence of bacterial colony on the surface of agar tested on Gram-positive (*S.*

Table 8
The results on formation of bacterial colony for Gram-positive

	Formation of bacterial colony		
	Guar gum	Manuka	Control (broth only)
Standard strain			
<i>S. aureus</i> ATCC6538	No	No	Yes
<i>S. pyogenes</i> ATCC19615	No	No	Yes
<i>E. faecalis</i> ATCC29212	No	Yes	Yes
Clinical isolated strain			
<i>S. aureus</i>	No	No	Yes
<i>S. hominis</i>	No	No	Yes
<i>S. pyogenes</i>	No	No	Yes
<i>S. agalactiae</i>	No	No	Yes
<i>S. haemolyticus</i>	No	No	Yes

Table 9
The results on formation of bacterial colony for Gram-negative bacteria

	Formation of bacterial colony		
	Guar gum	Manuka	Control (broth only)
Standard strain			
<i>E. coli</i> ATCC 8739	No	No	Yes
<i>S. typhimurium</i> ATCC14028	No	No	Yes
<i>K. pneumonia</i> ATCCBAA1144	No	No	Yes
<i>P. aeruginosa</i> ATCC27853	No	No	Yes
<i>P. mirabilis</i> ATCC12453	No	No	Yes
Clinical isolated strain			
<i>E. coli</i>	No	No	Yes
<i>Salmonella sp.</i>	No	No	Yes
<i>K. pneumonia</i>	No	No	Yes
<i>P. aeruginosa</i>	No	No	Yes
<i>E. clocae</i>	No	No	Yes
<i>E. aerogenes</i>	No	No	Yes
<i>P. vulgaris</i>	No	No	Yes
<i>P. mirabilis</i>	No	No	Yes
<i>A. baumannii</i>	No	No	Yes

aureus, *E. faecalis* ATCC 29212, *S. hominis*, and *S. haemolyticus*) and Gram-negative (*E. coli*, *P. aeruginosa*, *Salmonella* sp., and *K. pneumonia*) bacteria, respectively. Similar results were demonstrated by the preparation of manuka, except on *E. faecalis* ATCC

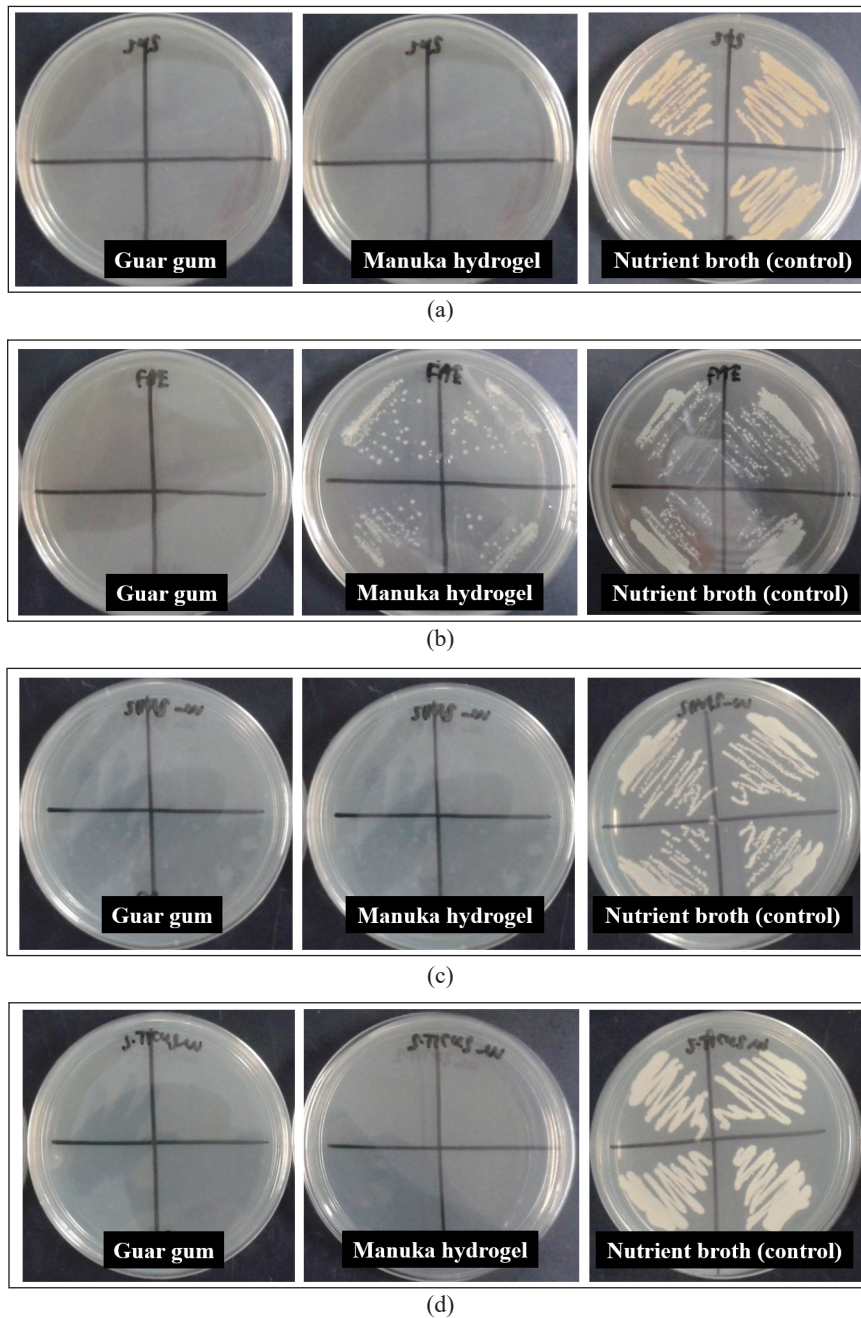


Figure 7. The results on formation of bacterial colony on the surface of agar for Gram-positive bacteria: (a) *S. aureus*; (b) *E. faecalis* ATCC 29212; (c) *S. hominis*; and (d) *S. haemolyticus*.

29212, where the formation of bacterial colonies was observed. The ability of *E. faecalis* to survive could be due to the development of a resistant mechanism, such as biofilm formation to combat the effectiveness of antibacterial agent (Gopinath & Prakash, 2013).

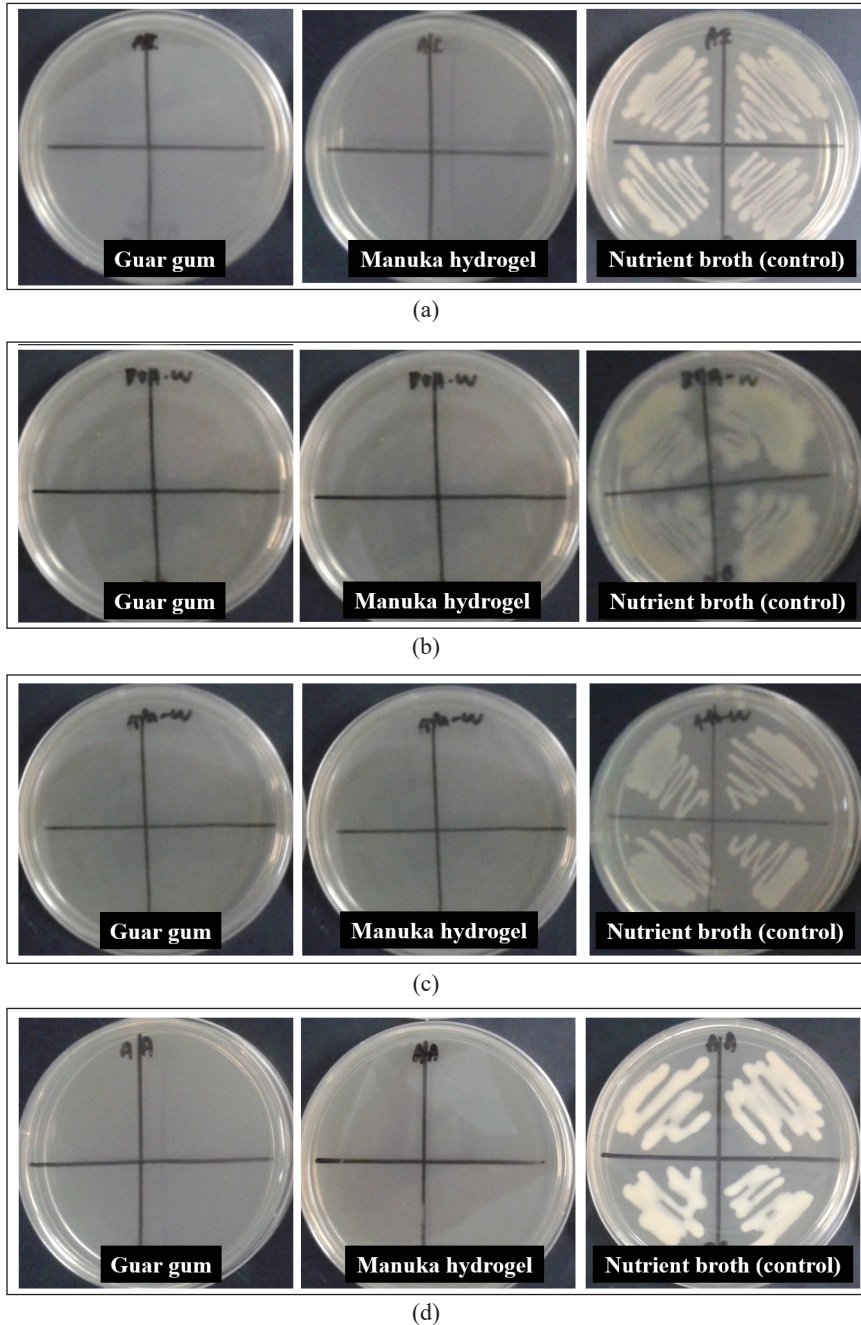


Figure 8. The results on formation of bacterial colony on the surface of agar for Gram-negative bacteria: (a) *E. coli*; (b) *P. aeruginosa*; (c) *Salmonella sp.*; and (d) *K. pneumonia*

The outcome was similar to those obtained from a previous study (Mohd-Aspar & Edros, 2019), which reported the highest concentration of manuka honey at 25% (w/v) required to kill *E. faecalis* compared to other bacterial species. In the control sample, where the bacteria were cultured in broth alone, the formation of bacteria colonies was observed for all 22 bacteria, indicating the absence of a bactericidal effect.

In many types of acute and chronic wounds, *S. aureus* and *P. aeruginosa* are usually isolated from infected wounds (Negut et al., 2018; Serra et al., 2015). These bacteria often cause biofilm development and chronic infections that may suppress immune activities and promote the development of antibiotic-resistant strains (Serra et al., 2015). Similar to *S. aureus* and *P. aeruginosa*, other wound-associated bacteria such as *E. coli*, *S. pyogenes*, *E. faecalis*, and *P. mirabilis* can also develop biofilms, antimicrobial inactivating enzymes, and other resistance mechanisms to eliminate the antibacterial action (Kim et al., 2018; Lu et al., 2014). In this study, 22 wound-associated bacteria, which include standard laboratory and clinical strains isolated from infected wounds, have been tested and were found to be susceptible to the preparation. This was proven by the formation of inhibition zone and the presence of bactericidal effect for both preparations against the tested bacteria. The results indicate that guar gum was effective in conveying the kelulut honey as a topical preparation without compromising its antibacterial properties.

Stability Study. The stability study was conducted by keeping the preparation at an extended period ($25^{\circ}\text{C} \pm 2/60\% \pm 5 \text{ RH}$) and accelerated storage ($40^{\circ}\text{C} \pm 2/75\% \pm 5 \text{ RH}$) conditions for six months. The physicochemical properties, i.e., colour, homogeneity, pH, and viscosity, and antibacterial efficacy (inhibition zone and formation of the bacterial colony) of the preparation was determined at 0, 1, 2, 3, and 6 months.

Physicochemical Properties. The results for the physicochemical properties of the preparation are shown in Table 10 for colour, homogeneity, and pH, and Figure 9 for viscosity, respectively. According to the results obtained, the colour, homogeneity, and pH of the preparation after six months of storage remained unchanged. The pH of the guar gum preparation was measured to be in the range between 3.41 ± 0.10 and 3.53 ± 0.10 . The difference between the lowest and highest pH levels was 4%. The ability to maintain the fundamental physicochemical properties indicates adequate and reliable preparation (Chen et al., 2016).

The viscosity of the guar gum preparation was inversely proportional with time. The highest viscosity of $2470 \pm 174.4 \text{ cps}$ for the long-term and $2533 \pm 285.0 \text{ cps}$ for the accelerated storage were measured at 0 months, respectively. After six months of storage, the lowest viscosity of $1247 \pm 130.5 \text{ cps}$ for the long-term and $800 \pm 200.0 \text{ cps}$ for the accelerated storage were recorded, respectively. The variation in viscosity between

Table 10

The results for colour, homogeneity, and pH during six months stability test of the preparation

	Long term - 25°C ± 2/60% RH ± 5					Accelerated - 40°C ± 2/75% RH ± 5				
	Months					Months				
	0	1	2	3	6	0	1	2	3	6
Color	Dark brown					Dark brown				
Homogeneity	Homogeneous					Homogeneous				
pH	3.53 ±0.06	3.51 ±0.06	3.52 ±0.07	3.47 ±0.06	3.43 ±0.04	3.47 ±0.17	3.45 ±0.10	3.43 ±0.08	3.45 ±0.09	3.41 ±0.10

The symbol ± represents the standard deviation which calculated between three biological replicates. Student's t-test shown significant differences for the pH-value measured.

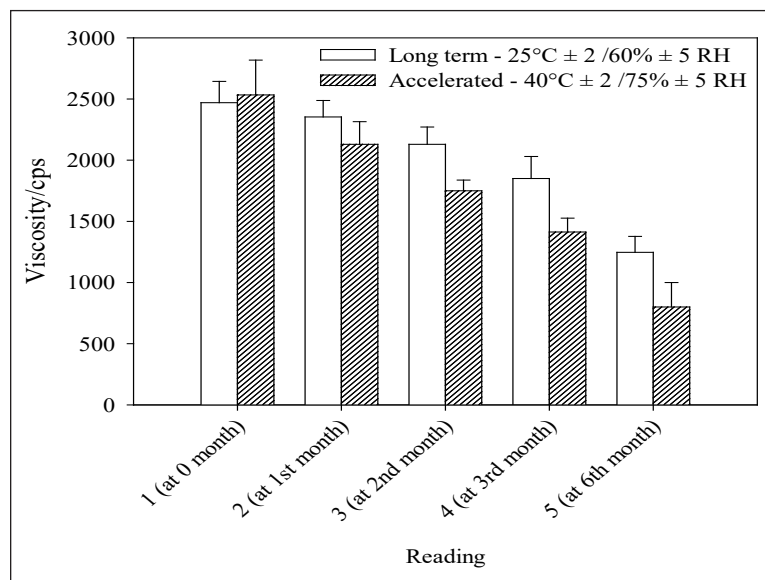


Figure 9. Viscosity of the preparation during the six-month of stability study after been stored at long term (25°C ± 2/60% ± 5 RH) and accelerated (40°C ± 2/75% ± 5 RH) storing conditions. Error bars symbolise the errors calculated from three biological replicates. Student's t-test shown significant differences for the data collected

measurements at 0 month and sixth month was 50% for the long-term and 68% for the accelerated storage.

A continuous reduction in viscosity within the six months of stability study, as demonstrated by the guar gum preparation, indicate an unstable preparation. This could be due to incomplete dispersal or solubility of guar gum to form a stable structure that resulted from the limited amount of water (Hemendrasinh & Dhruti, 2015) due to the reaction of guar gum molecules that compete with sugar for water availability (Mudgil et al., 2014). The temperature is another factor that affects the stability of the guar gum solution. The prolonged heat of guar gum solution may result in thermal degradation that leads to unstable

solubilisation of the guar gum (Mudgil et al., 2014; Yagoub & Nur, 2013). In this study, as the guar gum preparation was stored in extreme storage, the viscosity of the preparation was reduced, indicating an unstable preparation. The outcome is in congruent with the previous study that reported an unstable viscosity of guar gum preparation at high temperature (Yagoub & Nur, 2013). Storage at the ambient temperature (25°C) is considered sufficient for maintaining the viscosity of the guar gum preparation over long-term.

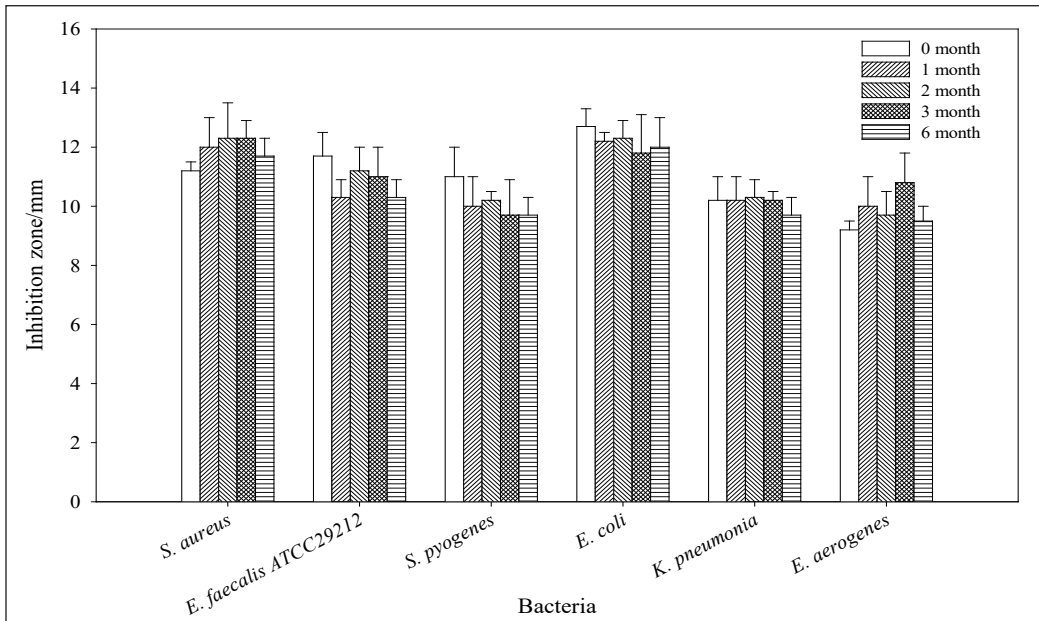
Antibacterial Efficacy. The antibacterial efficacy of the preparation within the six months of stability study was evaluated through the measurement of inhibition zone and formation of a bacterial colony. The measurement of the inhibition zone on Gram-positive and Gram-negative bacteria are shown in Figure 10 (a) and Figure 10 (b), respectively. Meanwhile, the results for the formation of the bacterial colony are tabulated in Table 11.

The inhibition zone measured for guar gum preparation ranged from 9.0 ± 0.00 mm to 12.8 ± 1.30 mm. The zone of inhibition showed an average variation of 7.8% between the initial and final measurements within the six-month stability study. As for the formation of a bacterial colony, the preparation remained valid to prevent the formation of the bacterial colony within the six months of the stability study. Based on the outcomes obtained from both evaluations, the efficacy of the preparation remained effective without a deficiency, indicating a stable and reliable preparation capable of maintaining its antibacterial properties over time (Irish et al., 2011).

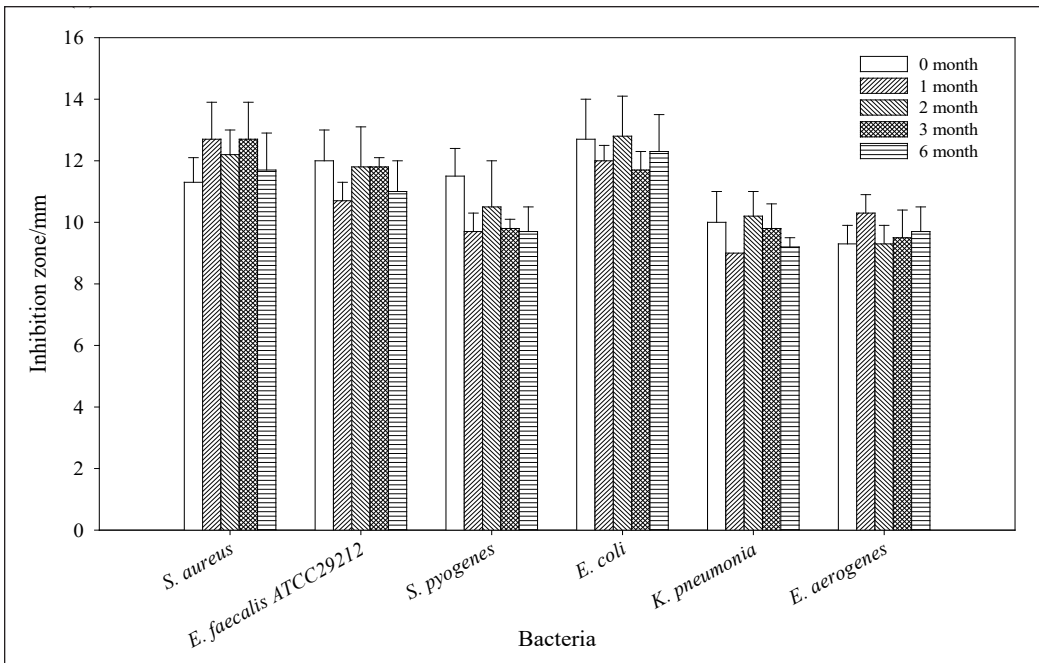
The synergistic interaction is considered positive if the therapeutic effect initially present in the preparation remains uninterrupted. The results indicated that the preparation prepared in this study is capable of retaining the antibacterial properties, as proven by the identical inhibition zone and bactericidal effect. The uninterrupted antibacterial properties could be explained by the stable polymeric agent to maintain the crosslinking network and uniformed dispersion of honey across the preparation (Sharma et al., 2015; Zhu et al., 2019). In addition, the interactions between the charges of the polymeric agent, i.e.,

Table 11
Bactericidal effect for the six-month of stability study for the optimal preparation

	Long-term 25°C ± 2 /60% ± 5 RH					Accelerated 40°C ± 2/75% ± 5 RH				
	Months					Months				
	0	1	2	3	6	0	1	2	3	6
<i>S. aureus</i>	Yes	Yes	Yes	Yes	Yes	Yes	Yes	Yes	Yes	Yes
<i>E. faecalis</i> ATCC 29212	Yes	Yes	Yes	Yes	Yes	Yes	Yes	Yes	Yes	Yes
<i>S. pyogenes</i>	Yes	Yes	Yes	Yes	Yes	Yes	Yes	Yes	Yes	Yes
<i>E. coli</i>	Yes	Yes	Yes	Yes	Yes	Yes	Yes	Yes	Yes	Yes
<i>K. pneumoniae</i>	Yes	Yes	Yes	Yes	Yes	Yes	Yes	Yes	Yes	Yes
<i>E. aerogenes</i>	Yes	Yes	Yes	Yes	Yes	Yes	Yes	Yes	Yes	Yes



(a)



(b)

Figure 10. Measurement of inhibition zone for the optimal preparation using guar gum after stored in: (a) long-term and $-25^{\circ}\text{C} \pm 2 / 60\% \pm 5 \text{ RH}$; and (b) accelerated $-40^{\circ}\text{C} \pm 2 / 75\% \pm 5 \text{ RH}$ storage conditions. Error bars symbolise the errors calculated from three biological replicates. One sample t-test represent significant differences between the mean of the sampled population and the hypothesised population mean ($P\text{-value} < 0.05$)

guar gum loaded with honey and the charges on the surface of the bacterial membrane formed a contact (Kaith et al., 2015) that allow the compounds such as phenolic acids and flavonoids to promote cell disruption and lysis to kill the bacteria (Henriques et al., 2010; Henriques et al., 2011). A similar finding with the positive synergistic effect of honey in preparation that led to more than 95% of drug release was demonstrated by the previous study (El-Kased et al., 2017).

CONCLUSION

The use of guar gum as a polymeric agent was appropriate for the preparation of kelulut honey as a topical preparation. The optimal preparation was finalised at pH 3.5, honey concentration of 90% (w/v), and guar gum concentration of 1.5% (w/v). The optimal preparation demonstrated reliable physicochemical properties, and most importantly, the potent antibacterial properties, including both bacteriostatic and bactericidal effects were retained on the 22 bacteria species after the honey was converted to a topical preparation. However, within the six months of stability study, the viscosity of the preparation was reduced to more than 50% between the initial (0 month) and final (6 months) measurements. Consideration of the addition of stabilising or preservative agent is recommended to overcome the reduction of viscosity over time.

ACKNOWLEDGEMENT

The authors would like to thank the Ministry of Education Malaysia in providing the fund for this project under the Fundamental Research Grant Scheme (FRGS; Grant Number: FRGS/1/2017/STG05/UMP/02/5) and Postgraduate Research Grant Scheme (PGRS190358), Universiti Malaysia Pahang (UMP) for the research facilities and IIUMC for providing the clinical bacterial strains.

REFERENCES

- Ammer, R. M., Zaman, S., Khalid, M., Bilal, M., Erum, S., Huang, D., & Che, S. (2016). Optimization of antibacterial activity of *Eucalyptus tereticornis* leaf extracts against *Escherichia coli* through response surface methodology. *Journal of Radiation Research and Applied Sciences*, 9(4), 376-385. doi: <https://doi.org/10.1016/j.jrras.2016.05.001>
- Anitha, G., & Pandey, V. P. (2016). Review on: Statistical designs and response surface methodology (RSM) as a tool for the optimization of HPLC methods. *International Journal of Pharmacy and Analytical Research*, 5(4), 552-569.
- Bakar, M. F. A., Sanusi, S. B., Bakar, F. I. A., Cong, O. J., & Mian, Z. (2017). Physicochemical and antioxidant potential of raw unprocessed honey from Malaysian stingless bees. *Pakistan Journal of Nutrition*, 16(11), 888-894. doi: <https://doi.org/10.3923/pjn.2017.888.894>

- Boukraâ, L. (Ed.). (2014). *Honey in traditional and modern medicine*. New York, USA: Taylor & Francis Group. doi: <https://doi.org/10.1201/b15608>
- Brudzynski, K., & Sjaarda, C. (2014). Antibacterial compounds of Canadian honeys target bacterial cell wall inducing phenotype changes, growth inhibition and cell lysis that resemble action of β -Lactam antibiotics. *PLoS One*, 9(9), 1-11. doi: <https://doi.org/10.1371/journal.pone.0106967.g003>
- Chen, M. X., Alexander, K. S., & Baki, G. (2016). Formulation and evaluation of antibacterial creams and gels containing metal ions for topical application. *Journal of Pharmaceutics*, 2016, 1-10. doi: <https://doi.org/10.1155/2016/5754349>
- Dantas, M. G. B., Reis, S. A. G., Damasceno, C. M. D., Rolim, L. A., Rolim-neto, P. J., Carvalho, F. O., ... & Almeida, J. R. G. da S. (2016). Development and evaluation of stability of a gel formulation containing the monoterpene borneol. *The Scientific World Journal*, 2016, 1-5. doi: <https://doi.org/10.1155/2016/7394685>
- Dewanjee, S., Maiti, A., Majumdar, R., Majumdar, A., & Mandal, S. C. (2008). Evaluation of antimicrobial activity of hydroalcoholic extract *Schima wallichii* bark. *Pharmacologyonline*, 1, 523-528.
- Dimeski, G., Solano, C., Petroff, M. K., & Hynd, M. (2011). Centrifugation protocols: Tests to determine optimal lithium heparin and citrate plasma sample quality. *Annals of Clinical Biochemistry*, 48(3), 218-222. doi: <https://doi.org/10.1258/acb.2010.010230>
- Dluya, T. (2016). Critical review: Antioxidant properties and antibiotic mechanism of honey against infectious diseases. *International Journal of Advances in Life Science and Technology*, 2, 16-24. doi: <https://doi.org/10.18488/journal.72/2015.2.2/72.2.16.24>
- El-Kased, R. F., Amer, R. I., Attia, D., & Elmazar, M. M. (2017). Honey-based hydrogel: *In vitro* and comparative *in vivo* evaluation for burn wound healing. *Scientific Reports*, 7(1), 1-11. doi: <https://doi.org/10.1038/s41598-017-08771-8>
- Franklin, R. C., Matthew, A. W., Jeff, A., Michael, N. D., George, M. E., Mary, J. F., ... & Barbara, L. Z. (2012). *Methods for dilution antimicrobial susceptibility tests for bacteria that grow aerobically: Approved standard — Ninth Edition* (Vol. 32). Wayne, USA. Retrieved July 20, 2020, from https://mafiadoc.com/download/methods-for-dilution-antimicrobial-susceptibility-tests-_5a19a8801723dd4f2ac359bc.html
- Gopinath, R., & Prakash, M. (2013). Antibacterial activity of three medicinal plants against clinically isolated multidrug resistant *Enterococcus faecalis* (MDRE). *International Journal of Current Microbiology and Applied Sciences*, 2(2), 6-14.
- Hemendrasinh, J. R., & Dhruvi, P. M. (2015). A review on pharmaceutical gel. *International Journal of Pharmaceutical Sciences*, 1(1), 33-47.
- Henriques, A. F., Jenkins, R. E., & Burton, N. F. (2010). The intracellular effects of manuka honey on *Staphylococcus aureus*. *European Journal of Clinical Microbiology & Infectious Diseases*, 29(1), 45-50. doi: <https://doi.org/10.1007/s10096-009-0817-2>
- Henriques, A. F., Jenkins, R. E., & Burton, N. F. (2011). The effect of manuka honey on the structure of *Pseudomonas aeruginosa*. *European Journal of Clinical Microbiology & Infectious Diseases*, 30(2), 167-171. doi: <https://doi.org/10.1007/s10096-010-1065-1>

- Iradhati, A. H., & Jufri, M. (2017). Formulation and physical stability test of Griseofulvin microemulsion gel. *International Journal of Applied Pharmaceutics*, 9(1), 7-10. doi: https://doi.org/10.22159/ijap.2017.v9s1.22_27
- Irish, J., Blair, S., & Carter, D. A. (2011). The antibacterial activity of honey derived from Australian flora. *PLoS One*, 6(3), 1-9. doi: <https://doi.org/10.1371/journal.pone.0018229>
- Ismail, W. I. W. (2016). A review on beekeeping in malaysia history, importance and future direction. *Journal of Sustainability Science and Management*, 11(2), 70-80.
- Jain, S., Rathod, N., Nagi, R., Sur, J., Laheji, A., Gupta, N., ... & Prasad, S. (2016). Antibacterial effect of aloe vera gel against oral pathogens: An in-vitro study. *Journal of Clinical and Diagnostic Research*, 10(11), 41-44. doi: <https://doi.org/10.7860/JCDR/2016/21450.8890>
- Jalil, M. A. A., Kasmuri, A. R., & Hadi, H. (2017). Stingless bee honey, the natural wound healer: A review. *Skin Pharmacology and Physiology*, 30(2), 66-75. doi: <https://doi.org/10.1159/000458416>
- Johnston, M., McBride, M., Dahiya, D., Owusu-apenten, R., & Nigam, P. S. (2018). Antibacterial activity of Manuka honey and its components: An overview. *AIMS Microbiology*, 4(4), 655-664. doi: <https://doi.org/10.3934/microbiol.2018.4.655>
- Jones, E. M., Cochrane, C. A., & Percival, S. L. (2015). The effect of pH on the extracellular matrix and biofilms. *Advances in Wound Care*, 4(7), 431-439. doi: <https://doi.org/10.1089/wound.2014.0538>
- Kaith, B. S., Sharma, R., & Kalia, S. (2015). Guar gum based biodegradable, antibacterial and electrically conductive hydrogels. *International Journal of Biological Macromolecules*, 75(April), 266-275. doi: <https://doi.org/10.1016/j.ijbiomac.2015.01.046>
- Kateel, R., Bhat, G., Baliga, S., Augustine, A. J., Ullal, S., & Adhikari, P. (2018). Antibacterial action of tropical honey on various bacteria obtained from diabetic foot ulcer. *Complementary Therapies in Clinical Practice*, 30(1), 29-32. doi: <https://doi.org/10.1016/j.ctcp.2017.11.001>
- Kim, C., Wilkins, K., Bowers, M., Wynn, C., & Ndegwa, E. (2018). Influence of pH and temperature on growth characteristics of leading foodborne pathogens in a laboratory medium and select food beverages. *Austin Food Sciences*, 3(1), 1-8.
- Lu, J., Turnbull, L., Burke, C. M., Liu, M., Carter, D. A., Schlothauer, R. C., ... & Harry, E. J. (2014). Manuka-type honeys can eradicate biofilms produced by *Staphylococcus aureus* strains with different biofilm-forming abilities. *Peer J*, 2(326), 1-25. doi: <https://doi.org/10.7717/peerj.326>
- Madiha, I. Y., Rukayadi, Y., & Norhayati, H. (2017). Effects of extraction conditions on yield, total phenolic contents and antibacterial activity of methanolic *Cinnamomum zeylanicum* blume leaves extract. *International Food Research Journal*, 24, 779-786.
- Majumdar, S., Roy, S., Gupta, R., & Khatun, N. (2018). Strategy for improving skin permeation by using topical nanoparticulate gel of aloe vera and in-vivo evaluation using wistar rats. *International Journal of Scientific and Research Publications*, 8(2), 323-339.
- Mohd-Aspar, M. A. S., & Edros, R. Z. (2019). Antibacterial properties of kelulut, tualang and acacia honey against wound-infecting bacteria. *Journal of Tropical Agricultural Science*, 42(4), 1185-1208.

- Morshedi, A., & Akbarian, M. (2014). Application of response surface methodology: Design of experiments and optimization: A mini review. *Indian Journal of Fundamental and Applied Life Sciences*, 4(S4), 2434-2439.
- Moussa, A., Noureddine, D., Mohamed, H. S., & Abdelmelek, M. (2012). Antibacterial activity of various honey types of Algeria against *Staphylococcus aureus* and *Streptococcus pyogenes*. *Asian Pacific Journal of Tropical Medicine*, 5(10), 773-776. doi: [https://doi.org/10.1016/S1995-7645\(12\)60141-2](https://doi.org/10.1016/S1995-7645(12)60141-2)
- Mudgil, D., Barak, S., & Khatkar, B. S. (2014). Guar gum: Processing, properties and food applications - A review. *Journal of Food Scientist & Technologists*, 51(3), 409-418.
- Mulye, S. P., Wadkar, K. A., & Kondawar, M. S. (2014). Formulation development and evaluation of Indomethacin emulgel. *Pelagia Research Library*, 4(5), 31-45.
- Negut, I., Grumezescu, V., & Grumezescu, A. M. (2018). Treatment strategies for infected wounds. *Molecules*, 23(9), 1-23. doi: <https://doi.org/10.3390/molecules23092392>
- Pande, V., Patel, S., Patil, V., & Sonawane, R. (2014). Design expert assisted formulation of topical bioadhesive gel of Sertaconazole Nitrate. *Advanced Pharmaceutical Bulletin*, 4(2), 121-130. doi: <https://doi.org/10.5681/apb.2014.019>
- Panther, D. J., & Jacob, S. E. (2015). The importance of acidification in atopic eczema: An underexplored avenue for treatment. *Journal of Clinical Medicine*, 4(5), 970-978. doi: <https://doi.org/10.3390/jcm4050970>
- Peacock, S. J., & Paterson, G. K. (2015). Mechanisms of methicillin resistance in *Staphylococcus aureus*. *Annual Review of Biochemistry*, 84(1), 577-601. doi: <https://doi.org/10.1146/annurev-biochem-060614-034516>
- Sanchez-Maldonado, A. F., Schieber, A., & Ganzle, M. G. (2011). Structure–function relationships of the antibacterial activity of phenolic acids and their metabolism by lactic acid bacteria. *Journal of Applied Microbiology*, 111(5), 1176-1184. doi: <https://doi.org/10.1111/j.1365-2672.2011.05141.x>
- Serra, R., Grande, R., Butrico, L., Rossi, A., Francesco, U., Settimio, ... & Francisisc, S. de. (2015). Chronic wound infections: The role of *Pseudomonas aeruginosa* and *Staphylococcus aureus*. *Expert Review of Anti-Infective Therapy*, 13(5), 605-613. doi: <https://doi.org/10.1586/14787210.2015.1023291>
- Shagana, J. A., & Geetha, R. (2017). Comparative analysis of antimicrobial activity of black tea, green tea and white tea extracts on *Streptococcus mutans* by tube dilution method. *Journal of Pharmaceutical Sciences and Research*, 9(9), 1581-1582.
- Shahzad, Y., Afreen, U., Shah, S. N. H., & Hussain, T. (2012). Applying response surface methodology to optimize nimesulide permeation from topical formulation. *Pharmaceutical Development and Technology*, 18(6), 1391-1398. doi: <https://doi.org/10.3109/10837450.2012.723721>
- Sharma, R., Kaith, B. S., Kalia, S., Pathania, D., Kumar, A., Sharma, N., ... & Schauer, C. (2015). Biodegradable and conducting hydrogels based on Guar gum polysaccharide for antibacterial and dye removal applications. *Journal of Environmental Management*, 162, 37-45. doi: <https://doi.org/10.1016/j.jenvman.2015.07.044>
- Shekar, P., Kumar, K. S., Jabasingh, S. A., Radhakrishnan, M., & Balagurunathan, R. (2014). Optimization of medium components for antibacterial metabolite production from marine *Streptomyces* sp. PUA2 using response surface methodology. *International Journal of Pharmacy and Pharmaceutical Sciences*, 6(7), 6-11.

- Sherlock, O., Dolan, A., Athman, R., Power, A., Gethin, G., Cowman, S., & Humphreys, H. (2010). Comparison of the antimicrobial activity of Ulmo honey from Chile and Manuka honey against methicillin-resistant *Staphylococcus aureus*, *Escherichia coli* and *Pseudomonas aeruginosa*. *BMC Complementary and Alternative Medicine*, 10(1), 1-5. doi: <https://doi.org/10.1186/1472-6882-10-47>
- Singh, M. P., Nagori, B. P., Shaw, N. R., Tiwari, M., & Jhanwar, B. (2013). Formulation development & evaluation of topical gel formulations using different gelling agents and its comparison with marketed gel formulation. *International Journal of Pharmaceutical Erudition*, 3(3), 1-10.
- Tan, H. T., Rahman, R. A., Gan, S. H., Halim, A. S., Hassan, S. A., Sulaiman, S. A., & Kirmpal-Kaur, B. S. (2009). The antibacterial properties of Malaysian tualang honey against wound and enteric microorganisms in comparison to manuka honey. *BMC Complementary and Alternative Medicine*, 9(1), 1-8. doi: <https://doi.org/10.1186/1472-6882-9-34>
- Tuksitha, L., Chen, Y. S., Chen, Y., Wong, K., & Peng, C. (2018). Antioxidant and antibacterial capacity of stingless bee honey from Borneo (Sarawak). *Journal of Asia-Pacific Entomology*, 21(2), 563-570. doi: <https://doi.org/10.1016/j.aspen.2018.03.007>
- Wang, Y., Fang, X., An, F., Wang, G., & Zhang, X. (2011). Improvement of antibiotic activity of *Xenorhabdus bovienii* by medium optimization using response surface methodology. *Microbial Cell Factories*, 10(1), 1-15. doi: <https://doi.org/10.1186/1475-2859-10-98>
- World Health Organisation. (2018). *WHO expert committee on specification for pharmaceutical preparations*. Geneva, Switzerland. Retrieved July 20, 2020, from <https://apps.who.int/iris/bitstream/handle/10665/272452/9789241210195-eng.pdf?ua=1>
- Yaacob, M., Rajab, N. F., Shahar, S., & Sharif, R. (2018). Stingless bee honey and its potential value: A systematic review. *Food Research*, 2(2), 124-133. doi: [https://doi.org/10.26656/fr.2017.2\(2\).212](https://doi.org/10.26656/fr.2017.2(2).212)
- Yagoub, N. A. G. A., & Nur, A. I. M. (2013). The influence of thermal treatment on physical properties of guar gum. *International Journal of Innovations in Pharmaceutical Sciences*, 2(6), 26-31.
- Zhu, T., Mao, J., Cheng, Y., Liu, H., Lv, L., Ge, M., ... & Lai, Y. (2019). Recent progress of polysaccharide-based hydrogel interfaces for wound healing and tissue engineering. *Advanced Materials Interfaces*, 6(17), 1-22. doi: <https://doi.org/10.1002/admi.201900761>

Identification and Antibiotic Resistance Profile of *Salmonella* spp. and *Citrobacter* spp. Isolated from Street-Vended Beverages

Siti Shahara Zulfakar^{1*}, Noraziah Mohamad Zin², Siti Nur Shafika Mat Zalami² and Nur Syakirah Mohd Nawawee¹

¹Environmental Health and Industrial Safety Program, Centre for Toxicology & Health Risk Studies, Faculty of Health Sciences, Universiti Kebangsaan Malaysia, 50300 UKM, Kuala Lumpur, Malaysia

²Programme of Biomedical Science, Faculty of Health Sciences, Universiti Kebangsaan Malaysia, 50300 UKM, Kuala Lumpur, Malaysia

ABSTRACT

The risk of foodborne diseases as well as the dissemination of antibiotic resistant bacteria increases with the consumption of street-vended food and beverages. This study investigated the prevalence of *Salmonella* spp. and *Citrobacter* spp. in street-vended beverages sold in Chow Kit, Kuala Lumpur, Malaysia. The Kirby-Bauer disk diffusion method was used to identify the antibiotic resistance profile of *Salmonella* spp. and *Citrobacter* spp. isolates towards 11 selected antibiotics. Six beverage samples were found positive for presumptive *Salmonella* spp. and *Citrobacter* spp. Upon confirmation via Microgen kit and PCR biochemical testing methods, only one isolate was confirmed to be *Salmonella enterica* serovar Derby while the other isolates were identified as *Citrobacter* spp. (n= 12; 2 isolates from each positive beverage sample). The antibiogram test showed that 58.3%, 16.7%, and 8.3% of the strains tested were resistance to tetracycline, cephalixin, and

ampicillin respectively, while all isolates were fully resistant toward penicillin and erythromycin. The isolate with the highest MAR index (0.45) was S23₁, with resistance to five of the tested antibiotics (penicillin, erythromycin, tetracycline, cephalixin, and ampicillin). Seven isolates had a MAR index of 0.27 and were resistant to three antibiotics, while the remaining four isolates had the lowest MAR index (0.18) and were resistant to only two antibiotics. This study shows that street-vended beverages have a

ARTICLE INFO

Article history:

Received: 22 July 2020

Accepted: 07 October 2020

Published: 22 January 2021

DOI: <https://doi.org/10.47836/pjst.29.1.31>

E-mail addresses:

sitishahara.zulfakar@ukm.edu.my (Siti Shahara Zulfakar)

noraziah.zin@ukm.edu.my (Noraziah Mohamad Zin)

fikasha096@gmail.com (Siti Nur Shafika Mat Zalami)

nursyakirah_mn@yahoo.com (Nur Syakirah Mohd Nawawee)

* Corresponding author

high risk of spreading antibiotic-resistant bacteria to the public and that *Citrobacter* spp. should be considered as emerging multidrug-resistant bacteria in the food production system.

Keywords: Antibiotic resistance, beverage, *Citrobacter* spp., *Salmonella* spp., street-vendor

INTRODUCTION

Ready-to-eat food and beverages sold by street hawkers are known as street-vended foods. Street food has been gaining popularity worldwide due to its unique taste, variety, and low price (Shagufta et al., 2017). Street hawkers commonly sell their food products in small stalls, portable tables, food trucks, or pushcarts (Das et al., 2010). However, the consumption of street-vended food and beverages increases the risk of foodborne diseases (Tambekar et al., 2009). There are many concerns surrounding the safety of street-vended food prepared by hawkers. In particular, street-vended food and drinks are usually synonymous with poor facilities. Besides, the hawkers do not have any environmental controls such as temperature and humidity control to guarantee the security or safety of their food products (Nawawee et al., 2019).

Food handlers are the primary source of contamination for foodborne diseases, as they can easily spread the bacteria to the food, especially via the faecal-oral route, open wounds, and dirty food contact surfaces (Abdul-Mutalib et al., 2015). In Malaysia, of every 100000 individuals, roughly 60.28 cases have been diagnosed with food and waterborne diseases, with typhoid fever being the most predominant (Woh et al., 2017). *Salmonella* spp. is a known foodborne pathogen that could also be found in drinking water and natural water resources (De Cesare, 2018; Shagufta et al., 2017; Tunung et al., 2007). In contrast, *Citrobacter* spp. are more commonly known as an opportunistic, nosocomial infection-causing microorganism that can be found in animal and human gastrointestinal, respiratory, and urinary tracts, and also in water and soil environments and food products (Trivedi et al., 2015). Although the presence of *Citrobacter* spp. in food products may not be routinely monitored due to its low incidence in Malaysia, this microorganism has been implicated in foodborne outbreaks elsewhere (Aminharati et al., 2019; Pletz et al. 2018; Tschape et al., 1995).

Bacterial infections can usually be treated with antibiotics. However, many bacterial strains have developed antibiotic resistance. Past studies in Malaysia have reported a high percentage of antibiotic resistance in pathogens isolated from food samples (Bahri et al., 2019; Chin et al., 2018; Odeyami & Sani, 2016; Tunung et al., 2007). The seriousness of this issue was further propounded by the World Health Organisation (WHO) declaring antibiotic resistance to be one of the most important public health threats of the 21st century.

This study tested for the presence of *Salmonella* spp. and *Citrobacter* spp. in drinks sold in the Chow Kit district in Kuala Lumpur, Malaysia. Presumptive isolates were then

confirmed via biochemical testing followed by 16S rRNA PCR and sequencing to further identify the bacteria. Then, the isolates' antimicrobial resistance to selected antibiotics was assessed.

MATERIALS AND METHODS

Sample Collection

Sampling procedures were as described in our previous study (Nawawee et al., 2019). Chow Kit, Kuala Lumpur, Malaysia was chosen as the sampling site due to its popularity among the locals and tourist for its markets and trading bazars. The sampling location was also located within 1 km distance from the research laboratory. The sample inclusion criteria were the drinks were kept in uncapped container before being poured into small plastic bags with ties cups purchased by the customer. This study did not include bottled, pre-packaged, or canned drinks. There were 17 street vendors that sold beverages that fitted these criteria. A total of 31 beverages comprising fresh fruit juice (sugarcane, coconut, watermelon) (n = 11), cordial-based drinks (n = 11), and milk-based drinks (n = 9) were purchased. Each sample were purchased on different days between 10-11 am. The drinks bought were kept in their normal packaging, placed in an icebox at 4°C, then moved to the laboratory and examined within the same day.

Experimental Procedures

All beverage samples were subjected to bacterial isolation of using culture method (Chong et al., 2017a; Thung et al., 2018). Presumptive isolates obtained from this method were then confirmed via Gram-staining procedures, a series of biochemical test as well as species identification via Polymerase Chain Reaction (PCR) method. All isolates were also subjected to antibiotic susceptibility test to determine the presence of resistant bacteria in the beverage samples.

Bacterial Isolation from Beverage Samples

Isolation of presumptive *Salmonella* spp. and *Citrobacter* spp. were conducted based on methods by Chong et al. (2017a) and Thung et al. (2018) with some modifications. First, 10 ml of the samples were homogenized with an equivalent volume of buffered peptone water (BPW) (Merck, Germany). A pre-enrichment step was then conducted, involving a 20-hr incubation of the sample at 37°C. Next, 10 ml of Rappaport-Vassiliadis soy broth (RVS broth) (Merck, Germany) was prepared to which a 0.1 ml aliquot of the pre-enriched samples were added. The mixture was then vortexed followed by a 24-hr incubation at 41.5°C. This step was followed with streaking a loopful of the enriched suspension onto Xylose Lysine Deoxycholate (XLD) agar (Merck, Germany) in triplicates, and 24-hr

incubation at 37°C. All black colonies or red colonies with black centres were considered as positive results in this study. Two colonies from each positive beverage sample were further analysed. For further analysis, isolated colonies were streaked onto Nutrient Agar (Merck, Germany) followed by 24-hr incubation at 37°C. A standard Gram-staining procedure was also conducted on the isolates.

Biochemical Test

Biochemical test for confirmation of the presumptive isolates was done using a Microgen GN-ID (GN A + B) system (Microgen Bioproducts Ltd, UK) in accordance with the manufacturer's procedure. In brief, a single colony from an 18–24 hr culture on Nutrient Agar was emulsified in 0.85% saline. A total of 0.1 ml of the bacterial suspension was then added to each well of the microwell test strips and incubated at 37°C for 18–24 hours. Additional reagents were added, and all colour changes were recorded according to the colour code provided by the manufacturer. Interpretations of the result and species identification were made using Microgen ID Software (MID-60).

Identification of Isolates via Polymerase Chain Reaction (PCR)

All isolates were grown in Nutrient Agar (Merck, Germany) for 18–24 hours at 37°C. DNA from the overnight culture was extracted using the boiling method (Zulfakar et al., 2019). A few loopful of bacterial culture were inoculated into 500 µl sterile distilled water. The suspension was then boiled at 95°C for 10 minutes, and quickly cooled at -20°C freezer for 10 minutes. Then, the suspension was centrifuged at 12 000 ×g for 5 minutes. The purity of the DNA template was determined by using a NanoDrop spectrophotometer (Thermoscientific, Model 2000) at $A_{260/280}$ and $A_{260/230}$. The supernatant containing DNA was used as the DNA template solution for PCR.

The 16S rDNA PCR was conducted using the universal primers, 27f (5'-AGA GTT TGA TCC TGG CTG AG-3') and 1492r (5'-GGT TAC CTT GTT ACG ACT T-3'), with the expected base pair of 1380 bp (Suardana, 2014). Amplification was carried out in a 50 µl reaction mixtures containing 5 µl of each primer, 25 µl of 1 X PCR Master Mix (First Base Asia, Singapore), 5 µl DNA template and 10 µl sterile distilled water. Next, amplification was applied on the mixture for 35 cycles, in a thermal cycler (Thermo Fisher Scientific, USA). Before the first cycle, the mixture was denatured for 2 min at 94°C. Each cycle comprised 1 min denaturation at 94°C, 1 min annealing at 45°C, 2 min elongation at 72°C, and a 10 min final elongation at 72°C. Next, 3 µl of the amplified PCR products were electrophoresed on 1% (wt/vol) agarose gel at 70 V for 30 minutes, pre-stained with non-ethidium bromide nucleic acid stain (First Base Asia), and then visualised under UV light using a UV transilluminator. The amplified products were then sent to First Base Sdn. Bhd., Malaysia, for DNA sequencing. The sequencing results were interpreted and

compared with the NCBI database using Basic Local Alignment Search Tool (BLAST) software.

Antibiotic Susceptibility Test

Standard Kirby-Bauer disc diffusion method (CLSI, 2012) was used to determine the antibiotic susceptibility of the isolates. First, 3-5 isolated colonies from a 24 hrs culture at 37°C on Nutrient Agar were chosen for each bacterial strain and transferred into 5 ml Mueller Hinton broth (Merck, Germany). The broth was then incubated at 37°C for 2 hrs and the turbidity of the culture were determined using a light spectrophotometer (PRIM 3649 Secomam, France) at 625nm. Then, the cultures with optical density readings between 0.08-0.13 nm were swabbed with a sterile cotton swab on Mueller Hinton Agar (MHA) plates (Merck, Germany) and left to dry for approximately 2 minutes. Following that, antibiotic discs were placed on the plates. The antibiotics tested were erythromycin (15 µg, E15), penicillin (10 µg, P10), chloramphenicol (30 µg, C30), sulfamethoxazole-trimethoprim (25 µg, SXT25), tetracycline (30 µg, TE30), amoxicillin (25 µg, AML25), ampicillin (10 µg, AMP10), cephalexin (30 µg, CL30), cefoxitin (30 µg, FDX30), cefotaxime (30 µg, CTX30), and ceftriaxone (30 µg, CRO30). After 24 hrs of incubation at 37°C, the isolates were rated as susceptible, intermediate, or resistant based on the measured inhibition zones. Finally, the formula below (Krumperman, 1983; Al-Dulaimi et al., 2019) was used to determine the multiple antibiotic resistance (MAR) index for each resistance pattern:

Multiple antibiotic resistance (MAR) index =

$$\frac{\text{Number of antibiotics to which a particular isolate was resistant (a)}}{\text{Total number of antibiotics tested (b)}}$$

RESULTS AND DISCUSSION

Out of 31 beverage samples tested, only 6 (19%) beverage samples were found positive for presumptive *Salmonella* and *Citrobacter* spp. based on the early identification on XLD agar. All positive samples showed pale to red colonies with black pigmentation in the centre of the colony. Although we have previously reported that milk-based drinks had the highest average total viable counts as compared to the other beverages (Nawawee et al., 2019), all of the milk-based drinks tested negative for both species in the current study. Meanwhile, cordial-based drinks and fruit juices each contributed three positive samples. Detection of pathogenic enterobacteriaceae bacteria have been reported in previous studies (Parish, 2008; Tribst et al., 2009). As fruits used to produce juices commonly do not undergo any heat treatments, therefore it is easily contaminated by microorganisms thus contaminating the beverages to be sold. Contamination of fruit juices could also occur due

to cross-contamination from the juice extractors and as well as utensils used to prepare the beverages (Chong et al., 2017b). Other possible sources that may contribute to the different results between the three type of beverages could be due to the handling practices by the street-vendors themselves as these beverages were bought from different street-vendors. Knowledge and application of safe food handling practices by the food handlers are essential in maintain the safety of food products sold to the consumers (Odeyami et al., 2019).

Gram-staining procedure confirmed that all strains are Gram-negative bacteria. Upon confirmation using the biochemical testing procedure with the commercial kit, it was identified that only 1 out of the 12 isolates was *Salmonella* spp. whereas the other isolates were positively identified as *Citrobacter* spp. (Table 1). Identification via the 16S rDNA PCR method further confirmed these results (Table 2). The isolated *Salmonella* strain was identified as *Salmonella enterica* subsp. *enterica* serovar Derby, whereas the other isolates were identified as *Citrobacter werkmanii* (9 isolates) and *Citrobacter freundii* (1 isolate), while the exact species for the remaining *Citrobacter* isolates are unknown.

Three critical characteristics are essential in the differentiation of *Salmonella* spp. colonies from *Citrobacter* spp. colonies on XLD agar; the ability to ferment xylose, the production of hydrogen sulphide, and the presence of lysine decarboxylase activity. Both *Salmonella* spp. and *Citrobacter* spp. are xylose fermenters that will cause acidification of the media to occur, causing the colour of the medium to change to yellow. Production of hydrogen sulphide would occur in *Salmonella* spp. and some *Citrobacter* spp., indicated by the presence of black pigmentation at the centre of the colonies. Lysine decarboxylase activities in *Salmonella* spp. strains will lead to cadaverine built-up causing alkalisation, thus neutralising the acidic condition caused by xylose degradation; hence, changing the media's colour back to red. The absence of this lysine decarboxylase reaction would cause the media colour to remain yellow (Powell & Marcon, 2012; Reller, 2012).

The presence of *Salmonella* spp. and *Citrobacter* spp. in street-vended beverages sold in the Chow Kit area may be attributed to the use of contaminated water sources that the vendors use to prepare their products (Levantesi et al., 2012). These microorganisms can be present as biofilm in the water distribution system and may be dispersed when the water from this distribution system is used to make beverages, as well as to wash vending utensils (Nemo et al., 2017). Lack of a freshwater supply system at every stall as observed in this study has forced some of the vendors to obtain their water supply elsewhere and they tend to keep any water they have in containers near the stall. If the safety of the stored water is not maintained, it can become contaminated. Apart from that, microorganisms could also be present in the edible ice served together with the beverages sold (Sunday et al., 2011).

Lack of hygienic control of the vending site and its surrounding area could also be one of the contributing factors of the presence of these microorganisms. We have reported previously that the cleanliness of the vending sites is not up to par (Nawawee et al., 2019). We also observed that the presence of uncovered trash cans was common at all stalls, which,

Table 1
Result for isolate identification by using Microgen GN-ID A+B kit

Sample ID	Test	Motility	Lysine	Ornithine	H ₂ S	Glucose	Mannitol	Xylose	ONPG	Indole	Urea	VP	Citrate	TDA	Gelatin	Malonate	Inositol	Sorbitol	Rhamnose	Sucrose	Lactose	Arabinose	Adonitol	Raffinose	Salicin	Arginine	Organism Ident.
DK ₃		+	+	+	+	+	+	+	-	-	-	-	+	-	-	-	-	+	+	-	-	+	-	-	-	+	<i>Salmonella enterica</i> Group 1
S13 ₂		+	-	-	+	+	+	+	+	-	+	-	+	-	-	+	-	-	+	-	-	-	-	-	-	+	<i>Citrobacter</i> spp.
S13 ₃		+	-	-	+	+	+	+	+	-	+	-	+	-	-	+	-	-	+	-	-	-	-	-	-	+	<i>Citrobacter</i> spp.
S22 ₁		+	-	-	+	+	+	+	+	-	+	-	+	-	-	+	-	-	+	-	-	-	-	-	-	+	<i>Citrobacter</i> spp.
S22 ₂		+	-	-	+	+	+	+	+	-	+	-	+	-	-	+	-	-	+	-	-	-	-	-	-	+	<i>Citrobacter</i> spp.
S23 ₁		+	-	-	+	+	+	+	+	-	+	-	+	-	-	+	-	-	+	-	-	-	-	-	-	+	<i>Citrobacter</i> spp.
S23 ₂		+	-	-	+	+	+	+	+	-	+	-	+	-	-	+	-	-	+	-	-	-	-	-	-	+	<i>Citrobacter</i> spp.
S27 ₂		+	-	-	+	+	+	+	+	-	+	-	+	-	-	+	-	-	+	-	-	-	-	-	-	+	<i>Citrobacter</i> spp.
S27 ₃		+	-	-	+	+	+	+	+	-	+	-	+	-	-	+	-	-	+	-	-	-	-	-	-	+	<i>Citrobacter</i> spp.
S29		+	-	-	+	+	+	+	+	-	+	-	+	-	-	+	-	-	+	-	-	-	-	-	-	+	<i>Citrobacter</i> spp.
S29 ₁		+	-	-	+	+	+	+	+	-	+	-	+	-	-	+	-	-	+	-	-	-	-	-	-	+	<i>Citrobacter</i> spp.
S30 ₂		+	-	-	+	+	+	+	+	-	+	-	+	-	-	+	-	-	+	-	-	-	-	-	-	+	<i>Citrobacter</i> spp.
CP		+	-	-	+	+	+	+	+	-	+	-	+	-	-	+	-	-	+	-	-	-	-	-	-	-	<i>Citrobacter</i> spp.

+: positive; -: negative; H₂S: Hydrogen sulphide; VP: Voges Proskauer; TDA: Tryptophan

Table 2
Bacterial identification of isolates via 16S rDNA PCR method

Isolate ID	Bacterial species	% Ident.
DKI ₃	<i>Salmonella enterica</i> subsp. <i>enterica</i> serovar Derby strain SeqrSC0080 16S ribosomal RNA gene, partial sequence	99.20%
S13 ₂	<i>Citrobacter werkmanii</i> strain BF-6, complete genome	99.93%
S13 ₃	<i>Citrobacter freundii</i> strain F-CF1 16S ribosomal RNA gene, partial sequence	99.39%
S22 ₁	<i>Citrobacter werkmanii</i> strain BF-6, complete genome	99.78%
S22 ₂	<i>Citrobacter werkmanii</i> strain BF-6, complete genome	99.71%
S23 ₁	<i>Citrobacter werkmanii</i> strain BF-6, complete genome	99.70%
S23 ₂	<i>Citrobacter werkmanii</i> strain BF-6, complete genome	99.93%
S27 ₂	<i>Citrobacter werkmanii</i> strain BF-6, complete genome	99.85%
S27 ₃	<i>Citrobacter sp.</i> UIWRF1266 16S ribosomal RNA gene, partial sequence	98.18%
S29	<i>Citrobacter werkmanii</i> strain BF-6, complete genome	99.70%
S29 ₁	<i>Citrobacter werkmanii</i> strain BF-6, complete genome	99.93%
S30 ₂	<i>Citrobacter werkmanii</i> strain BF-6, complete genome	99.85%

in turn, attracted pests such as flies to the area; thus disseminating microorganisms to the entire stall and inevitably to the beverages as well. The location of these vending sites at the roadside, the lack of adequate facilities for the vendors to wash their hands and to clean their vending area, and the lack of food hygiene practices among the vendors as observed by this study, will further expose the sold products to the risk of contamination as supported with findings by Andargie et al. (2008), Levantesi et al. (2012), and Odeyami et al. (2019).

Capita and Alonso-Calleja (2013) pointed out a major concern regarding the transmission of resistant bacteria through the food supply chain. Moreover, based on the results of the antibiotic susceptibility testing, all tested *Salmonella* and *Citrobacter* isolates showed resistance to penicillin and erythromycin (Table 3). Figure 1 shows a representative

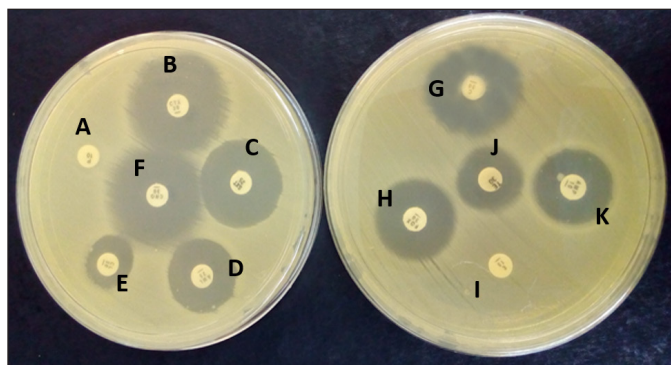


Figure 1. Antibiotic susceptibility testing result for S29₁ (*Citrobacter werkmanii*). A- Penicillin; B-Ceftriaxone; C- Trimethoprim-sulfamethoxazole; D-Ampicilin; E- Tetracycline; F- Cefotaxime; G-Chloramphenicol; H-Amoxycilin; I- Erythromycin; J- Cephalexin; K- Cefoxitin.

Table 3
Inhibition zone diameter (mm) for each isolates towards selected antibiotics

Isolate ID	E15	CRO30	CL30	SXT25	P10	AML25	CTX30	C30	FDX30	AMP10	TE30
DK I ₃	0 (R)	29 (S)	20 (S)	17 (S)	0 (R)	26 (S)	30 (S)	21 (S)	23 (S)	17 (S)	0 (R)
S13 ₂	0 (R)	30 (S)	16 (I)	26 (S)	0 (R)	21 (S)	32 (S)	24 (S)	21 (S)	18 (S)	8 (R)
S13 ₃	0 (R)	29 (S)	15 (I)	23 (S)	0 (R)	19 (S)	30 (S)	24 (S)	19 (S)	17 (S)	13 (I)
S22 ₁	0 (R)	29 (S)	15 (I)	25 (S)	0 (R)	20 (S)	30 (S)	20 (S)	19 (S)	18 (S)	11 (R)
S22 ₂	0 (R)	30 (S)	13 (R)	26 (S)	0 (R)	20 (S)	30 (S)	24 (S)	19 (S)	16 (S)	15 (S)
S22 ₃	0 (R)	31 (S)	14 (I)	27 (S)	0 (R)	23 (S)	31 (S)	24 (S)	21 (S)	18 (S)	10 (R)
S23 ₁	0 (R)	25 (S)	12 (R)	29 (S)	0 (R)	18 (S)	29 (S)	24 (S)	20 (S)	12 (R)	11 (R)
S23 ₂	0 (R)	30 (S)	14 (I)	27 (S)	0 (R)	21 (S)	30 (S)	26 (S)	20 (S)	17 (S)	10 (R)
S27 ₁	0 (R)	27 (S)	14 (I)	24 (S)	0 (R)	21 (S)	31 (S)	24 (S)	20 (S)	19 (S)	12 (I)
S27 ₂	0 (R)	30 (S)	14 (I)	25 (S)	0 (R)	19 (S)	31 (S)	25 (S)	21 (S)	15 (I)	17 (S)
S27 ₃	0 (R)	27 (S)	14 (I)	25 (S)	0 (R)	20 (S)	31 (S)	24 (S)	20 (S)	14 (I)	11 (R)
S29	0 (R)	28 (S)	14 (I)	24 (S)	0 (R)	20 (S)	30 (S)	23 (S)	20 (S)	19 (S)	16 (S)
S29 ₁	0 (R)	33 (S)	16 (I)	26 (S)	0 (R)	24 (S)	32 (S)	26 (S)	22 (S)	20 (S)	8 (R)
S29 ₂	0 (R)	29 (S)	16 (I)	25 (S)	0 (R)	22 (S)	30 (S)	24 (S)	21 (S)	15 (I)	8 (R)
S30	0 (R)	30 (S)	16 (I)	24 (S)	0 (R)	21 (S)	29 (S)	27 (S)	23 (S)	19 (S)	12 (I)
S30 ₂	0 (R)	32 (S)	18 (S)	30 (S)	0 (R)	28 (S)	36 (S)	24 (S)	24 (S)	14 (I)	18 (S)

E15: Erythromycin; CRO30: Ceftriaxone; CL30: Cephalaxin; SXT25: Trimethoprim-sulfamethoxazole; P10: Penicillin; AML25: Amoxicillin; CTX30: Cefotaxime; C30: Chloramphenicol; FDX30: Cefoxitin; AMP10: Ampicillin; TE30: Tetracycline.
(R): resistant; (I): Intermediate; (S): susceptible

Table 4
Antibiotic resistance profile for all tested bacterial isolates (n= 12)

Antibiotic	Bacterial isolates antibiogram profile	
	Resistant (%)	Sensitive (%)
Penicilin (P10)	12 (100)	0 (0)
Erythromycin (E15)	12 (100)	0 (0)
Ampicillin (AMP10)	1 (8.3)	11 (91.7)
Tetracycline (TE30)	7 (58.3)	5 (41.7)
Cephalexin (CL30)	2 (16.7)	10 (83.3)
Amoxicillin (AML25)	0 (0)	12 (100)
Chloramphenicol (C30)	0 (0)	12 (100)
Trimetoprim-sulfamethoxazole (SXT25)	0 (0)	12 (100)
Cefoxitin (FDX30)	0 (0)	12 (100)
Cefotaxime (CTX30)	0 (0)	12 (100)
Ceftriaxone (CRO30)	0 (0)	12 (100)

Table 5
Multiple Antibiotic Resistance (MAR) Index profile of tested bacterial isolates (n=12)

Isolate ID	Antibiotic Resistance Profile	MAR Index
S13 ₃ , S27 ₂ , S29, S30 ₂	E15, P10	0.18
S22 ₂	E15, P10, CL30	0.27
DKI ₃ , S13 ₂ , S22 ₁ , S23 ₂ , S27 ₃ , S29 ₁	E15, P10, TE30	0.27
S23 ₁	E15, P10, TE30, CL30, AMP10	0.45

E15: Erythromycin (15 µg); P10: Penicillin (10 µg); CL30: Cephalexin (30 µg); TE30: Tetracycline (30 µg); AMP10: Ampicillin (10 µg)

sample of the conducted antibiotic susceptibility testing. In particular, seven (58.3%) isolates were found resistant to tetracycline, two (16.7%) isolates exhibited resistance to cephalexin, and one (8.3%) was resistant to ampicillin (Table 4). Nevertheless, all of the isolates were sensitive to amoxicillin, chloramphenicol, trimethoprim-sulfamethoxazole, cefoxitin, cefotaxime, and ceftriaxone. The S23₁ (*Citrobacter werkmanii*) isolate exhibited the highest Multiple Antibiotic Resistance (MAR) index profile (0.45), signifying its resistance to five of the antibiotics tested (Table 5). Other than that, six isolates showed a MAR index of 0.27 (resistant toward 3 antibiotics) and the isolates with the lowest MAR index (0.18) recorded resistance to only two of the antibiotics. Bacterial isolates with a MAR index higher than 0.20 indicates that the isolate originated from an environment where various antibiotics were used.

High level of resistance showed by the isolates toward penicillin and erythromycin might be due to the widespread use of these antibiotics in the clinical setting (Fair & Tor, 2014). This resistance pattern is a result of selective pressures of antimicrobial use, changes in microbial characteristics, and technological changes that enhanced the modern

development and transmission of drug-resistant microbes (Walsh, 2000). It is important to note that the isolates from street food showed 83.3% multidrug-resistant toward three or more antibiotics compared to clinical samples (Tunung et al., 2007). The isolated *Salmonella* Derby strain in this study showed resistance toward tetracycline. High frequency of resistant *Salmonella* strains isolated from food in Malaysia toward tetracycline has been reported ranging from 72.7% to 77.3% (Thong & Modarressi, 2011).

In this study, the *Citrobacter* isolates showed resistance toward penicillin, erythromycin, cephalixin, tetracycline, and ampicillin. This finding was in concordance with studies by Leski et al. (2016) and Liu et al. (2017) who also reported the same finding, noting the resistance of *Citrobacter* spp. to many classes of antibiotics including β -lactam, tetracycline, and macrolides. Yang et al. (2018) also reported the resistance of *Citrobacter* spp. to almost all tested antibiotics, including aminoglycosides, cephalosporin, carbapenem, fluoroquinolone, and sulphonamide but the bacteria was still susceptible to tetracycline. However, the current findings show that except for cephalixin, 100% of the *Citrobacter* spp. isolates were sensitive to the later generation of cephalosporin, namely cefoxitin, cefotaxime, and ceftriaxone.

CONCLUSION

In conclusion, although the number of samples in this study may be limited, this study showed the presence of microbial contamination in street-vended beverages and revealed that *Citrobacter* spp. as having a potential role as an emerging multidrug-resistant bacterial species in the food production system. These findings also demonstrated the possible risk of street-vended beverages as a medium for the dissemination of antibiotic-resistant bacteria to the population. Besides the fundamental aspect of food safety and hygiene practices, awareness of the danger of antibiotic-resistant spread in food products should also be emphasised in the food safety training received by food handlers.

ACKNOWLEDGEMENT

Universiti Kebangsaan Malaysia provided partial support for this research under the GP-2019-K016381 fund scheme.

REFERENCES

- Abdul-Mutalib, N., Syafinaz, A., Sakai, K., & Shirai, Y. (2015). An overview of foodborne illness and food safety in Malaysia. *International Food Research Journal*, 22(3), 896-901.
- Al-Dulaimi, M. M. K., Mutalib, S. A., Ghani, M. A., Zaini, N. A. M., & Ariffin, A. A. (2019). Multiple antibiotic resistance (MAR), plasmid profiles, and DNA polymorphisms among *Vibrio vulnificus* isolates. *Antibiotics*, 8(2), 1-13. doi: <https://doi.org/10.3390/antibiotics8020068>

- Aminharati, F., Ehrampoush, M. H., Dallal, M. M. S., Yaseri, M., Tafti, A. A. D., & Rajabi, Z. (2019). *Citrobacter freundii* foodborne disease outbreaks related to environmental conditions in Yazd province, Iran. *Iran Journal of Public Health*, 48(6), 1099-1105.
- Andargie, G., Kassu, A., Moges, F., Tirunch, M., & Huruy, K. (2008). Prevalence of bacteria and intestinal parasites among food handlers in Gondar Town, Northwest Ethiopia. *Journal of Health, Population and Nutrition*, 26(4), 451-455. doi: 10.3329/jhpn.v26i4.1887
- Bahri, A. A., Salleh, W., Lani, M. N., & Abdullah, W. Z. W. (2019). Antimicrobial resistance of *Escherichia coli* isolated of *ulam* from supermarkets and wet markets in Kuala Terengganu, Malaysia. *Malaysian Applied Biology*, 48(3), 35-42.
- Capita, R., & Alonso-Calleja, C. (2013). Antibiotic-resistant bacteria: A challenge for the food industry. *Critical Reviews in Food Science and Nutrition*, 53(1), 11-48. doi: <https://doi.org/10.1080/10408398.2010.519837>
- Chin, P. S., Ang, G. Y., Yu, C. Y., Tan, E. L., Tee, K. K., Yin, W. F., ... & Tan, G. Y. A. (2018). Prevalence, antimicrobial resistance, and genetic diversity of *Listeria* spp. isolated from raw chicken meat and chicken-related products in Malaysia. *Journal of Food Protection* 81(2), 284-289. doi: <https://doi.org/10.4315/0362-028X.JFP-17-186>
- Chong, E. S., Bidin, Z. F., Bakar, N. F. A., & Zulfakar, S. S. (2017a). Bacterial contamination on beef carcass at selected abattoirs located in Selangor Malaysia. *Malaysian Applied Biology*, 46(1), 37-43
- Chong, S. Y., Rao, P. V., & Soon, J. M. (2017b). Identification of *Escherichia* spp. strains in street-vended beverages and associated preparation surfaces using 16S rRNA analysis. *International Food Research Journal*, 24, 1811-1818.
- Das, A., Nagananda, G. S., Bhattacharya, S., & Bhardwaj, S. (2010). Microbiology quality of street-vended Indian chaats sold in Bangalore. *Journal of Biological Sciences*, 10(3), 255-260.
- De Cesare, A. (2018). *Salmonella* in Foods: A reemerging problem. *Advances in Food and Nutrition Research*, 86, 137-179. doi: <https://doi.org/10.1016/bs.afnr.2018.02.007>
- Fair, R. J., & Tor, Y. (2014). Antibiotics and bacterial resistance in the 21st century. *Perspectives in Medicinal Chemistry*, 6, 25-64. doi: <https://doi.org/10.4137/PMC.S14459>
- Krumperman, P. H. (1983). Multiple antibiotic resistance indexing of *Escherichia coli* to identify high-risk sources of fecal contamination of foods. *Applied and Environmental Microbiology*, 46(1), 165-170.
- Leski, T. A., Taitt, C. R., Bangura, U., Stockelman, M. G., Ansumana, R., Cooper, W. H., ... & Vora, G. J. (2016). High prevalence of multidrug-resistant *Enterobacteriaceae* isolated from outpatient urine samples but not the hospital environment in Bo, Sierra Leone. *BMC Infectious Disease*, 16(1), 1-9. doi: <https://doi.org/10.1186/s12879-016-1495-1>
- Levantesi, C., Bonadonna, L., Briancesco, R., Grohmann, E., Toze, S., & Tandoi, V. (2012). *Salmonella* in surface and drinking water: Occurrence and water-mediated transmission. *Food Research International*, 45(2), 587-602. doi: <https://doi.org/10.1016/j.foodres.2011.06.037>
- Liu, L., Lan, R., Liu, L., Wang, Y., Zhang, Y., Wang, Y., & Xu, J. (2017). Antimicrobial resistance and cytotoxicity of *Citrobacter* spp. in Maanshan Anhui Province, China. *Frontiers in Microbiology*, 8, 1-12. doi: <https://doi.org/10.3389/fmicb.2017.01357>

- Nawawee, N. S. M., Bakar, N. F. A., & Zulfakar, S. S. (2019). Microbiological safety of street-vended beverages in Chow Kit, Kuala Lumpur. *International Journal of Environmental Research and Public Health*, *16*, 4463-4471. doi: <https://doi.org/10.3390/ijerph16224463>
- Nemo, R., Bacha, K., & Ketema, T. (2017). Microbiological quality and safety of some-street vended foods in Jimma Town, Southwestern Ethiopia. *African Journal of Microbiology Research*, *11*(14), 574-585. doi: <https://doi.org/10.5897/AJMR2014.7326>
- Odeyami, O. A., & Sani, N. A. (2016). Antibiotic resistance and burden of foodborne diseases in developing countries. *Future Science OA*, *2*(4), 1-4. doi: <https://doi.org/10.4155/fsoa-2016-0023>
- Odeyami, O. A., Sani, N. A., Obadina, A. O., Saba, C. K. S., Bamidele, F. A., Abughoush, M., ... & Aberoumand, A. (2019). Food safety knowledge, attitudes and practices among consumers in developing countries: An international survey. *Food Research International*, *116*, 1386-1390. doi: <https://doi.org/10.1016/j.foodres.2018.10.030>
- Parish, M. E. (2008). Food safety issues and the microbiology of fruit beverages and bottled water. In N. Heredia, I. Wesley & S. Garcia, (Eds.), *Microbiologically safe foods* (pp. 291-304). New York, USA: JohnWiley & Sons. doi: 10.1002/9780470439074
- Pletz, M. W., Wollny, A., Dobermann, U., Rödel, J., Neubauer, S., Stein, C., ... & Maschmann, J. (2018). A nosocomial foodborne outbreak of a VIM carbapenemase-expressing *Citrobacter freundii*. *Clinical Infectious Diseases*, *67*(1), 58-64. doi: <https://doi.org/10.1093/cid/ciy034>
- Powell, D. A., & Marcon, M. J. (2012). Etiologic agents of infectious diseases: *Citrobacter* species. In S. S. Long, L. K. Pickering & C. G. Prober (Eds.), *Principles and practice of pediatric infectious diseases* (pp. 806-807.). Edinburgh, NY: Elsevier.
- Reller, M. E. (2012). Etiologic agents of infectious diseases: *Salmonella* species. In S. Long, L. Pickering & C. Prober (Eds.), *Principles and practice of pediatric infectious diseases* (pp. 814-819). Philadelphia, USA: Saunders (Imprint).
- Shagufta, B., Sivakumar, M., Kumar, S., Agarwal, R. K., Bhilegaonkar, K. N., Kumar, A., & Dubal, Z. B. (2017). Antimicrobial resistance and typing of *Salmonella* isolated from street vended foods and associated environment. *Journal of Food Science and Technology*, *54*(8), 2532-2539. doi: <https://doi.org/10.1007/s13197-017-2698-1>
- Suardana, I. W. (2014). Analysis of nucleotide sequences of the 16S rRNA gene of novel *Escherichia coli* strains isolated from feces of human and Bali cattle. *Journal of Nucleic Acids*, *2014*, 1-7. doi: <https://doi.org/10.1155/2014/475754>
- Sunday, P. U., Nyaudoh, U. N., & Etido, J. U. (2011). Microbiological quality and safety evaluation of fresh juices and edible ice sold in Uyo Metropolis, South-South, Nigeria. *International Journal of Food Safety*, *13*, 374-378.
- Tambekar, D. H., Jaiswal, V. J., Dhanorkar, D. V., Gulhane, P. B., & Dudhane, M. N. (2009) Microbial quality and safety of street vended fruit juices: A case study of Amravati City. *International Journal of Food Safety*, *10*, 72-76.

- Thong, K. L., & Modarressi, S. (2011). Antimicrobial resistance genes associated with *Salmonella* from retail meats and street foods. *Food Research International*, 44(9), 2641-2646. doi: <https://doi.org/10.1016/j.foodres.2011.05.013>
- Thung, T. Y., Radu, S., Mahyudin, N. A., Rukayadi, Y., Zakaria, Z., Mazlan, N., ... & Chin, Y. Z. (2018). Prevalence, virulence genes and antimicrobial resistance profiles of *Salmonella* serovars from retail beef in Selangor, Malaysia. *Frontiers in Microbiology*, 8, 1-8. doi: <https://doi.org/10.3389/fmicb.2017.02697>
- Tribst, A. A. L., Sant'Ana, A. S., & Massaguer, P. R. (2009). Review: Microbiological quality and safety of fruit juices-past, present and future perspectives. *Critical Reviews in Microbiology*, 35, 310-339. doi: <https://doi.org/10.3109/10408410903241428>
- Trivedi, M. K., Branton, A., Trivedi, D., Nayak, G., Mondal, S. C., & Jana, S. (2015). Phenotyping and 16S rDNA analysis after biofield treatment on *Citrobacter braakii*: A urinary pathogen. *Journal of Clinical and Medical Genomics*, 3(1), 1-8. doi: <https://hal.archives-ouvertes.fr/hal-01435926>
- Tschape, H., Prager, R., Streckel, W., Fruth, A., Tietze, E., & Böhme, G. (1995). Verotoxinogenic *Citrobacter freundii* associated with severe gastroenteritis and cases of haemolytic uremic syndrome in a nursery school: Green butter as the infection source. *Epidemiology Infections*, 114(3), 441-450. doi: <https://doi.org/10.1017/S0950268800052158>
- Tunung, R., Chai, L., Usha, M., Lee, H., Fatimah, A., Farinazleen, M., & Son, R. (2007). Characterization of *Salmonella enterica* isolated from street food and clinical samples in Malaysia. *ASEAN Food Journal*, 14(3), 161-173.
- Walsh, C. (2000). Molecular mechanisms that confer antibacterial drug resistance. *Nature*, 406(6797), 775-781. doi: <https://doi.org/10.1038/35021219>
- Woh, P. Y., Thong, K. L., Behnke, J. M., Lewis, J. W., & Zain, S. N. M. (2017). Characterization of nontyphoidal *Salmonella* isolates from asymptomatic migrant food handlers in Peninsular Malaysia. *Journal of Food Protection*, 80(8), 1378-1383. doi: <https://doi.org/10.4315/0362-028X.JFP-16-342>
- Yang, L., Li, P., Liang, B., Hu, X., Li, J., Xie, J., ... & Song, H. (2018). Multidrug-resistant *Citrobacter freundii* ST139 co-producing NDM-1 and CMY-152 from China. *Scientific Reports*, 8(1), 1-7. doi: <https://doi.org/10.1038/s41598-018-28879-9>
- Zulfakar, S. S., Abu-Bakar, N. F., Aidilputra, A. A., Miatong, A., & Chong, E. S. (2019). Microbial contamination of meat contact surfaces at the selected beef processing plants in Selangor and its biofilm formation ability. *Pertanika Journal of Tropical Agricultural Science*, 42(2), 709-726.

Short Communication

In Silico Designing of a Multi-Epitope Based Vaccine Candidate Against Human Adenovirus Type B3 Respiratory Infections by Utilising Various Immunoinformatics Approaches

Somnath Panda¹, Urmila Banik² and Arun Kumar Adhikary^{1*}

¹*Unit of Microbiology, AIMST University, Faculty of Medicine, Jalan Bedong Semeling, 08100 Bedong, Kedah, Malaysia*

²*Unit of Pathology, AIMST University, Faculty of Medicine, Jalan Bedong Semeling, 08100 Bedong, Kedah, Malaysia*

ABSTRACT

Human adenovirus type B3 (HAdV-B3) causes severe respiratory infections, hence an efficient vaccine is required. Unfortunately, the presence of numerous hexon variations makes conventional vaccine designing difficult which warrants an alternative method. Therefore, an *in silico* multi-epitope vaccine had been constructed against appropriate hexon variants of HAdV-B3. The allergenicity, antigenicity, structure, physicochemical properties along with molecular docking with TLR-3 and TLR-9 had also been predicted.

The constructed vaccine had 23 different epitopes. It showed non-allergic but antigenic nature with 30 hours of half-life *in vitro* and exhibited thermostable nature. We anticipate that this will considerably reduce the time and expense of biological work needed for future vaccine development.

ARTICLE INFO

Article history:

Received: 8 September 2020

Accepted: 27 November 2020

Published: 22 January 2021

DOI: <https://doi.org/10.47836/pjst.29.1.32>

E-mail addresses:

somnathpanda86@yahoo.co.uk (Somnath Panda)

urmila_banik@yahoo.co.in (Urmila Banik)

arun_adhikary@msn.com (Arun Kumar Adhikary)

*Corresponding author

Keywords: Human adenovirus type B3, hypervariable regions, immunoinformatics, multi-epitope vaccine construct

INTRODUCTION

Human adenoviruses (HAdVs) possess a double stranded DNA without an envelope. As of today, 103 types of HAdVs had been categorized (<http://hadv.wg.gmu.edu/>) in accordance with their serological and genetic criteria and accordingly are organized into seven groups (A-G). Human adenovirus type B3 (HAdV-B3) causes respiratory infections, epidemic keratoconjunctivitis, pharyngoconjunctival fever, acute gastroenteritis, and also occasionally involve the nervous system (Harley et al., 2001).

The pediatric age group, predominantly, neonates are considered to be the primary targets for nosocomial and community-acquired pneumonia caused by HAdV-B3. The pneumonia can lead to respiratory or heart failure with fatal outcome. As per example, the epidemic of adenoviral pneumonia that occurred in Northern China recorded a fatality of up to 30% and HAdV-B3 along with B7 were recognized as the major causative agents (Dong, 2005). Moreover, HAdV-B3 also causes severe illness among immunocompromised patients with increased mortality (Lai et al., 2013). During recent years, the increasing number of detection of HAdV-B3 from respiratory samples supports that it is the most predominant form of HAdVs accountable for respiratory tract infections (Chen & Tian, 2018). It has been observed that HAdV-B3 could be responsible for up to 87% of all adenoviral respiratory infections (Lynch & Kajon, 2016).

In spite of its medical and epidemiological significance, there is no targeted antivirals or vaccines against HAdV-B3. A number of studies on antivirals showed that nucleoside analogues and protease inhibitors have some activity against some types of adenoviruses. But their clinical usefulness is still not well-proven (Lion, 2014). Currently, the mainstay for the management of adenoviral infections is symptomatic. Thus, a vaccine that is economical, efficacious, and also safe against HAdV-B3 is required.

It is well-known that antibodies against HAdV-B3 hexon protein can counteract the infectivity of HAdVs in a type-specific manner (Pichla-Gollon et al., 2007). The capsid of HAdVs is mainly formed by hexon which includes three identical units of the polypeptide consisting of 945 amino acids (AA) and its hypervariable regions (HVRs) contain the epitopes (Liu et al., 2018) which are especially significant for designing vaccine and developing novel therapeutic approaches. Recently, we found out that the HVRs of HAdV-B3 hexon was highly variable, and based upon those variations, the available field strains had been categorized into 25 hexon variants, 3Hv-1 to 3Hv-25, (Haque et al., 2018). As a result of this vast heterogeneity, conventional vaccine development remains challenging.

To overcome this challenge, we hypothesized that a novel multi-epitope vaccine would be a more cost-effective method and with reference to our current findings, four hexon variants (3Hv-1, 2, 3, and 4) were selected to form a multi-epitope vaccine construct (Panda et al., 2020). The objectives of the study were to predict suitable epitopes (B-cell

epitopes, Helper T Lymphocyte, and Cytotoxic T Lymphocyte epitopes) from the HVRs of those major variants with the help of various immunoinformatics tools and to construct and analyze a multi-epitope vaccine that could potentially be investigated for additional biological work for future vaccine development.

METHODOLOGY

HAdV-B3 Hexon Protein Sequence Selection for Vaccine Construct

In the HAdV-B3 prototype, the hypervariable regions comprise 319 amino acids and extend from 132 to 450 amino acids on hexon. After multisequence alignment, the HVRs associated with 3Hv-1, 2, 3, and 4 (the specific 319 amino acids long sequence), had been selected for further analysis. All the sequences (GenBank Accession Nos. AB330084, AF542106, DQ099432, KC456085, and AY854180), were gained from NCBI (National Centre for Biotechnology Information-<http://www.ncbi.nlm.nih.gov/>) and were analyzed further to predict the appropriate epitopes.

Linear B Cell Epitope (BCE) Prediction

BCE represents the antigen where B lymphocytes bind and carry out a fundamental role in vaccine construction. BCE were attained from BCEPRED (Prediction of B Cell Epitopes-<http://crdd.osdd.net/raghava/bcepred/>) database. It predicts according to the various physicochemical aspects of BCE and gives results with both graphical and tabular format. The graphical format assists the users in rapid visualization of BCE where the peaks above the default threshold (2.5) are considered as BCE. The tabular output gives a score established on various physical and biochemical aspects. The threshold (-3 to 3) including every other factor (hydrophilicity, accessibility, flexibility, antigenic propensity, and polarity) was fixed at default, and epitopes are indicated in blue color (Saha & Raghava, 2006b). All obtained BCE were incorporated in the concluding vaccine construct.

Helper T Lymphocyte (HTL) Epitopes Prediction

HTL responses play a significant role in the initiation of both humoral and cellular immune responses. Therefore, HTL epitopes are likely to be a fundamental element of vaccines. For this reason, HTL epitopes of 15 AA long was attained from the IEDB (<http://tools.iedb.org/mhcii/>) database following IEDB recommended method 2.22 for the 7-allele HLA (Human Leukocyte Antigen) reference set. The IEDB (Immune Epitope Database) is a freely available resource funded by NIAID (National Institute of Allergy and Infectious Diseases-<https://www.niaid.nih.gov/>). It catalogs experimental data on antibody and T cell epitopes studied in humans, non-human primates, and other animal species in the context of infectious disease, allergy, autoimmunity, and transplantation. It also hosts tools to

assist in the prediction and analysis of epitopes. HTL selection was established on their IC_{50} values; the peptides having maximum affinity have $IC_{50} < 50nM$, peptides having intermediate affinity have $IC_{50} < 500nM$, and peptides holding $IC_{50} < 5000nM$ show the lowest amount of affinity, therefore the lowermost IC_{50} value demonstrates the highest affinity (Wang et al., 2010).

Cytotoxic T Lymphocyte (CTL) Epitopes Prediction

CTLs are $CD8^+$ subset of T-cell responses to kill the cells having intracellular viral infections. During infection, when they encounter MHC-I mounted antigen, specific to their receptor, they transform into effector cells. Therefore, to design a vaccine, it is also crucial to predict CTL epitopes. For acquiring CTL epitopes, the selected AA sequence was uploaded on the NetCTL 1.2 (<http://www.cbs.dtu.dk/services/NetCTL/>) database. NetCTL 1.2 server predicts CTL epitopes in the input protein sequences and this method is established on three approaches: i) the transportation effectiveness of transporters in relation to antigen processing, ii) MHC-I attachment compatibility and iii) the proteasomal C-terminal dissociation. These three prediction outcomes are merged together, and specificity is determined from that merged score (Larsen et al., 2007). The cut-off score for identifying epitopes was prearranged at 0.75 and generally, a higher score designates higher specificity. HLA (Human Leukocyte Antigen) allele A1 supertype was selected for this prediction. The epitope prediction scores which are presented by a <-E sign designate that those epitopes are identified as MHC (Major Histocompatibility Complex) ligands.

Multi-epitope Vaccine Construction

To generate a multi-epitope vaccine construct, every projected BCE was chosen. Among all HTL epitopes, the ones acquiring IC_{50} values lesser than 50nM as determined by NN align (an artificial neural network-based method) score were selected. Overlapping HTL epitopes were merged together. Amongst the CTL epitopes, all the projected epitopes were nominated. To provide efficient separation and effective functioning, linkers have been inserted between two epitopes. β -defensin had been employed as an adjuvant. Naive T-cell and immature dendritic cells are recruited by β -defensin at the infection site and it also provides innate host response in microbial infections.

Prediction of Allergenicity and Antigenicity

To make sure the multi-epitope vaccine does not stimulate any allergenic response, the non-allergic and allergic behavior was forecasted using AlgPred (Prediction of Allergenic Proteins-<http://www.imtech.res.in/raghava/algpred/>) which depends on whether IgE epitopes are present on the input protein sequence. Altogether it implements four different

standards, IgE (Immunoglobulin E) epitope + MAST (Motif Alignment and Search Tool) + SVM (Support Vector Machine) + ARPs (Allergen Representative Peptides) BLAST (Basic Local Alignment Search Tool), for forecasting of allergenicity (Saha & Raghava, 2006a).

ANTIGENpro (<http://www.scratch.proteomics.ics.uci.edu/>) server was utilized for predicting the antigenicity. The predictions are established on the input sequence as well as machine learning algorithms. The accurateness of this server had been assessed to be 76% founded on cross-validation experiments (Magnan & Baldi, 2014). To reconfirm the antigenicity of the constructed multi-epitope vaccine, we also performed antigenicity analysis using the VaxiJen server. VaxiJen (<http://www.ddg-pharmfac.net/vaxijen/VaxiJen/VaxiJen.html>) is the first server for alignment-independent prediction of protective antigens. It allows antigen classification solely based on the physicochemical properties of proteins. The server performs well in cross-validations showing prediction accuracy from 70% to 89%. The threshold score for both the servers was 0.4.

Physicochemical Characterization of the Vaccine Construct

Various physicochemical features (molecular weight, sequence length, half-life, instability index, theoretical pI, aliphatic index as well as the grand average of hydropathicity or GRAVY) were further analyzed from the ProtParam tool (<http://web.expasy.org/protparam/>) (Gasteiger et al., 2005). Prediction results were established on the pK values of the AA.

Secondary Structure Prediction

PSIPRED (Position-Specific Iterative basic local alignment search tool based secondary structure PREDiction-<http://bioinf.cs.ucl.ac.uk/index.php?id=779>) server was implemented to determine the secondary structure (Jones, 1999). PSIPRED has two neural networks. The preliminary projection was achieved by its first network, which was then manipulated as input for the subsequent network. This server achieved an 81.6% Q₃ score established on the cross-validation method.

Tertiary Structure Prediction and Validation

The tertiary structure was constructed by means of the SWISS-MODEL (<https://swissmodel.expasy.org>) website (Waterhouse et al., 2018). The formation of the homology model contains four steps: (1) identification of templates, (2) alignment between target with the template, (3) model forming, and (4) quality assessment. The automated mode was commissioned for this to forecast the tertiary structure and was also validated from the Ramachandran plot.

Molecular Docking Between Vaccine Construct and Immune Receptor

To generate proper immune responses, the antigen along with the immune receptor has to

work together. For this, molecular docking was performed among the immune receptors (Toll-like receptor-3/TLR-3, PDB ID: 2A0Z and Toll-like receptor-9/TLR-9, PDB ID: 3WPF) with the ligand (the multi-epitope vaccine construct) with the help of PatchDock (<http://bioinfo3d.cs.tau.ac.il/PatchDock/>) server. It mainly holds 3 distinctive phases; demonstration of the molecular profile, matching the surface patch, and finally filtering and then scoring (Schneidman-Duhovny et al., 2005).

RESULTS

Multiple Sequence Alignment

The multiple sequence alignment of the amino acid sequence of the HVRs of the prototype (GB strain, GenBank Accession Nos. AB330084) and the four selected hexon variants of HAdV-B3 (3Hv-1, 2, 3, and 4, GenBank Accession Nos. AF542106, DQ099432, KC456085, and AY854180 respectively) are demonstrated in Figure 1.

```

GB-AB330084      TSQWIVTTNGDNAVTTTTNTFGIASMKGDNITKE KDITTEGEEKPIYADKTY EESWTDTDGTNEKF NIKGGQAKNRKVKPTTEGGVETEED
3Hv-1 AF542106  TSQWIVTTN[.]NAVTTTTNTFGIASMKGDNITKE KDITTEGEEKPIYADKTY EESWTDTD[.]TNEKF NIKGGQAKNRKVKPTTEGGVETEED
3Hv-2 DQ099432   TSQWIVTTN[.]NAVTTTTNTFGIASMKGDNITKE KDITTEGEEKPIYADKTY EESWTDTDGTNEKF NIKGGQAKNRKVKPTTEGGVETEED
3Hv-3 KC456085   TSQWIVTTN[.]NAVTTTTNTFGIASMKGDNITKE KDITTEGEEKPIYADKTY EESWTDTDGTNEKF NIKGGQAKNRKVKPTTEGGVETEED
3Hv-4 AY854180   TSQWIVTTN[.]NAVTTTTNTFGIASMKGDNITKE KDITTEGEEKPIYADKTY EESWTDTD[.]TNEKF NIKGGQAKNRKVKPTTEGGV[.]EED
.....
GB-AB330084      DGRDAVAGALAPEIVLYT ETSNNSHANLG NGIGPGHTYQGIKVKTTDDTNGWEKDANVAPANEITIGNNL
3Hv-1 AF542106   DGRDAVAGALAPEIVLYT [.]TS[.]NSHANLG [.]SIGPG[.]VQGIKVKTTDDTNGWEKDANVA[.]ANEI[.]IGNNL
3Hv-2 DQ099432   DGRDAVAGALAPEIVLYT [.]TS[.]NSHANLG [.]SIGPG[.]VQGIKVKTTDE[.]NGWEKDANVA[.]ANEI[.]IGNNL
3Hv-3 KC456085   DGRDAVAGALAPEIVLYT [.]TS[.]NSHANLG [.]SIGPGH[.]VQGIKVKTTDE[.]NGWEKDANV[.]ANEI[.]IGNNL
3Hv-4 AY854180   DGRDAVAGALAPEIVLYT [.]TS[.]NSHANLG [.]SIGPG[.]VQGIKVKTTDDTNGWEKDANVA[.]ANEI[.]IGNNL
.....
    
```

Figure 1. Multiple sequence alignment of the HVRs of the prototype (GB strain, GenBank Accession Nos. AB330084) and the four selected hexon variants of HAdV-B3 (3Hv-1, 2, 3, and 4, GenBank Accession Nos. AF542106, DQ099432, KC456085, and AY854180 respectively). The sequence variations as compared to the GB strain at different position of the HVRs are indicated with a dot at the bottom (and are also highlighted in green) and the homologies are represented by a star at the bottom.

Prediction of B-Cell Epitopes (BCE), Helper T Lymphocyte (HTL), and Cytotoxic T Lymphocyte (CTL) Epitopes

The HVRs of 3Hv-1, 2, 3, and 4 (GenBank Accession Nos. AF542106, DQ099432, KC456085, and AY854180 respectively), were analyzed for epitope prediction.

Altogether, 8 BCE were achieved from the HVRs of 3Hv-1 and 4, whereas, 7 BCE were achieved from the other 2 hexon variants (3Hv-2 and 3). For those epitopes with a similar sequence amongst all four hexon variants, only one was taken into account to construct the vaccine. The overall quantity of BCE incorporated was 9.

The HTL epitopes having IC₅₀ values lesser than 50nM (in accordance with NN align IC₅₀ score) were selected, depicting high affinity. The final selection was done depending on

the overlapping sequences which were then combined together to acquire the final epitopes. 5 HTL epitopes were nominated after merging the overlapping sequences.

Amongst all the achieved CTL epitopes, there were 9 from 3Hv-1 and 8 from the other 3 hexon variations (3Hv-2, 3, and 4) that were identified as MHC ligands (presented by a <-E sign). The different selected epitopes after merging their sequences are indicated in Table 1 and overall predictions are exhibited in supplementary data.

Table 1

The selected B-cell epitopes (BCE), HTL (Helper T Lymphocyte), and CTL (Cytotoxic T Lymphocyte) epitopes from the hypervariable regions (HVRs) of the four major hexon variant strains of HAdV-B3

BCE	HTL Epitopes	CTL Epitopes
WIVTTNR	DNFVGLMYYNSTGNMGVLAGQ	DTDVTNEKF
GIASMKG	DRNTELSYQLLLDSLWDRTRYFSMWKQAVDS	YTENVNLET
DITTEGEE	EGEEKPIYADKTYQPEPQ	ALAPEIVLY
VTNEKFG	LAPEIVLYTENVNLETP	ETPDSHVVY
TNIKGGQAKNRKVKPTT	NTELSYQLLLDSLGDRTYF	TSDNSHANL
VVYKPGTSDN		NTELSYQLL
VDLQDRN		WTDTDVTNE
IKVKTDDT		GIEDELPNY
SWTDTDGTNEKFG		DSLWDRTRY
9 BCE	5 HTL epitopes	9 CTL epitopes

Multi-epitope Vaccine Construction

This includes 9 linear BCE, 5 HTL, and 9 CTL epitopes and is exhibited in Figure 2. Linear BCE and HTL epitopes were attached together with GPGPG and the CTL epitopes were amalgamated with AAY linkers respectively. β -defensin (GIINTLQKYCRVRGGRCVLSCLPKEEQIGKCSTRGRKCCRK), which is 45 AA long, was further added by the EAAAK linker. Following the addition of linkers and adjuvant, the final vaccine construct sequence had 415 amino acids.

Allergenicity and Antigenicity Prediction

The final multi-epitope vaccine construct was not carrying any experimentally proven IgE epitopes, hence, it was considered as non-allergic (Supplementary Data).

The antigenicity probability was 0.938684 which designates an excellent antigenic feature of the vaccine construct. Reconfirming the antigenicity data from the Vaxijen server gave us an antigenicity probability score of 0.9306. Hence, the data from both the servers indicate that the multi-epitope vaccine construct is a good antigen.

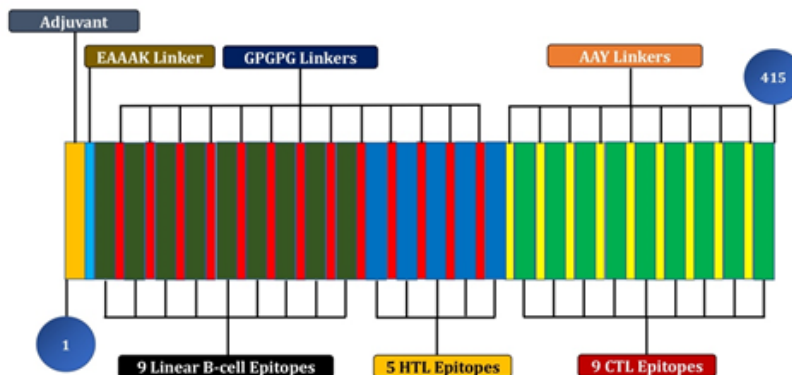


Figure 2. The multi-epitope vaccine construct consisting 9 linear (BCE) B-Cell Epitopes (dark green), 5 (HTL) Helper T Lymphocyte (blue) plus 9 (CTL) Cytotoxic T Lymphocyte (green) epitopes. The linear BCE and HTL epitopes were fused by GPGPG (red) linker and CTL epitopes were attached by AAY (yellow) linkers. β -defensin (orange) was associated with the EAAAK linker (light blue). Altogether, there were 23 different epitopes, 23 linkers, and 1 adjuvant comprising a total of 415 amino acids.

Physicochemical Evaluation of the Vaccine Construct

The molecular weight of the vaccine construct was 44 kDa which illustrates decent antigenic characteristics. The pI (Isoelectric point) value was 4.84 which designates the vaccine construct as acidic. The anticipated half-life was 30 hours *in vitro*, while the anticipated half-life was more than 20 and 10 hours in yeast and *E. coli* respectively. The expected aliphatic index was 59.04 which designates it as thermo-stable. GRAVY was measured to be -0.687 , and the instability index was computed as 22.13 (Supplementary Data).

Secondary and Tertiary Structure Estimation and Validation

In the projected secondary structure, coil, α -helix, and β -strands formation involved 268 AA, 86 AA and 61 AA respectively. Overall, it suggested that 64.57% were coils, 20.72% were helix, and 14.69% were stranded.

In tertiary structure prediction, 295 templates were located to match our target sequence, but the topmost 50 templates were filtered. The Global Model Quality Estimation (GMQE) score was 0.04 which reflects an accurate structure. The model achieved a QMEAN (Qualitative Model Energy ANalysis) Z-score of -2.76 which indicated the generated model was of extremely good quality. This was also highlighted by a “thumbs-up” symbol beside the score.

The Ramachandran plot showed a 79.07% favored region and 6.98% as outliers which were highest amongst the three predicted structures. There were no bad bonds present in the structure. The MolProbity score was 2.45. The secondary structure, tertiary structure and the Ramachandran plot are displayed in Figure 3 (a, b and c respectively).

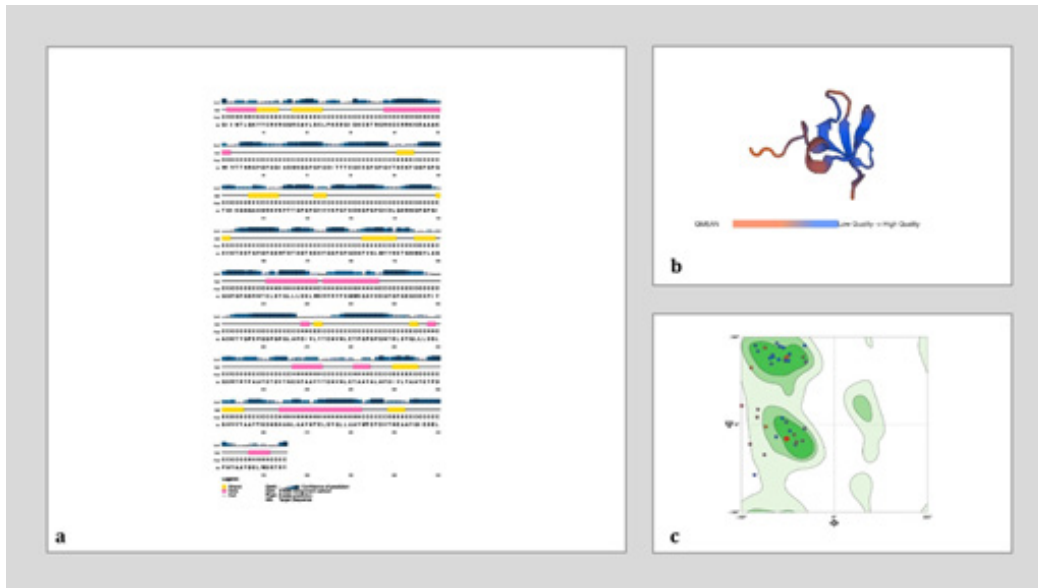


Figure 3. (a) The secondary conformational elements of the multi-epitope vaccine. The outcome indicated the organization of helix (pink colored bars), strands (yellow colored bars), and coils (black straight lines). (b) Tertiary folding of the vaccine. The orange to blue color grade bar below denotes the low quality to high quality of structure founded on QMEAN model schemes. (c) Tertiary structure validation by means of Ramachandran plot.

Molecular Docking Between Immunological Receptors (Toll-Like Receptor-3 and Toll-Like Receptor-9) and the Multi-epitope Vaccine Construct

Molecular docking generated several results among which the best 10 outcomes were sent to the FireDock server (Fast Interaction REfinement in molecular DOCKing-<http://bioinfo3d.cs.tau.ac.il/FireDock/php.php>) for enhancement and model number 10 was nominated as best depending on the collaborations between receptor and ligand. In Figure 4 (a) displays TLR-3 alone and (b) denotes the ligand-receptor docked complex. The geometric shape complementarity score of the best-docked model was estimated to be 12878, the calculated interface region of interaction was 1831.80. Also, the atomic contact energy (ACE) was 457.85. The global energy (binding energy of solution) of the best-docked model was 7.44.

On the other hand, Figure 4 (c) displays TLR-9 alone and (d) denotes the ligand-receptor docked complex. The geometric shape complementarity score of the best-docked model in this case was estimated to be 13944, the calculated interface region of interaction was 2231. Also, the atomic contact energy (ACE) was 448.23. The global energy (binding energy of solution) of the best-docked model was 7.94.

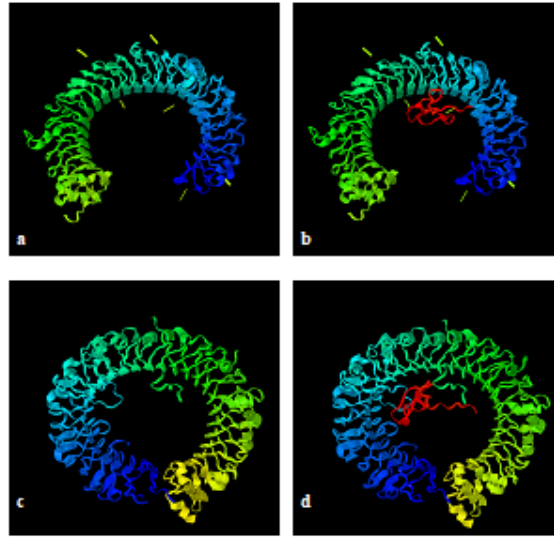


Figure 4. Comparison of Toll-like receptors-3 (TLR-3) and Toll-like receptor-9 (TLR-9) with the vaccine construct docked complex. (a) The rainbow-colored structure represents TLR-3 (PDB ID: 2A0Z), (b) The docked complex where the rainbow-colored structure is TLR-3 with the red colored structure denoting the multi-epitope vaccine construct, (c) The rainbow-colored structure represents Toll-like receptors-9/TLR-9 (PDB ID: 3WPF), and (d) The docked complex where the rainbow-colored structure is TLR-9 with the red colored structure denoting the multi-epitope vaccine construct.

DISCUSSION

HAdV-B3 causes respiratory infections with severe morbidity and mortality. It is generally considered as the most frequently identified HAdV type among pediatric age group with respiratory infections, requiring hospitalization. Over recent years, HAdV-B3 mediated respiratory illnesses have turned out as global health problem (Chen & Tian, 2018). Henceforth, the development of a vaccine is the key to encounter this health issue.

In an effort to prevent acute respiratory disease among military personnel, a live enteric-coated oral vaccine containing strains of HAdV-E4 and B7 was introduced in 1971 (Gurwith et al., 1989). Within the period of the vaccine use, the morbidity decreased by 50-60%, but later, many cases of HAdV-E4 and B7 mediated respiratory diseases had been detected among formerly vaccinated persons (Blasiolo et al., 2004). The detailed study revealed that major antigenic changes occurred due to single or multiple coding variations in HAdV-E4 and HAdV-B7 (Crawford-Miksza et al., 1999).

HVRs of hexon of HAdV-B3 are highly diverse in their antigenic areas (Haque et al., 2018). Since the epitopes of HAdVs are conformational, changes in single or multiple AA in HVRs might considerably affect the antigenic regions (Blasiolo et al., 2004). Hence, the antibody aimed at one variant may not offer a protective effect against additional existing variants of HAdV-B3.

Considering the epidemiological and clinical significance, an effective vaccine for HAdV-B3 is in demand to curb the infection and reduce health expenses. However, there are several challenges to create a vaccine against HAdV-B3 in a traditional way, for instance, (1) unavailability of all the strains reported so far due to the lack of culturing and isolation of the virus (Purcell et al., 2007), (2) strict biosecurity rules to transport the live virus (Salerno et al., 2007), (3) the huge amount of time essential for this (Purcell et al., 2007), and finally, (4) a chance of the emergence of a new recombinant strain when multiple strains are mixed together to generate a live vaccine (Sadanand, 2011). These challenges advocate that a newer approach to vaccine development is obligatory to bypass all these difficulties. Regarding this, a multi-epitope vaccine might be suitable as it allows to include numerous epitopes. This kind of vaccine was previously developed against many viruses namely human papillomavirus (Sabah et al., 2018) and dengue (Ali et al., 2017) which showed immense diversity in their neutralizing epitopes like HAdV-B3.

In the present study, first-ever against HAdV-B3, different immunoinformatics tools were applied to develop a multi-epitope vaccine construct. For this, different epitopes were predicted and a vaccine construct of 415 AA length was built carrying 9 linear BCE, 5 HTL, and 9 CTL epitopes conjugated with linkers. β -defensin was combined as an adjuvant since the peptides themselves are inadequately immunogenic. It recruits naive T-cell and immature dendritic cells at the site of infection through the CCR6 receptor (C-C Chemokine Receptor type 6), and provides adaptive and innate host response (Mohan et al., 2013).

The molecular weight of the newly developed vaccine construct was 44kDa which implied excellent antigenic properties as some higher molecular weight vaccines showed severe side effects. Previously, whole cells were used as vaccine candidates which were effective but some serious side effects were also associated. A well-known example is the vaccine against *Bordetella pertussis* having multiple pertussis antigens, where the molecular weight of the filamentous hemagglutinin and pertactin were 200kDa and 69kDa respectively (Kanra et al., 1993). The pI (Isoelectric point) value of the construct was 4.84 which denotes an acidic quality (Gasteiger et al., 2005). The pI of a protein is a good indicator of the protein's solubility as proteins tend to be the least soluble near their pI (Righetti et al., 1981). The Grand average of hydropathicity (GRAVY) value of our construct was -0.687 which designates hydrophilicity of the protein. The structure of the vaccine construct was stable since the instability index was 22.13. The aliphatic index of a protein is defined by the relative volume occupied by the aliphatic side chains (alanine, valine, isoleucine, and leucine) and high aliphatic index may be regarded as a positive factor for the increase of the thermostability (Ikai, 1980). The aliphatic index of the multi-epitope vaccine construct was 59.04 signifying that it is thermostable.

TLR-3 recognizes dsRNA, and thus, is involved in antiviral host immune responses (Alexopoulou et al., 2001). As dsRNA can potentially be generated during adenoviral

infection (Zhu et al., 2007), we have performed the docking of the multi-epitope vaccine construct with TLR-3. Moreover, TLR-3 has been shown to promote cross-priming to virus-infected cells (Schulz et al., 2005). The best-docked model with TLR-3 had a geometric shape complementarity score of 12878 and the global energy score was 7.44. However, HAdV-B3 activates innate immunity by its dsDNA through TLR-dependent pathway and the recognition of HAdV-B3 by the plasmacytoid dendritic cells is mediated by TLR-9 (Iacobelli-Martinez & Nemerow, 2007). Therefore, we had also performed the docking analysis of the multi-epitope vaccine construct with TLR-9. The best-docked model with TLR-9 had a geometric shape complementarity score of 13944 and the global energy score was 7.94.

Lastly, we believe that our newly proposed multi-epitope vaccine construct against HAdV-B3 could offer several advantages such as, (1) focusing an immune reaction concerning only the key neutralizing epitopes while circumventing the induction of antibodies that has no protective role and may even be harmful, (2) enable a more robust immune response capable of potentially accommodating mutations in neutralizing epitopes, (3) evading the hazard of handling live viruses, (4) it could be produced readily in the laboratory, (5) it can diminish the chances of co-infection as every possible epitope would be present and finally (6) if new hexon variants of HAdV-B3 appear in future, their epitopes could be easily incorporated in the existing vaccine.

CONCLUSION

Considering the heterogeneity of HAdV-B3 and the complexity of generating conventional vaccines, a multi-epitope vaccine construct incorporating all epitopes of four major HAdV-B3 hexon variants was built utilizing various immunoinformatics tools. We believe that this *in silico* multi-epitope vaccine construct will considerably reduce the time and expense of biological work essential for vaccine development with a better possibility of getting the desired solution by lessening the necessity for countless trial and error repeats of assays.

ACKNOWLEDGEMENT

A part of this project is supported by the Fundamental Research Grant Scheme (FRGS/1/2017/SKK11/AIMST/02/1) offered by the Ministry of Higher Education, Malaysia.

REFERENCES

- Alexopoulou, L., Holt, A. C., Medzhitov, R., & Flavell, R. A. (2001). Recognition of double-stranded RNA and activation of NF- κ B by Toll-like receptor 3. *Nature*, 413(6857), 732-738. doi: <https://doi.org/10.1038/35099560>

- Ali, M., Pandey, R. K., Khatoon, N., Narula, A., Mishra, A., & Prajapati, V. K. (2017). Exploring dengue genome to construct a multi-epitope based subunit vaccine by utilizing immunoinformatics approach to battle against dengue infection. *Scientific Reports*, 7(1), 1-13. doi: 10.1038/s41598-017-09199-w.
- Blasiolo, D. A., Metzgar, D., Daum, L. T., Ryan, M. A. K., Wu, J., Wills, C., ... & Russell, K. L. (2004). Molecular analysis of adenovirus isolates from vaccinated and unvaccinated young adults. *Journal of Clinical Microbiology*, 42(4), 1686-1693. doi: 10.1128/JCM.42.4.1686-1693.2004
- Chen, S., & Tian, X. (2018). Vaccine development for human mastadenovirus. *Journal of Thoracic Disease*, 10(Suppl 19), S2280-S2294. doi: 10.21037/jtd.2018.03.168.
- Crawford-Mikszka, L. K., Nang, R. N., & Schnurr, D. P. (1999). Strain variation in adenovirus serotypes 4 and 7a causing acute respiratory disease. *Journal of Clinical Microbiology*, 37(4), 1107-1112. doi: 10.1128/JCM.37.4.1107-1112.1999
- Dong, Y. S. (2005). Unite and devote to the works of pediatric clinical virology. *Zhonghua Er Ke Za Zhi = Chinese Journal of Pediatrics*, 43(1), 1-2.
- Gasteiger, E., Hoogland, C., Gattiker, A., Duvaud, S., Wilkins, M. R., Appel, R. D., & Bairoch, A. (2005). Protein identification and analysis tools on the ExpASY Server. In J. M. Walker (Ed.), *The Proteomics Protocols Handbook* (pp. 571-607). Totowa, New Jersey: Humana Press. doi: 10.1385/1-59259-890-0:571.
- Gurwith, M. J., Horwith, G. S., Impellizzeri, C. A., Davis, A. R., Lubeck, M. D., & Hung, P. P. (1989). Current use and future directions of adenovirus vaccine. *Seminars in Respiratory Infections*, 4(4), 299-303.
- Haque, E., Banik, U., Monowar, T., Anthony, L., & Adhikary, A. K. (2018). Worldwide increased prevalence of human adenovirus type 3 (HAdV-3) respiratory infections is well correlated with heterogeneous hypervariable regions (HVRs) of hexon. *PloS One*, 13(3), 1-12. doi: 10.1371/journal.pone.0194516.
- Harley, D., Harrower, B., Lyon, M., & Dick, A. (2001). A primary school outbreak of pharyngoconjunctival fever caused by adenovirus type 3. *Communicable Diseases Intelligence*, 25(1), 9-12.
- Iacobelli-Martinez, M., & Nemerow, G. R. (2007). Preferential activation of Toll-like receptor nine by CD46-utilizing adenoviruses. *Journal of Virology*, 81(3), 1305-1312. doi: 10.1128/JVI.01926-06
- Ikai, A. (1980). Thermostability and aliphatic index of globular proteins. *The Journal of Biochemistry*, 88(6), 1895-1898. doi: <https://doi.org/10.1093/oxfordjournals.jbchem.a133168>
- Jones, D. T. (1999). Protein secondary structure prediction based on position-specific scoring matrices. *Journal of Molecular Biology*, 292(2), 195-202. doi: 10.1006/jmbi.1999.3091.
- Kanra, G., Ceyhan, M., Vandevoorde, D., & Bogaerts, H. (1993). Acellular pertussis diphtheria-tetanus-pertussis vaccine containing separately purified pertussis toxoid, filamentous haemagglutinin and 69 kDa outer membrane protein as a booster in children. *European Journal of Pediatrics*, 152(6), 478-483. doi: <https://doi.org/10.1007/BF01955054>
- Lai, C. Y., Lee, C. J., Lu, C. Y., Lee, P. I., Shao, P. L., Wu, E. T., ... & Lin, J. J. (2013). Adenovirus serotype 3 and 7 infection with acute respiratory failure in children in Taiwan, 2010-2011. *PloS One*, 8(1), 1-7. doi: 10.1371/journal.pone.0053614.

- Larsen, M. V., Lundegaard, C., Lamberth, K., Buus, S., Lund, O., & Nielsen, M. (2007). Large-scale validation of methods for cytotoxic T-lymphocyte epitope prediction. *BMC Bioinformatics*, 8(1), 1-12. doi: 10.1186/1471-2105-8-424.
- Lion, T. (2014). Adenovirus infections in immunocompetent and immunocompromised patients. *Clinical Microbiology Reviews*, 27(3), 441-462. doi:10.1128/CMR.00116-13
- Liu, T., Fan, Y., Li, X., Gu, S., Zhou, Z., Xu, D., ... & Tian, X. (2018). Identification of adenovirus neutralizing antigens using capsid chimeric viruses. *Virus Research*, 256, 100-106. doi: 10.1016/j.virusres.2018.08.007.
- Lynch, J. P., & Kajon, A. E. (2016). Adenovirus: Epidemiology, global spread of novel serotypes, and advances in treatment and prevention. *Seminars in Respiratory and Critical Care Medicine*, 37(4), 586-602. doi: 10.1055/s-0036-1584923.
- Magnan, C. N., & Baldi, P. (2014). SSpro/ACCpro 5: Almost perfect prediction of protein secondary structure and relative solvent accessibility using profiles, machine learning and structural similarity. *Bioinformatics*, 30(18), 2592-2597. doi: 10.1093/bioinformatics/btu352.
- Mohan, T., Sharma, C., Bhat, A. A., & Rao, D. N. (2013). Modulation of HIV peptide antigen specific cellular immune response by synthetic α - and β -defensin peptides. *Vaccine*, 31(13), 1707-1716. doi: <https://doi.org/10.1016/j.vaccine.2013.01.041>.
- Panda, S., Banik, U., & Adhikary, A. K. (2020). Bioinformatics analysis reveals four major hexon variants of human adenovirus type-3 (HAdV-3) as the potential strains for development of vaccine and siRNA-based therapeutics against HAdV-3 respiratory infections. *Infection, Genetics and Evolution*, 85, 1-9. doi: 10.1016/j.meegid.2020.104439.
- Pichla-Gollon, S. L., Drinker, M., Zhou, X., Xue, F., Rux, J. J., Gao, G. P., ... & Bergelson, J. M. (2007). Structure-based identification of a major neutralizing site in an adenovirus hexon. *Journal of Virology*, 81(4), 1680-1689. doi: 10.1128/JVI.02023-06.
- Purcell, A. W., McCluskey, J., & Rossjohn, J. (2007). More than one reason to rethink the use of peptides in vaccine design. *Nature reviews Drug discovery*, 6(5), 404-414. doi: <https://doi.org/10.1038/nrd2224>
- Righetti, P. G., Tudor, G., & Ek, K. (1981). Isoelectric points and molecular weights of proteins: A new table. *Journal of Chromatography A*, 220(2), 115-194. doi: [https://doi.org/10.1016/S0021-9673\(00\)88456-3](https://doi.org/10.1016/S0021-9673(00)88456-3)
- Sabah, S. N., Gazi, M. A., Sthity, R. A., Husain, A. B., Quyyum, S. A., Rahman, M., & Islam, M. R. (2018). Designing of epitope-focused vaccine by targeting E6 and E7 conserved protein sequences: An immunoinformatics approach in Human Papilloma Virus 58 isolates. *Interdisciplinary Sciences, Computational Life Sciences*, 10(2), 251-260. doi: 10.1007/s12539-016-0184-5.
- Sadanand, S. (2011). Vaccination: the present and the future. *The Yale Journal of Biology and Medicine*, 84(4), 353-359.
- Saha, S., & Raghava, G. P. S. (2006a). AlgPred: Prediction of allergenic proteins and mapping of IgE epitopes. *Nucleic Acids Research*, 34(Web Server issue), W202-209. doi: 10.1093/nar/gkl343.

- Saha, S., & Raghava, G. P. S. (2006b). Prediction of continuous B-cell epitopes in an antigen using recurrent neural network. *Proteins*, 65(1), 40-48. doi: 10.1002/prot.21078.
- Salerno, R. M., Gaudioso, J., & Brodsky, B. H. (2007). *Laboratory biosecurity handbook*. Boca Raton, Florida: CRC press.
- Schulz, O., Diebold, S. S., Chen, M., Näslund, T. I., Nolte, M. A., Alexopoulou, L., ... & e Sousa, C. R. (2005). Toll-like receptor 3 promotes cross-priming to virus-infected cells. *Nature*, 433(7028), 887-892. doi: <https://doi.org/10.1038/nature03326>
- Schneidman-Duhovny, D., Inbar, Y., Nussinov, R., & Wolfson, H. J. (2005). PatchDock and SymmDock: Servers for rigid and symmetric docking. *Nucleic Acids Research*, 33(Web Server issue), W363-W367. doi: 10.1093/nar/gki481.
- Wang, P., Sidney, J., Kim, Y., Sette, A., Lund, O., Nielsen, M., & Peters, B. (2010). Peptide binding predictions for HLA DR, DP and DQ molecules. *BMC Bioinformatics*, 11(1), 1-12. doi: 10.1186/1471-2105-11-568.
- Waterhouse, A., Bertoni, M., Bienert, S., Studer, G., Tauriello, G., Gumienny, R., ... & Schwede, T. (2018). SWISS-MODEL: Homology modelling of protein structures and complexes. *Nucleic Acids Research*, 46(W1), W296-W303. doi: 10.1093/nar/gky427.
- Zhu, J., Huang, X., & Yang, Y. (2007). Innate immune response to adenoviral vectors is mediated by both Toll-like receptor-dependent and-independent pathways. *Journal of Virology*, 81(7), 3170-3180. doi: 10.1128/JVI.02192-06

SUPPLEMENTARY DATA

Menu

- Home
- Submission
- Help
- Algorithm
- Supplementary
- Related Links
- Acknowledgements
- Developers
- Contact

AllgPred: Prediction of Allergenic Proteins and Mapping of IgE Epitopes

Name of sequence	Protein
Length of Sequence	415
Predicted On	Mon Sep 23 09:06:47 2019
	NON ALLERGEN

Prediction by mapping of IgE epitope

The protein sequence does not contain experimentally proven IgE epitope

ExPASy ProtParam tool
18/09/2018, 5:33 PM

ProtParam

Home | [Contact](#)

ProtParam

User-provided sequence:

```

10      20      30      40      50      60
GIINTLQKY CRVRRGRCAN LSCLPKKEGI GKCTRGRKC CRKKEAAAK NIVTNRGPG
70      80      90     100     110     120
PGGIASRKG PPGDITITTE GEEGPGPVT NEKFGGPGP TNRKGGQAN RRVKPTTGP
130     140     150     160     170     180
PGVVYKPTS DMGPIQVDL QGRMGPGGI KVKTDGTPG FGSWTDGDT NEKFGGPGP
190     200     210     220     230     240
INPVULMYY STONKGLAG QGPGDGRNT ELSYQLLDS LMRTRYFSH NKQAVDSGP
250     260     270     280     290     300
PGEGEKP1Y ADKTYQPEP GPGPLAPEI VLYTENVLE TPGPGQNTS LSYQLLDSL
310     320     330     340     350     360
GDRTRYFAA DTDVINEKA AYTENVNLE TAAYALAPEI VLYAAYETP SHVVAAYTS
370     380     390     400     410
DNRANLAAY NTELSYQLA AYWTDGVTN EAAYIEDEL PNYAYDSLW DRTRY
    
```

References and documentation are available.

Number of amino acids: 415
Molecular weight: 44305.89
Theoretical pI: 4.84

Amino acid composition: [CSV format](#)

Ala (A)	31	7.5%
Arg (R)	17	4.1%
Asn (N)	23	5.5%
Asp (D)	25	6.0%
Cys (C)	6	1.4%
Gln (Q)	11	2.7%
Glu (E)	26	6.3%
Gly (G)	60	14.5%
His (H)	2	0.5%
Ile (I)	12	2.9%
Leu (L)	28	6.7%
Lys (K)	21	5.1%
Met (M)	4	1.0%
Phe (F)	6	1.4%
Pro (P)	37	8.9%
Ser (S)	17	4.1%
Thr (T)	36	8.7%
Trp (W)	6	1.4%
Tyr (Y)	27	6.5%
Val (V)	20	4.8%
Pro (P)	0	0.0%
Sec (U)	0	0.0%
(B)	0	0.0%
(Z)	0	0.0%
(X)	0	0.0%

<https://web.expasy.org/cgi-bin/protparam/protparam>
Page 1 of 2

In Silico Vaccine Against Human Adenovirus Type B3

ExPASy ProParam tool

18/09/2019, 5:33 PM

Total number of negatively charged residues (Asp + Glu): 51
Total number of positively charged residues (Arg + Lys): 38

Atomic composition:

Carbon	C	1951
Hydrogen	H	2979
Nitrogen	N	531
Oxygen	O	632
Sulfur	S	10

Formula: C₁₉₅₁H₂₉₇₉N₅₃₁O₆₃₂S₁₀
Total number of atoms: 6103

Extinction coefficients:

Extinction coefficients are in units of M⁻¹ cm⁻¹, at 280 nm measured in water.

Ext. coefficient 73605
Abs 0.1% (=1 g/l) 1.661, assuming all pairs of Cys residues form cystines

Ext. coefficient 73230
Abs 0.1% (=1 g/l) 1.653, assuming all Cys residues are reduced

Estimated half-life:

The N-terminal of the sequence considered is G (Gly).

The estimated half-life is: 30 hours (mammalian reticulocytes, in vitro).
>20 hours (yeast, in vivo).
>10 hours (Escherichia coli, in vivo).

Instability index:

The instability index (II) is computed to be 22.13
This classifies the protein as stable.

Aliphatic index: 59.04

Grand average of hydropathicity (GRAVY): -0.687

SB Swiss Institute of Bioinformatics | Decipher

<https://web.expasy.org/cgi-bin/protparam/protparam>

Page 2 of 2

The prediction of linear B-cell epitopes as obtained from the hypervariable regions (HVRs) of the four major hexon variant strains of HAdV-B3 by using the BCEPRED server

Strain	Predicted linear B-cell epitopes	Positions in HVR (132-450 AA)
3Hv-1	WIVTTNR	135-141
	GLASMKG	153-159
	DITTEGEE	172-180
	VTNEKFG	205-211
	TNIKGGQAKNRKVKPTT	232-248
	VVYKPGTSDN	294-303
	VDLQDRN	352-358
3Hv-2	IKVKTDDT	422-429
	WIVTTNR	135-141
	GLASMKG	153-159
	DITTEGEE	172-180
	SWTDTDGTNEKFG	199-211
	TNIKGGQAKNRKVKPTT	232-248
	VVYKPGTSDN	294-303
3Hv-3	VDLQDRN	352-358
	WIVTTNR	135-141
	GLASMKG	153-159
	DITTEGEE	172-180
	SWTDTDGTNEKFG	199-211
	TNIKGGQAKNRKVKPTT	232-248
	VVYKPGTSDN	294-303
3Hv-4	VDLQDRN	352-358
	WIVTTNR	135-141
	GLASMKG	153-159
	DITTEGEE	172-180
	VTNEKFG	205-211
	TNIKGGQAKNRKVKPTT	232-248
	VVYKPGTSDN	294-303

The prediction of Helper T Lymphocyte (HTL) epitopes as obtained from the hypervariable regions (HVRs) of the four major hexon variant strains of HAdV-B3 by using the IEDB server

HTL Epitopes	3Hv-1			
	Positions in HVR (132-450)	Allele	Percentile Rank	IC ₅₀ (nM)
VGLMYNSTGNMGVL	327-341	HLA-DRB1*07:01	1.10	12.60
GLMYNSTGNMGVLA	328-342	HLA-DRB1*07:01	1.30	14.00
FVGLMYNSTGNMGV	327-340	HLA-DRB1*07:01	1.80	17.10
LMYNSTGNMGVLAG	329-343	HLA-DRB1*07:01	2.20	19.50
RNTELSYQLLLDSLW	357-371	HLA-DRB4*01:01	0.87	25.30
FVGLMYNSTGNMGV	326-340	HLA-DRB1*15:01	1.40	25.60
NFVGLMYNSTGNMG	325-339	HLA-DRB1*15:01	1.50	25.70
DNFVGLMYNSTGNM	324-338	HLA-DRB1*15:01	1.50	26.30
VGLMYNSTGNMGVL	327-341	HLA-DRB1*15:01	1.70	28.50
NTELSYQLLLDSLWD	358-372	HLA-DRB4*01:01	1.20	29.00
MYNSTGNMGVLAGQ	330-344	HLA-DRB1*07:01	3.50	29.20
DRNTELSYQLLLDSL	356-370	HLA-DRB4*01:01	1.20	29.90
GEEKPIYADKTYQPE	178-192	HLA-DRB3*01:01	1.40	31.00
TELSYQLLLDSLWDR	359-373	HLA-DRB4*01:01	1.60	34.60
EKPIYADKTYQPEP	179-193	HLA-DRB3*01:01	1.60	36.00
LWDRTRYFSMWKQAV	370-384	HLA-DRB5*01:01	5.50	36.40

In Silico Vaccine Against Human Adenovirus Type B3

WDRTRYFSMWKQAVD	371-385	HLA- DRB5*01:01	5.60	37.00
EKPIYADKTYQPEPQ	180-194	HLA- DRB3*01:01	1.80	38.70
APEIVLYTENVNLET	275-289	HLA- DRB1*15:01	2.60	38.90
DRTRYFSMWKQAVDS	372-386	HLA- DRB5*01:01	6.10	40.70
PEIVLYTENVNLETP	276-290	HLA- DRB1*15:01	3.00	43.90
LAPEIVLYTENVNLE	274-288	HLA- DRB1*15:01	3.40	48.30
EGEEKPIYADKTYQP	177-191	HLA- DRB3*01:01	2.10	49.60
GLMYYNSTGNMGVLA	328-342	HLA- DRB1*15:01	3.50	49.70

3Hv-2				
HTL Eptopes	Positions in HVR (132- 450)	Allele	Percentile Rank	IC ₅₀ (nM)
VGLMYYNSTGNMGVL	327-341	HLA- DRB1*07:01	1.10	12.60
GLMYYNSTGNMGVLA	328-342	HLA- DRB1*07:01	1.30	14.00
FVGLMYYNSTGNMGV	327-340	HLA- DRB1*07:01	1.80	17.10
LMYYNSTGNMGVLAG	329-343	HLA- DRB1*07:01	2.20	19.50
RNTELSYQLLLDSL	357-371	HLA- DRB4*01:01	0.84	24.80
FVGLMYYNSTGNMGV	326-340	HLA- DRB1*15:01	1.40	25.60
NFVGLMYYNSTGNMG	325-339	HLA- DRB1*15:01	1.50	25.70
DNFVGLMYYNSTGNM	324-338	HLA- DRB1*15:01	1.50	26.30
VGLMYYNSTGNMGVL	327-341	HLA- DRB1*15:01	1.70	28.50
MYYNSTGNMGVLAGQ	330-344	HLA- DRB1*07:01	3.50	29.20
NTELSYQLLLDSLGD	358-372	HLA- DRB4*01:01	1.20	29.40
DRNTELSYQLLLDSL	356-370	HLA- DRB4*01:01	1.20	29.90
GEEKPIYADKTYQPE	178-192	HLA- DRB3*01:01	1.40	31.00
TELSYQLLLDSLGD	359-373	HLA- DRB4*01:01	1.70	35.50
EEKPIYADKTYQPEP	179-193	HLA- DRB3*01:01	1.60	36.00
EKPIYADKTYQPEPQ	180-194	HLA- DRB3*01:01	1.80	38.70
APEIVLYTENVNLET	275-289	HLA- DRB1*15:01	2.60	38.90
SYQLLLSLGDRTRY	362-376	HLA- DRB1*03:01	1.60	40.10
YQLLLSLGDRTRYF	363-377	HLA- DRB1*03:01	1.70	42.50
PEIVLYTENVNLETP	276-290	HLA- DRB1*15:01	3.00	43.90
LAPEIVLYTENVNLE	274-288	HLA- DRB1*15:01	3.40	48.30
EGEEKPIYADKTYQP	177-191	HLA- DRB3*01:01	2.10	49.60
GLMYYNSTGNMGVLA	328-342	HLA- DRB1*15:01	3.50	49.70

3Hv-3				
HTL Epitopes	Positions in HVR (132-450)	Allele	Percentile Rank	IC50(nM)
VGLMYNSTGNMGVL	327-341	HLA-DRB1*07:01	1.10	12.60
GLMYNSTGNMGVLA	328-342	HLA-DRB1*07:01	1.30	14.00
FVGLMYNSTGNMGV	327-340	HLA-DRB1*07:01	1.80	17.10
LMYYNSTGNMGVLAG	329-343	HLA-DRB1*07:01	2.20	19.50
RNTELSYQLLDLSLG	357-371	HLA-DRB4*01:01	0.84	24.80
FVGLMYNSTGNMGV	326-340	HLA-DRB1*15:01	1.40	25.60
NFVGLMYNSTGNMG	325-339	HLA-DRB1*15:01	1.50	25.70
DNFVGLMYNSTGNM	324-338	HLA-DRB1*15:01	1.50	26.30
VGLMYNSTGNMGVL	327-341	HLA-DRB1*15:01	1.70	28.50
MYNSTGNMGVLAG	330-344	HLA-DRB1*07:01	3.50	29.20
Q				
NTELSYQLLDLSLGD	358-372	HLA-DRB4*01:01	1.20	29.40
DRNTELSYQLLDLSL	356-370	HLA-DRB4*01:01	1.20	29.90
GEEKPIYADKTYQPE	178-192	HLA-DRB3*01:01	1.40	31.00
TELSYQLLDLSLGD	359-373	HLA-DRB4*01:01	1.70	35.50
EEKPIYADKTYQPEP	179-193	HLA-DRB3*01:01	1.60	36.00
EKPIYADKTYQPEPQ	180-194	HLA-DRB3*01:01	1.80	38.70
APEIVLYTENVNLET	275-289	HLA-DRB1*15:01	2.60	38.90
SYQLLDLSLGDRTRY	362-376	HLA-DRB1*03:01	1.60	40.10
YQLLDLSLGDRTRYF	363-377	HLA-DRB1*03:01	1.70	42.50
PEIVLYTENVNLETP	276-290	HLA-DRB1*15:01	3.00	43.90
LAPEIVLYTENVNLE	274-288	HLA-DRB1*15:01	3.40	48.30
EGEEKPIYADKTYQP	177-191	HLA-DRB3*01:01	2.10	49.60
GLMYNSTGNMGVLA	328-342	HLA-DRB1*15:01	3.50	49.70

3Hv-4				
HTL Epitopes	Positions in HVR (132-450)	Allele	Percentile Rank	IC50(nM)
VGLMYNSTGNMGVL	327-341	HLA-DRB1*07:01	1.10	12.60
GLMYNSTGNMGVLA	328-342	HLA-DRB1*07:01	1.30	14.00
FVGLMYNSTGNMGV	327-340	HLA-DRB1*07:01	1.80	17.10
LMYYNSTGNMGVLAG	329-343	HLA-DRB1*07:01	2.20	19.50
RNTELSYQLLDLSLG	357-371	HLA-DRB4*01:01	0.84	24.80
FVGLMYNSTGNMGV	326-340	HLA-DRB1*15:01	1.40	25.60
NFVGLMYNSTGNMG	325-339	HLA-DRB1*15:01	1.50	25.70
DNFVGLMYNSTGNM	324-338	HLA-DRB1*15:01	1.50	26.30
VGLMYNSTGNMGVL	327-341	HLA-DRB1*15:01	1.70	28.50
MYNSTGNMGVLAGQ	330-344	HLA-DRB1*07:01	3.50	29.20
NTELSYQLLDLSLGD	358-372	HLA-DRB4*01:01	1.20	29.40
DRNTELSYQLLDLSL	356-370	HLA-DRB1*15:01	1.20	29.90

In Silico Vaccine Against Human Adenovirus Type B3

GEEKPIYADKTYQPE	178-192	DRB4*01:01 HLA- DRB3*01:01	1.40	31.00
TELSYQLLLSLGDR	359-373	HLA- DRB4*01:01	1.70	35.50
EEKPIYADKTYQPEP	179-193	HLA- DRB3*01:01	1.60	36.00
EKPIYADKTYQPEPQ	180-194	HLA- DRB3*01:01	1.80	38.70
APEIVLYTENVNLET	275-289	HLA- DRB1*15:01	2.60	38.90
SYQLLLSLGDRTRY	362-376	HLA- DRB1*03:01	1.60	40.10
YQLLLSLGDRTRYF	363-377	HLA- DRB1*03:01	1.70	42.50
PEIVLYTENVNLETP	276-290	HLA- DRB1*15:01	3.00	43.90
LAPEIVLYTENVNLE	274-288	HLA- DRB1*15:01	3.40	48.30
EGEEKPIYADKTYQP	177-191	HLA- DRB3*01:01	2.10	49.60
GLMYNSTGNMGVLA	328-342	HLA- DRB1*15:01	3.50	49.70

The prediction of CTL epitopes based on MHC-I binding as obtained from the hypervariable regions (HVRs) of the four major hexon variant strains of HAdV-B3 by using the NetCTL 1.2 server

Hexon Variant	CTL Epitopes	Positions in HVR (132-450 AA)	Combined (COMB) Score
3Hv-1	DTDVTNEKF	202-210	2.0685
	YTENVNLET	281-289	1.9503
	ALAPEIVLY	273-281	1.6845
	ETPD SHV VY	288-296	1.6837
	TSDNSHANL	300-308	1.3163
	NTELSYQLL	358-366	1.1167
	WTD T DVTNE	200-208	0.9420
	GIEDELPNY	398-406	0.8811
	DSLWDRTRY	368-376	0.7810
	3Hv-2	YTENVNLET	281-289
DTDGTNEKF		202-210	1.6860
ALAPEIVLY		273-281	1.6845
ETPD SHV VY		288-296	1.6837
TSDNSHANL		300-308	1.3163
NTELSYQLL		358-366	1.1350
WTD T DGTNE		200-208	0.9130
GIEDELPNY		398-406	0.8811
YTENVNLET		281-289	1.9503
DTDGTNEKF		202-210	1.6860
3Hv-3	ALAPEIVLY	273-281	1.6845
	ETPD SHV VY	288-296	1.6837
	TSDNSHANL	300-308	1.3163
	NTELSYQLL	358-366	1.1350
	WTD T DGTNE	200-208	0.9130
	GIEDELPNY	398-406	0.8811
	DTDVTNEKF	202-210	2.0685
	YTENVNLET	281-289	1.9503
	ALAPEIVLY	273-281	1.6845
	ETPD SHV VY	288-296	1.6837
3Hv-4	TSDNSHANL	300-308	1.3163
	NTELSYQLL	358-366	1.1350
	WTD T DVTNE	200-208	0.9420
	GIEDELPNY	398-406	0.8811



Comparison of Proximate Composition of Raw and Cooked Intramuscle Tissue of *Thunnus tonggol* from Terengganu, Malaysia

Norhazirah Abd Aziz¹, Ahmad Shamsudin Ahmad¹, Adiana Ghazali¹, Nurul Izzah Ahmad², Ahmad Ali³ and Meng-Chuan Ong^{1,4,5*}

¹Faculty of Science and Marine Environment, Universiti Malaysia Terengganu, 21030 UMT, Kuala Nerus, Terengganu

²Environmental Health Research Centre, Institute for Medical Research, Aras 2, Blok C6 (C6-2-19), Kompleks NIH, No. 1, Jalan Setia Murni U13/52, Seksyen U13 Setia Alam, 40170 Shah Alam, Selangor, Malaysia

³Marine Fishery Resources Development and Management Department, Southeast Asian Fisheries Development Center (SEAFDEC), 21080 Chendering, Terengganu, Malaysia

⁴Institute of Oceanography and Environment, Universiti Malaysia Terengganu, 21030 UMT, Kuala Nerus, Terengganu, Malaysia

⁵Ocean Pollution and Ecotoxicology (OPEC) Research Group, Universiti Malaysia Terengganu, 21030 UMT, Kuala Nerus, Terengganu, Malaysia

ABSTRACT

A study was carried out to determine the effects of the steaming process on the proximate composition of the dark and white muscle tissue of *Thunnus tonggol* sampled from Terengganu waters. The mean percentage of moisture, ash, lipid, and protein of the raw dark muscle was 59.1%, 3.8%, 12.1% and 33.9%, while in the raw white muscle were 66.7%, 2.9%, 2.7% and 33.9%, respectively. Both types of muscle showed a significantly

different value in the lipid content. There was significant increase recorded in the protein content in both types of muscle after the steaming process (79.1% and 93.0% in dark and white muscles, respectively). Likewise, the percentage of ash showed some increment with 4.8% in the dark muscle and 7.9% in the white muscle. However, the cooking process decreased the percentage of moisture and lipid in both dark and white muscles. The percentage of moisture in dark muscle was reduced to

ARTICLE INFO

Article history:

Received: 19 August 2020

Accepted: 5 November 2020

Published: 22 January 2021

DOI: <https://doi.org/10.47836/pjst.29.1.33>

E-mail addresses:

aaziz@gmail.com (Norhazirah Abd Aziz)

sham@umt.edu.my (Ahmad Shamsudin Ahmad)

adiana@umt.edu.my (Adiana Ghazali)

nizzah.a@moh.gov.my (Nurul Izzah Ahmad)

aaseafdec@seafdec.org.my (Ahmad Ali)

ong@umt.edu.my (Meng-Chuan Ong)

*Corresponding author

7.7%, and 9.7% in white muscle. On the other hand, percentage of lipid content in both types of muscles after the steaming process was 0.43% in dark muscle and 0.03% in white muscle. This study reveals that the cooking process had considerable effects on the proximate composition of both dark and white muscles.

Keywords: Dark and white muscles, longtail tuna, proximate composition, raw and cooked, *Thunnus tonggol*

INTRODUCTION

Fish is known as the major source of food and essential nutrients to fulfil the nutritional requirements in most human populations of the world. Fish have been obtained a wide attraction as an excellent source of digestible protein, vitamins, and other minerals (Elmadfa & Meyer, 2017; Abraha et al., 2018; Mohanty et al., 2019). It has been reported that the population in eastern Asia consumed fish with rice daily or as part of a rice dish or as a side dish (Burger et al., 2003; Tang et al., 2015; Ahmad et al., 2016). The annual per capita fish consumption of Malaysian was the second highest after Japan when comparing among Asian nations or ranked number fifth throughout the world (York & Grossard, 2004). In particular, the consumption of fish among Malaysian has been recorded at least once a day in the amount of one and one-half medium size fish per day (Norimah et al., 2008; Ahmad et al., 2015).

Terengganu state situated at the east Peninsular of Malaysia has the longest coastline in Peninsular Malaysia around 244 km facing South China Sea waters. This region experienced monsoon seasons every year from November to March with a high density of rainfall, strong winds, and waves (Mohamed & Amil, 2005; Antonina et al., 2013; Daud et al., 2016). Terengganu is known as one of the centers of fisheries landing areas in Malaysia (Terengganu Tourism, 2018). In Terengganu, the most popular commercial fish species landed and consumed is Longtail tuna, *Thunnus tonggol* (Figure 1), or known as “*Ikan Tongkol*” (Basir et al., 2016; Azmi et al., 2019) by local communities. Terengganu people were estimated to consume this species 239.7 g per person and 1.83 times per week which is about 437.4g/person/week (Norhazirah et al., 2020). This species is among the smaller members of the Tuna family (Griffiths et al., 2010; Al-Mamari et al., 2014). In Terengganu, *Thunnus tonggol* is often served with a special local delicacy called *Nasi Dagang* cooked with curry gravy and served with glutinous rice. Another Terengganu’s popular *Thunnus tonggol* dish is *Singgang*, a healthy yet delicious fish soup prepared with turmeric, chili, garlic, and onion serve for lunch.

Despite its nutritional value and consumer preference, the effect of cooking on this species has been scarcely inscribed. Generally, the nutritional value in fishes can be altered by processing and heat applied through cooking methods (Alia et al. 2020). Therefore, it is

appropriate to undertake a thorough analysis of the proximate composition of this species' intramuscle, hence this research was accomplished.



Figure 1. The Longtail tuna (*Thunnus tonggol*) which is among the smaller members of the Tuna family and is in high abundance in Terengganu waters.

METHODOLOGY

Sample Preparation and Cooking

The fresh *Thunnus tonggol* fish samples with mean and length recorded were 1567 ± 107.3 g and 48.4 ± 1.3 cm respectively ($n = 25$) was obtained from the local fishermen from fish landing port at Pulau Kambing, Kuala Terengganu. Then the samples were transferred to the laboratory for further analysis. During transportation, the samples were kept in the icebox at low temperature, $\pm 4^{\circ}\text{C}$. On arrival at the laboratory, the fish samples were washed with distilled water three to four times to discard foreign substances and fish blood before the samples were eviscerated. The bone and skin were removed using a ceramic knife. Steaming of the samples were performed in a domestic steamer Pensonic PRC-25 G (Malaysia) at approximately 100°C for 20 minutes (Adepoju et al., 2017). The dark and white muscle were steamed separately. The raw and steamed samples were dried in the oven at 60°C for 12 hours as to express in dry basis. For steamed samples, the Longtail tuna muscles were steamed before undergoing the drying process. Then the dried samples were homogenized using a kitchen blender (Lombardo-Agüí et al., 2015; Gan et al., 2016) and analyzed to determine the proximate composition.

Proximate Composition

For further analysis, the moisture content of raw and steamed muscle samples was determined by oven-drying method at $95 - 105^{\circ}\text{C}$ for 24 hours. Crude protein content was calculated by converting the nitrogen content as determined by Kjeldahl's method (Gerhardt KBL40S and Foss Kjelttec 2100) using the conversion factor of 6.25 (Sullivan & Carpenter 1993). The lipid content was determined by the method described by AOAC (2006) using the Soxhlet system (Foss ST310). The Ash content in the muscles were gravimetrically determined by dry-ashing in a muffle furnace at 600°C for 6 hours.

Statistical Analysis

The normality test was run by using SPSS software where the p-value < 0.05, not normally distributed. A non-parametric Chi-square test was run to prove that the data was statistically significant where the p-value < 0.05.

RESULTS

The average percentage of proximate composition in raw and cooked *Thunnus tonggol* muscles were presented in Table 1. All the data were expressed in percentage dry basis. Generally, in raw muscles, the highest proximate composition was moisture with 59.1%, ranged from 58.5% to 59.5%, and 64.9%, ranged from 64.5% to 69.7% in dark and white muscle, respectively. The average ash content was slightly higher in the dark muscle which is 3.8% compared to 2.9% in white muscle. On the other hand, there was a significant distinction in the value of lipid content in both types of muscle, which the average value recorded was 12.1% and 2.7%. However, there were no significant differences in the average percentage of protein in both dark and white muscle.

Table 1

The mean and range percentage of lipid, moisture, ash and protein in raw muscle samples and cooked samples of Longtail tuna. All the values were expressed in percentage dry basis.

Proximate composition (% dry basis)	Moisture (%)	Ash (%)	Lipid (%)	Protein (%)	
Raw sample	Dark muscle	^a 58.5 – 59.5* ^b 59.1	3.6 – 4.2* 3.8	10.1 – 14.4 12.1	32.2 – 35.5 33.9
	White muscle	64.9 – 69.7* 66.7	2.9 – 3.1* 2.9	– 4.2 2.7	33.0- 35.6 33.9
Cooked sample	Dark muscle	6.1 – 7.2* 7.7	4.3 – 5.3* 4.8	0.38 – 0.47 0.43	78.5–79.6* 79.1
	White muscle	8.6 – 10.1* 9.7	7.5 – 8.6* 7.9	0.02 – 0.04 0.03	91.5- 94.4* 93

^aThe ranges percentage of proximate composition in intramuscle of raw and cooked samples.

^bThe averages percentages of proximate composition in intramuscle of raw and cooked samples

*Significantly different compared to the raw and cooked samples

Nevertheless, the cooking process reduced lipid content by 96.4% in dark muscle while 98.9% in white muscle. Apart from that, the moisture content also dropped after the cooking process in both types of muscle. However, the content of ash and protein showed an increment in dark and white muscle after being treated with the steamed process. The ash content raised by 63.3% in white muscle, while only 20.8% in dark muscle. Meanwhile, the protein values were increased tremendously after cooking treatment. The protein content in dark muscle increased by 133.3% while 174.3% in white muscle after the cooking process.

DISCUSSION

The nutritive values of the fish muscles may be altered by processing or cooking methods (García-Arias et al., 2003; Rahman et al., 2012; Moussa et al., 2014). The heat applied to the muscle may alter the content of moisture, ash, lipid, and protein (Feng et al., 2017; Abraha et al., 2018). Other than that, the structure of dark and white muscle may contribute to the changes of proximate composition in both raw and cooked samples.

In this study, both dark and white muscles of *Thunnus tonggol* were declining in the percentage of moisture by 87.0% and 85.5% in dark and white muscle, respectively, after been treated with the steaming process for 20 minutes. Water loss in both types of muscle was anticipated after the steaming phase as the heat was applied to them. This finding also agreed by other researchers (Ersoy & Ozeren 2009; Hosseini et al., 2014; Ersoy et al., 2016; Weber et al., 2018) in their studies where there was significant moisture loss in fish muscle after culinary treatment. The decrease in the percentage of moisture in both types of muscle through evaporation of dripping under heat condition may alter other components content such as protein and ash.

On the other hand, the protein content increased up to 93 % in both types of muscle. Protein increased in samples after cooking methods was derived from the loss of moisture (Eduardo et al., 2016; Ersoy & Ozeren, 2009). The declining of water content has been defined as the most factor that caused the protein and ash contents to increase significantly in the steamed fish (Arias et al., 2003; Weber et al., 2008). This is in accordance with the findings of Puwastien et al. (1999), Nalan et al. (2004), Weber et al. (2008), and Goswami and Manna (2020) where the cooked fish (steaming, boiling, and grilling) contained higher protein levels. Other than that, Ng and Rosman (2019) suggested that the increment of protein content possibly an effect of enzymatic hydrolysis, which might cause the free amino acids to discharge. On the other hand, the increased of protein content in cooked muscle sample might be due to the solubilization of some nitrogenous compounds (Mustafa et al., 2012).

The ash content in muscle samples indicated the information on the distribution of bony parts to the flesh (Sofoulaki et al., 2018). The increase of ash percentage indicated the larger skeletal mass of the fish (Rasmussen & Ostefeld, 2000; Daramola et al., 2007). Respecting the ash percentage, it consists mainly of minerals (Murray & Burt, 2001). In this

study, the increase of ash content by 63.3% in white muscle and 20.8% in dark muscle after the steaming process might be provoked by the remarkably dropping of moisture content.

On the other hand, the comparison data on the proximate composition analysis of few different fish species that treated with various cooking methods were demonstrated in Table 2. Rainbow trout (*Oncorhynchus mykiss*) treated with boiling, frying and grilling methods were analysed and the findings showed that there were changes occurred in proximate composition when compared to the raw sample. The moisture was decreased with all cooking treatments while ash, protein and lipid were increased in contents. Frying methods showed the great increment in lipid content from 3.44 ± 0.013 to 12.7 ± 0.08 % probably due to the usage of oil in the process. The frying methods that applied to the fish in few studies demonstrated the increment in lipid percentage due to the fat absorption by the fish (Nalan et al., 2004; Turkkan et al., 2008; Lira et al., 2017).

Moreover, study by Turkkan et al. (2008) presented the same pattern of proximate composition when cooking methods were applied to the seabass muscle samples. The increasing of lipid percentage in the samples after treated with frying method was 65.3 % while baked and microwaved methods were 40.7 and 23.2 %, respectively. Nonetheless, the research by Lira et al. (2017) determined the contradicting findings with other studies where the percentage of ash, and protein decreased. However, the various pattern found in that study might be controlled by the cooking methods and additional ingredients applied to the fish samples.

Table 2

The comparison data on the proximate composition analysis in various species of fish in raw and cooking treatment samples. All the data were expressed in mean percentage \pm sd.

Species	Cooking Treatment	Moisture (%)	Ash (%)
Rainbow trout (<i>Oncorhynchus mykiss</i>)	Raw	73.4 ± 0.015	1.35 ± 0.012
	Fried	62.7 ± 0.024	1.66 ± 0.006
	Boiled	69.2 ± 0.035	1.61 ± 0.02
	Grilled	65.8 ± 0.05	1.54 ± 0.025
Seabass (<i>Dicentrarchus labrax</i> , Linnaeus, 1758)	Raw	71.62 ± 0.23	0.92 ± 0.4
	Fried	62.9 ± 4.47	2.41 ± 0.49
	Baked	66.5 ± 3.08	2.18 ± 0.25
	Microwave-cooked	69.3 ± 0.38	2.90 ± 0.53
King mackerel (<i>Scomberomorus cavalla</i> , Cuvier, 1829)	Raw	-	5.15 ± 0.88
	Fried in coconut oil	-	5.03 ± 0.70
	Cooked in coconut milk	-	3.69 ± 0.26

Table 2 (Continued)

Species	Cooking Treatment	Protein (%)	Lipid (%)	References
Rainbow trout (<i>Oncorhynchus mykiss</i>)	Raw	19.8 ± 0.035	3.44 ± 0.013	Nalan et al. (2004)
	Fried	26.3 ± 0.23	12.7 ± 0.08	
	Boiled	20.7 ± 0.67	4.32 ± 0.75	
	Grilled	25 ± 0.41	5.95 ± 1.49	
Seabass (<i>Dicentrarchus labrax</i> , Linnaeus, 1758)	Raw	18.5 ± 0.43	4.18 ± 0.26	Turkkan et al. (2008)
	Fried	24.3 ± 0.67	6.91 ± 0.16	
	Baked	21.1 ± 0.65	5.88 ± 0.05	
	Microwave-cooked	26.5 ± 0.71	5.15 ± 0.22	
King mackerel (<i>Scomberomorus cavalla</i> , Cuvier, 1829)	Raw	92.4 ± 4.97	4.18 ± 1.63	Lira et al. (2017)
	Fried in coconut oil	82.4 ± 4.56	12.5 ± 3.75	
	Cooked in coconut milk	81.6 ± 5.74	14.8 ± 2.03	

CONCLUSION

The composition of fish is basically composed of water, lipid, and protein, which create the nutritional value, functional aspects, and sensory characteristics of the flesh. The cooking method that applied the increasing heat will definitely contribute to the changes of proximate composition of the fish due to the oxidation and evaporation process. Data resulting from this study can contribute to the nutrient information in the raw and cooked muscle of *Thunnus tonggol* from Terengganu, Malaysia. These data suggested that there was a significant alteration in the proximate composition of this species muscle after been treated with one type of culinary method, namely the steaming process. These data also accommodate the loss of water content might alter other proximate composition such as protein, lipid, and ash.

ACKNOWLEDGEMENT

This research was conducted with the funding from the Ministry of Higher Education Malaysia, under the Niche Area Research Grant Scheme (NRGS) project number 53131 and INOS under Higher Institution Centre of Excellence (HICoE, 66928). First, the authors wish to acknowledge their gratitude to the anonymous reviewers who gave freely time and effort, constructive recommendations that enhanced the value of this manuscript. The authors

also wish to express their gratitude to the Faculty of Fishery and Food Science, Universiti Malaysia Terengganu, and Mr. Zafrullah bin Abu Bakar for their contribution during the proximate analysis session. Their contribution to this work is very much appreciated.

REFERENCES

- Abraha, B., Admassu, H., Mahmud, A., Tsighe, N., Shui, X.W., & Fang, Y. (2018). Effect of processing methods on nutritional and physico-chemical composition of fish: A review. *MOJ Food Processing and Technology*, 6(4), 376-382. doi: 10.15406/mojfpt.2018.06.00191.
- Adepoju, M. A., Omitoyin, B. O., Mohan, C. O., & Zynudheen, A. A. (2017). Heat penetration attributes of milkfish (*Chanos chanos*) thermal processed in flexible pouches: A comparative study between steam application and water immersion. *Food Science Nutrition*, 5(3), 521-524. doi: 10.1002/fsn3.426.
- Ahmad, N. I., Noh, M. F. M., Mahiyuddin, W. R. W., Jaafar, H., Ishak, I., Azmi, W. N. F. W., ... & Hairi M. H. (2015). Mercury levels of marine fish commonly consumed in Peninsular Malaysia. *Environmental Science and Pollution Research*, 22, 3672-3686. doi: 10.1007/s11356-014-3538-8.
- Ahmad, N. I., Mahiyuddin, W. R. W., Mohamad, T. R. R., Ling, C. Y., Daud, S. F., Hussein, N. C., ... & Sulaiman, L. H. (2016). Fish consumption pattern among adults of different ethnics in Peninsular Malaysia. *Food Nutrition Research*, 60(1), 1-15. doi: 10.3402/fnr.v60.32697.
- Al-Mamari, D., Al-Kharusi, L., Al-Kiyumi, F., Al-Shogebai, S., Al-Anboori, I., Al-Seneadi, R., & Khrorv, S. (2014). Record of the largest longtail tuna, *Thunnus tonggol* (Bleeker 1851) from offshore Salalah in the Sultanate of Oman. *Journal of Fisheries*, 2(3), 215-216.
- Alia, T. T. N., Hing, L. S., Sim, S. F., Pradit, S., Ahmad, A., & Ong, M. C. (2020). Comparative study of raw and cooked farmed sea bass (*Lates calcarifer*) in relation to metal content and its estimated human health risk. *Marine Pollution Bulletin*, 153, 1-7. doi: 10.1016/j.marpolbul.2020.111009.
- Antonina, A. N., Shazili, N. A. M., Kamaruzzaman, B. Y., Ong, M. C., Rosnan, Y., & Sharifah, F. N. (2013). Geochemistry of the rare earth elements (REE) distribution in Terengganu coastal waters: A study case from Redang Island marine sediment. *Open Journal of Marine Science*, 3(3), 1-6. doi: 10.4236/ojms.2013.33017.
- AOAC Official Method 990.03. (2006). Protein (crude) in animal feed, combustion method, chapter 4. In W. Horowitz & G. W. Jr Latimer (Eds.), *Official methods of analysis of AOAC International* (18th Ed.) (pp. 30-31). Gaithersburg, Maryland: AOAC International.
- Arias, M. I. G., Pontes, E. A., Linares, M. C. G., Fernandez, M. C. G., & Muniz, F. J. S. (2003). Cooking-freezing-reheating (CFR) of sardine (*Sardina pilchardus*) fillets. Effect of different cooking and reheating procedures on the proximate and fatty acid compositions. *Food Chemistry*, 83(3), 349-356. doi: https://doi.org/10.1016/S0308-8146(03)00095-5
- Azmi, W. N. F. W., Ahmad, N. I., & Mahiyuddin, W. R. W. (2019). Heavy metal levels and risk assessment from consumption of marine fish in Peninsular Malaysia. *Journal of Environmental Protection*, 10(11), 1-22. doi: 10.4236/jep.2019.1011086.

- Basir, S., Jamon, S., Faizal, E. M., & Mokhtar, N. A. (2016). *Data collection system and tuna statistical in Malaysia* (IOTC-2013-WPDCS09-10). Malaysia National Report to the Scientific Committee of the Indian Ocean Tuna Commission for 2015. Retrieved August 19, 2020 from wqww.iotc.org.
- Burger, J., Stern, A. H., & Gochfeld, M. (2003). Mercury in commercial fish: Optimizing individual choices to reduce risk. *Environmental Health Perspective*, *113*, 266-271. doi: 10.1289/ehp.7315.
- Daramola, J. A., Fasakin, E. A., & Adeparusi, E. O. (2007). Changes in physiochemical and sensory characteristics of smoke-dried fish species stored at ambient temperature. *African Journal of Food, Agriculture, Nutrition and Development*, *7*(6), 1-16.
- Daud, N. R., Akhir, M. F., & Husain, M. L. (2016). Water circulation in the shallow shelf areas off the Terengganu coast affected by wind stress force using a hydrodynamic model. *Journal of Sustainability Science and Management*, *S11*, 81-92.
- Eduardo, T. V., Arlett, R. R., Lia, M., & Elena, P. (2016). Changes in fatty acids, sterols, pigments, lipid classes, and heavy metals of cooked or dried meals, compared to fresh marine by-product. *Animal Feed Science and Technology*, *221*, 195-205. doi: 10.1016/j.anifeedsci.2016.09.004.
- Elmadfa, I., & Meyer, A. L. (2017). Animal proteins as important contributors to a healthy human diet. *Annual Review of Animal Biosciences*, *5*, 111-131. doi: 10.1146/annurev-animal-022516-022943.
- Ersoy, B., & Ozeren, A. (2009). The effect of cooking methods on mineral and vitamin contents of African catfish. *Food Chemistry*, *115*(2), 419-422. doi: 10.1016/j.foodchem.2008.12.018.
- Ersoy, B., Yanar, Y., Aygul, K., & Mehmet, C. (2016). Effects of four cooking methods on the heavy metals concentrations of seabass fillets (*Dicentrarchus labrax* L. 1785). *Food Chemistry*, *99*(4), 748-751. doi: 10.1016/j.foodchem.2005.08.055
- Feng, X., Fu, C., & Yang, H. (2017). Gelatin addition improves the nutrient retention, texture, and mass transfer of fish balls without altering their nanostructure during boiling. *LWT*, *77*, 142-151. doi: 10.1016/j.lwt.2016.11.024.
- Gan, J., Lv, L., Peng, J. Li, J., Xiong, Z., Chen, D., & He, L. (2016). Multi-residue method for the determination of organofluorine pesticides in fish tissue by liquid chromatography triple quadrupole tandem mass spectrometry. *Food Chemistry*, *207*, 195-204. doi: 10.1016/j.foodchem.2016.02.098.
- García-Arias, M. T., Álvarez Pontes, E., García-Linares, M. C., García-Fernández, M. C., & Sánchez-Muniz, F. J. (2003). Cooking-freezing-reheating (CFR) of sardine (*Sardina pilchardus*) fillets. Effect of different cooking and reheating procedures on the proximate and fatty acid compositions. *Food Chemistry*, *83*(3), 349-356. doi: 10.1016/S0308-8146(03)00095-5.
- Goswami, S., & Manna, K. (2020). Comparison of the effects of cooking methods on nutritional composition of fresh and salted *Tenualosa ilisha*. *Aquaculture and Fisheries*, *5*(6), 294-299. doi: <https://doi.org/10.1016/j.aaf.2020.01.006>
- Griffiths, S. P., Fry, G. C., Manson, F. J., & Lou, D. C. (2010). Age and growth of longtail tuna (*Thunnus tonggol*) in tropical and temperate waters of the central Indo-Pacific. *ICES Journal of Marine Science*, *67*, 125-134. doi: 10.1093/icesjms/fsp223.

- Hosseini, H., Mahmoudzadeh, M., Rezaei, M., Mahmoudzadeh, L., Khaksar, R., Khoroshahi, N. K., & Badakhani, A. (2014). Effect of different cooking methods on minerals, vitamins, and nutritional quality indices of kutum roach (*Rutilus Frisii kutum*). *Food Chemistry*, *148*, 86-91. doi: 10.1016/j.foodchem.2013.10.012.
- Lira, G. M., Cabral, C. C. V. Q., Oliveira, I. B. A., Bruno, C. F., Simon, S. J. G. B., & Bragagnolo, N. (2017). Changes in the lipid fraction of king mackerel pan fried in coconut oil and cooked in coconut milk. *Food Research International*, *101*, 198-202. doi: <https://doi.org/10.1016/j.foodres.2017.08.070>
- Lombardo-Agüí, M., García-Campaña, A. M., Cruces-Blanco, C., & Gámiz-Gracia, L. (2015). Determination of quinolones in fish by ultra-high performance liquid chromatography with fluorescence detection using QuEChERS as sample treatment. *Food Control*, *50*, 864-868. doi: 10.1016/j.foodcont.2014.10.027.
- Mohamed, K. N., & Amil, R. (2005). Nutrients enrichment experiment on seawater samples at Pulau Perhentian, Terengganu. *Procedia Environmental Sciences*, *30*, 262-267. doi: 10.1016/j.proenv.2015.10.047.
- Mohanty, B. P., Ganguly, S., Mahanty, A., Mitra, T., Patra, S., Karunakaran, D., ... & Ayyappan, S. (2019). Fish in human health and nutrition. *Advances in Fish Research*, *7*, 189-218.
- Moussa, E. W. H., Shereen, A. N., Manal, A., Mehanni, A. E., & Rasha, A. E. (2014). Nutritional value and fatty acid composition of household cooking on fish fatty acids profile using atherogenicity and thrombogenicity indices. *Journal of Food Chemistry and Nutrition*, *2*(1), 27-41.
- Murray, J., & Burt, J. R. (2001). *The composition of fish* (Torry Advisory Note No. 38). Aberdeen, UK: Torry Research Station.
- Mustafa, M. G., Begum, S. R., Khaleque, M. A., Jannat, M., & Ahsan, D. A. (2012). Nutritional qualities of Hilsha and Sardina in different salt curing methods. *Dhaka University Journal of Biological Sciences*, *21*(1), 97-104. doi: <https://doi.org/10.3329/dujbs.v21i1.9749>
- Nalan, G., Pinar, Y., & Emel, C. (2004). Effects of cooking methods on the proximate composition and mineral contents of rainbow trout (*Oncorhynchus mykiss*). *Food Chemistry*, *84*, 19-22. doi: 10.1016/S0308-8146(03)00161-4.
- Ng, Z. X., & Rosman, N. F. (2019). In vitro digestion and domestic cooking improved the total antioxidant activity and carbohydrate-digestive enzymes inhibitory potential of selected edible mushroom. *Journal of Food Science and Technology*, *56*(2), 865-877. doi: <https://doi.org/10.1007/s13197-018-3547-6>
- Norhazirah, A. A., Adiana, G., Yunus, K., Annual, Z. F., Ahmad, A., & Ong, M. C. (2020). Longtail tuna (*Thunnus tonggol*) consumption frequency in Terengganu, Malaysia. *Open Journal of Marine Science*, *10*, 141-148. doi: 10.4236/ojms.2020.103011
- Norimah, A. K., Safiah, M., Jamal, K., Haslinda, S., Zuhaida, H., & Rohida, S. (2008). Food consumption patterns: Findings from the Malaysian Adult Nutrition Survey (MANS). *Malaysia Journal Nutrition*, *14*(1), 25-39.
- Puwastien, P., Judprasong, K., Kettwan, E., Vasanachitt, K., Yupaporn, N., & Bhattacharjee, L. (1999). Proximate composition on raw and cooked Thai freshwater and marine fish. *Journal of Food Composition and Analysis*, *12*, 9-16. doi: <https://doi.org/10.1006/jfca.1998.0800>

- Rahman, M. M., Zamri, M., & Fadilla, N. (2012). Effects of deep frying on proximate composition and micronutrient of Indian Mackerel (*Rastrelliger kanagurta*), Eel (*Monopterus albus*) and Cockle (*Anadara granosa*). *Pakistan Journal of Biological Sciences*, 15, 589-594. doi: 10.3923/pjbs.2012.589.594.
- Rasmussen, R. S., & Ostefeld, T. H. (2000). Effect of growth rate on quality traits and feed utilisation of rainbow trout (*Oncorhynchus mykiss*) and brook trout (*Salvelinus fontinalis*). *Aquaculture*, 184(3-4), 327-337. doi: 10.1016/S0044-8486(99)00324-5.
- Sofoulaki, K., Kalantzi, I., Machias, A., Mastoraki, M., Chatzifotis, S., Mylona, K., ... & Tzapakis, M. (2018). Metals and elements in sardine and anchovy: Species specific differences and correlation with proximate composition and size. *Science of the Total Environment*, 645, 329-338. doi: 10.1016/j.scitotenv.2018.07.133.
- Sullivan, D. M., & Carpenter, D. E. (1993). *Methods of analysis for nutrition labeling*. Arlington, USA: AOAC International.
- Tang, W., Cheng, J., Zhao, W., & Wang, W. (2015). Mercury levels and estimated total daily intakes for children and adults from an electronic waste recycling area in Taizhou, China: Key role of rice and fish consumption. *Journal of Environmental Sciences*, 34(1), 107-115. doi: 10.1016/j.jes.2015.01.029.
- Terengganu Tourism. (2018). *Reasons to visit Terengganu*. Retrieved August 19, 2020, from <http://terengganutourism.com>.
- Turkkan, A. U., Cakli, S., & Kilinc, B. (2008). Effects of cooking methods on the proximate composition and fatty acid composition of seabass (*Dicentrarchus labrax*, Linnaeus, 1758). *Food and Bioproducts Processing*, 86, 163-166.
- Weber, J., Bochi, V. C., Ribeiro, C. P., Victorio, A. D. M., & Emanuelli, T. (2018). Effect of different cooking methods on oxidation, proximate and fatty acid composition of silver catfish (*Rhamdia quelen*) fillets. *Food Chemistry*, 106, 140-146. doi: 10.1016/j.foodchem.2007.05.052.
- York, R., & Grossard, M. H. (2004). Cross-national meat and fish consumption: Exploring the effects of modernization and ecological context. *Ecological Economics*, 48, 293-302. doi: 10.1016/j.ecolecon.2003.10.009.



Distribution of Benthic Macroinvertebrates in Seafloor Northward of Pulau Indah, Klang

Mohd Sophian Mohd Kasihmuddin* and Zaidi Che Cob

Department of Earth Sciences and Environment, Universiti Kebangsaan Malaysia, 43600 UKM, Bangi, Selangor, Malaysia

ABSTRACT

An assessment of community of benthic macroinvertebrates in waters northwards of Pulau Indah, Klang was made with the main objective to determine distribution and diversity of benthic macroinvertebrates as well as to establish possible correlation between the community's distributions with environmental parameters. The sediments were obtained via Ponar Grab (0.023 m² mouth area), followed by filtration (500 µm) and laboratory sorting in order to extract all specimens from sediments. The specimens were identified to the lowest taxonomic hierarchy as possible. The physical parameters such as organic carbon (TOC) and grain size distributions were analysed. A total of 775 annelids, 15 arthropods, 12 echinoderms and 32 molluscs individuals were identified and recorded in six stations overall. Family Cirratulidae accounted to the highest numbers of the Annelids ($n=358$), whilst

Cerithidae recorded as highest numbers of Molluscs. Station 5, 6 and 1 recorded the highest diversity index ($H'=2.1845$), evenness index ($J'=0.6316$) and richness index ($D_{mn}=22.0454$) respectively. Principal Component Analysis indicated sediment particle size as the major connector on all stations, with different station correlated to certain sizes of sediment particle. Pearson correlation analysis showed positive correlations between environmental parameters with eight benthic taxa in this study, with most correlations were on

ARTICLE INFO

Article history:

Received: 13 August 2020

Accepted: 5 November 2020

Published: 22 January 2021

DOI: <https://doi.org/10.47836/pjst.29.1.34>

E-mail addresses:

sophianmkmaidin@gmail.com (Mohd Sophian Mohd

Kasihmuddin)

zdcc@ukm.edu.my (Zaidi Che Cob)

*Corresponding author

specific sediment particle size. As the study of benthic community is still inadequate in most of Malaysian waters, particularly in highly industrialised area such as waters in Port Klang, this study can serve as a starting point for any future studies concerning ecological disturbance affecting benthic community in Malaysian waters.

Keywords: Gastropod, Macrobenthos, Polychaete, Port Klang, Pulau Indah, Zooplankton

INTRODUCTION

Benthic macroinvertebrates are ubiquitous in seafloors all over the world. Their simple but unique lifeform enables them to adapt and survive in various conditions at the seafloor. They are regarded as ecosystem engineers, where they help ensuring the sediment environment habitable for other groups of marine organisms to thrive (Lu, 2005; Queirós et al., 2013).

Generally, benthic macroinvertebrates are found to be highly concentrated at soft-bottom sediment closer to the shore (Hossain, 2018) and also found along the continental shelves, where the region is still considered as euphotic zone and rich in nutrients (Vijapure et al., 2018). Peninsular Malaysia is well known to have shallower continental shelves and lesser water depth around it, especially at Straits of Malacca and Johor (Nakajima et al., 2009). These features grant numerous benefits to benthic community such as better foraging grounds and better establishment of guilds. Study in Sungai Pulai by Guan et al. (2014) estuary also shows variations in terms of spatial factor, where crustaceans and polychaetes were found to be highly concentrated in Tanjung Adang (located closer to land) and Merambong Shoal (located far off land) respectively. Their study area is known to have less human intrusion and populated by seagrasses but vulnerable to anthropogenic activities. Study by Mohammad and Jalal (2018) indicated that faunal variation in zones off human settlements in Kuala Pahang along Pahang Estuary was higher than the zones nearby Kuala Pahang itself. Their study recorded higher volume of polychaetes, gastropods and bivalves off Kuala Pahang but records otherwise around Kuala Pahang. Study by Sany et al. (2014) around West Port, Klang recorded 23 Molluscs, 3 Echinoderms, 4 Arthropods and 3 Annelids taxa in 9 stations across the West Port waterways, with molluscs and arthropods dominating stations closer to Pulau Kelang, which is known to have higher volume of mangrove trees and lesser human intrusions. Based on these studies, it could be deduced that spatial variations of benthic macroinvertebrates were influenced by nearby vicinities these benthic communities are located on. The number of benthic macroinvertebrate studies in Malaysian waters especially in areas with heavy anthropogenic activities are still lacking, especially in areas like ports and berths (Sany et al., 2014). As most assessments on benthic community in Malaysian waters were done via cluster sampling but limited to only one point source, this study focused not only utilizing similar sampling method, but also on multiple point comprising mangrove forests in Pulau Kelang, Sungai Klang

estuaries and waterways from Southpoint and North Port, and this study could serve as a useful reference when conducting cluster sampling in areas surrounded by various point sources such as mangrove estuaries (Al-Khayat et al., 2018; Taupp & Wetzel, 2018), ports and berths (Belal et al., 2020) and waterways (Arbi et al., 2017).

Environmental parameters also influence dispersion and dominance of macrobenthos in soft-bottom sediment. Macrobenthos in estuaries are generally highly diverse due to constant influx of nutrients from nearby mangrove areas, but any disturbance to the mangrove areas can directly affect the community as a whole (Lu, 2005). In Brazil, deforestation of mangrove forests effectively reduces the macrobenthos in the studied mudflat areas from 6000 individuals to less than 50 individuals (Bernadino et al., 2018). Deforestation that occurred in the study indicates alteration of the nature of sediment and lesser detritus which is necessary for macrobenthos to thrive. Mosbahi et al. (2019) showed higher diversity of macrobenthos off the coast of Sfax, Tunisia, attributed by lesser exposure to pollutants such as heavy metals further off the coast. Areas with higher heavy metal concentration consist of mostly opportunistic polychaetes such as *Cirratulus cirratus* and *Capitella capitata* whereas in areas with lesser heavy metal concentration consists of sensitive species such as *Euclymene oerstedii* and *Cymadusa filose*. These substrates may originate from the mainland or from certain point source such as fish farm and ports. Quimpo et al. (2020) related the impact of fish farm with lower rate of larval settlement for coral species, strongly implied influx of excess substrates such as unconsumed fish feed and fecal materials from the farm into the sediment. Consequently, this leads to introduction of uncontrollable dominance of algae, opportunistic polychaete and bacteria, in which makes the settlement of larval coral species difficult. In Malaysian waters, Zhen et al. (2020) focused on assessing macrobenthic community at three mudflat sites off Perak and Selangor. The study recorded Bagan Nakhoda Omar site as the highest taxa diversity due to higher chlorophyll-*a*, attributing to higher number of gastropods inhabiting the area, and another two sites, Bagan Sungai Buloh and Kuala Sangga Besar contained lower taxa diversity, attributed by higher ammonia level settling in sediment, possibly originating from nearby estuaries. Sany et al. (2015) made an ecological assessment to benthic macroinvertebrates in West Port, Port Klang. Their study shows contrasting diversity across the waterway of West Port, with lowest diversity but higher dominance of opportunistic gastropods and polychaetes at zones closer to berth lines, and higher diversity of ecologically-sensitive gastropods and echinoderms at southern end of West Port waterway, which has lesser human infrastructures in nearby.

Assessments made in this area (Port Klang) besides Sany et al. (2015) are still lacking overall if not, may not be contemporary with current state of pollution taking place around Port Klang in general. Data obtained from this study is may not tally with the current status of the benthic communities in this region. This study intends to establish connection of latest

distribution of benthic community in the region and relate with the current environmental conditions. This study can help us in identifying possible ecological stresses in the region and suggesting appropriate benthic bioindicator species inhabiting it, in which their population may indicate the current status of ecosystem health of the habitat. The outcome of this study may put ways for other specialized studies on sediments at waters of Port Klang such as heavy metal (ELturk et al., 2019), oil spill (Omar et al., 2018) and bacterial activities in response to presence of certain benthic organisms inhabiting the sediment (Hanapiah et al., 2018).

Therefore, the objectives of this study were to (1) determine distributional pattern of benthic macroinvertebrates inhabiting soft-bottom sediments of study areas northwards of Pulau Indah, Klang and (2) to establish correlation between the distribution and diversity of benthic macroinvertebrates with the corresponding environmental parameters in the study.

MATERIALS AND METHOD

Collection of Benthic Specimens and Sediment Samples

Sampling was performed one-time in six selected points in waters northwards of Pulau Indah (Figure 1). Station 1 was located north of Pulau Indah, closer to mouth of Sungai Klang. Stations 2 and 3 were located at east side of Pulau Indah and with close proximity to the mainland Selangor. Finally, stations 4 to 6 were located at west side of the island, with the station 4 located between the water passage from Northpoint port northwards and Southpoint port eastwards. Stations 5 and 6 were situated closer to smaller estuaries in the pristine and uninhabited Pulau Mat Zin.

Triplicates of sediment samples were taken using a Ponar grab with 0.023 m² mouth area for the purpose of assessing distribution of benthic macroinvertebrates, and another sediment sample was taken to assess the total organic carbon (TOC) and percentages of size particles of sediment (particle size distributon, PSD). Physical parameter such as salinity was taken using salinometer, while depth of water was taken using digital depth sounder. Sediments used for sorting specimens were filtered through 500 µm sieve before being transferred into double plastic bag and preserved using 5% formalin in seawater.

Sorting and Identification of Specimens and Analyses of Sediments

Sediment samples were transferred into Borgorov Box, where specimens were sorted out using forceps under the view of dissecting microscope and transferred into vials containing 70% ethanol to further preserve the specimens. Digital photos of specimens were taken using microscope imaging software (DinoCapture 2.0). Specimens were identified into lowest taxonomic level as possible, using reference such as Fauchald and Jumars (1977), Idris and Arshad (2013), Nakajima et al. (2009), Ng and Davie (2002), Ng (2017), Fujita and Irimura (2015), Ong and Wong (2015), Baharuddin et al. (2018) and others.

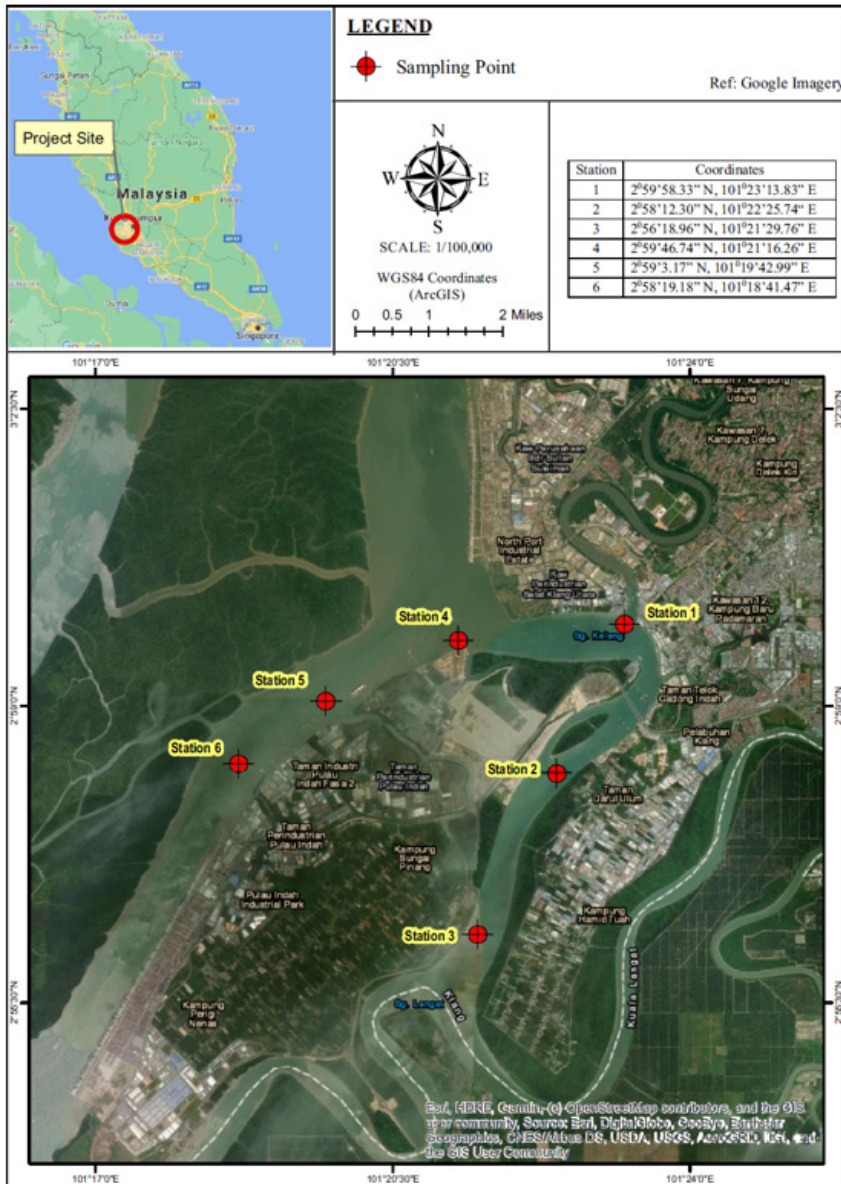


Figure 1. Location of all sampling points in this study

Sediments were stained with Rose Bengal solution, for easier identification under microscope due to pink coloration being applied onto specimens (Bernhard et al., 2006). Specimens were filtered immediately from sediments in the laboratory to reduce the abrasion effect by the sediment that could break specimens' body (Altuhaifi & Baudet 2011).

Loss of Ignition (LOI) method was used to assess the total organic carbon in each sediment samples. Sediments were dried thoroughly in an oven for three days in 60°C before incineration in muffle furnace (500°C) for four hours. The mass of sediment samples before and after burning were obtained and used to derive percentages of LOI and determine mass TOC in sediment in g. In TOC analysis, the sediments must be oven-dried for three days straight to ensure sediment contain zero moisture; thereby reducing measurement error during weighing after muffle furnace phase (Equations [1] to [2]).

$$\text{LOI}(\%) = \frac{(W_i - W_f)}{W_f} \times 100\% \quad [1]$$

$$\text{TOC (g)} = \text{LOI (\%)} \times 0.45 \quad [2]$$

A 0.45 coefficient was used as conversion factor for, based on standard carbon-nitrogen ratio in sediment (Huntington et al., 1988). For determination of percentage of particle size distribution, filtration method was used. Fifty (50) g of sediment samples were washed to remove impurities before passing through filtration set comprising a 2 mm sieve (for very fine sand), 1 mm sieve (for fine sand), 0.5 mm sieve (for medium-sized sand), 0.125 mm sieve (for coarse sand) and 0.063 mm sieve (for very coarse sand). The percentage of sediment samples were assessed by weighing the mass of sediment trapped in each level of the set.

Data Analysis

Ecological indices were calculated based on frequency distribution of macrobenthos organisms at each station. The Shannon-Wiener Diversity Index (H'), Pielou's Evenness Index (J') and Menhinick Richness Index (D_{mn}) were used to assess the state of ecosystem in each station. H' was used to assess diversity of taxa in one group, whereas J' assesses similarity of each taxon number in the group and D_{mn} assess number of individuals of all taxa found in the group (Equations [3], [4], and [5]) (Mason et al., 2005).

$$H' = \sum_{i=1}^s p_i \ln p_i \quad [3]$$

$$J' = \frac{H'}{H_{\max}} \quad [4]$$

$$D_{mn} = \frac{p_i}{\sqrt{N}} \quad [5]$$

Where p_i is individual number in one taxon, H_{\max} is $\ln(s)$ of species diversity in the community under maximum equitability conditions, and N is total number of individuals of

all taxa in one group. For statistical analysis, data derived from environmental parameters and macrobenthos population parameters were subjected to one-way ANOVA test to determine data differences between stations, respectively. For correlation analysis, both data from environmental parameters and macrobenthos population parameters were used for Pearson correlation analysis. Principal Component Analysis was plotted to identify relationship between stations and environmental parameters recorded in this study. In this study, PAST 4.03 was used to assess one-way ANOVA test and PCA, and SPSS 1.0.0.1406 was used to assess Pearson Correlation Analysis.

RESULT AND DISCUSSION

Distribution of Benthic Macroinvertebrates in Waters Surrounding Pulau Indah

A total of 834 macrobenthos individuals comprising of 4 phyla were recorded in this study (Table 1). In order of highest to lowest abundance, a total of 775 Annelids, 15 Arthropods, 12 Echinoderms and 32 Molluscs were found. In terms of species abundance per area, annelids recorded the highest, followed by molluscs, arthropods, and echinoderms (Figure 2). Annelids were found in all stations, but more prevalent in Stations 1 to 3. Polychaete *Caulleriella* and *Cirriformia* (Figure 3) from Family Cirratulidae are found highest in terms of abundance overall. Both polychaete genera dominate soft-bottom sediments in stations 1 and 2. Cirratulid polychaetes are very ubiquitous in soft-bottom sediment globally (Idris & Arshad 2013). However, their abundance is highest in regions susceptible to ecological stresses such as industrial and sewage areas where pollutions such as oil spill and release of heavy metal constituent generally occurs (Ferrando & Méndez, 2011). Both *Caulleriella* and *Cirriformia* polychaetes are found in other parts of waters surrounding Peninsular Malaysia such as in Merambong and Tanjung Adang Shoals (Guan et al., 2014) and Malaysian Exclusive Economic Zone in South China Sea (Rosli et al., 2018). *Mediomastus* (Family Capitellidae) and *Prionospio* (Family Spionidae) (Figure 3) polychaetes also account to higher abundance in station 1, and similar to Cirratulids polychaetes, they can be found in every soft-bottom sediment habitat and common in regions closer to shores and estuaries (Rehitha et al., 2017).

Molluscs were mostly found in Stations 1 to 3. *Cerithidea* snail (Figure 3) from Family Potamididae recorded the highest abundance in this phylum, and it was found in Station 1 and 2. *Cerithidea* snail is commonly found in soft-bottom sediment closer to estuaries and rocky shores and some species are found to attach themselves against human infrastructure such as dock and rock formations at beaches (Baharuddin et al., 2018 & Halim et al., 2019). *Cerithidea* can be found in other parts of waters of Peninsular Malaysia such as Penang (Gholizadeh et al., 2012), Pulau Bidong (Baharuddin et al., 2018) and also previously recorded in mangrove habitat in Pulau Klang, Pulau Ketam and Pulau Mat Zin, neighbouring islands to Pulau Indah (Singh & Baharin 2016). Arthropods were mostly found in Stations

Table 1

Checklist of benthic macroinvertebrate taxa found in all six stations in waters surrounding Pulau Indah, Klang

	St1	St2	St3	St4	St5	St6
Phylum Anelida						
Class Polychaeta						
Order Amphinomida						
Family Amphinomidae						
<i>Eurythoe</i>					1	
Order Capitellida						
Family Capitellidae						
<i>Capitella</i>	4					
<i>Mediomastus</i>	82		11			
<i>Notomastus</i>			33			
<i>Pulliola</i>			11			
Family Maldanidae			2	1	2	
Order Cossurida						
Family Cossuridae						
<i>Cossura</i>						1
Order Eunicida						
Family Eunicida						
<i>Eunice</i>		2	3			
Order Flabelligerida						
Family Flabelligeridae						
<i>Flabellina</i>	1					
Order Orbiniida						
Family Orbiniidae						
<i>Scolopella</i>		3	1			
Order Phyllodocida						
Suborder Aphroditiformia						
Family Sigalionidae						
<i>Sthenelanelia</i>		2			5	
Suborder Glyceriformia						
Family Glyceridae						
<i>Glycera</i>				2	4	6

Table 1 (Continued)

	St1	St2	St3	St4	St5	St6
Family Goniadidae						
<i>Goniada</i>				4	5	
Suborder Nereidiformia						
Family Hesionidae						
<i>Syllida</i>					1	
Family Pilargidae						
<i>Ancistrosyllis</i>		7				
<i>Sigambra</i>		5	34			
Suborder Phyllodociformia						
Family Phyllodocidae						
<i>Phyllodoce</i>	1					
Suborder Incertae Sedis						
Family Nephtyidae						
<i>Micronephthys</i>	9			3		
Order Spionida						
Suborder Spioniformia						
Family Poecilochaetidae						
<i>Poecilochaetus</i>	3		2			1
Family Spionidae						
<i>Prionospio</i>	157	3	3	10		4
Suborder Cirratuliformia						
Family Cirratulidae						
<i>Caulleriella</i>	83	98				4
<i>Cirriformia</i>	130	43				
Order Terebellida						
Family Terebellidae				1		
Phylum Arthropoda						
Order Amphipoda						
Family Scinidae						
<i>Scina</i>					3	
Order Decapoda						
Family Paraonoipectidae				1		

Table 1 (Continued)

	St1	St2	St3	St4	St5	St6
Family Xanthidae						
<i>Micropanope spinipes</i>					2	
Family Pontoporeiidae						
<i>Monoporeia</i>						3
Order Euphausiacea						
Family Euphasiidae						
<i>Thysanoessa</i>						2
Order Tanaidacea						
Family Tanaidae						
<i>Tanais</i>		1				3
Phylum Echinodermata						
Order Holothuroidea						
Family Cucumariidae						
<i>Thyonidium</i>					3	
Order Ophiuroidea						
Family Amphiuridae						
<i>Ophiothrix</i>		1				
Family Ophiactidae						
<i>Ophiactis</i>				3	3	2
Phylum Mollusca						
Order Caenogastropoda						
Family Cerithiidae						
<i>Cerithium</i>		4				
Family Potamididae						
<i>Cerithidea rhizophorarum</i>	5		5			
<i>Cerithidea rhizophorarum morchii</i> (var.)	8		2			
Order Littorinimorpha						
Family Rissoidae						
<i>Alvania</i>			7			
Order Neogastropoda						
Family Nassariidae						
<i>Nassarius</i>			1			

Distribution of Benthic Macroinvertebrates of Pulau Indah, Klang

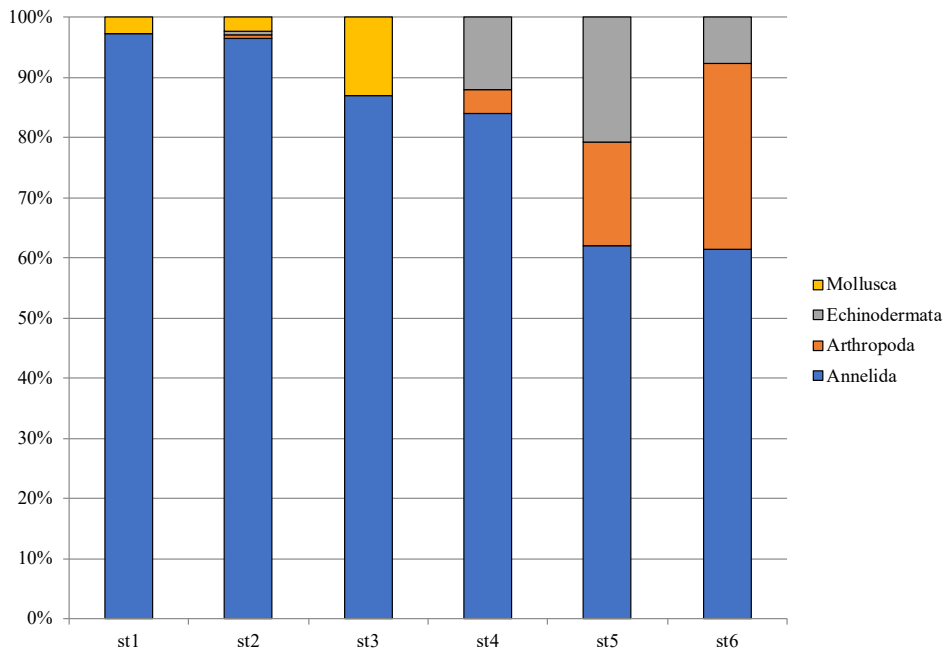


Figure 2. Taxa abundance percentage for all phyla in each station per square area.

4 to 6. Two families of crabs were identified, namely Family Paraonoipediae and Xanthidae (Figure 3). These crabs were found in Stations 4 and 5 respectively. These families of crab are well-known to inhabit in estuary areas and occasionally found at submerged part of port and berth (Ng & Davie 2002). Both families are common families of crab in Strait of Malacca and major waterways in Indonesia (Ng, 2017).

Zooplankton found in this study comprised amphipods, krills and tanaids (Figure 3). Like Brachyura crabs, majority of these individuals were found only in station 4 to 6. *Monoporeia* and *Scina* amphipods, *Thysanoessa* krills and *Tanais* tanaids are generally found only in nutrient-rich water, which in this case their abundance in these stations may be attributed to the stations' closer proximity to multiple small estuaries with rich mangrove covers (Nakajima et al., 2019). Distribution of sea cucumber *Thyodinium* and brittle stars *Ophiuthrix* and *Ophiactis* is commonly restricted to only areas rich in nutrients (Kamarudin et al., 2015; Gondim et al., 2013). Sea cucumber *Thyodinium* is previously reported as common in Tanjung Piai, Johor (Ong & Wong 2015), whereas *Ophiuthrix* and *Ophiactis* (Figure 3) are recorded in Strait of Johor (Fujita & Irimura, 2015). Studies showed that these organisms prefer environment with higher nutrient affluent and organic materials, and that closer the habitat to estuaries, the higher the abundance of these Echinoderms (Ong & Wong, 2015; Fujita & Irimura, 2015).

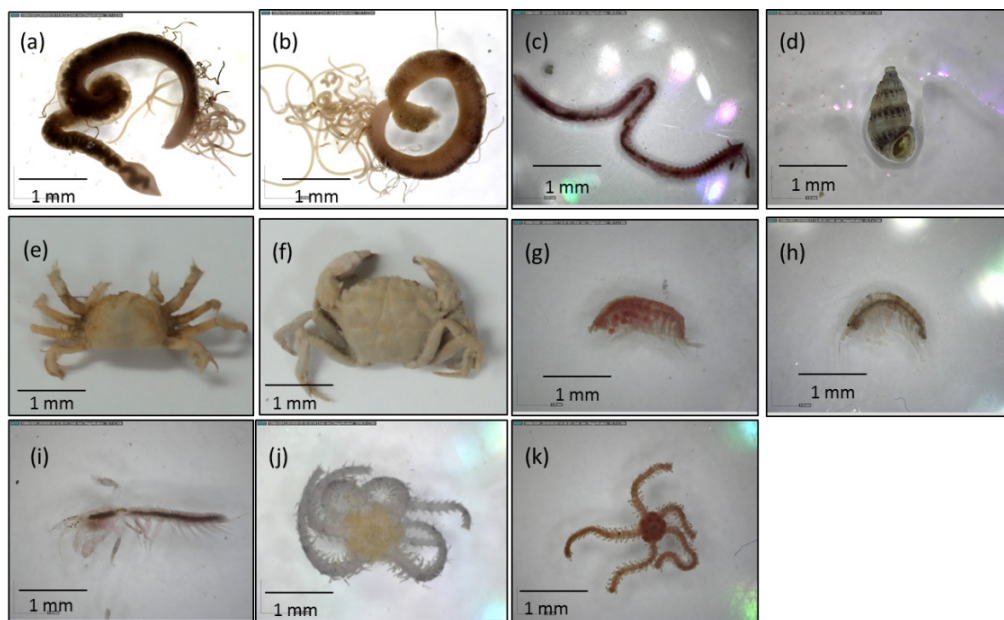


Figure 3. Assortment of representative genera found in this study. **Annelids:** (a) *Cirriformia* (b) *Caulleriella* (c) *Prionospio*; **Gastropods:** (d) *Cerithidea*; **Arthropods:** (e) Paraonoipediae crab (f) *Micropanope* (g) *Monoporeia* (h) *Scina* (i) *Tanais*; and **Echinoderms:** (j) *Ophiothrix* (k) *Ophiactis*

Taxonomic identification performed in this study was based on several studies such as Idris and Arshad (2013) for the annelids, Ong and Wong (2015) for the echinoderms, Ng (2017) for the arthropods and Baharuddin et al. (2018) for the molluscs. In addition, online websites such as WoRMS and MyBIS were also used as these online repositories are often updated by users all the time. Databases on online repositories may contain even more accurate location of targeted taxa as well as suitable naming nomenclature, biological traits, life cycle and even feeding behaviour (Horton et al., 2017).

Assessment of Ecological and Environmental Parameters

Table 2 shows ecological indices in terms of Shannon-Wiener Diversity Index (H'), Pielou's Evenness Index (J') and Menhinick's Richness Index (D_{mn}). For H' index, station 5 was the highest, followed by stations 6 and 3. Station 6 recorded the highest J' index value, while station 4 showed *vice versa*. Lastly, D_{mn} recorded station 1 as the highest in all station followed by station 2 and 3. Other stations, 4 to 6, showed almost similar D_{mn} index value. H' found in all stations especially in Station 5 was comparatively lower than the previous record of H' in Sany et al. (2014). Sany et al. (2014) focused on West Port, and Station 5 is located on it. Possible factor attributing to lower H' may be due to lower number of taxa found in this study compared to the number of taxa found in Sany et al. (2014). This study

also did sampling session only once, whilst Sany et al. (2014) performed the sampling in the region several times, possibly explaining higher taxa number and specimen counts than this study.

Table 2

Population parameters and ecological indices for overall benthic macroinvertebrates in respective stations

Stations	Taxa No.	Density (ind./m ²)	H'	J'	D_{mn}
1	11	21043.48	1.63	0.26	22.05
2	11	7347.83	1.38	0.27	13.15
3	13	5043.48	2.01	0.42	10.19
4	8	1086.96	1.76	0.55	5.00
5	10	1260.87	2.18	0.30	5.39
6	9	1130.43	2.06	0.63	5.10

As for environmental parameters, station 6 recorded the highest total organic carbon, followed by station 4 as the lowest record for the latter (Figure 5). As for sediment particle size assessment (Figure 4), stations 1 and 3 recorded highest percentage of coarse sand (0.5 mm) (52.24%, 49.16%). Stations 2, 4 and 5, on the other hand, recorded highest particle size percentage fine sand (67.13%, 84.61%, and 75.45%). Lastly, station 6 showed highest percentage of granule (2 mm) (17.70%).

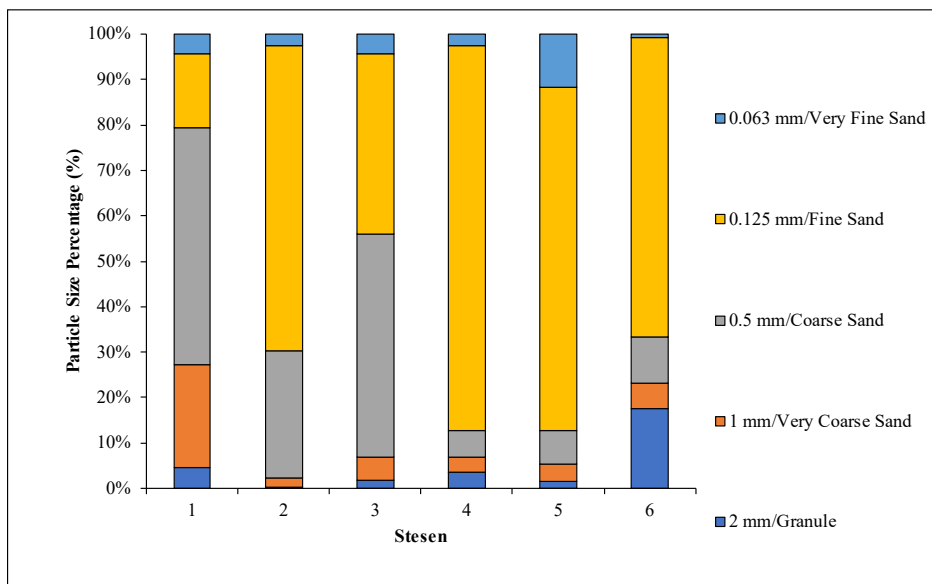


Figure 4. Percentages of sediment particle sizes in each respective station.

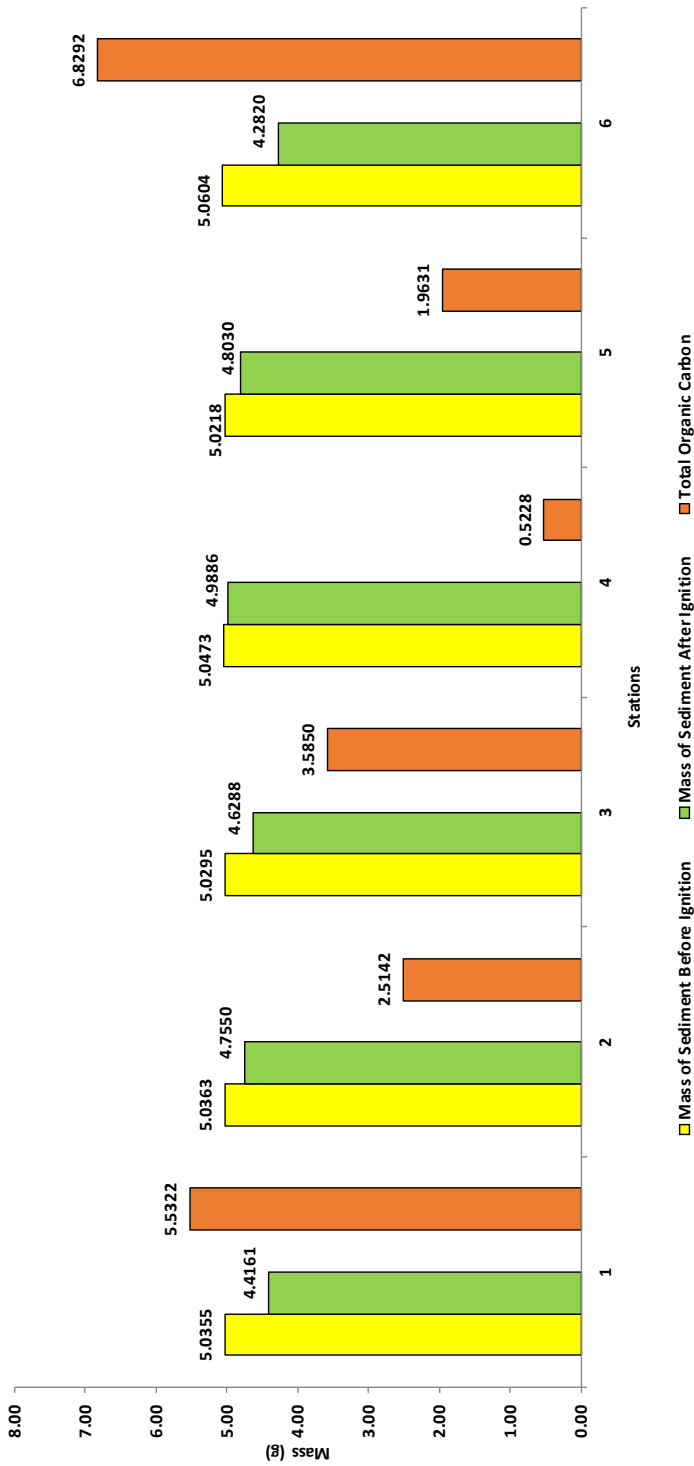


Figure 5. Mass of sediment before and after ignition, and Total Organic Carbon derived from LOI Method in each station in this study

Correlation of Distribution and Diversity of Benthic Macroinvertebrate Community with Environmental Parameter

Data Significance Between Stations. In terms of data significance, one-way ANOVA test showed no significant difference on both environmental parameters and benthic communities' abundance in all stations ($P > 0.05$).

Correlation Between Stations with Surrounding Environmental Parameters. Based on PCA analysis (Figure 6), stations 2, 4, and 5 were more attributed to fine sand (0.125 mm particle size sediment). These stations are located in between islands or mainland. Fine sand is common in this area. Bolam et al. (2016) reported aggregation of snails, polychaetes such as Spionids and Cirratulids and brittle star such as Ophiuroids in seafloor nearby a dredge disposal area, northeast coast of England, where active sedimentation process took place. Similarly, the coastline is also passed frequently by ships from other part of England. Benthic taxa found in Bolam et al. (2016) were smaller in size and their availability in sediments might be attributed to their ability to transverse across smaller-sized sediment to catch food and survivability from larger-sized predators such as crabs and Errantia polychaetes.

PCA analysis also showed that Station 1 and 3 were more attributed to coarse sand (0.5 mm sediment size). Station 1 is located nearby estuaries of Sungai Klang which is connected directly into Selangor inland, whilst station 3 is located nearby Sungai Langat. Sedimentation from these rivers were lower, hence might explain higher percentage of medium-sized sand but lesser extremities. Harris & Aris (2015) studied bioaccumulation of metals on these two rivers and reported lower sedimentation rate from both rivers inland. Polychaetes and gastropods were found in larger abundance in these two stations, with Sedentaria polychaetes (Capitellids, Cirratulids, Spionids) dominating the sediment by whole. Hill et al. (2013) conducted survey on dominance of these three polychaete family in Sydney Harbour, Australia, and associated large presence of these polychaete groups with presence of substrata in sediment such as PAH and heavy metals.

Lastly, PCA analysis indicated that station 6 was more attributed towards very fine sand (0.063 mm sediment size), very coarse sand (1 mm sediment size) and granules (2 mm sediment size), water depth, salinity and TOC. Station 6 is located closer to estuaries from Pulau Kelang, an island with mangrove biotope. Previous study by Sany et al. (2014) at shipping route nearby this study's station 6 recorded variation of Errantia polychaetes, gastropods and molluscs, and these variations were attributed to high concentration of organic nutrients such as phosphate and nitrate originating from estuaries of Pulau Kelang which might fuel phytoplankton leading to establishment of food web in the region by other organisms. Similarly, study by Barros et al. (2012) on mangrove estuaries in Brazil recorded highly diverse polychaete community, in which their occurrence were attributed to higher flux of organic carbon in sediment, originating from sediments drifting away from

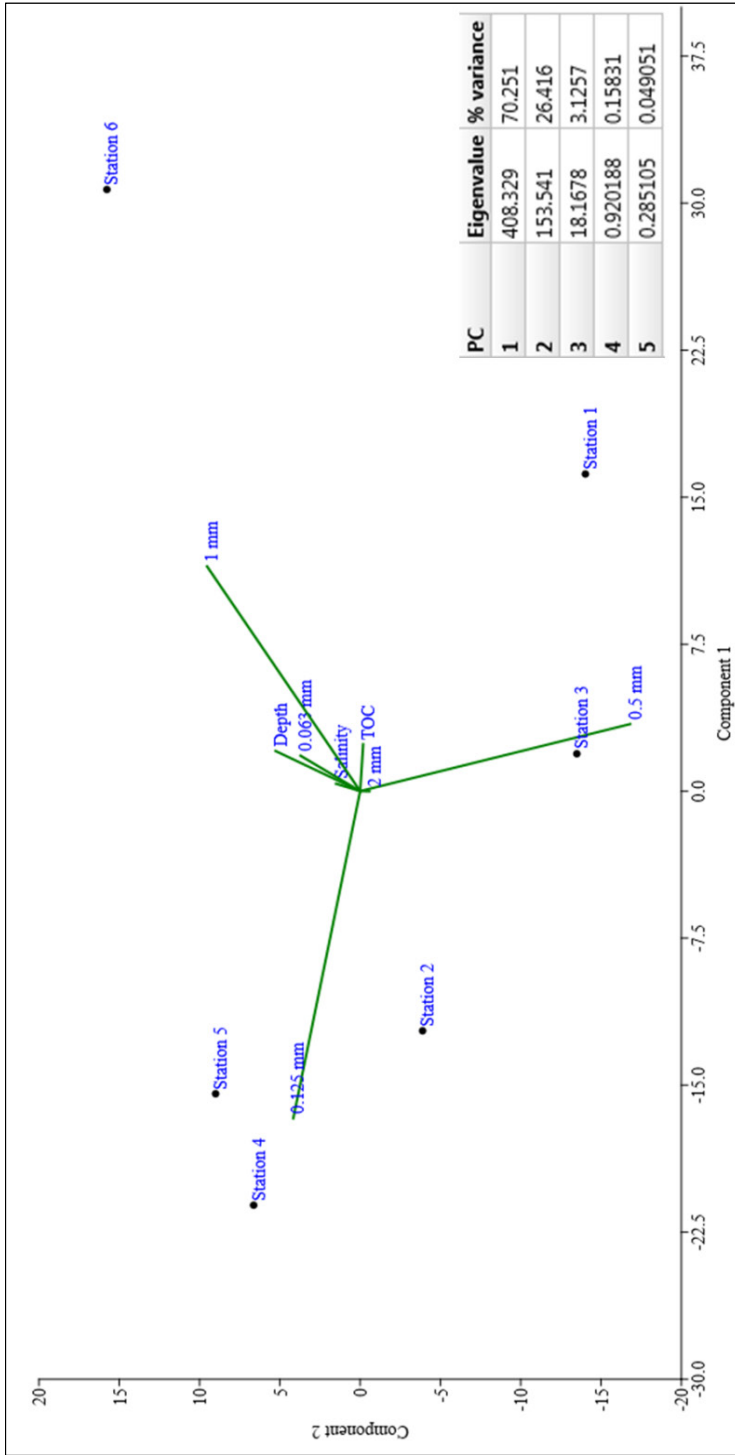


Figure 6. Principal Component Analysis (PCA) assessed on all stations with respect to environmental parameters in this study

mangrove roots. Their study also considered salinity as the driving factor for diversity of benthic community in the region. It may be possible that sedimentation process from Pulau Kelang mangrove estuaries might end up transporting more sediment offshore, in which sediment might contain enough organic materials for taxa in the region.

Correlation Between Benthic Taxa with Environmental Parameters. Pearson correlation analysis (refer to attached Excel file) indicated several genera of benthic macroinvertebrates had positive and negative correlations towards certain environmental parameters recorded in this study. For polychaete groups, *Cossura* had positive correlation with salinity, very fine sand (0.063 mm) and very coarse sand (1 mm); *Glycera* positively correlated to very fine sand (0.063 mm); *Micronephthys* positively correlated to 2 mm and *Poecilochaetus* positively correlated to coarse sand (0.5 mm). *Cossura* polychaete is commonly found in muddy sediment, and previously recorded in Bay of Bengal (Smitha et al., 2017) and in dredge disposal zone in Brazilian estuary (Sousa et al. 2019). *Glycera* bloodworm is common in smaller grain-sized sediment where it is easier to transverse to catch prey, and previously recorded in sediments of Sepetiba Bay, Brazil, with higher percentage on smaller-sized grain such as mud and silt (Mattos et al., 2013). *Micronephthys* is commonly found in sub-tidal areas where larger-sized sediment dominate the region (Murray et al., 2017), and previous report by Shakouri et al. (2017) showed records of the genus abundance in sub-tidal areas of Chabahar Bay, Iran. *Peocilochaetus* is common in sandy sediment closer to estuaries. Previous record by Raut et al. (2013) on east coast of India reported the finding of this genus in sediment closer to recently cleaned-up Boat Harbour.

In terms of Arthropod groups, both *Monoporeia* and *Thysanoessa* have positive correlation to salinity, very fine sand (0.063 mm) and very coarse sand (1 mm). *Tanais* was positively correlated to very coarse sand (1 mm). Previous records of these arthropods showed higher abundance of *Monoporeia* amphipod, *Thysanoessa* krill and *Tanais* tanaid in estuary and intertidal zones where salinity gradient was present along the zone, and higher percentage of smaller-sized grain sediment such as mud and silt present in the area (Wiklund & Andersson, 2014; Cabrol et al., 2019; Pandiyarajan et al., 2020).

For echinoderms, *Ophiactis*' abundance was negatively correlated to coarse sand (0.5 mm). Previous record on *Ophiactis* in Johor Straits showed higher abundance of the genus in mud and silts rather than in larger-sized sediment (Fujita & Irimura, 2015). Oppositely, mollusc *Cerithidea rizopharum* showed positive correlation to coarse sand (0.5 mm). *Cerithidea* is a common gastropod readily found in intertidal areas closer to port and berth where sands are in highest percentage of grain-size percentage (Reid & Claremont, 2014).

CONCLUSION

This study concludes that annelids were highest in terms distribution and diversity in all study areas, whilst distribution and diversity of other phyla were limited to certain study areas only. Ecological indices showed highest diversity index in Station 5, highest evenness in Station 6 and highest richness index in Station 1. Correlation study showed sediment particle size as a major factor that differentiated all stations in study, and also a major factor that correlated positively on eight benthic taxa in this study and another one taxon attained negative correlation on the same factor.

As benthic studies in Malaysia as a whole are still very inadequate, especially in areas with heavy human interference, this study can serve as a good starting point for more extensive studies regarding ecological stresses in benthic communities in other main ports in Sabah, Sarawak and Johor. Through this study, we can create a good comparison and generalization on conditions in benthic communities in these regions, and if possible, recommend actions to reduce any loss taxa of benthic community ecological stresses induced by pollutants such as heavy metal, oil spills and improper handling of domestic wastes.

ACKNOWLEDGEMENT

We sincerely thank Mr. Zuhaimi from the Marine Science Program, Universiti Kebangsaan Malaysia for his dedicated efforts on sample collection. This work was funded by Fundamental Research Grant, Ministry of Higher Education, Malaysia (Project No. FRGS/1/2017/STG03/UKM/02/5).

REFERENCES

- Al-Khayat, J. A., Abdulla, M. A., & Alatalo, J. M. (2018). Diversity of benthic macrofauna and physical parameters of sediments in natural mangroves and in afforested mangroves three decades after compensatory planting. *Aquatic Sciences*, *81*(1), 1-18. doi: <https://doi.org/10.1007/s00027-018-0599-7>
- Altuhafi, F., & Baudet, B. A. (2011). A hypothesis on the relative roles of crushing and abrasion in the mechanical genesis of a glacial sediment. *Engineering Geology*, *120*(1-4), 1-9. doi: <https://doi.org/10.1016/j.enggeo.2011.03.002>
- Arbi, I., Zhang, J., Liu, S., Wu, Y., & Huang, X. (2017). Benthic habitat health assessment using macrofauna communities of a sub-tropical semi-enclosed bay under excess nutrients. *Marine Pollution Bulletin*, *119*(2), 39-49. doi: <https://doi.org/10.1016/j.marpolbul.2017.03.042>
- Baharuddin, N., Basri, N. B., & Syawal, N. H. (2018). Marine gastropods (Gastropoda; mollusca) diversity and distribution on intertidal rocky shores of Terengganu, Peninsular Malaysia. *AACL Bioflux*, *11*(4), 1144-1154.

- Barros, F., de Carvalho, G. C., Costa, Y., & Hatje, V. (2012). Subtidal benthic macroinfaunal assemblages in tropical estuaries: Generality amongst highly variable gradients. *Marine Environmental Research*, 81, 43-52. doi: <https://doi.org/10.1016/j.marenvres.2012.08.006>
- Belal, A. A. M., Kelany, M. S., Hamed, M. M., & El-Fattah, L. S. A. (2020). Selected bacterial communities associated with macro-benthic fauna assemblages at the Timsah Lake and the Western Lagoon's sediments, Suez Canal, Egypt. *Egyptian Journal of Aquatic Research*, 46(2), 137-143. doi: <https://doi.org/10.1016/j.ejar.2020.02.003>
- Bernardino, A. F., de Oliveira Gomes, L. E., Hadlich, H. L., Andrades, R., & Correa, L. B. (2018). Mangrove clearing impacts on macrofaunal assemblages and benthic food webs in a tropical estuary. *Marine Pollution Bulletin*, 126, 228-235. doi: <https://doi.org/10.1016/j.marpolbul.2017.11.008>
- Bernhard, J. M., Ostermann, D. R., Williams, D. S., & Blanks, J. K. (2006). Comparison of two methods to identify live benthic foraminifera: A test between Rose Bengal and CellTracker Green with implications for stable isotope paleoreconstructions. *Paleoceanography*, 21(4), 1-8. doi: <https://doi.org/10.1029/2006PA001290>
- Bolam, S. G., McIlwaine, P. S. O., & Garcia, C. (2016). Application of biological traits to further our understanding of the impacts of dredged material disposal on benthic assemblages. *Marine Pollution Bulletin*, 105(1), 180-192. doi: <https://doi.org/10.1016/j.marpolbul.2016.02.031>
- Cabrol, J., Trombetta, T., Amaudrut, S., Aulanier, F., Sage, R., Tremblay, R., ... & Winkler, G. (2019). Trophic niche partitioning of dominant North-Atlantic krill species, *Meganyctiphanes norvegica*, *Thysanoessa inermis*, and *T. raschii*. *Limnology and Oceanography*, 64(1), 165-181. doi: <https://doi.org/10.1002/lno.11027>
- ELTurk, M., Abdullah, R., Zakaria, R. M., & Bakar, N. K. A. (2019). Heavy metal contamination in mangrove sediments in Klang estuary, Malaysia: Implication of risk assessment. *Estuarine, Coastal and Shelf Science*, 226, 1-7. doi: <https://doi.org/10.1016/j.ecss.2019.106266>
- Fauchald, K., Jumars, P.A. (1979). The diet of worms: A study of polychaete feeding guilds. *Oceanography Marine Biology Annual Review*, 17, 193-284.
- Ferrando, A., & Méndez, N. (2011). Efectos de la contaminación orgánica sobre la distribución de las comunidades de anélidos en la laguna costera "estero de urías" (Mexico) [Effects of organic pollution on the distribution of annelid communities in the coastal lagoon, *Urias estuary* (Mexico)]. *Scientia Marina*, 75(2), 351-358. doi: <https://doi.org/10.3989/scimar.2011.75n2351>
- Fujita, T., & Irimura, S. (2015). Preliminary list of ophiuroids (Echinodermata: Ophiuroidea) collected from the Johor Straits, Singapore. *Raffles Bulletin of Zoology*, 2015(31), 264-272.
- Gholizadeh, M., Yahya, K., Talib, A., & Ahmad, O. (2012). Effects of environmental factors on polychaete assemblage in Penang National Park, Malaysia. *World Academy of Science*, 72(December 2012), 669-672.

- Gondim, A. I., Alonso, C., Dias, T. L. P., Manso, C. L. C., & Christoffersen, M. L. (2013). A taxonomic guide to the brittle-stars (Echinodermata, Ophiuroidea) from the State of Paraíba continental shelf, Northeastern Brazil. *ZooKeys*, 307, 45-96. doi: <https://doi.org/10.3897/zookeys.307.4673>
- Guan, W. S., Ghaffar, M. A., Ali, M. M., & Cob, Z. C. (2014). The Polychaeta (Annelida) communities of the Merambong and Tanjung Adang Shoals, Malaysia, and its relationship with the environmental variables. *Malayan Nature Journal*, 66(1-2), 168-183.
- Halim, S. S. A., Shuib, S., Talib, A. & Yahya, K. (2019). Species composition, richness, and distribution of molluscs from intertidal areas at Penang Island, Malaysia. *Songklanakarin Journal of Science and Technology*, 41(1), 165-173.
- Hanapiah, M., Zulkifli, S. Z., Mustafa, M., Mohamat-Yusuff, F., & Ismail, A. (2018). Isolation, characterization, and identification of potential Diuron-degrading bacteria from surface sediments of Port Klang, Malaysia. *Marine Pollution Bulletin*, 127, 453-457. doi: <https://doi.org/10.1016/j.marpolbul.2017.12.015>
- Harris, H. & Aris, A. Z. (2015). Distribution of metals and quality of intertidal surface sediment near commercial port and estuaries of urbanized rivers in Port Klang, Malaysia. *Environmental Earth Sciences*, 73, 7205-7218. doi: 10.1007/s12665-014-3900-7
- Hill, N. A., Simpson, S. L., & Johnston, E. L. (2013). Beyond the bed: Effects of metal contamination on recruitment to bedded sediments and overlying substrata. *Environmental Pollution*, 173, 182-191. doi: <https://doi.org/10.1016/j.envpol.2012.09.029>
- Horton, T., Gofas, S., Kroh, A., Poore, G. C. B., Read, G., Rosenberg, G., ... & Vranken, S. E. (2017). Improving nomenclatural consistency: A decade of experience in the World Register of Marine Species. *European Journal of Taxonomy*, 2017(389), 1-24. doi: <https://doi.org/10.5852/ejt.2017.389>
- Hossain, M. B. (2018). Trophic functioning of macrobenthic fauna in a tropical acidified Bornean estuary (Southeast Asia). *International Journal of Sediment Research*, 34(1), 48-57. doi: <https://doi.org/10.1016/j.ijsrc.2018.08.002>
- Huntington, T. G., Ryan, D. F., & Hamburg, S. P. (1988). Estimating soil nitrogen and carbon pools in a northern hardwood forest ecosystem. *Soil Science Society of America Journal*, 52(4), 1162-1167. doi: <https://doi.org/10.2136/sssaj1988.03615995005200040049x>
- Idris, I., & Arshad, A. (2013). Checklist of polychaetous annelids in Malaysia with redescription of two commercially exploited species. *Asian Journal of Animal and Veterinary Advances*, 8(3), 409-436. doi: 10.3923/ajava.2013.409.436
- Kamarudin, K. R., Usup, G., Hashim, R., & Rehan, M. M. (2015). Sea cucumber (Echinodermata: Holothuroidea) species richness at selected localities in Malaysia. *Pertanika Tropical Agricultural Science*, 38(1), 7-32.
- Lu, L. (2005). Seasonal variation of macrobenthic infauna in the Johor Strait, Singapore. *Aquatic Ecology*, 39(1), 107-111. doi: <https://doi.org/10.1007/s10452-004-7111-2>

- Mason, N. W. H., Mouillot, D., Lee, W. G., & Wilson, J. B. (2005). Functional richness, functional evenness and functional divergence: The primary components of functional diversity. *Oikos*, *111*(1), 112-118. doi: <https://doi.org/10.1111/j.0030-1299.2005.13886.x>
- Mattos, G., Cardoso, R. S., & Santos, A. S. D. (2013). Environmental effects on the structure of polychaete feeding guilds on the beaches of Sepetiba Bay, south-eastern Brazil. *Journal of the Marine Biological Association of the United Kingdom*, *93*(4), 973-980. doi: <https://doi.org/10.1017/S0025315412000707>
- Mohamamad, A., & Jalal, K. C. A. (2018). Macrobenthic diversity and community composition in the Pahang Estuary, Malaysia. *Journal of Coastal Research*, *82*(4), 206-211. doi: <https://doi.org/10.2112/SI82-030.1>
- Mosbahi, N., Serbaji, M. M., Pezy, J. P., Neifar, L., & Dauvin, J. C. (2019). Response of benthic macrofauna to multiple anthropogenic pressures in the shallow coastal zone south of Sfax (Tunisia, central Mediterranean Sea). *Environmental Pollution*, *253*, 474-487. doi: <https://doi.org/10.1016/j.envpol.2019.06.080>
- Murray, F., Solan, M., & Douglas, A. (2017). Effects of algal enrichment and salinity on sediment particle reworking activity and associated nutrient generation mediated by the intertidal polychaete *Hediste diversicolor*. *Journal of Experimental Marine Biology and Ecology*, *495*, 75-82. doi: [10.1016/j.jembe.2017.06.002](https://doi.org/10.1016/j.jembe.2017.06.002)
- Nakajima, R., Yoshida, T., Othman, B. H. R., & Toda, T. (2009). Diel variation of zooplankton in the tropical coral-reef water of Tioman Island, Malaysia. *Aquatic Ecology*, *43*(4), 965-975. doi: <https://doi.org/10.1007/s10452-008-9208-5>
- Ng, P. K. L. (2017). On the identities of the highland vampire crabs, *Geosesarma foxi* (Kemp, 1918) and *G. serenei* Ng, 1986, with description of a new phytotelmic species from Penang, Peninsular Malaysia (Crustacea: Decapoda: Brachyura: Sesarmidae). *Raffles Bulletin of Zoology*, *65*, 226-242.
- Ng, P. K. L., & Davie, P. J. F. (2002). A checklist of the brachyuran crabs of Phuket and Western Thailand. *Phuket Marine Biological Center Special Publication*, *23*(2), 369-384.
- Omar, T. F. T., Aris, A. Z., Yusoff, F. M., & Mustafa, S. (2018). Occurrence, distribution, and sources of emerging organic contaminants in tropical coastal sediments of anthropogenically impacted Klang River estuary, Malaysia. *Marine Pollution Bulletin*, *131*, 284-293. doi: <https://doi.org/10.1016/j.marpolbul.2018.04.019>
- Ong, J. Y., & Wong, H. P. S. (2015). Sea cucumbers (Echinodermata: Holothuroidea) from the Johor Straits, Singapore. *Raffles Bulletin of Zoology*, *2015*(31), 273-291.
- Pandiyarajan, R. S., Jyothibabu, R., Jagadeesan, L., & Arunpandi, N. (2020). Ecology and distribution of tanaids in a large tropical estuary along the Southwest Coast of India. *Regional Studies in Marine Science*, *33*(2020), 1-12. doi: <https://doi.org/10.1016/j.rsma.2019.101032>
- Queirós, A. M., Birchenough, S. N. R., Bremner, J., Godbold, J. A., Parker, R. E., Romero-Ramirez, A., ... & Widdicombe, S. (2013). A bioturbation classification of European marine infaunal invertebrates. *Ecology and Evolution*, *3*(11), 3958-3985. doi: <https://doi.org/10.1002/ece3.769>
- Quimpo, T. J. R., Ligson, C. A., Manogan, D. P., Requilme, J. N. C., Albelda, R. L., Conaco, C., & Cabaitan, P. C. (2020). Fish farm effluents alter reef benthic assemblages and reduce coral settlement. *Marine Pollution Bulletin*, *153*, 1-7. doi: <https://doi.org/10.1016/j.marpolbul.2020.111025>

- Raut, D., Raman, P. E., Raman, A. V., & Patnaik, L. (2013). Assessment of Benthic community alterations in relation to pollution in a boat harbor in Visakhapatnam, East Coast of India. *The Ecoscan*, 7(1&2), 51-56.
- Rehitha, T. V., Ullas, N., Vineetha, G., Benny, P. Y., Madhu, N. V., & Revichandran, C. (2017). Impact of maintenance dredging on microbenthic community structure of a tropical estuary. *Ocean and Coastal Management*, 144(2017), 71-82.
- Reid, D. G., & Claremont, M. (2014). The genus *Cerithideopsis* Thiele, 1929 (Gastropoda: Potamididae) in the Indo-West Pacific region. *Zootaxa*, 3779(1), 61-80. doi: <https://doi.org/10.11646/zootaxa.3779.1.8>
- Rosli, N. S., Yahya, N., Idris, I., & Bachok, Z. (2018). Polychaetous annelid community structure in relation to soft bottom sediment characteristics in continental shelf of the southern South China Sea. *Journal of Sustainability Science and Management*, 13(5), 125-146.
- Shakouri, A., Mortimer, K., & Dehani, E. (2017). A new species and new records of Magelona (Annelida: Magelonidae) from Chabahar Bay, Gulf of Oman, South-eastern Iran. *Journal of the Marine Biological Association of the United Kingdom*, 97(7), 1537-1552. doi: <https://doi.org/10.1017/S002531541600076X>
- Singh, H. R., & Baharin, N. K. (2016). Gastropod community structure from varying levels of mangrove disturbance in Selangor, Malaysia. *Malaysian Forester*, 79(1-2), 54-63.
- Smitha, C. K., Raveendran, T. V., Rosamma, P., & Damodaran, R. (2017). First Record of the polychaete *Cossura aciculata* from Indian Waters. *Journal on New Biological Reports*, 6(2), 82-85.
- Sousa, L. K. S., Júnior, M. N., Cutrim, M. V. J., & de Oliveira, V. M. (2019). *Cossura yacy* sp. nov. (cossuridae, annelida) from a tropical brazilian estuary. *Iheringia - Serie Zoologia*, 109, 1-9.
- Sany, S. B. T., Hashim, R., Salleh, A., Rezayi, M., & Safari, O. (2015). Ecological quality assessment based on macrobenthic assemblages indices along West Port, Malaysia coast. *Environmental Earth Sciences*, 74(2), 1331-1341. doi: 10.1007/s12665-015-4122-3
- Sany, S. B. T., Rezayi, M., Hashim, R., Salleh, A., & Safari, O. (2014). Diversity and distribution of benthic invertebrates. *International Journal of Environmental, Ecological, Geological and Mining Engineering*, 8(7), 458-461.
- Taupp, T., & Wetzel, M. A. (2018). Functionally similar but taxonomically different: Benthic communities in 1889 and 2006 in an industrialized estuary. *Estuarine, Coastal and Shelf Science*, 217, 292-300. doi: <https://doi.org/10.1016/j.ecss.2018.11.012>
- Vijapure, T., Sukumaran, S., Neetu, S., & Chandel, K. (2018). Macrobenthos at marine hotspots along the northwest Indian inner shelf: Patterns and drivers. *Marine Environmental Research*, 144(December 2018), 111-124. doi: <https://doi.org/10.1016/j.marenvres.2018.12.007>
- Wiklund, A. K. E., & Andersson, A. (2014). Benthic competition and population dynamics of *Monoporeia affinis* and *Marenzelleria* sp. in the northern Baltic Sea. *Estuarine, Coastal and Shelf Science*, 144, 46-53. doi: <https://doi.org/10.1016/j.ecss.2014.04.008>
- Zhen, W. L., Teoh, H. W., Lee, C. W., Lee, S. L., Saito, H., & Chong, V. C. (2020). Macrobenthic community associated with semi-cultured blood cockles (*Tegillarca granosa*) in tropical mudflats. *Continental Shelf Research*, 195, 1-11. doi: <https://doi.org/10.1016/j.csr.2020.104061>

Flood-Modeling and Risk Map Simulation for Mae Suai Dam-Break, Northern Thailand

Anurak Busaman, Somporn Chuai-Aree, Salang Musikasuwan and Rhysa McNeil*

*Department of Mathematics and Computer Science, Faculty of Science and Technology,
Prince of Songkla University, Pattani 94000, Thailand
Centre of Excellence in Mathematics, CHE, Si Ayutthaya Rd., Bangkok, 10400, Thailand*

ABSTRACT

Dam-break floods are a serious disaster. This study aims to simulate and model the Mae Suai dam-break flood using shallow water equations (SWE) with an adaptive tree grid finite volume method, and determine the relationship between the initial water levels in the dam and the simulation results set regarding arrival times and maximum water depths using a polynomial model. We used elevation data obtained from the Shuttle Radar Topography Mission. The method was evaluated using the Xe-Pian dam-break flood simulation. The numerical results of water propagation was in agreement with the satellite image. The SWE and numerical algorithm was then used for the Mae Suai dam-break flood simulation. The numerical solution sets were approximated by a polynomial function of appropriate degree for flood arrival times and maximum water depth. Comparisons showed that the polynomial model results were similar to the SWE results; however, the proposed method was more efficient and can obtain a flood risk map without the need to fully solve the SWE. The method can also be applied for dam-break flood simulations and models in other regions using information from the dam.

Keywords: Dam break, modeling, polynomial function, shallow water equations, simulation

ARTICLE INFO

Article history:

Received: 26 July 2020

Accepted: 28 October 2020

Published: 22 January 2021

DOI: <https://doi.org/10.47836/pjst.29.1.35>

E-mail addresses:

anurak.b@psu.ac.th (Anurak Busaman)

schuaiaree@gmail.com (Somporn Chuai-Aree)

salang.m@psu.ac.th (Salang Musikasuwan)

rhysa.m@psu.ac.th (Rhysa McNeil)

* Corresponding author

INTRODUCTION

Dam-break floods are serious disasters. In 1959 the Malpasset dam-break in southern France, caused about 68 million dollars in terms of economic loss and resulted in 421 deaths (Goodman, 2013). In 2005, the Taum Sauk dam-break flood in the United States

caused 1,100 fatalities (NOAA, 2005). In 2018, the Xe-Pian Xe-Namnoy dam-break flood in Laos resulted in 6,600 people becoming homeless and 98 people missing (Gong, 2018). Simulation and modeling of dam-break floods are necessary in order to provide information for planning, preparation, prevention and evacuation. For the simulation and modeling of the dam-break, George (2011) simulated Malpasset dam-break flood by solving the shallow-water equations with a finite a volume method and block-structured dynamic adaptive mesh refinement (AMR), while Dat et al. (2019) simulated dam-break flood inundation for a case study of DakDrinh Reservoir in Vietnam using 1D and 2D models of MIKE FLOOD. Moreover, Latrubesse et al. (2020) studied the cause of the Xe-Pian Xe-Namnoy dam breach, and assessed the hydrologic and geomorphic impact of the flood using the HEC-RAS 2D model to study flooding dynamics and dam-break flow.

Most of the dam-break simulations used numerical methods for solving the shallow water equations, which is time-consuming. And since the dam-break flood is a sudden flood, the results of the simulations may not be available in real-time. A mathematical model that can be run without fully running the numerical methods would be more practical. This can be performed by solving the model equations using the numerical method for some flood events and finding the relationship of the solution in the form of a simple model that can create the information for the dam-break in real-time.

In Thailand, an earthquake with a magnitude of 6.3 on the Richter scale occurred at Payao breakage in northern Thailand. The Payao breakage may have been caused by the earthquake and the dam-break at the nearby Mae Suai dam. This study was conducted for flood simulation and modeling for the case of Mae Suai dam break.

In a previous study, Busaman et al. (2015) developed the program to simulate and visualize the overland water flows by solving the shallow water equations using an adaptive tree grid finite volume method. This study modified this method in application for the dam-break flood simulation and modeling. Therefore, the objective of the study was to simulate Mae Suai dam-break flood using the shallow water equations with adaptive tree grid finite volume method, and assessed the relationship between initial water levels in the dam and the Mae Suai dam-break flood simulation results set regarding arrival times and maximum water depths using polynomial modeling.

MATERIALS AND METHODS

This study used a computational program (Busaman et al., 2015) written in Delphi Version 7 which could simulate and visualize in two and three dimensions animated views using the Open Graphics Library interface, including automatic generation of Keyhole Markup Language files for showing results via the Google Earth program. The program consists of numerical models and algorithms used to simulate and visualize the overland water flow.

Equations

For the numerical models, the system of shallow water equations (SWE) was used to determine the behavior of overland water flow. The shallow water equations can be written as Equations 1, 2 and 3 (Cushman-Roisin & Beckers, 2011).

$$\frac{\partial h}{\partial t} + \frac{\partial uh}{\partial x} + \frac{\partial vh}{\partial y} = 0 \tag{1}$$

$$\frac{\partial uh}{\partial t} + \frac{\partial(u^2h + \frac{g}{2}h^2)}{\partial x} + \frac{\partial uvh}{\partial y} = -gh \frac{\partial z}{\partial x} - gh \frac{n^2 u \sqrt{u^2 + v^2}}{h^{4/3}} \tag{2}$$

$$\frac{\partial vh}{\partial t} + \frac{\partial uvh}{\partial x} + \frac{\partial(v^2h + \frac{g}{2}h^2)}{\partial y} = -gh \frac{\partial z}{\partial y} - gh \frac{n^2 v \sqrt{u^2 + v^2}}{h^{4/3}} \tag{3}$$

In the above equations, h is the water depth, uh and vh represent the water discharge in the x and y directions, respectively, u and v are depth-averaged velocities in x and y direction respectively. For other variables, g is gravitational acceleration, z is topographic height, t is time, and n is the Manning’s roughness coefficient. The equation can be written in a vector form as Equation 4:

$$\partial_t H + \partial_x f(H) + \partial_y g(H) = -Z(H) - S(H) \tag{4}$$

where $H = [h \quad uh \quad vh]^T$ is the dependent variable. $f(H) = [uh \quad u^2h + \frac{g}{2}h^2 \quad uvh]^T$ and $g(H) = [vh \quad uvh \quad v^2h + \frac{g}{2}h^2]^T$ are the flux functions in x and y directions, respectively. For the source terms, the gravity forces $Z(H)$ and friction forces $S(H)$ are represent by Equation 5:

$$Z(H) = \left[0 \quad gh \frac{\partial z}{\partial x} \quad gh \frac{\partial z}{\partial y} \right]^T \tag{5}$$

and Equation 6

$$S(H) = \left[0 \quad gh \frac{n^2 u \sqrt{u^2 + v^2}}{h^{4/3}} \quad gh \frac{n^2 v \sqrt{u^2 + v^2}}{h^{4/3}} \right]^T \tag{6}$$

Computational Details

The shallow water equations were solved using a finite volume method. We adopted Addusse’s discretization scheme (Audusse et al., 2004; Delestre et al., 2008). However, since the accuracy of overland water flow simulation depends widely on the usage of fine

terrain grids, two dynamic grid techniques were adopted in our algorithm. First technique is to use a dynamically adaptive tree grid method, where the method continuously adjusts grid resolutions to follow features in the flow on the terrain. Second technique is the dynamic domain defining method (dynamic DDM) described by Yamaguchi et al. (2007). In this method, during the simulation, the area computation is expanded or shrunk to exclude dry grid cells. We developed the computational program by modifying adaptive tree grid techniques for rectangular quad tree grids, and combining them with the dynamic DDM.

For the computational program, Addusse’s scheme can be applied for the discretization scheme on adaptive tree grids as Equation 7:

$$H_i^{t+\Delta t} = H_i^t - \frac{\Delta t}{\Delta_i} \sum_k \hat{F}_k^t \cdot n_k \Delta \tau_k - \Delta t S_i^t \tag{7}$$

where Δt is the time step size; the subscript i is the spatial index of each cell; Δ_i is the cell area; the subscript k is the index for each sub interfaces over boundary between the cell and its neighbor, and $\Delta \tau_k$ is the width of the sub interface; \hat{F} is the numerical fluxes, depending upon the chosen scheme; n is the unit outward normal vector. In the discrete form, the gravity force is distributed to the numerical fluxes for each sub interfaces.

This method preserves the non-negative solutions of the water depth and also conserves the total water depth. Moreover, the scheme can compute dry states, and satisfies the still water properties.

The numerical scheme includes various techniques for best estimation. These techniques include a reconstruction procedure where each grid cell is estimated using the various quantities at interfaces between two adjacent cells using a min-mod slope limiter (Hagen et al., 2005) as Equation 8:

$$Q_k^- = Q_i + \sigma_k(x_k - x_i) + \delta_k(y_k - y_i) \tag{8}$$

where $Q = [h \quad u \quad v \quad h+z]^T$ is the interpolated variable at each interface k . (x_i, y_i) is the position of the cell, while (x_k, y_k) is the position of each interface k . σ_k and δ_k are minmod slope limiters at the position (x_k, y_k) in x and y directions, respectively. The reconstruction procedure is performed for second order accurate scheme in space and helps to preserve the steady state and non-negativity of water depth. These quantities at interfaces are used for flux computation based on Harten, Lax and van Leer (HLL) flux as Equation 9:

$$\hat{F}_k \cdot n_k = \frac{\alpha_+ \hat{F}(U_k^-) - \alpha_- \hat{F}(U_k^+) + \alpha_+ \alpha_- (U_k^+ - U_k^-)}{\alpha_+ - \alpha_-} + \hat{Z}(U_k^-) \cdot n_k \tag{9}$$

where $\alpha_{\pm} = \pm \max \left\{ \pm q_k^- \cdot n + \sqrt{g \hat{h}_k^-}, \pm q_k^+ \cdot n + \sqrt{g \hat{h}_k^+}, 0 \right\}$ are the wave speeds with the velocity vector, $q = [u \ v]^T$ and the vector of flux function $\hat{F}(U) = [f(U) \ g(U)]^T$. In here, $\hat{Z}(U) = [z_x \ z_y]^T$ is the term to satisfy the balance of momentum flux and momentum gravity forces in the Audusse's scheme, when (Equation 10):

$$z_x = \left[0, \frac{g}{2} (h_k^-)^2 - \frac{g}{2} (\hat{h}_k^-)^2 + gh_i z_k^-, 0 \right]^T, \quad z_y = \left[0, 0, \frac{g}{2} (h_k^-)^2 - \frac{g}{2} (\hat{h}_k^-)^2 + gh_i z_k^- \right]^T \quad [10]$$

In these equations, $U_k^{\pm} = [\hat{h}_k^{\pm}, (u\hat{h})_k^{\pm}, (v\hat{h})_k^{\pm}]^T$ is the vector defined by the Audusse's scheme with the hydrostatic reconstruction (Zanotti & Manca, 2010) given by Equation 11:

$$\hat{h}_k^{\pm} = \max \left\{ 0, h_k^{\pm} + z_k^{\pm} - \max \{ z_k^-, z_k^+ \} \right\} \quad [11]$$

For second order accurate scheme in time is obtained using the second order total variation diminishing (TVD) method as Equation 12:

$$\begin{aligned} H_i^1 &= H_i^t - \Phi(H_i^t) \\ H_i^2 &= H_i^1 - \Phi(H_i^1) \\ H_i^{t+\Delta t} &= \frac{H_i^t + H_i^2}{2} \end{aligned} \quad [12]$$

where $\Phi(H_i) = -\frac{\Delta t}{\Delta_i} \sum_k \hat{F}_k \cdot n_k \Delta \tau_k$ is the process of the numerical fluxes, the superscript 1 and 2 are the iteration steps. The TVD method can help reduce oscillation in the solution.

Moreover, in order to ensure stability, we also used a semi-implicit method for the friction forces (Delestre et al., 2008) as Equation 13:

$$uh_i^{t+\Delta t} \leftarrow \frac{uh_i^{t+\Delta t}}{1 + \Delta t \frac{gn^2 \sqrt{(u_i^t)^2 + (v_i^t)^2}}{(h_i^{t+\Delta t})^{4/3}}}, \quad vh_i^{t+\Delta t} \leftarrow \frac{vh_i^{t+\Delta t}}{1 + \Delta t \frac{gn^2 \sqrt{(u_i^t)^2 + (v_i^t)^2}}{(h_i^{t+\Delta t})^{4/3}}} \quad [13]$$

For boundaries conditions, the opened boundaries conditions were used in this work as Equation 14:

$$h_m = h_n, u_m = u_n, v_m = v_n, z_m = z_n \quad [14]$$

where the subscripts m is the spatial index of the boundary cells, and n are referred to as fictitious cells outside the computational domain.

This numerical algorithm is more efficient because it reduces the number of computational grid cells and computational times while preserving accuracy. The content in detail of the numerical schemes and algorithms for our software has been proposed by Busaman (2014). The adaptive tree grid finite volume algorithm was used in this work for solving SWE for Mae-suai dam-break simulation for each initial dam water levels of 472 to 509 meters. These initial water levels were set following historical data from Mae-suai dam, which were 427m for the lowest water level and 509m for the spillway level. The SWE simulation results set would be adopted for finding the relationship between the arrival times and maximum water depths using polynomial models as presented in the next section.

Arrival Time Model

For arrival times, we created a model using a 5-degree polynomial applied for each grid point. The arrival time is shown by Equation 15:

$$A_{i,j}(W) = \beta_{5,i,j}W^5 + \beta_{4,i,j}W^4 + \beta_{3,i,j}W^3 + \beta_{2,i,j}W^2 + \beta_{1,i,j}W + \beta_{0,i,j} \quad [15]$$

where $A_{i,j}(W)$ is the arrival time at each grid point (i,j) for an initial water level in the dam W and $\beta_{0,i,j}, \beta_{1,i,j}, \dots, \beta_{5,i,j}$ are the coefficients of the model for each (i,j) .

Maximum Water Depth Model

The maximum water depth can be modeled using a 5-degree polynomial applied for each grid point. The maximum water depth is shown in Equation 16:

$$M_{i,j}(W) = \gamma_{5,i,j}W^5 + \gamma_{4,i,j}W^4 + \gamma_{3,i,j}W^3 + \gamma_{2,i,j}W^2 + \gamma_{1,i,j}W + \gamma_{0,i,j} \quad [16]$$

where $M_{i,j}(W)$ is the maximum water depth at (i,j) for an initial water level in the dam W and $\gamma_{0,i,j}, \gamma_{1,i,j}, \dots, \gamma_{5,i,j}$ are the coefficients of the model for each (i,j) .

Flow Diagram of Simulation

This simulation was divided into two parts as shown in Figure 1. The first part was the SWE simulation for initial dam water levels of 472 to 509 meters, and consisted of 4 steps as follows. Step 1: solving the results from SWE for each initial water level in the dam.

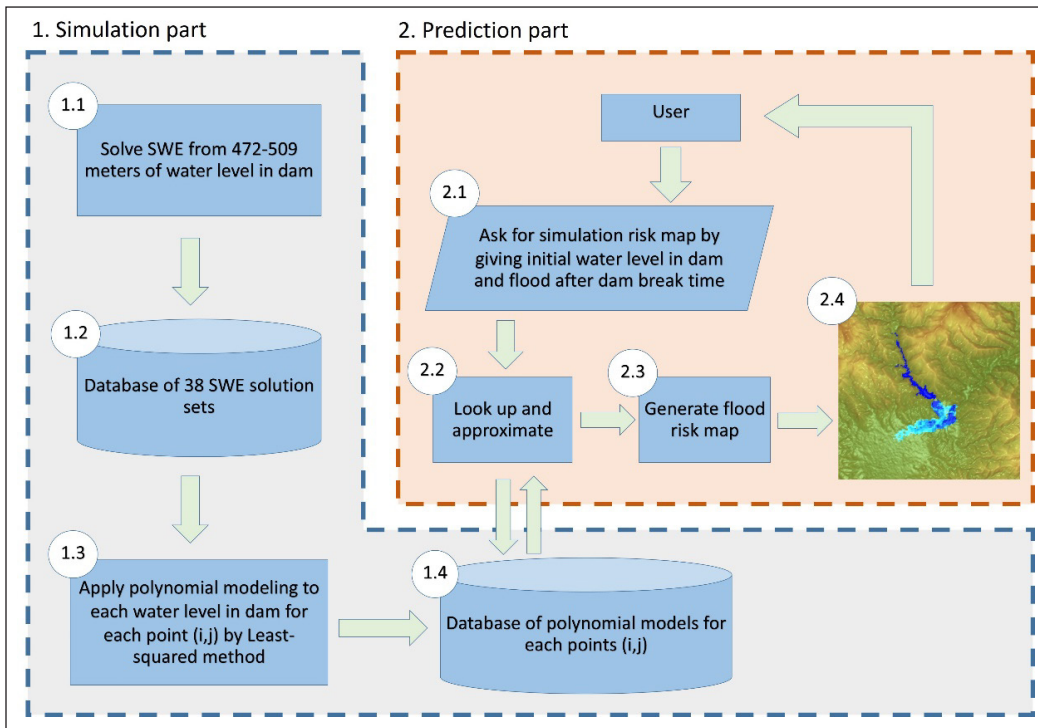


Figure 1. Flow diagram of simulation

Step 2: storing the arrival times and maximum water depth of the results in step 1 for each initial water level in the dam. Step 3: using least squares for parameter estimation of the coefficient value in the polynomial Equations 5 and 6 for each grid point (i, j), and Step 4: storing the coefficient values in a database for implementation in the second part. For the second part, there are 4 steps. Step 1: allowing the user to define inputs, which are the initial water level in the dam and flood after time the dam-break. Step 2: to approximate the arrival times and maximum water depth using the polynomial models stored in the database from Step 4 part 1. Step 3: to generate a flood risk map using the polynomial model results. Finally, Step 4 shows the flood risk map results to the user.

Simulation for Mae Suai Dam-Break flood

The simulation used digital terrain data $54,000 \text{ m} \times 54,000 \text{ m}$, generated from the SRTM data source. The data grid size was 600×600 cells. The location of Mae Suai dam and the land use map for this simulation is shown in Figure 2. Each of the grid cells are defined using Manning's coefficients by land use types as shown in Table 1 (Hunukumbura et al., 2007).

For the numerical solutions, the shallow water equations were solved using the adaptive finite volume method. The simulation was performed on the domain

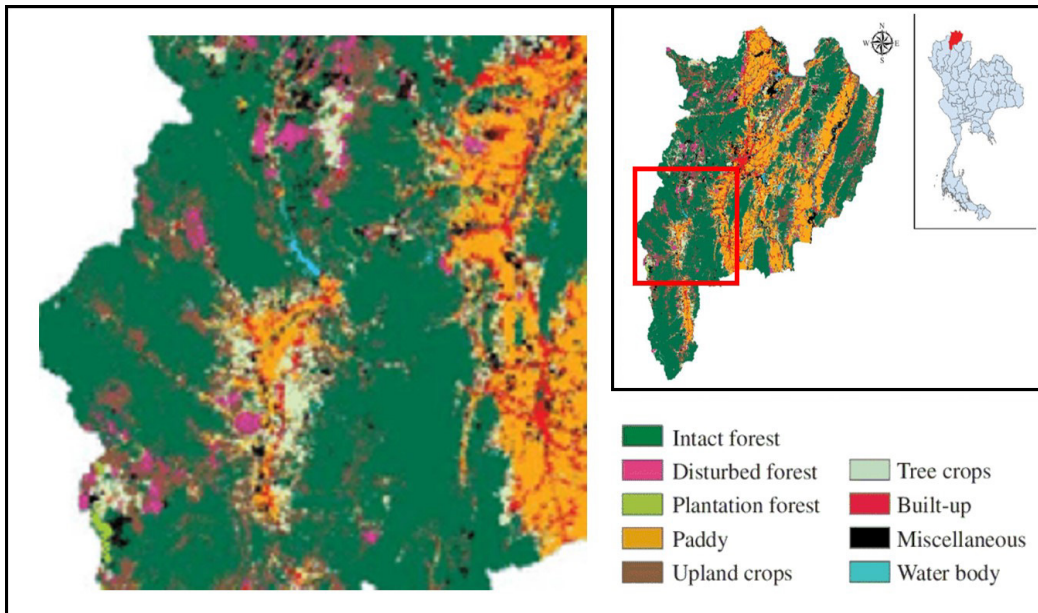


Figure 2. Location of Mae Suai dam and land use map for this simulation

Table 1
Manning's coefficients for land use type

Land use type	Coefficient	Land use type	Coefficient
Intact forest	0.80	Tree crops	0.17
Disturbed forest	0.80	Built-up	0.011
Plantation forest	0.80	Miscellaneous	0.01
Paddy field	0.17	Water body	0.01
Upland crops	0.06		

of adaptive tree grid, set as follows. There were 4 tree grid level with resolutions $1800\text{ m} \times 1800\text{ m}$, $360\text{ m} \times 360\text{ m}$, $180\text{ m} \times 180\text{ m}$ and $90\text{ m} \times 90\text{ m}$ for levels 1, 2, 3 and 4, respectively. Therefore, level 1 had the initial grid containing 30×30 cells. The topography values were provided for levels 1-4. The tree grid cells for children were designed as 5×5 , 2×2 and 2×2 for levels 1, 2 and 3, respectively, while level 4 cells had no children. The numerical experiment was simulated for 36,000 seconds with the boundary conditions defined as open boundaries.

In order to validate and evaluate the shallow water model and the program for dam break flood events, the program was used to simulate the water flow after the Xe-Pian dam break that occurred in Laos on 23 July 2018. We also simulated the Mae Suai dam-break flood for various initial water levels in the dam.

RESULTS

Xe-Pian Dam-Break Flood Simulation

The simulation of Xe-Pian dam break was performed on the domain of digital terrain data $16,200 \text{ m} \times 19,800 \text{ m}$, generated from the Shuttle Radar Topography Mission (SRTM) data source. We assumed that the free surface elevation of the reservoir behind the dam was 805m. The whole process took 5 hours to simulate the first 24-hour period of the flood event. In this experiment, we defined the Manning's coefficient to be 0.035, where the boundary condition is considered as open following Busaman (2014).

For the initial grid of the simulation, the finest grid cells were generated at the boundary of the reservoir. The maximum tree grid level was 4 with resolutions of $720 \text{ m} \times 720 \text{ m}$, $360 \text{ m} \times 360 \text{ m}$, $180 \text{ m} \times 180 \text{ m}$, and $90 \text{ m} \times 90 \text{ m}$ for levels 1, 2, 3, and 4, respectively. Therefore, the initial grid level 1 had 70×95 cells. The topography values were automatically obtained via the bilinear interpolation. The tree grid cells for children were 2×2 for level 1-3, while no children from level 4 cells.

The results are presented at different points in time as shown in Figure 3. The color bars at top left corner of each images indicate the depth of flooding (in meters). To check the accuracy of the model, we compared the simulation result with the satellite image as shown in Figure 4. The simulation of flooding area is nearly the same as that obtained from the satellite image. This suggests that the simulation program is reasonably accurate and has potential for practical usage.

Mae Suai Dam-Break Flood Simulation

We simulated the Mae Suai dam-break flood for various initial water levels in the dam. The initial minimum and maximum water levels from the mean sea level in the dam were set for each simulation from 472 m (lowest water level) to 509 m (spillway level). Therefore, the 38 SWE solution sets were simulated by adaptive grid finite volume method related to initial water level from 472 to 509 m using 1-meter increments for each simulation. Some examples of the dam-break simulation for different initial water levels in the dam are illustrated in Figure 5.

From Figure 5, it can be seen that the flood results depended on the initial water level in the dam. By this reasoning, we used the relation between polynomial modeling and simulation results to model the flood risk information regarding arrival times, maximum water depths and flood map. The details of the modeling and results are presented in the following section.

The simulation result, obtained by the SWE, were estimated using polynomial modeling (Equation 4). In Figure 6, comparisons between the polynomial models and the SWE simulation results are shown for arrival times (left panel) and maximum water depth

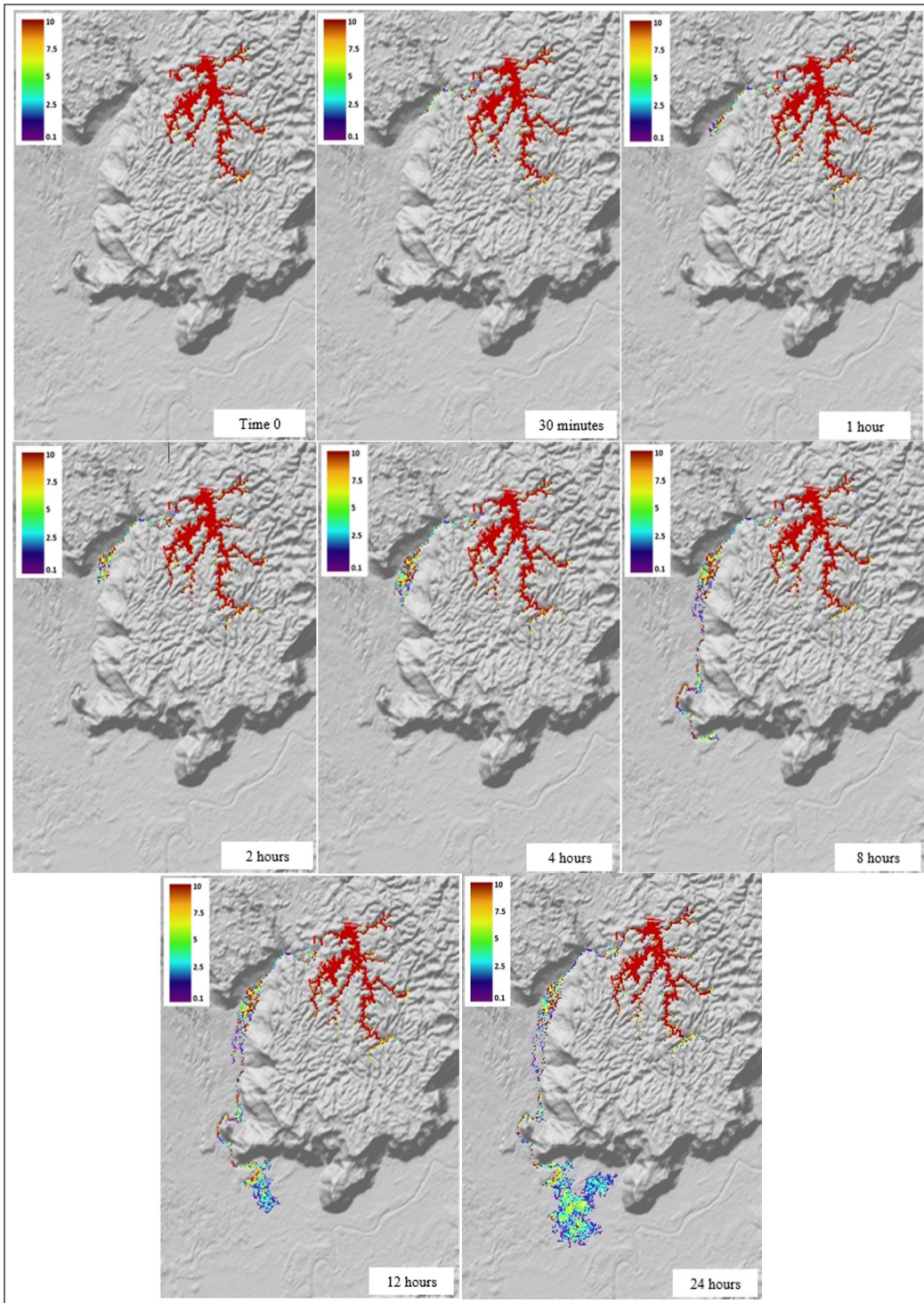


Figure 3. Simulation results of Xe-pian dam break at different points in times (0, 30 minutes, 1 hour, 2 hours, 4 hours, 8 hours, 12 hours and 24 hours). Depth of flooding (in meters) is shown in the legends

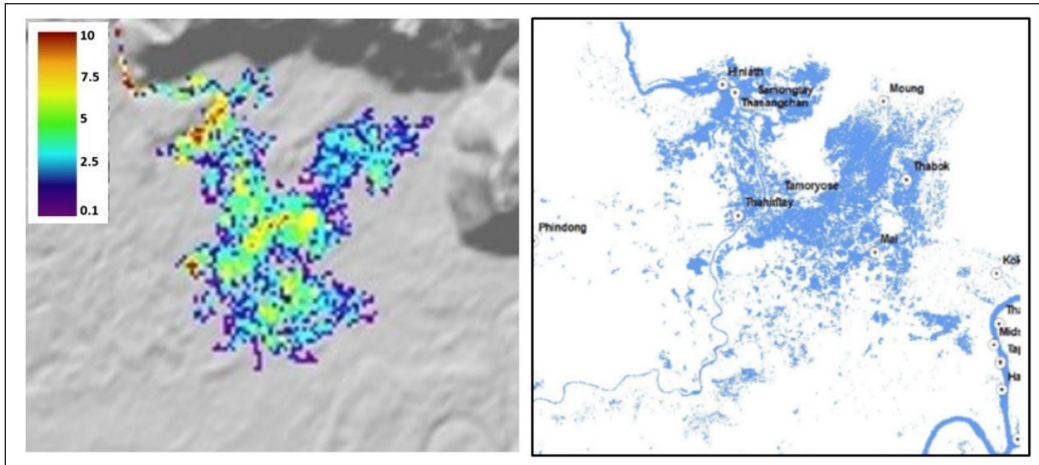


Figure 4. Comparison of the numerical simulation (left) and the satellite image (right) for the Xe-Pian dam break in Laos

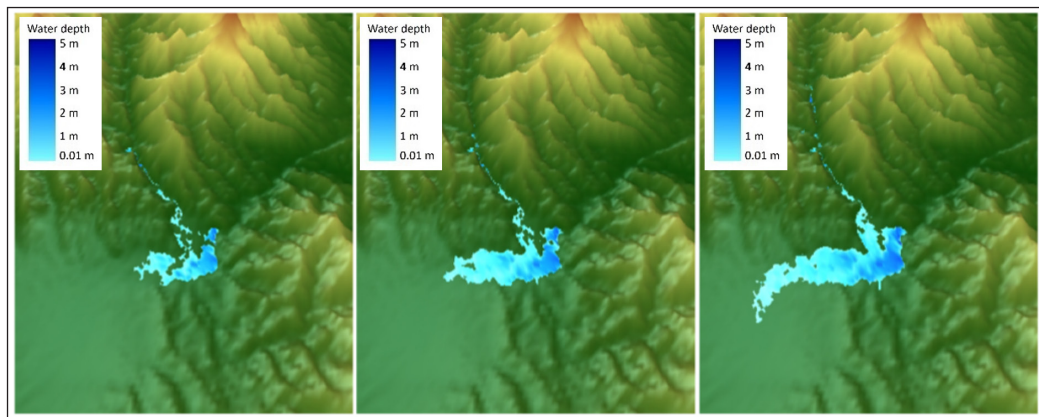


Figure 5. 3D visualization of dam-break flow simulation at 36000 seconds for different initial water levels: 490 m (left), 500 m (middle) and 509 m (right).

(right panel). Figure 6 shows that the arrival times and the maximum water depth from the polynomial model are consistent with the SWE simulation.

In this section, the results of the flood map prediction are presented. We used the polynomial models to predict and visualize the flood map of Mae Suai dam break for an initial water level in the dam set at 505.5 meters. To assess the accuracy of the SWE simulation, the color in each grid cell was compared with each corresponding grid cell from the flood map created by the polynomial model. The comparison is that if the simulation time is greater than the flow arrival time at the cell, the flood area is expanded to the cell, and colored by its maximum water depth value. Figure 7 shows results for the polynomial model at various time points compared with the SWE simulation. As the two results are very similar, the polynomial model can be used to predict areas at high risk of flooding.

For quantitative comparison, we calculated the mean relative absolute error between the polynomial model and the SWE simulation for arrival time and maximum water depth. The mean relative absolute error of arrival time was 12.01%, while maximum water depth was

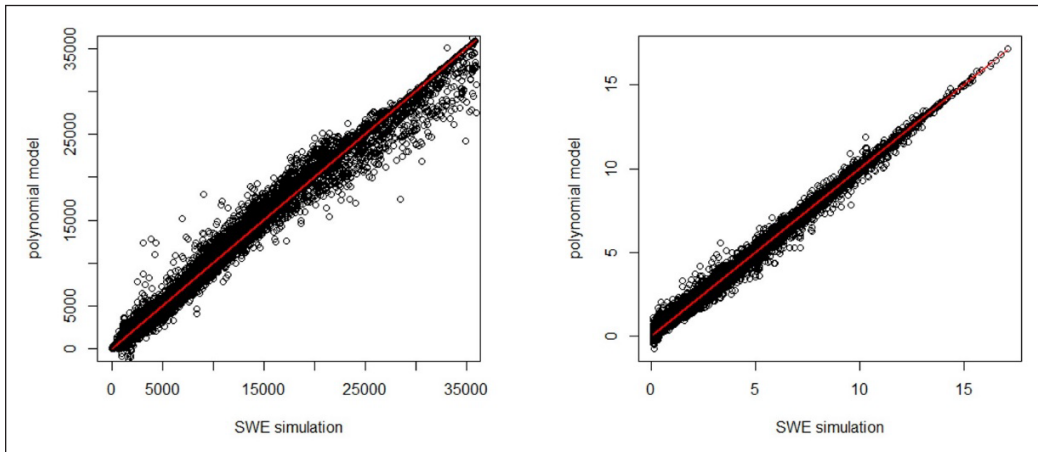


Figure 6. Comparison of arrival times (left) and maximum water depths (right) obtained by the polynomial model and the SWE simulation.

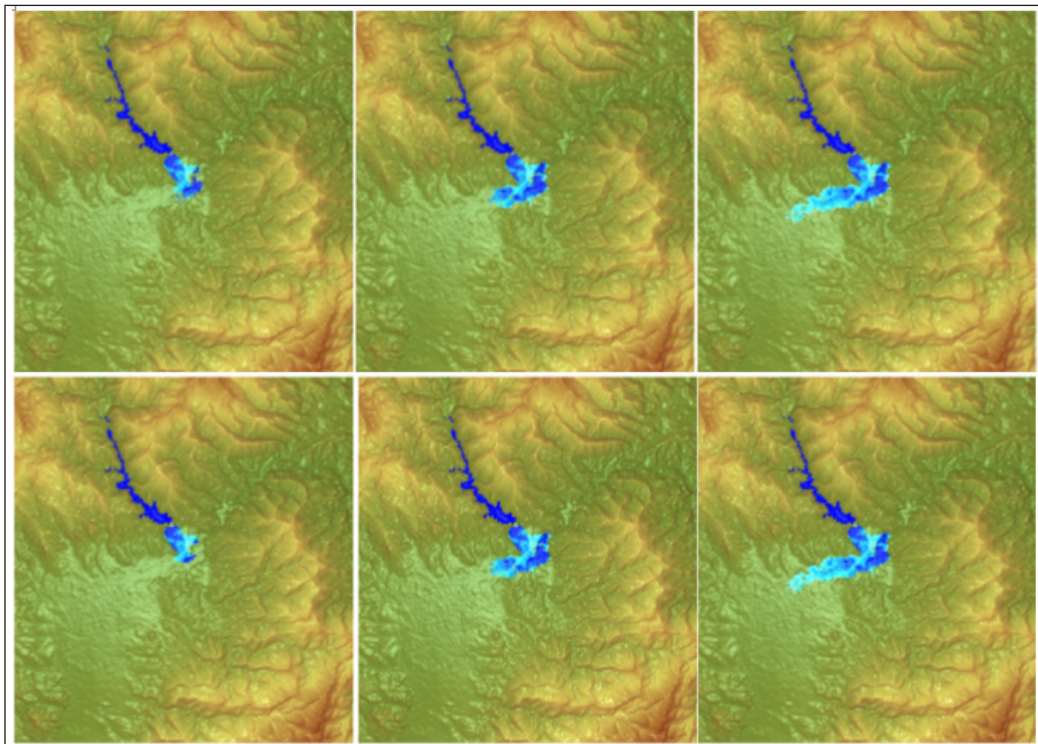


Figure 7. Visualization of flood map using polynomial model (top) and SWE simulation (bottom) for each time point: 1500 second (left), 6,000 second (middle), 36,000 second (right)

2.81%. Thus, the accuracy of the polynomial model compared with the SWE simulation was 87.99% for arrival time results and 97.19% for maximum water depth results.

CONCLUSION

In this study, we validated the shallow water equations with an adaptive tree grid finite volume algorithm using the Xe-pian dam-break flood simulation. The numerical results of the water propagation was in agreement with the satellite image. This shows that the numerical algorithm has the potential for dam-break flood simulations. The numerical algorithm can thus be used to simulate the Mae Suai dam-break flood for various initial dam water levels. The result sets were approximated using a polynomial model and the results were similar to the results from the SWE. Moreover, the flood risk map can be generated using the arrival times and maximum water depths models. A comparison of the flood risk map created by the polynomial and SWE models were similar, indicating that the polynomial model can be useful for Mae Suai dam-break flood risk assessment and flood preparation. The proposed method is more efficient and a flood risk map can be obtained without the need to fully solve the shallow water equations. The method can also be applied for other dams and floods in regions where information of that area is available.

ACKNOWLEDGMENTS

We would like to thank the Centre of Excellence in Mathematics, the Commission on Higher Education, Thailand for supporting this research.

REFERENCES

- Audusse, E., Buchut, F., Bristeau, M. O., Klein, R., & Perthame, B. (2004). A fast and stable well-balanced scheme with hydrostatic reconstruction for shallow water flows. *SIAM Journal on Scientific Computing*, 25(6), 2050-2065. doi: 10.1137/S1064827503431090
- Busaman, A. (2014). *Dynamically adaptive tree grid technique for flood simulation* (Doctoral thesis). Chulalongkorn University, Bangkok, Thailand.
- Busaman, A., Mekchay, K., Siripant, S., & Chuai-Aree, S. (2015). Dynamically adaptive tree grids modeling for simulation and visualization of rain-water overland flow. *International Journal for Numerical Methods in Fluids*, 79(11), 559-579. doi: <https://doi.org/10.1002/flid.4064>
- Cushman-Roisin, B., & Beckers, J. M. (2011). *Introduction to geophysical fluid dynamics: Physical and numeric aspects*. Oxford, UK: Academic Press.
- Dat, T. T., Tri, D. Q., Truong, D. D., & Hoa, N. N. (2019). Application of mike flood model in inundation simulation with the Dam-break Scenarios: A case study of Dak-Drinh Reservoir in Vietnam. *International Journal of Earth Sciences and Engineering*, 12(01), 60-70. doi: 10.21276/ijee.2019.12.0106

- Delestre, O., Cordier, S., James, F., & Darboux, F. (2008, June 9-13). Simulation of rain-water overland-flow. In *Proceedings of the 12th International Conference on Hyperbolic Problems* (pp. 537-546). University of Maryland, College Park, USA.
- George, D. L. (2011). Adaptive finite volume methods with well-balanced Riemann solvers for modeling floods in rugged terrain: Application to the Malpasset dam-break flood (France, 1959). *International Journal for Numerical Methods in Fluids*, 66(8), 1000-1018. doi: <https://doi.org/10.1002/fld.2298>
- Gong, L. (2018). Laos dam collapse: Regional response. *Khmer Times*. Retrieved August 23, 2019, from <https://www.khmertimeskh.com/525750/laos-dam-collapse-regional-response>
- Goodman, R. (2013). On the failure of Malpasset Dam. *AEG Shlemon specialty Conference: Dam failures and incidents*. Denver, Colorado: Association of Environmental and Engineering Geologists.
- Hagen, T. R., Hjelmervik, J. M., Lie, K. A., Natvig, J. R., & Henriksen, M. O. (2005). Visual simulation of shallow water waves. *Simulation Modelling Practice and Theory: Special Issue on Programmable Graphics Hardware*, 13(8), 716-726. doi: <https://doi.org/10.1016/j.simpat.2005.08.006>
- Hunukumbura, P. B., Weerakoon, S. B., & Herath, S. (2007). Development of a cell-based model to derive direct Runoff Hydrgraphs for Ungauged mountainous basins. *Journal of Mountain Science*, 4(4), 309-320. doi: <https://doi.org/10.1007/s11629-007-0309-8>
- Latrubesse, E. M., Park, E., Sieh, K., Dang, T., Lind, Y. N., & Yun, S. (2020). Dam failure and a catastrophic flood in the Mekong basin (Bolaven Plateau), southern Laos, 2018. *Geomorphology*, 362, 1-16. doi: <https://doi.org/10.1016/j.geomorph.2020.107221>
- NOAA. (2005). *Taum Sauk dam failure December 15th 2005*. National Weather Service St. Louis Missouri. Retrieved December 1st, 2019, from https://www.weather.gov/media/lxx/Events/12_15_2005.pdf
- Yamaguchi, S., Ikeda, T., Iwamura, K., Naono, K., Ninomiya, A., Tanaka, K., & Takahashi, H. (2007, September 4-5). Development of GIS-based flood-simulation software and application to flood-risk assessment. In *2nd IMA International Conference on Flood Risk Assessment* (pp. 4-5). University of Plymouth, UK.
- Zanotti, O., & Manca, G. M. (2010). *A very short introduction to Godunov methods*. Caen, France: Lecture Notes for the COMPSTAR School on Computational Astrophysics.

Differentiation Unclean and Cleaned Edible Bird's Nest using Multivariate Analysis of Amino Acid Composition Data

Nurul Alia Azmi¹, Ting Hun Lee^{1,2*}, Chia Hau Lee¹, Norfadilah Hamdan¹ and Kian Kai Cheng²

¹*School of Chemical and Energy Engineering, Faculty of Engineering, Universiti Teknologi Malaysia, 81310 UTM, Skudai, Johor, Malaysia*

²*Innovation Centre in Agritechnology for Advanced Bioprocessing (ICA), Universiti Teknologi Malaysia – Pagoh, Jalan Edu Hub UTM 2, Hub Pendidikan Tinggi Pagoh, 84600 Pagoh, Johor, Malaysia*

ABSTRACT

Edible Bird's Nest (EBN) has been used as a health modulator for many centuries. Nutrient degradation in EBN always happen during cleaning process due to many factors such as temperature and long soaking time in water. The present study attempts to find the difference between unclean and cleaned EBN in their amino acid composition. A total of 65 EBN samples were collected directly from swiftlet premises in 13 states of Malaysia to ensure the coverage of geographical location differences. A standardized cleaning method had been adapted from the industry to clean the collected EBN sample in the lab. Then it was analysed for amino acids composition. After that OPLS-DA multivariate model was used to discriminate the unclean and cleaned EBN on 18 types of amino acids composition. The model was robust with classification and predictive ability of 76.1% and 64.5%, respectively. The model was further validated with sample blind test and 100% of the sample was accurately fall into their respective cluster, unclean and cleaned EBN. The findings

suggest that three major amino acids with the highest VIP value were Aspartic acid, Methionine and Glutamic acid and proposed as the marker for discriminating the unclean and cleaned EBN.

ARTICLE INFO

Article history:

Received: 09 September 2020

Accepted: 05 November 2020

Published: 22 January 2021

DOI: <https://doi.org/10.47836/pjst.29.1.36>

E-mail addresses:

nurulalia95@gmail.com (Nurul Alia Azmi)

leetinghun@utm.my (Ting Hun Lee)

leechiahau0506@gmail.com (Chia Hau Lee)

fadilahamdan87@gmail.com (Norfadilah Hamdan)

chengkiankai@utm.my (Kian Kai Cheng)

* Corresponding author

Keywords: Cleaning process, edible bird's nest (EBN), orthogonal partial least square discriminant analysis (OPLS-DA)

INTRODUCTION

Edible Bird's Nest (EBN) is produced by the regurgitated secretion of swiftlets, *Aerodramus fuchiphagus* (Shim et al., 2016). It is a delicacy and food tonic that is popular, especially among the Chinese community all over the world. It has been used as a Traditional Chinese Medicine (TCM) since the Tang Dynasty (618-907) A.D (Lim, 2007; Marcone, 2005). According to the Compendium of Materia Medica "Ben Cao Gang Mu" written by Li Shizhen, EBN is an energy tonic that reinforces energy, nourishes lung, helps to maintain a youthful and radiant complexion (Li & Wu, 2010). Yida et al. (2015) reported that Chinese also used EBN for general well-being purpose such as, fasten the recovery of postpartum for women, enhance renal function, boost the immune system, regulate blood circulation, increase energy and also increase metabolic rate.

EBN is a very complicated industry that involving too many uncertainties, parties, location, or even bird's species are not certainly clear. Apart from the variance that is not able to control by humans such as swiftlets habitat, location and environmental factor, some areas should be closely monitored, and stringent guideline should be recommended to industries. It is the 'gray area' that many malpractices including adulteration and negligent handling of this precious health modulating animal bioproduct especially during the cleaning process. Previously the composition of EBN nutrients was based on different colors, production sites and geographical origins (Halimi et al., 2014; Lukman & Wibawan, 2018; Norhayati et al., 2010; Saengkrajang et al., 2013; Seow et al., 2016a; Seow et al., 2016b). However, none of these literatures reported the difference content in EBN on unclean and cleaned. The focus should be aimed at the content to provide a clearer understanding on its content. Further investigation on unclean and cleaned EBN should also be researched to see the nutrient change and provide as a guideline to the industries on cleaning or processing to enhance EBN content.

During the early 70's, EBN cleaning industries was a highly kept secrets, and no information was able to obtain from any source including literature. When the house variety of EBN emerged and became popular in the 80's, the EBN cleaning process has become an industry need. Due to lack of research and development, the industry through trial and error searched for an effective cleaning method without considering much on EBN nutrient changes. During that time or earlier, the well-known bleaching technique used a bleaching agent to "clean" the EBN. By using this bleaching technique, the fine feather was bleached to off white and resemble EBN colour. It is efficient, fast, and economy despite not knowing the biochemical properties change and bleaching chemical residual, toxicity and other problem lying beneath. This technique, however, is bad for the consumer. Eventually the cleaning method became unacceptable. Other problem includes excessive soaking in water, steaming and even boiling during the cleaning process might affect some nutrient content change in EBN. It has been reported that EBN is sensitive towards heat, and the composition of its active compounds could be changed (Shim et al., 2016).

The cleaning process of EBN may trigger the breakdown and denaturation of the polymer such as protein and carbohydrate into amino acids and saccharide, respectively (Chua et al., 2015). It causes the inaccuracy in quantify of the polymer. Based on the literature study, protein is the main component that plays an important role in regulating some metabolism or pathway which contribute to the therapeutic effects (Abidin et al., 2011; Chua et al., 2015; Chua et al., 2013; Chua & Zukefli, 2016; Wong, 2013). Amino acids are the building block of protein, and these compounds can be a promising indicator for the classification of EBN (Chua et al., 2015; Quek et al., 2018). Results from various researchers and our study have shown that there are 18 types of amino acid detected from EBN and it is well established (Hun et al., 2015; Marcone, 2005; Su et al., 1998). The quantification and qualification of the amino acids are more accurate compared to protein. It is because protein is not stable and easily degraded at high temperature (Chua et al., 2015; Chua et al., 2013). However, at higher temperature (too high), the amino acids itself will denature thus indicating the EBN is over-process and do not have any protein-related nutrient in EBN (Erik et al., 2015). Despite all these discoveries, little is known on the content changes of unclean and cleaned EBN, and to date, the scientific evidence-based studies on this topic have yet been reported. The data on the amino acid composition of unclean and cleaned EBN may give some insights for the better understanding of EBN cleaning process. It is also extremely important to preserve the valuable content of this all rounded therapeutic compound.

This study aimed to investigate the changes of amino acids composition before and after the cleaning process and further identify the amino acids markers for unclean and cleaned EBN. This present study also revealed the distribution of important amino acids. A novel classification method using Orthogonal Partial Latent Square Discriminant Analysis (OPLS-DA) to categorise the unclean and cleaned EBN samples based on its amino acid composition. It is the first study to be reported on an attempt to use the amino acids composition in EBN to differentiate the unclean and cleaned EBN. This finding can be a reference for EBN industries in order to check on their incoming and outgoing product quality. Also, the authority could use these amino acids composition to be a standard to inspect on the malpractice of EBN processors.

MATERIALS AND METHODS

Sample Preparation

A total of 65 EBN samples were collected on 1st January to 31st December 2016 from different states in Malaysia (5 for each state) to ensure the coverage of geographical location differences. The source for EBN could be an important factor in confirming the variant in EBN constituent. The sample collected from the swiftlet premises were labelled with Radio Frequency Identification marked by Department of Veterinary Services Malaysia.

However, the identification number is not disclosed here to protect the premises owner's privacy. All samples collected were genuine and directly from the licensed swiftlets premises at a different location that has been used as the reference standard. There were two similar sample set of ENB, consisted of 65 sample each. The first set of ENB undergone the cleaning process with the method according to Good Manufacturing Practice (GMP) of industrial cleaning method [Raw-Unclean and Raw-Clean Edible Bird's Nest (MS 2333:2010)], labelled as cleaned ENB sample. Other set of ENB sample did not go through any cleaning process, labelled as unclean ENB sample. The sample that had undergone cleaning process was ensured to be same as unclean ENB for analysis. This ensured that unclean and cleaned ENB were from the same source and minimized the location variant.

Cleaning Method

Good Manufacturing Practice (GMP) of industrial cleaning method [Raw-Unclean and Raw-Clean Edible Bird's Nest (MS 2333:2010)] was adapted and standardized for all samples. Briefly, the collected ENB was moisturized with reverse osmosis water, and a pair of forceps was used to separate the feathers, eggshells, dirt and other impurities by human labour. After the cleaning process, the ENB was dried in the oven (Mettler, Schwabach, Germany) at 45°C for 2 hours. The total sample for this study was 130 samples, consisting of 65 unclean and cleaned samples each.

Amino Acids Analysis

All amino acids detection was carried out using acid hydrolysis method except Tryptophan. (Oda et al., 1998; Su et al., 1998). 0.3 g of ground ENB samples were weighed and transferred into hydrolyzing bottles. 15 ml of 6 N HCl was added and sealed tightly. Then, the samples were hydrolyzed in a convection oven (Mettler, Schwabach, Germany) for 24 h at 40°C.

While Tryptophan was determined by using alkaline hydrolysis because it is not stable and may destroy in acid condition (Reverter et al., 1997). The ground ENB (0.1 g) was placed in an evacuated tube and added with 15 mL of 4.3N lithium hydroxide (LiOH. H₂O). The mixture was flushed with N₂ gas and heated in an oven (Mettler, Schwabach, Germany) at 120°C for 16 hours. The pH of the sample was adjusted to 4.5, with a diluted hydrochloric acid solution (0.1M).

Derivation step of amino acids was done with the aid of AccQ.Fluor Reagent kit (Waters Corporation, Massachusetts, USA). The derivatized samples were filtered using syringe filter (0.45 µm pore size hydrophilic PVDF) before being injected into the Waters e2695 High-Performance Liquid Chromatography instrument (Waters Corporation,

Massachusetts, USA), fitted with AccQ. Tag 3.9×150 mm column (Waters Corporation, Milford, Massachusetts, USA). Then, the detection was done using a Waters 2475 fluorescence detector (Waters Corporation, Milford, Massachusetts, USA) at 254 nm. All targeted compounds were identified base on the retention time of the corresponding standard. Then, they were quantified using the internal standard method adapted from Khaleduzzaman et al. (2008) except Tryptophan. The internal standard used was α Amino Butyric Acid (AABA). The quantity of Tryptophan in sample was compared to a calibration curve of Tryptophan standard.

Statistical Analysis

SPSS v20 for Windows (SPSS Inc., Chicago United States) was used to analyzed experimental data and subjected to independent sample T-test and Pearson Correlation analysis.

Orthogonal Partial Latent Square Discriminate Analysis

The chemometric analysis was done using SIMCA software (version 14.1.0, Umetric, Sweden) while Orthogonal Partial Latent Square Discrimination Analysis (OPLS-DA) performed the classification. OPLS-DA is the supervised statistical analysis method that predicts the variable Y (unclean and cleaned EBN) by explanatory quantitative variables X (18 types of amino acids). It can separate the systematic variation in X variable into two-part, one part is X variable correlated to Y variable; and second part is X variable orthogonal to Y variable, which does not contribute to discrimination of unclean and cleaned EBN (Blasco et al., 2015). The robustness of the model was interpreted after seven-fold internal cross-validation by cumulative goodness of fit (R^2Y), goodness of prediction (Q^2) and Cross-Validation Analysis of Coefficient Variance (CV-ANOVA) (Beauclercq et al., 2019).

OPLS-DA model is statistically reliable if CV-ANOVA, $p < 0.05$. The model can be interpreted as robust if the Q^2 (cum) > 0.4 and R^2Y (cum) > 0.5 (Blasco et al., 2015). Each X variable that contributes to the OPLS-DA model was summarized by Variable Importance Projection (VIP) value. High VIP value indicates, high contribution of the X variable to discriminate the unclean and cleaned EBN on the OPLS-DA model (Beauclercq et al., 2019). High VIP value combining with small Jackknife confident interval can be potential marker to discriminate the unclean and cleaned EBN sample (Beauclercq et al., 2019). The basic method of Jackknife is by removing one sample in the dataset and replacing it with the blind sample in the population to recompute the mean and obtain the confident interval. The small Jackknife confident interval value indicates that the dataset is approximately correct and has no bias (Blasco et al., 2015).

RESULT AND DISCUSSION

Amino Acids Composition

Figure 1 shows a typical chromatogram of EBN amino acids and ammonia obtained from the acid hydrolysate extract. There were 17 types of amino acids found in the analyzed EBN samples. However, ammonia was not accounted in this study as it is not an amino acid. Besides Figure 2 shows, the chromatogram of EBN sample from alkaline hydrolysate extract. Based on the result, all analyzed EBN samples contained Tryptophan.

Serine was the highest amino acid in unclean EBN with 3.72 ± 0.36 w/w% and followed by Aspartic acid with 3.51 ± 0.41 w/w% (Figure 3). Meanwhile, for cleaned EBN, Phenylalanine was the highest amino acid with 4.21 ± 0.32 w/w% and next most abundant amino acid was Serine with 4.06 ± 0.42 w/w% (Figure 3). These results agree with Ali et al. (2019), Chua et al. (2015) and Marcone (2005). Their analyses showed that the most abundant amino acids of EBN were Serine, Aspartic acid, and Phenylalanine.

This study found that Tryptophan, Methionine and Alanine were the lowest amino acids in both unclean and cleaned EBN (Figure 3). These results were in line with the previous finding from Ali et al. (2019) and Chua et al. (2015), where these three amino acids were among the lowest amino acids in EBN. However, this is contradicting to the previous study by Saengkrajang et al. (2013) which found that Methionine was the highest amino acid in EBN. One possible reason that could make the difference is due to the origin of the EBN collected and also the cleaning method employed.

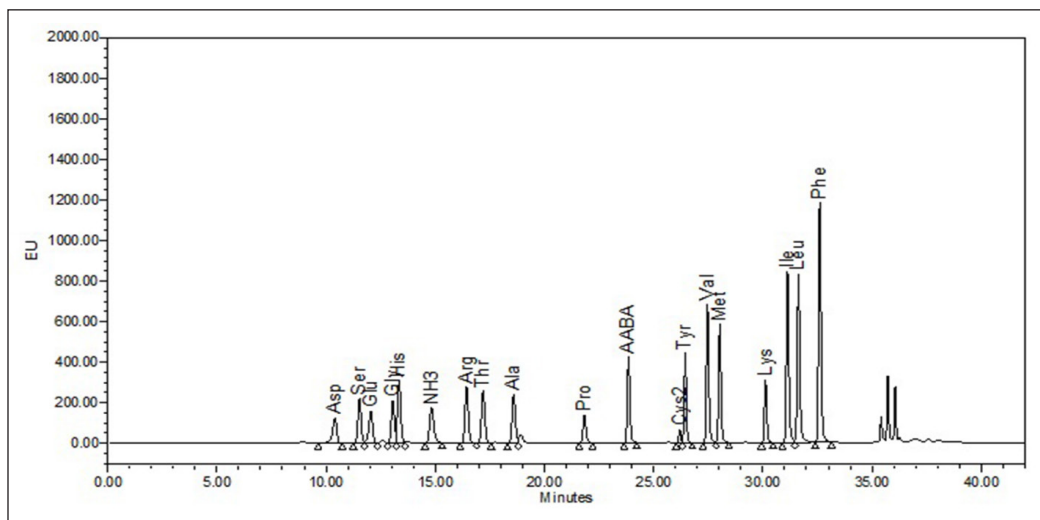


Figure 1. Typical chromatogram of the 17 types of amino acids from acid hydrolysate EBN sample including the internal standard (AABA) and ammonia, adapted from Hun et al. (2020). Abbreviation: Asp, Aspartic acid; Ser, Serine; Glu, Glutamic acid; Gly, Glycine; His, Histidine; NH₃, Ammonia; Arg, Arginine; Thr, Threonine; Ala, Alanine; Pro, Proline; AABA, Alpha Amino Butyric Acid, Cys, Cysteine; Tyr, Tyrosine; Val, Valine; Met, Methionine; Lys, Lysine; Ile, Isoleucine; Leu, Leucine; Phe, Phenylalanine

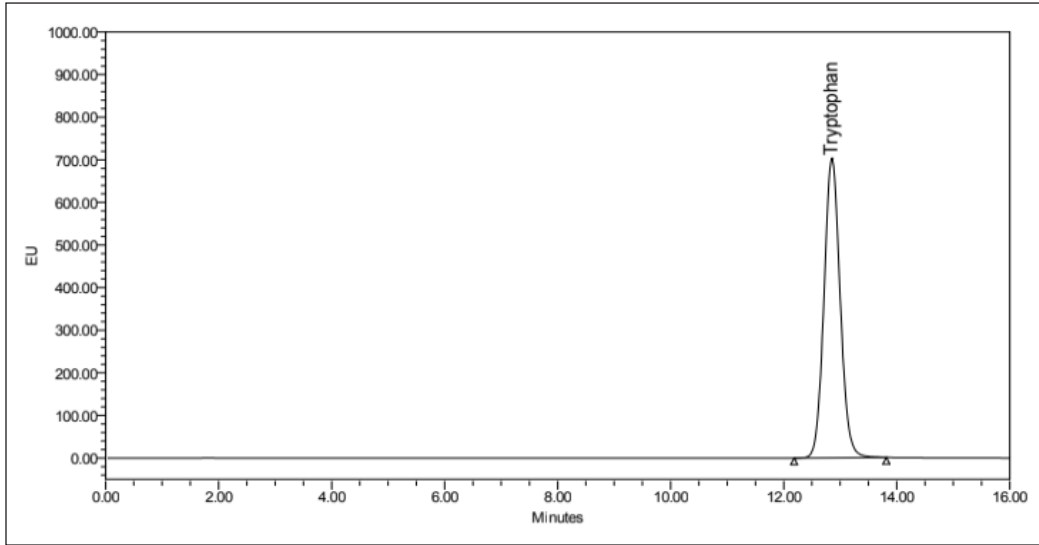


Figure 2. Typical chromatogram of Tryptophan in EBN sample from alkaline hydrolysate extract

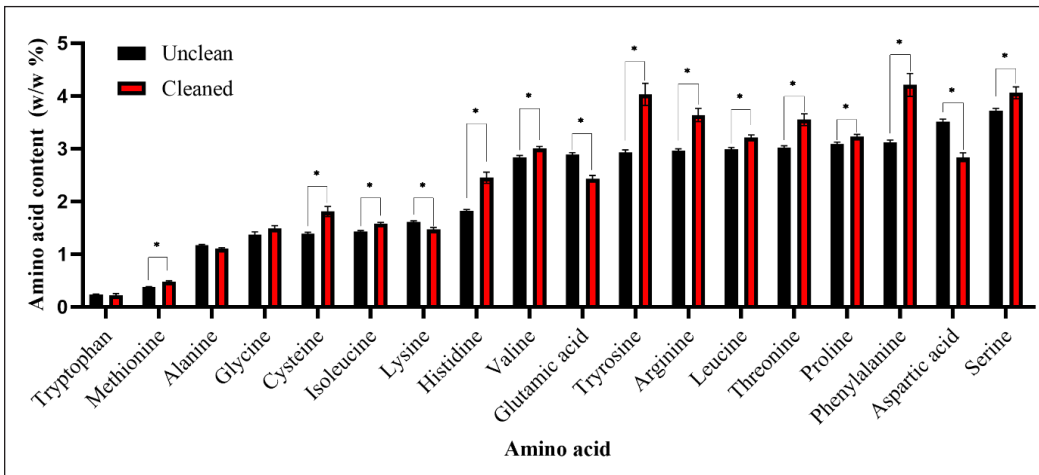


Figure 3. Amino acids composition of unclean and cleaned EBN. The data shown the mean of 65 independent samples \pm Standard Deviation (SD). Asterisk (*) represent significant difference between unclean and cleaned EBN ($p < 0.05$)

Effect of EBN Cleaning Process in Amino Acids Content

The results obtained revealed that the total amount of amino acid content in cleaned EBN was significantly higher ($p < 0.05$) compared to unclean EBN with 44.8 ± 1.05 w/w% ($n=65$) and 40.4 ± 1.32 w/w% ($n=65$) respectively. Figure 3 shows 18 amino acids content in unclean and cleaned EBN samples. From the result obtained, this study shows that the cleaning process affected the amino acids content in EBN. This study revealed most individual amino acid content increased after cleaning process except Lysine, Aspartic

acid, Glutamic acid, Alanine and including Tryptophan, although it showed very little difference in content. The increment of amino acids content could be due to the key factor of drying temperature (40°C) during the cleaning process that breakdown the protein into amino acids. The heat could cause additional energy that changed the protein structure, characteristic and molecule arrangement (Mauer, 2003). This present study is in agreement with Aluko (2018) that found the optimum temperature to breakdown the protein into amino acids was between 37°C to 50°C.

There are some amino acids content decreased significantly after the cleaning process including, Lysine, Aspartic acid, and Glutamic acid. According to Erik et al. (2015), Aspartic acid and Glutamic acid are categorized under charged and acidic amino acid and, these types of amino acids contain high propensity and energetically favorable contact with water. Furthermore, data from Del et al. (2009), found that, these amino acids contained lateral chain that allowed the formation of zwitterionic function to solubilize the amino acid in water. The zwitterionic formed when an amino acid has the amino group (negative charge) and carboxylic group (positive charge) in ion form. During the cleaning process, a large amount of water was in contact with the EBN for 5-6 hours. This could be the major reason that promotes Aspartic acid and Glutamic acid to dissolve into water. Tripathy et al. (2018) revealed that Glutamic acid had good solubility in water compared to other amino acids, and it could be leached when contact with water during the cleaning process of EBN. Lysine in cleaned EBN was also significantly lower compared to unclean EBN. This might due, this amino acid is sensitive to multi stimuli such as temperature and pH (Tripathy et al., 2018). A study done by Tulbek et al. (2017) found that, the Lysine content in cooked pea bean was significantly lower compared to uncook pea bean. It could be the reason that, why Lysine content decreased after the cleaning process.

The EBN cleaning process has made the content of the amino acids changed significantly (Figure 3). This showed that it is important to monitor the key compound of EBN before and after the cleaning process. There were 15 amino acids that changed significantly, and only 3 are not. Further research on the molecular level could be explored to find the theory behind this.

Discrimination of Unclean and Cleaned EBN

The OPLS-DA model performance was based on 18 types of amino acids content from unclean and cleaned EBN. Figure 4 shows 85% of the randomly selected original data (55 samples each from both classes, 110 samples) as a predictive model and remaining 15 % of the sample was used for testing set to project into predictive model to validate the accuracy (Seow et al., 2016a). The predictive variation given by (R^2X_{cum}) between X (amino acids) and Y (EBN sample), the best model used five components, and interprets 95 % of the total variation in X. OPLS-DA developed a three-component model based on the data set. In

addition, robustness of the model explained by 76.1 % of the differences between the two groups (R^2Y_{cum}), clearly separating the unclean and cleaned EBN samples. The model has high predictive ability with 64.5 % (Q^2_{cum}) and it was validated by cross-validated variance analysis (CV-ANOVA) with a P-value of $6.07/10^{20}$. Seven-fold cross-validation used as internal validating method to validate the prediction ability of the model (Beauclercq et al., 2019). Figure 4 shows, the model plot of score scatters indicate that sample classification was highly sensitive to classified unclean and cleaned EBN. Repetitive dots of different groups mapped on OPLS-DA model score plot showed a strong separation suggesting that the unclean and cleaned EBN could be differentiated based on their respective amino acids observed.

Several studies have reported on the application of OPLS-DA method to classify the distinctive category of the sample (Cavanna et al., 2019; Phua et al., 2014; Song et al., 2013). This shows that the OPLS-DA is robust and reliable to separate the sample according to the specific category. Phua et al. (2014) reported an important discovery where they classified the colorectal cancer cell and the healthy cell based on the metabolite compounds by using OPLS-DA. Cavanna et al. (2019) successfully classified the chicken egg based on its freshness. The most recent application of OPLS-DA on EBN sample was reported by Seow et al. (2016a) where they successfully discriminated the cave and house EBN with predictive power (Q^2_{cum}) of 76.1%. The developed OPLS-DA model from our study and Seow et al. (2016a) can be used to classify unknown EBN sample in future.

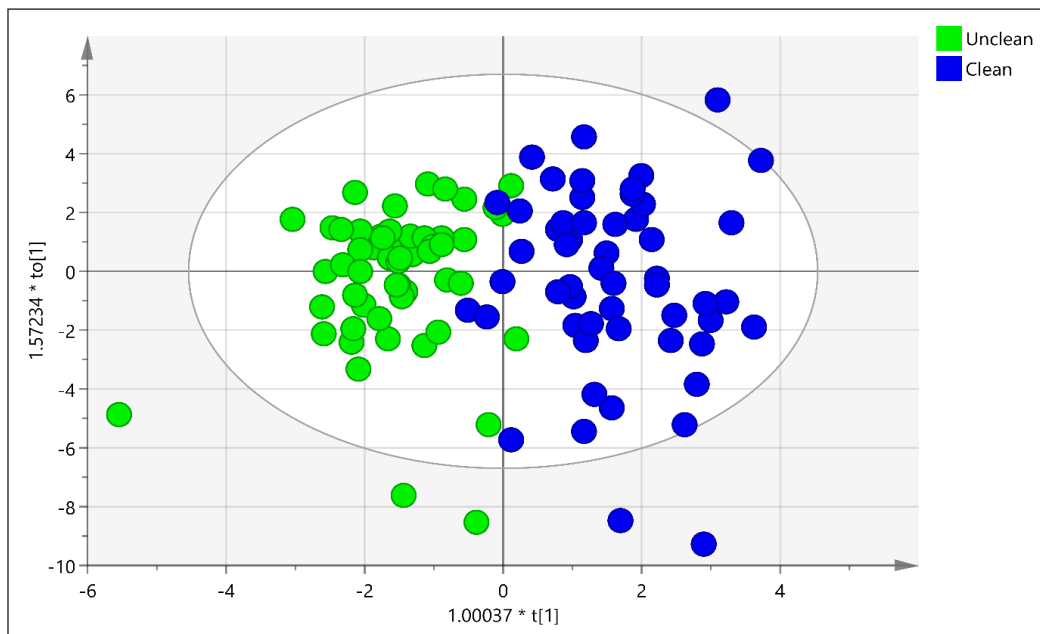


Figure 4. OPLS-DA model score plot for 85% training set (n=110) of 18 variables (amino acids) for unclean and cleaned EBN sample. A score plot for unclean EBN (n=55, green dot) and cleaned EBN (n=55, blue dot)

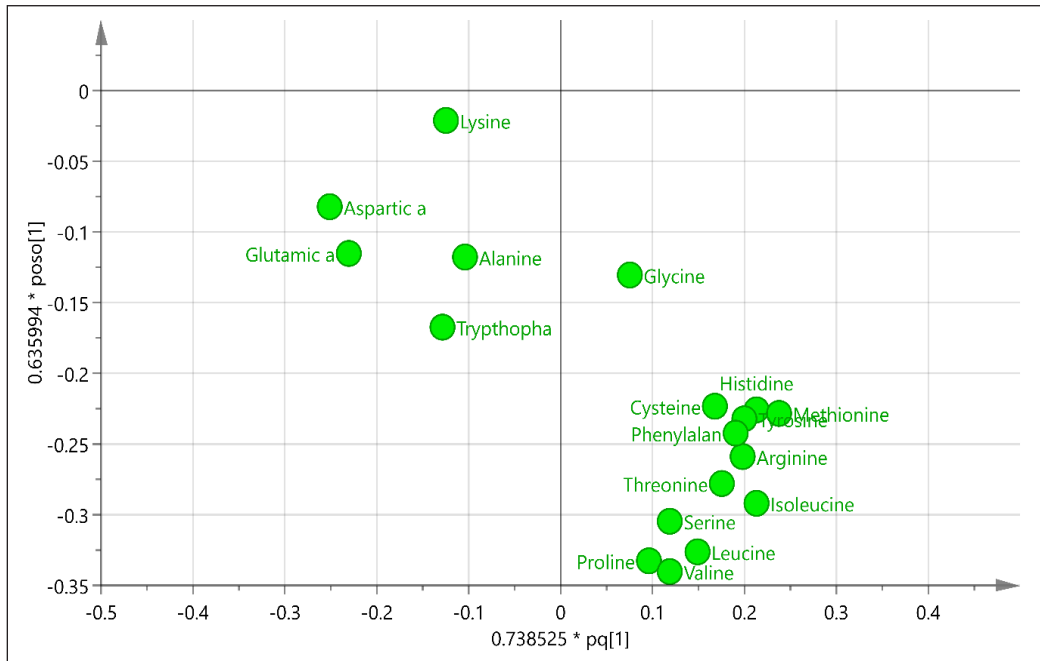


Figure 5. Loading plot for OPLS-DA overview based on the OPLS-DA model including 18 type of amino acids

Figure 5 shows the loading plot of the model, where variable was expressed differently between unclean and cleaned EBN samples to confirm the score plot result. Five amino acids Lysine, Aspartic acid, Glutamic acid, Alanine and Tryptophan are on the same side of the unclean class in the score plot of the model (Figure 4). It was shown that these five amino acids were dominant in unclean EBN. Data have shown that these five amino acids were reduced after the cleaning process (Figure 3).

Evaluation of Predictive Model Robustness and Model Validation for Discrimination of Unclean and Cleaned EBN

The predictive model robustness was assessed by using external validation and the remaining 15 % of the 130 EBN sample as a testing set. They have been treated as ‘unknown’ sample to validate the sample classification in exact cluster and not overfitting to the predictive model. The model classified all 20 samples correctly (Figure 6) and the 10 each unclean and cleaned EBN samples were grouped into their respective clusters exactly. Blind test sample classification accuracy was 100%, and the ‘unknown’ EBN samples fall into their exact cluster.

Figure 7 shows the value of Variable Projection Influence (VIP) suggested weightage of each variable within the model to effectively differentiate between the two classes on the basis of their differences. Variables that are weak predictive reliability, whether with low VIP value magnitude or with their Jackknife confidence interval crossing zero, are low

Differentiation Unclean and Cleaned EBN

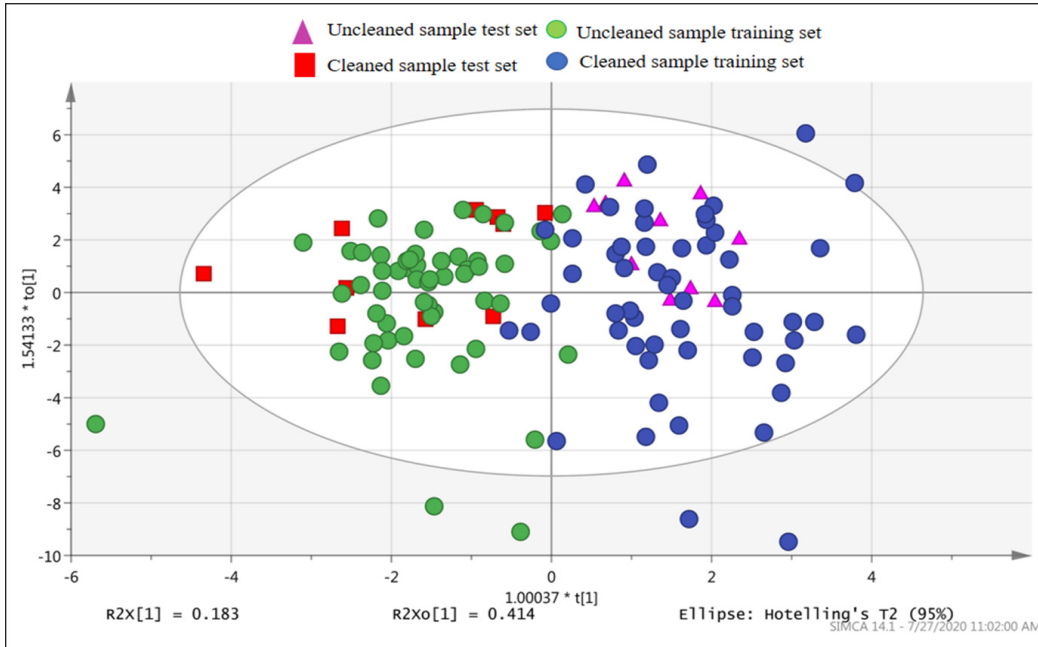


Figure 6. Predicted score plot for 15 % testing set and 85 % of training set of EBN samples. A total of 20 unclean and cleaned samples test set fell into their accurate classes

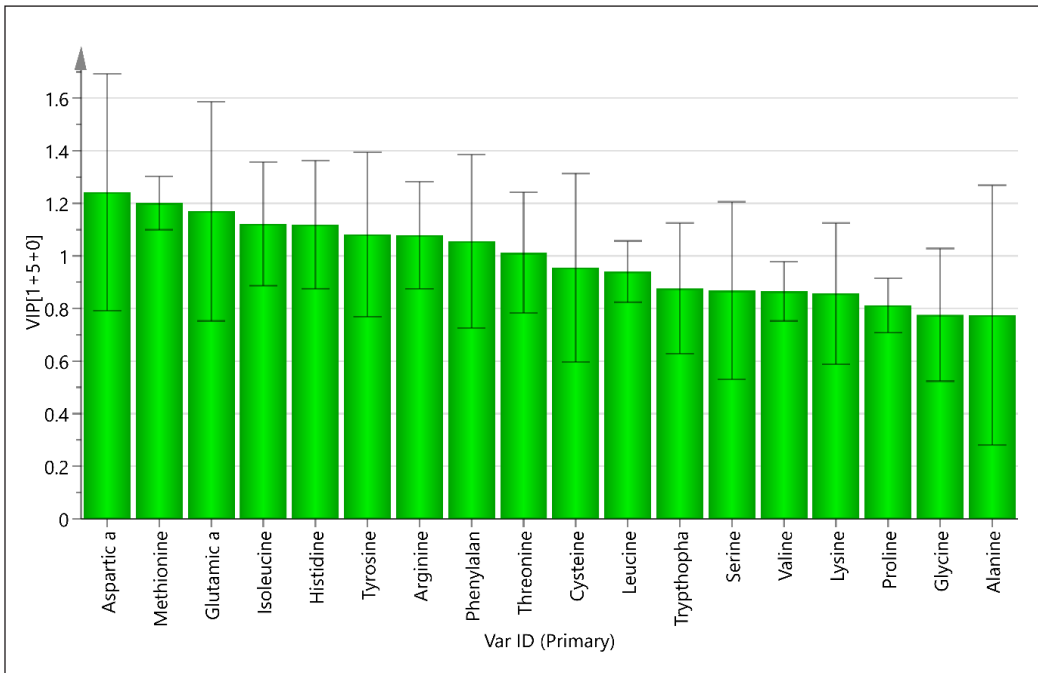


Figure 7. Variable on Projection (VIP) plot of OPLS-DA with Jackknife confident interval. The variables were sort from the highest to lowest VIP value. The highest VIP value indicates the most important variable for discriminating unclean and cleaned EBN sample into the OPLS-DA model score plot

reliability in prediction and not robust (Seow et al., 2016a). VIP was then used to select those compounds possessing the highest discrimination i.e. unclean and cleaned potential in the predictive model (VIP score > 1). The three highest VIP variables namely Aspartic acid, Methionine and Glutamic acid were proposed as primary markers that could be used to differentiate unclean and cleaned EBN (Blasco et al., 2015; Marcone, 2005; Senizza et al., 2019). Based on the predictive model and the blind test results, the primary markers are valid.

CONCLUSION

The EBN cleaning process has changed the amino acid composition of EBN. It was found that only Glutamic acid, Aspartic acid, and Lysine were significantly decreased after the cleaning process whereas the others have increased. Eighteen types of amino acids were found in both unclean and cleaned EBN samples. EBN can be differentiated between unclean and cleaned based on their amino acid composition. The model developed has successfully distinguished and further classified the EBN samples into unclean and cleaned classes based on amino acids composition. Aspartic acid, Methionine and Glutamic acid can be used as the markers with the highest discriminative weightage to distinguish between the unclean and cleaned EBN samples according to its class as proposed by the model developed in this study.

ACKNOWLEDGMENT

The authors would like to thank Universiti Teknologi Malaysia (UTM) for providing necessary facilities to complete experimental work. The research was funded by Universiti Teknologi Malaysia (UTM) via research grant (R.J130000.7846.4J273). The authors also would like to thank John Wiley and Sons Publisher for giving us the permission to re-use the Figure 1 image from the manuscript entitled “Characterization of Polar and Non-Polar Compounds of House Edible Bird’s Nest (EBN) from Johor, Malaysia” (Hun et al., 2020).

REFERENCES

- Abidin, F. Z., Hui, C. K., Luan, N. S., Ramli, E. S. M., Hun, L. T., & Ghafar, N. A. (2011). Effects of edible bird’s nest (EBN) on cultured rabbit corneal keratocytes. *BMC Complementary and Alternative Medicine*, *11*(1), 1-10. doi: <https://doi.org/10.1186/1472-6882-11-94>
- Ali, A. A. M., Noor, H. S. M., Chong, P., Babji, A. S., & Lim, S. (2019). Comparison of amino acids profile and antioxidant activities between edible bird nest and chicken egg. *Malaysian Applied Biology*, *48*(2), 63-66.
- Aluko, R. (2018). Food protein-derived peptides: Production, isolation, and purification. In *Proteins in Food Processing* (2nd Ed., pp. 389-412). Amsterdam, Netherlands: Woodhead Publishing. doi: <https://doi.org/10.1016/B978-0-08-100722-8.00016-4>

- Beauclercq, S., Lefèvre, A., Montigny, F., Collin, A., Tesseraud, S., Leterrier, C., ... & Guilloteau, L. A. (2019). A multiplatform metabolomic approach to characterize fecal signatures of negative postnatal events in chicks: A pilot study. *Journal of Animal Science and Biotechnology*, *10*(1), 1-12. doi: <https://doi.org/10.1186/s40104-019-0335-8>
- Blasco, Błaszczczyński, J., Billaut, J. C., Nadal-Desbarats, L., Pradat, P. F., Devos, D., ... & Corcia, P. (2015). Comparative analysis of targeted metabolomics: Dominance-based rough set approach versus orthogonal partial least square-discriminant analysis. *Journal of Biomedical Informatics*, *53*, 291-299. doi: <https://doi.org/10.1016/j.jbi.2014.12.001>
- Cavanna, D., Zanardi, S., Dall'Asta, C., & Suman, M. (2019). Ion mobility spectrometry coupled to gas chromatography: A rapid tool to assess eggs freshness. *Food Chemistry*, *271*, 691-696. doi: <https://doi.org/10.1016/j.foodchem.2018.07.204>
- Chua, Y. G., Chan, S. H., Bloodworth, B. C., Li, S. F. Y., & Leong, L. P. (2015). Identification of edible bird's nest with amino acid and monosaccharide analysis. *Journal of Agricultural and Food Chemistry*, *63*(1), 279-289. doi: <https://doi.org/10.1021/jf503157n>
- Chua, K. H., Lee, T. H., Nagandran, K., Yahaya, N. H. M., Lee, C. T., Tjih, E. T. T., & Aziz, R. A. (2013). Edible bird's nest extract as a chondro-protective agent for human chondrocytes isolated from osteoarthritic knee: *In vitro* study. *BMC Complementary and Alternative Medicine*, *13*(1), 1-9. doi: <https://doi.org/10.1186/1472-6882-13-19>
- Chua, L. S., & Zukefli, S. N. (2016). A comprehensive review of edible bird nests and swiftlet farming. *Journal of Integrative Medicine*, *14*(6), 415-428. doi: [https://doi.org/10.1016/S2095-4964\(16\)60282-0](https://doi.org/10.1016/S2095-4964(16)60282-0)
- Del, C. C. P., Garde-Cerdán, T., Sánchez, A. M., Maggi, L., Carmona, M., & Alonso, G. L. (2009). Determination of free amino acids and ammonium ion in saffron (*Crocus sativus* L.) from different geographical origins. *Food Chemistry*, *114*(4), 1542-1548. doi: <https://doi.org/10.1016/j.foodchem.2008.11.034>
- Erik, V. D., Hoogeveen, A., & Abeln, S. (2015). The hydrophobic temperature dependence of amino acids directly calculated from protein structures. *PLoS Computational Biology*, *11*(5), 1-17. doi: <https://doi.org/10.1371/journal.pcbi.1004277>
- Halimi, N. M., Kasim, Z. M., & Babji, A. S. (2014). Nutritional composition and solubility of edible bird nest (*Aerodramus fuchiphagus*). In *AIP Conference Proceedings* (Vol. 1614, No. 1, pp. 476-481). New York, USA: AIP Publishing LLC.
- Hun, L. T., Lee, C. H., Azmi, N. A., Kavita, S., Wong, S., Znati, M., & Jannet, H. B. (2020). Characterization of polar and non-polar compounds of house edible bird's nest (EBN) from Johor, Malaysia. *Chemistry and Biodiversity*, *17*(1), 1-10. doi: <https://doi.org/10.1002/cbdv.201900419>
- Hun, L. T., Wani, W. A., Tjih, E. T. T., Adnan, N. A., Ling, Y. L., & Aziz, R. A. (2015). Investigations into the physicochemical, biochemical and antibacterial properties of edible bird's nest. *Journal of Chemical and Pharmaceutical Research*, *7*(7), 228-247.
- Khaleduzzaman, A., Khandaker, Z., Khan, M., Banu, L., & Khan, M. (2008). Evaluation of a high performance liquid chromatography (Hplc) method for amino acid analysis in feed with precolumn derivatization and fluorescence detection. *Bangladesh Journal of Animal Science*, *37*(2), 66-73. doi: <https://doi.org/10.3329/bjas.v37i2.9883>

- Li, Y., & Wu, Y. L. (2010). A golden phoenix arising from the herbal nest-A review and reflection on the study of antimalarial drug Qinghaosu. *Frontiers of Chemistry in China*, 5(4), 357-422. doi: <https://doi.org/10.1007/s11458-010-0214-5>
- Lim, C. (2007). *Make millions from swiftlet farming: A definitive guide*. Kuala Lumpur, Malaysia: True Wealth.
- Lukman, W., & Wibawan, I. W. T. (2018). Protein profile of edible bird's nest origin Kalimantan and Java Islands Indonesia. *Journal of Agriculture and Veterinary Sciences*, 11(5), 69-73. doi: 10.9790/2380-1105026973
- Marcone, M. F. (2005). Characterization of the edible bird's nest the "Caviar of the East". *Food Research International*, 38(10), 1125-1134. doi: <https://doi.org/10.1016/j.foodres.2005.02.008>
- Mauer, L. (2003). Heat treatment for food proteins. In *Protein* (pp. 4868-4872). Amsterdam, Netherland: Woodhead Publishing.
- Norhayati, M. K., Azman, O., & Nazaimoon, W. M. (2010). Preliminary study of the nutritional content of Malaysian edible bird's nest. *Malaysian Journal of Nutrition*, 16(3), 389-396.
- Oda, M., Ohta, S., Suga, T., & Aoki, T. (1998). Study on food components: The structure of N-linked asialo carbohydrate from the edible bird's nest built by *Collocalia fuciphaga*. *Journal of Agricultural and Food Chemistry*, 46(8), 3047-3053. doi: <https://doi.org/10.1021/jf980094k>
- Phua, L. C., Chue, X. P., Koh, P. K., Cheah, P. Y., Ho, H. K., & Chan, E. C. Y. (2014). Non-invasive fecal metabonomic detection of colorectal cancer. *Cancer Biology and Therapy*, 15(4), 389-397. doi: <https://doi.org/10.4161/cbt.27625>
- Quek, M. C., Chin, N. L., Yusof, Y. A., Law, C. L., & Tan, S. W. (2018). Pattern recognition analysis on nutritional profile and chemical composition of edible bird's nest for its origin and authentication. *International Journal of Food Properties*, 21(1), 1680-1696. doi: <https://doi.org/10.1080/10942912.2018.1503303>
- Reverter, M., Lundh, T., & Lindberg, J. E. (1997). Determination of free amino acids in pig plasma by precolumn derivatization with 6-N-aminoquinolyl-N-hydroxysuccinimidyl carbamate and high-performance liquid chromatography. *Journal of Chromatography B: Biomedical Sciences and Applications*, 696(1), 1-8. doi: [https://doi.org/10.1016/S0378-4347\(97\)00217-X](https://doi.org/10.1016/S0378-4347(97)00217-X)
- Saengkrajang, W., Matan, N., & Matan, N. (2013). Nutritional composition of the farmed edible bird's nest (*Collocalia fuciphaga*) in Thailand. *Journal of Food Composition and Analysis*, 31(1), 41-45. doi: <https://doi.org/10.1016/j.jfca.2013.05.001>
- Senizza, B., Rocchetti, G., Ghisoni, S., Busconi, M., De Los Mozos Pascual, M., Fernandez, J. A., ... & Trevisan, M. (2019). Identification of phenolic markers for saffron authenticity and origin: An untargeted metabolomics approach. *Food Research International*, 126(2019), 1-7. doi: <https://doi.org/10.1016/j.foodres.2019.108584>
- Seow, E. K., Ibrahim, B., Muhammad, S. A., Lee, L. H., & Cheng, L. H. (2016a). Differentiation between house and cave edible bird's nests by chemometric analysis of amino acid composition data. *Lebensmittel-Wissenschaft und Technologie - Food Science and Technology*, 65, 428-435. doi: <https://doi.org/10.1016/j.lwt.2015.08.047>

- Seow, E. K., Ibrahim, B., Muhammad, S. A., Lee, L. H., Lalung, J., & Cheng, L. H. (2016b). Discrimination between cave and house-farmed edible bird's nest based on major mineral profiles. *Pertanika Journal of Tropical Agricultural Science*, 39(2), 181-195.
- Shim, E. K., Chandra, G. F., Pedireddy, S., & Lee, S. Y. (2016). Characterization of swiftlet edible bird's nest, a mucin glycoprotein, and its adulterants by Raman Microspectroscopy. *Journal of Food Science and Technology*, 53(9), 3602-3608. doi: <https://doi.org/10.1007/s13197-016-2344-3>
- Song, H. H., Kim, D. Y., Woo, S., Lee, H. K., & Oh, S. R. (2013). An approach for simultaneous determination for geographical origins of Korean Panax ginseng by UPLC-QTOF/MS coupled with OPLS-DA models. *Journal of Ginseng Research*, 37(3), 341-348. doi: 10.5142/jgr.2013.37.341
- Su, S. C., Yu, P. C., Liu, C. H., Shiau, H. W., Lee, S. C., & Chou, S. S. (1998). Application of capillary electrophoresis for identification of the authenticity of bird's nests. *Journal of Food and Drug Analysis*, 6(1), 455-464.
- Tripathy, D. B., Mishra, A., Clark, J., & Farmer, T. (2018). Synthesis, chemistry, physicochemical properties and industrial applications of amino acid surfactants: A review. *Comptes Rendus Chimie*, 21(2), 112-130. doi: <https://doi.org/10.1016/j.crci.2017.11.005>
- Tulbek, M., Lam, R., Asavajaru, P., & Lam, A. (2017). Pea: A sustainable vegetable protein crop. In *Sustainable Protein Sources* (pp. 145-164). Amsterdam, Netherland: Woodhead Publishing. doi: <https://doi.org/10.1016/B978-0-12-802778-3.00009-3>
- Wong, R. S. (2013). Edible bird's nest: Food or medicine. *Chinese Journal of Integrative Medicine*, 19(9), 643-649. doi: <https://doi.org/10.1007/s11655-013-1563-y>
- Yida, Z., Imam, M. U., Ismail, M., Ooi, D. J., Sarega, N., Azmi, N. H., ... & Yusuf, N. B. (2015). Edible bird's nest prevents high fat diet-induced insulin resistance in rats. *Journal of Diabetes Research*, 2015, 1-11. doi: <https://doi.org/10.1155/2015/760535>



Effect of Sodium Hydroxide (NaOH) Treatment on Coconut Coir Fibre and its Effectiveness on Enhancing Sound Absorption Properties

Ida Norfaslia Nasidi, Lokman Hakim Ismail and Emedya Murniwaty Samsudin*

Faculty of Civil Engineering and Built Environment, Universiti Tun Hussein Onn Malaysia, 86400 Parit Raja, Batu Pahat, Johor, Malaysia

ABSTRACT

Natural fibre has been conventionally and widely utilised as a sound absorber in order to replace the traditional synthetic absorber materials. In this study, coir fibre (CF) was prepared as an acoustic absorber and subjected to an additional surface treatment by using sodium hydroxide (NaOH) at various concentrations ranging from 1% to 8%. This was geared towards analysing the effect of alkalisation on the fibre morphology, diameter, and changes occurring in the CF functional groups, thus resulting in enhanced sound absorption properties. To this end, the fibre surface was analysed using a scanning electron microscopy (SEM) to study the surface morphology of treated and untreated CF materials, whereas the implementation of Fourier-transform infrared (FTIR) allowed an analysis of CF characterisation. The absorber sample was fabricated at a constant thickness of 45mm and a density of 0.4g/cm³ density prior to testing for the sound absorption coefficient (SAC) by using an impedance tube. The morphology of CF revealed the treated fibres to be free of impurities including lignin and hemicellulose layer, which were removed from their surface. This finding was supported by the peak changes observed on the FTIR spectra. Furthermore, the fibre diameter was reduced as the concentrations of NaOH increased. The

results conclusively indicated that treated CF at the concentrations of 7% and 8% NaOH gained the highest SAC values across the low and high-frequency ranges, yielding an α coefficient average of 0.9 and above.

Keywords: Coir, fiber diameter, fourier transform infrared (FTIR), sodium hydroxide, sound absorption coefficient, surface morphology

ARTICLE INFO

Article history:

Received: 23 July 2020

Accepted: 12 October 2020

Published: 22 January 2021

DOI: <https://doi.org/10.47836/pjst.29.1.37>

E-mail addresses:

idalia_nasidi@yahoo.com.my (Ida Norfaslia Nasidi)

lokman@uthm.edu.my (Lokman Hakim Ismail)

emedya@uthm.edu.my (Emedya Murniwaty Samsudin)

* Corresponding author

INTRODUCTION

Today's modern era has resulted in the development of noise from the environment and transportation alike to become a source of pollution for mankind. As noise is inherently present in the physical surrounding, one cannot escape from this element; however, it should be noted that different people are not equally affected by the same noise. Regardless, excessive noise may affect human health and yield different psychological effects, which include insomnia, heart attack, and hypertension (Memon et al., 2015; Shiney & Premlet, 2014). Collectively, these problems lead to public awareness and concerns regarding noise pollution. Following this, demands for a solution in order to counter-act against such issue has been raised, underlining the need for proper noise control to ensure human comfort, especially in a building compartment. To this end, improving the human quality of life and growing general awareness towards the environment have spurred much interest in sustainable materials such as natural fibre by previous researchers as the sound-absorbing materials as opposed to traditional synthetic materials, such as glass wool, minerals fibres, and fibreglass. In fact, the recent decades have been associated with natural fibre and its popularity over synthetic fibre due to its low cost, lightweight attribute, ample supply as a natural and renewable resource, and good mechanical properties (Berardi & Iannace, 2015). This allowing the increasing development of more sustainable materials and support sustainability initiative. Additionally, natural fibre is a fibrous material, which can result in porous sound-absorbing materials offering excellent acoustic absorption attribute at a high-frequency range (Tang & Yan, 2017).

According to Abdullah et al. (2015) higher fibre volume yields better absorptive properties compared to a lesser fibre volume of banana fibre and sugarcane bagasse fibre. Moreover, the combination for both types of fibre show a beneficial outcome in sound absorption improvement compared to a single fibre usage. Meanwhile, Santoni et al. (2019) had assessed the effect of treatment on the physical characteristics of a material and the effect of sound absorption performance when utilising hemp fibre. They found, finer fibre diameter due to the treatment increased the sound absorption coefficient compared to thicker fibre diameter. In another study, Taban et al. (2019) found that coir fibre with thickness 45 mm produced higher sound absorption than thinner sample of 25 mm and 35 mm with SAC value of 0.97 at 1000 Hz. Next, the introduction of air gap during the experimental analysis at 10, 20, and 30 mm resulted in a significantly increased SAC at a low-frequency range. Same observations made by Ying et al. (2016), where the thicker samples and the introduction of air gap exhibited higher sound absorption of coir fibre.

Theoretically, natural fibres are commonly known as a lignocellulosic material predominantly made up of cellulose, which is the most abundant biopolymer component present on earth (Kabir et al., 2012; Naidu et al., 2017). It can also be defined as a fibrous material due to its complex internal structure, thereby forming the cell wall of a plant

(Hassan & Badri, 2014). Despite natural fibre being acknowledged with properties such as good mechanical attributes, easy processing, occupational health benefits, and reduced environmental effect (Chandramohan & Marimuthu, 2011), it is also associated with various well-documented drawbacks. Such disadvantages include moisture absorption, low thermal stability, and poor compatibility with a hydrophobic polymer matrix (Akhtar et al., 2016). To counter-act the aforementioned weaknesses, several studies have opted to investigate the properties of natural fibre for its improvement, namely via natural fibre surface modification by using either physical, chemical, or biological treatment.

Nevertheless, alkali treatment by using sodium hydroxide (NaOH) is well-known as a commonly employed chemical treatment for natural fibre and typically yields good fibre-matrix adhesion and improves the thermal and mechanical properties of composite (Jayabal et al., 2012). The reaction between NaOH and natural fibre is as shown in Equation 1.



Alkali treatment of NaOH eliminate impurities and reduces diameter of fiber by removal the lignin and hemicellulose layer on fiber surface (Senthamaraikannan & Kathiresan, 2018). Despite, NaOH treatment would also maximize the mechanical strength of kenaf fibre and PALF reinforced composites (Feng et al., 2020). Using 5% of NaOH solution, alkali-treated *Ziziphus Mauritiana* fibers improved on the surface roughness and influenced the bonding behavior due to the reduction of amorphous constituents (Vinod et al., 2020).

Therefore, this current work focus to find an alternate materials which was sustainable to replace synthetic sound absorber. Although a number of studies has been devoted towards exploring the usage of natural fibre as a sound absorber, the effect of its surface treatment via NaOH across different concentrations is seldom reported, especially in the context of Malaysian natural fibre and natural fibre waste. Hence, this paper attempts to observe the morphological changes of coir fibre structure and its fibre diameter changes after being subjected to NaOH treatment in order to enhance the sound absorption properties of coconut coir fibre (CF).

MATERIALS AND METHODS

Material Preparations

Raw CF was supplied by a local agricultural waste supplier, namely Sarjani Agro Shop Sdn. Bhd. located in Sri Medan, Batu Pahat. The CF sample was then cut to a shorter length of ± 2 cm to 5 cm for easy processing during the fabrication stage. To analyse the morphological and chemical changes occurring in the fibre structure and their effects towards sound absorption performance, the CF sample was treated using NaOH of different concentrations. Therefore, the control sample consisted of untreated coir fibre, while eight

different concentrations of NaOH were utilised, namely 1%, 2%, 3%, 4%, 5%, 6%, 7%, and 8%, respectively. Next, the fibre-to-solution ratio was set to 1:20 so as to ensure the fibres were fully submerged in the NaOH solution and soaked for two hours. Following this, they were washed under running water for several times to eliminate any NaOH residue on the fibre strands, until no change in colour was observed in the drained water. Subsequently, the process of drying the fibres commenced, which was done under the sun for 2 to 3 days depending on the weather condition, before they were oven-dried for 30 minutes at the heating temperature of $110^{\circ}\text{C} \pm 5^{\circ}\text{C}$.

Sample Preparation

In this study, 15% of urea formaldehyde (UF) was utilised as the main adhesive material for the formation of the acoustic samples (Nasidi et al., 2018). It was provided by Evergreen Adhesive & Chemical Sdn. Bhd., which is a prominent company specialising in wood-working adhesives and located at Parit Raja, Batu Pahat, Johor. Then, the CF sample was fabricated at a constant density of 0.4 g/cm^3 and 45 mm thickness (Samsudin et al., 2017). In particular, two sample diameters were fabricated, specifically 28 mm and 100 mm, which were then fit into the prepared mould and compressed by using a hot compression machine for 15 min at 180°C using 1000 psi. Following this, the samples were removed from the machine and left at room temperature for cooling down (Figure 1), it should be noted that this was done before they were taken out from the mould to prevent any damage. In total, six samples (three samples for the 29 mm diameter and three samples for 100 mm diameters) for each concentration were subjected to testing in the impedance tube to determine their respective acoustic absorption coefficient.



Figure 1. CF sample

Fibre Diameter

The diameter measurement of CF samples was carried out by using a Digital Microscope Image Analyser, whereby 100 single-fibre strands were randomly selected for each concentration of treatment. Due to their irregular shapes, measurement of a single fibre was carried out in three positions, namely at the top, middle, and bottom of the fibre (Sanjay et al., 2019). Every fibre measured was cut according



Figure 2. CF under Digital Microscope Image Analyser

to the average length of each fibre type in order to calculate its average diameter at the three aforementioned positions to yield the actual fibre diameter. Figure 2 shows the CF diameter measurement conducted using the Digital Microscope Image Analyser.

Surface Morphology Analysis

The element of CF surface morphology was examined in this study by employing a scanning electron microscopy (SEM) using HITACHI SUI510 model. Prior to observation, the samples were coated with gold three times for 90 s. Following this, the surface morphology analysis was carried out with an accelerating voltage of 15 kV and 63.0 μ A emission, whereas the observation was undertaken at 500 \times magnification focused on the fibre structure and silica bodies present on its surface.

FTIR Analysis

Fourier-transform infrared (FTIR) is a cost-effective, rapid, non-destructive, simple, and appropriate tool for analysing the changes in fibre functional groups, whether in untreated or treated fibres alike. To this end, untreated and treated CF spectra were determined accordingly using Perkin Elmer FTIR Spectrometer LR 64912C, N3896, FTIR software V1.3.2 Perkin Elmer LX100877-1 made in the U.S.A., which was equipped with an ATR sample holder. To achieve this, the CF samples were ground into powder form less than 100 microns, which was next inserted into the powder plate until it covered the crystal glass and was slowly compacted. The process was carried out at a wavenumber ranging between 4000 cm^{-1} to 600 cm^{-1} and operated at a resolution of 4 cm^{-1} , whereby 32 scans were collected for each sample.

Sound Absorption Test

The next phase consisted of CF sample measurement by using an impedance tube in accordance to BS ISO 10534-2 in order to measure the sound absorption coefficient (SAC). This equipment and its method of measurement are well-known as a simple approach, which is easily conducted and convenient in determining the α value. Measurement equipped with tubes (SCS9020B/TL), two-unit microphones, one speaker and one computer to analyse the data. The process was carried out within the range of frequency from 100 Hz to 5000 Hz in 1/3 octave band. In particular, the low-frequency range testing employed a large tube with a 100 mm tube diameter at the frequencies spanning from 100 Hz to 1600 Hz, whereas high-frequency range testing spanned from 1500 Hz to 5000 Hz by using a small tube with a 29 mm diameter tube size. Then, measuring the absorption coefficient in order to assess the sound absorption performance was done by placing a loudspeaker at one end of the impedance tube and a sample at its other end. During the testing, the sound waves were propagated within the tube to strike between the sample and sound source, which then reflected as a standing wave.

RESULT AND DISCUSSION

Coir Fibre Diameter

Table 1 details a summary of the results obtained from laboratory measurements of the CF diameter. Physically, CF revealed an almost regular diameter along the entirety of the fibre strands. However, the measurement was also taken at three different locations of the strand, allowing the calculation of a mean value. The values in Table 1 reveal a larger fibre diameter for the untreated CF sample compared to the treated fibre. In particular, untreated CF yielded an average diameter ranging between 46.7 µm and 260.0 µm, whereas its average diameter value was 124.27 µm. A similar result had been reported by Chen et al. (2016) when bamboo fibres were subjected to varying concentrations of NaOH, while studies by Dittenber and Gangaroa (2012) and Geethamma et al. (1998) had observed their raw CCF diameter that ranged from 100 µm to 460 µm. Next, the mean CF diameter was reduced after the samples were treated with different concentrations of NaOH, which spanned from low to high concentrations. In particular, the diameter value was reduced by approximately 22.9 % when its values were juxtaposed across untreated fibre to those subjected to 8% NaOH concentration. Such decrement in fibre diameter is typically caused by the removal of lignin, which is generally found on the fibre surface (Hashim et al., 2017). This is supported by Pouriman et al. (2017), whereby the average diameter of a single salogo fibre was reduced from 6.23 µm to 4.23 µm. Similarly, the alkali treatment subjected to the sample had removed some of the cellulose and lignin contents on the fibre structure, thereby causing the fibre diameter reduction.

Figure 3 depicts the cumulative distribution of 100 fibre strands of CF. The findings clearly showed a decreased fibre diameter when the alkali concentrations were increased. Furthermore, untreated fibre and those subjected to 1% NaOH resulted in a larger fibre diameter, whereby the line in Figure 4 is located slightly to the right side. Meanwhile, fibres treated with 2% and 3% NaOH straddled the middle range between the thicker and thinner fibre diameters, whereas NaOH concentration increments from 4% to 8% yielded barely-seen changes in the fibre diameter. However, it should be noted that the 7% and 8% NaOH concentrations were characterised with graph lines located at the outer part of the group on the left side.

Table 1
Range of diameter and average diameter of untreated and treated CCF samples

Fiber	CF 0%	CF 1%	CF 2%	CF 3%	CF 4%	CF 5%	CF 6%	CF 7%	CF 8%
Range of diameter (µm)	46.7–260.0	36.7–346.7	40.0–306.5	30.0–270.0	30.0–261.2	36.9–260.8	36.2–216.7	20.0–326.7	26.7–360.1
Average Diameter (µm)	124.3	123.9	112.9	105.9	104.8	103.4	101.1	98.8	95.8

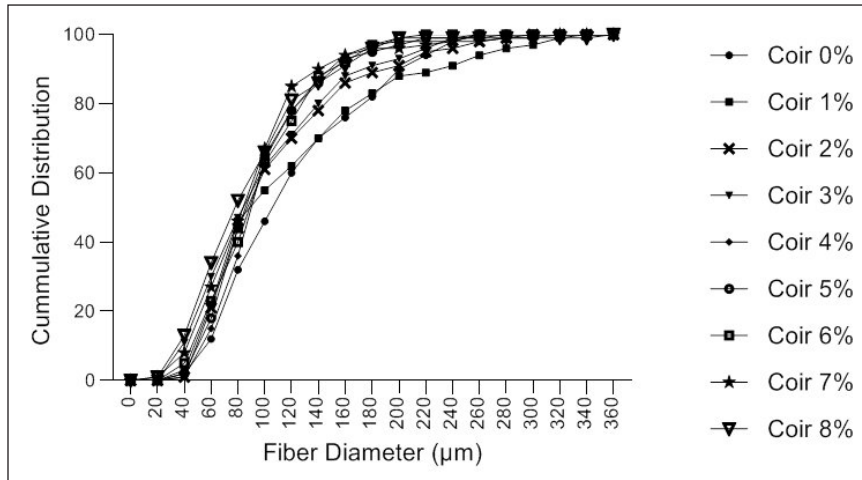


Figure 3. Cumulative distribution of CF

Surface Morphology of CCF

Figures 4 (a) - (i) reveal the surface morphologies of untreated and treated CF samples ranging from 1% to 8% NaOH concentrations, which were analysed using SEM. For example, the untreated CF fibre strand is shown in Figure 4(a) in which it is fully covered by impurities and has uneven surfaces. Besides, its components included pectin, wax, lignin, and silica bodies, which paralleled the observations of Ng et al. (2018). Removal of impurities could be seen as compared to the untreated fibers. It shows gradual changes in the effect of NaOH treatment on the coir fiber surface. Meanwhile, treated CCF samples subjected to NaOH concentrations ranging from 1% to 3% (Figure 4 (b)-(d)) showed a partial removal of the impurities, including silica bodies, which left tiny holes on the sample surfaces. These tiny holes are associated with the creation of microcompartments, which are good for sound dissipation purposes (Mercado et al., 2018). Therefore, this shows that a low concentration of NaOH does not significantly affect the removal of impurities present on the fibre (Hashim et al., 2017). Subsequently, an increased concentration of NaOH treatments subjected to higher concentrations from 4% (Figure 4(e)) to 6% (Figure 4(g)) allowed the remaining silica bodies to be completely removed. As a result, it created pores that appeared due to the removal of the silica bodies, which looked larger with an uneven depth. Similar findings had also been discovered by Ng et al. (2018), which further increased the mechanical bonding between the coir fibre and matrix during the fabrication process (Karthikeyan et al., 2014). Additionally, some longitudinal pits were observed along the fibre strands assessed in this study, thereby paralleling the same phenomenon described by (Manjula et al., 2017). However, as the NaOH concentrations increased to 7% and 8% (Figure 4 (h)-(i)), these previously created pores disappeared almost completely. This may be attributable to the surface layer CF removal (Leão et al., 2015) Besides, the

morphological results indicated the CF fibres had rough surfaces and were clean from any impurities as the NaOH concentration was increased. To support the argument regarding alkali treatment effectiveness, FTIR spectroscopy was employed to investigate the structural changes observed on the CF sample surface before and after treatment.

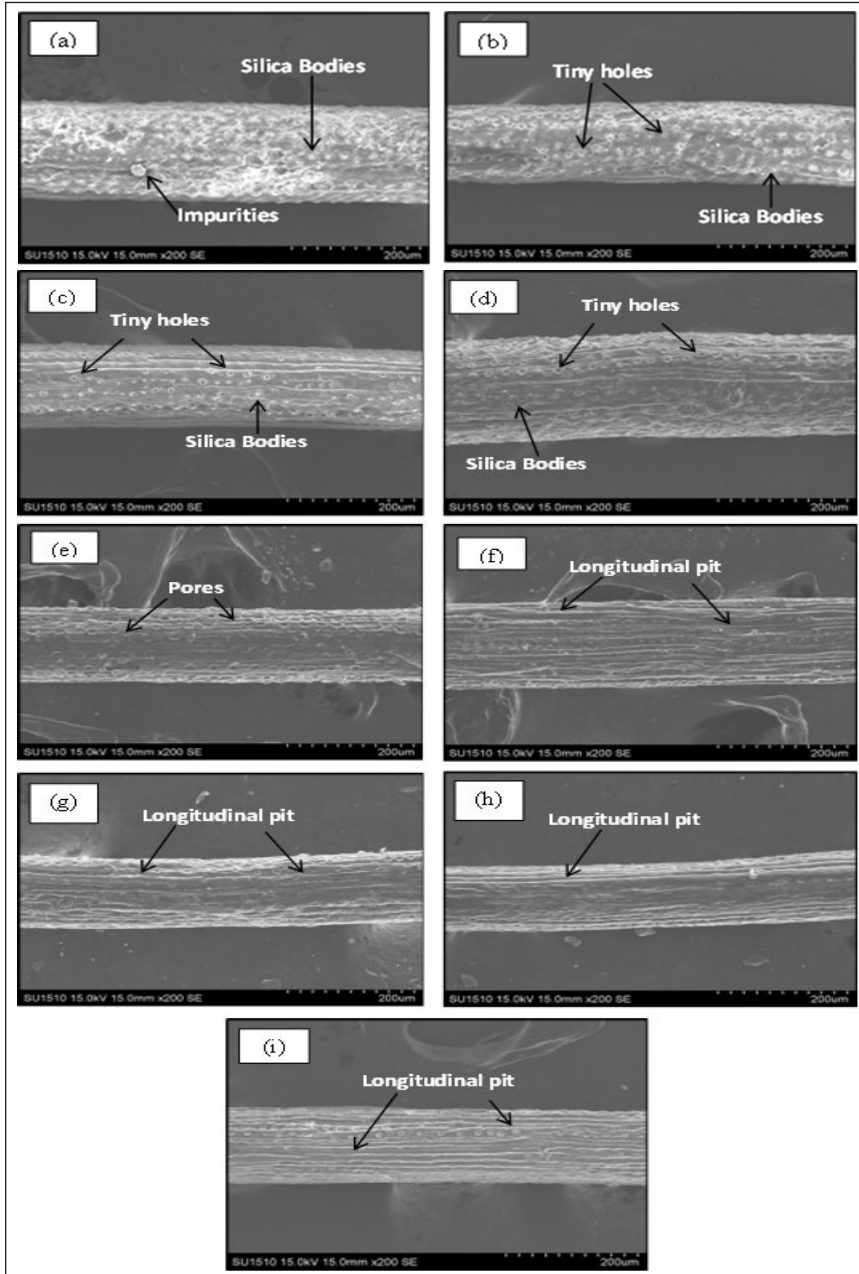


Figure 4. SEM images on surface of CF : (a) CF0%, (b) CF1% (c) CF2%, (d) CF3%, (e) CF4%, (f) CF5%, (g) CF6%, (h) CF7%, and (i) CF8%

FTIR Analysis

Figure 5 represents the FTIR spectra observed for the untreated and treated CF samples, ranging from 1% to 8% concentrations. First, the peak ranging from 3000 cm^{-1} to 3700 cm^{-1} corresponded to the O – H stretching of hydroxyl groups (Krishnan & Ramesh, 2013; Siakeng et al., 2018). In this study, the untreated CF gained its O – H peak at band 3345 cm^{-1} in which the observations clearly and contrastingly depicted a significantly reduced intensity for alkali-treated sample. The diminished intensity may be attributed to the breaks of hydrogen bonding present in OH groups during the NaOH treatments (Yew et al., 2019). Meanwhile, the absorption band corresponding to the C = O stretching of carboxyl and acetyl groups in the hemicellulose yielded the raw CF peak band at 1735 cm^{-1} . However, it disappeared when the fibres were treated with NaOH, which could be linked to hemicellulose solubility property in an alkaline solution and thus caused its disappearance (Yew et al., 2019). The same observations had also been made by Abraham et al. (2013), wherein a peak was present at band 1249 cm^{-1} for the untreated CF sample and attributable to the aromatic ring skeletal vibration and C = O stretching of lignin. However, the peak for treated fibre samples was not completely removed; its intensity was merely decreased. Therefore, this is indicative of some lignin and hemicellulose content removed via the NaOH treatment from the fibre surfaces and supports the fibre diameter decrements outcomes observed after subjected to the treatment.

Sound Absorption Coefficient (SAC)

Figure 6 illustrates the sound absorption performance generated by untreated and NaOH-treated CF samples, which range from 1% to 8%. The findings revealed that as the frequency increased, the SAC values were also amplified in line with the outcomes from (Taban et

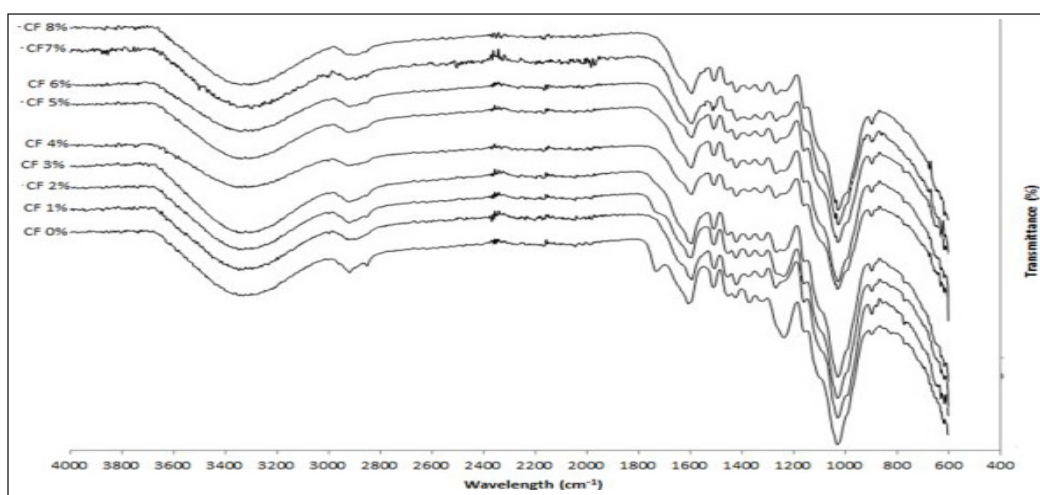


Figure 5. FTIR spectrum of raw and alkali treated CF

al., 2019). Furthermore, the result shows that from, untreated and treated CF samples alike yielded superior acoustic absorption ability at the frequency ranging from 500 Hz to 5000 Hz. Besides, the SAC values obtained for all samples were higher than 0.5, thereby indicating that over 50% of the incident sound was absorbed. The figure further shows that the peak absorption at a lower frequency region is gained by CF samples treated with high NaOH concentrations. In particular, samples subjected to 7% and 8% NaOH yielded $\alpha = 0.98$ at the frequency of 1250 Hz. Upon entering the middle frequency region, the SAC value for all CF samples was decreased, revealing the least absorptive value as low as 0.72. In contrast, the highest sound absorption performance was obtained by an untreated CF sample in the middle frequency range, indicating its status as a good absorber from the middle to the beginning of the high-frequency range in comparison with treated fibres. Here, the SAC values recorded ranged from 0.83 to 0.96 at frequencies between 2000 Hz to 4000 Hz. Lastly, the high-frequency sector revealed the highest SAC values obtained at the higher NaOH concentrations (i.e. 7% and 8%), while other samples also observed an increased sound absorption performance. This outcome is significantly attributable to the finest diameter of fibre treated with the highest NaOH concentrations through the removal of impurities, lignin and hemicellulose layer on fiber surfaces, thus enhancing the SAC outcomes at the low and high-frequency ranges (Wang et al., 2015). Similar outcome was discovered by Samaei et al. (2020), where the decrement on fiber diameter due to NaOH treatment increased the sound absorption performances of kenaf fiber at constant thickness and density. Theoretically, fiber diameter was the one factor that influencing the sound absorption of fibrous materials. This was due to the more tortuous path and higher airflow

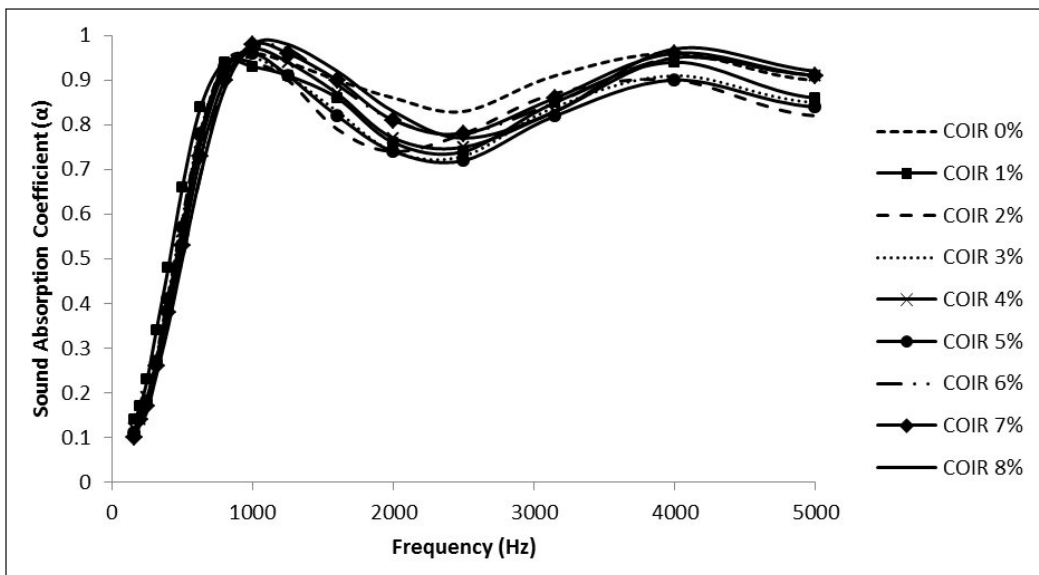


Figure 6. Sound absorption performance of CF at different concentrations of NaOH treatment

resistance caused by higher fibre volume needed to reach equal volume of fibre with same thickness and density (Seddeq, 2009). Further analysis was made to see the correlation between acoustical performances and fibre diameter of coir fibre. It was observed that there was a positive correlation between the two variables where $r = 0.754$. Overall, CF implementation led to good absorption performance and the material was thus considered a good absorber.

CONCLUSION

In this work, CF was utilised as a sound absorber material, whereby its surface fibre was subjected to treatment using 1% to 8% NaOH concentrations. Accordingly, the morphological changes, fibre diameter, and fibre composition were observed and analysed in evaluating its characteristics and sound absorption performance. In brief, NaOH-treated CF samples yielded enhanced sound absorption performances in comparison with the untreated sample, whereby a higher NaOH concentration led to better performance. This is caused by its finer fibre diameter in which an absorber sample requires a higher amount of fibre to have the same weight as a thicker fibre sample, thus allowing more sound energy to be dissipated. Furthermore, the average fibre size decreased when the alkali concentrations were increased, whereas the surface morphology analysis revealed the partial removal of certain impurities at a certain amount from the fibre surface, which included lignin and hemicellulose. Up until 8% NaOH concentration, clear fibre was observed and supported further by the accompanying FTIR peak spectra results. Hence, the results obtained in this study suggested for the use of 7% and 8% NaOH concentrations in order to optimally implement a coconut fibre treatment approach geared for maximum sound absorption performance.

ACKNOWLEDGMENTS

Special thanks to Research Management Centre (RMC) Universiti Tun Hussein Onn Malaysia, for the funding of this research under vote E15501 and vote U791.

REFERENCES

- Abdullah, A. H., Azharia, A., & Salleh, F. M. (2015). Sound absorption coefficient of natural fibres hybrid reinforced polyester composites. *Jurnal Teknologi*, 76(9), 31-36. doi: 10.11113/jt.v76.5643
- Abraham, E., Deepa, B., Pothen, L. A., Cintil, J., Thomas, S., John, M. J., ... & Narine, S. S. (2013). Environmental friendly method for the extraction of coir fibre and isolation of nanofibre. *Carbohydrate Polymers*, 92, 1477-1483. doi: <https://doi.org/10.1016/j.carbpol.2012.10.056>
- Akhtar, M. N., Sulong, A. B., Radzi, M. K. F., Ismail, N. F., Raza, M. R., Muhamad, N., & Khan, M. A. (2016). Influence of alkaline treatment and fiber loading on the physical and mechanical properties of kenaf/

- polypropylene composites for variety of applications. *Progress in Natural Science: Materials International*, 26(6), 657-664. doi: <https://doi.org/10.1016/j.pnsc.2016.12.004>
- Berardi, U., & Iannace, G. (2015). Acoustic characterization of natural fibers for sound absorption applications. *Building and Environment*, 94, 840-852. doi: <https://doi.org/10.1016/j.buildenv.2015.05.029>
- Chandramohan, D., & Marimuthu, K. (2011). A review on natural fibers. *International Journal of Research and Reviews in Applied Sciences*, 8(2), 194-206.
- Chen, H., Yu, Y., Zhong, T., Wu, Y., Li, Y., Wu, Z., & Fei, B. (2016). Effect of alkali treatment on microstructure and mechanical properties of individual bamboo fibers. *Cellulose*, 24(1), 333-347. doi: <https://doi.org/10.1007/s10570-016-1116-6>
- Dittenber, D. B., & Gangarao, H. V. S. (2012). Critical review of recent publications on use of natural composites in infrastructure. *Composites: Part A*, 43(8), 1419-1429. doi: <https://doi.org/10.1016/j.compositesa.2011.11.019>
- Feng, N. L., Malingam, S. D., Razali, N., & Subramonian, S. (2020). Alkali and silane treatments towards exemplary mechanical properties of kenaf and pineapple leaf fibre-reinforced composites. *Journal of Bionic Engineering*, 17, 380-392. doi: <https://doi.org/10.1007/s42235-020-0031-6>
- Geethamma, V. G., Mathew, K. T., Lakshminarayanan, R., & Thomas, S. (1998). Composite of short coir fibres and natural rubber: effect of chemical modification, loading and orientation of fibre. *Polymer*, 39(6-7), 1483-1491. doi: [https://doi.org/10.1016/S0032-3861\(97\)00422-9](https://doi.org/10.1016/S0032-3861(97)00422-9)
- Hashim, M. Y., Amin, A. M., Marwah, O. M. F., Othman, M. H., Yunus, M. R. M., & Ng, C. H. (2017). The effect of alkali treatment under various conditions on physical properties of kenaf fiber. *Journal of Physics: Conference Series*, 914, 1-15. doi: <https://doi.org/10.1088/1742-6596/914/1/012030>
- Hassan, N. S., & Badri, K. (2014). Lignin recovery from alkaline hydrolysis and glycerolysis of oil palm fiber. *AIP Conference Proceedings* 1614(1), 433-438. doi: <https://doi.org/10.1063/1.4895236>
- Jayabal, S., Sathiyamurthy, S., Loganathan, K. T., & Kalyanasundaram, S. (2012). Effect of soaking time and concentration of NaOH solution on mechanical properties of coir-polyester composites. *Bulletin of Materials Science*, 35(4), 567-574. doi: <https://doi.org/10.1007/s12034-012-0334-2>
- Kabir, M. M., Wang, H., Lau, K. T., & Cardona, F. (2012). Chemical treatments on plant-based natural fibre reinforced polymer composites: An overview. *Composites: Part B*, 43, 2883-2892. doi: <https://doi.org/10.1016/j.compositesb.2012.04.053>
- Karthikeyan, A., Balamurugan, K., & Kalpana, A. (2014). The effect of SLS treatment on tensile property of coconut fiber reinforced epoxy composites. *Transactions of Mechanical Engineering*, 38(1), 157-166.
- Krishnan, V. N., & Ramesh, A. (2013). Synthesis and characterization of cellulose nanofibers from coconut coir fibers. *IOSR Journal of Applied Chemistry (IOSR-JAC)*, 6(3), 18-23.
- Leão, R. M., Luz, S. M., Araujo, J. A., & Novack, K. (2015). Surface treatment of coconut fiber and its application in composite materials for reinforcement of polypropylene. *Journal of Natural Fibers*, 12(6), 574-586. doi: <https://doi.org/10.1080/15440478.2014.984048>

- Manjula, R., Raju, N., Chakradhar, R., & Johns, J. (2017). Effect of thermal aging and chemical treatment on tensile properties of coir fiber. *Journal of Natural Fibers*, 15(1), 112-121. doi: <https://doi.org/10.1080/15440478.2017.1321513>
- Memon, H., Abro, Z. A., Ahmed, A., & Khoso, N. A. (2015). Considerations while designing acoustic home textiles: A review. *Journal of Textile and Apparel, Technology and Management*, 9(3), 1-29.
- Mercado, R. D. T., Ureta, R. M., & Templo, R. J. D. (2018). The potential of selected agricultural wastes fibers as acoustic absorber and thermal insulator based on their surface morphology via scanning electron microscopy. *World News of Natural Sciences*, 20, 129-147.
- Naidu, A. L., Jagadeesh, V., & Bahubalendruni, M. V. A. R. (2017). A review on chemical and physical properties of natural fiber reinforced composites. *International Journal of Advanced Research in Engineering and Technology (IJARET)*, 8(1), 56-68.
- Nasidi, I. N., Ismail, L. H., Samsudin, E. M., Abdul Khodir, M. F., & Kamarozaman, M. A. (2018). The Effect of Different Fibre Length and Different Urea Formaldehyde (UF) content on Sound Absorption Performance of Empty Fruit Bunch (EFB). *MATEC Web of Conferences*, 150, 1-5. doi: <https://doi.org/10.1051/mateconf/201815003003>
- Ng, Y. R., Shahid, S. N. A. M., & Nordin, N. I. A. A. (2018). The effect of alkali treatment on tensile properties of coir / polypropylene biocomposite. *IOP Conference Series: Materials Science and Engineering*, 368, 1-8. doi: <https://doi.org/10.1088/1757-899X/368/1/012048>
- Pouriman, M., Caparanga, A. R., Ebrahimi, M., & Dahresobh, A. (2017). Characterization of untreated and alkaline-treated salago fibers (*Genus wikstroemia* spp.). *Journal of Natural Fibers*, 15(2), 296-307. doi: <https://doi.org/10.1080/15440478.2017.1329105>
- Samaei, S. E., Mahabadi, H. A., Mousavi, S. M., Khavanin, A., Faridan, M., & Taban, E. (2020). The influence of alkaline treatment on acoustical, morphological, tensile, and thermal properties of Kenaf natural fibers. *Journal of Industrial Textiles*, 0(0), 1-25. doi: <https://doi.org/10.1177/1528083720944240>
- Samsudin, E. M., Ismail, L. H., Kadir, A. A., & Nasidi, I. N. (2017, July 23-27). Thickness, density, and porosity relationship towards sound absorption performance of mixed palm oil fibers. In *24th International Congress on Sound and Vibration* (pp. 1-8). London, UK.
- Sanjay, M. R., Siengchin, S., Parameswaranpillai, J., Jawaid, M., Pruncu, C. I., & Khan, A. (2019). A comprehensive review of techniques for natural fibers as reinforcement in composites: Preparation, processing and characterization. *Carbohydrate Polymers*, 207, 108-121. doi: <https://doi.org/10.1016/j.carbpol.2018.11.083>
- Santoni, A., Bonfiglio, P., Fausti, P., Marescotti, C., Mazzanti, V., Mollica, F., & Pompoli, F. (2019). Improving the sound absorption performance of sustainable thermal insulation materials: Natural hemp fibres. *Applied Acoustics*, 150, 279-289. doi: <https://doi.org/10.1016/j.apacoust.2019.02.022>
- Seddeq, H. S. (2009). Factors influencing acoustic performance of sound absorptive materials. *Australian Journal of Basic and Applied Sciences*, 3(4), 4610-4617.
- Senthamaraiannan, P., & Kathiresan, M. (2018). Characterization of raw and alkali treated new natural cellulosic fiber from *Coccinia grandis*. L. *Carbohydrate Polymers*, 186, 332-343. doi: <https://doi.org/10.1016/j.carbpol.2018.01.072>

- Shiney, A., & Premlet, B. (2014). Acoustic properties of composite coir mats. *IOSR Journal of Applied Physics*, 6(3), 18-23.
- Siakeng, R., Jawaid, M., Ariffin, H., & Salit, M. S. (2018). Effects of surface treatments on tensile, thermal, and fibre-matrix bond strength of coir and pineapple leaf fibres with poly lactic acid. *Journal of Bionic Engineering*, 15(6), 1035-1046. doi: <https://doi.org/10.1007/s42235-018-0091-z>
- Taban, E., Tajpoor, A., Faridan, M., Samaei, S. E., & Beheshti, M. H. (2019). Acoustic absorption characterization and prediction of natural coir fibers. *Acoustics Australia*, 47(1), 67-77. doi: <https://doi.org/10.1007/s40857-019-00151-8>
- Tang, X., & Yan, X. (2017). Acoustic energy absorption properties of fibrous materials: A review. *Composites Part A: Applied Science and Manufacturing*, 101, 360-380. doi: <https://doi.org/10.1016/j.compositesa.2017.07.002>
- Vinod, A., Vijay, R., Singaravelu, D. L., Khan, A., Sanjay, M., Siengchin, S., ... & Asiei, A. M. (2020). Effect of alkali treatment on performance characterization of *Ziziphus mauritiana* fiber and its epoxy composites. *Journal of Industrial Textiles*, 0(0), 1-3. doi: <https://doi.org/10.1177/1528083720942614>
- Wang, X., Li, Y., Chen, T., & Ying, Z. (2015). Research on the sound absorption characteristics of porous metal materials at high sound pressure levels. *Advances in Mechanical Engineering*, 7(5), 1-7. doi: <https://doi.org/10.1177/1687814015575429>
- Yew, B. S., Muhamad, M., Mohamed, S. B., & Wee, F. H. (2019). Effect of alkaline treatment on structural characterisation, thermal degradation, and water absorption ability of coir fibre polymer composites. *Sains Malaysiana*, 48(3), 653-659. doi: <http://dx.doi.org/10.17576/jsm-2019-4803-19>
- Ying, L. Z., Putra, A., Nor, M. J. M., Muhammad, N., & Yaakob, M. Y. (2016, July 10-14). Sound absorption of multilayer natural coir and kenaf fibers. In *23rd International Congress on Sound and Vibration* (pp. 1-7). Athens, Greece.

REFEREES FOR THE PERTANIKA JOURNAL OF SCIENCE AND TECHNOLOGY

VOL. 29 (1) JAN. 2021

The Editorial Board of Pertanika Journal of Science and Technology wishes to thank the following:

Abdul Salam Babji <i>(UKM, Malaysia)</i>	Chuan Zun Liang <i>(UMP, Malaysia)</i>	Khairul Hamimah Abas <i>(UTM, Malaysia)</i>
Abdullah Hisam Omar <i>(UTM, Malaysia)</i>	Darren Ong Chung Lee <i>(XMU, Malaysia)</i>	Koo Lee Feng <i>(UPM, Malaysia)</i>
Achutha Kini <i>(MIT, India)</i>	Dharini Pathmanathan <i>(UM, Malaysia)</i>	Lai Kee Huong <i>(Sunway University, Malaysia)</i>
Adem Kilicman <i>(UPM, Malaysia)</i>	Effariza Hanafi <i>(UM, Malaysia)</i>	Lam Man Kee <i>(UTP, Malaysia)</i>
Ahmad Fikri Abdullah <i>(UPM, Malaysia)</i>	Elysha Nur Ismail <i>(UPM, Malaysia)</i>	Lee Nung Kion <i>(UNIMAS, Malaysia)</i>
Ahmad Ramli Mohd Yahya <i>(USM, Malaysia)</i>	Eris Elianddy Supeni <i>(UPM, Malaysia)</i>	Lee Sin Chang <i>(UPM, Malaysia)</i>
Ahmed Jalal Khan Chowdhury <i>(IIUM, Malaysia)</i>	Fam Soo Fen <i>(UTeM, Malaysia)</i>	Lim Gin Keat <i>(USM, Malaysia)</i>
Aidi Hizami Alias <i>(UPM, Malaysia)</i>	Farzaneh Mohamadpour <i>(USB, Iran)</i>	Lim Yoke Mui <i>(USM, Malaysia)</i>
Amin Ismail <i>(UPM, Malaysia)</i>	Ghufran Redzwan <i>(UM, Malaysia)</i>	Md Abul Kalam <i>(UM, Malaysia)</i>
Aminuddin Ab Ghani <i>(USM, Malaysia)</i>	Hanani Ahmad Yusof@Hanafi <i>(IIUM, Malaysia)</i>	Md Faisal Md Basir <i>(UTM, Malaysia)</i>
Ang Bee Chin <i>(UM, Malaysia)</i>	Hanizam Awang <i>(USM, Malaysia)</i>	Md. Noordin Abu Bakar <i>(USM, Malaysia)</i>
Arien Heryansyah <i>(UTM, Malaysia)</i>	Hashibah Hamid <i>(UUM, Malaysia)</i>	Mohamad Kamarol Mohd Jamil <i>(USM, Malaysia)</i>
Ariffin Abdul Mutalib <i>(UUM, Malaysia)</i>	Hedzlin Zainuddin <i>(UiTM, Malaysia)</i>	Mohamad Yusof Maskat <i>(UKM, Malaysia)</i>
Ashrafi Seyed Mohammad <i>(SCU, Iran)</i>	Isa Bala Muhammad <i>(FUTMinna, Nigeria)</i>	Mohamadarriff Othman <i>(UM, Malaysia)</i>
Azmah Hanim Mohamed Ariff <i>(UPM, Malaysia)</i>	Jayaraj Vijaya Kumaran <i>(UMK, Malaysia)</i>	Mohammed Alias Yusof <i>(UPNM, Malaysia)</i>
Che Zalina Zulkifli <i>(UPSI, Malaysia)</i>	Kamarul Ariffin Noordin <i>(UM, Malaysia)</i>	Mohd Hudzari Haji Razali <i>(UiTM, Malaysia)</i>
Chiuan Yee Leow <i>(USM, Malaysia)</i>	Kasturi Dewi Varathan <i>(UM, Malaysia)</i>	Mohd Shahrul Nizam Mohd Danuri <i>(KUIS, Malaysia)</i>
Chuah Joon Huang <i>(UM, Malaysia)</i>	Kek Sie Long <i>(UTHM, Malaysia)</i>	Mohd Shamsul Anuar <i>(UPM, Malaysia)</i>

Muhammad Azril Hezmi
(UTM, Malaysia)

Muhammad Ekhlasar Rahman
(Curtin University, Malaysia)

Muhammad Hafiz Borkhanuddin
(UMT, Malaysia)

Muhammad Heikal Ismail
(UPM, Malaysia)

Nadiatul Adilah Ahmad Abdul
Ghani
(UMP, Malaysia)

Nasir Ganikhodjaev
(IIUM, Malaysia)

Noorashrina, A. Hamid
(USM, Malaysia)

Nor Amaiza Mohd Amin
(UPM, Malaysia)

Nor Khaizura Mahmud@Ab
Rashid
(UPM, Malaysia)

Noramalina Abdullah
(USM, Malaysia)

Norharyati Harum
(UTeM, Malaysia)

Normah Maan
(UTM, Malaysia)

Norzalilah Mohamad Nor
(USM, Malaysia)

Nur Anisah Mohamed Rahman
(UM, Malaysia)

Nur Fadhilah Ibrahim
(UMT, Malaysia)

Nurul Hashimah Ahamed
Hassain Malim
(USM, Malaysia)

Nurulhuda Khairuddin
(UPM Malaysia)

Othman A. Karim
(UKM, Malaysia)

Pah Chin Hee
(IIUM, Malaysia)

Pin Kar Yong
(FRIM, Malaysia)

Puay How Tion
(USM, Malaysia)

Rabiah Abdul Kadir
(UKM, Malaysia)

Rafeah Wahid
(UNIMAS, Malaysia)

Rita Hayati
(Unsyiah, Indonesia)

Riza Wirawan
(UNJ, Indonesia)

Rohazila Mohamad Hanafiah
(USIM, Malaysia)

Roseliza Kadir Basha
(UPM, Malaysia)

Rozaini Zohdi
(UiTM, Malaysia)

Salina Abdul Samad
(UKM, Malaysia)

Sarina Sulaiman
(IIUM, Malaysia)

Shamima Abdul Rahman
(University of Cyberjaya, Malaysia)

Shanmughasundaram
Palanisamy
(KCE, India)

Shariza Jamek
(UMP, Malaysia)

Shuhaida Shuib
(USM, Malaysia)

Siti Nurbaya Oslan
(UPM, Malaysia)

Suraya Mohd Tahir
(UPM, Malaysia)

Suryani Kamarudin
(UPM, Malaysia)

Tan Cheng Siang
(UNIMAS, Malaysia)

Wang Seok Mui
(UiTM, Malaysia)

Woon Kai Lin
(UM, Malaysia)

Yap Wei Boon
(UKM, Malaysia)

Zabidin Salleh
(UMT, Malaysia)

Zulkurnain Abdul-Malek
(UTM, Malaysia)

FRIM – Forest Research Institute Malaysia
FUTMinna – Federal University of Technology Minna
IIUM – International Islamic University Malaysia
KCE – Karpagam College of Engineering
KUIS – Kolej Universiti Islam Antarabangsa Selangor
MIT – Manipal Institute of Technology
SCU – Shahid Chamrani University of Ahvaz
UiTM – Universiti Teknologi MARA
UKM – Universiti Kebangsaan Malaysia
UM – Universiti Malaya
UMK – Universiti Malaysia Kelantan
UMP – Universiti Malaysia Pahang
UMT – Universiti Malaysia Terengganu
UNIMAS – Universiti Malaysia Sarawak

UNJ – Universitas Negeri Jakarta
Unsyiah – Universitas Syiah Kuala
UPM – Universiti Putra Malaysia
UPNM – Universiti Pertahanan Nasional Malaysia
UPSI – University Pendidikan Sultan Idris
USB – University of Sistan & Baluchistan
USIM – Universiti Sains Islam Malaysia
USM – Universiti Sains Malaysia
UTeM – Universiti Teknikal Malaysia Melaka
UTHM – Universiti Tun Hussein Onn Malaysia
UTM – Universiti Teknologi Malaysia
UTP – Universiti Teknologi Petronas
ULUM – Universiti Utara Malaysia
XMU – Xiamen University

While every effort has been made to include a complete list of referees for the period stated above, however if any name(s) have been omitted unintentionally or spelt incorrectly, please notify the Chief Executive Editor, *Pertanika* Journals at executive_editor.pertanika@upm.edu.my

Any inclusion or exclusion of name(s) on this page does not commit the *Pertanika* Editorial Office, nor the UPM Press or the University to provide any liability for whatsoever reason.

Pertanika Journal of Science & Technology

Our goal is to bring high-quality research to the widest possible audience

INSTRUCTIONS TO AUTHORS

(REGULAR ISSUE)

(Manuscript Preparation & Submission Guide)

Revised: November 2020

Please read the *Pertanika* guidelines and follow these instructions carefully. The Chief Executive Editor reserves the right to return manuscripts that are not prepared in accordance with these guidelines.

MANUSCRIPT PREPARATION Manuscript Types

Pertanika accepts submission of mainly 4 types of manuscripts

- that have not been published elsewhere (including proceedings)
- that are not currently being submitted to other journals

1. Regular article

Regular article is a full-length original empirical investigation, consisting of introduction, methods, results, and discussion. Original research work should present new and significant findings that contribute to the advancement of the research area. *Analysis and Discussion* must be supported with relevant references.

Size: Generally, each manuscript is **not to exceed 6000 words** (excluding the abstract, references, tables, and/or figures), a maximum of **80 references**, and **an abstract of less than 250 words**.

2. Review article

A review article reports a critical evaluation of materials about current research that has already been published by organising, integrating, and evaluating previously published materials. It summarises the status of knowledge and outlines future directions of research within the journal scope. A review article should aim to provide systemic overviews, evaluations, and interpretations of research in a given field. Re-analyses as meta-analysis and systemic reviews are encouraged.

Size: Generally, it is expected **not to exceed 6000 words** (excluding the abstract, references, tables, and/or figures), a maximum of **80 references**, and **an abstract of less than 250 words**.

3. Short communications

Each article should be timely and brief. It is suitable for the publication of significant technical advances and maybe used to:

- (a) reports new developments, significant advances and novel aspects of experimental and theoretical methods and techniques which are relevant for scientific investigations within the journal scope;
- (b) reports/discuss on significant matters of policy and perspective related to the science of the journal, including 'personal' commentary;
- (c) disseminates information and data on topical events of significant scientific and/or social interest within the scope of the journal.

Size: It is limited to **3000 words** and have a maximum of **3 figures and/or tables, from 8 to 20 references, and an abstract length not exceeding 100 words**. The information must be in short but complete form and it is not intended to publish preliminary results or to be a reduced version of a regular paper.

4. Others

Brief reports, case studies, comments, concept papers, letters to the editor, and replies on previously published articles may be considered.

Language Accuracy

Pertanika emphasises on the linguistic accuracy of every manuscript published. Articles can be written in **English** or **Bahasa Malaysia** and they must be competently written and presented in clear and concise grammatical English/Bahasa Malaysia. Contributors are strongly advised to have the manuscript checked by a colleague with ample experience in writing English manuscripts or a competent English language editor. For articles in Bahasa Malaysia, the title, abstract and keywords should be written in both English and Bahasa Malaysia.

Author(s) **may be required to provide a certificate** confirming that their manuscripts have been adequately edited. **All editing costs must be borne by the authors.**

Linguistically hopeless manuscripts will be rejected straightaway (e.g., when the language is so poor that one cannot be sure of what the authors are really trying to say). This process, taken by authors before submission, will greatly facilitate reviewing, and thus, publication.

MANUSCRIPT FORMAT

The paper should be submitted in **one-column format** with 1.5 line spacing throughout. Authors are advised to use Times New Roman 12-point font and *MS Word* format.

1. Manuscript Structure

The manuscripts, in general, should be organised in the following order:

Page 1: Running title

This page should **only** contain the running title of your paper. The running title is an abbreviated title used as the running head on every page of the manuscript. The running title **should not exceed 60 characters, counting letters and spaces.**

Page 2: Author(s) and Corresponding author's information

General information: This page should contain the **full title** of your paper **not exceeding 25 words**, with the name of all the authors, institutions and corresponding author's name, institution and full address (Street address, telephone number (including extension), handphone number, and e-mail address) for editorial correspondence. **The corresponding author must be clearly indicated with a superscripted asterisk symbol (*).**

Authors' name: The names of the authors should be named **in full without academic titles.** For Asian (Chinese, Korean, Japanese, Vietnamese), please write first name and middle name before surname (family name). The last name in the sequence is considered the surname.

Authors' addresses: Multiple authors with different addresses must indicate their respective addresses separately by superscript numbers.

Tables/figures list: A list of the number of **black and white/colour figures and tables** should also be indicated on this page. See "**5. Figures & Photographs**" for details.

Example (page 2):

Fast and Robust Diagnostic Technique for the Detection of High Leverage Points

Habshah Midi^{1,2*}, Hasan Talib Hendi¹, Jayanthi Arasan² and Hassan Uraibi³

¹*Institute for Mathematical Research, Universiti Putra Malaysia, 43400 UPM, Serdang, Selangor, Malaysia*

²*Department of Mathematics, Faculty of Science, Universiti Putra Malaysia, 43400 UPM, Serdang, Selangor, Malaysia*

³*Department of Statistics, University of Al-Qadisiyah, 88 -Al-Qadisiyah -Al-Diwaniyah, Iraq*

E-mail addresses

habshah@upm.edu.my (Habshah Midi)

h.applied.t88@gmail.com (Hasan Talib Hendi)

jayanthi@upm.edu.my (Jayanthi Arasan)

hssn.sami1@gmail.com (Hassan Uraibi)

*Corresponding author

List of Table/Figure: Table 1.

Figure 1.

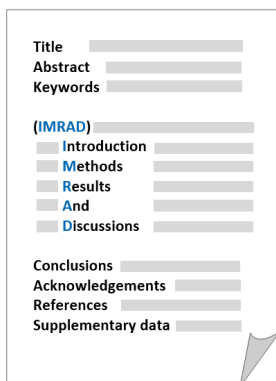
Page 3: Abstract

This page should **repeat** the **full title** of your paper with only the **Abstract**, usually in one paragraph and **Keywords**.

Keywords: *Not more than 8 keywords in alphabetical order must be provided to describe the content of the manuscript.*

Page 4: Text

A regular paper should be prepared with the headings *Introduction, Materials and Methods, Results and Discussions, Conclusions, Acknowledgements, References, and Supplementary data* (if any) in this order. The literature review may be part of or separated from the *Introduction*.



Title _____
 Abstract _____
 Keywords _____

(IMRAD)

Introduction _____
 Methods _____
 Results _____
 And _____
 Discussions _____

Conclusions _____
 Acknowledgements _____
 References _____
 Supplementary data _____

MAKE YOUR ARTICLES AS CONCISE AS POSSIBLE

Most scientific papers are prepared according to a format called IMRAD. The term represents the first letters of the words Introduction, Materials and Methods, Results, And, Discussion. It indicates a pattern or format rather than a complete list of headings or components of research papers; the missing parts of a paper are: Title, Authors, Keywords, Abstract, Conclusions, and References. Additionally, some papers include Acknowledgments and Appendices.

The Introduction explains the scope and objective of the study in the light of current knowledge on the subject; the Materials and Methods describes how the study was conducted; the Results section reports what was found in the study; and the Discussion section explains meaning and significance of the results and provides suggestions for future directions of research. The manuscript must be prepared according to the Journal's instructions to authors.

2. Levels of Heading

Level of heading	Format
1 st	LEFT, BOLD, UPPERCASE
2 nd	Flush left, Bold, Capitalise each word
3 rd	Bold, Capitalise each word, ending with .
4 th	Bold italic, Capitalise each word, ending with .

3. Equations and Formulae

These must be set up clearly and should be typed double-spaced. Numbers identifying equations should be in square brackets and placed on the right margin of the text.

4. Tables

- All tables should be prepared in a form consistent with recent issues of *Pertanika* and should be numbered consecutively with Roman numerals (Table 1, Table 2).
- A brief title should be provided, which should be shown at the top of each table (APA format):

Example:

Table 1

PVY infected Nicotiana tabacum plants optical density in ELISA

- Explanatory material should be given in the table legends and footnotes.
- Each table should be prepared on a new page, embedded in the manuscript.
- Authors are advised to keep backup files of all tables.

**** Please submit all tables in Microsoft word format only, because tables submitted as image data cannot be edited for publication and are usually in low-resolution.**

5. Figures & Photographs

- Submit an original figure or photograph.
- Line drawings must be clear, with a high black and white contrast.
- Each figure or photograph should be prepared on a new page, embedded in the manuscript for reviewing to keep the file of the manuscript under 5 MB.
- These should be numbered consecutively with Roman numerals (Figure 1, Figure 2).
- Provide a brief title, which should be shown at the bottom of each table (**APA format**):

Example: Figure 1. PVY-infected in vitro callus of Nicotiana tabacum

- If a figure has been previously published, acknowledge the original source, and submit written permission from the copyright holder to reproduce the material.
- Authors are advised to keep backup files of all figures.

**** Figures or photographs must also be submitted separately as TIFF or JPEG, because figures or photographs submitted in low-resolution embedded in the manuscript cannot be accepted for publication. For electronic figures, create your figures using applications that are capable of preparing high-resolution TIFF files.**

6. Acknowledgement

Any individuals and entities who have contributed to the research should be acknowledged appropriately.

7. References

References begin on their own page and are listed in alphabetical order by the first author's last name. Only references cited within the text should be included. All references should be in 12-point font and double-spaced. If a Digital Object Identifier (DOI) is listed on a print or electronic source, it is required to include the DOI in the reference list. Use Crossref to find a DOI using author and title information.

NOTE: When formatting your references, please follow the **APA-reference style** (7th edition) (refer to the examples). Ensure that the references are strictly in the journal's prescribed style, failing which your article will **not be accepted for peer-review**. You may refer to the *Publication Manual of the American Psychological Association* (<https://apastyle.apa.org/>) for further details.

Examples of reference style are given below:

Books		
	Insertion in text	In reference list
Book/E-Book with 1-2 authors	<p>Information prominent' (the author's name is within parentheses):</p> <p>... (Staron, 2020)</p> <p>... (Darus & Rasdi, 2019)</p> <p>... Or</p> <p>'Author prominent' (the author's name is outside the parentheses):</p> <p>(Starron, 2020)...</p> <p>Darus and Rasdi (2019) ...</p>	<p>Staron, M. (2020). <i>Action research in software engineering</i>. Springer International Publishing. https://doi.org/10.1007/978-3-030-32610-4</p> <p>Darus, A., & Rasdi, I. (2019). <i>Introduction to occupational health a workbook</i>. UPM Press.</p>
Book/E-Book with 3 or more authors	<p><i>For all in-text references, list only the first author's family name and followed by 'et al.'</i></p> <p>Information prominent' (the author's name is within parentheses):</p> <p>... (Yusof et al., 2020)</p> <p>... Or</p> <p>'Author prominent' (the author's name is outside the parentheses):</p> <p>Yusof et al. (2020) ...</p>	<p>Yusof, N. A., Azmi, U. Z. M., Ariffin, N., & Rahman, S. F. A. (2020). <i>Biosensors and chemical sensors: A practical approach</i>. UPM Press.</p>
Book/E-Book with more than 20 authors		<p>For books with more than 20 authors, please follow the guidelines for journal articles with more than 20 authors.</p>
Chapter in an edited Book/E-Book	<p>Information prominent' (the author's name is within parentheses):</p> <p>... (Mainzer, 2020) ...</p> <p>... (Tang et al., 2020) ...</p> <p>Or</p> <p>'Author prominent' (the author's name is outside the parentheses):</p> <p>Mainzer (2020) ...</p> <p>Tang et al. (2020) ...</p>	<p>Mainzer, K. (2020). Logical thinking becomes automatic. In K. Mainzer (Ed.), <i>Artificial intelligence-When do machines take over?</i> (pp. 15-45). Springer. https://doi.org/10.1007/978-3-662-59717-0_3</p> <p>Tang, W., Khavarian, M., Yousefi, A., & Cui, H. (2020). Properties of self-compacting concrete with recycled concrete aggregates. In R. Siddique (Ed.), <i>Self-Compacting Concrete: Materials, Properties, and Applications</i> (pp. 219-248). Woodhead Publishing. https://doi.org/10.1016/B978-0-12-817369-5.00009-X</p>

	Insertion in text	In reference list
Editor	<p>Information prominent' (the author's name is within parentheses): ... (Kesharwani, 2020) (Lanza et al., 2020) ... Or 'Author prominent' (the author's name is outside the parentheses): Kesharwani (2020) ... Lanza et al. (2020) ...</p>	<p>Kesharwani, P. (Ed.). (2020). <i>Nanotechnology based approaches for tuberculosis treatment</i>. Academic Press.</p> <p>Lanza, R., Langer, R., Vacanti, J. P., & Atala, A. (Eds.). (2020). <i>Principles of tissue engineering</i>. Academic press. https://doi.org/10.1016/C2018-0-03818-9</p>
Several works by the same author in the same year	<p>Information prominent' (the author's name is within parentheses): ... (Aggarwal & Aggarwal, 2020a, 2020b) ... Or 'Author prominent' (the author's name is outside the parentheses): Aggarwal & Aggarwal (2020a, 2020b) ...</p>	<p>Aggarwal, P., & Aggarwal, Y. (2020a). Strength properties of SCC. In R. Siddique (Ed.), <i>Self-Compacting Concrete: Materials, Properties, and Applications</i> (p. 83-115). Woodhead Publishing. doi: https://doi.org/10.1016/B978-0-12-817369-5.00004-0</p> <p>Aggarwal, P., & Aggarwal, Y. (2020b). Carbonation and corrosion of SCC. In R. Siddique (Ed.), <i>Self-Compacting Concrete: Materials, Properties, and Applications</i> (p. 147-193). Woodhead Publishing. doi: https://doi.org/10.1016/B978-0-12-817369-5.00007-6</p>
Journals		
Journal article with 1-2 authors	<p>Information prominent' (the author's name is within parentheses): ... (Laan & Fox, 2019) ... Or 'Author prominent' (the author's name is outside the parentheses): Laan and Fox (2019) ...</p>	<p>Laan, E., & Fox, J. W. (2019). An experimental test of the effects of dispersal and the paradox of enrichment on metapopulation persistence. <i>Oikos</i>, 129(1), 49-58. https://doi.org/10.1111/oik.06552</p>
Journal article with 3 or more authors	<p><i>For all in-text references, list only the first author's family name and followed by 'et al.'</i> Information prominent' (the author's name is within parentheses): ... (Midi et al., 2020) (Shagufta et al., 2017) ... Or 'Author prominent' (the author's name is outside the parentheses): Midi et al. (2020) ... Shagufta et al. (2017) ...</p>	<p>Midi, H., Hendi, H. T., Arasan, J., & Uraibi, H. (2020). Fast and Robust Diagnostic Technique for the Detection of High Leverage Points. <i>Pertanika Journal of Science & Technology</i>, 28(4), 1203-1220.</p> <p>Shagufta, B., Sivakumar, M., Kumar, S., Agarwal, R. K., Bhilegaonkar, K. N., Kumar, A., & Dubal, Z. B. (2017). Antimicrobial resistance and typing of Salmonella isolated from street vended foods and associated environment. <i>Journal of Food Science and Technology</i>, 54(8), 2532-2539. doi: https://doi.org/10.1007/s13197-017-2698-1</p>
Journal article with more than 20	<p>Information prominent' (the author's name is within parentheses): ... (Wiskunde et al., 2019) ... Or 'Author prominent' (the author's name is outside the parentheses): Wiskunde et al. (2019) ...</p>	<p>Wiskunde, B., Arslan, M., Fischer, P., Nowak, L., Van den Berg, O., Coetzee, L., Juárez, U., Riyaziyyat, E., Wang, C., Zhang, I., Li, P., Yang, R., Kumar, B., Xu, A., Martinez, R., McIntosh, V., Ibáñez, L. M., Mäkinen, G., Virtanen, E., ... Kovács, A. (2019). Indie pop rocks mathematics: Twenty One Pilots, Nicolas Bourbaki, and the empty set. <i>Journal of Improbable Mathematics</i>, 27(1), 1935-1968. https://doi.org/10.0000/3mp7y-537</p>
Journal article with an article number	<p>Information prominent' (the author's name is within parentheses): ... (Roe et al., 2020) ... Or 'Author prominent' (the author's name is outside the parentheses): Roe et al. (2020) ...</p>	<p>Roe, E. T., Bies, A. J., Montgomery, R. D., Watterson, W. J., Parris, B., Boydston, C. R., Sereno, M. E., & Taylor, R. P. (2020). Fractal solar panels: Optimizing aesthetic and electrical performances. <i>Plos One</i>, 15(3), Article e0229945. https://doi.org/10.1371/journal.pone.0229945</p>
Journal article with missing information	<p>Information prominent' (the author's name is within parentheses): ... (Alfirevic et al., 2017) (Hayat et al., 2020) (Fan et al., 2020) ...</p>	<p>Missing volume number Alfirevic, Z., Stampalija, T., & Dowswell, T. (2017). Fetal and umbilical Doppler ultrasound in high-risk pregnancies (review). <i>Cochrane Database of Systematic Reviews</i>, (6), 1-163. https://doi.org/10.1002/14651858.CD007529.pub4. Copyright</p>

	Insertion in text	In reference list
Journal article with missing information	Or 'Author prominent' (the author's name is outside the parentheses): Alfirevic et al. (2017) ... Hayat et al. (2020) ... Fan et al. (2020) ...	Missing issue number Hayat, A., Shaishta, N., Mane, S. K. B., Hayat, A., Khan, J., Rehman, A. U., & Li, T. (2020). Molecular engineering of polymeric carbon nitride based Donor-Acceptor conjugated copolymers for enhanced photocatalytic full water splitting. <i>Journal of colloid and interface science</i> , 560, 743-754. https://doi.org/10.1016/j.jcis.2019.10.088 Missing page or article number Fan, R. G., Wang, Y. B., Luo, M., Zhang, Y. Q., & Zhu, C. P. (2020). SEIR-Based COVID-19 Transmission Model and Inflection Point Prediction Analysis. <i>Dianzi Keji Daxue Xuebao/Journal of the University of Electronic Science and Technology of China</i> , 49(3). https://doi.org/10.12178/1001-0548.9_2020029
Several works by the same author in the same year	Information prominent' (the author's name is within parentheses): ... (Chee et al., 2019a, 2019b) ... Or 'Author prominent' (the author's name is outside the parentheses): Chee et al. (2019a, 2019b) ...	Chee, S. S., Jawaid, M., Sultan, M. T. H., Alothman, O. Y., & Abdullah, L. C. (2019a). Accelerated weathering and soil burial effects on colour, biodegradability and thermal properties of bamboo/kenaf/epoxy hybrid composites. <i>Polymer Testing</i> , 79, Article 106054. https://doi.org/10.1016/j.polymeresting.2019.106054 Chee, S. S., Jawaid, M., Sultan, M. T. H., Alothman, O. Y., & Abdullah, L. C. (2019b). Evaluation of the hybridization effect on the thermal and thermo-oxidative stability of bamboo/kenaf/epoxy hybrid composites. <i>Journal of Thermal Analysis and Calorimetry</i> , 137(1), 55-63. https://doi.org/10.1007/s10973-018-7918-z
Newspaper		
Newspaper article – with an author	... (Shamshuddin, 2019) ... Or ... Shamshuddin (2019) ...	Shamshuddin, J. (2019, September 23). Lynas plant waste residue can be used to boost oil palm growth? <i>New Straits Times</i> . https://www.nst.com.my/opinion/letters/2019/09/523930/lynas-plant-waste-residue-can-be-used-boost-oil-palm-growth
Newspaper article – without an author	("Zoonotic viruses," 2017). OR "Zoonotic viruses" (2017) ... Use a shortened title (or full title if it is short) in Headline Case enclosed in double quotation marks.	Zoonotic viruses like swine flu are ticking time bombs, say experts. (2020, July 4). <i>New Straits Times</i> , 3.
Dissertation/Thesis		
Published Dissertation or Thesis References	... (Rivera, 2016) ... Or ... Rivera (2016) ...	Rivera, C. (2016). <i>Disaster risk management and climate change adaptation in urban contexts: Integration and challenges</i> [Doctoral dissertation, Lund University]. Lund University Publications. https://lup.lub.lu.se/search/ws/files/5471705/8570923.pdf
Unpublished Dissertation or Thesis References	... (Brooks, 2014) ... Or ... Brooks (2014) ...	Brooks, J. D. (2015). <i>Bamboo as a strengthening agent in concrete beams for medium height structures</i> [Unpublished Doctoral dissertation]. The University of Washington.
Conference/Seminar Papers		
Conference proceedings published in a journal	... (Duckworth et al., 2019) ... Or Duckworth et al. (2019) ...	Duckworth, A. L., Quirk, A., Gallop, R., Hoyle, R. H., Kelly, D. R., & Matthews, M. D. (2019). Cognitive and noncognitive predictors of success. <i>Proceedings of the National Academy of Sciences, USA</i> , 116(47), 23499-23504. https://doi.org/10.1073/pnas.1910510116
Conference proceedings published as a book chapter	... (Bedenel et al., 2019) ... Or Bedenel et al. (2019) ...	Bedenel, A. L., Jourdan, L., & Biernacki, C. (2019). Probability estimation by an adapted genetic algorithm in web insurance. In R. Battiti, M. Brunato, I. Kotsireas, & P. Pardalos (Eds.), <i>Lecture notes in computer science: Vol. 11353. Learning and intelligent optimization</i> (pp. 225-240). Springer. https://doi.org/10.1007/978-3-030-05348-2_21

	Insertion in text	In reference list
Online	... (Gu et al., 2018) ... Or Gu et al. (2018) ...	Gu, X., Yu, J., Han, Y., Han, M., & Wei, L. (2019, July 12-14). <i>Vehicle lane change decision model based on random forest</i> . [Paper presentation]. 2019 IEEE International Conference on Power, Intelligent Computing and Systems (ICPICS), Shenyang, China. https://doi.org/10.1109/ICPICS47731.2019.8942520
Government Publications		
Government as author	First in-text reference: Spell out the full name with the abbreviation of the body. ... National Cancer Institute (2019) ... Or ... (National Cancer Institute, 2019) ... Subsequent in-text reference: ... NCI (2019) ... Or ... (NCI, 2019) ...	National Cancer Institute. (2019). <i>Taking time: Support for people with cancer</i> (NIH Publication No. 18-2059). U.S. Department of Health and Human Services, National Institutes of Health. https://www.cancer.gov/publications/patient-education/takingtime.pdf

8. General Guidelines

Abbreviations: Define alphabetically, other than abbreviations that can be used without definition. Words or phrases that are abbreviated in the *Introduction* and following text should be written out in full the first time that they appear in the text, with each abbreviated form in parenthesis. Include the common name or scientific name, or both, of animal and plant materials.

Authors' Affiliation: The primary affiliation for each author should be the institution where the majority of their work was done. If an author has subsequently moved to another institution, the current address may also be stated in the footer.

Co-Authors: The commonly accepted guideline for authorship is that one must have substantially contributed to the development of the paper and share accountability for the results. Researchers should decide who will be an author and what order they will be listed depending upon their order of importance to the study. Other contributions should be cited in the manuscript's *Acknowledgements*.

Similarity Index: All articles received must undergo the initial screening for originality before being sent for peer review. *Pertanika* does not accept any article with a similarity index exceeding **20%**.

Copyright Permissions: Authors should seek necessary permissions for quotations, artwork, boxes or tables taken from other publications or other freely available sources on the Internet before submission to *Pertanika*. The *Acknowledgement* must be given to the original source in the illustration legend, in a table footnote, or at the end of the quotation.

Footnotes: Current addresses of authors if different from heading may be inserted here.

Page Numbering: Every page of the manuscript, including the title page, references, and tables should be numbered.

Spelling: The journal uses American or British spelling and authors may follow the latest edition of the Oxford Advanced Learner's Dictionary for British spellings. Each manuscript should follow one type of spelling only.

SUBMISSION OF MANUSCRIPTS

All submissions must be made electronically using the **ScholarOne™ online submission system**, a web-based portal by Clarivate Analytics. For more information, go to our web page and click "**Online Submission (ScholarOne™)**".

Submission Checklist

1. MANUSCRIPT:

Ensure your manuscript has followed the *Pertanika* style particularly the first-4-pages as explained earlier. The article should be written in a good academic style and provide an accurate and succinct description of the contents ensuring that grammar and spelling errors have been corrected before submission. It should also not exceed the suggested length.

2. DECLARATION FORM:

Author has to sign a declaration form. In signing the form, authors declare that the work submitted for publication is original, previously unpublished, and not under consideration for any publication elsewhere.

Author has to agree to pay the publishing fee once the paper is accepted for publication in *Pertanika*.

3. COVER LETTER:

In Step 6 of the ScholarOne system, author is asked to upload a cover letter in *Pertanika* format. Please ignore this instruction and replace the cover letter with the **Declaration Form**.

Note:

COPYRIGHT FORM: Author will be asked to sign a copyright form when the paper is accepted. In signing the form, it is assumed that authors have obtained permission to use any copyrighted or previously published material. All authors must read and agree to the conditions outlined in the form and must sign the form or agree that the corresponding author can sign on their behalf. Articles cannot be published until a signed form (original pen-to-paper signature) has been received.

Visit our Journal's website for more details at <http://www.pertanika.upm.edu.my/>.

ACCESS TO PUBLISHED MATERIALS

Under the journal's open access initiative, authors can choose to download free material (via PDF link) from any of the journal issues from *Pertanika*'s website. Under "**Browse Journals**" you will see a link, "*Regular Issue*", "*Special Issue*" or "*Archives*". Here you will get access to all current and back-issues from 1978 onwards. No hard copy of journals or offprints are printed.

Visit our Journal's website at:

http://www.pertanika.upm.edu.my/regular_issues.php for "Regular Issue"

http://www.pertanika.upm.edu.my/cspecial_issues.php for "Special Issue"

http://www.pertanika.upm.edu.my/journal_archives.php for "Archives"

PUBLICATION CHARGE

Upon acceptance of a manuscript, a processing fee of RM 750 / USD 250 will be imposed on authors; RM 750 for any corresponding author affiliated to an institution in Malaysia; USD 250 for any corresponding author affiliated to an institution outside Malaysia. Payment must be made online at <https://paygate.upm.edu.my/action.do?do=>

Any queries may be directed to the **Chief Executive Editor's** office via email to executive_editor.pertanika@upm.edu.my

Medical and Health Sciences

Molecular Markers and Phylogenetic Analysis of UPMT27, a Field Isolate of the Malaysian Fowl Adenovirus Associated with Inclusion Body Hepatitis 547
Salisu Ahmed, Abdul Razak Mariatulqabtiyah, Mohd Hair Bejo, Abdul Rahman Omar, Aini Ideris and Nurulfiza Mat Isa

Optimisation and Evaluation of Antibacterial Topical Preparation from Malaysian Kelulut Honey using Guar Gum as Polymeric Agent 565
Mohd Amir Shahlan Mohd-Aspar, Raihana Zahirah Edros and Norul Amilin Hamzah

Identification and Antibiotic Resistance Profile of *Salmonella* spp. and *Citrobacter* spp. Isolated from Street-Vended Beverages 593
Siti Shahara Zulfakar, Noraziah Mohamad Zin, Siti Nur Shafika Mat Zalami and Nur Syakirah Mohd Nawawee

Short Communication

In Silico Designing of a Multi-Epitope Based Vaccine Candidate Against Human Adenovirus Type B3 Respiratory Infections by Utilising Various Immunoinformatics Approaches 607
Somnath Panda, Urmila Banik and Arun Kumar Adhikary

Earth Sciences

Comparison of Proximate Composition of Raw and Cooked Intramuscle Tissue of *Thunnus tonggol* from Terengganu, Malaysia 629
Norhazirah Abd Aziz, Ahmad Shamsudin Ahmad, Adiana Ghazali, Nurul Izzah Ahmad, Ahmad Ali and Meng-Chuan Ong

Distribution of Benthic Macroinvertebrates in Seafloor Northward of Pulau Indah, Klang 641
Mohd Sophian Mohd Kasihmuddin and Zaidi Che Cob

Flood-Modeling and Risk Map Simulation for Mae Suai Dam-Break, Northern Thailand 663
Anurak Busaman, Somporn Chuai-Aree, Salang Musikasuwan and Rhysa McNeil

Chemical Sciences

Differentiation Unclean and Cleaned Edible Bird's Nest using Multivariate Analysis of Amino Acid Composition Data 677
Nurul Alia Azmi, Ting Hun Lee, Chia Hau Lee, Norfadilah Hamdan and Kian Kai Cheng

Material Sciences

Effect of Sodium Hydroxide (NaOH) Treatment on Coconut Coir Fibre and its Effectiveness on Enhancing Sound Absorption Properties 693
Ida Norfaslia Nasidi, Lokman Hakim Ismail and Emedya Murniwaty Samsudin

Shoreline Change and its Impact on Land use Pattern and Vice Versa-A Critical Analysis in and Around Digha Area between 2000 and 2018 using Geospatial Techniques <i>Anindita Nath, Bappaditya Koley, Subhajit Saraswati, Basudeb Bhatta and Bidhan Chandra Ray</i>	331
Surface Treatment of Cement based Composites: Nano Coating Technique <i>Isam Mohamad Ali, Tholfekar Habeeb Hussain and Ahmed Samir Naje</i>	349
Environmental Sciences	
Quantifying Suspended Sediment using Acoustic Doppler Current Profiler in Tidung Island Seawaters <i>Henry Munandar Manik and Randi Firdaus</i>	363
Carbon Footprint of Built Features and Planting Works during Construction, Maintenance and Renewal Stages at Urban Parks in Petaling Jaya, Selangor <i>Nurzuliza Jamirsah, Ismail Said, Badrulzaman Jaafar and Mohd Haniff Mohd Hassani</i>	387
Optimisation of Culture Conditions for PLA-food-packaging Degradation by <i>Bacillus</i> sp. SNRUSA4 <i>Suwapha Sawiphak and Aroon Wongjiratthiti</i>	407
Synthesis of Magnetic Activated Carbon Treated with Sodium Dodecyl Sulphate <i>Palsan Sannasi Abdullah, Huda Awang and Jayanthi Barasarathi</i>	427
Information, Computer & Communication Technologies	
<i>Review Article</i>	
Multilingual Sentiment Analysis: A Systematic Literature Review <i>Nur Atiqah Sia Abdullah and Nur Ida Aniza Rusli</i>	445
<i>Review Article</i>	
Internet of Things (IoT) Implementation in Learning Institutions: A Systematic Literature Review <i>Ruth Chweya and Othman Ibrahim</i>	471
LTE Network Analysis in Frequency Reuse Recycling Techniques <i>Muhammad Sabir Hussain, Nasri Suleiman and Nor Kamariah Noordin</i>	519
Algorithm for B-scan Image Reconstruction in Optical Coherence Tomography <i>Kranti Patili, Anurag Mahajan, Balamurugan Subramani, Arulmozhivarman Pachiyappan and Roshan Makkar</i>	533

Bifurcation Analysis of an Exothermic Biocatalytic Reaction System <i>'Afifi Md Desa, Mohd Hafiz Mohd and Mohamad Hekarl Uzir</i>	165
Mathematical Sciences	
Predictive Performance of Logistic Regression for Imbalanced Data with Categorical Covariate <i>Hezlin Aryani Abd Rahman, Yap Bee Wah and Ong Seng Huat</i>	181
Elastic-Net Regression based on Empirical Mode Decomposition for Multivariate Predictors <i>Abdullah Suleiman Al-Jawarneh and Mohd. Tahir Ismail</i>	199
A New Parametric Function-Based Dynamic Lane Changing Trajectory Planning and Simulation Model <i>Md. Mijanoor Rahman, Mohd. Tahir Ismail, Norhashidah Awang and Majid Khan Majahar Ali</i>	217
Combined Impacts of Predation, Mutualism and Dispersal on the Dynamics of a Four-Species Ecological System <i>Murtala Bello Aliyu and Mohd Hafiz Mohd</i>	233
Revisited the Critical Load Assessment of Huang et al. on Willems Tested Beck Column <i>Peter Praveen Jakkana, Nageswara Rao Boggarapu, Mahaboob Bodanapu, Appa Rao Bhogapurapu Venkata, Narayana Cherukuri and Harnath Yeddala</i>	251
Modelling High Dimensional Paddy Production Data using Copulas <i>Nuranisyha Mohd Roslan, Wendy Ling Shinyie and Sim Siew Ling</i>	263
Logic Learning in Adaline Neural Network <i>Nadia Athirah Norani, Mohd Shareduwan Mohd Kasihmuddin, Mohd. Asyraf Mansor and Noor Saifurina Nana Khurizan</i>	285
Applied Sciences and Technologies	
Improvement of Bioethanol Production in Consolidated Bioprocessing (CBP) via Consortium of <i>Aspergillus niger</i> B2484 and <i>Trichoderma asperellum</i> B1581 <i>Mona Fatin Syazwane Mohamed Ghazali, Muskhazli Mustafa, Nur Ain Izzati Mohd Zainudin and Nor Azwady Abd Aziz</i>	301
Drying Characteristics of Jackfruit and Snake Fruit using Freeze Dryer <i>Joko Nugroho Wahyu Karyadi, Siti Rahma, Ronal Sitindaon, Dionisia Gusda Primadita Putri and Dwi Ayuni</i>	317

Contents

Foreword <i>Abu Bakar Salleh</i>	i
Engineering Sciences	
<i>Review Article</i>	
Former and Current Trend in Subsurface Irrigation Systems <i>Yasir Layth Alrubaye and Badronnisa Yusuf</i>	1
Forecasting Wind Speed in Peninsular Malaysia: An Application of ARIMA and ARIMA-GARCH Models <i>Nor Hafizah Hussin, Fadhilah Yusof, 'Aaishah Radziah Jamaludin and Siti Mariam Norrulashikin</i>	31
Harmonic Current Distortion Using the Linear Quadratic Regulator for a Grid-Connected Photovoltaic System <i>Oscar Andrew Zongo and Anant Oonsivilai</i>	59
Statistical Analysis of AC Dielectric Strength for Palm Oil under the Influence of Moisture <i>Muhammad Safwan Shukri, Norhafiz Azis, Jasronita Jasni, Robiah Yunus and Zaini Yaakub</i>	77
Performance Analysis of the Linear Launcher Motor via Modelling and Simulation for Light Electric Vehicles <i>Norramlee Mohamed Noor, Ishak Aris, Norhisam Misron, Suhaidi Shafie and Parvez Iqbal</i>	95
Implementation of Artificial Neural Network to Predict the Permeability and Solubility Models of Gypseous Soil <i>Imad Habeeb Obead, Hassan Ali Omran and Mohammed Yousif Fattah</i>	107
Public Tendering Practices, Issues and Directions - A Case of Pakistan Construction Sector <i>Ali Raza Khoso, Md Aminah Yusof, Muhammad Aslam Leghari, Fida Siddiqui and Samiullah Sohu</i>	123
Modeling of Inactivation of Biofilm Composing Bacteria with Low Intensity Electric Field: Prediction of Lowest Intensity and Mechanism <i>Mokhamad Tirono and Suhariningsih</i>	149



Pertanika Editorial Office, Journal Division
Putra Science Park
1st Floor, IDEA Tower II
UPM-MTDC Technology Centre
Universiti Putra Malaysia
43400 UPM Serdang
Selangor Darul Ehsan
Malaysia

<http://www.pertanika.upm.edu.my/>
E-mail: executive_editor.pertanika@upm.edu.my
Tel: +603 9769 1622

PENERBIT
UPM
UNIVERSITI PUTRA MALAYSIA
PRESS

<http://penerbit.upm.edu.my>
E-mail: penerbit@upm.edu.my
Tel: +603 9769 8851

